Lecture Notes in Control and Information Sciences

412

Leonid Fridman
Jaime Moreno
Rafael Iriarte (Eds.)

Sliding Modes after the First Decade of the 21st Century

State of the Art

Lecture Notes
in Control and Information Sciences 412

Editors: M. Thoma, F. Allgöwer, M. Morari

Leonid Fridman, Jaime Moreno,
and Rafael Iriarte (Eds.)

Sliding Modes after the First Decade of the 21st Century

State of the Art

Springer

Editors

Prof. Leonid Fridman
Universidad Nacional Autonoma de Mexico
Ciudad Universitaria, Instituto de Ingenieria
Departamento de Ingenieria de Control y Robotica
Division de Ingenieria Electrica
04510 Mexico, D.F.
Mexico
E-mail: lfridman@servidor.unam.mx

Prof. Jaime Moreno
Universidad Nacional Autonoma de Mexico
Ciudad Universitaria
Instituto de Ingenieria
04510 Mexico, D.F.
Mexico

Prof. Rafael Iriarte
Universidad Nacional Autonoma
de Mexico
Ciudad Universitaria,
Instituto de Ingenieria
Departamento de Ingenieria de
Control y Robotica
Division de Ingenieria Electrica
04510 Mexico, D.F.
Mexico

ISBN 978-3-642-22163-7 e-ISBN 978-3-642-22164-4

DOI 10.1007/978-3-642-22164-4

Lecture Notes in Control and Information Sciences ISSN 0170-8643

Library of Congress Control Number: 2011931876

Typeset & Cover Design: Scientific Publishing Services Pvt. Ltd., Chennai, India.

Printed on acid-free paper

9 8 7 6 5 4 3 2 1

springer.com

Lecture Notes in Control and Information Sciences

Edited by M. Thoma, F. Allgöwer, M. Morari

Further volumes of this series can be found on our homepage:
springer.com

Vol. 412: Fridman, L., Moreno, J., Iriarte R. (Eds.):
Sliding Modes after the First Decade of the 21st Century
595 p. 2011 [978-3-642-22163-7]

Vol. 411: Kaczorek, T.;
Selected Problems of Fractional Systems Theory
344 p. 2011 [978-3-642-20501-9]

Vol. 410: Bourlès, H., Marinescu, B.;
Linear Time-Varying Systems
637 p. 2011 [978-3-642-19726-0]

Vol. 409: Xia, Y., Fu, M., Liu, G.-P.;
Analysis and Synthesis of Networked Control Systems
198 p. 2011 [978-3-642-17924-2]

Vol. 408: Richter, J.H.;
Reconfigurable Control of Nonlinear Dynamical Systems
291 p. 2011 [978-3-642-17627-2]

Vol. 407: Lévine, J., Müllhaupt, P.:
Advances in the Theory of Control, Signals and Systems with Physical Modeling
380 p. 2010 [978-3-642-16134-6]

Vol. 406: Bemporad, A., Heemels, M., Johansson, M.:
Networked Control Systems
appro. 371 p. 2010 [978-0-85729-032-8]

Vol. 405: Stefanovic, M., Safonov, M.G.:
Safe Adaptive Control
appro. 153 p. 2010 [978-1-84996-452-4]

Vol. 404: Giri, F.; Bai, E.-W. (Eds.):
Block-oriented Nonlinear System Identification
425 p. 2010 [978-1-84996-512-5]

Vol. 403: Tóth, R.;
Modeling and Identification of Linear Parameter-Varying Systems
319 p. 2010 [978-3-642-13811-9]

Vol. 402: del Re, L.; Allgöwer, F.; Glielmo, L.; Guardiola, C.; Kolmanovsky, I. (Eds.):
Automotive Model Predictive Control
284 p. 2010 [978-1-84996-070-0]

Vol. 401: Chesi, G.; Hashimoto, K. (Eds.):
Visual Servoing via Advanced Numerical Methods
393 p. 2010 [978-1-84996-088-5]

Vol. 400: Tomás-Rodríguez, M.; Banks, S.P.:
Linear, Time-varying Approximations to Nonlinear Dynamical Systems
298 p. 2010 [978-1-84996-100-4]

Vol. 399: Edwards, C.; Lombaerts, T.; Smaili, H. (Eds.):
Fault Tolerant Flight Control
appro. 350 p. 2010 [978-3-642-11689-6]

Vol. 398: Hara, S.; Ohta, Y.; Willems, J.C.; Hisaya, F. (Eds.):
Perspectives in Mathematical System Theory, Control, and Signal Processing
appro. 370 p. 2010 [978-3-540-93917-7]

Vol. 397: Yang, H.; Jiang, B.; Cocquempot, V.:
Fault Tolerant Control Design for Hybrid Systems
191 p. 2010 [978-3-642-10680-4]

Vol. 396: Kozlowski, K. (Ed.):
Robot Motion and Control 2009
475 p. 2009 [978-1-84882-984-8]

Vol. 395: Talebi, H.A.; Abdollahi, F.; Patel, R.V.; Khorasani, K.:
Neural Network-Based State Estimation of Nonlinear Systems
appro. 175 p. 2010 [978-1-4419-1437-8]

Vol. 394: Pipeleers, G.; Demeulenaere, B.; Swevers, J.:
Optimal Linear Controller Design for Periodic Inputs
177 p. 2009 [978-1-84882-974-9]

Vol. 393: Ghosh, B.K.; Martin, C.F.; Zhou, Y.:
Emergent Problems in Nonlinear Systems and Control
285 p. 2009 [978-3-642-03626-2]

Vol. 392: Bandyopadhyay, B.; Deepak, F.; Kim, K.-S.: Sliding Mode Control Using Novel Sliding Surfaces
137 p. 2009 [978-3-642-03447-3]

Vol. 391: Khaki-Sedigh, A.; Moaveni, B.: Control Configuration Selection for Multivariable Plants
232 p. 2009 [978-3-642-03192-2]

Vol. 390: Chesi, G.; Garulli, A.; Tesi, A.; Vicino, A.: Homogeneous Polynomial Forms for Robustness Analysis of Uncertain Systems
197 p. 2009 [978-1-84882-780-6]

Vol. 389: Bru, R.; Romero-Vivó, S. (Eds.): Positive Systems
398 p. 2009 [978-3-642-02893-9]

Vol. 388: Jacques Loiseau, J.; Michiels, W.; Niculescu, S-I.; Sipahi, R. (Eds.): Topics in Time Delay Systems
418 p. 2009 [978-3-642-02896-0]

Vol. 387: Xia, Y.; Fu, M.; Shi, P.: Analysis and Synthesis of Dynamical Systems with Time-Delays
283 p. 2009 [978-3-642-02695-9]

Vol. 386: Huang, D.; Nguang, S.K.: Robust Control for Uncertain Networked Control Systems with Random Delays
159 p. 2009 [978-1-84882-677-9]

Vol. 385: Jungers, R.: The Joint Spectral Radius
144 p. 2009 [978-3-540-95979-3]

Vol. 384: Magni, L.; Raimondo, D.M.; Allgöwer, F. (Eds.): Nonlinear Model Predictive Control
572 p. 2009 [978-3-642-01093-4]

Vol. 383: Sobhani-Tehrani E.; Khorasani K.; Fault Diagnosis of Nonlinear Systems Using a Hybrid Approach
360 p. 2009 [978-0-387-92906-4]

Vol. 382: Bartoszewicz A.; Nowacka-Leverton A.; Time-Varying Sliding Modes for Second and Third Order Systems
192 p. 2009 [978-3-540-92216-2]

Vol. 381: Hirsch M.J.; Commander C.W.; Pardalos P.M.; Murphey R. (Eds.) Optimization and Cooperative Control Strategies: Proceedings of the 8th International Conference on Cooperative Control and Optimization
459 p. 2009 [978-3-540-88062-2]

Vol. 380: Basin M. New Trends in Optimal Filtering and Control for Polynomial and Time-Delay Systems
206 p. 2008 [978-3-540-70802-5]

Vol. 379: Mellodge P.; Kachroo P.; Model Abstraction in Dynamical Systems: Application to Mobile Robot Control
116 p. 2008 [978-3-540-70792-9]

Vol. 378: Femat R.; Solis-Perales G.; Robust Synchronization of Chaotic Systems Via Feedback
199 p. 2008 [978-3-540-69306-2]

Vol. 377: Patan K. Artificial Neural Networks for the Modelling and Fault Diagnosis of Technical Processes
206 p. 2008 [978-3-540-79871-2]

Vol. 376: Hasegawa Y. Approximate and Noisy Realization of Discrete-Time Dynamical Systems
245 p. 2008 [978-3-540-79433-2]

Vol. 375: Bartolini G.; Fridman L.; Pisano A.; Usai E. (Eds.) Modern Sliding Mode Control Theory
465 p. 2008 [978-3-540-79015-0]

Vol. 374: Huang B.; Kadali R. Dynamic Modeling, Predictive Control and Performance Monitoring
240 p. 2008 [978-1-84800-232-6]

Vol. 373: Wang Q.-G.; Ye Z.; Cai W.-J.; Hang C.-C. PID Control for Multivariable Processes
264 p. 2008 [978-3-540-78481-4]

Vol. 372: Zhou J.; Wen C. Adaptive Backstepping Control of Uncertain Systems
241 p. 2008 [978-3-540-77806-6]

Vol. 371: Blondel V.D.; Boyd S.P.; Kimura H. (Eds.) Recent Advances in Learning and Control
279 p. 2008 [978-1-84800-154-1]

Vol. 370: Lee S.; Suh I.H.; Kim M.S. (Eds.) Recent Progress in Robotics: Viable Robotic Service to Human
410 p. 2008 [978-3-540-76728-2]

Preface

This book is a collection of the Plenary and Semiplenary talks in the joint 11^{th} IEEE Workshop on Variable Structure Systems (VSS2010) and the principal meeting for the international project supported by *Fondo de Cooperación Internacional en Ciencia y Tecnología Unión Europea - México (FONCICYT)* 93302 "Automatization and Monitoring of Energy Production Processes via Sliding Mode Control". As the workshop organisers, together with the IEEE Technical Committee on Variable Structure Systems (VSS) and Sliding Modes (SM), we invited the heads of the 21 leading groups working in the fields of VSS and SM to present the recent contributions of their groups.

The book consists of three main parts:

Part I: VSS and SM Algorithms and their Analysis
Part II: Design Methods
Part III: Applications

The first part of the book (Part I: VSS and SM Algorithms and their Analysis) opens with a tutorial by Prof. Fridman. He presents the principal algorithms of sliding mode (SM) enforcement developed during the last 20 years. The history, advantages and disadvantages of second order and arbitrary order sliding mode algorithms, Lyapunov-based approach for second order SM, chattering investigation in higher order sliding mode (HOSM) controllers, HOSM-based observation and identification, integral sliding modes, adaptive SM controllers, HOSM-controllers-based uncertainties compensation, SM control for hybrid systems, output-based LQ control, relay delay control and SM control for distributed parameter systems are discussed. Furthermore, this chapter formulates and discusses important open problems.

Chapter 2, by Arie Levant, develops robust exact differentiators based on the homogeneity approach in order to produce robust output-feedback controllers. The chapter also presents simulation results and applications in the fields of control, signal and image processing.

The third chapter, by Igor M. Boiko, gives an overview of some available and emerging frequency domain methods of analysis of systems having conventional and

second-order sliding modes. The method of analysis of transient oscillations is given in detail. Furthermore, a frequency-domain criterion of finite-time convergence is presented in the chapter.

Chapter 4, by Jaime A. Moreno, presents advances in the design of Second Order Sliding Modes algorithms using Lyapunov methods, based on recently developed Lyapunov functions for some of these algorithms.

In the fifth chapter a new sliding mode control technique for a class of SISO dynamic systems is presented by Zhihong Man, Suiyang Khoo, Xinghuo Yu, Chunyan Miao, Jiong Jin and Feisiang Tay. An intelligent sliding mode controller is designed, for both stable and unstable closed-loop systems, which uses a recursive learning structure to assure that no chattering occurs in the sliding mode control system. The proposed controller design does not require a priori information on the upper and/or the lower bounds of the unknown system parameters and uncertain system dynamics.

Chapter 6, by Alessandro Pisano, Milan Rapaić and Elio Usai, outlines some results concerning the application of second-order sliding-mode techniques in the framework of control and estimation problems for some classes of fractional-order systems. Through the use of fractional-order sliding manifolds the authors present results concerning control, estimation and observation problems. The applicability of this theory in the framework of fault detection is also presented in the experimental section.

In Chapter 7, by Lei Yu, Jean-Pierre Barbot, Djamila Benmerzouk, Driss Boutat, Thierry Floquet and Gang Zheng, the authors discuss relations between first and high order sliding mode algorithms and both types of Zeno behaviors of switched dynamical systems. The finite time error convergence of a super-twisting based observer is studied, making use of the Henstock-Kurzweil integral. Finally, a two-tanks example is included to highlight the main ideas of the chapter.

As the start to the second part of the book (Part II: Design Methods), Chapter 8 by Xiaoran Han, Emilia Fridman and Sarah K. Spurgeon considers the development of sliding mode control strategies for linear, time delay systems with bounded disturbances that are not necessarily matched. A static output feedback sliding mode control design is considered in which Linear Matrix Inequalities (LMIs) are derived to compute solutions to both the existence problem and the finite time reachability problem that minimize the ultimate bound of the reduced-order sliding mode dynamics in the presence of time varying delay and unmatched disturbances. The emphasis of the chapter is on the development of frameworks that are constructive and applicable to real problems.

Next, in Chapter 9 by Hebertt Sira Ramírez, Alberto Luviano Juárez and John Cortés Romero, a new feedback controller design approach, devoid of state measurements, for the sliding mode control of a large class of linear switched systems is proposed. The approach regards the average Generalized Proportional Integral (GPI) output feedback controller design as a guide for defining the sliding mode features. It is assumed that the available output signal coincides with the system's flat output, an output capable of parameterizing all the variables in the system and exhibits no zero dynamics. Simulation results are presented along with experimental

results for the trajectory tracking problem on a popular DC-to-DC switched power converter of the "buck" type.

Chapter 10, by Liu Hsu, Eduardo V. L. Nunes, Tiago Roux Oliveira, Alessandro Jacoud Peixoto, José Paulo V. S. Cunha, Ramon R. Costa and Fernando Lizarralde, describes the main results developed by the authors in the area of output-feedback sliding mode control with a focus on SISO nonlinear systems. A linear growth restriction on the unmeasured states is assumed, while less restrictive conditions are imposed on the growth of nonlinearities depending on the measured output for the systems under consideration. Different tracking controllers for plants with arbitrary relative degree are presented and several approaches to overcome the relative degree obstacle are considered. Some experimental results are presented to illustrate the applicability of the control schemes in real systems.

In Chapter 11, by Christopher Edwards, Halim Alwi, Chee P. Tan and José Manuel Andrade da Silva, the use of sliding mode ideas for fault detection leading to fault tolerant control is described. The chapter discusses how sliding mode control and observer design methods can be advantageously used towards this end. A sliding mode observer is used to robustly estimate any unknown fault signal existing within the system based on appropriate scaling of the equivalent output estimation error injection signal. One advantage of these sliding mode methods over more traditional residual based observer schemes is that because the faults are reconstructed, both the "shape" and size of the faults are preserved. A further benefit of this approach is that because faults are reconstructed, these signals can be used to correct a faulty sensor; for example, to maintain reasonable performance until appropriate maintenance may be undertaken. This "virtual sensor" can be used in the control algorithm to form the output tracking error signal which is processed to generate the control signal. A recent application of sliding mode controllers for fault tolerant control is also presented.

The mean-square and mean-module filtering problems for a linear system with Gaussian white noises are then addressed in Chapter 12 by Michael Basin. Here, it is shown that the designed sliding mode mean-square filter generates the mean-square estimate, which has the same minimum estimation error variance as the best estimate given by the classical Kalman-Bucy filter, although the gain matrices of both filters are different. Furthermore, the designed sliding mode mean-module filter generates a mean-module estimate with a better value of the mean-module criterion in comparison to the mean-square Kalman-Bucy filter. The theoretical result is complemented with an illustrative example verifying performance of the designed filters. The paper then addresses the optimal controller problem for a linear system over linear observations with respect to different Bolza-Meyer criteria. The optimal solutions are obtained as sliding mode controllers, each consisting of a sliding mode filter and a sliding mode regulator. Performance of the obtained optimal controllers is verified in the illustrative example against the conventional LQG controller that is optimal for the quadratic Bolza-Meyer criterion.

Yuri Shtessel, Simon Baev, Christopher Edwards, Sarah Spurgeon and Alan Zinober study the problem of causal output tracking and observation in non-minimum phase nonlinear systems in Chapter 13. The extended method of Stable System

Center (ESSC) is used in two-fold manner: i) to generate reference profile for unstable internal states; ii) to estimate states of unstable internal dynamics. Two applications of the proposed technique are considered for illustration purposes: output voltage tracking in a nonminimum phase DC/DC electric power converter and output tracking in SISO systems with time-delayed output feedback. Numerical simulations are used to illustrate theoretical results.

Part II closes with Chapter 14 by Bijnan Bandyopadhyay and Fulwani Deepak. In this chapter, a nonlinear sliding surface is discussed to improve the transient response for general discrete-time MIMO linear systems with matched perturbations. The nonlinear surface modulates the closed-loop damping ratio from an initially low to final high value to achieve better transient performance. The control law is based on the discrete-time sliding mode equivalent control and thus eliminates chattering. The control law is proposed for both the case when the disturbance bound is known and the case when it is not. Multirate output feedback is used to relax the need of the entire state vector for implementation of the control law. A possible extension of the nonlinear surface to input-delay systems is also presented.

The last part of the book (Part III: Applications) opens with Chapter 15 by Michael Defoort, Thierry Floquet, Anne-Marie Kokosy and Wilfrid Perruquetti. This chapter derives a scheme for real time motion planning and robust control of a swarm of nonholonomic mobile robots evolving in an uncertain environment. This scheme consists of two main parts: (i) a real time collision-free motion planner; (ii) a trajectory tracking controller. In implementation, the motion planner dynamically generates the optimal trajectory while the robot runs. High precision motion tracking is achieved by the design of a higher order sliding mode controller based on geometric homogeneity properties. Experiments demonstrate the effectiveness of the proposed strategy.

Chapter 16, by Domingo Biel, Arnau Dòria-Cerezo, Enric Fossas, Raúl S. Muñoz-Aguilar and Rafael Ramos-Lara, reports two applications of SMC in power electronics: energy generation using a wound rotor synchronous machine and chattering reduction in a buck converter. In the former, three control schemes are analyzed, each with a particular sliding surface, while the latter uses Field Parallel Gate Arrays (FPGA) to reduce chattering in a buck converter based on a paper by V. Utkin; simulations and experimental results are included in both applications.

In Chapter 17 Franck Plestan, Vincent Brégeault, Alain Glumineau, Yuri Shtessel and Emmanuel Moulay present advanced control methodologies of uncertain nonlinear systems. The authors first propose an adaptive sliding mode controller that preserves the robustness of the system in the presence of bounded uncertainties/perturbations with unknown bounds. Due to the on-line adaptation, the proposed approach allows reducing control chattering. Then, a high order sliding mode control strategy that features a priory knowledge of the convergence time is presented. Finally, an output feedback second order sliding mode controller is presented and discussed. The control algorithms are applied to experimental set-up equipped by electrical or electropneumatic actuators.

Chapter 18 by Jesús de León Morales presents some control applications for electromechanical systems. This chapter intends to show the advantages of using sliding

mode techniques for control and observer design purposes oriented towards implementation. These domains are related with the research topics of the Mechatronics laboratory in the CIIDIT-UANL Research Institute, Nuevo Leon University.

Luis Martínez-Salamero and Angel Cid-Pastor study the use of sliding motions in converters in Chapter 19. This control strategy allows a systematic design of the three canonical elements for power processing, i.e., DC transformer, power gyrator and loss-free resistor (LFR). A search of candidates is performed by studying a great number of converters with topological constraints imposed by the nature of each canonical element. Several examples ranging from DC impedance matching by means of a DC transformer to LFR-based power factor correction illustrate the application of the synthesis.

Chapter 20, by Antonella Ferrara and Luca Massimiliano Capisani, address the use of higher order sliding modes to design robotic controllers. The chapter presents the application of the Second Order Sliding Mode (SOSM) design methodology to the control and supervision of industrial manipulators by proposing a robust control scheme and a diagnostic scheme to detect and, possibly, isolate and identify faults acting on the components of the system. The proposed SOSM motion controller and the SOSM observers designed to construct the diagnostic scheme are theoretically developed, and their practical application is described. Lastly, the authors experimentally verify the proposed approaches on a COMAU SMART3-S2 industrial robot manipulator.

In the closing chapter of the book, Chapter 21, Alexander G. Loukianov, Jose M. Cañedo, B. Castillo-Toledo and Edgar N. Sánchez present the systematic design of robust stabilizing nonlinear controllers for electric machines (synchronous and induction) in continuous and discrete time. This design is based on the combination of the Block Control feedback linearization, Sliding Mode (SM) and Neural Network (NN) control techniques. The Block Control technique is used to design a nonlinear sliding manifold in order to achieve error tracking. Then an SM algorithm, including integral and discrete time SMs, is implemented to ensure finite time convergence of the state vector to the designed SM manifold in the presence of matched and unmatched perturbations. This control scheme is the extended by including an NN identifier designed in the NBC form and used instead of the physical model.

It is our hope that this book will provide a clear and complete picture on the current state-of-the-art of VSS and SM theory.

Finally, we would like to thank Alfredo Sosa, a postgraduate student at the National Autonomous University of Mexico (UNAM), for all his work during the editing process of this book.

Mexico City, 2010

Leonid Fridman
Jaime Moreno
Rafael Iriarte

Contents

Part I: VSS and SM Algorithms and Their Analysis

1 Sliding Mode Enforcement after 1990: Main Results and Some Open Problems 3
L. Fridman
1.1 Sliding Mode Control Up until 1990 3
1.2 Second Order Sliding Modes: First Generation 4
1.2.1 Twisting Algorithm 4
1.2.2 The First Criticism of SOSM 5
1.2.3 The Super-Twisting Algorithm 5
1.2.4 The Sub-Optimal Algorithm 7
1.2.5 Recapitulations 7
1.3 Second Generation: Arbitrary Order Sliding Mode Controllers 8
1.3.1 Discussion on the Definition of r-th Order Sliding Motions 8
1.3.2 Arbitrary Order Sliding Mode Controllers 9
1.3.3 Black-Box Control 11
1.4 Terminal Sliding Mode Control 12
1.5 Third Generation: Non-Homogeneous HOSMs 15
1.6 Lyapunov Based Approach 15
1.7 Chattering Problem and HOSM 16
1.7.1 Chattering Analysis in the Frequency Domain 17
1.7.2 Singularly Perturbed Analysis of Homogeneous Sliding Modes in the Presence of Fast Actuators 22
1.7.3 Energy Based Approach 25
1.7.4 Recapitulation 26
1.7.5 Open Problems 26
1.8 HOSM Observation and Identification 26
1.8.1 HOSM Observation and Unknown Inputs Identification 27

1.8.2 Time Invariant Parameter Identification 30
1.8.3 Further Development 32
1.8.4 Recapitulation 32
1.8.5 Open Problems 33
1.9 Integral Sliding Mode Control 33
1.10 HOSM Output Based Control 35
1.10.1 Open Problems 37
1.11 Adaptive Sliding Mode Control 37
1.11.1 ASMC with Known Bounds for the Disturbance 37
1.11.2 ASMC without Known Bounds for the Disturbance 38
1.12 HOSM Based Unmatched Uncertainties Compensation 38
1.12.1 Black Box Control via HOSM 39
1.12.2 Model Based Application of HOSM 39
1.12.3 Exact Unmatched Uncertainties Compensation Based on HOSM Observation 40
1.12.4 Conclusions 41
1.13 VSS Methods for Hybrid Systems 42
1.13.1 Hybrid Nonlinear Systems 42
1.13.2 Hybrid Linear Systems 42
1.13.3 Open Problems 42
1.14 Relay Control with Delay 43
1.14.1 Oscillatory Nature of Relay Delayed Systems 43
1.14.2 Methods of the Relay Delayed Control Design 45
1.14.3 Prediction Method 45
1.14.4 Methods of Oscillation Control 46
1.14.5 Open Problems 47
1.15 Distributed Parameter Systems 47
References 49

2 Finite-Time Stability and High Relative Degrees in Sliding-Mode Control 59
Arie Levant
2.1 Introduction 59
2.2 Preliminaries 62
2.3 SISO Regulation Problem 63
2.3.1 Standard SISO Regulation Problem and the Idea of Its Solution 63
2.4 Homogeneity, Finite-Time Stability and Accuracy 64
2.5 Homogeneous Sliding Modes 67
2.5.1 Second Order Sliding Mode Controllers 67
2.5.2 Arbitrary Order Sliding Mode Controllers 69
2.6 Differentiation and Output-Feedback Control 72
2.6.1 Arbitrary Order Robust Exact Differentiation 72
2.6.2 Output-Feedback Control 73
2.7 Adjustment of the Controllers 75

2.7.1 Control Magnitude Adjustment 75
2.7.2 Parameter Adjustment 76
2.8 Advanced Issues 77
2.8.1 Chattering Analysis 77
2.8.2 Robustness Issues 81
2.8.3 Choosing the Parameters 82
2.9 Application and Simulation Examples 82
2.9.1 Control Simulation 82
2.9.2 Signal Processing: Real-Time Differentiation 86
2.9.3 Image Processing 88
2.10 Conclusions 90
References 90

3 Frequency-Domain Methods in Conventional and Higher-Order Sliding Mode Control 93
Igor M. Boiko
3.1 Introduction 93
3.2 Ideal and Real Sliding Modes: Poincare Maps and Frequency-Domain Approach 94
3.3 Analysis of Convergence – Quasi-Static DF Approach 96
3.4 Frequency-Domain Characteristics and Convergence Rate 102
3.5 Extension to Higher-Order Plants 106
3.6 Extention to Other Types of Controllers 109
3.7 Conclusions 111
References 112

4 Lyapunov Approach for Analysis and Design of Second Order Sliding Mode Algorithms 113
Jaime A. Moreno
4.1 Introduction 113
4.2 Problem Statement and Main Results 116
4.3 Finite Time Convergence of Unperturbed GSOA with Constant Gains 119
4.3.1 Stability Analysis without Perturbations: An ALE Approach 119
4.3.2 Convergence Time 120
4.4 Robustness and Exactness of the Perturbed GSOA with Constant Gains 121
4.4.1 The Class of Perturbations 121
4.4.2 Robust Stability Analysis: A Riccati Inequality Approach 122
4.4.3 Practical Stability 123
4.4.4 Frequency Domain Interpretation: The Circle Criterium 124

4.5 Uniformity of the GSOA with Constant Gains 126
4.5.1 A Non Quadratic Strong Lyapunov Function for the GSOA 126
4.5.2 Uniformity in the Convergence 127
4.5.3 An Alternative Robust Lyapunov Function 128
4.6 The GSOA with Variable Gains 128
4.7 Conclusions 129
4.8 Appendix 130
4.8.1 Proof of Theorem 4.1 132
4.8.2 Proof of Proposition 4.1 134
4.8.3 Proof of Theorem 4.2 135
4.8.4 Proof of Theorem 4.3 135
4.8.5 Proof of Theorem 4.4 138
4.8.6 Proof of Proposition 4.2 141
4.8.7 Proof of Proposition 4.3 143
4.8.8 Proof of Theorem 4.5 146
References 147

5 A New Design of Sliding Mode Control Systems 151
Zhihong Man, Suiyang Khoo, Xinghuo Yu, Chunyan Miao, Jiong Jin, Feisiang Tay
5.1 Introduction 152
5.2 Problem Formulation 154
5.3 Convergence Analysis 157
5.4 A Simulation Example 161
5.5 Conclusions 165
References 166

6 Second-Order Sliding Mode Approaches to Control and Estimation for Fractional Order Dynamics 169
A. Pisano, M. Rapaić, E. Usai
6.1 Introduction 169
6.2 Preliminaries on Fractional Calculus 171
6.3 Second-Order Sliding Mode Controllers for Multivariable Linear FOS 173
6.3.1 Sliding Manifold Design 174
6.3.2 Control-Input Design 177
6.3.3 Implementation Issues 178
6.3.4 Simulation Results 180
6.4 Second-Order Sliding Mode Based Observation and Estimation for FOS 181
6.4.1 Disturbance Observer for FOS 181
6.4.2 Discrete-Mode Identification for Switched FOS 184
6.4.3 Simulation Results 189
6.4.4 Disturbance Estimation Test 189

6.4.5 Discrete State Estimation Test 190
6.5 Experimental Fault Detection of a Hydraulic Plant 192
6.6 Conclusions 194
References 194

7 Discussion about Sliding Mode Algorithms, Zeno Phenomena and Observability 199
L. Yu, J.-P. Barbot, D. Benmerzouk, D. Boutat, T. Floquet, G. Zheng
7.1 Discussion on Zeno and Sliding Mode Behavior 200
7.2 Zeno Types 201
7.3 Mathematical Recalls of H-K Integral 202
7.4 Observability and Observer Design for Some Classes of Hybrid Dynamical System 205
7.4.1 First Basic Observability Form 205
7.4.2 Second Basic Observability Form 205
7.4.3 Extended Observability Form 205
7.4.4 Discussion on the Observability of the First Basic Observability Form 206
7.4.5 Discussion on the Observability of the Second Basic Observability Form 206
7.4.6 Observability for the Extended Observability Form 209
7.5 The Two Tanks Example 211
7.6 Conclusion 217
References 217

Part II: Sliding Mode Control Design

8 Output Feedback Sliding Mode Control of Uncertain Systems in the Presence of State Delay with Applications 223
X. Han, E. Fridman, S.K. Spurgeon
8.1 Introduction 223
8.2 Problem Formulation 226
8.3 A General Framework for Design 226
8.4 Existence Problem 227
8.5 Reachability Problem 232
8.6 Liquid Monopropellant Rocket Motor Control 238
8.7 Conclusion 242
References 242

9 Sliding Mode Controller Design: An Input-Output Approach 245
Hebertt Sira-Ramírez, Alberto Luviano-Juárez, John Cortés-Romero
9.1 Introduction 245
9.2 An Introductory Example 247
9.2.1 An Average GPI Controller Design Devoid of Observers 247

9.2.2 A Switched Control Interpretation of the Average Design . . . 249
9.2.3 A GPI Observer Based Approach . . . 250
9.3 Definitions and Main Results . . . 254
9.4 An Application Example with Simulations . . . 257
9.4.1 An Observer-Free Approach . . . 258
9.4.2 A GPI Observer Based Approach . . . 259
9.5 A "Buck" Converter Example with Experimental Results . . . 261
9.5.1 The Buck Converter Model . . . 262
9.5.2 The GPI Sliding Mode Controller . . . 263
9.5.3 Experimental Results . . . 264
9.6 Conclusions . . . 267
References . . . 268

10 Output Feedback Sliding Mode Control Approaches Using Observers and/or Differentiators . . . 269
Liu Hsu, Eduardo V.L. Nunes, Tiago Roux Oliveira, Alessandro Jacoud Peixoto, José Paulo V.S. Cunha, Ramon R. Costa, Fernando Lizarralde
10.1 Introduction . . . 270
10.2 Preliminaries . . . 271
10.3 Problem Statement . . . 271
10.3.1 Basic Assumptions . . . 272
10.3.2 Control Objective . . . 273
10.4 Output Tracking Error Equation . . . 273
10.4.1 Output Feedback Model Matching Control . . . 273
10.4.2 Error Equation and Equivalent Nonlinear Input Disturbance . . . 274
10.5 Norm State Observer and Norm Bound for Equivalent Disturbance . . . 274
10.6 Output Feedback Sliding Mode Controller . . . 275
10.7 Relative Degree Compensation . . . 276
10.7.1 Linear Lead Filter . . . 276
10.7.2 Variable Structure Lead Filter . . . 276
10.7.3 High-Gain Observers . . . 278
10.7.4 Hybrid Estimation Scheme . . . 282
10.8 Peaking Phenomena Avoidance . . . 284
10.9 Chattering Alleviation . . . 285
10.10 Binary Model Reference Adaptive Control . . . 286
10.11 Experimental Results . . . 287
10.12 Concluding Remarks . . . 289
References . . . 290

11 Sliding Modes for Fault Detection and Fault Tolerant Control 293
C. Edwards, H. Alwi, C.P. Tan, J.M. Andrade da Silva
11.1 Introduction 294
11.2 Sliding Mode Observers for Fault Detection 295
11.3 A Cascade Based Robust Fault Reconstruction Scheme 297
11.3.1 Summary of Fault Reconstruction Algorithm 298
11.3.2 Design Example 303
11.4 Reconstruction of Incipient Sensor Faults 305
11.4.1 Simulation Results 310
11.5 Unmatched Parametric Uncertainty 311
11.6 Fault Tolerant Control 313
11.6.1 Design Procedures 314
11.6.2 Benchmark Simulation Results 317
11.7 Conclusions 320
References 321

12 Applying Sliding Mode Technique to Optimal Filter and Controller Design 325
Michael Basin
12.1 Introduction 326
12.2 Optimal Filtering Problem 327
12.2.1 Problem Statement 327
12.3 Mean-Square Filter Design 328
12.3.1 Example 1 329
12.3.2 Appendix 1 330
12.4 Mean-Module Filter Design 332
12.4.1 Example 2 332
12.4.2 Appendix 2 333
12.5 Optimal Controller Problem 335
12.5.1 Problem Statement 335
12.6 Mean-Square Controller Design 337
12.6.1 Separation Principle. I 337
12.6.2 Optimal Controller Problem Solution. I 339
12.6.3 Example 3 340
12.7 Mean-Module Controller Design 342
12.7.1 Separation Principle. II 342
12.7.2 Optimal Controller Problem Solution. II 343
12.7.3 Example 4 344
12.8 Conclusions 347
References 348

13 Output Tracking and Observation in Nonminimum Phase Systems via Classical and Higher Order Sliding Modes 351
Y. Shtessel, S. Baev, C. Edwards, S. Spurgeon, A. Zinober
13.1 Introduction 352

13.2 System Description . . . 353
13.3 Problem Formulation . . . 355
13.4 Sliding Mode Control Design . . . 355
13.4.1 The Extended Method of Stable System Center . . . 355
13.4.2 Sliding Variable and Sliding Mode Control . . . 361
13.4.3 The Nonminimum Phase System Output Tracking Error Dynamics in the Sliding Mode . . . 362
13.5 Observer for the Unstable Internal Dynamics . . . 363
13.5.1 Luenberger Observer Design . . . 363
13.5.2 Reconstruction of the Internal State . . . 364
13.5.3 Reconstruction of the External Disturbance . . . 364
13.6 Case Study 1: Output Voltage Tracking in Nonminimum Phase DC/DC Electric Power Converter . . . 364
13.6.1 Model of the Boost DC/DC Converter . . . 365
13.6.2 The Problem Formulation . . . 367
13.6.3 Sliding Mode Controller Design . . . 367
13.6.4 Generation of a Bounded Profile η_c . . . 368
13.6.5 Sliding Mode Parameter Observer . . . 368
13.6.6 Numerical Simulations . . . 369
13.7 Case Study 2: SISO Output Tracking in Systems with Time Delay in Control Feedback . . . 371
13.7.1 Preliminaries . . . 372
13.7.2 Problem Formulation . . . 373
13.7.3 Padé Approximation . . . 373
13.7.4 Design of a Sliding Mode Controller for Causal Output Tracking . . . 374
13.7.5 Numerical Example . . . 376
13.8 Conclusions . . . 378
References . . . 378

14 Discrete-Time Sliding Mode Control Using Output Feedback and Nonlinear Surface . . . 381
Bijnan Bandyopadhyay, Fulwani Deepak
14.1 Introduction . . . 381
14.2 Multirate Output Feedback . . . 384
14.3 Nonlinear Sliding Surface . . . 386
14.4 Control Laws . . . 390
14.4.1 Control Law Based on Reaching Law Approach . . . 391
14.4.2 Control Law with Disturbance Observer . . . 393
14.5 Extension to Input-Delay Systems . . . 394
14.6 Magnetic Tape Position Tracking . . . 395
14.6.1 Comparison with Different Linear Sliding Surfaces . . . 400
14.6.2 Nonlinear Sliding Surface with Disturbance . . . 401
14.7 Summary . . . 403
References . . . 403

Part III: Applications

15 Higher Order Sliding Modes in Collaborative Robotics 409
Michael Defoort, Thierry Floquet, Anne-Marie Kökösy, Wilfrid Perruquetti
15.1 Introduction 409
15.2 Some Contributions on Higher Order Sliding Mode 412
15.2.1 Problem Formulation 412
15.2.2 Design of a Higher Order Sliding Mode Controller 414
15.3 Collaborative Robotics Issues 417
15.3.1 Context 417
15.3.2 Control Issues 417
15.3.3 Problem Formulation and Navigation Strategy 418
15.3.4 Path Planning 421
15.3.5 Path Tracking 426
15.3.6 Experimental Results 431
15.4 Conclusion 434
References 435

16 Two Applications of Sliding Mode Control in Energy Generation and Power Electronics 439
D. Biel, A. Dòria-Cerezo, E. Fossas, R.S. Muñoz-Aguilar, R. Ramos-Lara
16.1 Introduction 439
16.2 Sliding Mode Control of a Wound Rotor Synchronous Generator 440
16.2.1 System Description 441
16.2.2 Direct Sliding Mode Controller 442
16.2.3 Sliding Mode Control with an Outer-PI Loop 445
16.2.4 Dynamic Sliding Mode Controller 446
16.2.5 Simulations 447
16.2.6 Experimental Results 449
16.3 Implementing ON/OFF Controllers by Field Parallel Gate Arrays (FPGA) 451
16.3.1 Chattering Reduction 452
16.3.2 A $m-$Phases Parallel Buck Converter 455
16.4 Conclusions 457
References 463

17 Advances in High Order and Adaptive Sliding Mode Control – Theory and Applications 465
F. Plestan, V. Brégeault, A. Glumineau, Y. Shtessel, E. Moulay
17.1 Introduction 465
17.2 Problem Statement 466
17.3 Adaptive Sliding Mode Control 469

17.4 High Order Sliding Mode Control 472
17.4.1 A Unified Approach 472
17.4.2 Control Solutions and Design of Functions $\mathscr{F}$ 474
17.4.3 Second Order Sliding Mode Control by Static Output Feedback 478
17.5 Applications 480
17.5.1 Control of Electropneumatic Actuator 480
17.5.2 Control of Induction Motor 486
17.6 Conclusion 490
References 491

18 Sliding Mode Controllers and Observers for Electromechanical Systems 493
J. de Leon-Morales
18.1 Introduction 493
18.1.1 Application Domains of Sliding Mode 494
18.1.2 Paper Structure 495
18.2 Power Systems: Synchronous Machine and Multi-machine Systems 495
18.2.1 Synchronous Machine 495
18.2.2 One Axes Model 497
18.2.3 Sliding-Mode Controller Design 498
18.2.4 Multi-machine Mathematical Model 501
18.3 Helicopter: Twin Rotor System 506
18.3.1 Dynamical Model of a Twin Rotor System 506
18.4 Teleoperation Bilateral: Master-Slave Systems 510
18.4.1 Introduction 510
18.4.2 Teleoperation System 510
18.4.3 Controller Design 512
18.4.4 Super Twisting Observer Design 513
18.4.5 Simulation Results 514
18.5 Conclusions 515
References 515

19 Synthesis of Canonical Elements for Power Processing Based on Sliding-Mode Control 517
Luis Martínez-Salamero and Angel Cid-Pastor
19.1 Introduction 517
19.2 Power Processing Systems 519
19.3 Generalized Canonical Element 520
19.4 Synthesis of DC Transformers 521
19.5 Power Gyrator 527
19.6 Loss-Free Resistors 528
19.7 Impedance Matching 529
19.8 DC-AC Conversion 534

19.9 Power Distribution 536
19.10 Power Factor Correction 537
19.11 Conclusions 538
References 539

20 Second Order Sliding Modes to Control and Supervise Industrial Robot Manipulators 541
Antonella Ferrara, Luca Massimiliano Capisani
20.1 Introduction 541
20.2 Problem Formulation 542
20.2.1 The Manipulator Model 543
20.3 Solution to the Problem 1: Robust Motion Control for Robot Manipulators 543
20.3.1 Design of the Inverse Dynamics Part of the Control Scheme 544
20.3.2 Design of the Proposed Second Order Sliding Mode Controller 544
20.4 Experimental Results on Motion Control 546
20.4.1 The Considered Industrial Robot 547
20.4.2 The Experiments 548
20.4.3 Comparison with the Super Twisting Second Order Sliding Mode Algorithm 553
20.5 Solution to Problem 2: Fault Diagnosis for Robot Manipulators 555
20.5.1 The Considered Fault Scenarios 555
20.5.2 Actuator and Sensor Faults 555
20.5.3 The Proposed Diagnostic Scheme 555
20.5.4 Actuator Faults Detection Strategy 556
20.5.5 Sensor Faults Detection Strategy 557
20.5.6 Residual Generation 559
20.5.7 Fault Isolation for Single Faults 560
20.5.8 Experimental Results on Fault Diagnosis 561
20.5.9 Experimental Test in Presence of Actuator Faults 561
20.5.10 Experimental Tests in Presence of Sensor Faults 562
20.6 Conclusions 563
References 564

21 Sliding Block Control of Electrical Machines (Motors and Generators) 569
Alexander G. Loukianov, Jose M. Cañedo, B. Castillo-Toledo, Edgar N. Sanchez
21.1 Introduction 569
21.2 Synchronous Motor SM Block Control 570
21.2.1 Plant Model 570
21.2.2 The Flux Linkage ψ_{fd} Control Loop 571

21.2.3 The Current i_d Control Loop 572
21.2.4 The Speed ω_m Control Loop 572
21.3 The Synchronous Generator Control 573
21.3.1 Plant Model 573
21.3.2 The Idea of Block Integral SM Controllers 574
21.3.3 Block Integral SM Speed Stabilizer 576
21.3.4 SM Voltage Regulator 578
21.3.5 Control Switching Logic 579
21.4 Induction Motor with Magnetic Saturation Control 579
21.4.1 Mathematical Model of Induction Motor with Saturation 580
21.5 Induction Motor Discrete Time Control 581
21.5.1 Plant Model 581
21.5.2 Control Algorithm 584
21.6 Induction Motor Hybrid Control 588
21.6.1 Discrete–Time Controller 589
21.7 Induction Motor Neural Network SM Block Control 591
21.7.1 Identification 591
21.7.2 Controller Design 593
References 594

Part I
VSS and SM Algorithms and Their Analysis

Chapter 1
Sliding Mode Enforcement after 1990: Main Results and Some Open Problems

L. Fridman

The objective of this chapter is to try to analyze the main stages in the development of sliding mode enforcing control algorithms, starting from the first Variable Structure Systems workshop (VSS90). I would like to underline that this is my personal opinion, I am just trying to understand the steps we have made as a community during the last twenty years after VSS90 as well as which problems still remain open. Of course, generally I will concentrate the chapter on results in open problems I have discovered working with my group and coauthors.

1.1 Sliding Mode Control Up until 1990

The history of VSS up until the early 70's has been described in [148]. By 1980, the main part of classical SMC theory had been finished and later reported in Prof. Utkin's monograph in Russian in 1981 (English version [151]). In this monograph (see also accomplished result [46]), the two-step procedure for sliding mode control design was clearly stated:

1. Sliding surface design;
2. Discontinuous(relay or unit) controllers ensuring the sliding modes.

The main advantages of SMC were the following:

- exact compensation (insensitivity) w.r.t. bounded matched uncertainties;
- reduced order of sliding equations;
- finite-time convergence to the sliding surface.

However, the following disadvantages were evident:

- chattering;
- insensitivity only w.r.t. matched perturbations;

L. Fridman
Department of Control Engineering and Robotics
National Autonomous University of Mexico (UNAM)

L. Fridman et al. (Eds.): Sliding Modes, LNCIS 412, pp. 3–57.
springerlink.com

- the sliding variables converge in finite-time: however, the state variables only converge asymptotically;
- non-ideal closed-loop performance in presence of parasitic dynamics, discretization and noises;
- the sliding surface design is restricted to have relative degree one with respect to the control, i.e. higher order derivatives are required for the sliding surface design.

It is impossible to observe all the papers devoted to sliding surface design. That is why I will concentrate this chapter on the development of control algorithms, enforcing sliding motions.

1.2 Second Order Sliding Modes: First Generation

By the early 80's, the control community had understood that the main disadvantage of SMC is the "chattering" effect [151]. It has been shown that this effect is mainly caused by unmodelled cascade dynamics which increase the system's relative degree and perturb the ideal sliding mode existing in the system [31].

In order to overcome the chattering problem in the sliding mode, the second order sliding mode (SOSM) concept was introduced in the Ph.D. dissertation of A. Levant (Levantovskii).

Definition ([51]). The point $(x,\ \dot{x}) = (0,0)$ is called a second order sliding mode point if it is a solution of system

$$\ddot{x} = f(t,x,\dot{x}) + g(t,x,\dot{x})u \qquad x,(t),f(t),g(t) \in \mathbb{R}$$

in the Filippov [57] sense.

1.2.1 Twisting Algorithm

The first and simplest SOSM algorithm is the so-called "twisting algorithm"(TA). For a relative degree two system the TA takes the form:

$$u = -a\text{sign}(\dot{x}) - b\text{sign}(x),\ b > a$$

where $u,x \in \mathbb{R}$. Under the assumption of known bounds for f and g and with parameters a and b of the controller chosen appropriately [51], the twisting algorithm ensures the finite time exact convergence of both x and $\dot{x}$, i.e. there exists $T > 0$ such that for all $t > T$, $x(t) = \dot{x}(t) = 0$. Thus the TA is said to be a SOSM control algorithm since it provides the existence of a (stable) "second order sliding mode" at the origin $(x,\ \dot{x}) = (0,0)$.

With the use of the TA, the *sliding surface design is no longer needed for one degree of freedom mechanical systems*. Moreover, the TA collapses *the dynamics of such systems!*

Under additional assumptions regarding the smoothness of the system, the algorithm has been used to attenuate chattering in relative degree one systems by including an integrator in the control input

$$\begin{aligned}\dot{x} &= f(t,x)+g(t,x)u,\\ \dot{u} &= v,\\ v &= -a\text{sign}(\dot{x})-b\text{sign}(x),\end{aligned}$$

and in this way, the actual control u is absolutely continuous.

1.2.2 The First Criticism of SOSM

On the end of 80th the SOSM was criticized. The main two points of criticism was the following:

1. Definition 1.2 of a SOSM does not provide a clear difference between a first (or traditional) and second order sliding mode. To see this, let us consider the case of a traditional sliding mode on a stable linear surface $\dot{x}+cx=0$. In this case, the origin $(\dot{x},x)=(0,0)$ consists of an integral curve corresponding to the initial conditions $x(0)=0,\dot{x}(0)=0$. Thus, according to Definition 1.2, a traditional (or first order) sliding mode also contains a second order sliding mode in the origin.
2. The anti-chattering strategy for a first order sliding mode makes use of the derivative $\dot{x}$. Thus, if by any reason it is possible to measure $\dot{x}$ and additionally $g(t,x)$ is also known, then the uncertainty $f=\dot{x}-gu$ is also known and can be compensated without any discontinuous control! In this case, what is the reason for the use of a SMC?

Both of these points will be addressed later on.

1.2.3 The Super-Twisting Algorithm

As we have discussed, the use of the twisting algorithm in a system with relative degree one allowed to exactly compensate a (absolutely continuous) disturbance by means of an absolutely continuous control. However, this approach required the derivative $\dot{x}$. At the end of 80's, the main issue was the question if this was actually possible without the use of derivatives.

The super twisting algorithm (STA):

$$\begin{aligned}\dot{x} &= f(t,x)+g(t,x)u,\\ u &= -k_1|x|^{\frac{1}{2}}\text{sign}(x)+v,\\ \dot{v} &= -k_2\text{sign}(x),\end{aligned}\tag{1.1}$$

for any f is Lipshitz bounded uncertainty/disturbance for some constants k_1 and k_2 ensures [89] exact finite time convergence to the second sliding mode set $x(t)=\dot{x}(t)=0,\forall t\geq T$ without usage of $\dot{x}$. If we consider system (1.1) as having x as the measured output, the STA is an output-feedback controller.

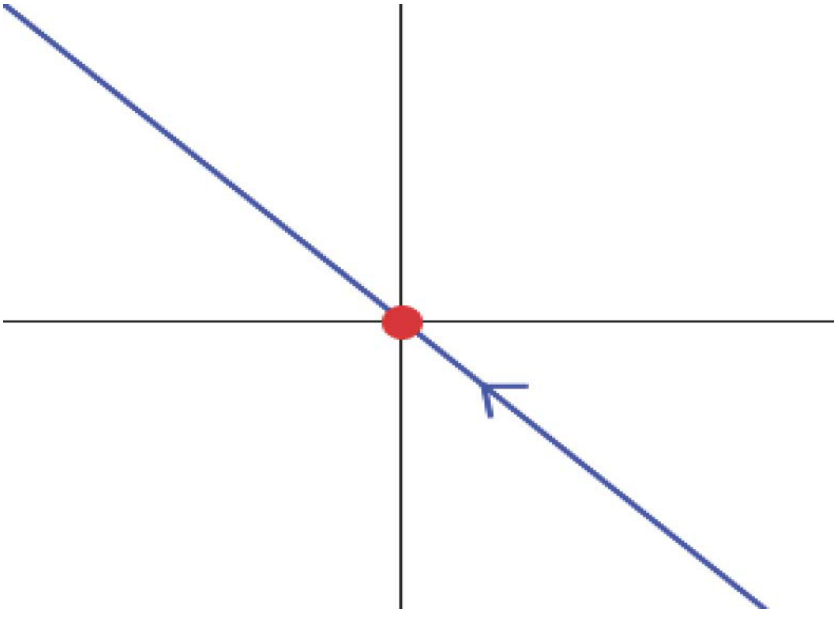

Fig. 1.1 Existence of first and second order sliding modes: first order sliding modes (on the line), a second order sliding mode (at the origin)

This last property of the STA allowed to construct a second-order sliding mode differentiator [90] and gave further impetus to the development of the mathematical theory and applications of SOSM algorithms. We now briefly describe the idea behind it. Let $f(t)$ be a signal to be differentiated and assume that $|\ddot{f}(t)| \leq L$, with L being a known constant. Take $x_1 = f, x_2 = \dot{f}$; then the problem can be reformulated as finding an observer for

$$\dot{x}_1 = x_2, \quad \dot{x}_2 = \ddot{f}, \quad y = x_1,$$

where $\ddot{f}(t)$ is considered as a bounded perturbation. Since the STA does not require derivatives, which in this case would be the state x_2, it only uses output injection and results particularly useful in the form of a STA observer

$$\begin{aligned} \dot{\hat{x}}_1 &= -k_1 |\hat{x}_1 - y|^{\frac{1}{2}} \operatorname{sign}(\hat{x}_1 - y) + \hat{x}_2, \\ \dot{\hat{x}}_2 &= -k_2 \operatorname{sign}(\hat{x}_1 - y), \end{aligned}$$

Once the constants k_1 and k_2 are appropriately chosen, the convergence of the STA ensures that the equalities $(f - \hat{x}_1) = (\dot{f} - \hat{x}_2) = 0$ are established after a finite-time transient. Thus $\hat{x}_2$ is an estimate for the derivative $\dot{f}(t)$ and turns out to be the best possible one ([90]) in the sense of [84] when (bounded Lebesgue-measurable) noise or discretization are present. However, the difficult geometrical proof of the

STA convergence remained as the main disadvantage for this algorithm, thereby preventing further generalizations.

1.2.4 The Sub-Optimal Algorithm

SOSM attracted the full attention of the international control community after a presentation at the Third IEEE Workshop on Variable Structure and Lyapunov Theory [65] and the publication of the first tutorial paper on High Order Sliding Modes (HOSMs) [66]. Since 1996 the number of publications on second order sliding modes theory and applications has grown exponentially, generally through the efforts of Professor Bartolini and his group (see for instance [12] and references therein and also [112] with the similar idea). The results of Prof. Bartolini's group are based on another SOSM controller that does not (explicitly) need derivatives, the Sub-Optimal Algorithm(SOA):

$$\begin{aligned} \ddot{x} &= f(t,x,\dot{x}) + g(t,x,\dot{x})u, \\ u &= -U_m \text{sign}(x - \tfrac{1}{2}x^*), \end{aligned}$$

where x^* is the last extrema of the curve $x(t)$. The SOA algorithm is also able to guarantee the finite time exact convergence $x(t) = \dot{x}(t) = 0, \forall t \geq T$ once the parameter U_m has been tuned large enough. This SOA algorithm has been used to solve numerous relevant control problems, see for instance [11] or [16] and the references therein. To smooth out the control law for relative degree one systems, the SOA can be used in the same manner as the TA (1.2.1).

1.2.5 Recapitulations

The use of the Super Twisting and Sub-Optimal SOSM algorithms for smooth systems allows substituting the use of a discontinuous control by means of an absolutely continuous one. Additionally, their use offers:

1. Chattering attenuation (but not its complete removal [27, 26, 29, 28]).
2. Differentiator obtained using the STA and SOA:

   - finite-time exact estimation of derivatives under ideal conditions, i.e. in the absence of both noise and sampling;
   - the best possible approximation in the sense of [84] of order $O(\delta)$ w.r.t. discrete sampling and of order $O(\sqrt{\varepsilon})$ w.r.t. deterministic Lebesgue-measurable noise bounded by ε.

For relative degree 2 systems, the use of the TA and the SOA allows:

- Reducing the order of the sliding dynamics up to $(n-2)$ but the design of the sliding surface of order $(n-2)$ is still necessary;
- For one degree of freedom mechanical systems, both the SOA and the TA provide dynamic collapse, i.e. the sliding surface design is no longer needed.

However, the following problems remain open:

3. The problem of exact finite-time stabilization (dynamic collapse) and exact disturbance compensation for SISO systems with arbitrary relative degree.
4. The performance under noise and sampling during the cascade use of these algorithms provides a precision of order $O(\delta^{\frac{1}{2^{r-1}}})$ w.r.t. the sampling step and $O(\varepsilon^{\frac{1}{2^r}})$ w.r.t. deterministic Lebesgue-measurable noise bounded by ε but can not provide the best possible asymptotic accuracy for the higher order derivatives in the sense of [84]. The construction of a high order differentiator providing the best possible asymptotic accuracy in the sense of [84] remains open as well.

1.3 Second Generation: Arbitrary Order Sliding Mode Controllers

Let

$$\begin{aligned} &\dot{x} = f(t,x) + g(t,x)u, \qquad x \in \mathbb{R}^n \\ &\sigma = \sigma(x,t), \end{aligned}$$

where $\sigma \in \mathbb{R}$ is an output to be exactly stabilized in finite-time at $\sigma = 0$, $u \in \mathbb{R}$ is the control input and $x \in \mathbb{R}^n$ is the state. Let the output σ have a fixed and known relative degree $r \in \mathbb{R}^n$. In such a case, the control problem is translated into the finite-time stabilization of an uncertain differential equation or, equivalently, of the following differential inclusion

$$\sigma^{(r)} \in [-C, C] + [K_m, K_M]u, \tag{1.2}$$

where C, K_m and K_M are known constants parameterizing the uncertainty of the original system. If $r \leq 2$, the first order SM or SOSM controllers are able to solve the problem. However, the case when $r > 2$ in the end of 90th remained as open issue.

1.3.1 Discussion on the Definition of r-th Order Sliding Motions

First, an analogous definition of an r-th order sliding mode was required. Let the r-th order sliding set $\mathscr{S}_r$ be determined by the following equalities

$$\sigma = \dot{\sigma} = \cdots = \sigma^{(r-1)} = 0.$$

The following definition was introduced in [91]:

Definition 1.1. The set $\mathscr{S}_r$ is said to contain an r-th order sliding mode if it consists (locally) of integral curves of the system in Filippov's sense.

Now let us recall the discussion on Subsection 1.2.1 about the ambiguity between the definitions of a first and second order sliding mode. In fact, the same situation is

also present with Definition 1.1 of an r-th order sliding motion. Indeed, if a stable first order sliding mode is induced on a linear surface $c_0\sigma^{(r)}+c_1\sigma^{(r-1)}+\cdots+c_r\sigma=0$ the point $\sigma=\dot{\sigma}=\cdots=\sigma^{(r-1)}=0$ consists of an integral curve of the system given by the conditions $\sigma(0)=\cdots=\sigma^{(r-1)}(0)=0$. In this sense, the first order sliding mode also contains an r-th order sliding mode at the origin. To prevent this situation, the following definition in the spirit of [47] is proposed:

Definition 1.2. The set $\mathscr{S}_r$ is said to contain an r-th order sliding mode if it consists of integral curves of the system in Filippov's sense and there exists a vicinity $\mathscr{N}\subseteq\mathbb{R}^n$ of $\mathscr{S}_r$ in which the shift operator is not invertible.

This last definition is equivalent to the following definition:

Definition 1.3. The set $\mathscr{S}_r$ is said to contain an r-th order sliding mode if there exists a vicinity $\mathscr{N}\subseteq\mathbb{R}^n$ of $\mathscr{S}_r$ such that for any initial condition from $\mathscr{N}$ the trajectories of the system (in Filippov's sense) converge to $\mathscr{S}_r$ in finite-time.

The problem of defining vector order sliding modes for the MIMO systems remained to be open.

1.3.2 Arbitrary Order Sliding Mode Controllers

In 2001, the first arbitrary order SM controller was introduced in [91]. Such controllers allowed solving the finite-time enforcement of an r-th order sliding mode and exact matched perturbation/ uncertainties compensation.

Given the relative degree r of the output, HOSM controllers are constructed using a recursion. The following is the recursion for the first reported kind of HOSM controllers: the so-called "nested" ones [91]. Let p be the least common multiple of $1,2,\ldots,r$. Also let

$$\varphi_{0,r}=\sigma, \qquad N_{1,r}=|\sigma|^{\frac{r-1}{r}},$$
$$\varphi_{i,r}=\sigma^{(i)}+\beta_i N_{i,r}\operatorname{sign}(\varphi_{i-1,r}),\ N_{i,r}=\left(|\sigma|^{\frac{p}{r}}+\cdots+|\sigma^{(i-1)}|^{\frac{p}{r-1+1}}\right)^{\frac{r-i}{p}},$$

and the r-th order sliding mode controller

$$u=-\alpha\operatorname{sign}\left(\varphi_{r-1,r}(\sigma,\dot{\sigma},\ldots,\sigma^{(r-1)})\right). \tag{1.3}$$

be applied to system (1.1). Then this algorithm provides for the finite-time stabilization of $\sigma,\dot{\sigma}=0$ and,therefore, of its successive derivatives up to $\sigma^{(r-1)}$. Thus it provides for the existence of an r-th order sliding mode in the set $\mathscr{S}_r$. The parameters β_i can be selected in advance in such a way that only the gain of the controller α has to be selected large enough.

Since controller (1.3) uses the output and it successive derivatives, the HOSM arbitrary order differentiator, introduced in [92], was instrumental for the applicability of HOSM controllers. Let $\sigma(t)$ be a signal to be differentiated $k-1$ times and

assume that $|\sigma^{(k)}| \leq L$, with L being a known constant. Then, the $(k-1)$-th order HOSM differentiator takes the following form

$$\begin{aligned}
\dot{z}_0 &= v_0 = -\lambda_k L^{\frac{1}{k+1}} |z_0 - \sigma|^{\frac{k}{k+1}} \operatorname{sign}(z_0 - \sigma) + z_1, \\
\dot{z}_1 &= v_1 = -\lambda_{k-1} L^{\frac{1}{k}} |z_1 - v_0|^{\frac{k-1}{k}} \operatorname{sign}(z_1 - v_0) + z_2, \\
&\vdots \\
\dot{z}_{k-1} &= v_{k-1} = -\lambda_1 L^{\frac{1}{2}} |z_{k-1} - v_{k-2}|^{\frac{1}{2}} \operatorname{sign}(z_{k-1} - v_{k-2}) + z_k, \\
\dot{z}_k &= -\lambda_0 L \operatorname{sign}(z_k - v_{k-1}).
\end{aligned} \tag{1.4}$$

where z_i is the estimation of the true derivative $\sigma^{(i)}(t)$. The differentiator ensures the finite-time exact differentiation under ideal conditions of exact measurement in continuous time. The only information needed is upper bound, L, for $|\sigma^{(k+1)}|$. Then a parametric sequence $\{\lambda_i\} > 0$, $i = 0, 1, \ldots, k$, is recursively built, which provides for the convergence of the differentiators for each order k. In particular, the parameters $\lambda_0 = 1.1$, $\lambda_1 = 1.5$, $\lambda_2 = 2$, $\lambda_3 = 3$, $\lambda_4 = 5$, $\lambda_5 = 8$ are enough up until the 5-th differentiation order. With discrete sampling, the differential equations are replaced by their Euler approximations. This differentiator provides for the best possible asymptotic accuracy in the presence of input noises or discrete sampling [92, 84] for the rth derivative:

- order $O(\delta)$ with respect to discrete sampling,
- order $O(\varepsilon^{\frac{1}{r+1}})$ with respect to bounded deterministic Lebesgue measurable noise.

The use of the HOSM arbitrary order differentiator together with the HOSM arbitrary order controller allowed the design and the implementation of a universal arbitrary-order HOSM output-feedback controller for uncertain single-input single-output (SISO) systems ensuring the finite-time output stabilization in spite of disturbances. At this point, the advantage of using homogeneity properties in the system in order to systematize the controller design became evident, and in fact all previous existing algorithms turned out to be also homogeneous [93].

It was also pointed out [93] that any exact controller must be discontinuous at least in the set $\sigma = \dot{\sigma} = \cdots = \sigma^{(r-1)} = 0$ to be able to compensate exactly for the class of bounded matched perturbation/uncertainties. The Quasi-Continuous HOSM controllers [95, 94] are continuous everywhere except in such point. They are also constructed using a recursion:

$$\varphi_{0,r} = \sigma, \qquad N_{0,r} = |\sigma|, \qquad \Psi_{0,r} = \frac{\varphi_{0,r}}{N_{0,r}} = \operatorname{sign}\sigma,$$
$$\varphi_{i,r} = \sigma^{(i)} + \beta_i N_{i-1,r}^{\frac{r-i}{r-i+1}} \Psi_{i-1,r}, \; N_{i,r} = |\sigma^{(i)}| + \beta_i N_{i-1,r}^{\frac{r-i}{r-i+1}}, \; \Psi_{i,r} = \frac{\varphi_{i,r}}{N_{i,r}},$$

and

$$u = -\alpha \Psi_{r-1,r}(\sigma, \dot{\sigma}, \ldots, \sigma^{(r-1)}). \tag{1.5}$$

The advantage of Quasi-Continuous controllers with respect to Nested ones strives in the chattering reduction due to the decrease of discontinuities in the controller ([95, 94]).

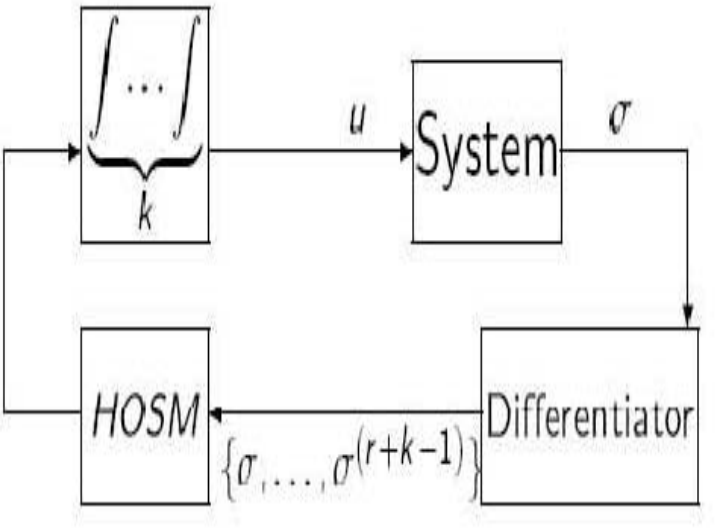

Fig. 1.2 Black box control diagram

At this point, it is worth remarking that several other approaches for the design of arbitrary order sliding mode controllers have been proposed ever since. For instance, results based on minimum-time optimal controllers and integral sliding modes have been developed in [85, 112, 15] as well as the use of homogeneous finite-time convergent controllers [23] with robustness provided by first order SM [44].

1.3.3 Black-Box Control [92]

HOSM approach allows to solve the problem of finite-time output stabilization of a black box system(see Figure 1.2). The only information needed from the system is:

- the upper bound for the relative degree r of the plant;
- the level of the smoothness k for the control signal for which the actuators hardware is tolerant;
- the bounds for the differential inclusion (1.2).
  In this case only one parameter, α, has to be tuned large enough in order to provide either a finite time exact stabilization of the output or a finite time exact tracking. Moreover, if σ is known to be $(r+k-1)$ times differentiable, the controller can be k times differentiable by including k integrators in the control input and thus attenuating chattering (it is reasonable to put $k = 0, 1$ only).

However, the following points for HOSM controllers remained to be unsolved:

- The homogeneity features of the system, that were essential in the convergence proof, were destroyed if an adaptation of the gain of the controller was attempted. Thus it was not possible to reduce the gain of the controller once the system approached the origin, a desirable feature which would allow to decrease chattering.
- The time constant for finite time convergence is tending to infinity together with growing of the norm of initial conditions.
- Only asymptotic accuracy ensured by HOSM controllers and differentiators is proved. The constants for estimations of accuracy need to be computed.

1.4 Terminal Sliding Mode Control

The idea of the terminal sliding mode control was first reported in [152, 105, 106], where a terminal sliding variable (vector) with a nonlinear term is proposed for a second-order nonlinear system as well as an n-link rigid robotic manipulator system with uncertain dynamics, to solve the finite time error convergence problem, after the closed-loop error dynamics reaches and then remains on the terminal sliding mode surface. The basic principle of the terminal sliding mode control is described as follows. Consider the second order linear or nonlinear system

$$\begin{aligned} \dot{x}_1 &= x_2 \\ \dot{x}_2 &= f(x_1, x_2) + b(x_1, x_2)\, u(t) \end{aligned} \tag{1.6}$$

where x_1 and x_2 are the system states, $f(\cdot)$ and $b(\cdot) \neq 0$ are linear or nonlinear functions of x_1 and x_2, and u is the control input. In order to achieve the finite time convergence of the state variables, the following first-order terminal sliding variable is defined:

$$s = x_2 + \beta x_1^{q/p}$$

where $\beta > 0$, p and q are positive odd integers with

$$p > q \tag{1.7}$$

With a properly designed sliding mode controller of the form:

$$u(x) = \begin{cases} u^+(x) \text{ if } s > 0 \\ u^-(x) \text{ if } s < 0 \end{cases}$$

the terminal sliding variable s can be driven to the terminal sliding mode surface $s = 0$ in a finite time. On the terminal sliding mode surface, the system dynamics are then determined by the following nonlinear differential equation:

$$\dot{x}_1 = -\beta x_1^{q/p} \tag{1.8}$$

It has been shown in [162] and [163] that $x_1 = 0$ is the terminal attractor of the system (1.6). Indeed, if the initial value of x_1 at $t = 0$ is $x_1(0)\,(\neq 0)$ and two positive odd integers p and q satisfy (1.7), the relaxation time t_1 for a solution of the system (1.6) is then given by

$$t_1 = -\beta^{-1} \int_{x_1(0)}^{0} \frac{dx_1}{x_1^{q/p}} = \frac{|x_1(0)|^{1-q/p}}{\beta\,(1-q/p)} \tag{1.9}$$

Expression (1.9) means that the system state x_1 converges to zero in a finite time on the terminal sliding mode surface (1.8), and the system state x_2 also converges to zero in a finite time identically. For the terminal sliding mode tracking control of an n-link robotic manipulator in [105, 106] and [107], the terminal sliding variable vector S is defined as:

$$S = C\tilde{e}$$

where

$$C = \begin{bmatrix} C_1 & C_2 \end{bmatrix} = \begin{pmatrix} c_{11} & & 1 & \\ & \ddots & & \ddots \\ & & c_{nn} & & 1 \end{pmatrix}$$

with $c_{ii} > 0$ for $i = 1, \cdots n$, and

$$\tilde{e} = \left[\varepsilon_1^{p_2/p_2} \;\cdots\; \varepsilon_n^{p_2/p_2} \;\dot{\varepsilon}_1 \;\cdots\; \dot{\varepsilon}_n \right]^T$$

with ε_i the tracking error between the i-th joint angle and the desired reference signal [105]. The input torque vector of the robotic manipulator can then be designed, using the system states and the upper and the lower bounds of unknown system parameters and unknown system uncertainties, to drive the sliding variable vector S to the sliding mode surface $S = 0$, and on the sliding mode surface, the system tracking error dynamics satisfy the following relationship:

$$c_{ii}\varepsilon_i^{p_2/p_2} + \dot{\varepsilon}_i = 0 \quad \text{for} \quad i = 1, \cdots n$$

and then the tracking error converges to zero in a finite time. In [158], the terminal sliding mode control was extended to control a class of high-order SISO system:

$$\dot{x}_i = x_{i+1}\; i = 1, \cdots n-1$$

$$\dot{x}_n = \sum_{j=1}^{n} a_j x_j \; + u(t)$$

with the following hierarchical terminal sliding mode structure:

$$s_1 = \dot{s}_0 + \beta_1 s_0^{q_1/p_1}$$

$$s_2 = \dot{s}_1 + \beta_2 s_1^{q_2/p_2}$$

$$\vdots$$

$$s_{n-1} = \dot{s}_{n-2} + \beta_{n-1} s_{n-2}^{q_{n-1}/p_{n-1}}$$

where $s_0 = x_1$, $\beta_i > 0$, $p_i > q_i$, p_i and q_i are positive odd integers. As shown in [158], the controller is designed to drive the sliding variable s_{n-1} to zero in a finite time. Considering the chain-like structure of the sliding mode surface, the sliding variables $s_{n-2}, \cdots s_0$ can then converge to zero in a finite time sequentially. In [159], the terminal sliding mode control of the following MIMO linear systems was considered:

$$\dot{X}_1 = A_{11}X_1 + A_{12}X_2$$

$$\dot{X}_2 = A_{21}X_1 + A_{22}X_2 + B_2U$$

where $X_1 \in R^{n-m}$ and $X_2 \in R^m$ are the system states, $A_{11} \in R^{(n-m)\times(n-m)}$, $A_{12} \in R^{(n-m)\times m}$, $A_{21} \in R^{m\times(n-m)}$, $A_{22} \in R^{m\times m}$ and $B_2 \in R^{m\times m}$ are the system parameter matrices, the pair (A_{11}, A_{12}) is controllable, B_2 is non-singular, and $n-m \leq m$. The new terminal sliding mode structure, developed by adding a nonlinear term to the conventional linear sliding mode surface, is of the form:

$$S = C_1X_1 + C_2X_2 + C_3X_1^{q/p}$$

where $C_1 \in R^{m\times(n-m)}$, $C_2 \in R^{m\times m}$ and $C_3 \in R^{m\times(n-m)}$ are the terminal sliding mode parameter matrices, the matrix C_2 is full rank of m, the odd positive integers p and q satisfy the following condition together with (1.7):

$$2q > p$$

and $X_1^{q/p}$ is a vector defined as

$$X_1^{q/p} = \left[x_1^{q/p}\ x_2^{q/p}\ \cdots\ x_{n-m}^{q/p}\right]^T$$

It has been shown in [153] that, if the sliding mode parameter matrices are chosen in that

$$A_{11} - A_{12}C_2^{-1}C_1 = 0$$

and

$$A_{12}C_2^{-1}C_3 = diag\,(\beta_i)$$

with $\beta_i > 0$, $i = 1, 2, \cdots, n-m$, the sliding mode controller can be designed to drive the sliding variable S to the sliding mode surface $S = 0$ in a finite time, and then the system states X_1 and X_2 converge to zero in a finite time. It was noted by many researchers that the terminal sliding mode control methods developed in [105] and [159] have the singularity problem. The research in [153] and [55] discussed the singularity issue in detail and proposed a global non-singular terminal sliding mode control, where the first-order terminal sliding mode variable is defined as:

$$s = x_1 + \frac{1}{\beta} x_2^{p/q} \tag{1.10}$$

where the constant β ¿0, p and q are positive odd integers satisfy (1.7). It was also noted that, as the closed-loop dynamics with the terminal sliding mode controllers [152, 105] is far away from the system origin, the convergence speed is relatively low, compared with the conventional linear sliding mode control. In order to improve the convergence, a new terminal sliding variable based on [153] was developed in [160, 156] and [54] with the following form:

$$s = \dot{x}_1 + \alpha x_1 + \beta x_2^{q/p}$$

where $\alpha > 0$, parameters β, p and q are chosen as in (1.10). Although the terminal sliding mode technique has been widely applied to the control of mechanical systems, electrical systems, aircraft systems and other complex systems, as seen in [82, 83, 146, 161, 157], the development of this technique is still at its initial stage, and many theoretical researches need to be done in the near future.

1.5 Third Generation: Non-Homogeneous HOSMs

In [98], HOSM controllers were extended to include a variable gain and thus became non-homogeneous. In this case the controller takes the form

$$u = -\alpha \Phi(t,x) \Psi_{r-1,r}(\sigma, \dot{\sigma}, \ldots, \sigma^{(r-1)}), \tag{1.11}$$

where the "gain function" $\Phi(t,x) > 0$ can be selected to solve the problem for the case when the boundaries of the differential inclusion (1.2) are not constant. This feature also allows a reduction in the chattering by decreasing the amplitude of the controller.

1.6 Lyapunov Based Approach

As we have pointed out, in [96] the design of SOSMs was systematized using a homogeneity point of view. However this approach, based on geometric methods, prevented further generalizations of the algorithms.

Due to this, there were several attempts to give an analytic proof for the convergence of SOSM algorithms. At the beginning only weak (semidefinite negative) Lyapunov functions were reported for the TA (see for instance [119]). A strong Lyapunov function for both the TA and the STA was reported in [130, 131], obtained using a modification of Zubov's method [166]. However, this Lyapunov function was so intricate that it also prevented exploring new modifications to the algorithms.

In that same year (2009) Prof. Moreno presented a simpler Lyapunov function for the super-twisting algorithm that had the structure of a quadratic function [111, 39] of the terms forming STA. This function provided an estimate for the convergence time and also allowed to make the first modification of the STA by including linear

terms that improved its convergence and robustness properties [39]. Moreover, the approach proposed in [39] allowing to use well known Lyapunov equations and LMI solutions for STA analysis.

In this section we will recall another interesting modification of the STA that was possible due to a Lyapunov analysis: the STA with variable gains [40]. It is well known that first order SM algorithms with variable gains improve the performance of the system by decreasing the amplitude of the control signal and thus of the chattering [151]. The STA with variable gains (VGSTA) has the following structure

$$\begin{aligned}\dot{x}_1 &= -k_1(t,x)\phi_1(x_1) + x_2 + g_1(t,x),\\ \dot{x}_2 &= -k_2(t,x)\phi_2(x_1) + g_2(t,x)\end{aligned}$$

where the functions g_1 and g_2 are disturbances and the VGSTA is composed of the gain functions $k_1(t,x)$, $k_2(t,x)$ and of the functions

$$\begin{aligned}\phi_1(x_1) &= |x_1|^{\frac{1}{2}}\text{sign}(x_1) + k_3 x_1, \quad k_3 > 0,\\ \phi_2(x_1) &= 0.5\text{sign}(x_1) + 1.5k_3|x_1|^{\frac{1}{2}}\text{sign}(x_1) + k_3^2 x_1\end{aligned}$$

Under the assumption that the disturbances satisfy the bounds

$$|g_1(t,x)| \le \rho_1(t,x)|\phi_1(x_1)|, \quad |g_2(t,x)| \le \rho_2(t,x)|\phi_2(x_1)|$$

for some known continuous functions ρ_1, ρ_2 and that the gains are selected to satisfy

$$\begin{aligned}k_1(t,x) &> \left[\tfrac{1}{4\varepsilon}\left[2\varepsilon\rho_1 + \rho_2\right]^2 + 2\varepsilon\rho_2 + \varepsilon + \left[2\varepsilon + \rho_1(t,x)\right]\left(\beta + 4\varepsilon^2\right)\right],\\ k_2(t,x) &> 4\varepsilon^2 + 2\varepsilon k_1(t,x)\ ,\end{aligned}$$

for some $\varepsilon > 0$, then the finite-time stability of $x_1 = 0$ is ensured.

This approach may be widely exploited in the near future because it allows:

- designing absolutely continuous SM controllers capable of compensating Lipshitz continuous perturbations/uncertainties which may grow together with the states;
- adaptation of the control law.

1.7 Chattering Problem and HOSM

The main motivation for the development of SOSM control algorithms was the elimination of chattering. The chattering phenomenon is caused by the inevitable existence of the so-called *parasitic* or *unmodelled* dynamics that exist along with the *principal dynamics* of the plant, thereby increasing the relative degree of output. Thus, in traditional sliding modes, chattering appears due to the fact that s (the sliding variable) is too small, but $\dot{s}$ is not; this causes a high frequency motion to appear in the system.

When second order sliding modes appeared in the 80's, along with their boom in the last half of the 90's, it was thought that the problem of chattering was solved.

This was not completely true: a chattering reduction is achieved, but nevertheless a high frequency phenomenon still appears. In fact, the claimed chattering-free property associated with SOSM algorithms has not been and cannot be achieved even in the case of continuous SOSM algorithms [26].

In this section we present three different approaches to the chattering problem. The first one [26], [27], [28] uses frequency domain methods to show the existence of periodic motions in first order and also higher order sliding mode algorithms. This approach leads to the conclusion that even though SOSM algorithms are able to adjust chattering, they do not provide chattering free control.

The second approach based on the singularly perturbed analysis to the chattering problem [97].

The third approach [3] is devoted to a formal definition of chattering and its classification according to the amount of energy that it dissipates. It allows to analyze the differences between first and high order sliding motions and also with respect to other approaches like high-gain control.

1.7.1 Chattering Analysis in the Frequency Domain

The *methodology* presented in this section is based on the describing function (DF) method, which provides only approximate solutions. The DF method provides a simple, efficient solution of the periodic problem. The accuracy of the obtained results can always be assessed via simulations. The DF method is reasonably precise for chattering analysis because chattering means the high frequency oscillations,

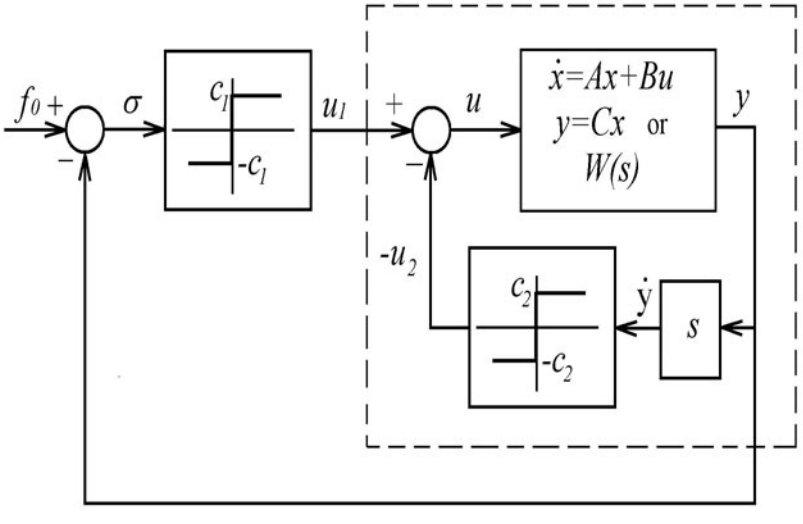

Fig. 1.3 Block diagram of the system governed by TA

i.e. higher harmonics should to be filtered out by the plant and consequently the system satisfies the filter hypothesis.

The use of the DF method will, therefore, be justified in the section devoted to examples and simulations.

For exact frequency-domain analysis of chattering and approximate frequency-domain analysis of transients in SM control systems, please refer to [24] and the chapter of Dr. I. Boiko in this book, respectively.

1.7.1.1 Twisting Algorithm and Its DF Analysis

Let the plant (or the plant plus actuator) be given by the following differential equations:

$$\dot{x} = Ax + Bu, \quad y = Cx \tag{1.12}$$

where A and B are matrices of respective dimensions; $x \in \mathbb{R}^n$ and $y \in \mathbb{R}$ may be treated either as the sliding variable or as the system output. We assume that the plant is asymptotically stable, apart from some possible integrating terms, and that it is a low-pass filter. We shall also use the plant description in the form of a transfer function $W(s) := C(Is - A)^{-1}B$.

Let the control be the twisting algorithm [51, 89]:

$$u = -c_1 \text{sign}(y) - c_2 \text{sign}(\dot{y}), \tag{1.13}$$

where c_1 and c_2 are positive values, $c_1 > c_2 > 0$.

Assume that a periodic motion occurs in the system with the twisting algorithm and find the parameters of this periodic motion. As normally accepted in the DF analysis, we assume that the harmonic response of the plant is that of a low-pass filter, such that the output of the plant is a harmonic oscillation. The DF of the twisting algorithm, denoted by $N(a_1)$, is the first harmonic of the periodic control signal divided by the amplitude of $y(t)$ [7]:

$$N = \frac{4}{\pi a_1}(c_1 + jc_2), \tag{1.14}$$

where a_1 is the amplitude of the input to the nonlinearity (of $y(t)$ in our case). Let us note that the DF of the twisting algorithm only depends on the value of the amplitude. This suggests finding the parameters of the limit cycle via the solution of the harmonic balance equation [7]:

$$W(j\Omega)N(a) = -1, \tag{1.15}$$

where a is the generic amplitude of the oscillation at the input of the nonlinearity and $W(j\Omega)$ is the complex frequency response characteristic (Nyquist plot) of the plant. Using the notation of the twisting algorithm this equation can be rewritten as follows:

$$W(j\Omega) = -\frac{1}{N(a_1)}, \tag{1.16}$$

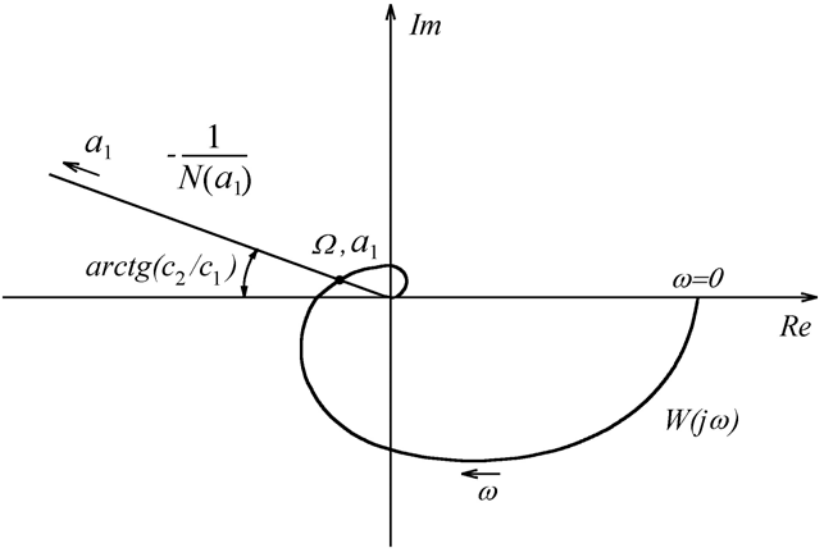

Fig. 1.4 Solving the harmonic balance equation for TA

where the function on the right-hand side is given by:

$$-\frac{1}{N} = \pi a_1 \frac{-c_1 + jc_2}{4(c_1^2 + c_2^2)}.$$

Equation (1.15) is equivalent to the condition of the complex frequency response characteristic of the open-loop system intersecting the real axis at the point $(-1, j0)$. The graphical illustration of the technique of solving equation (1.15) is given in Fig. 1.4. The function $-\frac{1}{N}$ is a straight line, the slope of which depends on the c_2/c_1 ratio. This line is located in the second quadrant of the complex plane. The point of intersection of this function and the Nyquist plot $W(j\varpi)$ provides the solution of the periodic problem. This point gives the frequency of the oscillation and the amplitude a_1. Therefore, if the transfer function of the plant (or plant plus actuator) has relative degree higher than *two,* then a periodic motion may occur in such a system. For that reason, if an actuator of first or higher order is added to the plant of relative degree *two* driven by the twisting controller a periodic motion may occur in the system.

The conditions for the existence of a periodic solution in a system with the twisting controller can be derived from the analysis of Fig. 1.4. Obviously, every system with a plant of relative degree *three* or higher would have a point of intersection with the negative reciprocal of the DF of the twisting algorithm and, therefore, a periodic solution would exist.

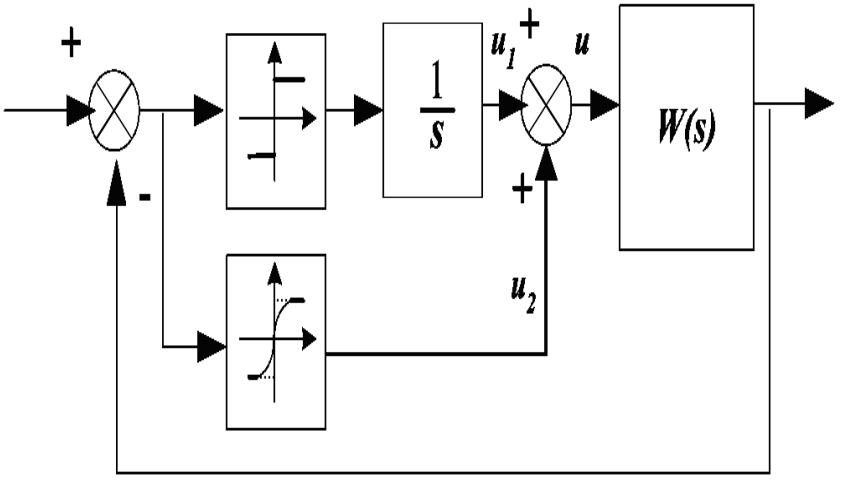

Fig. 1.5 Block diagram of the system governed by STA

This is applicable to so called " twisting as a filter" algorithm. The introduction of the integrator in series with the plant makes the relative degree of this part of the system equal to two. As a result, any actuator introduced in the loop increases the overall relative degree to at least three. In this case, there always exists a point of intersection of the Nyquist plot of the series connection of the actuator, the plant and the integrator and of the negative reciprocal of the DF of the twisting algorithm. Thus, if an actuator of first or higher order is added to the plant with relative degree one a periodic motion may occur in the system with the twisting as a filter algorithm.

1.7.1.2 Super-Twisting Algorithm and Its DF Analysis

A similar approach as in the last section can be used to perform a DF analysis for the super-twisting algorithm:

$$u = -k_1 \text{sign}(y) + v, \quad \dot{v} = -k_2 |y|^{\frac{1}{2}} \text{sign}(y),$$

The DF of the STA is given by

$$N = N_1 + N_2 = \frac{4k_1}{\pi a_y} \frac{1}{j\Omega} + \frac{1.1128 k_2}{\sqrt{a_y}}. \tag{1.17}$$

where a_y is the amplitude of the output oscillations. Let us note that the DF of the super-twisting algorithm depends on the values of both the amplitude, a_y, and the frequency, Ω. The parameters of the limit cycle may be found via the solution of the harmonic balance equation (1.15), where the DF N is given by (1.17).

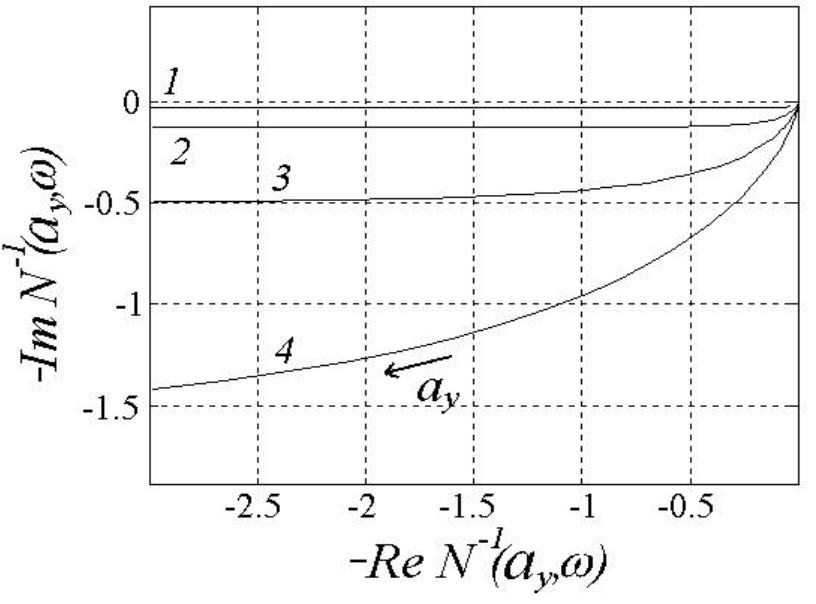

Fig. 1.6 Level curves for $-1/N$ in the super-twisting case

The DF of the STA can be depicted as a number of plots representing the dependency on the amplitude, with each of those plots corresponding to a certain frequency. The frequency range of interest lies below the frequency corresponding to the intersection of the Nyquist plot and the real axis. The plots of the function $-1/N$ are depicted in Fig. 1.6. Plots 1-4 correspond to four different frequencies with the following relationship: $\Omega_1 > \Omega_2 > \Omega_3 > \Omega_4$. Each of those plots represents the dependence of the DF on the amplitude value.

By solving the harmonic balance equation (1.15), it is possible to prove the existence of a periodic solutions:

Proposition 1.1. *If the relative degree of the plant is* ***two*** *or higher and the plant does not have double zero poles then at least one solution may exist of the equation (1.16) for the super-twisting algorithm.*

It is important that the point of intersection be located in the third quadrant of the complex plane. Therefore, if the transfer function of the plant (or plant plus actuator) has relative degree higher than one, a periodic motion may occur in such a system. For that reason, if *parasitic dynamics* of first or higher order are added to the *principal dynamics* of relative degree *one* driven by the super-twisting controller then, once again, a periodic motion may occur in the system. Moreover, the frequency of the periodic solution for the super-twisting algorithm is always lower than the frequency of the periodic motion in the system with the classical first order

SM relay controller since the latter is determined by the point of the intersection of the Nyquist plot and the real axis.

In [80, 81, 30] different SOSM controllers are studied in terms of their transfer properties, which allows investigating the response of the system to an external signal representing either a disturbance, which the system is supposed to reject, or the reference input, which the system is supposed to track. An approach based on the Locus of a Perturbed Relay System (LPRS) [24] is developed making reference to linear plant/actuator sensor dynamics and to the "generalized sub-optimal" second-order sliding mode control algorithm in the closed loop [30].

1.7.2 Singularly Perturbed Analysis of Homogeneous Sliding Modes in the Presence of Fast Actuators

Till now, the robustness of homogeneous sliding modes had been proven with respect to switching imperfections, small delays and noises [93]. In reality, the control affects a plant by means of an actuator. A proper mathematical model of the actuator is often uncertain, and, as a result, it is not accounted for at the control-design stage. The purpose of the actuator is to properly transmit the input, and it does so when the input changes smoothly and slowly. For this reason the actuator needs to be fast, exact and stable. Unfortunately, high-frequency discontinuous inputs cause uncontrolled vibrations of the actuator and of the closed SOSM system (see [27], [26], [28] and references therein).

That is why the proper way to describe the behavior of control systems with fast actuators is through the singularly perturbed technique. For first order sliding mode systems the singularly perturbed analysis of chattering was proposed and developed in [60], [61]. For the SOSM such analysis is performed in [29], [28].

Most of known HOSM controllers are homogeneous [96], [93]. Here, following [97], we will analyze the accuracy of homogeneous HOSMs with respect to the presence of unaccounted-for fast stable actuators.

Let a smooth dynamic system with a smooth output function σ be closed by some possibly-dynamic discontinuous feedback and be understood in the Filippov sense [57]. Then, provided that the successive total time derivatives $\sigma, \dot{\sigma}, ..., \sigma^{(r-1)}$ be continuous functions of the closed-system state-space variables and the set $\sigma = \dot{\sigma} =, ..., = \sigma^{(r-1)} = 0$ be a non-empty integral set, the motion on the set is called a sliding (rth order sliding) mode [92], [93]. Sliding modes used in most variable structure systems are of the first order.

Let the dynamic system and the output (sliding variable) σ have the form

$$\dot{x} = a(t,x) + b(t,x)v, \quad \sigma = \sigma(t,x) \tag{1.18}$$

where $x \in R^n$, $t \in R$, $\sigma \in R$, the $r-1$ total time derivatives are measured in real time, $v \in \mathbb{R}$ is the input, and n is uncertain. Provided an r-sliding mode $\sigma = 0$ is established in (1.18), asymptotic of σ are to be estimated in the presence of unaccounted-for fast stable actuators.

Assumption 1.1. *The smooth, uncertain functions a, b and σ are defined in some open region $\Omega_x \in R^{n+1}$. It is supposed that, provided the input v be a Lebesgue-measurable function of time, $|v| \le v_M$, all solutions starting from an open region $\Omega_x \in R^n$ at $t = t_a$ can be extended in time up to $t = t_b > t_a$ without leaving Ω. The constant $v_M > 0$ is introduced in Assumption 1.4.*

Existence of such t_b is trivial for any $v_M > 0$ and bounded Ω_x.

Assumption 1.2. *The relative degree r of the system is assumed to be constant and known. That means that for the first time the input variable v explicitly appears in the rth total time derivative of σ. It is possible to verify that*

$$\sigma^{(r)} = h(t,x) + g(t,x)\, v \tag{1.19}$$

where $h(t,x) = \sigma^{(r)}|v = 0$, $g(t,x) = (\partial/\partial v)\,\sigma^{(r)}$ are some unknown smooth functions. The set Ω_x is supposed to contain rsliding points at the time $t = t_a$, i.e. points satisfying $\sigma = \dot{\sigma} = , ..., = \sigma^{(r-1)} = 0$.

Assumption 1.3. *It is supposed that the inequalities*

$$0 < K_m \le \frac{\partial}{\partial v}\sigma^{(n)} \le K_M, \qquad \left|\sigma^{(r)}\right|_{v=0} \le C \tag{1.20}$$

hold in Ω for some K_m, K_M, $C > 0$. Conditions (1.20) are formulated in terms of input-output relations.

The actuator model is described by the equations

$$\mu \dot{z} = f(z,u), \qquad v = v(z) \tag{1.21}$$

where $z \in R$, $u \in R$ are the control and the input of the actuator respectively, output $v(z)$ is continuous, $f \in (z,u)$ is a locally bounded Borel-measurable function and the time constant $\mu > 0$ is a small parameter. Recall that all differential equations are understood in the Filippov sense [57].

The control u is determined by a feedback of the form

$$u = U\left(\sigma, \dot{\sigma}, ..., \sigma^{(r-1)}\right) \tag{1.22}$$

where U is a function, continuous almost everywhere, bounded by some constant $u_M > 0$ in its absolute value.

When applied directly to (1.18), i.e. with

$$v = u \tag{1.23}$$

this control is supposed to locally establish the r-sliding mode $\sigma = 0$ (see also Assumption 1.6 below). In order to apply (1.22) one needs to measure or estimate $r-1$ derivatives of σ.

Assumption 1.4. *The initial values of actuator (1.21) belong to a compact region Ω_{z0}. The actuator features Bounded-Input-Bounded-State (BIBS) property for some*

value of μ. As $|u| \le u_M$, this provides for the infinite extension in time of any solution of (1.21) and z belonging to another compact region Ω_z independent of μ. Indeed, μ can be excluded by the time transformation $\tau = t/\mu$. This assumption also causes the actuator output v to be bounded in its absolute value by some constant $v_M > 0$.

Assumption 1.5. *The dynamic output-feedback (1.22) is supposed to be $r-$sliding homogeneous [93], which means that the identity*

$$U\left(\sigma, \dot{\sigma}, ..., \sigma^{(r-1)}\right) = U\left(\kappa^r \sigma, \kappa^{r-1}\dot{\sigma}, ..., \kappa\sigma^{(r-1)}\right) \tag{1.24}$$

is kept for any. It is also assumed that the control function U is locally Lipschitzian everywhere except in a finite number of smooth manifolds comprising the closed set Γ in the space with coordinates $\Sigma = \left(\sigma, \dot{\sigma}, ..., \sigma^{(r-1)}\right)$. Note that, due to homogeneity property (1.24), set Γ contains the origin $\Sigma = 0$, where function U is inevitably discontinuous [93].

Assumption 1.6. *It is assumed that with control (1.22) applied directly to the inclusion, a finite-time stable inclusion (1.22), (1.23) is created.*

Assumption 1.7. *The actuator is assumed exact in the following sense. With $\mu = 1$ and any constant value of u, $|u| \le u_M$, the output v uniformly tends to u. In other words, for any $\delta > 0$ there exists $T > 0$ such that with any u, $u = const$, $|u| \le u_M$, $z(0) \in \Omega_z$, the inequality $|v - u| \le \delta$ is kept after the transient time T. It is also required that the function $f(z,u)$ in (1.21) be uniformly continuous in u, which means that $\|f(z,u) - f(z,u+\Delta u)\|$ tends to 0 with $\Delta u \to 0$ uniformly in $z \in \Omega_z$, $|u| \le u_M$.*

Assumption 1.8. *It is supposed that the change of (1.22), (1.23) at the set Γ to*

$$v \in \begin{cases} U(\Sigma), & \Sigma \notin \Gamma \\ [-v_M, v_M], & \Sigma \in \Gamma \end{cases} \tag{1.25}$$

does not destroy the finite-time convergence, i.e. (1.19),(1.25) is also finite time stable.

The asymptotic sliding accuracy is calculated in the following main Lemma.

Lemma 1.1. *Under Assumptions 1.1-1.6 suppose that for some $\mu = \mu_0$ there exists a ball, B, centered at $\Sigma = 0$ and a bounded invariant set, Θ, which in finite time attracts all trajectories of the inclusion (1.21), (1.22) starting within $B \times \Omega_{z0}$. Then there exist a time moment $t_1 \in (t_a, t_b)$, $a_0, a_1, ..., a_{r-1} > 0$, and a vicinity Q of the r-sliding set in Ω_x at $t = t_a$, such that with a sufficiently small $\mu > 0$ the inequalities $|\sigma| < a_0\mu^r$, $|\dot{\sigma}| < a_1\mu^{r-1}, ..., \left|\sigma^{(r-1)}\right| < a_{r-1}\mu$ are kept with $t \ge t_1$ for any trajectory of (1.18), (1.21), (1.22) starting within Q at $t = t_a$.*

Theorem 1.1. *Let Assumptions 1.1-1.8 hold. Then the conditions of Lemma 1.1 hold and the corresponding asymptotic sliding accuracy is obtained.*

1.7.3 Energy Based Approach [3]

Consider an absolutely continuous scalar signal $\xi(t) \in \mathbb{R}$, $t \in [0,T]$. Also let $\bar{\xi}$ be an absolutely continuous "nominal signal" such that ξ is considered as its perturbed value. Let $\Delta\xi = \xi - \bar{\xi}$, and introduce virtual dry (Coloumb) friction, which is a force of constant magnitude k directed against the motion vector $\Delta\dot{\xi}$. Its work or "heat release" during an infinitesimal time increment dt equals $-k\text{sign}(\Delta\dot{\xi})\Delta\dot{\xi}dt = -k|\Delta\dot{\xi}|dt$. Define the L_1-chattering of the signal $\xi(t)$ with respect to $\bar{\xi}(t)$ as the energy required to overcome such friction with $k = 1$, i.e.

$$L_1\text{-chat}\left(\xi,\bar{\xi};0,T\right) := \int_0^T |\dot{\xi}(t) - \dot{\bar{\xi}}|dt$$

In other words, L_1-chattering is the distance between $\dot{\xi}$ and $\dot{\bar{\xi}}$ in the L_1-metric, or the variation of the signal difference $\Delta\xi$. Similarly, considering virtual viscous friction proportional to $\Delta\xi$, obtain

$$L_2\text{-chat}\left(\xi,\bar{\xi};0,T\right) = \left[\int_0^T |\dot{\xi}(t) - \dot{\bar{\xi}}|^2 dt\right]^{1/2}.$$

Let $x(t) \in \mathbb{R}^n$, $t \in [0,T]$, be an absolutely continuous vector function, and $M(t,x)$ be some positive-definite continuous symmetric matrix with a determinant different from 0. The chattering of the trajectory $x(t)$ with respect to $\bar{x}(t)$ is defined as

$$L_p\text{-chat}\left(x,\bar{x};0,T\right) = \left[\int_0^T \left[\left(\dot{x}(t) - \dot{\bar{x}}(t)\right)M(t,x)\left(\dot{x}(t) - \dot{\bar{x}}(t)\right)\right]^p dt\right]^{1/p}$$

Matrix M is introduced here to take into account a local metric. Note that with $M = I$ the L_1-chattering is the length of the curve $x(t) - \bar{x}(t)$.

1.7.3.1 Classification: Chattering Family

The notions introduced depend on the time scale and the space coordinates. The following notions are free of this drawback.

Consider a family of absolutely continuous trajectories (signals) $x(t,\varepsilon) \in \mathbb{R}^n$, $t \in [0,T]$, $\varepsilon \in \mathbb{R}^l$. The family of chattering parameters ε_i measure some imperfections and tend to zero. Define the nominal trajectory (signal) as the limit trajectory (signal) $\bar{x}(t) := \lim_{\varepsilon\to 0} x(t,\varepsilon)$, $t \in [0,T]$. Chattering is not defined in the case when the limit trajectory $\bar{x}(t)$ does not exist or is not absolutely continuous. For chattering classification the well known L_p technique is used.

Definition 1.4. L_p-chattering is said to be

i) infinitesimal, if the "heat release" is infinitesimal, i.e.

$$\lim_{\varepsilon\to 0} L_p\text{-chat}\,(x,\bar{x};0,T)=0,$$

ii) bounded if the "heat release" is bounded, i.e.

$$\lim_{\varepsilon\to 0} L_p\text{-chat}\,(x,\bar{x};0,T)>0,$$

iii)unbounded if the "heat release" is not bounded, i.e.

$$\lim_{\varepsilon\to 0} L_p\text{-chat}\,(x,\bar{x};0,T)=\infty.$$

The last two chattering types are to be considered as potentially destructive.

In [3] it is shown that high gain controller design can cause unbounded "heat release".

1.7.4 Recapitulation

1. The use of phrases such as *chattering free* or *chattering elimination*i s not correct. Continuous HOSM based controllers can eliminate chattering in the mathematical model of the system but not in the system itself, i.e. they can only adjust chattering, not eliminate it.
2. Chattering in continuous high gain controllers may have unbounded heat release.

1.7.5 Open Problems

- estimation of HOSMs accuracy in smooth controllers in the presence of fast actuators;
- compensator design for SOSM and HOSM controllers (e.g. [134] for the twisting controller);
- finding the solutions which will allow the adjustment of chattering by system design;
- for the observer-based case, find the sufficient and necessary conditions for chattering adjustment and accuracy for the observer-based approach suggested in [31](see also [151]).

1.8 HOSM Observation and Identification

The problems of state observation and unknown input estimation have been actively developed using the Sliding Mode approach (see, for example, the corresponding chapters in the [151] and the recent tutorials [58, 50, 132, 144]). The first sliding modes observers (SMO) were designed for systems with relative degree one with respect to the unknown inputs [50]. Generally, they were developed for systems

which satisfy the necessary and sufficient conditions to estimate the entire state vector without differentiation of the output (i.e., for the systems with relative degree one w.r.t. the unknown inputs) (see also [145]). A recent and most complete tutorial, about such kind of observers is made by Prof. S. Spurgeon [144].

It turns out that the conditions to estimate the entire state vector without differentiation of the output are not satisfied for the state observation of a mechanical system where only positions are measured [41], [43]. To overcome the restriction of relative degree one w.r.t the unknown inputs, an idea was suggested: to transform the system into a triangular form and use a step by step sliding mode observer based on the successive reconstruction of each element of the transformed state vector with filtration in each step (see, e.g., [75, 1]).

The design of the observers that need a regular form is restricted to the fulfillment of a specific relative degree condition [58]. The essence of the observers that use the triangular form is to recover information from the derivatives of the output of the system which are not affected by the unknown inputs. Such derivatives can be estimated via a second order sliding mode technique, specifically by the super-twisting algorithm. In the last two decades some second-order sliding-mode algorithms have been designed. However, they still require consecutive differentiations.

One of the problems with the recently proposed SMO is that the differentiation procedure is done step-by-step using the super-twisting algorithm which increases the error due to the sample time of sensors or computer calculations. Also, as in the majority of exact sliding mode observers, it is assumed that the unknown input vector is uniformly bounded. Three kinds of sliding mode observers has been proposed recently for overcoming such a problem. In [33], [19], [20] an algebraic observer was suggested which made use of the STA in each differentiation step. The authors of [59] proposed first using a step-by step differentiation process to generate a new system output, and then designing a first order sliding mode. The second approach was proposed in [68, 67, 17, 63] allowing the use of arbitrary order robust exact differentiators providing the best possible accuracy of the observer w.r.t. the sampling step and bounded deterministic noise in the sense of [84]. Furthermore, in [17] it is no longer necessary to have bounded unknown inputs.

One of the important properties of SMO is that they allow reconstructing the unknown inputs which, depending of their nature, allow the use of observers for fault detection and isolation ([137, 145]), identification of uncertain parameters ([43, 19]) and compensation of disturbances ([56]). However, all the mentioned observers consider that in order to estimate the unknown inputs it is necessary to estimate the state vector first. In [21], necessary and sufficient conditions were given for the estimation of unknown inputs, which do not require the state to be estimated.

1.8.1 HOSM Observation and Unknown Inputs Identification

Let Σ be a linear system whose dynamics are governed by the following equations:

$$\Sigma : \begin{cases} \dot{x}(t) = Ax(t) + Dw(t) \\ y(t) = Cx(t) + Fw(t) \end{cases} \tag{1.26}$$

The state vector is represented by $x(t) \in \mathbb{R}^n$, $w(t) \in \mathbb{R}^m$ represents the unknown input vector and $y(t) \in \mathbb{R}^p$ is the system output. Without loss of generality, it is assumed that rank $\begin{bmatrix} D \\ F \end{bmatrix} = m$.

Definition 1.5. Σ is called strongly observable if $y(t) = 0$ for all $t \geq 0$ implies $x(t) = 0$ for all $t \geq 0$.

To overcome the restriction of consecutive differentiation the following observer design was proposed in [17] for strongly observable systems. The extension to strongly detectable systems is also given in that paper.

In the next lines we give a simplified design of the observer. The main idea is to express x as a differentiation operator to y. Let the matrices M_{k+1} be defined by means of the following algorithm:

$$\begin{aligned} M_{k+1} &= N_{k+1}^{\perp\perp} N_{k+1}, \quad M_1 = \left(F^{\perp}C\right)^{\perp\perp} F^{\perp}C \\ N_{k+1} &= T_k \begin{pmatrix} M_k A \\ D \end{pmatrix}, T_k = \begin{pmatrix} M_k D \\ F \end{pmatrix}^{\perp} \end{aligned} \tag{1.27}$$

Defining $\Phi_1 := J_1 y$, where[1] $J_1 := \left(F^{\perp}C\right)^{\perp\perp} F^{\perp}$, leads to

$$\Phi_1 = \left(F^{\perp}C\right)^{\perp\perp} F^{\perp}Cx = M_1 x \tag{1.28}$$

Now with $\Phi_2 := N_2^{\perp\perp} T_1 \begin{bmatrix} \frac{d}{dt} M_1 x \\ y \end{bmatrix}$, and moving the differentiation operator outside of the parenthesis, the following identity is obtained[2]

$$\Phi_2 = M_2 x = \frac{d}{dt} N_2^{\perp\perp} T_1 \begin{bmatrix} J_1 & 0 \\ 0 & I \end{bmatrix} \begin{bmatrix} y \\ y^{[1]} \end{bmatrix} = \frac{d}{dt} J_2 \begin{bmatrix} y \\ y^{[1]} \end{bmatrix}$$

Matrix J_2 is defined by the previous identity. Then, we can generalize the procedure as follows: defining $\Phi_k := N_k^{\perp\perp} T_{k-1} \begin{bmatrix} \frac{d}{dt} M_{k-1} x \\ y \end{bmatrix}$ $(k = 2, \ldots, n-1)$, the identity

[1] The notation $X^{\perp}$ means a full row rank orthogonal matrix to X, i.e. $X^{\perp}X = 0$ and $\text{rank}X^{\perp} = n - \text{rank}X$. The matrix $X^{\perp\perp}$ must satisfy the conditions $\text{rank}X^{\perp\perp} = \text{rank}X$ and $\det \begin{bmatrix} X^{\perp} \\ X^{\perp\perp} \end{bmatrix} \neq 0$.

[2] Let $f(t)$ be a vector function, $f^{[k]}$ represents the k-th anti-differentiator of $f(t)$, i.e. $f^{[k]}(t) = \int_0^t \int_0^{\tau_1} \cdots \int_0^{\tau_{k-1}} f(\tau_k) d\tau_k \cdots d\tau_2 d\tau_1$, $f^{[0]}(t) = f(t)$.

$$\Phi_k = M_k x = \frac{d^{k-1}}{dt^{k-1}} N_k^{\perp\perp} T_{k-1} \begin{bmatrix} J_{k-1} & 0 \\ 0 & I \end{bmatrix} \begin{bmatrix} y \\ y^{[1]} \\ \vdots \\ y^{[k-1]} \end{bmatrix} = \frac{d^{k-1}}{dt^{k-1}} J_k \begin{bmatrix} y \\ y^{[1]} \\ \vdots \\ y^{[k-1]} \end{bmatrix} \tag{1.29}$$

holds, where $J_k = N_k^{\perp\perp} T_{k-1} \begin{bmatrix} J_{k-1} & 0 \\ 0 & I \end{bmatrix}$.

Thus, the state vector x can be expressed by the identity

$$x = \frac{d^{n-1}}{dt^{n-1}} M_n^{-1} J_n \begin{bmatrix} y \\ y^{[1]} \\ \vdots \\ y^{[n-1]} \end{bmatrix} \tag{1.30}$$

By defining $H(t)$ as

$$H(t) = M_n^{-1} J_n \begin{bmatrix} y \\ y^{[1]} \\ \vdots \\ y^{[n-1]} \end{bmatrix} \tag{1.31}$$

we obtain that $x(t) = \dfrac{d^{n-1}}{dt^{n-1}} H(t)$. Then, vector $x(t)$ can be obtain by means of a high order differentiator [92].

Thus, the j-th term of $x(t)$ can be estimated in the following way

$$\begin{array}{rcl} \dot{z}_{j,0} & = & \lambda_0 \left| z_{j,0} - H_j \right|^{\frac{n-1}{n}} \operatorname{sign}\left(z_{j,0} - H_j \right) + z_{j,1} \\ \dot{z}_{j,1} & = & \lambda_1 \left| z_{j,1} - \dot{z}_{j,0} \right|^{\frac{n-2}{n-1}} \operatorname{sign}\left(z_{j,1} - \dot{z}_{j,0} \right) + z_{j,2} \\ & \vdots & \\ \dot{z}_{j,n-2} & = & \lambda_{n-2} \left| z_{j,n-2} - \dot{z}_{j,n-3} \right|^{1/2} \operatorname{sign}\left(z_{j,n-2} - \dot{z}_{j,n-3} \right) + z_{j,n-1} \\ \dot{z}_{j,n-1} & = & \lambda_{n-1} \operatorname{sign}\left(z_{j,n-1} - \dot{z}_{j,n-2} \right) \end{array} \tag{1.32}$$

With the proper selection of constants λ_i $(i = 0, \cdots, \bar{n}_H - 1)$, there exists a finite time t_j such that the identity $z_{j,n-1}(t) = \frac{d^{n-1}}{dt^{n-1}} H_j(t)$ is achieved for all $t \geq t_j$. The constants λ_i can be calculated in the following form, $\lambda_i = \lambda_{0i} K^{1/(\bar{n}_H - i)}(t)$, where $K(t)$ is a continuous function and, at time t, $K(t)$ is a known local Lipschitz constant for $x(t)$ and λ_{0i} is calculated for the case when $K(t) = 1$ (λ_{0i} may be calculated through simulations). A value of λ_{0i} $(i = 0, \cdots, \bar{n}_H - 1)$ for a fifth order differentiator was given in [92], with $\lambda_{00} = 12$, $\lambda_{01} = 8$, $\lambda_{02} = 5$, $\lambda_{03} = 3$, $\lambda_{04} = 1.5$, and $\lambda_{05} = 1.1$.

Remark 1.1. The restriction over the boundedness of $x(t)$ can be avoided by means of a more elaborated technique, using a linear compensator and defining an extended vector which includes the perturbations. For more details see [17].

Thus, defining the vector $z_{n-1} = \left[z_{1,n-1} \ \cdots \ z_{l,n-1} \right]^T$, we achieve in a finite time the identity

$$z_{n-1}(t) = x(t)$$

If we assume that $w(t)$ is differentiable with a bounded derivative then we can extended the state vector as

$$x_{\text{ex}}(t) = \begin{bmatrix} x(t) \\ w(t) \end{bmatrix}$$

In such a way, the previous procedure can be applied to the extended vector $x_{\text{ex}}(t)$. If we define $\bar{n} = n + m$, and we use a differentiator of order $\bar{n} - 1$, we obtain the following identities,

$$z_{\bar{n}-1}(t) = x_{\text{ex}}(t)$$

Remark 1.1. Indeed, if we consider that $D = B$, then we can use the estimated unknown input in the control law to compensate the effects of the matched disturbances [56].

1.8.2 Time Invariant Parameter Identification

Let us assume that we have reconstructed $w(t)$, the complementary part of the extended state vector $x_{ex}(t)$, by means of an adaptable variable $\hat{w}(t)$. Using regressor notation, we can write $w(t)$ as

$$w(t) = \theta(t)\varphi(t,x,u)$$

where $\theta(t) \in \mathbb{R}^{n \times l}$ is a matrix composed by the value of the uncertain parameters and $\varphi(t,x,u) \in \mathbb{R}^l$ is a known nonlinear function vector.

Through a shorter notation, function $\varphi(t,x,u)$ will be referred to as $\varphi(t)$. Now, using the auxiliary variable σ for integration in time, we have that

$$\frac{1}{t}\int_0^t \hat{w}(\sigma)\varphi^T(\sigma)d\sigma = \theta\frac{1}{t}\int_0^t \varphi(\sigma)\varphi(\sigma)^T d\sigma \tag{1.33}$$

Therefore, the system parameters can be estimated from (1.33) by

$$\hat{\theta}(t) = \left[\int_0^t \hat{w}(\sigma)\varphi^T(\sigma)d\sigma\right]\left[\int_0^t \varphi(\sigma)\varphi^T(\sigma)d\sigma\right]^{-1} \tag{1.34}$$

where $\hat{\theta}$ is the estimation of θ. For any square matrix the next equalities holds

$$\begin{gathered} \Gamma^{-1}(t)\Gamma(t) = I, \\ \Gamma^{-1}(t)\dot{\Gamma}(t) + \dot{\Gamma}^{-1}(t)\Gamma(t) = 0 \end{gathered} \tag{1.35}$$

Let us define $\Gamma(t) = \left[\int_0^t \varphi(\sigma)\varphi^T(\sigma)d\sigma\right]^{-1}$. Using (1.35) we can rewrite (1.34) in the form:

$$\dot{\hat{\theta}} = \left[\int_0^t \hat{w}(\sigma)\varphi^T(\sigma)d\sigma\right]\dot{\Gamma}(t) + \hat{w}(t)\varphi^T(t)\Gamma(t)$$

Now, using equation (1.34) we can write

$$\dot{\widehat{\theta}} = \widehat{\theta}\Gamma^{-1}(t)\dot{\Gamma}(t) + \hat{w}(t)\varphi^T(t)\Gamma(t)$$

The equalities (1.35) allow us to write a dynamic expression to compute θ as

$$\dot{\widehat{\theta}} = \left[-\widehat{\theta}\varphi(t) + \hat{w}(t)\right]\varphi^T(t)\Gamma(t). \tag{1.36}$$

In the same way, a dynamic form to find $\Gamma(t)$ is given by

$$\dot{\Gamma}(t) = -\Gamma(t)\varphi(t)\varphi^T(t)\Gamma(t) \tag{1.37}$$

The average values of the real $w(t)$ satisfy the equality

$$\int_0^t w(\sigma)\varphi^T(\sigma)d\sigma = \theta\int_0^t \varphi(\sigma)\varphi^T(\sigma)d\sigma$$

then

$$\theta = \left[\int_0^t w(\sigma)\varphi^T(\sigma)d\sigma\right]\Gamma(t).$$

Taking into account that in practice $\hat{w} = w + \varepsilon$, we have the following identity for θ:

$$\theta = \left[\int_0^t \hat{w}(\sigma)\varphi^T(\sigma)d\sigma + \int_0^t \varepsilon(\sigma)\varphi^T(\sigma)d\sigma\right]\Gamma(t). \tag{1.38}$$

Let us assume $\hat{w} = \widehat{\theta}\varphi(t)$. In this case equation (1.38) becomes

$$\theta = \left[\widehat{\theta}\int_0^t \varphi(\sigma)\varphi^T(\sigma)d\sigma + \int_0^t \varepsilon(\sigma)\varphi^T(\sigma)d\sigma\right]\Gamma(t),$$

which may be rewritten as

$$\theta = \widehat{\theta} + \left[\int_0^t \varepsilon(\sigma)\varphi^T(\sigma)d\sigma\right]\Gamma(t). \tag{1.39}$$

Thus, it is possible to define the convergence conditions

$$\sup||t\Gamma(t)|| < \infty, \tag{1.40}$$

$$||\frac{1}{t}\int_0^t \varepsilon(\sigma)\varphi^T(\sigma)d\sigma|| \to 0 \quad \text{as} \quad t \to \infty. \tag{1.41}$$

Condition (1.40), known as the persistent excitation condition, requires the non-singularity of the matrix $\Gamma^{-1}(t) = \int_0^t \varphi(\sigma)\varphi^T(\sigma)d\sigma$. To avoid this restriction let us introduce the term ρI where $0 < \rho << 1$ and I is the unit matrix and redefine $\Gamma^{-1}(t)$ as

$$\Gamma^{-1}(t) = \int_0^t \left(\varphi(\sigma)\varphi^T(\sigma)d\sigma\right) + \rho I$$

In this case the value of $\Gamma^{-1}(t)$ is always non-singular.

Notice that the introduction of the term ρI is equivalent to setting the initial conditions of (1.37) as

$$\Gamma(0) = \rho^{-1} I, \quad 0 < \rho\text{-small enough}$$

The introduction of the term ρ ensures that the condition $\sup ||t\Gamma(t)|| < \infty$ be satisfied, but it does not guarantee the convergence of the estimated parameters to the real values. The convergence of the estimated values to the real ones is ensured by the *persistent excitation condition*

$$\liminf_{t\to\infty} \frac{1}{t} \int_0^t \left(\varphi(\sigma)\varphi(\sigma)^T d\sigma\right) > 0$$

Condition (1.41) refers to the unknown input estimation process, and it gives the convergence quality of the identification. The estimated parameters will tend to the real parameters values as fast as the term $\frac{1}{t}\int_0^t \varepsilon(\sigma)\varphi(\sigma)^T d\sigma$ converges to zero.

In [43] the continuous time version of the forgetting factor method(FFM) is suggested.

1.8.3 Further Development

This obviously will increase the sort of systems that can be considered. A procedure to reconstruct the unknown inputs by means of sliding mode differentiators was also proposed. Then, in future research, the possibility of using unknown input estimators (without state observation) for fault detection and isolation, for example, should be considered.

For nonlinear systems there also exists a variety of works dedicated to the design of SMO. Unlike in the case of linear systems, almost all of them use a sufficient condition (of triangularization and relative degree) for the observer design. For instance, affine nonlinear systems with scalar output and relative degree equal to the dimension of the state [154], complete vector relative degree and a transformation [69] and complete relative degree without transformation [42]. In [9] a more general class of systems is considered. Here, the basic idea is that when the triangular form can not be achieved, an extended triangular form is proposed. The most general observer is given in [6] for affine nonlinear systems with meromorphic vector fields and without known inputs. In this last work, an observer using the output and its derivatives (estimated using the HOSM differentiator) is constructed under almost sufficient and necessary structural conditions.

1.8.4 Recapitulation

1. HOSM observers were designed ensuring:

- the finite time theoretically exact identification of smooth unknown inputs for strongly observable systems;

- the best possible asymptotic accuracy of unknown inputs estimation in the sense of [84];
- the theoretically exact identification of smooth unknown inputs for strongly detectable systems;
- the continuous version of the least square method providing asymptotic parameter identification
- the continuous version of the forgetting factor method ([43], [19]).

1.8.5 Open Problems

1. HOSMOs ensure finite time exact convergence but they still can not ensure the separation principle because the convergence time is unknown. Moreover, in the case when the initial conditions tend to infinity the convergence time grows to infinity. That is why the design of uniformly convergent HOSMO observers with prescribed convergence time is desired. The first paper about uniform exact observability is published in VSS10 [38].

2. HOSMOs are designed for a wide class of nonlinear systems, but not for the most general cases. This is why the following are still needed:

- HOSMO design for nonlinear MIMO systems without a strong restriction on the relative degree,
- HOSMO design for nonlinear MIMO systems without transformations;
- HOSMO design for distributed parameters systems;

3. Modifications of the least square method providing parameter identification in finite time.

1.9 Integral Sliding Mode Control

Integral sliding modes [109,150,149] were suggested as a tool to reach the following goals:

- compensation of matched perturbations starting form the initial moment, i.e. ensuring the sliding mode starting form the initial moment;
- preservation of the dimension of the initial system, i.e. saving the system dynamics previously designed for the ideal case (without perturbation).
  These two attractive properties of ISM allows them to be successfully used in different kinds of applications, e.g. robotics (see, for example [45]) and design problems (see, for example [35]).

Suppose that a control law $u = u_0(x,t)$ achieving the control objective (e.g. steering, stabilization or tracking) is already available for an ideal, nominal system

$$\dot{x} = f(x,t) + B(x)u\,, \quad x \in R^n\,, u \in R^m\,. \tag{1.42}$$

Furthermore, suppose that instead of the ideal system (1.42), one has a perturbed system

$$\dot{x} = f(x,t) + B(x)(u+\delta) + \phi_{um}\,,$$

where δ is a matched disturbance and ϕ_{um} is an unmatched disturbance. Then, a sliding mode control law $u_1(x,t)$ can be easily included such that the closed-loop

$$\dot{x} = f(x,t) + B(x)(u_0+u_1+\delta) + \phi_{um}$$

is insensitive to δ.

One begins by constructing the sliding variable

$$s(x,t) = g(x) - z(t)\,, \quad s(x,t) \in R^m\,,$$

where

$$z(t) = g(x_0) + \int_{t_0}^{t} G(x)\left[f(x,\tau) + B(x)u_0(x,\tau)\right] \quad G(x) = \frac{\partial g}{\partial x}(x)$$

(gradients are regarded as row vectors) and $g(x)$ is any function such that $G(x)B(x)$ is invertible.

Notice first that, at $t = t_0$, we have $s = 0$, thus the system starts at the sliding surface (there is no reaching time). Let us now compute the time derivative of s:

$$\begin{aligned}\dot{s} &= G(x)\left[f(x,t) + B(x)(u_0+u_1+\delta) + \phi_{um} - f(x,t) - B(x)u_0\right]\\ &= G(x)B(x)(u_1+\delta) + G(x)\phi_{um}\,.\end{aligned}$$

It can be readily seen that if δ and ϕ_{um} are bounded by known functions, then it is possible to construct a unit control u_1 ensuring $\dot{s} = 0$. The equivalent control is

$$u_{eq} = -\delta - (G(x)B(x))^{-1}G(x)\phi_{um}\,,$$

so the trajectories of the system at the sliding surface are given by

$$\dot{x} = f(x,t) + B(x)u_0 + \left[I - B(x)(G(x)B(x))^{-1}G(x)\right]\phi_{um}\,,$$

which shows the insensitivity with respect to δ.

It is clear that the projection matrix $G(x)$ should

- not amplify the remnant perturbation

$$\phi_{sm} = \left[\underbrace{I - B(x)(G(x)B(x))^{-1}G(x)}_{\Gamma(x)}\right]\phi_{um}\,, \tag{1.43}$$

- minimize (1.43).

It has been shown in [35] that, if $B(x)$ is constant ($B(x) = B$), then G may be chosen such that it minimizes the norm of the projection matrix

$$\Gamma(x) = \left[I - B(GB)^{-1}G\right] \tag{1.44}$$

In the optimal case,

$$G = B^{+}$$

(B^{+} is the Moore-Penrose pseudo inverse of B), the Euclidean norm of ϕ_{sm} is minimal, and $\phi_{sm} = \phi_{\phi m}$, i.e. the unmatched perturbation is not amplified.

This result has been extended in [135] to systems which do not posses a constant $B(x)$, but that have a certain regular form. Under certain integrability conditions on $B(x)$, the optimal can be found for systems which are not necessarily in regular form. To further attenuate ϕ_r one can design u_0 using $\mathscr{H}_\infty$ techniques [34, 35].

1.10 HOSM Output Based Control

High Order Sliding Modes allowed solving the finite-time output regulation and exact disturbance compensation problem for single-input single-output (SISO) systems. After this, the question was the applicability of the HOSM approach to multi-input multi-output (MIMO) systems and for state stabilization. Let us consider the case of a linear system

$$\begin{aligned} \dot{x} &= Ax + B[u + w(t)], \\ y &= Cx, \end{aligned} \tag{1.45}$$

where $x \in \mathbb{R}^n$, $y \in \mathbb{R}^p$, $u, w \in \mathbb{R}^m$ are the state, measured output, controlled input and disturbance, respectively.

The first natural extension of the HOSM methodology was to consider a MIMO system with vector relative degree. In such case, each output can be controlled independently as a SISO system and the exact finite-time output regulation problem is solvable using HOSMs. Moreover, if the relative degree is complete (i.e. the sum of the individual relative degrees is equal to the state dimension), then the finite-time output stability yields finite-time state stabilization.

However, in a more general case where the system has more outputs than inputs or simply when the system does not have vector relative degree, a more detailed structural analysis of the system is required in order to apply the HOSM approach. Since, in general, we can expect that HOSM controllers are able to provide finite-time stabilization of the output, we should assume that the finite-time output stabilization of $y = 0$ has to yield finite-time state stabilization of $x = 0$ in spite of disturbances. This, for linear systems, turns out to be equivalent to the absence of invariant zeros or of the strong observability of the system [76] with respect to the measured output y. Unfortunately, it is not possible to control the output y directly every time, especially when there exist more outputs than inputs. However, strong observability offers a short-come to this problem by providing necessary and sufficient conditions for estimating the state (in finite-time) using only the measured

output (and its derivatives estimated by HOSM differentiators) in spite of the inputs. Once the state has been estimated in finite-time, the controllability of the system ensures the existence of a "fictitious" output with full vector relative degree [103] that can be easily controlled with the use of HOSMs to provide the finite-time stabilization of the state.

The extension to the MIMO case has been done in [13, 49, 44, 5, 6]. The whole state is assumed to be known in [13], and the traditional sign function of the first order sliding modes (1-SMs) is replaced with a 2-SM controller. The resulting control is both robust and exact, but there is no finite-time stable output regulation and the whole state is used, not only the output. The case of well-defined vector relative degree is considered in [44, 49], and an output based controller is developed. Only asymptotic stability is ensured in [49], and moreover the system has to be BIBS stable with respect to a smooth disturbance. Only the output regulation problem is considered in [44]. In [5], the general case for a controllable and strongly observable linear system is considered and solved obtaining the finite-time exact state stabilization based on output feedback. In [6] the notion of strong observability is extended and characterized for a fairly wide class of nonlinear systems and it allows obtaining the finite-time exact state stabilization of strongly observable and flat nonlinear systems.

Another aspect of this problem arises due to the interaction between the controller and the observer (or differentiator). In general, it is necessary to turn on the controller once the differentiator has converged. Since the HOSM differentiator converges in finite-time this problem can be solved by waiting a sufficient amount of time and then turning on the controller. The problem of real time detection of the convergence time of the HOSM differentiator is considered in [4] where a criterion is developed and used to turn on the controller at an appropriate time.

One way to avoid any initialization phase is by using a hybrid differentiator scheme [114, 113]. The idea is to design a switching law to select between some general estimator, that provides an input-to-state practical stability property for any plant/controller initial conditions, and a locally exact differentiator in such a way that global stability properties are achieved and in addition exact tracking is ultimately achieved.

Other approaches for output feedback SMC are also outlined in the Chapter by prof. Liu Hsu and co-workers. For the sake of simplicity, the focus is maintained on single-input-single-output (SISO) nonlinear systems, although several results have been extended to the control of multi-input-multi-output (MIMO) systems [78, 117, 116]. For the considered class of nonlinear systems, linear growth restriction on the unmeasured states is assumed, while less restrictive conditions are imposed to the growth of nonlinearities depending on the measured output. Moreover, the high frequency gain (HFG) is uncertain in norm but with known sign. The case of unknown HFG sign (unknown control direction) can be coped with the monitoring function approach presented in [114]. Alternative tracking controllers for plants with arbitrary relative degree using different approaches to overcome the relative degree obstacle are briefly described: linear or variable structure lead

filters [77], high-gain observers with constant or dynamic gain [128], hybrid estimation schemes combining lead filters or observers with locally exact differentiators based on high-order sliding mode [114, 113].

The proposed output feedback controllers discussed employ linear lead filters or HGO only to generate the switching law. The modulation function (variable gain) in the control law is synthesized using signals from the standard input-output filters from MRAC which are free of peaking. The dwell-time strategy for control activation introduced in [115] is another approach for peaking avoidance. The dwell-time method allows the inclusion of more general class of uncertain strongly nonlinear systems. It can also enhance the stability and performance of the HGO based controllers.

1.10.1 Open Problems

- uniformly convergent observation and control algorithms are needed,
- relationship between controllability, strong observability and flatness.

1.11 Adaptive Sliding Mode Control

Adaptive control is usually used in order to achieve a desired state or output tracking performance(chattering adjustement). When the HOSMs algorithms were developed it was common opinion that adaptive sliding mode control(ASMC) is not needed anymore. The reason was the following: applying ASMC we only can adjust the discontinuous control gain but the control is still discontinuous. Applying HOSM controllers (STA for the case of relative degree one) for the case when the perturbation is Lipshitz continuous we can have absolutely continuous controller adjusting chattering, i. e. having self adaptation property and avoid filtration of the outputs.

However, there are 2 principal cases when the usage of ASMC seems to be reasonable.

1. When the perturbations/uncertainties are discontinuous but their bounds of are known.
2. When the bounds of the perturbations/uncertainties are known.

1.11.1 ASMC with Known Bounds for the Disturbance

It is acknowledged fact that adaptive sliding mode control (ASMC) techniques are useful in estimating uncertainties/disturbances, even with known bounds, in order to compensate them explicitly while relaxing the burden on the high frequency portion of the SMC, which in turn yields chattering reduction. This kind of ASMCs have been successfully applied to robotic control with unmodelled dynamics [164], for friction identification and compensation [143] and for coupling identification and compensation in MEMS gyroscopes [53]. These ASMC techniques include:

- A gain adaptation algorithm in the 2-sliding mode controller that allowed achieving improved accuracy of the sliding variable stabilization typical of 3-sliding mode [14],
- ASMC that have been applied for estimation and compensation of the sensor's disturbance terms and the external disturbances acting on the plant with aerospace applications [74, 138],
- Fuzzy logic ASMC techniques, but usually they can only guarantee zone convergence; see, for instance, [100],
- An ASMC method proposed in [10], [86] allows adapting the SMC control gain. The idea is based on estimating the equivalent control: once the sliding mode occurs, the disturbance magnitude may be evaluated and allows an adequate tuning of the control gain. This approach requires the knowledge of the uncertainties/perturbations bounds and the use of a low-pass filter, which introduces signal magnitude attenuation, delay, and transient behavior when disturbances are acting.
- The output-feedback model-reference sliding mode controller (MRAC) for multivariable linear systems based on the adaptive control formulation and on the unit vector control approach is presented in [127]. The high frequency gain matrix of the plant is not assumed to be known.

1.11.2 ASMC without Known Bounds for the Disturbance

The case when the boundaries of disturbances/uncertainties exist but are unknown is of extreme importance for developing new ASMC techniques from a theoretical and applications viewpoint. These ASMC techniques include

- ASMC presented in [79], where the gain dynamics directly depend on the sliding variable: the control gain is increased until the sliding mode is not established. Once this is the case, the gain dynamics equal 0. The main drawback to this approach is the gain over-estimation with respect to the uncertainties bound.
- Adaptive continuous control with the asymptotic sliding mode that is robust to actuator failures, nonlinear perturbations, and bounded external disturbances with unknown bounds is presented in [110].
- A gain adaptation technique for traditional SMC that does not overestimate the control gain has been proposed and applied to an electropneumatic actuator in [32]
- A gain adaptation technique for 2- SMC that does not overestimate the control gain has been proposed in [139]
- An adaptive continuous/smooth finite reaching time 2-SMC is proposed in [138]

1.12 HOSM Based Unmatched Uncertainties Compensation

It is a known issue that classical sliding mode (SM) control [151] is not able to compensate both matched and unmatched perturbations [48]. Nevertheless, controllers

based on HOSM algorithms may be applied in order to reject the effect of unmatched perturbations. Next, some of this schemes are presented.

1.12.1 Black Box Control via HOSM

Consider a Single-Input-Single-Output system of the form

$$\begin{aligned} \dot{x}_1 &= f_1(x_1,t) + B_1(x_1,t)x_2 + \omega_1(x_1,t) \\ \dot{x}_i &= f_i(\bar{x}_i,t) + B_i(\bar{x}_i,t)x_{i+1} + \omega_i(\bar{x}_i,t) \\ \dot{x}_n &= f_n(x,t) + B_n(x,t)u + \omega_n(x,t) \\ i &= 2,...,n-1 \\ \sigma &: (t,\xi) \mapsto \sigma(t,\xi) \in R \end{aligned} \tag{1.46}$$

where $x \in R^n$ is the state vector, $x_i \in R$, $\bar{x}_i = [x_1 \dots x_i]^T$, and $u \in R$ is the control. Moreover f_i and B_i are smooth scalar functions, ω_i is a bounded unknown perturbation term due to parameter variations and external disturbances with at least $n-i$ bounded derivatives w.r.t. system (1.46), $B_i \neq 0 \quad \forall x \in X \subset R^n, t \in [0,\infty)$ and σ is the measured output. The task is to achieve $\sigma \equiv 0$.

It is assumed that system (1.46) has a constant and known relative degree r. Then it follows that $\sigma^{(r)} = h(t,\xi) + g(t,\xi)u, \quad g(t,\xi) \neq 0$ holds, where $h(t,\xi) = \sigma^{(r)}|_{u=0}$, $g(t,\xi) = \frac{\partial}{\partial u}\sigma^{(r)}$ if the inequalities $0 < K_m \leq \frac{\partial}{\partial u}\sigma^{(r)} \leq K_M$, $|\sigma^{(r)}|_{u=0}| \leq C$ are fulfilled for some $K_m, K_M, C > 0$. The trajectories of (1.46) are assumed infinitely extendible in time for any Lebesgue-measurable bounded control $u(t,x)$. The next differential inclusion is implied

$$\sigma^{(r)} \in [-C,C] + [K_m,K_M]u \tag{1.47}$$

As it was described earlier, the above problem may be solved by the Quasi-Continuous controller [95], which is constructed to ensure that $\sigma = \dot{\sigma} = \ldots = \sigma^{(r-1)} = 0$ is established in finite time.

In [101] compensation of unmatched perturbations is tackled using the block control approach combined with HOSM algorithms in order to consider unmodelled actuators in the controller design.

1.12.2 Model Based Application of HOSM

In [52] a new design algorithm for systems in strict-feedback form, a special case of the BC-form, is proposed. This algorithm achieves finite-time **exact** tracking of the desired output in the presence of smooth unmatched perturbations. These features are accomplished via the use of quasi-continuous high-order sliding modes (HOSM) and a hierarchical design approach. In the first step the desired dynamic for the first state is defined by the desired tracking signal. After the first step, the desired dynamic for each state is defined by the previous one. Each virtual control is divided into two parts, the first one is intended to compensate the nominal nonlinear part of

the system and the second one is aimed at achieving the desired dynamics in spite of perturbations.

Consider the class of systems of equation (1.46), with the output $y = x_1$. The control problem is to design a controller such that the output y tracks a smooth desired reference y_d with bounded derivatives, in spite of the presence of unknown bounded perturbations. The whole state vector x is assumed to be known.

At each step i the constraint $\sigma_i = 0$ is established and kept by means of the virtual control $x_{i+1} = \phi_i$, which forms the constraint $\sigma_{i+1} = x_{i+1} - \phi_i$ for the next step.

Step 1. Defining $x_2 = \phi_1$, the next virtual controller is constructed

$$\begin{aligned} \phi_1(x_1,t,u_1) &= B_1(x_1,t)^{-1}\{-f_1(x_1,t)+u_1\} \\ u_1^{(n-1)} &= -\alpha_1 H_n(\sigma_1,\dot{\sigma}_1,\ldots,\sigma_1^{(n-1)}) \end{aligned} \tag{1.48}$$

where $\sigma_1 = x_1 - y_d$ and H_n is an n-th order sliding mode algorithm that is introduced in ϕ_1 through $n-1$ integrators. The derivatives $\sigma_1, \dot{\sigma}_1, \ldots, \sigma_1^{(n-1)}$ are calculated by means of robust differentiators with finite-time convergence [92].

Step i. The remaining virtual controls are constructed as follows.

$$\begin{aligned} \phi_i(\overline{x}_i,t,u_i) &= B_i(\overline{x}_i,t)^{-1}\{-f_i(\overline{x}_i,t)+u_i\} \\ u_i^{(n-i)} &= -\alpha_i H_{n-i+1}(\sigma_i,\dot{\sigma}_i,\ldots,\sigma_i^{(n-i)}) \\ \sigma_i &= x_i - \phi_{i-1}; \quad i = 2,\ldots,n. \end{aligned} \tag{1.49}$$

where H_{n-i+1} is an $n-i+1$-th order sliding algorithm. Notice that in *step n*, the real control is calculated i.e. $\phi_n = u$.

$$u = B_n(x,t)^{-1}\{-f_n(x,t)+u_n\};\ u_n = -\alpha_n \mathrm{sign}(\sigma_n).$$

It is possible to smooth out the control signal by raising the order of the QC controller in each ϕ. If this is done, the super-twisting algorithm can also be used in u_n. The following theorem describes the result.

Theorem 1.2. *Provided that $\omega_i(\overline{x}_i,t)$ in system (1.46) and y_d are smooth functions with $n-i$ and n bounded derivatives respectively the above hierarchic design results in an ultimate controller u, providing for the finite time stability of $\sigma_1 = x_1 - y_d = \dot{\sigma}_1 = \ldots = \sigma_1^{(n-1)} = 0$ in system (1.46).*

1.12.3 Exact Unmatched Uncertainties Compensation Based on HOSM Observation

Let us consider a linear time invariant system with unknown inputs

$$\begin{aligned} \dot{x} &= Ax + Bu + Dw(t), \\ y &= Cx, \end{aligned}$$

where $x \in \mathbb{R}^n$, $u \in \mathbb{R}^m$, $y \in \mathbb{R}^p$ and $w \in \mathbb{R}^q$ are the state vector, the control, the measured output of the system and the unknown input (or disturbance), respectively. In addition, and without loss of generality, let us assume that rank$C = p$, rank$B = m$, rank$D = q$ and that the triplet (A, D, C) is strongly observable, such that the state $x(t)$ may be recovered in finite-time using only the output and its derivatives (through the use of the HOSM differentiator). Under the additional assumption on the smoothness of the unknown input w, i.e. $|\dot{w}(t)| \leq L$, an extra derivative of the estimated state can be computed, thus obtaining an estimate for $\dot{x}$. Under these considerations, an estimate for the unknown input may be obtained as

$$\hat{w} = D^{+}\left[\dot{x} - Ax - Bu\right],$$

With this estimate of the unknown input, it is natural to try to compensate the effect of the unknown input in the system as much as possible. Direct compensation of the part of w that is matched to u is direct. To see this apply the state transformation $T = \begin{bmatrix} B^{\perp} \\ B^{+} \end{bmatrix}$ which allows to rewrite the system as

$$\begin{aligned} \dot{x}_1 &= A_{11}x_1 + A_{12}x_2 + D_1 w, \\ \dot{x}_2 &= A_{21}x_2 + A_{22}x_2 + D_2 w + u \end{aligned} \tag{1.50}$$

with $x_1 \in \mathbb{R}^{n-m}$, $x_2 \in \mathbb{R}^m$. If

$$D_1 \in \text{span}A_{12}, \tag{1.51}$$

then taking

$$u = -D_2\hat{w} + v,$$

the effect of matched disturbances can be reduced and theoretically (if all the derivatives are exact) completely removed without the direct application of a discontinuous control signal.

Another option is to consider the estimate of the disturbance into the sliding surface design as $s = x_2 + Kx_1 + G\hat{w}$, where matrices K and G are to be designed to provide for both stability and performance and the control is constructed as an unitary control

$$u = -\rho(x)\frac{s}{\|s\|}.$$

1.12.4 Conclusions

Three methods for finite time compensation of unmatched perturbations of inputs are suggested.

Open problems

1. Design a global compensation technique joining the Lyapunov backstepping techniques together with HOSM techniques.

2.Observer based compensation for the case when condition (1.51) is not satisfied.

1.13 VSS Methods for Hybrid Systems

A variety of sliding mode observers can be found in the literature of the last two decades. Firstly, the observation process was followed by means of classical sliding modes. Then, when second and higher order sliding modes were introduced, the observers were designed for a larger class of systems. This allows removing the relative degree restriction w.r.t. the unknown inputs required when using classical sliding modes. Furthermore, when using high order sliding mode observers (HOSMOs), the unknown inputs can be reconstructed in finite time. These characteristics make high order sliding mode observers an attractive option when the reconstruction of the state and/or unknown inputs is needed.

1.13.1 Hybrid Nonlinear Systems

The finite-time convergence and exact disturbance compensation of HOSMOs makes them ideal for implementation in hybrid systems. One of the main properties that makes HOSMO ideal for hybrid systems is that one can make the observer converge before a switching occurs, provided that a minimum dwell time exists. Since the class of hybrid systems is quite big, HOSMOs have been used in different forms.

- For nonlinear autonomous switching systems with jumps, an observer has been designed which allows the simultaneous reconstruction of the continuous state vector, the discrete state vector and even the unknown inputs [8].
- For Lagrangian systems an observer has been designed allowing the reconstruction of the state vector in finite time in [136], where the HOSMO was copied from [41].

1.13.2 Hybrid Linear Systems

There is still a few number of papers that can be found in the literature of sliding mode observers of hybrid linear systems. We can find the following works:

- A HOSMO is designed in [18] for switched linear systems where the mechanism that activates the switching event is completely unknown (discrete state is unknown). There, by means of a HOSMO, both the discrete and continuous state can be reconstructed in finite time.
- A HOSMO is designed for linear switched systems with unknown inputs in [22]. The discrete events are assumed to be known. This allows designing an observer that does not lose convergence at any switching instant.

1.13.3 Open Problems

The following are some of the still unsolved, but actual, problems of research in sliding mode observation of hybrid systems.

Global Observation. One of the drawbacks that still has not been solved is the global convergence w.r.t. the initial conditions. Due to the restrictions of high order sliding modes, one has to know a region where the state vector begins. That is why a design of global observers seems to be an interesting challenge. A possible solution is the use of the new uniform HOSMO proposed in [38], [37].

Zenon Phenomenon. The case when the Zenon phenomenon appears is another problem to be solved when HOSMO are designed; some efforts have been done in this sense by Prof. Barbot and his collaborators [155].

Parameter estimation The estimation of parameter uncertainties is yet another problem to be solved. This problem is still in the early stages of investigation, but already some efforts have been made and soon results might be shown.

We can continue talking about particular problems that can be tackled using HOSMO, but it is enough to say that all that has been done up until now using HOSMO may be investigated for the case of hybrid systems with all the possibilities this type of systems allows, i.e. switched systems, autonomous switching systems, systems with jumps, chaotic hybrid systems, etc. Therefore, we can say that SM observation is still in the beginning of its development and is thus a promissory topic of research.

1.14 Relay Control with Delay

Relay control systems occur in many industrial applications. They are simple in realization, cheap, very effective and sometimes have better dynamics than traditional linear systems [147]. The *relay* nature may be inherent in both sensors and controllers. For example, the HEGO-sensor in the air-to-fuel ratio control system of automobile engine is a relay measurer [36], while the control systems of electric drives have *on-off* "switches"as relay control inputs [149]. The preferable control strategy essentially depends on the device (sensor and/or controller) having the relay nature.

On the other hand, *time delays* that usually take place in feedback control systems can not be ignored, because they lead to "unmodelled" oscillations (such as "chattering" [149]) and/or system instability [104]. This phenomenon is typical of relay control systems [149], [64]. The presence of time delays, together with system uncertainties (such as external disturbances, errors in system parameters estimations, unknown and variable time delay), makes the problem of the control design and the stability analysis of relay control systems essentially complex.

1.14.1 Oscillatory Nature of Relay Delayed Systems

The equation

$$\dot{x}(t) = -\text{sign}\,(x(t-1)) \tag{1.52}$$

has a 4-periodic solutions

$$g_0(t) = \begin{cases} t \text{ for } -1 \le t \le 1, \\ 2-t \text{ for } 1 \le t \le 3. \end{cases}$$

$$g_0(t+4k) = g_0(t)\ , \quad k \in \mathbf{Z}.$$

Since

$$\dot{g}_0(t) = -\text{sign}[g_0(t-1-4n)]$$

and transforming t to $(4n+1)t$ we obtain

$$\frac{1}{4n+1}[g_0((4n+1)t)]' = -\text{sign}\,\frac{1}{4n+1}g_0((4n+1)(t-1)).$$

This means that there exists a countable set of periodic solutions, *steady modes*, or more concisely, a SM. Namely, it is easy to verify that the $4/(4n+1)$-periodic function

$$g_n(t) = \frac{1}{4n+1}g_0((4n+1)t)\ , \quad t \in \mathbf{R}$$

is a solution of (1.52) for each integer $n \ge 1$. It is necessary to remark that the initial function φ_n, which generates the corresponding steady mode g_n, has $2n$ zeros on the time interv al $(-1,0)$.

In [64] it was shown that each solution $x(t) \not\equiv 0$ of (1.52), after a finite time, coincides with one of the $g_n(t+\alpha)$ for some $n \ge 0$, $\alpha \in \mathbf{R}$. Consequently, in the simplest scalar relay delayed control system, only oscillatory solutions can occur. Moreover, a solution $g_n(t)$ is stable for $n = 0$, and unstable for $n \ge 1$.

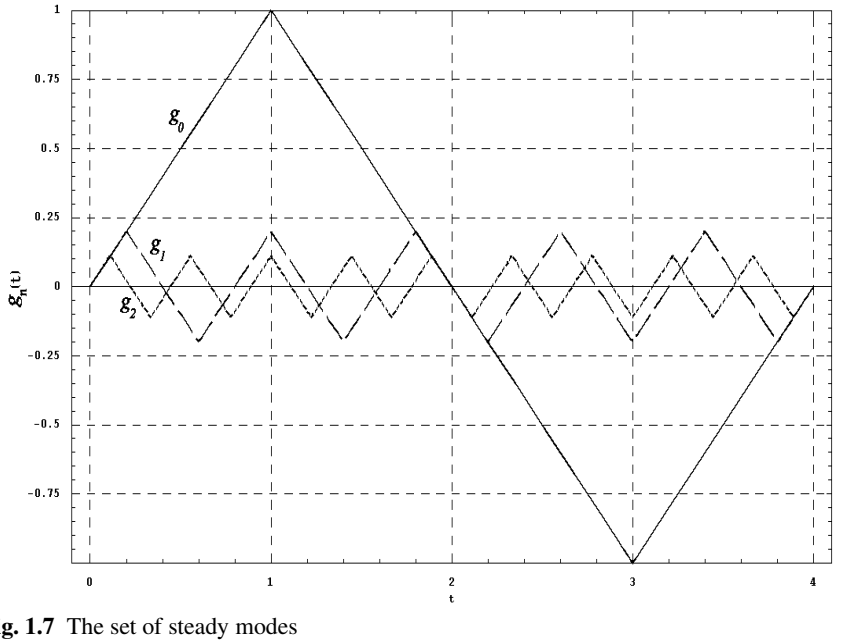

Fig. 1.7 The set of steady modes

1.14.2 Methods of the Relay Delayed Control Design

Time delay compensation (or prediction) and the control of system oscillations are two modern approaches to the problem of control design for time delay systems.

1.14.3 Prediction Method

Pade approximation of delay that reduces the relay delay output tracking problem to the sliding mode control for nonminimum phase system was suggested in [140]. In [133], [102], [99] some implementations of a prediction method for sliding mode control design can be found.

Consider the time delayed control system of the form

$$\dot{x}(t) = Ax(t) + Bu(t-h) + Df(t) \tag{1.53}$$

where $x \in \mathbb{R}^n$ is the vector of the system state, $A \in \mathbb{R}^{n\times n}$ is the system matrix, $u \in \mathbb{R}^m$ is the vector of control inputs, $B \in R^{n\times m}$ is the matrix of the control gains, and $h > 0$ is a time delay *input* assumed to be known.

The typical prediction equation [99,102] for system (1.53) has the form

$$y(t) = e^{Ah}x(t) + \int_{-h}^{0} e^{-\theta A}Bu(t+\theta)d\theta \tag{1.54}$$

Obviously, the calculation of *the prediction variable* $y(t)$ requires information about the control forces $u(t)$ generated during the time interval $[t-h,t)$. We assume that such information can be stored and used for the control purpose.

In this case the predictor variable $y(t)$ satisfies the following equation

$$\dot{y}(t) = Ay(t) + Bu(t) + e^{Ah}Df(t) \tag{1.55}$$

According to the predictor method [108, 133, 102], in order to stabilize the original system (1.53) we need to design the stabilizing controller for the prediction system (1.55). Unfortunately, in the disturbed case ($f \neq 0$) the property $y(t) \to 0$ does not imply $x(t) \to 0$, even when the matching condition $range\,(D) \subseteq range(B)$ holds. The integral term in formula (1.54) is non-zero in the general case (see, for example, [62]). Particularly, for the sliding mode controller application we have $u(t) = u_{eq}(t) \neq 0$, where $u_{eq}(t)$ is an equivalent control. Moreover, the property $y(t) \to 0$ can be guaranteed by implementing the sliding mode control algorithm in the predictor system (1.55) only in the case when $range\,(e^{Ah}D) \subseteq range(B)$.

Therefore, the proposed technique *does not allow* to realize a sliding mode in the system state space [142]; it may ensure the sliding motion *only* in the predictor space [62] and leaves the system state oscillations produced by uncertainties without consideration.

1.14.4 Methods of Oscillation Control

PI control algorithms for amplitude control of one dimensional relay systems with delay in the input was suggested in [2]. Methods for relay control of system oscillations can be found in [70], [71], [141], [129].

Consider the control system with time delay of the form

$$\dot{x}(t) = Ax(t) + Bu(x(t-h(t))) + f(t,x(t)) \tag{1.56}$$

where $x \in \mathrm{R}^n$ is a state space vector, the system matrix $A \in \mathrm{R}^{n\times n}$ is allowed to be *unstable*, $B \in \mathrm{R}^{n\times m}$ is a control gain matrix, $u \in \mathrm{R}^n$ is a vector of control inputs, $h(t)$ is a time delay and the unknown function $f(t,x(t))$ describes system uncertainties.

We suggest that the full state space vector be available for measurement with an *unknown but bounded time delay* $h(t)$

$$0 \le h(t) \le h_0 \tag{1.57}$$

where h_0 is known. The function $h(t)$ is supposed to be piece-wise continuous. System (1.56) is considered under initial conditions of the form

$$x(t) = \varphi(t), \text{ for } t \in [-h_0, 0]$$

where $\varphi(t)$ is an arbitrary function of time.

The control $u(\cdot)$ in system (1.56) is a *relay*

$$u(\cdot) = (-p_1 \mathrm{sign}[S_1(\cdot)], ..., -p_m \mathrm{sign}[S_m(\cdot)])^T \tag{1.58}$$

where the positive parameters $p_i > 0, (i = 1,2,...,m)$ and the *linear* mappings $S_i : \mathrm{R}^n \to \mathrm{R}, (i = 1,2,...,m)$ should be designed.

All existing control algorithms for uncertain relay delayed systems do not guarantee system stability in the traditional sense [102], [70], [71]. They only provide *practical* stability, such as convergence to a certain zone. Therefore, below we introduce two special definitions of practical stability for relay delayed control systems.

Definition 1.6. System (1.56) is called ε - stabilizable, if for some fixed $\varepsilon > 0$ there exists a control $u(\cdot)$ of the form (1.58) and a $\delta > 0$, such that any solution $x_\varphi(t)$ of system (1.56) with the initial function $\varphi(t) : \|\varphi(0)\| < \delta$ is bounded

$$\left\|x_\varphi(t)\right\| < \varepsilon \text{ for } \forall t \ge 0$$

In other words, system (1.56) is ε - stable, if the designed control holds any system solution inside the given ε - neighborhood of the origin. Such system motion is typical for relay time delayed systems [64] and completely differs from Lyapunov stability since the control $u(\cdot)$ and $\delta > 0$ may not exist for all $\varepsilon > 0$.

Definition 1.7. System (1.56) is called $R\varepsilon$ - stabilizable if, for some fixed $\varepsilon > 0$ and fixed $R > \varepsilon$, there exist a control $u(\cdot)$ of the form (1.58) and a time instant $T > 0$

such that any solution $x_\varphi(t)$ of system (1.56) with the initial function $\varphi(t) : \|\varphi(0)\| < R$ *converges to zone* ε *in a finite time* T

$$\left\|x_\varphi(t)\right\| < \varepsilon \text{ for } \forall t \geq T$$

This stability form is similar to that of semiglobal *stability* with only one difference: asymptotic convergence to origin replaced by finite time convergence to a zone. Therefore, it can be also called *practical semiglobal stability* [71].

In [64] the necessary condition

$$\lambda h_0 < \ln(2) \tag{1.59}$$

was given for the existence of *nontrivial bounded solutions* for a *scalar* system

$$\dot{x} = \lambda x - p\,\text{sign}[x(t-h_0)], \lambda, p, h_0 > 0 \tag{1.60}$$

Condition (1.59) is a necessary and sufficient condition for the ε- stabilization of system (1.60). The condition (1.59) analyzed was discovered by I. Boiko using frequency methods [25].

Papers [70], [129] extend this result to the case of vector control systems.

The methods of $R\varepsilon$ - stabilization are also presented in [71,141]. They are based on control gain adaptation and need a multi-step property of the control inputs (i.e. each relay control input may have some finite or discrete set of values). These methods typically require a stronger stabilization condition, such as $\lambda h_0 \leq \frac{1}{2}\ln(2)$.

1.14.5 Open Problems

1. Generalize conditions of stabilization and gain adaptation algorithms for the nonlinear case.
2. Extension of the Lyapunov methods for relay delay systems allowing to generalize the gain adaptation methods.

1.15 Distributed Parameter Systems

Many important plants, such as time-delay systems, flexible manipulators and structures as well as heat transfer processes, combustion, and fluid mechanical systems, are governed by functional and partial differential equations or, more generally, equations in a Hilbert space. As these systems are often described by models with a significant degree of uncertainties, it is of interest to develop consistent stabilization methods that are capable of utilizing time-delay and distributed parameter models and providing the desired system performance in spite of the model uncertainties. The presence of an unbounded operator in the state equation precludes from a simple extension of finite-dimensional control algorithms.

Theoretical results obtained in an abstract infinite - dimensional setting [87, 88, 120, 118, 126, 165] were further supported by applications to distributed parameter and time delay systems.

A stabilizing discontinuous control law, developed for infinite dimensional systems [118, 125, 126, 121], was obtained from the Lyapunov min-max approach, the origins of which may be found in [72, 73]. It was synthesized to guarantee that the time derivative of a Lyapunov functional, selected for a nominal system, remain negative definite on the trajectories of the system with perturbations caused by uncertainties of a plant operator and environment conditions. The approach gave rise to a so-called *unit feedback signal*, whose norm is equal to one everywhere with the exception of the sliding surface where it undergoes discontinuities.

In [121] the unit feedback synthesis was developed for a class of linear infinite-dimensional systems with a finite-dimensional unstable part using finite-dimensional sensing and actuation. An output feedback controller is synthesized by coupling an infinite-dimensional Luenberger state observer and a unit state feedback controller. In order to obtain the fully practical finite-dimensional framework for controller synthesis a finite-dimensional approximation of the Luenberger observer, as well as a continuous approximation of the unit feedback controller, is carried out at the implementation stage.

Implementation, performance and robustness issues of the unit output feedback control design are illustrated in a simulation study of the linearization of the Kuramoto–Sivashinsky equation (KSE) around the spatially-uniform steady-state solution with periodic boundary conditions. While unforced, the KSE describes incipient instabilities in a variety of physical and chemical systems and a control problem that arises here is to avoid the appearance of instabilities in the closed-loop system.

In [120], the unit control approach was extended to Hilbert space-valued minimum phase semilinear systems. The control algorithms presented ensured asymptotic stability, global or local accordingly, as state feedback or output feedback is available. The desired robustness properties of the closed-loop system against external disturbances with an *a priori* known norm bounds made the algorithms extremely suited for stabilization of the underlying system operating under uncertainty conditions. It was particularly shown that discontinuous feedback stabilization was constructively available in the case where complex nonlinear dynamics of the uncertain system did not admit factoring out a destabilizing nonlinear gain and thus the destabilizing gain could not be handled through nonlinear damping.

The theory was applied to the stabilization of chemical processes around prespecified steady-state temperature and concentration profiles corresponding to a desired coolant temperature. Performance issues of the unit feedback design were illustrated in a simulation study of the plug flow reactor.

In the recent publications [122, 123, 124], the second order sliding mode control (twisting and supertwisting) algorithms were generalized towards the infinite-dimensional setting and applied for controlling heat and wave processes, operating under uncertainty conditions.

Acknowledgements. I really appreciate the help of my students and ex-students M.T. Angulo, A. Estrada, Dr. F.J. Bejarano, Dr. F. Castaños and Dr. A. Polyakov, and Professors L.Hsu, Z. Man, J. Moreno, Y. Orlov , Y.Shtessel and E. Usai and Dr. I. Boiko in the preparation of this paper.

This chapter was supported by FONCICyT, grant 93302.

References

1. Ahmed-Ali, T., Lamnabhi-Lagarrigue, F.: Sliding observer-controller design for uncertain triangular nonlinear systems. IEEE Transaction on Automatic Control 44(6), 1244–1249 (1999)
2. Akian, M., Bliman, P., Sorine, M.: Control of delay systems with relay. IMA Journal on Mathematical Control and Information 19, 133–155 (2002)
3. Levant, A.: Chattering analysis. IEEE Trans. Autom. Control 55(6), 1380–1389 (2010)
4. Angulo, M., Levant, A.: On robust output based finite-time control of LTI systems using HOSMs. International Journal of Systems Science (2011), doi: http://dx.doi.org/10.1080/00207721.2011.564676
5. Angulo, M.T., Fridman, L.: Output-based finite time control of LTI systems with matched perturbations using HOSM. In: Proceedings of the 48th IEEE Conference on Decision and Control 2009, pp. 6095–6100 (2009)
6. Angulo, M.T., Fridman, L., Moog, C., Moreno, J.: Output feedback design for exact state stability of flat nonlinear systems. In: Proceedings of 11th Workshop on Varibale Structure Systems (VSS 2010), pp. 32–38 (2010)
7. Atherton, D.P.: Nonlinear Control Engineering - Describing Function Analysis and Design. Van Nostrand Company Limited, Workingham (1975)
8. Barbot, J., Saadaoui, H., Djema, M., Manamanni, N.: Nonlinear observer for autonomous switching systems with jumps. Nonlinear Analysis: Hybrid Systems 1(4), 537–547 (2007)
9. Barbot, J.P., Boutat, D., Floquet, T.: An observation algorithm for nonlinear systems with unknown inputs. Automatica 45, 1970–1974 (2009)
10. Bartolini, G., Ferrara, A., Pisano, A., Usai, E.: Adaptive reduction of the control effort in chattering free sliding mode control of uncertain nonlinear systems. Journal of Applied Mathematics and Computer Science 8(1), 51–71 (1998)
11. Bartolini, G., Ferrara, A., Punta, E.: Multi-input second-order sliding-mode hybrid control of constrained manipulators. Dyn. Control 10(3), 277–296 (2000)
12. Bartolini, G., Ferrara, A., Usai, E.: Output tracking control of uncertain nonlinear second-order systems. Automatica 33(12), 2203–2212 (1997)
13. Bartolini, G., Ferrara, A., Usai, E., Utkin, V.: On multi-input chattering-free second order sliding mode control. IEEE Transactions on Automatic Control 45(9), 1711–1717 (2000)
14. Bartolini, G., Levant, A., Pisano, A., Usai, E.: 2-sliding mode with adaptation. In: Proceedings of the Seventh IEEE Mediterranean Conference on Control and Systems (1999)
15. Bartolini, G., Pillosu, S., Pisano, A., Usai, E.: Time-optimal stabilization for a third-order integrator: a robust state-feedback implementation. In: Colunius, F., Grne, L. (eds.) Bifurcation and Control. LNCIS, vol. 273, pp. 83–108. Springer, Heidelberg (2002)

16. Bartolini, G., Pisano, A., Punta, E., Usai, E.: A survey of applications of second-order sliding mode control to mechanical systems. International Journal of Control 45(9/10), 875–892 (2003)
17. Bejarano, F., Fridman, L.: High order sliding mode observer for linear systems with unbounded unknown inputs. International Journal of Control 83(9), 1920–1929 (2010)
18. Bejarano, F., Fridman, L.: State exact reconstruction for switched linear systems via a super-twisting algorithm. International Journal of Systems Science 42(5), 717–724 (2011)
19. Bejarano, F., Fridman, L., Poznyak, A.: Exact state estimation for linear systems with unknown inputs based on hierarchical super-twisting algorithm. International Journal of Robust and Nonlinear Control 17(18), 1734–1753 (2007)
20. Bejarano, F., Fridman, L., Poznyak, A.: Hierarchical second-order sliding-mode observer for linear time invariant systems with unknown inputs. International Journal of Systems Science 38(10), 793–802 (2007)
21. Bejarano, F., Fridman, L., Poznyak, A.: Unknown input and state estimation for unobservable systems. SIAM Journal on Control and Optimization 48(2), 1155–1178 (2009)
22. Bejarano, F., Pisano, A., Usai, E.: Finite-time converging jump observer for linear switched systems with unknown inputs. Nonlinear Analysis: Hybrid Systems 5(2), 174–188 (2011)
23. Bhat, S., Bernstein, D.: Finite-time stability of continuous autonomous systems. SIAM Journal on Control and Optimization 38(3), 751–766 (2000)
24. Boiko, I.: Discontinuous Control Systems. Birkhäuser, Boston (2009)
25. Boiko, I.: Oscillations and transfer properties of relay feedback systems with time-delay linear plants. Automatica 45(12), 1127–1135 (2009)
26. Boiko, I., Fridman, L.: Analysis of chattering in continuous sliding-mode controllers. IEEE Transactions on Automatic Control 50(9), 1442–1446 (2005)
27. Boiko, I., Fridman, L., Castellanos, M.I.: Analysis of second order sliding mode algorithms in the frequency domain. IEEE Transactions on Automatic Control 49(6), 946–950 (2004)
28. Boiko, I., Fridman, L., Pisano, A., Usai, E.: Analysis of chattering in systems with second order sliding modes. IEEE Trans. Autom. Control 52(11), 2085–2102 (2007)
29. Boiko, I., Fridman, L., Pisano, A., Usai, E.: Performance analysis of second-order sliding-mode control systems with fast actuators. IEEE Trans. Autom. Control 52(6), 1053–1059 (2007)
30. Boiko, I., Fridman, L., Pisano, A., Usai, E.: On the transfer properties of the generalized sub-optimal second-order sliding mode control algorithm. IEEE Transactions on Automatic Control 54(2), 399–403 (2009)
31. Bondarev, A.G., Bondarev, S.A., Kostylyeva, N.Y., Utkin, V.I.: Sliding modes in systems with asymptotic state observers. Automatica i Telemechanica (Automation and Remote Control) 46(5), 679–684 (1985)
32. Bregeault, V., Plestan, F., Shtessel, Y., Poznyak, A.: Adaptive sliding mode control for an electropneumatic actuator. In: Proceedings of VSS, pp. 260–265 (2010)
33. Cannas, B., Cincotti, S., Usai, E.: An algebraic observability approach to chaos synchronisation by sliding differentiators. IEEE Transactions on Circuits and Systems I: Fundamental Theory and Applications 49(7), 1000–1006 (2002)
34. Cao, W.J., Xu, J.X.: Nonlinear integral-type sliding surface for both matched and unmatched uncertain systems. IEEE Trans. Automatic Control 49(8), 1355–1360 (2004)
35. Castaños, F., Fridman, L.: Analysis and design of integral sliding manifolds for systems with unmatched perturbations. IEEE Trans. Automatic Control 51(5), 853–858 (2006)

36. Choi, S.B., Hedrick, J.K.: Robust throttle control of automotive engines. ASME Journal of Dynamic Systems, Measurement, and Control 18, 92–98 (1996)
37. Cruz, E., Moreno, J., Fridman, L.: Uniform robust exact differentiator. In: Proceedings of 2010 49th IEEE Conference on Decision and Control, pp. 102–107 (2010)
38. Cruz, E., Moreno, J., Fridman, L.: Uniform second-order sliding mode observer for mechanical systems. In: Proceedings of 11th IEEE Workshop in Variable Structure Sytems, pp. 14–19 (2010)
39. Davila, A., Moreno, J., Fridman, L.: Optimal Lyapunov function selection for reaching time estimation of super twisting algorithm. In: Proc. 48th Conference on Decision and Control, pp. 8405–8410 (2009)
40. Davila, A., Moreno, J., Fridman, L.: Optimal Lyapunov function selection for reaching time estimation of super twisting algorithm. In: Proc. American Control Conference (ACC2010), pp. 968–973 (2010)
41. Davila, J., Fridman, L., Levant, A.: Second order sliding mode observer for mechanical systems. IEEE Transactions on Automatic Control 50(11), 1785–1789 (2005)
42. Davila, J., Fridman, L., Pisano, A., Usai, E.: Finite-time state observation for nonlinear uncertain systems via higher-order sliding modes. International Journal of Control 82(8), 1564–1574 (2009)
43. Davila, J., Fridman, L., Poznyak, A.: Observation and identification of mechanical systems via second order sliding modes. International Journal of Control 79(10), 1251–1262 (2006)
44. Defoort, M., Floquet, T., Kokosy, A., Perruquetti, W.: A novel higher order sliding mode control scheme. Syst. Control Lett. 58(2), 102–108 (2009)
45. Defoort, M., Perruquetti, T.F.W.: Decentralized tracking for a class of interconnected nonlinear systems using variable structure control. Informatics in Control, Automation and Robotics 13, 277–288 (2006)
46. Drakunov, S.V., Izosimov, D.B., Loukyanov, A.G., Utkin, V.A., Utkin, V.I.: Block control principle. Automation and Remote Control 51(5), 601–609 (1990)
47. Drakunov, S.V., Utkin, V.I.: Sliding mode control in dynamic systems. International Journal of Control 55(7), 1029–1037 (1992)
48. Drazenovic, B.: The invariance conditions in variable structure systems. Automatica 5(3), 287–295 (1969)
49. Edwards, C., Floquet, T., Spurgeon, S.: Circumventing the relative degree condition in sliding mode design. In: Modern Sliding Mode Control Theory New Perspectives and Applications. LNCIS, vol. 375, pp. 137–158 (2008)
50. Edwards, C., Spurgeon, S., Hebden, R.: On development and applications of sliding mode observers. In: Xu, J., Xu, Y. (eds.) Variable Structure Systems:Towards XXIst Century. LNCIS, pp. 253–282. Springer, Berlin (2002)
51. Emel'yanov, S.V., Korovin, S.K., Levantovsky, L.V.: Second order sliding modes in controlling uncertain processes. Soviet Journal of Computer and System Science 24(4), 63–68 (1986)
52. Estrada, A., Fridman, L.: Exact compensation of unmatched perturbations via HOSM. In: Proceedings of the 47th IEEE Conference on Decision and Control, pp. 278–282 (2008)
53. Fei, J., Batur, C.: Adaptive sliding mode control with sliding mode observer for a micro-electro-mechanical vibratory gyroscope. Proceedings of the Institution of Mechanical Engineers, Part I: Journal of Systems and Control Engineering 222(8), 839–847 (2008)
54. Feng, Y., Yu, X., Man, Z.: Control of nonlinear systems using terminal sliding modes. In: Proc. Conference on Decision and Control (CDC 2001), Orlando, pp. 4021–4026 (2001)

55. Feng, Y., Yu, X., Man, Z.: Non-singular terminal sliding mode control of rigid manipulators. Automatica 38, 2159–2167 (2002)
56. Ferreira, A., Bejarano, F.J., Fridman, L.: Robust control with exact uncertainties compensation: With or without chattering? IEEE Transactions of Control Systems Technology (2011), doi: http://dx.doi.org/10.1109/TCST.2010.2064168
57. Filippov, A.: Differential equations with discontinuous right-hand side. Kluwer, Dordrecht (1988)
58. Floquet, T., Barbot, J.: A canonical form for the design of unknown input sliding mode observers. In: Edwards, C., Fossas, E., Fridman, L. (eds.) Advances in Variable Structure and Sliding Mode Control. LNCIS, vol. 334, pp. 271–292. Springer, Heidelberg (2006)
59. Floquet, T., Edwards, C., Spurgeon, S.: On sliding mode observers for systems with unknown inputs. Int. J. Adapt. Control Signal Process. 21(8-9), 638–656 (2007)
60. Fridman, L.: An averaging approach to chattering. IEEE Trans. Autom. Control 46(8), 1260–1265 (2001)
61. Fridman, L.: Singularly perturbed analysis of chattering in relay control systems. IEEE Transactions on Automatic Control 47(12), 2079–2084 (2002)
62. Fridman, L., Acosta, P., Polyakov, A.: Robust eigenvalue assignment for uncertain delay control systems. In: Proceedings of 3rd IFAC Workshop on Time Delay Systems, pp. 239–244 (2001)
63. Fridman, L., Davila, J., Levant, A.: High-order sliding-mode observation for linear systems with unknown inputs. Nonlinear Analysis: Hybrid Systems (2011), doi: http://dx.doi.org/10.1016/j.nahs.2010.09.003
64. Fridman, L., Fridman, E., Shustin, E.: Steady modes and sliding modes in relay control systems with delay. In: Barbot, J., Perruquetti, W. (eds.) Sliding Mode Control In Engineering, pp. 263–294. Marcel Dekker, New York (2002)
65. Fridman, L., Levant, A.: Higher order sliding modes as the natural phenomena of control theory. In: Proceedings of the Workshop on Variable Structure and Lyapunov Technique, pp. 302–309 (1994)
66. Fridman, L., Levant, A.: Higher order sliding modes as the natural phenomena of control theory. In: Garofalo, F., Glielmo, G. (eds.) Robust Control Variable Structure and Lyapunov Techniques. LNCIS, vol. 217, pp. 107–133. Springer, Heidelberg (1996)
67. Fridman, L., Levant, A., Davila, J.: Observation and identification via high-order sliding modes. In: Bartolini, G., Fridman, L., Pisano, A., Usai, E. (eds.) Modern Sliding Mode Control Theory New Perspectives and Applications. LNCIS, vol. 375, pp. 293–320
68. Fridman, L., Levant, A., Davila, J.: Observation of linear systems with unknown inputs via high-order sliding-mode. International Journal of Systems Science 38(10), 773–791 (2007)
69. Fridman, L., Shtessel, Y., Edwards, C., Yan, X.G.: Higher-order sliding-mode observer for state estimation and input reconstruction in nonlinear systems. International Journal of Robust and Nonlinear Control 18(4-5), 399–412 (2008)
70. Fridman, L., Strygin, V., Polyakov, A.: Stabilization of amplitude of oscillations via relay delay control. Int. J. Control 76(8), 770–780 (2003)
71. Fridman, L., Strygin, V., Polyakov, A.: Stabilization via delayed relay control rejecting uncertainty in a time delay. Int. J. Robust Nonlinear Control 14(1), 15–37 (2004)
72. Gutman, S.: Uncertain dynamic systems - a Lyapunov min-max approach. IEEE Trans. Autom. Control 24(3), 437–449 (1979)
73. Gutman, S., Leitmann, G.: Stabilizing feedback control for dynamic systems with bounded uncertainties. In: Proceedings of the 15th Conference on Decision and Control, pp. 94–99 (1976)

74. Hall, C., Shtessel, Y.: Sliding mode disturbance observer-based control for a reusable launch vehicle. AIAA J. Guidance, Control and Dynamics 29(6), 1315–1328 (2006)
75. Hashimoto, H., Utkin, V., Xu, J., Suzuki, H., Harashima, F.: VSS observer for linear time varying system. In: Procedings of IECON 1990, pp. 34–39. Pacific Grove, CA (1990)
76. Hautus, M.: Strong detectability and observers. Linear Algebra and its Applications 50, 353–468 (1983)
77. Hsu, L., Lizarralde, F., Araújo, A.D.: New results on output-feedback variable structure model-reference adaptive control: design and stability analysis. IEEE Trans. Autom. Control 42(3), 386–393 (1997)
78. Hsu, L., Peixoto, A.J., Cunha, J.P.S., Costa, R.R., Lizarralde, F.: Output feedback sliding mode control for a class of uncertain multivariable systems with unmatched nonlinear disturbances. In: Variable Structure Systems, Sliding Mode and Nonlinear Control, Advances in Variable Structure and Sliding Mode Control, pp. 195–225. Springer, Berlin (2006)
79. Huang, Y.J., Kuo, T.C., Chang, S.H.: Adaptive sliding-mode control for nonlinear systems with uncertain parameters. IEEE Trans. Syst. Man, and Cybernetics-Part B: Cybernetics 38(2), 534–539 (2008)
80. Boiko, I., Castellanos, M., Fridman, L.: Describing function analysis of second-order sliding mode observers. Intern. Journ. of Systems Science 38(10), 817–824 (2007)
81. Boiko, I., Castellanos, M., Fridman, L.: Analysis of response of second-order sliding mode controllers to external inputs in frequency domain. International Journal on Robust and Nonlinear Control 38(4-5), 502–514 (2008)
82. Khoo, S., Trinh, H., Man, Z., Shen, W.: Fast finite-time consensus of a class of high-order uncertain nonlinear systems. In: Proc. 5th IEEE Conference on Industrial Electronics and Applications (ICIEA 2010), pp. 2076–2081 (2010)
83. Khoo, S., Xie, L., Man, Z.: Robust finite-time consensus tracking algorithm for multi-robot systems. IEEE/ASME Transactions on Mechatronics 14(2), 219–228 (2009)
84. Kolmogorov, A.N.: On inequalities between upper bounds of consecutive derivatives of an arbitrary function defined on an infinite interval. Amer. Math. Soc. Transl. 2(9), 233–242 (1962)
85. Laghrouche, S., Plestan, F., Glumineau, A.: Higher order sliding mode control based on integral sliding mode. Automatica 43(3), 531–537 (2007)
86. Lee, H., Utkin, V.: Chattering suppression methods in sliding mode control systems. Annual Reviews in Control 31, 179–188 (2007)
87. Levaggi, L.: Infinite dimensional systems sliding motions. European Journal of Control 8, 508–518 (2002)
88. Levaggi, L.: Infinite dimensional systems sliding motions. Differential Integral Equations 15, 167–189 (2002)
89. Levant, A.: Sliding order and sliding accuracy in sliding mode control. International Journal of Control 58(6), 1247–1263 (1993)
90. Levant, A.: Robust exact differentiation via sliding mode technique. Automatica 34(3), 379–384 (1998)
91. Levant, A.: Universal SISO sliding-mode controllers with finite-time convergence. IEEE Transactions on Automatic Control 46(9), 1447–1451 (2001)
92. Levant, A.: High-order sliding modes: differentiation and output feedback control. International Journal of Control 76(9-10), 924–941 (2003)
93. Levant, A.: Homogeneity approach to high-order sliding mode design. Automatica 41(5), 823–830 (2005)

94. Levant, A.: Quasi-continuous high-order sliding-mode controllers. IEEE Trans. Autom. Control 50(11), 1812–1816 (2005)
95. Levant, A.: Homogeneous quasi-continuous sliding-mode control. In: Advances in Variable Structure and Sliding Mode Control. LNCIS, vol. 334, pp. 143–168 (2006)
96. Levant, A.: Principles of 2-sliding mode design. Automatica 43(4), 576–586 (2007)
97. Levant, A., Fridman, L.: Accuracy of homogeneous sliding modes in the presence of fast actuators. IEEE Transactions on Automatic Control 55(3), 810–814 (2010)
98. Levant, A., Michael, A.: Adjustment of high-order sliding-mode controllers. International Journal of Robust and Nonlinear Control 19(15), 1657–1672 (2009)
99. Li, X., Yurkovitch, S.: Sliding mode control of systems with delayed states and controls. In: Young, K.D., Ozguner, U. (eds.) Variable Structure Systems, Sliding Mode and Nonlinear Control. LNCIS, pp. 93–108. Springer, London (1999)
100. Lin, W.S., Chen, C.S.: Robust adaptive sliding mode control using fuzzy modeling for a class of uncertain MIMO nonlinear systems. IEE Proceedings of Control Theory Applications 149, 193–201 (2002)
101. Loukianov, A., Fridman, L., Canedo, J., Sanchez, E., Soto-Cota, A.: Higher order sm block-control of nonlinear systems with unmodeled actuators: Application to electric power systems and electrohydraulic servo-drives. In: Bartolini, G., Fridman, L., Pisano, A., Usai, E. (eds.) Modern Sliding Mode Control Theory New Perspectives and Applications. LNCIS, pp. 401–426. Springer, London (2008)
102. Loukianov, A.G., Espinosa-Guerra, O., Castillo-Toledo, B., Utkin, V.A.: Integral sliding mode control for systems with time delay. In: Proceedings of 9th IEEE Workshop on Variable Structure Systems, pp. 256–261 (2006)
103. Luenberguer, D.G.: Canonical forms for linear multivariable systems. IEEE Transactions on Automatic Control 12(3), 290–293 (1967)
104. Malek-Zaverei, M., Jamshidi, M.: Time-Delay Systems Analysis Optimization and Applications. Elsevier Science Ltd, New York (1987)
105. Man, Z., Paplinski, A.P., Wu, H.R.: A robust MIMO terminal sliding mode control scheme for rigid robotic manipulators. IEEE Trans. Automatic Control 39, 2464–2469 (1994)
106. Man, Z., Yu, X.: Adaptive terminal sliding mode tracking control for rigid robotic manipulators with uncertain dynamics. JSME Int. J. of Mechanical Systems, Machine Elements and Manufacturing 40(3), 493–502 (1997)
107. Man, Z., Yu, X., O'Day, M.: A robust adaptive terminal sliding mode control for rigid robotic manipulators. J. of Intelligent and Robotic Systems 24(3), 23–41 (1999)
108. Manitius, A., Olbrot, A.: Finite spectrum assignment problem for systems with delay. IEEE Trans. on Automatic Control 24(4), 541–553 (1979)
109. Matthews, G.P., DeCarlo, R.A.: Decentralized tracking for a class of interconnected nonlinear systems using variable structure control. Automatica 24, 187–193 (1988)
110. Mirkin, B., Gutman, P.O., Shtessel, Y.: Adaptive continuous control with sliding mode for plants under nonlinear perturbations, external disturbances and actuator failures. In: Proceedings of VSS, pp. 250–255 (2010)
111. Moreno, J.: A linear framework for the robust stability analysis of a generalized supertwisting algorithm. In: Proc. 6th Int. Conf. Elect. Eng., Comp. Sci. and Aut. Cont. (CCE 2009), Mexico, pp. 12–17 (2009)
112. Newman, W.: Robust sub-optimal control. IEEE Transactions on Automatic Control 35(7), 841–844 (1990)
113. Nunes, E.V.L., Hsu, L., Lizarralde, F.: Global exact tracking for uncertain systems using output-feedback sliding mode control. IEEE Trans. Autom. Control 54(5), 1141–1147 (2009)

114. Oliveira, T., Peixoto, A., Nunes, E., Hsu, L.: Control of uncertain nonlinear systems with arbitrary relative degree and unknown control direction using sliding modes. Int. J. Adaptive Control Signal Process. 21(8/9), 692–707 (2007)
115. Oliveira, T.R., Hsu, L.: Dwell-time and monitoring schemes for peaking avoidance in high-gain observer based output-feedback control. In: Proc. of 48th IEEE Conf. on Decision and Control (CDC 2009), Shanghai, pp. 7557–7562 (2009)
116. Oliveira, T.R., Peixoto, A.J., Costa, R.R., Hsu, L.: New results on output-feedback variable structure model-reference adaptive control: design and stability analysis. Dynamics of Continuous, Discrete and Impulsive Systems. Series B: Applications and Algorithms 17(6), 839–874 (2010)
117. Oliveira, T.R., Peixoto, A.J., Hsu, L.: Sliding mode control of uncertain multivariable nonlinear systems with unknown control direction via switching and monitoring function. IEEE Trans. Autom. Control 55(4), 1028–1034 (2010)
118. Orlov, Y.: Discontinuous unit feedback control of uncertain infinite-dimensional systems. IEEE Transactions on Automatic Control 45(5), 834–843 (2000)
119. Orlov, Y.: Discontinuous Systems: Lyapunov Analysis and Robust Synthesis under Uncertainty Conditions. Springer, London (2008)
120. Orlov, Y., Dochain, D.: Discontinuous feedback stabilization of minimum-phase semilinear infinite-dimensional systems with application to chemical tubular reactor. IEEE Trans. Autom. Control 47(8), 1293–1304 (2002)
121. Orlov, Y., Lou, Y., Christofides, P.: Sliding mode control synthesis of uncertain time-delay systems. Int. J. Contr. 77, 1115–1136 (2004)
122. Orlov, Y., Pisano, A., Usai, E.: Continuous state-feedback tracking of an uncertain heat diffusion process. Systems and Control Letters 59(12), 754–759 (2010)
123. Orlov, Y., Pisano, A., Usai, E.: Exponential stabilization of the uncertain wave equation via distributed dynamic input extension. IEEE Transactions on Automatic Control 56(1), 212–217 (2011)
124. Orlov, Y., Pisano, A., Usai, E.: Tracking control of the uncertain heat and wave equation via power-fractional and sliding-mode techniques. SIAM Journal on Control and Optimization 49(2), 363–382 (2011)
125. Orlov, Y., Utkin, V.: Sliding mode control in infinite-dimensional systems. Automatica 23, 1127–1135 (1987)
126. Orlov, Y., Utkin, V.: Unit sliding mode control in infinite-dimensional systems. Applied Math. and Computer Science 8, 7–20 (1987)
127. Paulo, J., Cunha, V.S., Hsu, L., Costa, R., Lizarralde, F.: Output-feedback model-reference sliding mode control of uncertain multivariable system. IEEE Transactions on Automatic Control 48(12), 2245–2250 (2003)
128. Peixoto, A.J., Oliveira, T.R., Hsu, L.: Global tracking output-feedback sliding mode control design via norm estimators and variable high gain observer. In: Proc. of 48th IEEE Conf. on Decision and Control (CDC 2009), Shanghai, pp. 6083–6088 (2009)
129. Polyakov, A.: Robust eigenvalue assignment for uncertain delay control systems. In: Proc. 47th Conference on Decision and Control, pp. 5306–5311 (2008)
130. Polyakov, A., Poznyak, A.: Lyapunov function design for finite-time convergence analysis: Twisting controller for second order sliding mode realization. Automatica 45, 444–448 (2009)
131. Polyakov, A., Poznyak, A.: Reaching time estimation for super-twisting second order sliding mode controller via Lyapunov function designing. IEEE Trans. Automatic Control 45(8), 1951–1955 (2009)

132. Poznyak, A.: Deterministic output noise effects in sliding mode observation. In: Sabanovic, A., Fridman, L., Spurgeon, S. (eds.) Variable Structure Systems: from Principles to Implementation. IEE Control Engineering Series, pp. 45–80. IEE, London (2004)
133. Roh, Y.H., Oh, J.H.: Robust stabilization of uncertain input delay systems by sliding mode control with delay compensation. Automatica 35(12), 1861–1865 (1999)
134. Rosales, J., Boiko, I., Fridman, L.: Design of compensators for second order sliding modes. In: Proc. of 11th International Workshop on Variable Structure Systems (VSS 2010), Mexico, pp. 20–25 (2010)
135. Rubagotti, M., Estrada, A., Castaños, F., Ferrara, A., Fridman, L.: Optimal disturbance rejection by integral sliding mode control for systems in regular form. In: Proc. of the Variable Structure Systems Workshop, Mexico City, Mexico, pp. 78–82 (2010)
136. Saadaoui, H., Manamanni, N., Djema, M., Barbot, J., Floquet, T.: Exact differentiation and sliding mode observers for switched Lagrangian systems. Nonlinear Analysis: Hybrid Systems and Applications 65, 1050–1069 (2006)
137. Saif, M., Xiong, Y.: Sliding mode observers and their application in fault diagnosis. In: Caccavale, F., Villani, L. (eds.) Fault Diagnosis and Fault Tolerance for Mechatronic Systems: Recent Advances. Springer Tracts in Advanced Robotics, pp. 1–52. Springer, Berlin (2003)
138. Shtessel, Y., Edwards, C., Spurgeon, S., Kochalummoottil, J.: Adaptive continuous finite reaching time control and second order sliding modes. In: Proceedings of VSS, pp. 266–271 (2010)
139. Shtessel, Y., Moreno, J., Plestan, F., Fridman, L., Poznyak, A.: Super-twisting adaptive sliding mode control: a Lyapunov design. In: 49th IEEE Conference on Decision and Control, pp. 5109–5113 (2010)
140. Shtessel, Y., Zinober, A., Shkolnikov, I.: Sliding mode control for nonlinear systems with output delay via method of stable system centre. ASME Journal of Dynamic Systems, Measurement and Control 25(2), 253–257 (2003)
141. Shustin, E., Fridman, L., Fridman, E., Castanos, F.: Robust semiglobal stabilization of the second order system by relay feedback with an uncertain variable time delay. SIAM J. Control Optim. 47(1), 196–217 (2008)
142. Sing, K.N.: Comments on robust stabilization of uncertain input delay systems by sliding mode control with delay compensation. Automatica 37, 73–84 (2001)
143. Song, G., Cai, L., Wang, Y., Longman, R.: A sliding mode based smooth adaptive robust controller for friction compensation. Int. J. Robust Nonlinear Control 8, 725–739 (1998)
144. Spurgeon, S.: Sliding mode observers - a survey. International Journal of Systems Science 39(8), 751–764 (2008)
145. Tan, C., Edwards, C.: Sliding mode observers for robust detection and reconstruction of actuator and sensor faults. International Journal of Robust and Nonlinear Control 13, 443–463 (2003)
146. Tan, C., Yu, X., Man, Z.: Terminal sliding mode observers for a class of nonlinear systems. Automatica 46(8), 1401–1404 (2010)
147. Tsypkin, Y.: Relay Control Systems. Cambridge University Press, Cambridge (1984)
148. Utkin, V.: First stage of VSS: People and events. In: Yu, X., Xu, J.-X. (eds.) Variable Structure Systems: Towards the 21st Century. LNCIS, vol. 274, pp. 1–32. Springer, London (2002)
149. Utkin, V., Guldner, J., Shi, J.: Relay Control Systems. Taylor and Francis, Taylor (1999)
150. Utkin, V., Shi, J.: Integral sliding mode in systems operating under uncertainty conditions. In: Proceedings of the 35th Conference on Decision and Control, Kobe, Japan, pp. 4591–4596 (1996)

151. Utkin, V.I. (ed.): Sliding Modes in Control Optimization. Springer, Heidelberg (1992)
152. Venkataraman, S.T., Gulati, S.: Control of nonlinear systems using terminal sliding modes. In: Proc. American Control Conference, pp. 891–893 (1992)
153. Wu, Y., Yu, X., Man, Z.: Terminal sliding mode control design for uncertain dynamic systems. Systems and Control Letters 34, 281–287 (1998)
154. Xiong, Y., Saif, M.: Sliding mode observer for nonlinear uncertain systems. IEEE Transaction on Automatic Control 46(12), 2012–2017 (2001)
155. Yu, L., Barbot, J.P., Boutat, D., Benmerzouk, D.: Observability normal forms for a class of switched systems with Zeno phenomena. In: ACC 2009: Proceedings of the 2009 American Control Conference, pp. 1766–1771. IEEE Press, Piscataway (2009)
156. Yu, S., Yu, X., Man, Z.: A fuzzy neural network approximator with fast terminal sliding mode and its applications. Fuzzy Sets and Systems 148(3), 469–486 (2005)
157. Yu, X., Kaynak, O.: Sliding mode control with soft computing: A survey. IEEE Transactions on Industrial Electronics 56(9), 3275–3285 (2010)
158. Yu, X., Man, Z.: Model reference adaptive control systems with terminal sliding modes. Int. J. Control 64, 1165–1176 (1996)
159. Yu, X., Man, Z.: Model reference adaptive control systems with terminal sliding modes. IEEE Trans. Circuits and Systems-I 44(11), 1065–1070 (1997)
160. Yu, X., Man, Z.: Non-singular terminal sliding mode control of rigid manipulators. IEEE Transactions on Circuits and Systems, Part 1 49(2), 261–264 (2002)
161. Yu, X., Wang, B., Batsukh, B., Wang, L., Man, Z.: An improved training algorithm for feedforward neural network learning based on terminal attractors. Journal of Global Optimization (2011), doi: 10.1007/s10898–010–9597–6
162. Zak, S.: Terminal atractors for addressable memory in neural network. Physics Letters A 133(1,2), 18–22 (1988)
163. Zak, S.: Terminal attractors in neural networks. Neural Networks 133(2), 259–274 (1989)
164. Zhihong, M., O'day, M., Yu, X.: A robust adaptive terminal sliding mode control for rigid robotic manipulators. J. Intell. Robotics Syst. 24(1), 23–41 (1999)
165. Zolezzi, T.: Variable structure control of semilinear evolution equations. In: Partial differential equations and the calculus of variations: Essays in Honor of Ennio De Giorgi, pp. 997–1018. Birkhäuser, Basel (1989)
166. Zubov, V.: Methods of A.M. Lyapunov and their applications. Noordhoff, Groningen (1964)

Chapter 2
Finite-Time Stability and High Relative Degrees in Sliding-Mode Control

Arie Levant

Abstract. Establishing and exactly keeping constraints of high relative degrees is a central problem of the modern sliding-mode control. Its solution in finite-time is based on so-called high-order sliding modes, and is reduced to finite-time stabilization of an auxiliary uncertain system. Such stabilization is mostly based on the homogeneity approach. Robust exact differentiators are also developed in this way and are used to produce robust output-feedback controllers. The resulting controllers feature high accuracy in the presence of sampling noises and delays, ultimate robustness to the presence of unaccounted-for fast stable dynamics of actuators and sensors, and to small model uncertainties affecting the relative degrees. The dangerous types of the chattering effect are removed artificially increasing the relative degree. Parameters of the controllers and differentiators can be adjusted to provide for the needed convergence rate, and can be also adapted in real time. Simulation results and applications are presented in the fields of control, signal and image processing.

2.1 Introduction

Sliding mode (SM) control is used to cope with heavy uncertainty conditions. The corresponding approach [18,56,58] is based on the exact keeping of a properly chosen function (sliding variable) at zero by means of high-frequency control switching. Although very robust and accurate, the approach also features certain drawbacks. The standard sliding mode may be implemented only if the relative degree of the sliding variable is 1, i.e. control has to explicitly appear already in its first total time derivative. Another problem is that the high-frequency control switching may cause dangerous vibrations called the chattering effect [14, **?**,23].

Arie Levant
Applied Mathematics Department,
Tel-Aviv University, Tel-Aviv, Israel
e-mail: levant@post.tau.ac.il

L. Fridman et al. (Eds.): Sliding Modes, LNCIS 412, pp. 59–92.
springerlink.com

The issues can be settled in a few ways. High-gain control with saturation is used to overcome the chattering effect approximating the sign-function in a narrow boundary layer around the switching manifold [54], the sliding-sector method [24] avoids chattering in control of disturbed linear time-invariant systems. This paper surveys the sliding-mode order approach [30] which addresses both the chattering and the relative-degree restrictions, while preserving the sliding-mode features and improving the accuracy in the presence of small imperfections.

Establishing the needed constraint $\sigma = 0$ requires the stabilization of the sliding variable σ at zero. The corresponding auxiliary dynamic system is of the order of the relative degree and is typically uncertain. Theoretically it also allows feedback linearization [25], though the system uncertainty prevents its direct utilization. Finite-time stabilization is preferable, since it provides for higher robustness, simpler overall performance analysis, and, as it is further shown, for higher accuracy in the presence of small sampling noises and delays. With the relative degree 1 such finite-time stabilization is easily obtained by means of the relay control, which is widely used in the standard sliding-mode control. With higher relative degrees the problem is much more complicated. The standard sliding-mode design suggests choosing a new auxiliary sliding variable of the first relative degree. That variable is usually a linear combination of the original sliding variable σ and its successive total time derivatives [54, 52], which leads to only exponential stabilization of σ. The finite-time stabilization corresponds to the high-order sliding-mode (HOSM) approach [30, 45, 4].

HOSM actually is a motion on the discontinuity set of a dynamic system understood in Filippov's sense [20]. The sliding order characterizes the dynamics smoothness degree in the vicinity of the mode. Let the task be to make some smooth scalar function σ vanish, keeping it at zero afterwards. Then successively differentiating σ along trajectories, a discontinuity will be encountered sooner or later in the general case. Thus, a sliding mode $\sigma = 0$ may be classified by the number r of the first successive total time derivative $\sigma^{(r)}$ which is not a continuous function of the state space variables or does not exist due to some reason, like trajectory nonuniqueness. That number is called the sliding order [30, 32]. If σ is a vector, also the sliding order is a vector.

The words "rth order sliding" are often abridged to "r-sliding". The term "r-sliding controller" replaces the longer expression "finite-time-convergent r-sliding mode controller". The sliding order usually coincides with the relative degree, provided the control is discontinuous and the relative degree exists.

The standard sliding mode, on which most variable structure systems (VSS) are based, is of the first order ($\dot{\sigma}$ is discontinuous). The standard-sliding-mode precision $\sup|\sigma|$ is proportional to the time interval between the measurements or to the switching delay. Asymptotically stable HOSMs arise in systems with traditional sliding-mode control, if the relative degree of the sliding variable σ is higher than 1. The limit sliding-accuracy asymptotics is the same in that case, as of the standard 1-sliding mode [54]. The asymptotic convergence to the constraint inevitably complicates the overall system performance analysis.

Actually r-sliding controllers' design [32,33,45] requires only the knowledge of the system relative degree r. The produced control is a discontinuous function of σ and of its real-time-calculated successive derivatives $\dot{\sigma}, \ldots, \sigma^{(r-1)}$. Realizations of r-sliding mode provide for the sliding precision of up to the rth order with respect to sampling intervals and delays [30].

Since the HOSM method is developed for arbitrary relative degree, one just needs to consider the control derivative of some order as a new virtual control in order to get the needed smoothness degree of the real control and to diminish the chattering [30, 4, 5]. Indeed the procedure was recently theoretically proved to only leave the non-harmful chattering of infinitesimal energy [36]. While finite-time-convergent arbitrary-order sliding-mode controllers are still mostly theoretically studied [17, 16,21,32,33,35], 2-sliding controllers are already successfully implemented for the solution of practical problems [1,6,11,12,15,19,26,29,44,48, **?**,53,51,55], hundreds of references are available.

In order to stabilize the sliding variable dynamics in finite time, one usually needs to use the homogeneity approach [3,13]. As a result, almost all known r-sliding controllers possess specific homogeneity called the r-sliding homogeneity [33]. The homogeneity makes the convergence proofs of the HOSM controllers standard and provides for the highest possible asymptotic accuracy [30] in the presence of measurement noises, delays and discrete measurements. Thus, with τ being the sampling interval, the accuracy $\sigma = O(\tau^r)$ is attained [33]. These asymptotical features are preserved, when a robust exact homogeneous differentiator of the order $r-1$ [32] is applied as a standard part of the homogeneous output-feedback r-sliding controller.

While most results were obtained for the Single-Input Single-Output (SISO) case, a few theoretical results were obtained for the Multi-Input Multi-Output (MIMO) case [5,16] with a well-defined vector relative degree.

The standard SISO r-SM control problem statement assumes the uniform boundedness of the functional coefficients appearing in the rth derivative of the sliding variable. Such assumptions usually only apply to bounded operational regions. These restrictions have been recently removed [8, 42]. Similarly the requirement of the highest derivative boundedness has been removed from the HOSM differentiators [34]. Thus, global applications of HOSM controllers and observers becomes possible. Such global versions of HOSM controllers and differentiators are inevitably not homogeneous, but they usually remain homogeneous in a small vicinity of HOSM.

The recent results prove the ultimate robustness of the homogeneous sliding modes with respect to various dynamic perturbations, including singular perturbations corresponding to the dynamics of fast stable actuators and sensors [36,41] and small perturbations changing the system relative degree [39].

Simulation demonstrates the practical applicability of the approach in control, signal and image processing.

2.2 Preliminaries

Definition 2.1. A differential inclusion $\dot{x} \in F(x), x \in \mathbb{R}^n$, is further called a Filippov differential inclusion [20] if the vector set $F(x)$ is non-empty, closed, convex, locally bounded and upper-semicontinuous. The latter condition means that the maximal distance of the points of $F(x)$ from the set $F(y)$ vanishes when $x \to y$. Solutions are defined as absolutely-continuous functions of time satisfying the inclusion almost everywhere.

Such solutions always exist and have most of the well-known standard properties except the uniqueness [20].

Definition 2.2. It is said that a differential equation $\dot{x} = f(x), x \in \mathbb{R}^n$, with a locally-bounded Lebesgue-measurable right-hand side is understood in the Filippov sense [20], if it is replaced by a special Filippov differential inclusion $\dot{x} \in F(x)$, where

$$F(x) = \bigcap_{\delta>0} \bigcap_{\mu N=0} \overline{co} f(O_\delta(x) \backslash N).$$

Here μ is the Lebesgue measure, $O_\delta(x)$ is the δ-vicinity of x, and $\overline{co}M$ denotes the convex closure of M. In the most usual case, when f is continuous almost everywhere, the procedure is to take $F(x)$ being the convex closure of the set of all possible limit values of f at a given point x, obtained when its continuity point y tends to x. In the general case approximate-continuity [50] points y can be taken (one of the equivalent definitions by Filippov [20]). A solution of $\dot{x} = f(x)$ is defined as a solution of $\dot{x} \in F(x)$. Obviously, values of f on any set of the measure 0 do not influence the Filippov solutions. Note that with continuous f the standard definition is obtained.

In order to better understand the definition note that any possible Filippov velocity has the form $\dot{x} = \lambda_1 f_1 + \ldots + \lambda_{n+1} f_{n+1}, \lambda_1 + \ldots + \lambda_n + 1 = 1, \lambda_i \geq 0$, where $f_1, \ldots, f_{n+1}$ are some values of f obtained as limits at the point x along sequences of continuity (approximate continuity) points. Thus, $\dot{x}$ can be considered as a mean value of the velocity taking on the values f_i during the time share $\lambda_i \Delta t$ of a current infinitesimal time interval Δt.

Definition 2.3. Consider a discontinuous differential equation $\dot{x} = f(x)$ (Filippov differential inclusion $\dot{x} \in F(x)$) with a smooth output function $\sigma = \sigma(x)$, and let it be understood in the Filippov sense. Then, provided that

1. successive total time derivatives $\sigma, \dot{\sigma}, \ldots, \sigma^{(r-1)}$ are continuous functions of x,
2. the set

$$\sigma = \dot{\sigma} = \ddot{\sigma} = \ldots = \sigma^{(r-1)} = 0 \tag{2.1}$$

   is a non-empty integral set,
3. the Filippov set of admissible velocities at the r-sliding points (2.1) contains more than one vector,

the motion on set (2.1) is said to exist in r-sliding (rth-order sliding) mode [30, 31]. Set (2.1) is called r-sliding set. It is said that the sliding order is strictly r, if the next derivative $\sigma^{(r)}$ is discontinuous or does not exist as a single-valued function of x. The non-autonomous case is reduced to the considered one introducing the fictitious equation $\dot{t} = 1$.

Note that the third requirement is not standard and means that set (2.1) is a discontinuity set of the equation. It is only introduced here to exclude extraneous cases of integral manifolds of continuous differential equations. The standard sliding mode used in the traditional VSSs is of the first order (σ is continuous, and $\dot{\sigma}$ is discontinuous). The notion of the sliding order appears to be connected with the relative degree notion.

Definition 2.4. A smooth autonomous SISO system $\dot{x} = a(x) + b(x)u$ with the control u and output σ is said to have the relative degree r, if the Lie derivatives locally satisfy the conditions [25]

$$L_b\sigma = L_aL_b\sigma = \ldots = L_a^{r-2}L_b\sigma = 0, L_a^{r-1}L_b\sigma \neq 0.$$

It can be shown that the equality of the relative degree to r actually means that the successive total time derivatives $\sigma, \dot{\sigma}, \ldots, \sigma^{(r-1)}$ do not depend on control and can be taken as a part of new local coordinates, and $\sigma^{(r)}$ linearly depends on u with the nonzero coefficient $L_a^{r-1}L_b\sigma$. Also here the non-autonomous case is reduced to the autonomous one introducing the fictitious equation $\dot{t} = 1$.

2.3 SISO Regulation Problem

First consider an uncertain smooth nonlinear Single-Input Single-Output (SISO) system $\dot{x} = f(t,x,u), x \in \mathbb{R}^n, t,u \in \mathbb{R}$ with a smooth output $s(t,x) \in \mathbb{R}$. Let the goal be to make the output s(t, x) to track some real-time-measured smooth signal $s_c(t)$. Introducing a new auxiliary control $v \in \mathbb{R}, \dot{u} = v$, and the output $\sigma(t,x) = s(t,x) - s_c(t)$, obtain a new affine-in-control system $\frac{d}{dt}(x,u)^t = (f(t,x,u),0)^t + (0,1)^t v$ with the control task to make $\sigma(t,x)$ vanish. Therefore, the further consideration is restricted only to systems affine in control.

2.3.1 Standard SISO Regulation Problem and the Idea of Its Solution

Consider a dynamic system of the form

$$\dot{x} = a(t,x) + b(t,x)u, \quad \sigma = \sigma(t,x), \tag{2.2}$$

where $x \in \mathbb{R}^n, a, b$ and $\sigma : \mathbb{R}^{n+1} \to \mathbb{R}$ are unknown smooth functions, $u \in \mathbb{R}$, the dimension n might be also uncertain. Only measurements of σ are available in real time. The task is to provide in finite time for exactly keeping $\sigma \equiv 0$. The relative

degree r of the system is assumed to be constant and known. In other words, for the first time the control explicitly appears in the rth total time derivative of σ and

$$\sigma^{(r)} = h(t,x) + g(t,x)u, \tag{2.3}$$

where $h(t,x) = \sigma^{(r)}|_{u=0}, g(t,x) = \frac{\partial}{\partial u}\sigma^{(r)} \neq 0$. It is supposed that for some $K_m, K_M, C > 0$

$$0 < Km \leq \frac{\partial}{\partial u}\sigma^{(r)} \leq KM, \quad \left|\sigma^{(r)}|_{u=0}\right| \leq C, \tag{2.4}$$

which is always true at least in compact operation regions. Trajectories of (2.2) are assumed infinitely extendible in time for any Lebesgue-measurable bounded control $u(t,x)$. Finite-time stabilization of smooth systems at an equilibrium point by means of continuous control is considered in [3,13]. In our case any continuous control

$$u = \phi\left(\sigma, \dot{\sigma}, \ldots, \sigma^{(r-1)}\right) \tag{2.5}$$

providing for $\sigma \equiv 0$, should satisfy the equality $\phi(0,0,\ldots,0) = -h(t,x)/g(t,x)$, whenever (2.1) holds. Since the problem uncertainty prevents it, the control has to be discontinuous at least on the set (2.1). Hence, the r-sliding mode $\sigma = 0$ is to be established. As follows from (2.3), (2.4)

$$\sigma^{(r)} \in [-C,C] + [K_m, K_M]u. \tag{2.6}$$

The differential inclusion (2.5), (2.6) is understood here in the Filippov sense, which means that the right-hand vector set is enlarged at the discontinuity points of (2.5), in order to satisfy the convexity and semicontinuity conditions from Definition 1. The Filippov procedure from Definition 2 is applied for this aim to the function (2.5), and the resulting scalar set is substituted for u in (2.6). The obtained inclusion does not "remember" anything on system (2.2) except the constants r, C, K_m, K_M. Thus, provided (2.4) holds, the finite-time stabilization of (2.6) at the origin simultaneously solves the stated problem for all systems (2.2). Note that the realization of this plan requires real-time differentiation of the output. The controllers, which are designed in this paper, are *r-sliding homogeneous* [33]. The corresponding notion is introduced below.

2.4 Homogeneity, Finite-Time Stability and Accuracy

Definition 2.5. A function $f : \mathbb{R}^n \to \mathbb{R}$ (respectively a vector-set field $F(x) \subset \mathbb{R}^n, x \in \mathbb{R}^n$, or a vector field $f : \mathbb{R}^n \to \mathbb{R}^n$) is called *homogeneous of the degree* $q \in \mathbb{R}$ *with the dilation*

$$d_\kappa : (x_1, x_2, \ldots, x_n) \mapsto (\kappa^{m_1} x_1, \kappa^{m_2} x_2, \ldots, \kappa^{m_n} x_n)$$

[3], where $m1, \ldots, m_n$ are some positive numbers (*weights*), if for any $\kappa > 0$ the identity $f(x) = \kappa^{-q} f(d_\kappa x)$ holds (respectively $F(x) = \kappa^{-q} d_\kappa^{-1} F(d_\kappa x)$, or $f(x) =$

$\kappa^{-q} d_\kappa^{-1} f(dx)$). The non-zero homogeneity degree q of a vector field can always be scaled to ± 1 by an appropriate proportional change of the weights $m_1, \ldots, m_n$.

Note that the homogeneity of a vector field $f(x)$ (a vector-set field $F(x)$) can equivalently be defined as the invariance of the differential equation $\dot{x} = f(x)$ (differential inclusion $\dot{x} \in F(x)$) with respect to the combined time-coordinate transformation

$$G_\kappa : (t,x) \mapsto (\kappa^p t, d_\kappa x),$$

where $p, p = -q$, might naturally be considered as the weight of t. Indeed, the homogeneity condition can be rewritten as

$$\dot{x} \in F(x) \Leftrightarrow \frac{d(d_\kappa x)}{d(\kappa^p t)} \in F(d_\kappa x).$$

Examples. In the following the weights of x_1, x_2 are 3 and 2 respectively. Then the function $x_1^2 + x_2^3$ is homogeneous of the weight (degree) 6: $\left(\kappa^3 x_1\right)^2 + \left(\kappa^2 x_2\right)^3 = \kappa^6 \left(x_1^2 + x_2^3\right)$. The differential inequality $|\dot{x}_1| + \dot{x}_2^{4/3} \le x_1^{4/3} + x_2^2$ corresponds to the homogeneous differential inclusion

$$(\dot{x}_1, \dot{x}_2) \in (z_1, z_2) : |z_1| + z_2^{4/3} \le x_1^{4/3} + x_2^2$$

of the degree +1. The system of differential equations

$$\begin{cases} \dot{x}_1 = x_2 \\ \dot{x}_2 = -x_1^{1/3} - |x_2^{1/2}| \mathrm{sign} x_2 \end{cases} \tag{2.7}$$

is of the degree -1 and is finite-time stable [13].

1°. A differential inclusion $\dot{x} \in F(x)$ (equation $\dot{x} = f(x)$) is further called *globally uniformly finite-time stable* at 0, if $x(t) = 0$ is a Lyapunov-stable solution and for any $R > 0$ exists $T > 0$ such that any trajectory starting within the disk $||x|| < R$ stabilizes at zero in the time T. **2°**. A differential inclusion $\dot{x} \in F(x)$ (equation $\dot{x} = f(x)$) is further called *globally uniformly asymptotically stable* at 0, if it is Lyapunov stable and for any $R > 0, \varepsilon > 0$ exists $T > 0$ such that any trajectory starting within the disk $||x|| < R$ enters the disk $||x|| < \varepsilon$ in the time T to stay there forever. A set D is called *dilation retractable* if $d_\kappa D \subset D$ for any $\kappa \in [0,1]$. In other words with any its point x it contains the whole line $d_\kappa x, \kappa \in [0,1]$. **3°**. A homogeneous differential inclusion $\dot{x} \in F(x)$ (equation $\dot{x} = f(x)$) is further called *contractive* if there are 2 compact sets D_1, D_2 and $T > 0$, such that D_2 lies in the interior of D_1 and contains the origin; D_1 is dilation-retractable; and all trajectories starting at the time 0 within D_1 are localized in D_2 at the time moment T.

Theorem 2.1. *[33]. Let $\dot{x} \in F(x)$ be a homogeneous Filippov inclusion with a negative homogeneous degree $-p$, then properties $1^o, 2^o$ and 3^o are equivalent and the maximal settling time is a continuous homogeneous function of the initial conditions of the degree p.*

Finite-time stability of homogeneous discontinuous differential equations was also considered in [47].

Proof. Obviously, both 1^o and 2^o imply 3^o , and 1^o implies 2^o . Thus, it is enough to prove that 3^o implies 1^o . All trajectories starting in the set D_1 concentrate in a smaller set D_2 in time T. Applying the homogeneity transformation obtain that the same is true with respect to the sets $d_\kappa D_1, d_\kappa D_2$ and the time κT for any $\kappa > 0$. An infinite collapsing chain of embedded regions is now constructed, such that any point belongs to one of the regions, and the resulting convergence time is majored by a geometric series. □

Due to the continuous dependence of solutions of the Filippov inclusion $\dot{x} \in F(x)$ on its graph $\Gamma = (x,y)|y \in F(x)$ [20], the contraction feature 3^o is obviously robust with respect to perturbations causing small changes of the inclusion graph in some vicinity of the origin.

Corollary 2.1. *[33] The global uniform finite-time stability of homogeneous differential equations (Filippov inclusions) with negative homogeneous degree is robust with respect to locally small homogeneous perturbations.*

Let $\dot{x} \in F(x)$ be a homogeneous Filippov differential inclusion. Consider the case of "noisy measurements" of x_i with the magnitude $\beta_i \tau^{m_i}, \beta_i, \tau > 0$,

$$\dot{x} \in F(x_1 + \beta_1[-1,1]\tau^{m_1}, \ldots, x_n + \beta_n[-1,1]\tau^{m_n}).$$

Successively applying the global closure of the right-hand-side graph and the convex closure at each point x, obtain some new Filippov differential inclusion $\dot{x} \in F_\tau(x)$.

Theorem 2.2. *[33]. Let $\dot{x} \in F(x)$ be a globally uniformly finite-time stable homogeneous Filippov inclusion with the homogeneity weights $m_1, \ldots, m_n$ and the degree $-p < 0$, and let $\tau > 0$. Suppose that a continuous function $x(t)$ be defined for any $t \geq -\tau^p$ and satisfy some initial conditions $x(t) = \xi(t), t \in [-\tau^p, 0]$. Then if $x(t)$ is a solution of the disturbed differential inclusion*

$$\dot{x}(t) \in F_\tau(x(t + [-\tau^p, 0])), \quad 0 < t < \infty,$$

the inequalities $|x_i| < \gamma_i \tau^{m_i}$ are established in finite time with some positive constants γ_i independent of τ and ξ.

Note that Theorem 2.2 covers the cases of retarded or discrete noisy measurements of all, or some of the coordinates, and any mixed cases. In particular, infinitely extendible solutions certainly exist in the case of noisy discrete measurements of some variables or in the constant time-delay case. For example, with small delays of the order of τ introduced in the right-hand side of (2.7) the accuracy $x_1 = O(\tau^3), \dot{x}_1 = x_2 = O(\tau^2)$ is obtained. As follows from Corollary 2.1, with sufficiently small ε the addition of the term $\varepsilon x_1^{2/3}$ in the first equation of (2.7) disturbs neither the finite-time stability, nor the above asymptotic accuracy.

2.5 Homogeneous Sliding Modes

Suppose that feedback (2.5) imparts homogeneity properties to the closed-loop inclusion (2.5), (2.6). Due to the term $[-C,C]$, the right-hand side of (2.5) can only have the homogeneity degree 0 with $C \neq 0$. Indeed, with a positive degree the right hand side of (2.5), (2.6) approaches zero near the origin, which is not possible with $C \neq 0$. With a negative degree it is not bounded near the origin, which contradicts the local boundedness of ϕ. Thus, the homogeneity degree of $\sigma^{(r-1)}$ is to be opposite to the degree of the whole system. Scaling the system homogeneity degree to -1, achieve that the homogeneity weights of $t,\sigma,\dot{\sigma},\ldots,\sigma^{(r-1)}$ are $1,r,r-1,\ldots,1$ respectively. This homogeneity is further called the *r-sliding homogeneity*. The inclusion (2.5), (2.6) is called *r-sliding homogeneous* if for any $\kappa > 0$ the combined time-coordinate transformation

$$G_\kappa : (t,\sigma,\dot{\sigma},\ldots,\sigma^{(r-1)}) \mapsto (\kappa t,\kappa^r\sigma,\kappa^{r-1}\dot{\sigma},\ldots,\kappa\sigma^{(r-1)}) \tag{2.8}$$

preserves the closed-loop inclusion (2.5), (2.6). Note that the Filippov differential inclusion corresponding to the closed-loop inclusion (2.5), (2.6) is also r-sliding homogeneous.

Transformation (2.8) transfers (2.5), (2.6) into

$$\frac{d^r(\kappa^r\sigma)}{(d\kappa t)^r} \in [-C,C] + [K_m,K_M]\phi(\kappa^r\sigma,\kappa^{r-1}\dot{\sigma},\ldots,\kappa\sigma^{(r-1)}).$$

Hence, (2.5), (2.6) is r-sliding homogeneous if

$$\phi(\kappa^r\sigma,\kappa^{r-1}\dot{\sigma},\ldots,\kappa\sigma^{(r-1)}) \equiv \phi(\sigma,\dot{\sigma},\ldots,\sigma^{(r-1)}). \tag{2.9}$$

Definition 2.6. Controller (2.5) is called r-sliding homogeneous (rth order sliding homogeneous) if (2.9) holds for any $(\sigma,\dot{\sigma},\ldots,\sigma^{(r-1)})$ and $\kappa > 0$. The corresponding sliding mode is also called homogeneous (if exists).

Such a homogeneous controller is inevitably discontinuous at the origin $(0,\ldots,0)$, unless ϕ is a constant function. It is also uniformly bounded, since it is locally bounded and takes on all its values in any vicinity of the origin. Recall that the values of ϕ on any zero-measure set do not affect the corresponding Filippov inclusion.

Almost all known r-sliding controllers, $r \geq 2$, are r-sliding homogeneous. The only important exception is the terminal 2-sliding controller maintaining 1-sliding mode $\dot{\sigma}+\beta\sigma^\rho \equiv 0$, where $\rho = (2k+1)/(2m+1), \beta > 0, k < m$, and k,m are natural numbers [45]. Indeed, the homogeneity requires $\rho = 1/2$ and $\sigma \geq 0$.

2.5.1 Second Order Sliding Mode Controllers

Let $r = 2$. As follows from the previous Section it is sufficient to construct a 2-sliding-homogeneous contractive controller. Their discrete-sampling versions provide for the accuracy described in Theorem 2.2, i.e. $\sigma = O(\tau^2), \dot{\sigma} = O(\tau)$. Similarly,

the noisy measurements lead to the accuracy $\sigma = O(\varepsilon), \dot{\sigma} = O(\varepsilon^{1/2})$, if the maximal errors of σ and $\dot{\sigma}$ sampling are of the order of ε and $\varepsilon^{1/2}$ respectively.

Design of such 2-sliding controllers is greatly facilitated by the simple geometry of the 2-dimensional phase plane with coordinates σ, $\dot{\sigma}$: any smooth curve locally divides the plane in two parts. It is easy to construct any number of such controllers [37]. Only few controllers are presented here.

The twisting controller [30]

$$u = -(r_1 \mathrm{sign}\sigma + r_2 \mathrm{sign}\dot{\sigma}),$$

has the convergence conditions

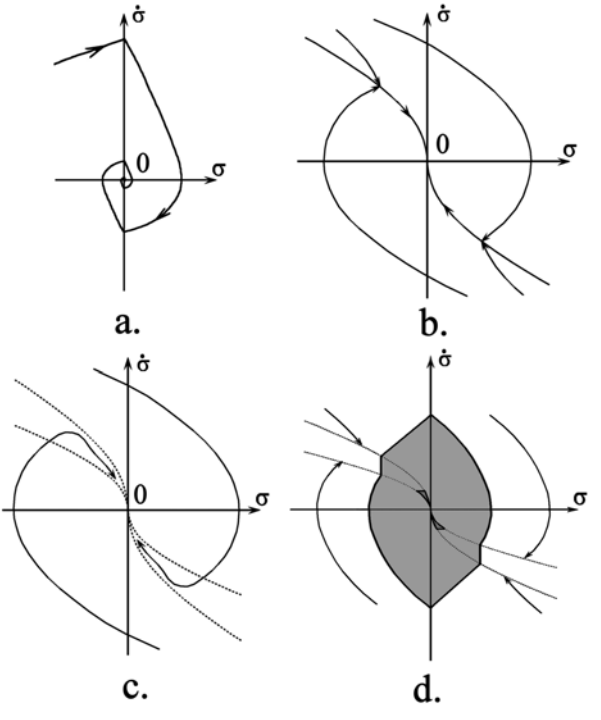

Fig. 2.1 Convergence of various 2-sliding homogeneous controllers

$$(r_1 + r_2)K_m - C > (r_1 - r_2)K_M + C, (r_1 - r_2)K_m > C.$$

Its typical trajectory in the plane σ, $\dot{\sigma}$ is shown in Fig. 2.1a. A homogeneous form of the controller with prescribed convergence law (Fig. 2.1b; [30])

$$u = -\alpha \mathrm{sign}(\dot{\sigma} + \beta|\sigma|^{1/2}\mathrm{sign}\sigma), \alpha K_m - C > \beta^2/2$$

is a 2-sliding homogeneous analogue of the terminal sliding mode controller originally featuring a singularity at $\sigma = 0$ [45]. The 2-sliding stability analysis is based on the fact that all the trajectories in the plane $\sigma, \dot{\sigma}$ which pass through a given continuity point of $u = \phi(\sigma, \dot{\sigma})$ are confined between the properly chosen trajectories of the homogeneous differential equations $\ddot{\sigma} = \pm C + K_M \phi(\sigma, \dot{\sigma})$ and $\ddot{\sigma} = \pm C + K_m \phi(\sigma, \dot{\sigma})$. These border trajectories cannot be crossed by other paths, if ϕ is locally Lipschitzian, and may be often chosen as boundaries of appropriate dilation-retractable regions [37]. A region is dilation-retractable iff, with each its point $(\sigma, \dot{\sigma})$, it contains all the points of the parabolic segment $(\kappa^2\sigma, \kappa\dot{\sigma}), 0 \le \kappa \le 1$. The popular sub-optimal controller [4,5,6,7] is defined by the formula

$$u = -r_1 \mathrm{sign}(\sigma - \sigma^*/2) + r_2 \mathrm{sign}\sigma^*, r_1 > r_2 > 0,$$

where σ^* is the value of σ detected at the closest time in the past when $\dot{\sigma}$ was 0. The initial value of σ^* is 0. The corresponding convergence conditions are

$$2[(r_1 + r_2)K_m - C] > (r_1 - r_2)K_M + C, (r_1 - r_2)K_m > C.$$

Usually the moments when $\dot{\sigma}$ changes its sign are detected using finite differences. The control u depends actually on the whole history of measurements of $\dot{\sigma}$ and σ, and does not have the feedback form (2.5). Nevertheless, with $r = 2$ the homogeneity transformation (2.8) preserves its trajectories, and it is natural to call it 2-sliding homogeneous in the broad sense. Also the statements of Theorems 2.1, 2.2 remain valid for this controller.

An important class of HOSM controllers comprises recently proposed so-called *quasi-continuous* controllers. Controller (2.5) is called *quasi-continuous* [35], if it can be redefined according to continuity everywhere except the r-sliding manifold $\sigma = \dot{\sigma} = \ldots = \sigma^{(r-1)} = 0$. Due to always present disturbances and noises, in practice, with the sliding order $r > 1$ the general-case trajectory does never hit the r-sliding manifold, for the r-sliding condition has the codimension r. Hence, the control practically remains continuous function of time all the time. As a result, the chattering is significantly reduced. Following is a 2-sliding controller with such features [35]:

$$u = -\alpha \frac{\dot{\sigma} + \beta |\sigma|^{1/2} \mathrm{sign}\sigma}{\dot{\sigma} + \beta |\sigma|^{1/2}}, \beta > 0.$$

This control is continuous everywhere except the origin. It vanishes on the parabola $\dot{\sigma} + \beta |\sigma|^{1/2} \mathrm{sign}\sigma = 0$. With sufficiently large α there are such numbers $\rho_1, \rho_2, 0 < \rho_1 < \beta < \rho_2$ that all the trajectories enter the region between the curves $\dot{\sigma} + \rho_t |\sigma|^{1/2} \mathrm{sign}\sigma = 0$ and cannot leave it (Fig. 2.1c). The contractivity property of the controller is demonstrated in Fig. 2.1d.

2.5.2 *Arbitrary Order Sliding Mode Controllers*

Following are two most known r-sliding controller families [32,35]. The controllers of the form

$$u = -\alpha \Psi_{r-1,r}(\sigma, \dot{\sigma}, \ldots, \sigma^{(r-1))},$$

are defined by recursive procedures, have the magnitude $\alpha > 0$, and solve the general output regulation problem from Section 2.3. The parameters of the controllers can be chosen in advance for each relative degree r. Only the magnitude α is to be adjusted for any fixed C, K_m, K_M, most conveniently by computer simulation, avoiding complicated and redundantly large estimations. Obviously, α is to be negative with $(\partial/\partial u)\sigma^{(r)} < 0$. In the following $\beta_1, \ldots, \beta_{r-1} > 0$ are the controller parameters, and $i = 1, \ldots, r-1$.

1. The following procedure defines the "nested" r-sliding controller [32], based on a pseudo-nested structure of 1-sliding modes. Let $q > 1$. The controller is built by the following recursive procedure:

$$N_{i,r} = (|\sigma|^{q/r} + |\dot{\sigma}|^{q/(r-1)} + \ldots + |\sigma^{(}i-1)|^{q/(r-i+1)})^{(r-i)/q};$$

$$\Psi_{0,r} = \mathrm{sign}\sigma, \phi_{i,r} = \sigma^{(i)} + \beta_i N_{i,r} \Psi_{i-1,r} \quad \Psi_{i,r} = \mathrm{sign}\phi_{i,r}; u = -\alpha \Psi_{r-1,r}.$$

   Following are the nested sliding-mode controllers (of the first family) for $r \le 4$ with tested β_i and q being the least multiple of $1, \ldots, r$:

   a. $u = -\alpha \mathrm{sign}\sigma$,
   b. $u = -\alpha \mathrm{sign}(\dot{\sigma} + |\sigma|^{1/2}\mathrm{sign}\sigma)$,
   c. $u = -\sigma \mathrm{sign}(\ddot{\sigma} + 2(|\dot{\sigma}|^3 + |\sigma|^2)^1/6 \mathrm{sign}(\dot{\sigma} + |\sigma|^{2/3}\mathrm{sign}\sigma))$,
   d.

$$u = -\alpha \mathrm{sign}\left(\dddot{\sigma} + 3(\ddot{\sigma}^6 + \dot{\sigma}^4 + |\sigma|^3)^{1/12} \mathrm{sign}\left[\ddot{\sigma} + (\dot{\sigma}^4 + |\sigma|^3)^{1/6} \mathrm{sign}(\dot{\sigma} + 0.5|\sigma|^{3/4}\mathrm{sign}\sigma)\right]\right).$$

   Though these controllers can be given an intuitive inexact explanation based on recursively nested standard sliding modes, the proper explanation is more complicated [32], since no sliding mode is possible on discontinuous surfaces, and a complicated motion arises around the control discontinuity set.

   The discontinuity set of nested sliding-mode controllers is a complicated stratified set with codimension varying in the range from 1 to r, which causes certain transient chattering. To avoid it one needs to artificially increase the relative degree.

2. Quasi-continuous r-sliding controller is a feedback function of $\sigma, \dot{\sigma}, \ldots, \sigma^{(r-1)}$ being continuous everywhere except the manifold $\sigma = \dot{\sigma} = \ldots = \sigma^{(r-1)}$ of the r-sliding mode. In the presence of errors in evaluation of σ and its derivatives, these equalities never take place simultaneously with $r > 1$. Therefore, control practically turns to be a continuous function of time. The following procedure defines a family of such controllers [35]:

$$\phi_{0,r} = \sigma, N_{0,r} = |\sigma|, \quad \Psi_{0,r} = \phi_{0,r}/N_{0,r} = \mathrm{sign}\sigma,$$

$$\phi_{i,r} = \sigma^{(i)} + \beta_i N_{i-1,r}^{(r-i)/(r-i+1)} \Psi_{i-1,r},$$

$$N_{i,r} = |\sigma^{(i)}| + \beta_i N_{i-1,r}^{(r-i)/(r-i+1)}, \Psi_{i,r} = \phi_{i,r}/N_{i,r}. \quad u = -\alpha \Psi_{r-1,r}$$

Following are quasi-continuous controllers with $r \leq 4$ and simulation-tested β_i.

a. $u = -\alpha \text{sign}\sigma$,
b. $u = -\alpha(\dot{\sigma} + |\sigma|^{1/2}\text{sign}\sigma)/(\dot{\sigma} + |\sigma|^{1/2})$,
c. $u = -\alpha[\ddot{\sigma} + 2(|\dot{\sigma}|^{2/3})^{-1/2}(\dot{\sigma} + |\sigma|^{2/3}\text{sign}\sigma)]/[\ddot{\sigma} + 2(|\dot{\sigma}|^{2/3})^{1/2}]$,
d.

$$\phi_{3,4} = \dddot{\sigma} + 3[\ddot{\sigma} + (|\dot{\sigma}| + 0.5|\sigma|^{3/4})^{-1/3}(\dot{\sigma} + 0.5|\sigma|^{3/4}\text{sign}\sigma)]$$
$$[|\ddot{\sigma} + (|\dot{\sigma}| + 0.5|\sigma|^{3/4})^{2/3}]^1/2,$$

$$N_{3,4} = |\dddot{\sigma}| + 3[|\ddot{\sigma} + (|\dot{\sigma}| + 0.5|\sigma|^{3/4})^{2/3}]^1/2, \qquad u = -\alpha \phi_{3,4}/N_{3,4}.$$

It is easy to see that the sets of parameters β_i are chosen the same for both families with $r \leq 4$. Note that while enlarging α increases the class (2.4) of systems, to which the controller is applicable, parameters β_i, are tuned to provide for the needed convergence rate [42]. The author considers the second family as the best one. In addition to the reduced chattering, another advantage of these controllers is the simplicity of their coefficients' adjustment (Section 2.7).

Theorem 2.3. *Each representative of the order r of the above two families of arbitrary-order sliding-mode controllers is r-sliding homogeneous. A finite-time stable r-sliding mode is established with properly chosen parameters.*

The proof of the Theorem is based on Theorem 2.1, i.e. on the proof of the contractivity property. Asymptotic accuracies of these controllers are readily obtained from Theorem 2.2. In particular $\sigma^{(i)} = O(\tau^{r-i}), i = 0, 1, \ldots, r-1$, if the measurements are performed with the sampling interval τ. A controller providing for the time-optimal stabilization of the inclusion (2.6) under the restriction $|u| \leq \alpha$ was recently proposed [17]. Such controllers are also r-sliding homogeneous providing for the accuracies corresponding to Theorem 2.2. Unfortunately, in practice they are only available for $r \leq 3$.

Chattering Attenuation. The standard chattering attenuation procedure is to consider the control derivative as a new control input, increasing the relative degree and the sliding order by one [30, 5, 6]. That procedure is studied in Section 2.8. It was many times successfully applied in practice [8, 26, 44], etc, though formally the convergence is only locally ensured in some vicinity of the $(r+1)$-sliding mode $\sigma \equiv 0$. Global convergence can be easily obtained in the case of the transition from the relative degree 1 to 2 [30, 37]; semi-global convergence can be assured with higher relative degrees [40].

2.6 Differentiation and Output-Feedback Control

Any r-sliding homogeneous controller can be complemented by an $(r-1)$th order differentiator [2,7,27,29,57] producing an output-feedback controller. In order to preserve the demonstrated exactness, finite-time stability and the corresponding asymptotic properties, the natural way is to calculate $\dot{\sigma},\dots,\sigma^{(r-1)}$ in real time by means of a robust finite-time convergent exact *homogeneous* differentiator [31,32]. Its application is possible due to the boundedness of $\sigma^{(r)}$ provided by the boundedness of the feedback function ϕ in (2.5).

2.6.1 Arbitrary Order Robust Exact Differentiation

Let the input signal $f(t)$ be a function defined on $[0,\infty)$ and consisting of a bounded Lebesgue-measurable noise with unknown features, and of an unknown base signal $f_0(t)$, whose kth derivative has a known Lipschitz constant $L>0$. The problem of finding real-time robust estimations of $\dot{f}_0(t),\ddot{f}_0(t),\dots,f0(k)(t)$ being exact in the absence of measurement noises is solved by the differentiator [33]

$$\dot{z}_0 = v_0, v_0 = -\lambda_k L^{1/(k+1)}|z_0 - f(t)|^{k/(k+1)}\mathrm{sign}(z_0 - f(t)) + z_1, \tag{2.10}$$

$$\dot{z}_1 = v_1, v_1 = -\lambda_{k-1} L^{1/k}|z_1 - v_0|^{(k-1)/k}\mathrm{sign}(z_1 - v_0) + z_2, \tag{2.11}$$

$$\dots \tag{2.12}$$

$$\dot{z}_{k-1} = v_{k-1}, v_{k-1} = -\lambda_1 L^{1/2}|z_{k-1} - v_{k-2}|^{1/2}\mathrm{sign}(z_{k-1} - v_{k-2}) + z_k, \tag{2.13}$$

$$\dot{z}_k = -\lambda_0 L\mathrm{sign}(z_k - v_{k-1}). \tag{2.14}$$

The parameters $\lambda_0,\lambda_1,\dots,\lambda_k > 0$ being properly chosen, the following equalities are true in the absence of input noises after a finite time of the transient process:

$$z_0 = f_0(t); z_i = v_{i-1} = f_0^{(i)}(t), i = 1,\dots,k.$$

Note that the differentiator has a recursive structure. Once the parameters $\lambda_0,\lambda_1,\dots,\lambda_{k-1}$ are properly chosen for the $(k-1)$th order differentiator with the Lipschitz constant L, only one parameter λ_k is needed to be tuned for the kth order differentiator with the same Lipschitz constant. The parameter λ_k is just to be taken sufficiently large. Any $\lambda_0 > 1$ can be used to start this process. Such differentiator can be used in any feedback, trivially providing for the separation principle [2,33].

Proof. Denote $\sigma_i = (z_i - f^{(i)}(t))/L$. Dividing by L all equations and subtracting $f^{(i+1)}(t)/L$ from both sides of the equation with $\dot{z}_i$ on the left, $i = 0,\dots,k$, obtain

$$\begin{aligned}
\dot{\sigma}_0 &= -\lambda_k|\sigma_0|^{k/(k+1)}\mathrm{sign}(\sigma_0) + \sigma_1,\\
\dot{\sigma}_1 &= -\lambda_{k-1}|\sigma_1 - \dot{\sigma}_0|^{(k-1)/k}\mathrm{sign}(\sigma_1 - \dot{\sigma}_0) + \sigma_2,\\
\dot{\sigma}_{k-1} &= -\lambda_1|\sigma_{k-1} - \dot{\sigma}_{k-2}|^{1/2}\mathrm{sign}(\sigma_{k-1} - \dot{\sigma}_{k-2}) + \sigma_k,\\
\dot{\sigma}_k &\in -\lambda_0\mathrm{sign}(\sigma_k - \dot{\sigma}_{k-1}) + [-1,1].
\end{aligned}$$

where the inclusion $f^{(k+1)}(t)/L \in [-1,1]$ is used in the last line. This differential inclusion is homogeneous with the homogeneity degree -1 and the weights $k+1,k,\ldots,1$ of $0,1,\ldots,k$ respectively. The finite time convergence of the differentiator follows from the contractivity property of this inclusion [32] and Theorem 2.1. □

Thus an infinite sequence of parameters λ_i can be built, valid for all k. In particular, one can choose $\lambda 0 = 1.1, \lambda 1 = 1.5, \lambda 2 = 2, \lambda 3 = 3, \lambda 4 = 5, \lambda 5 = 8$, which is enough for $k \leq 5$. Another possible choice of the differentiator parameters with $k \leq 5$ is $\lambda 0 = 1.1, \lambda 1 = 1.5, \lambda 2 = 3, \lambda 3 = 5, \lambda 4 = 8, \lambda 5 = 12$ [35, 34]. Theorem 2.2 provides for the asymptotic accuracy of the differentiator. Let the measurement noise be any Lebesgue-measurable function with the magnitude not exceeding ε. Then the accuracy $|z_i(t) - f_0^{(i)}(t)| = O(\varepsilon^{(k+1-i)/(k+1)})$ is obtained. That accuracy is shown to be the best possible [28, 31]. It was recently proved that the differentiator continues to locally converge in finite time also in the case, when $L = L(t)$ is a continuous function of time [34]. If L is absolutely continuous and the logarithmical derivative $\dot{L}/L$ is uniformly bounded, then the convergence region is constant and can be done arbitrarily large increasing L; moreover in the presence of a Lebesgue-measurable sampling noise with the magnitude $L(t,x)$ the accuracy $|z_i(t) - f_0^{(i)}(t)| = O(\varepsilon^{(k-i+1)/(k+1)})L(t,x)$ is obtained. If the sampling interval is τ, differential equations (2.10) should be replaced by their Euler approximations. In that case the accuracy $|z_i(t) - f_0^{(i)}(t)| = O(\tau^{(k-i+1)})L(t,x)$ is obtained. Differentiators (2.10) with constant and variable parameters L have been already proved useful for global exact observation [10, 12].

2.6.2 Output-Feedback Control

Suppose that the assumptions of the standard SISO regulation problem (Section 2.3.1) are satisfied. Introducing the above differentiator of the order $r-1$ in the feed-back, obtain an output-feedback r-sliding controller

$$u = \phi(z_0, z_1, \ldots, z_{r-1}), \tag{2.15}$$

$$\begin{aligned}
&\dot{z}_0 = v_0, v_0 = -\lambda_{r-1} L^{1/r} |z_0 - \sigma|^{(r-1)/r} \operatorname{sign}(z_0 - \sigma) + z_1,\\
&\dot{z}_1 = v_1, v_1 = -\lambda_{r-2} L^{1/(r-1)} |z_1 - v_0|^{(r-2)/(r-1)} \operatorname{sign}(z_1 - v_0) + z_2,\\
&\ldots\\
&\dot{z}_{r-2} = v_{r-2}, v_{r-2} = -\lambda_1 L^{1/2} |z_{r-2} - v_{r-3}|^{1/2} \operatorname{sign}(z_{r-2} - v_{r-3}) + z_{r-1},\\
&\dot{z}_{r-1} = -\lambda_0 L \operatorname{sign}(z_{r-1} - v_{r-2}),
\end{aligned} \tag{2.16}$$

where L is constant, $L \geq C + \sup|\phi| K_M$, and parameters λ_i of differentiator (2.16) are chosen in advance (Subsection 2.6.1).

Theorem 2.4. *Let controller (2.5) be r-sliding homogeneous and finite-time stable, and the parameters of the differentiator (2.15) be properly chosen with respect to the upper bound of $|\phi|$. Then in the absence of measurement noises the output-feedback controller (2.15), (2.16) provides for the finite-time convergence of each trajectory to the r-sliding mode $\sigma = 0$; otherwise convergence to a set defined by the inequalities $|\sigma| < \gamma_0\varepsilon, |\dot\sigma| < \gamma_1\varepsilon^{(r-1)/r}, \dots, \sigma^{(r-1)} < \gamma_{r-1}\varepsilon^{1/r}$ is ensured, where ε is the unknown measurement noise magnitude and $\gamma_0, \gamma_1, \dots, \gamma_{r-1}$ are some positive constants.*

Proof. Denote $s_i = z_i - \sigma^{(i)}$. Then using $\sigma^{(i)} \in [-L, L]$ controller (2.15), (2.16) can be rewritten as

$$u = -\alpha\phi(s_0 + \sigma, s_1 + \dot\sigma, \dots, s_{r-1} + \sigma^{(r-1)}), \tag{2.17}$$

$$\begin{aligned}
\dot s_0 &= -\lambda_{r-1}L^{1/r}|s_0|^{(r-1)/r}\operatorname{sign}(s_0) + s_1,\\
\dot s_1 &= -\lambda_{r-2}L^{1/(r-1)}|s_1 - \dot s_0|(r-2)/(r-1)\operatorname{sign}(s_1 - \dot s_0) + s_2,\\
&\dots\\
\dot s_{r-2} &= -\lambda_1 L^{1/2}|s_{r-2} - \dot s_{r-3}|^{1/2}\operatorname{sign}(s_{r-2} - \dot s_{r-3}) + s_{r-1},\\
\dot s_{r-1} &\in -\lambda_0 L\operatorname{sign}(s_r - \dot s_{r-2}) + [-L, L].
\end{aligned} \tag{2.18}$$

Solutions of (2.3), (2.15), (2.16) correspond to solutions of the Filippov differential inclusion (2.6), (2.17), (2.18). Assign the weights $r-i$ to $s_i, \sigma^{(i)}, i = 0, 1, \dots, r-1$, and obtain a homogeneous differential inclusion (2.6), (2.17), (2.18) of the degree -1. Let the initial conditions belong to some ball in the space $s_i, \sigma^{(i)}$. Due to the finite-time stability of the differentiator part (2.18) of the inclusion, it collapses in a bounded finite time, and the controller becomes equivalent to (2.5), which is uniformly finite-time stabilizing by assumption. Due to the boundedness of the control no solution leaves some larger ball till the moment, when $s \equiv 0, \dots, s_{r-1} \equiv 0$ is established. Hence, (2.6), (2.17), (2.18) is also globally uniformly finite-time stable. Theorems 2.1, 2.2 finish the proof. □

In the absence of measurement noises the convergence time is bounded by a continuous function of the initial conditions in the space $\sigma, \dot\sigma, \dots, \sigma^{(r-1)}, s_0, s_1, \dots, s_{r-1}$. This function is homogeneous of the weight 1 and vanishes at the origin (Theorem 2.1). Let σ measurements be carried out with a sampling interval τ, or let them be corrupted by a noise being an unknown bounded Lebesgue-measurable function of time of the magnitude ε, then solutions of (2.3), (2.15), (2.16) are infinitely extendible in time under the assumptions of Section 2.2, and the following Theorem is a simple consequence of Theorem 2.2.

Theorem 2.5. *The discrete-measurement version of the controller (2.15), (2.16) with the sampling interval provides in the absence of measurement noises for the inequalities*

$$|\sigma| < \delta_0\varepsilon, |\dot\sigma| < \delta_1\varepsilon^{(r-1)}, \dots, \sigma^{(r-1)} < \delta_{r-1}$$

for some $\gamma_0, \gamma_1, \ldots, \gamma_{r-1} > 0$. *In the presence of a measurement noise of the magnitude* ε *the accuracies*

$$|\sigma| < \sigma_0 \varepsilon, |\dot{\sigma}| < \delta_1 \varepsilon^{(r-1)/r}, \ldots, \sigma^{(r-1)} < \delta_{r-1} \varepsilon^{1/r}$$

are obtained for some $\delta_0, \delta_1, \ldots, \delta_{r-1} > 0$.

The asymptotic accuracy provided by Theorem 2.5 is the best possible with discontinuous $\sigma^{(r)}$ and discrete sampling [32]. A Theorem corresponding to the case of discrete noisy sampling is also easily formulated basing on Theorem 2.2. Note that the lacking derivatives can be also estimated by means of divided finite differences, providing for robust control with homogeneous sliding modes [38]. The results of this Section are also valid for the sub-optimal controller [4]. Hence, actually the problem stated in Section 2.2 is solved.

2.7 Adjustment of the Controllers

It is shown here that the control amplitude can be taken variable, and a procedure is presented for the adjustment of the coefficients in order to get a needed convergence rate.

2.7.1 Control Magnitude Adjustment

Condition (2.4) is rather restrictive and is mostly only locally fulfilled, which implies only local (or semi-global) applicability of the described approach in practice. Indeed, one needs to take the control magnitude large enough for the whole operational region. Consider a more general case, when as previously

$$\sigma^{(r)} = h(t,x) + g(t,x)u,$$

but h might be not bounded, and g might be not separated from zero. Instead, assume that a locally bounded Lebesgue-measurable non-zero function $\Phi(t,x)$ be available, such that for any positive d with sufficiently large α the inequality

$$\alpha g(t,x)\Phi(t,x) > d + |h(t,x)|$$

holds for any t,x. The goal is to make the control magnitude a feedback adjustable function. It is also assumed that, if σ remains bounded, trajectories of (2.1) are infinitely extendible in time for any Lebesgue-measurable control $u(t,x)$ with bounded quotient u/Φ. This assumption is needed only to avoid finite-time escape. In practice the system is often required to be weakly minimum phase. Note also that actuator presence might in practice prevent effectiveness of any global control due to saturation effects. For simplicity the full information on the system state is assumed available. In particular, t,x,σ and its $r-1$ successive derivatives are measured. Consider the controller

$$u = -\alpha\Phi(t,x)\Psi_{r-1,r}(\sigma, \dot{\sigma}, \ldots, \sigma^{(r-1)}), \tag{2.19}$$

where $\alpha > 0$, and $\Psi_{r-1,r}$ is one of the two r-sliding homogeneous controllers introduced in Subsection 2.5.2.

Theorem 2.6. *[42]. With properly chosen parameters of the controller Ψ_{r-1},r and sufficiently large $\alpha > 0$ controller (2.19) provides for the finite-time establishment of the identity $\sigma \equiv 0$ for any initial conditions. Moreover, any increase of the gain function Φ does not interfere with the convergence.*

While the function Φ can be chosen large to control exploding systems, it is also reasonable to make the function Φ decrease and even vanish, when approaching the system operational point, therefore reducing the chattering [42, 44]. Note that controller (2.19) is not homogeneous. The global-convergence differentiator (2.10) with variable parameter L [34] can be implemented here resulting in an output feedback.

2.7.2 Parameter Adjustment

Controller parameters presented in Section 2.5 provide for the formal solution of the stated problem. Nevertheless, in practice one often needs to adjust the convergence rate, either to slow it down relaxing the requirements to actuators, or to accelerate it in order to meet some system requirements. Note in that context that redundantly enlarging the magnitude parameter of controllers from Section 2.5 does not accelerate the convergence, but only increases the chattering, while its reduction may lead to the convergence loss. The main procedure is to take the controller

$$u = \lambda^r \alpha \Psi_{r-1,r}(\sigma, \dot{\sigma}/\lambda, \ldots, \sigma^{(r-1)}/\lambda^{r-1}), \quad \lambda > 0.$$

instead of

$$u = -\alpha \Psi_{r-1,r}(\sigma, \dot{\sigma}, \ldots, \sigma^{(r-1)})$$

providing for the approximately λ times reduction of the convergence time. Exact formulations (Levant et al., 2006b) are omitted here in order to avoid unnecessary complication. In the case of quasi-continuous controllers (Section 2.5) the form of controller is preserved. The new parameters $\tilde{\beta}_1, \ldots, \tilde{\beta}_{r-1}, \tilde{\alpha}$ are calculated according to the formulas $\tilde{\beta}_1 = \lambda\beta_1, \tilde{\beta}_2 = \lambda^{r/(r-1)}\beta_2, \ldots, \tilde{\beta}_{r-1} = \lambda^{r/2}\beta_{r-1}, \tilde{\alpha} = \lambda^r\alpha$. Following are the resulting quasi-continuous controllers with $r \leq 4$, simulation-tested β_i and a general gain function Φ:

1. $u = -\alpha\Phi \mathrm{sign}\sigma$
2. $u = -\alpha\Phi(\dot{\sigma} + \lambda|\sigma|^{1/2}\mathrm{sign}\sigma)/(|\dot{\sigma}| + \lambda|\sigma|^{1/2})$,
3. $u = -\alpha\Phi[\ddot{\sigma} + 2\lambda^{3/2}(|\dot{\sigma}| + \lambda|\sigma|^{2/3})^{-1/2}(\dot{\sigma} + \lambda|\sigma|^{2/3}\mathrm{sign}\sigma)]/[|\ddot{\sigma}| + 2\lambda^{3/2}(|\dot{\sigma}| + \lambda|\sigma|^{2/3})^{1/2}]$,
4. $\phi_{3,4} = \dddot{\sigma} + 3\lambda^2[\ddot{\sigma} + \lambda^{4/3}(|\dot{\sigma}| + 0.5\lambda|\sigma|^{3/4})^{-1/3}(\dot{\sigma} + 0.5\lambda|\sigma|^{3/4}\mathrm{sign}\sigma)]$
$[|\ddot{\sigma}| + \lambda^{4/3}(|\dot{\sigma}| + 0.5\lambda|\sigma|^{3/4})^{2/3}]^{-1/2}$,

$$N_{3,4} = |\dddot{\sigma}| + 3\lambda^2[|\ddot{\sigma}| + \lambda^{4/3}(|\dot{\sigma}| + 0.5\lambda|\sigma|^{3/4})^{2/3}]^{1/2},$$
$$u = -\alpha\Phi\phi_{3,4}/N_{3,4}.$$

2.8 Advanced Issues

Chattering analysis and attenuation, robustness issues, and choosing the controller parameters are considered here.

2.8.1 Chattering Analysis

The following presentation follows [36]. The notion of mathematical chattering inevitably depends on the time and coordinate scales. For example, the temperature measured at some fixed place in London does not fluctuate much in one hour, but if the time is measured in years, then the chattering is very apparent. At the same time, compared with the temperature on Mercury, these vibrations are negligible. Thus, the chattering of a signal is to be considered with respect to some nominal signal, which is known from the context. Consider an absolutely continuous scalar signal $\xi(t) \in \mathbb{R}, t \in [0,T]$. Also let $\bar{\xi}$ be an absolutely continuous nominal signal, such that ξ is considered as its disturbance. Let $\Delta\xi = \xi - \bar{\xi}$, and introduce virtual dry (Coloumb) friction, which is a force of constant magnitude k directed against the motion vector $\Delta\dot{\xi}(t)$. Its work ("heat release") during an infinitesimal time increment dt equals $-k\text{sign}(\Delta\dot{\xi})\Delta\dot{\xi}dt = -k|\Delta\dot{\xi}|dt$. Define the L_1-chattering of the signal $\xi(t)$ with respect to $\bar{\xi}(t)$ as the energy required to overcome such friction with $k = 1$, i.e.

$$L_1 - \text{chat}(\xi, \bar{\xi}; 0, T) = \int_0^T |\dot{\xi}(t) - \dot{\bar{\xi}}|dt.$$

In other words, L_1-chattering is the distance between $\dot{\xi}$ and $\dot{\bar{\xi}}$ in the L_1-metric, or the variation of the signal difference $\Delta\xi$. Similarly, considering virtual viscous friction proportional to $\Delta\dot{\xi}$, obtain L_2-chattering. Other power models of friction produce L_p-chattering, p ¿ 1, which is defined in the obvious way. If the nominal signal $\bar{\xi}$ is not defined, the linear signal $\xi(0) + t(\xi(T) - \xi(0))/T$ is naturally used for the comparison. The three last arguments of the chattering function can be omitted in the sequel, if they are known from the context. Let $x(t) \in \mathbb{R}^n, t \in [0,T]$, be an absolutely continuous vector function, and $M(t,x)$ be some positive-definite continuous symmetric matrix with the determinant separated from 0. The chattering of the trajectory $x(t)$ with respect to $\bar{x}(t)$ is defined as

$$L_p - \text{chat}(x, \bar{x}, 0, T) = \{\int_0^T [(\dot{x}^t(t) - \dot{\bar{x}}^t)M(t,x)(\dot{x}(t) - \dot{\bar{x}})]^{p/2}dt\}^{1/p}.$$

The matrix M is introduced here to take into account a local metric. Note that with $M = I$ the L_1-chattering is the length of the curve $x(t) - \bar{x}(t)$.

Chattering Family. The notions introduced depend on the time scale and the space coordinates. The following notions are free of this drawback. Consider a family of absolutely continuous trajectories (signals) $x(t,\varepsilon) \in \mathbb{R}^n, t \in [0,T], \varepsilon \in \mathbb{R}^l$. The

family *chattering parameters* ε_i measure some imperfections and tend to zero. Define the nominal trajectory (signal) as the limit trajectory (signal) $\bar{x}(t) = \lim\limits_{\varepsilon\to 0} x(t,\varepsilon)$, $t \in [0,T]$. Chattering is not defined in the case when the limit trajectory $\bar{x}(t)$ does not exist or is not absolutely continuous.

- L_p-chattering is classified as infinitesimal, if the "heat release" is infinitesimal, i.e. $\lim\limits_{\varepsilon\to 0} L_p - \mathrm{chat}(x,\bar{x};0,T) = 0$;
- L_p-chattering is classified as bounded if $\overline{\lim\limits_{\varepsilon\to 0}} L_p - \mathrm{chat}(x,\bar{x};0,T) > 0$;
- L_p-chattering is classified as unbounded if the "heat release" is not bounded, i.e $\overline{\lim\limits_{\varepsilon\to 0}} Lp - \mathrm{chat}(x,\bar{x};0,T) = \infty$.

The last two chattering types are to be considered as potentially destructive. Obviously, if L_1-chattering is infinitesimal, the length of the trajectory $x(t,\varepsilon)$ tends to the length of $\bar{x}(t)$. The chattering is bounded or unbounded iff the length of $x(t,\varepsilon)$ is respectively bounded or unbounded when $\varepsilon \to 0$.

Proposition 2.1. *Let $x(t,\varepsilon)$ uniformly tend to $\bar{x}(t)$ with $\varepsilon \to 0$. Then the above classification of chattering is invariant with respect to smooth transformations of time and coordinates, and to the choice of a continuous positive-definite symmetric matrix M.*

Proof. Indeed, it follows from the uniform convergence that the trajectories are confined to a compact region. The proposition now follows from the boundedness from above and from below of the norm of the Jacobi matrix of the transformation. □

Proposition 2.2. *Let $x(t,\varepsilon)$ uniformly tend to $\bar{x}(t)$ with $\varepsilon \to 0$. Then the chattering is infinitesimal, iff the chattering of all coordinates of $x(t,\varepsilon)$ is infinitesimal. The chattering is unbounded iff the projection to some subset of the coordinates has unbounded chattering. The chattering is bounded iff it is not unbounded, and the projection to some subset of the coordinates has bounded chattering.*

Proof. This is a simple consequence of Proposition 2.2. □

Suppose now that the mathematical model of a closed-loop control system is decoupled into two subsystems,

$$\dot{x} = X_\xi(t,x,y), \dot{y} = Y_\xi(t,x,y),$$

where ε is a chattering parameter. Consider any local chattering family of that system. Then, similarly to Proposition 2.2, the above classification of the chattering of the vector coordinate x does not depend on any smooth state coordinate transformation of the form $\tilde{x} = \tilde{x}(t,x), \tilde{y} = \tilde{y}(t,x,y)$.

Assume that the chattering of the vector coordinate x of the first subsystem is considered dangerous, while the chattering of the second subsystem is not important for some practical reason. In particular, this can be the case when the vector coordinate y of the second subsystem corresponds to some internal computer variables. In the following, the first subsystem is called **main** and may contain the models of any

chattering-sensitive devices including actuators and sensors; the second subsystem is called **auxiliary**.

It is said that there is **infinitesimal** (L_p-)chattering in a closed-loop control system depending on a small vector chattering parameter if any local chattering family of *the main-subsystem* trajectories features infinitesimal chattering. The chattering is called **unbounded** if there exists a local chattering family of the main subsystem with unbounded chattering. The chattering is called **bounded** if it is not unbounded and there exists a local chattering family of the main subsystem with bounded chattering.

The least possible chattering in this classification is the infinitesimal one. In other words, infinitesimal chattering is present in any real control system, as a result of infinitesimal disturbances of a different nature. The prefix L_p- is omitted in the cases when the corresponding statement on chattering does not depend on $p \leq 1$. This is true everywhere in the sequel.

Examples. It can be shown [36] that only infinitesimal heat release is possible in mechanical systems with infinitesimal chattering. Consider a smooth dynamic system

$$\dot{x} = a(t,x) + b(t,x)u, \tag{2.20}$$

where $x \in \mathbb{R}^n, u \in R^m$.

Continuous feedback. Let system (2.20) be closed by some continuous feedback $u = U(t,x)$, and ε be the maximal magnitude of the measurement noise and control delays. Then only *infinitesimal chattering* is present in the system.

Standard sliding mode. Let $\sigma(t,x) = 0, \sigma \in \mathbb{R}^m$, be a vector constraint to be kept in the standard sliding mode. Let the vector relative degree of σ be $(1,1,\ldots,1)$, which means that

$$\dot{\sigma} = \Theta_1(t,x) + \Theta_2(t,x)u, \tag{2.21}$$

with some smooth Θ_1, Θ_2 and $\det \Theta_2 \neq 0$. Taking

$$u = -K\Theta_2^{-1}\sigma/||\sigma||, K > \sup||\Theta_1||, \tag{2.22}$$

obtain a local first-order sliding mode $\sigma \equiv 0$. Consider any regularization parameter ε having the physical sense of switching imperfections, such as switching delays, small measurement errors, hysteresis etc., which vanish when $\varepsilon = 0$. Then the VSS (2.20) - (2.22) features *bounded chattering*.

Now let (2.20) be a Single-Input Single-Output (SISO) system, $u \in \mathbb{R}, \sigma \in \mathbb{R}$, and let the relative degree be r, which means that the system can be rewritten in the form

$$\sigma^{(r)} = h(t,\theta,\Sigma) + g(t,\theta,\Sigma)u, \quad K_M \geq g \geq K_m > 0, \tag{2.23}$$

$$\dot{\theta} = \Theta(t,\theta,\Sigma), \quad \zeta \in \mathbb{R}^{n-r} \tag{2.24}$$

where $\Sigma = (\sigma, \dot{\sigma}, \ldots, \sigma^{(r-1)})$, and, without any loss of generality, the function g is assumed positive. Suppose that h be uniformly bounded in any bounded region of the space ζ, Σ and (2.24) features the Bounded-Input-Bounded-State (BIBS) property with Σ considered as the input.

High-gain control. In the case when the functions g and h are uncertain, a high-gain feedback is applied,

$$u = -ks, s = \sigma^{(r-1)} + \beta_1 \sigma^{(r-2)} + \ldots + \beta_{r-1}\sigma, \tag{2.25}$$

where $\lambda^{r-1} + \beta_1 \lambda^{r-2} + \ldots + \beta_{r-1}\lambda$ is a Hurwitz polynomial. It can be shown that, provided k is sufficiently large, such feedback provides for the semi-global convergence into a set $||\Sigma|| \leq d, d = O(1/k)$. System (2.23)-(2.25) features infinitesimal chattering with any fixed k and small noises. In order to improve the performance, one needs to increase k. It is easy to show that with the chattering parameter $\mu = 1/k \to 0$, a system with infinitesimal chattering is obtained in the absence of noise.

Now introduce some infinitesimal noise of the magnitude $\varepsilon \to 0$ in the measurements of the function s. Let possible noises be any smooth functions of time of the magnitude ε. Then the chattering in system (2.23) - (2.25) is *unbounded* with the chattering parameters $\mu = 1/k \to 0$ and $\varepsilon \to 0$. The reason is that $\sigma^{(r)}$ can start to follow the noise with $\mu = o(\varepsilon)$. This result applies also to the estimation of the chattering of multi-input multi-output (MIMO) systems. Indeed, it is sufficient to fix all feedback components except one in order to prove the possibility of unbounded chattering. Introduction of control saturation turns the chattering into *bounded*.

HOSM control. Suppose that the assumptions of Section 2.5 hold. Apply r-sliding homogeneous control (2.5). Suppose that $\sigma^{(i)}, i = 0, 1, \ldots, r-1$, is measured with noises of the magnitudes $\tilde{\gamma}_i \varepsilon^{r-i}$, and variable delays not exceeding $\tilde{\gamma}_i \varepsilon$, where $\tilde{\gamma}_i, \gamma_i$ are some positive constants. Then (Sections 2.5, 2.6) the accuracy $|\sigma| < a_0 \varepsilon^r, |\dot{\sigma}| < a_1 \varepsilon^{r-1}, \ldots, |\sigma^{(r-1)}| < a_{r-1}\varepsilon$ is established in finite time with some positive constants $a_0, a_1, \ldots, a_{r-1}$ independent of ε. The result does not change when only σ is measured and all its derivatives are estimated by means of an (r-1)th order robust differentiator. Note that with $\varepsilon = 0$ the exact r-sliding mode $\sigma \equiv 0$ is established. The above connection between the measurement noise magnitudes and delays is not restrictive, since in reality there are concrete noises and delays, which can be considered as samples of a virtual family indexed by ε in a non-unique way. Moreover, actual noise magnitudes can be lower, preserving the same upper estimations and the worst-case asymptotics. Following from the above result, there is no unbounded chattering in the system (2.2), (2.5). Indeed, after the coordinates are chosen as in (2.23), (2.24), it is obvious that the only coordinate which can reveal bounded or unbounded chattering is $\sigma^{(r-1)}$. Its chattering function is bounded due to the boundedness of $\sigma^{(r)}$. Thus, unbounded chattering is impossible. In fact there is *bounded* chattering in that case.

Chattering Attenuation. The chattering attenuation procedure [30, 36] is based on treating the derivative $u^{(l)}$ as a new control. As a result, the relative degree is artificially increased to $r + l$, and $u^{(i)}, i = 0, \ldots, l-1$, are included in the set

of coordinates. Global ($r = l = 1$) [30, 34] or semiglobal [40] convergence is ensured for the $(r+l)$-sliding mode. As follows from Sections 2.5, 2.6 the accuracies $\sigma = O(\varepsilon^{r+l}), \dot{\sigma} = O(\varepsilon^{r+l-1}), \ldots, \sigma^{(r)} = O(\varepsilon^{l})$ are obtained with time delays of the order of ε and the measurement errors of $\sigma^{(i)}$ being $O(\varepsilon^{r+l-i})$. Thus, only infinitesimal chattering takes place in that case. Moreover, chattering functions of the plant trajectories are of the order $O(\varepsilon^{l})$. These results are trivially extended to the MIMO case with a vector relative degree and a vector sliding order.

2.8.2 Robustness Issues

Practical application of any control approach requires its robustness to be shown with respect to inevitably present imperfections. In more general perspective such robustness can be considered as an important case of the approximability property [9]. In reality the control u affects the system via an additional dynamic system called actuator, while the sliding variable is estimated by another system called sensor. Also the main system does not exactly describe the real process, i.e. small perturbations exist; small delays and noises corrupt the connections (Fig. 2.2).

Moreover, the very division of a controlled system into an actuator, a plant and a sensor is not unique. For example, any actuator or sensor can always be integrated in the plant drastically changing the relative degree. Often a model with the smallest possible relative degree is chosen at the design stage. That is the main reason, why in practice relative degrees usually equal 2 or 3 and almost never exceed 5.

As it was shown, most HOSM controllers feature homogeneity properties. The robustness of homogeneous sliding modes with respect to the presence of switching imperfections, small delays, noises was proved in Sections 2.5, 2.6. The performance has recently also been shown to be robust with respect to the presence of unaccounted-for fast stable actuators and sensors [41], i.e. under the assumptions of Section 2.5 the functions $\sigma, \dot{\sigma}, \ldots, \sigma^{(r-1)}$ remain infinitesimally small. Thus, the conclusion is that such singular perturbations do not amplify the chattering, if the internal variables of actuators and sensors are excluded from the main system.

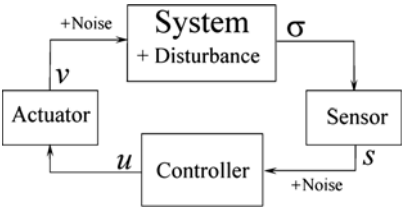

Fig. 2.2 Disturbed control system

A well-known weak point of the HOSM applications is the requirement that the relative degree of the sliding variable be well-defined, constant and known. Any small general perturbation or model inaccuracy can lead to the decrease of the relative degree, or even to its disappearance.

It is proved in the paper presented at VSS'2010 by A. Levant that the robustness is preserved when all mentioned disturbances are present simultaneously, provided an output-feedback homogeneous controller (2.15), (2.16) is applied, making use of a finite-time-stable differentiator. The differentiator is needed, though it already does not estimate derivatives of σ, since, due to the system disturbance, the output σ might be not differentiable. Also in that case the chattering is not amplified. In other words the chattering attenuation procedure is still effective.

2.8.3 Choosing the Parameters

Let the relative degree be r. Recall that the recursive construction procedures for the nested SM controllers and the quasi-continuous controllers (Section 2.5.2) involve the construction of the functions $\phi_{i,r}, i = 1,\dots,r-1$, depending on the parameters $\beta_j > 0, j = 1,\dots,i$.

Theorem 2.7. *[43] Let for some $i = 1,\dots,r-2$ the equality*

$$\phi_{i-1,r}(\sigma,\dot{\sigma},\dots,\sigma^{(i-1)}) = 0$$

define a finite-time stable differential equation, then with any sufficiently large β_i also $\phi_{i-1,r}(\sigma,\dot{\sigma},\dots,\sigma^{(i)}) = 0$ is finite-time stable. Parameters $\beta_i, i = 1,\dots,r-1$, constitute a proper choice of parameters for the corresponding r-SM controller, if the differential equation $\phi_{r-1,r}(\sigma,\dot{\sigma},\dots,\sigma^{(r-1)}) = 0$ is finite time stable.

It follows from the theorem that the parameters $\beta_1,\dots,\beta_{r-1}$ can be chosen one-by-one by means of relatively simple simulation of concrete differential equations.

2.9 Application and Simulation Examples

Only the main points of the presented results are demonstrated.

2.9.1 Control Simulation

Practical application of HOSM control is presented in a lot of papers, only to mention here [1, 6, 15, 19, 26, 44, 46, 53, 51]. Consider a simple kinematic model of car control

$$\dot{x} = V cos\phi, \dot{y} = V\sin\phi, \dot{\phi} = \tfrac{V}{\Delta}\tan\theta, \dot{\theta} = v,$$

where x and y are Cartesian coordinates of the rear-axle middle point, ϕ is the orientation angle, V is the longitudinal velocity, Δ is the length between the two axles and θ is the steering angle (i.e. the real input) (Fig. 2.3), ε is the disturbance parameter, v is the system input (control). The task is to steer the car from a given initial position to the trajectory $y = g(x)$, where $g(x)$ and y are assumed to be available in real time.

Define $\sigma = y - g(x)$. Let $V = \text{const} = 10m/s, \Delta = 5m, x = y = \phi = \theta = 0$ at $t = 0, g(x) = 10\sin(0.05x) + 5$.

The relative degree of the system is 3 and the quasi-continuous 3-sliding controller (Section 2.5.2) solves the problem. It was taken $\alpha = 2, L = 400$. The resulting output-feedback controller (2.15), (2.16) is

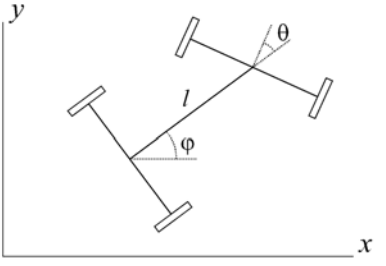

Fig. 2.3 Kinematic car model

$$v = -2[s_2 + 2(|s_1| + |s_0|^{2/3})^{-1/2}(s_1 + |s_0|^{2/3}\text{sign}s_0)]/[|s_2| + 2(|s_1| + |s_0|^{2/3})^{1/2}],$$
$$\dot{s}_0 = \varpi_0, \quad \varpi_0 = -14.74|s_0 - \sigma|^{2/3}\text{sign}(s_0 - \sigma) + s_1,$$
$$\dot{s}_1 = \varpi_1, \varpi_1 = -30|s_1 - \varpi_0|^{1/2}\text{sign}(s_1 - \varpi_0) + s_2, \dot{s}_2 = -440\text{sign}(s_2 - \varpi_1).$$

The controller parameter α is convenient to find by simulation. The differentiator parameter $L = 400$ is taken deliberately large, in order to provide for better performance in the presence of measurement errors ($L = 25$ is also sufficient, but is much worse with sampling noises). The control was applied only from $t = 1$, in order to provide some time for the differentiator convergence. The integration was carried out according to the Euler method (the only reliable integration method with discontinuous dynamics), the sampling step being equal to the integration step $\tau = 10^{-}4$. In the absence of noises the tracking accuracies $|\sigma| \le 5.4 \cdot 10^{-7}, |\dot{\sigma}| \le 2.4 \cdot 10^{-4}, |\ddot{\sigma}| \le 0.042$ were obtained. With $\tau = 10^{-5}$ the accuracies $|\sigma| \le 5.6 \cdot 10^{-10}, |\dot{\sigma}| 1.4 \cdot 10^{-5}, |\ddot{\sigma}| \le 0.0042$ were attained, which mainly corresponds to the asymptotics stated in Theorem 2.5. The car trajectory, 3-sliding tracking errors, steering angle θ and its derivative u are shown in Fig. 2.4a, b, c, d respectively. It is seen from Fig. 2.4c that the control u remains continuous until the very entrance into the 3-sliding mode. The steering angle θ remains rather smooth and is quite feasible.

Robustness of HOSM. Consider now a disturbed kinematic model

$$\dot{x} = V(\cos\phi + \varepsilon\sin(\theta + v + 0.1)), \dot{y} = V(\sin\phi - \varepsilon\sin(\theta + v - 0.1)),$$
$$\dot{\phi} = \frac{V}{\Delta}\tan\theta, \dot{\theta} = v,$$

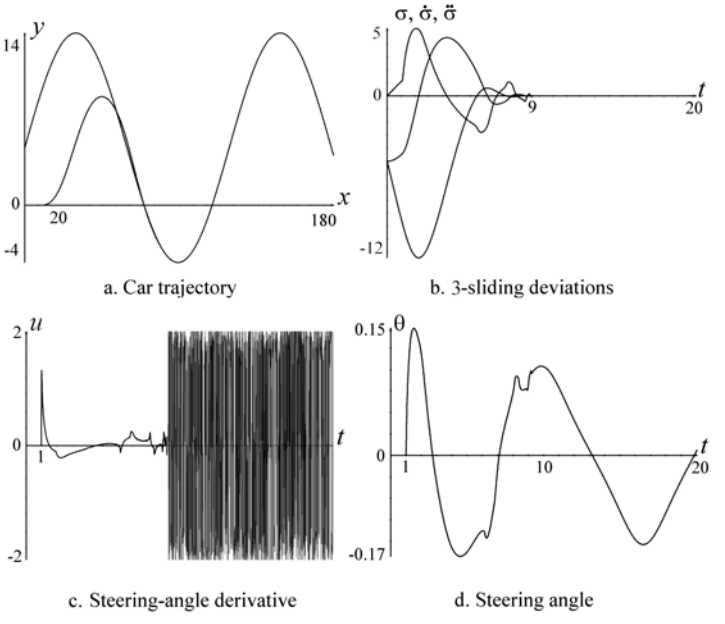

Fig. 2.4 Quasi-continuous 3-sliding car control

where ε is the disturbance magnitude and apply the same control. Let the actuator and the sensor be described by the systems

$$\begin{aligned}
&\mu\dot{z}_1 = z_2,\\
&\mu\dot{z}_2 = -2(2-0.5\sin(t+1))\mathrm{sign}(z_1-u) - 3z_2, v = z_1+\eta_1(t);\\
&\lambda\dot{\zeta}_1 = \zeta_2,\\
&\lambda\dot{\zeta}_2 = -(\zeta_1-x)^3 + (\zeta_1-x) + (1+0.2\cos t)\zeta_2,\\
&\quad s = \zeta_1 - g(x) + \eta_2(t).
\end{aligned}$$

Here u, v are the input and the output of the actuator, s is the sensor output, to be substituted for σ into the differentiator. It is taken $\zeta_1 = -10, \zeta_2 = 20, u(0) = 0, z_1(0) = z_2(0) = 0$ at $t = 0, \eta_i$ are noises, $|\eta_1| \le \varepsilon_1, |\eta_2| \le \varepsilon_2$. The actual "generalized" relative degree now is 1 (the system is not affine in control anymore). The discontinuous derivative of the steering angle directly affects the car coordinates x and y. The maximal tracking error does not exceed 0.5 meters with $\varepsilon = 0.05, \lambda = \mu = 0.02, \varepsilon_1 = 0, \varepsilon_2 = 0.1$ (Fig. 2.5). The error does not exceed 0.05 meters with $\varepsilon = 0.05, \lambda = \mu = 0.01, \varepsilon_1 = \varepsilon_2 = 0$; and 0.005m with $\varepsilon = \lambda = \mu = 0.001, \varepsilon_1 = \varepsilon_2 = 0$.

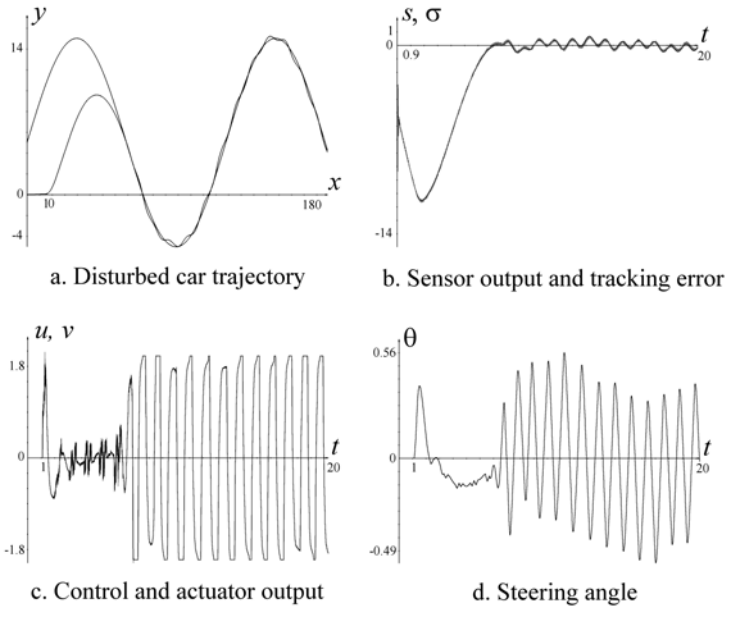

Fig. 2.5 Output regulation of the perturbed model with $\varepsilon = 0.05, \lambda = \mu = 0.02, \varepsilon_1 = 0, \varepsilon_2 = 0.1$

Chattering of Aircraft Pitch Control. The chattering of a mechanical actuator is demonstrated here. A practical aircraft control problem [44] is to get the pitch angle θ of a flying platform to track some signal θ_c given in real time. The actual nonlinear dynamic system is given by its linear 5-dimensional approximations, calculated for 42 equilibrium points within the Altitude - Mach flight envelope and containing significant uncertainties. The relative degree is 2. Details are presented in [44]. The actuator (stepper motor servo) output v is to follow the input u. The output v changes its value 512 times per second with a step of ± 0.2, or remains the same. It gets the input 64 times per second and stops to react for 1/32 s each time, when $\text{sign}(u - v)$ changes. The actuator output has the physical meaning of the horizontal stabilizer angle, and its significant chattering is not acceptable.

Following are unpublished simulation results (1994) revealing the chattering features of a linear dynamic control based on the H_∞ approach and a 3-sliding-mode control practically applied afterwards in the operational system (1997). In order to produce a Lipschitzian control, the 3-sliding-mode controller was constructed according to the described chattering attenuation procedure. The comparison of the performances is shown in Fig. 2.6. The control switches from the linear control to the 3-sliding-mode control at $t = 31.5$. The chattering is caused by the inevitably relatively large linear-control gain.

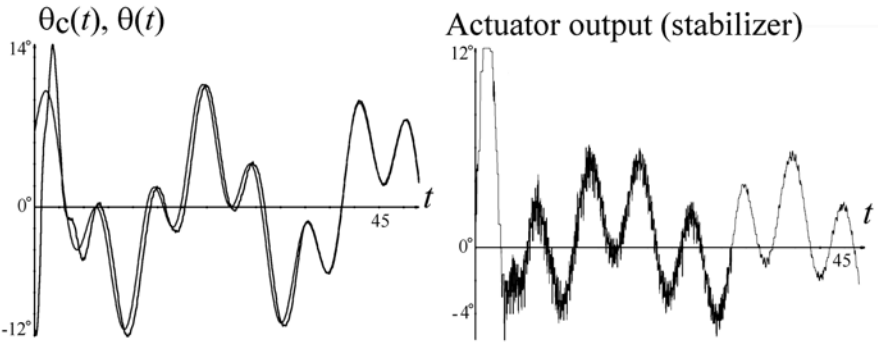

Fig. 2.6 Chattering of the aircraft horizontal stabilizer: a switch from a linear control to a 3-sliding one

2.9.2 *Signal Processing: Real-Time Differentiation*

Following is the 5th order differentiator:

$$\begin{aligned}
\dot{z}_0 &= v_0, v_0 = -8L^{1/6}|z_0 - f(t)|^{5/6}\mathrm{sign}(z_0 - f(t)) + z_1,\\
\dot{z}_1 &= v_1, v_1 = -5L^{1/5}|z_1 - v_0|^{4/5}\mathrm{sign}(z_1 - v_0) + z_2,\\
\dot{z}_2 &= v_2, v_2 = -3L^{1/4}|z_2 - v_1|^{4/5}\mathrm{sign}(z_2 - v_1) + z_3,\\
\dot{z}_3 &= v_3, v_3 = -2L^{1/3}|z_3 - v_2|^{4/5}\mathrm{sign}(z_3 - v_2) + z_4,\\
\dot{z}_4 &= v_4, v_4 = -1L^{1/2}|z_4 - v_3|^{4/5}\mathrm{sign}(z_4 - v_3) + z_5,\\
\dot{z}_5 &= -1.1L\mathrm{sign}(z_5 - v_4); \quad f^{(6)} \le L.
\end{aligned}$$

It is applied with $L = 1$ for the differentiation of the function

$$f(t) = \sin 0.5t + \cos 0.5t, |f^{(6)}| \le L = 1.$$

The initial values of the differentiator variables are taken zero. In practice it is reasonable to take the initial value of z_0 equal to the current sampled value of $f(t)$, significantly shortening the transient. Convergence of the differentiator is demonstrated in Fig. 2.7. The 5th derivative is not exact due to the software restrictions (insufficient number of valuable digits within the long double precision format). Higher order differentiation requires special software to be used.

Differentiation with Variable Parameter L. Consider a differential equation

$$y^{(4)} + \dddot{y} + \ddot{y} + \dot{y} = (\cos 0.5t + 0.5\sin t + 0.5)(\dddot{y} - 2\dot{y} + y)$$

with initial values $y(0) = 55, \dot{y}(0) = -100, \ddot{y}(0) = -25, \dddot{y}(0) = 1000$. The measured output is $y(t)$, the parametric function

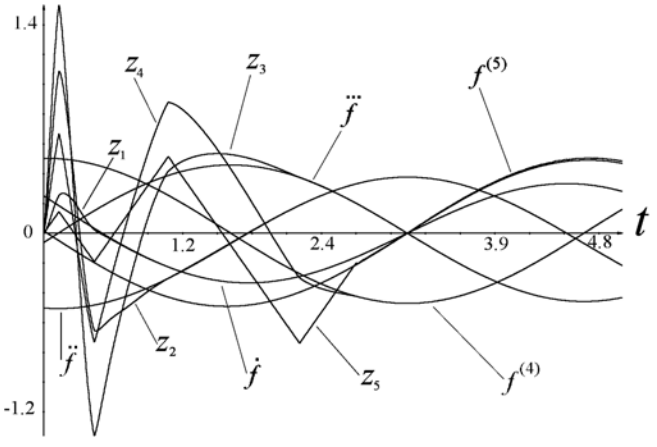

Fig. 2.7 5th order differentiation

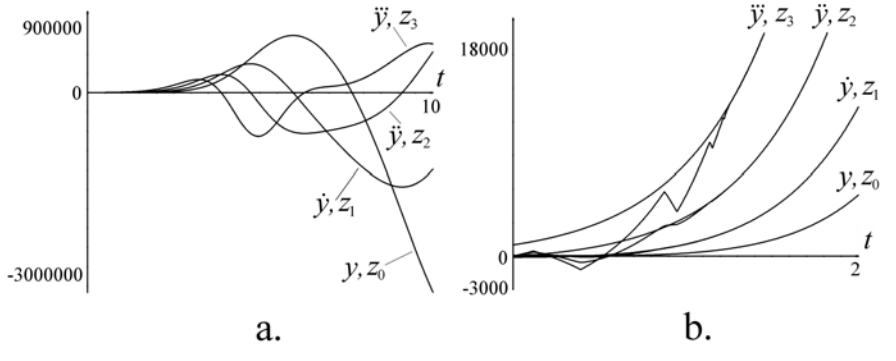

Fig. 2.8 Variable parameter L. The input signal and its derivatives (a), convergence of the differentiator (b)

$$L(t) = 3(y^2 + \dot{y}^2 + \ddot{y}^2 + \dddot{y}^2 + 36)^{1/2}$$

is taken. The third order differentiator (2.10) is taken with $\lambda_0 = 1.1, \lambda_1 = 1.5, \lambda_2 = 2, \lambda_3 = 3$. The initial values of the differentiator are $z_0(0) = 10, z_1(0) = z_2(0) = z_3(0) = 0$. The graphs of $y, \dot{y}, \ddot{y}, \dddot{y}$ are shown in Fig. 2.8a. It is seen that the functions tend to infinity fast. In particular they are "measured" in millions, and $y^{(4)}$ is about $7.5 \cdot 10^6$ at $t = 10$. The accuracies $|z_0 - y| \le 6.0 \cdot 10^{-6}, |z_1 - \dot{y}| \le 1.1 \cdot 10^{-4}, |z_2 - \ddot{y}| \le 0.97, |z_3 - \dddot{y}| \le 4.4 \cdot 10^3$ are obtained with $\tau = 10^{-4}$. In the graph scale of Fig. 2.8a the estimations z_0, z_1, z_2, z_3 cannot be distinguished respectively from $y, \dot{y}, \ddot{y}, \dddot{y}$. Convergence of the differentiator outputs during the first

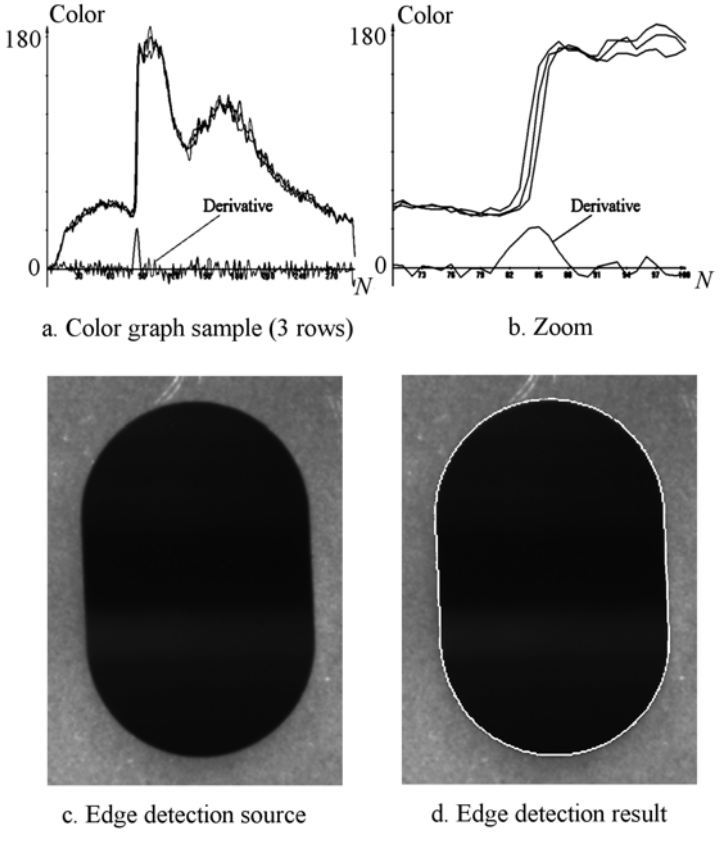

Fig. 2.9 Edge detection

2 time units is demonstrated in Fig. 2.8b. Note that also here the graph of z_0 cannot be distinguished from the graph of y. The normalized coordinates $\sigma_0(t) = (z_0(t) - y(t))/L(t), \sigma_1(t) = (z_1(t) - \dot{y}(t))/L(t), \sigma_2(t) = (z_2(t) - \ddot{y}(t))/L(t), \sigma_3(t) = (z_3(t) - \dddot{y}(t))/L(t)$ get the accuracies $|\sigma_0| \le 6.9 \cdot 10^{-16}, |\sigma_1| \le 1.2 \cdot 10^{-11}, |\sigma_2| \le 1.0 \cdot 10^{-7}, |\sigma_3| \le 4.6 \cdot 10^{-4}$ with $\tau = 10^{-4}$. With $\tau = 10^{-3}$ the accuracies change to $|\sigma_0| \le 2.0 \cdot 10^{-12}, |\sigma_1| \le 5.0 \cdot 10^{-9}, |\sigma_2| \le 5.2 \cdot 10^{-6}, |\sigma_3| \le 2.4 \cdot 10^{-3}$.

2.9.3 Image Processing

A gray image is represented in computers as a noisy function given on a planar grid, which takes integer values in the range 0 - 255. In particular, 0 and 255 correspond to the black and to the white respectively. An edge point is defined as a point of the maximal gradient. Samples of 3 successive rows from a real gray photo are presented in Fig. 2.9a together with the results of the first-order differentiation (2.10)

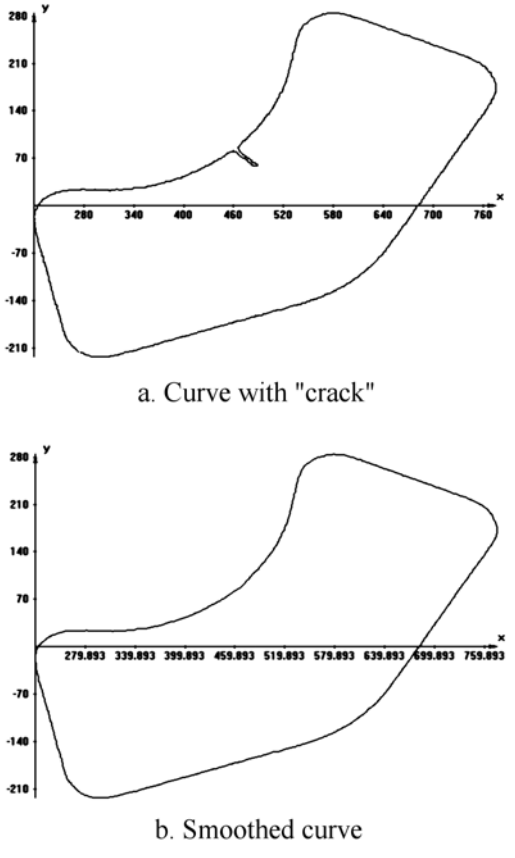

Fig. 2.10 Smoothing a curve

of their arithmetical average, $L = 3$. The differentiation was carried out in both directions, starting from each row end, and the arithmetical average was taken exterminating lags. A zoom of the same graph in a vicinity of an edge point is shown in Fig. 2.9b. Some results of the edge detection are demonstrated in Fig. 2.9c,d. These results were obtained by the author in the framework of a practical research project fulfilled by the Institute of Industrial Mathematics (Beer-Sheva, Israel, 2000) for Cognitense Ltd. The simplicity of the differentiator application allows easy tangent line calculation for a curve in an image. It is shown in Fig. 2.10 how a crack of the edge of a piece given by a photo is found and eliminated (the edge was already previously found, and its points were numbered).

2.10 Conclusions

The sliding-mode order approach allows the exact finite-time stabilization at zero of sliding variables with high relative degrees. Homogeneity features of dynamical systems and differential inclusions greatly simplify the proofs of finite-time convergence and provide for the easy calculation of the asymptotical accuracy in the presence of delays and measurement errors. The homogeneity approach provides a convenient effective framework for the design of high-order sliding mode controllers. Dangerous forms of the chattering effect are effectively treated without compromising the main advantages of sliding-mode control. The approach features ultimate robustness with respect to the presence of unaccounted-for fast dynamics of stable actuators and sensors, model inaccuracies changing the relative degrees, measurement errors and delays. Non-homogeneous versions of the developed controllers and differentiators provide for the global applications removing the boundedness conditions.

References

1. Aguilar-Lopez, R., Martinez-Guerra, R., Puebla, H., Hernandez-Suerez, R.: High order sliding-mode dynamic control for chaotic intracellular calcium oscillations. Nonlinear Analysis: Real World Applications 11(1), 217–231 (2010)
2. Atassi, A.N., Khalil, H.K.: Separation results for the stabilization of nonlinear systems using different high-gain observer designs. Systems & Control Letters 39 (2000)
3. Bacciotti, A., Rosier, L.: Liapunov functions and stability in control theory. Springer, London (2005)
4. Bartolini, G., Ferrara, A., Usai, E.: Chattering avoidance by second-order sliding mode control. IEEE Transaction on Automatic Control 43(2), 241–246 (1998)
5. Bartolini, G., Ferrara, A., Usai, E., Utkin, V.: On multi-input chattering-free second-order sliding mode control. IEEE Transaction on Automatic Control 45(9), 1711–1717 (2000)
6. Bartolini, G., Pisano, A., Punta, E., Usai, E.: A survey of applications of second-order sliding mode control to mechanical systems. International Journal of Control 76(9/10), 875–892 (2003)
7. Bartolini, G., Pisano, A., Usai, E.: First and second derivative estimation by sliding mode technique. Journal of Signal Processing 4(2), 167–176 (2000)
8. Bartolini, G., Pisano, A., Usai, E.: Global stabilization for nonlinear uncertain systems with unmodeled actuator dynamics. IEEE Transaction on Automatic Control 46(11), 1826–1832 (2001)
9. Bartolini, G., Punta, E., Zolezzi, T.: Approximability properties for second-order sliding mode control systems. IEEE Transaction on Automatic Control 52(10), 1813–1825 (2007)
10. Bejarano, F., Fridman, L.: Unbounded unknown inputs estimation based on high-order sliding mode differentiator. In: Proc. of 48th IEEE CDC, Shanghai, China (2009)
11. Beltran, B., Ahmed-Ali, T., Benbouzid, M.: High-order sliding-mode control of variable-speed wind turbines. IEEE Transaction on Automatic Control 56(11), 3314–3321 (2009)
12. Benallegue, A., Mokhtari, A., Fridman, L.: High-order sliding-mode observer for a quadrotor UAV. International Journal of Robust Nonlinear Control 18(4), 427–440 (2008)

13. Bhat, S., Bernstein, D.: Finite time stability of continuous autonomous systems. SIAM J. Control Optim. 38(3), 751–766 (2000)
14. Boiko, I., Fridman, L.: Analysis of chattering in continuous sliding-mode controllers. IEEE Transaction on Automatic Control 50(9), 1442–1446 (2005)
15. Daniele, B., Capisani, M., Ferrara, A., Pisu, P.: Fault Detection for Robot Manipulators via Second-Order Sliding Modes. IEEE Transactions on Industrial Electronics 55(11), 3954–3963 (2008)
16. Defoort, M., Floquet, T., Kokosy, A., Perruquetti, W.: A novel higher order sliding mode control scheme. Systems & Control Letters 58, 102–108 (2009)
17. Dinuzzo, F., Ferrara, A.: Higher order sliding mode controllers with optimal reaching. IEEE Transaction on Automatic Control 54(9), 2126–2136 (2009)
18. Edwards, C., Spurgeon, S.K.: Sliding Mode Control: Theory and Applications. Taylor & Francis, Abington (1998)
19. Evangelista, C., Puleston, P., Valenciaga, F.: Wind turbine efficiency optimization. Comparative study of controllers based on second order sliding modes. International Journal of Hydrogen Energy 35(11), 5934–5939 (2010)
20. Filippov, A.F.: Differential Equations with Discontinuous Right-Hand Side. Kluwer, Dordrecht (1988)
21. Floquet, T., Barbot, J.P., Perruquetti, W.: Higher-order sliding mode stabilization for a class of nonholonomic perturbed systems. Automatica 39, 1077–1083 (2003)
22. Fridman, L.: An averaging approach to chattering. IEEE Transactions on Automatic Control 46, 1260–1265 (2001)
23. Fridman, L.: Chattering analysis in sliding mode systems with inertial sensors. International Journal of Control 76(9/10), 906–912 (2003)
24. Furuta, K., Pan, Y.: Variable structure control with sliding sector. Automatica 36, 211–228 (2000)
25. Isidori, A.: Nonlinear Control Systems, 2nd edn. Springer, New York (1989)
26. Kaveh, P., Shtessel, Y.B.: Blood glucose regulation using higher-order sliding mode control. International Journal of Robust and Nonlinear Control 18(4-5), 557–569 (2008)
27. Kobayashi, S., Suzuki, S., Furuta, K.: Adaptive vs differentiator, advances in variable structure systems. In: Proc. of the 7th VSS Workshop. Sarajevo (2002)
28. Kolmogoroff, A.N.: On inequalities between upper bounds of consecutive derivatives of an arbitrary function defined on an infinite interval. Amer. Math. Soc. Transl. 2, 233–242 (1962)
29. Krupp, D., Shkolnikov, I.A., Shtessel, Y.B.: 2-sliding mode control for nonlinear plants with parametric and dynamic uncertainties. In: Proceedings of AIAA Guidance, Navigation, and Control Conference, Denver, CO (2000)
30. Levant, A.: Sliding order and sliding accuracy in sliding mode control. International Journal of Control 58(6), 1247–1263 (1993)
31. Levant, A.: Robust exact differentiation via sliding mode technique. Automatica 34(3), 379–384 (1998)
32. Levant, A.: Higher-order sliding modes, differentiation and output-feedback control. International Journal of Control 76(9/10), 924–941 (2003)
33. Levant, A.: Homogeneity approach to high-order sliding mode design. Automatica 41(5), 823–830 (2005)
34. Levant, A.: Exact differentiation of signals with unbounded higher derivatives. In: Procedings of the 45th IEEE Conference on Decision and Control CDC 2006, San-Diego, CA, USA (2006)
35. Levant, A.: Quasi-continuous high-order sliding-mode controllers. IEEE Transaction on Automatic Control 50(11), 1812–1816 (2006)

36. Levant, A.: Chattering analysis. IEEE Transactions on Automatic Control 55(6), 1380–1389 (2010)
37. Levant, A.: Construction principles of 2-sliding mode design. Automatica 43(4), 576–586 (2007)
38. Levant, A.: Finite differences in homogeneous discontinuous control. IEEE Transaction on Automatic Control 52(7), 1208–1217 (2007)
39. Levant, A.: Robustness of homogeneous sliding modes to relative degree fluctuations. In: Proceeding of the 6th IFAC Symposium on Robust Control Design, Haifa, Israel (2009)
40. Levant, A., Alelishvili, L.: Integral high-order sliding modes. IEEE Transaction on Automatic Control 52(7), 1278–1282 (2007)
41. Levant, A., Fridman, L.: Accuracy of homogeneous sliding modes in the presence of fast actuators. IEEE Transactions on Automatic Control 55(3), 810–814 (2010)
42. Levant, A., Michael, A.: Adjustment of high-order sliding-mode controllers. International Journal of Robust Nonlinear Control 19(15), 1657–1672 (2009)
43. Levant, A., Pavlov, Y.: Generalized homogeneous quasi-continuous controllers. International Journal of Robust Nonlinear Control 18(4-5), 385–398 (2008)
44. Levant, A., Pridor, A., Gitizadeh, R., Yaesh, I., Ben-Asher, J.: Aircraft pitch control via second order sliding technique. J. of Guidance, Control and Dynamics 23(4), 586–594 (2000)
45. Man, Z., Paplinski, A., Wu, H.: A robust MIMO terminal sliding mode control for rigid robotic manipulators. IEEE Transaction on Automatic Control 39(12), 2464–2468 (1994)
46. Massey, T., Shtessel, Y.: Continuous traditional and high order sliding modes for satellite formation control. AIAA J. Guidance, Control, and Dynamics 28(4), 826–831 (2005)
47. Orlov, Y.: Finite time stability and robust control synthesis of uncertain switched systems. SIAM J. Control Optim. 43(4), 1253–1271 (2005)
48. Orlov, Y., Aguilar, L., Cadiou, J.C.: Switched chattering control vs. back-lash/friction phenomena in electrical servo-motors. International Journal of Control 76(9/10), 959–967 (2003)
49. Pisano, A., Davila, J., Fridman, L., Usai, E.: Cascade control of PM DC drives via second-order sliding-mode technique. IEEE Transactions on Industrial Electronics 55(11), 3846–3854 (2008)
50. Saks, S.: Theory of the Integral. Dover Publ. Inc., New York (1964)
51. Shtessel, Y., Shkolnikov, I.: Aeronautical and space vehicle control in dynamic sliding manifolds. International Journal of Control 76(9/10), 1000–1017 (2003)
52. Sira-Ramirez, H.: On the dynamical sliding mode control of nonlinear systems. International Journal of Control 57(5), 1039–1061 (1993)
53. Sira-Ramirez, H.: Dynamic Second-Order Sliding Mode Control of the Hovercraft Vessel. IEEE Transactions On Control Systems Technology 10(6), 860–865 (2002)
54. Slotine, J.J., Li, W.: Applied Nonlinear Control. Prentice-Hall Inc., London (1991)
55. Spurgeon, S., Goh, K., Jones, N.: An application of higher order sliding modes to the control of a diesel generator set (genset). In: Yu, X., Xu, J.X. (eds.) Proc. of the 7th VSS Workshop on Advances in Variable Structure Systems (2002)
56. Utkin, V.: Sliding Modes in Optimization and Control Problems. Springer, New York (1992)
57. Yu, X., Xu, J.: An adaptive signal derivative estimator. Electronic Letters 32(16) (1996)
58. Zinober, A.: Variable Structure and Lyapunov Control. Springer, Berlin (1994)

Chapter 3
Frequency-Domain Methods in Conventional and Higher-Order Sliding Mode Control

Igor M. Boiko

Abstract. Sliding mode control has become a mature theory and found a number of useful applications. The theory of sliding mode control is based on mostly state space models and Lyapunov approach to analysis of the convergence of the system states to the sliding surface. This approach often limits the analysis to the second-order systems. Frequency-domain methods could potentially overcome the above-mentioned limitation of the state-space approach. Yet they find limited applications in sliding mode control theory. The present article is aimed at giving an overview of some available and emerging frequency domain methods of analysis of systems having conventional and second-order sliding modes. The method of analysis of transient oscillations is given in detail. A frequency-domain criterion of finite-time convergence is presented.

3.1 Introduction

Sliding mode control theory has become a mature theory and found a number of useful applications. The theory of sliding mode (SM) control is mostly based on state space models and the Lyapunov approach to analysis of the convergence of the system states to the sliding surface. This approach often limits the analysis to the second-order systems. Frequency domain methods could potentially overcome the above-mentioned limitation inherent in the state-space approach. Yet they find limited applications in SM control theory despite introduction of these methods into SM control at the time of the initial phase of the development of the SM control theory [21,17]. The approach of [21,17] was based on the describing function method. With respect to analysis of SM control systems, methods [18,10] can be mentioned too – as allowing for frequency-domain analysis of chattering in SM control systems

Igor M. Boiko
Honeywell and University of Calgary
2500 University Dr.
NW Calgary, Alberta, T2N 1N4, Canada

L. Fridman et al. (Eds.): Sliding Modes, LNCIS 412, pp. 93–112.
springerlink.com

having relay control and affected by parasitic dynamics. It is worth noting that the above-mentioned methods can be applied to the analysis of real (non-ideal) sliding modes, which occur in the systems affected by parasitic dynamics of various kinds (of sensors and actuators, for example), and revealed as self-excited oscillations or chattering. The modification of the describing function analysis presented in [9], vice versa, could potentially be applied to analysis of ideal sliding modes. After a long period of lack of interest to frequency domain methods from the SM control community, some new developments emerged in [5], and with respect to the new class of sliding mode control systems – higher-order sliding mode control systems – in [7,6].

The present article is aimed at giving a brief overview of available and perspective frequency domain methods of analysis of systems having conventional and second-order sliding modes (SOSM) and presenting a new development of the frequency-domain techniques to analysis of transient modes in SM systems.

3.2 Ideal and Real Sliding Modes: Poincare Maps and Frequency-Domain Approach

According to the SM control theory (see [19]) the system has two modes of operation: the convergence of the states to the sliding surface (the reaching phase) and the sliding along the sliding surface after the reaching phase is finished. It is also known that if the system includes some kind of parasitic dynamics then the ideal sliding along the sliding surface cannot be achieved, and high-frequency self-excited oscillations in the vicinity of the sliding surface (chattering) occur instead. The same chattering process exists not only around the sliding surface but also in the vicinity of the origin after all transients caused by the initial conditions of the system end. Generally, for the two considered cases, the system trajectories in the vicinity of the sliding surface either reveal the Lyapunov stable finite-time convergence (ideal SM) or the existence of an invariant set (SM system having parasitic dynamics) [19]. It can be shown that the size of this invariant set depends on the contribution of the parasitic dynamics, which can be estimated, for example, by the values of the time constants associated with these parasitic dynamics [8]. If instead of the state variables, the so-called sliding variable (which may be defined as a weighted sum of all the state variables) is considered then the convergence process in the system can be considered as the convergence process of the sliding variable.

The frequency-domain approach and related to this approach the Poincare map analysis use a different concept. In the case of the ideal SM, the Poincare map of the system is a series of convergent points, so that a fixed point does not exist. In the case of non-ideal SM, due to the existence of parasitic dynamics, a fixed point does exist, which corresponds to a limit cycle or a periodic motion of a certain frequency. Fig. 3.1 illustrates these two cases.

Therefore, there exist two different analysis problem related to SM control systems: analysis of the transient processes of convergence of the states in the system

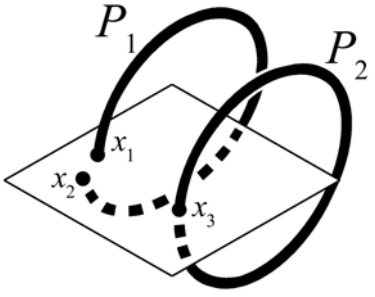

Fig. 3.1 Poincare maps: for process without limit cycle (P_1) and for process with limit cycle ($P2$)

with ideal SM, and analysis of the real SM, which occurs in the system with parasitic dynamics. The latter includes analysis of the parameters of chattering and of the input-output properties of the system (response to external disturbances and signals). It can be noted that the first problem is much more complex than the second one from the perspective of the application of frequency domain methods. In the problem of analysis of chattering or input-output properties in the system in which chattering takes place, the frequency-domain approach is a "natural" tool because a periodic process of certain frequency exists. Frequency-domain methods provide significant advantages over other methods of analysis. Among frequency-domain methods intended for this type of analysis are both approximate [9, 2] and exact [5] methods. For the analysis of convergence in the systems with ideal SM, the frequency-domain methods do not provide such visible advantages as in the former case. However, the natural feature of the frequency-domain methods of being "system order independent" may result in noticeable advantages as far as the system order is higher than two (especially if it is a high number). The following sections of the present article provide some elaboration on that. The relationship of problems and frequency-domain methods in SM control can be illustrated by the following diagram (Fig. 3.2).

Frequency-domain methods of analysis of SM in systems with parasitic dynamics, both conventional SM and second-order SM systems, were presented in a number of recent publications (see [5, 7, 6] and references within). On the contrary, frequency-domain methods of analysis of ideal sliding modes, and, therefore, analysis of transient modes (because the steady oscillatory modes do not occur) in conventional and second-order SM systems is a new area, which to our best knowledge has not been presented so far in the literature.

The following material of this article is aimed at the development of the frequency-domain approach to the analysis of transient modes in conventional and second-order SM systems, in particular at the analysis of the conditions of finite-time and asymptotic convergence.

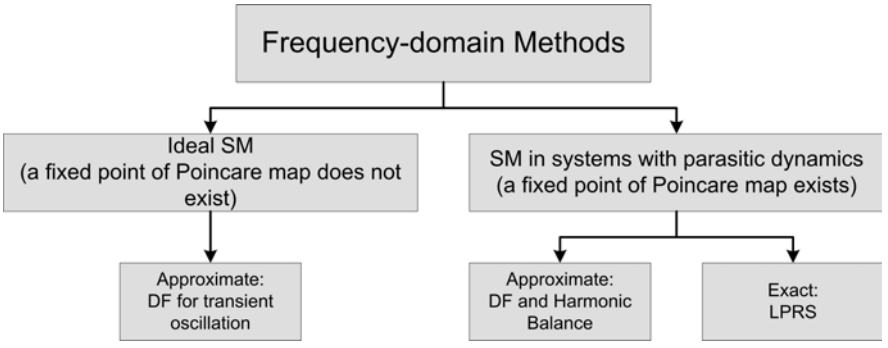

Fig. 3.2 Problems and frequency-domain methods in SM control

3.3 Analysis of Convergence – Quasi-Static DF Approach

The problems of finite-time convergence in the analysis of conventional sliding-mode (SM) and second-order sliding mode (SOSM) control systems are of great importance. In fact, an algorithm cannot be legitimately called a SOSM without proof of the finite-time convergence. There are a number of SOSM algorithms available now, for which the property of finite-time convergence has been proved, and others for which this property is still awaiting for the proof. The most popular SOSMs are "twisting", "super-twisting", "twisting-as-a-filter" [12,13], "sub-optimal" [4,3], and some others [16]. The problems of finite-time convergence and convergence rate are valid problems in the conventional SM control [19] and "terminal SM" [15,20] control too. Recently, an interest to frequency-domain analysis of SOSM systems using the describing function (DF) method [2] and other approaches was shown [7,6]. These and other publications, however, concern the problem of finding periodic motions in SOSM systems affected by parasitic dynamics of sensors and actuators. If only the principal dynamics of the system are taken into account the SOSM systems reveal converging transient motions, analysis of which requires a different approach. There exists an approach to analysis of *transient oscillations* in non-linear systems that are still based on the DF method [9]. It can be considered an extension of method [11]. The term *transient oscillations* can be used to describe a process that is oscillatory in nature and is given by a sinusoid with slowly changing frequency and amplitude, which very precisely fits the character of transients in SOSM systems. The use of a frequency-domain approach for analysis of convergence type of SOSM systems would provide a number of advantages over the direct solution of the differential equations or methods based on Lyapunov techniques. The most important one is the unification of the treatment of all the algorithms based on some frequency-domain characteristics. This in turn may lead to the formulation of some criteria that should be satisfied for a SOSM algorithm to provide a finite-time convergence, and simple rules that would allow one to develop new SOSM algorithms.

The article is organized as follows. At first we are going to consider and analyze a system comprising the twisting SOSM controller and a second-order plant – via the *quasi-static* DF approach. The frequency and the amplitude of the oscillations are found as functions of time. Then analysis of the type of convergence is considered. After that the developed approach is extended to a higher-order plant. We shall give examples throughout the article.

Filtering Hypothesis for Transient Oscillations.
One of the conditions of the applicability and validity of the DF method to analysis of self-excited oscillations is the condition of the low-pass filtering properties of the linear part (plant) of the system to be valid. In fact, the condition of the ideal low-pass filtering is assumed, so that no higher harmonics are propagated through the plant. In the case of a transient oscillation, this hypothesis cannot be directly applied because the transient oscillation is not a periodic signal and cannot be expanded into a Fourier series. Therefore, some modification and reformulation of the filtering hypothesis becomes necessary.

We will use the following transformation of the time coordinate that will allow us to obtain the oscillation of certain constant frequency (which may not be a periodic motion, as the amplitude may still be a function of time). However, for the sake of illustration of the idea we disregard the cases of variable amplitude and assume that the amplitude of the input to the nonlinearity remains constant. We consider the following input to the nonlinearity:

$$y(t) = a \sin \Psi(t) \tag{3.1}$$

where $\Psi(t) = \int_0^t \Omega(\tau) d\tau + \varphi$ is the *instantaneous phase*, is selected to satisfy the initial conditions, and $\Omega(t) = \dot{\Psi}(t)$ is the *instantaneous frequency*. The nonlinearity $u = f(y)$ produces the output $u(t) = f(y(t))$ as the reaction to the input (3.1). We formulate the filtering hypothesis as follows.

Definition 3.1. If (a) there is a system comprising serially connected nonlinearity and linear dynamics, with $y(t)$ being the input to the nonlinearity, $u(t) = f(y(t))$ being the output of the nonlinearity (input to the linear dynamics), and $y_1(t)$ being the output of the linear dynamics, and (b) there exists a transformation of time $\tau = g(t)$, $t \in [t_0; t_1]$, where t_1 can be either finite value or infinity, such that $y(\tau)$ is a periodic function of frequency $\tilde{\Omega}$, and $u(\tau) = f(y(\tau))$ can be expanded into the Fourier series as follows:

$$u(\tau) = \frac{A_0}{2} + \sum_{k=1}^{\infty} \left(A_k \cos \tilde{\Omega} \tau + B_k \sin \tilde{\Omega} \tau \right),$$

where A_k and B_k are the coefficient of the Fourier series that are calculated through known formulas, and (c) the linear dynamics have ideal low-pass filtering properties with respect to signal $u(\tau)$, so that

$$y_1(\tau) \approx a_u K_l \sin(\tilde{\Omega} t + \phi_l), \tag{3.2}$$

where $a_u = \sqrt{{A_k}^2 + {B_k}^2}$ is the amplitude of the first harmonic of the control signal, K_l is the gain of the linear dynamics (at frequency $\tilde{\Omega}$), ϕ_l is the phase shift (lag) of the linear dynamics (at frequency $\tilde{\Omega}$), then we say that the linear dynamics possess the *ideal low-pass filtering* (LPF) property.

We should note that no frequency-dependent amplitude attenuation and phase lag is assumed in formula (3.2), which cannot be true in real life. For that reason it is termed as the *ideal low-pass filtering*. Fig. 3.3 illustrates the idea of the first harmonic in a signal of time-varying frequency and the ideal LPF for a transient oscillation. Every linear dynamics that have LPF property also have frequency-dependent amplitude attenuation (which in fact is the same property: the former follows from the latter). Therefore, practical (or real) LPF property will be different from the ideal one because gain K_l and phase lag ϕ will be frequency-dependent. The output of the linear dynamics that possess real LPF property as a function of the original time is given by the following formula:

$$y_1(t) \approx a K_l(\Omega, a, \dot{a}) \sin(\Psi(t) + \phi_l(\Omega, a, \dot{a})), \tag{3.3}$$

where $\Omega(t) = \dot{\Psi}(t)$, and $K_l(\Omega, a, \dot{a})$ is the gain of the linear dynamics, $\phi_l(\Omega, a, \dot{a})$ is the phase shift (lag) of the linear dynamics.

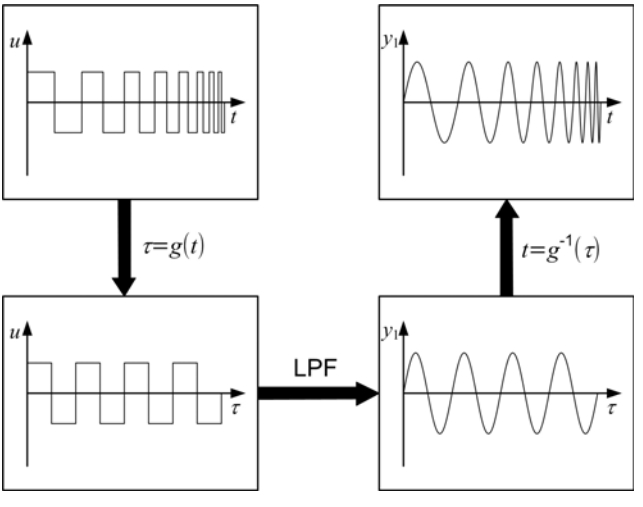

Fig. 3.3 First harmonic and ideal low-pass filtering for signal of variable frequency

Formula (3.3) constitutes the quasi-static formulation of the real LPF property of the linear dynamics, which enables us to use the so-called quasi-static approach to the DF analysis of transient oscillations [9].

Describing Function Analysis of Second-Order Systems with SOSM.
We now carry out a frequency-domain analysis of the transient process in a SOSM control system. Let the plant be given as follows:

$$\begin{aligned} \dot{\mathbf{x}} &= \mathbf{A}\mathbf{x} + \mathbf{B}u \\ y &= \mathbf{C}\mathbf{x}, \end{aligned} \tag{3.4}$$

and the controller be the "twisting" SOSM controller [12] given as follows:

$$u = -c_1 \cdot \operatorname{sign} y - c_2 \cdot \operatorname{sign} \dot{y}, \tag{3.5}$$

We shall first consider the case of the second-order system with

$$\mathbf{A} = \begin{bmatrix} 0 & 1 \\ -a_1 & -a_2 \end{bmatrix}, \mathbf{B} = \begin{bmatrix} 0 & b_2 \end{bmatrix}^{\mathrm{T}}, \mathbf{C} = \begin{bmatrix} 1 & 0 \end{bmatrix}, a_1 \geq 0, a_2 > 0, b_2 > 0.$$

We shall also use the transfer function of the plant determined in accordance with (3.4) as $W_l(s) = b_2/(s^2 + a_2 s + a_1)$. However, we note that the transfer function is used as a format of the dynamics description rather than as a method of analysis and it is only used as a method of analysis where it is explicitly stated. We apply the describing function method (DF) in the following *quasi-static* formulation [9]. Assume that the plant is a low-pass filter, and $y(t)$ is a damped oscillation of variable frequency, so that $a(t)$ is the *instantaneous amplitude* and $\Psi(t)$ is the *instantaneous phase* of oscillations of $y(t)$:

$$y(t) = a(t) \sin \Psi(t), \tag{3.6}$$

with the same meaning of the variables as in formula (3.1). Replace the nonlinearities in equation (3.5) with their DFs – like in [8]. For the first relay:

$$N_1(a) = \frac{4c_1}{\pi a}, \tag{3.7}$$

and for the second relay

$$N_2(a^*) = \frac{4c_2}{\pi a^*}, \tag{3.8}$$

where a^* is the instantaneous amplitude of $\dot{y}(t)$, which still needs to be obtained. Find amplitude a^* via differentiating (3.6).

$$\dot{y}(t) = a(t) \left[\sigma(t) \sin \Psi(t) + \Omega(t) \cos \Psi(t) \right], \tag{3.9}$$

where $\sigma(t) = \dot{a}(t)/a(t)$ is the *instantaneous decay*. Therefore, $a^* = a\sqrt{\sigma^2(t) + \Omega^2(t)}$, and the DF for the second relay can be rewritten as

$$N_2(a) = \frac{4c_2}{\pi a \sqrt{\sigma^2 + \Omega^2}}. \tag{3.10}$$

Now we write the formula for the transfer function of the closed-loop system via replacing the nonlinearities with respective DFs:

$$W_{cl}(s) = \frac{(N_1(a) + sN_2(a))b_2}{s^2 + (a_2 + N_2(a)b_2)s + a_1 + N_1(a)b_2}.$$

The characteristic equation of the closed-loop system is, therefore,

$$s^2 + 2\xi\omega_n s + {\omega_n}^2 = 0, \tag{3.11}$$

where $\xi = 0.5(a_2 + N_2(a)b_2)/\sqrt{a_1 + N_1(a)b_2}$, $\omega_n = \sqrt{a_1 + N_1(a)b_2}$. (Note: the characteristic equation can also be obtained through other approaches; finding the denominator of the transfer function of the closed-loop system is only one of them. We emphasize that this transfer function cannot be used for analysis of the propagation of the signals through the closed-loop system; it is used here as a means of deriving the characteristic equation). The instantaneous decay is:

$$\sigma(t) = -\xi\omega_n = -0.5(a_2 + N_2(a)b_2) \tag{3.12}$$

By definition, the instantaneous decay provides the instantaneous rate of the amplitude change: $\sigma(t) = \dot{a}(t)/a(t)$. The instantaneous amplitude can be found via solving the following differential equation:

$$\dot{a}(t) = a(t)\sigma(t), \quad a(0) = a_0. \tag{3.13}$$

The formulas for the instantaneous decay and instantaneous frequency are as follows.

$$\sigma(t) = -0.5\left(a_2 + \frac{4c_2b_2}{\pi a(t)\sqrt{\sigma^2(t) + \Omega^2(t)}}\right), \tag{3.14}$$

$$\Omega(t) = 0.5\sqrt{4\left(a_1 + \frac{4c_1b_2}{\pi a(t)}\right) - \left(a_2 + \frac{4c_2b_2}{\pi a(t)\sqrt{\sigma^2(t) + \Omega^2(t)}}\right)^2}. \tag{3.15}$$

The formulas for the instantaneous amplitude (3.13), instantaneous decay (3.14) and instantaneous frequency (3.15) make a set of one differential and two algebraic equations. The proposed solution algorithm is as follows. Express Ω from (3.14):

$$\Omega = \sqrt{\frac{16{c_2}^2{b_2}^2}{\pi^2a^2(2\sigma + a_2)^2} - \sigma^2} \tag{3.16}$$

and substitute the expression in formula (3.15). Solve this equation for σ.

$$\sigma = -\frac{2c_2b_2}{\sqrt{\pi^2a^2a_1 + 4\pi ac_1b_2}} - \frac{a_2}{2} \tag{3.17}$$

Substitution of (3.17) in (3.13) yields the following differential equation for $a(t)$.

$$\dot{a} = -\frac{2c_2b_2a}{\sqrt{\pi^2a^2a_1 + 4\pi ac_1b_2}} - \frac{a_2}{2}a, \quad a(0) = a_0. \tag{3.18}$$

Formula (3.18) is a first-order nonlinear differential equation of the type:

$$\dot{z} = -\lambda z - g(z), \quad z(0) = z_0 > 0, \tag{3.19}$$

where $g(z) = \frac{\alpha}{\sqrt{1+\beta/z}}$, $\alpha = \frac{2c_2b_2}{\pi\sqrt{a_1}}$, $\beta = \frac{4c_1b_2}{\pi a_1}$, $\lambda = \frac{a_2}{2}$, $z = a$. The nonlinear function $g(z)$ has infinite derivative at $z = 0$, which makes the finite-time convergence of the process given by (3.18) possible. Prove it and assess the convergence time. At first prove an auxiliary lemma.

Lemma 3.1. *For the first-order nonlinear differential equation*

$$\dot{z} = -g(z), \tag{3.20}$$

where $g(z) > 0$ for all $z > 0$, and $g(0) = 0$, and the initial condition $z(0) = z_0 > 0$ the following holds. If there exists a function $h(z)$, such that $h(z) \le g(z)$ for all $z \in [0; z_0]$, $h(z) > 0$, and $h(0) = 0$, so that a finite-time convergence to zero in the equation

$$\dot{z} = -h(z) \tag{3.21}$$

takes place $\left(z(T_h) = 0, z \in [0; z_0]\right)$ then the finite-time convergence to zero in the original equation takes place too, with the convergence time $T_g \le T_h$.

Proof. Transform equation (3.20) into an equation with z being an independent variable and time being a dependent variable: $dt/dz = -1/g(z)$, from which the time can be found as $t(z) = -\int_{z_0}^{z} \frac{1}{g(z)}dz$, and the convergence time as: $T_g = -\int_{z_0}^{0} \frac{1}{g(z)}dz = \int_{0}^{z_0} \frac{1}{g(z)}dz$. Now, since $h(z) \le g(z)$ and $g(z) > 0$, $h(z) > 0$ for all $z > 0$, the following inequality holds: $T_h = -\int_{z_0}^{0} \frac{1}{h(z)}dz = \int_{0}^{z_0} \frac{1}{h(z)}dz \ge T_g$. □

Theorem 3.1. *The process of conversion of the amplitude described by (3.18) from the initial value a_0 provides finite-time conversion with the conversion time not exceeding*

$$T^* = \frac{2}{\lambda}\left(\ln\left(\lambda\sqrt{z_0} + \frac{\alpha}{\sqrt{z_0+\beta}}\right) - \ln\frac{\alpha}{\sqrt{z_0+\beta}}\right) \tag{3.22}$$

Proof. Consider equation (3.19), which is a reformulated (3.18). Replace nonlinearity $g(z)$ in it with another nonlinearity $h(z)$ such that $h(z) \le g(z), \quad z \in [0; z_0]$,

for which the finite-time conversion property can be (has been) proved. Select $h(z)$ to be $h(z) = \rho\sqrt{z}, \quad \rho > 0$. Select parameter $\rho = \frac{\alpha}{\sqrt{z_0+\beta}}$ to satisfy the requirement $h(z) \le g(z), \quad z \in [0; z_0]$. Also, note that $h(z_0) = g(z_0)$. Therefore, since $g^2(z) = \frac{\alpha^2 z}{z+\beta}$ and $h^2(z) = \frac{\alpha^2 z}{z_0+\beta}$, $g^2(z) \ge h^2(z)$ for all $z \in [0; z_0]$. Via the substitute $z_1 = \sqrt{z}$, and respectively $\dot{z} = 2z_1\dot{z}_1$, the equation containing the square root function is transformed into a linear equation: $\dot{z}_1 = -0.5\rho z_1 - 0.5\lambda$, which has a solution $z_1(t) = -\frac{\rho}{\lambda}(1 - e^{-0.5\lambda t}) + z_1(0)e^{-0.5\lambda t}$. By solving the equation $z_1(T*) = 0$ find $T*$ as given by (3.22). □

Corollary 3.1. *We also note that if parameter $c_2 = 0$ in (3.5) then, according to Theorem 3.2, $T^* \to \infty$ and asymptotic convergence takes place. In this case we have the so-called asymptotic second-order sliding mode.*

The nonlinear functions $g(z)$ and $h(z)$ for $c_1 = 50$, $c_2 = 5$ and other parameters of the above example are presented in Fig. 3.4. The considered first-order system with the square root nonlinearity (assuming also symmetric properties of the square root function for negative z) is known as having a *terminal sliding mode* (or *power-fractional sliding mode*) [15, 20], which has finite-time convergence. Since $h(z) \le g(z), \quad z \in [0; z_0]$, according to Lemma 3.1, the system (3.19) provides a faster convergence than the system with the square root nonlinearity. Time T^* serves as a higher estimate of the convergence time in system (3.18).

An example of analysis of the system with the linear plant $W_l(s) = 1/(s^2 + s + 1)$ and the twisting controller with $c_1 = 50$, $c_2 = 5$ is given in Fig. 3.5. The theoretical value of the higher estimate of the convergence time is $T^* = 4.85$, which is close to the theoretical convergence time due to closeness of functions $g(z)$ and $h(z)$ (Fig. 3.4). The theoretical analysis is given along with the simulations. One can see that the proposed approach provides a good estimate of the SOSM transient dynamics.

3.4 Frequency-Domain Characteristics and Convergence Rate

The approach to analysis of convergence of the SOSM-controlled system given above involves consideration of instantaneous amplitude, frequency and decay. Now, with those methodology and results available, we look at the problem of the existence of periodic motions, asymptotic and finite time convergence considering the condition of the harmonic balance in the system. Periodic motions can exist in the system if the Nyquist plot of the plant $W(j\omega)$ intersects the negative reciprocal of the DF $-N^{-1}(a)$ (Fig. 3.6). In Fig. 3.6, two Nyquist plots corresponding to the second- $W_1(j\omega)$ and third-order $W_2(j\omega)$ plants and two negative reciprocal DF corresponding to the relay control $-{N_1}^{-1}(a)$ and to the twisting algorithm $-{N_2}^{-1}(a)$ [7] are depicted. Intersection of $W_2(j\omega)$ with either of the DFs provides a periodic solution (points A or B) of finite frequency and amplitude. Plot $W_1(j\omega)$ does not have any points of intersection with either $-{N_1}^{-1}(a)$ or $-{N_2}^{-1}(a)$ except the origin. However, the character of the process in the system is different – depending on whether the control is an ideal relay (plot $-{N_1}^{-1}(a)$) or the SOSM control

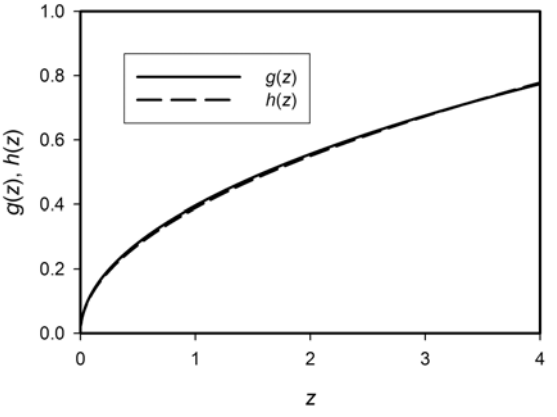

Fig. 3.4 Functions $g(z)$ and $h(z)$ of differential equation for amplitude

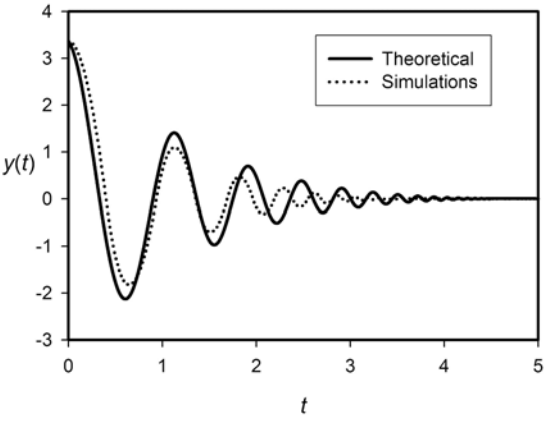

Fig. 3.5 Example of analysis of twisting SOSM controlled system

(plot $-N_2{}^{-1}(a)$). In the former case the convergence is asymptotic (see Corollary 3.1), in the second one – it is finite-time.

Let us consider the condition of the phase balance that is a part of the harmonic balance condition. For a periodic motion to occur in the system the following condition must hold:

$$\phi_l(\Omega) + \arg N(a) = -\pi, \tag{3.23}$$

where Ω is the frequency and a is the amplitude of the self-excited periodic motion, $\phi_l(\omega) = \arg W_l(j\omega)$ is the phase characteristic of the plant. Considering the plant with $W_1(j\omega)$ we should note that there is a significant difference between the

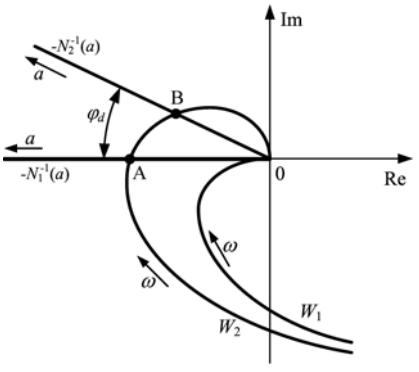

Fig. 3.6 Determination of periodic motions and decaying oscillations

controls with DFs $-{N_1}^{-1}(a)$ and $-{N_2}^{-1}(a)$. In the first case, formally speaking, there is a frequency at which the phase balance condition (3.23) holds. This frequency is $\Omega = \infty$. Therefore, we might say that in the system with $W_1(j\omega)$ and $-{N_1}^{-1}(a)$, a periodic motion of infinite frequency occurs. In the second case, a periodic motion cannot occur at any frequency (including $\Omega = \infty$). There is a condition that we shall further refer as a *phase deficit*. Quantitatively, let us term the *phase deficit* as the minimum phase value that needs to be added (with the negative sign) to the phase characteristic of the plant to make the phase balance condition hold at some frequency (including the case of $\Omega = \infty$). Note: we do not consider now the case of possibly non-monotone frequency characteristics. The phase deficit is depicted in Fig. 3.6 as ϕ_d. Therefore,

$$\phi_l(\Omega) - \phi_d + \arg N(a) = -\pi, \tag{3.24}$$

assuming that $\phi_d \geq 0$ and $\arg N(a) \geq 0$ for SOSM.

Now consider controllers that include a nonlinearity with infinite derivative in zero. For this type of nonlinearity, the DF $N(a) \to \infty$ if $a \to 0$ and, therefore, $-N^{-1}(a) \to 0$ if $a \to 0$. Also, assume that $-N^{-1}(a)$ is a straight line in the complex plane (other types of $-N^{-1}(a)$ will be considered below). Formulate the following theorem.

Theorem 3.2. *For the second-order plant given by (3.4) and the controller having the describing function $N(a)$ that satisfies the condition: $\frac{\mathrm{Im}N(a)}{\mathrm{Re}N(a)} = const$ (the negative reciprocal DF of the controller is a straight line in the complex plane), the following three modes of oscillations can occur (necessary conditions).*

A. A periodic motion occurs only if the phase deficit value is negative.
B. An oscillation having asymptotic convergence of the amplitude to zero (periodic process of infinite frequency and zero amplitude) occurs only if the phase deficit value is zero.

C. *An oscillation having finite-time convergence of the amplitude to zero occurs only if the phase deficit value is positive.*

Proof. A. If the phase deficit is negative there always exists a point of intersection of the Nyquist plot of the plant and of the negative reciprocal of the DF of the controller (follows from the definition of the phase deficit). Therefore, there is a solution of the harmonic balance equation [9, 2], and a self-excited periodic motion occurs.

C. It follows from the definition of the nonlinearity of the controller that

$$N(a) = \frac{k_1}{r(a)} + j\frac{k_2}{r(a)}, \tag{3.25}$$

where $k_1 > 0$, $k_2 > 0$ are constant coefficients, $r(a)$ is an increasing function of the amplitude a: $\frac{dr(a)}{da} > 0$ for all $a \in [0;\infty)$, such that $r(0) = 0$ (examples of this function can be $r(a) = a$, $r(a) = \sqrt{a}$, etc.). The negative reciprocal of (3.25) becomes

$$-N^{-1}(a) = -\frac{r(a)}{{k_1}^2 + {k_2}^2}(k_1 - jk_2)$$

Therefore, the *phase deficit* for this system is $\phi_d = \arctan(k_2/k_1)$. Considering that $y(t) = a(t)\sin\Psi(t)$ and $\dot{y}(t) = a(t)[\sigma(t)\sin\Psi(t) + \Omega(t)\cos\Psi(t)]$ represent the response of the nonlinear controller to signal $y(t)$ as an expansion in the basis of functions $y(t)$, $\dot{y}(t)$ (weighted sum), the following holds:

$$u(t) \approx -\left(p_1 y(t) + \frac{p_2}{\Omega}\dot{y}(t)\right) = -a\left((p_1 + p_2\frac{\sigma}{\Omega})\sin\Psi + p_2\cos\Psi\right), \tag{3.26}$$

where the sign "-" is attributed to the negative feedback, the "approximate equality" is due to the use of the approximate DF method. (Note: that basis would be an orthogonal one if the decay were zero.) The weight $p_2 = k_2/r(a)$; the weight p_1 can be determined for a particular controller. It reduces to $p_1 = k_1/r(a)$ when $\sigma = 0$. It follows from (3.26) that the controller output can be represented as follows:

$$u(t) \approx -\left(p_1 + \frac{p_2}{\Omega}s\right)y(t),$$

where $s = \frac{d}{dt}$. Similar to (3.19), we can write the following formula for the instantaneous decay:

$$\sigma = -0.5\left(a_2 + \frac{p_2(a)}{\Omega}b_2\right) = -0.5\left(a_2 + \frac{k_2}{r(a)\Omega}b_2\right) \tag{3.27}$$

and instantaneous frequency (similar to (3.14), (3.15)):

$$\Omega = 0.5\sqrt{4(a_1 + p_1(a)b_2) - \left(a_2 + \frac{k_2}{r(a)\Omega}b_2\right)^2}.$$

As an auxiliary result, find the following limit from the last formula:

$$\lim_{a\to 0} r(a)\Omega = \lim_{a\to 0} 0.5r(a)\sqrt{4\left(a_1 + p_1(a)b_2\right) - \left(a_2 + \frac{k_2}{r(a)\Omega}b_2\right)^2} = 0,$$

considering that $\Omega \to \infty$ when $a \to 0$ and $r(0) = 0$. Therefore, considering the differential equation for the amplitude

$$\dot{a} = a\sigma = -\frac{k_2}{2r(a)\Omega}b_2 a - \frac{a_2}{2}a, \tag{3.28}$$

one can see that the nonlinearity present in this equation is the one with $g(0) = 0$ and infinite derivative at $a = 0$: $g(a) = \frac{k_2 b_2 a}{2r(a)\Omega}$, $\lim\limits_{a\to 0} g(a) = 0$ (follows from $\frac{dr(a)}{da} > 0$), $g'(a) = \frac{k_2 b_2}{2}\left(\frac{1}{r(a)\Omega} - \frac{ar'(a)}{r^2(a)\Omega} - \frac{a^{d\Omega}/_{da}}{r(a)\Omega^2}\right)$, $\lim\limits_{a\to 0} g'(a) = \infty$ (due to the first term in the brackets; considering also boundedness on the second term, and the derivative $d\Omega/da < 0$). These dynamics define a terminal sliding mode and finite convergence time [6]. This completes the proof for option C.

B. For this option, coefficient k_2 in (3.25) is zero. As follows from (3.28) $\dot{a} = -0.5a_2 a$, thus, providing exponential (asymptotic) convergence.

□

It follows from (3.22) and (3.28) that within the finite-time convergence option, the convergence time depends on k_2 and, therefore, on the phase deficit value. When the *phase deficit* tends to zero the convergence time tends to infinity.

3.5 Extension to Higher-Order Plants

Relationship between the frequency-response properties of the plant and controller, and the transient process convergence rate was investigated for second-order systems. One would legitimately expect similar properties from a higher-order system as far as relative degree of the plant remains the same (two) because the convergence properties depend on the high-frequency part of the frequency response. We now carry out this analysis from a different, however, point of view. We shall now formulate and prove the following statement, which is the extension of the properties considered above to higher-order plants.

Theorem 3.3. *In the system* (3.4) *controlled by the twisting controller* (3.5)*, asymptotic convergence takes place only if* $c_2 = 0$*, and finite-time convergence takes place only if* $c_2 > 0$*.*

Proof. Prove the theorem via assuming that the harmonic balance condition holds in the origin and showing that this is a valid assumption for $c_2 = 0$, which leads to the conclusion about the asymptotic convergence, and invalid assumption for $c_2 > 0$ necessitating finite-time convergence (proof by contradiction). Assume that the harmonic balance condition of the following form holds in the origin:

$$[N_1(a_{01}) + j\Omega_0 \cdot N_2(a_{02})]\, W_l(j\Omega_0) = -1, \tag{3.29}$$

where $a_{01} \to 0$, $a_{02} \to 0$, $\Omega_0 \to \infty$, subscript "0" denotes the variable in the origin. We investigate convergence of the transient process in the vicinity of the origin by giving the amplitude a small increment and analyzing the type of convergence from this disturbed initial point. We shall consider that the harmonic balance equation will still be valid at small increments of the amplitude – similarly to how it is done for oscillations of finite frequency [14,1]:

$$\begin{aligned}&[N_1(a_{01}+\Delta a_1) + (\Delta\sigma + j(\Omega_0+\Delta\Omega)) \cdot N_2(a_{02}+\Delta a_2)]\\ &\quad \cdot W_l(\Delta\sigma + j(\Omega_0+\Delta\Omega)) = -1\end{aligned} \tag{3.30}$$

Taking the derivative with respect to a_1 from both sides of (3.30) yields:

$$\begin{aligned}&\left.\frac{\partial N_1}{\partial a_1}\right|_{a_1=0} \cdot W_l(j\Omega_0) + j\Omega_0 \left.\frac{\partial N_2}{\partial a_1}\right|_{a_1=0} \cdot W_l(j\Omega_0)\\ &\quad + \left.\frac{\partial W_l}{\partial s}\right|_{s=j\Omega_0} \frac{ds}{da_1} N_1(a_{01}) + N_2(a_{02}) \frac{ds}{da_1} W_l(j\Omega_0)\\ &\quad + j\Omega_0 N_2(a_{02}) \left.\frac{\partial W_l}{\partial s}\right|_{s=j\Omega_0} \frac{ds}{da_1} = 0\end{aligned} \tag{3.31}$$

where $s = \Delta\sigma + j(\Omega_0 + \Delta\Omega)$ is the Laplace variable; the derivatives $\frac{\partial N_1}{\partial a_1}$ and $\frac{\partial N_2}{\partial a_1}$ can be obtained by differentiating (3.7) and (3.10), respectively, as follows:

$$\frac{\partial N_1}{\partial a_1} = -\frac{4c_1}{\pi a_1^2}, \quad \frac{\partial N_2}{\partial a_1} = -\frac{4c_2}{\pi\Omega a_1^2}.$$

Express the quantity $\frac{ds}{da_1}$ from equation (3.31).

$$\frac{ds}{da_1} = \frac{1}{a_1 \left\{ \left.\frac{\partial \ln W_l}{\partial s}\right|_{s=j\Omega_0} + \frac{c_2}{\Omega_0} \frac{c_1 - jc_2}{c_1^2+c_2^2} \right\}}.$$

Considering that $s = \Delta\sigma + j(\Omega_0 + \Delta\Omega)$ and, therefore, $\frac{ds}{da_1} = \frac{d(\Delta\sigma)}{da_1} + j\frac{d(\Delta\Omega)}{da_1} = \frac{d\sigma}{da_1} + j\frac{d\Omega}{da_1}$, we can write the following expression for the derivative of the decay:

$$\begin{aligned}\frac{d\sigma}{da_1} &= \mathrm{Re}\, \frac{1}{a_1 \left\{ \left.\frac{\partial \ln W_l}{\partial s}\right|_{s=j\Omega_0} + \frac{c_2}{\Omega_0} \frac{c_1 - jc_2}{c_1^2+c_2^2} \right\}}\\ &= \frac{1}{a_1} \frac{\frac{\partial \arg W_l}{\partial \ln \Omega_0} + \frac{c_1 c_2}{c_1^2+c_2^2}}{\left\{ \frac{\partial \arg W_l}{\partial \ln \Omega_0} + \frac{c_1 c_2}{c_1^2+c_2^2} \right\}^2 + \left\{ \frac{\partial \ln |W_l|}{\ln \Omega_0} + \frac{c_2^2}{c_1^2+c_2^2} \right\}^2}\end{aligned} \tag{3.32}$$

where

$$\frac{\partial \ln|W_l|}{\partial \ln \Omega_0} = \frac{\partial \ln|W_l|}{\partial \ln \omega}\bigg|_{\omega=\Omega_0} = \lim_{\omega\to\infty} \frac{\partial \ln|W_l|}{\partial \ln \omega} = -r, \tag{3.33}$$

r is the relative degree of the plant transfer function, which reflects the fact of the existence of high-frequency asymptotes of the Bode magnitude plot,

$$\frac{\partial \arg W_l}{\partial \ln \Omega_0} = \frac{\partial \arg W_l}{\partial \ln \omega}\bigg|_{\omega=\Omega_0} = \lim_{\omega\to\infty} \frac{\partial \arg W_l}{\partial \ln \omega} = 0- \tag{3.34}$$

With account of (3.33) and (3.34), formula (3.32) can be rewritten as follows:

$$\frac{d\sigma}{d\ln a_1} = \frac{\frac{c_1c_2}{c_1^2+c_2^2} + 0-}{\left\{\frac{c_1c_2}{c_1^2+c_2^2}\right\}^2 + \left\{-r + \frac{c_2^2}{c_1^2+c_2^2}\right\}^2}. \tag{3.35}$$

It follows from formula (3.35) that if $c_2 = 0$ then $\frac{d\sigma}{d\ln a_1} = 0$ and if $c_2 > 0$ then $\frac{d\sigma}{d\ln a_1} > 0$. Before interpreting these conclusions, we analyse the derivative $\frac{d\sigma}{d\ln a_1}$. By definition $\sigma = \dot{a}_1/a_1$ and, therefore,

$$\frac{d\sigma}{d\ln a_1} = a_1\frac{d\sigma}{da_1} = a_1\frac{d\left(\dot{a}_1/a_1\right)}{da_1} = \frac{d\dot{a}_1}{da_1} - \frac{\dot{a}_1}{a_1} \tag{3.36}$$

We can interpret (3.36) as the second-order differential equation with state variables a_1 and $\dot{a}_1$ without explicit time and draw the phase portrait of this second-order system in the phase plane using the isoclines technique (Fig. 3.7).

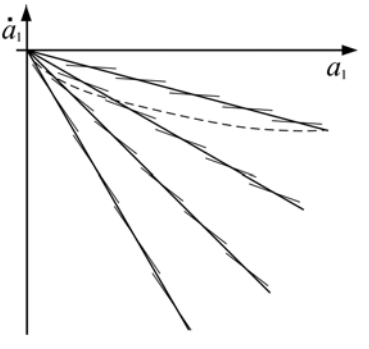

Fig. 3.7 Phase trajectory of system (3.36) with isoclines shown

Denote two angles (their tangents) as $\tan\phi = \frac{d\dot{a}_1}{da_1}$ and $\tan\psi = \frac{\dot{a}_1}{a_1}$; ϕ gives the slope of the tangent line in a point of the phase portrait and ψ gives the slope of the vector from the origin to a point of the phase portrait. The condition $\frac{d\sigma}{d\ln a_1} = 0$

means that the angles ϕ and ψ must be equal, which means in turn that the phase portrait is a strait line and $\dot{a}_1/a_1 = const$. The last condition constitutes the asymptotic convergence of a_1 to 0.

In the case when $c_2 > 0$, the angle Φ (absolute value) is always greater than the angle ϕ (absolute value). In fact, the difference between the tangents of these angles is equal to $q = \frac{\frac{c_1 c_2}{c_1^2+c_2^2}}{\left\{\frac{c_1 c_2}{c_1^2+c_2^2}\right\}^2 + \left\{-r+\frac{c_2^2}{c_1^2+c_2^2}\right\}^2}$ in any point of the phase portrait. Therefore, the phase trajectories of the system $\frac{d\dot{a}_1}{da_1} - \frac{\dot{a}_1}{a_1} = q$ look like in Fig. 3.7 (the example of $c_1 = 10$, $c_2 = 10$, $r = 2$, and $q = 0.2$), with the trajectory schematically shown by the dash line. The fact that the difference between the tangents of the angles ϕ and Φ must be constant and equal to q in all points (including the origin) results in the infinite slope of the phase trajectories in the origin (the difference of two infinite values still gives q, which would be impossible with finite slopes). Therefore, in the vicinity of the origin, the differential equation for the amplitude is $\dot{a}_1 = h(a_1)$, with function $h(a_1) \leq 0$ having infinite slope at $a_1 \to 0$.

Now prove that the equation $\dot{a}_1 = h(a_1)$, with function $h(a_1) \leq 0$ having infinite slope at $a_1 \to 0$, features finite-time convergence. Define a majoring nonlinearity as $h_2(a_1) = -\beta a_1^{\alpha}$ for the function $h(a_1)$ through the selection of values α and β in such a way that in the initial point the following two equalities hold: $h_2(a_1) = h(a_1)$ and $\frac{dh_2(a_1)}{da_1} = \frac{dh(a_1)}{da_1}$. This results in the following two equations: $\frac{d\dot{a}_1}{da_1} = q + \frac{\dot{a}_1}{a_1} = -\alpha\beta a_1^{\alpha-1}$ and $\tan\psi = \frac{\dot{a}_1}{a_1} = -\beta {a_1}^{\alpha-1}$. Solution of these equations results in the following expressions: $\alpha = 1 - \frac{q}{\tan\psi}$, $\beta = {a_{10}}^{\alpha-1}\tan\psi$, where a_{10} is the value of a_1 in the initial point. It follows from the last formulas if α and β are selected to ensure the same initial point and the same initial slope for the original and the majoring nonlinearities then in all other points corresponding to any selected $\psi$the slope (absolute value) of the original nonlinearity is steeper than the slope of the majoring nonlinearity. Therefore, $h(a_1) = h_2(a_1) < 0$ for all $a_1 \in (0; a_{10})$. Since differential equation $\dot{a}_1 = -\beta a_1^{\alpha}$ has finite-time convergence [15, 20], according to Theorem 3.1, the original equation $\dot{a}_1 = h(a_1)$ (or $\frac{\dot{a}_1}{a_1} = \sigma \to -\infty$) has finite-time convergence of a_1 to 0.

Because we assumed the existence of a periodic solution in the origin, which requires the fulfilments of the condition $\sigma = 0$ at $a_1 \to 0$, and we also showed that it is the case only if $c_2 = 0$, and therefore, our assumption was not valid for $c_2 > 0$, we can now conclude that asymptotic convergence of the transient oscillation takes place only if $c_2 = 0$, and finite-time convergence takes place if $c_2 > 0$. □

3.6 Extention to Other Types of Controllers

The relationship between the DF of the controller and the possibility of a particular mode of the transient process to occur was established above. However, this was done for a particular type of controllers – namely the one that satisfies the

condition $\mathrm{Im}N(a)/\mathrm{Re}N(a) = const$. This holds for the twisting controller [12], the sub-optimal algorithm [4,3], and possibly some other controllers/algorithm that can be designed in the future. Yet, it is not a condition that is always satisfied. However, only values of the amplitude $a \leq a_0$ are realized in the convergence process, and, respectively, only the low-amplitude segment of the function $-N^{-1}(a)$ is utilized. Therefore, the fact of finite-time convergence depends on the shape of $-N^{-1}(a)$ only in the vicinity of the origin (in the complex plane), so that if the process starts from certain amplitude, only the amplitudes in the range from the initial one to zero will be attained. Furthermore, if the process starts at some finite amplitude, the time over which it reaches another smaller finite amplitude will always be finite. Therefore, to establish the fact of finite time convergence one needs to analyse only a very small vicinity of the origin, and consequently, what is important in that respect is the location of the low amplitude asymptote of the plot $-N^{-1}(a)$.

Let us reformulate the definition of the *phase deficit* and define it as the minimum phase value that needs to be added (with the negative sign) to the phase characteristic of the plant to make the high-frequency asymptote of the Nyquist plot of the plant to coincide with the low-amplitude asymptote of the negative reciprocal DF of the controller. The noted property can also be extended to plants of higher order and relative degree two – as considered above: a higher-order system would exhibit the properties of the corresponding second-order system at high enough frequencies. We illustrate this statement through analysis of two different controllers. Let the plant be the one that was considered in the above examples, and the control be

$$u = -c_1 \cdot \mathrm{sign} y - c_2 \cdot f(\dot{y}), \tag{3.37}$$

with nonlinear function $f(\dot{y})$ being in the first case $f(\dot{y}) = f_I(\dot{y}) = \mathrm{sign}(\dot{y})$ and in the second case $f(\dot{y}) = f_{II}(\dot{y}) = \mathrm{sign}(\dot{y}) \cdot (\dot{y})^2$. The DF formula for the second nonlinearity is: $N_{II}(a) = \frac{2}{\pi a}\int\limits_0^{\pi} (a\sin\theta)^2 \sin\theta d\theta = \frac{2a}{3\pi}$. Also, the DF of the

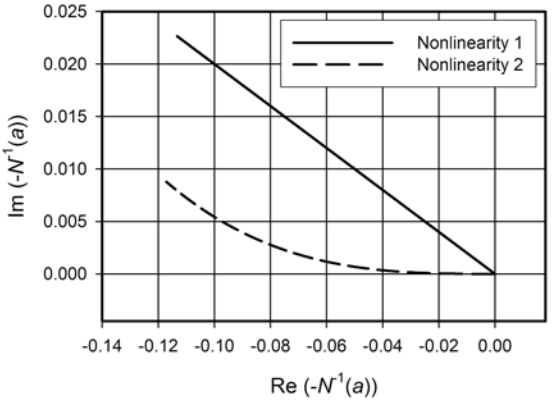

Fig. 3.8 Negative reciprocal of $N_1(a)$ and $N_2(a)$

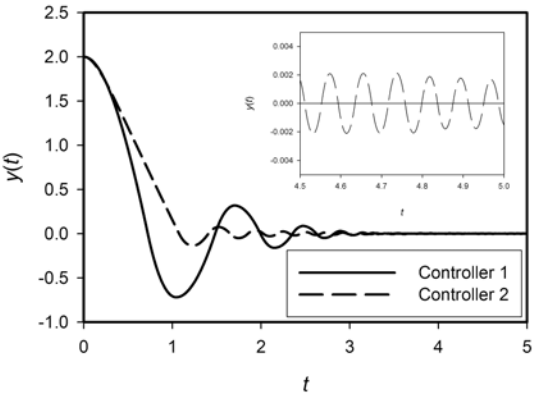

Fig. 3.9 Transients in the system with controllers 1 and 2; zoomed picture for time 4.5s-5.0s

relay function is given by formula (3.7). Therefore, the DF of the first controller is $N_1(a) = \frac{4c_1}{\pi a} + j\frac{4c_2}{\pi a}$, and of the second controller is $N_2(a) = \frac{4c_1}{\pi a} + j\frac{2ac_2}{3\pi}$. Select $c_1 = 10, c_2 = 2$ and compute and plot the negative reciprocal functions of $N_1(a)$ and $N_2(a)$ (Fig. 3.8). Indeed, the system with controller having the DF $N_1(a)$ reveals a finite time convergence, while the controller with DF $N_2(a)$ shows asymptotic convergence (Fig. 3.9). A zoomed image shows the process after 4.5s, which reveals the type of convergence.

3.7 Conclusions

The article provides an overview of the frequency-domain methods in sliding mode control. It is pointed out that there exist two problems: analysis of sliding modes in the systems affected by parasitic dynamics and analysis of ideal sliding modes. These two problems require two different frequency-domain approaches to the analysis: the one based on the assumption of the existence of a fixed point of the Poincare map and the other one for the case of the absence of any fixed point of Poincare map. A frequency-domain approach to analysis of transient oscillatory processes in systems with SOSM (which corresponds to the second case) is presented in detail. The approach involves application of the describing function method in the quasi-static formulation to analysis of the transient oscillation and consideration of the instantaneous values of the frequency, amplitude and decay of the oscillations. The presented development leads to a simple criterion of the existence of a finite-time or asymptotic conversion, which involves just one characteristic – the phase deficit. The presented methodology can be used for the development of new SOSM algorithms.

References

1. Aguilar, L., Boiko, I., Fridman, L., Iriarte, R.: Generating self-excited oscillations via two-relay controller. IEEE Transaction on Automatic Control 54(2), 416–420 (2009)
2. Atherton, D.: Nonlinear Control Engineering - Describing Function Analysis and Design. Van Nostrand Company Limited, Workingham (1975)
3. Bartolini, G., Ferrara, A., Levant, A., Usai, E.: On Second Order Sliding Mode Controllers. In: Young, K., Ozguner, U. (eds.) Variable Structure Systems, Sliding Mode and Nonlinear. LNCIS, vol. 247, Springer, London (1999)
4. Bartolini, G., Ferrara, A., Usai, E.: Chattering Avoidance by Second-Order Sliding Mode Control. IEEE Transactions on Automatic Control 43(2), 241–246 (1998)
5. Boiko, I.: Discontinuous Control Systems: Frequency-Domain Analysis and Design. Birkhauser, Boston (2009)
6. Boiko, I., Fridman, L.: Analysis of chattering in continuous sliding-mode controllers. IEEE Transaction on Automatic Control 50(9), 1442–1446 (2005)
7. Boiko, I., Fridman, L., Castellanos, M.: Analysis of second order sliding mode algorithms in the frequency domain. IEEE Transaction on Automatic Control 49(6), 946–950 (2004)
8. Fridman, L.: Singularly perturbed analysis of chattering in relay control systems. IEEE Transactions on Automatic Control 47(12), 2079–2084 (2002)
9. Gelb, A., Velde, W.V.: Multiple-Input Describing Functions and Nonlinear System Design. McGraw-Hill, New York (1968)
10. Hamel, B.: Contribution a l'etude mathematique des systemes de reglage par tout-ourien. Service Technique Aeronautique 17 (1949)
11. Krylov, N., Bogoliubov, N.: Introduction to Nonlinear Mechanics. Princeton University Press, Princeton (1947)
12. Levant, A.: Sliding order and sliding accuracy in sliding mode control. International Journal of Control 58(6), 1247–1263 (1993)
13. Levant, A.: Universal SISO sliding-mode controllers with finite-time convergence. IEEE Transactions on Automatic Control 46(9), 1447–1451 (2001)
14. Loeb, J.M.: Advances in nonlinear servo theory. In: Frequency Response, pp. 260–268 (1956)
15. Man, Z., Poplinsky, A., Wu, H.: A robust MIMO terminal sliding mode control for rigid robotic manipulators. IEEE Transaction on Automatic Control 39(12), 2464–2468 (1994)
16. Shtessel, Y., Shkolnikov, I., Brown, M.: An asymptotic second-order smooth sliding mode control. Asian Journal of Control 5(4), 498–504 (2003)
17. Starikova, M.: Analysis of Control Systems Having Logical Control Devices. Mashinostroenie, Moscow (1978)
18. Tsypkin, Y.: Relay Control Systems. Cambridge University Press, Cambridge (1984)
19. Utkin, V.: Sliding Modes in Control and Optimization. Springer, Heidelberg (1992)
20. Yu, X., Wu, Y., Man, Z.: On global stabilization of nonlinear dynamical systems. In: Young, K., Ozguner, U. (eds.) Variable Structure Systems, Sliding Mode and Nonlinear Control. LNCIS, vol. 247, pp. 109–122. Springer, London (1999)
21. Zhiltsov, K.: Approximate Methods for Variable Structure Systems Analysis. Energia, Moscow (1974)

Chapter 4
Lyapunov Approach for Analysis and Design of Second Order Sliding Mode Algorithms

Jaime A. Moreno

Abstract. Lyapunov functions are a basic tool for analysis and design in the modern control theory, and there are many different design methodologies based on Lyapunov theory. Second Order Sliding Modes, and in particular, the Super-Twisting Algorithm (STA), are a powerful tool for the design of controllers, observers and differentiators having very attractive dynamic features: they converge in finite time, even in presence of persistently acting bounded perturbations. This property, that we will call *exactness*, can be achieved because of the discontinuous nature of the STA. The design of control or observation algorithms based on Second Order Sliding Modes has been performed until now using either geometric or homogeneous approaches, but not Lyapunov methods. The reason for this situation is simple: only recently has been possible to find adequate Lyapunov functions for some of these algorithms. In this paper some recent advances in this direction will be presented and extended.

Index terms: Sliding Modes, Variable Structure Control, Lyapunov Methods, Riccati Equations.

4.1 Introduction

The *Super-Twisting Algorithm* (STA) is a well-known second order sliding modes (SOSM) algorithm introduced by [16]. It was first designed as an absolutely continuous control law, allowing to compensate Lipschitz perturbations exactly and ensuring finite time convergence. This algorithm is widely used to substitute discontinuous controllers by continuous ones and it has been widely used for control [2, 7, 16, 18, 19, 12] (see also [4], [38], [13]). In [16] a controlled system given

Jaime A. Moreno
Eléctrica y Computación, Instituto de Ingeniería
Universidad Nacional Autónoma de México,
04510 México D.F., Mexico
e-mail: JMorenoP@ii.unam.mx

L. Fridman et al. (Eds.): Sliding Modes, LNCIS 412, pp. 113–149.
springerlink.com

by $\dot{\xi}(t) = u(t) + \varphi(t)$ is considered, where ξ is the scalar state variable, and $\pi(t)$ is an unknown input or perturbation. The STA proposed in [16] is the control algorithm described by

$$\begin{aligned} &u(t) = u_1(t) + u_2(t) \ , \\ &u_1(t) = -k_1 |\xi|^{1/2} \operatorname{sign}(\xi) \ , \ \dot{u}_2(t) = -k_2 \operatorname{sign}(\xi) \ , \end{aligned} \tag{4.1}$$

that, under some conditions on k_1, k_2, is a second-order sliding algorithm, that is robust against a perturbation $\pi(t)$ with a bounded derivative $|\dot{\pi}(t)| \leq L$, and that does not require the derivative of ξ for its implementation. The properties of STA control in the frequency domain are studied in [8], [15].

The algorithm received another meaning when it was first used to design robust exact differentiators [17,37], [18] and observers ([9], [5], [11]), providing finite time convergence for the observer even in the presence of unknown inputs. For observer design or robust exact differentiators a more appropriate form is

$$\begin{aligned} \dot{x}_1 &= -k_1 |x_1|^{1/2} \operatorname{sign}(x_1) + x_2 + \rho_1(x,t) \\ \dot{x}_2 &= -k_2 \operatorname{sign}(x_1) + \rho_2(x,t) \end{aligned} \tag{4.2}$$

where x_i are the scalar state variables, k_i are gains to be designed, and ρ_i are the perturbation terms. The change of variables $x_1 = \xi$, $x_2 = u_2$ shows the equivalence of (4.1) and (4.2), with $\rho_1(x,t) = 0$, $\rho_2(x,t) = \dot{\pi}(t)$. Since the righthand side of (4.2) is discontinuous, its solutions will be understood in the sense of Filippov [10].

Finite time convergence and robustness for the STA has been proved by geometrical methods [16], [9], [19], or by means of the Homogeneity properties [3] of the algorithm [18, 34], [19], [35]. These methods are very restricted for analysis and design of the algorithms. For example, an estimation of the convergence time is not possible by any of them, and the design of the gains is not possible by means of Homogeneity methods.

Lyapunov functions have became a basic tool for analysis and design in modern control theory, so it is natural to look for Lyapunov functions for the STA. It is well-known that $V_w(x) = k_2 |x_1| + \frac{1}{2} x_2^2$ is a *weak* Lyapunov function for the system (4.2) without perturbations, since $\dot{V}(x) = -k_1 k_3 |x_1|^{1/2}$ is only negative semidefinite. (Finite time) convergence can only be asserted by using a generalization of LaSalle's invariance principle for discontinuous systems [34], but it is not possible to provide robustness results, or to estimate the convergence time from it. By a detailed analysis of the weak Lyapunov function $\sqrt{V_w(x)}$ in [41], finite time and robust convergence for the STA is proved. A *strict* (or strong) Lyapunov function, i.e. a positive definite (p.d.) function with negative definite (n.d.) derivative, has been proposed in [39], from which an estimation of the convergence time for the perturbed STA is drawn. However, the form of the function makes it difficult to operate with it for applications or further developments.

In contrast, the strict Lyapunov functions proposed in [20] are very simple, since they are Quadratic-like functions, similar to the ones usually employed for linear systems. In that paper a modification to the STA is introduced, consisting in the

addition of linear correction terms to the purely nonlinear terms of the STA. These extra degrees of freedom provide a stronger attraction force to the algorithm, when the trajectories are far away from the origin. This is the case since the added linear terms are stronger than the nonlinear ones far from the origin. So a faster convergence and an enhanced robustness of the stability to a wider class of perturbations is obtained. Since the modified algorithm is not homogeneous it is not possible to use the homogeneity theory [3, 18, 19, 35] to prove convergence and stability robustness. The Lyapunov function introduced in [39] is also not appropriate for this case. In [20] a strong and robust Lyapunov function is introduced, but its handling, although simple, is cumbersome.

In [23] a Generalized STA (GSTA) is introduced, that includes the classical STA and the modified STA introduced in [20]. For the GSTA a linear framework for the design of quadratic Lyapunov functions is developed in [23]. This means that, for the nominal case without perturbations, Algebraic Lyapunov Equations (ALE) are used for the design of a family of quadratic Lyapunov functions, and each member of the family assures the convergence in finite time and gives an estimate of that convergence time. When perturbations satisfying sector-like conditions are considered, a family of robust Lyapunov functions are designed using Algebraic Riccati Inequalities (ARI), or the corresponding LMIs. Its frequency domain interpretations, as the circle criterion, can also be used to study the robust stability of the STA when bounded perturbations act on it.

In [21] an optimal estimation of the convergence time, based on the quadratic Lyapunov functions of [23], is provided. In [28, 29] it was shown that the convergence time of the STA can be made independent (uniform) of the initial condition, if high-order terms are added to the algorithm. To establish this uniform property the quadratic Lyapunov functions from [23] are not appropriate, so that a non-quadratic Lyapunov function has to be introduced. A STA with variable gains (VGSTA) has been introduced in [25], which allows to robustify the algorithm against perturbations, for which a time and/or state dependent upper bound is known. A further application of the VGSTA is for adaptive control purposes [26]. All these algorithms are easily designed by means of their Lyapunov functions, and they can find different applications [24, 27, 28, 29, 30, 33]. Lyapunov functions for other algorithms are also under study [32, 31].

In this paper, all these results of Lyapunov functions for the STA are unified and extended. We consider a general second order algorithm, that includes *discontinuous* algorithms such as the STA and the GSTA, but also *continuous* algorithms, that have been used for control or observation purposes (with arbitrary order), with special emphasis in obtaining finite-time convergence [1, 36]. For this generalized algorithm, with or without considering perturbations, we provide a unified method to design quadratic or non-quadratic Lyapunov functions, when the gains are considered constant. For the case of variable gains, quadratic Lyapunov functions are proposed. From the Lyapunov functions conditions for the finite time convergence or the uniform convergence (in the initial state) are derived, and estimates of the convergence time are derived. The robustness properties can also be obtained. This

allows to design the gains of the algorithm to attain desired robustness and convergence properties. For the design of quadratic Lyapunov functions a linear framework, as the one proposed for the GSTA in [23], can be provided for the whole family of algorithms. Moreover, the method also provides Chetaev's functions to prove instability. This is a distinguishing feature of our method compared to the ones in the literature for continuous and homogeneous algorithms [1, 36]. Although our Lyapunov functions are very simple, and are simple to handle, they have a striking property: they are continuous, but not Lipschitz continuous. This means that standard Lyapunov theorems cannot be applied. However, it is shown that they can be used in the usual form in order to provide stability results. Finally, an important result is obtained for the STA, or in general, for the discontinuous algorithms in the family: they are the only ones in the whole family that provide convergence to the origin in finite-time and despite of perturbations that do not vanish at the origin. This is a distinguishing feature of the class of STA, that is due to its discontinuous nature.

4.2 Problem Statement and Main Results

In this paper we consider a second order system, named here as Generic Second Order Algorithm (GSOA), and described by the differential equation

$$\begin{aligned} \dot{x}_1 &= -k_1(t)\,\phi_1(x_1) + x_2 + \rho_1(t,x) \\ \dot{x}_2 &= -k_2(t)\,\phi_2(x_1) + \rho_2(t,x)\ , \end{aligned} \tag{4.3}$$

where x_i, $i = 1,2$, are the scalar state variables, $k_i(t)$ are positive, continuous gain functions to be designed, $\rho_i(t,x)$, $i = 1,2$, are time-varying and/or nonlinear perturbations, and the nonlinearities $\phi_1(x_1)$ and $\phi_2(x_1)$ are

$$\phi_1(x_1) = \mu_1 |x_1|^p \operatorname{sign}(x_1) + \mu_2 |x_1|^q \operatorname{sign}(x_1)\ ,\ \mu_1\ ,\ \mu_2 \geq 0\,, \tag{4.4a}$$

$$\begin{aligned} \phi_2(x_1) = {} & \mu_1^2 p\,|x_1|^{2p-1} \operatorname{sign}(x_1) + \mu_1\mu_2\,(p+q)\,|x_1|^{p+q-1} \operatorname{sign}(x_1) + \\ & + \mu_2^2 q\,|x_1|^{2q-1} \operatorname{sign}(x_1)\ , \end{aligned} \tag{4.4b}$$

with μ_1, $\mu_2 \geq 0$ non negative constants and $q \geq 1 \geq p \geq \frac{1}{2}$ are real numbers. Note that $\phi_1(x_1)$ and $\phi_2(x_1)$ are monotone increasing continuous functions for all $p > \frac{1}{2}$, but when $p = \frac{1}{2}$ the function $\phi_2(x_1)$ has a (bounded) discontinuity at $x_1 = 0$. Since $\phi_2(x_1)$ is not necessarily a continuous function, in general the differential equation (4.3) does not have classical solutions, so that solutions of (4.3) are all trajectories in the sense of Filippov [10]. The cases with $0 < p < \frac{1}{2}$ will be excluded, since $\phi_2(x_1)$ has an unbounded discontinuity at $x_1 = 0$.

For different values of the parameters $(\mu_1,\ \mu_2,\ p,\ q)$ some important particular cases are recovered:

(L) A linear algorithm is recovered when $(\mu_1,\ \mu_2,\ p,\ q) = (1,\ 0,\ 1,\ 1)$, so that $\phi_1(x_1) = x_1$, $\phi_2(x_1) = x_1$.

(STA). The classical Super-Twisting Algorithm (STA), originally proposed in [16], is obtained by setting $(\mu_1,\ \mu_2,\ p,\ q) = \left(1,\ 0,\ \frac{1}{2},\ q\right)$, so that $\phi_1(x_1) = |x_1|^{\frac{1}{2}} \operatorname{sign}(x_1)$, $\phi_2(x_1) = \frac{1}{2}\operatorname{sign}(x_1)$. Note that in this case $\phi_2(x_1)$ is a discontinuous function.

(H). A Homogeneous Algorithm is obtained if $\phi_1(x_1) = |x_1|^p \operatorname{sign}(x_1)$, $\phi_2(x_1) = p|x_1|^{2p-1} \operatorname{sign}(x_1)$, for $p \geq \frac{1}{2}$. When $p = \frac{1}{2}$ the previous ST algorithm is recovered. In this case system (4.3) is homogeneous [3,18].

(GSTA). For $p = \frac{1}{2}$ and $q = 1$ the Generalized Super-Twisting Algorithm (GSTA) proposed in [23] is obtained.

All these algorithms use *constant* gains k_1, k_2. However, a Variable Gain Super-Twisting Algorithm (VGSTA) has been proposed in [25], that corresponds to the GSTA with variable gains $k_i(t)$.

Note that the GSO Algorithm (4.3) has a lower order term $\mu_1|x_1|^p \operatorname{sign}(x_1)$, where $1 \geq p \geq \frac{1}{2}$, and a higher order term $\mu_2|x_1|^q \operatorname{sign}(x_1)$, with $q \geq 1$. The convergence properties of the algorithm (4.3), with and without perturbations, are highly dependent on the values of p and q.

Several Types of (asymptotic) Stability will be considered:

Definition 4.1. The origin $x = 0$ for system (4.3) is (locally) globally

- *Finite-time stable*, if all trajectories starting in (a neighborhood of $x = 0$) $\mathbb{R}^2$ converge to $x = 0$ in finite time.
- *Exponentially stable*, if all trajectories starting in (a neighborhood of $x = 0$) $\mathbb{R}^2$ converge to $x = 0$ exponentially.
- *Asymptotically stable*, if all trajectories starting in (a neighborhood of $x = 0$) $\mathbb{R}^2$ converge to $x = 0$ asymptotically.
- *Uniformly stable*, if all trajectories starting in $\mathbb{R}^2$ converge to a neighborhood of $x = 0$ in finite time, and the convergence time is uniformly (upper) bounded with respect to the initial condition.
- *Robustly stable*, if all trajectories starting in (a neighborhood of $x = 0$) $\mathbb{R}^2$ converge to $x = 0$ for a family of perturbations vanishing at the origin.
- *Exactly stable*, if all trajectories starting in (a neighborhood of $x = 0$) $\mathbb{R}^2$ converge to $x = 0$ in finite time, for a family of perturbations that is non vanishing at the origin.
- *Practically stable*, if all trajectories starting in (a neighborhood of $x = 0$) $\mathbb{R}^2$ converge to a neighborhood of $x = 0$ in finite time, for a family of perturbations non vanishing at the origin.

In this paper we provide a rather complete characterization of the properties of the GSOA for all values $q \geq 1 \geq p \geq \frac{1}{2}$. The main features are:

- Families of *strict (or strong)* Lyapunov functions, i.e. whose derivative is negative definite, are constructed for the GSOA, with and without perturbations, for all values of (p,q). These Lyapunov functions are simple (for example, of quadratic type).

- The construction of the Lyapunov functions is systematic, and they provide the full set of stabilizing (constant) gains (k_1, k_2).
- The type of stability (finite-time, exponential, asymptotic, uniform) and its robustness properties, are characterized by means of the Lyapunov functions.
- An estimation of the (finite-time) convergence time is provided by means of the Lyapunov function.

Low order term p	High order term q	Stability Type	
$p = 1$	$q = 1$	Exponential Robust	Non Uniform Practical
$\frac{1}{2} < p < 1$	$q = 1$	Finite-Time Robust	Non Uniform Practical
$p = \frac{1}{2}$	$q = 1$	Finite-Time **Exact**	Non Uniform Practical
$p = 1$	$q > 1$	Exponential Robust	Uniform Practical
$\frac{1}{2} < p < 1$	$q > 1$	Finite-Time Robust	Uniform Practical
$p = \frac{1}{2}$	$q > 1$	Finite-Time **Exact**	**Uniform** Practical

It is well known that for $p = q = 1$ the linear algorithm converges exponentially for adequately selected gains k_1, k_2, and in the presence of perturbations either exponential stability or practical stability will be reached, depending on the characteristics of the perturbation term. In presence of bounded perturbations, not vanishing at the origin, only practical stability can be achieved. From the previous Table it is clear that:

- The low order term is responsible for the type of stability: if $p = 1$ convergence is exponential, for $p > 1$ convergence is asymptotic and for $\frac{1}{2} \leq p < 1$ convergence is in finite-time.
- The high order term is responsible for the uniformity of the convergence with respect to the initial condition: if $q \leq 1$ there is no uniformity, and for $q > 1$ the convergence is uniform.
- For $p = \frac{1}{2}$ robustness of the stability with respect to perturbations is exact, a distinguishing feature, since for no other value of p this property is obtained. Since this is the only value of p for which the algorithm GSOA is discontinuous, this strong robustness property is a consequence of the discontinuous control. This unique and strong robustness feature distinguishes the STA (or GSTA) from all other algorithms.

In what follows several stability and robustness results for the GSOA will be presented. The case with constant gains will be considered in detail, and then a brief extension to the varying gain case will be given. Due to space limitations, only some proofs of the results will be provided in the Appendix.

4.3 Finite Time Convergence of Unperturbed GSOA with Constant Gains

In this section it is shown that for $\frac{1}{2} \leq p < 1$ all trajectories of the GSOA (4.3) with constant gains k_1, k_2, converge robustly and in finite time to the origin. Moreover, for $p = \frac{1}{2}$ the convergence is exact, meaning that the origin is reached in finite time despite of bounded perturbations, a unique feature of this algorithm. A quadratic (robust) Lyapunov function will be constructed to characterize these properties. The values of the gains (k_1, k_2) to achieve these properties can be calculated by means of an Algebraic Lyapunov Equation (ALE) in the unperturbed case, or by means of an Algebraic Riccati Inequality (ARI) for the perturbed case, resembling the methods used for Linear Time Invariant systems in classical linear control theory. Moreover, these conditions are necessary to achieve stability, and the convergence time can be estimated from the Lyapunov function.

4.3.1 Stability Analysis without Perturbations: An ALE Approach

For system (4.3) without perturbations, when $k_1, k_2 > 0$ are positive *constants*, the quadratic form

$$V_Q(x) = \zeta^T P \zeta \ , \tag{4.5}$$

where

$$\zeta^T = \Phi^T(x) = \left[\phi_1(x_1) \ , \ x_2\right] \ , \tag{4.6}$$

and matrix $P = P^T > 0$ is the unique symmetric and positive definite solution of the Algebraic Lyapunov Equation (ALE)

$$A^T P + PA = -Q \tag{4.7}$$

with the Hurwitz matrix

$$A = \begin{bmatrix} -k_1 & , & 1 \\ -k_2 & & 0 \end{bmatrix} \ , \tag{4.8}$$

and an *arbitrary* symmetric and positive definite matrix $Q = Q^T > 0$, provides a *family* of *strong (strict)* Lyapunov functions for (4.3), when $\mu_1 > 0$. Notice that $\Phi(x)$ is a global homeomorphism for every (p, q), with $\frac{1}{2} \leq p \leq 1$, and for $p = 1$ it is a diffeomorphism.

Remark 4.1. Since $V_Q(x)$ (4.5) (and also $V_N(x)$ (4.20) introduced below) is continuous but not locally Lipschitz, the usual versions of Lyapunov Theorem [10, 3, 34] cannot be used here. However, it is possible to show that $V_Q(\varphi(t, x_0))$ is an absolutely continuous (AC) function of time along the state trajectories $\varphi(t, x_0)$ of the differential equation (4.3). This implies that it is differentiable almost everywhere, and on those points the derivative can be calculated in the usual way, i.e. applying the chain rule. Moreover, if the derivative $\dot{V}_Q$ is negative definite almost everywhere, then $V_Q(\varphi(t, x_0))$ is monotone decreasing and converges to zero, what is the

condition required by Zubov's Theorem [40, Theorem 20.2, p. 568.]. The same argument is also valid for all the proofs of the present paper.

Theorem 4.1. *Consider the system (4.3) with $\mu_1 > 0$, and constant gains k_1 , k_2. The following statements are equivalent:*

(i) The origin $x = 0$ of (4.3) is asymptotically stable.
(ii) Matrix A (4.8) is Hurwitz, i.e. all its eigenvalues have negative real parts.
(iii) The constant gains are positive, i.e. $k_1 > 0$, $k_2 > 0$.
(iv) For every *symmetric and positive definite matrix $Q = Q^T > 0$, the ALE (4.7) has a unique symmetric and positive definite solution $P = P^T > 0$.*

In this case the function (4.5) is a global, strong Lyapunov function *for system (4.3). The time derivative $\dot{V}_Q$ of the Lyapunov function, taken along the trajectories of the system, satisfy the differential inequality*

$$\dot{V}_Q \leq -\gamma_1 (Q, \mu_1) V_Q^{\frac{3p-1}{2p}} (x) - \gamma_2 (Q, \mu_2) |x_1|^{q-1} V_Q (x) \ , \tag{4.9}$$

where

$$\gamma_1 (Q, \mu_1) \triangleq \mu_1^{\frac{1}{p}} p \frac{\lambda_{\min} \{Q\} \lambda_{\min}^{\frac{1-p}{2p}} \{P\}}{\lambda_{\max} \{P\}} \ , \ \gamma_2 (Q, \mu_2) \triangleq \mu_2 q \frac{\lambda_{\min} \{Q\}}{\lambda_{\max} \{P\}}$$

are scalars depending on the selection of the matrix Q and μ_1, μ_2.

In the proof of the Theorem it is shown that the stability of the equilibrium $x = 0$ of (4.3) is completely determined by the stability of the matrix A, i.e. of the associated LTI system $\dot{\xi} = A\xi$: if A is stable or unstable, then so is the equilibrium point of (4.3). This is a remarkable fact.

4.3.2 Convergence Time

From Lyapunov's inequality (4.9) it is possible to conclude that: (i) the GSOA converges to the origin in *finite time* when $\frac{1}{2} \leq p < 1$ ($\mu_1 > 0$), and (ii) an upper bound for the convergence time can be estimated.

Proposition 4.1. *Suppose that $k_1 > 0$, $k_2 > 0$, and $\mu_2 \geq 0$. Then a trajectory of the STA (4.3) starting at $x_0 \in \mathbb{R}^2$ converges to the origin in finite time if $\frac{1}{2} \leq p < 1$ ($\mu_1 > 0$), and it reaches that point at most after a time*

$$T (x_0) = \begin{cases} \frac{2p}{(1-p)\gamma_1 (Q,\mu_1)} V_Q^{\frac{1-p}{2p}} (x_0) & \text{if } \mu_2 = 0 \text{ or } q > 1 \\ \frac{2p}{(1-p)\gamma_2 (Q,\mu_2)} \ln \left(1 + \frac{\gamma_2 (Q,\mu_2)}{\gamma_1 (Q,\mu_1)} V_Q^{\frac{1-p}{2p}} (x_0) \right) & \text{if } \mu_2 > 0 \text{ and } q = 1 \end{cases} \ , \tag{4.10}$$

where $V_Q (x)$, $\gamma_1 (Q, \mu_1)$ and $\gamma_2 (Q, \mu_2)$ are given in Proposition 4.1. When $p = 1$ ($\mu_1 > 0$) the convergence is exponential.

4.4 Robustness and Exactness of the Perturbed GSOA with Constant Gains

Consider now the GSOA with constant gains, when time-varying and/or nonlinear perturbations ($\rho_i(t,x)$, $i=1,2$) are present,

$$\begin{aligned}\dot{x}_1 &= -k_1\phi_1(x_1)+x_2+\rho_1(t,x)\\ \dot{x}_2 &= -k_2\phi_2(x_1)+\rho_2(t,x)\ .\end{aligned} \tag{4.11}$$

Using the vector ζ (4.6) it is possible to write (4.11) as

$$\dot{\zeta}=\phi_1'(x_1)\begin{bmatrix}-k_1\phi_1(x_1)+x_2+\rho_1(t,x)\\ -k_2\phi_1(x_1)+\frac{\rho_2(t,x)}{\phi_1'(x_1)}\end{bmatrix}=\phi_1'(x_1)\left(A\zeta+\tilde{\rho}\right)\ ,$$

with A as in (4.8) and

$$\tilde{\rho}(t,\zeta)=\left[\begin{array}{c}\rho_1(t,x)\\ \left(\frac{1}{p\mu_1|x_1|^{p-1}+q\mu_2|x_1|^{q-1}}\right)\rho_2(t,x)\end{array}\right]_{x=\varphi^{-1}(\zeta)}\ .$$

4.4.1 The Class of Perturbations

In the forthcoming analysis it will be assumed that the components of the (transformed) perturbation term $\tilde{\rho}(t,\zeta)$ satisfy the sector conditions (for $i=1,2$ and $\forall t\geq 0$ and $\forall\zeta\in\mathbb{R}^2$)

$$\omega_i(\tilde{\rho}_i,\zeta)=-\tilde{\rho}_i^2(t,\zeta)+g_i^2\zeta_1^2=\begin{bmatrix}\tilde{\rho}_i\\ \zeta\end{bmatrix}^T\begin{bmatrix}-1 & 0\\ 0 & g_i^2C^TC\end{bmatrix}\begin{bmatrix}\tilde{\rho}_i\\ \zeta\end{bmatrix}\geq 0\ ,$$

where $C=[1\ ,\ 0]$. This is equivalent to $|\tilde{\rho}_i(t,\zeta)|\leq g_i|\zeta_i|$, with $g_i>0$, or, in original variables, to $|\rho_i(t,x)|\leq g_i|\phi_i(x_1)|$. It follows that

$$\omega(\tilde{\rho},\zeta)=\theta_1\omega_1(\tilde{\rho}_1,\zeta)+\theta_2\omega_2(\tilde{\rho}_2,\zeta)\geq 0\ ,\ \forall\theta_i\geq 0\ ,\ i=1,2\ ,$$

and $\omega(\tilde{\rho},\zeta)$ can be written in a quadratic form as

$$\omega(\tilde{\rho},\zeta)=\begin{bmatrix}\tilde{\rho}(t,\zeta)\\ \zeta\end{bmatrix}^T\begin{bmatrix}-\Theta & 0\\ 0 & R\end{bmatrix}\begin{bmatrix}\tilde{\rho}(t,\zeta)\\ \zeta\end{bmatrix}\geq 0\ ,$$

where

$$\Theta=\begin{bmatrix}\theta_1 & 0\\ 0 & \theta_2\end{bmatrix}\ ,\ R=\left(\theta_1g_1^2+\theta_2g_2^2\right)C^TC\ .$$

In the next paragraph it will be shown that the GSOA (4.3) is *robust* against perturbations satisfying these restrictions, when the (constant) gains (k_1,k_2) are selected appropriately. Note that

$$|\rho_1(t,x)| \leq g_1\left(\mu_1 |x_1|^p + \mu_2 |x_1|^q\right) \tag{4.12a}$$

$$|\rho_2(t,x)| \leq g_2\left(p\mu_1^2 |x_1|^{2p-1} + (p+q)\mu_1\mu_2 |x_1|^{p+q-1} + q\mu_2^2 |x_1|^{2q-1}\right) \tag{4.12b}$$

so that both $\rho_1(t,x)$ and $\rho_2(t,x)$ have to vanish at the origin, i.e. $\rho_1(t,0) = 0$ and $\rho_2(t,0) = 0$ for all values $q \geq 1 \geq p > \frac{1}{2}$. However, for $p = \frac{1}{2}$, as in the (Generalized) STA,

$$-\frac{1}{2}g_2\mu_1^2 \leq \rho_2(t,0) \leq \frac{1}{2}g_2\mu_1^2$$

the perturbation $\rho_2(t,x)$ does not have to vanish at the origin, so that it can withstand persistently exciting perturbation terms!, a property that is only possible by using discontinuous control. The growth of the perturbation for large values of x is given by the degree q of the high order term. Other perturbations, for example depending on x_2, can also be considered by using different sectors (see [23]).

4.4.2 Robust Stability Analysis: A Riccati Inequality Approach

It is possible to construct a robust, quadratic Lyapunov function to ensure the convergence in finite time (when $1 > p \geq \frac{1}{2}$ and $\mu_1 > 0$) and to estimate it, when certain conditions are satisfied.

Theorem 4.2. *Suppose that there exist a symmetric and positive definite matrix $P = P^T > 0$, positive constants $\theta_i > 0$, $i = 1,2$, and $\varepsilon > 0$ so that the matrix inequality (MI)*

$$\begin{bmatrix} A^TP + PA + \varepsilon P + R & PB \\ B^TP & -\Theta \end{bmatrix} \leq 0\,, \tag{4.13}$$

or equivalently, the Algebraic Riccati Inequality (ARI)

$$A^TP + PA + \varepsilon P + R + PB\Theta^{-1}B^TP \leq 0\,, \tag{4.14}$$

are satisfied, where

$$B = \begin{bmatrix} 1 & 0 \\ 0 & 1 \end{bmatrix}\,,\; B = \begin{bmatrix} 1 \\ 0 \end{bmatrix}\,,\; B = \begin{bmatrix} 0 \\ 1 \end{bmatrix}\,,$$

depending on whether $\rho_1(t,x)$ and $\rho_2(t,x)$, only $\rho_1(t,x)$, or only $\rho_2(t,x)$ are present, respectively. In this case the origin is globally, robustly stable, so that all trajectories of system (4.11) converge to the origin for all perturbations satisfying (4.12), and the quadratic form $V_Q(x) = \zeta^T P\zeta$ is a strong, robust Lyapunov function *for system (4.11). For $1 > p \geq \frac{1}{2}$ and $\mu_1 > 0$ every trajectory reaches the origin in a finite-time smaller than*

$$T(x_0) = \begin{cases} \dfrac{2}{(1-p)\varepsilon\mu_1^{\frac{1}{p}}\lambda_{\min}^{\frac{1-p}{2p}}\{P\}} V_Q^{\frac{1-p}{2p}}(x_0) & \text{if } \mu_2 = 0 \text{ or } q > 1 \\ \dfrac{2p}{(1-p)q\varepsilon\mu_2} \ln\left(1 + \dfrac{q\mu_2}{p\mu_1^{\frac{1}{p}}\lambda_{\min}^{\frac{1-p}{2p}}\{P\}} V_Q^{\frac{1-p}{2p}}(x_0)\right) & \text{if } \mu_2 > 0 \text{ and } q = 1 \end{cases}, \tag{4.15}$$

where x_0 is the initial state. For $p = 1$ and $\mu_1 > 0$ convergence is exponential. When $p = \frac{1}{2}$ the origin is exactly stable.

The previous result shows how to analyze the robust stability of the GSTA: given certain gains k_1, k_2 of the GSTA and given the perturbation terms if the ARI (4.14), or equivalently, the Matrix Inequality (8.15) are feasible, then the robust finite time stability of the algorithm is assured, and a Strong Lyapunov Function can be calculated. Note that in (8.15) one can replace the term εP by εI without altering the solvability conditions. In that case (8.15) is a Linear Matrix Inequality in the unknowns, so that efficient algorithms can be used for solving it.

However, a very important application of the Theorem is for design purposes: given the perturbation terms find gains k_1, k_2 of the GSTA, if they exist, so that robust finite time stability of the algorithm is assured and a certain convergence time T_d is met (for all initial states in a compact set). In order to find such gains let us write

$$A = \begin{bmatrix} -k_1 & 1 \\ -k_2 & 0 \end{bmatrix} = A_0 - KC\ ,\ A_0 = \begin{bmatrix} 0 & 1 \\ 0 & 0 \end{bmatrix}\ ,\ C = \begin{bmatrix} 1 & 0 \end{bmatrix}\ ,\ K = \begin{bmatrix} k_1 \\ k_2 \end{bmatrix}\ .$$

In this case the problem is to find a symmetric and positive definite matrix $P = P^T > 0$, positive constants $\theta_i > 0$, $i = 1, 2$, a gain matrix K and $\varepsilon > 0$ so that the matrix inequality

$$\begin{bmatrix} A_0^T P + PA_0 - C^T K^T P - PKC + \varepsilon P + R & PB \\ B^T P & -\Theta \end{bmatrix} \leq 0 \tag{4.16}$$

is feasible. Again, replacing εP by εI in (4.16) does not affect its solvability. (4.16) is then a LMI in the unknowns P, PK, ε, Θ.

4.4.3 Practical Stability

When the perturbation is large then convergence to the origin can be lost. However, "practical" stability, i.e. ultimate and uniform boundedness [14, Section 4.8], can still be achieved.

Theorem 4.3. *Suppose that the perturbation terms of the system (4.2) are globally bounded by*

$$|\rho_1| \leq \delta_1\ ,\ |\rho_2| \leq \delta_2\ , \tag{4.17}$$

for some constants $\delta_1, \delta_2 \geq 0$, that the gains $k_1 > 0$, $k_2 > 0$ are positive, that $q \geq 1$, and $\mu_1 > 0$. Then the trajectories are ultimate and uniformly bounded, i.e. the system is practically stable, if one of the following conditions are satisfied:

1. $\mu_2 = 0,\ \ p = \frac{1}{2},\ \delta_1 \geq 0$ *is arbitrary and*

$$\delta_2 < \frac{\mu_1^2 \lambda_{\min}\{Q\}}{4\lambda_{\max}\{P\}}\,. \tag{4.18}$$

2. $\mu_2 = 0,\ \frac{1}{2} < p \leq 1$ *and* $\delta_1,\ \delta_2$ *are arbitrary.*
3. $\mu_2 > 0$*and* $\delta_1,\ \delta_2$ *are arbitrary.*

Note that for the classic STA (where $p = \frac{1}{2}$ and $\mu_2 = 0$) the trajectories of the system do not remain bounded for every bounded (4.17) perturbation: for this it is required that δ_2 satisfies (4.18), i.e. that the perturbation ρ_2 is small enough. This is due to the boundedness of $\phi_2(x_1)$. However, the algorithms with $\frac{1}{2} < p \leq 1$ have bounded trajectories for arbitrarily bounded perturbations (4.17), i.e. there are no restrictions on the values of δ_1, δ_2. If there is a linear or a higher order term in $\phi_1(x_1)$, i.e. $\mu_2 > 0$ and $q \geq 1$, then all algorithms have bounded trajectories for arbitrarily bounded perturbations (4.17), with no restrictions on the values of δ_1, δ_2.

4.4.4 *Frequency Domain Interpretation: The Circle Criterium*

An important and recurrent topic in linear control theory is the interpretation of analysis and design methods in the frequency domain. There are also classical relationships between LMIs as (8.15) or Riccati inequalities as (4.14) and certain Frequency domain inequalities. These connections can therefore be used for the analysis or the design of GSOA. Instead of dealing with the general theory in this paragraph this possibility will be illustrated by means of an example.

Consider the GSOA with constant gains and a perturbation term

$$\begin{aligned} \dot{x}_1 &= -k_1\phi_1(x_1) + x_2 \\ \dot{x}_2 &= -k_2\phi_2(x_1) + \rho_2(t,x)\ , \end{aligned}$$

where $\phi_1(x_1)$ and $\phi_2(x_1)$ are as in (4.4), and it is assumed that the perturbation $\rho_2(t,x)$ is bounded by (4.12b), where we use $g = g_2$. The robust stability analysis can be performed through the LMI (in this case Θ is scalar and can be set to one without loss of generality)

$$\begin{bmatrix} A^TP + PA + \varepsilon P + g^2C^TC & PB \\ B^TP & -1 \end{bmatrix} \leq 0\ ,\ B = \begin{bmatrix} 0 \\ 1 \end{bmatrix}\ . \tag{4.19}$$

Using the classical circle criterium [14] the Linear Matrix Inequality (4.19) will be satisfied if and only if the Nyquist diagram of the transfer function $G(s) = C(sI - A)^{-1}B = 1/\left(s^2 + k_1 s + k_2\right)$ is contained in the circle centered at the origin and with radius g, that is, iff

$$\max_{\omega} |G(j\omega)|^2 = \left\{ \begin{array}{ll} \frac{1}{k_2^2} & \text{if } k_2 - \frac{1}{2}k_1^2 < 0 \\ \frac{1}{k_1^2\left(k_2 - \frac{1}{4}k_1^2\right)} & \text{if } k_2 - \frac{1}{2}k_1^2 > 0 \end{array} \right| < \frac{1}{g^2}\ .$$

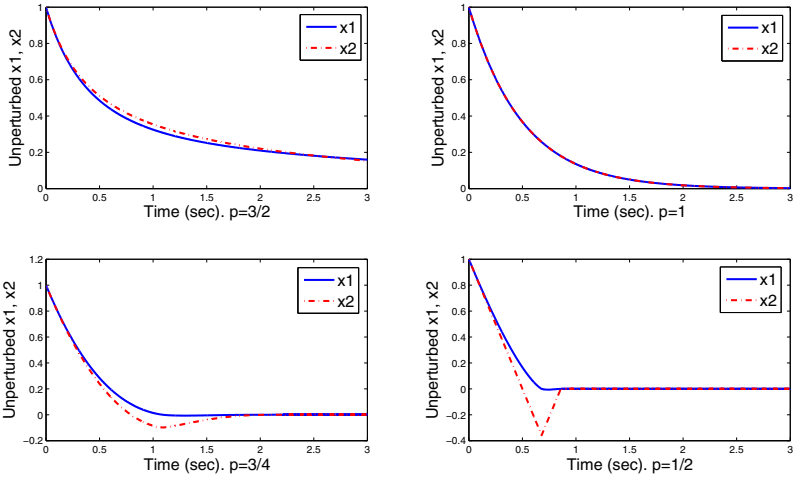

Fig. 4.1 States of the GSO Algorithm without perturbation and for different values of p

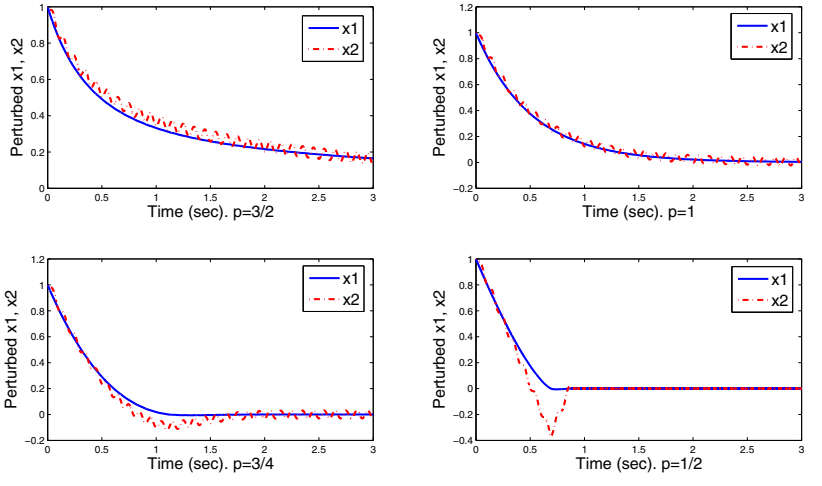

Fig. 4.2 States of the GSO Algorithm with a persistent perturbation $\rho_2(t,x) = 1.9\sin(10t)$, for different values of p

For design purposes it follows that there are two possibilities of selecting the gains $k_1 > 0, k_2 > 0$ so that the GSOA will converge to the origin, despite of a perturbation bounded by g:

- Select k_2 such that $k_2 > g$ and then select $k_1^2 > 2k_2$.
- Select k_1 and k_2 such that both inequalities $k_1^2\left(k_2 - \frac{1}{4}k_1^2\right) > g^2$ and $2k_2 > k_1^2$ are satisfied. This is the case if, for example, one selects $k_1 > g$ and $k_2 > \frac{1}{2}k_1^2 + 1$.

For a selection of the gains as $k_2 = 2$ and $k_1 = 3$ the simulated state trajectories, without and with a perturbation $\rho_2(t,x) = 1.9\sin(10t)$, are presented in Figures 4.1 and 4.2, respectively, for four values of $p = \left(\frac{3}{2}\ ,\ 1\ ,\ \frac{3}{4}\ ,\ \frac{1}{2}\right)$. Note in Figure 4.1 that for $p = \frac{3}{2}$ the convergence is asymptotic, and for $p = 1$ the trajectories converge exponentially. For $p = \frac{3}{4}$ and $p = \frac{1}{2}$ trajectories converge in finite-time. Under a persistent and bounded perturbation (see Figure 4.2) the trajectories are finally and uniformly bounded for the values of $p = \left(\frac{3}{2}\ ,\ 1\ ,\ \frac{3}{4}\right)$. However, for $p = \frac{1}{2}$, that corresponds to the STA, the convergence is *exact*: the trajectories converge to zero in finite-time despite of the bounded perturbation.

4.5 Uniformity of the GSOA with Constant Gains

In the previous section it was shown that global and robust finite-time stability of the origin of the GSOA can be proved when $1 > p \geq \frac{1}{2}$ and $\mu_1 > 0$. Instead, exponential stability is obtained if $p = 1$ and $\mu_1 > 0$. In these results the value of q, the degree of the high order term, is of no importance. In fact, as can be seen in (4.9), the q-dependent term in $\dot{V}_Q$ is only negative semidefinite, except when $q = 1$, and so it is not possible to show that the convergence velocity is increased by the presence of this term, using the quadratic Lyapunov function V_Q (4.5). In this section we will show that the presence of a high order term $\mu_2 |x_1|^q \operatorname{sign}(x_1)$ can indeed highly accelerate the convergence to zero of the trajectories. In fact, if $q > 1$ this acceleration is so strong that the convergence becomes *uniform* in the initial condition (see Definition 4.1), that is, the time to reach a neighborhood of the origin (or the origin itself if $p < 1$) is uniformly bounded by a constant! Since this rather strong convergence property cannot be characterized by the quadratic Lyapunov function V_Q, and alternative strict or strong (non quadratic) Lyapunov function $V_N(x)$ for the GSOA (4.3) will be introduced here. The use of $V_N(x)$ allows us to characterize the uniform convergence property for the GSOA. Moreover, combining the quadratic V_Q and the non quadratic V_N strong Lyapunov functions for the GSOA all properties of the algorithm can be established. Note that for $V_N(x)$ the observations in Remark 4.1 are important.

4.5.1 A Non Quadratic Strong Lyapunov Function for the GSOA

We consider an alternative strong Lyapunov function for the system.

Theorem 4.4. *Consider the system (4.3) with $k_1 > 0$, $k_2 > 0$ constant. The continuous function*

$$V_N(x) = \alpha |\phi_1(x_1)|^2 - \beta |\phi_1(x_1)|^{\frac{1}{q}} \operatorname{sign}(x_1) |x_2|^{\frac{2q-1}{q}} \operatorname{sign}(x_2) + \delta x_2^2 , \qquad (4.20)$$

where $\alpha = k_2\delta$, $\beta = 1$, $\delta > 0$, *is a global,* strong Lyapunov function *for system (4.3) for* δ *sufficiently large. Moreover, the derivative* $\dot{V}_N$ *of the Lyapunov function satisfies the differential inequality*

$$\dot{V}_N \leq -\frac{1}{q}\nu_{\min}\left(\frac{1}{4\delta\max\{1,k_2\}}\right)^{\frac{3q-1}{2q}} V_N^{\frac{3q-1}{2q}}(x) \ , \tag{4.21}$$

where

$$\nu_{\min} \triangleq \min_{x_1\in\mathbb{R}} \frac{p\mu_1|x_1|^{p-q}+q\mu_2}{\left(\mu_1|x_1|^{p-q}+\mu_2\right)^{\frac{q-1}{q}}} \ . \tag{4.22}$$

For $q > 1$ *and* $\mu_2 > 0$ *global asymptotic stability of the origin is assured.*

It is interesting to note, that V_N (4.20) is also a strong (strict) Lyapunov function for system (4.3). Compared to V_Q, whose derivative $\dot{V}_Q$ (4.9) is bounded by a negative definite term containing the power $\frac{3p-1}{2p}$ of V_Q that is smaller than 1 for $p < 1$, the derivative $\dot{V}_N$ (4.21) is bounded by a negative definite term containing the power $\frac{3q-1}{2q}$ that is greater than 1 for $q > 1$. And therefore, both Lyapunov functions reflect different properties of the algorithm.

4.5.2 Uniformity in the Convergence

When $p < 1 < q$ the convergence will be uniform and in finite time, this means that every trajectory converges to zero in a time smaller than a constant, independent of the initial condition! This result will be established using $W(x) = V_Q(x) + V_N(x)$, the sum of the quadratic $V_Q(x)$ (4.5) and the non quadratic $V_N(x)$ (4.20) Lyapunov functions, as a Lyapunov function for the GSOA.

Proposition 4.2. *Suppose that* $k_1 > 0$, $k_2 > 0$, $\mu_1, \mu_2 > 0$ *and* $\frac{1}{2} \leq p < 1 < q$. *Then a trajectory of the GSOA (4.3) starting at* $x_0 \in \mathbb{R}^2$ *converges to the origin in finite time and it reaches that point at most after a time*

$$T(x_0) = \frac{2q}{(q-1)\kappa_2}\left(\frac{1}{\mu^{\frac{q-1}{2q}}} - \frac{1}{W^{\frac{q-1}{2q}}(x_0)}\right) + \frac{2p}{(1-p)\kappa_1}\mu^{\frac{1-p}{2p}} \ , \tag{4.23}$$

where $W(x) = V_Q(x) + V_N(x)$, μ *is any value satisfying* $0 < \mu < W(x_0)$, *and* κ_1, κ_2 *are constants given in (4.30a,4.30b). Moreover, the convergence time is uniformly bounded by*

$$T_{\max} = \frac{2q}{(q-1)\kappa_2}\left(\frac{\kappa_2}{\kappa_1}\right)^{\frac{q-p}{p(q-1)}} + \frac{2p}{(1-p)\kappa_1}\left(\frac{\kappa_1}{\kappa_2}\right)^{\frac{q(1-p)}{q-p}} \ , \tag{4.24}$$

i.e. any trajectory converges to $x = 0$ *in a time smaller than* $T_{\max}$.

4.5.3 An Alternative Robust Lyapunov Function

When perturbation terms satisfying the conditions (4.12) are present, it is possible to show that the non quadratic function (4.20) is a robust, strong Lyapunov function.

Proposition 4.3. *Consider the system (4.3) with perturbations satisfying (4.12), and with constant gains k_1, k_2 sufficiently large. Then the continuous function $V_N(x)$ (4.20), where $\alpha = k_2\delta$, $\beta = 1$, $\delta > 0$, is a global,* robust, strong Lyapunov function *for system (4.3) for δ sufficiently large. Moreover, the derivative $\dot{V}_N$ of the Lyapunov function satisfies the differential inequality*

$$\dot{V}_N \leq -2\psi_{\min} v_{\min} \left(\frac{1}{4\delta \max\{1, k_2\}} \right)^{\frac{3q-1}{2q}} V_N^{\frac{3q-1}{2q}}(x) \ , \tag{4.25}$$

where $v_{\min}$ is as in (4.22) and $\psi_{\min}$ is as in (4.33). For $q > 1$ and $\mu_2 > 0$ robust, and global asymptotic stability of the origin is assured. Moreover, if $\mu_1, \mu_2 > 0$ and $\frac{1}{2} \leq p < 1 < q$ the origin is robust and uniformly stable, and for $p = \frac{1}{2}$ the origin is exactly stable. In these cases the expressions for the reaching time (4.23), and its upper bound (4.24) are also valid, if the values for the constants κ_1, κ_2 are modified appropriately.

Using the non quadratic Lyapunov function it is possible to show that Theorem 4.3 is valid for every $q \geq 1$. This means that a higher order term allows the algorithms to have bounded trajectories for every bounded perturbation.

4.6 The GSOA with Variable Gains

In the previous sections the GSOA (4.3) has been considered with constant gains (k_1, k_2). Our aim in this section is to allow the gains $(k_1(t), k_2(t))$ to be time-varying (or in fact, to be functions of other variables). The main advantage of having variable gains consists in being able to "adapt" on line the values of the gains to external perturbations, when a varying bound of the perturbation is known.

Consider the GSOA (4.3) with variable gains

$$\begin{aligned} \dot{x}_1 &= -k_1(t)\,\phi_1(x_1) + x_2 + \rho_1(t,x) \\ \dot{x}_2 &= -k_2(t)\,\phi_2(x_1) + \rho_2(t,x) \ , \end{aligned}$$

where $\phi_1(x_1)$ and $\phi_2(x_1)$ are as in (4.4). Assume that the perturbations are bounded as (compare to (4.12))

$$|\rho_1(t,x)| \leq g_1(t,x)\,|\phi_1(x_1)| \tag{4.26a}$$

$$|\rho_2(t,x)| \leq g_2(t,x)\,|\phi_2(x_1)| \ , \tag{4.26b}$$

where $g_1(t,x) \geq 0$, $g_2(t,x) \geq 0$ are known continuous functions. It will be shown by means of a *constant*, strong, quadratic Lyapunov function (4.5), that an appropriate

selection of the gains, according to the variation of the perturbations, renders the origin globally and robustly stable. Moreover, when $p = \frac{1}{2}$ it is *exactly* stable.

Theorem 4.5. *Consider the GSOA (4.3), and suppose that the perturbations satisfy (4.26) for some known continuous functions $g_1(t,x) \geq 0$, $g_2(t,x) \geq 0$. Choose the (variable) gains as*

$$\begin{aligned} k_1(t,x) &= \delta + \frac{1}{\beta}\left\{\frac{1}{4\varepsilon}\left[2\varepsilon g_1 + g_2\right]^2 + 2\varepsilon g_2 + \varepsilon + \left[2\varepsilon + g_1(t,x)\right]\left(\beta + 4\varepsilon^2\right)\right\} \\ k_2(t,x) &= \beta + 4\varepsilon^2 + 2\varepsilon k_1(t,x)\ , \end{aligned} \tag{4.27}$$

where $\beta > 0$, $\varepsilon > 0$, $\delta > 0$ are arbitrary positive constants. Then $x = 0$ is a globally, robustly stable point, so that all trajectories of system (4.3) converge to the origin for all perturbations, and the quadratic form $V_Q(x) = \zeta^T P \zeta$ (4.5) is a strong, robust Lyapunov function. *For $1 > p \geq \frac{1}{2}$ and $\mu_1 > 0$ every trajectory reaches the origin in a finite-time smaller than*

$$T(x_0) = \begin{cases} \frac{2p}{(1-p)\gamma_1} V_Q^{\frac{1-p}{2p}}(x_0) & \text{if } \mu_2 = 0 \text{ or } q > 1 \\ \frac{2p}{(1-p)\gamma_2} \ln\left(1 + \frac{\gamma_2}{\gamma_1} V_Q^{\frac{1-p}{2p}}(x_0)\right) & \text{if } \mu_2 > 0 \text{ and } q = 1 \end{cases}, \tag{4.28}$$

where γ_1 and γ_2 are as in (4.35), and x_0 is the initial state. For $p = 1$ and $\mu_1 > 0$ convergence is exponential. When $p = \frac{1}{2}$ the origin is exactly *stable.*

4.7 Conclusions

In this paper a Generalized Second Order Algorithm (GSOA) (4.3) has been introduced, that includes several Second Order Sliding Modes Algorithms of the STA type, and many other continuous algorithms, with constant or time-varying gains, and considering perturbations. For this (large) family of algorithms two different strong (strict) and robust Lyapunov functions are developed: a quadratic and a non-quadratic one. Each of them is useful to establish different properties of the algorithms. The quadratic Lyapunov functions are used to determine finite-time convergence and to estimate the convergence time from every initial condition. Moreover, robustness for perturbations strong near the origin can be established. For the quadratic one a linear framework has been developed, that makes it very easy to design the gains in order to achieve some convergence or robustness properties. In this linear framework the calculations are done in the same fashion as for LTI systems, where Algebraic Lyapunov Equations have to be solved to find the Lyapunov function in the unperturbed case, or Algebraic Riccati Inequalities in the perturbed case. Also frequency domain interpretations are possible, such as the classical Circle Criterion. The non-quadratic Lyapunov functions are used to determine uniform convergence properties, that is, when the convergence of the trajectories has an upper bound for every initial condition. The (uniform) convergence time can be

estimated from these non quadratic Lyapunov functions and robustness against perturbations. For time-varying gains (constant) quadratic Lyapunov functions have been designed, that allow to adapt the gains of the converging algorithms.

One distinguishing feature of the Lyapunov functions proposed here is that they are very simple, but they are also non-smooth. This means that classical Lyapunov theorems cannot be used to prove the convergence. Despite of this, it is shown that one can use these functions in much the same form as with classical (smooth) Lyapunov functions. The user, in fact, can forget the non smoothness issue, and operate with the functions as usual.

An important result of the paper is that the discontinuous algorithms, in particular the Super-Twisting Algorithm (STA), have a unique and distinguishing property among all other (continuous) algorithms: the origin is *exactly* stable, that means, that the equilibrium point is reached in *finite-time* and despite of perturbations that are *non vanishing* at the origin! This important property cannot be achieved by continuous functions.

We expect that the Lyapunov functions proposed in this paper will facilitate the analysis and design of systems with STA-like algorithms. Among other possibilities opened by the Lyapunov treatment is the study of interconnected systems, what is a very interesting topic for analysis and design. There are many other algorithms and topics not considered in this paper, and that deserve particular attention. Although Lyapunov functions for non-homogeneous STA-type algorithms have been considered in [31], there are still many open questions. Initial steps for Lyapunov analysis of second order algorithms of the Twisting-Algorithm type have been done in [32]. An important direction is the Lyapunov analysis for Higher Order Sliding Modes Algorithms.

Acknowledgements. The author gratefully acknowledge the financial support from CONACyT (Consejo Nacional de Ciencia y Tecnologia) , grant 51244, and Programa de Apoyo a Proyectos de Investigación e Innovación Tecnológica (PAPIIT) , UNAM, grant IN117610.

4.8 Appendix

In this appendix we collect the proofs of the results. From the classical Young's inequality it is easy to show the following

Lemma 4.1. *For every real numbers $a>0$, $b>0$, $c>0$, $p>1$, $q>1$, with $\frac{1}{p}+\frac{1}{q}=1$ the following inequality is satisfied*

$$ab \leq c^p \frac{a^p}{p} + c^{-q} \frac{b^q}{q} .$$

The next result justifies the use of continuous but non-locally Lipschitz Lyapunov functions to prove the stability of the origin of (4.3). Denote as $\varphi(t,x_0)$ any (absolutely continuous) solution of the differential inclusion (4.3).

Lemma 4.2. *Consider a continuous, positive definite function* $W : \mathbb{R}^2 \to \mathbb{R}$, *and suppose that it can be written as the*

$$W(x) = \sum_{i=1}^{N} \alpha_i(x_1)\,\beta_i(x_2)\,,$$

where $\beta_i(x_2)$ *are continuously differentiable and* $\alpha_i(x_1)$ *are absolutely continuous (AC) functions. Suppose furthermore that* $\alpha_i(x_1)$ *are continuously differentiable everywhere, except on the point* $x_1 = 0$. *Moreover, assume that when a trajectory* $\varphi(t,x_0)$ *of system (4.3) is in* $\mathscr{R}$, *a domain in* $\mathbb{R}^2$, *and it reaches the set* $\mathscr{S} = \{(x_1,x_2) \in \mathbb{R}^2 \mid x_1 = 0\}$, *i.e.* $\varphi_1(T,x_0) = 0$, *there is a time interval* $\Delta_T = (T-\tau, T+\tau)$ *for which* $|\varphi_2(t,x_0)| > |\rho_1(t,x)|$ *when* $t \in \Delta_T$. *Under these conditions the function* $W(t) = W(\varphi(t,x_0))$, *evaluated along a trajectory of system (4.3), is absolutely continuous when* $\varphi(t,x_0) \in \mathscr{R}$. *The derivative* $\dot{W}(t)$ *exists almost everywhere and, on the set* $\mathscr{R} \setminus \mathscr{S}$, *it can be calculated in the usual form applying the chain rule*

$$\dot{W} = \frac{\partial W(x)}{\partial x} \begin{bmatrix} -k_1(t)\,\phi_1(x_1) + x_2 + \rho_1(t,x) \\ -k_2(t)\,\phi_2(x_1) + \rho_2(t,x) \end{bmatrix}\,,\ \forall x \in \mathscr{R} \setminus \mathscr{S}\,.$$

If $\dot{W}(t) \leq 0 \quad (\geq 0),\ \forall x \in \mathscr{R} \setminus \mathscr{S}$, *then* $W(\varphi(t,x_0))$ *is non-increasing (non-decreasing) as long as* $\varphi(t,x_0) \in \mathscr{R}$. *Moreover, if*

$$\dot{W}(\varphi(t,x_0)) \leq -\gamma(W(\varphi(t,x_0)))$$

for $t \in [t_0,T]$, *with* $T > t_0$, *then*

$$W(\varphi(t,x_0)) \leq W(\varphi(t_0,x_0)) - \int_{t_0}^{t} \gamma(W(\varphi(\tau,x_0)))\,d\tau\,,\ \forall t \in [t_0,T]\,.$$

Proof. Because of the lack of differentiability of $W(x)$ the usual Lyapunov's Theorem [14] cannot be applied. However, a continuous $W(x)$ can be used as a Lyapunov function, in the same spirit as in the theorem of Zubov [40, Theorem 20.2, p. 568.], if it is possible to show that it decreases monotonically along the trajectories of the system, and converges to zero, what we will show next.

Since the state trajectories $\varphi(t,x_0)$ of the differential inclusion (4.3) are AC functions of time, and $W(x)$ is AC, it follows that $W(\varphi(t,x_0))$ is a continuous function of time. Since, in general, the composition of two AC functions $h \circ g$ fails to be AC [6, p. 391], except when h is Lipschitz or g is monotone [6, p. 391], it is not possible to ensure that $V(\varphi(t,x_0))$ is AC. Since $\beta_i(x_2)$ are continuously differentiable, and therefore Lipschitz, it follows that $\beta_i(\varphi_2(t,x_0))$ is AC. The same is true for $\alpha_i(\varphi_1(t,x_0))$, except when $\varphi_1(t,x_0) = 0$. However, in this case, due to the fact that $|\varphi_2(t,x_0)| > |\rho_1(t,x)|$ when $t \in \Delta_T$, it follows form the differential equation $\dot{x}_1 = -k_1(t)\,\phi_1(x_1) + x_2 + \rho_1(t,x)$ that, when x_1 is in a neighborhood of 0, $\dot{x}_1 > 0$ (or $\dot{x}_1 < 0$), so that $\varphi_1(t,x_0)$ will be monotone increasing (or monotone decreasing) during the interval $t \in \Delta_T$. This shows that $\alpha_i(\varphi_1(t,x_0))$ is AC. Since the sum and

product of AC functions is AC $W(\varphi(t,x_0))$ is AC, as long as $\varphi(t,x_0) \in \mathscr{R}$, and it has a derivative almost everywhere. This derivative can be calculated by the chain rule, where the function is continuously differentiable, that is, on the set $\mathscr{R} \setminus \mathscr{S}$. If $\mathscr{R}$ contains the origin, and $x = 0$ is an equilibrium point for the system, then if the origin is reached, then $W(0) = 0$ and the constant function is AC. It is well-known [6,3], that if an AC function satisfies $\dot{W}(t) \leq 0$ (or ≥ 0) almost everywhere, then it is non-increasing (or non-decreasing). Finally, since an AC function is the integral of its derivative [6], then

$$W(\varphi(t,x_0)) - W(\varphi(t_0,x_0)) = \int_{t_0}^{t} \dot{W}(\varphi(\tau,x_0))\,d\tau \leq -\int_{t_0}^{t} \gamma(W(\varphi(\tau,x_0)))\,d\tau\ .$$

□

4.8.1 *Proof of Theorem 4.1*

Equivalence of items (ii), (iii) and (iv) is a well-known fact from Lyapunov stability of Linear Time Invariant Systems. Now it will be shown that (ii) $\Longrightarrow$ (i). For any $Q = Q^T > 0$, with A Hurwitz, it follows that P, the solution of the ALE (4.7), satisfies the stated properties [14]. $V_Q(x)$ (4.5) is AC and continuously differentiable everywhere except on the set $\mathscr{S} = \{(x_1,x_2) \in \mathbb{R}^2 \mid x_1 = 0\}$. Moreover, for P positive definite it is a positive definite and radially unbounded function in $\mathbb{R}^2$. Suppose that $\varphi_2(T,x_0) \neq 0$ at the instant $t = T$, when $\varphi_1(t,x_0)$ crosses zero. Then from the differential inclusion $\dot{x}_1 \in -k_1\phi_1(x_1) + x_2$ follows that $\varphi_1(t,x_0)$ will be monotonically increasing or decreasing during an interval containing T. If $\varphi_2(t,x_0) = 0$ when $\varphi_1(t,x_0)$ crosses zero, then $\varphi_1(t,x_0)$ will stay in zero. Lemma 4.2 is satisfied, with $\mathscr{R} \setminus \mathscr{S} = \mathbb{R}^2 \setminus \mathscr{S}$.

Note that one can write $\phi_2(x_1) = \phi_1'(x_1)\,\phi_1(x_1)$, where $\phi_1'(x_1) = p\mu_1 |x_1|^{p-1} + q\mu_2 |x_1|^{q-1}$. Since

$$\dot{\zeta} = \begin{bmatrix} \phi_1'(x_1)\{-k_1\phi_1(x_1) + x_2\} \\ -k_2\phi_2(x_1) \end{bmatrix} = \phi_1'(x_1) \begin{bmatrix} -k_1 & , & 1 \\ -k_2 & , & 0 \end{bmatrix} \zeta = \phi_1'(x_1) A \zeta\ ,$$

the derivative of the candidate Lyapunov function is

$$\dot{V}_Q(x) = \dot{\zeta}^T P\zeta + \zeta^T P\dot{\zeta} = \phi_1'(x_1)\,\zeta^T \left(A^T P + PA\right)\zeta = -\phi_1'(x_1)\,\zeta^T Q\zeta$$

where Q satisfies the ALE (4.7). Recall the standard inequality for quadratic forms

$$\lambda_{\min}\{P\}\,\|\zeta\|_2^2 \leq \zeta^T P\zeta \leq \lambda_{\max}\{P\}\,\|\zeta\|_2^2\ ,$$

where

$$\|\zeta\|_2^2 = \phi_1^2(x_1) + x_2^2 = \mu_1^2 |x_1|^{2p} + 2\mu_1\mu_2 |x_1|^{p+q} + \mu_2^2 |x_1|^{2q} + x_2^2$$

is the Euclidean norm of ζ, and note that the inequality

$$|x_1|^{1-p} \leq \left(\frac{1}{\mu_1}|\phi_1(x_1)|\right)^{\frac{1-p}{p}} \leq \left(\frac{1}{\mu_1}\|\zeta\|_2\right)^{\frac{1-p}{p}} \leq \left(\frac{V_Q^{\frac{1}{2}}(x)}{\mu_1 \lambda_{\min}^{\frac{1}{2}}\{P\}}\right)^{\frac{1-p}{p}} \tag{4.29}$$

is satisfied for every $\frac{1}{2} \leq p < 1$ and $\mu_1 > 0$, and therefore

$$-|x_1|^{p-1} \leq -\left(\frac{V_Q^{\frac{1}{2}}(x)}{\mu_1 \lambda_{\min}^{\frac{1}{2}}\{P\}}\right)^{\frac{p-1}{p}}.$$

This shows that

$$\dot{V}_Q \leq -\lambda_{\min}\{Q\}\phi_1'(x_1)\|\zeta\|_2^2 \leq -\lambda_{\min}\{Q\}\left(\mu_1 p|x_1|^{p-1} + \mu_2 q|x_1|^{q-1}\right)\|\zeta\|_2^2$$

$$\leq -\mu_1 \frac{p\lambda_{\min}\{Q\}\left(\mu_1 \lambda_{\min}^{\frac{1}{2}}\{P\}\right)^{\frac{p-1}{p}}}{\lambda_{\max}\{P\}} V_Q^{\frac{3p-1}{2p}}(x) - \mu_2 \frac{\lambda_{\min}\{Q\} q}{\lambda_{\max}\{P\}}|x_1|^{q-1} V_Q(x),$$

so that $V(\varphi(t,x_0))$ is monotonically decreasing, and by Zubov's Theorem [40, Theorem 20.2, p. 568.], the origin is asymptotically stable. This shows that $V_Q(x)$ is a strong Lyapunov function when $\mu_1 > 0$ or $\mu_2 > 0$ and $q = 1$. Note that $\frac{1}{2} \leq \frac{3p-1}{2p} \leq 1$, so that for $\mu_1 > 0$ and $\frac{1}{2} \leq p < 1$ the convergence is in finite time. For $\mu_1 > 0$ and $p = 1$ and when $\mu_1 = 0$, $\mu_2 > 0$ and $q = 1$ the convergence is also exponential. If $\mu_1 = 0$, $\mu_2 > 0$ and $q > 1$ the Lyapunov function is weak, since the derivative is negative semidefinite.

Now we show that (i) $\Longrightarrow$ (ii), or equivalently, that $\sim$(ii) $\Longrightarrow$ $\sim$(i). So assume that A is not Hurwitz, so we will show that $x = 0$ is not assymptotically stable for (4.3). Several cases are possible here.

1. The ALE (4.7) does not have a unique solution P for every Q: This is the case if the eigenvalues $\lambda_1(A)$, $\lambda_2(A)$ of A are such that $\lambda_1(A) + \lambda_2(A) = 0$. It is easy to prove that this is the case if and only if $k_1 = 0$. Consider three subcases:
   a. $k_2 > 0$. The eigenvalues of A are imaginary. $P = \begin{bmatrix} k_2 & 0 \\ 0 & 1 \end{bmatrix}$, and $Q = 0$ are solutions of (4.7). So that $V_Q(x)$ is p.d. and $\dot{V}_Q(x) = 0$. This means that $V(\varphi(t,x_0))$ remains constant along the solutions of the system, and so it does not converge to zero.
   b. $k_2 = 0$. A has two eigenvalues at the origin with Jordan form $J = \begin{bmatrix} 0 & 1 \\ 0 & 0 \end{bmatrix}$.
   c. $k_2 < 0$. The eigenvalues of A are real, with the same magnitude but different signs. In this and the preceeding case $P = \begin{bmatrix} p_1 & 0 \\ 0 & p_2 \end{bmatrix} > 0$, and

$Q = \begin{bmatrix} 0 & k_2 p_2 - p_1 \\ k_2 p_2 - p_1 & 0 \end{bmatrix}$ are solutions of (4.7). Using Lemma 4.2, instability can be proved by a simple extension of the proof of Chetaev's theorem for linear systems [14].

2. The ALE (4.7) does have a unique solution P for every Q: This is the case if $\lambda_1(A) + \lambda_2(A) \neq 0$, that is $k_1 \neq 0$. Consider two subcases:
   a. Matrix A is Antihurwitz, that is, both eigenvalues have positive real parts. In this case the ALE (4.7) has a positive definite solution P for every negative definite matrix Q. In this case $V_Q(x) > 0$ has a p.d. derivative $\dot{V}_Q(x) > 0$. Using Lemma 4.2, instability can be proved by a simple extension of the proof of Chetaev's Theorem for linear systems [14].
   b. The eigenvalues of A are real, one positive and the other negative or zero. Using Lemma 4.2, instability can be proved by a simple extension of the proof of Chetaev's Theorem for linear systems [14].

□

4.8.2 *Proof of Proposition 4.1*

Note that the solution of the differential equation

$$\dot{v} = -\gamma_1 v^{\frac{3p-1}{2p}}, \quad v(0) = v_0 \geq 0$$

is given by

$$v(t) = \left(v_0^{\frac{1-p}{2p}} - \left(1 - \frac{3p-1}{2p}\right)\gamma_1 t \right)^{\frac{2p}{1-p}} \text{ if } \gamma_1 > 0\,,\ \frac{1}{2} \leq p < 1\,.$$

More over, the DE

$$\dot{v} = -\gamma_1 v^{\frac{3p-1}{2p}} - \gamma_2 v\,, \quad v(0) = v_0 \geq 0$$

using the transformation $w(t) = \exp(\gamma_2 t)\, v(t)$ leads to

$$\dot{w} = \gamma_2 \exp(\gamma_2 t)\, v + \exp(\gamma_2 t)\left(-\gamma_1 v^{\frac{3p-1}{2p}} - \gamma_2 v\right) = -\gamma_1 \exp(\gamma_2 t)\left(\exp(-\gamma_2 t)\, w\right)^{\frac{3p-1}{2p}}$$
$$= -\gamma_1 \exp\left(\frac{1-p}{2p}\gamma_2 t\right) w^{\frac{3p-1}{2p}}\,, \quad w(0) = v_0 \geq 0\,.$$

Its solution, found by separation of variables,

$$\int_{w(0)}^{w(t)} \frac{dw}{w^{\frac{3p-1}{2p}}} = -\gamma_1 \int_0^t \exp\left(\frac{1-p}{2p}\gamma_2 \tau\right) d\tau$$

is given by

$$\frac{2p}{1-p}w^{\frac{1-p}{2p}}(t)=\frac{2p}{1-p}w^{\frac{1-p}{2p}}(0)-\frac{2p\gamma_1}{(1-p)\gamma_2}\left[\exp\left(\frac{1-p}{2p}\gamma_2 t\right)-1\right]$$

and therefore

$$v(t)^{\frac{1-p}{2p}}=\exp\left(-\frac{1-p}{2p}\gamma_2 t\right)v_0^{\frac{1-p}{2p}}-\frac{\gamma_1}{\gamma_2}\exp\left(-\frac{1-p}{2p}\gamma_2 t\right)\left[\exp\left(\frac{1-p}{2p}\gamma_2 t\right)-1\right].$$

It follows from (4.9) and the Lemma 4.2 that $V_Q(t)\leq v(t)$ when $V_Q(x_0)\leq v_0$. Therefore, $x(t)$ converges to zero in finite time (when $\mu_1>1$) and reaches that value at most after a time given by (4.10). □

4.8.3 Proof of Theorem 4.2

The derivative of the candidate Lyapunov function along the trajectories of the perturbed system (4.11) is

$$\begin{aligned}\dot{V}_Q&=\phi_1'(x_1)\left\{\zeta^T\left(A^TP+PA\right)\zeta+\tilde{\rho}^TB^TP\zeta+\zeta^TPB\tilde{\rho}\right\}\\&=\phi_1'(x_1)\begin{bmatrix}\zeta\\\tilde{\rho}\end{bmatrix}^T\begin{bmatrix}A^TP+PA & PB\\B^TP & 0\end{bmatrix}\begin{bmatrix}\zeta\\\tilde{\rho}\end{bmatrix}\\&\leq\phi_1'(x_1)\left\{\begin{bmatrix}\zeta\\\tilde{\rho}\end{bmatrix}^T\begin{bmatrix}A^TP+PA & PB\\B^TP & 0\end{bmatrix}\begin{bmatrix}\zeta\\\tilde{\rho}\end{bmatrix}+\omega(\tilde{\rho},\zeta)\right\}\\&=\phi_1'(x_1)\begin{bmatrix}\zeta\\\tilde{\rho}\end{bmatrix}^T\begin{bmatrix}A^TP+PA+R & PB\\B^TP & -\Theta\end{bmatrix}\begin{bmatrix}\zeta\\\tilde{\rho}\end{bmatrix}\leq-\phi_1'(x_1)\varepsilon V_Q\end{aligned}$$

$$\begin{aligned}\dot{V}_Q&\leq-p\varepsilon\mu_1|x_1|^{p-1}V_Q-q\varepsilon\mu_2|x_1|^{q-1}V_Q\\&\leq-p\varepsilon\mu_1^{\frac{1}{p}}\lambda_{\min}^{\frac{1-p}{2p}}\{P\}V_Q^{\frac{3p-1}{2p}}(x)-q\varepsilon\mu_2|x_1|^{q-1}V_Q(x)\end{aligned}$$

By similar arguments as the ones in Theorem 4.1 and Proposition 4.1, it can be shown that the state converges to zero in finite time, at most after $T(x_0)$ (4.15) units of time.

Using the Schur complement it is easy to see that the Matrix Inequality (8.15) and the Algebraic Riccati Inequality (4.14) are equivalent. □

4.8.4 Proof of Theorem 4.3

Consider a $P=P^T>0$ such that (4.5) is a Lyapunov function for the unperturbed system. Given some perturbation constants δ_1,δ_2 there is a set $\mathscr{R}=\left\{x\in\mathbb{R}^2\mid\|\zeta\|_2>r\right\}$ such that $\varphi_1(t,x_0)$ is monotone when it crosses zero in $\mathscr{R}$.

Therefore, from Lemma 4.2, it follows that $V_Q(\varphi(t,x_0))$ is AC, and $\dot{V}_Q$ along the solutions of the perturbed system (4.2), where it exists, is given by (when $q=1$)

$$\begin{aligned}
\dot{V}_Q &= -\phi_1'(x_1)\left\{\zeta^T Q\zeta - \left[\rho_1\ 0\right]P\zeta\right\} + 2\left[0\ \rho_2\right]P\zeta \\
&\leq -\phi_1'(x_1)\left\{\lambda_{\min}\{Q\}\|\zeta\|_2^2 - \delta_1\lambda_{\max}\{P\}\|\zeta\|_2\right\} + 2\delta_2\lambda_{\max}\{P\}\|\zeta\|_2 \\
&\leq -\left(p\mu_1|x_1|^{p-1}+\mu_2\right)\left\{\lambda_{\min}\{Q\}\|\zeta\|_2^2 - \delta_1\lambda_{\max}\{P\}\|\zeta\|_2\right\} + 2\delta_2\lambda_{\max}\{P\}\|\zeta\|_2 \\
&\leq -p\mu_1|x_1|^{p-1}\left\{\lambda_{\min}\{Q\}\|\zeta\|_2^2 - \delta_1\lambda_{\max}\{P\}\|\zeta\|_2\right\} - \mu_2\lambda_{\min}\{Q\}\|\zeta\|_2^2 + \\
&+ (\mu_2\delta_1 + 2\delta_2)\lambda_{\max}\{P\}\|\zeta\|_2 \\
&\leq -p\mu_1\left(\frac{1}{\mu_1}\|\zeta\|_2\right)^{\frac{p-1}{p}}\left\{\lambda_{\min}\{Q\}\|\zeta\|_2^2 - \delta_1\lambda_{\max}\{P\}\|\zeta\|_2\right\} - \mu_2\lambda_{\min}\{Q\}\|\zeta\|_2^2 + \\
&+ (\mu_2\delta_1 + 2\delta_2)\lambda_{\max}\{P\}\|\zeta\|_2 \\
&\leq -p\mu_1^{\frac{1}{p}}\lambda_{\min}\{Q\}\|\zeta\|_2^{\frac{3p-1}{p}} + p\mu_1^{\frac{1}{p}}\delta_1\lambda_{\max}\{P\}\|\zeta\|_2^{\frac{2p-1}{p}} - \mu_2\lambda_{\min}\{Q\}\|\zeta\|_2^2 + \\
&+ (\mu_2\delta_1 + 2\delta_2)\lambda_{\max}\{P\}\|\zeta\|_2 \ ,
\end{aligned}$$

where the inequality (obtained from (4.29)), and valid for $\frac{1}{2} \leq p \leq 1$ and $\mu_1 > 0$,

$$-|x_1|^{p-1} \leq -\left(\frac{1}{\mu_1}\|\zeta\|_2\right)^{\frac{p-1}{p}}$$

has been used. If $p=\frac{1}{2}$ and $\mu_2 = 0$ this becomes

$$\dot{V}_Q \leq -\left(\frac{1}{2}\mu_1^2\lambda_{\min}\{Q\} - 2\delta_2\lambda_{\max}\{P\}\right)\|\zeta\|_2 + \frac{1}{2}\mu_1^2\delta_1\lambda_{\max}\{P\} \ .$$

When

$$\delta_2 < \frac{\mu_1^2\lambda_{\min}\{Q\}}{4\lambda_{\max}\{P\}}$$

$$\begin{aligned}
\dot{V}_Q \leq &-\kappa\left(\frac{1}{2}\mu_1^2\lambda_{\min}\{Q\} - 2\delta_2\lambda_{\max}\{P\}\right)\|\zeta\|_2 - (1-\kappa)\left(\frac{1}{2}\mu_1^2\lambda_{\min}\{Q\} - 2\delta_2\lambda_{\max}\{P\}\right)\|\zeta\|_2 + \\
&+ \frac{1}{2}\mu_1^2\delta_1\lambda_{\max}\{P\}
\end{aligned}$$

$$\dot{V}_Q \leq -\kappa\frac{\left(\frac{1}{2}\mu_1^2\lambda_{\min}\{Q\} - 2\delta_2\lambda_{\max}\{P\}\right)}{\lambda_{\max}^{\frac{1}{2}}\{P\}}V_Q^{\frac{1}{2}}(x) \ ,$$

$$\forall\|\zeta\|_2 > \frac{\mu_1^2\delta_1\lambda_{\max}\{P\}}{2(1-\kappa)\left(\frac{1}{2}\mu_1^2\lambda_{\min}\{Q\} - 2\delta_2\lambda_{\max}\{P\}\right)} \ ,$$

for any $0 < \kappa < 1$. This shows the practical stability, i.e. the final and uniform boundedness of the trajectories if δ_2 is small enough.

If $\frac{1}{2} < p \leq 1$, $\mu_1 > 0$ and $\mu_2 = 0$ then

$$\dot{V}_Q \leq -p\mu_1^{\frac{1}{p}} \lambda_{\min}\{Q\} \|\zeta\|_2^{\frac{3p-1}{p}} + 2\delta_2 \lambda_{\max}\{P\} \|\zeta\|_2 + p\mu_1^{\frac{1}{p}} \delta_1 \lambda_{\max}\{P\} \|\zeta\|_2^{\frac{2p-1}{p}}$$

and

$$\frac{3p-1}{p} > 1 > \frac{2p-1}{p} .$$

This implies that for any $0 < \kappa < 1$

$$\begin{aligned} \dot{V}_Q &\leq -\kappa p\mu_1^{\frac{1}{p}} \lambda_{\min}\{Q\} \|\zeta\|_2^{\frac{3p-1}{p}} , \ \forall \|\zeta\|_2 \notin \mathscr{B} , \\ &\leq -\frac{\kappa p\mu_1^{\frac{1}{p}} \lambda_{\min}\{Q\}}{\lambda_{\max}^{\frac{3p-1}{2p}}\{P\}} V_Q^{\frac{3p-1}{2p}}(x) , \ \forall \|\zeta\|_2 \notin \mathscr{B} , \end{aligned}$$

where $\mathscr{B}$ is the compact set given by

$$\mathscr{B} = \left\{ x \in \mathbb{R}^2 \mid 2\delta_2 \lambda_{\max}\{P\} + p\mu_1^{\frac{1}{p}} \delta_1 \lambda_{\max}\{P\} \|\zeta\|_2^{\frac{p-1}{p}} \geq (1-\kappa) p\mu_1^{\frac{1}{p}} \lambda_{\min}\{Q\} \|\zeta\|_2^{\frac{2p-1}{p}} \right\} .$$

Note that for $\frac{1}{2} < p \leq 1$ the set $\mathscr{B}$ contains the origin, and, since $\frac{2p-1}{p} > \frac{p-1}{p}$, it is bounded. This implies that the trajectories of the system are "practically" stable, i.e. they are finally and uniformly bounded.

Finally, when $\mu_2 > 0$ then

$$\begin{aligned} \dot{V}_Q \leq &-\left(\mu_2 \|\zeta\|_2^{\frac{1-p}{p}} + p\mu_1^{\frac{1}{p}} \right) \lambda_{\min}\{Q\} \|\zeta\|_2^{\frac{3p-1}{p}} + p\mu_1^{\frac{1}{p}} \delta_1 \lambda_{\max}\{P\} \|\zeta\|_2^{\frac{2p-1}{p}} + \\ &+ (\mu_2 \delta_1 + 2\delta_2) \lambda_{\max}\{P\} \|\zeta\|_2 , \end{aligned}$$

what implies that for any $0 < \kappa < 1$

$$\begin{aligned} \dot{V}_Q &\leq -\kappa \left(\mu_2 \|\zeta\|_2^{\frac{1-p}{p}} + p\mu_1^{\frac{1}{p}} \right) \lambda_{\min}\{Q\} \|\zeta\|_2^{\frac{3p-1}{p}} , \ \forall \|\zeta\|_2 \notin \mathscr{D} , \\ &\leq -\kappa \frac{p\mu_1^{\frac{1}{p}} \lambda_{\min}\{Q\}}{\lambda_{\max}^{\frac{3p-1}{2p}}\{P\}} V_Q^{\frac{3p-1}{2p}}(x) - \kappa \frac{\mu_2 \lambda_{\min}\{Q\}}{\lambda_{\max}\{P\}} V_Q(x) , \ \forall \|\zeta\|_2 \notin \mathscr{D} , \end{aligned}$$

where $\mathscr{D}$ is the compact set given by

$$\begin{aligned} \mathscr{D} = \Bigg\{ x \in \mathbb{R}^2 \mid &(\mu_2 \delta_1 + 2\delta_2) \lambda_{\max}\{P\} + p\mu_1^{\frac{1}{p}} \delta_1 \lambda_{\max}\{P\} \|\zeta\|_2^{\frac{p-1}{p}} \\ &\geq (1-\kappa) \left(\mu_2 \|\zeta\|_2^{\frac{1-p}{p}} + p\mu_1^{\frac{1}{p}} \right) \lambda_{\min}\{Q\} \|\zeta\|_2^{\frac{2p-1}{p}} \Bigg\} . \end{aligned}$$

This implies that the trajectories of the system are "practically" stable, i.e. they are finally and uniformly bounded. □

4.8.5 *Proof of Theorem 4.4*

The derivative of $V_N(x)$ is given by

$$\dot{V}_N(x) = -|\phi_1(x_1)|^{\frac{1-q}{q}}\phi_1'(x_1)\left\{2\alpha k_1|\phi_1(x_1)|^{\frac{3q-1}{q}} - 2(\alpha - k_2\delta)\phi_1^{\frac{2q-1}{q}}(x_1)x_2 + \right.$$
$$\left. -\frac{1}{q}\beta k_1\phi_1(x_1)|x_2|^{\frac{2q-1}{q}}\operatorname{sign}(x_2) - k_2\frac{2q-1}{q}\beta|\phi_1(x_1)|^2|x_2|^{\frac{q-1}{q}} + \frac{1}{q}\beta|x_2|^{\frac{3q-1}{q}}\right\}$$

If $q = 1$

$$\dot{V}_N(x) = -\phi_1'(x_1)\left\{(2\alpha k_1 - k_2\beta)|\phi_1(x_1)|^2 - 2\left(\alpha - k_2\delta + \frac{1}{2}\beta k_1\right)\phi_1(x_1)x_2 + \beta|x_2|^2\right\}$$
$$\leq -\mu_2\zeta^T\begin{bmatrix}(2\alpha k_1 - k_2\beta) & -\left(\alpha - k_2\delta + \frac{1}{2}\beta k_1\right)\\ -\left(\alpha - k_2\delta + \frac{1}{2}\beta k_1\right) & \beta\end{bmatrix}\zeta$$

where $\zeta^T = \left[\phi_1(x_1)\ , x_2\right]$, and the last inequality follows from $\phi_1'(x_1) = \left(p\mu_1|x_1|^{p-1} + \mu_2\right) \geq \mu_2$. $\dot{V}(x)$ is negative definite iff

$$(2\alpha k_1 - k_2\beta)\beta - \left(\alpha - k_2\delta + \frac{1}{2}\beta k_1\right)^2 > 0\,.$$

Setting $\alpha = k_2\delta$ one obtains

$$\delta > \frac{\beta}{2}\left(\frac{1}{k_1} + \frac{k_1}{4k_2}\right)\,.$$

When $q > 1$, from Lemma 4.1 it follows that

$$\phi_1^{\frac{2q-1}{q}}(x_1)x_2 \leq |\phi_1(x_1)|^{\frac{2q-1}{q}}|x_2| \leq \frac{\gamma_1^{\frac{3q-1}{2q-1}}}{\frac{3q-1}{2q-1}}|\phi_1(x_1)|^{\frac{2q-1}{q}\frac{3q-1}{2q-1}} + \frac{\gamma_1^{-\frac{3q-1}{q}}}{\frac{3q-1}{q}}|x_2|^{\frac{3q-1}{q}}\ ,$$

$$|\phi_1(x_1)||x_2|^{\frac{2q-1}{q}} \leq \frac{\gamma_2^{\frac{3q-1}{q}}}{\frac{3q-1}{q}}|\phi_1(x_1)|^{\frac{3q-1}{q}} + \frac{\gamma_2^{-\frac{3q-1}{2q-1}}}{\frac{3q-1}{2q-1}}|x_2|^{\frac{2q-1}{q}\frac{3q-1}{2q-1}}\ ,$$

$$|\phi_1(x_1)|^2|x_2|^{\frac{q-1}{q}} \leq \frac{\gamma_3^{\frac{3q-1}{2q}}}{\frac{3q-1}{2q}}|\phi_1(x_1)|^{2\frac{3q-1}{2q}} + \frac{\gamma_3^{-\frac{3q-1}{q-1}}}{\frac{3q-1}{q-1}}|x_2|^{\frac{q-1}{q}\frac{3q-1}{q-1}}\ ,$$

are valid for $\left\{\frac{3q-1}{2q-1} > 1, \frac{3q-1}{q} > 1, \frac{3q-1}{2q} > 1\right\}$, that is $\left\{q > \frac{1}{2}, q > \frac{1}{2}, q > 1\right\}$, and every $\gamma_1, \gamma_2, \gamma_3 > 0$. Using these three inequalities one obtains

$$\dot{V}_N(x) \leq -|\phi_1(x_1)|^{\frac{1-q}{q}}\phi_1'(x_1)\{$$
$$\left[2\alpha k_1 - 2|(\alpha - k_2\delta)|\frac{\gamma_1^{\frac{3q-1}{2q-1}}}{\frac{3q-1}{2q-1}} - \frac{1}{q}\beta k_1\frac{\gamma_2^{\frac{3q-1}{q}}}{\frac{3q-1}{q}} - k_2\frac{2q-1}{q}\beta\frac{\gamma_3^{\frac{3q-1}{2q}}}{\frac{3q-1}{2q}}\right]|\phi_1(x_1)|^{\frac{3q-1}{q}} +$$
$$+\left[\frac{1}{q}\beta - 2|(\alpha - k_2\delta)|\frac{\gamma_1^{-\frac{3q-1}{q}}}{\frac{3q-1}{q}} - \frac{1}{q}\beta k_1\frac{\gamma_2^{-\frac{3q-1}{2q-1}}}{\frac{3q-1}{2q-1}} - k_2\frac{2q-1}{q}\beta\frac{\gamma_3^{-\frac{3q-1}{q-1}}}{\frac{3q-1}{q-1}}\right]|x_2|^{\frac{3q-1}{q}}\Bigg\}$$

Choosing

$$\alpha = k_2\delta$$

then

$$\dot{V}_N(x) \leq -|\phi_1(x_1)|^{\frac{1-q}{q}}\phi_1'(x_1)\left\{\left[2\delta k_1 k_2 - \frac{1}{3q-1}\beta k_1\gamma_2^{\frac{3q-1}{q}} - 2k_2\frac{2q-1}{3q-1}\beta\gamma_3^{\frac{3q-1}{2q}}\right]\times\right.$$
$$\left.|\phi_1(x_1)|^{\frac{3q-1}{q}} + \frac{1}{q}\beta\left[1 - k_1\frac{2q-1}{3q-1}\gamma_2^{-\frac{3q-1}{2q-1}} - k_2\frac{(2q-1)(q-1)}{3q-1}\gamma_3^{-\frac{3q-1}{q-1}}\right]|x_2|^{\frac{3q-1}{q}}\right\}.$$

Note that

$$\nu(x_1) \triangleq |\phi_1(x_1)|^{\frac{1-q}{q}}\phi_1'(x_1) = \left(\mu_1|x_1|^p + \mu_2|x_1|^q\right)^{\frac{1-q}{q}}\left(p\mu_1|x_1|^{p-1} + q\mu_2|x_1|^{q-1}\right)$$
$$= \frac{p\mu_1|x_1|^{p-q} + q\mu_2}{\left(\mu_1|x_1|^{p-q} + \mu_2\right)^{\frac{q-1}{q}}} = \frac{\frac{p\mu_1}{|x_1|^{q-p}} + q\mu_2}{\left(\frac{\mu_1}{|x_1|^{q-p}} + \mu_2\right)^{\frac{q-1}{q}}}.$$

It follows that

$$\nu(x_1) > 0\ ,\ \forall x_1\ ,\ \lim_{|x_1|\to\infty}\nu(x_1) = q\mu_2^{\frac{1}{q}}\ ,$$
$$\lim_{|x_1|\to 0}\nu(x_1) = \lim_{|x_1|\to 0}\frac{p\mu_1^{\frac{1}{q}}}{|x_1|^{(q-p)\frac{1}{q}}} = \infty\ ,$$

and $\nu_{\min} = \min_{x_1\in\mathbb{R}}\nu(x_1)$, the minimum of $\nu(x_1)$ exists and $\nu_{\min} > 0$.

Choosing $\gamma_2, \gamma_3 > 0$ such that

$$1 > \frac{2q-1}{3q-1}\left(k_1\gamma_2^{-\frac{3q-1}{2q-1}} + k_2(q-1)\gamma_3^{-\frac{3q-1}{q-1}}\right)\ ,$$

what is always possible, and choosing

$$\delta > \frac{\beta}{2k_1k_2(3q-1)}\left(k_1\gamma_2^{\frac{3q-1}{q}} + 2k_2(2q-1)\gamma_3^{\frac{3q-1}{2q}}\right)$$

it follows that $\dot{V}_N(x)$ is negative definite. In particular, if

$$\gamma_2 = \left(4\frac{2q-1}{3q-1}k_1\right)^{\frac{2q-1}{3q-1}} \ , \ \gamma_3 = \left(4\frac{2q-1}{3q-1}k_2\left(q-1\right)\right)^{\frac{q-1}{3q-1}}$$

and

$$\delta > \frac{\beta}{2k_1k_2\left(3q-1\right)}\left(k_1\gamma_2^{\frac{3q-1}{q}} + 2k_2\left(2q-1\right)\gamma_3^{\frac{3q-1}{2q}}\right) + \frac{1}{2q}\frac{\beta}{2k_1k_2}$$

one finally obtains that

$$\dot{V}_N\left(x\right) \leq -\frac{1}{2q}\beta\nu_{\min}\left(\left|\phi_1\left(x_1\right)\right|^{\frac{3q-1}{q}} + \left|x_2\right|^{\frac{3q-1}{q}}\right) < 0 \, .$$

To show positive definiteness of V_N note that $\forall\gamma_4 > 0$, $q > \frac{1}{2}$

$$\left|\phi_1\left(x_1\right)\right|^{\frac{1}{q}}\left|x_2\right|^{\frac{2q-1}{q}} \leq \frac{\gamma_4^{2q}}{2q}\left|\phi_1\left(x_1\right)\right|^{\frac{1}{q}2q} + \frac{\gamma_4^{-\frac{2q}{2q-1}}}{\frac{2q}{2q-1}}\left|x_2\right|^{\frac{2q-1}{q}\frac{2q}{2q-1}} \ ,$$

and therefore

$$V_N\left(x\right) \leq \left(\alpha + \beta\frac{\gamma_4^{2q}}{2q}\right)\left|\phi_1\left(x_1\right)\right|^2 + \left(\delta + \frac{2q-1}{2q}\beta\gamma_4^{-\frac{2q}{2q-1}}\right)x_2^2$$

$$V_N\left(x\right) \geq \left(\alpha - \beta\frac{\gamma_4^{2q}}{2q}\right)\left|\phi_1\left(x_1\right)\right|^2 + \left(\delta - \frac{2q-1}{2q}\beta\gamma_4^{-\frac{2q}{2q-1}}\right)x_2^2 \qquad .$$

If

$$\alpha > \beta\frac{\gamma_4^{2q}}{2q} \ , \ \delta > \frac{2q-1}{2q}\beta\gamma_4^{-\frac{2q}{2q-1}}$$

or, equivalently

$$\left(\frac{2q-1}{2q}\frac{\beta}{\delta}\right)^{\frac{2q-1}{2q}} < \gamma_4 < \left(\frac{2q\alpha}{\beta}\right)^{\frac{1}{2q}} \ .$$

Such a γ_4 exists if and only if

$$\beta < \left(\frac{1}{2q-1}\right)^{\frac{2q-1}{2q}} 2q\delta^{\frac{2q-1}{2q}}\alpha^{\frac{1}{2q}} \ .$$

In this case $V_N\left(x\right)$ is positive definite.

Setting (without loss of generality) $\beta = 1$, and since $\alpha = k_2\delta$, it is required to choose

$$\delta > \max\left\{\frac{\left(2q-1\right)^{\frac{2q-1}{2q}}}{2qk_2^{\frac{1}{2q}}} \ , \ \frac{1}{2k_1k_2\left(3q-1\right)}\left(k_1\gamma_2^{\frac{3q-1}{q}} + 2k_2\left(2q-1\right)\gamma_3^{\frac{3q-1}{2q}}\right) + \frac{1}{2q}\frac{1}{2k_1k_2}\right\}$$

so that $V_N\left(x\right)$ is positive definite and $\dot{V}_N\left(x\right)$ is negative definite and

$$V_N(x) \le 2\delta\left(k_2|\phi_1(x_1)|^2 + x_2^2\right) \le 2\delta\max\{1,k_2\}\left(|\phi_1(x_1)|^2 + x_2^2\right)$$
$$\dot{V}_N(x) \le -\frac{1}{2q}\nu_{\min}\left(|\phi_1(x_1)|^{\frac{3q-1}{q}} + |x_2|^{\frac{3q-1}{q}}\right) < 0\,.$$

Note that for $q > 1$, $\frac{3q-1}{q} > 2$, and using the standard inequality

$$\left[\frac{1}{2}\left(|\phi_1(x_1)|^2 + x_2^2\right)\right]^{\frac{1}{2}} \le \left[\frac{1}{2}\left(|\phi_1(x_1)|^{\frac{3q-1}{q}} + |x_2|^{\frac{3q-1}{q}}\right)\right]^{\frac{q}{3q-1}}$$

it follows that

$$\left(\frac{1}{2}\right)^{\frac{q-1}{2q}}\left(|\phi_1(x_1)|^2 + x_2^2\right)^{\frac{3q-1}{2q}} \le \left(|\phi_1(x_1)|^{\frac{3q-1}{q}} + |x_2|^{\frac{3q-1}{q}}\right)$$

and therefore

$$\begin{aligned}\dot{V}_N(x) &\le -\frac{1}{2q}\nu_{\min}\left(|\phi_1(x_1)|^{\frac{3q-1}{q}} + |x_2|^{\frac{3q-1}{q}}\right)\\ &\le -\frac{1}{2q}\left(\frac{1}{2}\right)^{\frac{q-1}{2q}}\nu_{\min}\left(|\phi_1(x_1)|^2 + x_2^2\right)^{\frac{3q-1}{2q}}\\ &\le -\frac{1}{q}\nu_{\min}\left(\frac{1}{4\delta\max\{1,k_2\}}\right)^{\frac{3q-1}{2q}} V_N^{\frac{3q-1}{2q}}(x)\,.\end{aligned}$$

Since for $q > 1$, $\frac{3q-1}{2q} > 1$ asymptotic convergence to the origin is assured. □

4.8.6 *Proof of Proposition 4.2*

Consider as a Lyapunov function the sum of both Lyapunov functions (4.5) and (4.20)

$$W(x) = V_Q(x) + V_N(x)\,.$$

It is clear that

$$\dot{W}(x) \le -\gamma_1(Q,\mu_1)V_Q^{\frac{3p-1}{2p}}(x) - \frac{1}{q}\nu_{\min}\left(\frac{1}{4\delta\max\{1,k_2\}}\right)^{\frac{3q-1}{2q}} V_N^{\frac{3q-1}{2q}}(x)\,.$$

Recall that $\|\zeta\|_2^2 = \phi_1^2(x_1) + x_2^2$ and

$$\lambda_{\min}\{P\}\|\zeta\|_2^2 \le V_Q(x) \le \lambda_{\max}\{P\}\|\zeta\|_2^2$$
$$\theta_{\min}\|\zeta\|_2^2 \le V_N(x) \le 2\delta\max\{1,k_2\}\|\zeta\|_2^2$$

so that

$$W(x) \le [\lambda_{\max}\{P\} + 2\delta\max\{1,k_2\}]\|\zeta\|_2^2$$

and therefore

$$\begin{aligned}\dot{W}(x) &\leq -\gamma_1(Q,\mu_1)\lambda_{\min}^{\frac{3p-1}{2p}}\{P\}\|\zeta\|_2^{\frac{3p-1}{p}} - \frac{1}{q}\nu_{\min}\left(\frac{1}{4\delta\max\{1,k_2\}}\right)^{\frac{3q-1}{2q}}\theta_{\min}^{\frac{3q-1}{2q}}\|\zeta\|_2^{\frac{3q-1}{p}} \\ &\leq -\kappa_1 W^{\frac{3p-1}{2p}}(x) - \kappa_2 W^{\frac{3q-1}{2q}}(x)\ ,\end{aligned}$$

where

$$\kappa_1 = \frac{\gamma_1(Q,\mu_1)\lambda_{\min}^{\frac{3p-1}{2p}}\{P\}}{\left[\lambda_{\max}\{P\}+2\delta\max\{1,k_2\}\right]^{\frac{3p-1}{2p}}}\ , \tag{4.30a}$$

$$\kappa_2 = \frac{1}{q}\nu_{\min}\left(\frac{\theta_{\min}}{4\delta\max\{1,k_2\}\left[\lambda_{\max}\{P\}+2\delta\max\{1,k_2\}\right]}\right)^{\frac{3q-1}{2q}}\ . \tag{4.30b}$$

Note that the solution of the differential equation

$$\dot{v} = -\kappa_2 v^{\frac{3q-1}{2q}}\ ,\quad v(0) = v_0 \geq 0$$

is given by

$$v(t) = \frac{1}{\left(\frac{1}{v_0^{\frac{q-1}{2q}}} + \left(\frac{q-1}{2q}\right)\kappa_2 t\right)^{\frac{2q}{q-1}}} \text{ if } \kappa_2 > 0\ ,\ 1 < q\ .$$

Since W satisfies both differential inequalities $\dot{W}(x) \leq -\kappa_1 W^{\frac{3p-1}{2p}}(x)$ and $\dot{W}(x) \leq -\kappa_2 W^{\frac{3q-1}{2q}}(x)$ the value of W is below the solution of any of both inequalities. So

$$W(t) \leq \min\left\{\left(W^{\frac{1-p}{2p}}(x_0) - \left(\frac{1-p}{2p}\right)\kappa_1 t\right)^{\frac{2p}{1-p}}\ ,\ \frac{1}{\left(\frac{1}{W^{\frac{q-1}{2q}}(x_0)} + \left(\frac{q-1}{2q}\right)\kappa_2 t\right)^{\frac{2q}{q-1}}}\right\}.$$

From this expression it is possible to estimate the convergence time, in the following form: consider a trajectory starting at point x_0, at an energy level $W(x_0)$. An upper bound $T_1(x_0)$ of the time at which it reaches the surface level $W(x) = \mu$, for some $0 < \mu < W(x_0)$, can be calculated from

$$\frac{1}{\left(\frac{1}{W^{\frac{q-1}{2q}}(x_0)} + \left(\frac{q-1}{2q}\right)\kappa_2 T_1(x_0)\right)^{\frac{2q}{q-1}}} = \mu$$

as

$$T_1(x_0) = \frac{2q}{(q-1)\kappa_2}\left(\frac{1}{\mu^{\frac{q-1}{2q}}} - \frac{1}{W^{\frac{q-1}{2q}}(x_0)}\right)$$

Now starting from this surface μ an upperbound $T_2(x_0)$ to reach the origin can be calculated from

$$\left(\mu^{\frac{1-p}{2p}} - \left(\frac{1-p}{2p}\right)\kappa_1 T_2(x_0)\right)^{\frac{2p}{1-p}} = 0$$

as

$$T_2(x_0) = \frac{2p}{(1-p)\kappa_1}\mu^{\frac{1-p}{2p}}.$$

And therefore the (total) time to reach the origin can be estimated as

$$T(x_0) = T_1(x_0) + T_2(x_0) = \frac{2q}{(q-1)\kappa_2}\left(\frac{1}{\mu^{\frac{q-1}{2q}}} - \frac{1}{W^{\frac{q-1}{2q}}(x_0)}\right) + \frac{2p}{(1-p)\kappa_1}\mu^{\frac{1-p}{2p}},$$

for every $0 < \mu < W(x_0)$. From this expression it is clear that (i) every trajectory converges to zero in finite time, and (ii) the convergence time is uniformly upper bounded by a constant, that can be estimated as

$$T_{\max}(\mu) = \frac{2q}{(q-1)\kappa_2}\frac{1}{\mu^{\frac{q-1}{2q}}} + \frac{2p}{(1-p)\kappa_1}\mu^{\frac{1-p}{2p}}.$$

This function achieves a minimum at

$$\mu = \left(\frac{\kappa_1}{\kappa_2}\right)^{\frac{2pq}{q-p}},$$

so that the best estimate of the uniform convergence time is

$$T_{\max} = \frac{2q}{(q-1)\kappa_2}\left(\frac{\kappa_2}{\kappa_1}\right)^{\frac{q-p}{p(q-1)}} + \frac{2p}{(1-p)\kappa_1}\left(\frac{\kappa_1}{\kappa_2}\right)^{\frac{q(1-p)}{q-p}}.$$

□

4.8.7 *Proof of Proposition 4.3*

Since the perturbation terms are bounded as $|\rho_1(t,x)| \leq g_1|\phi_1(x_1)|$, $|\rho_2(t,x)| \leq g_2|\phi_2(x_1)|$, then there exist functions $\tilde{g}_1(t)$, $\tilde{g}_2(t)$ such that $\rho_1(t,x) = \tilde{g}_1(t)\phi_1(x_1)$, $\rho_2(t,x) = \tilde{g}_2(t)\phi_2(x_1)$, with $|\tilde{g}_1(t)| \leq g_1$, and $|\tilde{g}_2(t)| \leq g_2$. The derivative of $V_N(x)$ is given by

$$\dot{V}_N(x) = -|\phi_1(x_1)|^{\frac{1-q}{q}}\phi_1'(x_1)\Big\{2\alpha\hat{k}_1(t)|\phi_1(x_1)|^{\frac{3q-1}{q}} + \\ -2\left(\alpha-\hat{k}_2(t)\delta\right)|\phi_1(x_1)|^{\frac{2q-1}{q}}\operatorname{sign}(x_1)x_2 - \frac{1}{q}\beta\hat{k}_1(t)\phi_1(x_1)|x_2|^{\frac{2q-1}{q}}\operatorname{sign}(x_2) + \\ -\hat{k}_2(t)\frac{2q-1}{q}\beta|\phi_1(x_1)|^2|x_2|^{\frac{q-1}{q}} + \frac{1}{q}\beta|x_2|^{\frac{3q-1}{q}}\Big\},$$

where $\hat{k}_1(t) = k_1 - \tilde{g}_1(t)$, $\hat{k}_2(t) = k_2 - \tilde{g}_2(t)$. In a similar form as in the proof of Theorem 4.4 (using Lemma 4.1) one obtains

$$\dot{V}_N(x) \leq -|\phi_1(x_1)|^{\frac{1-q}{q}}\phi_1'(x_1)\left\{\psi_1(t)|\phi_1(x_1)|^{\frac{3q-1}{q}} + \psi_2(t)|x_2|^{\frac{3q-1}{q}}\right\},$$

where

$$\psi_1(t) = 2\alpha\hat{k}_1(t) - 2\left|\left(\alpha-\hat{k}_2(t)\delta\right)\right|\frac{2q-1}{3q-1}\gamma_1^{\frac{3q-1}{2q-1}} - \beta\hat{k}_1(t)\frac{1}{3q-1}\gamma_2^{\frac{3q-1}{q}} + \\ -2\beta\hat{k}_2(t)\frac{2q-1}{3q-1}\gamma_3^{\frac{3q-1}{2q}}$$

$$\psi_2(t) = \frac{1}{q}\beta - 2\left|\left(\alpha-\hat{k}_2(t)\delta\right)\right|\frac{q}{3q-1}\gamma_1^{-\left(\frac{3q-1}{q}\right)} - \frac{1}{q}\beta\hat{k}_1(t)\frac{2q-1}{3q-1}\gamma_2^{-\left(\frac{3q-1}{2q-1}\right)} + \\ -\beta\hat{k}_2(t)\frac{2q-1}{q}\frac{q-1}{3q-1}\gamma_3^{-\left(\frac{3q-1}{q-1}\right)}.$$

For negative definiteness it is required that $\psi_1(t) > 0$ and $\psi_2(t) > 0$. Assuming that $k_1 > b_1 g_1$ and $k_2 > b_2 g_2$ it follows that $k_1 - g_1 \leq \hat{k}_1(t) \leq k_1 + g_1$, $k_2 - g_2 \leq \hat{k}_2(t) \leq k_2 + g_2$ and

$$\left|\left(\alpha-\tilde{k}_2(t)\delta\right)\right| = |\alpha - k_2\delta + \tilde{g}_2(t)\delta| \leq |\alpha - k_2\delta| + g_2\delta.$$

Choosing $\alpha = k_2\delta$ it follows that

$$\psi_1(t) \geq \beta\Upsilon_1 - 2g_2\delta\frac{2q-1}{3q-1}\gamma_1^{\frac{3q-1}{2q-1}},\ \psi_2(t) \geq \frac{1}{q}\beta\Upsilon_2 - 2g_2\delta\frac{q}{3q-1}\gamma_1^{-\left(\frac{3q-1}{q}\right)},$$

$$\Upsilon_1 = 2k_2\bar{k}_1\frac{\delta}{\beta} - \bar{k}_1\frac{1}{3q-1}\gamma_2^{\frac{3q-1}{q}} - 2\bar{k}_2\frac{2q-1}{3q-1}\gamma_3^{\frac{3q-1}{2q}},$$

$$\Upsilon_2 = 1 - \bar{k}_1\frac{2q-1}{3q-1}\gamma_2^{-\left(\frac{3q-1}{2q-1}\right)} - \bar{k}_2\frac{(2q-1)(q-1)}{3q-1}\gamma_3^{-\left(\frac{3q-1}{q-1}\right)}$$

where $\bar{k}_1 = k_1 - g_1$, $\bar{k}_2 = k_2 - g_2$. $\psi_1(t) > 0$ and $\psi_2(t) > 0$ if

$$\beta\Upsilon_1 > 2g_2\delta\frac{2q-1}{3q-1}\gamma_1^{\frac{3q-1}{2q-1}},\ \frac{1}{q}\beta\Upsilon_2 > 2g_2\delta\frac{q}{3q-1}\gamma_1^{-\left(\frac{3q-1}{q}\right)}$$

or equivalently

$$\left(\frac{q^2}{3q-1}\frac{2g_2\delta}{\beta\Upsilon_2}\right)^{\frac{q}{3q-1}} < \gamma_1 < \left(\frac{3q-1}{2q-1}\frac{\beta\Upsilon_1}{2g_2\delta}\right)^{\frac{2q-1}{3q-1}} .$$

Such a γ_1 exists iff

$$\left(\frac{q^2}{3q-1}\frac{2g_2\delta}{\beta\Upsilon_2}\right)^{\frac{q}{3q-1}} < \left(\frac{3q-1}{2q-1}\frac{\beta\Upsilon_1}{2g_2\delta}\right)^{\frac{2q-1}{3q-1}} ,$$

or

$$2\frac{q^{\frac{2q}{3q-1}}(2q-1)^{\frac{2q-1}{3q-1}}}{3q-1}g_2\frac{\delta}{\beta} < \Upsilon_2^{\frac{q}{3q-1}}\Upsilon_1^{\frac{2q-1}{3q-1}} \tag{4.31}$$

Choosing, for example, γ_2 and γ_3 such that

$$\bar{k}_1\frac{2q-1}{3q-1}\gamma_2^{-\left(\frac{3q-1}{2q-1}\right)} = \frac{1}{4} , \ \bar{k}_2\frac{(2q-1)(q-1)}{3q-1}\gamma_3^{-\left(\frac{3q-1}{q-1}\right)} = \frac{1}{4}$$

then $\Upsilon_2 = 1/2$ and (4.31) becomes

$$\frac{2^{\frac{4q-1}{2q-1}}q^{\frac{2q}{2q-1}}(2q-1)}{(3q-1)^{\frac{3q-1}{2q-1}}}g_2^{\frac{3q-1}{2q-1}}\left(\frac{\delta}{\beta}\right)^{\frac{3q-1}{2q-1}} + \frac{(4(2q-1))^{\frac{2q-1}{q}}}{(3q-1)^{\frac{3q-1}{q}}}\bar{k}_1^{\frac{3q-1}{q}}$$
$$+ 2(4(q-1))^{\frac{q-1}{2q}}\frac{(2q-1)^{\frac{3q-1}{2q}}}{(3q-1)^{\frac{3q-1}{2q}}}\bar{k}_2^{\frac{3q-1}{2q}} < 2\bar{k}_1k_2\frac{\delta}{\beta} .$$

Selecting, for example,

$$\frac{\delta}{\beta} = \eta\bar{k}_1^{\frac{2q-1}{q}} , \ \eta > 0 \tag{4.32}$$

the previous inequality becomes

$$\bar{k}_1 > \frac{2^{\frac{2q-1}{3q-1}}(q-1)^{\frac{q-1}{2(3q-1)}}(2q-1)^{\frac{1}{2}}}{(3q-1)^{\frac{1}{2}}\left[2\eta k_2 - \left(\frac{2^{\frac{4q-1}{2q-1}}q^{\frac{2q}{2q-1}}(2q-1)}{(3q-1)^{\frac{3q-1}{2q-1}}}g_2^{\frac{3q-1}{2q-1}}\eta^{\frac{3q-1}{2q-1}} + \frac{(4(2q-1))^{\frac{2q-1}{q}}}{(3q-1)^{\frac{3q-1}{q}}}\right)\right]^{\frac{q}{3q-1}}}\bar{k}_2^{\frac{1}{2}} ,$$

that can be always satisfied selecting k_2 large enough, so that the denominator is positive, and then making $\bar{k}_1$ large enough. Setting

$$\psi_{\min} = \min\{\psi_1(t) , \psi_2(t)\} \tag{4.33}$$

and with $\nu_{\min}$ defined in (4.22), one finally obtains that

$$\dot{V}_N(x) \leq -\psi_{\min}\nu_{\min}\left(|\phi_1(x_1)|^{\frac{3q-1}{q}} + |x_2|^{\frac{3q-1}{q}}\right) < 0 .$$

Recall from Theorem 4.4 that V_N is positive definite if (using $\alpha = k_2\delta$)

$$\frac{(2q-1)^{\frac{2q-1}{2q}}}{2qk_2^{\frac{1}{2q}}} < \frac{\delta}{\beta}\,.$$

This condition and (4.32) can be satisfied simultaneously if η and/or $\bar{k}_1$ are selected large enough. It follows that

$$\dot{V}_N(x) \leq -2\psi_{\min}\nu_{\min}\left(\frac{1}{4\delta\max\{1,k_2\}}\right)^{\frac{3q-1}{2q}} V_N^{\frac{3q-1}{2q}}(x)\,.$$

Since for $q>1$, $\frac{3q-1}{2q}>1$ asymptotic convergence to the origin is assured.

The last part of the Proposition can be proved in a similar form as Proposition 4.2, noting that $W(x)=V_Q(x)+V_N(x)$ is a robust Lyapunov function for the system.

If $q=1$

$$\begin{aligned}\dot{V}_N(x) &= -\phi_1'(x_1)\left\{\left(2\alpha\tilde{k}_1(t)-\tilde{k}_2(t)\beta\right)|\phi_1(x_1)|^2+\right.\\ &\left.-2\left(\alpha-\tilde{k}_2(t)\delta+\frac{1}{2}\beta\tilde{k}_1(t)\right)\phi_1(x_1)x_2+\beta|x_2|^2\right\}\\ &\leq -\mu_2\zeta^T\begin{bmatrix}\left(2\alpha\tilde{k}_1(t)-\tilde{k}_2(t)\beta\right) & -\left(\alpha-\tilde{k}_2(t)\delta+\frac{1}{2}\beta\tilde{k}_1(t)\right)\\ -\left(\alpha-\tilde{k}_2(t)\delta+\frac{1}{2}\beta\tilde{k}_1(t)\right) & \beta\end{bmatrix}\zeta\end{aligned}$$

where $\zeta^T=\left[\phi_1(x_1)\ ,x_2\right]$, and the last inequality follows from $\phi_1'(x_1)=\left(p\mu_1|x_1|^{p-1}+\mu_2\right)\geq\mu_2$. $\dot{V}(x)$ is negative definite iff

$$\begin{aligned}\left(2\alpha\tilde{k}_1(t)-\tilde{k}_2(t)\beta\right)\beta-\left(\alpha-\tilde{k}_2(t)\delta+\frac{1}{2}\beta\tilde{k}_1(t)\right)^2 &\geq (2\alpha(k_1-g_1)-(k_2+g_2)\beta)\beta+\\ -\left(\left|\alpha-k_2\delta+\frac{1}{2}\beta k_1\right|+g_2\delta+\frac{1}{2}\beta g_1\right)^2 &>0\,.\end{aligned}$$

Setting $\alpha=k_2\delta$ one obtains

$$2k_2\frac{\delta}{\beta}(k_1-g_1)>(k_2+g_2)+\left(\frac{1}{2}k_1+\frac{1}{2}g_1+g_2\frac{\delta}{\beta}\right)^2\,. \qquad \square$$

4.8.8 *Proof of Theorem 4.5*

Consider as a candidate Lyapunov function the quadratic form (4.5), with the *constant*, positive definite matrix $P=P^T$, given by

$$P=\begin{bmatrix}p_1 & p_3\\ p_3 & p_2\end{bmatrix}=\begin{bmatrix}\beta+4\varepsilon^2 & -2\varepsilon\\ -2\varepsilon & 1\end{bmatrix}\,, \tag{4.34}$$

with arbitrary positive constants $\beta>0$, $\varepsilon>0$. Note that due to (4.26) we can write $\rho_1(t,x)=\alpha_1(t,x)\phi_1(x_1)$, and $\rho_2(t,x)=\alpha_2(t,x)\phi_2(x_1)$ for some functions

$|\alpha_1(t,x)| \leq g_1(t,x)$ and $|\alpha_2(t,x)| \leq g_2(t,x)$. Using these functions and noting that $\phi_2(x_1) = \phi_1'(x_1)\,\phi_1(x_1)$ one can show that

$$\dot{\zeta} = \phi_1'(x_1) \begin{bmatrix} -(k_1(t,x) - \alpha_1(t,x)) & , & 1 \\ -(k_2(t,x) - \alpha_2(t,x)) & & 0 \end{bmatrix} \zeta = \phi_1'(s)\,\mathscr{A}(t,x)\,\zeta\,.$$

for every point in $\mathbb{R}^2 \backslash \mathscr{S}$, where this derivative exists. Similarly one can calculate the derivative of $V(x)$ on the same set as

$$\dot{V}_Q = \phi_1'(s)\,\zeta^T \left(\mathscr{A}^T(t,x)P + P\mathscr{A}(t,x)\right)\zeta = -\phi_1'(s)\,\zeta^T Q(t,x)\,\zeta$$

where

$$Q(t,x) = \begin{bmatrix} 2(k_1(t,x) - \alpha_1(t,x))\,p_1 + 2(k_2(t,x) - \alpha_2(t,x))\,p_3 & \bigstar \\ (k_1(t,x) - \alpha_1(t,x))\,p_3 + (k_2(t,x) - \alpha_2(t,x))\,p_2 - p_1\,, & -2p_3 \end{bmatrix}.$$

With the selection of P in (4.34) and the gains in (4.27) it follows that (the arguments of the functions were left out)

$$\begin{aligned} Q - 2\varepsilon\mathbb{I} &= \begin{bmatrix} 2\beta k_1 + 4\varepsilon(2\varepsilon k_1 - k_2) - 2\left(\beta + 4\varepsilon^2\right)\alpha_1 + 4\varepsilon\alpha_2 - 2\varepsilon & \bigstar \\ k_2 - 2\varepsilon k_1 - \left(\beta + 4\varepsilon^2\right) + 2\varepsilon\alpha_1 - \alpha_2\,, & 2\varepsilon \end{bmatrix} \\ &= \begin{bmatrix} 2\beta k_1 - \left(\beta + 4\varepsilon^2\right)(4\varepsilon + 2\alpha_1) + 4\varepsilon\alpha_2 - 2\varepsilon & \bigstar \\ 2\varepsilon\alpha_1 - \alpha_2\,, & 2\varepsilon \end{bmatrix} \end{aligned}$$

that is positive definite for every value of (t,x). This shows that

$$\dot{V}_Q = -\phi_1'(x_1)\,\zeta^T Q(t,x)\,\zeta \leq -2\varepsilon\phi_1'(x_1)\,\zeta^T\zeta \leq -\gamma_1 V_Q^{\frac{3p-1}{2p}} - \gamma_2 |x_1|^{q-1} V_Q\,,$$

where

$$\gamma_1 = 2\mu_1 \frac{p\varepsilon\left(\mu_1 \lambda_{\min}^{\frac{1}{2}}\{P\}\right)^{\frac{p-1}{p}}}{\lambda_{\max}\{P\}}\,,\quad \gamma_2 = 2\mu_2 \frac{\varepsilon q}{\lambda_{\max}\{P\}}\,. \tag{4.35}$$

The rest of the proof is analogous to the proofs of Theorem 4.1 and Proposition 4.1. □

References

1. Andrieu, V., Praly, L., Astolfi, A.: Homogeneous approximation, recursive observer design and output feedback. SIAM Journal of Control and Optimization 47(4), 1814–1850 (2008)
2. Bartolini, G., Ferrara, A., Usai, E., Utkin, V.: On Multi-Input Chattering-Free Second-Order Sliding Mode Control. IEEE Transactions on Automatic Control 45(9), 1711–1719 (2000)
3. Baccioti, A., Rosier, L.: Lyapunov functions and stability in control theory, 2nd edn. Springer, New York (2005)

4. Baev, S., Shtessel, Y., Shkolnikov, I.: Nonminimum-phase output tracking in causal systems using higher order sliding modes. International Journal of Robust and Nonlinear Control, Special Issue on Advances in Higher Order Sliding Mode Control 18(4-5), 454–467 (2008)
5. Bejarano, J.F., Fridman, L., Poznyak, A.: Exact state estimation for linear systems with unknown inputs based on hierarchical super-twisting algorithm. International Journal on Robust and Nonlinear Control 17(18), 1734–1753 (2007)
6. Bogachev, V.I.: Measure Theory, vol. I, p. 491. Springer, Berlin (2007)
7. Boiko, I., Fridman, L.: Analysis of Chattering in Continuous Sliding-Mode Controllers. IEEE Transactions on Automatic Control 50(9), 1442–1446 (2005)
8. Boiko, I.: Discontinuous Systems. Birkhuser, Boston (2008)
9. Davila, J., Fridman, L., Levant, A.: Second-Order Sliding- Modes Observer for Mechanical Systems. IEEE Transactions on Automatic Control 50(11), 1785–1789 (2005)
10. Filippov, A.F.: Differential equations with discontinuous right-hand side. Kluwer Academic Publishers, Dordrecht (1988)
11. Floquet, T., Barbot, J.P.: Super twisting algorithm-based step-by-step sliding mode observers for nonlinear systems with unknown inputs. International Journal of Systems Science 38(10), 803–815 (2007)
12. Fridman, L., Levant, A.: Higher order sliding modes. In: Barbot, J.P., Perruquetti, W. (eds.) Sliding Mode Control in Engineering, pp. 53–101. Marcel Dekker, New York (2002)
13. Kaveh, P., Shtessel, Y.: Blood Glucose Regulation Using Higher Order Sliding Mode Control. International Journal of Robust and Nonlinear Control, Special Issue on Advances in Higher Order Sliding Mode Control 18(4-5), 557–569 (2008)
14. Khalil, H.K.: Nonlinear Systems, 3rd edn., p. 750. Prentice-Hall (2002)
15. Kobayashi, S., Furuta, K.: Frequency characteristics of Levant's differentiator and adaptive sliding mode differentiator. International Journal of Systems Science 38(10), 825–832 (2007)
16. Levant, A.: Sliding order and sliding accuracy in sliding mode control. International Journal of Control 58(6), 1247–1263 (1993)
17. Levant, A.: Robust Exact Differentiation via Sliding Mode Technique. Automatica 34(3), 379–384 (1998)
18. Levant, A.: Homogeneity approach to high-order sliding mode design. Automatica 41, 823–830 (2005)
19. Levant, A.: Principles of 2-sliding mode design. Automatica 43, 576–586 (2007)
20. Moreno, J.A., Osorio, M.: A Lyapunov approach to second-order sliding mode controllers and observers. In: 47th IEEE Conference on Decision and Control CDC 2008, pp. 2856–2861 (2008)
21. Davila, A., Moreno, J.A., Fridman, L.: Optimal Lyapunov function selection for reaching time estimation of supertwisting algorithm. In: Proceedings of the 48th IEEE Conference on Decision and Control, Shangai, China, pp. 8405–8410 (December 2009)
22. Moreno, J.A., Osorio, M.: Strict Lyapunov Functions for the Super-Twisting Algorithm. Submitted to the IEEE Transactions on Automatic Control (2010)
23. Moreno, J.A.: A Linear Framework for the Robust Stability Analysis of a Generalized Supertwisting Algorithm. In: Proc. 6th Int. Conf. Elect. Eng., Comp. Sci. and Aut. Conf. (CCE 2009), Mexico, November 10-13, 2009, pp. 12–17 (2009)
24. Moreno, J.A., Alvarez, J., Rocha-Cozatl, E., Diaz-Salgado, J.: Super-Twisting Observer-Based Output Feedback Control of a Class of Continuous Exothermic Chemical Reactors. In: 2010 IFAC 9th International Symposium on Dynamics and Control of Process Systems, DYCOPS 2010, Leuven, Belgium, July 5-7 (2010)

25. Davila, A., Moreno, J.A., Fridman, L.: Variable Gains Super-Twisting Algorithm: A Lyapunov Based Design. In: American Control Conference - ACC 2010, Baltimore, MA, USA, June 30-July 2 (2010)
26. Shtessel, Y.B., Moreno, J.A., Plestan, F., Fridman, L.M., Poznyak, A.S.: Super-twisting Adaptive Sliding Mode Control: a Lyapunov Design. Submitted to the 49th IEEE Conference on Decision and Control, Atlanta, Georgia, USA, December 15-17 (2010)
27. Guzman-Baltazar, E., Moreno, J.A.: Dissipative Design of Adaptive Observers for Systems with Multivalued Nonlinearities. In: Submitted to the 49th IEEE Conference on Decision and Control, Atlanta, Georgia, USA, December 15-17 (2010)
28. Cruz-Zavala, E., Moreno, J.A., Fridman, L.: Uniform Robust Exact Differentiator. Submitted to the 49th IEEE Conference on Decision and Control. Atlanta, Georgia, USA. December 15-17 (2010)
29. Cruz-Zavala, E., Moreno, J.A., Fridman, L.: Uniform Second-Order Sliding Mode Observer for Mechanical Systems. In: IFAC 11th International Workshop on Variable Structure Systems -VSS 2010, Mexico City, Mexico, June 26-28 (2010)
30. Salgado, I., Chairez Oria, I., Moreno, J.A., Fridman, L.M.: Sampled Output Based Continuous Second Order Sliding Mode Observer. In: IFAC 11th International Workshop on Variable Structure Systems -VSS 2010, Mexico City, Mexico, June 26-28 (2010)
31. Moreno, J.A.: Lyapunov Analysis of Non Homogeneous Super-Twisting Algorithms. In: IFAC 11th International Workshop on Variable Structure Systems -VSS 2010, Mexico City, Mexico, June 26-28 (2010)
32. Santiesteban, R., Moreno, J.A., Fridman, L.M.: Finite-Time Convergence Analysis for "Twisting" Controller via a Strict Lyapunov Function. In: IFAC 11th International Workshop on Variable Structure Systems -VSS 2010, Mexico City, Mexico, June 26-28 (2010)
33. Angulo, M.T., Fridman, L.M., Moog, C., Moreno, J.A.: Output Feedback Design for Robust Finite-Time State Stability of Flat Nonlinear Systems. In: IFAC 11th International Workshop on Variable Structure Systems -VSS 2010, Mexico City, Mexico, June 26-28 (2010)
34. Orlov, Y.: Finite Time Stability and Robust Control Synthesis of Uncertain Switched Systems. SIAM Journal of Control and Optimization 43(4), 1253–1271 (2005)
35. Orlov, Y.: Discontinuous Control. Springer, Berlin (2009)
36. Perruquetti, W., Floquet, T., Moulay, E.: Finite-Time Observers: Application to Secure Communication. IEEE Transactions on Automatic Control 53(1), 356–359 (2008)
37. Pisano, A., Usai, E.: Globally convergent real-time differentiation via second order sliding modes. International Journal of Systems Science 38(10), 833–844 (2007)
38. Pisano, A., Usai, E.: Contact force regulation in wire-actuated pantographs via variable structure control and frequency-domain techniques. International Journal of Control 81(11), 1747–1762 (2008)
39. Polyakov, A., Poznyak, A.: Reaching Time Estimation for Super-Twisting Second Order Sliding Mode Controller via Lyapunov Function Designing. IEEE Transactions on Automatic Control 54(8), 1951–1955 (2009)
40. Poznyak, A.S.: Advanced Mathematical Tools for Automatic Control Engineers. Deterministic Techniques, vol. 1, p. 774. Elsevier, Amsterdam (2008)
41. Utkin, V., Guldner, J., Shi, J.: Sliding Mode Control in Electro-Mechanical Systems, 2nd edn. CRC Press, Taylor & Francis (2009)

Chapter 5
A New Design of Sliding Mode Control Systems

Zhihong Man, Suiyang Khoo, Xinghuo Yu, Chunyan Miao, Jiong Jin, and Feisiang Tay

Abstract. A new sliding mode control technique for a class of SISO dynamic systems is presented in this chapter. It is seen that the stability status of the closed-loop system is first checked, based on the approximation of the most recent information of the first-order derivative of the Lyapunov function of the closed-loop system, an intelligent sliding mode controller can then be designed with the following intelligent features: (i) If the closed-loop system is stable, the correction term in the controller will continuously adjust control signal to drive the closed-loop trajectory to reach the sliding mode surface in a finite time and the desired closed-loop dynamics with the zero-error convergence can then be achieved on the sliding mode surface. (ii) If, however, the closed-loop system is unstable, the correction term is capable of modifying the control signal to continuously reduce the value of the derivative of the Lyapunov function from the positive to the negative and then drives the closed-loop trajectory to reach the sliding mode surface and ensures that the desired closed-loop

Zhihong Man · Feisiang Tay
Faculty of Engineering and Industrial Sciences,
Swinburne University of Technology,
VIC 3122, Australia

Suiyang Khoo
School of Engineering, Deakin University, VIC 3217, Australia

Xinghuo Yu
Platform Technologies Research Institute, RMIT University,
VIC 3001, Australia

Chunyan Miao
School of Computer Engineering,
Nanyang Technological University, Singapore, 639798

Jiong Jin
Department of Electrical and Electronic Engineering,
The University of Melbourne,
VIC 3010, Australia

L. Fridman et al. (Eds.): Sliding Modes, LNCIS 412, pp. 151–167.
springerlink.com

dynamics can be obtained on the sliding mode surface. The main advantages of this new sliding mode control technique over the conventional one are that no chattering occurs in the sliding mode control system because of the recursive learning control structure; the system uncertainties are embedded in the Lipschitz-like condition and thus, no priori information on the upper and/or the lower bounds of the unknown system parameters and uncertain system dynamics is required for the controller design; the zero-error convergence can be achieved after the closed-loop dynamics reaches the sliding mode surface and remains on it. The performance for controlling a third-order linear system is evaluated in the simulation section to show the effectiveness and efficiency of the new sliding mode control technique.

5.1 Introduction

Since 1950s, sliding mode control has been extensively investigated and successfully applied for controlling linear systems, nonlinear systems and complex systems with unknown system parameters, uncertain dynamics and external disturbances [25, 10, 20, 5, 24, 18, 17, 6, 26, 19, 13, 16, 8, 1, 12, 3, 7, 4, 2, 14]. Generally speaking, if the information on the upper and/or the lower bounds of the unknown system parameters, uncertain dynamics and the external disturbances is known, a high-speed switching sliding mode controller can be designed to drive the closed-loop trajectory to reach the sliding mode surface and then remain on it to ensure that the desired closed-loop dynamics with the zero-error convergence can be achieved, which is insensitive to the unknown system parameters, uncertain dynamics and the external disturbances.

Switching/chattering of sliding mode control signals crossing the sliding mode surfaces is an important characteristic in all current sliding mode control systems. It has been well-known that, in order to eliminate the effects of uncertainties and guarantee the zero-error convergence on the sliding mode surface, a switching process, which keeps the closed-loop dynamics on the sliding mode surface, is necessary. However, the chattering issue has largely restricted the applications of the sliding mode control technique in practice, since the high-speed chattering control signals require that the controlled systems have a wide frequency band in order to response the high frequency control actions efficiently, and also, the chattering control signals may excite some undesired high frequency mode in the closed-loop systems, which may not be considered and included in the system models. Although the boundary-layer technique can be used to eliminate the chattering as seen in [20, 5, 24, 18, 17, 6, 26], the property of the zero-error convergence is lost as the sign function is replaced by the sigmoid function in sliding mode control signals. In fact, for more than 50 years, the researchers in the area of sliding mode control systems have been exploring the possibility of developing a new sliding mode control technique which ensures both the zero-error convergence and the chattering-free characteristics in sliding mode control systems with uncertainties.

In this chapter, we present a new sliding mode control technique for a class of SISO dynamic systems. The new sliding mode controller has an intelligent recursive-learning structure, consisting of a most recent control signal and a correction term [21, 9, 22, 23]. However, the correction term of the new sliding mode controller in this paper is updated by using the estimate of the most recent information on the gradient of the Lyapunov function, in order to continuously adjust the stability and convergence of the closed-loop system. For instance, if the closed-loop system is stable, the correction term in the controller will continuously adjust the control signal in the sense that the closed-loop system trajectory can reach the sliding mode surface in a finite time and remains on it, the desired closed-loop dynamics with the zero-error converge can then be achieved on the sliding mode surface. However, if the closed-loop system is unstable, the correction term in the controller will correct the control signal to continuously reduce the value of the derivative of the Lyapunov function from the positive to the negative, and then drives the closed-loop trajectory to reach the sliding mode surface in a finite time and guarantees that the desired closed-loop dynamics with the zero-error converge can be achieved on the sliding mode surface. Because of the recursive learning structure of the new sliding mode controller, after the closed-loop system trajectory reaches the sliding mode surface, the sliding variable does not cross the sliding mode surface with the zigzag motion, and therefore no chattering occurs in the closed-loop sliding mode control system.

Another distinguishing characteristic of this new sliding mode control technique is that the ***Lipschitz-like condition***, describing the important dynamic property of the closed-loop system with or without uncertain dynamics, is proposed, which states that the difference between the current value of the first-order derivative of the Lyapunov function and its most recent value is sufficiently small as the sampling period is sufficiently small. It will be seen that, as the Lipschitz-like condition is used for designing the sliding mode controller, the information of the uncertain system dynamics is embedded in the Lipschitz-like condition, and thus, the upper and/or the lower bounds of the unknown system parameters and the uncertain system dynamics are not required. It will be further seen from next few sections that the sliding mode control design is greatly simplified and many desired properties such as the chattering-free and zero-error convergence and robustness with respect to uncertain dynamics can all be achieved in the new sliding mode control systems.

The rest of the chapter is organized as follows: In Section 5.2, the SISO dynamic system model, the state equation of the sliding variable and its derivatives, and the new sliding mode control structure are formulated. In Section 5.3, the convergence analysis of the closed-loop dynamics equipped with the new sliding mode controller is studied in detail, and some important properties on the intelligent learning, robustness, and chattering-free are also addressed. In Section 5.4, a simulation example for controlling a third-order uncertain linear system is presented to show the effectiveness and efficiency of the proposed new sliding mode control technique. Section 5.5 concludes with some further work.

5.2 Problem Formulation

Consider a class of SISO dynamic systems described by the following differential equation:

$$x^{(n)} = f\left(x(t), \dot{x}(t), \cdots, x^{(n-2)}(t), x^{(n-1)}(t)\right) + b\left(x(t), \dot{x}(t), \cdots, x^{(n-2)}(t), x^{(n-1)}(t)\right) u(t) \quad (5.1)$$

where t is the time, $x(t)$ is the system output, $x^{(i)}(t)\,(i = 1, 2, , n)$ is the ith-order derivative of $x(t)$, $u(t)$ is the control input, $f\left(x(t), \dot{x}(t), \cdots, x^{(n-2)}(t), x^{(n-1)}(t)\right)$ and $b\left(x(t), \dot{x}(t), \cdots, x^{(n-2)}(t), x^{(n-1)}(t)\right)$ are the unknown linear or nonlinear functions. For simplicity, in the following analysis we use $f(t)$ and $b(t)$ to replace $f\left(x(t), \dot{x}(t), \cdots, x^{(n-2)}(t), x^{(n-1)}(t)\right)$ and $b\left(x(t), \dot{x}(t), \cdots, x^{(n-2)}(t), x^{(n-1)}(t)\right)$, respectively.

In this chapter, we assume that the SISO dynamic system in (5.1) is controllable with $b(t) = b\left(x(t), \dot{x}(t), \cdots, x^{(n-2)}(t), x^{(n-1)}(t)\right) > 0$. As in [15, 11], we define a simple first-order sliding variable $s(t)$ for the nth-order SISO system in (5.1) as follows:

$$s(t) = \dot{x}(t) + \lambda x(t) \quad (5.2)$$

where λ is a positive constant.

Remark 5.1. It is easy to understand that, if a controller $u(t)$ can be designed to drive the first-order sliding variable $s(t)$ in (5.2) to zero in a finite time, the system output $x(t)$ can then exponentially converge to zero on the sliding mode surface $s(t) = 0$.

For the further process, differentiating the sliding variable $s(t)$ with respect to the time t for $n-1$ times, we obtain the following equations:

$$\begin{aligned} \dot{s}(t) &= \ddot{x}(t) + \lambda \dot{x}(t) \\ \ddot{s}(t) &= (t) + \lambda \ddot{x}(t) \\ &\vdots \\ s^{(n-1)}(t) &= x^{(n)}(t) + \lambda x^{(n-1)}(t) \\ &= f\left(x(t), \dot{x}(t), \cdots x^{(n-1)}(t)\right) + b\left(x(t), \dot{x}(t), \cdots x^{(n-1)}(t)\right) u(t) + \lambda x^{(n-1)}(t) \end{aligned} \quad (5.3)$$

Defining the following state variable vector:

$$z(t) = \left[s(t)\ \dot{s}(t)\ \cdots\ s^{(n-2)}(t)\right]^T \quad (5.4)$$

we can represent (5.3) in the following matrix form:

$$\begin{bmatrix} \dot{s}(t) \\ \ddot{s}(t) \\ \vdots \\ s^{(n-2)}(t) \\ s^{(n-1)}(t) \end{bmatrix} = \begin{bmatrix} 0 & 1 & 0 & \cdots & 0 \\ 0 & 0 & 1 & 0 \cdots & 0 \\ \vdots & & & \vdots & \\ 0 & 0 & \cdots & 0 & 1 \\ 0 & 0 & \cdots & 0 & 0 \end{bmatrix} \begin{bmatrix} s(t) \\ \dot{s}(t) \\ \vdots \\ s^{(n-3)}(t) \\ s^{(n-2)}(t) \end{bmatrix} + \begin{bmatrix} 0 \\ 0 \\ \vdots \\ 0 \\ f(t) \end{bmatrix}$$

$$+ \begin{bmatrix} 0 \\ 0 \\ \vdots \\ 0 \\ b(t) \end{bmatrix} u(t) + \begin{bmatrix} 0 \\ 0 \\ \vdots \\ 0 \\ \lambda x^{(n-1)}(t) \end{bmatrix} \tag{5.5}$$

or more compactly

$$\dot{z}(t) = Az(t) + F(t) + B(t)u(t) + P(t) \tag{5.6}$$

where

$$A = \begin{bmatrix} 0 & 1 & 0 & \cdots & 0 \\ 0 & 0 & 1 & 0 \cdots & 0 \\ \vdots & & & \vdots & \\ 0 & 0 & \cdots & 0 & 1 \\ 0 & 0 & \cdots & 0 & 0 \end{bmatrix}, \quad F(t) = \begin{bmatrix} 0 \\ 0 \\ \vdots \\ 0 \\ f(t) \end{bmatrix}, \quad B(t) = \begin{bmatrix} 0 \\ 0 \\ \vdots \\ 0 \\ b(t) \end{bmatrix}$$

and

$$P(t) = \begin{bmatrix} 0 \\ 0 \\ \vdots \\ 0 \\ \lambda x^{(n-1)}(t) \end{bmatrix} \tag{5.7}$$

The sliding mode controller proposed in this chapter is of the form:

$$u(t) = u(t-\tau) - \Delta u(t) \tag{5.8}$$

with the correction term:

$$\Delta u(t) = \begin{cases} \frac{s^{(n-2)}(t)}{\left|s^{(n-2)}(t)\right|^2} \left(\eta_1 \hat{V}(t-\tau) + \beta \left| \hat{V}(t-\tau) \right| + \eta_2 \left| \hat{V}(t-2\tau) \right| \right) & s^{(n-2)}(t) \neq 0 \\ 0 & s^{(n-2)}(t) = 0 \end{cases} \tag{5.9}$$

where $\hat{\dot{V}}(t-\tau)$ is the approximation of $\dot{V}(t-\tau)$, $\dot{V}(t)$ is the first-order derivative of the Lyapunov function candidate $V(t) = z^T(t)z(t)/2$, chosen for the closed-loop system, and computed as follows:

$$\begin{aligned}\dot{V}(t) = \varphi(\phi(t), u(t)) = z(t)^T \dot{z}(t) = z(t)^T [Az(t) + F(t) + B(t)u(t) + P(t)] \\ = z(t)^T Az(t) + z(t)^T F(t) + z(t)^T P(t) + z(t)^T B(t)u(t)\end{aligned} \quad (5.10)$$

$\hat{\dot{V}}(t-\tau)$, the estimate of $\dot{V}(t-\tau)$, is computed as:

$$\hat{\dot{V}}(t-\tau) = \frac{V(t) - V(t-\tau)}{\tau} \quad (5.11)$$

with the time-delay τ chosen to be sufficiently small in the sense that there exist a large positive number $M >> 1$ and a small positive constant β_1, such that the following inequalities are held:

$$|\varphi(\phi(t), u(t-\tau)) - \varphi(\phi(t-\tau), u(t-\tau))| < \frac{1}{M}|\varphi(\phi(t-\tau), u(t-\tau))| \quad (5.12)$$

for both $\varphi(\phi(t), u(t-\tau)) \neq 0$ and $\varphi(\phi(t-\tau), u(t-\tau)) \neq 0$, and

$$|\delta(\dot{V}(t-\tau))| = \left|\dot{V}(t-\tau) - \hat{\dot{V}}(t-\tau)\right| \leq \beta_1 \left|\hat{\dot{V}}(t-\tau)\right| \neq 0 \quad (5.13)$$

the control parameters η_1 and β in the correction term of the controller and the scalar β_1 in (5.13) are chosen to satisfy the following inequalities:

$$\frac{1}{M} < \eta_1 b(t) < 1 - \frac{1}{M} \quad (5.14)$$

and

$$\beta > \eta_1 \beta_1 \quad (5.15)$$

the positive constant control parameter η_2 in the correction term in (5.9) will be determined later.

Remark 5.2. Since the time delay τ is chosen to be sufficiently small in this paper, we can reasonably assume that

- $\hat{\dot{V}}(t-\tau)$ is nonzero when the closed-loop dynamics is not constrained on the sliding mode surface s(t) = 0.
- $\dot{V}(t-\tau)$ and $\hat{\dot{V}}(t-\tau)$ have the same sign for $\dot{V}(t-\tau) \neq 0$, that is,

$$\text{sign}(\dot{V}(t-\tau)) = \text{sign}\left(\hat{\dot{V}}(t-\tau)\right) \quad (5.16)$$

Remark 5.3. Using (5.14) in (5.12), we obtain

$$|\varphi(\phi(t), u(t-\tau)) - \varphi(\phi(t-\tau), u(t-\tau))| < \eta_1 b(t) \left|\dot{V}(t-\tau)\right| \tag{5.17}$$

for both $\varphi(\phi(t), u(t-\tau)) \neq 0$ and $\varphi(\phi(t-\tau), u(t-\tau)) \neq 0$.

(5.17) is called the Lipschitz-like condition, which states that the difference between the current value of the gradient of the Lyapunov function and its most recent value is very small as the time delay τ is sufficiently small. It will be seen from the next section that it is because of the use of the Lipschitz-like condition that no information on the upper and/or the lower bounds of the unknown system parameters and the uncertain dynamics is required for designing sliding mode controller, and the Lipschitz-like condition also plays a very important role in the convergence analysis of the closed-loop sliding mode control system with uncertain dynamics and guarantees that the controller $u(t)$, updated using the most recent information on $\hat{V}(t-\tau)$ and $\hat{V}(t-2\tau)$, can correct the motion of the closed-loop dynamics and drives the state variable vector $z(t)$ to converge to zero in a finite time, and then the system output $x(t)$ exponentially converges to zero on the sliding mode surface $s(t) = 0$. The detailed convergence analysis is given in the next section.

5.3 Convergence Analysis

Theorem 5.1. *Consider the state equation in (5.6) for a class of SISO dynamic systems in (5.1). The system output $x(t)$ asymptotically converges to zero if the control input $u(t)$ is designed as in (5.8) with the correction term in (5.9).*

Proof. Differentiating the Lyapunov function $V(t) = z(t)^T z(t)/2$ with respect to the time t and using (5.8) and (5.9), we have

$$\begin{aligned}
\dot{V}(t) &= z(t)^T [Az(t) + F(t) + B(t)u(t) + P(t)] \\
&= z(t)^T Az(t) + z(t)^T F(t) + z(t)^T P(t) + z(t)^T B(t)u(t) \\
&= z(t)^T Az(t) + z(t)^T F(t) + z(t)^T P(t) + z(t)^T B(t)u(t-\tau) \\
&- z(t)^T B(t) \frac{s^{(n-2)}(t)}{\left|s^{(n-2)}(t)\right|^2} \left(\eta_1 \hat{\dot{V}}(t-\tau) + \beta \left|\hat{\dot{V}}(t-\tau)\right| + \eta_2 \hat{\dot{V}}(t-2\tau)\right)
\end{aligned} \tag{5.18}$$

It is noted that

$$z(t)^T B(t) \frac{s^{(n-2)}(t)}{\left|s^{(n-2)}(t)\right|^2} = b(t) \tag{5.19}$$

(5.18) can then be further expressed as:

$$\begin{aligned}
\dot{V}(t) &= \left[z(t)^T A z(t) + z(t)^T F(t) + z(t)^T P(t) + z(t)^T B(t) u(t-\tau)\right] \\
&\quad -\eta_1 b(t) \hat{V}(t-\tau) - \beta b(t) \left|\hat{V}(t-\tau)\right| - \eta_2 b(t) \left|\hat{V}(t-2\tau)\right| \\
&= \left[z(t)^T A z(t) + z(t)^T F(t) + z(t)^T P(t) + z(t)^T B(t) u(t-\tau)\right] \\
&\quad -\eta_1 b(t) \left(\dot{V}(t-\tau) - \delta\left(\dot{V}(t-\tau)\right)\right) - \beta b(t) \left|\hat{V}(t-\tau)\right| - \eta_2 b(t) \left|\hat{V}(t-2\tau)\right| \\
&\quad - \left[z(t-\tau)^T A z(t-\tau) + z(t-\tau)^T F(t-\tau) + z(t-\tau)^T P(t-\tau) + z(t-\tau)^T B(t-\tau) u(t-\tau)\right] \\
&\quad + \left[z(t-\tau)^T A z(t-\tau) + z(t-\tau)^T F(t-\tau) + z(t-\tau)^T P(t-\tau) + z(t-\tau)^T B(t-\tau) u(t-\tau)\right] \\
&= \varphi(\phi(t), u(t-\tau)) - \eta_1 b(t) \dot{V}(t-\tau) + \eta_1 b(t) \delta\left(\dot{V}(t-\tau)\right) - \beta b(t) \left|\hat{V}(t-\tau)\right| \\
&\quad -\eta_2 b(t) \left|\hat{V}(t-2\tau)\right| - \varphi(\phi(t-\tau), u(t-\tau)) + \varphi(\phi(t-\tau), u(t-\tau)) \\
&= \dot{V}(t-\tau) - \left[\eta_1 b(t) \dot{V}(t-\tau) - [\varphi(\phi(t), u(t-\tau)) - \varphi(\phi(t-\tau), u(t-\tau))]\right] \\
&\quad +\eta_1 b(t) \delta\left(\dot{V}(t-\tau)\right) - \beta b(t) \left|\hat{V}(t-\tau)\right| - \eta_2 b(t) \left|\hat{V}(t-2\tau)\right|
\end{aligned} \tag{5.20}$$

From the Lipschitz-like condition in (5.17), we see that $\dot{V}(t-\tau)$ and the term $\eta_1 b(t) \dot{V}(t-\tau) - [\varphi(\phi(t), u(t-\tau)) - \varphi(\phi(t-\tau), u(t-\tau))]$ have the same sign. Thus, for the case that $\dot{V}(t-\tau) < 0$,

$$\begin{aligned}
0 > \eta_1 b(t) \dot{V}(t-\tau) - [\varphi(\phi(t), u(t-\tau)) - \varphi(\phi(t-\tau), u(t-\tau))] \\
> 2\eta_1 b(t) \dot{V}(t-\tau)
\end{aligned} \tag{5.21}$$

then $\dot{V}(t)$ in (5.20) satisfies the following inequality:

$$\dot{V}(t) < \dot{V}(t-\tau) + \eta_1 b(t) \delta\left(\dot{V}(t-\tau)\right) - \beta b(t) \left|\hat{V}(t-\tau)\right| - \eta_2 b(t) \left|\hat{V}(t-2\tau)\right| \tag{5.22}$$

It is noted that

$$\begin{aligned}
&-\beta b(t) \left|\hat{V}(t-\tau)\right| + \eta_1 b(t) \delta\left(\dot{V}(t-\tau)\right) \\
&\leq -\beta b(t) \left|\hat{V}(t-\tau)\right| + \eta_1 b(t) \left|\delta\left(\dot{V}(t-\tau)\right)\right| \\
&\leq -\beta b(t) \left|\hat{V}(t-\tau)\right| + \eta_1 b(t) \beta_1 \left|\hat{V}(t-\tau)\right| \\
&= -(\beta - \eta_1 \beta_1) b(t) \left|\hat{V}(t-\tau)\right| < 0
\end{aligned} \tag{5.23}$$

Using (5.23) in (5.22), we have

$$\dot{V}(t) < \dot{V}(t-\tau) < 0 \tag{5.24}$$

Since $\left|\dot{V}(t)\right| > \left|\dot{V}(t-\tau)\right| > 0$ and $\dot{V}(t)$ is more negative as the time t is increased, $V(t)$ will converge to zero in a finite time, that is, the closed-loop dynamics reaches

the sliding mode surface $s(t) = 0$ in a finite time, and thus, the system output $x(t)$ will asymptotically converge to zero on the sliding mode surface $s(t) = 0$.

For the case that $\dot{V}(t-\tau) > 0$, based on (5.17), we have

$$0 < \eta_1 b(t)\dot{V}(t-\tau) - [\varphi(\phi(t), u(t-\tau)) - \varphi(\phi(t-\tau), u(t-\tau))] < 2\eta_1 b(t)\dot{V}(t-\tau) \quad (5.25)$$

then (5.20) can be expressed as:

$$\begin{aligned}
\dot{V}(t) &< \dot{V}(t-\tau) + \eta_1 b(t)\,\delta\left(\dot{V}(t-\tau)\right) - \beta b(t)\left|\hat{V}(t-\tau)\right| - \eta_2 b(t)\left|\hat{V}(t-2\tau)\right| \\
&\le \dot{V}(t-\tau) + \eta_1 b(t)\left|\delta\left(\dot{V}(t-\tau)\right)\right| - \beta b(t)\left|\hat{V}(t-\tau)\right| - \eta_2 b(t)\left|\hat{V}(t-2\tau)\right| \\
&\le \dot{V}(t-\tau) + \eta_1\beta_1 b(t)\left|\hat{V}(t-\tau)\right| - \beta b(t)\left|\hat{V}(t-\tau)\right| - \eta_2 b(t)\left|\hat{V}(t-2\tau)\right| \\
&= \dot{V}(t-\tau) - (\beta - \eta_1\beta_1) b(t)\left|\hat{V}(t-\tau)\right| - \eta_2 b(t)\left|\hat{V}(t-2\tau)\right| \\
&< \dot{V}(t-\tau) - \eta_2 b(t)\left|\hat{V}(t-2\tau)\right| < \dot{V}(t-\tau)
\end{aligned} \quad (5.26)$$

(5.26) indicates that the sliding mode control law in (5.8) continuously makes $\dot{V}(t)$ smaller than $\dot{V}(t-\tau)$ when $\dot{V}(t-\tau) > 0$.

Suppose that, at the time $t = t_1$, $\dot{V}(t)$ is driven to zero, that is,

$$\dot{V}(t_1) = \varphi(\phi(t_1), u(t_1)) = 0 \quad (5.27)$$

At $t = t_1 + \tau$, (5.20) can be expressed as:

$$\begin{aligned}
\dot{V}(t_1+\tau) &= \dot{V}(t_1) - \left[\eta_1 b(t_1+\tau)\dot{V}(t_1) - [\varphi(\phi(t_1+\tau), u(t_1)) - \varphi(\phi(t_1), u(t_1))]\right] \\
&\quad + \eta_1 b(t_1+\tau)\,\delta\left(\dot{V}(t_1)\right) - \beta\, b(t_1+\tau)\left|\hat{V}(t_1)\right| - \eta_2 b(t_1+\tau)\left|\hat{V}(t_1-\tau)\right| \\
&= \varphi(\phi(t_1+\tau), u(t_1)) - \eta_2 b(t_1+\tau)\left|\hat{V}(t_1-\tau)\right| \\
&\quad - \beta\, b(t_1+\tau)\left|\hat{V}(t_1)\right| + \eta_1 b(t_1+\tau)\,\delta\left(\dot{V}(t_1)\right)
\end{aligned} \quad (5.28)$$

It is noted that

$$\begin{aligned}
&-\beta\, b(t_1+\tau)\left|\hat{V}(t_1)\right| + \eta_1 b(t_1+\tau)\,\delta\left(\dot{V}(t_1)\right) \\
&\le -\beta\, b(t_1+\tau)\left|\hat{V}(t_1)\right| + \eta_1 b(t_1+\tau)\beta_1\left|\hat{V}(t_1)\right| \\
&= -(\beta - \eta_1\beta_1) b(t_1+\tau)\left|\hat{V}(t_1)\right| < 0
\end{aligned} \quad (5.29)$$

In addition, $\varphi(\phi(t_1+\tau), u(t_1))$ is upper bounded and $\left|\hat{V}(t_1-\tau)\right|$ is nonzero. Thus, there exists a positive number η_2 such that the following inequality is held:

$$\varphi\left(\phi\left(t_1+\tau\right),u\left(t_1\right)\right)-\eta_2 b\left(t_1+\tau\right)\left|\hat{\dot{V}}\left(t_1-\tau\right)\right|<0 \tag{5.30}$$

Therefore, using (5.29) and (5.30) in (5.28), we obtain

$$\begin{aligned}\dot{V}\left(t_1+\tau\right)\leq&-\left(\beta-\eta_1\right)b\left(t_1+\tau\right)\left|\hat{\dot{V}}\left(t_1\right)\right|\\&+\left[\varphi\left(\phi\left(t_1+\tau\right),u\left(t_1\right)\right)-\eta_2 b\left(t_1+\tau\right)\left|\hat{\dot{V}}\left(t_1-\tau\right)\right|\right]<0\end{aligned} \tag{5.31}$$

(5.31) means that

$$\dot{V}\left(t\right)<0 \quad \text{for} \quad t>t_1 \tag{5.32}$$

The analysis from (5.25) to (5.32) shows that the sliding mode controller in (5.8) is capable of continuously reducing the value of $\dot{V}\left(t\right)$ from the positive to the negative, and the closed-loop trajectory can then be driven to the sliding mode surface in a finite time, as discussed for the case that $\dot{V}\left(t-\tau\right)<0$, and guarantees that the system output $x(t)$ asymptotically converges to zero on the sliding mode surface $s(t)=0$.

In summary, based on the analysis from (5.18) to (5.32), we conclude that the new sliding mode controller in (5.8) guarantees that the closed-loop system trajectory reaches the sliding mode surface $s(t)=0$ in a finite time and the system output $x(t)$ can then asymptotically converge to zero on the sliding mode surface. □

Remark 5.4. It should be noted that, if $s^{(n-2)}\left(t\right)\neq 0$ at $t=0^+$, the control process with the controller in (5.8) guarantees that, for $t>0^+$, $s^{(n-2)}\left(t\right)$ cannot be zero in any time interval. This is because, if $s^{(n-2)}\left(t\right)$ equals zero in a time interval, the signals $s^{(n-3)}\left(t\right)$, $s^{(n-4)}\left(t\right)$, , $s\left(t\right)$ will all go infinity. This contradicts to the facts that (i) the controller u(t) in (5.8) can drive the state variable vector $z(t)$ to converge to zero in a finite time if $\dot{V}\left(t-\tau\right)<0$ and (ii) the controller $u(t)$ is capable of continuously reducing the value of $\dot{V}\left(t\right)$ from the positive to the negative and then drives the state variable vector $z(t)$ to converge to zero in a finite time, as shown in the analysis of Theorem 5.1. However, it is possible for $s^{(n-2)}\left(t\right)$ to be zero at some single points that are neither the local minima nor the global minimum. Since the system trajectory cannot remain at these points, it must move toward the system origin.

Remark 5.5. The intelligent learning capability of the proposed sliding mode control technique has been clearly seen from the proof of Theorem 5.1. The primary information to help the controller to make decision at the time t is the value of $\hat{\dot{V}}\left(t-\tau\right)$, the approximation of $\dot{V}\left(t-\tau\right)$, which is the most recent information of the gradient of the Lyapunov function at the time $t-\tau$ with the property that $\text{sign}\left(\hat{\dot{V}}\left(t-\tau\right)\right)=\text{sign}\left(\dot{V}\left(t-\tau\right)\right)$, for $\dot{V}\left(t-\tau\right)\neq 0$, as the time delay τ is sufficiently small. In particular, if $\dot{V}\left(t-\tau\right)<0$, the controller ensures that $\dot{V}\left(t\right)<\dot{V}\left(t-\tau\right)<0$ and $\dot{V}\left(t\right)$ is more negative as the time t is increased. Thus, the closed-loop trajectory reaches the sliding mode surface in a finite time. On the other hand, if $\dot{V}\left(t-\tau\right)>0$, the controller will gradually reduce the value of $\dot{V}\left(t\right)$ from the positive to the negative

and then drives the closed-loop trajectory to reach the sliding mode surface in a finite time. On the sliding mode surface, the system output asymptotically converges to zero.

Remark 5.6. It is seen that the control component $\eta_2 \left|\dot{V}(t-2\tau)\right|$ in the correction term in (5.9) makes the $\dot{V}(t)$ more negative and thus speeds up the convergence of the state variable vector z(t) toward the sliding mode surface. However, the most important role of the term $\eta_2 \left|\dot{V}(t-2\tau)\right|$ in this new sliding mode control system is that, at the points where $\dot{V}(t)=0$ but $V(t)\neq 0$, it is able to drive $\dot{V}(t)$ to cross the zero from the positive to the negative and then guarantees the closed-loop dynamics to reach the sliding mode surface in a finite time, as discussed from (5.25) to (5.32).

Remark 5.7. It should be highlighted that the sliding mode controller in (5.8) does not require any information about the upper and/or the lower bounds of the uncertain system parameters and the uncertain dynamics, and is designed based only on the current measurements of the state variables and the most recent information about the system input and output as well as the estimate of the gradient of the Lyapunov function. Therefore, the proposed sliding mode control technique is robust with respect to system uncertainties.

5.4 A Simulation Example

In order to illustrate the performance of the proposed sliding mode control technique, we consider the following third-order linear system:

$$(t) = -a_1 x(t) - a_2 \dot{x}(t) - a_3 \ddot{x}(t) + bu(t) \tag{5.33}$$

where system parameters and the initial values of the state variables are $a_1 = 6$, $a_2 = 11$, $a_3 = 6$, $b = 1$, $x(0) = 0.3$, $\dot{x}(0) = 0$ and $\ddot{x}(0) = 0$, respectively. Defining the following first-order sliding variable:

$$s(t) = \dot{x}(t) + \lambda x(t) \tag{5.34}$$

and differentiating $s(t)$ with respect to the time t for two times, we obtain the following state equation:

$$\begin{bmatrix} \dot{s}(t) \\ \ddot{s}(t) \end{bmatrix} = \begin{bmatrix} 0 & 1 \\ 0 & 0 \end{bmatrix} \begin{bmatrix} s(t) \\ \dot{s}(t) \end{bmatrix} + \begin{bmatrix} 0 \\ f(t) \end{bmatrix} + \begin{bmatrix} 0 \\ 2 \end{bmatrix} u(t) + \begin{bmatrix} 0 \\ \lambda \dot{x}(t) \end{bmatrix} \tag{5.35}$$

with

$$f(t) = -\left(6x(t) + 11\dot{x}(t) + 6\ddot{x}(t)\right) \tag{5.36}$$

Based on (5.8), we design the sliding mode controller as follows:

$$u(t) = u(t-\tau) - \frac{\dot{s}(t)}{\left|\dot{s}(t)\right|^2}\left(\eta_1 \hat{\dot{V}}(t-\tau) + \beta \left|\hat{\dot{V}}(t-\tau)\right| + \eta_2 \left|\hat{\dot{V}}(t-2\tau)\right|\right) \tag{5.37}$$

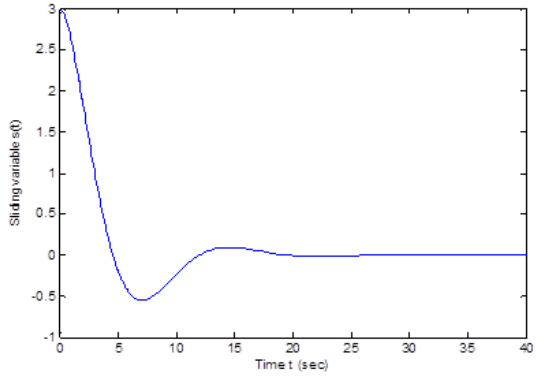

(a) The sliding variable $s(t)$

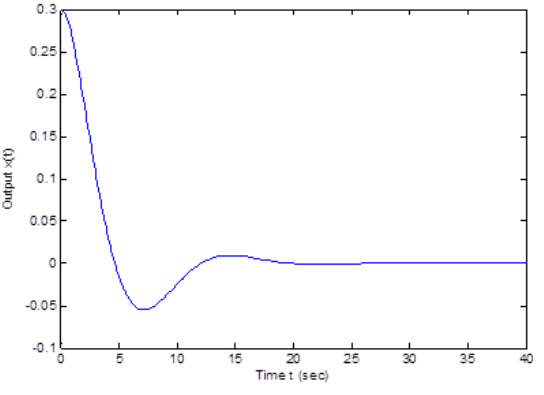

(b) The system output $x(t)$

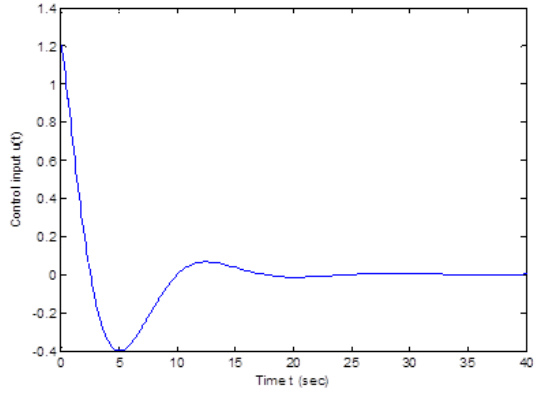

(c) The control input $u(t)$

Fig. 5.1 $x_0 = [0.3 \quad 0 \quad 0], \tau = 0.01s$.

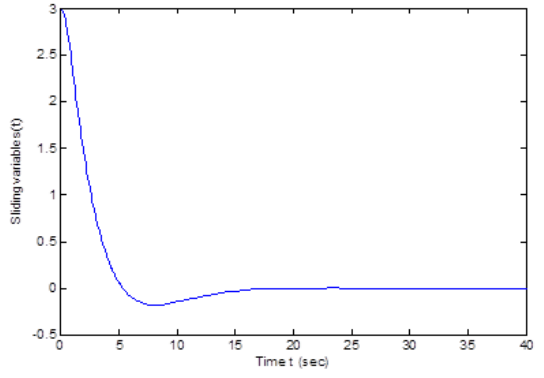

(a) The sliding variable $s(t)$

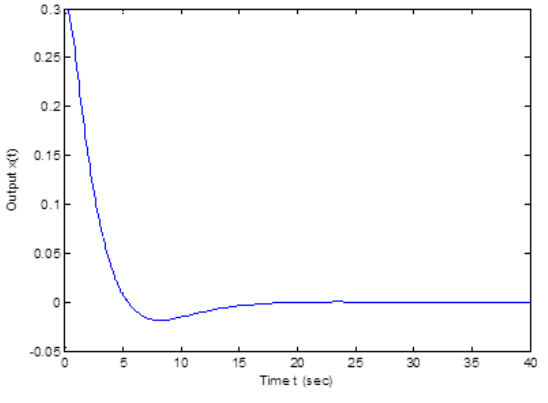

(b) The system output $x(t)$

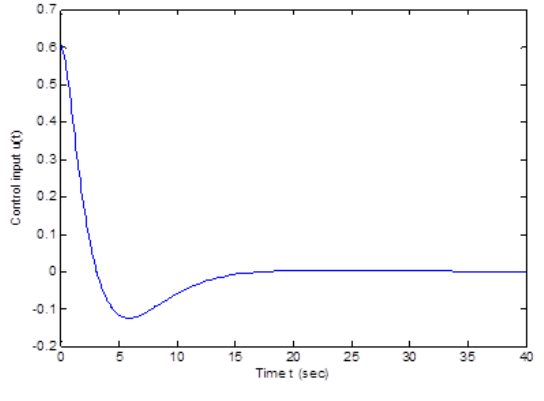

(c) The control input $u(t)$

Fig. 5.2 Increased sampled period from $\tau = 0.01s$ to $\tau = 0.02s$

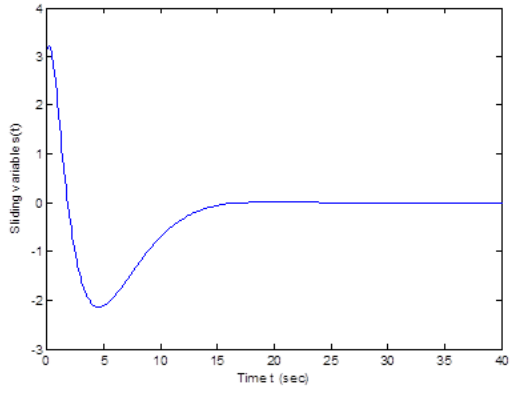

(a) The sliding variable $s(t)$

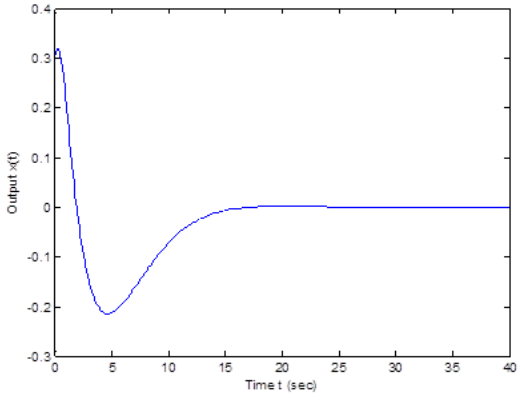

(b) The system output $x(t)$

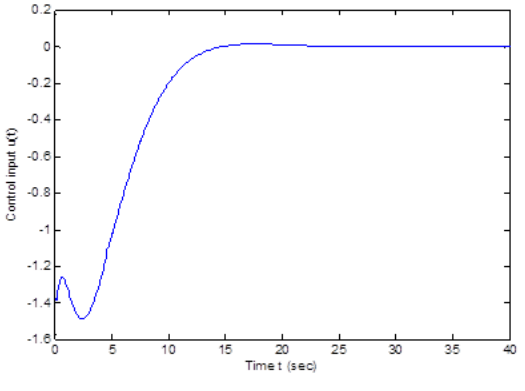

(c) The control input $u(t)$

Fig. 5.3 Nonzero initial velocity $\dot{x}(0) = 0.1$

The Runge-Kutta method is used to solve the closed-loop nonlinear differential equation numerically. Figure 5.1(a) - Figure 5.1(c) show the sliding variable $s(t)$, the system output $x(t)$ and the control signal $u(t)$, respectively, where the sliding mode parameter is chosen as $\lambda = 10$, the sampling period $\Delta T = 0.01s$, the time delay $\tau = 0.01s$, and the control parameters in the correction term are set to $\eta_1 = 0.0025$, $\beta_1 = 0.003$ and $\eta_2 = 0.005$, and scalar β in (5.13) is computed using (5.15) as: $\beta = 2\eta_1\beta_1 = 0.00015$. It is seen that the sliding variable $s(t)$ converges to zero in a finite time, the system output $x(t)$ then exponentially converges to zero on the sliding mode surface, and the control signal $u(t)$ is completely chattering-free.

Figure 5.2(a) - Figure 5.2(c) show the sliding variable $s(t)$, the system output $x(t)$ and the control signal $u(t)$, respectively, where the sliding mode parameter λ, the control parameters η_1, β_1 and η_2 and the scalar β are the same as the ones in Figure 5.1(a) - Figure 5.1(c), but the sampling period (the time delay τ) is increased from $0.01s$ to $0.02s$. It is seen that the system performance does not degenerated by the lower sampling frequency, instead, the overshoots are greatly reduced and the convergence is faster than the one in Figure 5.1(a) - Figure 5.1(c).

Figure 5.3(a) - Figure 5.3(c) show the sliding variable $s(t)$, the system output $x(t)$ and the control signal $u(t)$, respectively, where the sliding mode parameter λ, the control parameters η_1, β_1, η_2 and the scalar β, the sampling period (the time delay τ), the initial values of the position $x(t)$ and the acceleration $\ddot{x}(t)$ are the same as the ones in Figure 5.2(a) - Figure 5.2(c), but the initial value of the velocity signal $\dot{x}(t)$ is chosen as $\dot{x}(0) = 0.1$. It is seen that, although the controller takes more time to handle the effect of the non-zero $\dot{x}(0)$ and the large overshoots of both $s(t)$ and $x(t)$ occur in Figure 5.3(a) and Figure 5.3(b), respectively, both the sliding variable $s(t)$ and the system output $x(t)$ converge to zero, and the control signal remains the chattering-free.

5.5 Conclusions

In this chapter, a new sliding mode control technique with a learning control structure has been developed. The theoretical analysis and the simulation results have shown that the new sliding mode control technique can not only drive the closed-loop trajectory to reach the sliding surface in a finite time and guarantee the desired closed-loop dynamics with the zero-error convergence on the sliding mode surface, but also have the privilege of chattering-free characteristic, which makes the proposed sliding mode control potentially have a wide range of applications in the near future. The further work for using the proposed new sliding mode control technique to control MIMO linear and nonlinear systems, sampled data systems, dynamical fuzzy systems and consensus networks is under the authors' investigation.

References

1. Adamy, J., Flemming, A.: Soft variable-structure controls: A survey. Automatica 40, 1821–1844 (2004)
2. Bartolini, G., Ferrara, A., Utkin, V., Zolezzi, T.: A control vector simplex approach to variable structure control of nonlinear systems. International Journal of Robust Nonlinear Control 7, 321–335 (1997)
3. Bartolini, G., Pisano, A., Punta, E., Usai, E.: A survey of applications of second-order sliding mode control to mechanical systems. International Journal of Control 76, 875–892 (2003)
4. Bonivento, C., Marconi, L., Zanasi, R.: Output regulation of nonlinear systems by sliding mode. Automatica 37, 535–542 (2001)
5. Decarlo, R.A., Zak, S.H., Mathews, G.P.: Variable structure control of nonlinear multivariable systems: A tutorial. Proceedings of the IEEE 76, 212–232 (1998)
6. Dorling, C.M., Zinober, A.: Two approaches to hyperplane design in multivariable variable structure control systems. International Journal of Control 44, 65–82 (1986)
7. El-Ghezawi, O.M.E., Zinober, A.S.I., Billings, S.A.: Analysis and design of variable structure systems using a geometric approach. International Journal of Control 38, 657–671 (1983)
8. Ferrara, A., Utkin, V.: Constrained optimization via sliding modes in dynamic linear systems. pp. 2977–2981 (2003)
9. Gopinath, S., Kar, I.N.: Iterative learning control scheme for manipulators with actuator dynamics. Automatica 39, 1367–1384 (2004)
10. Hung, J.Y., Gao, W., Huang, J.C.: Variable structure control: A survey. IEEE Transaction on Industrial Electronics 40, 2–22 (1993)
11. Levant, A.: High-order sliding modes: differentiation and output feedback control. International Journal of Control 76, 924–941 (2003)
12. Levant, A., Fridman, L.: Robustness issues of 2-sliding mode control. In: Variable Structure Systems: From Principles to Implementation, Stevenage, U.K (2004)
13. Man, Z., Palaniswami, M.: Robust tracking control for rigid robotic manipulators. IEEE Transaction on Automatic Control 39, 154–158 (1994)
14. Nunes, E.V.L., Hsu, L., Lizarralde, F.: Global exact tracking for uncertain systems using output-feedback sliding mode control. IEEE Transaction on Automatic Control 54, 1141–1147 (2009)
15. Rodrigueza, A., De Leóna, J., Fridman, L.: Quasi-continuous high-order sliding-mode controllers for reduced-order chaos synchronization. International Journal of Control 43, 948–961 (2008)
16. Seshagiri, S., Khalil, H.K.: On Introducing integral action in sliding mode control. pp. 1473–1478 (2002)
17. Slotine, J.J.E.: Sliding controller design for nonlinear systems. International Journal of Control 40, 421–434 (1984)
18. Slotine, J.J.E., Sastry, S.S.: Tracking control of nonlinear system using sliding surface with application to robotic manipulators. International Journal of Control 40, 46–92 (1983)
19. Utkin, V.: Sliding Modes in Control and Optimization. Springer, Berlin (1992)
20. Utkin, V., Young, K.D.: Methods for constructing discontinuity planes in multidimensional variable structure systems. Automat. Remote Contr. 39, 1466–1470 (1978)
21. Wang, D.: A simple iterative learning controller for manipulators with flexible joints. Automatica 31, 1341–1344 (1995)

22. Xu, J., Qu, Z.: Robust iterative learning control for a class of nonlinear systems. Automatica 34, 983–988 (1998)
23. Xu, J., Yan, R.: Iterative learning control design without a priori knowledge of the control direction. Automatica 40, 1803–1809 (2004)
24. Young, K.D.: Design of variable structure model following control system. IEEE Transaction on Automatic Control 23, 1079–1085 (1978)
25. Yu, X., Kaynak, O.: Sliding mode control with soft computing: A survey. IEEE Transaction on Industrial Electronics 56, 3275–3285 (2009)
26. Zinober, A.: Introduction to variable structure control. Deterministic Nonlinear Control. Peregrinus, U.K (1990)

Chapter 6
Second-Order Sliding Mode Approaches to Control and Estimation for Fractional Order Dynamics

A. Pisano, M. Rapaić, and E. Usai

Abstract. This chapter outlines some results concerning the application of second-order sliding-mode techniques in the framework of control and estimation problems for some classes of fractional-order systems (FOS). Concerning the control problems, a second-order sliding mode control approach is developed to stabilize a class of linear uncertain multivariable fractional-order dynamics. Concerning estimation and observation problems, two main results are illustrated. A method for reconstructing in finite time an external disturbance acting on a known FOS is presented, and, as a second instance, a method for estimating the discrete state of a switched FOS is discussed. Both the schemes make use of second-order sliding mode observers. The method for discrete state reconstruction in switched FOS find useful application in the framework of fault detection, as shown in the experimental section part. Key point of all the approaches herein presented is the use of fractional-order sliding manifolds. Simple controller/observer tuning formulas are constructively developed along the paper by Lyapunov analysis. Simulation and experimental results confirm the expected performance.

6.1 Introduction

Fractional–order systems, i.e. dynamical systems described using fractional (or, more precisely, non-integer) order derivative and integral operators, are studied with

A. Pisano · E. Usai
Universitá degli studi di Cagliari
Dipartimento di Ingegneria Elettrica ed Elettronica (DIEE),
Cagliari, Italy
e-mail: pisano@diee.unica.it, eusai@diee.unica.it

M. Rapaić
University of Novi Sad
Automation and Control Systems Department, Novi Sad, Serbia
e-mail: rapaja@uns.ac.rs

L. Fridman et al. (Eds.): Sliding Modes, LNCIS 412, pp. 169–197.
springerlink.com

growing interest in recent years [16,25,44,41,14], and it has become apparent that a large number of physical phenomena can be modeled by fractional–order models in the areas of bioengineering [30], transport phenomena [4], economy [45] and mechanics [1,5,43], medical sciences [17] and others (see [44]).

The pioneering applications of fractions calculus in control theory date back to the sixties [31]. In the nineties, Oustaloup proposed a non-integer robust control strategy named CRONE (*Commande Robuste d'Ordre Non-Entier*) [37]. Another well known fractional control algorithm is the fractional PID (FPID, or $PI^{\lambda}D^{\mu}$) controller introduced by Podlubny [41,42], and its "partial" versions PI^{λ} and PD^{μ} (see e.g. the recent paper [29]).

Recently, optimal control theory has been generalized to incorporate models of fractional order [1,2,3,24] and fractional calculus is penetrating other nonlinear control paradigms such as the model-reference adaptive control [23,52,26], or flatness-based control [32].

In the present chapter we deal with several classes of uncertain *commensurate* fractional-order linear systems, including both time-invariant and switched dynamics. Commensurate FOS are vastly studied in the literature [23,11,48] and can been seen as the natural generalization of state-space models of conventional, integer-order, systems.

Although fractional calculus has been previously combined with sliding mode (SM) techniques [49,50] in controlling linear and nonlinear integer-order systems [10,19], SM techniques have been applied to control fractional-order systems only recently, see [46,20,47]. In [46] perfectly known linear MIMO dynamics were studied, and a first-order sliding mode stabilizing controller was suggested, while in [20] nonlinear single-input fractional-order dynamics expressed in a form that can be considered as a fractional-order version of the chain-of-integrators "Brunowsky" normal form were studied. Sliding manifolds containing fractional-order derivatives were used in both works [46,20]. In [47] the control of a special class of Single Input Single Output (SISO) switched fractional order systems (SFOS) is addressed from the viewpoints of the Generalized Proportional Integral (GPI) feedback control approach and a sliding mode based $\Sigma - \Delta$ modulation implementation of an average model based designed feedback controller. In [15] an application of SMC to fractional order dynamics arising in economics was presented.

The main drawback of sliding mode control is the so-called "chattering" phenomenon, namely the occurrence of undesirable high-frequency vibrations of the system variables which are caused by the discontinuous high-frequency nature of first-order sliding-mode control signals. The second (and higher) order sliding mode control (2-SMC) approach is a recent and quite active area of investigation in the sliding mode control theory [6,27,7]. It was developed starting from the mid eighties [21,22] to the main aim of improving the control accuracy and alleviating the undesired chattering effect by removing the control discontinuity while keeping similar properties of robustness analogous as those featured by the conventional first-order sliding mode approach.

The design of nonlinear (possibly discontinuous) observers for FOS is a topic not yet addressed in the literature. Although some results are known about the estimation and compensation of disturbances [12], the state observer design is up to now limited to the standard application of Luenberger-like observers for perfectly known FOS [13], and basic issues of observability are still under study [9, 35].

In the present paper, the second-order sliding mode approach is applied for control and estimation purposes in the framework of FOS. A key point of the proposed approaches is the use of special fractional-order sliding variables whose first-order total time derivatives contain integer derivatives of the state variables only, thus being manageable by conventional Lyapunov theory.

As for controller design, we revise the results achieved in the recent authors' work [40]. As for the observer design we present original material concerning two distinct problems. A method for reconstructing in finite time an external disturbance acting on a known FOS is presented, and, furthermore, a method for estimating the discrete state of a switched FOS is discussed. Both the schemes make use of second-order sliding mode observers. The method for discrete state reconstruction in switched FOS find useful application in the framework of fault detection, as shown in the experimental section part. The proposed controllers and observers are very simple to implement and characterized by simple and constructive tuning conditions.

The outline of the paper is as follows. The next Section 6.2 recalls some preliminaries on fractional calculus. Section 6.3 contains the problem formulation of the control problem dealt with, namely the stabilization of perturbed linear multivariable FOS, along with the suggested procedures for sliding manifold design (Subsect. 6.3.1), controller design (Subsect. 6.3.2), and simulation results. Section 6.4 contains the proposed results concerning estimation and observation, namely a method for disturbance estimation in a class of FOS (Subsect. 6.4.1), and a method for discrete state identification in switched FOS (Subsect. 6.4.2), along with the corresponding Simulation results (Subsect. 6.4.3). Section 6.5 presents an experimental application of the approach in Subsection 6.4.2 to a problem of fault diagnosis in a hydraulic system. Section 6.6 draws finally some concluding remarks.

6.2 Preliminaries on Fractional Calculus

Fractional calculus (FC) is a remarkably old topic. Its origins can be traced back to the end of seventeenth century, to the famous correspondence between Marquise de L'Hospital and G. W. Leibnitz in 1695. Since than it has been addressed by many famous mathematicians, including Euler, Lagrange, Laplace, Fourier and others. However, in consequent centuries it remained a purely theoretical topic, with little if any connections to practical problems in physics and engineering. In recent decades, FC is found to be a valuable tool in many applied disciplines, ranging from mechanics and elasticity to control theory and signal processing. The first text devoted solely to fractional calculus is the book by Oldham and Spanier [36] published in 1974. Since then, numerous texts emerged (see e.g. [41, 25]).

Several definitions of fractional operators appear in literature. In the present chapter the so called **Riemann–Liouville** approach is adopted. The Riemann–Liouville **fractional integral** of order $\alpha \geq 0$ is defined as

$$I^{\alpha}x(t) = \frac{1}{\Gamma(\alpha)} \int_0^t x(\tau)(t-\tau)^{\alpha-1} d\tau \tag{6.1}$$

where $x(t)$ is a scalar or a vector signal and $\Gamma(\alpha)$ is the Euler's Gamma function

$$\Gamma(\alpha) = \int_0^{\infty} v^{\alpha-1} e^{-v} dv. \tag{6.2}$$

For integer values of integration order α Riemann–Liouville fractional integral is equivalent to the classical n-fold integral. In fact, in such a case eq. (6.1) reduces to the well known Cauchy formula

$$I^{n}x(t) = \frac{1}{(n-1)!} \int_0^t x(\tau)(t-\tau)^{n-1} d\tau. \tag{6.3}$$

The Riemann–Liouville **fractional derivative** of order $\alpha \geq 0$ is defined as

$$D^{\alpha}x(t) = \frac{d^n}{dt^n} I^{n-\alpha} \tag{6.4}$$

where n is the integer number such that $n-1 < \alpha \leq n$. It can be proven, although this is not trivial, that for integer values of α fractional derivative coincides with the classical one. Within the current paper $\alpha \in (0,1)$ is of primary interest. For such values of α the definition (6.4) becomes

$$D^{\alpha}x(t) = \frac{1}{\Gamma(1-\alpha)} \frac{d}{dt} \int_0^t \frac{x(\tau)}{(t-\tau)^{\alpha}} d\tau \tag{6.5}$$

Let us prove the following statement that will be used in the sequel.

Lemma 6.1. *Consider a vector signal $z(t) \in \mathbb{R}^m$. Let $\alpha \in (0,1)$. If there exists $t_1 < \infty$ such that*

$$I^{\alpha}z(t) = 0 \qquad \forall t \geq t_1 \tag{6.6}$$

then

$$\lim_{t \to \infty} z(t) = 0. \tag{6.7}$$

Proof of Lemma 6.1. To prove the claim, first note that (6.6) is equivalent to $I^{\alpha}z(t) = a(t)$ where $a(t)$ is an arbitrary function identically equal to zero for $t \geq t_1$. On the other hand, since the fractional derivative is the left inverse of the fractional integral [25], this is equivalent to saying that $z(t) = D^{\alpha}a(t)$, or

$$z(t) = \frac{1}{\Gamma(1-\alpha)} \frac{d}{dt} \int_0^t \frac{a(\tau)}{(t-\tau)^{\alpha}} d\tau \tag{6.8}$$

For large values of t, in fact for all $t \geq t_1$, this reduces to

$$z(t) = \frac{1}{\Gamma(1-\alpha)} \frac{d}{dt} \int_0^{t_1} \frac{a(\tau)}{(t-\tau)^{\alpha}} d\tau \tag{6.9}$$

because $a(t)$ clips the upper limit of the integral. The time variable t can now be seen as a parameter, and under mild regularity conditions for the function $a(\tau)$ (namely, function $g(t,\tau) = a(\tau)(t-\tau)^{-\alpha}$ must be absolutely integrable in the interval $\tau \in [0,t_1]$) the derivative operator can be brought inside the integral, yielding

$$z(t) = \frac{1}{\Gamma(1-\alpha)} \int_0^{t_1} a(\tau) \frac{\partial}{\partial t} \frac{1}{(t-\tau)^{\alpha}} d\tau = \frac{-\alpha}{\Gamma(1-\alpha)} \int_0^{t_1} a(\tau) \frac{1}{(t-\tau)^{\alpha+1}} d\tau \tag{6.10}$$

Now, it is clear that

$$|z(t)| \leq \frac{\alpha}{\Gamma(1-\alpha)} \int_0^{t_1} |a(\tau)| \frac{1}{|t-\tau|^{\alpha+1}} d\tau \tag{6.11}$$

and, since the right hand side tends to zero when t approaches infinity, $|z(t)|$ must be also. Lemma 6.1 is proven. □

The conditions for the asymptotic stability of fractional order dynamics are well understood for **commensurate** linear time-invariant FOS

$$D^{\alpha} z = Az, \quad z \in R^m, \quad \alpha \in (0,1) \tag{6.12}$$

for which the necessary and sufficient condition is known in terms of a constraint on the eigenvalues of the system characteristic matrix. The following Lemma holds:

Lemma 6.2. *[11, 48] Consider system (6.12), and let $\lambda_i(A)$ $(i = 1,2,...,m)$ be the eigenvalues of matrix A. The system is asymptotically stable if and only if the following condition holds*

$$|arg(\lambda_i(A))| > \alpha \frac{\pi}{2}, \quad i = 1,2,...,m \tag{6.13}$$

The above Lemma recovers the well known results of classical control theory when $\alpha = 1$, and interestingly states that asymptotically FOS are allowed to have eigenvalues with positive real part, provided that the imaginary part is sufficiently large in magnitude.

6.3 Second-Order Sliding Mode Controllers for Multivariable Linear FOS

Consider a fractional-order linear multivariable system affected by a matched unknown perturbation

$$D^{\alpha} x(t) = Ax(t) + B(u(t) + d(t)) \qquad 0 < \alpha < 1 \tag{6.14}$$

where $x(t) \in \mathbb{R}^n$ represents the "state" vector, which is supposed to be available for measurement, $u(t) \in \mathbb{R}^m$ represents the input vector, A and B are the characteristic and control matrices, having appropriate dimensions, and $d(t)$ is an uncertain, sufficiently smooth, disturbance. The class of fractional-order dynamics (6.14) is called commensurate because all internal variables $x(t)$ are differentiated with the same order α. In this paper, we consider only the commensurate case. However, this is not a major restriction, since a variety of fractional order models are in fact commensurate. For example, all input/ouput models with fractional derivatives of rational order can be seen as commensurate, with α equal to the reciprocal value of the least common multiple of denominators of all derivatives appearing in the model.

As noted earlier, (6.14) can be seen as a generalization of classical state-space model. However, fractional order systems are inherently infinite dimensional, and therefore the components of $x(t)$ can not be seen as *states* of the considered systems. To emphasize this, and in accordance to [23], the term *vector-space model* will be used in the sequel to denote (6.14). The components of $x(t)$ will be denoted as the *internal variables*.

Let us introduce the following assumptions:

Assumption $\mathbf{A_1}$. (A,B) is a controllable pair, with the matrix B being full rank $(rank(B) = m)$

Assumption $\mathbf{A_2}$. A known constant d_{Md} exists such that $\|\frac{d}{dt}d(t)\| \leq d_{Md}$

The control task is the asymptotic stabilization of the system (6.14).

We define the m-dimensional sliding manifold in the form

$$\sigma = CI^{1-\alpha}x = 0 \tag{6.15}$$

where $\sigma \in \mathbb{R}^m$ and $C \in \mathbb{R}^{m\times n}$ is a constant matrix.

6.3.1 Sliding Manifold Design

This step concerns the design of the matrix C in order to assign a prescribed stable sliding mode dynamics.

The "sliding mode dynamics" is the dynamics of the original system after that it has been constrained to evolve on the sliding manifold $\sigma = 0$. Considering the special form (17.2) for the selected sliding manifold, the sliding mode dynamics is actually described by a fractional-order integro-differential system of the type

$$\begin{aligned} D^{\alpha}x &= Ax + B(u+d) \\ \sigma &= CI^{1-\alpha}x = 0 \end{aligned} \tag{6.16}$$

with $\sigma = [\sigma_1\ \sigma_2\ \ldots\ \sigma_m]$.

The standard approaches to sliding mode dynamics analysis for linear MIMO systems [18] do not readily apply to the considered case because of the sliding variable σ do not contain x directly, but its fractional integral of order $(1-\alpha)$ instead.

From the linearity of the fractional integral operator, the sliding manifold can be written in the form

$$\sigma = I^{1-\alpha}(Cx) = 0 \tag{6.17}$$

The integral of order $(1-\alpha)$ of every component of vector Cx is steered to zero. This means, according to Lemma 6.1, that every component of vector Cx tends to zero asymptotically starting from the moment at which σ is identically zero.

The analysis of the sliding mode dynamics can then refer to the following system

$$D^{\alpha}x = Ax + B(u+d) \tag{6.18}$$

$$Cx = \eta(t) \tag{6.19}$$

where $\eta(t)$ is an asymptotically vanishing term. Let matrix C be selected in such a way that the square matrix CB, of order m, be nonsingular.

Since $rank(B) = m$ there exist an invertible transformation matrix T such that

$$TB = \begin{bmatrix} 0 \\ B_2 \end{bmatrix} \tag{6.20}$$

where $B_2 \in \mathbb{R}^{m\times m}$ is nonsingular. The transformed internal vector z can be constructed as

$$z = Tx \tag{6.21}$$

with $z = [z_1^T\, z_2^T]^T$, $z_1 \in \mathbb{R}^{n-m}$, $z_2 \in \mathbb{R}^m$, such that the transformed system dynamics is

$$D^{\alpha}z_1 = A_{11}z_1 + A_{12}z_2 \tag{6.22}$$

$$D^{\alpha}z_2 = A_{21}z_1 + A_{22}z_2 + B_2(u+d) \tag{6.23}$$

$$CT^{-1}z = \eta(t) \tag{6.24}$$

with the matrices A_{ij} such that

$$TAT^{-1} = \begin{bmatrix} A_{11} & A_{12} \\ A_{21} & A_{22} \end{bmatrix} \tag{6.25}$$

Actually, the output map equation (6.24) of the transformed system represents an m-dimensional algebraic constraint involving the system internal variables $x_i(t)$ that reduces the order of the sliding mode dynamics with respect to that of the original plant. Let us partition matrix CT^{-1} as

$$CT^{-1} = [C_1 \;\; C_2] \tag{6.26}$$

in such a way that

$$CT^{-1}z = C_1z_1 + C_2z_2 \tag{6.27}$$

The assumption that the matrix product CB is nonsingular implies that the matrix C_2 is nonsingular too [18]. One can rewrite the output equation as

$$z_2 = -C_2^{-1}C_1 z_1 + C_2^{-1}\eta(t) \tag{6.28}$$

By considering (6.28) into the first of (6.24) it yields the following sliding mode dynamics governing equation

$$D^\alpha z_1 = (A_{11} - A_{12}C_2^{-1}C_1)z_1 + A_{12}C_2^{-1}\eta(t) \tag{6.29}$$
$$z_2 = -C_2^{-1}C_1 z_1 + C_2^{-1}\eta(t) \tag{6.30}$$

Thus, the criteria for selecting the C matrix are as follows:
- CB must be nonsingular
- $M = C_2^{-1}C_1$ must be such that the following dynamics is asymptotically stable

$$D^\alpha z_1 = (A_{11} - A_{12}M)z_1 + A_{12}C_2^{-1}\eta(t) = \bar{A}z_1 + A_{12}C_2^{-1}\eta(t) \tag{6.31}$$

with implicit definition of matrix $\bar{A} = A_{11} - A_{12}M$. Since signal $\eta(t)$ is asymptotically vanishing, the asymptotic stability properties of system (6.31) will be governed by its characteristic matrix $\bar{A}$ only. Once the asymptotic convergence to zero of vector z_1 is ensured by the appropriate selection of the matrix M, the successive asymptotic vanishing of vector z_2 trivially results from (6.30).

Thus, by Lemma 6.2, the matrix M should be designed to place the eigenvalues of the matrix $\bar{A} = A_{11} - A_{12}M$ according to the restriction (6.13). The possibility of assigning the eigenvalues of the matrix $\bar{A} = A_{11} - A_{12}M$ is grant by the following Proposition.

Proposition 6.1. *[18, p. 39] The matrix pair (A_{11}, A_{12}) is controllable if and only if the matrix pair (A, B) is controllable.*

It should be noted that the above design procedure, fixing $M = C_2^{-1}C_1$ only, does not uniquely determine matrix C. A computationally convenient way to set the matrices C_1 and C_2 is according to $C_2 = I_m$, $C_1 = M$, which gives rise to

$$C = [M \;\; I_m]T \tag{6.32}$$

where I_m is the m-th order identity matrix.

Remark 6.1. A possible choice for the transformation matrix T is

$$T = \begin{bmatrix} B^\perp \\ T_1 \end{bmatrix} \tag{6.33}$$

where $B^\perp$ is a matrix such that $B^\perp B = 0$ and $B^\perp$ is linearly independent of B, and T_1 is any matrix that makes T and $T_1 B$ nonsingular. A possible choice for T_1 is

$$T_1 = (B^T B)^{-1} B^T \tag{6.34}$$

Clearly, this choice guarantees the decomposition (6.20), with $B_2 = T_1 B = I$.

6.3.2 Control-Input Design

This step concerns the design of a control input vector $u(t)$ steering the system (6.14) in finite time onto the sliding manifold (17.2). The task is not trivial due to, both, the presence of the unknown disturbance and the fractional-order nature of the system dynamics. By (6.4) it yields that

$$\dot{\sigma} = C\frac{d}{dt}I^{1-\alpha}x = CD^{\alpha}x \tag{6.35}$$

In light of the plant equation (6.14) it follows that the dynamics of the sliding variable σ is of integer order and uniform vector relative degree one.

$$\dot{\sigma} = CAx + CB(u+d) \tag{6.36}$$

The control vector $u = [u_1\ u_2\ \dots\ u_m]$ is expressed as follows

$$u = (CB)^{-1}v \tag{6.37}$$

$$v = -CAx(t) - k_1\sigma - k_2|\sigma|^{1/2}\text{sign}(\sigma) + w \tag{6.38}$$

$$\dot{w} = -k_3\text{sign}(\sigma) \tag{6.39}$$

where the following notation is used to give (6.38)-(6.39) a more compact representation.

$$|\sigma|^{1/2}\text{sign}(\sigma) = [\sqrt{|\sigma_1|}\text{sign}(\sigma_1), \dots, \sqrt{|\sigma_m|}\text{sign}(\sigma_m)]^T \tag{6.40}$$

The next Theorem is proven.

Theorem 6.1. *Consider system (6.14) satisfying the Assumptions A_1, A_2, and the sliding manifold (17.2) with the C matrix designed according to the procedure given in the Section 6.3.1. Then, the control law (6.37)-(6.40), with the scalar parameters k_1, k_2, k_3 fulfilling the following tuning conditions*

$$k_1 > 2\sqrt{\rho} \quad k_2 > 0 \quad k_3 > \rho\sqrt{k_1} \quad \rho = \|CB\|d_{Md} \tag{6.41}$$

will steer the system (6.14) asymptotically to the origin.

Proof. The closed loop system dynamics is obtained as follows considering (6.37) into (6.36)

$$\begin{aligned} \dot{\sigma} &= CBd - k_1\sigma - k_2|\sigma|^{1/2}\text{sign}(\sigma) + w \\ \dot{w} &= -k_3\text{sign}(\sigma) \end{aligned} \tag{6.42}$$

Define the following new variable $z = w + CBd$, and rewrite system (6.42) in the new $\sigma - z$ coordinates

$$\begin{aligned} \dot{\sigma} &= -k_1\sigma - k_2|\sigma|^{1/2}\text{sign}(\sigma) + z \\ \dot{z} &= -k_3\text{sign}(\sigma) + CB\tfrac{d}{dt}d(t) \end{aligned} \tag{6.43}$$

The dynamics of the variable pairs $(\sigma_i, z_i) \in \mathbb{R}^2$, $i = 1,2,...,m$, are decoupled one each other, then to simplify the stability analysis it is convenient to refer to the decoupled systems independently

$$\begin{aligned} \dot{\sigma}_i &= -k_1\sigma_i - k_2|\sigma_i|^{1/2}\text{sign}(\sigma_i) + z_i \qquad i = 1,2,...,m \\ \dot{z}_i &= -k_3\text{sign}(\sigma_i) + c_i B\frac{d}{dt}d(t) \end{aligned} \tag{6.44}$$

with c_i being the i-th row of matrix C. For the uncertain term $c_i B\frac{d}{dt}d(t)$ the following bound holds by virtue of assumption A_3

$$\left| c_i B\frac{d}{dt}d(t) \right| \leq \|CB\| d_{Md} \tag{6.45}$$

The dynamics (6.44)-(6.45) is a special case of the more general second-order dynamics studied in [34, Theorem 5]. The same Lyapunov function as that used in [34] is considered:

$$V_i = 2k_3|\sigma_i| + \frac{1}{2}z_i^2 + \frac{1}{2}\left(k_1|\sigma_i|^{1/2}\text{sign}(\sigma_i) + k_1\sigma_i - z_i\right)^2 \tag{6.46}$$

which can be rewritten as follows

$$V_i = \xi_i^T H \xi_i \tag{6.47}$$

$$\xi_i = \begin{bmatrix} |\sigma_i|^{1/2}\text{sign}(\sigma_i) \\ \sigma_i \\ z_i \end{bmatrix} \quad H = \begin{bmatrix} (4k_3 + k_2^2) & k_1k_2 & -k_2 \\ k_1k_2 & k1^2 & -k_1 \\ -k_2 & -k_1 & 2 \end{bmatrix} \tag{6.48}$$

By evaluating the derivative of (6.47)-(6.48) along the trajectories of system (6.44)-(6.45), and considering the tuning rules (6.41), it can be found two positive constants γ_1 and γ_2 such that

$$\dot{V}_i \leq -\gamma_1 V_i - \gamma_2\sqrt{V_i} \tag{6.49}$$

which easily implies, by simple application of the comparison Lemma, that all the V_i Lyapunov functions, $i = 1,2,...,m$, tend to zero in a finite time, and the same holds for the vector σ. As shown in the Section 6.4, the finite time vanishing of the sliding vector variable σ guarantees that all the $x(t)$ solutions of the uncertain system (6.14) will tend globally and asymptotically to zero. This proves the Theorem. □

6.3.3 Implementation Issues

In general, fractional order dynamics describe the behavior of infinite dimensional systems by means of a finite-dimensional vector whose components are related one each other by fractional-order differential relationships. In the present chapter it is shown that if the desired sliding surface is also defined in the fractional manner (17.2) then its derivative can be exactly expressed as in (6.36) through the

linear right-hand side of the commensurate fractional-order dynamics (6.14). Starting from this place, all specifics related to the fractional calculus completely disappear, and never appear again. This means that the stability of an infinite dimensional system has been converted into standard sliding-mode analysis of a finite-dimensional dynamics.

The proposed approach requires the availability of the sliding variable (17.2) which is related to the vector space via a fractional order integration operator of order $(1-\alpha)$. Fractional order operators are infinite dimensional ones that do not allow an exact algorithmic on-line computation. Thus, it is impossible to measure exactly the sliding variable vector. However, numerical approximations are available that allow to obtain an estimate of the fractional-order integral of an available signal. Among the most well-known ones are the methods based on Oustaloup's rational approximation. This and other analogue realizations of fractional-order operators were discussed in [38]. Different numerical approximations are reported in [51,8]. By means of these methods, rational approximations of fractional-order operators are obtained in the form of FIR or IIR digital filters. By choosing filters of sufficiently high order, the approximation error can be made arbitrarily small in a desired frequency range.

In this chapter the fractional integrals were computed numerically in a "general purpose" fashion (i.e. with no pre-specified frequency range of interest), using the left Euler approximation of the fractional integral (6.1). The entire time interval $[0,t]$, with $t = NT$, is divided into segments of length T, and the sampling instants $t_n = nT$ $(n = 0,1,...,N)$ will be considered in the approximate formula explained as follows

$$\begin{aligned} I^{\alpha}x(t_n) &= \frac{1}{\Gamma(\alpha)}\int_0^{t_n} x(\tau)(t_n-\tau)^{\alpha-1}d\tau \\ &= \frac{1}{\Gamma(\alpha)}\sum_{k=0}^{n}\int_{kT}^{(k+1)T} x(\tau)(nT-\tau)^{\alpha-1}d\tau \\ &\approx \frac{1}{\Gamma(\alpha)}\sum_{k=0}^{n} x(kT)\int_{kT}^{(k+1)T}(nT-\tau)^{\alpha-1}d\tau \\ &= \sum_{k=0}^{n} x(kT)w(nT-kT), \end{aligned} \tag{6.50}$$

where,

$$w(nT-kT) = \frac{1}{\Gamma(\alpha)}\int_{kT}^{(k+1)T}(nT-\tau)^{\alpha-1}d\tau. \tag{6.51}$$

The above approximation to the fractional integral retains the hereditary properties of fractional operators: the entire process history is taken into consideration. However, if the sampling time T is small, the number of terms in the approximation sum (6.50) may become unreasonably high even for relatively small values of time t. Therefore, the maximal number of terms was limited, and the approximation used in the sequel is

$$I^{\alpha}x(t_n) = \sum_{k=max(0,n-N)}^{n} x(kT)w(nT-kT), \tag{6.52}$$

with $n_{max} = 5000$. Fractional derivatives were approximated according to (6.4), where the first order derivative was approximated by finite differences. The resulting approximate formulas implement, therefore, high-order FIR filters.

The overall approximation error in the sliding variable estimation can be understood as an additive measurement noise corrupting the sliding variable. As it is well known, sliding-mode based variable structure control algorithms feature good properties of robustness against the measurement noise and discretization effects.

6.3.4 Simulation Results

Distributed parameters processes, heat transfer in particular, constitute a rich area of application of fractional calculus. Recently, Melchior and coworkers [[44], page 493] considered a test bench involving a long aluminum rod heated from one of its sides, and showed a good agreement between the experimental data and a commensurate fractional-order linear model of the system. The input $u(t)$ to such model is the thermal flux applied at one end of the rod, and the output is the actual temperature at a prescribed section of the rod. The obtained model is commensurate, and its vector-space formulation is as follows

$$D^{0.5}x(t) = \begin{bmatrix} 0 & 1 & 0 \\ 0 & 0 & 1 \\ 0 & -0.0601251 & -0.42833 \end{bmatrix} x(t) + \begin{bmatrix} 0 \\ 0 \\ 1 \end{bmatrix} u(t). \tag{6.53}$$

In the sequel, we will assume that all of the vector-space variables are accessible for measurement and will use this model to test the control strategies discussed previously. We also added a matching disturbance

$$d(t) = 0.9sin(0.2\pi t) \tag{6.54}$$

as in (6.14) to test the robustness properties of the suggested sliding mode controllers. Clearly, the bounding constant d_{Md} in the Assumption A_2 can be the selected as

$$d_{Md} = 1 \tag{6.55}$$

In order to design the vector C defining the sliding manifold the transformation matrix T is computed first according to (6.33)-(8.1). It yields

$$T = \begin{bmatrix} 0 & 1 & 0 \\ -1 & 0 & 0 \\ 0 & 0 & 1 \end{bmatrix} \tag{6.56}$$

The resulting decomposition (6.25) yields

$$A_{11} = \begin{bmatrix} 0 & 0 \\ -1 & 0 \end{bmatrix}, \quad A_{21} = \begin{bmatrix} 0 \\ 0 \end{bmatrix}, \quad A_{12} = \begin{bmatrix} -0.0601 & 0 \end{bmatrix}, \quad A_{12} = -0.4283 \tag{6.57}$$

The matrix $M = [5 \ -6]$ places the eigenvalues of matrix $A_{11} - A_{12}M$ in the location $[-2 - 3]$, which is selected according to the stability condition (6.13) of Lemma 6.2. Vector C defining the chosen sliding manifold is then derived according to (6.32) as $C = [6\ 5\ 1]$. Since $CB = 1$ the norm of CB, which is involved in the controller tuning formulas, takes also unit value,i.e. $\|CB\| = 1$. The suggested second order sliding mode control algorithm (6.37)-(6.38) has been implemented with the following parameter values, that are selected according to the tuning inequalities (6.41): $\rho = 1$, $k_1 = 3$, $k_2 = 3$, $k_3 = 2$.

In all tests, the sampling period $T_s = 0.0001s$ has been used. The fractional order dynamics is simulated by first computing the fundamental matrix $\Phi(t)$, equal to the inverse Laplace transform of $(s^{0.5}I - A)^{-1}$, where s is the Laplace variable and I is the unit matrix of appropriate size. The inverse Laplace transform was calculated using the series expansion method introduced by Atanacković *et al.* [4]. The vector-space response is then calculated according to

$$x(t) = \Phi(t)I_0 + \int_0^t \Phi(t-\tau)Bu(\tau)d\tau \tag{6.58}$$

with $I_0 = \lim_{t\to 0} D^{\alpha-1}x(t)$ being the initial condition (not equal to $x(0)$). In the following simulations I_0 was set to $[0\ 0\ 1]$.

The Figure 6.1 shows the time evolution of the three internal variables. The figure 6.2 displays the control input $u(t)$ which is a **continuous** function of time. The time history of the sliding variable $\sigma(t)$ is reported in the Figure 6.3. The test confirms the good robustness properties of the approach.

6.4 Second-Order Sliding Mode Based Observation and Estimation for FOS

Two distinct problems shall be addressed later on. A method for reconstructing in finite time an external disturbance acting on a known FOS is presented, and, furthermore, a method for estimating the discrete state of a switched FOS is discussed. Both the schemes make use of second-order sliding mode observers, and, in particular, the latter will be experimentally verified through its application to a problem of fault diagnosis (Section 6.5).

6.4.1 Disturbance Observer for FOS

Consider now a generalized form of the fractional-order system (6.14):

$$D^{\alpha}x(t) = Ax(t) + Bu(t) + F + d(t) \qquad 0 < \alpha < 1 \tag{6.59}$$

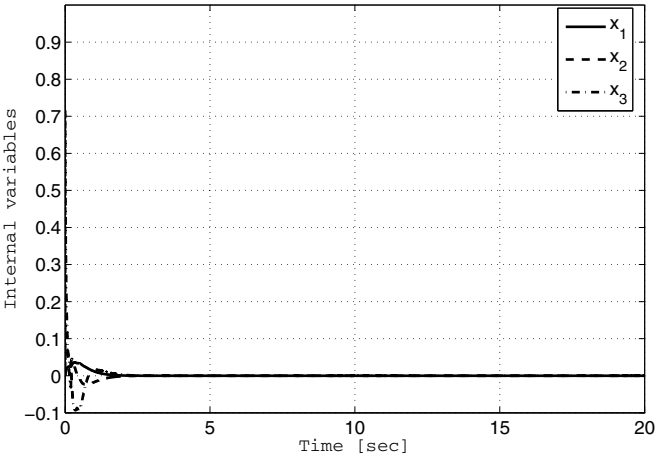

Fig. 6.1 The internal variables x_1, x_2, x_3.

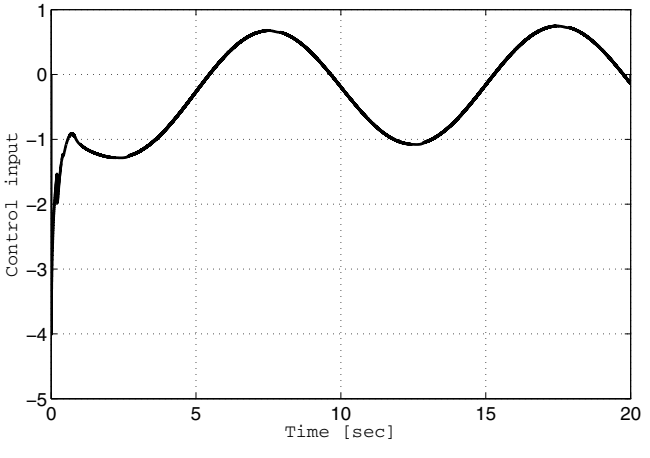

Fig. 6.2 The control input u.

where $x(t) \in \mathbb{R}^n$ represents the system's *vector-space model* [23], whose components (the *internal variables*) are supposed to be available for measurement, $u(t) \in \mathbb{R}^m$ represents the known input vector, A and B are the characteristic and control matrices and F is an affine term, having appropriate dimensions, and $d(t) \in \mathbb{R}^n$ is a sufficiently smooth uncertain disturbance.

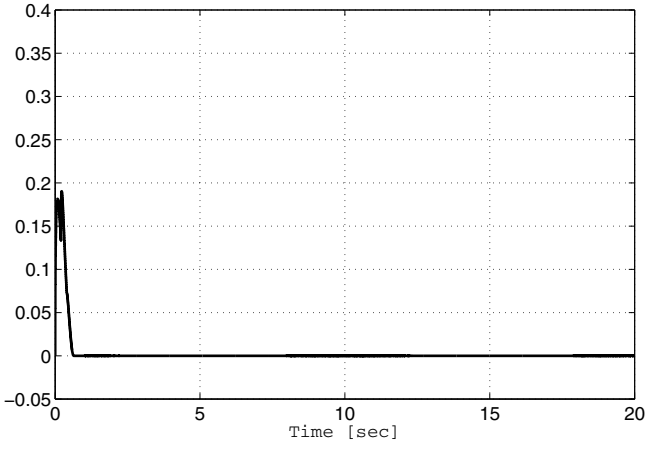

Fig. 6.3 The sliding variable σ.

The problem of reconstructing the disturbance $d(t)$ is tackled.
Assume what follows
Assumption A_3. It can be found a constant d_{Md} such that

$$\left\| \frac{d}{dt} d(t) \right\| \leq d_{Md} \tag{6.60}$$

It is proposed the next observer

$$D^{\alpha}\hat{x}(t) = Ax(t) + Bu(t) + F + w(t) \tag{6.61}$$

where the observer injection input term $w(t)$ is computed by means of the dynamical super-twisting plus linear controller:

$$\varepsilon = I^{1-\alpha}(\hat{x} - x) \tag{6.62}$$

$$w = w_1 + w_2 \tag{6.63}$$

$$w_1 = -k_1\varepsilon - k_2|\varepsilon|^{1/2}\text{sign}(\varepsilon) \tag{6.64}$$

$$\dot{w}_2 = -k_3\text{sign}(\varepsilon) \tag{6.65}$$

By a proper generalization of the stability results demonstrated in the Theorem 6.1, it can be shown that under the Assumption A_3 the system (6.61)-(6.65) with appropriate observer gains permits the reconstruction of the disturbance since the next equality holds starting from a finite time instant T in accordance with:

$$w_2(t) = d(t), \qquad t \geq T \tag{6.66}$$

Theorem 6.2. *Consider system (6.59) fulfilling the Assumption A_3 along with the observer (6.61)-(6.65) with the gain parameters chosen according to the next inequalities:*

$$k_1 > 2\sqrt{\rho} \quad k_2 > 0 \quad k_3 > \rho\sqrt{k_1} \quad \rho = d_{Md} \tag{6.67}$$

Then, there is a finite $T > 0$ such that the relation (6.66) holds.

Proof of Theorem 6.2. The time derivative of the error variable ε (6.62) is:

$$\dot{\varepsilon} = D^{\alpha}\hat{x}(t) - D^{\alpha}x(t) \tag{6.68}$$

which, considering the plant and observer dynamics (6.59)-(6.65) yields the following:

$$\dot{\varepsilon} = w(t) - d(t) = -k_1\varepsilon - k_2|\varepsilon|^{1/2}\text{sign}(\varepsilon) + w_2(t) - d(t) \tag{6.69}$$

By making the change of variable

$$z(t) = w_2(t) - d(t) \tag{6.70}$$

one can augment and rewrite (6.69) as

$$\begin{aligned} \dot{\varepsilon} &= w(t) - d(t) = \\ &= -k_1\varepsilon - k_2|\varepsilon|^{1/2}\text{sign}(\varepsilon) + z(t) \end{aligned} \tag{6.71}$$

$$\dot{z} = -k_3\text{sign}(\varepsilon) - \frac{d}{dt}d(t) \tag{6.72}$$

System (6.71)-(6.72) is equivalent to the system (6.43) that was dealt with in the proof of Theorem 6.1. Therefore, the asymptotic stability of (6.71)-(6.72) follows by the same Lyapunov analysis made in the proof of Theorem 6.1 using the functions

$$V_i = \xi_i^T H \xi_i, \quad i = 1, 2, ..., n \tag{6.73}$$

$$\xi_i = \begin{bmatrix} |\varepsilon_i|^{1/2}\text{sign}(\varepsilon_i) \\ \varepsilon_i \\ z_i \end{bmatrix} \quad H = \begin{bmatrix} (4k_3 + k_2^2) & k_1k_2 & -k_2 \\ k_1k_2 & k1^2 & -k_1 \\ -k_2 & -k_1 & 2 \end{bmatrix} \tag{6.74}$$

where ε_i and z_i are generic entries of ε and z ($i = 1, 2, ..., n$). It turns out that the tuning conditions (6.67) guarantee the attainment of condition

$$\dot{V}_i \leq -\gamma_1 V_i - \gamma_2\sqrt{V_i}, \quad \gamma_1, \gamma_2 > 0 \tag{6.75}$$

that guarantees the **finite time** convergence of ε and z to zero starting from some finite moment $T > 0$. By the definition (6.70) of $z(t)$, it directly follows the condition (6.66) . Theorem 6.2 is proven. □

6.4.2 Discrete-Mode Identification for Switched FOS

Consider now a switched and unperturbed version of system (6.59)

$$D^{\alpha}x(t) = A_{j(t)}x(t) + B_{j(t)}u(t) + F_{j(t)} \quad 0 < \alpha < 1 \quad j(t) \in \{1,2,...,q\} \tag{6.76}$$

where $x(t) \in \mathbb{R}^n$, $u(t) \in \mathbb{R}^m$, and where the so-called "commutation signal" (or "discrete state") $j(t)$ determines the actual system dynamics among the possible q "operation mode" represented by the triplets (A_i, B_i, F_i), $i = 1,2,...,q$.

Consider the next expression for the piecewise constant commutation signal

$$j(t) = j_k, \quad t_{k-1} \leq t < t_k, \quad k = 1,2,...,\infty \tag{6.77}$$

where $t_0 = 0$ and t_k are the "switching times" at which the discrete state is changing.

Let the next **dwell-time** restriction holds for the switching sequence

$$t_k - t_{k-1} \geq \Delta, \quad k = 1,2,...,\infty \tag{6.78}$$

The dwell time restrictions inhibits the occurrence of the so-called "Zeno phenomenon" for the considered switched dynamics, namely the occurrence of infinitely fast changes in the system modes. Note, however, that if the control matrix B is constant (i.e., if $B_1 = B_2 = ... = B_q = B$) then the control input $u(t)$ can be discontinuous and of arbitrarily high (theoretically infinite) switching frequency.

Some specific operation modes in the set $\{1,2,...,q\}$ are supposed to correspond to **faulty conditions** for system (6.76) that need to be detect for real-time monitoring and fault diagnosis purposes. The pair $(x(t), u(t))$ is supposed to be accessible for measurements. The task is to reconstruct the unknown discrete state $j(t)$. The logic that drives the mode switchings can be either driven by internal system's variables or driven by an external supervisor, in any case it is unknown to the designer. Then, the identification of the correct mode after the switching times will require a transient. This transient should be faster that the Δ value involved in dwell time restriction, otherwise the estimation will be use-less.

A parallel stage containing q observers, one for each of the possible modes of operation, is suggested:

$$D^{\alpha}\hat{x}_i(t) = A_i x(t) + B_i u(t) + F_i + v_i, \quad i = 1,2,...,q \tag{6.79}$$

where v_i is the injection input for the $i-th$ observer, to be designed.

Denote the observation error for the i-th observer as

$$e_i = \hat{x}_i - x_i \tag{6.80}$$

Then the switched and fractional order error dynamics will be given by

$$D^{\alpha}e_i(t) = (A_i - A_{j(t)})x(t) + (B_i - B_{j(t)})u(t) + (F_i - F_{j(t)}) + v_i(t) \tag{6.81}$$

It can be then separated the error dynamics of the "**correct**" observer (i.e., that having the index i which matches the current mode of operation $j(t)$):

$$D^{\alpha}e_i(t) = v_i(t), \quad i = j(t) \tag{6.82}$$

and the error dynamics of the remaining "**wrong**" observers:

$$D^{\alpha}e_i(t) = (A_i - A_{j(t)})x(t) + (B_i - B_{j(t)})u(t) + (F_i - F_{j(t)}) + v_i(t), \quad i \neq j(t) \tag{6.83}$$

Denote

$$\Delta A_i^j = A_i - A_{j(t)} \tag{6.84}$$

$$\Delta B_i^j = B_i - B_{j(t)} \tag{6.85}$$

$$\Delta F_i^j = F_i - F_{j(t)} \tag{6.86}$$

and

$$\varphi_i^j(x,u,t) = \Delta A_i^j x(t) + \Delta B_i^j u(t) + \Delta F_i^j \tag{6.87}$$

then (6.83) is rewritten as

$$D^{\alpha}e_i(t) = \varphi_i^j(x,u,t) + v_i(t), \quad i \neq j(t) \tag{6.88}$$

Concerning the state- and input-dependent functions $\varphi_i^j(x,u,t)$ entering the dynamics (6.88) of the wrong observers, in order to guarantee the identifiability of the correct mode they should not be identically zero. Then it is made the next

Assumption A_4**.**

$$\left\| \varphi_i^j(x,u,t) \right\| \neq 0, \quad \forall i,j = 1,2,...,q, \;\; i \neq j \tag{6.89}$$

The above assumption A_4 should be understood as a constraint on the dynamics of the switched system and in particular on the resulting $(x-u)$ time evolutions. In other words it could be said that the manifolds $\varphi_i^j(x,u,t) = 0$ should not contain admissible $x(t) - u(t)$ trajectories of the switched system.

Functions $\varphi_i^j(x,u,t)$ are also supposed to be smooth enough according to the next

Assumption A_5**.** There is a constant Φ such that

$$\left\| \frac{d}{dt}\varphi_i^j(x,u,t) \right\| \leq \Phi, \quad \forall i,j = 1,2,...,q \tag{6.90}$$

Clearly, the above Assumption implies a bounded, although arbitrarily large, admissible domain for the evolution of the (x,u) trajectories in the respective space. This gives **semi-global** validity to the presented discrete mode observer.

The design of the observer injection terms is carried out by the same technique adopted in the previous subsection:

$$\sigma_i = I^{1-\alpha}(\hat{x}_i - x) \tag{6.91}$$

$$v_i = v_{1i} + v_{2i} \tag{6.92}$$

$$v_{1i} = -k_1\sigma_i - k_2|\sigma_i|^{1/2}\text{sign}(\sigma_i) \tag{6.93}$$

$$\dot{v}_{2i} = -k_3\text{sign}(\sigma_i) \tag{6.94}$$

The new error variables σ_i are introduced in (6.91), which involves a non-integer order integration of the original error variables e_i. It is worth to note that the dynamics of the variable σ_i is of integer order:

$$\dot{\sigma}_i = \begin{cases} v_i(t) & i = j(t) \\ \varphi_i^j(x,u,t) + v_i(t) & i \neq j(t) \end{cases} \tag{6.95}$$

It can be defined a unique set of tuning rules for all the gains of the q observers. Consider the next inequalities involving the tuning coefficients:

$$k_1 > 2\Phi \quad k_2 > 0 \quad k_3 > \Phi\sqrt{k_1} \tag{6.96}$$

The main idea behind the proposed observer structure is that, after a finite transient starting at any switching times, the injection input $v_{2i}(t)$ will be identically zero for the *correct* observer and will be separated from zero for the *wrong* observers. This can be obtained, by virtue of Assumption A_4, if the **finite-time convergence to zero of σ_i and $\dot{\sigma}_i$** is provided for all the q observers ($i = 1,2,...,q$).

Let the maximal finite transient duration be denoted as T. Then, in that case, provided that $T < \Delta$, the next relationship directly derives by the achieved conditions $\sigma_1 = \dot{\sigma}_1 = \dot{\sigma}_2 = ... = \dot{\sigma}_q = 0$:

$$v_{2i}(t) = \begin{cases} 0 & i = j(t) \\ -\varphi_i^j(x,u,t) & i \neq j(t) \end{cases} \qquad t_{k-1} + T \leq t \leq t_k, \quad k = 1,2,... \tag{6.97}$$

On the basis of (6.95), and by taking into account the Assumption A_4 as well, it can be developed a simple method for estimating the actual discrete state $j(t)$ by comparing the norms of the the observer signals $v_{21}(t)$, $v_{22}(t)$, ..., $v_{2q}(t)$ looking for the closest to zero:

$$\hat{j}(t) = \arg\min_i \|v_{2i}(t)\| \tag{6.98}$$

The proposed scheme for the identification of the discrete state in the switched FOS (6.76) is summarized in the next Theorem:

Theorem 6.3. *Consider the switched FOS (6.76), fulfilling the Assumptions A_4 and A_5, and the observers (6.79), (6.91)-(6.94) with the observer gains chosen according to (6.96). Then, the discrete state estimation (6.98) will be such that*

$$\hat{j}(t) = j(t), \qquad t_{k-1} + T \leq t \leq t_k, \quad k = 1,2,... \tag{6.99}$$

Proof of Theorem 6.3. By combining (6.82) and (6.83), the dynamics of the error variables e_i is given by:

$$D^\alpha e_i(t) = \begin{cases} v_i(t) & i = j(t) \\ \varphi_i^j(x,u,t) + v_i(t) & i \neq j(t) \end{cases} \tag{6.100}$$

Then, by (6.62) the dynamics of the modified error variables σ_i is of integer order, and it is given by (6.95). By (6.77), during the first switching interval $t \in (0,t_1)$ the actual mode is $j(t) = j_1$. Then (6.95) specializes as

$$\dot{\sigma}_{j_1} = v_{j_1}(t) \tag{6.101}$$

$$\dot{\sigma}_i(t) = \varphi_i^j(x,u,t) + v_i(t), \quad i = 1,2,...,q, \quad i \neq j_1 \tag{6.102}$$

Considering (6.92)-(6.65) into (6.101) yields

$$\dot{\sigma}_{j_1}(t) = -k_1\sigma_{j_1} - k_2|\sigma_{j_1}|^{1/2}\text{sign}(\sigma_{j_1}) + v_{2,j_1}(t) \tag{6.103}$$

$$\dot{v}_{2,j_1} = -k_3\text{sign}(\sigma_{j_1}) \tag{6.104}$$

$$\dot{\sigma}_i(t) = -k_1\sigma_i - k_2|\sigma_i|^{1/2}\text{sign}(\sigma_i) + v_{2,i}(t) + \varphi_i^j(x,u,t) \tag{6.105}$$

$$\dot{v}_{2,i} = -k_3\text{sign}(\sigma_i) \quad i = 1,2,...,q, \quad i \neq j_1 \tag{6.106}$$

By introducing the new coordinates

$$z_i(t) = v_{2,i}(t) + \varphi_i^j(x,u,t) \tag{6.107}$$

one can augment and rewrite (6.105)-(6.106) as

$$\dot{\sigma}_i = -k_1\sigma_i - k_2|\sigma_i|^{1/2}\text{sign}(\sigma_i) + z_i(t) \tag{6.108}$$

$$\dot{z}_i = -k_3\text{sign}(\sigma_i) + \frac{d}{dt}\varphi_i^j(x,u,t) \quad i = 1,2,...,q, \quad i \neq j_1 \tag{6.109}$$

In light of the assumption A_5, systems (6.103)-(6.104) and (6.108)-(6.109) are equivalent to the system (6.43) that was dealt with in the proof of Theorem 6.1. Therefore, taking into account the observer tuning conditions (6.67), the finite time convergence to zero of σ_i $(i = 1,2,...n)$, v_{2,j_1}, and z_i $(i = 1,2,...,q, \quad i \neq j_1)$ can be demonstrated following by the same Lyapunov analysis made in the proof of Theorem 6.1.

Let $T > 0$ be the transient time. By increasing the Φ constant in the tuning formulas, the transient time can be made as small as desired [28, 39], and in particular such that $T << \Delta$.

Then, considering (6.70), during the first switching interval the next conditions are achieved:

$$v_{2j_1}(t) = 0 \qquad T < t < t_1 \tag{6.110}$$

$$v_{2i}(t) = -\varphi_i^j(x,u,t), \quad i = 1,2,...,q, \quad i \neq j_1 \tag{6.111}$$

In light of the assumption A_4, the residual-based estimation logic (6.98) provides the reconstruction of the discrete state after the transient time T, i.e.

$$\hat{j}(t) = j_1, \qquad 0 + T \leq t \leq t_1 \tag{6.112}$$

At the time moment $t = T_1$ the discrete state will be changing. A new transient of length T is activated for the observer error dynamics, at the end of which the next conditions will be in force:

$$v_{2j_2}(t) = 0 \qquad t_1 + T < t < t_2 \tag{6.113}$$

$$v_{2i}(t) = -\varphi_i^j(x,u,t), \quad i = 1,2,...,q, \quad i \neq j_2 \tag{6.114}$$

Thus the estimation logic (6.98) still provides the reconstruction of the discrete state after the transient time, i.e.

$$\hat{j}(t) = j_2, \qquad t_1 + T < t < t_2 \tag{6.115}$$

By iteration on the successive switching intervals, condition (6.99), and so Theorem 6.3, is proven. □

Remark 6.1. The logic (6.98) appears not completely effective, since in some case it can happen that Assumption A_4 is violated and, as a result, also the wrong residuals $v_{2i}(t)$ $(i \neq j(t))$ can occasionally cross the zero value. Note that this event becomes highly improbable when the order n of the systems is growing.

On the other hand, only the correct residual $(i = j(t))$ can stay at (or, more realistically, close to) zero for long time intervals. Hence the next averaged residuals can be considered

$$R_i(t) = \int_{t-\delta}^{t} \|v_{2i}(\tau)\| d\tau. \tag{6.116}$$

where δ is a small time delay (the width of a receding horizon window of observation for the residuals $\|v_{2i}\|$), along with the corresponding modified discrete state evaluation strategy

$$\hat{j}(t) = \arg\min_i R_i(t) \tag{6.117}$$

6.4.3 Simulation Results

Some simulation examples will be presented and discussed to illustrate the effectiveness of the presented disturbance and discrete-state observers.

6.4.4 Disturbance Estimation Test

Let us consider first the disturbance estimation problem. Consider the commensurate perturbed fractional-order system

$$D^{0.6}\mathbf{x} = \begin{bmatrix} -1 & 0 \\ 0 & -2 \end{bmatrix} \mathbf{x} + \begin{bmatrix} 1 \\ 1 \end{bmatrix} \mathbf{u} + \mathbf{d} \tag{6.118}$$

where $\mathbf{d}$ is a vector of unmeasurable disturbances to be estimated. For the purpose of the current example, let us assume that the disturbance signal is

$$\mathbf{d}(t) = \begin{bmatrix} 1 \\ \sin(t) \end{bmatrix} h(t - 0.5), \tag{6.119}$$

with h being the unit step signal. Clearly system (6.118)-(6.119) belongs to the class of systems (6.59), and the Assumption A_3 is fulfilled at any $t \geq 0.5$ with the value $d_{Md} = 1$.

The state is assumed to be fully available and the algorithm (6.61)-(6.65) can be used for state estimation. The sampling time was chosen to be $T = 1ms$, while the parameters of the disturbance estimation algorithm were selected as $k_1 = 1.5$, $k_2 = 0.25$ and $k_3 = 2$ in accordance with the tuning formulas (6.67).

Figure 6.4 depicts the components of the actual and estimated disturbance signal. The solid line represents the actual profile of the disturbance signals acting on the dynamics of the first and second internal variable, respectively. The estimated disturbances are plotted with dashed lines.

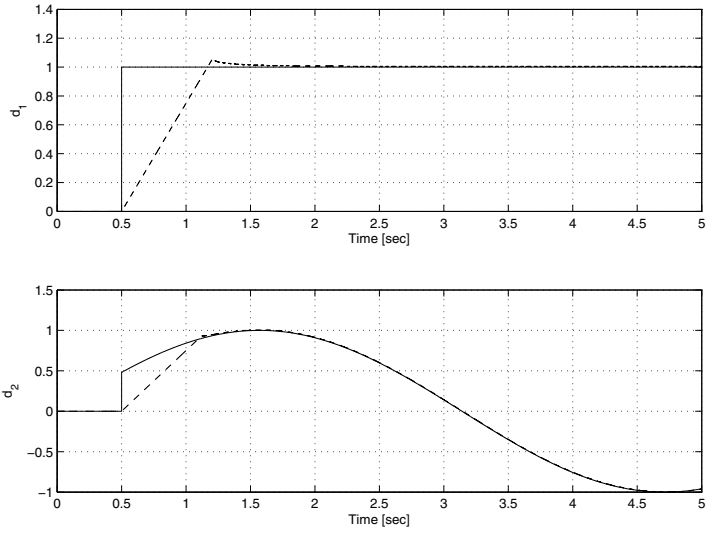

Fig. 6.4 Disturbance estimation test. Actual and estimated disturbance.

6.4.5 Discrete State Estimation Test

Now let us consider the discrete state estimation problem for the affine switched FOS (6.76) with the order of differentiation $\alpha = 0.6$ and $q = 3$ distinct sub-models defined by the matrix triplets

$$A_1 = \begin{bmatrix} -1 & 0 \\ 0 & -2 \end{bmatrix}, \qquad B_1 = \begin{bmatrix} 1 \\ 1 \end{bmatrix}, \qquad F_1 = \begin{bmatrix} 0 \\ 0 \end{bmatrix} \tag{6.120}$$

$$A_2 = \begin{bmatrix} 0 & 1 \\ -2 & 0 \end{bmatrix}, \quad B_2 = \begin{bmatrix} 1 \\ 0 \end{bmatrix}, \quad F_2 = \begin{bmatrix} 0 \\ 0 \end{bmatrix} \tag{6.121}$$

$$A_3 = \begin{bmatrix} -6 & -4 \\ 1.5 & -1 \end{bmatrix}, \quad B_3 = \begin{bmatrix} 0 \\ 1 \end{bmatrix}, \quad F_3 = \begin{bmatrix} 0 \\ 0 \end{bmatrix} \tag{6.122}$$

The discrete state is changed according to the next rule

$$j(t) = \begin{cases} 1 & 0 \leq t < 2 \\ 2 & 2 < t \leq 4 \\ 3 & 4 < t <\leq 6 \end{cases} \tag{6.123}$$

The parallel stage of observers (6.79), (6.91)-(6.94) have been implemented with the gains $k_1 = 2$, $k_2 = 2$ $k_3 = 2$. The discrete state and the residual signals $\|v_{21}\|$, $\|v_{22}\|$, $\|v_{23}\|$ corresponding to the different observers are presented in Figure 6.5. It can be noted that the "correct" residuals tend to zero in the corresponding time intervals, while the "wrong" residual keep always separated from zero except some isolated time instant (the residual of mode 1 becomes zero around $t = 5.5$, however promptly leaving the zero value). To cope with this fact, the modified residual evaluation strategy (6.116)-(6.117) has been implemented, with the length of the time window chosen as $\delta = 0.1s$. The actual and discrete state are depicted in the Figure 6.6 which confirms the correct performance of the discrete mode observer.

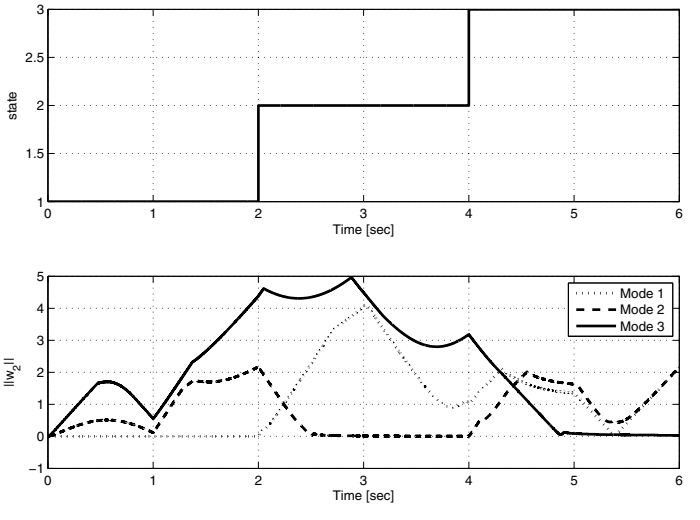

Fig. 6.5 Discrete state estimation test. The residuals $\|v_{21}\|$, $\|v_{22}\|$, $\|v_{23}\|$.

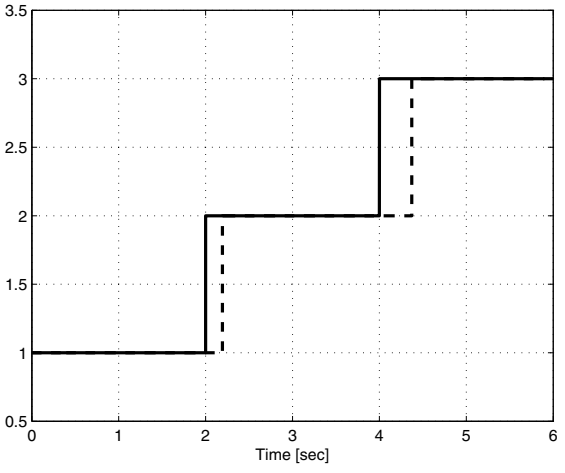

Fig. 6.6 Discrete state estimation test. Actual and estimated discrete state.

6.5 Experimental Fault Detection of a Hydraulic Plant

The discrete state estimation algorithm previously described will now be exploited to detect certain faults in a laboratory hydraulic system. The experimental hydraulic setup is shown in Figure 6.7. The centrifugal pump (**P**) draws the water from the lower tank (**TL**) into the upper tank (**TU**). The flow is adjusted by the electrical servo valve (**FV**). The flow is measured using the flow meter and the pulse flow transmitter (**FT**). The level in the upper tank is measured by the float level sensor and transmitter (**LT**).

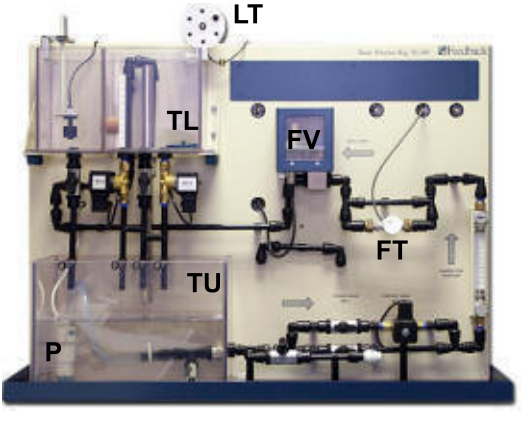

Fig. 6.7 "Feedback" Level/Flow Process Control System, PROCON 38-001

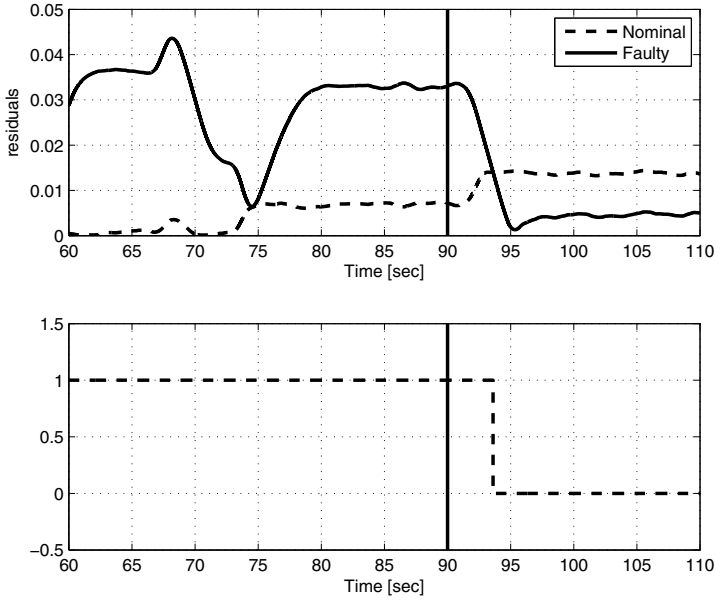

Fig. 6.8 Pump fault detection test. The residuals $R_1(t)$ and $R_2(t)$ (upper plot) and the estimated discrete state (lower plot)

The considered fault is a reduction of the pump rotating speed, which reduces the amount of flow. The fault has been reproduced in the experimental setup by reducing the pump control signals from the nominal value (healthy condition) to the 70% (faulty condition). Two fractional order models have been derived via least square identification for the healthy and faulty behaviour. Then, the suggested method for discrete state reconstruction can be applied as a fault diagnosis logic, by identifying whether the actual mode of operation is the nominal or faulty one.

Before any processing the measurements were scaled into the $[0,1]$ interval, with 0 and 1 denoting the minimal and maximal measured value of the physical quantity. Denote the normalized flow measurements by $f(t)$ and the normalized pump control signal by $v(t)$. The measurement sampling time was selected as $T_s = 10ms$.

A scalar ($n = m = 1$) affine model has been identified for the nominal and faulty working regimes. The **nominal regime model** is

$$D^{0.9} f(t) = -0.0186 f(t) + 0.03 v(t) - 0.0043 \tag{6.124}$$

and the **faulty regime model** was

$$D^{0.9} f(t) = -0.6532 f(t) + 0.1412 v(t) + 0.5082 \tag{6.125}$$

The parallel stage of observers (6.79), (6.62)-(6.94) has been implemented with the gains $k_1 = 1$, $k_2 = 2$ $k_3 = 0.5$. As before, the residual signal was chosen as the integral of $\|v_{21}\|$ and $\|v_{22}\|$ in a receding horizon time window of width $\delta = 1s$, according to the modified residual evaluation strategy (6.116)-(6.117).

During the experimental test, the fault is activated at time $t = 90$. The residuals corresponding to the two observers are presented in Figure 6.8 along with the estimated discrete state where "1" stands for the nominal behaviour, and "0" stands for the faulty one. In both plots, the solid vertical line denotes the instant at which the fault occurs. The fault is identified after less than 4 seconds.

6.6 Conclusions

Second-order sliding mode techniques have been suggested in order to solve control and estimation problems for certain classes of fractional-order dynamics. The core of the proposed approaches, for both the control and estimation problems addressed, was the selection of special **fractional-order** sliding variables. The presented results show that "fractional-order" second-order sliding mode control has a good potential in the field of control and estimation for FOS. Among the possible lines of improvement of the presented results, more general classes of linear FOS (e.g. the non-commensurate ones), as well as some classes of nonlinear fractional-order dynamics could be studied. Taking into account non-matching uncertainties and disturbances in the models is another important subject to be tackled in next research activities, both for the control and observation tasks, which can be possibly achieved by developing a fractional-order version of the the integral sliding mode approach and/or by generalizing to the FOS the concepts of strong observability [33].

Ackowledgements. The authors gratefully acknowledge the financial support from the FP7 European Research Projects "PRODI - Power plants Robustification by fault Diagnosis and Isolation techniques", grant no.224233 and by European-Mexico Cooperation Program (Foncicyt grant n 93302).

References

1. Agrawal, O.P.: Formulation of Euler-Lagrange equations for fractional variational problems. Journal of Mathematical Analysis and Applications 272, 368–379 (2002)
2. Agrawal, O.P.: A general formulation and solution for fractional optimal control problems. Nonlinear Dynamics 38, 323–337 (2004)
3. Agrawal, O.P., Baleanu, D.: A Hamiltonian Formulation and a Direct Numerical Scheme for Fractional Optimal Control Problems. Journal of Vibrations and Control 13, 1269–1281 (2007)
4. Atanacković, T.M., Pilipović, S., Zorica, D.: A diffusion wave equation with two fractional derivatives of different order. Journal of Physics A 40, 5319–5333 (2007)
5. Atanacković, T.: On Distributed Derivative Model of a Viscoelastic Body. C. R. Mecanique 331, 687–692 (2003)

6. Bartolini, G., Ferrara, A., Levant, A., Usai, E.: On Second Order Sliding Mode Controllers. In: Young, K.D., Ozguner, U. (eds.) Variable Structure Systems, Sliding Mode and Nonlinear Control. LNCIS, vol. 247, pp. 329–350. Springer, Heidelberg (1999)
7. Bartolini, G., Fridman, L., Pisano, A., Usai, E.: Modern Sliding Mode Control Theory. In: New Perspectives and Applications. LNCIS, vol. 375. Springer, Heidelberg (2008)
8. Barbosa, R.S., Tenreiro Machado, J.A., Silva, M.F.: Time-Domain Design of Fractional Differintegrators using Least Squares. Signal Processing 86, 2567–2581 (2006)
9. Bettayeb, M., Djennoune, S.: A note on the controllability and the observability of fractional dynamical systems. In: Proc. 2nd IFAC Workshop on Fractional Differentiation and its Applications, Porto, Portugal, pp. 506–511 (2006)
10. Calderon, A.J., Vinagre, B.M., Felix, V.: On Fractional Sliding Mode Control. In: 7th Portuguese Conference on Automatic Control (CONTROLO 2006), Lisbon, Portugal (2006)
11. Chen, Y., Ahn, H.S., Podlubny, I.: Robust stability check of fractional order linear time invariant systems with interval uncertainties. Signal Processing 86, 2611–2618 (2006)
12. Chen, Y., Vinagre, B.M., Podlubny, I.: On fractional order disturbance observers. In: Proc. of The First IFAC Symposium on FOS, Chicago (US), pp. 1–8 (2003)
13. Dzieliski, A., Sierociuk, D.: Observer for discrete fractional order systems. In: Proc. 2nd IFAC Workshop on Fractional Differentiation and its Applications, Porto, Portugal, pp. 524–529 (2006)
14. Das, S.: Functional Fractional Calculus for System Identification and Controls. Springer, Berlin (2008)
15. Dadras, S., Momeni, H.R.: Control of a fractional-order economical system via sliding mode. Physica A 389(12), 2434–2442 (2010)
16. Debnath, L.: A brief historical introduction to fractional calculus. Int. J. Math. Educ. Sci. Technl. 35(4), 487–501 (2004)
17. Ding, Y., Ye, H.: A fractional-order differential equation model of HIV infection of CD4+ T-cells. Mathematical and Computer Modelling 50(3), 386–392 (2009)
18. Edwards, C., Spurgeon, S.K.: Sliding Mode Control: Theory And Applications. Taylor and Francis, Abington (1998)
19. Efe, M.O., Kasnakoğlu, C.: A Fractional Adaptation Law for Sliding Mode Control. International Journal of Adaptive Control and Signal Processing 22, 968–986 (2008)
20. Efe, M.O.: Fractional Order Sliding Mode Controller Design for Fractional Order Dynamic Systems. In: Gven, Z.B., Baleanu, D., Tenreiro Machado, J.A. (eds.) New Trends in Nanotechnology and Fractional Calculus Applications (2009); manuscript presented during Fractional Differentiation and Its Applications, Ankara, Turkey (November 2008)
21. Emelyanov, S.V., Korovin, S.K., Levant, A.: Higher-order sliding modes in control systems. Differential Equations 29(11), 1627–1647 (1993)
22. Emelyanov, S.V., Korovin, S.K.: Control complex and uncertain systems: new types of feed back. Springer Communication and Control Engineering Series, vol. 302 (2000)
23. Hartley, T.T., Lorenzo, C.F.: Dynamics and Control of Initialized Fractional-Order Systems. Nonlinear Dynamics 29, 201–233 (2002)
24. Jeličić, Z.D., Petrovački, N.: Optimality conditions and a solution scheme for fractional optimal control problems. Structural and Multidisciplinary Optimization 38, 571–581 (2009)
25. Kilbas, A.A., Srivastava, H.M., Trujillo, J.J.: Theory and Applications of Fractional Differential Equations. Elsevier, B.V, Amsterdam (2006)
26. Ladaci, S., Charef, A.: On fractional adaptive control. Nonlinear Dynamics 43(4), 365–378 (2006)

27. Levant, A.: Sliding order and sliding accuracy in sliding mode control. Int. J. Control 58, 1247–1263 (1993)
28. Levant, A.: Higher-order sliding modes, differentiation and output-feedback control. Int. J. Control 76, 924–941 (2003)
29. Luo, Y., Chen, Y.Q.: Fractional order proportional-derivative controller for a class of fractional order systems. Automatica 45(10), 2446–2450 (2009)
30. Magin, R.L.: Fractional Calculus in Bioengineering. Begell House, New Yark (2006)
31. Manabe, S.: The non-integer integral and its application to control systems. Electrotechnical Journal of Japan 6(3-4), 83–87 (1961)
32. Melchior, P., Cugnet, M., Sabatier, J., Poty, A., Oustaloup, A.: Flatness Control of a Fractional Thermal System. In: Sabatier, J., Agrawal, O.P., Tenreiro Machado, J.A. (eds.) Advances in Fractional Calculus. Theoretical Developments and Applications in Physics and Engineering. Springer, Heidelberg (2007)
33. Molinari, B.P.: A strong contollability and observability in linear multivariable control. IEEE Transaction on Automatic Control 21(5), 761–764 (1976)
34. Moreno, J.A., Osorio, M.: A Lyapunov approach to second-order sliding mode controllers and observers. In: 47th IEEE Conference on Decision and Control, Cancun, MX (2008)
35. Mozyrska, D., Bartosiewicz, Z.: Observability Concepts for Nonlinear Discrete-Time Fractional Order Control Systems. In: Proc. 3rd IFAC Workshop on Fractional Differentiation and its Applications, Ankara, Turkey (2008)
36. Oldham, K.B., Spanier, J.: The Fractional Calculus. Academic Press, London (1974)
37. Oustaloup, A., Moreau, X., Nouillant, M.: The CRONE Suspension. Control Engineering Practice 4(8), 1101–1108 (1996)
38. Petráš, I., Podlubny, I., O'Leary, P., Dorcak, L., Vinagre, B.: Analogue Realizations of Fractional-Order Controllers. In: FBERG, TU Kosice, Kosice (2002)
39. Polyakov, A., Poznyak, A.: Lyapunov function design for finite- time convergence analysis: "Twisting" controller for second-order slidingmode realization. Automatica 45(2), 444–448 (2009)
40. Pisano, A., Rapaic, M., Jelecic, Z., Usai, E.: Sliding mode control approaches to the robust regulation of linear multivariable fractional-order dynamics. International Journal of Robust and Nonlinear Control (2010), doi:10.1002/rnc.1565 (published online on April 9, 2010)
41. Podlubny, I.: Fractional Differential Equations. Academic Press, London (1999)
42. Podlubny, I.: Fractional Order Systems and $PI^{\lambda}D^{\mu}$-Controllers. IEEE Transactions on Automatic Control 44(1), 208–214 (1999)
43. Riewe, F.: Nonconservative Lagrangian and Hamiltonian mechanics. Physical Review E 53(2), 1890–1899 (1995)
44. Sabatier, J., Agrawal, O.P., Tenreiro Machado, J.A.: Advances in Fractional Calculus - Theoretical Developments and Applications in Physics and Engineering. Springer, Heidelberg (2007)
45. Scalas, E.: On the Application of Fractional Calculus in Finance and Economics. Plenary Lecture paper. In: Proc. 3rd IFAC Workshop on Fractional Differentiation and its Applications, Ankara, Turkey (2008)
46. Si-Ammour, A., Djennoune, S., Bettayeb, M.: A sliding mode control for linear fractional systems with input and state delays. Communications in Nonlinear Science and Numerical Simulation 14(5), 2310–2318 (2009)

47. Sira-Ramírez, H., Feliu-Battle, V.: A Generalized PI Sliding Mode and PWM Control of Switched Fractional Systems. In: Bartolini, G., Fridman, L., Pisano, A., Usai, E. (eds.) Modern Sliding Mode Control Theory. New Perspectives and Applications. LNCIS, vol. 375, pp. 215–236. Springer, Heidelberg (2008)
48. Tavazoei, M.H., Haeri, M.: A note on the stability of fractional order systems. Mathematics and Computers in Simulation 79, 1566–1576 (2009)
49. Utkin, V.I.: Sliding Modes in Control and Optimization. Springer, Berlin (1992)
50. Young, K.D., Özgüner, U., Utkin, V.I.: A Control Engineer's Guide to Sliding Mode Control. IEEE Trans. Control Systems Technology 7, 328–342 (1999)
51. Vinagre, B.M., Chen, Y.Q., Petráš, I.: Two Direct Tustin Discretization Methods for Fractional-Order Differentiator/Integrator. Journal of the Franclin Institute 34, 349–362 (2003)
52. Vinagre, B.M., Petracs, I., Podlubny, I., Chen, Y.Q.: Using fractional order adjustment rules and fractional order reference models in model reference adaptive control. Nonlinear Dyn. 29(1-4), 269–279 (2002)

Chapter 7
Discussion about Sliding Mode Algorithms, Zeno Phenomena and Observability

L. Yu, J.-P. Barbot, D. Benmerzouk, D. Boutat, T. Floquet, and G. Zheng

Abstract. This chapter is devoted to a discussion about the relations between first and high order sliding mode algorithms and both types of Zeno (Chattering and Genuinely) behaviors of switched dynamical systems. Firstly, the Henstock-Kurzweil integral is recalled in order to set up the problem of switched systems with Zeno phenomena, which enables to include Filippov solution and take into account some

L. Yu
Signal Processing Laboratory, Electronic and Information School,
Wuhan University, China, and ECS ENSEA, 6 Avenue du Ponceau, 95014 Cergy-Pontoise, France and Project ALIEN, INRIA Lille - Nord Europe
e-mail: lei.yu@ensea.fr

J.-P. Barbot
ECS ENSEA, 6 Avenue du Ponceau, 95014 Cergy-Pontoise, France and
Project ALIEN, INRIA Lille - Nord Europe
e-mail: barbot@ensea.fr

D. Benmerzouk
Department of Mathematics, Tlemcen University, Algeria
e-mail: d_benmerzouk@yahoo.fr

D. Boutat
PRISME ENSIB, 10 Boulevard de Lahitolle, 18020 Bourges, France
e-mail: driss.boutat@ensi-bourges.fr

T. Floquet
LAGIS, UMR FRE 3303, Ecole Centrale de Lille, Cité Scientifique,
BP 48, 59651 Villeneuve-d'Ascq Cedex, France and Project ALIEN,
INRIA Lille - Nord Europe
e-mail: thierry.floquet@ec-lille.fr

G. Zheng
Project ALIEN,
INRIA Lille - Nord Europe, 40, avenue Halley,
59650 Villeneuve d'Ascq, France
e-mail: gang.zheng@inria.fr

L. Fridman et al. (Eds.): Sliding Modes, LNCIS 412, pp. 199–219.
springerlink.com

singularities. Then, observer designs based on the well-known super twisting algorithm are proposed. For this kind of problems, the importance of finite time convergence of the observation error is studied, and some simulations are given to highlight the discussion. Lastly, the two tanks example is given in order to point out the differences between both Zeno phenomena types, to show that there is life after Zeno and that a higher order sliding mode observer can be efficient before, during and after both Zeno phenomena types.

7.1 Discussion on Zeno and Sliding Mode Behavior

First order sliding mode concept has been well-known in control system theory for at least fifty years, especially since the book of Filippov [14]. A system exhibiting a first order sliding mode behavior can be seen as a variable structure system converging in finite time towards some constraint manifold and then sliding on this manifold by means of permanent switches at an infinite frequency between two system structures. Commutations at infinite frequency between two subsystems is named as Zeno[1] phenomena in the hybrid dynamical system theory. The relation between first order sliding mode and Zeno phenomena generates a huge set of questions, such as:

1. Is first order sliding mode the only Zeno phenomena?
2. Do all Zeno phenomena always exhibit a sliding mode?
3. Is it possible to use a sliding mode approach in the context of hybrid dynamical systems?
4. Is there life after Zeno?
5. Are specific mathematical tools required?

The answer to the first question is no. In fact, since at least the pioneer works of S. Emelyanov, S. Korovin and A. Levant [13], [26], a new type of sliding modes has been introduced called higher order sliding modes. This type of sliding mode ensures a finite time convergence onto a constraint manifold defined by the vanishing of some constraint variable s and at least its first derivative $\dot{s}$ along the system trajectories. The requirement that $\dot{s}$ must be also equal to zero in finite time has an important consequence on the qualitative behavior of Zeno phenomena. For example, in [31] Chapter 8 page 228, it is proved that the twisting algorithm generates an infinite number of commutation in finite time, where any dwell time[2] is strictly different to zero. Actually, one can distinguish different qualitative behaviors such as the chattering Zeno phenomena and the genuinely Zeno phenomena, see Ames *et al.* [2]. Roughly speaking, the chattering Zeno phenomena is equivalent to obtain a dwell time equal to zero after a finite number of commutations, as it is exactly the case for first order sliding mode. On the other hand, the genuinely Zeno phenomena corresponds to obtain an infinity of commutation before obtaining a dwell time equal to zero, and this is exactly the case of the twisting algorithm.

[1] This refers to Zeno of Elea and its paradoxes, see for example “Achille and the tortoise”.

[2] Time interval between two switching instants.

The answer to the second question is also no. For instance, consider the bouncing ball example (see [2] and [20]). This is a switched system with jumps (actually an impact system [6]) that exhibits a Zeno phenomena. This kind of system has only one dynamic and has a jump state at the impact instant before to roll on the floor. It is shown in [2] that the bouncing ball case generates a genuinely Zeno phenomena and that the solution after the Zeno point (impact accumulation point) satisfies a holonomic constraint which is different from the Filippov solution.

The answer to the third question is yes. This will be proved in Section 7.4 where a sliding mode observer for a particular class of hybrid systems will be designed on the basis of our previous work [34].

The answer to the fourth question is also yes. In the example of the bouncing ball, even if the model changes after the Zeno time, meaning in some sense that "there is no life of the original model after Zeno", it will be shown that it is not the case for the two tanks example.

The answer to the fifth question is also yes. In fact, in order to consider the most general class of systems, the most general definition of integral has to be considered. To the best of our knowledge, the most general integral definition is the Henstock-Kurzweil-Pettis integral (H-K-P integral). Nevertheless, for the sake of simplicity, this chapter will only deal with the Henstock-Kurzweil integral (H-K integral) [18] which is recalled in the Section 7.3.

7.2 Zeno Types

In this chapter, we will consider Hybrid Dynamical Systems belonging to the following class of switched systems without state jump:

$$\begin{cases} \dot{x} = f(x) + g(x)\,q = f(x) + \sum_{i=1}^{n} g_i(x)\,q_i \\ y = h(x) \end{cases} \tag{7.1}$$

where $x \in U \subset R^n$ is the set of admissible continuous state, $y \in R$ is the measured output and where the vector fields $f : U \to R^n$, $g_i : U \to R^n$ and $h : U \to R$ are sufficiently smooth. Moreover $q_i : R^+ \to Q = \{0,1\}$ is the discrete component of the discrete vector q.

The definition of time trajectory and Zeno phenomenon given in [28, 23] can be stated as follows:

Definition 7.1. A time trajectory is a finite or infinite sequence of intervals $T_N = \{I_i\}_{i=0}^{N}$, where $N \in \mathbb{N}$, such that:

- $I_i = [\tau_i, \tau_{i+1}]$, $\tau_i \leq \tau_{i+1}$ for all $0 \leq i \leq N$.
- If N is limited, either $I_N = [\tau_N, \tau_{N+1}]$ with $\tau_N \leq \tau_{N+1}$ and τ_∞ bounded or $I_N = [\tau_N, \tau_{N+1}[$ for $\tau_N \leq \tau_{N+1} \leq \infty$.
- For all i corresponds a discrete transition $q_i(t)$ such that $q_i(t)$ is constant for $t \in [\tau_i, \tau_{i+1}]$.
- For all i and $t \in [\tau_i, \tau_{i+1}]$ corresponds a continuous evolution $x(t)$.

Definition 7.2
A dynamical system is called Zeno if $t_\infty := \sum_{i=0}^{\infty} (\tau_{i+1} - \tau_i)$ is bounded.

This means that the system takes an infinite amount of discrete transitions in a finite amount of time, in this case the time t_∞ is called Zeno time.

It is known that there exist two fundamental types of Zeno:

Definition 7.3

- **Chattering Zeno:** There exist a finite number $C \in \mathbb{N}$ and a bounded value t_∞ such that:
  $t_\infty = \sum_{i=0}^{\infty} (\tau_{i+1} - \tau_i) \quad \text{and} \quad \forall j > C, \quad [t_{j+1} - t_j] = 0.$
- **Genuinely Zeno:** There exist $C \in \mathbb{N}$ and a bounded value t_∞ such that:
  $t_\infty = \sum_{i=0}^{\infty} (\tau_{i+1} - \tau_i) \quad \text{and} \quad \forall j > C, \quad [t_{j+1} - t_j] > 0.$

Consider for example the twisting algorithm [13, 17, 26]. It is clear that the convergence on the constrained manifold given by $s = \dot{s} = 0$ is due to a Genuinely Zeno phenomenon [31]. Nevertheless, after the finite time convergence on this manifold, the Zeno behavior is a chattering phenomenon. So, for the twisting algorithm the Zeno type changes but the process never leaves the Zeno behavior.

7.3 Mathematical Recalls of H-K Integral

The H-K integral, also known as the gauge integral, the generalized Riemann integral, was defined independently by Henstock and Kurzweil in the 1950's. Let us recall both the definitions related to the Riemann integral and the H-K integral in order to clarify their differences.

Definition 7.4. Consider a real function f defined on an interval $[a,b] \subset R$. For any tagged partition P of $[a,b]$ such as $a = x_0 < x_1 < x_2 < \cdots < x_n = b$, and $\tau_i \in [x_{i-1}, x_i] \subset [a,b]$, consider

$$f(P) := \sum_{i=1}^{n} f(\tau_i)(x_i - x_{i-1}).$$

For any given function $\delta : [a,b] \to R_+^*$, P is said to be a δ-fine tagged partition of $[a,b]$ if $h_i := x_i - x_{i-1} < \delta(\tau_i)$ where δ is called a gauge for each i.

Definition 7.5. A number I is called the Riemann integral (respectively the H-K integral) of $f : [a,b] \to R$ if for each constant $\varepsilon > 0$, there exists a constant δ (respectively a function $\delta : [a,b] \to R_+^*$), such that whenever P is a δ-fine tagged partition of $[a,b]$, one has $|I - f(P)| < \varepsilon$.

Roughly speaking, the integral of f on $[a,b]$ is obtained by approximating the region under the curve defined on $[a,b]$ as a union of small rectangles. The Riemann integral requires that all those rectangles depend on a constant δ while the H-K integral

uses a more sophisticated δ (δ depends on τ_i). In fact, when a function f oscillates more quickly at some points of the interval $[a,b]$, one has to tighten the step h_i at these points in order to approximate more accurately the associated surface. This is possible by choosing $h_i < \delta(\tau_i)$ such that $\delta(\tau_i)$ is a sufficiently small positive value that depends on the place from where the rectangle of height $f(\tau_i)$ is considered (see Fig. 7.1).

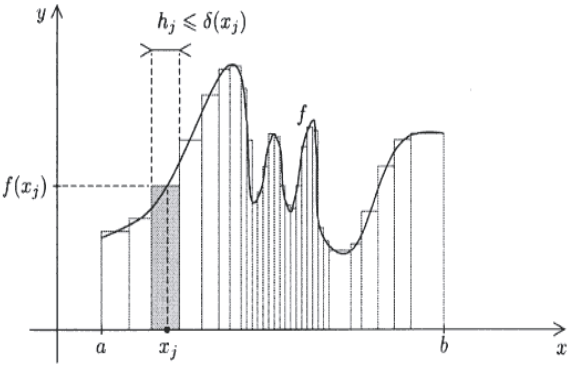

Fig. 7.1 Illustrative explanation of H-K Gauge

To highlight the principle of the H-K integral, consider the two following examples.

Example 7.1. Consider the function f defined on $[0,1]$ as follows:

$$f(x) = \begin{cases} x^{-1}\sin(x^{-2}) & \text{on }]0,1] \\ 0 & \text{for } x = 0. \end{cases}$$

This function is neither Riemann nor Lebesgue integrable, but H-K integrable, and this can be proved by using a special choice of gauge (that requires skill and effort) given as follows:

$$\delta(\tau) = \begin{cases} \sqrt{\varepsilon} & \text{if } \tau = 0 \\ min\left\{\frac{\tau}{2}, \frac{\varepsilon\tau^4}{24}\right\} & \text{if } 0 < \tau \leq 1. \end{cases}$$

Example 7.2. Consider the function g defined on $[0,1]$ as follows:

$$g(x) = \begin{cases} x & \text{if } x \in \mathcal{Q} \\ 0 & \text{if } x \notin \mathcal{Q} \end{cases}$$

where $\mathcal{Q}$ represents the set of rationales. This function is discontinuous everywhere, and thus it is not Riemann integrable but H-K integrable. It can be proved that its value is equal to 0 by using a special choice of the gauge given by:

$$\delta(\tau) = \begin{cases} 2^{-j-1}\varepsilon & \texttt{if } \tau = p_j \\ 1 & \texttt{if } \tau \notin \mathscr{Q} \end{cases}$$

where $p_1, p_2, \ldots, p_j, \ldots$ are the rationales.

Thus, taking a more general form of the gauge δ (instead of δ constant) yields a richer class of possible integrands and permits to obtain that:

Riemann integrable functions $\subset$ Lebesgue integrable functions $\subset$ H-K integrable functions

Note that the H-K integral can also be generalized to bounded or unbounded sets in R^n and to more general spaces such as Banach spaces or ordered spaces. The most important feature of the H-K integral is its wider applicability. Moreover, it can avoid abstract notions such as set theory, σ algebras or inner and outer measures. This can be seen from the equivalence:

a set $E \subset [a,b]$ is Lebesgue integrable $\iff$ its characteristic function is H-K integrable

Moreover, many classical results formulated in the framework of the Lebesgue theory, such as the Lemma of Fatou or the fundamental theorem of calculus, can be simplified (assumptions on continuity for example are omitted when H-K integrability is considered) [18].

Another important result is the Hake's Theorem which states that it is not necessary to consider "improper" H-K integral (as it is the case of Riemann integral) because the construction of the H-K integral makes any "improper" H-K integral be a "proper" integral. Note also that other integrals, such as Denjoy integral, Perron integral, Lee and Vyborny integral, all turn out to be "equivalent" to the H-K integral.

Some authors proposed an extension of the H-K integral, called Kurzweil-Henstock-Pettis integral (H-K-P integral) (see [8]) which offers an interesting possible applicability to Fourier analysis and differential equations. In this case, the solution of a Cauchy problem given by:

$$\dot{X} = f(t, X(t)) \quad \texttt{with } X(0) = X_0$$

is studied as the solution of the following integral equation:

$$X(t) = X_0 + \int_0^t f(\mu, X(\mu))d\mu$$

where the integral is in the sense of H-K. It does not require strong assumptions on the considered system. So it can be seen as a tool that defines more accurately (and take into account) the specific and quick oscillations of the considered dynamics.

7.4 Observability and Observer Design for Some Classes of Hybrid Dynamical System

The following three classes of switched systems without jump are considered.

7.4.1 First Basic Observability Form

The first proposed observability form is:

$$\begin{pmatrix} \dot{z}_1 \\ \dot{z}_2 \\ \dot{z}_3 \\ \vdots \\ \dot{z}_n \end{pmatrix} = \begin{pmatrix} 0 & \cdots & 0 & 0 & 0 \\ 1 & \ddots & 0 & 0 & 0 \\ 0 & \ddots & 0 & 0 & 0 \\ \vdots & \ddots & \ddots & \ddots & \vdots \\ 0 & \cdots & 0 & 1 & 0 \end{pmatrix} \begin{pmatrix} z_1 \\ z_2 \\ z_3 \\ \vdots \\ z_n \end{pmatrix} + \begin{pmatrix} \tilde{f}_q \\ 0 \\ 0 \\ \vdots \\ 0 \end{pmatrix} \tag{7.2}$$

$$y = \tilde{h}(z) = z_n \tag{7.3}$$

where q is the discrete vector and $\tilde{f}_q$ is a continuous function with respect to z and parameterized by q. This system is regularly weakly locally observable and the observability is independent from the discrete vector q.

7.4.2 Second Basic Observability Form

The second proposed observability form is:

$$\dot{z} = \alpha_0(z) + \gamma_q(y), \quad q \in Q \tag{7.4}$$

$$y = \tilde{h}(z) = z_n \tag{7.5}$$

where $z \in \mathbb{R}^n$ and $y \in \mathbb{R}$

Assumption 7.1. *The pair $(\alpha_0(z), y)$ is regularly locally weakly observable*[3].

7.4.3 Extended Observability Form

The following extended observability form includes both previous forms:

[3] In addition to the classical locally weakly observability condition (see [19]), the first $n-1$ derivatives in the rank condition are requested to be regular i.e.

$$Rank \begin{pmatrix} d\tilde{h} \\ \vdots \\ dL_{\alpha_0}^{n-1}\tilde{h} \end{pmatrix} |_Z = n$$

$$\begin{pmatrix} \dot{\xi}_1 \\ \vdots \\ \dot{\xi}_{r-1} \end{pmatrix} = \begin{pmatrix} 0\,1\,0\,\ldots\,0 \\ 0\,0\,1\,\ldots\,0 \\ \vdots\,\vdots\,\vdots\,\ddots\,\vdots \\ 0\,0\,0\,\ldots\,1 \end{pmatrix} \begin{pmatrix} \xi_1 \\ \vdots \\ \xi_{r-1} \\ \xi_r \end{pmatrix} \tag{7.6}$$

$$\dot{\eta}_1 = \dot{\xi}_r = \alpha_0(\xi,\eta) + \gamma_q(\xi) \tag{7.7}$$

$$\dot{\tilde{\eta}} = \beta_0(\xi,\eta) + \delta_q(\xi) \tag{7.8}$$

$$y = \xi_1 \tag{7.9}$$

where $\xi = (\xi_1 \cdots \xi_r)^T$, $\eta = (\eta_1, \cdots, \eta_{n-r+1})^T$ and $\tilde{\eta} = (\eta_2, \cdots, \eta_{n-r+1})^T$.

Assumption 7.2.
The pair $\left(\begin{pmatrix} \alpha_0(\xi,\eta) \\ \beta_0(\xi,\eta) \end{pmatrix}, \eta_1 \right)$ *is uniformly weakly locally observable*[4].

In this paper, any consideration on the existence of the diffeomorphisms which transform a switched system into one of these forms is given, nevertheless sufficient conditions may be found in our previous work [34].

7.4.4 Discussion on the Observability of the First Basic Observability Form

For the form (7.2)-(7.3), an estimate of the continuous state ξ can be obtained *via* an algebraic estimator as defined in [29, 30], a sliding mode observer ([3, 12]), or a high order sliding mode observer [9, 16, 27, 32], because y and the $n-1$ first time derivatives of y provide sufficient information in order to estimate the continuous state.

7.4.5 Discussion on the Observability of the Second Basic Observability Form

In the form (7.4)-(7.5), the discrete state q is not considered as an unknown perturbation but as an input, consequently the following assumption is requested:

Assumption 7.3.
The discrete state q is known and $\gamma_q(y)$ *is Henstock-Kurzweil-Pettis integrable*[5] *(see [18], [8], [33]) or NV-Integrable [10].*

Clearly, this assumption can not be satisfied in the case of Zeno phenomena, such as for the Chattering Zeno (i.e. after some time the dwell time is exactly equal to zero) or for the Genuinely Zeno (i.e. the dwell time is never equal to zero) [2]. So, in

[4] Uniformly with respect to ξ.
[5] See also Denjoy-Khinchine integrable.

practice, it is only possible to obtain the filtered discrete state q_f, instead of the real discrete state q. Consequently, Assumption 7.3 is replaced by the following one:

Assumption 7.4.

- *a- The system (7.4)-(7.5) is affine with respect to the discrete state q, i.e.* $\gamma_q(y) = \gamma(y)q$*, where* γ *is at least a* C^1 *function of y.*
- *b- The functions* $\gamma(y)q$ *and* $\gamma(y)q_f$ *are Henstock-Kurzweil-Pettis integrable and the mean value* q_f *is measured* via *a low pass filter with a large enough bandwidth on the time interval* $[0, \alpha]$.

Moreover, consider the following system:

$$\dot{z} = \alpha_0(z) \tag{7.10}$$
$$y = \tilde{h}(z) = z_n \tag{7.11}$$

and assume that:

Assumption 7.1. *For the system (7.10)-(7.11), there exists an observer such that the continuous state observation error (i.e. the difference between the continuous state ant its estimate) is exponentially stable.*

Remark 7.1. Under some specific assumptions such as Lipschitz condition or persistent excitation, it is possible to design classical high gain observers [4] or adaptive observers [7]. Without the perturbation term, those observers can guarantee the exponential stability of the continuous state observation error.

Then, it is possible to set the following proposition:

Proposition 7.1.

- *A) Under Assumptions 7.1, 7.3 and 7.1, system (7.4)-(7.5) with Zeno phenomenon is observable*[6].
- *B) Under Assumptions 7.1, 7.4 and 7.1, system (7.4)-(7.5) with Zeno phenomenon is practically observable*[7].

Proof. Proof of part *A*: there exists an observer of the form:

$$\dot{\hat{z}} = \beta(\hat{z}, y, \hat{y}) \tag{7.12}$$
$$\hat{y} = \hat{z}_n \tag{7.13}$$

which ensures the exponential stability of the continuous state observation error $e = z - \hat{z}$ for system (7.10), (7.11). Consequently, there exists a Lyapunov function $V(e)$ with respect to (7.10), (7.11) and (7.12), (7.13) such that:

$$\dot{V} = \frac{\partial V}{\partial e}(\alpha_0(z) - \beta(\hat{z}, y, \hat{y})) < -KV \tag{7.14}$$

[6] The observation error can be assigned to zero.

[7] The observation error can be constrained to lie within any measurable vicinity of zero but not zero.

with $K > 0$.
Modifying (7.12), (7.13) as follows:

$$\dot{\hat{z}} = \beta(\hat{z}, y, \hat{y}) + \gamma_{q_f}(y) \quad \text{with } \gamma_{q_f}(y) = \gamma(y) q_f \tag{7.15}$$

$$\hat{y} = z_n \tag{7.16}$$

the state observation error for system (7.4)-(7.5) and observer (7.15)-(7.16) is exponentially stable. Using the previous Lyapunov function, one has:

$$\dot{V} = \frac{\partial V}{\partial e}(\alpha_0(z) - \beta(\hat{z}, y, \hat{y}) + \gamma_q(y) - \gamma_{q_f}(y)) < -K'V$$

where $K' = K + sup_{t\in[0,\alpha]}\{|o(y(t))|\}$.
Proof of part B: the observation error for systems (7.4)-(7.5) and (7.15)-(7.16) becomes:

$$\dot{e} = \alpha_0(z) - \beta(\hat{z}, y, \hat{y}) + \gamma(y)(q - q_f)$$

From condition b) of Assumption 7.4, one obtains that

$$\dot{p} = \gamma(y) p \qquad \text{with} \quad p = q - q_f$$

is a Cauchy problem for each fixed initial value p_0 in the sense of Henstock-Kurzweil-Pettis integrals.

Using the same method as Filippov in [15] page 17 and setting $\varepsilon = e - p$, one has:

$$\dot{\varepsilon} = \alpha_0(z) - \beta(\hat{z}, y, \hat{y}) \tag{7.17}$$

which admits a local solution in the Carathéodory sense for $t \in [0, \Gamma] \subset [0, \alpha]$. Moreover, Assumption 7.1 and the observer (7.12)-(7.13) ensure that there exists a Lyapunov function $V(e)$ for (7.10)-(7.11) which satisfies (7.14). Consequently, derivation of $V(\varepsilon)$ with respect to (7.17) gives:

$$\dot{V} = \frac{\partial V}{\partial \varepsilon}(\alpha_0(z) - \beta(\hat{z}, y, \hat{y})) \tag{7.18}$$

Since $\varepsilon = e - p$, one has $\frac{\partial V}{\partial \varepsilon}|_\varepsilon = \frac{\partial V}{\partial e}|_\varepsilon$ and from Assumption 7.1, it is possible to rewrite (7.18) as follows:

$$\begin{aligned}\dot{V} = & \frac{\partial V}{\partial e}|_e(\alpha_0(z) - \beta(\hat{z}, y, \hat{y})) \\ & -\frac{1}{2}\frac{\partial^2 V}{\partial e^2}|_e[O(p) \otimes (\alpha_0(z) - \beta(\hat{z}, y, \hat{y}))] + O(p^2)\end{aligned}$$

with $\lim_{p\to 0} O(p) = 0$.
As for all $\varepsilon > 0$, there exists a filter and $t_1 \geq 0$ such that $\forall t > t_1$, we have

$$\|p\| = \sup_{0\leq t\leq \Gamma} \left| \int_{t_1}^{t} \gamma(y(\sigma))(q(\sigma) - q_f(\sigma)) d\sigma \right| < \varepsilon$$

one obtains

$$\dot{V}(\varepsilon) \leq -K'V(\varepsilon) + \frac{1}{2}\left|\frac{\partial^2 V}{\partial e^2}|_e[O(p)\otimes(\alpha_0(z)-\beta(\hat{z},y,\hat{y}))]\right| + |O(||p||^2)| \tag{7.19}$$

Consequently, it is possible, for each $V_d > 0$, to set $\varepsilon << \frac{V_d}{2}$ and the inequality (7.19) becomes

$$\dot{V}(\varepsilon) \leq -K'V(\varepsilon) + |O(\varepsilon)|$$

So, one can conclude that for $e \notin E_{V_d} := \{e : V(e) < V_d\}$, one has:

$$\dot{V}(\varepsilon) \leq -\frac{K''}{2}V(\varepsilon) \qquad \text{for some} \quad K'' > 0$$

because $\varepsilon << \frac{V_d}{2}$ guarantees that $|O(\varepsilon)| < \frac{V_d}{2}$. □

7.4.6 *Observability for the Extended Observability Form*

For system (11.55)-(7.9), according to the previous discussion on the observability for the two basic forms, one can easily conclude:

Corollary 7.1.
Under Assumptions 7.2, 7.4 and 7.1, the system (11.55)-(7.9) with Zeno phenomenon is practically observable.

Consequently, it is possible to design an hybrid observer for this system: for the observation of ξ, a step-by-step high order sliding mode observer can be designed to obtain a finite time estimate of ξ. So, after the convergence of ξ, ξ_r (or η_1) can be considered as an output, and one can design an asymptotic observer (for example a high gain observer) to estimate η, as shown in Figure 7.2.

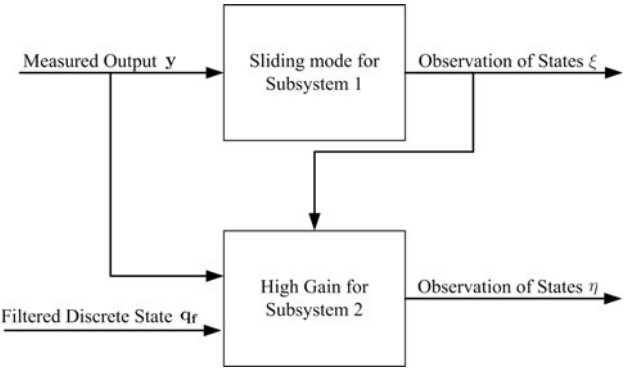

Fig. 7.2 Hybrid observer scheme.

Example 7.3. Consider the following system:

$$\begin{cases} \dot{z}_1 = z_2 \\ \dot{z}_2 = z_3 - z_2^3 + \frac{3}{2}z_2 + \frac{1}{2}\gamma_q(z_2) \\ \dot{z}_3 = -z_2 \\ y = z_1 \end{cases} \tag{7.20}$$

with $\gamma_q(z_2) = sign(w) \cdot z_2$, where w is a high frequency noise. This form of q theoretically leads to a Zeno phenomena.

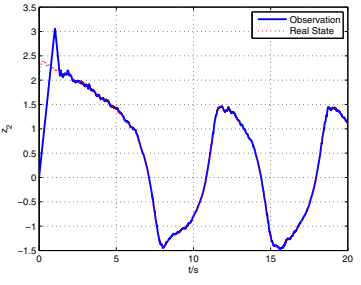

Fig. 7.3 Results of Observer for system (7.20) for z_2.

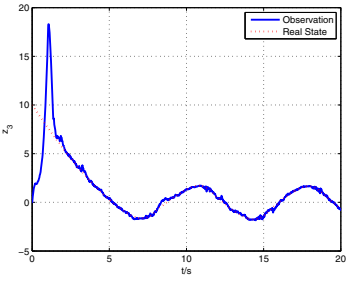

Fig. 7.4 Results of Observer for system (7.20) for z_3.

For this example, one can follow the scheme shown in Fig. 7.2 to build an hybrid observer. First, one considers the states z_1 and z_2, where z_1 is known and z_2 is observed through a sliding mode observer. Denote $\hat{z}_2$ as the observation of z_2. Then the remaining state dynamics has the following form:

$$\begin{cases} \dot{z}_2 = z_3 - z_2^3 + \frac{3}{2}z_2 + \frac{1}{2}\gamma_q(z_2) \\ \dot{z}_3 = -z_2 \\ y' = z_2 \end{cases}$$

where the value of z_2 is taken as the output of the subsystem (7.21), i.e. $y' = \hat{z}_2$. One can observe the state z_3 using a high gain observer. The performances are shown

in Fig. 7.3 and 7.4, where Fig. 7.3 shows the state z_2 and the observed state $\hat{z}_2$ and where Fig. 7.4 depicts the same for z_3. In fact, the high gain observer (with $\hat{z}_2$ as output and z_2, z_3 as states) must be switched on only after the convergence of the finite time sliding mode observer (with z_1 as output and z_1, z_2 as states). Hence one can assign $\hat{z}_3$ to be zero at the beginning of the observation procedure.

7.5 The Two Tanks Example

consider the two water tanks example [21] in Fig. 7.5, which is a typical switched system where Zeno behavior may exist if the commutation of the water distribution between both tanks is considered instantaneous with respect to the other dynamics.

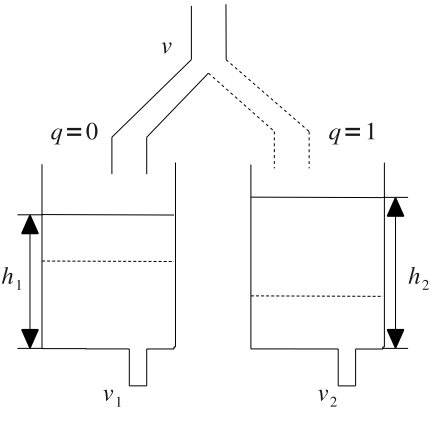

Fig. 7.5 Two water tanks system

The simplified model of the two water tanks system described in Fig. 7.5 is given by:

$$\begin{pmatrix} \dot{h}_1 \\ \dot{h}_2 \end{pmatrix} = \begin{pmatrix} v - v_1 \\ -v_2 \end{pmatrix} + \begin{pmatrix} -v \\ v \end{pmatrix} q$$

where h_1, h_2 are the water levels for each tanks, v_1, v_2 are the flows of water out of the tanks, v is a constant input flow of water which goes through a pipe and into either tank at any particular time point, and q is the switching state of the pipe which is determined by the transient conditions (see Fig. 7.6 and Fig. 7.7 for two different cases).

By considering Torricelli's law, one has $v_1 = \sqrt{2gh_1}$ and $v_2 = \sqrt{2gh_2}$, where g is the gravity. Then the dynamic can be rewritten as

$$\begin{pmatrix} \dot{h}_1 \\ \dot{h}_2 \end{pmatrix} = \begin{pmatrix} v - \sqrt{2gh_1} \\ -\sqrt{2gh_2} \end{pmatrix} + \begin{pmatrix} -v \\ v \end{pmatrix} q \tag{7.21}$$

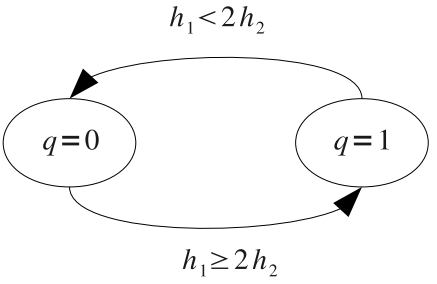

Fig. 7.6 The transient of discrete state for the case 1 ($h_1 = 2h_2$).

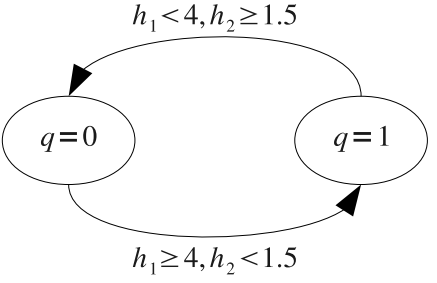

Fig. 7.7 The transient of discrete state for the case 2 ($h_1 = 4$ and $h_2 = 1.5$).

Assume that the only measured signal is $y = h_1 + h_2$ (v and q are supposed to be unknown). Then the system is regularly locally weakly observable:

$$rank \begin{pmatrix} dy \\ d\dot{y} \end{pmatrix} = rank \begin{pmatrix} 1 & 1 \\ \frac{-1}{\sqrt{2gh_1}} & \frac{-1}{\sqrt{2gh_2}} \end{pmatrix} = 2 \tag{7.22}$$

excepted on the set S_O

$$S_O = \{(h_1, h_2)^T : h_1 = h_2\}.$$

This set is a set of observability singularities and it is a manifold of dimension $n - 1 = 1$. Moreover, S_O separates the state space in two parts. It is important to note that S_O characterizes the singularity observability considering only y and $\dot{y}$. However, there exist several different observability definitions for nonlinear systems and hybrid systems [5], [11], [20], [22], [25], involving high order output derivatives with order greater than the dimension of the state space.

Moreover, the system satisfies the observability matching condition [31].[8]

[8] Considering a system of the following form:

$$\dot{x} = f(x) + g(x)q$$
$$y = h(x)$$

the observability matching condition with respect to q is satisfied if $L_g h = ... = L_g^{n-2} h = 0$.

$$\frac{\partial y}{\partial q} = \frac{\partial \dot{y}}{\partial q} = 0 \tag{7.23}$$

Conditions (7.22) and (7.23) are necessary and sufficient conditions for the existence of a diffeomorphism which transforms, at least locally, the system (7.21) into the first basic normal form. Then, under the diffeomorphism $\xi = \phi(h_1, h_2)$ with $\phi_1(h_1, h_2) = h_1 + h_2$ and $\phi_2(h_1, h_2) = v - \sqrt{2gh_1} - \sqrt{2gh_2}$, the system is locally transformed into the first basic normal form (7.2)-(7.3):

$$\begin{aligned} \dot{\xi}_1 &= \xi_2 \\ \dot{\xi}_2 &= -\sqrt{\frac{g}{2}} \left(\frac{(v - \sqrt{2gh_1} - vq)}{\sqrt{h_1}} + \frac{(vq - \sqrt{2gh_2})}{\sqrt{h_2}} \right) \\ y &= \xi_1 \end{aligned} \tag{7.24}$$

where

$$h_1 = \frac{1}{4} \left(\frac{v - \xi_2}{\sqrt{2g}} + \mu \sqrt{2\xi_1 - \frac{(v - \xi_2)^2}{2g}} \right)^2,$$

$$h_2 = \frac{1}{4} \left(\frac{v - \xi_2}{\sqrt{2g}} - \mu \sqrt{2\xi_1 - \frac{(v - \xi_2)^2}{2g}} \right)^2.$$

Using this state transformation, one has to choose either the trajectories are in the subspaces $S_O^+ = \{(h_1, h_2) : h_1 > h_2\}$ or $S_O^- = \{(h_1, h_2) : h_1 < h_2\}$, where S_O is the boundary between both of them. Thus, $\mu = 1$ if the state is in S_O^+ and $\mu = -1$ if the state is in S_O^-. In both cases given in Fig. 7.6 and Fig. 7.7, the system behavior is principally or exclusively in the subspace $h_1 > h_2$. Then the appropriate change of coordinates is $\mu = 1$. This highlights the fact that the diffeomorphism is only a local transformation and in this case the validity domains are strongly related to S_O.

Regarding the particular properties of the hybrid dynamical system (observability matching condition and regularly locally weakly observability) and taking advantage of the basic normal form (7.24), a higher order sliding mode observer [9,16,27] only made here of one super twisting algorithm step because the knowledge of the discrete state q is not required. The proposed observer is the following:

$$\begin{aligned} \dot{\hat{\xi}}_1 &= \hat{\xi}_2 + \lambda |y - \hat{\xi}_1|^{\frac{1}{2}} \mathtt{sign}(y - \hat{\xi}_1) \\ \dot{\hat{\xi}}_2 &= \alpha \mathtt{sign}(y - \hat{\xi}_1) \\ \hat{y} &= \hat{\xi}_1 \end{aligned} \tag{7.25}$$

Setting $e_1 = \xi_1 - \hat{\xi}_1$ and $e_2 = \xi_2 - \hat{\xi}_2$, the observation error dynamics is:

$$\begin{aligned} \dot{e}_1 &= e_2 - \lambda |e_1|^{\frac{1}{2}} \mathtt{sign}(e_1) \\ \dot{e}_2 &= \dot{\xi}_2 - \alpha \mathtt{sign}(e_1) \end{aligned} \tag{7.26}$$

which is stable for appropriate values of α and λ [27, 32]. In the given simulations, $\lambda = 5$, $\alpha = 40$ and a computation step equal to $10^{-5}s$ is used with the solver ode5 of Matlab.

Case 1. (Fig. 7.6) exhibits a chattering Zeno phenomena ($I_{min} = 0$ when the state behavior reaches the sliding manifold $h_1 = 2h_2$ approximatively at time $t = 0.2s$) and the system slides on the switching manifold until $h_1 \simeq 2.5$ and $h_2 \simeq 1.25$ (see the green trajectory in Fig. 7.8 and Fig 7.9). Note that the Zeno time t_∞ in this case is not unique, because during all the period the system slides on the switching manifold, there is an infinite number of commutations in every small time interval. The fact that the Zeno behavior is not restricted to a particular time instant t_∞, but appears during a finite or infinite time interval is characteristic of a sliding mode behavior. Here, when the system has reached the switched manifold given by $h_1 = 2h_2$, the system never leaves the constrained manifold (it is an invariant one).

The system behavior (in green) and the observer behavior (in red) are given in Fig. 7.8 and Fig. 7.9 for an appropriate choice of coordinate and a wrong choice of coordinate, respectively.

The observation errors in original coordinates are given in Fig 7.10. As the original behavior does not cross S_O (in blue in Fig. 7.8 and Fig. 7.9), the observer (7.25) converges and it is not at all influenced by the Zeno behavior of the observed system (even if it is a chattering Zeno which slides on the switching manifold).

Case 2. (Fig. 7.7) exhibits a genuinely Zeno phenomena. Roughly speaking, the system switches more and more quickly and infinitely until the time $t_\infty \simeq 1.6$ which corresponds to the time when the state is equal to the desired one ($h_1 = 4$ and $h_2 = 1.5$). After that, there is *still life* [2] (see the green trajectory in Fig. 7.12). The system trajectories in the phase plane are given in Fig. 7.11 and Fig. 7.12 with an appropriate and a wrong choice of coordinate, respectively. Life after Zeno is due

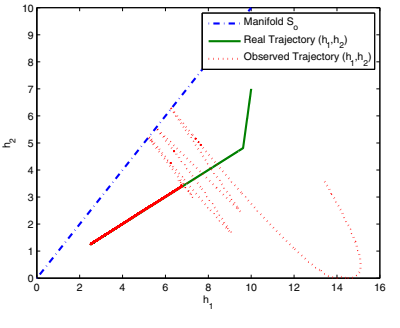

Fig. 7.8 The phase plane with an appropriate choice of coordinate.

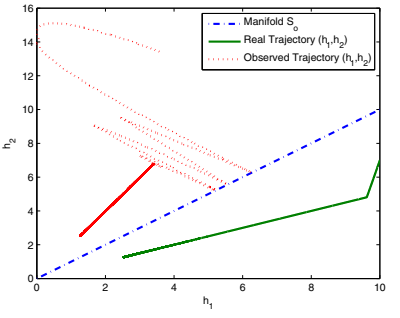

Fig. 7.9 he phase plane with a wrong choice of coordinate.

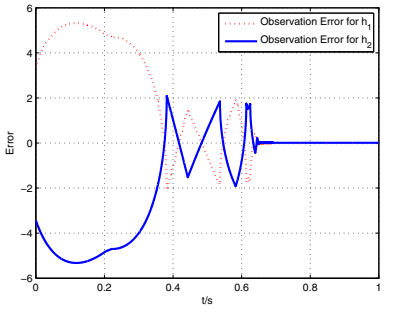

Fig. 7.10 The observation errors in the original coordinates.

to the fact that the input v is strictly smaller than $v_1 + v_2$ (the desired point is semi attractive, in fact the state behavior reaches ($h_1 = 4$, $h_2 = 1.5$) only if the initial conditions verify $h_1 + h_2 \gg 5.5$). Since the original system trajectory (in green) crosses the observability singularity set S_O, the observer trajectory diverges when the trajectory is in the opposite subspace. Moreover, when the system trajectory is close to the observability singularity set S_O, the observation errors increase even if the coordinates choice is correct.

The observation errors in the canonical coordinates ξ are given in Fig. 7.13 ($e_1 = \xi_1 - \hat{\xi}_1$ in blue and $e_2 = \dot{\xi}_1 - \dot{\hat{\xi}}_1$ in red). The observation errors are shown only during the first second, because the higher order sliding mode observer (7.25) converges in a finite time $\simeq 0.1s$ and is not substantially perturbed by the S_O crossing or by the Zeno behavior of the original system. The observation errors in the original coordinates (h_1, h_2) are given in Fig. 7.14 and it is clear, for such coordinates, that the error dynamics are strongly influenced by the crossing of S_O. The Zeno time is $t_\infty \simeq 1.6s$ (when $h_1 = 4$ and $h_2 = 1.5$). Then, the system converges to a limit cycle and the observer works well in both coordinates (original coordinates with appropriate choice and canonical coordinates) because the limit cycle does not cross S_O.

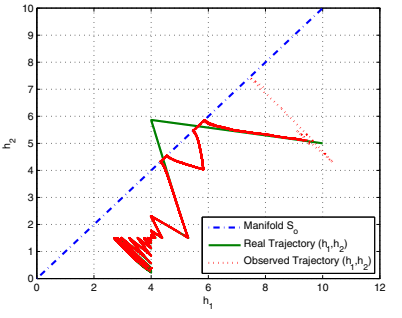

Fig. 7.11 The phase plane with an appropriate choice of coordinate.

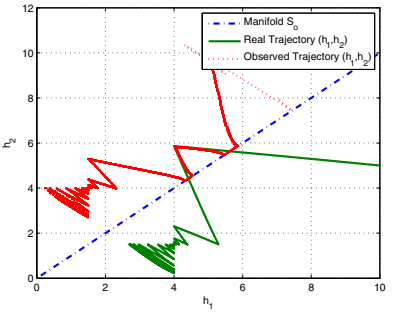

Fig. 7.12 The phase plane with a wrong choice of coordinate.

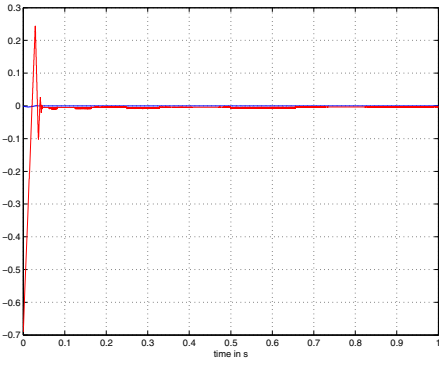

Fig. 7.13 The observation errors in the canonical coordinates.

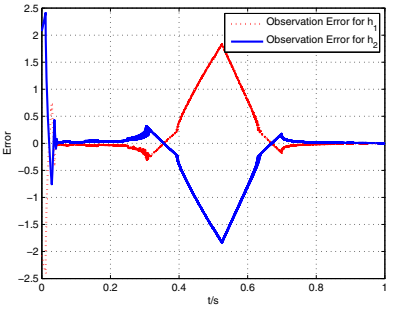

Fig. 7.14 The observation error in the original coordinates.

7.6 Conclusion

In this chapter, the links between sliding mode and Zeno phenomenon have been highlighted and it can be thought that many tools and methods of sliding mode theory could be successfully used for hybrid dynamical system under Zeno phenomenon (even if sliding mode control does not consider state jump as it is the case for example of the bouncing ball). Moreover, it is probably interesting to find new sliding mode controls inspired by some "physical" systems which exhibits Zeno behaviors [1], [28]. In order to emphasis again the links between Zeno phenomenon and sliding mode, note that, for physical systems, Zeno phenomenon is due to model approximations [24] while sliding mode control is based on an actuator idealization, and that both simulations can be very difficult [21].

References

1. Ames, A., Abate, A., Sastry, S.: Sufficient Conditions for the Existence of Zeno Behavior in Nonlinear Hybrid Systems via Constant Approximations. In: 44th IEEE CDC and ECC, pp. 4033–4038 (2005)
2. Ames, A., Zheng, H., Gregg, R., Sastry, S.: Is there life after Zeno? Taking executions past the breaking (zeno) point. In: IEEE ACC, Mineapolis (2006)
3. Barbot, J.-P., Boukhobza, T., Djemaï, M.: Sliding mode observer for triangular input form. In: IEEE Conf. Decision Control, Kobe (1996)
4. Besançon, G., Zhang, Q., Hammouri, H.: High-Gain Observer based State and Parameter Estimation in Nonlinear System. In: 6th IFAC Symposium on Nonlinear Control Systems (2004)
5. Boutat, D., Benali, A., Barbot, J.-P.: About the observability of piecewise dyamical system. In: 6th IFAC Symposium on Nonlinear Control Systems (2004)
6. Brogliato, B.: Nonsmooth Impact Mechanics: Models, Dynamics and Control. LNCIS, vol. 220. Springer, Heidelberg (1996)
7. Busawon, K., de Leon Morales, J.: An observer design for uniformly observable nonlinear systems. Int. J. of Control 73(15), 1357–1381 (2000)

8. Cichon, M., Kubiaczyk, I., Sikorska, A.: The Henstock-Kurweil-Pettis integral and exsitence theorems for the Cauchy problem. Czeckoslovak Mathematical Journal 54, 279–289 (2004)
9. Davila, J., Fridman, L., Pisano, A., Usai, E.: Finite-time state observation for non-linear uncertain systems via higher-order sliding modes. International Journal of Control 8, 1564–1574 (2009)
10. De Fogio, S.: The NV-Integrals, AMS Special Session on Nonabsolute Integration, Toronto (2000)
11. Diop, S., Fliess, M.: On nonlinear observability. In: Proc. 1st Europ. Control Conf., Hermès, pp. 152–157 (1991)
12. Drakunov, S., Utkin, V.: Sliding mode observer: Tutorial. In: Proc. of the 34th IEEE CDC 1995 (1995)
13. Emelyanov, S.V., Korovin, S.K.: Applying the principle of control by deviation to extend the set of possible feedback types. Soviet Physics, Doklady 26(6), 562–564 (1981)
14. Filippov, A.F.: Classical solutions of differential equations with multi-valued right-hand sides. SIAM J. Control 5, 609–621 (1967)
15. Filippov, A.F.: Differential Equations with Discontinuous Righthand sides. Kluwer Academic Publishers, Dordrecht (1988)
16. Floquet, T., Barbot, J.-P.: Super twisting algorithm-based step-by-step sliding mode observers for nonlinear systems with unknown inputs. International Journal of Systems Science 38(10), 803–815 (2007)
17. Fridman, L., Levant, A.: Higher order sliding modes as the natural phenomenon in control theory. In: Robust Control via Variable Structure and Lyapunov Techniques, vol. 217, pp. 107–133. Springer, Heidelberg (1996)
18. Henstock, R.: The General Theory of Integration. Oxford Mathematical Monographs. Clarendon Press, Oxford (1991)
19. Hermann, R., Krener, A.J.: Nonlinear controllability and observability. IEEE Transactions on Automatic Control 22, 728–740 (1977)
20. Heymann, M., Lin, F., Meyer, G., Resmerita, S.: Analysis of Zeno behaviours in hybrid systems. In: Proc. of 41th IEEE CDC, Las Vegas (2002)
21. Johansson, K.H., Lygeros, J., Sastry, S., Egerstedt, M.: Simulation of zeno hybrid automata. In: Proc. 38th Conference on Decision and Control, vol. 4, pp. 3538–3543 (1999)
22. Kang, W., Barbot, J.-P., Xu, L.: On the observability of nonlinear and switched system. Springer, Heidelberg (2010) (in press) (The book dedicated to Dr Wijesuriya P. Dayawansa)
23. Goebel, R., Hespanha, J., Teel, A.R., Cai, C., Sanfelice, R.: Hybrid systems: generalized solutions and robust stability. In: Proceedings of IFAC, Nolcos (2004)
24. Goebel, R., Sanfelice, R., Teel, A.: Hybrid Dynamical systems. IEEE Control Systems Magazine 29(2), 28–93 (2009)
25. Leonov, G., Nijmeijer, H., Pogromsky, A., Fradkov, A.: Dynamics and Control of Hybrid Mecanical Systems. World Scientific Series on Nonlinear Science, Serie B 14 (2010)
26. Levant, A.: Sliding order and sliding accuracy in sliding mode control. Int. J. of Control 58(6), 1253–1253 (1993)
27. Levant, A.: Robust Extract Differentiation via Sliding mode Technique. Automatica 34(3), 379–384 (1998)
28. Lygeros, J., Johansson, H.K., Simic, S.N., Zhang, J., Sastry, S.S.: Dynamical Properies of Hybrid Automata. IEEE Trans. on Autom. Control 48(1), 2–17 (2003)
29. Mboup, M., Join, C., Fliess, M.: A revised look at numerical differentiation with an application to nonlinear feedback control. In: The 15th Mediterrean Conference on Control and Automation (2007)

30. Mboup, M.: Parameter estimation via differential algebra and operational calculus, Rapport de Recherche (2007), http://hal.inria.fr/inria-00138294/fr
31. Perruquetti, W., Barbot, J.-P.: Sliding Mode Control in Engineering. Marcel Dekker, New York (2002)
32. Saadaoui, H., Manamani, N., Djemai, M., Barbot, J.P., Floquet, T.: Exact differentiation and Sliding mode observer for switched Lagrangian systems. Nonlinear Analysis: Theory, Methods & Applications 65(5), 1050–1069 (2006)
33. Talvila, E.: Estimates of the remainder in Taylors theorem using the Henstock. Czeckoslovak Mathematical Journal 55, 933–940 (2005)
34. Yu, L., Barbot, J.-P., Boutat, D., Benmerzouk, D.: Observability Normal Forms for a Class of Switched Systems with Zeno Phenomena. In: IEEE ACC (2009)

Part II
Sliding Mode Control Design

Chapter 8
Output Feedback Sliding Mode Control of Uncertain Systems in the Presence of State Delay with Applications

X. Han, E. Fridman, and S.K. Spurgeon

Abstract. This chapter considers the development of sliding mode control strategies for linear, time delay systems with bounded disturbances that are not necessarily matched. The emphasis is on the development of frameworks that are constructive and applicable to real problems. For many systems it may not be practical to measure all the system states and therefore a static output feedback sliding mode control design paradigm is considered. The novel feature of the method is that Linear Matrix Inequalities (LMIs) are derived to compute solutions to both the existence problem and the finite time reachability problem that minimize the ultimate bound of the reduced-order sliding mode dynamics in the presence of time varying delay and unmatched disturbances. The methodology is therefore constructive and provides guarantees on the level of closed-loop performance that will be achieved by uncertain systems which experience delay. An uncertain model with both matched and unmatched disturbances from the literature provides a tutorial example of the proposed method. A case study involving the practical application of the design methodology in the area of liquid monopropellant rocket motor control is also presented.

8.1 Introduction

The control of time-delay systems is known to be of industrial and applications significance. Such problems largely fall into two main categories. The first category

X. Han · S.K. Spurgeon
Instrumentation, Control and Embedded Systems Research Group,
School of Engineering and Digital Arts
Kent University, Canterbury, Kent, CT2 7NZ
e-mail: xh25@kent.ac.uk, S.K.Spurgeon@kent.ac.uk

E. Fridman
School of Electrical Engineering
Tel Aviv University, Tel Aviv, 69978, Israel
e-mail: emilia@eng.tau.ac.il

L. Fridman et al. (Eds.): Sliding Modes, LNCIS 412, pp. 223–244.
springerlink.com

arises because of the need to model systems more accurately given increasing performance expectations. Many processes, such as manufacturing processes and the internal combustion engine, include such after effect phenomena in their inner dynamics and time delay is also produced via the actuators, sensors and field networks involved in the practical implementation of feedback control strategies. The second class of problems arises when time delays are used as a modelling tool to simplify some infinite dimensional systems. This tool is used for constructing models of distributed systems modelled by partial differential equations where a set of finite dimensional state variables with appropriate time delay characteristics can be used to represent heat exchange processes, for example.

The application of sliding mode control to the problem of systems with time-delay is a far from trivial problem generically, involving the combination of delay phenomenon with relay actuators which has the potential to induce oscillations around the sliding surface during the sliding mode. There are a number of papers which have considered the problem. The development of sliding mode controllers for operation in the presence of single or multiple, constant or time-varying state delays was solved by [14]. This uses the usual regular form method of solution and the uncertainty is assumed to be matched, so that the effects will be rejected by an appropriately designed sliding mode control strategy. The work assumed full state availability. The problem was also considered by [19] where a class of uncertain time delay systems with multiple fixed delays in the system states is considered. The paper considers unmatched and time varying parameter uncertainties together with matched and bounded external disturbances, but again full state information is assumed to be available to the controller. Work in [18] considers sliding mode control of an uncertain system in the presence of fixed state-delay, but again full-state feedback is assumed.

The assumption of full-state feedback is a limiting one in practice as it may be prohibitively expensive, and indeed, sometimes impossible, to measure all the state variables. One approach to solve this problem is to implement the controller with an observer, where the observer provides state estimates for use by the controller. However, the implementation of the controller-observer is more involved and the theoretical frameworks to ensure stability across the range of practical operation of the plant may be challenging. A more straightforward approach is to use only the subset of state information that is available, i.e. the measured output, within the control design paradigm. This chapter will provide an insight into what can be achieved via a sliding mode approach to output feedback control of time delay systems, which may experience both matched and unmatched uncertainty.

It is known that in the presence of bounded disturbances that do not vanish as the state approaches an equilibrium point, asymptotic stability is, in general, not possible. However, under certain conditions, the *ultimate boundedness* of the system's trajectories can be achieved [2]. Sliding Mode Control (SMC) is known for its complete robustness to so-called matched uncertainties and disturbances [22], as demonstrated in the work of [14] referenced above, but the closed-loop performance will be affected by the presence of unmatched uncertainty. For example, in [10] robustness properties of integral sliding-mode controllers are studied where

the euclidean norm of the unmatched perturbation is minimized by selecting a projection matrix. The approach articulated in this chapter will employ tools of ultimate boundedness to develop a framework for output feedback sliding mode control of time delay systems which experience unmatched uncertainty.

There are typically two facets to the design of a static output feedback sliding mode control. One is the existence problem, i.e., the design of a switching surface in the output vector space which is usually of lower order than the state vector space. Consider first the switching surface design problem for uncertain systems, where time-delay effects are not considered. Two different methods of designing sliding surfaces using eigenvalue assignment and eigenvector techniques were proposed in [9], [25]. A canonical form via which the static output feedback sliding mode control design problem is converted to a static output feedback stabilization problem for a particular subsystem triple was provided in [8]. However, the solution to the general static output feedback problem, even for linear time-invariant systems, is still open. Iterative LMI approaches have been exploited to solve the static output feedback problem using a bilinear matrix inequality formulation, see [3], [17], [4]. In [6], where the regular form was not used for synthesization of the control law, LMIs were derived for switching function design whilst minimizing the cost function associated with the control. Sufficient conditions for static output feedback controller design using LMIs have also been sought. Although only sufficient, the solutions have the advantage of being linear and, hence, easily tractable using standard optimization techniques, see, [20], [5]. The second facet in the design of a sliding mode output feedback controller is the control, or reachability, synthesis problem whereby a control is determined to ensure the sliding surface is attractive. It is non-trivial to synthesize a control law only using the output vector, even for the situation where time-delay effects are not considered, since the derivative of the sliding surface is always related to the unmeasured states and this derivative appears in the reachability condition. As well within the existence problem, LMI methods have also been considered within the context of developing a sliding mode control strategy which solves the reachability problem for a given sliding surface. For example, LMI methods which yield reachability conditions for designing static sliding mode output feedback controllers were presented in [7].

In the context of output feedback sliding mode control for time-delay systems, the existence and reachability problems for systems in the presence of matched uncertainty are considered in [15]. The delay is assumed to be time-varying and bounded where the upper bound is known. In line with the development of output feedback controllers in the non-delayed case, LMIs are used to select all the parameters of the closed-loop sliding mode controller. Central to the work is the descriptor Lyapunov-Krasovskii functional method from [11], which is used to design a switching function and verify that the magnitude of the linear gain used to construct the controller is an appropriate solution to the reachability problem.

Central to the work presented in this chapter is the same descriptor approach [11] [15], which is applied to derive LMIs for the solution of the sliding mode output feedback control problem in the presence of both matched and *unmatched* disturbances and time varying state delays. It is demonstrated that the state trajectories

of the system converge towards a ball with a prespecified exponential convergence rate. In Section 8.2 the problem formulation is described and an appropriate general framework to accomplish the output feedback sliding mode control design is described in Section 8.3. A constructive solution to the existence problem is presented in Section 8.4 and Section 8.5 shows the formulation of the reachability problem which will ensure that the sliding mode is reached. A problem from the literature is used to provide a tutorial example of how the paradigm can be used to solve both the existence and reachability problems for practical design. A case study relating to the control of a liquid monopropellant rocket motor system is used to further illustrate the design process in Section 8.6.

Notation. $\mathscr{R}^n$ denotes the n dimensional Euclidean space with vector norm $\|\cdot\|$ or the induced matrix norm, $\mathscr{R}^{n\times m}$ is the set of all $n\times m$ real matrices. $P>0$, for $P\in\mathscr{R}^{n\times n}$, means that P is symmetric and positive definite whereas $*$ means the symmetric entries of a LMI.

8.2 Problem Formulation

Consider an uncertain dynamical system of the form

$$\begin{aligned}\dot{x}(t) &= Ax(t)+A_dx(t-\tau(t))+Bu(t)+B_1w(t)\\ y(t) &= Cx(t)\\ x(t_0-\tau(t)) &= \phi(\tau(t)) \quad for \quad \tau(t)\in[0\ \ h]\end{aligned} \tag{8.1}$$

where $x\in\mathscr{R}^n$, $u\in\mathscr{R}^m, w\in\mathscr{R}^k$ and $y\in\mathscr{R}^p$ with $m<p<n$, ϕ is absolutely continuous with square integrable $\dot{\phi}$, h is an upper-bound on the time-delay function $(0\le\tau(t)\le h,\ \forall t\ge 0)$. The time-varying delay may be either slowly varying (i.e. a differentiable delay with $\dot{\tau}(t)\le d<1$) or fast varying (piecewise continuous delay). Assume that the nominal linear system (A,A_d,B,B_1,C) is known and that the input and output matrices B and C are both of full rank. The disturbance is assumed to be bounded whereby $\|w(t)\|\le\Delta$ with a known upper bound $\Delta>0$. A control strategy will be sought which induces an ideal sliding motion with desirable performance characteristics on the surface

$$\mathscr{S}=\{x\in\mathscr{R}^n : s(t)=FCx(t)=0\} \tag{8.2}$$

for some selected matrix $F\in\mathscr{R}^{m\times p}$ so that the motion, when restricted to $\mathscr{S}$, is stable.

8.3 A General Framework for Design

The first problem considered is how to choose F, which parameterises the switching surface in (8.2) and hence the dynamic performance of the system in the sliding mode, so that the associated sliding motion is stable. A control law will then be determined to guarantee the existence of a sliding motion. A convenient system

representation closely allied to the usual regular form used for sliding mode control design is employed. It can be shown that if $rank(CB) = m$ and system triple $(A,\ B,\ C)$ are minimum phase, there exists a coordinate system $x_r = T_r x$, $x_r = [x_1\ \ x_2]^T$, in which the system (A,A_d,B,B_1,C) has the transformed structure

$$A_r = \begin{bmatrix} A_{11}\ A_{12} \\ A_{21}\ A_{22} \end{bmatrix} A_{d_r} = \begin{bmatrix} A_{d11}\ A_{d12} \\ A_{d21}\ A_{d22} \end{bmatrix} B_r = \begin{bmatrix} 0 \\ B_2 \end{bmatrix} B_{1_r} = \begin{bmatrix} B_{11} \\ B_{12} \end{bmatrix} C_r = \begin{bmatrix} 0\ T \end{bmatrix} \quad (8.3)$$

where $B_2 \in \mathscr{R}^{m\times m}$ is non-singular and $T \in \mathscr{R}^{p\times p}$ is orthogonal [8]. Furthermore, A_{11}, $A_{d11} \in \mathscr{R}^{(n-m)\times(n-m)}$ and the remaining sub-blocks are partitioned accordingly. Let

$$\begin{bmatrix} F_1\ F_2 \end{bmatrix} = FT \quad (8.4)$$

where $F_1 \in \mathscr{R}^{m\times(p-m)}$ and $F_2 \in \mathscr{R}^{m\times m}$. As a result

$$FC_r = \begin{bmatrix} F_1C_1\ F_2 \end{bmatrix} \quad (8.5)$$

where

$$C_1 = \begin{bmatrix} 0_{(p-m)\times(n-p)}\ I_{(p-m)} \end{bmatrix} \quad (8.6)$$

It is straightforward to see that $FC_rB_r = F_2B_2$ and the square matrix F_2 is nonsingular. By assumption, the system contains both matched and unmatched uncertainties and therefore the sliding motion is independent of the matched uncertainty but dependent on the unmatched uncertainty. In terms of the coordinate framework defined above, the reduced-order sliding mode dynamics are governed by the following reduced order system

$$\dot{x}_1(t) = (A_{11} - A_{12}KC_1)x_1(t) + (A_{d11} - A_{d12}KC_1)x_1(t-\tau(t)) + B_{11}w(t) \quad (8.7)$$

The response of this system must therefore be ultimately bounded, where $K = F_2^{-1}F_1$, and the problem of hyperplane design is equivalent to a static output feedback problem for the system $(A_{11},\ A_{d11},\ A_{12},\ A_{d12},\ C_1)$, where $(A_{11}+A_{d11},\ A_{12}+A_{d12})$ is assumed controllable and $(A_{11}+A_{d11},\ C_1)$ observable. Note that the presence of the unmatched uncertainty means that, in general, asymptotic stability cannot be attained by the system (8.7). This is formalised in terms of the existence problem, which must be solved to determine the switching surface, in the next section.

8.4 Existence Problem

It will be shown that the system (8.3) is exponentially attracted to a bounded region in $\mathscr{R}^n$ if the reduced-order system (8.7) is exponentially attracted to a bounded domain in $\mathscr{R}^{n-m}$. Consider the Lyapunov-Krasovskii functional below for the exponential stability analysis of (8.7)

$$V(t) = x_1^T(t)Px_1(t) + \int_{t-h}^{t} e^{\alpha(s-t)}x_1^T(s)Ex_1(s)ds + \int_{t-\tau(t)}^{t} e^{\alpha(s-t)}x_1^T(s)Sx_1(s)ds + h\int_{-h}^{0}\int_{t+\theta}^{t} e^{\alpha(s-t)}\dot{x}_1^T(s)R\dot{x}_1(s)dsd\theta \tag{8.8}$$

with $(n-m)\times(n-m)$-matrices $P>0$ and $E\geq 0, S\geq 0, R\geq 0$. To prove exponential stability of the system (8.7) using (8.8), it is necessary to use the following lemma.

Lemma 8.1. *[112] Let $V:[0,\infty)\rightarrow R^+$ be an absolutely continuous function. If there exist $\alpha>0$ and $b>0$ such that the derivative of V satisfies almost everywhere the inequality*

$$\frac{d}{dt}V(t)+\alpha V(t)-b\|w(t)\|^2\leq 0$$

then it follows that for all $\|w(t)\|\leq\Delta$

$$V(t)\leq e^{-\alpha(t-t_0)}V(t_0)+\frac{b}{\alpha}\Delta^2,\quad t\geq t_0.$$

Differentiating $V(t)$ from (8.8) yields

$$\begin{aligned} M = {} & 2x_1^T(t)P\dot{x}_1(t)+h^2\dot{x}_1{}^T(t)R\dot{x}_1(t) \\ & -he^{-\alpha h}\textstyle\int_{t-h}^{t}\dot{x}_1{}^T(s)R\dot{x}_1(s)ds+x_1^T(t)(E+S)x_1(t) \\ & -x_1^T(t-h)Ex_1(t-h)e^{-\alpha h}+\alpha x_1^T(t)Px_1(t) \\ & -(1-\dot{\tau}(t))x_1^T(t-\tau(t))Sx_1(t-\tau(t))e^{-\alpha\tau(t)} \\ & -bw^T(t)w(t). \end{aligned} \tag{8.9}$$

Further using the identity

$$\begin{aligned} & -h\textstyle\int_{t-h}^{t}\dot{x}_1{}^T(s)R\dot{x}_1(s)ds \\ & =-h\textstyle\int_{t-h}^{t-\tau(t)}\dot{x}_1{}^T(s)R\dot{x}_1(s)ds-h\int_{t-\tau(t)}^{t}\dot{x}_1{}^T(s)R\dot{x}_1(s)ds \end{aligned} \tag{8.10}$$

and applying Jensen's inequality

$$\textstyle\int_{t-\tau(t)}^{t}\dot{x}_1{}^T(s)R\dot{x}_1(s)ds\geq\frac{1}{h}\int_{t-\tau(t)}^{t}\dot{x}_1{}^T(s)dsR\int_{t-\tau(t)}^{t}\dot{x}_1(s)ds \tag{8.11}$$

and

$$\textstyle\int_{t-h}^{t-\tau(t)}\dot{x}_1{}^T(s)R\dot{x}_1(s)ds\geq\frac{1}{h}\int_{t-h}^{t-\tau(t)}\dot{x}_1{}^T(s)dsR\int_{t-h}^{t-\tau(t)}\dot{x}_1(s)ds. \tag{8.12}$$

then equation (8.9) becomes

$$\begin{aligned} & M\leq 2x_1^T(t)P\dot{x}_1{}^T(t)+\alpha x_1^T(t)Px_1(t)+h^2\dot{x}_1{}^T(t)R\dot{x}_1(t) \\ & -[\big(x_1(t)-x_1(t-\tau(t))\big)^TR\big(x_1(t)-x_1(t-\tau(t))\big)- \\ & \big(x_1(t-\tau(t))-x_1(t-h)\big)^TR\big(x_1(t-\tau(t))-x_1(t-h)\big)]e^{-\alpha h} \\ & +x_1^T(t)(E+S)x_1(t)-x_1^T(t-h)Ex_1(t-h)e^{-\alpha h} \\ & -(1-d)x_1^T(t-\tau(t))Sx_1(t-\tau(t))e^{-\alpha h}-bw^T(t)w(t) \end{aligned} \tag{8.13}$$

Using the descriptor method as in [11] and the free-weighting matrices technique from [16]

$$\begin{aligned} 0 \equiv\ & 2(x_1^T(t)P_2^T + \dot{x_1}^T(t)P_3^T)[-\dot{x_1}(t) + (A_{11} - A_{12}KC_1) \\ & x_1(t) + (A_{d11} - A_{d12}KC_1)x_1(t-\tau(t)) + B_{11}w(t)] \end{aligned} \tag{8.14}$$

where matrix parameters P_2, $P_3 = \varepsilon P_2 \in \mathscr{R}^{n-m}$ are added to the right-hand side of (8.13). Setting $\eta(t) = col\{x_1(t), \dot{x_1}(t), x_1(t-h), x_1(t-\tau(t)), w(t)\}$, then $M \leq \eta^T(t)\Theta\eta(t) \leq 0$ if the matrix $\Theta < 0$. Multiplying matrix Θ from the right and the left by $diag\{P_2^{-1}, P_2^{-1}, P_2^{-1}, P_2^{-1}, I\}$ and its transpose respectively and denoting

$$Q_2 = P_2^{-1}, \widehat{P} = Q_2^T P Q_2,\ \widehat{R} = Q_2^T R Q_2,\ \widehat{E} = Q_2^T E Q_2,\ \widehat{S} = Q_2^T S Q_2$$

it follows $\Theta < 0 \Leftrightarrow \widehat{\Theta} < 0$ where

$$\widehat{\Theta} = \begin{bmatrix} \widehat{\theta}_{11} & \widehat{\theta}_{12} & 0 & \widehat{\theta}_{14} & \widehat{\theta}_{15} \\ * & \widehat{\theta}_{22} & 0 & \widehat{\theta}_{24} & \widehat{\theta}_{25} \\ * & * & \widehat{\theta}_{33} & \widehat{\theta}_{34} & 0 \\ * & * & * & \widehat{\theta}_{44} & 0 \\ * & * & * & * & \widehat{\theta}_{55} \end{bmatrix} < 0 \tag{8.15}$$

and

$$\begin{aligned} \widehat{\theta}_{11} &= (A_{11} - A_{12}KC_1)Q_2 + \alpha\widehat{P} + Q_2^T(A_{11} - A_{12}KC_1)^T + \widehat{E} + \widehat{S} - \widehat{R}e^{-\alpha h} \\ \widehat{\theta}_{12} &= \widehat{P} - Q_2 + \varepsilon Q_2^T(A_{11} - A_{12}KC_1)^T \\ \widehat{\theta}_{14} &= (A_{d11} - A_{d12}KC_1)Q_2 + \widehat{R}e^{-\alpha h} \\ \widehat{\theta}_{15} &= B_{11} \qquad\qquad \widehat{\theta}_{22} = -\varepsilon Q_2 - \varepsilon Q_2^T + h^2\widehat{R} \\ \widehat{\theta}_{24} &= \varepsilon(A_{d11} - A_{d12}KC_1)Q_2 \qquad \widehat{\theta}_{25} = \varepsilon B_{11} \\ \widehat{\theta}_{33} &= -(\widehat{E} + \widehat{R})e^{-\alpha h} \qquad \widehat{\theta}_{34} = \widehat{R}e^{-\alpha h} \\ \widehat{\theta}_{44} &= -2e^{-\alpha h}\widehat{R} - (1-d)\widehat{S}e^{-\alpha h} \qquad \widehat{\theta}_{55} = -bI \end{aligned} \tag{8.16}$$

Select the LMI variable Q_2 in the following form

$$Q_2 = \begin{bmatrix} Q_{11} & Q_{12} \\ Q_{22}\mathscr{M} & \delta Q_{22} \end{bmatrix} \tag{8.17}$$

where Q_{22} is a $(p-m) \times (p-m)$ matrix, $\mathscr{M}$ is a $(p-m) \times (n-p)$ tuning matrix and δ is a tuning parameter to be selected by the designer. It follows that

$$KC_1Q_2 = \begin{bmatrix} KQ_{22}\mathscr{M} & \delta KQ_{22} \end{bmatrix}$$

Defining $Y = KQ_{22}$ it follows that

$$KC_1Q_2 = \begin{bmatrix} Y\mathscr{M} & \delta Y \end{bmatrix} \tag{8.18}$$

To construct K, substitute (8.18) into (8.16) to yield

$$\begin{aligned}
&\widehat{\theta}_{11} = A_{11}Q_2 - A_{12}[Y \quad \delta Y] + Q_2^T A_{11}^T + \alpha\widehat{P} - [Y\mathscr{M} \quad \delta Y]^T A_{12}^T + \widehat{E} + \widehat{S} - \widehat{R}e^{-\alpha h} \\
&\widehat{\theta}_{12} = \widehat{P} - Q_2 + \varepsilon Q_2^T A_{11}^T - \varepsilon[Y\mathscr{M} \quad \delta Y]^T A_{12}^T \\
&\widehat{\theta}_{14} = A_{d11}Q_2 - A_{d12}[Y\mathscr{M} \quad \delta Y] + \widehat{R}e^{-\alpha h} \\
&\widehat{\theta}_{15} = B_{11} \qquad\qquad \widehat{\theta}_{22} = -\varepsilon Q_2 - \varepsilon Q_2^T + h^2\widehat{R} \\
&\widehat{\theta}_{24} = \varepsilon A_{d11}Q_2 - \varepsilon A_{d12}[Y\mathscr{M} \quad \delta Y] \quad \widehat{\theta}_{25} = \varepsilon B_{11} \\
&\widehat{\theta}_{33} = -(\widehat{E} + \widehat{R})e^{-\alpha h} \qquad \widehat{\theta}_{34} = \widehat{R}e^{-\alpha h} \\
&\widehat{\theta}_{44} = -2e^{-\alpha h}\widehat{R} - (1-d)\widehat{S}e^{-\alpha h} \qquad \widehat{\theta}_{55} = -bI
\end{aligned} \tag{8.19}$$

The following Proposition can now be stated:

Proposition 8.1. *Given scalars $h > 0$, $d < 1$, $\alpha > 0$, ε, δ, b and a matrix $\mathscr{M} \in \mathscr{R}^{(p-m)\times(n-p)}$, if there exist $(n-m)\times(n-m)$ matrices $\widehat{P} > 0$, $\widehat{E} \geq 0$, $\widehat{S} \geq 0$, $\widehat{R} \geq 0$ and matrices $Q_{22} \in \mathscr{R}^{(p-m)\times(p-m)}$, $Q_{11} \in \mathscr{R}^{(n-p)\times(n-p)}$, $Q_{12} \in \mathscr{R}^{(n-p)\times(p-m)}$, $Y \in \mathscr{R}^{m\times(p-m)}$ such that the LMI (8.15) with matrix entries (8.19) holds, then the reduced order system (8.7), where $K = YQ_{22}^{-1}$, is exponentially attracted to the ellipsoid*

$$x_1^T(t)Px_1(t) \leq \frac{b}{\alpha}\Delta^2 \tag{8.20}$$

where $P = Q_2^{-T}\widehat{P}Q_2^{-1}$, for all differentiable delays $0 \leq \tau(t) \leq h$, $\dot{\tau}(t) \leq d < 1$. Moreover, the reduced order dynamics (8.7) is exponentially stable for all piecewise-continuous delays $0 \leq \tau(t) \leq h$, if the LMI (8.15) is feasible with $\widehat{S} = 0$.

Once K is obtained the sliding function matrix is defined as

$$F = \begin{bmatrix} K & I_m \end{bmatrix} T^{-1}$$

where T is from matrix C_r in (8.3). From (8.20) the reduced order sliding mode dynamics are ultimately bounded by

$$\|x_1(t)\|^2 \leq \frac{b}{\alpha\underline{\lambda}(P)}\Delta^2 \tag{8.21}$$

where $\underline{\lambda}(P)$ denotes the minimum eigenvalue of matrix P. It follows from the transformed structure that the output equation is

$$y(t) = C_r x_r(t) \tag{8.22}$$

In the ideal sliding mode

$$x_2(t) = -KC_1x_1(t) \tag{8.23}$$

Substituting from (8.23) in (8.22) and denoting the upperbound of $\|x_1(t)\|^2$ as $t \to \infty$ by $\gamma = \frac{b}{\alpha \underline{\lambda}(P)} \Delta^2$, the corresponding bound on the output during the ideal sliding mode is given by

$$\|y(t)\|^2 \leq \|C_r\|^2 (\|KC_1\|^2 + 1)\gamma \tag{8.24}$$

Example 8.1. Consider a third order system from [23] which incorporates both matched and unmatched disturbances. Two different solutions to the existence problem demonstrate how the ultimate bound of the sliding mode dynamics can be minimized, according to Proposition 8.1. Consider the system

$$\begin{aligned} \dot{x}(t) &= \begin{bmatrix} -3 & 0 & 1 \\ 1 & 2 & 0 \\ 0 & 1 & -2 \end{bmatrix} x(t) + \begin{bmatrix} 0 \\ 1 \\ 0 \end{bmatrix} u(t) + \begin{bmatrix} 2 \\ 1 \\ 0 \end{bmatrix} sin(t) \\ y(t) &= \begin{bmatrix} 0 & 1 & 0 \\ 1 & 1 & 0 \end{bmatrix} x(t) \end{aligned} \tag{8.25}$$

The transformed structure of (8.25) according to the representation (8.3) is

$$\begin{aligned} A_r &= \begin{bmatrix} -2 & -0.71 & 1 \\ 0.71 & -3 & 0 \\ 0.5 & -2.12 & 2 \end{bmatrix}, \; B_r = \begin{bmatrix} 0 \\ 0 \\ 1 \end{bmatrix}, \; B_{1_r} = \begin{bmatrix} 0 \\ 1.41 \\ 2 \end{bmatrix} \\ C_r &= \begin{bmatrix} 0 & -0.71 & 1 \\ 0 & 0.71 & 1 \end{bmatrix} \end{aligned} \tag{8.26}$$

Subsystem $(A_{11}, A_{12}, B_{11}, C_1)$ is given by

$$A_{11} = \begin{bmatrix} -2 & -0.71 \\ 0.71 & -3 \end{bmatrix}, \; A_{12} = \begin{bmatrix} 1 \\ 0 \end{bmatrix}, \; B_{11} = \begin{bmatrix} 0 \\ 1.41 \end{bmatrix}, \; C_1 = \begin{bmatrix} 0 & 1 \end{bmatrix} \tag{8.27}$$

The switching surface design problem is solved by developing a static output feedback controller for this subsystem. Choosing the tuning parameter in the LMI (8.15) with entries (8.19) as $\delta = 0.9$, $\varepsilon = 0.34$, $M = .1$ and choosing $\alpha = 4$, $b = 0.000005$, then it is obtained that $K = -0.29$. Define

$$F = \begin{bmatrix} -0.29 & 1 \end{bmatrix} T^{-1}, \quad \text{where } T = \begin{bmatrix} -0.71 & 1 \\ 0.71 & 1 \end{bmatrix}$$

The poles of the reduced order system $A_{11} - A_{12}KC_1$ are given by $\begin{bmatrix} -2.5 \pm j0.22 \end{bmatrix}$, and by Proposition 8.1 the states of the reduced order system and the outputs in the ideal sliding mode are ultimately bounded by $\|x_1(t)\| \leq 2.57$, $\|y(t)\| \leq 3.78$ respectively.

Choosing different parameter settings as $\alpha = 0.04$, $b = 5$, $\delta = 0.9$, $\varepsilon = 0.4$, $M = 1$, then a second parameterization of the switching surface is obtained as $\hat{K} = -1.58$. The second switching function is then given by

$$\hat{F} = \begin{bmatrix} -1.58 & 1 \end{bmatrix} T^{-1}$$

The poles of the reduced order sliding mode dynamics $A_{11} - A_{12}\hat{K}C_1$ are $\begin{bmatrix} -1.57, & -3.43 \end{bmatrix}$. The ultimate bounds on the states of the reduced order system and on the outputs in the ideal sliding mode in this case are $\|x_1(t)\| \leq 33.7$ and $\|y(t)\| \leq 89$ respectively. As can be seen, the ultimate bound on the trajectories $\|y(t)\|$ obtained by using K is smaller than that obtained by using $\hat{K}$, and we intuitively expect the first switching function to provide better sliding mode performance than the second. This will be verified in the later simulations.

Having addressed the existence problem and formulated a methodology to prescribe the ideal sliding mode dynamics, it is now necessary to develop a control strategy to ensure the sliding mode is attained.

8.5 Reachability Problem

It is first necessary to perform a coordinate transformation which will express the system dynamics in terms of the states of the reduced order sliding mode dynamics and the dynamics of the sliding variables, $s(t)$. This facilitates solution of the reachability problem. It can be shown [7] that the following system transformation and control structure exist such that $z(t) = T_1 x_r(t)$, where $T_1 = \begin{bmatrix} I_{n-m} & 0 \\ KC_1 & I_m \end{bmatrix}$ so that the system $(\bar{A}, \bar{A}_d, \bar{B}, F\bar{C})$ has the property

$$\bar{A} = \begin{bmatrix} \bar{A}_{11} & \bar{A}_{12} \\ \bar{A}_{21} & \bar{A}_{22} \end{bmatrix} \bar{A}_d = \begin{bmatrix} \bar{A}_{d11} & \bar{A}_{d12} \\ \bar{A}_{d21} & \bar{A}_{d22} \end{bmatrix} \bar{B} = \begin{bmatrix} 0 \\ I_m \end{bmatrix} \bar{B}_1 = \begin{bmatrix} \bar{B}_{11} \\ \bar{B}_{12} \end{bmatrix} F\bar{C} = \begin{bmatrix} 0 & I_m \end{bmatrix} \quad (8.28)$$

where $z_1(t) = x_1(t)$, $z_2(t) = s(t)$. Note that $\bar{A}_{11} = A_{11} - A_{12}KC_1$ and $\bar{A}_{d11} = A_{d11} - A_{d12}KC_1$ exhibit the reduced order sliding-mode dynamics. Also, $\bar{C} = [0 \quad \bar{T}]$, where $\bar{T} \in \mathscr{R}^{p \times p}$ is nonsingular. The control law is defined by

$$u(t) = -Gy(t) - v_y(t) \quad (8.29)$$

where

$$G = \begin{bmatrix} G_1 & G_2 \end{bmatrix} \bar{T}^{-1} \quad (8.30)$$

$$v_y(t) = \begin{cases} \rho \frac{Fy(t)}{\|Fy(t)\|} & \text{if } Fy(t) \neq 0 \\ 0 & \text{otherwise} \end{cases} \quad (8.31)$$

where $G_1 \in \mathscr{R}^{m \times (p-m)}$, $G_2 \in \mathscr{R}^{m \times m}$, $F = \begin{bmatrix} K & I_m \end{bmatrix} T^{-1}$. The uncertain system (8.1) in the z coordinate system becomes

$$\dot{z}(t) = \bar{A}z(t) + \bar{A}_d z(t - \tau(t)) + \bar{B}u(t) + \bar{B}_1 w(t) \quad (8.32)$$

Closing the loop in the system (8.32) with the control law (8.29) yields

$$\dot{z}(t) = A_0 z(t) + \bar{A}_d z(t-\tau(t)) - \bar{B} v_y(t) + \bar{B}_1 w(t) \tag{8.33}$$

where $A_0 = \bar{A} - \bar{B}G\bar{C}$. Let $\bar{P}$ be a symmetric positive definite matrix partitioned conformably with (8.28) so that $\bar{P} = \begin{bmatrix} \bar{P}_1 & 0 \\ 0 & \bar{P}_2 \end{bmatrix}$. It follows that $\bar{P}\bar{B} = (F\bar{C})^T P_2$ and from (8.28) $Fy(t) = z_2(t)$. It can be shown that

$$\begin{aligned} \psi &= \bar{P}A_0 + A_0^T \bar{P} \\ &= \begin{bmatrix} \bar{P}_1\bar{A}_{11} + \bar{A}_{11}^T\bar{P}_1 & \bar{P}_1\bar{A}_{12} + (\bar{A}_{21} - G_1C_1)^T\bar{P}_2 \\ * & \bar{P}_2\bar{A}_{22} + \bar{A}_{22}^T\bar{P}_2 - \bar{P}_2G_2 - (\bar{P}_2G_2)^T \end{bmatrix} \\ &= \begin{bmatrix} \bar{P}_1\bar{A}_{11} + \bar{A}_{11}^T\bar{P}_1 & \bar{P}_1\bar{A}_{12} + \bar{A}_{21}^T\bar{P}_2 - (L_1C_1)^T \\ * & \bar{P}_2\bar{A}_{22} + \bar{A}_{22}^T\bar{P}_2 - L_2 - (L_2)^T \end{bmatrix} \end{aligned} \tag{8.34}$$

where $L_1 = \bar{P}_2G_1$ and $L_2 = \bar{P}_2G_2$. A stability condition for the full order closed loop system can be derived using the following Lyapunov-Krasovskii functional

$$\begin{aligned} V(t) &= z^T(t)\bar{P}z(t) + \int_{t-h}^{t} e^{\bar{\alpha}(s-t)} z^T(s)\bar{E}z(s)ds + \int_{t-\tau(t)}^{t} e^{\bar{\alpha}(s-t)} z^T(s)\bar{S}z(s)ds \\ &+ h\int_{-h}^{0}\int_{t+\theta}^{t} e^{\bar{\alpha}(s-t)} \dot{z}^T(s)\bar{R}\dot{z}(s)dsd\theta \end{aligned} \tag{8.35}$$

where $\bar{E} \geq 0$, $\bar{S} \geq 0$ and $\bar{R} = \begin{bmatrix} \bar{R}_1 & 0 \\ 0 & 0 \end{bmatrix}$ where $\bar{R}_1 \geq 0$ (as it is desired to determine a stability condition for the time delay system which is delay-independent of $z_2(t)$). Then

$$\begin{aligned} \bar{M} &= \dot{V} + \bar{\alpha}V - \bar{b}w^T(t)w(t) \\ &\leq 2z^T(t)\bar{P}\dot{z}^T(t) + \bar{\alpha}z^T(t)\bar{P}z(t) + h^2\dot{z}^T(t)\bar{R}\dot{z}(t) \\ &- [(z(t) - z(t-\tau(t)))^T\bar{R}(z(t) - z(t-\tau(t))) \\ &+ (z(t-\tau(t)) - z(t-h))^T\bar{R}(z(t-\tau(t)) - z(t-h))]e^{-\bar{\alpha}h} \\ &+ z^T(t)(\bar{E} + \bar{S})z(t) - z^T(t-h)\bar{E}z(t-h)e^{-\bar{\alpha}h} \\ &- (1-d)z^T(t-\tau(t))\bar{S}z(t-\tau(t))e^{-\bar{\alpha}\tau(t)} - \bar{b}w^T(t)w(t) \end{aligned} \tag{8.36}$$

Substitute the right-hand side of equation (8.33) into (8.36). Setting $\varsigma(t) = col\{z(t), z(t-h), z(t-\tau(t)), w(t)\}$, then

$$\dot{V}(t) \leq \varsigma(t)^T\Phi_h\varsigma(t) + h^2\dot{z}^T(t)\bar{R}\dot{z}(t) + 2z^T\bar{P}\bar{B}(\bar{B}_{12}w(t) - v_y(t)) < 0 \tag{8.37}$$

is satisfied if $\varsigma^T(t)\Phi_h\varsigma(t) + h^2\dot{z}^T(t)\bar{R}\dot{z}(t) < 0$ and $2z^T\bar{P}\bar{B}(\bar{B}_{12}w(t) - v_y(t)) < 0$, where

$$\Phi_h = \begin{bmatrix} \phi_{11} & 0 & \bar{P}\bar{A}_d + \bar{R}e^{-\bar{\alpha}h} & \begin{bmatrix} \bar{P}_1\bar{B}_{11} \\ 0 \end{bmatrix} \\ * & \phi_{22} & \bar{R}e^{-\bar{\alpha}h} & 0 \\ * & * & -2e^{-\bar{\alpha}h}\bar{R} - (1-d)\bar{S}e^{-\bar{\alpha}h} & 0 \\ * & * & * & -\bar{b}I \end{bmatrix} \tag{8.38}$$

with

$$\phi_{11} = \psi + \bar{\alpha}\bar{P} + \bar{S} + \bar{E} - \bar{R}e^{-\bar{\alpha}h}; \quad \phi_{22} = -(\bar{E} + \bar{R})e^{-\bar{\alpha}h}$$

Setting $\xi(t) = col\{z(t), z(t-h), z(t-\tau(t)), w(t), v_y(t)\}$ and $\overline{I} = \begin{bmatrix} I_{(n-m)} & 0 \end{bmatrix}^T$, it is obtained that

$$\begin{aligned} h^2\dot{z}^T(t)\bar{R}\dot{z}(t) &= [z^T(t)A_0^T + z^T(t-\tau(t))\bar{A}_d^T - v_y^T(t)\bar{B}^T + w^T(t)\bar{B}_1^T]h^2\bar{R}[A_0 z(t) \\ &\quad + \bar{A}_d z(t-\tau(t)) - \bar{B}v_y(t) + \bar{B}_1 w(t)] \\ &= \xi^T(t)\begin{bmatrix} A_0^T \\ 0 \\ \bar{A}_d^T \\ \bar{B}_1^T \\ \bar{B}^T \end{bmatrix} \overline{I}h^2\bar{R}_1\overline{I}^T \begin{bmatrix} A_0^T \\ 0 \\ \bar{A}_d^T \\ \bar{B}_1^T \\ \bar{B}^T \end{bmatrix}^T \xi(t) \end{aligned} \tag{8.39}$$

Using the Schur complement, $\xi^T(t)\Phi_h\xi(t) + h^2\dot{z}^T(t)\bar{R}\dot{z}(t) < 0$ holds if

$$\begin{bmatrix} & & hA_0^T\begin{bmatrix} I_{(n-m)} \\ 0 \end{bmatrix}\bar{R}_1 \\ & & 0 \\ \Phi_h & & h\bar{A}_d^T\begin{bmatrix} I_{(n-m)} \\ 0 \end{bmatrix}\bar{R}_1 \\ & & h\bar{B}_1^T\begin{bmatrix} I_{(n-m)} \\ 0 \end{bmatrix}\bar{R}_1 \\ * * * * & & -\bar{R}_1 \end{bmatrix} < 0 \tag{8.40}$$

for some $\bar{\alpha} > 0$, $\bar{b} > 0$ and $0 \le \tau(t) \le h$, i.e. to ensure the exponential attractiveness of (8.33) to the ellipsoid $z^T(t)\bar{P}z(t) \le \frac{\bar{b}}{\bar{\alpha}}\Delta^2$. Given the control structure in (8.30) then

$$\begin{aligned} &2z^T(t)\bar{P}\bar{B}(\bar{B}_{12}w(t) - v_y(t)) \\ &= 2z_2^T(t)\bar{P}_2(\bar{B}_{12}w(t) - v_y(t)) \\ &\le -2\rho\bar{P}_2\|z_2(t)\| + 2\bar{P}_2\|\bar{B}_{12}\|\|z_2(t)\|\Delta \\ &< 0 \end{aligned}$$

The latter inequality implies exponential attractivity of the ellipsoid $z^T(t)\bar{P}z(t) \le \frac{\bar{b}}{\bar{\alpha}}\Delta^2$, thus for $t \to \infty$, $z^T(t-\tau(t))\bar{P}z(t-\tau(t)) \le \frac{\bar{b}}{\bar{\alpha}}\Delta^2$ holds. The following proposition can now be stated:

Proposition 8.2. *Given scalars $h > 0$, $d < 1$, $\bar{\alpha} > 0$, $\bar{b} > 0$, assume there exist $n \times n$ matrices $\bar{P} = diag\{\bar{P}_1, \bar{P}_2\} > 0$ with $P_2 \in \mathscr{R}^{m\times m}$, $\bar{E} \geq 0$, $\bar{S} \geq 0$, a $(n-m)\times(n-m)$-matrix $\bar{R}_1 \geq 0$, $L_1 \in \mathscr{R}^{m\times(p-m)}$, $L_2 \in \mathscr{R}^{m\times m}$ such that LMI (8.40) is feasible. Then for $\rho > \|\bar{B}_{12}\|\Delta$ the closed-loop system (8.33), where $G_1 = \bar{P}_2^{-1}L_1$, $G_2 = \bar{P}_2^{-1}L_2$, is exponentially attracted to the ellipsoid $z^T(t)\bar{P}z(t) \leq \frac{\bar{b}}{\bar{\alpha}}\Delta^2$ for all $\tau(t) \in [0,h]$. Consequently it also holds that $z^T(t-\tau(t))\bar{P}z(t-\tau(t)) \leq \frac{\bar{b}}{\bar{\alpha}}\Delta^2$ for $t \to \infty$.*

Denote

$$A_0^L = [0\ I_m]A_0;\ \ \bar{A}_d^L = [0\ I_m]\bar{A}_d;\quad \beta = \frac{\bar{b}}{\bar{\alpha}}\Delta^2 \tag{8.41}$$

given $\bar{\delta} > 0$, conditions will now be derived that guarantee the solutions of (8.28) satisfy the bound

$$\|A_0^L z(t)\| + \|A_d^L z(t-\tau(t))\| < \bar{\delta} \tag{8.42}$$

for $t \to \infty$. Note that

$$\begin{aligned} &z^T(t)(A_0^L)^T(A_0^L)z(t) \leq \bar{\delta}_1^2\frac{z^T(t)\bar{P}z(t)}{\beta} \\ &z^T(t-\tau(t))(A_d^L)^T(A_d^L)z(t-\tau(t)) \leq \bar{\delta}_2^2\frac{z^T(t-\tau(t))\bar{P}z(t-\tau(t))}{\beta} \end{aligned} \tag{8.43}$$

where $\bar{\delta} = \bar{\delta}_1 + \bar{\delta}_2$. Hence, the following inequalities hold

$$(A_0^L)^T(A_0^L) \leq \frac{\bar{\delta}_1^2\bar{P}}{\beta};\quad (A_d^L)^T(A_d^L) \leq \frac{\bar{\delta}_2^2\bar{P}}{\beta} \tag{8.44}$$

and, by Schur complements, the following inequalities

$$\begin{bmatrix} -\frac{\bar{\delta}_1^2\bar{P}}{\beta} & (A_0^L)^T \\ * & -I \end{bmatrix} < 0;\quad \begin{bmatrix} -\frac{\bar{\delta}_2^2\bar{P}}{\beta} & (A_d^L)^T \\ * & -I \end{bmatrix} < 0 \tag{8.45}$$

guarantee that for all the solutions, the bound in equation (8.42) holds for $t \to \infty$.

Corollary 8.1. *Given scalars $\bar{\alpha} > 0$, $\bar{b} > 0$, let there exist $n \times n$ matrices $\bar{P} = diag\{\bar{P}_1, \bar{P}_2\} > 0$, $\bar{E} \geq 0$, $\bar{S} \geq 0$, a $(n-m)\times(n-m)$-matrix $\bar{R}_1 \geq 0$, $L_1 \in \mathscr{R}^{m\times(p-m)}$, $L_2 \in \mathscr{R}^{m\times m}$ such that the LMI (8.40) is feasible for $0 \leq \tau(t) \leq h$, $\dot{\tau}(t) \leq d < 1$. Let $\bar{\delta}_1$ and $\bar{\delta}_2$ satisfy (8.45) with the notation given in (8.41). Then for*

$$\rho > \|B_{12}\|\Delta + \bar{\delta} \tag{8.46}$$

an ideal sliding motion takes place on the surface $\mathscr{S}$.

Proof. Substituting the control law it follows from (8.32) that

$$\dot{s}(t) = F\bar{C}A_0 z(t) + F\bar{C}\bar{A}_d z((t-\tau(t)) + (\bar{B}_{12}w(t) - v_y(t))$$

Let $V_c : \mathscr{R}^m \to \mathscr{R}$ be defined by $V_c(s) = 2s^T(t)\bar{P}_2 s(t)$. It follows that

$$\bar{P}_2 F\bar{C}A_0 = \bar{P}_2 A_0^L;\quad \bar{P}_2 F\bar{C}A_d = \bar{P}_2 A_d^L$$

Starting from initial condition $z(t_0)$, it can be verified that there exists $t_1 > 0$ such that for all $t \geq t_1$,

$$\begin{aligned}\dot{V}_c(s) &= 2s^T(t)\bar{P}_2A_0^Lz(t) + 2s^T(t)\bar{P}_2A_d^Lz(t-\tau(t)) + 2s^T(t)\bar{P}_2(\bar{B}_{12}w(t) - v_y(t)) \\ &\leq 2\|s(t)\|\|\bar{P}_2\|(\|A_0^Lz(t)\| + \|A_d^Lz(t-\tau(t))\|) - 2\bar{\delta}\|s(t)\|\|\bar{P}_2\| \\ &< -2\eta\|s(t)\| \end{aligned} \tag{8.47}$$

where $\eta = \bar{\delta} - \|A_0^Lz(t)\| - \|A_d^Lz(t-\tau(t))\|$. A sliding motion will thus be attained in finite time.

□

Example 8.2. Two solutions to the reachability problem will now be performed for the uncertain system (8.25) corresponding to the existence problem solutions proposed in Example 8.1 with K, $\hat{K}$ respectively. A control gain G is designed based on K, which brings the full order closed-loop system into a bounded region centered about the sliding surface. Setting $\bar{\alpha} = 1$, $\bar{b} = 0.004$ in Proposition 8.2, then

$$G = \begin{bmatrix} 6.3, & 1.9 \end{bmatrix}$$

The closed-loop poles of $A - BGC$ are $\begin{bmatrix} -6.3, & -2.5, & -2.4 \end{bmatrix}$. The switching gain $\rho = 2.5$ which is derived from LMI (8.45) will ensure the sliding surface is reached

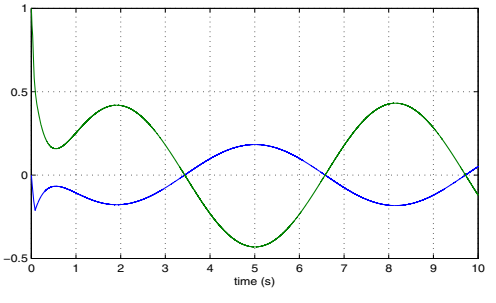

(a) Outputs

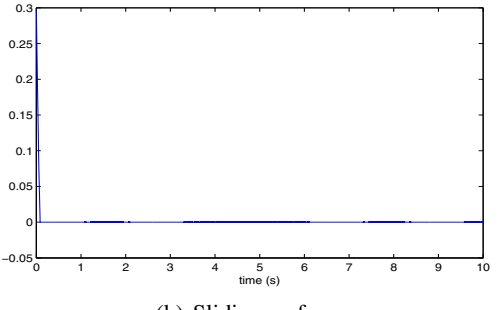

(b) Sliding surface

Fig. 8.1 Closed-loop response of system (8.25) with the first controller

in finite time. It was observed in the simulation that the bound on the reduced order sliding dynamics is $\|x_1(t)\| \leq 0.44$ which compares favourably with the estimated bound $\|x_1(t)\| \leq 2.57$. As may be expected, the theoretical bounds are conservative. Figure 8.1 shows that the outputs of the system are stable with ultimate bound $\|y(t)\| \leq 0.47$ in the simulation plots. The sliding surface is reached in finite time.

Based on $\hat{K}$ with $\bar{\alpha} = 1$, $\bar{b} = 0.004$,

$$\hat{G} = \begin{bmatrix} 55.5, & -18.7 \end{bmatrix}$$

The closed-loop poles of $A - B\hat{G}C$ are $\begin{bmatrix} -34.7, & -3.4, & -1.6 \end{bmatrix}$. The switching gain $\hat{\rho} = 7.23$. It was observed in the simulation that the bound on $\|x_1(t)\| \leq 0.5$ whereas the estimated bound was $\|x_1(t)\| \leq 33.7$. Figure 8.2 shows that the outputs of the system are stable with ultimate bound $\|y(t)\| \leq 1.15$.

Recall from Example 8.1 that the estimated ultimate bound of the closed loop trajectories $\|y(t)\|$ obtained by using K is smaller than that computed for $\hat{K}$. It is thus expected that the ultimate bound on $\|y(t)\|$ will be smaller using K than using $\hat{K}$. This can be verified in Figure 8.1 and Figure 8.2 where the actual bounds on the output $y(t)$ are less using K and both bounds lie within the theoretical predictions.

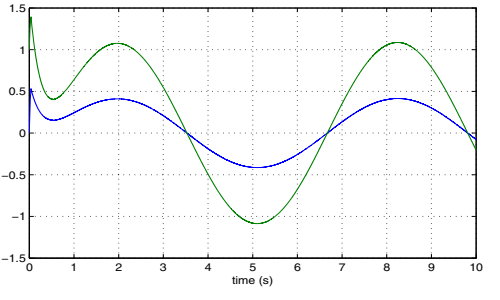

(a) Outputs

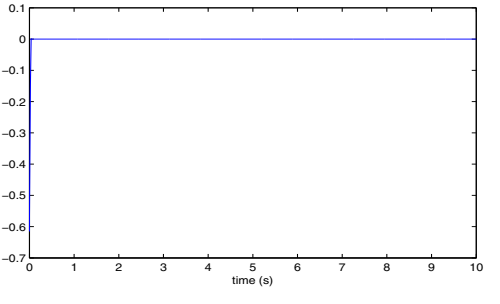

(b) Sliding surface

Fig. 8.2 Closed-loop response of system (8.25) with the second controller

8.6 Liquid Monopropellant Rocket Motor Control

Control of a liquid monopropellant rocket motor with a pressure feeding system is a challenging problem as the system is an unstable, time delay system. When it is stabilised via linear state feedback, the robustness of the system is unsatisfactory and [26] have demonstrated the advantage of applying a state feedback sliding mode control in this regard. The case study presented here will consider output feedback sliding mode control of the system using the methodology described in the chapter.

The model of the liquid monopropellant rocket motor has been previously considered in [26] [24]. The model assumes nonsteady flow and takes account of nonuniform lag to form a linearised model of the combustion chamber and feeding system. The states are given by

$x_1(t)$ relative deviation of the instantaneous combustion chamber pressure from its steady-state value
$x_2(t)$ relative deviation of the instantaneous mass flow upstream of the capacitance from its steady-state value
$x_3(t)$ relative deviation of the instantaneous mass flow rate of the injected propellant from its steady-state value
$x_4(t)$ ratio between the deviation of the instantaneous pressure at a point from its steady-state value and twice the injector pressure drop in steady-state operation

The outputs have been chosen to be the second and fourth states. With the pressure exponent of the combustion process assumed to be 0.8 the system description is given from [24] as

$$A = \begin{bmatrix} -0.2 & 0 & 0 & 0 \\ 0 & 0 & 0 & -1 \\ -1 & 0 & -1 & 1 \\ 0 & 1 & -1 & 0 \end{bmatrix} \; A_d = \begin{bmatrix} -0.8 & 0 & 1 & 0 \\ 0 & 0 & 0 & 0 \\ 0 & 0 & 0 & 0 \\ 0 & 0 & 0 & 0 \end{bmatrix} \; B = \begin{bmatrix} 0 \\ 1 \\ 0 \\ 0 \end{bmatrix} \; C = \begin{bmatrix} 0 & 1 & 0 & 0 \\ 0 & 0 & 0 & 1 \end{bmatrix} \quad (8.48)$$

The transformed system used to solve the existence problem is given by

$$A_r = \begin{bmatrix} -0.2 & 0 & 0 & 0 \\ -1 & -1 & 1 & 0 \\ 0 & -1 & 0 & 1 \\ 0 & 0 & -1 & 0 \end{bmatrix} \; A_{d_r} = \begin{bmatrix} -0.8 & 1 & 0 & 0 \\ 0 & 0 & 0 & 0 \\ 0 & 0 & 0 & 0 \\ 0 & 0 & 0 & 0 \end{bmatrix} \; B_r = \begin{bmatrix} 0 \\ 0 \\ 0 \\ 1 \end{bmatrix} \; C_r = \begin{bmatrix} 0 & 0 & 0 & 1 \\ 0 & 0 & 1 & 0 \end{bmatrix} \quad (8.49)$$

and the reduced subsystem matrices are

$$A_{11} = \begin{bmatrix} -0.2 & 0 & 0 \\ -1 & -1 & 1 \\ 0 & -1 & 0 \end{bmatrix} \; A_{12} = \begin{bmatrix} 0 \\ 0 \\ 1 \end{bmatrix} \; A_{d11} = \begin{bmatrix} -0.8 & 1 & 0 \\ 0 & 0 & 0 \\ 0 & 0 & 0 \end{bmatrix} \; A_{d12} = \begin{bmatrix} 0 \\ 0 \\ 0 \end{bmatrix} \; C_1 = \begin{bmatrix} 0 & 0 & 1 \end{bmatrix} \quad (8.50)$$

Suppose the initial conditions $x(t_0) = \begin{bmatrix} 1, -1, 5, 20 \end{bmatrix}^T$ in the simulation. To construct K for the reduced order system (8.7) according to the Proposition 8.1, the parameter settings in the LMI (8.15) with entries (8.19) are selected with the delay-upperbound $h = 0.82s$ and the rate of change of the time varying delay $\dot{\tau}(t) \leq d = 0.1$. If for $\delta = 40$, $\varepsilon = 0.9$, $M = \begin{bmatrix} 5, 2 \end{bmatrix}$ and choosing $\alpha = 0.1, b = 0.005$, then it is obtained that the LMI variable $K = 6.93$. The sliding function matrix is therefore

$$F = \begin{bmatrix} 1, 6.93 \end{bmatrix}$$

which provides stable sliding mode dynamics where the poles of the non delayed dynamics $A_{11} - A_{12}KC_1$ are

$$\begin{bmatrix} -6.75, -1.17, -0.2 \end{bmatrix} \tag{8.51}$$

Following the solution of the existence problem, which will provide stable sliding mode dynamics, reachability of the sliding surface must be considered. Setting $\bar{\alpha} = 0.04$, $\bar{b} = 2$ in Proposition 8.2, it is obtained that

$$G = \begin{bmatrix} 23.2, 115.5 \end{bmatrix} \tag{8.52}$$

The closed-loop poles of $A - BGC$ are

$$\begin{bmatrix} -15.9, -7.03, -1.25, -0.2 \end{bmatrix} \tag{8.53}$$

A switching gain $\rho = 0.1$, which satisfies the LMI (8.45), will ensure the finite time reachability to the sliding surface, as seen in Figure 8.3, where asymptotic stability of the system outputs is observed.

Control design without taking account of possible occurrences of disturbances can lead to undesirable performance. Unlike matched uncertainties whose effects on the system can be directly rejected by use of an appropriate sliding mode control, unmatched uncertainties or disturbances affect the dynamics in the sliding mode. The corresponding effects on the states may lead to violation of the finite time reachability of the sliding surface as demonstrated below. Assume that the control design above has been performed and an unmatched, unknown but bounded disturbance occurs at $35s$ with disturbance distribution $B_1 = \begin{bmatrix} 1 & 0 & 0 & 0 \end{bmatrix}^T w(t)$ where $\|w(t)\| \leq 2$. Note the value of $w(t)$ is taken to be large enough to demonstrate the potential effect of the disturbance to the system and the advantage of taking knowledge of the disturbance into the design process in the proposed scheme. As can be seen from Fig 8.4, the sliding surface is reached and maintained until $35s$ after which time the dynamic response is disturbed and lies within a boundary of the ideal sliding surface. Outputs become ultimately bounded due to the effects of the unmatched disturbances.

By using knowledge of the unknown but bounded disturbance, then the following design is performed. Construct K for the reduced order system (8.7) with delay

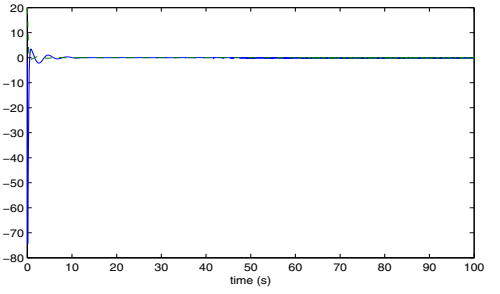

(a) Outputs

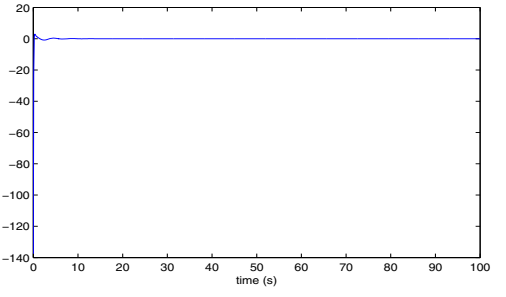

(b) Sliding surface

Fig. 8.3 Closed-loop response of (8.48) with varying delay $\tau(t) \leq 0.82s$

and unmatched disturbance B_1 according to Proposition 8.1. Parameter settings in the LMI (8.15) with entries (8.19) are selected this time the same as for the initial design, where the effects of the disturbance were not considered. Therefore setting delay-upperbound $h = 0.82s$, rate of change of the time varying delay $\dot{\tau}(t) \leq d = 0.1$, $\delta = 40$, $\varepsilon = 0.9$, $M = \begin{bmatrix} 5, 2 \end{bmatrix}$, $\alpha = 0.1$, $b = 0.005$, it is obtained that $K = 7$ and the sliding function matrix is given by

$$F = \begin{bmatrix} 1, 7 \end{bmatrix}$$

The poles of the subsystem $A_{11} - A_{12}KC_1$ are

$$\begin{bmatrix} -6.82, -1.17, -0.2 \end{bmatrix}$$

It is known that the performance of the closed loop system will be affected by both matched and unmatched disturbances during the transient period to the sliding surface, but will be unaffected by matched disturbances after the sliding surface is reached. Therefore taking account the bound of the unmatched disturbance into the LMIs design, a control G with larger gain will be derived which yields a shorter

transient time from the initial states to the sliding surface to minimize the effects of the disturbances. Choose the same setting as before $\bar{\alpha} = 0.04$, $\bar{b} = 2$ in Proposition 8.2, it is obtained that

$$G = \left[2880,\ 20132\right] \tag{8.54}$$

The closed-loop poles of $A - BGC$ are

$$\left[-2873.2,\ -6.8,\ -1.2,\ -0.2\right] \tag{8.55}$$

A switching gain $\rho = 14000$ derived from the LMI (8.45) is seen to be large in order to ensure the finite time reachability condition is satisfied. Figure 8.5 shows that sliding surface is reached in finite time and remains on it afterwards despite the unmatched disturbance. However the outputs of the system still remain ultimately bounded due to the effects of unmatched bounded disturbances with the bound $\|y(t)\| \leq 1.6$. The design proposes a methodology which allows systematic synthesis of a sliding mode control for a system with delay and both matched and unmatched disturbances, through a set of LMIs conditions to derive the switching gain which ensures the finite time reachability of the sliding surface.

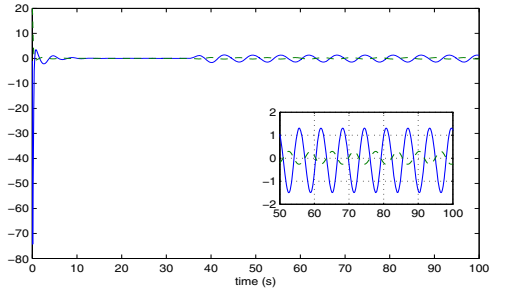

(a) Outputs

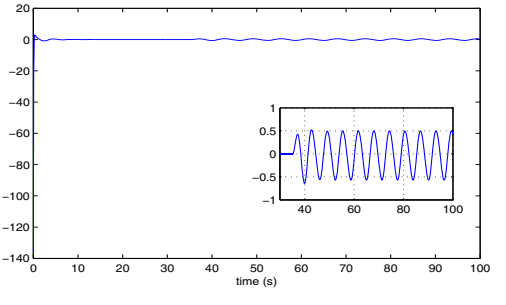

(b) Sliding surface

Fig. 8.4 Closed loop response disturbed by unmatched disturbance $w(t)$ at $t = 35s$

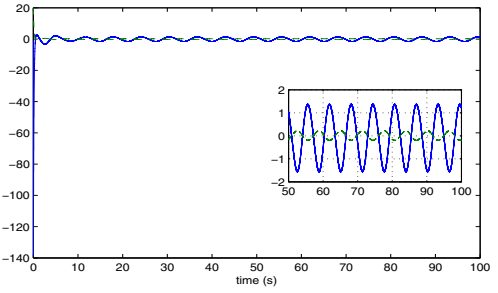

(a) Outputs

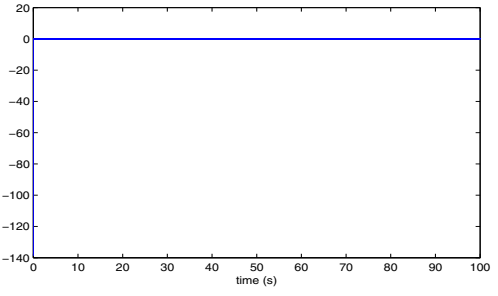

(b) Sliding surface

Fig. 8.5 Closed-loop response of (8.48) with varying delay $\tau(t) \leq 0.82s$ and unmatched disturbance $\|w(t)\| \leq 2$.

8.7 Conclusion

The development of output feedback based sliding mode schemes for systems in the presence of state delay and both matched and unmatched disturbances has been presented. A descriptor Lyapunov functional approach has been used for switching function design. The methodology has been implemented using LMIs and can give desirable static output feedback sliding mode control dynamics with guaranteed ultimate bound. A novel feature of the method is that the switching control gain as well as the switching surface is determined using LMIs. A numerical example as well as an application study on a liquid monopropellant rocket motor demonstrates the methodology and its effectiveness.

References

1. Benton, R.E., Smith, D.A.: A static-output feedback design procedure for robust emergency lateral control of a highway vehicle. IEEE Trans. Automatic Control Syst. Technol. 13, 618–623 (2005)

2. Brockman, M.L., Corless, M.: Quadratic boundedness of nominally linear systems. Int. J. Control 71, 1105–1117 (1998)
3. Cao, Y.Y., Lam, J., Sun, Y.X.: Static output feedback stabilization: An ILMI approach. Automatica 34, 1641–1645 (1998)
4. Choi, H.H.: Variable structure output feedback control for a class of uncertain dynamic systems. Automatica 38, 335–341 (2002)
5. Crusius, C.A.R., Trofino, A.: Sufficient LMI conditions for output feedback control problems. IEEE Trans. Automatic Control 44, 1053–1057 (1999)
6. Edwards, C.: A practical method for the design of sliding mode controllers using linear matrix inequalities. Automatica 40, 1761–1769 (2004)
7. Edwards, C., Akoachere, A., Spurgeon, S.K.: Sliding mode output feedback controller design using linear matrix inequalities. IEEE Trans. Automatic Control 46, 115–119 (2001)
8. Edwards, C., Spurgeon, S.K.: Sliding mode stabilization of uncertain systems using only output information. Int. J. Control 62, 1129–1144 (1995)
9. El-Khazali, R., Decarlo, R.A.: Output feedback variable sturcture controllers. IEEE Trans. Automatic Control 31, 805–816 (1995)
10. Fernando, C., Fridman, L.: Analysis and Design of Integral Sliding Manifolds for Systems With Unmatched Perturbations. IEEE Trans. Automatic Control 51, 853–858 (2006)
11. Fridman, E.: New Lyapunov-Krasovskii functionals for stability of linear retarded and neutral type systems. Systems Control Letters 42, 233–240 (2001)
12. Fridman, E., Dambrine, M.: Control under Quantization, Saturation and Delay: A LMI approach. Automatica 10, 2258–2264 (2009)
13. Fridman, E., Dambrine, M., Yeganefar, N.: On matrix inequalities approach to input to state stability. Automatica 44, 2364–2369 (2008)
14. Gouaisbaut, F., Dambrine, M., Richard, J.P.: Robust control of delay systems: a sliding mode control design via LMI. Systems and Control Letters 46, 219–230 (2002)
15. Han, X., Fridman, E., Spurgeon, S.K., Edwards, C.: On the design of sliding mode static output feedback controllers for systems with state delay. IEEE Trans. Industrial Electronics 56, 3656–3664 (2009)
16. He, Y., Wang, Q.G., Lin, C., Wu, M.: Delay range dependent stability for systems with time-varying delay. Automatica 43, 371–376 (2007)
17. Huang, D., Nguang, S.K.: Robust H_∞ static output feedback control of fuzzy systems: An ILMI approach. IEEE Trans. Syst. 36, 216–222 (2006)
18. Jafarov, E.M.: Robust sliding mode controller design techniques for stabilisation of multivariable time-delay systems with parameter perturbations and external disturbances. International Journal of Systems Science 36, 433–444 (2005)
19. Li, X., DeCarlo, R.A.: Robust sliding mode control of uncertain time delay systems. Int. J. Control 76, 1296–1305 (2003)
20. Shaked, U.: An LPD approach to robust H_2 and H_∞ static output feedback design. IEEE Trans. Automatic Control 48, 866–872 (2003)
21. Seuret, A., Edwards, C., Spurgeon, S., Fridman, E.: Static output feedback sliding mode control design via an artificial stabilizing delay. IEEE Trans. Automatic Control 54, 256–265 (2009)
22. Utkin, V.I.: Sliding Modes in Control and Optimization. Springer, New York (1992)

23. Xiang, J., Wei, W., Su, H.: An ILMI approach to robust static output feedback sliding mode control. Int. J. Control 79, 1930–1935 (2006)
24. Xie, L., Fridman, E., Shaked, U.: Robust H_∞ control of distributed delay systems with application to combustion control. IEEE Trans. Automatic Conrol 46, 1930–1935 (2001)
25. Zak, S.H., Hui, S.: On variable structure output feedback controllers for uncertain dynamic systems. IEEE Trans. Automatic Control 38, 1509–1512 (1993)
26. Zheng, F., Cheng, M., Gao, W.: Variable Structure Control of Time-delay Systems with a Simulation Study on Stabilizing Combustion in Liquid Propellant Rocket Motors. Automatica 31, 1031–1037 (1995)

Chapter 9
Sliding Mode Controller Design: An Input-Output Approach

Hebertt Sira-Ramírez, Alberto Luviano-Juárez, and John Cortés-Romero

Abstract. In this chapter, we propose a new feedback controller design approach for the sliding mode control of a large class of linear switched systems. The method is devoid of state measurements, and it efficiently extends the sliding mode control methodology to traditional input-output descriptions of the plant. The approach is based on regarding the average Generalized Proportional Integral (GPI) output feedback controller design as a guide for defining the sliding mode features. Throughout, it is assumed that the available output signal coincides with the system's flat output, an output capable of completely differentially parameterizing all the variables in the system (inputs, original outputs and state variables) and exhibits no zero dynamics. Encouraging simulation results are presented in connection with a tutorial example. Experimental results are also presented for the trajectory tracking problem on a popular DC-to-DC switched power converter of the "buck" type.

9.1 Introduction

Sliding mode control has undergone a substantial development since its early inception in the former Soviet Union. For a detailed survey of the many early contributions and the fundamental theoretical aspects of this field, the reader is invited to revise the authoritative book by Prof. V. Utkin [2]. Recent books by Edwards and Spurgeon [3] and by Utkin *et al.* [4] depict the breath of the theory and the efficient possibilities for practical applications. Sliding mode control, however, is intimately tied to the state variable formulation of dynamical systems. The need

Hebertt Sira-Raírez · Alberto Luviano-Juárez
Departamento de Ingeniería Eléctrica, Sección de Mecatrónica
Cinvestav IPN, Av. IPN No. 2508, México, D.F.

John Cortés-Romero
Departamento de Ingeniería Eléctrica, Sección de Mecatrónica
Cinvestav IPN, Av. IPN No. 2508, México, D.F.
Universidad Nacional de Colombia, Bogotá, Colombia

L. Fridman et al. (Eds.): Sliding Modes, LNCIS 412, pp. 245–268.
springerlink.com

for often unavailable states, or unmeasured output phase variables, leads to the use of asymptotic observers. These facts substantially limit the applicability of sliding mode control, specially in the realm of nonlinear systems where, we should recall, asymptotic observers represent an issue which has not been entirely resolved. A contribution towards using sliding mode control without state measurements was given by H. Sira-Ramírez and R. Silva-Ortigoza [5] in the context of *sigma-delta* modulation. In this approach to sliding mode control, an average output feedback controller design is produced which induces a desirable closed loop behavior. This closed loop behavior is enforced as the zero dynamics of an exogenous sliding mode behavior, imposed on a first order nonlinear dynamics defining the sigma-delta modulator. These devices were commonly used in communications systems for translating continuous signals into discrete valued signals (See the pioneering work of Steele [6], and the book by Norsworthy *et al.* [7] for the natural implications in analog to digital conversion. The output of the modulator is, thus, the switching input signal directly affecting the plant. The robustness, or lack thereof, of the average design is directly bestowed on the sigma-delta modulation implementation.

In this chapter, we propose a robust Generalized Proportional Integral (GPI) approach for sliding mode controller design on switched systems. GPI control has been established as an efficient linear control technique that circumvents the need for asymptotic observers (See Fliess *et al.* [8]) and it has been shown, in [5], to be intimately related to classical compensator networks design. Here, we advocate the creation of sliding motion behavior on a sliding surface obtained by integration from the explicit expression of the robust average GPI feedback control input. The average input is to be viewed as a desirable *equivalent control*, which is a fundamental concept in sliding mode control, (Utkin [2]). The proposed method does not resort to asymptotic state observers and efficiently extends the sliding mode control methodology to traditional input-output, frequency domain, descriptions of the average model of the given switched plant. The underlying design task reduces to that of a robust average output feedback control scheme and it is found to be intimately related to the sigma-delta modulation scheme. The proposed GPI approach to sliding mode design is based on a key observation regarding the switched control interpretation of the robust GPI controller designed for the smooth regulation of the average model of the given switched plant. Our proposal states that the average GPI controller design is to be viewed as an equivalent control, arising from an ideal sliding dynamics, whose corresponding sliding surface coordinate function is to be determined. The resulting sliding surface coordinate function turns out to be a low pass filtered stable output tracking error differential polynomial. The main limitation of the new approach lies in the assumption that the available output signal coincides with the system's flat output (See Fliess *et al.* [9], and also Sira-Ramírez and Agrawal [10]) and, hence, the underlying average linear system is, both, controllable and, also, observable from this special output. Nevertheless, this limitation is easily lifted in the more general case of minimum phase, input-output, systems with unavailable flat outputs. A simulation examples is presented, and, also, an experimental result is reported solving a trajectory tracking problem on a popular DC-to-DC power converter of the "buck" type.

Section 9.6 contains an introductory example which presents, in a tutorial fashion, the fundamental idea behind the GPI based sliding mode control design methodology. Generally speaking, there exist two alternative approaches for the average robust GPI controller design: an observer-free approach and a GPI observer-based approach. Here we explain and develop both design approaches. Section 9.4 presents a simulation example directly applying the results of the tutorial example in Section 9.6. Section 9.5 deals with the design of a sliding mode controller for a "buck" converter plant in a trajectory tracking task within a DC to AC output voltage conversion scheme and presents the corresponding experimental results. The conclusions and suggestions for further work are collected at the end of the chapter.

9.2 An Introductory Example

Consider a perturbed, switched controlled, third order integrating plant of the form:

$$y^{(3)} = \kappa u + \xi(t),\ u \in \{0,1\} \tag{9.1}$$

where u is a discrete valued signal representing a switching action taking values in the discrete set $\{0,1\}$. The perturbation input signal, $\xi(t)$, is completely unknown but uniformly, absolutely, bounded by some real number *a priori* unknown. The parameter κ is assumed to be a known scalar constant.

Suppose it is desired to track a given smooth reference trajectory $y^*(t)$ from arbitrary initial conditions based, solely, on the knowledge of the control input u and of the output y.

We set, in relation to the given switched controlled plant, the following perturbed *average system* model in which u is replaced by a smooth signal u_{av} bounded in the closed interval $[0,1]$ of the real line, and the corresponding output signal is replaced by y_{av}. In other words, we set the perturbed average system as,

$$y_{av}^{(3)} = \kappa u_{av} + \xi(t),\ \ u_{av} \in [0,1] \tag{9.2}$$

We now pose, on the perturbed average system model (9.2), the problem of accurately tracking the given smooth reference signal, $y^*(t)$, via a suitable output feedback control design, in spite of the unkwnon but bounded perturbation input $\xi(t)$. It is further assumed that the viability of tracking the given reference signal, $y^*(t)$, is assessed by the fact that the corresponding (unperturbed) open loop average control input, $u_{av}^*(t)$, off-line computed as: $u_{av}^*(t) = \ddot{y}^*(t)$, is comfortably bounded by the closed interval $[0,1]$. Note that the nominal average control input must ignore, for lack of knowledge, the presence of the perturbation input.

9.2.1 An Average GPI Controller Design Devoid of Observers

A GPI controller for the tracking of the reference signal, $y^*(t)$, in the average system (9.2) proceeds as follows:

1) Compute the open loop, perturbed, average tracking error dynamics as,

$$e_{y,av}^{(3)} = \kappa e_{u,av} + \xi(t) \tag{9.3}$$

where $e_{y,av} = y_{av} - y^*(t)$ and $e_{u,av} = u_{av} - u_{av}^*(t)$. We denote, henceforth, $u_{av}^*(t)$ simply as $u^*(t)$.

2) Build a robust linear output feedback controller for the average system, under the assumption that the perturbation input, $\xi(t)$, exhibits negligible higher order derivatives, say, of fourth order, thus it may be locally approximated by an arbitrary element of a family of fixed, third degree, Taylor time-polynomial. The robust GPI controller is then given by,

$$e_{u,av} = -\frac{1}{\kappa}\left[\frac{k_6 s^6 + k_5 s^5 + \cdots + k_1 s + k_0}{s^4(s^2 + k_8 s + k_7)}\right] e_{y,av} \tag{9.4}$$

The closed loop tracking error system is thus, dominantly, governed by the slightly right-hand-side perturbed version of the following linear, homogeneous, system,

$$e_{y,av}^{(9)} + k_8 e_{y,av}^{(8)} + \cdots + k_1 \dot{e}_{y,av} + k_0 e_{y,av} = 0 \tag{9.5}$$

whose coefficients may be readily determined so that $e_{y,av}(t)$ asymptotically, exponentially decays to zero in an ideal fashion. However, due to the presence of the small residual of the perturbation input, not completely canceled by the fourth order derivation operation explicitly appearing in the denominator of the proposed controller (9.4), one may only guarantee asymptotic exponential convergence to the interior of a disk, of small radius, in the average tracking error phase space. The radius of this disk can be made as small as desired by choosing the set of gains: $\{k_8, k_7, \ldots, k_1, k_0\}$, so that the roots of the corresponding characteristic polynomial to (9.5) are located *deep* into the left half of the complex plane.

The figure below depicts the interpretation of (9.4) as a block diagram where a saturation block has been included to emphasize the fact that: $u_{av} \in [0, 1]$.

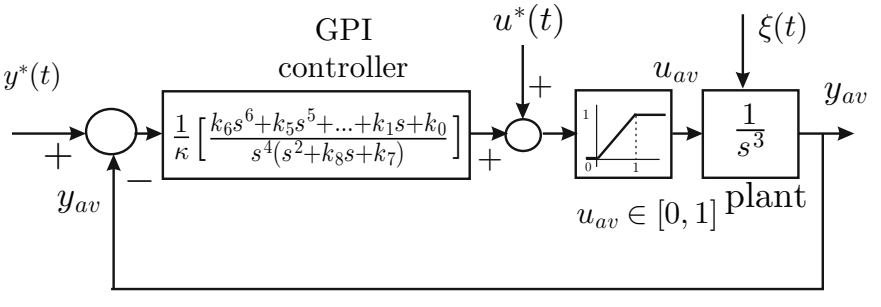

Fig. 9.1 GPI average control scheme for a third order perturbed integrator plant.

Letting z be defined as

$$z = -\frac{1}{\kappa}\left[\frac{1}{s^4(s^2+k_8 s+k_7)}\right](y_{av}(s)-y^*(s)) \tag{9.6}$$

Let u_δ, be suggestive of a correction input term, complementing the faulty nominal control input $u^*(t)$ and actually representing the *output* of the linear compensator acting on the output error signal: $-(y_{av}-y^*(t))/\kappa$. We have,

$$u_{av}-u^*(t) = u_\delta = k_6\dot{z}_6 + k_5 z_6 + \cdots + k_1 z_2 + k_0 z_1 \tag{9.7}$$

where,

$$\begin{aligned}
\dot{z}_1 &= z_2\\
\dot{z}_2 &= z_3\\
&\vdots\\
\dot{z}_5 &= z_6\\
\dot{z}_6 &= -k_8 z_6 - k_7 z_5 - \frac{1}{\kappa}(y_{av}-y^*(t))\\
z &= z_1
\end{aligned} \tag{9.8}$$

In terms of a canonical state space realization of the dynamic output feedback controller (9.4), the average control input, u_{av}, results in the following expression:

$$\begin{aligned}
u_{av} = {} & u^*(t) + (k_5 - k_6 k_8)z_6 + (k_4 - k_6 k_7)z_5 + k_3 z_4 + k_2 z_3 + k_1 z_2 + k_0 z_1\\
& -\frac{k_6}{\kappa}(y_{av}-y^*(t))
\end{aligned} \tag{9.9}$$

It is convenient to take all the initial conditions of the dynamic output feedback controller to be zero.

Since the average controller is a high-gain controller one easily avoids large transients leading to possible controller output saturations by smoothly "clutching" the output reference trajectory, $y^*(t)$, via multiplication by a smooth interpolating polynomial factor of the Bézier type. A second alternative, with similar effects, is based on the traditional *anti-reset windup* strategy applied to the multiple integration term in the controller (See Aström and Murray [11]), for enlightening details)

9.2.2 A Switched Control Interpretation of the Average Design

As far as the control of the switched system (9.1) is concerned, we would like to bestow, or, somehow, impose, on its sliding mode controlled closed loop system, the nice average asymptotic stability features of the previously designed average GPI dynamical feedback controller in an *equivalent control* sense. One may then regard the average control input, u_{av}, as an equivalent control, u_{eq}, whose corresponding sliding surface coordinate function, σ, needs to be determined. Thus we let, for the switched system,

$$u_{eq} = u^*(t) + (k_5 - k_6 k_8) z_6 + (k_4 - k_6 k_7) z_5 + k_3 z_4 + k_2 z_3 + k_1 z_2 + k_0 z_1 - \frac{k_6}{\kappa}(y - y^*(t)) =: u^*(t) + u_\delta \tag{9.10}$$

where y_{av} has been replaced by the actual system output y. Clearly, the equation generating the equivalent control, u_{eq}, arises, primarily, from the well known *invariance condition*: $\dot{\sigma} = 0$, particularized at $\sigma = 0$. We thus find, via a single integration operation, with zero initial conditions on the controller state variables: z_j, $j = 1, ..., 6$, the following convenient integral expression for the sliding surface coordinate function σ:

$$\sigma = \int_0^t [u^*(\tau) + u_\delta(\tau) - u] \, d\tau \tag{9.11}$$

In other words,

$$\dot{\sigma} = u^*(t) + u_\delta - u = u_{av}(t) - u \tag{9.12}$$

It is assumed that the sum, $u^*(t) + u_\delta$, that we still, abusively, call: $u_{av}(t)$, is uniformly bounded by the interval $[0, 1]$. It is, then, easy to establish the existence of a sliding regime on the *zero level set* of the sliding surface coordinate function, σ, i.e., on $\sigma = 0$. For this, we propose to use the following discontinuous feedback control strategy for the switched control input u.

$$u = \frac{1}{2}[1 + \text{sign } \sigma] \tag{9.13}$$

which precisely corresponds to the feedback control scheme shown in Figure 9.2. Note that, from (9.12) and (9.13), if and only if, $0 < u_{av}(t) = u^*(t) + u_\delta < 1$, then,

$$\sigma \dot{\sigma} = \sigma \left(u_{av}(t) - \frac{1}{2}[1 + \text{sign } \sigma] \right) < 0 \tag{9.14}$$

and a sliding regime exists on $\sigma = 0$ (See Utkin [2]).

It is easy to see that the three integrations in the block diagram of Figure 9.2 can be equivalently carried out with a single integration performed just before the switching law inside the nonlinear block synthesizing the actual control input u. The scheme shown in Figure 9.3 entirely coincides with the $\Sigma - \Delta$ modulation implementation of the average GPI controller on the switched system as advocated in Sira-Ramírez and Ortigoza (see [12] and, also, [5]).

9.2.3 A GPI Observer Based Approach

Consider, again, the average output trajectory tracking error perturbed system, treated in the previous section,

$$e_{y,av}^{(3)} = \kappa e_{u,av} + \xi(t) \tag{9.15}$$

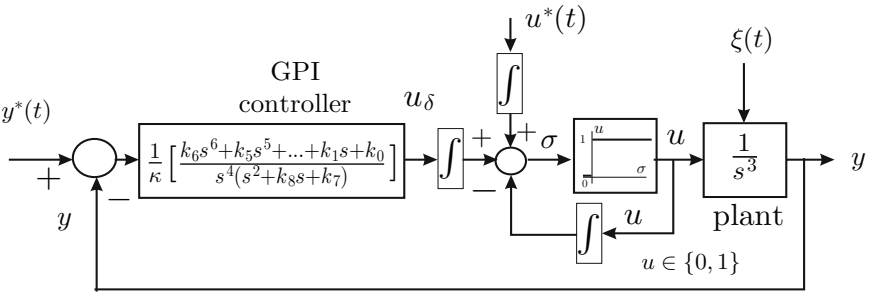

Fig. 9.2 GPI based sliding mode control scheme for a third order switched perturbed integrator plant.

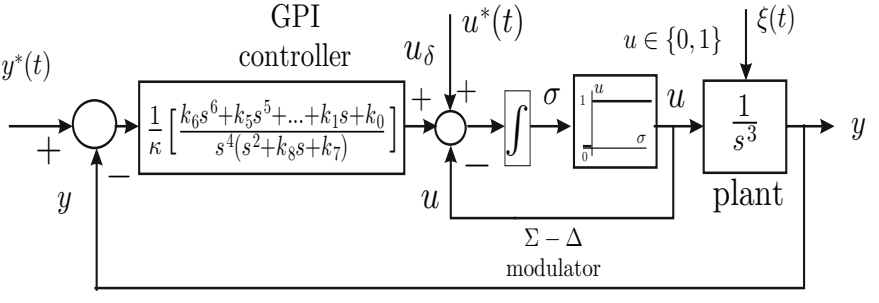

Fig. 9.3 GPI based $\Sigma-\Delta$ sliding mode control scheme for a third order switched perturbed integrator plant.

Independently of the structural nature of, $\xi(t)$, regarding a possible state dependent nature, or its characterization as a purely exogenous time disturbance input, we regard $\xi(t)$ as a smooth, uniformly absolutely bounded time input signal which, as in the previous developments, is treated as an arbitrary element of a family of local, fixed degree, Taylor time-polynomial inputs. The fundamental difference is that instead of attempting a direct canceling of this input from a controller with sufficient integrations, we now attempt to on-line estimate the signal, $\xi(t)$, by means of a, sufficiently high gain, asymptotic linear observer. This observer, however, is equipped with an internal self-updating local internal model of, $\xi(t)$, of polynomial character and of fixed order. As before, we take this polynomial to be a fourth degree time polynomial denoted by the variable z_1. Clearly, we assume that, ideally, in the adopted model, $z_1^{(4)} = 0$. However, for analysis purposes on the effects of the actual perturbation input, we take: $z_1^{(4)} = \varphi^{(4)}(t)$, to be a uniformly, absolutely, bounded signal.

We thus consider the state space representation of the average tracking error perturbed dynamics, (9.15). The state space model is, thus,

$$\begin{aligned}
\dot{e}_1 &= e_2 \\
\dot{e}_2 &= e_3 \\
\dot{e}_3 &= \kappa e_{u,av} + z_1 \\
\dot{z}_1 &= z_2 \\
\dot{z}_2 &= z_3 \\
\dot{z}_3 &= z_4 \\
\dot{z}_4 &= 0
\end{aligned} \tag{9.16}$$

where $e_1 = e_{y,av}$, $e_2 = \dot{e}_{y,av}$, $e_3 = \ddot{e}_{y,av}$ and where the observer signal, z_1, locally approximates $\varphi(t)$ in a fixed degree time-polynomial fashion.

An asymptotic observer for the given tracking error dynamics, based on the model (9.16), is just given by

$$\begin{aligned}
\dot{\hat{e}}_1 &= \hat{e}_2 + \lambda_6(e_1 - \hat{e}_1) \\
\dot{\hat{e}}_2 &= \hat{e}_3 + \lambda_5(e_1 - \hat{e}_1) \\
\dot{\hat{e}}_3 &= \kappa e_{u,av} + \hat{z}_1 + \lambda_4(e_1 - \hat{e}_1) \\
\dot{\hat{z}}_1 &= \hat{z}_2 + \lambda_3(e_1 - \hat{e}_1) \\
\dot{\hat{z}}_2 &= \hat{z}_3 + \lambda_2(e_1 - \hat{e}_1) \\
\dot{\hat{z}}_3 &= \hat{z}_4 + \lambda_1(e_1 - \hat{e}_1) \\
\dot{\hat{z}}_4 &= \lambda_0(e_1 - \hat{e}_1)
\end{aligned} \tag{9.17}$$

Let $\tilde{e}_1 = \tilde{e} = e_1 - \hat{e}_1 = e_{y,av} - \hat{e}_1$, denote the, redundant, observer reconstruction error of the average output tracking error e_1. Also, let $\tilde{z}_1 = \varphi(t) - \hat{z}_1$ denote the actual disturbance reconstruction error, associated with the signal $z_1 = \varphi(t)$. Clearly, $\tilde{z}_2 = \dot{\varphi}(t) - \hat{z}_2$, etc. The reconstruction error evolves according to,

$$\begin{aligned}
\dot{\tilde{e}}_1 &= \tilde{e}_2 - \lambda_6\tilde{e}_1 \\
\dot{\tilde{e}}_2 &= \tilde{e}_3 - \lambda_5\tilde{e}_1 \\
\dot{\tilde{e}}_3 &= \tilde{z}_1 - \lambda_4\tilde{e}_1 \\
\dot{\tilde{z}}_1 &= \tilde{z}_2 - \lambda_3\tilde{e}_1 \\
\dot{\tilde{z}}_2 &= \tilde{z}_3 - \lambda_2\tilde{e}_1 \\
\dot{\tilde{z}}_3 &= \tilde{z}_4 - \lambda_1\tilde{e}_1 \\
\dot{\tilde{z}}_4 &= \varphi^{(4)}(t) - \lambda_0\tilde{e}_1
\end{aligned} \tag{9.18}$$

$$\tilde{e}^{(7)} + \lambda_6\tilde{e}^{(6)} + \lambda_5\tilde{e}^{(5)} + \lambda_4\tilde{e}^{(4)} + \lambda_3\tilde{e}^{(3)} + \lambda_2\tilde{e}^{(2)} + \lambda_1\tilde{e}^{(1)} + \lambda_0\tilde{e} = \varphi^{(4)}(t) \tag{9.19}$$

It follows that if $\varphi^{(4)}(t)$ is an absolutely, uniformly, bounded time signal, and provided the choice of the design parameters $\{\lambda_7, ..., \lambda_0\}$, is made in such a manner that the roots of the associated characteristic polynomial in the complex variable s,

$$p_o(s) = s^7 + \lambda_6 s^6 + \lambda_5 s^5 + \lambda_4 s^4 + \lambda_3 s^3 + \lambda_2 s^2 + \lambda_1 s + \lambda_0 \tag{9.20}$$

are located deep into the left half of the complex plane, then the reconstruction error trajectories, $\tilde{e}_1(t) = \tilde{e}(t)$, and those of its time derivatives, converge towards a small as desired disk, of radius ε, around the origin of the observer reconstruction error state space. In fact, the quantity, ε, is inversely related to the modulus of the smallest assigned root of $p_o(s)$ (see [1] for details). Clearly, if $\tilde{e}$ and its time derivatives, $\tilde{e}^{(i)}$, $i = 1,2,...$, can be made uniformly absolutely bounded, in a small as desired neighborhood of the origin, then the difference: $\tilde{z}_1 = \varphi(t) - z_1 = \tilde{\dot{e}}_3 + \lambda_4 \tilde{e}_1$ is also uniformly, absolutely, bounded by a small positive constant. This means that, z_1, closely estimates, $\varphi(t)$, for appropriately chosen observer design constants. Moreover, respectively $\hat{e}_j, j = 2,3$ closely reconstructs the tracking error derivatives, e_j, $j = 2,3$. This information, provided by the GPI observer, is most useful in the construction of an average output tracking error based dynamical feedback controller.

The average feedback controller is then proposed to be:

$$e_{u,av} = \frac{1}{\kappa}\left[-\hat{z}_1 - k_2\hat{e}_3 - k_1\hat{e}_2 - k_0 e_1\right] \tag{9.21}$$

After convergence of the estimated tracking error derivatives to a small neighborhood of their actual values, the average closed loop system is approximately governed by the following dynamics

$$e^{(3)}_{y,av} + k_2\ddot{e}_{y,av} + k_1\dot{e}_{y,av} + k_0 e_{y,av} = \varphi(t) - \hat{\varphi}(t) + \zeta(t) \tag{9.22}$$

where $\zeta(t)$ summarizes the joint contribution of the tracking error derivatives small estimation errors. It follows that if the average feedback control gains: $\{k_2, k_1, k_0\}$, are chosen in such a manner that the roots of the associated characteristic polynomial,

$$p_c(s) = s^3 + k_2 s^2 + k_1 s + k_0 \tag{9.23}$$

are located deep into the left half of the complex plane, then the average tracking error $e_{y,av}$ and its time derivatives, converge towards a small as desired disk around the origin of the tracking error state space where all tracking error trajectories remain uniformly, absolutely, bounded. As a consequence, the output, $y(t)$, of the system closely follows the given output reference trajectory, $y^*(t)$.

The average control input is then expressed as:

$$u_{av} = u^*(t) - \frac{1}{\kappa}\left[\hat{z}_1 + k_2\hat{e}_3 + k_1\hat{e}_2 + k_0 e\right] = u^*(t) - u_\delta \tag{9.24}$$

where u_δ is the dynamic feedback correction term, complementing the nominal control input $u^*(t)$.

Interpreting, as in the previous section, the average control input as the equivalent control of a sliding regime defined on a certain sliding surface coordinate function σ, yet to be determined, a viable expression from where the equivalent control input might have been solved for, is given by the invariance condition:

$$\begin{aligned}\dot{\sigma} &= -u + u^*(t) - \frac{1}{\kappa}\left[\hat{z}_1 + k_2\hat{e}_3 + k_1\hat{e}_2 + k_0 e\right] \\ &= -u + u^*(t) - u_\delta = 0 \end{aligned} \tag{9.25}$$

We denote, with an abuse of notation, $u_{av} = u^*(t) - u_\delta$. We assume that, in steady state, $u_{av}(t)$ is uniformly bounded within the closed interval, $[0,1]$, of the real line.

The sliding surface coordinate signal is obtained via direct integration, with respect to time, of the previous expression. We have

$$\sigma = \int_0^t \left[u_{av}(\tau) - u\right] d\tau \tag{9.26}$$

In the immediate vicinity of the sliding surface $\sigma = 0$, one has

$$\sigma\dot{\sigma} = \sigma\left(u_{av}(t) - u\right) \tag{9.27}$$

The fact that, uniformly in time, $u_{av}(t)$ satisfies: $0 < u_{av}(t) < 1$, then, the choice,

$$u = \frac{1}{2}(1 + \operatorname{sign}\sigma) \tag{9.28}$$

guarantees that sufficiently close to the sliding surface $\sigma = 0$, the inequality, $\sigma\dot{\sigma} < 0$, is satisfied and a sliding regime exists on $\sigma = 0$, in finite time.

As a consequence of the sliding motion, occurring in finite time, on the exogenous sliding surface $\sigma = 0$, the invariance condition: $\dot{\sigma} = 0$, is ideally satisfied. As a consequence, the equivalent control input, u_{eq}, associated with this exogenous sliding motion, is given by

$$u_{eq} = u_{av} = u^*(t) - u_\delta \tag{9.29}$$

The crucial importance of the average controller design becomes clear, as it represents the equivalent control of the sliding motions taking place on $\sigma = 0$. The ideal sliding dynamics, corresponding to the sliding regime on $\sigma = 0$, coincides with the average closed loop controlled responses.

9.3 Definitions and Main Results

Let $x \in \mathbb{R}^n$ and $u \in \{0,1\}$. Consider the linear, time-varying, switched, system: $\dot{x} = A(t)x + b(t)u$, $y = c(t)x$, with $A(t)$, $b(t)$ and $c(t)$ matrices of appropriate dimensions, whose elements take values in the set of continuous functions defined on the real line. We define the average system associated with the switched system the system described by $\dot{z} = A(t)z + b(t)u_{av}$, $y_{av} = c(t)z$, where u_{av} is a continuous function bounded in the closed interval $[0,1]$. Under such circumstances, the vector z represents the averaged state function corresponding to x and the average output y_{av} corresponds with y.

We say the switched system, $\dot{x} = A(t)x + b(t)u$, $y = c(t)x$, is, on the average, uniformly controllable and uniformly observable if the pairs $(A(t), b(t))$ and $(c(t), A(t))$

are, respectively, uniformly controllable and uniformly observable pairs, i.e., if $\dot{z} = A(t)z + b(t)u_{av}$, $y_{av} = c(t)z$ is uniformly controllable and uniformly observable with u_{av} unrestricted. We assume, however, that the uniform controllability property locally holds when the values of the average control input, $u_{av}(t)$, are uniformly bounded within the compact interval $[0,1]$.

The system $\dot{z} = A(t)z + b(t)u_{av}$, $y = c(t)z$ is said to flat, with flat output y, if all the components of the state functions $z(t)$ and the unrestricted control input u_{av} are parameterizable in terms of y and a finite number of its time derivatives. Flatness is equivalent to uniform controllability. Moreover, the system is uniformly observable from the flat output.

We generalize the developments in the example of the previous section as follows:

Proposition 9.1. *We are given an n-dimensional, single-input single-output (SISO), switched, linear, on the average uniformly observable, and uniformly controllable system of the form,*

$$\dot{x} = A(t)x + b(t)u + \zeta(t), \;\; y = c(t)x \tag{9.30}$$

where $x \in \mathbb{R}^n$, $u \in \{0,1\}$ and $\zeta(t)$ is an "unmatched", smooth, external perturbation input (i.e., $\zeta(t)$ is not in the image of $b(t)$). Let the output, y, be a flat output *of the system,. Under such circumstances, consider the associated simplified average scalar input-output system,*

$$y^{(n)} = \kappa(t)u_{av} + \xi(t) \tag{9.31}$$

where $\xi(t)$ is a, possibly, state dependent perturbation input, including the effect of the unmatched external perturbation inputs $\zeta(t)$. and assumed to be locally approximated by a Taylor time-polynomial model of degree m. The perturbation input $\xi(t)$ is, hence, assumed to exhibit finitely uniformly, absolutely, bounded time derivatives beyond, and including, the order m. Suppose it is desired to have the output y of the system, track a given smooth output reference trajectory $y^*(t)$, within a small as desired error $e_y(t) = y(t) - y^*(t)$, i.e., the tracking error $e_y(t)$ is to uniformly remain absolutely bounded by a small, constant, quantity ε, i.e., $|e_y(t)| < \varepsilon$. Let $u^*(t)$ denote the unperturbed nominal input trajectory, faulty computed as $u^*(t) = \frac{1}{\kappa(t)}[y^*(t)]^{(n)}$. Then, the following scalar controller, written, with an abuse of notation combining signals in the frequency domain and in the time domain, as:

$$u_{av} = u^*(t) - \frac{1}{\kappa(t)}\left[\frac{k_{n+m}s^{n+m} + \cdots + k_1 s + k_0}{s^{m+1}(s^{n-1} + k_{2n+m-1}s^{n-2} + \cdots + k_{n+m+1})}\right](y - y^*(t)) \tag{9.32}$$

asymptotically exponentially, uniformly, forces the closed loop system trajectories to converge towards the interior of a disk, centered around the origin in the tracking error space of phase coordinates, provided the set of coefficients: $\{k_{2n+m-1}, ..., k_1, k_0\}$, are chosen in such a way that the polynomial, $p(s)$, in the complex variables s, defined by,

$$p(s) = s^{2n+m} + k_{2n+m-1}s^{2n+m-2} + \cdots + k_1 s + k_0 \tag{9.33}$$

is a Hurwitz polynomial, with roots located well to the left of the imaginary axis of the complex plane.

The switched implementation of the above average output feedback controller is carried out through a $\Sigma - \Delta$ modulator. All robustness features of the average design are bestowed into the switched implementation through the corresponding ideal sliding dynamics.

Proof. The proof is obtained by direct calculation of the closed loop system perturbed characteristic differential equation. Notice that uniform local controllability of the average system prevents the scalar function $\kappa(t)$ to cross, or adopt in any open interval of time, the value of zero. Hence, multiplicative cancelation of $\kappa(t)$, by its inverse, is a uniformly well defined operation. We have, with $k_{2n+m} = 1$,

$$e_y^{2n+m} + k_{2n+m-1} e_y^{2n+m-2} + \cdots + k_1 \dot{e}_y + k_0 e_y = \sum_{j=0}^{n} k_{2n+m-j} \frac{d^{m+n-j}}{dt^{m+n-j}} \xi(t)$$

In accordance with the assumption that $\xi(t)$ is locally approximated by an element of a family of Taylor time-polynomials of fixed degree m, we have that time derivatives beyond the order m result in a small perturbation input exciting the left hand side of the closed loop dynamics of the system. As long as the roots of the dominant closed loop characteristic polynomial, $p(s)$, are chosen to lay sufficiently far into the left half of the complex plane, the time response of the output of the closed loop system converges, in an asymptotically exponential fashion, to a small disk around the origin of the tracking error phase space. The larger the modulus of the imposed closed loop system poles, the smaller the neighborhood delimited by the disk around the origin. The details of the proof may be found in [1]. The second part of the proposition follows from well known results about $Sigma - \Delta$ modulation in sliding mode control (see [12] and [5] for details). □

A second possibility, already explored in the previous section, is to implement a traditional average state feedback controller, through a GPI observer, which simultaneously estimates the state dependent plus external perturbation input and allows its efficient on-line cancelation in a rather approximate manner. We state the result as follows:

Proposition 9.2. *Suppose all hypothesis on the given switched system remain valid. Consider, as before, the non-phenomenological average model of a linear time-varying, non-matching, externally perturbed switched system,*

$$y^{(n)} = \kappa(t) u_{av} + \xi(t)$$

where $\xi(t)$ is a, possibly, state dependent perturbation input, including the effect of the unmatched external perturbation inputs $\zeta(t)$. Let e_1 denote the tracking error $(y - y^*(t))$, $e_2 = \dot{e}_1$, $e_3 = \ddot{e}_1$, etc. Then, the following scalar estimated state average feedback controller:

$$u_{av} = u^*(t) - \frac{1}{\kappa(t)}\left[\hat{z}_1 + k_{n-1}\hat{e}_n + \ldots + k_1\hat{e}_2 + k_0 e_1\right] \tag{9.34}$$

with coefficients chosen so that the roots of the associated characteristic polynomial $p_c(s)$ *given by*

$$p_c(s) = s^n + k_{n-1}s^{n-1} + \ldots + k_1 s + k_0 \tag{9.35}$$

and variables $\hat{e}_j$*, j=2,...n-1, given by the following observer,*

$$\begin{aligned}
\dot{\hat{e}}_1 &= \hat{e}_2 + \lambda_{n+m-1}(e_1 - \hat{e}_1)\\
\dot{\hat{e}}_2 &= \hat{e}_3 + \lambda_{n+m-2}(e_1 - \hat{e}_1)\\
&\vdots =\\
\dot{\hat{e}}_n &= \hat{e}_{n-1} + \kappa(t)u + \hat{z}_1 + \lambda_m(e_1 - \hat{e}_1)\\
\dot{\hat{z}}_1 &= \hat{z}_2 + \lambda_{m-1}(e_1 - \hat{e}_1)\\
&\vdots =\\
\dot{\hat{z}}_{m-1} &= \hat{z}_{m-2} + \lambda_1(e_1 - \hat{e}_1)\\
\dot{\hat{z}}_m &= \lambda_0(e_1 - \hat{e}_1)
\end{aligned} \tag{9.36}$$

asymptotically exponentially, uniformly, forces the tracking error estimates, $\hat{e}_1$*,...,*$\hat{e}_n$*, and the disturbance estimate,* $\hat{z}_1$*, to converge arbitrarily close towards the actual corresponding values of the tracking errors, its time derivatives and the actual disturbance signal* $\xi(t)$*. In other words, the estimation errors, of the tracking errors, converge towards the interior of a disk, centered around the origin of the phase space of the reconstruction error, provided the set of coefficients:* $\lambda_{n+m-1},\ldots,\lambda_1,\lambda_0$*, are chosen in such a way that the polynomial,* $p_o(s)$*, in the complex variables s, defined by,*

$$p_o(s) = s^{n+m} + \lambda_{n+m-1}s^{n+m-1} + \cdots + \lambda_1 s + \lambda_0 \tag{9.37}$$

is a Hurwitz polynomial, with roots located well to the left of the imaginary axis of the complex plane. Moreover, the static average feedback controller forces the output tracking error, and its time derivatives, to a vicinity of zero in the tracking error phase space, provided the set of coefficients $\{k_0,\ldots,k_{n-1}\}$ *are chosen in such a manner that* $p_c(s)$ *is a Hurwitz polynomial.*

9.4 An Application Example with Simulations

In this section we present an illustrative example of the average GPI based controller design method and its corresponding switched interpretation. We deal with a linear composite system of the cascade type. We explore both, the state free approach, and the observer based approach for the average designs. Simulations results are included to assess the validity of the proposed approaches.

9.4.1 An Observer-Free Approach

Consider a third order linear dynamic system modeling a normalized 3-compartment cascade process (see [13]).

$$\begin{aligned} \dot{\theta}_1 &= \theta_2 - \theta_1 \\ \dot{\theta}_2 &= \theta_1 - 2\theta_2 + \theta_3 \\ \dot{\theta}_3 &= \theta_2 - 2\theta_3 + u \\ y &= \theta_1 \end{aligned} \tag{9.38}$$

where the input variable, u, takes values in the discrete set $\{0,1\}$. The equilibrium point for the system is characterized by $\theta_1 = \theta_2 = \theta_3 = \Theta$ with $u = \Theta$. We assume the equilibrium point satisfies $0 < \Theta < 1$.

It is desired to smoothly rise from a given output equilibrium point, $\theta_1 = \theta_2 = \theta_3 = \Theta_{init}$, with, $0 < \Theta_{init} < 1$, to a final desired equilibrium point, $0 < \Theta_{final} < 1$, within a finite time interval $[0, T]$.

The input output model is readily obtained to be

$$y^{(3)} + 5\ddot{y} + 6\dot{y} + y = u \tag{9.39}$$

We thus consider the simplified model as a perturbed chain of integrators

$$y^{(3)} = u + \xi(t) \tag{9.40}$$

where $\xi(t) = -5\ddot{y} - 6\dot{y} - y$ is a state-dependent perturbation input of unknown but bounded nature[1]. However, in order to make the controller task more challenging, we addition to the state dependent perturbation input, $\xi(t)$, a rather wild external perturbation input. We set

$$\xi(t) = -5\ddot{y} - 6\dot{y} - y + 0.3e^{-\sin^2(3t)}\cos(0.1t\sqrt{t}) \tag{9.41}$$

Since the system conforms, exactly, to the tutorial example in the previous section, with $\kappa = 1$, we directly use the GPI based switching controller designed there. Figure 9.4 depicts the performance of the proposed GPI based sliding mode controller on the simulation example. The perturbation input ξ results to be large, as compared to the output and control input variables of the system. We emphasize that such a large perturbation cannot be handled by traditional, state dependent, sliding mode control without running into control input saturations or locality of the existence of the sliding regime.

[1] The idea of regarding state-dependent perturbations as unknown but bounded time signals that need to be directly overcome, or, else, estimated and then canceled, is extensively used in sliding mode control [2]. It has also been advocated, as *active disturbance rejection* by the late Prof. J. Han in a number of academic and successful industrial applications [14], it is also at the core of *intelligent PID control* recently introduced by Fliess and Join [15] and it has been advocated by Prof. C.D. Johnson since the seventies under the name of *disturbance accommodation*(see, for instance, [16]).

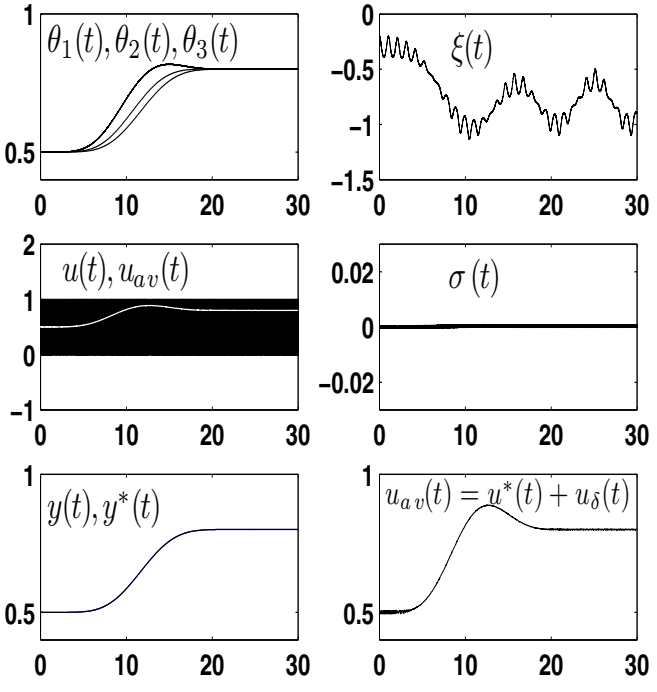

Fig. 9.4 Performance of GPI based sliding mode controller for a 3-compartment cascade switched system

The GPI controller parameters were chosen in accordance with the asymptotic exponential stability of (9.5) by gathering the parameters from the desired closed loop characteristic polynomial, $p(s)$, given by

$$p(s) = (s^2 + 2\zeta\omega_n s + \omega_n^2)^4 (s + p) \tag{9.42}$$

with $\zeta = 1$, $\omega_n = 10$, $p = 10$. The output reference trajectory $y^*(t)$ was set to be a Bézier interpolating polynomial smoothly connecting the initial equilibrium $\Theta_{init} = 0.5$ to the desired final equilibrium point $\Theta_{final} = 0.8$ in $T = 25$ normalized time units. The nominal control input, $u^*(t)$, was set to be $u^*(t) = 0.5 + [y^*]^{(3)}(t)$ in order to reflect the impossibility of its accurate, *a priori* computation. The constant term was added to guarantee the initial state and control input equilibrium.

9.4.2 A GPI Observer Based Approach

Consider the tracking error system corresponding to the simplified dynamics (9.42)

$$e_y^{(3)} = e_{u,av} + \xi(t) \tag{9.43}$$

with $e_y = y_{av} - y^*(t)$ and $e_{u,av} = u_{av} - u^*(t)$. As before, and due to the fact that the state-dependent perturbation input $\xi(t)$ is assumed to be unknown, the nominal average control input, $u^*(t)$, is computed on the basis of the unperturbed simplified system. In other words, we take $u^*(t) = [y^*_{av}(t)]^{(3)}$. The discrepancies between this adopted nominal control input and the actual nominal control input, are relegated to the uncertain signal $\xi(t)$.

The tracking error model, including the approximate internal model for the perturbation input $\xi(t)$ is just

$$\begin{aligned}
\dot{e}_1 &= e_2 \\
\dot{e}_2 &= e_3 \\
\dot{e}_3 &= e_{u,av} + z_1 \\
\dot{z}_1 &= z_2 \\
\dot{z}_2 &= z_3 \\
\dot{z}_3 &= z_4 \\
\dot{z}_4 &= 0 \\
e_y &= e_1
\end{aligned} \tag{9.44}$$

where we have used a third degree, self-updating, time-polynomial approximation, z_1, as the internal model of $\xi(t)$ in the tracking error model.

As in the previous section, the tracking error system and its approximate model conforms, exactly, to the general third order example treated before, with $\kappa = 1$. We, thus, directly propose the GPI observer based switching controller designed in that section. A GPI observer for the, simplified, approximate, average perturbed tracking error system corresponding to (9.44) is given by,

$$\begin{aligned}
\dot{\hat{e}}_1 &= \hat{e}_2 + \lambda_6(e_1 - \hat{e}_1) \\
\dot{\hat{e}}_2 &= \hat{e}_3 + \lambda_5(e_1 - \hat{e}_1) \\
\dot{\hat{e}}_3 &= e_{u,av} + \hat{z}_1 + \lambda_4(e_1 - \hat{e}_1) \\
\dot{\hat{z}}_1 &= \hat{z}_2 + \lambda_3(e_1 - \hat{e}_1) \\
\dot{\hat{z}}_2 &= \hat{z}_3 + \lambda_2(e_1 - \hat{e}_1) \\
\dot{\hat{z}}_3 &= \hat{z}_4 + \lambda_1(e_1 - \hat{e}_1) \\
\dot{\hat{z}}_4 &= \lambda_0(e_1 - \hat{e}_1)
\end{aligned} \tag{9.45}$$

The observer based controller is then given by

$$e_{u,av} = [-\hat{z}_1 - k_2\hat{e}_3 - k_1\hat{e}_2 - k_0 e_1] \tag{9.46}$$

The average control input is then obtained as:

$$u_{av} = u^*(t) - [\hat{z}_1 + k_2\hat{e}_3 + k_1\hat{e}_2 + k_0 e_1] \tag{9.47}$$

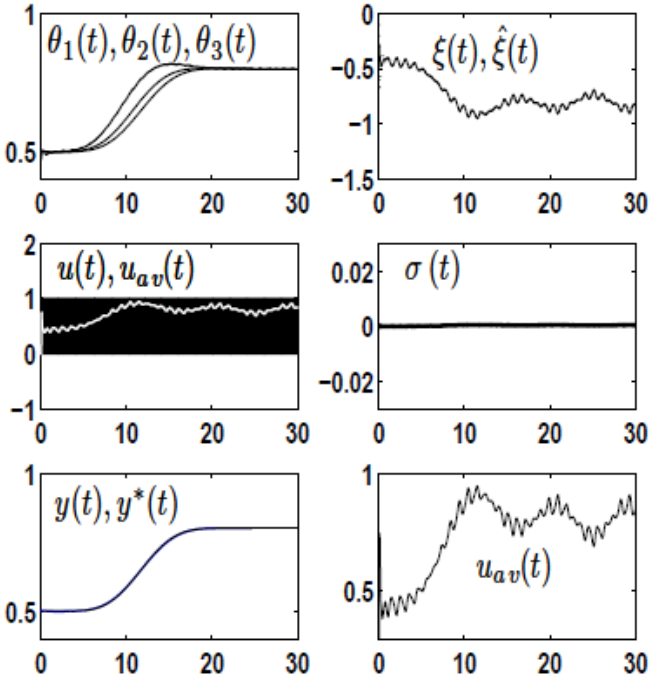

Fig. 9.5 Performance of GPI observer based sliding mode controller for a 3-compartment cascade switched system

Figure 9.5 depicts the performance of the proposed GPI based sliding mode controller on the simulation example.

In this instance the seventh order characteristic polynomial of the estimation error dynamics was determined with the help of the desired characteristic polynomial $(s^2 + 2\zeta_o \omega_{no} s + \omega_{no}^2)^3 (s + p_o)$ with $z = 1$, $\omega_{no} = p_o = 20$. The gains of the steady state characteristic polynomial for the closed loop dynamics: $s^3 + k_2 s^2 + k_1 s + k_0$ were set in accordance with $(s^2 + 2\zeta_c \omega_{nc} s + \omega_{nc}^2)(s + p_c)$, with $\zeta_c = 1$, $\omega_{nc} = p_c = 1$. The state-dependent unknown perturbation input $\xi(t)$ is, as before, given by $\xi(t) = -5\ddot{y} - 6\dot{y} - y + 0.1 \exp(-\sin^2(3t)) \cos(0.1t\sqrt{t})$.

9.5 A "Buck" Converter Example with Experimental Results

In this section, we devote attention to the experimental implementation of the proposed input-output control scheme for switched systems, which is based on the average GPI controller design. Due to space limitations, we describe below the technical details of the laboratory implementation for the case of the observer-free approach.

The results obtained with the observer approach are similar and, in fact, rather effective too.

9.5.1 The Buck Converter Model

Consider the "buck" converter circuit shown in Figure 9.6. The system of differential equations which ideally describes the converter dynamics is given by:

$$\begin{aligned} \frac{di}{dt} &= \frac{1}{L}(-v+uE), \\ \frac{dv}{dt} &= \frac{1}{C}\left(i-\frac{v}{R}\right), \\ y &= v \end{aligned} \tag{9.48}$$

where i describes the inductor current and v represents the output capacitor voltage. The parameters L and C represent, respectively, the inductance and the capacitance of the elements in the circuit. E is the constant voltage of the battery feeding the system. The control input u represents the switch position function and it takes values in the discrete set $\{0,1\}$. The previous system is addressed as the "switched model".

Notice that the ideal model (9.48) does not incorporate the parasitic semiconductor voltages in the diodes, the conducting resistances in the transistors, nor the internal resistance of the battery or of the inductor element. All these unknown terms will be lumped into a single, un-modeled, state-dependent, yet bounded, perturbation input, $\xi(t)$, affecting the simplified input-output dynamics.

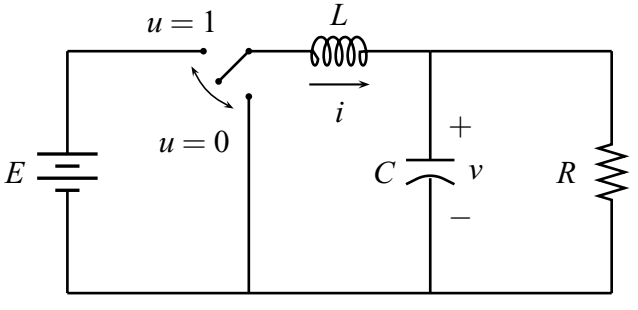

Fig. 9.6 "Buck" converter circuit

The input-output representation of the average idealized model of the converter, with $u_{av} \in [0,1]$, is described by,

$$\ddot{y}_{av} + \frac{1}{RC}\dot{y}_{av} + \frac{1}{LC}y_{av} = \frac{E}{LC}u_{av} \tag{9.49}$$

This average model can be further simplified to be considered as a perturbed second order integrator, with constant input gain, of the form:

$$\ddot{y}_{av} = \kappa u_{av} + \xi(t), \quad \kappa = \frac{E}{LC} \tag{9.50}$$

The perturbation input, $\xi(t)$, is an unknown, state-dependent, perturbation input of the form:

$$\xi(t) = -(1/RC)\dot{y}_{av} - (1/LC)y_{av} + \varphi(t), \tag{9.51}$$

with $\varphi(t)$ representing all the parasitic resistances and the un-modeled voltage sources in the circuit.

9.5.2 The GPI Sliding Mode Controller

It is desired to have the output voltage, $y = v$, of the converter track a biased sinusoidal reference signal of the form $y^*(t) = A + B\sin(\omega t + \phi)$. The coefficients A and B are chosen so that the viability condition is satisfied, at least, by the ill-computed average nominal control input, $u^*(t) = (1/\kappa)\ddot{y}^*(t)$, is bounded within the interval $[0,1]$ of the real line.

A robust average GPI controller for the second order dynamics can be readily designed by taking the perturbation input, $\xi(t)$, to be locally approximated by, say, an element of a family of fixed, second degree, Taylor time-polynomials. The average robust GPI controller is simply given by,

$$\begin{aligned}
u_{av} &= u^*(t) + u_\delta \\
u_\delta &= [k_4\dot{z}_4 + k_3 z_4 + k_2 z_3 + k_1 z_2 + k_0 z_1] \\
\dot{z}_1 &= z_2 \\
\dot{z}_2 &= z_3 \\
\dot{z}_3 &= z_4 \\
\dot{z}_4 &= -k_5 z_4 - \frac{LC}{E}(y - y^*(t))
\end{aligned} \tag{9.52}$$

or, equivalently, in the frequency domain

$$u_{av}(s) = u^*(s) - \frac{LC}{E}\left[\frac{k_4 s^4 + \ldots + k_1 s + k_0}{s^3(s + k_5)}\right](y(s) - y^*(s)) \tag{9.53}$$

This controller yields the average closed loop system

$$e^{(6)}_{y,av} + k_5 e^{(5)}_{y,av} + k_4 e^{(4)}_{y,av} + \ldots + k_1 \dot{e}_{y,av} + k_0 e_{y,av} \approx 0 \tag{9.54}$$

The GPI controller gains $\{k_5, k_4, \ldots, k_0\}$ are chosen so that the prevailing linear behavior, comprised in the dominant closed loop characteristic polynomial, $p(s) = s^6 + k_5 s^5 + \ldots + k_1 s + k_0$ exhibits all its roots deep in the left half of the complex

plane. One, customarily, identifies such gains, by equating $p(s)$ to a desired polynomial of the form $p_d(s) = (s^2 + 2\zeta\omega_n s + \omega_n^2)^3$, with $0 < \zeta < 1$, $\omega_n > 0$.

The sliding mode controller is then readily synthesized as

$$u = \frac{1}{2}(1 + \text{sign}\,\sigma)$$
$$\sigma = \int_0^t [u^*(\tau) + u_\delta(\tau) - u(\tau)]\, d\tau \tag{9.55}$$

Note that the resistor load parameter R is unknown to the controller and, in fact, if time variations do exist on this parameter, then the perturbation input $\xi(t)$ turns out to be,

$$\xi(t) = -\left(\frac{1}{R(t)C}\right)\dot{y}_{av} - \left(\frac{1}{LC} - \frac{\dot{R}(t)}{R^2(t)C}\right) y_{av} + \varphi(t) \tag{9.56}$$

and the same proposed GPI based sliding mode controller still applies.

9.5.3 Experimental Results

Some experiments were carried out to assess the performance of the proposed GPI based discontinuous feedback control scheme on an actual "buck" converter plant. A buck converter prototype (see figure 9.11) was designed with the following parameters: $E = 15$ [V], $L = 16$ [mH], $C = 5$ [μF], $R = 25$ [Ω]. The switching action was performed by means of a MOSFET transistor (NTE2984), as depicted in figure 9.8 with an isolation circuit based on a TTL optocoupler (NTE3087). Since the optocoupler inverts the logical input, it is necessary to invert previously the input signal in the control algorithm. The isolation schematics is shown in figure 9.9. The controller was devised in a MATLAB - xPC Target environment using a sampling period of 60 [μs]. The communication between the "buck" circuit and the controller was performed by a National Instruments PCI-6025E data acquisition card, where a digital output was used as control signal and one analog input was taken for the buck voltage adquisition. A voltage conditioning circuit consisting in a scaling of the capacitor voltage, besides an operational amplifier isolation module was implemented. In this case, we used a scaling factor of $1/3$. Figure 9.10 reproduces the

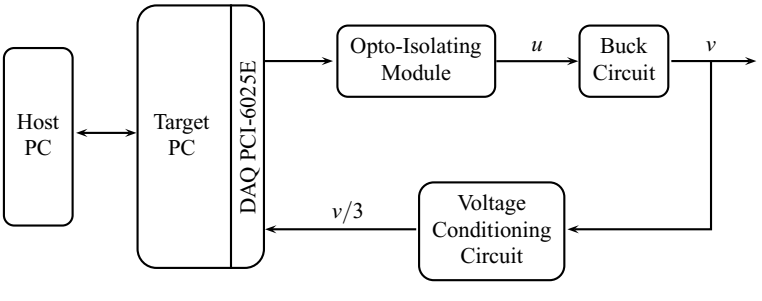

Fig. 9.7 Block diagram of the control system

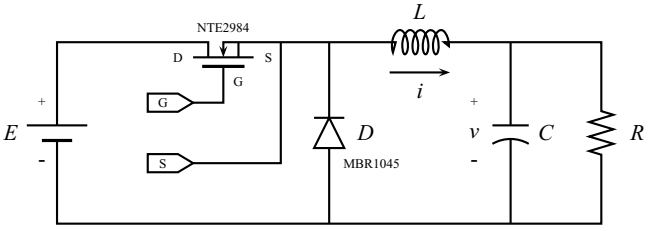

Fig. 9.8 Semiconductor realization of the Buck converter.

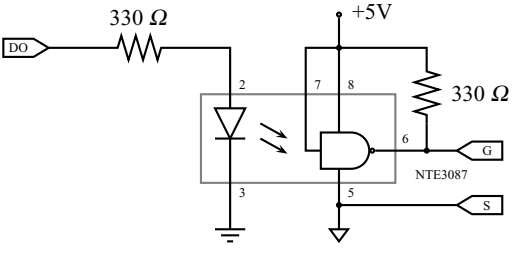

Fig. 9.9 Opto-isolation circuit.

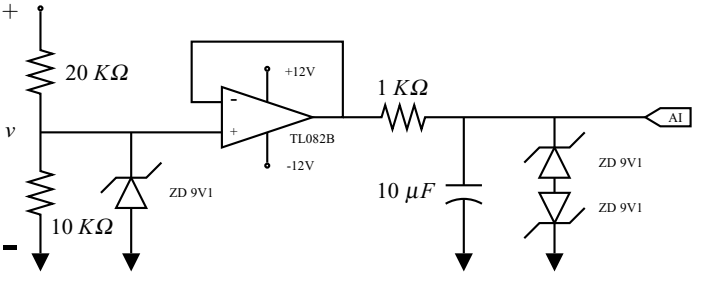

Fig. 9.10 Voltage conditioning circuit.

schematics of the conditioning circuit. The interconnection of the modules can be appreciated in a block diagram form as depicted in figure 9.7. The output reference trajectory to be tracked, $y^*(t) = v^*(t)$, was set to be a biased sinusoidal signal of the form:

$$v^*(t) = 8 + 4\sin\left(10\pi t + \frac{3\pi}{2}\right)$$

Figure 9.12, shows the fast output reference trajectory tracking process achieved by the proposed GPI sliding mode controller. The sliding behavior, characterized by high frequency input switchings, arises immediately after the controller is activated. The voltage $y(t) = v(t)$ tracks the desired output reference trajectory $y^*(t)$, with negligible tracking error in spite of all uncertainties. In order to further test the

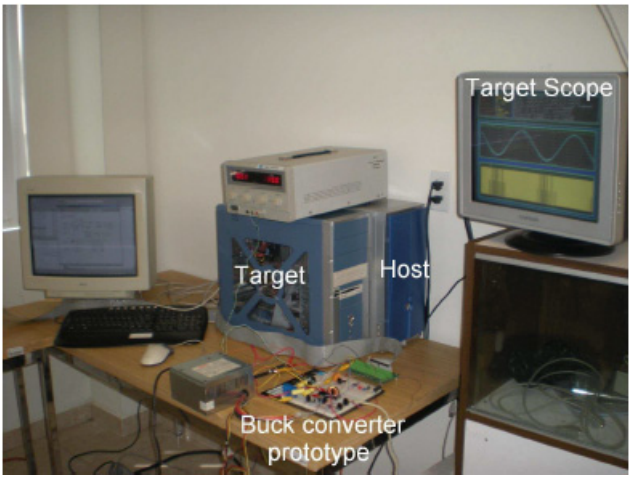

Fig. 9.11 Experimental prototype.

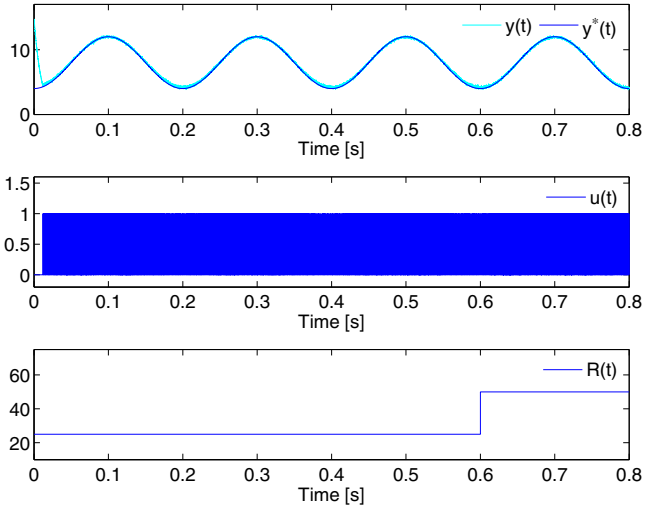

Fig. 9.12 Experimental results using the GPI sliding strategy in a trajectory tracking task, under unexpected load changes.

robustness features of the proposed output feedback discontinuous control scheme, we devised a large, un-modeled, load variation exhibiting an abrupt, step-like, change of a 100% of its nominal value. We allowed the load parameter perturbation to be of the following form:

$$R = 25 + 25\,\mathscr{U}(t - 0.6) \tag{9.57}$$

where $\mathscr{U}(t)$ stands for the unit step function.

9.6 Conclusions

In this article, we have proposed a switch-mode robust output feedback controller design approach for the regulation, and trajectory tracking, of controllable linear switched systems described by traditional input-output, frequency domain, representations. The proposed discontinuous feedback controllers lead the closed loop system towards a robust sliding mode behavior capable of sustaining large unknown perturbation inputs. As such, the proposed design methodology does not require the availability of state variables, nor the explicit use of traditional asymptotic state observers. The approach is fundamentally based on the GPI controller design methodology for the smooth regulation of the average model of the given linear, switched, plant. The proposed approach, most naturally applies to the class of flat linear systems with measurable flat output, i.e., controllable linear systems whose measured output is precisely given by the flat output. These systems are naturally devoid of any zero dynamics. The method may also be easily extended to minimum phase linear systems, whose available output does not coincide with the flat output. Experimental results were also presented for a DC-to-AC power conversion scheme involving a suitable trajectory tracking problem on a popular switched DC-to-DC electronic power converter of the "buck" type. The proposed, state-free, sliding mode control design method is easily extended to nonlinear switched systems, with enhanced robustness features that largely allow for the simplification of the nonlinear output dynamics to that of a linear chain of perturbed integrators with possibly nonlinear input gains (see Sira-Ramírez *et al.* [17] for an induction motor example).

A topic that deserves utmost attention, in the upcoming future, is the extension of the proposed sliding mode controller design method to the class of nonlinear systems exhibiting input delays (an example, dealing with delays, out of the sliding mode context may be found in Sira-Ramírez *et al.* [19])

The proposed, state-free, sliding mode control design method is easily extended to nonlinear switched systems, with enhanced robustness features that largely allow for the simplification of the nonlinear output dynamics to that of a linear chain of perturbed integrators with possibly nonlinear input gains (see Sira-Ramírez *et al.* [17] for an induction motor example). This development requires, in the average design, the combination of suitable linear GPI observers, which are the dual counterparts of GPI controllers, and traditional estimated states linear feedback controllers (see Sira-Ramírez *et al.* [18] for a mechanical system example). A fundamental limitation of this extension is the need to have a minimum-phase plant. Flatness, however, may allow for an elegant circumvention of the problem. This will be the topic of future publications. A topic that deserves utmost attention is the extension of the proposed sliding mode controller design method to the class of nonlinear systems exhibiting input delays (an example may be found in Sira-Ramírez *et al.* [19])

References

1. Luviano-Juárez, A., Cortés-Romero, J., Sira-Ramírez, H.: Synchronization of Chaotic Oscillators by means of Generalized Proportional Integral Observers. International Journal of Bifurcations and Chaos in Engineering Systems 20(5) (May 2010) (to appear)
2. Utkin, V.: Sliding modes and their application in variable structure systems. Mir, Moskow (1978)
3. Edwards, C., Spurgeon, S.: Sliding mode control: theory and applications. Systems and Control Series. Taylor and Francis, London (1998)
4. Utkin, V., Guldner, J., Shi, J.: Sliding Mode Control in Electromecanical Systems. System and Control Series. CRC Press, Boca Raton (1999)
5. Sira-Ramírez, H., Silva-Ortigoza, R.: Control design techniques in power electronics devices. Power Systems Series. Springer, London (2006)
6. Steele, R.: Delta Modulation Systems. Pentech Press, London (1978)
7. Norsworthy, S.R., Shreirer, R., Themes, G.C.: Delta-Sigma Data Converters: Theory, Design, and Simulation. Electrical Engineering Series. IEEE Press, Piscataway (1997)
8. Fliess, M., Marquez, R., Delaleau, E., Sira-Ramírez, H.: Correcteurs proportionnels integraux generallises. ESAIM: Control, Optimisation and Calculus of Variations 7, 23–41 (2002)
9. Fliess, M., Levine, J., Martin, P., Rouchon, P.: Flatness and defect of non-linear systems: introductory theory and examples. International Journal of Control 61(6), 1327–1361 (1995)
10. Sira-Ramírez, H., Agrawal, S.: Differentially flat systems. Marcel Dekker Inc., New York (2004)
11. Åström, K.J., Murray, R.: Feedback Systems: An Introduction for Scientists and Engineers. Princeton University Press, Princeton (2008)
12. Sira-Ramírez, H., Silva-Ortigoza, R.: Sliding mode, sigma-delta modulation control of the boost converter. Asian Journal of Control 7(4), 349–355 (2005)
13. Martin, P., Murray, R., Rouchon, P.: Flat systems, equivalence and trajectory generation, Caltech, Technical Report. CDS-2003-008 (2003), http://www.cds.caltech.edu/reports/
14. Han, J.: From pid to active disturbance rejection control. IEEE Transactions on Industrial Electronics 56(3), 900–906 (2009)
15. Fliess, M., Join, C.: Intelligent pid controllers. In: 16th Mediterranean Conference on Control and Automation, Ajaccio, Corsica, France (2006)
16. Parker, G.L., Johnson, C.D.: Decoupling linear dynamical systems using disturbance accomodation control theory. In: 41st. Southeastern Symposium on System Theory, March 15-17, University of Tenessee Space Institute, Tullahoma (2009)
17. Sira-Ramírez, H., Beltrán-Carbajal, F., Blanco-Ortega, A.: Robust generalized proportional integral controller for the induction motor. In: Proc. of the The 10th International Workshop on Variable Structure Systems, Antalya, Turkey, June 8-10 (2008)
18. Sira-Ramírez, H., Beltrán-Carvajal, F., Blanco-Ortega, A.: A Generalized Proportional Integral Output Feedback Controller for the Robust Perturbation Rejection in a Mechanical System. e-STA Revue des Sciences et Technologies de l'Automatique 5(4) (2008) (Fourth Trimester)
19. Sira-Ramírez, H., Velasco-Villa, M., Rodríguez-Angeles, A.: Trajectory tracking control of an input delayed monocycle. In: American Control Conference, Baltimore, MD (June-July 2010)

Chapter 10
Output Feedback Sliding Mode Control Approaches Using Observers and/or Differentiators

Liu Hsu, Eduardo V.L. Nunes, Tiago Roux Oliveira, Alessandro Jacoud Peixoto, José Paulo V.S. Cunha, Ramon R. Costa, and Fernando Lizarralde

Abstract. This chapter briefly describes the main results developed by the authors in the area of output feedback sliding mode control. For the sake of simplicity, the focus is maintained on uncertain single-input-single-output (SISO) nonlinear systems, although several results have been extended to the control of multi-input-multi-output (MIMO) systems. For the considered class of nonlinear systems, linear growth restriction on the unmeasured states is assumed, while less restrictive conditions are imposed to the growth of nonlinearities depending on the measured output. We present different tracking controllers for plants with arbitrary relative degree. We consider several approaches to overcome the relative degree obstacle: linear or variable structure lead filters, high-gain observers with constant or dynamic gain, global hybrid estimation schemes combining lead filters or observers with locally exact differentiators based on high-order sliding mode. Global or semi-global stability properties can be proved either for asymptotic exact tracking or for tracking within a small residual error. Some experimental results are presented to illustrate the applicability of the control schemes in real systems.

Liu Hsu · Ramon R. Costa · Fernando Lizarralde
COPPE/Federal University of Rio de Janeiro, Brazil
e-mail: {liu,ramon,fernando}@coep.ufrj.br

Eduardo V.L. Nunes
Dept. of Electronics and Computer Eng., Federal University of Rio de Janeiro, Brazil
e-mail: eduardo@coep.ufrj.br

Tiago Roux Oliveira · José Paulo V.S. Cunha
Dept. of Electronics and Telecom. Eng., State University of Rio de Janeiro, Brazil
e-mail: tiagoroux@uerj.br, jpaulo@ieee.org

Alessandro Jacoud Peixoto
Celso Suckow da Fonseca Federal Center of Technology, Brazil
e-mail: jacoud@me.com

L. Fridman et al. (Eds.): Sliding Modes, LNCIS 412, pp. 269–292.
springerlink.com

10.1 Introduction

The research in output feedback sliding mode control (SMC) has been intensified over the last two decades. This has been motivated by the need to overcome practical difficulties in implementing conventional variable structure controllers, which rely on state feedback. In early attempts to circumvent this problem, lead filters were used to reconstruct the unmeasured states. However, this usually led to control chattering that severely limited the potential advantages of ideal SMC [51].

The pioneering work [3] proposed the use of asymptotic observers to cope with the lack of full state measurements. The main idea was to reformulate the switching functions in terms of the observed states. It was shown that chattering could thereby be avoided even in the presence of unmodeled dynamics since an ideal SMC loop around the discontinuous function could be preserved through the observer. However, in this seminal paper, the plant model was assumed known and no external disturbances were included.

Other papers followed in the direction of including plant uncertainties and disturbances. In [18], [16] and [22], the variable structure model-reference adaptive controller (VS-MRAC) was proposed for uncertain linear plants as a robust alternative to MRAC based on parameter adaptation. Robust state estimators were also used to deal with uncertainties, for instance, high-gain observers (HGOs) [11] and sliding mode observers [52, 8].

As a more recent trend, a new class of output feedback SMC schemes based on higher-order sliding mode for plants of arbitrary relative degree has been considered by several authors [32, 1, 14]. One tool for the implementation of higher-order SMC is the so called robust exact differentiator (RED) [32]. Theoretically, controllers based on this differentiator, may lead to exact output tracking. However, the RED can only guarantee local/semi-global closed-loop stability properties, since it requires a uniform constant Lipschitz bound for the n-th derivative of the input signal, which is not valid for arbitrary initial conditions in closed-loop applications.

The present chapter briefly describes the main results developed by the authors in the area of output feedback sliding mode control. For the sake of simplicity, the focus is maintained on single-input-single-output (SISO) systems, although several works have already considered the control of multi-input-multi-output (MIMO) systems, e.g., [21, 20, 23, 42]. Moreover, we restrict ourselves to a class of uncertain nonlinear systems with linear growth restriction on the unmeasured states, while less restrictive conditions are imposed to the measured output. As a consequence, finite-time escape is not precluded for the open-loop system.

Different output feedback sliding mode controllers for the output tracking of a reference model are presented, considering several approaches for the recovery of unmeasured states and relative degree compensation: linear or variable structure lead filters, high-gain observers with constant or dynamic gain, global hybrid estimation schemes combining lead filters or observers with locally exact differentiators based on high-order sliding mode. Global or semi-global stability properties have been obtained with some residual tracking error or even with asymptotic exact tracking.

This chapter is organized as follows. Section 10.2 presents some preliminary concepts, definitions, notations and properties. Section 10.3 describes the plant, the reference model and the control objective. A parametrization for the output feedback model matching control and the output error equations are described in Section 10.4. In Section 10.5, a norm state observer and a norm bound for the equivalent disturbance are derived. Section 10.6 presents the conventional sliding mode design. Several relative degree compensation schemes are discussed in Section 10.7. Some alternatives to avoid the peaking phenomena are briefly discussed in Section 10.8. In Section 10.9 a brief discussion about chattering alleviation is presented. Section 10.10 describes a binary model-reference adaptive controller (B-MRAC) which applies VSC concepts to improve the robustness and transient performance of a parameter adaptation control algorithm. Experimental results are discussed in Section 10.11 and some conclusions are presented in Section 10.12.

10.2 Preliminaries

- The Euclidean norm of a vector x and the corresponding induced norm of a matrix A are denoted by $\|x\|$ and $\|A\|$, respectively.
- The symbol "s" represents either the Laplace variable or the differential operator "d/dt", according to the context.
- The output of a linear system with transfer function $H(s)$ and input u is written $H(s)u$. Pure convolution $h(t)*u(t)$ is denoted by $H(s)*u$, with $h(t)$ being the impulse response of $H(s)$.
- Classes $\mathscr{K}$, $\mathscr{K}_\infty$ functions are defined as usual [30, p. 144].
- ISS and ISpS mean Input-to-State-Stable (or Stability) and Input-to-State-Practical-Stability, respectively [29].
- Filippov's definition for the solution of discontinuous differential equations is assumed throughout the paper [12]. In order to avoid clutter, the symbol u alone, without the argument t, represents a switching control law which is not a usual function of t when sliding mode takes place. On the other hand, we denote the extended equivalent control [50], [21, Sec. 2.3] by $u(t)$ (instead of $u_{eq}(t)$) which, by definition, is piece-wise continuous. Note that u can always be replaced by $u(t)$ in the right-hand side of the differential equations.

10.3 Problem Statement

Consider a single-input-single-output nonlinear uncertain plant described by

$$\begin{aligned} \dot{x} &= f_p(x,t) + bu\,, \qquad f_p(x,t) = Ax + \phi(x,t)\,, \\ y &= h^T x\,, \end{aligned} \tag{10.1}$$

where $x \in \mathbb{R}^n$ is the state, $u \in \mathbb{R}$ is the control input, $y \in \mathbb{R}$ is the measured output and $\phi : \mathbb{R}^n \times \mathbb{R}^+ \to \mathbb{R}^n$ is a state dependent uncertain nonlinear disturbance, possibly unmatched. The triple $\{A, b, h^T\}$ is in the canonical controllable form with uncertain

constant matrices A (lower companion form) and $h^T = [h_1\ h_2\ \ldots\ h_{(n-n^*+1)}\ 0\ \ldots\ 0]$. Note that $h_{(n-n^*+1)} = h^T A^{n^*-1} b$, which coincides with the general expression for the high frequency gain of the linear subsystem $\{A,b,h^T\}$ [30, p. 512].

10.3.1 Basic Assumptions

Without loss of generality, we assume that the initial time is $t = 0$. All uncertain parameters belong to some compact set Ω_p such that the necessary uncertainty bounds, to be defined later, are available for design. In Ω_p we assume that: (i) ϕ is locally Lipschitz in x ($\forall x$), piecewise continuous in t ($\forall t$) and sufficiently smooth; (ii) $\{A,b,h^T\}$ represents a linear plant which is minimum-phase, observable, has known order n and known *relative degree* n^*, as is usual in Model Reference Adaptive Control (MRAC) [26]. Our main additional assumptions are:

(A1) There exists a global diffeomorphism $(\bar{x},t) = T(x,t)$, $\bar{x}^T := [\eta^T\ \xi^T]$, $\eta \in \mathbb{R}^{n-n^*}$, which transforms (10.1) into the *normal form* [30, p. 516], with $\xi = [y\ \dot{y} \ldots y^{(n^*-1)}]^T$ and

$$\begin{aligned} \dot{\eta} &= F_0(\eta,\xi)\,, \\ \dot{\xi} &= A_r\xi + B_r k_p[u + d(x,t)]\,, \\ y &= \xi_1\,, \end{aligned}$$

where $k_p := h^T A^{n^*-1} b = h_{(n-n^*+1)}$ is the *constant* plant high frequency gain (HFG) with known sign, A_r, B_r is in the Brunovsky's controller form and the η-dynamics is ISS from ξ to η (minimum-phase condition).

According to (A1), the plant (10.1) has relative degree n^* and the HFG k_p is uncertain in norm but with known sign. The case of unknown HFG sign (unknown control direction) can be coped with the monitoring function approach presented in [43] and [53].

The above assumption is satisfied, for instance, by systems (10.1) with $\phi(x,t) = [\phi_1(x_1,y,t)\ \ \phi_2(x_1,x_2,y,t)\ \ \cdots\ \ \phi_n(x_1,\ldots,x_n,y,t)]^T$ triangular in the unmeasured states. We further assume that:

(A2) The term ϕ is norm bounded by $\|\phi(x,t)\| \le k_x\|x\| + \varphi(y,t)$, $\forall x,t$, where $k_x \ge 0$ is a *known* scalar and $\varphi : \mathbb{R}\times\mathbb{R}^+ \to \mathbb{R}^+$ is a known function piecewise continuous in t and continuous in y, and $\varphi(y,t) \le \Psi_\varphi(|y|) + k_\varphi$, where $\Psi_\varphi \in \mathscr{K}_\infty$ is locally Lipschitz and $k_\varphi > 0$ is a constant.

According to (A2), no particular growth condition, such as linear growth or existence of a global Lipschitz constant, is imposed on φ. Therefore, nonlinearities like $\varphi(y) = y^2$ can be included and thus, finite-time escape is not precluded *a priori* and for each solution of (10.1) there exists a maximal time interval of definition given by $[0,t_M)$, where t_M may be finite or infinite.

10.3.2 Control Objective

The aim is to achieve global or semi-global stability properties in the sense of uniform signal boundedness and asymptotic output tracking, i.e., the *output tracking error*

$$e(t) = y(t) - y_m(t) \tag{10.2}$$

should asymptotically tend to zero (exact tracking) or at least to a small residual set. The *desired trajectory* $y_m(t)$ is assumed to be generated by a *reference model* of the form:

$$y_m = M(s)r = \frac{k_m}{L(s)(s+a_m)}\, r\,, \quad L(s) = s^{(n^*-1)} + \sum_{i=2}^{n^*} l_{n^*-i}\, s^{(n^*-i)}\,, \tag{10.3}$$

where $k_m > 0$, $a_m > 0$, the *reference signal* $r(t)$ is assumed piecewise continuous and uniformly bounded and $L(s)$ is a Hurwitz polynomial.

10.4 Output Tracking Error Equation

In this section, an output feedback model matching control u^* is derived so that, when $u = u^*$, the transfer function of the closed loop system is the same as that of the model. Then, the relevant output error equation is obtained. To this end, a key idea is to transform ϕ to an input (matched) disturbance.

10.4.1 Output Feedback Model Matching Control

In order to obtain an output feedback model matching control, we first introduce the *regressor vector* $\omega := [\omega_1^T \ \omega_2^T \ y \ r]^T$, using the following input and output (I/O) filters of MRAC design [26]:

$$\dot{\omega}_1 = \Lambda\omega_1 + gu\,, \qquad \dot{\omega}_2 = \Lambda\omega_2 + gy\,, \tag{10.4}$$

where $\Lambda \in \mathbb{R}^{(n-1)\times(n-1)}$ is Hurwitz and g is a constant vector such that $\{\Lambda, g\}$ is controllable. Such filters are needed due to the lack of full state measurement of the plant and replace a state observer. Then, the model matching control is parametrized as

$$u = \theta^T\omega\,, \qquad \theta^T := [\theta_1^T \ \theta_2^T \ \theta_3 \ \theta_4]\,. \tag{10.5}$$

If $\phi \equiv 0$, the closed loop transfer function from r to y is denoted by $G_c(s,\theta)$. As is well known [26], there exists a constant vector θ^* which solves the equation $G_c(s,\theta) = M(s)$ provided that the zeros of the model are eigenvalues of Λ. Thus, if $\phi \equiv 0$, a *model matching control law* is given by $u^* = \theta^{*T}\omega$. Further, θ^* is unique if the model is of order n. In particular, model matching requires $\theta_4^* = k_m/k_p$. Since the plant parameters are uncertain, θ^* is not available. However, we assume that θ^*

is elementwise bounded by a known constant vector $\bar{\theta}$ ($|\theta_i^*| \leq \bar{\theta}_i, \forall i$). Thus, u^* can also be norm bounded by available signals.

10.4.2 Error Equation and Equivalent Nonlinear Input Disturbance

Considering $X^T := [x^T \ \omega_1^T \ \omega_2^T]$, with u replaced by $u - u^* + u^*$, and noting that, for appropriate matrices Ω_1 and Ω_2, $\omega = \Omega_1 X + \Omega_2 r$, one can write the state space representation of (10.1) and (10.4) as [20, Sec. 6.2]

$$\dot{X} = A_c X + b_c r + b_c k^* [u - u^*] + B_\phi \phi, \qquad y = h_c^T X, \tag{10.6}$$

where $B_\phi = [I \ 0 \ 0]^T$ and $k^* := 1/\theta_4^*$. Note that $\{A_c, b_c, h_c^T\}$ is a non-minimal stable realization of $M(s)$. The desired trajectory y_m can also be generated by:

$$\dot{X}_m = A_c X_m + b_c k^* [\theta_4^* r - d_\phi] + B_\phi \phi, \qquad y_m = h_c^T X_m, \tag{10.7}$$

where the *equivalent input disturbance* $d_\phi = (k^* M(s))^{-1} h_c^T (sI - A_c)^{-1} B_\phi \phi$ can be written as

$$d_\phi := W_{n^*-1} \phi^{(n^*-1)} + \ldots + W_1 \dot{\phi} + W_0 \phi + \bar{W}_\phi(s) * \phi, \tag{10.8}$$

with $\bar{W}_\phi$ being a row vector of strictly proper and bounded-input-bounded-output stable transfer functions and $W_i \in \mathbb{R}^n$ are constant row vectors obtained from the model parameters and the Markov parameters corresponding to $h_c^T (sI - A_c)^{-1} B_\phi$. Note that from the relative degree assumption of (A1), u does not appear in d_ϕ which involves the derivatives of the output y only up to order $n^* - 1$.

Now, from (10.6)–(10.7), one has

$$\dot{X}_e = A_c X_e + b_c k^* [u - \bar{u}], \qquad e = h_c^T X_e, \qquad X_e := X - X_m, \tag{10.9}$$

$$e = k^* M(s)[u - \bar{u}], \qquad \bar{u}(t) := \theta^{*T} \omega(t) - d_\phi, \tag{10.10}$$

where $\bar{u}$ is the model matching control in the presence of ϕ [23].

10.5 Norm State Observer and Norm Bound for Equivalent Disturbance

Since we assume sufficient differentiability for ϕ, one can find $\Psi_\phi \in \mathcal{K}$ and a constant $k_\phi > 0$ such that $|d_\phi| \leq \Psi_\phi(\|x\|) + \bar{W}_\phi(s) * \|\phi\| + k_\phi$. Considering (A2) and applying [20, Lemma 3] to (10.6), it is possible to find $k_x^* > 0$ such that, for $k_x \in [0, k_x^*]$ a norm bound for X and x can be obtained through *first order approximation filters* (FOAFs) (see details in [20]) similarly to norm state observers [48, 31, 40, 42]. Therefore, one has $\|x(t)\| \leq \hat{x}(t) + \hat{\pi}(t)$, where

$$\hat{x}(t) := \frac{1}{s+\lambda_x}[c_1\varphi(y,t) + c_2\|\omega(t)\|], \tag{10.11}$$

with $c_1, c_2, \lambda_x > 0$ being appropriate constants that can be computed by the optimization methods described in [6]. The exponentially decaying term $\hat{\pi}$ accounts for initial conditions [20]. Moreover, from (A2) and (10.11), one has $\|\phi(x,t)\| \leq k_x\hat{x}(t) + \varphi(y,t)$, *modulo* $\hat{\pi}$ term, and one can write $|d_\phi| \leq \hat{d}_\phi + \hat{\pi}_\phi$, where $\hat{\pi}_\phi$ is a decaying term,

$$\hat{d}_\phi(t) := \Psi_\phi(|\hat{x}(t)|) + \frac{c_\phi}{s+\gamma_\phi}[k_x\hat{x}(t) + \varphi(y,t)] + k_\phi, \tag{10.12}$$

and $\frac{c_\phi}{s+\gamma_\phi}$ is a FOAF designed for $\bar{W}_\phi(s)$, with appropriate positive constants c_ϕ and γ_ϕ.

10.6 Output Feedback Sliding Mode Controller

For plants with $n^* = 1$, $M(s)$ in (10.3) is strictly positive real (SPR). Applying [22, Lemma 1] to the error equation in (10.10), global exponential stability and finite-time exact tracking is guaranteed with $u = -[\text{sgn}(k_p)]f(t)\text{sgn}(e)$ where the *modulation function* $f(t)$ satisfies $f(t) \geq |\bar{u}| + \delta$, with $\bar{u}$ defined in (10.10) and δ being a positive constant, which can be arbitrarily small.

A possible choice for a modulation function $f(t)$ to satisfy the latter inequality, *modulo* exponentially decaying terms, is given by

$$f(t) = \bar{\theta}^T|\omega(t)| + |\hat{d}_\phi(t)| + \delta, \tag{10.13}$$

with $\hat{d}_\phi$ given in (10.12). Thus, $f(t)$ can be implemented using only available signals.

For the case of plants with $n^* > 1$, the modulation function design can be repeated, but $M(s)$ is not SPR. However, with the multiplier $L(s)$, $M(s)L(s)$ is SPR and from (10.10):

$$\sigma = k^*M(s)L(s)[u - \bar{u}], \tag{10.14}$$

with

$$\sigma = L(s)e = e^{(n^*-1)} + l_{n^*-2}e^{(n^*-2)} + \ldots + l_1\dot{e} + l_0e. \tag{10.15}$$

Thus, using $u = -[\text{sgn}(k_p)]f(t)\text{sgn}(\sigma)$ we recover the $n^* = 1$ case results. The problem is that the *ideal sliding variable* σ is not available since $L(s)$ is non-causal. In order to overcome this problem the following control law is considered:

$$u = -[\text{sgn}(k_p)]f(t)\,\text{sgn}(\hat{\sigma}), \tag{10.16}$$

where $\hat{\sigma}$ is an estimate for σ obtained from one of the following relative degree compensation strategies.

10.7 Relative Degree Compensation

In this section, some alternatives are proposed to estimate σ and to provide a surrogate for the non-causal operator $L(s)$ (10.3) by means of: (a) ordinary or variable structure lead filters, (b) high-gain observers with constant or dynamic gain and (c) a hybrid estimation scheme which combines, via a suitable switching rule, one of the previous compensation alternatives with a local robust exact differentiator based on high-order sliding mode.

10.7.1 Linear Lead Filter

The linear lead filter is given by:

$$\hat{\sigma}_l = L_a(s)e\,, \qquad L_a(s) = \frac{L(s)}{F(\tau s)}\,, \tag{10.17}$$

where $\tau > 0$ is a sufficiently small constant, and $F(\tau s)$ is a Hurwitz polynomial with $F(0) = 1$, for instance $F(\tau s) = (\tau s + 1)^{(n^*-1)}$. As τ tends to zero, $L_a(s)$ and $\hat{\sigma}_l$ approximate $L(s)$ and σ, respectively. Replacing the ideal sliding variable σ by its estimate $\hat{\sigma} = \hat{\sigma}_l$ in the control law (10.16), global/semi-global stability properties can be guaranteed [43, 37]. However, the linear lead filter cannot provide the exact estimate of σ, and is well known to lead to control chattering with residual tracking error since the *ideal sliding loop* (ISL) [51] around the switching function of the variable structure system is destroyed due to the small lag introduced by $F^{-1}(\tau s)$. On the other hand, if a prediction error loop is used as detailed in [15], the ISL can be preserved and control chattering is theoretically avoided.

10.7.2 Variable Structure Lead Filter

Variable structure lead filters (VSLF) had been proposed by Ezerov and Utkin [16, 28]. A solution to robust model reference control based on VSLF's and the *prediction error* [16] given by

$$\hat{e} = k^{nom} M(s)L(s)\left(u_0 - L^{-1}(s)u_N\right)\,, \tag{10.18}$$

where $k^{nom} := k_p^{nom}/k_m$, k_p^{nom} is a nominal value for k_p, was extensively explored in the VS-MRAC controller presented by [16, 22, 21, 23] and illustrated in Figures 10.1 and 10.2.

In this case, the operator $L(s)$ can be written as $L(s) = L_1(s)\ldots L_N(s)$, where $L_i(s) = s + \alpha_i$, $\alpha_i > 0$, and $N := n^* - 1$, is chosen such that $M(s)L(s)$ is SPR. In Figure 10.1, the operator $\mathscr{L}$ is an approximation of $L(s)$ realized by the chain of VSLF's depicted in Fig. 10.2. If $n^* = 1$, $L(s) = \mathscr{L} = 1$, then the prediction error becomes null, i.e., $\hat{e} \equiv 0$ and one can remove the internal loops passing by $k^{nom}M(s)L(s)$.

The *averaging filters* $F_i^{-1}(\tau s)$ in Figure 10.2 are low-pass filters with unit DC gain, where $F_i(\tau s)$ are Hurwitz polynomials in τs and $F_i(0) = 1$, e.g.,

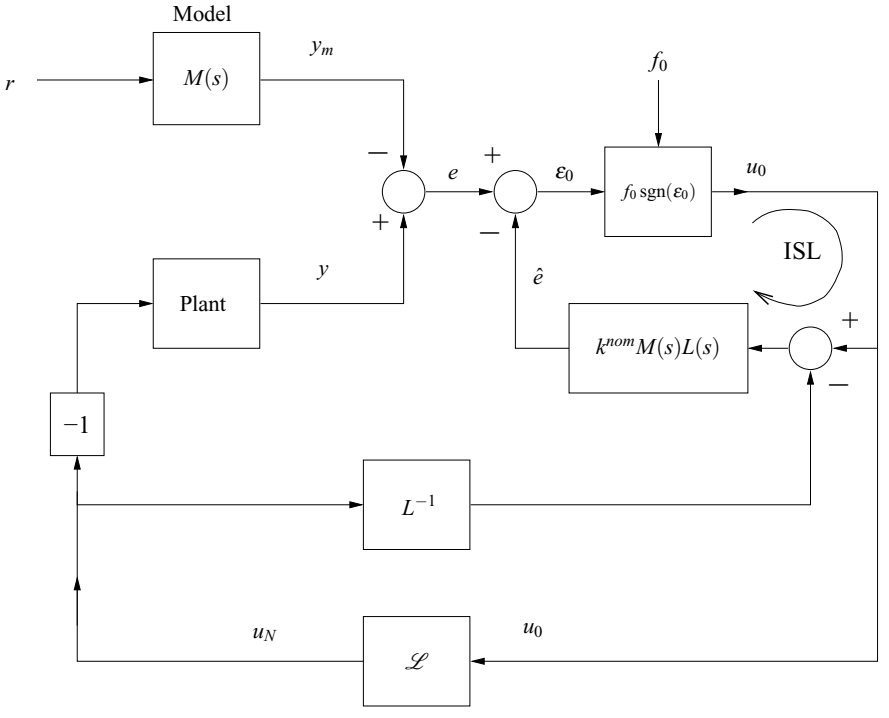

Fig. 10.1 Block diagram of the VS-MRAC. The I/O filters and the computation of the modulation function f_0 are omitted to avoid clutter. The realization of $\mathscr{L}$ is presented in Figure 10.2.

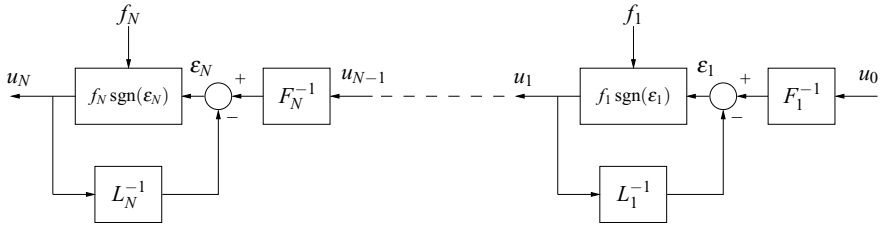

Fig. 10.2 Implementation of the operator $\mathscr{L}$ via variable structure lead filters.

$F_i(\tau s) = \tau s + 1$. When the time constant τ is sufficiently small, they give an approximation of the *equivalent control* signals $(u_i)_{eq}$ [50]. Indeed, this control system for linear systems is globally exponentially stable with respect to a small residual set of order $\mathscr{O}(\tau)$ as had been proved in [22].

In spite of the more involved implementation of the VSLF's, which requires several filters for the computation of the modulation functions $f_1, \ldots, f_N$ for the relays,

they are less noise sensitive when compared to standard linear lead filters, as is discussed in [15].

10.7.3 High-Gain Observers

The strong impact of HGO theory can be easily verified from the literature. Of particular interest in high-gain control designs, which include sliding mode control, is the fact that HGO can provide approximations of the output time-derivatives preserving a high frequency loop [3,15] that is absent when using cascaded linear lead filters. As a consequence, HGO based sliding mode control may be designed so that ideal sliding mode can be produced thus avoiding prohibitive low frequency chattering which may occur, e.g., with lead filters [10,33].

10.7.3.1 High-Gain Observer with Constant Gain

To develop a model-reference controller based on an HGO, a natural idea would be to estimate the plant state, as in the robust stabilization controller of [38]. However, in the trajectory tracking controller [39] and in the model-reference controller [7], the state of an error equation is estimated rather than the plant state. In this way, the reference model (stable and perfectly known) is used instead of the plant model (uncertain and possibly unstable) for the estimator, since the design of an observer for the reference model is easier than the design of an observer for the plant [4]. For this purpose, we rewrite (10.10) as the minimal order error equation

$$\dot{x}_e = A_M x_e + B_M k^* \left[u - \bar{u} + \pi_e \right], \tag{10.19}$$

$$e = C_M x_e, \tag{10.20}$$

where x_e is the new error state and

$$A_M = \begin{bmatrix} -a_{n^*-1} & 1 & \cdots & 0 \\ \vdots & & \ddots & \vdots \\ -a_1 & 0 & & 1 \\ -a_0 & 0 & \cdots & 0 \end{bmatrix}, \quad B_M = \begin{bmatrix} 0 \\ \vdots \\ 0 \\ k_M \end{bmatrix}, \quad C_M = \begin{bmatrix} 1 & 0 & \cdots & 0 \end{bmatrix}, \tag{10.21}$$

is the minimal realization of $M(s) = k_m/(s^{n^*} + a_{n^*-1}s^{n^*-1} + \ldots + a_1 s + a_0)$ in the observer canonical form. The exponentially decaying scalar signal π_e in (10.19) represents the effects of uncontrollable states of the complete error equation (10.9).

It is possible to design a matrix $S \in \mathbb{R}^{1\times n^*}$, which defines the ideal sliding surface $\sigma = Sx_e = 0$ with x_e from (10.19), such that $\{A_M, B_M, S\}$ is a realization of the transfer function $M(s)L(s)$, which has relative degree one [7, eq. (17)]. Since the state x_e is not measured, the proposed control law is given in (10.16) with the modulation function (10.13) and the sliding variable $\hat{\sigma}$ given by

$$\hat{\sigma}_o = S\hat{x}_e, \tag{10.22}$$

where $\hat{x}_e$ is an estimate for the state error x_e provided by the HGO:

$$\dot{\hat{x}}_e = A_M \hat{x}_e + B_M k^{\text{nom}} u - \left[\alpha(\varepsilon^{-1}) - a_M\right] \tilde{e}\,, \tag{10.23}$$

$$\tilde{e} = C_M \hat{x}_e - e\,, \tag{10.24}$$

where $\tilde{e}$ is the observer output error, and $a_M = [a_{n^*-1}, \ldots, a_1, a_0]^T$. The coefficients α_i in the observer feedback vector [34]

$$\alpha(\varepsilon^{-1}) = \left[\frac{\alpha_{n^*-1}}{\varepsilon} \cdots \frac{\alpha_1}{\varepsilon^{n^*-1}} \frac{\alpha_0}{\varepsilon^{n^*}}\right]^T \tag{10.25}$$

must be chosen so that the characteristic polynomial of the closed-loop observer is Hurwitz, which holds if $N_\alpha(s) = s^{n^*} + \alpha_{n^*-1} s^{n^*-1} + \cdots + \alpha_0$ is Hurwitz and $\varepsilon > 0$. Since it is desired that the uncertainties and disturbances have negligible effects in the estimated state $\hat{x}_e$, the norm of the observer feedback vector ($\|\alpha(\varepsilon^{-1})\|$) should be large, which requires ε to be sufficiently small.

The proposed controller can be represented by the diagram in Fig. 10.3. For linear systems, this controller is globally exponentially stable with respect to a small residual set of order $\mathcal{O}(\varepsilon)$ [7]. For nonlinear systems of the class satisfying assumptions (A1) and (A2), this controller can be designed such that the closed-loop system is semi-globally stable [40, 41].

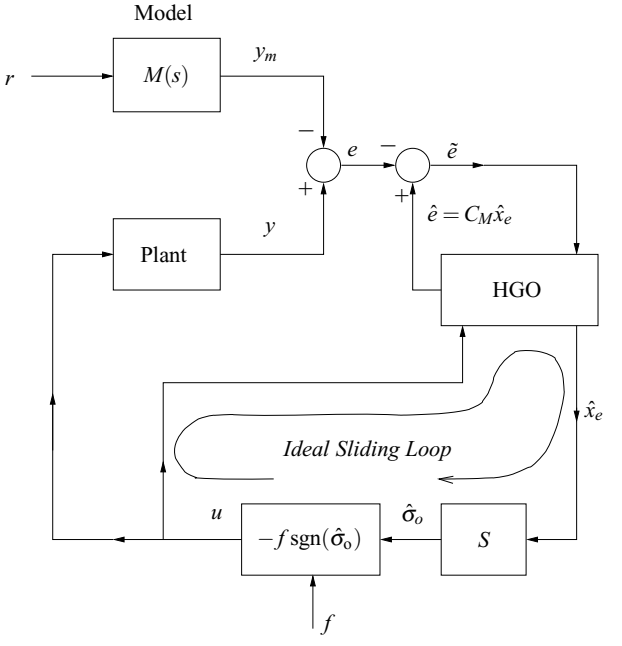

Fig. 10.3 Model-reference sliding mode controller based on a high-gain observer for systems with relative degree $n^* \geq 2$. The I/O filters and the synthesis of the modulation function f are not shown to avoid clutter.

10.7.3.2 High-Gain Observer with Dynamic Gain

Most available output feedback SMC designs, including the previous approaches mentioned above, achieves global results only under rather stringent assumptions such as linearly or uniformly globally bounded vector fields. In the recent years, Praly [46] and then several others have shown that, by using dynamic observer gain, global results can be achieved without invoking the global Lipschitz conditions or "output feedback" forms [27].

In [44, 45], it is shown that an output feedback SMC strategy based on an HGO with dynamic observer gain in conjunction with norm state observers can also be used for a state of the art class of nonlinear systems to guarantee global practical tracking. Such a class encompasses, for example, uncertain systems (10.1) satisfying assumptions (A1) and (A2) or systems in lower triangular form [27] where:

$$|\phi_i| \leq k_x(\eta, y, t)\ [|x_1| + \ldots + |x_i|] + \varphi(\eta, y, t), \qquad i = 1, \ldots, n^*, \tag{10.26}$$

that is, the nonlinearities ϕ_i have linear growth condition in the unmeasured states and growth rate k_x possibly depending on the inverse dynamics unmeasured state η in (A1), on the system output y and time. Strong polynomial nonlinearities φ in the inverse dynamics state and in the output system are also allowed.

Unlike the previous section, the HGO provides an estimate $\hat{\xi}$ for the partial plant state ξ in (A1). In this case, the HGO is given by

$$\dot{\hat{\xi}} = A_r \hat{\xi} + B_r u + H_\varepsilon L_o (y - C_r \hat{\xi}), \tag{10.27}$$

where $C_r := [1\ 0\ \ldots\ 0]$ and L_o and H_ε are defined as

$$L_o := [\, l_1\ \ldots\ l_{n^*}\,]^T, \quad \text{and} \quad H_\varepsilon := \operatorname{diag}(\varepsilon^{-1}, \ldots, \varepsilon^{-n^*}). \tag{10.28}$$

The observer gain L_o is such that $s^{n^*} + l_1 s^{n^*-1} + \ldots + l_{n^*}$ is Hurwitz. On the other hand, instead of using a constant ε, we introduce a *variable* parameter $\varepsilon(t) > 0$, $\forall t \in [0, t_M)$, of the form

$$\varepsilon(\hat{x}, t) := \frac{\bar{\varepsilon}}{1 + \psi_\varepsilon(\hat{x}, t)}, \tag{10.29}$$

where ψ_ε, named *domination function*, is non-negative and continuous in its arguments, $\hat{x}$ is the norm bound for the plant state x given in (10.11) and $\bar{\varepsilon} > 0$ is a design constant.

The HGO gain is inversely proportional to the small parameter ε which is time-varying due to the domination function $\psi_\varepsilon(\hat{x}, t)$ in (10.29). In [45], properties for $\psi_\varepsilon(\hat{x}, t)$ were established so that one can prove that the HGO estimation error is ultimately small, provided $\bar{\varepsilon}$ is chosen sufficiently small.

For each system trajectory, ε is absolutely continuous and $\varepsilon \leq \bar{\varepsilon}$. Note that ε is bounded for t in any finite sub-interval of $[0, t_M)$. Therefore,

$$\varepsilon(\hat{x}, t) \in [\underline{\varepsilon}, \bar{\varepsilon}], \quad \forall t \in [t_*, t_M), \tag{10.30}$$

for some $t_* \in [0, t_M)$ and $\underline{\varepsilon} \in (0, \bar{\varepsilon})$.

The proposed control law is given in (10.16) with the modulation function (10.13) and the sliding variable $\hat{\sigma}$ given by

$$\hat{\sigma} = S(\hat{\xi} - \xi_m), \tag{10.31}$$

where $\xi_m := [\, y_m \ \dot{y}_m \ \ldots \ y_m^{(n^*-1)} \,]^T$ and S is designed as in HGO with constant gain case. Then, by means of a novel ISS lemma for output feedback [45, Lemma 1], we can conclude global practical tracking. Thus, we could apply the dynamic gain HGO proposed in [44, 45] and peaking free norm state observers in order to extend the global tracking results via output feedback SMC to the class of nonlinear plants considered here.

In order to illustrate the time varying behavior of the variable parameter $\varepsilon(t)$, we consider the following simple academic case with no zeros dynamics and relative degree two ($n^* = 2$):

$$\begin{aligned} \dot{x}_1 &= x_2\,, \\ \dot{x}_2 &= -\delta_1 x_2 + k_p u + \delta_2 y^2 + \delta_3 \sin(2\pi\delta_4 t)\,, \\ y &= x_1\,. \end{aligned}$$

The plant is in the normal form given in (A1), with $k_p d = -\delta_1 x_2 + \delta_2 y^2 + \delta_3 \sin(2\pi\delta_4 t)$. The uncertain parameters are: $1 \le k_p \le 2$, $1 \le \delta_1, \delta_2 < 3$, $0.5 \le \delta_3 < 2$ and $8 \le \delta_4 \le 10$ (Hz). The *actual* plant parameters, assumed unknown, are $k_p = 2$, $\delta_1 = 2$, $\delta_2 = 1$, $\delta_3 = 0.7$ and $\delta_4 = 10$. Note that, since $x_1 = y$ is measured, only a norm bound for $x_2 = \dot{y}$ is needed. Moreover, by noting that $\delta_1 > 0$ a norm bound for $x_2 = \dot{y}$ can be easily obtained from the x_2-dynamics. The norm bound for the plant state $\hat{x} = 2|v_1| + |v_2| + |y|$ is valid *modulo* exponentially decaying terms, where v_1 and v_2 are such that: $\dot{v}_1 = -v_1 + u$ and $\dot{v}_2 = -v_2 + 8|v_1| + 3y^2 + 2$ (for details see [45]). The desired trajectory y_m is generated with $M(s) = \frac{4}{(s+2)^2}$ and $r = \operatorname{sgn}(\sin(0.5\pi t))$. The modulation and the HGO domination function are given by $f = 15|v_1| + 7.4|v_2| + 4.4|y| + 3y^2 + 4|r| + 2.1$ and $\psi_\varepsilon = 56|v_1| + 28|v_2| + 13|y| + 15y^2 + \|y_t\|\mathrm{e}^{-t} + 22$, respectively, where $\|y_t\|$ denotes the $\mathscr{L}_{\infty e}$ norm of the signal $y(t)$. Moreover, the HGO and the sliding surface are implemented with $l_1 = 2$, $l_2 = 1$ and $S = [\, 2 \ 1 \,]$.

For $y(0) = 0$ and $\dot{y}(0) = 0$ and with a constant and large value of $\varepsilon(t) = \bar{\varepsilon} = 1$ an apparent degradation in the closed loop tracking accuracy (y does not even converge to y_m) is observed in Fig. 10.4 (a). Moreover, for $y(0) = 5$ and $\dot{y}(0) = 0$, the plant output escapes at $t \approx 1.79$ seconds (not shown). On the other hand, when the time varying $\varepsilon(t)$ is implemented with the same large value for $\bar{\varepsilon} = 1$, the plant output converges to the desired trajectory from $y(0) = 5$, as shown in Fig. 10.4 (b). In this case, the time evolution of $\varepsilon(t)$ is shown in Fig. 10.4 (c), from which one can verify that a constant $\varepsilon = \bar{\varepsilon} = 0.0005$ could be used. However, this value is not known *a priori*. Moreover, care must be taken in reducing $\bar{\varepsilon}$, since there exists a trade off between measurement noise reduction and tracking accuracy.

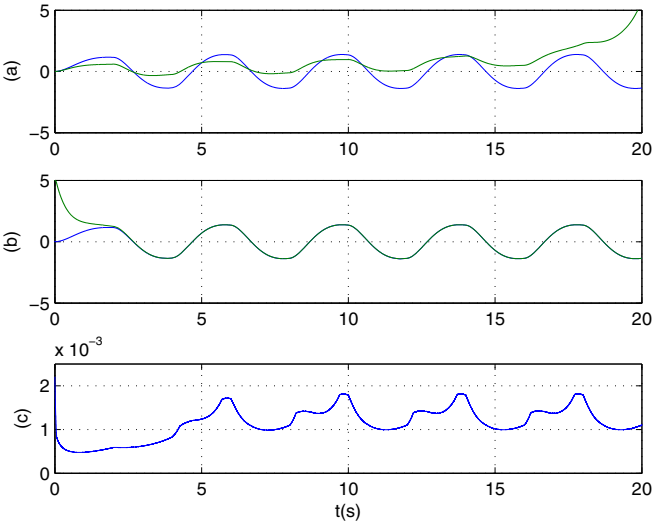

Fig. 10.4 Simulation results: (a) y, y_m when ε is held constant at $\varepsilon = 1$, with $y(0) = 0$ and $\dot{y}(0) = 0$; (b) y, y_m when $\varepsilon(t)$ is time-varying according to (10.29) with $\bar{\varepsilon} = 1$, $y(0) = 5$ and $\dot{y}(0) = 0$; (c) the time varying $\varepsilon(t)$.

10.7.4 Hybrid Estimation Scheme

Here, we restrict the class of plants, requiring that the term $\phi(x,t)$ in (10.1) to be given by $\phi(x,t) = bd(x,t)$, where $d(x,t)$ is assumed to be uncertain, locally integrable and uniformly bounded by $|d(x,t)| \leq \bar{d}(t)$, $\forall t$, with $\bar{d}(t)$ being known. In this case, the SMC using a lead filter can provide global stability properties, even in the presence of an additive disturbance β_α of order $\mathscr{O}(\tau)$ in the output of the estimator $\hat{\sigma}_l$ [37, 43]. A similar result can be derived for the other previously presented relative degree compensation strategies. However, if lead filters or high-gain observers are used to generate the sliding function [13, 2], one cannot ensure exact tracking for plants with relative degree greater than one.

In order to recover exact tracking, one can use the following differentiator based on higher-order sliding mode [32]:

$$\begin{aligned}
\dot{\eta}_0 &= v_0, \qquad v_0 = -\lambda_0 |\eta_0 - e(t)|^{\frac{n}{n+1}} \operatorname{sgn}(\eta_0 - e(t)) + \eta_1 , \\
&\vdots \\
\dot{\eta}_i &= v_i, \qquad v_i = -\lambda_i |\eta_i - v_{i-1}|^{\frac{n-i}{n-i+1}} \operatorname{sgn}(\eta_i - v_{i-1}) + \eta_{i+1} , \\
&\vdots \\
\dot{\eta}_n &= -\lambda_n \operatorname{sgn}(\eta_n - v_{n-1}) .
\end{aligned} \tag{10.32}$$

According to [32, Theorem 1], if the parameters λ_i $(i=0,\ldots,n)$ are properly chosen, (10.32) can provide the exact derivatives, in the absence of noise, after a finite-time transient process. Then, $\eta_0 = e$, $\eta_1 = \dot{e}$, etc. Hence, a RED of order (n^*-1) can be used to estimate σ (10.14) as follows:

$$\hat{\sigma}_r = \eta_{n^*-1} + l_{n^*-2}\eta_{n^*-2} + \cdots + l_1\eta_1 + l_0\eta_0\,, \tag{10.33}$$

If the control law $u = -[\mathrm{sgn}(k_p)]f(t)\,\mathrm{sgn}(\hat{\sigma}_r)$ is used, only local/semi-global stability properties could be guaranteed, even for linear systems, since [32, Theorem 1] requires that $e^{(n^*)}(t)$ should be uniformly bounded, which cannot be guaranteed *a priori* in the closed-loop system.

It should be noted that a modified version of the RED with time-dependent parameters, which allows differentiation of signals with unbounded higher derivatives, was proposed in [33]. However, if such modified RED were used in closed-loop control, its parameters could became quite large to ensure stability, making the RED exceedingly sensitive to noise and discretization [32, 33].

In the following, a hybrid estimation scheme is designed, trying to combine the desirable features of the RED and the previous estimation schemes.

The idea is to design a switching law to select between some general estimator (referred to as ISpS estimator), that provides an input-to-state practical stability property, with a locally exact differentiator in such a way that the stability properties are preserved and, in addition, exact tracking is achieved. More precisely, the ISpS estimator is such that the stability property of the closed-loop system is preserved, even in the presence of a bounded additive disturbance β_α at the output of the estimator, i.e., the closed-loop system is ISpS with respect to the disturbance β_α [37]. For instance, the lead filter and the high-gain observer satisfy this ISpS property.

The objective is to design a control scheme so as to achieve global exact tracking. To this end, we propose a hybrid estimator, named GRED, which consists of a convex combination of the estimate $\hat{\sigma}_e$ provided by the ISpS estimator and the RED estimate $\hat{\sigma}_r$ according to (see Figure 10.5):

$$\hat{\sigma}_g = \alpha(\tilde{\sigma}_{re})\hat{\sigma}_e(t) + [1-\alpha(\tilde{\sigma}_{re})]\,\hat{\sigma}_r(t)\,, \tag{10.34}$$

where $\tilde{\sigma}_{re} = \hat{\sigma}_r - \hat{\sigma}_e$ is the difference between both estimators. The switching function $\alpha(\tilde{\sigma}_{re})$ is a continuous, state dependent modulation which assumes values in the interval $[0,1]$ and allows the controller to smoothly change from one estimator to the other.

We now propose the following switching law for α:

$$\alpha(\tilde{\sigma}_{re}) = \begin{cases} 0\,, & \text{if } |\tilde{\sigma}_{re}| < \varepsilon_M - c\,, \\ (|\tilde{\sigma}_{re}| - \varepsilon_M + c)/c\,, & \text{if } \varepsilon_M - c \le |\tilde{\sigma}_{re}| < \varepsilon_M\,, \\ 1\,, & \text{if } |\tilde{\sigma}_{re}| \ge \varepsilon_M\,, \end{cases} \tag{10.35}$$

where $0 < c < \varepsilon_M$ is a boundary layer used to smoothen the switching function, and ε_M is an appropriate positive design parameter.

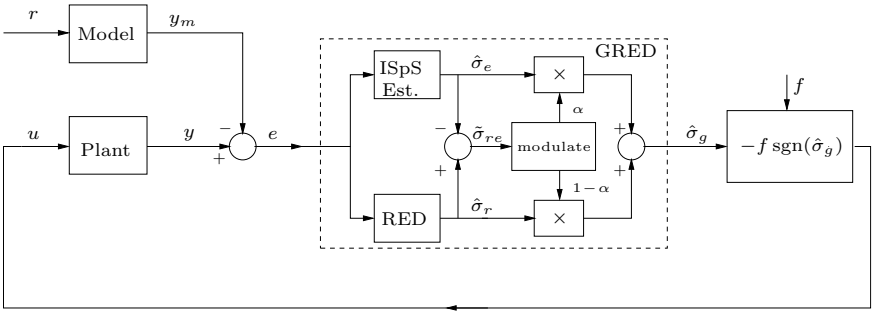

Fig. 10.5 Global RED based Sliding Mode Controller (GRED-SMC).

From (10.34), it can be concluded that $\beta_\alpha := \hat{\sigma}_g - \hat{\sigma}_e = (1-\alpha)\tilde{\sigma}_{re}$ and, with (10.35), one has

$$\hat{\sigma}_g = \hat{\sigma}_e + \beta_\alpha\,, \quad \text{and} \quad |\beta_\alpha| \leq \varepsilon_M\,, \tag{10.36}$$

which means that the resulting system is equivalent to a SMC using an ISpS estimator in the presence of the output disturbance β_α, which is uniformly bounded. Thus, global stability properties of the overall closed loop system can be assured and ultimately exact estimation of σ can be obtained [36, 37].

If we consider a broader class of plants, allowing a term ϕ that satisfies Assumption (A2), then only the SMC using a modified HGO with a dynamically variable gain can ensure global stability properties. However, this approach cannot guarantee exact tracking. To this end, we can implement the hybrid estimation scheme using this modified HGO, according to [36].

10.8 Peaking Phenomena Avoidance

It is well known that HGOs and linear lead filters may generate peaking in their signals. *Peaking phenomena* may be destabilizing and even provoke finite-time escape in closed-loop nonlinear systems [49]. Even for linear systems, peaking may lead to unacceptable transient performance [7].

For the case of real eigenvalues, the sliding variable $\hat{\sigma}_l(t)$ of (10.17) generated by the lead filter as well as $\hat{\sigma}_o(t)$ in (10.22) generated by the HGO contain a transient term of the form

$$\frac{a}{\mu^b}\,\mathrm{e}^{-\frac{ct}{\mu}}\,,$$

for some appropriate constants $a, b, c > 0$ possibly depending on the system initial conditions. The small parameter μ represents the time constant τ in the linear lead filter or ε in the HGO. Thus, the sliding variables $\hat{\sigma}_l(t)$ and $\hat{\sigma}_o(t)$ eventually exhibit an impulsive-like transient behavior, as $\mu \to 0$, where the transient peaks to $\mathscr{O}(1/\mu)$ values before decaying rapidly to zero [30], which is the origin of *peaking phenomena*.

Some alternatives for peaking alleviation developed by other researchers are the following:

1. The amplitude of the control signal can be globally bounded through saturation [38, 39]. This may restrict stability to become local or semi-global and precludes global stabilization of unstable linear systems;
2. The HGO *free of peaking* proposed by [5], which is based on a time-varying observer gain. Initially, the observer gain vector has small norm such that peaking is avoided. Thereafter, the observer gain vector converges exponentially to some specified high-gain vector such that the estimation error becomes small after the initial transient has vanished. However, this algorithm may fail in actual systems since disturbances may excite peaking when the observer gain is large, as recognized in [5].
3. The *semi-high-gain observer* [34], which is an HGO with a non conservative value for the observer gain, computed such that the closed-loop stability is guaranteed. However, this procedure, which was developed for stabilization purposes, seems inadequate for tracking applications where the observer gain must be large enough to keep the residual output error small.

The proposed output feedback controllers discussed in this chapter employ linear lead filters or HGO only to generate the switching law. The modulation function in the control law is synthesized using signals from the I/O filters which are free of peaking. This will lead us to obtain global (or semi-global) stability without peaking phenomena in the plant and control signals. It is remarkable that the original VS-MRAC [16, 22] developed for linear systems is intrinsically free of peaking since it is based on variable structure lead filters.

The dwell-time strategy for control activation introduced in [41, 40] is another approach for peaking avoidance. In this strategy, we only use the HGO estimates in the modulation function after a certain *dwell-time* τ_D, which is chosen large enough to allow the peaking transients of the HGO state to settle down, and small enough to ensure that the system trajectories do not leave a small prescribed compact set, thus avoiding finite-time escape. For $t \leq \tau_D$, we set $u := 0$. Other possibilities for assigning the value of u during the dwell-time could of course be envisaged.

The dwell-time method allows the inclusion of a more general class of uncertain strongly nonlinear systems satisfying a polynomial type growth even in the unmeasured state, not only in the measured output. It can also enhance the stability and performance of the HGO based controllers.

10.9 Chattering Alleviation

The importance of the existence of *ideal sliding mode* has been discussed in several works, e.g., [51, p. 210], [3], [15]. In the absence of measurement noise, the switching frequency can be arbitrarily increased by reducing the sampling period in practical real-time computer implementation of the control scheme or by reducing the delay of switching devices in the case of analog implementation. In many

applications, such as in electrical drives or converters, high frequency switching is acceptable and, therefore, the advantages of sliding mode control are preserved. In contrast, when using linear differentiators to replace the states required in the switching function $\hat{\sigma}$, inevitable small lags are introduced in the high-frequency loop and this usually leads to *chattering* with limited frequency, almost independent of the sampling period or switching delay, thus deteriorating the performance of sliding mode control. Achieving the *ideal sliding mode* avoids chattering in the sense that its effect would not be noticed at the plant output since chattering would occur with infinite frequency. Of course, noise, delay or unmodeled dynamics are ubiquitous in practical applications. So, as a rule, perfect tracking is not achievable in practice. However, when a given controller theoretically guarantees the existence of ideal sliding mode in the absence of such "imperfections", one should expect better performance in practice. Several ways to alleviate chattering were proposed in the literature. For the VS-MRAC, the introduction of a fast low pass filter was proposed to obtain what was called "Smooth Sliding Control", preserving an ideal sliding loop [15].

In the next section, we present the binary adaptive controller which bridges the parameter adaptive control with the SMC. The interest is that, through the increase of the adaptation gain, one can make the adaptive controller tend to the SMC. A compromise between the control precision and the level of chattering can be found by tuning the gain. Indeed, when the adaptation gain is sufficiently low, chattering does not occur but the performance may not be satisfactory. Hence such gain can be tuned so as to get the best from both approaches while avoiding their drawbacks, e.g., chattering.

10.10 Binary Model Reference Adaptive Control

The well known error equation of MRAC for linear plants of relative degree $n^* = 1$ is of the form (see eq. (10.9))

$$\begin{aligned} \dot{X}_e &= A_c X_e + b_c k^* \left[u - \theta^{*T} \omega \right], \\ e &= y - y_m = h_c^T X_e, \\ u &= \theta^T \omega, \end{aligned} \tag{10.37}$$

where $\{A_c, b_c, h_c^T\}$ is an appropriate nonminimal realization of the reference model transfer function assumed SPR.

The gradient adaptation law with a σ-modification [25] is given by

$$\dot{\theta} = -\sigma\theta - \gamma e\, \omega, \quad \sigma > 0, \tag{10.38}$$

with adaptation gain $\gamma > 0$. In variable structure adaptive control, according to [16], the input u can be

$$u = -f(t)\,\mathrm{sgn}(e), \qquad f(t) > \left| \theta^{*^T} \omega \right|. \tag{10.39}$$

For instance, $u = -M_\theta \|\omega\| \operatorname{sgn}(e)$, with $M_\theta > \|\theta^*\|$.

A binary version of (10.39) is given in [9] as follows

$$u = M_\theta \|\omega\| \mu(t), \tag{10.40}$$

$$\dot{\mu}(t) = \begin{cases} -\alpha \operatorname{sgn}(e), & \text{if } |\mu(t)| \leq 1, \\ -\beta \mu(t), & \text{if } |\mu(t)| > 1, \end{cases} \tag{10.41}$$

$t \geq 0$, $|\mu(0)| \leq 1$, where α and β are positive constants. It can be shown that all such solutions satisfy $|\mu(t)| \leq 1, \forall t > 0$ and, moreover, when $\alpha \to +\infty$, (10.41) becomes the bang-bang law $\mu = -\operatorname{sgn}(e)$. Thus, the binary MRAC (B-MRAC) (10.40) and (10.41) tends to the VSC law (10.39) as $\alpha \to +\infty$, in some sense.

It was proved in [19] that a B-MRAC with predictable and uniform transient behavior can be derived from the MRAC by using a projection factor and by (essentially) increasing the speed of adaptation, while keeping the adjustable parameter vector θ inside some finite ball of appropriate radius. The projection factor is given by:

$$\sigma = \begin{cases} 0, & \text{if } \|\theta\| < M_\theta \text{ or } \sigma_{eq} < 0, \\ \sigma_{eq}, & \text{if } \|\theta\| \geq M_\theta \text{ and } \sigma_{eq} \geq 0, \end{cases} \tag{10.42}$$

where $\sigma_{eq} = 1 - \gamma e \theta^T \omega / \|\theta\|^2$ and $M_\theta > \|\theta^*\|$ is constant. Let $B_\theta = \{\theta : \|\theta\| \leq M_\theta\}$. Assuming that $\theta(0) \in B_\theta$, the projection factor acts as follows. If at any time $\theta(t)$ is on the sphere $\|\theta\| = M_\theta$ and the term $-\gamma \omega^T e$ points outwards such sphere, the update vector is projected onto the tangent plane of the sphere; alternatively, if it points inwards, the σ-factor is equal to zero and $\theta(t)$ moves to the interior of the sphere. Then, it is straightforward to prove that the closed ball B_θ is invariant [17], i.e., $\theta(t) \in B_\theta, \forall t \geq 0$.

The B-MRAC has excellent adaptation properties for large enough γ. This results from the fact if $M_\theta > \|\theta^*\|$, then $\|X_e(t)\|$ tends exponentially fast to some residual set of order $O(\sqrt{1/\gamma})$. The foregoing properties were proved in [19] and [24] for the case of arbitrary relative degree.

10.11 Experimental Results

In this section, experiments with a DC motor are presented in order to illustrate the applicability of some of the proposed strategies to actual systems. Here, we restrict ourselves to some of the considered relative degree compensation schemes. Other experimental results can be found in [7,35].

The experiments were performed using a laboratory prototype based on a permanent magnet DC motor 2342024CR from MicroMo Electronics, Inc., with built in gear box (1:43). The control algorithm was implemented on a motion control system (Arcs Inc.) based on a digital signal processor (DSP) hosted in a microcomputer. The control signal u is the armature voltage, which is generated by a 12-bit digital-to-analog converter connected to a linear power amplifier (motor driver). The sampling frequency is 2.5 kHz. The motor angular position is measured by an incremental

optical encoder with resolution 1000 *counts per revolution* (cpr). The resolution of the measured angular position of the load is 172000 cpr due to the gear box and the electronics on the card.

The following nominal relative degree two model of the DC motor is used, neglecting the small electrical time constant

$$G_p(s) = \frac{y}{u} = \frac{k_p}{s(s+10)}, \tag{10.43}$$

where y is the angular position in degrees, u is the armature voltage in volts and the gain $k_p \in [600, 1000]$ is uncertain.

The aim of the experiment discussed here is to evaluate the practical advantage of RED ($\alpha = 0$), compared to a linear lead filter, in a real application, which also justifies the combination of the lead filter plus RED in order to obtain precise tracking with global stability properties.

In this experiment, the reference model is $M(s) = \frac{20}{(s+5)(s+20)}$ and the linear lead filter is given by $\frac{L}{F} = \frac{(s+5)}{(\tau s+1)}$, with $\tau = 2$ ms. The nonlinear lead filter (RED) is implemented as in (10.32) with $\lambda_0 = 100$ and $\lambda_1 = 2500$.

In order to simplify the control implementation, a constant modulation function was chosen to be $f(t) = 5$ which is sufficient enough to guarantee the model following. In what follows, we discuss in detail the results of the experiment.

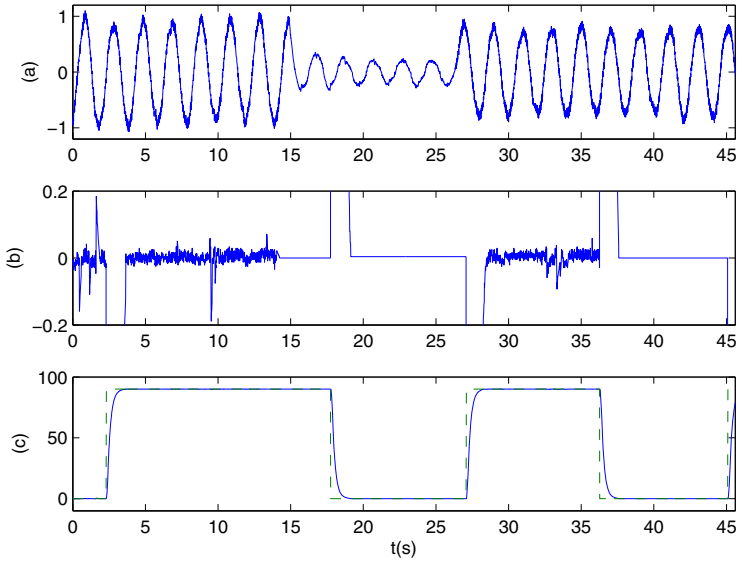

Fig. 10.6 Experiments using linear lead filter or RED based nonlinear lead filter: (a) output error e (tracking a sinusoid); (b) output error e in response to step inputs; (c) y (solid) and reference step inputs (dashed). All angles are expressed in degrees.

In Figure 10.6(a), the linear lead filter is applied for $t \in [0, 16)$ seconds. Then for $t \in [16, 26]$ seconds, it was manually switched to the nonlinear lead filter ($\alpha = 0$) and finally, it was switched back to the linear lead filter. One can clearly note the better performance of the RED based (nonlinear) filter and the performance degradation caused by the phase lag of the linear lead filter, with $\tau = 2$ ms. This time constant was *experimentally* tuned as small as possible so that the control chattering was acceptable.

Figures 10.6(b) and 10.6(c) present the response of the system to step changes in the reference input. For $t \in [14, 28]$ seconds and $t \in [37, 45]$ seconds, only the nonlinear lead filter is used, while in the remaining intervals of time, the linear lead filter is used. Noticeable chattering results in the latter case, during the steady state in the step following experiment. In contrast, the chattering is practically eliminated in the case of the nonlinear lead filter. Thus, remarkably superior *regulation* performance is observed when the RED based nonlinear lead filter is used.

10.12 Concluding Remarks

In this chapter, output feedback sliding mode controllers for output tracking of a reference model were presented. After a brief overview of the main approaches and results available in the literature, the focus was maintained on the controller named variable structure model-reference adaptive controller (VS-MRAC), which is a robust alternative to the well known model-reference adaptive controller (MRAC) based on parameter adaptation. More recently [53], the VS-MRAC has been referred as the variable structure model reference robust control (VS-MRRC) since it is based on signal synthesis without the need of parameter adaptation.

Several approaches for unmeasured states estimation have been considered to implement the switching laws. The control signals are free of peaking since the modulation functions use conventional input-output filters usual in the MRAC framework. Global or semi-global closed-loop stability properties are achieved for a class of uncertain nonlinear systems with arbitrary relative degree and linear growth restriction on the unmeasured states. It is noteworthy that less restrictive conditions are imposed to the measured output.

Exact output tracking is achieved by means of a hybrid compensator which combines linear lead filters or high-gain observers (HGO) with robust exact differentiators based on high-order sliding mode. For the class of nonlinear plants considered here, which encompasses minimum-phase systems with nonlinearities affinely norm bounded by unmeasured states with constant growth rate, global output tracking is achieved by using an HGO with dynamic gain. Experimental results are provided to show the applicability of some of the proposed methods.

Further developments could include the combination of the hybrid compensator and the dynamic HGO in order to obtain global exact output tracking. A well known limitation of model-reference control is that the plant is required to be minimum phase [26]. Output stabilization/tracking of uncertain nonminimum-phase plants is still an interesting contemporary issue. On the other hand, the adaptive pole

placement control (APPC) can be applied to nonminimum phase plants, since it has been developed in an indirect approach and does not require the cancellation of plant zeros. The Variable Structure Adaptive Pole Placement Control developed by [47] is based on new switching laws which replace the traditional integral adaptive laws. This new controller has significant performance improvements, such as fast transient and robustness to parametric uncertainties and disturbances.

Acknowledgements. This work was partially supported by CNPq, FAPERJ and CAPES (Brazil).

References

1. Bartolini, G., Levant, A., Pisano, A., Usai, E.: Higher-order sliding modes for the output-feedback control of nonlinear uncertain systems. In: Yu, X., Xu, J.-X. (eds.) Variable Structure Systems: Towards the 21st Century, pp. 83–108. Springer, Berlin (2002)
2. Boiko, I., Fridman, L.: Analysis of chattering in continuous sliding mode controllers. IEEE Trans. Aut. Contr. 50(9), 1442–1446 (2005)
3. Bondarev, A.G., Bondarev, S.A., Kostyleva, N.E., Utkin, V.I.: Sliding modes in systems with asymptotic state observers. Autom. Remote Control 46(6), 679–684 (1985)
4. Chang, P.H., Lee, J.W.: A model reference observer for time-delay control and its application to robot trajectory control. IEEE Trans. Contr. Syst. Tech. 4(1), 2–10 (1996)
5. Chitour, Y.: Time-varying high-gain observers for numerical differentiation. IEEE Trans. Aut. Contr. 47(9), 1565–1569 (2002)
6. Cunha, J.P.V.S., Costa, R.R., Hsu, L.: Design of first-order approximation filters for sliding-mode control of uncertain systems. IEEE Trans. Ind. Electronics 55(11), 4037–4046 (2008)
7. Cunha, J.P.V.S., Costa, R.R., Lizarralde, F., Hsu, L.: Peaking free variable structure control of uncertain linear systems based on a high-gain observer. Automatica 45(5), 1156–1164 (2009)
8. Edwards, C., Spurgeon, S.K.: Sliding Mode Control: Theory and Applications. Taylor & Francis Ltd., Taylor (1998)
9. Emelyanov, S.V.: Binary Automatic Control Systems. MIR Publishers, Moscow (1987)
10. Emelyanov, S.V., Korovin, S.K., Nersisian, A.L., Nisenzon, Y.Y.: Discontinuous output feedback stabilizing an uncertain MIMO plant. Int. J. Contr. 55(1), 83–107 (1992)
11. Esfandiari, F., Khalil, H.K.: Output feedback stabilization of fully linearizable systems. Int. J. Contr. 56(5), 1007–1037 (1992)
12. Filippov, A.F.: Differential equations with discontinuous right-hand side. American Math. Soc. Translations 42(2), 199–231 (1964)
13. Fridman, L.: An averaging approach to chattering. IEEE Trans. Aut. Contr. 46(8), 1260–1264 (2001)
14. Fridman, L., Levant, A.: Higher order sliding modes. In: Perruquetti, W., Barbot, J.B. (eds.) Sliding Mode Control in Engineering, ch. 3. Marcel Dekker, New York (2002)
15. Hsu, L.: Smooth sliding control of uncertain systems based on a prediction error. Int. J. on Robust and Nonlinear Control 7, 353–372 (1997)
16. Hsu, L., Araújo, A.D., Costa, R.R.: Analysis and design of I/O based variable structure adaptive control. IEEE Trans. Aut. Contr. 39(1), 4–21 (1994)
17. Hsu, L., Costa, R.R.: Adaptive control with discontinuous σ-factor and saturation for improved robustness. Int. J. Contr. 45(3), 843–859 (1987)

18. Hsu, L., Costa, R.R.: Variable structure model reference adaptive control using only input and output measurement: Part I. Int. J. Contr. 49(2), 399–416 (1989)
19. Hsu, L., Costa, R.R.: Binary control approach to design globally exponential stable systems. In: Proc. 7th Int. Conf. on Systems Engineering, Las Vegas, USA (1990)
20. Hsu, L., Costa, R.R., Cunha, J.P.V.S.: Model-reference output-feedback sliding mode controller for a class of multivariable nonlinear systems. Asian Journal of Control 5(4), 543–556 (2003)
21. Hsu, L., Cunha, J.P.V.S., Costa, R.R., Lizarralde, F.: Multivariable output-feedback sliding mode control. In: Yu, X., Xu, J.-X. (eds.) Variable Structure Systems: Towards the 21st Century, pp. 283–313. Springer, Berlin (2002)
22. Hsu, L., Lizarralde, F., Araújo, A.D.: New results on output-feedback variable structure model-reference adaptive control: design and stability analysis. IEEE Trans. Aut. Contr. 42(3), 386–393 (1997)
23. Hsu, L., Peixoto, A.J., Cunha, J.P.V.S., Costa, R.R., Lizarralde, F.: Output feedback sliding mode control for a class of uncertain multivariable systems with unmatched nonlinear disturbances. In: Edwards, C., Colet, F.E., Fridman, L. (eds.) Advances in Variable Structure and Sliding Mode Control, pp. 195–225. Springer, Berlin (2006)
24. Hsu, L., Real, J.A., Costa, R.R.: Dual mode adaptive control. In: Proc. IFAC 1999 World Congress, Beijing, vol. k, pp. 339–344 (July 1999)
25. Ioannou, P.A., Kokotovic, P.V.: Robust redesign of adaptive control. IEEE Trans. Aut. Contr. 29(3), 202–211 (1984)
26. Ioannou, P.A., Sun, J.: Robust Adaptive Control. Prentice-Hall, Englewood Cliffs (1996)
27. Isidori, A.: Nonlinear Control Systems II. Springer, London (1999)
28. Itkis, U.: Control Systems of Variable Structure. Wiley, New York (1976)
29. Jiang, Z.P., Teel, A.R., Praly, L.: Small-gain theorem for ISS systems and applications. Math. Control Signals Systems 7, 95–120 (1994)
30. Khalil, H.K.: Nonlinear Systems, 3rd edn. Prentice-Hall, Englewood Cliffs (2002)
31. Krichman, M., Sontag, E.D., Wang, Y.: Input-output-to-state stability. SIAM J. Contr. Optim. 39(6), 1874–1928 (2001)
32. Levant, A.: Higher-order sliding modes, differentiation and output-feedback control. Int. J. Contr. 76(9), 924–941 (2003)
33. Levant, A.: Exact differentiation of signals with unbounded higher derivatives. In: Proc. IEEE Conf. on Decision and Control, San Diego, CA, pp. 5585–5590 (December 2006)
34. Lu, X.-Y., Spurgeon, S.K.: Output feedback stabilization of SISO nonlinear systems via dynamic sliding modes. Int. J. Contr. 70(5), 735–759 (1998)
35. Nunes, E.V.L., Hsu, L., Lizarralde, F.: Output-feedback sliding mode control for global asymptotic tracking of uncertain systems using locally exact differentiators. In: Proc. American Contr. Conf. Minneapolis, pp. 5407–5412 (2006)
36. Nunes, E.V.L., Hsu, L., Lizarralde, F.: Global output feedback tracking controller based on hybrid estimation for a class of uncertain nonlinear systems. In: Proc. 10th Int. Workshop on Variable Structure Sys., Antalya, Turkey, pp. 141–146 (2008)
37. Nunes, E.V.L., Hsu, L., Lizarralde, F.: Global exact tracking for uncertain systems using output-feedback sliding mode control. IEEE Trans. Aut. Contr. 54(5), 1141–1147 (2009)
38. Oh, S., Khalil, H.K.: Output feedback stabilization using variable structure control. Int. J. Contr. 62(4), 831–848 (1995)
39. Oh, S., Khalil, H.K.: Nonlinear output-feedback tracking using high-gain observer and variable structure control. Automatica 33(10), 1845–1856 (1997)
40. Oliveira, T.R., Peixoto, A.J., Costa, R.R., Hsu, L.: Dwell-time and disturbance monitoring for peaking avoidance and performance improvement in high-gain observer based sliding mode control. In: Dynamics of Continuous, Discrete and Impulsive Systems Series B: Applications and Algorithms (2010) (to be published)

41. Oliveira, T.R., Peixoto, A.J., Hsu, L.: Peaking free output-feedback sliding mode control of uncertain nonlinear systems. In: Proc. American Contr. Conf., Seattle (WA), pp. 389–394 (June 2008)
42. Oliveira, T.R., Peixoto, A.J., Hsu, L.: Sliding mode control of uncertain multivariable nonlinear systems with unknown control direction via switching and monitoring function. IEEE Trans. Aut. Contr. 55(4), 1028–1034 (2010)
43. Oliveira, T.R., Peixoto, A.J., Nunes, E.V.L., Hsu, L.: Control of uncertain nonlinear systems with arbitrary relative degree and unknown control direction using sliding modes. Int. J. Adaptive Contr. Signal Process. 21(8/9), 692–707 (2007)
44. Peixoto, A.J., Hsu, L., Costa, R.R., Lizarralde, F.: Global tracking sliding mode control for uncertain nonlinear systems based on variable high gain observer. In: Proc. IEEE Conf. on Decision and Control, New Orleans (LA), pp. 2041–2046 (December 2007)
45. Peixoto, A.J., Oliveira, T.R., Hsu, L., Lizarralde, F., Costa, R.R.: Global tracking sliding mode control for a class of nonlinear systems via variable gain observer. Int. J. of Robust and Nonlinear Control (2010) (to be published)
46. Praly, L., Jiang, Z.: Linear output feedback with dynamic high gain for nonlinear systems. Systems & Contr. Letters 53, 107–116 (2004)
47. Silva Jr., F.C., Araújo, A.D.: Variable structure adaptive pole placement control. In: Proc. IEEE Conf. Decision and Control and the European Control Conf., Seville, Spain, pp. 2859–2864 (2005)
48. Sontag, E.D., Wang, Y.: Output-to-state stability and detectability of nonlinear systems. Systems & Contr. Letters 29, 279–290 (1997)
49. Sussmann, H.J., Kokotović, P.V.: The peaking phenomenon and the global stabilization of nonlinear systems. IEEE Trans. Aut. Contr. 36(4), 424–440 (1991)
50. Utkin, V.I.: Sliding Modes and Their Application in Variable Structure Systems. MIR Publishers, Moscow (1978)
51. Utkin, V.I.: Sliding Modes in Control and Optimization. Springer, Heidelberg (1992)
52. Walcott, B.L., Żak, S.: Combined observer-controller synthesis for uncertain dynamical systems with applications. IEEE Trans. Syst. Man. and Cyber. 18(1), 88–104 (1988)
53. Yan, L., Hsu, L., Costa, R.R., Lizarralde, F.: A variable structure model reference robust control without a prior knowledge of high frequency gain sign. Automatica 44(4), 1036–1044 (2008)

Chapter 11
Sliding Modes for Fault Detection and Fault Tolerant Control

C. Edwards, H. Alwi, C.P. Tan, and J.M. Andrade da Silva

Abstract. This chapter will describe the use of sliding mode ideas for fault detection leading to fault tolerant control. The fundamental purpose of a fault detection and isolation (FDI) scheme is to generate an alarm when a fault occurs and to pinpoint the source. Fault tolerant control (FTC) systems seek to provide, at worst, a degraded level of performance (compared to the fault free situation) in the event of a fault or failure developing in the system. This chapter will discuss how sliding mode methods for control system design and observer design, can be advantageously used for such schemes. The sliding mode observer FDI schemes seek to robustly estimate any unknown fault signal existing within the system based on appropriate scaling of the equivalent output estimation error injection signal. Both actuator fault and sensor fault problems are considered. One advantage of these sliding mode methods over more traditional residual based observer schemes is that because the faults are reconstructed, both the 'shape' and size of the faults are preserved. In the absence of modelling discrepancies, the faults would be reconstructed perfectly. In the uncertain case, the thresholds set for the reconstruction signals for alarm purposes, correspond directly to the level of faults than can (or must) be tolerated. A further benefit of this approach is that because faults are reconstructed, these signals can be used to correct a faulty sensor for example, to maintain reasonable performance until appropriate maintenance could be undertaken. This 'virtual sensor' can be used in the control algorithm to form the output tracking error signal which is processed to generate the control signal. In particular the chapter discusses recent advances which seek to obviate the traditional relative degree one minimum phaseness

C. Edwards · H. Alwi · J.M. Andrade da Silva
Control Group, University of Leicester
e-mail: {chris.edwards,ha18,jma28}@le.ac.uk

C.P. Tan
School of Engineering, Monash University, Malaysia
e-mail: tan.chee.pin@eng.monash.edu.my

L. Fridman et al. (Eds.): Sliding Modes, LNCIS 412, pp. 293–323.
springerlink.com

conditions. Also the effects of unmatched uncertainty are discussed. In all the methods proposed, efficient Linear Matrix Inequality methods are employed to synthesis the required gains. A recent application of sliding mode controllers for fault tolerant control is also presented. Here the inherent robustness properties of sliding modes to matched uncertainty are exploited. Although sliding mode controllers can cope easily with faults, they are not able to directly deal with failures – i.e. the total loss of an actuator. In order to overcome this, the integration of a sliding mode scheme with a control allocation framework is considered whereby the effectiveness level of the actuators is used by the control allocation scheme to redistribute the control signals to the 'healthy' actuators when a fault occurs.

11.1 Introduction

The fundamental purpose of a fault detection and isolation (FDI) scheme is to generate an alarm when a fault occurs and to pin-point the source [38]. Fault tolerant control (FTC) systems seek to provide, at worst, a degraded level of performance (compared to the fault free situation) in the event of a fault or failure developing in the system. Most existing FDI schemes in the literature are concerned with the design of so-called residuals. These residual signals are used as 'alarms' to indicate the occurrence of a fault, and if properly designed, give information from which the source of the fault may be identified. In analytic redundancy approaches, the residuals are (usually dynamic) weightings of the difference between the measured plant output and the output of a model of the system. Many fault detection methods are observer based; the observer will usually be designed from a model which will inevitably not be a perfect representation of the real system. In terms of the observer design, the plant/model mismatch will usually be encapsulated as uncertainty. The design procedure for the FDI scheme must then seek to minimize the effect of the uncertainty in an effort to minimize false alarms and missed faults when the scheme is implemented on a real system [12].

In the last decade the use of *sliding mode observers* for FDI has been explored. The novelty of the approach lies in the ability of sliding mode observers to reconstruct un-measurable signals within a process by appropriate scaling and filtering of the so-called 'equivalent output error injection' [23]. This is a unique property of sliding mode observers, which emanates from the fact that the introduction of a sliding motion forces the outputs of the observer to perfectly track the plant measurements [23]. Reconstruction approaches attempt to capture both the magnitude and 'shape' of the faults, which can be advantageous. The fact that even in the presence of faults the output of the sliding mode observer still perfectly follows the plant output, means residuals formulated in the usual way – i.e. as functions of the output estimation error – would always be zero. As a consequence, the effect of the faults is seen through the fact that the equivalent output error injection term must compensate for the fault in order to maintain sliding.

11.2 Sliding Mode Observers for Fault Detection

A relevant model of the problem may be posed as

$$\dot{x} = Ax + Q\xi(x,t) + Mf(u,t) \tag{11.1}$$
$$y = Cx, \tag{11.2}$$

where $A \in \mathbb{R}^{n\times n}$, $Q \in \mathbb{R}^{n\times h}$, $M \in \mathbb{R}^{n\times q}$ and $C \in \mathbb{R}^{p\times n}$. The state $x(t)$ is assumed to be unknown. The bounded unknown function $f(u,t)$ represents the actuator fault to be estimated. The term $\xi(x,t)$ represents uncertainty affecting the system and is assumed to satisfy

$$\|\xi(x,t)\| \leq k_1\|u(t)\| + \alpha(t,y(t)) + k_2 \tag{11.3}$$

where k_1 and k_2 are scalars and $\alpha(\cdot)$ is a known function. In [21], under passivity-like conditions for the system $((A-GC),M,C)$, where G represents a design gain in the observer, it was shown the sliding mode dynamics associated with the observer error can be decoupled from the uncertainty/faults. Unlike existing work where only estimates of the faults are obtained, here the fault can be precisely reconstructed, i.e. asymptotically estimated with an arbitrary level of accuracy. The same class of systems is considered in [23] but a more flexible stance is adopted. Two assumptions are made:

A1) rank(CM)=rank(M)
A2) the invariant zeros of the matrix triple (A,M,C) lie in the left half plane.

In [21] an observer of the form

$$\dot{\hat{x}}(t) = A\hat{x}(t) + Bu(t) - G_l e_y(t) + G_n \nu \tag{11.4}$$
$$\hat{y}(t) = C\hat{x}(t) \tag{11.5}$$

where $G_l \in \mathbb{R}^{n\times p}$ and $G_n \in \mathbb{R}^{n\times p}$ are gain matrices to be designed. The output error injection vector $\nu \in \mathbb{R}^p$, which induces a sliding motion, is given by

$$\nu = \begin{cases} -\rho(t,y(t),u(t))\dfrac{P_2 e_y(t)}{\|P_2 e_y(t)\|} & \text{if } e_y(t) \neq 0 \\ 0 & \text{otherwise} \end{cases} \tag{11.6}$$

where $e_y(t) = \hat{y}(t) - y(t)$ is the output estimation error. In the above, $P_2 \in \mathbb{R}^{p\times p}$ is a symmetric positive definite (s.p.d.) matrix. The function $\rho : \mathbb{R}_+ \times \mathbb{R}^p \times \mathbb{R}^m \to \mathbb{R}_+$ is chosen to satisfy

$$\rho(t,y,u) \geq k_1\|u(t)\| + \alpha(t,y(t)) + k_2 + \eta \tag{11.7}$$

where $\eta \in \mathbb{R}_+$. An estimate of the unknown fault is then postulated as

$$\hat{f}(t) = W\nu_{eq}(t) \tag{11.8}$$

where v_{eq} represents the equivalent injection necessary to maintain a sliding motion and $W \in \mathbb{R}^{q \times p}$. The idea is to synthesize the gains G_l, G_n and W so that

- in the absence of uncertainty $\hat{f} \to f$ as $t \to \infty$;
- if uncertainty is present then $\|\hat{f} - f\|$ is minimized in an appropriate norm.

The synthesis of the observer design parameters can be posed as a convex optimization problem and solved using Linear Matrix Inequality (LMI) techniques [8] in a systematic way. If 'precise' fault reconstruction is not possible, the LMI optimization seeks to minimize the effect of the uncertainty on the reconstruction. Robustness to the uncertainty in the modelling process is vital. The disturbances corrupt the reconstruction, and could produce a significantly nonzero reconstruction when there are no faults, or worse, mask the effect of a fault. Edwards *et al.* [23,22] used a sliding mode observer [21] to reconstruct faults, in which there was no explicit consideration of the disturbances or uncertainty. Tan & Edwards [43] built on the work in [22,23] and presented a design algorithm for the observer, using LMIs, such that the $\mathscr{L}_2$ gain from the disturbances to the fault reconstruction is minimized. Saif & Guan [39] aggregated the faults and disturbances to form a new augmented 'fault' vector and used a linear unknown input observer to reconstruct the new 'fault' vector. A necessary condition in [23,22,43,39] is that the first Markov parameter of the system connecting the fault to the output must be full rank. This limits the class of systems to which [23,22,43,39] are applicable.

Recently, there have been developments in fault reconstruction for systems whose first *Markov parameter is not full rank*. Floquet & Barbot [26] transformed the system into an 'output information' form such that existing sliding mode observer techniques can be implemented to estimate the states in finite time and reconstruct the faults. However, in [26] there is no explicit consideration of disturbances or uncertainty. Higher order sliding mode schemes have been suggested by [5,14,29]. The work in [29] uses the concept of 'strong observability' together with higher order sliding mode observers. Strong observability has also been exploited in [5] using a hierarchy of observers. Chen & Saif advocate a bank of high-order sliding-mode differentiators to obtain derivatives of the outputs and then estimate the faults from these signals [14]. Floquet *et.al* suggest the use of exact differentiators to generate derivatives of the measurements to 'create' additional outputs [27] to circumvent relative degree assumptions. However all the work in [26,14,27,5,29] does not consider uncertainty – unless the faults and uncertainty are augmented and treated as 'unknown inputs'. In this case the number of disturbances plus faults must not exceed the number of outputs. This results in strong constraints which must be satisfied, and hence a smaller class of systems for which the results are applicable. Ng *et al.* [37] extended the work in [43] exploiting two sliding mode observers in cascade; known signals from the first observer were considered as outputs of a 'fictitious' system which has a full rank (first) Markov parameter; then a second sliding mode observer is designed based on the fictitious system to reconstruct the fault. This enables robust fault reconstruction for systems where the number of disturbances and faults exceed the number of outputs (which cannot be achieved by [26,14]). The next section builds on [37] using multiple observers in cascade.

11.3 A Cascade Based Robust Fault Reconstruction Scheme

The use of sliding mode observers in a cascade framework for unknown input estimation is not new [40,34,33,35]. However the work in [33] assumes full state measurement, whilst [34] does not consider any external disturbances. Although [40] considers both faults and uncertainties, they are aggregated and are both treated as unknown inputs – this introduces considerable conservatism. Here the faults and disturbances are treated differently. Using similar techniques as in [37], measurable signals from an observer are used as outputs of a fictitious system; the next observer is designed for the fictitious system and the known signals from this observer are used as outputs of another fictitious system. The process is repeated until a fictitious system whose (first) Markov parameter is full rank is obtained. The technique proposed in [43] is then used to robustly reconstruct the fault. This results in robust fault reconstruction applicable to a wider class of systems than in [37]. The final fictitious system is found to be in the same framework as [43] which minimizes the $\mathscr{L}_2$ gain from the disturbances to the fault reconstruction; this enables the algorithm to be applicable for systems when the number of outputs are less than the sum of faults and disturbance channels. In addition, it is found that the design of previous observers does not affect the sliding motion of the final observer, which implies that the $\mathscr{L}_2$ gain from the disturbances to the fault reconstruction is not affected. First re-write the system in (11.1)-(11.2) as

$$\dot{x}^1 = A^1 x^1 + M^1 f^1 + Q^1 \xi^1 \tag{11.9}$$

$$y^1 = C^1 x^1 \tag{11.10}$$

where $x^1 \in \mathbb{R}^{n^1}$ are the states, $y^1 \in \mathbb{R}^p$ are the outputs and $f^1 \in \mathbb{R}^q$ are unknown faults. The signals $\xi^1 \in \mathbb{R}^h$ are uncertainties or dynamics that represent the mismatch between the linear model (11.9) and the real plant. Assume without loss of generality $rank(M^1) = q, rank(C^1) = p$ and $rank(C^1 M^1) = \bar{r}^1 < q$, implying that $\bar{r}^1 \leq \min\{p,q\}$. Since $rank(C^1) = p$, then C^1 can be written without loss of generality in the form $C^1 = \begin{bmatrix} 0 & I_p \end{bmatrix}$.

The objective is to reconstruct f^1 whilst minimizing the effects of ξ^1 on the fault reconstruction. If $h + q > p$ and $\bar{r}^1 < q$, then the approaches suggested in [23,22,39,43,40,5,14,29,26,27] are *not applicable*. In this situation, the following section proposes the cascade observer scheme.

For the algorithm which will be described in the sequel, partition the matrices from (11.9) as

$$A^1 = \begin{bmatrix} A_1^1 & A_2^1 \\ A_3^1 & A_4^1 \end{bmatrix}, \; M^1 = \begin{bmatrix} M_1^1 \\ M_2^1 \end{bmatrix}, \; Q^1 = \begin{bmatrix} Q_1^1 \\ Q_2^1 \end{bmatrix} \begin{matrix} \updownarrow n^1 - p \\ \updownarrow p \end{matrix}$$

where A_1^1 is square. Since by assumption $C^1 = \begin{bmatrix} 0 & I_p \end{bmatrix}$ and $rank(C^1 M^1) = \bar{r}^1$, then it follows that $rank(M_2^1) = \bar{r}^1$. In the above, Q^1 has no particular structure.

11.3.1 Summary of Fault Reconstruction Algorithm

The fault reconstruction method can be summarized in the following steps. Set $i = 1$ and enter the following algorithm:

1. Consider the generic uncertain faulty system

$$\dot{x}^i = A^i x^i + M^i f^i + Q^i \xi^i \tag{11.11}$$
$$y^i = C^i x^i \tag{11.12}$$

and define $\bar{r}^i := rank(C^i M^i)$.

   a. If $rank(C^i M^i) = rank(M^i)$, set $i = k$ and jump to step 7.
   b. If $rank(C^i M^i) < rank(M^i)$ and $i = n^1$, then the method cannot be used to reconstruct the faults [44] and terminate the algorithm.

   If neither (a) nor (b) are satisfied, proceed to the next step.
2. For the case when $i = 1$, define the following

$$\bar{M}_{11}^0 := M_1^1, \bar{M}_{12}^0 := M_2^1, m^1 := p, \bar{r}^0 := 0 \tag{11.13}$$

$$\tilde{A}_{13}^0 := A_3^1, \tilde{A}_{11}^0 := A_1^1, \ \bar{A}_{\Omega}^0 = \alpha^0 = \bar{M}_{22}^0 = \phi \tag{11.14}$$

where ϕ is the empty matrix. Then A^i and M^i can be expanded as

$$\left[\begin{array}{cc|ccc} \bar{A}_{\Omega}^{i-1} & 0 & \star & 0 & 0 \\ \star & \tilde{A}_{11}^{i-1} & \star & 0 & 0 \\ \hline \star & \tilde{A}_{13}^{i-1} & \star & 0 & 0 \\ \star & 0 & \star & -\alpha^{i-1} I & 0 \\ \star & \star & \star & 0 & -\alpha^{i-1} I \end{array}\right] \quad M^i = \left[\begin{array}{cc} 0 & 0 \\ \bar{M}_{11}^{i-1} & 0 \\ \hline \bar{M}_{12}^{i-1} & 0 \\ 0 & 0 \\ 0 & \alpha^{i-1} \bar{M}_{22}^{i-1} \end{array}\right] \begin{array}{l} \updownarrow (i-1)h \\ \updownarrow n^i - p - (i-1)h \\ \updownarrow m^i \\ \updownarrow p - \bar{r}^{i-1} - m^i \\ \updownarrow \bar{r}^{i-1} \end{array} \tag{11.15}$$

3. Define orthogonal matrices $D^i \in \mathbb{R}^{m^i \times m^i}$ and $T_2^i \in \mathbb{R}^{(q-\bar{r}^{i-1}) \times (q-\bar{r}^{i-1})}$ such that

$$\left[\begin{array}{cc} I & 0 \\ 0 & (D^i)^{-1} \end{array}\right] \left[\begin{array}{c} \bar{M}_{11}^{i-1} \\ \bar{M}_{12}^{i-1} \end{array}\right] (T_2^i)^{-1} = \left[\begin{array}{cc} M_{11}^i & M_{12}^i \\ \hline 0 & 0 \\ 0 & M_{22}^i \end{array}\right] \tag{11.16}$$

and $M_{22}^i \in \mathbb{R}^{r^i \times r^i}$ is invertible. Let $T_1^i := T_{11}^i \times diag\left\{I_{n^i-p}, (D^i)^{-1}, I_{p-m^i}\right\}$ where

$$T_{11}^i = \left[\begin{array}{cc|ccc} I & 0 & 0 & 0 & 0\ 0 \\ 0 & I & 0 & -M_{12}^i (M_{22}^i)^{-1} & 0\ 0 \\ \hline 0 & 0 & I & 0 & 0\ 0 \\ 0 & 0 & 0 & 0 & I\ 0 \\ 0 & 0 & 0 & I & 0\ 0 \\ 0 & 0 & 0 & 0 & 0\ I \end{array}\right] \begin{array}{l} \updownarrow h \\ \updownarrow n^i - p - h \\ \updownarrow m^i - r^i \\ \updownarrow p - m^i - \bar{r}^{i-1} \\ \updownarrow r^i \\ \updownarrow \bar{r}^{i-1} \end{array} \tag{11.17}$$

Define

$$\tilde{A}_3^i := (D^i)^{-1}\tilde{A}_{13}^{i-1} = \begin{bmatrix} \tilde{A}_{31}^i \\ \tilde{A}_{32}^i \end{bmatrix} \begin{matrix} \updownarrow m^i - r^i \\ \updownarrow r^i \end{matrix} \tag{11.18}$$

and

$$\tilde{A}_1^i := \tilde{A}_{11}^{i-1} - M_{12}^i (M_{22}^i)^{-1}\tilde{A}_{32}^i \tag{11.19}$$

Perform the coordinate transformation

$$x^i \mapsto T_1^i x^i,\ f^i \mapsto f^{i+1} := \underbrace{\begin{bmatrix} T_2^i & 0 \\ 0 & I_{\bar{r}^{i-1}} \end{bmatrix}}_{T_f^i} f^i \tag{11.20}$$

then the matrix triple (A^i, M^i, C^i) will have the form

$$\begin{bmatrix} A_1^i & A_2^i \\ A_3^i & A_4^i \end{bmatrix} = \left[\begin{array}{cc|c} \bar{A}_\Omega^{i-1} & 0 & \star \\ \star & \tilde{A}_1^i & \star \\ \hline \star & \tilde{A}_{31}^i & \star \\ \star & 0 & \star \\ \star & \star & \star \end{array}\right] \quad \begin{bmatrix} M_1^i \\ M_2^i \end{bmatrix} = \left[\begin{array}{cc} 0 & 0 \\ M_{11}^i & 0 \\ \hline 0 & 0 \\ 0 & 0 \\ 0 & \bar{M}_{22}^i \end{array}\right] \begin{matrix} \updownarrow (i-1)h \\ \updownarrow n^i - p - (i-1)h \\ \updownarrow m^i - r^i \\ \updownarrow p - m^i - \bar{r}^{i-1} \\ \updownarrow \bar{r}^i \end{matrix} \tag{11.21}$$

(11.22)

where $C^i = \begin{bmatrix} 0 & C_2^i \end{bmatrix}$ and

$$\bar{M}_{22}^i = \begin{bmatrix} M_{22}^i & 0 \\ 0 & \alpha^{i-1}\bar{M}_{22}^{i-1} \end{bmatrix} \begin{matrix} \updownarrow r^i \\ \updownarrow \bar{r}^{i-1} \end{matrix} \text{ and } C_2^i = diag\left\{D^i, I_{p-m^i}\right\} \begin{bmatrix} I & 0 & 0 & 0 \\ 0 & 0 & I & 0 \\ 0 & I & 0 & 0 \\ 0 & 0 & 0 & I \end{bmatrix} \begin{matrix} \updownarrow m^i - r^i \\ \updownarrow p - \bar{r}^{i-1} - m^i \\ \updownarrow r^i \\ \updownarrow \bar{r}^{i-1} \end{matrix}$$

4. Assume ξ^i satisfies

$$\dot{\xi}^i = A_\Omega^i \xi^i + B_\Omega^i \xi^{i+1} \tag{11.23}$$

Augment (11.23) with (11.11) to obtain

$$\dot{\bar{x}}^i = \bar{A}^i \bar{x}^i + \bar{M}^i f^{i+1} + \bar{Q}^i \xi^{i+1} \tag{11.24}$$

$$y^i = \bar{C}^i \bar{x}^i \tag{11.25}$$

where

$$\bar{A}^i = \left[\begin{array}{cccc|c} A_\Omega^i & 0 & 0 & 0 & \\ \star & \bar{A}_\Omega^{i-1} & 0 & \star & \\ \star & \star & \tilde{A}_1^i & \star & \\ \hline \star & \star & \tilde{A}_{31}^i & \star & \\ \star & \star & 0 & \star & \\ \star & \star & \star & \star & \end{array}\right] \begin{matrix} \updownarrow h \\ \updownarrow (i-1)h \\ \updownarrow n^i - p - (i-1)h \\ \updownarrow m^i - r^i \\ \updownarrow p - m^i - \bar{r}^{i-1} \\ \updownarrow \bar{r}^i \end{matrix} \quad \bar{M}^i = \left[\begin{array}{cc} 0 & 0 \\ M_{11}^i & 0 \\ \hline 0 & 0 \\ 0 & \bar{M}_{22}^i \end{array}\right] \begin{matrix} \updownarrow ih \\ \updownarrow n^1 - p - (i-1)h \\ \updownarrow p - \bar{r}^i \\ \updownarrow \bar{r}^i \end{matrix}$$

Define

$$\bar{A}^i_\Omega := \begin{bmatrix} A^i_\Omega & 0 \\ \star & \bar{A}^{i-1}_\Omega \end{bmatrix} \quad \Rightarrow \quad \bar{A}^i = \left[\begin{array}{cc|c} \bar{A}^i_\Omega & 0 & 0 \\ \star & \tilde{A}^i_1 & \star \\ \hline \bar{Q}^i_{21} & \tilde{A}^i_{31} & \star \\ \star & 0 & \star \\ \star & \star & \star \end{array}\right] \begin{array}{l} \updownarrow ih \\ \updownarrow n^i - p - (i-1)h \\ \updownarrow m^i - r^i \\ \updownarrow p - m^i - \bar{r}^{i-1} \\ \updownarrow \bar{r}^i \end{array}$$

5. Define $m^{i+1} := rank(\tilde{A}^i_{31})$. If $m^{i+1} < q - \bar{r}^i$, then the fault can never be fully reconstructed [44] and terminate the algorithm. Otherwise, let U^i_1 and U^i_2 be invertible matrices of dimension $m^i - r^i$ and $n^i - p - (i-1)h$ such that

$$U^i_1 \tilde{A}^i_{31} (U^i_2)^{-1} = \begin{bmatrix} 0 & I_{m^{i+1}} \\ 0 & 0 \end{bmatrix}, \; U^i_1 \bar{Q}^i_{21} = \begin{bmatrix} \bar{Q}^i_{211} \\ \bar{Q}^i_{212} \end{bmatrix} \tag{11.26}$$

where $\bar{Q}^i_{211}, \bar{Q}^i_{212}$ are matrices with no particular structure. Also partition

$$U^i_2 \tilde{A}^i_1 (U^i_2)^{-1} = \begin{bmatrix} \tilde{A}^i_{11} & \tilde{A}^i_{12} \\ \tilde{A}^i_{13} & \tilde{A}^i_{14} \end{bmatrix} \begin{array}{l} \updownarrow n^i - p - m^{i+1} - (i-1)h \\ \updownarrow m^{i+1} \end{array} \tag{11.27}$$

Define a transformation $\bar{x}^i \mapsto \bar{T}^i \bar{x}^i$ where $\bar{T}^i := diag\left\{I_{ih}, U^i_2, U^i_1, I_{p+r^i-m^i}\right\} \bar{T}^i_1$ with

$$\bar{T}^i_1 := \left[\begin{array}{ccc|c} I & 0 & 0 & 0 \\ 0 & I & 0 & 0 \\ \bar{Q}^i_{211} & 0 & I & 0 \\ \hline 0 & 0 & 0 & I \end{array}\right] \begin{array}{l} \updownarrow ih \\ \updownarrow n^i - p - (i-1)h - m^{i+1} \\ \updownarrow m^{i+1} \\ \updownarrow p \end{array} \tag{11.28}$$

then $\bar{A}^i, \bar{M}^i, \bar{C}^i$ are transformed to be

$$\begin{bmatrix} \bar{A}^i_1 & \bar{A}^i_2 \\ \bar{A}^i_3 & \bar{A}^i_4 \end{bmatrix} = \left[\begin{array}{ccc|c} \bar{A}^i_\Omega & 0 & 0 & \star \\ \star & \tilde{A}^i_{11} & \tilde{A}^i_{12} & \star \\ \star & \tilde{A}^i_{13} & \tilde{A}^i_{14} & \star \\ \hline 0 & 0 & I & \star \\ \star & \star & \star & \star \\ \star & \star & \star & \star \end{array}\right] \quad \begin{bmatrix} \bar{M}^i_1 \\ \bar{M}^i_2 \end{bmatrix} = \left[\begin{array}{cc} 0 & 0 \\ \bar{M}^i_{11} & 0 \\ \bar{M}^i_{12} & 0 \\ \hline 0 & 0 \\ 0 & \bar{M}^i_{22} \end{array}\right] \begin{array}{l} \updownarrow ih \\ \updownarrow n^i - p - m^{i+1} - (i-1)h \\ \updownarrow m^{i+1} \\ \updownarrow p - \bar{r}^i \\ \updownarrow \bar{r}^i \end{array} \tag{11.29}$$

and

$$\bar{C}^i = \begin{bmatrix} 0 & \bar{C}^i_2 \end{bmatrix} \quad \text{where } \det \bar{C}^i_2 \neq 0 \tag{11.30}$$

Finally partition

$$\bar{A}^i_3 = \begin{bmatrix} \bar{A}^i_{31} \\ \bar{A}^i_{32} \end{bmatrix} \begin{array}{l} \updownarrow m^{i+1} \\ \updownarrow p - m^{i+1} \end{array} \tag{11.31}$$

which from (11.29) results in $\bar{A}^i_{31} = \begin{bmatrix} 0 & I_{m^{i+1}} \end{bmatrix}$.

6. A sliding mode observer [21] for the system (11.24) - (11.25) is

$$\dot{\hat{x}}^i = \bar{A}^i \hat{\bar{x}}^i - \bar{G}_l^i \bar{e}_y^i + \bar{G}_n^i \bar{v}^i \tag{11.32}$$

$$\hat{y}^i = \bar{C}^i \bar{x}^i \tag{11.33}$$

where $\hat{\bar{x}}^i \in \mathbb{R}^{\bar{n}^i}$ is the estimate of $\bar{x}^i$ and $\bar{e}_y^i = \hat{y}^i - y^i$ is the output estimation error. The matrices $\bar{G}_l^i, \bar{G}_n^i \in \mathbb{R}^{\bar{n}^i \times p}$ are observer gains (to be designed). In the coordinate system of (11.29) - (11.30), $\bar{G}_n^i$ will be assumed to have the structure

$$\bar{G}_n^i = \begin{bmatrix} -\bar{L}^i \\ I_p \end{bmatrix} (\bar{P}_o^i \bar{C}_2^i)^{-1}, \quad \bar{L}^i = \begin{bmatrix} \bar{L}_o^i & 0 \end{bmatrix} \tag{11.34}$$

where $\bar{P}_o^i \in \mathbb{R}^{p \times p}$ is a s.p.d matrix, $\bar{L}^i \in \mathbb{R}^{(\bar{n}^i - p) \times p}$ and $\bar{L}_o^i \in \mathbb{R}^{(\bar{n}^i - p) \times m^{i+1}}$. The term $\bar{v}^i$ in (11.32) is a discontinuous term defined by

$$\bar{v}^i = -\bar{\rho}^i \frac{\bar{e}_y^i}{\|\bar{e}_y^i\|}, \ \bar{\rho}^i \in \mathbb{R}_+ \tag{11.35}$$

Define $\bar{e}^i := \hat{\bar{x}}^i - \bar{x}^i$ as the state estimation error, and combine equations (11.24), (11.25) and (11.32) - (11.33) to obtain the error system

$$\dot{\bar{e}}^i = (\bar{A}^i - \bar{G}_l^i \bar{C}^i)\bar{e}^i + \bar{G}_n^i \bar{v}^i - \bar{M}^i f^{i+1} - \bar{Q}^i \xi^{i+1} \tag{11.36}$$

Proposition 11.1. *[43] Consider a s.p.d. matrix*

$$\bar{P}^i = \begin{bmatrix} \bar{P}_1^i & \bar{P}_1^i \bar{L}^i \\ (\bar{P}_1^i \bar{L}^i)^T & (\bar{C}_2^i)^T \bar{P}_o^i \bar{C}_2^i + (\bar{L}^i)^T \bar{P}_1^i \bar{L}^i \end{bmatrix} \tag{11.37}$$

where $\bar{P}_1^i \in \mathbb{R}^{(\bar{n}^i - p) \times (\bar{n}^i - p)}$. Assume that

$$\bar{P}^i (\bar{A}^i - \bar{G}_l^i \bar{C}^i) + (\bar{A}^i - \bar{G}_l^i \bar{C}^i)^T \bar{P}^i < 0 \tag{11.38}$$

Then, for a large enough $\bar{\rho}^i$ in (11.35), an ideal sliding motion takes place on $\bar{\mathbb{S}}^i = \{\bar{e}^i : \bar{C}^i \bar{e}^i = 0\}$ in finite time.

Apply a change of coordinates T_L^i to (11.29) - (11.30) and $\bar{G}_n^i$ in (11.34) where

$$T_L^i := \begin{bmatrix} I_{\bar{n}^i - p} & \bar{L}^i \\ 0 & \bar{C}_2^i \end{bmatrix}$$

then $\bar{A}^i, \bar{M}^i, \bar{C}^i, \bar{Q}^i$ from (11.29) - (11.30) and $\bar{G}_n^i$ are transformed to have the structures

$$\bar{A}^i \to \begin{bmatrix} \bar{A}_1^i + \bar{L}_o^i \bar{A}_{31}^i & \star \\ \bar{C}_2^i \bar{A}_3^i & \star \end{bmatrix}, \ \bar{M}^i \to \begin{bmatrix} \bar{M}_1^i \\ \bar{C}_2^i \bar{M}_2^i \end{bmatrix} \tag{11.39}$$

$$\bar{C}^i \to \begin{bmatrix} 0 & I_p \end{bmatrix}, \ \bar{Q}^i \to \begin{bmatrix} \bar{Q}_1^i & 0 \end{bmatrix}, \ \bar{G}_n^i \to \begin{bmatrix} 0 \\ (\bar{P}_o^i)^{-1} \end{bmatrix} \tag{11.40}$$

Assume that a sliding motion is taking place on $\bar{\mathbb{S}}^i$ so that $\bar{e}_y^i = \dot{\bar{e}}_y^i = 0$, then (11.36) can be partitioned in the new coordinates associated with (11.39) - (11.40) as

$$\dot{\bar{e}}_1^i = (\bar{A}_1^i + \bar{L}_o^i \bar{A}_{31}^i)\bar{e}_1^i - \bar{M}_1^i f^{i+1} - \bar{Q}_1^i \xi^{i+1} \tag{11.41}$$

$$0 = \bar{C}_2^i \bar{A}_3^i \bar{e}_1^i - \bar{C}_2^i \bar{M}_2^i f^{i+1} + (\bar{P}_o^i)^{-1} \bar{v}_{eq}^i \tag{11.42}$$

where $\bar{v}_{eq}^i$ is the equivalent output error injection required to maintain a sliding motion [23, 22]. As the term $\bar{e}_y^i$ is a measurable signal, the signal $\bar{v}_{eq}^i$ is computable online and is available for use in an online FDI scheme [23, 22].

Define $w^i := -\bar{e}_1^i$ and re-arrange (11.41) - (11.42) to obtain

$$\dot{w}^i = (\bar{A}_1^i + \bar{L}_o^i \bar{A}_{31}^i)w^i + \bar{M}_1^i f^{i+1} + \bar{Q}_1^i \xi^{i+1} \tag{11.43}$$

$$(\bar{P}_o^i \bar{C}_2^i)^{-1} \bar{v}_{eq}^i = \bar{A}_3^i w^i + \bar{M}_2^i f^{i+1} \tag{11.44}$$

and let

$$z^i := (\bar{P}_o^i \bar{C}_2^i)^{-1} \bar{v}_{eq}^i = \begin{bmatrix} z_1^i \\ z_2^i \end{bmatrix} \begin{matrix} \updownarrow m^{i+1} \\ \updownarrow p - m^{i+1} \end{matrix}$$

Note, as argued above, z_1^i and z_2^i are available in real time. Substituting for $\bar{A}_3^i$ from (11.31) results in

$$z_1^i = \begin{bmatrix} 0 & I_{m^{i+1}} \end{bmatrix} w^i \tag{11.45}$$

$$z_2^i = \bar{A}_{32}^i w^i + \begin{bmatrix} 0 & 0 \\ 0 & \bar{M}_{22}^i \end{bmatrix} f^{i+1} \tag{11.46}$$

Define a signal z_f^i, (also available in real time), as an output from a stable filter

$$\dot{z}_f^i := -\alpha^i z_f^i + \alpha^i z_2^i \tag{11.47}$$

where $\alpha^i \in \mathbb{R}_+$. From (11.46) and (11.47):

$$\dot{z}_f^i = -\alpha^i z_f^i + \alpha^i \bar{A}_{32}^i w^i + \begin{bmatrix} 0 & 0 \\ 0 & \alpha^i \bar{M}_{22}^i \end{bmatrix} f^{i+1} \tag{11.48}$$

Combining (11.43), (11.45) and (11.48) the following state-space system

$$\dot{x}^{i+1} = A^{i+1} x^{i+1} + M^{i+1} f^{i+1} + Q^{i+1} \xi^{i+1} \tag{11.49}$$

$$y^{i+1} = C^{i+1} x^{i+1} \tag{11.50}$$

can be obtained where $x^{i+1} := col(w^i, z_f^i)$ and $y^{i+1} := col(z_1^i, z_f^i)$ and

$$A^{i+1} := \begin{bmatrix} \bar{A}_1^i + \bar{L}_o^i \bar{A}_{31}^i & 0 \\ \alpha^i \bar{A}_{32}^i & -\alpha^i I_{p-m^{i+1}} \end{bmatrix} \quad M^{i+1} := \begin{bmatrix} \bar{M}_1^i \\ \begin{bmatrix} 0 & 0 \\ 0 & \alpha^i \bar{M}_{22}^i \end{bmatrix} \end{bmatrix} \quad Q^{i+1} := \begin{bmatrix} \bar{Q}_1^i \\ 0 \end{bmatrix} \tag{11.51}$$

and

$$C^{i+1} := \begin{bmatrix} 0 & I_p \end{bmatrix} \tag{11.52}$$

Notice that (11.49) is in the form of (11.9) and C^{i+1} and C^i have the same structure. It is clear that $f^{i+1} \in \mathbb{R}^q, \xi^{i+1} \in \mathbb{R}^h$. Let $x^{i+1} \in \mathbb{R}^{n^{i+1}}, y^{i+1} \in \mathbb{R}^p$ and define $\bar{r}^{i+1} := rank(C^{i+1}M^{i+1})$. Note that $\bar{r}^{i+1} \leq q$. It can be seen that

$$n^{i+1} = n^i + h - m^{i+1} \tag{11.53}$$

Increment the counter i by 1 and return to step 1.

7. Since $rank(C^k M^k) = rank(M^k)$, then the robust fault reconstruction approach from [43] may be adopted to estimate f^k, which minimizes the effect of the disturbance ξ^k. Define $\hat{f}^k$ to be the estimate of f^k, then the reconstruction of f^1 can be obtained from

$$\hat{f}^1 := (T_f^k)^{-1} \ldots (T_f^2)^{-1} (T_f^1)^{-1} \hat{f}^k \tag{11.54}$$

where the T_f^i are defined in (11.20).

Remarks 11.1.

- Notice from the structure of A^i in (11.15), the matrix $\bar{L}_o^{i-1}$ appears only in the last p columns of A^i. From the structure of C^i in (11.52), it is clear that $\bar{L}_o^{i-1}$ affects only the p output states of x^i, and hence $\bar{L}_o^{i-1}$ will not affect the reduced order sliding motion of observer i and also all subsequent observers. From [43], the quality of the fault reconstruction depends on the sliding motion of observer k, which is independent of $\bar{L}_o^i$ from previous observers.
- The equivalent output error injection in (11.42) can be obtained by approximating the discontinuous term in (11.35) using a smoothing function or by low pass filtering [20]. In a cascade observer scheme, inaccuracies due to the approximations will be compounded and this could adversely affect the quality of the fault reconstruction. A solution to this would be to use second order sliding mode approaches which do not require approximations to obtain the equivalent output error injection [5]. This can be done by replacing the discontinuous term in (35) with the supertwisting structure [5]. Details of this approach are described in [44].

11.3.2 Design Example

The method described above will now be demonstrated using a model of a civil aircraft [19] whose matrices are given as follows:

$$A^1 = \begin{bmatrix} -0.5137 & -0.5831 & -0.6228 & 0.0004 & 0 \\ 1.0064 & -0.6284 & -0.0352 & -0.0021 & 0 \\ 0 & 0 & -37.0000 & 0 & 0 \\ 0 & 1.7171 & 0 & -0.0166 & -9.8046 \\ 1.0000 & 0 & 0 & 0 & 0 \end{bmatrix}, \; M^1 = \begin{bmatrix} 0 \\ 0 \\ 37 \\ 0 \\ 0 \end{bmatrix}$$

where the states are q, α, elevator position, V_{tas}, θ. The input is the elevator command. It is assumed that the first and second rows of the matrix A^1 contain uncertainties. The problem is to reconstruct actuator faults using only measurement of speed and pitch angle. Notice that the method in [26] cannot be used on this system as there is no consideration of the disturbance ξ^1. If the signals f^1 and ξ^1 are augmented to form a new 'fault' vector, this results in the new 'fault' vector having 3 components. The number of outputs in this system is only 2, and hence the methods in [26, 40] are not applicable. It can be established that $n^1 = 5, p = 2, q = 1, h = 2, \bar{r}^1 = 0$.

The filter matrices that appropriately describe the characteristics of ξ^1 are chosen here as $A^1_\Omega = -10I_2, B^1_\Omega = 10I_2$. Note this choice is not unique: in this example, first order linear filter realizations have been chosen, although higher order filters could equally well have been used. The crucial decision is the choice of the filter bandwidth and not the particular choice of filter itself. With this choice of filter, it can be shown that $C^2M^2 = 0$, and hence $\bar{r}^2 = 0$ which results in $r^2 = 0$. Here the matrices A^2_Ω, B^2_Ω that describe ξ^2 are chosen as $A^2_\Omega = -10I_2, B^2_\Omega = 10I_2$. It can be shown this gives $m^3 = 1$ and $rank(C^3M^3) = rank(M^3)$. Finally, the robust sliding mode observer can be designed based on A^3, M^3, C^3, Q^3 using Step 7 of the algorithm.

Figure 11.1 shows the nominal case when there is no uncertainty. The left subfigure of Figure 11.2 shows the disturbances ξ^1 that impact on the system, and the right subfigure shows ξ^3 which is the fictitious disturbance signal obtained from ξ^1 by performing the operation $\xi^2 = \frac{1}{10}\dot{\xi}^1 + \xi^1, \xi^3 = \frac{1}{10}\dot{\xi}^2 + \xi^2$ (which is the reverse of the filtering process of ξ^3 used to obtain ξ^1. It can be seen in Figure 11.2 that ξ^3 is visually identical to ξ^1 which implies the weighting function for the disturbance

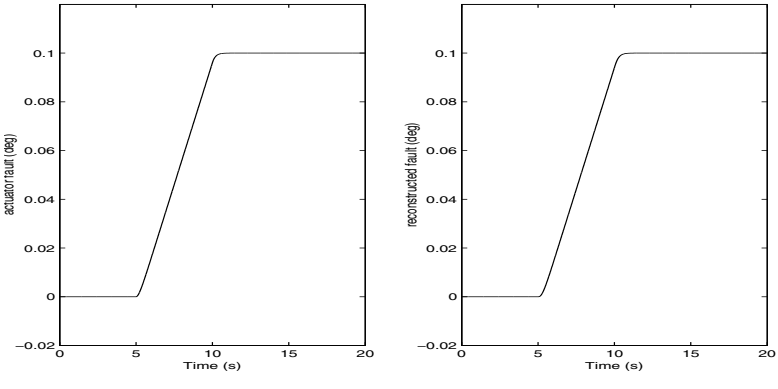

Fig. 11.1 The fault applied to the actuator (left) and its reconstruction (right) for the case when $\Delta A^1 = 0$ i.e. when there is no uncertainty.

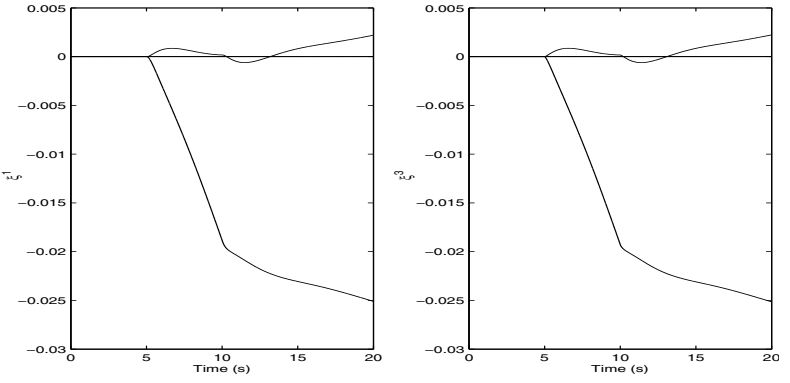

Fig. 11.2 The components of ξ^1 (left) and the fictitious signal ξ^3 (right)

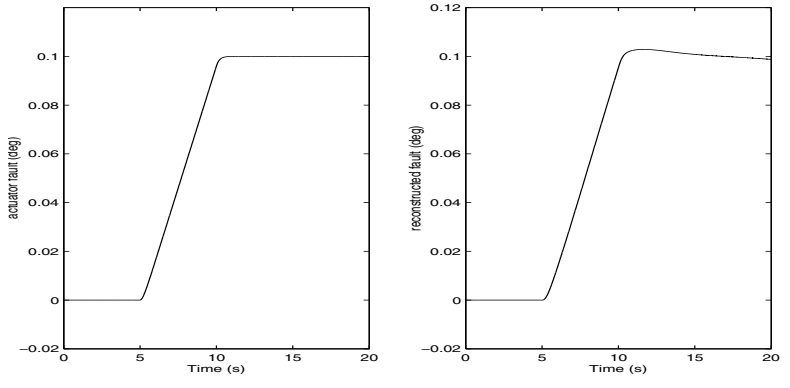

Fig. 11.3 The fault reconstruction in the presence of uncertainty in A^1.

using the values of $A^1_\Omega = A^2_\Omega = -10I_2, B^1_\Omega = B^2_\Omega = 10I_2$ is valid for this example. The right subfigure of Figure 11.3 shows the fault reconstruction. Although there is a slight degradation due to ΔA^1, the reconstruction is not severely affected by ξ^1 (which is significant – being more than 10% of the magnitude of the fault).

11.4 Reconstruction of Incipient Sensor Faults

The methods for sensor fault estimation proposed in [43, 42] require one (testable) assumption, to guarantee the existence of the observer design. A sufficient condition in [43, 42] is that the system needs to be open-loop stable in order to robustly estimate the sensor faults. Open-loop stability is not a necessary condition, but for open-loop unstable systems with certain classes of faults, examples can be constructed such that the methods in [43, 42] are not applicable. Note that

classical linear unknown input observers (UIO) also *cannot* be employed in this situation [24, 11, 13, 17, 39].

This section discusses a new observer design for sensor fault reconstruction which addresses this restriction. In particular the proposed observer designs are applicable for open-loop stable and unstable systems. Consider initially[1] a nominal dynamical system affected by sensor faults modelled as

$$\dot{x}(t) = Ax(t) + Bu(t) \tag{11.55}$$

$$y(t) = Cx(t) + Ff_o(t) \tag{11.56}$$

where $A \in \mathbb{R}^{n\times n}, B \in \mathbb{R}^{n\times m}, C \in \mathbb{R}^{p\times n}$ and $F \in \mathbb{R}^{p\times q}$, with $n \geq p > q$. Assume that the matrices C and F have full row and column rank respectively. Without loss of generality, it can be assumed that the outputs of the system have been reordered (and scaled if necessary) so that the matrix F has a structure

$$F = \begin{bmatrix} 0 \\ I_q \end{bmatrix} \tag{11.57}$$

The function $f_o : \mathbb{R}_+ \to \mathbb{R}^q$ is unknown but smooth and bounded. The signal $f_o(t)$ represents (additive) sensor faults and F represents a distribution matrix, which indicates which of the sensors providing measurements are prone to possible faults.

The objective is to design a sliding mode observer to reconstruct the faults $f_o(t)$ using only $y(t)$ and $u(t)$. Suppose the signal f_o is smooth and assume

$$\varphi(t) := \dot{f}_o(t) \tag{11.58}$$

It is assumed that the sensor faults are incipient and so $\|\varphi(t)\|$ is small in magnitude, but over time the effects of the fault increment, and become significant. Equations (11.55) and (11.58) can be combined to give a system of order $n+q$ with states $x_a := \mathrm{col}(x, f_o)$ in the form

$$\begin{bmatrix} \dot{x}(t) \\ \dot{f}_o(t) \end{bmatrix} = \underbrace{\begin{bmatrix} A & 0 \\ 0 & 0 \end{bmatrix}}_{A_a} \begin{bmatrix} x(t) \\ f_o(t) \end{bmatrix} + \underbrace{\begin{bmatrix} B \\ 0 \end{bmatrix}}_{B_a} u(t) + \underbrace{\begin{bmatrix} 0 \\ I_q \end{bmatrix}}_{F_a} \varphi(t) \tag{11.59}$$

$$y(t) = \underbrace{\begin{bmatrix} C & F \end{bmatrix}}_{C_a} \begin{bmatrix} x(t) \\ f_o(t) \end{bmatrix} \tag{11.60}$$

Equations (11.59) and (11.60) represent an *unknown input problem* for (A_a, F_a, C_a) driven by the unmeasurable signal $\varphi(t)$. From (11.60), and based on the structure of F in (11.57),

$$C_a = \begin{bmatrix} C & F \end{bmatrix} = \begin{bmatrix} C_1 & 0 \\ C_2 & I_q \end{bmatrix} \tag{11.61}$$

[1] An extension to uncertain systems is discussed in [4].

where $C_1 \in \mathbb{R}^{p-q\times n}$ and $C_2 \in \mathbb{R}^{q\times n}$. Notice (A_a, F_a, C_a) is inherently relative degree one since $C_a F_a = F$ and $\text{rank}(F) = q$ by assumption.

Lemma 11.1. *[4] The triple (A_a, F_a, C_a) is minimum phase iff (A, C_1) is detectable.*

Lemma 11.2. *[4] The pair (A_a, C_a) is observable if (A, C_1) does not have an unobservable mode at zero or if the open loop system in (11.55) is stable.*

Assume without loss of generality that C from (11.56) is given as

$$C = \begin{bmatrix} C_1 \\ C_2 \end{bmatrix} = \begin{bmatrix} 0 & 0 & I_{p-q} \\ 0 & I_q & 0 \end{bmatrix} \tag{11.62}$$

For any system with C of full rank, this canonical form can be achieved by a change of coordinates. Change coordinates in (11.59) and (11.60) according to $x_a \mapsto T x_a$ where

$$T = \begin{bmatrix} I_n & 0 \\ C_2 & I_q \end{bmatrix} \tag{11.63}$$

The triple in the new coordinates is $(TA_aT^{-1}, TF_a, C_aT^{-1})$ where

$$TA_aT^{-1} = \begin{bmatrix} A & 0 \\ C_2A & 0 \end{bmatrix} \quad C_aT^{-1} = \begin{bmatrix} 0 & I_p \end{bmatrix} \quad TF_a = F_a = \begin{bmatrix} 0 \\ I_q \end{bmatrix} \tag{11.64}$$

from the definition of C_1 in (11.62). In the x_a coordinates

$$f_o(t) = C_f x_a(t) \tag{11.65}$$

where

$$C_f := \begin{bmatrix} 0_{q\times n} & I_q \end{bmatrix} \tag{11.66}$$

After the change of coordinates $x_a \mapsto T x_a$ the new matrix relating the states to the fault signals f_o is

$$C_f T^{-1} = \begin{bmatrix} 0 & I_q \end{bmatrix} \begin{bmatrix} I & 0 \\ -C_2 & I_q \end{bmatrix} = \begin{bmatrix} 0_{q\times(n-p)} & -I_q & 0_{q\times(p-q)} & I_q \end{bmatrix} \tag{11.67}$$

using C_2 as defined in (11.62). Write

$$A_a = \begin{bmatrix} A_{11} & A_{12} \\ A_{21} & A_{22} \end{bmatrix} = \left[\begin{array}{c|c} A_{11} & A_{12} \\ \hline A_{211} & \\ A_{212} & A_{22} \end{array}\right] \tag{11.68}$$

where $A_{11} \in \mathbb{R}^{(n+q-p)\times(n+q-p)}$. Define A_{211} as the top $p-q$ rows of A_{21}. By construction, the unobservable modes of (A_{11}, A_{211}) are the invariant zeros of (A_a, F_a, C_a) [23]. Also define $F_2 \in \mathbb{R}^{p\times q}$ as the bottom p rows of F_a so that

$$F_2 = \begin{bmatrix} 0_{(p-q)\times q} \\ I_q \end{bmatrix} \tag{11.69}$$

Assumption 1: Assume that the triple (A,B,C) is such that the new pair (A,C_1) associated with (11.59)-(11.61) does not have unobservable modes at the origin.

For the system in (11.59) - (11.60) consider a sliding mode observer of the form given in (11.4)-(11.5). An appropriate gain G_n for the nonlinear injection term ν in (11.4) is

$$G_n = \begin{bmatrix} -L \\ I_p \end{bmatrix} \quad \text{where} \quad L = \begin{bmatrix} L_1 \; L_2 \end{bmatrix} \tag{11.70}$$

and $L_1 \in \mathbb{R}^{(n+q-p)\times(p-q)}$ and $L_2 \in \mathbb{R}^{(n+q-p)\times q}$ represent design freedom [21,45]. If $e := z - x_a$ then

$$\dot{e}(t) = (A_a - G_l C_a)e(t) - F_a\varphi + G_n\nu \tag{11.71}$$

where φ is defined in (11.58). For an appropriate choice of $\rho(t,y,u)$ in (11.6), it can be shown that an ideal sliding motion takes place on $\mathscr{S} = \{e : C_a e = 0\}$ in finite time: for details see [43]. The sliding motion is governed by

$$\dot{e} = (A_a - G_n(C_aG_n)^{-1}C_aA_a)e - (F_a - G_n(C_aG_n)^{-1}C_aF_a)\varphi \tag{11.72}$$

Partition the state error vector e from (11.71), conformably with the canonical form in (11.68), as $\mathrm{col}(e_1,e_y)$. To identify the reduced order sliding motion, perform a further change of coordinates according to the nonsingular matrix

$$T_L = \begin{bmatrix} I_{n+q-p} & L \\ 0 & I_p \end{bmatrix} \tag{11.73}$$

so that

$$e = (e_1,e_y) \to (e_1 + Le_y, e_y) \equiv (\tilde{e}_1, e_y) =: \tilde{e} \tag{11.74}$$

It can be easily verified that in the coordinate system in (11.74), during the sliding motion, the error system (i.e. the reduced order sliding motion) can be written as

$$\dot{\tilde{e}}_1(t) = \big(A_{11} + L_1A_{211} + L_2A_{212}\big)\tilde{e}_1(t) + L_2\varphi \tag{11.75}$$

$$\dot{e}_y(t) = e_y(t) = 0 \tag{11.76}$$

The matrices L_1 and L_2 needed to be chosen to ensure $A_{11} + LA_{211} + L_2A_{212}$ is stable for the sliding motion to be stable. The effect of φ on the estimation $\hat{f}_o$ is given by $C_f e = \tilde{C}_f\tilde{e}$ where $\tilde{C}_f = C_f T_L^{-1}$ and C_f is given in (11.66). It can be verified

$$\tilde{C}_f = \begin{bmatrix} 0_{n-p\times q} \; I_q \; * \end{bmatrix} \tag{11.77}$$

where $*$ represents a matrix which plays no part in the subsequent analysis. During the sliding motion,

$$\tilde{C}_f\tilde{e} = \begin{bmatrix} 0_{n-p\times q} \; I_q \big| * \end{bmatrix} \begin{bmatrix} \tilde{e}_1 \\ e_y \end{bmatrix} = \underbrace{\begin{bmatrix} 0_{n-p\times q} \; I_q \end{bmatrix}}_{C_e} \tilde{e}_1 \tag{11.78}$$

since $e_y = 0$ during sliding. The effect of φ on the reconstruction is $\tilde{G}(s)\varphi$ where

$$\tilde{G}(s) := \left[\begin{array}{c|c} A_{11}+L_1A_{211}+L_2A_{212} & L_2 \\ \hline C_e & 0 \end{array}\right] \tag{11.79}$$

and C_e is defined in (11.78). Since the pair (A_{11},A_{211}) is observable, from the partition of A_{21} in (11.68) to obtain A_{211} and A_{212}, it follows that there exist L_1 and L_2 so that $A_{11}+L_1A_{211}+L_2A_{212}$ is stable. Furthermore:

Proposition 11.2. *[4] If (A_a,F_a,C_a) from (11.55)-(11.56) is minimum phase, then a sliding mode observer of the form in (11.4)-(11.5) exists such that $\hat{f}_o = C_f x_a \to f_o$ as $t \to \infty$.*

Proposition 11.3. *[4] If the system matrix A from (11.55) is stable, $\hat{f}_o = C_f z_a \to f_o$ as $t \to \infty$.*

Remark 11.1. If A from (11.55) is unstable then for certain fault conditions, (A,C_1) may be unobservable and perfect reconstruction is not possible. Furthermore if (A,C_1) is undetectable making (A_a,F_a,C_a) nonminimum phase, then as argued in [24], unknown input observers cannot be employed to reject φ (see for example [39, 17, 13, 11]).

Define a Lyapunov matrix for the error system in (11.71) of the form

$$P = \begin{bmatrix} P_{11} & P_{12} \\ P_{12}^{\mathrm{T}} & P_{22} \end{bmatrix} \tag{11.80}$$

where $P_{11} \in \mathbb{R}^{(n+q-p)\times(n+q-p)}$ is s.p.d. Let $G_l \in \mathbb{R}^{(n+q)\times p}$ be a matrix satisfying

$$P(A_a - G_lC_a) + (A_a - G_lC_a)^{\mathrm{T}}P < 0 \tag{11.81}$$

Here, the design of G_l from (11.4) will be chosen to satisfy

$$\begin{bmatrix} P(A_a - G_lC_a) + (A_a - G_lC_a)^{\mathrm{T}}P & P(G_lD - B_d) & E^{\mathrm{T}} \\ (G_lD - B_d)^{\mathrm{T}}P & -\gamma_0 I_{p+q} & 0 \\ E & 0 & -\gamma_0 I_q \end{bmatrix} < 0 \tag{11.82}$$

The matrices $B_d \in \mathbb{R}^{(n+q)\times(p+q)}$, $D \in \mathbb{R}^{p\times(p+q)}$ in (11.82) are defined as

$$B_d := \begin{bmatrix} 0 & F_a \end{bmatrix} \tag{11.83}$$

$$D := \begin{bmatrix} D_1 & 0 \end{bmatrix} \tag{11.84}$$

where $D_1 \in \mathbb{R}^{p\times p}$ and

$$E = \begin{bmatrix} C_e & F_2^{\mathrm{T}} \end{bmatrix} \tag{11.85}$$

where C_e is defined in (11.78). Formally the design problem is:

For given D_1 and γ_0: minimize γ with respect to P, subject to (11.82) and

$$\begin{bmatrix} X_{11} & -P_{122} & C_e \\ -P_{122}^{\mathrm{T}} & -\gamma I_q & 0 \\ C_e & 0 & -\gamma I_q \end{bmatrix} < 0 \tag{11.86}$$

$$P > 0 \tag{11.87}$$

This is a convex optimization problem. Standard LMI software such as [30] can be used to synthesize numerically γ and P. Once P has been determined, L can be determined as $L = P_{11}^{-1} P_{12}$. As argued in [42] a possible choice of the s.p.d matrix P_0 associated with the unit-vector term (11.6) is $P_0 = P_{22} - P_{21} P_{11}^{-1} P_{12}$.

11.4.1 Simulation Results

The ADMIRE model represents a small rigid fighter aircraft with a delta-canard configuration. Details of the model can be found in [28]. The linear model used for design has been obtained at a low speed flight condition of Mach 0.22 at an altitude of 3000m and is similar to the one in [32]. The states are $x = [\alpha\ \beta\ p\ q\ r]^{\mathrm{T}}$ with controlled outputs α, β, p; where α is angle of attack (AoA) (rad), β is sideslip angle (rad), p is roll rate (rad/sec), q is pitch rate (rad/sec) and r is yaw rate (rad/sec).

The linear model is open-loop unstable, which is a typical characteristic of fighter aircraft to allow high manoeuvrability. It is assumed that the sensor for the pitch rate (q) is prone to faults. It can be shown the associated augmented system (A_a, F_a, C_a)

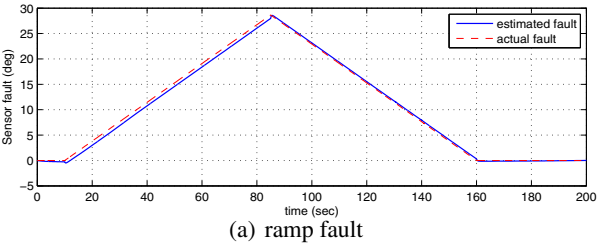

(a) ramp fault

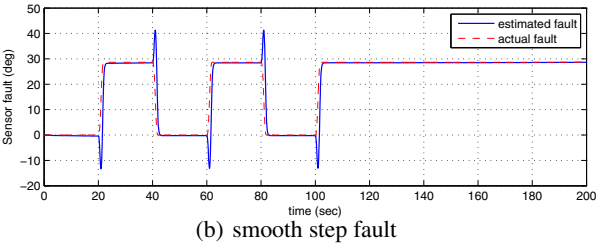

(b) smooth step fault

Fig. 11.4 Sensor fault reconstruction on the pitch rate (q) sensor on ADMIRE full nonlinear model

is non–minimum phase [4]. The design parameters for the observer were chosen as, $\gamma_0 = 10$ from (11.82) and $D_1 = I_3$ from (11.84); this yields $\|\tilde{G}(s)\|_\infty = 1.2212$.

The simulation in Figure 11.4 has been obtained from the full nonlinear ADMIRE model with the aircraft undergoing a banking manoeuvre and change in altitude. Figure 11.4 shows the results of the fault reconstruction using different sensor fault shapes, to show the effectiveness of the method. In both conditions, the proposed scheme provides satisfactory fault reconstructions on the q sensor when tested on the full nonlinear model. As expected, perfect fault estimation cannot be achieved.

11.5 Unmatched Parametric Uncertainty

This section considers the effect of parametric uncertainty on state estimation. Consider

$$\dot{x}(t) = \big(A + \Delta A(t)\big)x(t) + B\big(u(t) + \xi(t,x,u)\big) \tag{11.88}$$

$$y(t) = Cx(t) \tag{11.89}$$

where $A \in \mathbb{R}^{n\times n}$, $B \in \mathbb{R}^{n\times m}$ and $C \in \mathbb{R}^{p\times n}$. The uncertain system matrix $\Delta A(t)$ depends upon the time-varying uncertain vector $\theta(t) : \mathbb{R}_+ \to \Theta$, where $\Theta \subseteq \mathbb{R}^r$ is the parameter space. In this section it is again assumed that A1 holds, i.e $rank(CB) = m$. If the state estimation error is defined as

$$e(t) = \hat{x}(t) - x(t) \tag{11.90}$$

then, it follows from (11.88) and (11.4) that the error system dynamics are governed by

$$\dot{e}(t) = \big(A - G_l C\big)e(t) - \Delta A(t)x(t) + G_n \nu - B\xi(\cdot) \tag{11.91}$$

Note the effect of the mismatched uncertainty contained in $\Delta A(t)$ cannot be rejected. The problem to be addressed consists of synthesizing a sliding mode observer defined in (11.4)-(11.5) which guarantees robust stable error system dynamics and the existence of a stable sliding motion, despite the uncertainties present in the system (11.88)-(11.89), in finite time on the sliding hyperplane

$$\mathscr{S}_{Obs} = \big\{e(t) \in \mathbb{R}^n : e_y(t) = Ce(t) = 0\big\} \tag{11.92}$$

Under assumption A1 it can be assumed the system in (11.88)- (11.89) has the structure

$$A = \begin{bmatrix} A_{11} & A_{12} \\ A_{21} & A_{22} \end{bmatrix} \quad B = \begin{bmatrix} 0 \\ B_2 \end{bmatrix} \quad C = \begin{bmatrix} 0 & T \end{bmatrix} \tag{11.93}$$

where $B_2 \in \mathbb{R}^{m\times m}$ and $T \in \mathbb{R}^{p\times p}$. The gain associated with the nonlinear injection can be parameterized as

$$G_n = \begin{bmatrix} -LT^T \\ T^T \end{bmatrix} \text{ where } L = \begin{bmatrix} L_1 & 0 \end{bmatrix}$$

and $L_1 \in \mathbb{R}^{(n-p)\times(p-m)}$. The error system dynamics given in (11.91) are clearly influenced by the effect of the mismatched uncertainty. The next lemma is concerned

with the uniform ultimate boundedness of the uncertain error system (11.91). Let ΔA_u represent the unmatched component of ΔA then

Lemma 11.3. *[16] Let $\Omega_e \subset \mathbb{R}^n$ be a bounded set defined by*

$$\Omega_e = \left\{ e(t) \in \mathbb{R}^n : \|e(t)\| < 2\|\Delta A_u(t)x(t)\|\gamma_\lambda^{-1} + \gamma_e \right\} \tag{11.94}$$

where $\gamma_\lambda \in \mathbb{R}_+$, and $\gamma_e \in \mathbb{R}_+$ is a small design scalar. Assuming $\|\Delta A_u(t)x(t)\|$ is bounded, the estimation error $e(t)$ is ultimately bounded with respect to the set Ω_e.

From the change of coordinates $e \mapsto T_L e = \tilde{e}$, where

$$T_L = \begin{bmatrix} I_{n-p} & L \\ 0 & T \end{bmatrix}$$

the uncertain error system dynamics can be written as follows

$$\dot{\tilde{e}}_1(t) = \tilde{A}_{11}\tilde{e}_1(t) + \Delta A_u(t)x(t) \tag{11.95}$$

$$\dot{e}_y(t) = \tilde{A}_{21}\tilde{e}_1(t) + A_{22}^{stb}e_y(t) + \nu - \tilde{B}_2\xi_\Delta(t,x,u) \tag{11.96}$$

where $\tilde{A}_{11}$ is stable. Define $(\tilde{e}_1, e_y) := \tilde{e}$ where $\tilde{e}_1 \in \mathbb{R}^{n-p}$ then

Lemma 11.4. *[16] A sliding motion takes place in finite time t_σ on the sliding surface $\mathscr{S}_{Obs}$ within the domain*

$$\Omega_\sigma = \left\{ \left(\tilde{e}_1(t), e_y(t)\right) : \|T\tilde{A}_{21}\tilde{e}_1(t)\| < \|\tilde{B}_2\|\eta - \gamma_\sigma \right\} \tag{11.97}$$

where $\gamma_\sigma \in \mathbb{R}_+$ is a small design scalar.

An LMI-based approach is proposed using a polytopic description involving the mismatched uncertainty to synthesize the gains. The following additional assumption is employed throughout this section:

A3) The matrix $\Delta A_u(t)$, defined in (11.95), is affine with respect to the uncertain parameters denoted in vector form by $\theta(t) = [\theta_1(t)\ \ \theta_2(t)\ \ \cdots\ \ \theta_r(t)]^{\mathrm{T}}$. These uncertain parameters satisfy

$$\underline{\theta}_i \leqslant \theta_i \leqslant \overline{\theta}_i \quad \text{for} \quad i = 1, \ldots, r \tag{11.98}$$

and define a convex set in the parameter space $\Theta \subseteq \mathbb{R}^r$.

From the assumption above, the uncertain reduced-order output error system (11.95) admits a polytopic representation given by

$$\mathscr{P}_L^{Obs} = \left\{ \sum_{j=1}^{N} \mu_j \Phi_j : \sum_{j=1}^{N} \mu_j = 1, \mu_j \geq 0 \text{ for } j = 1, \ldots, N \right\} \tag{11.99}$$

where $N = 2^r$ is the number of vertices of $\mathscr{P}_L^{Obs}$ and

$$\Phi_j = \left[\begin{array}{c|c} \left(A_{11} + L_1 A_{211}\right) & \Delta A_{u_j} \\ \hline I_{(n-p)} & 0 \end{array}\right] \tag{11.100}$$

for $j = 1,\ldots,N$. Let γ_0 be a positive scalar. Then (11.95) is stable and satisfies

$$\|\tilde{e}_1(t)\|_2 < \gamma_0 \|x(t)\|_2 \tag{11.101}$$

if and only if there exists a s.p.d. matrix $P_1 \in \mathbb{R}^{(n-p)\times(n-p)}$ such that

$$\begin{bmatrix} (A_{11}+L_1A_{211})^{\mathrm{T}}P_1 + P_1(A_{11}+L_1A_{211}) + I_{(n-p)} & P_1\Delta A_{uj} \\ (P_1\Delta A_{uj})^{\mathrm{T}} & -\gamma_0^2 I_n \end{bmatrix} < 0 \tag{11.102}$$

for $j = 1,\ldots,N$

Proposition 11.4. *[16] Consider a reduced-order output error system matrix given by*

$$\Phi_{\tilde{e}_1 x}(t) = \left[\begin{array}{c|c} (A_{11}+L_1A_{211}) & \Delta A_u(t) \\ \hline I_{(n-p)} & 0 \end{array}\right] \tag{11.103}$$

where A_{11} and A_{211} are known matrices such that the pair (A_{11}, A_{211}) is detectable. Then, the solution of the optimization problem: minimize γ_0 with respect to Q_1 and F_L subject to

$$\begin{bmatrix} A_{11}^{\mathrm{T}}Q_1 + Q_1A_{11} + A_{211}^{\mathrm{T}}F_L^{\mathrm{T}} + F_LA_{211} & Q_1\Delta A_{uj} & I_{(n-p)} \\ (Q_1\Delta A_{uj})^{\mathrm{T}} & -\gamma_0 I_n & 0 \\ I_{(n-p)} & 0 & -\gamma_0 I_{(n-p)} \end{bmatrix} < 0 \tag{11.104}$$

$$Q_1 > 0 \tag{11.105}$$

guarantees

$$\|\tilde{e}_1(t)\|_2 < \gamma_0 \|x(t)\|_2 \tag{11.106}$$

The gain matrix L_1 can be straightforwardly computed as

$$L_1 = Q_1^{-1}F_L \tag{11.107}$$

Once $L_1 \in \mathbb{R}^{(n-p)\times(p-m)}$ is designed the observer gain matrices can be computed.

11.6 Fault Tolerant Control

The inherent robustness properties of sliding modes to matched uncertainty make it a natural candidate for passive fault tolerant control. It is argued in [1] that a broad class of actuator faults can be accommodated by an appropriate scheme which monitors quantitatively the extent to which a sliding motion (in a control context) is being attained and then triggers an adaptive mechanism if there is deterioration in performance. The controller is based around a state-feedback sliding mode scheme and the gain associated with the nonlinear term is allowed to adaptively increase when the onset of a fault is detected. Compared to other FTC schemes, the controller is simple and yet is shown to work across the entire 'up and away' flight envelope.

Although the controller in [1] copes easily with faults, it is not able to directly deal with failures – i.e. the total loss of an actuator. In order to overcome this, the

integration of a sliding mode scheme with a control allocation framework has been considered in [2] where the effectiveness level of the actuators is used by the control allocation scheme to redistribute the control signals to the 'healthier' actuators when a fault occurs.

One of the challenges of using traditional control ideas for systems with redundancy, i.e. over-actuated systems, is how to deal with these additional degrees of freedom. Control allocation (CA) has emerged as one of the most studied techniques when dealing with such problems (see for example [25, 7, 10, 18]). One benefit of using CA structure for fault tolerant control (FTC) is that the controller remains the same and the control effort is distributed to all available actuators without reconfiguration. This is vital in terms of simplicity of design. Recently, [2] developed a rigorous design procedure from a theoretical perspective to achieve FTC while proving stability for a class of faults and failures. The work in [2] has been used to design lateral and longitudinal controllers for the GARTEUR FM-AG16 benchmark problem ([41]). The GARTEUR FM-AG16 action group has undertaken an extensive study to establish the benefits of using state of the art fault detection and FTC methods for aerospace systems ([19, 46, 15, 36, 31]). The control allocation scheme described here uses actuator effectiveness levels to redistribute the control signals to the functioning healthy actuators when a fault or failure occurs ([2]).

11.6.1 Design Procedures

Consider a situation where a fault associated with the actuators develops in a system. It will be assumed that the system subject to actuator faults or failures about a trim condition, can be written as

$$\dot{x}(t) = Ax(t) + Bu(t) - BK(t)u(t) + BK(t)d(t) \tag{11.108}$$

where $A \in \mathbb{R}^{n\times n}$ and $B \in \mathbb{R}^{n\times m}$. The unknown input $d(t)$ represents the effect of faults which appear if $K(t) \neq 0$, and models, for example, an additional moment generated by a control surface stuck in a non-neutral position. The effectiveness gain $K(t) = \text{diag}(k_1(t), \ldots, k_m(t))$ where the $k_i(t)$ are scalars satisfying $0 \leq k_i(t) \leq 1$. These scalars model a decrease in effectiveness of a particular actuator. If $k_i(t) = 0$, the ith actuator is working perfectly whereas if $k_i(t) > 0$, a fault is present. If $k_i(t) = 1$ the actuator has failed completely. Here the control is distributed based on the efficiency of the actuators through $K(t)$, and redistributed to the remaining 'healthy' ones when faults/failures occur [2].

The idea is that if an actuator fault occurs, the control input $u(t)$ is reallocated to minimize the use of the faulty control surfaces. This section considers the design of a controller of the form

$$u(t) = N(k_1, \ldots, k_m)v(t) \tag{11.109}$$

where $N \in \mathbb{R}^{m\times l}$ with $l < m$ is a matrix which depends on the effectiveness levels of the actuators and $v(t) \in \mathbb{R}^l$ is a sliding mode based controller. The steps to synthesize the controller are given below:

11.6.1.1 Pre–design Calculations

This subsection outlines the sliding mode CA controller development from [2].

1. Make a re–ordering of the states in (11.108) so that the input distribution matrix B is partitioned as:
$$B = \begin{bmatrix} B_1 \\ B_2 \end{bmatrix} \tag{11.110}$$
where $B_1 \in \mathbb{R}^{(n-l)\times m}$ and $B_2 \in \mathbb{R}^{l\times m}$ has rank l. Typically in aircraft systems, B_2 is associated with angular acceleration in roll, pitch and yaw ([32]).
2. Scale the states so that $B_2 B_2^{\mathrm{T}} = I$ and $\|B_2\| = 1$.
3. Let the 'virtual control'
$$\nu(t) := B_2 u(t) \tag{11.111}$$
By direct manipulation, the true control signal $u(t)$ is recovered as
$$u(t) = B_2^{\dagger}\nu(t) \tag{11.112}$$
where $B_2^{\dagger} \in \mathbb{R}^{m\times l}$ is a right pseudo-inverse of the matrix B_2. In [2], the pseudo-inverse was chosen as
$$B_2^{\dagger} := W B_2^{\mathrm{T}}(B_2 W B_2^{\mathrm{T}})^{-1} \tag{11.113}$$
where $W \in \mathbb{R}^{m\times m}$ is a s.p.d diagonal matrix. It can be shown that the pseudo-inverse in (11.113) arises from the optimization problem
$$\min_u \; u^{\mathrm{T}} W^{-1} u \quad \text{subject to } B_2 u = \nu \tag{11.114}$$
The work in [2] advocates the choice
$$W := I - K \tag{11.115}$$
and so $W = \mathrm{diag}\{w_1, \ldots, w_m\}$ where $w_i = 1 - k_i$. Note in a fault free situation $W = I$. As $k_i \to 1$, $w_i \to 0$ and so the associated component u_i in (11.114) is weighted heavily since $\frac{1}{w_i}$ becomes large.
4. For analysis purposes, $d(t)$ from (11.108) will be considered as zero since, as an exogenous signal, it plays no part in determining closed loop stability, and represents the trim point correction which needs to be compensated for by the pilot.
5. Define
$$\hat{\nu}(t) := (B_2 W^2 B_2^{\mathrm{T}})(B_2 W B_2^{\mathrm{T}})^{-1}\nu(t) \tag{11.116}$$
and change the coordinates of the system in (11.108) using the linear transformation $x(t) \mapsto \hat{x}(t) = T_r x(t)$ where
$$T_r := \begin{bmatrix} I & -B_1 B_2^{\mathrm{T}} \\ 0 & I \end{bmatrix} \tag{11.117}$$

to achieve the canonical form given by

$$\begin{bmatrix} \dot{\hat{x}}_1 \\ \dot{\hat{x}}_2 \end{bmatrix} = \underbrace{\begin{bmatrix} \hat{A}_{11} & \hat{A}_{12} \\ \hat{A}_{21} & \hat{A}_{22} \end{bmatrix}}_{\hat{A}} \begin{bmatrix} \hat{x}_1 \\ \hat{x}_2 \end{bmatrix} + \underbrace{\begin{bmatrix} 0 \\ I_l \end{bmatrix}}_{\hat{B}} \hat{v} + \begin{bmatrix} B_1 B_2^N B_2^+ \\ 0 \end{bmatrix} \hat{v} \tag{11.118}$$

where

$$B_2^+ := W^2 B_2^{\mathrm{T}} (B_2 W^2 B_2^{\mathrm{T}})^{-1} \tag{11.119}$$

and

$$B_2^N := (I - B_2^{\mathrm{T}} B_2) \tag{11.120}$$

6. Compute the smallest possible scalar γ_0 such that

$$\|B_2^+\| = \|W^2 B_2^{\mathrm{T}} (B_2 W^2 B_2^{\mathrm{T}})^{-1}\| < \gamma_0 \tag{11.121}$$

for all $0 < W \leq I$. A finite value of γ_0 is guaranteed to exist ([2]).

The virtual control law will now be designed based on the fault-free condition ($K = 0$) in which the top partition of the last term in (11.118) is zero since $B_1 B_2^N B_2^+|_{W=I} = 0$. The selection of the sliding surface is the first part of sliding mode controller design and defines the system's closed–loop performance. Define the switching function $\sigma(t) : \mathbb{R}^n \to \mathbb{R}^l$ to be $\sigma(t) = Sx(t)$ where $S \in \mathbb{R}^{l \times n}$ and $\det(SB_v) \neq 0$. The matrix S represents design freedom. Define a hyperplane

$$\mathscr{S} = \{x(t) \in \mathbb{R}^n \ : \ Sx(t) = 0\}$$

In the $\hat{x}(t)$ coordinates in (11.118), a choice for the sliding surface is

$$\hat{S} := S T_r^{-1} = \begin{bmatrix} M & I_l \end{bmatrix} \tag{11.122}$$

where $M \in \mathbb{R}^{l \times (n-l)}$ represents design freedom. The objective is to compute M from (11.122) so that $\tilde{A}_{11} := \hat{A}_{11} - \hat{A}_{12} M$ is stable. If $(\hat{A}, \hat{B})$ is controllable, then $(\hat{A}_{11}, \hat{A}_{12})$ is controllable ([20]) and a matrix M can always be found to make $\tilde{A}_{11}$ stable.

Proposition 11.5. *[2] During a fault or failure condition, for any combination of $0 < w_i \leq 1$, the closed–loop system will be stable if*

$$0 \leq \frac{\gamma_2 \gamma_0}{1 - \gamma_1 \gamma_0} < 1 \tag{11.123}$$

where the scalar γ_0 is defined in (11.121), γ_1 is defined as

$$\gamma_1 := \|M B_1 B_2^N\| \tag{11.124}$$

while

$$\gamma_2 := \|G(s)\|_\infty \tag{11.125}$$

where $G(s) := \tilde{A}_{21}(sI - \tilde{A}_{11})^{-1} B_1 B_2^N$ and the matrix $\tilde{A}_{21} := M\tilde{A}_{11} + \hat{A}_{21} - \hat{A}_{22} M$. By construction the transfer function $G(s)$ is stable.

The matrix M has been chosen using the following procedure:

1. Compute γ_0 to satisfy (11.121).
2. Compute and check if $\gamma_1 := \|MB_1B_2^N\| < \frac{1}{\gamma_o}$ is satisfied. Otherwise re–design the matrix M.
3. Calculate the transfer function matrix $G(s)$, then if $\|G(s)\|_\infty := \gamma_2 < \frac{1}{\gamma_0} - \gamma_1$, the closed–loop is guaranteed to be stable $\forall\ 0 < W \leq I$. Otherwise consider re–designing the matrix M.

11.6.1.2 The Control Law

The proposed control law from [2] has a structure $\hat{v}(t) = \hat{v}_l(t) + \hat{v}_n(t)$ where

$$\hat{v}_l(t) := -\tilde{A}_{21}\hat{x}_1(t) - \tilde{A}_{22}\sigma(t) \tag{11.126}$$

and $\tilde{A}_{22} := M\hat{A}_{12} + \hat{A}_{22}$. The nonlinear component is defined to be

$$\hat{v}_n(t) := -\rho(t,x)\frac{\sigma(t)}{\|\sigma(t)\|} \qquad \text{for } \sigma(t) \neq 0 \tag{11.127}$$

where $\sigma(t) = \hat{S}\hat{x}(t)$. The non-linear gain

$$\rho(t,x) := \frac{\gamma_1\gamma_0\|\hat{v}_l(t)\| + \eta}{1 - \gamma_1\gamma_0} \tag{11.128}$$

ensures a sliding motion occurs on $\mathscr{S}$ in finite time. The final control law is

$$u(t) = WB_2^{\mathrm{T}}(B_2W^2B_2^{\mathrm{T}})^{-1}\hat{v}(t) \tag{11.129}$$

11.6.2 Benchmark Simulation Results

The results considered here are all based on the GARTEUR FM-AG16 benchmark problem [41, 3]. The information necessary to compute W *on–line in real time will be supplied by assuming a measurement of the actual actuator deflection is available*. This is not an unrealistic assumption in aircraft systems [9]. Alternatively a fault reconstruction scheme (e.g. [43] or [47]) can also be used.

The controller design objective considered here is to bring a faulty aircraft to a near landing condition. This can be achieved by a change of direction through a 'banking turn' manoeuvre, followed by a decrease in altitude and speed. This can be achieved by tracking appropriate roll angle (ϕ) and sideslip angle (β) commands (laterally), and tracking flight path angle (FPA) and airspeed (V_{tas}) commands (longitudinally).

A linearization of the benchmark model ([41]) has been obtained around a fault free operating condition of 263,000Kg, 92.6m/s true airspeed, and an altitude of 600m at 25.6% of maximum thrust and at a 20° flap position. For design purposes, four longitudinal states ($x_{long} = [q\ V_{tas}\ \alpha\ \theta]^{\mathrm{T}}$ which represent pitch rate, true airspeed, angle of attack, pitch angle respectively) are considered, together with four

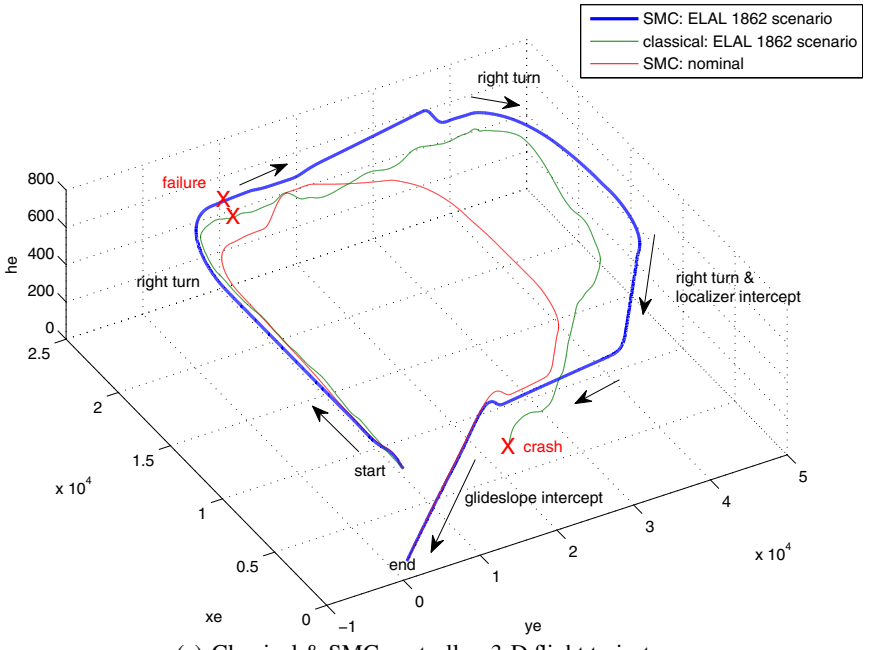

(a) Classical & SMC controller: 3-D flight trajectory

(b) SIMONA flight motion simulator (outside view)

(c) Pilot view inside SIMONA during landing manoeuvre

Fig. 11.5 ELAL 1862 failure tests on SIMONA simulator (pictures courtesy of the International Research Institute for Simulation, Motion and Navigation (SIMONA))

lateral states ($x_{lat} = [p\ r\ \beta\ \phi]^{\mathrm{T}}$ which represent roll rate, yaw rate, sideslip angle and roll angle). After some aggregation, the lateral control surfaces are

$$\delta_{lat} = [\delta_{air}\ \delta_{ail}\ \delta_{aor}\ \delta_{aol}\ \delta_{sp1-4}\ \delta_{sp5}\ \delta_{sp8}\ \delta_{sp9-12}\ \delta_r,\ e1_{lat}\ e2_{lat}\ e3_{lat}\ e4_{lat}]^{\mathrm{T}}$$

which represent aileron deflection (right & left - inner & outer)(rad), spoiler deflections (left: 1-4 & 5 - right: 8 & 9-12) (rad), rudder deflection (rad) and lateral engine pressure ratios (EPR). The longitudinal control surfaces are

$$\delta_{long} = [\delta_e \ \delta_s \ e1_{long} \ e2_{long} \ e3_{long} \ e4_{long}]^{\mathrm{T}}$$

which represent elevator deflection (rad), horizontal stabilizer deflection (rad), and longitudinal EPR.

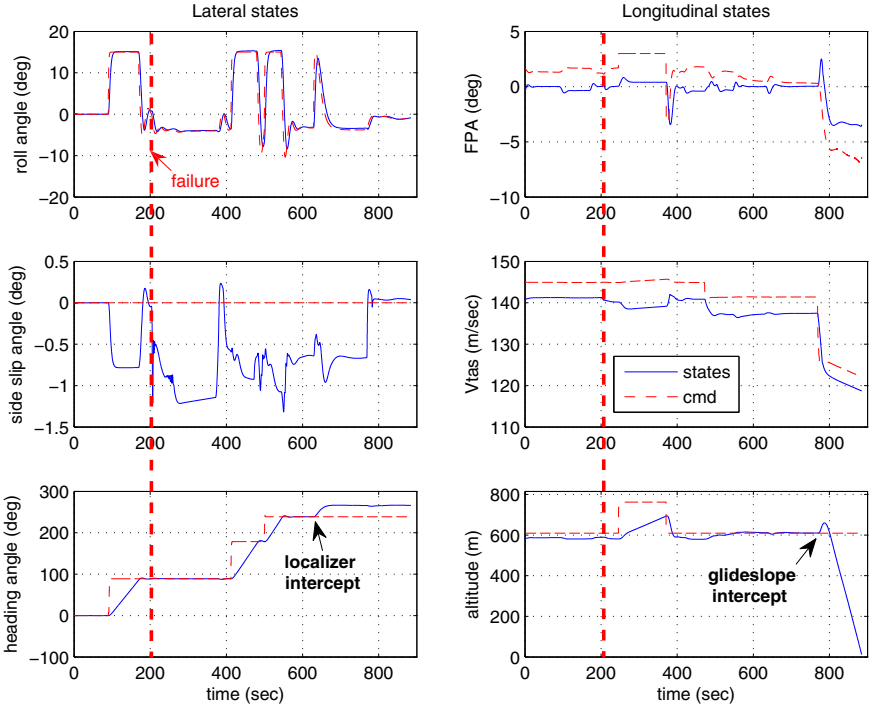

Fig. 11.6 ELAL 1862 scenario: SMC controller: controlled states

The proposed scheme was implemented on the SIMONA flight simulator at Delft University of Technology [6]. Figure 11.5 summarizes the results of piloted tests based on the ELAL 1862 failure scenario in which engines no. 3 and 4 detached and caused significant damage to the right wing [41]. Figure 5(a) shows the comparisons between the implemented sliding mode CA scheme and the piloted classical controller. Figure 5(a) clearly shows that the proposed scheme manages to maintain nominal performance and achieve safe near landing condition. Meanwhile, the piloted classical controller crashes during the final stage of the test flight before lining up with the runway. Figure 5(c) shows the actual pilot's view inside the SIMONA cockpit near to landing. Details of the states and control surface deflections are shown below in Figures 11.6 and 11.7.

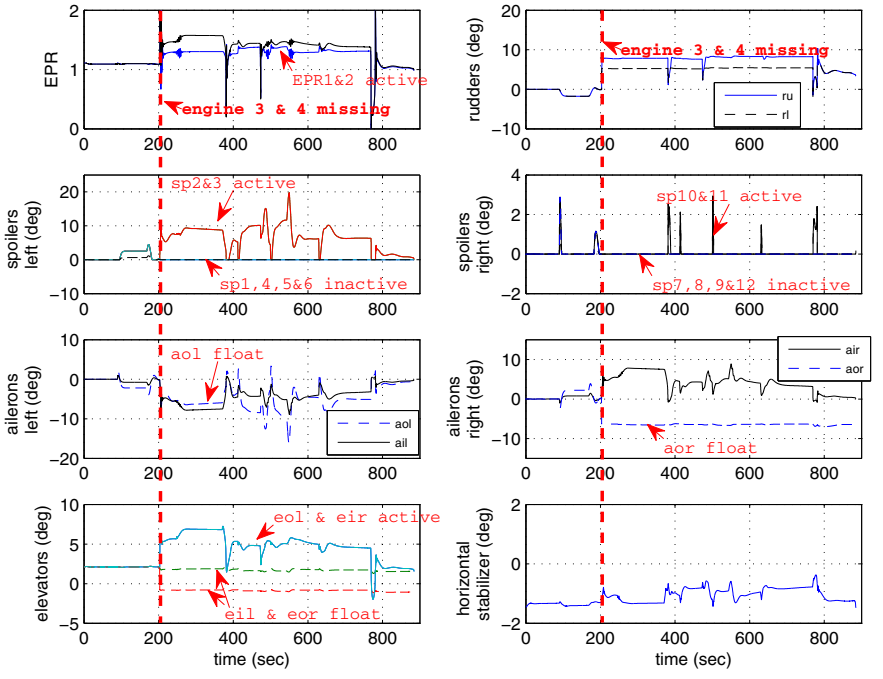

Fig. 11.7 ELAL 1862 scenario: SMC controller: control surfaces deflection

11.7 Conclusions

This chapter described the use of sliding mode ideas for fault detection leading to fault tolerant control. The sliding mode observer FDI schemes robustly estimate any unknown fault signal existing within the system based on appropriate scaling of the equivalent output estimation error injection signal. One advantage of these sliding mode methods over more traditional residual based observer schemes is that because the faults are reconstructed, both the 'shape' and size of the faults are preserved. A further benefit of this approach is that because faults are reconstructed, these signals can be used to correct a faulty sensor for example, to maintain reasonable performance until appropriate maintenance could be undertaken. In particular the chapter discussed recent advances to obviate the traditional relative degree one minimum phase conditions. Also the effects of unmatched uncertainty were discussed. In all the methods proposed, efficient Linear Matrix Inequality methods can be employed to synthesis the required gains. A recent application of sliding mode controllers for fault tolerant control was presented in which the inherent robustness properties of sliding modes to matched uncertainty were exploited. In order to cope with total failures, the integration of a sliding mode scheme with a control allocation framework was considered whereby the effectiveness level of the actuators was used by

the control allocation scheme to redistribute the control signals to the 'healthy' ones when a fault occurs.

References

1. Alwi, H., Edwards, C.: Fault detection and fault-tolerant control of a civil aircraft using a sliding-mode-based scheme. IEEE Transactions on Control Systems Technology 16(3), 499–510 (2008)
2. Alwi, H., Edwards, C.: Fault tolerant control using sliding modes with on-line control allocation. Automatica 44(7), 1859–1866 (2008)
3. Alwi, H., Edwards, C., Stroosma, O., Mulder, J.A.: Piloted sliding mode FTC simulator evaluation for the ELAL Flight 1862 incident. AIAA Journal of Guidance Control and Dynamics 33(3), 677–694 (2010)
4. Alwi, H., Edwards, C., Tan, C.P.: Sliding mode estimation schemes for incipient sensor faults. Automatica 45(7), 1679–1685 (2009)
5. Bejarano, F.J., Fridman, L., Poznyak, A.: Hierarchical observer for strongly detectable systems via second order sliding mode. In: Proceedings of the IEEE CDC 2007, New Orleans, pp. 3709–3713 (2007)
6. Berkouwer, W.R., Stroosma, O., van Paassen, M.M.R., Mulder, M., Mulder, J.A.B.: Measuring the performance of the SIMONA research simulator's motion system. In: AIAA Modeling and Simulation Technologies Conference (2005)
7. Bošković, J.D., Mehra, R.K.: Control allocation in overactuated aircraft under position and rate limiting. In: Proceedings of the American Control Conference, pp. 791–796 (2002)
8. Boyd, S.P., El-Ghaoui, L., Feron, E., Balakrishnan, V.: Linear Matrix Inequalities in Systems and Control Theory. SIAM, Philadelphia (1994)
9. Brière, D., Traverse, P.: Airbus A320/A330/A340 electrical flight controls: A family of fault-tolerant systems. In: Digest of Papers FTCS-23 The Twenty-Third International Symposium on Fault-Tolerant Computing, pp. 616–623 (1993)
10. Buffington, J., Chandler, P., Pachter, M.: On-line system identification for aircraft with distributed control effectors. International Journal of Robust and Nonlinear Control 9, 1033–1049 (1999)
11. Chen, J., Patton, R., Zhang, H.: Design of unknown input observers and robust fault detection filters. International Journal of Control 63, 85–105 (1996)
12. Chen, J., Patton, R.J.: Robust model-based fault diagnosis for dynamic systems. Kluwer Academic Publishers, Boston (1999)
13. Chen, J., Zhang, H.: Robust detection of faulty actuators via unknown input observers. International Journal of Systems Science 22, 1829–1839 (1991)
14. Chen, W., Saif, M.: Actuator fault diagnosis for uncertain linear systems using a high-order sliding-mode robust differentiator (hosmrd). Int. J. Robust and Nonlinear Control 18, 413–426 (2007)
15. Cieslak, J., Henry, D., Zolghadri, A., Goupil, P.: Development of an active fault-tolerant flight control strategy. AIAA Journal of Guidance, Control and Dynamics 31(1), 135–147 (2008)
16. Andrade da Silva, J.M., Edwards, C.: Sliding mode observer for systems with mismatched uncertainties. In: Proceedings of the 11th Int. Workshop on Variable Structure Systems (VSS 2010), Mexico (2010)
17. Darouach, M.: On the novel approach to the design of unknown input observers. IEEE Transactions on Automatic Control 39, 698–699 (1994)

18. Davidson, J.B., Lallman, F.J., Bundick, W.T.: Real-time adaptive control allocation applied to a high performance aircraft. In: 5th SIAM Conference on Control & Its Application (2001)
19. Edwards, C., Lombaerts, T.J.J., Smaili, H. (eds.): Fault Tolerant Flight Control:A Benchmark Challenge. LNCIS, vol. 399. Springer, Heidelberg (2010)
20. Edwards, C., Spurgeon, S.K.: Sliding Mode Control: Theory and Applications. Taylor & Francis, Taylor (1998)
21. Edwards, C., Spurgeon, S.K.: On the development of discontinuous observers. Int. J. Control 59, 1211–1229 (1994)
22. Edwards, C., Spurgeon, S.K.: A sliding mode observer based FDI scheme for the ship benchmark. European J. Control 6, 341–356 (2000)
23. Edwards, C., Spurgeon, S.K., Patton, R.J.: Sliding mode observers for fault detection. Automatica 36, 541–553 (2000)
24. Edwards, C., Tan, C.P.: A comparison of sliding mode and unknown input observers for fault reconstruction. European Journal of Control 16, 245–260 (2006)
25. Enns, D.: Control allocation approaches. In: AIAA Guidance, Navigation and Control Conference and Exhibit, pp. 98–108 (1998)
26. Floquet, T., Barbot, J.P.: An observability form for linear systems with unknown inputs. International Journal Control 79, 132–139 (2006)
27. Floquet, T., Edwards, C., Spurgeon, S.K.: On sliding mode observers for systems with unknown inputs. Int. J. Adaptive Control and Signal Processing 21, 638–656 (2007)
28. Forssell, L., Nilsson, U.: ADMIRE, the aero-data model in a research environment version 4.0, model description. Technical Report FOI-R-1624–SE, Swedish Defence Agency, FOI (2005)
29. Fridman, L., Davila, J., Levant, A.: High-order sliding-mode observation and fault detection. In: Proceedings of the IEEE Conference on Decision and Control, New Orleans, pp. 4317–4322 (2007)
30. Gahinet, P., Nemirovski, A., Laub, A.J., Chilali, M.: LMI Control Toolbox, Users Guide. The MathWorks, Inc. (1995)
31. Hallouzi, R., Verhaegen, M.: Fault-tolerant subspace predictive control applied to a Boeing 747 model. AIAA Journal of Guidance, Control and Dynamics 31(4), 873–883 (2008)
32. Härkegård, O., Glad, S.T.: Resolving actuator redundancy - optimal control vs. control allocation. Automatica 41(1), 137–144 (2005)
33. Haskara, I., Ozguner, U., Utkin, V.: On sliding mode observers via equivalent control approach. Int. J. Control 71, 1051–1067 (1998)
34. Wang, J., Tsang, K.M., Li, G., Zhang, L.: Cascade observer-based fault diagnosis for nonlinear systems. In: Proc. of the IASTED International Conference on Modelling, Simulation and Optimization, Banff, Alberta, Canada, pp. 253–258 (2003)
35. Krasnova, S.A., Utkin, V.A., Mikheev, Y.V.: Cascade design of state observers. Automation and Remote Control 62, 207–226 (2001)
36. Lombaerts, T.J.J., Huisman, H.O., Chu, Q.P., Mulder, J.A., Joosten, D.A.: Flight control reconfiguration based on online physical model identification and nonlinear dynamic inversion. In: AIAA Guidance, Navigation and Control Conference and Exhibit, vol. 7435 (2008)
37. Ng, K.Y., Tan, C.P., Edwards, C., Kuang, Y.C.: New results in robust actuator fault reconstruction in linear uncertain systems. Int. J. Robust and Nonlinear Control 17, 1294–1319 (2007)
38. Patton, R.J., Frank, P.M., Clark, R.N.: Fault Diagnosis in Dynamic Systems: Theory and Application. Prentice-Hall, New York (1989)

39. Saif, M., Guan, Y.: A new approach to robust fault detection and identification. IEEE Transactions on Aerospace and Electronic Systems 29, 685–695 (1993)
40. Sharam, R., Aldeen, M.: Fault detection in nonlinear systems with unknown inputs using sliding mode observer. In: Proc. of American Control Conference, New York, pp. 432–437 (2007)
41. Smaili, H., Breeman, J., Lombaerts, T., Joosten, D.: RECOVER: A benchmark for integrated fault tolerant flight control evaluation. In: Edwards, C., Lombaerts, T., Smaili, H. (eds.) Fault Tolerant Flight Control. LNCIS, vol. 399, pp. 171–221. Springer, Heidelberg (2010)
42. Tan, C.P., Edwards, C.: Sliding mode observers for detection and reconstruction of sensor faults. Automatica, 1815–1821 (2002)
43. Tan, C.P., Edwards, C.: Sliding mode observers for robust detection and reconstruction of actuator and sensor faults. International Journal of Robust and Nonlinear Control 13, 443–463 (2003)
44. Tan, C.P., Edwards, C.: Robust fault reconstruction in uncertain linear systems using multiple sliding mode observers in cascade. IEEE Transactions on Automatic Control 55(4), 855–867 (2010)
45. Utkin, V.I.: Sliding Modes in Control Optimization. Springer, Berlin (1992)
46. Varga, A.: Fault detection and isolation of actuator failures for a large transport aircraft. In: Proceeding First CEAS European Air and Space Conference (2007)
47. Zhang, Y.M., Jiang, J.: Active fault-tolerant control system against partial actuator failures. IEE Proceedings: Control Theory & Applications 149, 95–104 (2002)

Chapter 12
Applying Sliding Mode Technique to Optimal Filter and Controller Design

Michael Basin

Abstract. This paper addresses the mean-square and mean-module filtering problems for a linear system with Gaussian white noises. The obtained solutions contain a sliding mode term, signum of the innovations process. It is shown that the designed sliding mode mean-square filter generates the mean-square estimate, which has the same minimum estimation error variance as the best estimate given by the classical Kalman-Bucy filter, although the gain matrices of both filters are different. The designed sliding mode mean-module filter generates the mean-module estimate, which yields a better value of the mean-module criterion in comparison to the mean-square Kalman-Bucy filter. The theoretical result is complemented with an illustrative example verifying performance of the designed filters. It is demonstrated that the estimates produced by the designed sliding mode mean-square filter and the Kalman-Bucy filter yield the same estimation error variance, and there is an advantage in favor of the designed sliding mode mean-module filter. Then, the paper addresses the optimal controller problem for a linear system over linear observations with respect to different Bolza-Meyer criteria, where 1) the integral control and state energy terms are quadratic and the non-integral term is of the first degree or 2) the control energy term is quadratic and the state energy terms are of the first degree. The optimal solutions are obtained as sliding mode controllers, each consisting of a sliding mode filter and a sliding mode regulator, whereas the conventional feedback LQG controller fails to provide a causal solution. Performance of the obtained optimal controllers is verified in the illustrative example against the conventional LQG controller that is optimal for the quadratic Bolza-Meyer criterion. The simulation results confirm an advantage in favor of the designed sliding mode controllers.

Michael Basin
Department of Physical and Mathematical Sciences
Autonomous University of Nuevo Leon, San Nicolas de los Garza, Nuevo Leon, Mexico
e-mail: mbasin@fcfm.uanl.mx, mbasin2007@gmail.com

L. Fridman et al. (Eds.): Sliding Modes, LNCIS 412, pp. 325–349.
springerlink.com

12.1 Introduction

Since the sliding mode control was invented in the beginning of 1970s (see a historical review in [1,2,3]), it has been applied to solve several classes of problems. For instance, the sliding mode control methodology has been used in stabilization [4,5], tracking [6,7], observer design [8,9], frequency domain analysis [10], and other control problems. Promising modifications of the original sliding mode concept, such as integral sliding mode [11] and higher order sliding modes [12,3], have been developed. The sliding mode optimal regulators has been recently designed for linear systems with son-quadratic Bolza-Meyer criteria [13,14]. Application of the sliding mode method is extended even to stochastic systems [15,16,17] and stochastic filtering problems [18,19]. However, to the best of authors' knowledge, that no sliding mode filtering algorithms solving the mean-square or mean-module filtering and controller problems have been designed even for linear systems. Meanwhile, simply the fact that the sliding mode control has a transparent physical sense [1] and is successfully applied to many technical problems [4] leads to a conjecture that the sliding mode mean-square and mean-module filters, dual to sliding mode regulators obtained in [13] and [14], should exist. Furthermore, combining the sliding mode mean-square and mean-module filters to be designed with the sliding mode regulators obtained in [13] and [14] leads to the design of the sliding mode mean-square and mean-module controllers providing solutions to the optimal control problems if the system state is not directly measured.

This paper presents the solutions to the mean-square and mean-module filtering problems for linear systems, which contain a sliding mode term, signum of the innovations process. It is shown that the designed sliding mode mean-square filter generates the mean-square estimate, which has the same minimum estimation error variance as the best estimate given by the classical Kalman-Bucy filter [20], although the gain matrices of both filters are different. To the best of our knowledge, this is the first designed sliding mode filter that is optimal with respect to the mean-square criterion and yields the estimate with the same structural properties as the conventional optimal filter. On the other hand, the designed sliding mode filter generates the mean-module estimate, which yields a better value of the mean-module criterion in comparison to the mean-square Kalman-Bucy filter. To the best of our knowledge, this is the first designed sliding mode filter that is optimal with respect to the mean-module criterion. The theoretical result is complemented with an illustrative example verifying performance of the designed filters. It is demonstrated that the estimates produced by the designed filter and the Kalman-Bucy filter yield the estimate with the same minimum estimation error variance, whereas there is an advantage in favor of the designed sliding mode mean-module filter.

Then, the paper presents the solutions to the optimal controller problems for a linear system over linear observations with respect to different Bolza-Meyer criteria, where 1) the integral control and state energy terms are quadratic and the non-integral term is of the first degree or 2) the control energy term is quadratic and the state energy terms are of the first degree. That type of criteria would be useful in the joint control and parameter identification problems where the objective

should be reached for a finite time. The theoretical results are complemented with illustrative examples verifying performance of the designed controller algorithms. The designed sliding mode controllers are compared to the feedback LQG controller corresponding to the quadratic Bolza-Meyer criterion, which is based on the Kalman-Bucy filter [20] and the conventional LQ regulator [21,22]. The simulation results confirm an advantage in favor of the designed sliding mode controllers.

The paper is organized as follows. Section 12.2 states the mean-square and mean-module filtering problems for linear systems with Gaussian white noises. The sliding mode solutions to the mean-square and mean-module filtering problems are given in Sections 12.3 and 12.4, respectively, which also contain illustrative examples. The proofs of the obtained results are given in Appendices 1 and 2. Section 12.5 states the corresponding optimal controller problems for linear systems over linear observations with non-quadratic Bolza-Meyer criterions. The sliding mode solutions to the controller problems based on the mean-square and mean-module filtering problems are given in Sections 12.6 and 12.7, respectively, which also contain illustrative examples. Section 12.8 presents conclusions to this study.

12.2 Optimal Filtering Problem

12.2.1 Problem Statement

Let (Ω, F, P) be a complete probability space with an increasing right-continuous family of σ-algebras $F_t, t \geq t_0$, and let $(W_1(t), F_t, t \geq t_0)$ and $(W_2(t), F_t, t \geq t_0)$ be independent standard Wiener processes. The F_t-measurable random process $(x(t), y(t))$ is described by a linear differential equation for the system state

$$dx(t) = (a_0(t) + a(t)x(t))dt + b(t)dW_1(t), \quad x(t_0) = x_0, \tag{1}$$

and a linear differential equation for the observation process

$$dY(t) = A(t)x(t)dt + B(t)dW_2(t). \tag{2}$$

Here, $x(t) \in R^n$ is the state vector and $y(t) \in R^m$, $m \leq n$, is the observation process. The initial condition $x_0 \in R^n$ is a Gaussian vector such that x_0, $W_1(t)$, and $W_2(t)$ are independent. It is assumed that $B(t)B^T(t)$ is a positive definite matrix. All coefficients in (1)–(2) are deterministic functions of time of appropriate dimensions.

The state and observation equations can also be written in an alternative form

$$\dot{x}(t) = a_0(t) + a(t)x(t) + b(t)\psi_1(t), \quad x(t_0) = x_0, \tag{1*}$$

$$y(t) = A(t)x(t) + B(t)\psi_2(t), \tag{2*}$$

where $y(t) = \dot{Y}(t)$, and $\psi_1(t)$ and $\psi_2(t)$ are white Gaussian noises, which are the weak mean square derivatives of standard Wiener process $W_1(t)$, and $W_2(t)$ (see [23]). The representations (1),(2) and (1*),(2*) are equivalent ([24]). The equations

$(1^*),(2^*)$ present the conventional form for the equations (1),(2), which is actually used in practice.

The estimation problem is to find the estimate $\hat{x}(t)$ of the system state $x(t)$, based on the observation process $Y(t) = \{y(s), t_0 \le s \le t\}$, that minimizes the mean-square norm

$$J = E[(x(t) - \hat{x}(t))^T (x(t) - \hat{x}(t)) \mid F_t^Y] \tag{3}$$

at every time moment t. Here, $E[z(t) \mid F_t^Y]$ means the conditional expectation of a stochastic process $z(t) = (x(t) - \hat{x}(t))^T (x(t) - \hat{x}(t))$ with respect to the σ - algebra F_t^Y generated by the observation process $Y(t)$ in the interval $[t_0, t]$. As known [23], this estimate is given by the conditional expectation

$$\hat{x}(t) = m(t) = E(x(t) \mid F_t^Y)$$

of the system state $x(t)$ with respect to the σ - algebra F_t^Y generated by the observation process $Y(t)$ in the interval $[t_0, t]$. As usual, the matrix function

$$P(t) = E[(x(t) - m(t))(x(t) - m(t))^T \mid F_t^Y]$$

is the estimation error variance.

The well-known solution to the stated filtering problem is the Kalman-Bucy filter [20]. An alternative solution involving the sliding mode term is given in Section 12.3 and then proved in Appendix 1. As demonstrated, the obtained sliding mode filter is optimal with respect to the criterion (3).

This paper also addresses the mean-module filtering problem to find the estimate $\hat{x}(t)$ of the system state $x(t)$, based on the observation process $Y(t) = \{y(s), t_0 \le s \le t\}$, that minimizes the mean-module norm

$$J = E[(\mid x(t) - \hat{x}(t) \mid) \mid F_t^Y] \tag{4}$$

at every time moment t. Here, $\mid x \mid = [\mid x_1 \mid, \ldots, \mid x_n \mid] \in R^n$ is defined as the vector of absolute values of the components of the vector $x \in R^n$.

The solution to the stated filtering problem, involving the sliding mode term, is given in Section 12.4 and then proved in Appendix 2. As demonstrated, the obtained sliding mode filter is optimal with respect to the criterion (4).

12.3 Mean-Square Filter Design

The solution to the mean-square filtering problem for the linear system (1) and the criterion (3) is given as follows. The mean-square estimate satisfies the differential equation with the sliding mode term

$$\dot{m}(t) = a_0(t) + a(t)m(t) + Q(t)A^T(t)(B(t)B^T(t))^{-1} \times \tag{5}$$

$$A(t)\mathrm{sign}[A^T(t)(A(t)A^T(t))^{-1}y(t) - m(t)],$$

with the initial condition $m(t_0) = E(x(t_0) \mid F_{t_0}^Y)$. Here, the Signum function of a vector $x = [x_1, \ldots, x_n] \in R^n$ is defined as $\text{sign}[x] = [\text{sign}(x_1), \ldots, \text{sign}(x_n)] \in R^n$, and the signum function of a scalar x is defined as $\text{sign}(x) = 1$, if $x > 0$, $\text{sign}(x) = 0$, if $x = 0$, and $\text{sign}(x) = -1$, if $x < 0$ ([25]).

The matrix function $Q(t)$ satisfies the matrix equation with time-varying coefficients

$$\dot{Q}(t) = (b(t)b^T(t)) * \mid A^T(t)(A(t)A^T(t))^{-1}y(t) - m(t) \mid + a(t)Q(t), \tag{6}$$

with the initial condition

$$Q(t_0) = E[(x(t_0) - m(t_0)(x(t_0) - m(t_0)^T \mid F_{t_0}^Y] *$$
$$\mid A^T(t_0)(A(t_0)A^T(t_0))^{-1}y(t_0) - m(t_0) \mid$$

.

Here, $\mid x \mid = [\mid x_1 \mid, \ldots, \mid x_n \mid] \in R^n$ is defined as the vector of absolute values of the components of the vector $x \in R^n$, and $A * b$ denotes a product between a matrix $A \in R^{n \times n}$ and a vector $b \in R^n$, that results in the matrix defined as follows: all entries of the j-th column of the matrix A are multiplied by the j-th component of the vector b, $j = 1, \ldots, n$.

The presented result is formulated in the following theorem and proved in Appendix 1.

Theorem 12.1. *The mean-square filter for the linear system state (1) over the linear observations (2) is given by the equation (5) for the estimate $m(t) = E(x(t) \mid F_t^Y)$ and the equation (6) for the filter gain matrix $Q(t)$.*

12.3.1 Example 1

This section presents an illustrative example of designing the mean-square sliding mode filter for a linear system (1),(2), using the filtering equations (5),(6).

Consider a scalar linear unmeasured state

$$\dot{x}(t) = x(t) + \psi_1(t), \quad x(0) = x_0, \tag{7}$$

and the scalar linear observation process

$$y(t) = x(t) + \psi_2(t), \tag{8}$$

where $\psi_1(t)$ and $\psi_2(t)$ are white Gaussian noises, which are the weak mean square derivatives of standard Wiener processes (see [23]). The equations (7),(8) correspond to the alternative conventional form (1^*),(2^*) for the equations (1),(2).

The filtering problem is to find the mean-square estimate for the linear state (7), using linear observations (8) confused with independent and identically distributed disturbances modeled as white Gaussian noises.

The filtering equations (5),(6) take the following particular form for the system (7),(8)

$$\dot{m}(t) = m(t) + Q(t)\text{sign}[y(t) - m(t)], \tag{9}$$

with the initial condition $m(0) = E(x(0) \mid y(0)) = m_0$,

$$\dot{Q}(t) = Q(t) + \mid y(t) - m(t) \mid, \tag{10}$$

with the initial condition $Q(0) = E((x(0) - m(0))(x(0) - m(0))^T \mid y(0)) * \mid y(0) - m(0) \mid$.

The estimates obtained upon solving the equations (9),(10) are compared to the estimates satisfying the Kalman-Bucy filtering equations [20] for the linear system (7),(8)

$$\dot{m}_K(t) = m_K(t) + P(t)[y(t) - m_K(t)], \tag{11}$$

with the initial condition $m(0) = E(x(0) \mid y(0)) = m_0$,

$$\dot{P}(t) = 1 + 2P(t) - P^2(t), \tag{12}$$

with the initial condition $P(0) = E((x(0) - m(0))(x(0) - m(0))^T \mid y(0))$.

Numerical simulation results are obtained solving the systems of filtering equations (9),(10) and (11),(12). The obtained values of the estimates $m(t)$ and $m_K(t)$ satisfying the equations (9) and (11), respectively, are compared to the real values of the state variables $x(t)$ in (7).

For each of the two filters (9),(10) and (11),(12) and the reference system (7),(8), involved in simulation, the following initial values are assigned: $x_0 = 1$, $m_0 = 10$, $P(0) = 100$, $Q(0) = 866.9$. The filtering horizon is set to $T = 0.4$. Gaussian disturbances $\psi_1(t)$ and $\psi_2(t)$ in (7),(8) are realized using the built-in MatLab white noise function.

The following graphs are obtained: graphs of the reference state $x(t)$, satisfying the equation (7), the mean-square sliding mode filter estimate $m(t)$, satisfying the equations (9), and the Kalman-Bucy filter estimate $m_K(t)$, satisfying the equation (11), are shown in the entire simulation interval $[0, 0.4]$ in Fig. 1. In addition, the graph of the mean-square sliding mode filter estimate $m(t)$ averaged by a Butterworth filter and all the variables of Fig. 1 are shown in detail in the interval $[0.2, 0.4]$ in Fig. 2.

It can be observed that the estimates given by both filters generate the same minimum estimation error variance, although the gain matrices $Q(t)$ and $P(t)$ are different.

12.3.2 Appendix 1

Proof of Theorem 12.1. The well-known classical solution to the filtering problem for a linear system (1^*) over linear observations (2^*) with respect to the mean-square criterion (3) is given by the Kalman-Bucy filter [20]. The mean-square estimate $m(t) = E(x(t) \mid F_t^Y)$ is governed by the equation

$$\dot{m}(t) = a_0(t) + a(t)m(t) + P(t)A^T(t)(B(t)B^T(t))^{-1}\times \tag{13}$$
$$A(t)[A^T(t)(A(t)A^T(t))^{-1}y(t) - m(t)].$$

with the initial condition $m(t_0) = E(x(t_0) \mid F_{t_0}^Y)$. The mean-square estimation error variance matrix $P(t)$ satisfies the Riccati equation

$$\dot{P}(t) = a(t)P(t) + P(t)a^T(t) + b(t)b^T(t) -$$
$$P(t)A^T(t)(B(t)B^T(t))^{-1}A(t)P(t), \tag{14}$$

with the initial condition $P(t_0) = E[(x(t_0) - m(t_0)(x(t_0) - m(t_0)^T \mid F_{t_0}^Y]$.

Let us show that the Kalman-Bucy filter (13),(14) coincides with the designed mean-square filter (5),(6). Indeed, upon introducing the new gain matrix $Q(t) = P(t) * \mid A^T(t)(A(t)A^T(t))^{-1}y(t) - m(t) \mid$, the estimate equation (13) coincides with the equation (5). Furthermore, in view of (14),(1), and the equality

$$A(t)(A^T(t)(A(t)A^T(t))^{-1}y(t) - m(t)) =$$
$$= A(t)(x(t) - m(t) + A^T(t)(A(t)A^T(t))^{-1}B(t)\psi_2(t)),$$

the newly introduced gain matrix $Q(t)$ satisfies the equation

$$\dot{Q}(t) = E(\dot{Q}(t) \mid F_t^Y) = E\big(\frac{d(P(t) * \mid A^T(t)(A(t)A^T(t))^{-1}y(t) - m(t) \mid)}{dt} \mid F_t^Y\big) =$$
$$E\big(\frac{dP(t)}{dt} * \mid A^T(t)(A(t)A^T(t))^{-1}y(t) - m(t) \mid +$$
$$P(t) * \frac{d(\mid A^T(t)(A(t)A^T(t))^{-1}y(t) - m(t) \mid)}{dt} \mid F_t^Y\big) =$$
$$E\big((P(t)a^T(t) + a(t)P(t) + b(t)b^T(t) -$$
$$P(t)A^T(t)(B(t)B^T(t))^{-1}A(t)P(t)) * \mid A^T(t)(A(t)A^T(t))^{-1}y(t) - m(t) \mid +$$
$$(-P(t)a^T(t) * \mid A^T(t)(A(t)A^T(t))^{-1}y(t) - m(t) \mid +$$
$$P(t)A^T(t)(B(t)B^T(t))^{-1}A(t)P(t) * \mid A^T(t)(A(t)A^T(t))^{-1}y(t) - m(t) \mid) \mid F_t^Y\big) =$$
$$b(t)b^T(t) * \mid A^T(t)(A(t)A^T(t))^{-1}y(t) - m(t) \mid +$$
$$a(t)P(t) * \mid A^T(t)(A(t)A^T(t))^{-1}y(t) - m(t) \mid =$$
$$b(t)b^T(t) * \mid A^T(t)(A(t)A^T(t))^{-1}y(t) - m(t) \mid + a(t)Q(t),$$

with the initial condition

$Q(t_0) = E[(x(t_0) - m(t_0)(x(t_0) - m(t_0)^T \mid F_{t_0}^Y] * \mid A^T(t_0)(A(t_0)A^T(t_0))^{-1}y(t_0) - m(t_0) \mid$, which coincides with (6). The theorem is proved. □

12.4 Mean-Module Filter Design

The solution to the mean-module filtering problem for the linear system (1) and the criterion (4) is given as follows. The mean-module estimate satisfies the differential equation with the sliding mode term

$$\dot{m}(t) = a_0(t) + a(t)m(t) + Q(t)A^T(t)(B(t)B^T(t))^{-1} \times \tag{15}$$
$$A(t)\text{sign}[A^T(t)(A(t)A^T(t))^{-1}y(t) - m(t)].$$

with the initial condition $m(t_0) = E(x(t_0) \mid F^Y_{t_0})$, where the Signum function is defined as in Section 12.3.

The matrix function $Q(t)$ satisfies the matrix equation with time-varying coefficients

$$\dot{Q}(t) = b(t)b^T(t) + a(t)Q(t), \tag{16}$$

with the initial condition
$Q(t_0) = E[(x(t_0) - m(t_0))(\text{sign}(A^T(t_0)(A(t_0)A^T(t_0))^{-1}A(t_0)x(t_0) - m(t_0)))^T \mid F^Y_{t_0}]$.

The presented result is formulated in the following theorem and proved in Appendix 2.

Theorem 12.2. *The mean-module filter for the linear system state (1) over the linear observations (2) is given by the equation (15) for the estimate $m(t)$ and the equation (16) for the filter gain matrix $Q(t)$.*

12.4.1 Example 2

This section presents an illustrative example of designing the mean-module sliding mode filter for a linear system (1),(2), using the filtering equations (15),(16).

Consider again a scalar linear unmeasured state

$$\dot{x}(t) = x(t) + \psi_1(t), \quad x(0) = x_0, \tag{17}$$

and the scalar linear observation process

$$y(t) = x(t) + \psi_2(t), \tag{18}$$

where $\psi_1(t)$ and $\psi_2(t)$ are white Gaussian noises.

The filtering problem is to find the mean-module estimate for the linear state (17), using linear observations (18) confused with independent and identically distributed disturbances modeled as white Gaussian noises.

The filtering equations (15),(16) take the following particular form for the system (17),(18)

$$\dot{m}(t) = m(t) + Q(t)\text{sign}[y(t) - m(t)], \tag{19}$$

with the initial condition $m(0) = E(x(0) \mid y(0)) = m_0$,

$$\dot{Q}(t) = Q(t) + 1, \tag{20}$$

with the initial condition $Q(0) = E((x(0) - m(0))(\text{sign}(x(0) - m(0)))^T \mid y(0))$.

The estimates obtained upon solving the equations (19),(20) are also compared to the estimates satisfying the Kalman-Bucy filtering equations (11),(12).

For each of the two filters (19),(20) and (11),(12) and the reference system (17),(18), involved in simulation, the following initial values are assigned: $x_0 = 1$, $m_0 = 10$, $P(0) = Q(0) = 100$. The filtering horizon is set to $T = 0.4$.

Note that the initial conditions $P(0)$ and $Q(0)$ are assigned equal for simulation purposes, since the results should be compared with respect to the mean-module criterion (4). If the initial value for Q is assigned as $Q(0) = 10$, the Kalman-Bucy filter would yield a better result as the best mean-square linear filter.

The following graphs are obtained: graphs of the reference state $x(t)$, satisfying the equation (17), the mean-module sliding mode filter estimate $m(t)$, satisfying the equations (19), and the mean-square Kalman-Bucy filter estimate $m_K(t)$, satisfying the equation (12), are shown in the entire simulation interval $[0, 0.4]$ in Fig. 3.

It can be observed that the mean-module sliding mode filter (19),(20) yields a certainly better value of the mean-module criterion (4) in comparison to the Kalman-Bucy filter (11),(12).

Note that the comparison of the designed mean-module sliding mode filter (19),(20) to the best mean-square Kalman-Bucy filter (11),(12) with respect to the criterion (4) is conducted for illustration purposes, since the filter (19),(20) should theoretically yield a better result, as follows from Theorem 12.2.

12.4.2 Appendix 2

Proof of Theorem 12.2. According to the general filtering theory based on the innovations process [23], the optimal estimate is a linear function of the minimized residual criterion. For instance, the mean-square Kalman-Bucy estimate linearly depends on the integral of $x(t) - E(x(t) \mid F_t^Y)$, which is the derivative of the minimized mean-square residue $(1/2)(x(t) - E(x(t) \mid F_t^Y))^T (x(t) - E(x(t) \mid F_t^Y))$, given that the right-side of the Kalman-Bucy filter estimate equation linearly includes the derivative term $x(t) - E(x(t) \mid F_t^Y)$ (see [20]). Similarly, the mean-module estimate equation linearly includes the derivative $\text{sign}(x(t) - E(x(t)) \mid F_t^Y)$ of the minimized mean-module residue $\mid x(t) - E(x(t) \mid F_t^Y) \mid$ in the criterion (4). Therefore, the mean-module estimate can be represented by the equation (15)

$$\dot{m}(t) = a_0(t) + a(t)m(t) + Q(t)A^T(t)(B(t)B^T(t))^{-1} \times$$

$$A(t)\text{sign}[A^T(t)(A(t)A^T(t))^{-1}y(t) - m(t)].$$

with the initial condition $m(t_0) = E(x(t_0) \mid F_{t_0}^Y)$. Here, the gain matrix $Q(t)$ should be selected to minimize the conditional variance of the estimation error produced by the estimate $m(t)$. According to the Ito formula (see, for example, [23]), the equation for

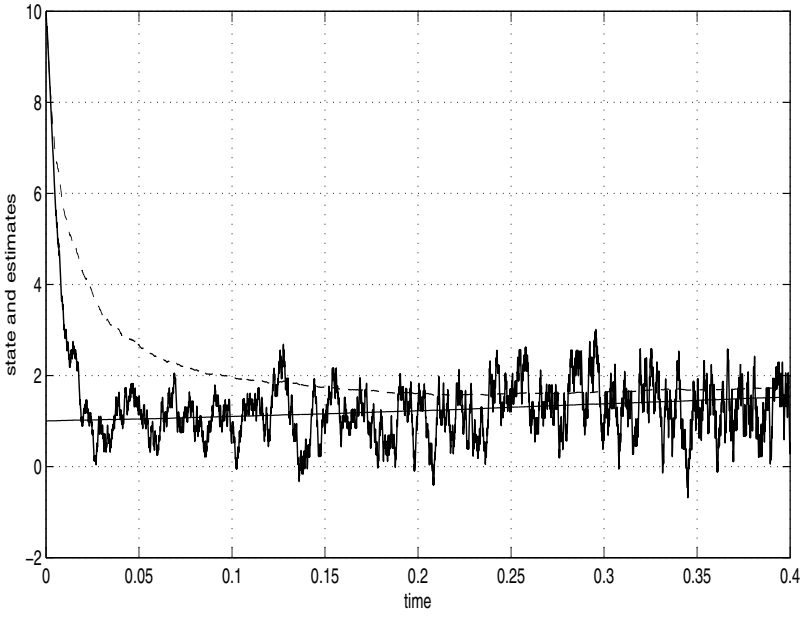

Fig. 12.1 Graphs of the unmeasured state (7) $x(t)$ (thin solid), the mean-square sliding mode estimate (9) $m(t)$ (thick solid), and the Kalman-Bucy estimate (11) $m_K(t)$ (dashed) in the interval $[0, 0.4]$.

the estimation error conditional variance $P(t) = E[(x(t) - m(t))(x(t) - m(t))^T \mid F_t^Y]$, produced by the estimate $m(t)$, takes the form

$$\dot{P}(t) = a(t)P(t) + P(t)a^T(t) + b(t)b^T(t) - Q(t)A^T(t)(B(t)B^T(t))^{-1}A(t)\times$$

$$E(\text{sign}(A^T(t)(A(t)A^T(t))^{-1}A(t)x(t) - m(t))(x(t) - m(t))^T \mid F_t^Y) -$$

$$E((x(t) - m(t))(\text{sign}(A^T(t)(A(t)A^T(t))^{-1}A(t)x(t) - m(t))^T \mid F_t^Y)\times$$

$$A^T(t)(B(t)B^T(t))^{-1}A(t)Q^T(t) + Q(t)A^T(t)(B(t)B^T(t))^{-1}A(t)Q^T(t).$$

As follows from the preceding equation, the variable $P(t)$ is minimized, if the gain matrix $Q(t)$ is assigned as

$$Q(t) = E((x(t) - m(t))(\text{sign}(A^T(t)(A(t)A^T(t))^{-1}A(t)x(t) - m(t)))^T \mid F_t^Y).$$

In view of the Ito formula, the equation for $Q(t)$ is given by (16), with the initial condition $Q(t_0) = E[(x(t_0) - m(t_0))(\text{sign}(A^T(t_0)(A(t_0)A^T(t_0))^{-1}A(t_0)x(t_0) - m(t_0)))^T \mid F_{t_0}^Y]$. The theorem is proved. □

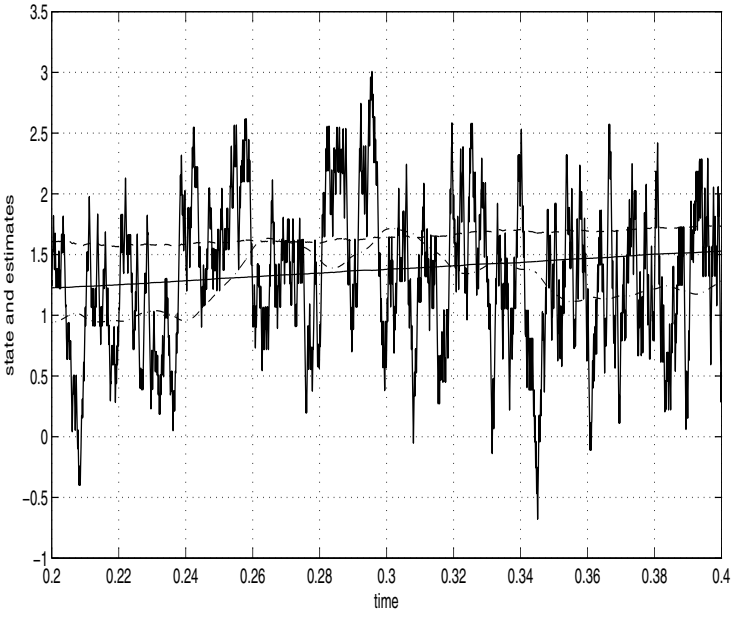

Fig. 12.2 Graphs of the unmeasured state (7) $x(t)$ (thin solid), the mean-square sliding mode estimate (9) $m(t)$ (thick solid), the mean-square sliding mode estimate (9) $m(t)$ averaged by a Butterworth filter (dashed and dotted), and the Kalman-Bucy estimate (11) $m_K(t)$ (dashed) in the interval $[0.2, 0.4]$.

12.5 Optimal Controller Problem

12.5.1 Problem Statement

Let (Ω, F, P) be a complete probability space with an increasing right-continuous family of σ-algebras $F_t, t \geq t_0$, and let $(W_1(t), F_t, t \geq t_0)$ and $(W_2(t), F_t, t \geq t_0)$ be independent Wiener processes. The F_t-measurable random process $(x(t), y(t))$ is described by a linear differential equation for the system state

$$dx(t) = a(t)x(t)dt + B(t)u(t)dt + b(t)dW_1(t), \quad x(t_0) = x_0, \tag{21}$$

and a linear differential equation for the observation process

$$dy(t) = A(t)x(t)dt + G(t)dW_2(t). \tag{22}$$

Here, $x(t) \in R^n$ is the state vector, $u(t) \in R^l$ is the control input, and $y(t) \in R^m$ is the linear observation vector, $m \leq n$. The initial condition $x_0 \in R^n$ is a Gaussian vector such that x_0, $W_1(t) \in R^p$, and $W_2(t) \in R^q$ are independent. The observation matrix $A(t) \in R^{m \times n}$ is not supposed to be invertible or even square. It is assumed that

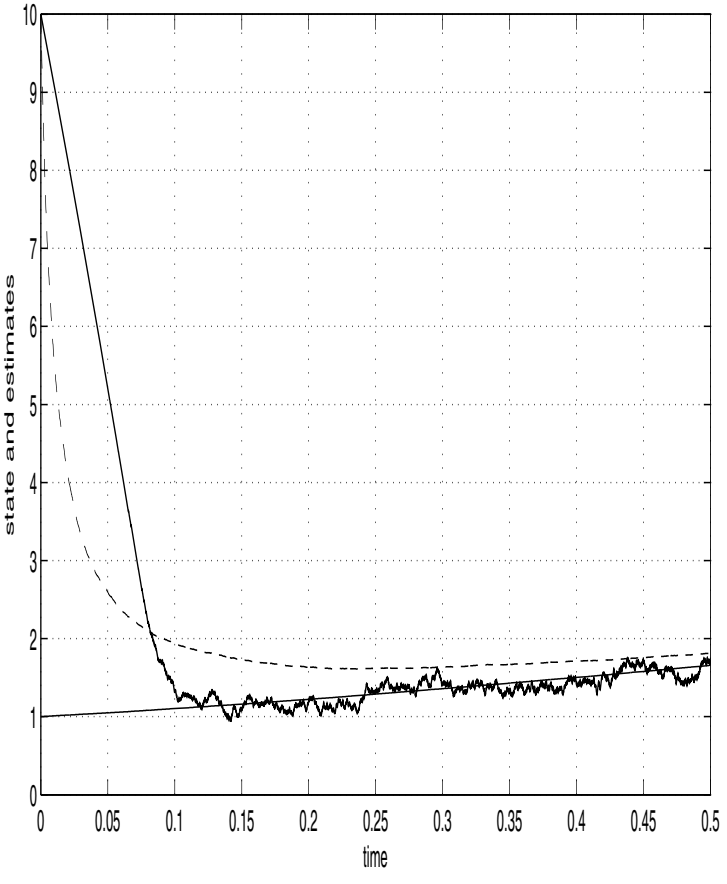

Fig. 12.3 Graphs of the unmeasured state (15) $x(t)$ (thin solid), the mean-module sliding mode estimate (17) $m(t)$ (thick solid), and the Kalman-Bucy estimate (11) $m_K(t)$ (dashed) in the interval $[0, 0.4]$.

$G(t)G^T(t)$ is a positive definite matrix, therefore, $m \leq q$. All coefficients in (21)–(22) are deterministic functions of appropriate dimensions. Without loss of generality, the system (1) (pair $(a(t), B(t))$) is assumed to be controllable for almost all $t \geq t_0$, i.e, the uncontrollable state components are removed from the consideration.

The state and observation equations can also be written in an alternative form

$$\dot{x}(t) = a(t)x(t) + B(t)u(t) + b(t)\psi_1(t), \quad x(t_0) = x_0, \tag{21*}$$

$$y(t) = A(t)x(t) + B(t)\psi_2(t), \tag{22*}$$

where $y(t) = \dot{Y}(t)$, and $\psi_1(t)$ and $\psi_2(t)$ are white Gaussian noises, which are the weak mean square derivatives of standard Wiener process $W_1(t)$, and $W_2(t)$ (see

[23]). The representations (21),(22) and (21*),(22*) are equivalent ([24]). The equations (21*),(22*) present the conventional form for the equations (21),(22), which is actually used in practice.

In the classical linear optimal controller problem [21,22], the criterion to be minimized is defined as a quadratic Bolza-Meyer functional:

$$J_3 = E[\frac{1}{2}[x(T)]^T \psi[x(T)] + \frac{1}{2}\int_{t_0}^{T}(u^T(s)R(s)u(s) + x^T(s)L(s)x(s))ds],$$

where $R(t)$ is positive and ψ, $L(t)$ are nonnegative definite symmetric matrix functions, and $T > t_0$ is a certain time moment. The symbol $E[f(x)]$ means the expectation (mean) of a function f of a random variable x, and a^T denotes transpose to a vector (matrix) a. The solution to this problem is well-known [21,22] and considered fundamental for the optimal linear systems theory.

In this paper, the criteria to be minimized include a non-quadratic terminal term or both non-quadratic state energy terms and are defined as follows:

$$J_1 = E[\sum_{i=1}^{n}\psi_{ii} \mid x_i(T) \mid + \frac{1}{2}\int_{t_0}^{T}(u^T(s)R(s)u(s) + x^T(s)L(s)x(s))ds], \tag{23}$$

$$J_2 = E[\sum_{i=1}^{n}\psi_{ii} \mid x_i(T) \mid + \int_{t_0}^{T}\frac{1}{2}(u^T(s)R(s)u(s))ds + \sum_{i=1}^{n}L_{ii}(s) \mid x_i(s) \mid ds], \tag{24}$$

where $R(s)$ is positive and $L(s)$ is a nonnegative definite continuous symmetric matrix functions, ψ is a diagonal nonnegative definite matrix, and $\mid x_i \mid$ denotes the absolute value of the component x_i of the vector $x \in R^n$.

The optimal controller problem is to find the control $u^*(t)$, $t \in [t_0, T]$, that minimizes the criterion J along with the unobserved trajectory $x^*(t), t \in [t_0, T]$, generated upon substituting $u^*(t)$ into the state equation (21).

Solutions to the stated optimal control problems are given in the next sections.

12.6 Mean-Square Controller Design

12.6.1 Separation Principle. I

Solving the first problem, in accordance with the separation principle for linear stochastic systems (see [21,22]), the unmeasured linear state $x(t)$, satisfying (21), is replaced with its mean-square estimate $m(t)$ over linear observations $y(t)$ (22), which is obtained using the mean-square sliding mode filter (5),(6)

$$\dot{m}(t) = a(t)m(t) + B(t)u(t) + K(t)A^T(t)(B(t)B^T(t))^{-1}\times \tag{25}$$

$$A(t)\text{sign}[A^T(t)(A(t)A^T(t))^{-1}y(t) - m(t)].$$

$$m(t_0) = m_0 = E(x(t_0) \mid F_{t_0}^Y),$$

$$\dot{K}(t) = (b(t)b^T(t))* \mid A^T(t)(A(t)A^T(t))^{-1}y(t) - m(t) \mid + a(t)K(t), \tag{26}$$
$$K(t_0) = E[(x(t_0) - m(t_0)(x(t_0) - m(t_0)^T \mid F_{t_0}^Y]*$$
$$\mid A^T(t_0)(A(t_0)A^T(t_0))^{-1}y(t_0) - m(t_0) \mid .$$

Here, the Signum function of a vector $x = [x_1, \ldots, x_n] \in R^n$ is defined as $\text{sign}[x] = [\text{sign}(x_1), \ldots, \text{sign}(x_n)] \in R^n$, and the signum function of a scalar x is defined as $\text{sign}(x) = 1$, if $x > 0$, $\text{sign}(x) = 0$, if $x = 0$, and $\text{sign}(x) = -1$, if $x < 0$ ([25]). A vector $\mid x \mid = [\mid x_1 \mid, \ldots, \mid x_n \mid] \in R^n$ is defined as the vector of absolute values of the components of the vector $x \in R^n$, and $A * b$ denotes a product between a matrix $A \in R^{n \times n}$ and a vector $b \in R^n$, that results in the matrix defined as follows: all entries of the j-th column of the matrix A are multiplied by the j-th component of the vector b, $j = 1, \ldots, n$.

Recall that $m(t)$ is the mean-square estimate for the state vector $x(t)$, based on the observation process $Y(t) = \{y(s), t_0 \le s \le t\}$, that minimizes the mean-square norm

$$H = E[(x(t) - m(t))^T(x(t) - m(t)) \mid F_t^Y]$$

at every time moment t. Here, $E[\xi(t) \mid F_t^Y]$ means the conditional expectation of a stochastic process $\xi(t) = (x(t) - m(t))^T(x(t) - m(t))$ with respect to the σ - algebra F_t^Y generated by the observation process $Y(t)$ in the interval $[t_0, t]$. As known [23], this optimal estimate is given by the conditional expectation

$$m(t) = E(x(t) \mid F_t^Y)$$

of the system state $x(t)$ with respect to the σ - algebra F_t^Y generated by the observation process $Y(t)$ in the interval $[t_0, t]$. As usual, the matrix function

$$P(t) = E[(x(t) - m(t))(x(t) - m(t))^T \mid F_t^Y]$$

is the estimation error variance.

It is readily verified (see [21,22]) that the optimal control problem for the system state (21) and cost function (23) is equivalent to the optimal control problem for the estimate (25) and the cost function J_1 represented as

$$J_1 = \sum_{i=1}^{n} \psi_{ii} \mid m_i(T) \mid + \frac{1}{2}\int_{t_0}^{T} (u^T(s)R(s)u(s) + m^T(s)L(s)m(s))ds +$$
$$\frac{1}{2}\int_{t_0}^{T} tr[P(s)L(s)]ds + tr[P^{-1}(T)K(T)\psi], \tag{27}$$

where $tr[A]$ denotes trace of a matrix A. Since the latter part of J_1 does not depend on control $u(t)$ or state $x(t)$, the reduced effective cost function M_1 to be minimized takes the form

$$M_1 = \sum_{i=1}^{n} \psi_{ii} \mid m_i(T) \mid + \frac{1}{2}\int_{t_0}^{T} (u^T(s)R(s)u(s) + m^T(s)L(s)m(s))ds. \tag{28}$$

Thus, the solution to the optimal control problem specified by (21),(23) can be found solving the optimal control problem given by (24),(28). Finally, the minimal value of the criterion J_1 should be determined using (27). This conclusion presents the separation principle for linear systems with a non-quadratic criterion (23).

12.6.2 Optimal Controller Problem Solution. I

The optimal solution to the control problem defined by (24),(28) is given in [13]. Applying the separation principle from the previous subsection to the sliding mode mean-square filter (25),(26) and the sliding mode optimal regulator in [13], the optimal controller solving the original problem (21)–(23) is given by the following theorem.

Theorem 12.3. *The optimal controller for a linear system (21) over linear observations (22) with respect to a non-quadratic criterion (23) is given by the control law*

$$u(t) = R^{-1}(t)B^T(t)Q(t)sign[m(t)], \tag{29}$$

where the matrix function $Q(t)$ is the solution of the matrix equation

$$\dot{Q}(t) = L(t) * \mid m(t) \mid -a^T(t)Q(t). \tag{30}$$

The terminal condition for the equation (30) is defined as $Q(T) = -\psi$, if the state $m(t)$ does not reach the sliding manifold $m(t) = 0$ within the time interval $[t_0, T]$, $m(t) \neq 0, t \in [t_0, T]$. Otherwise, if the state $m(t)$ reaches the sliding manifold $m(t) = 0$ within the time interval $[t_0, T]$, $m(t) = 0$ for some $t \in [t_0, T]$, then $Q(t)$ is set equal to a matrix function $Q_0(t)$ that is such a solution of (30) that $m(t)$ reaches the sliding manifold $m(t) = 0$ under the control law (28) with the matrix $Q_0(t)$ exactly at the final time moment $t = T$, $m(T) = 0$, but $m(t) \neq 0$, $t < T$.

Upon substituting the optimal control (29) into the equation (25), the following optimally controlled state estimate equation is obtained

$$\dot{m}(t) = a(t)m(t) + B(t)R^{-1}(t)B^T(t)Q(t)\text{sign}[m(t)] +$$

$$K(t)A^T(t)(B(t)B^T(t))^{-1}A(t)\text{sign}[A^T(t)(A(t)A^T(t))^{-1}y(t) - m(t)], \tag{31}$$

with the initial condition $m(t_0) = E(x(t_0) \mid F_t^Y)$.

Proof. Readily follows applying the separation principle from the previous subsection to the sliding mode mean-square filter (25),(26) and the sliding mode optimal regulator in [13]. □

Thus, the optimally controlled estimate equation (31), the control gain matrix equation (30), the optimal control law (29), and the filter gain matrix equation (25) give the complete solution to the optimal controller problem for linear systems over linear observations and a non-quadratic cost function (23).

12.6.3 Example 3

This section presents an example of designing the optimal sliding mode controller for a linear system (21) over linear observations (22) with a non-quadratic criterion (23), using the controller (26),(29)–(31), and comparing it to the best available LQG controller.

Consider a linear state equation

$$\dot{x}(t) = x(t) + u(t) + \psi_1(t), \quad x(0) = 1, \tag{32}$$

and a linear observation process

$$y(t) = x(t) + \psi_2(t), \tag{33}$$

where $\psi_1(t)$ and $\psi_2(t)$ are white Gaussian noises, which are the weak mean square derivatives of standard Wiener processes (see [23]). The equations (32),(33) correspond to the alternative conventional form (21*),(22*) for the equations (21),(22).

The controller problem is to find the control $u(t)$, $t \in [0,T]$, $T = 1.2$, that minimizes the criterion

$$J_1 = 50 \mid x(T) \mid + \frac{1}{2}\int_0^T (u^2(t) + x^2(t))dt, \tag{34}$$

In other words, the control problem is to minimize the overall energy of the state x using the minimal overall energy of control u.

Applying the sliding-mode controller (26),(29)–(31), the control law (29) is given by

$$u(t) = Q(t)\text{sign}[x(t)], \tag{35}$$

where $m(t)$ satisfies the equation

$$\dot{m}(t) = m(t) + u(t) + K(t)\text{sign}[y(t) - m(t)], \tag{36}$$

with the initial condition $m(0) = E(x(0) \mid y(0)) = m_0$, $K(t)$ satisfies the equation

$$\dot{K}(t) = K(t) + \mid y(t) - m(t) \mid, \tag{37}$$

with the initial condition $K(0) = E((x(0) - m(0))(x(0) - m(0))^T \mid y(0))* \mid y(0) - m(0) \mid$, and $Q(t)$ satisfies the equation

$$\dot{Q}(t) = \mid m(t) \mid - Q(t), \tag{38}$$

with the terminal condition $Q(1.2) = -50$, if $m(t) \neq 0$ for any $t < 5$, and $Q^*(t^*) = 0$, where t^* is the time that the estimate $m(t)$ reaches the sliding manifold $m = 0$ at the final moment $t = T$, otherwise.

Upon substituting the control (35) and the obtained expressions for $K(t)$ and $Q(t)$ into (36), the optimally controlled state estimate equation takes the form

$$\dot{m}(t) = m(t) + Q(t)\text{sign}[m(t)] + K(t)\text{sign}[y(t) - m(t)], \tag{39}$$

with the initial condition $m(0) = E(x(0) \mid y(0)) = m_0$. The obtained system (37)–(39) can be solved using simple numerical methods, such as "shooting." This method consists in varying initial conditions of (18) until the given terminal condition is satisfied.

For numerical simulation of the system (32),(33) and the controller (35)–(39), the initial values $x(0) = 1$, $m(0) = 10$, and $P(0) = 866.25$ are assigned. The final time is set to $T = 1.2$. The disturbances $\psi_1(t)$ in (32) and $\psi_2(t)$ in (33) are realized using the built-in MatLab white noise function.

The system (37)–(39) is first simulated with the terminal condition $Q^*(1.2) = -50$. As the simulation shows, the state $m(t)$ reaches zero before the final moment $T = 1.2$. Accordingly, the terminal condition for the equation (38) is reset to $Q^*(1.2) = -\psi_0$ such that $m(1.2) = 0$, and the system (37)–(39) is simulated again. The results obtained applying the controller (35)–(39) to the system (12) are shown in Fig. 4, which presents the graphs of the controlled state (32) $x(t)$, the controlled estimate (39) $m(t)$, the control (35) $u(t)$, and the criterion (34) $J_1(t)$ in the interval $[0, 1.2]$. The value of the criterion (34) at the final moment $T = 1.2$ is $J_1(1.2) = 4.985$.

The designed sliding mode controller (26),(29)–(31) is compared to the best linear controller for the criterion J_3 with the quadratic non-integral term

$$J_3 = 25x^2(T) + \frac{1}{2}\int_0^T (u^2(t) + x^2(t))dt, \tag{40}$$

As follows from the optimal LQG theory [21,22], the linear control law is given by

$$u(t) = Q(t)m(t), \tag{41}$$

where where $m(t)$ satisfies the equation

$$\dot{m}(t) = m(t) + u(t) + P(t)[y(t) - m(t)], \tag{42}$$

with the initial condition $m(0) = E(x(0) \mid y(0)) = m_0$, the variance $P(t)$ satisfies the Riccati equation

$$\dot{P}(t) = 1 + 2P(t) - P^2(t), \tag{43}$$

with the initial condition $P(0) = E((x(0) - m(0))(x(0) - m(0))^T \mid y(0))$, and $Q(t)$ satisfies the Riccati equation

$$\dot{Q}(t) = 1 - 2Q(t) - Q^2(t), \quad Q(1.2) = -50. \tag{44}$$

Upon substituting the control (41) and the obtained expressions for $P(t)$ and $Q(t)$ into (42), the optimally controlled state estimate equation takes the form

$$\dot{m}(t) = m(t) + Q(t)m(t) + P(t)[y(t) - m(t)], \tag{45}$$

with the initial condition $m(0) = E(x(0) \mid y(0)) = m_0$.

Note that the comparison of the designed sliding mode controller (26),(29)–(31) to the best LQG controller (41)–(45) with respect to the criterion (34) is conducted for illustration purposes, since the controller (26),(29)–(31) should theoretically yield a better result, as follows from Theorem 12.3.

The results obtained applying the controller (26),(29)–(31) to the system (32),(33) are shown in Fig. 4, which presents the graphs of the controlled state (32) $x(t)$, the controlled estimate (35) $m(t)$, the control (31) $u(t)$, and the criterion (34) $J_1(t)$ in the interval $[0, 1.2]$. The value of the criterion (34) at the final moment $T = 1.2$ is $J_1(1.2) = 7.51$.

It can be observed that the sliding mode controller (26),(29)–(31) yields a certainly better value of the criterion (34) in comparison to the linear feedback LQG controller (41)–(45). Note that the classical linear feedback LQG controller fails to provide a causal optimal control for the criterion (34).

12.7 Mean-Module Controller Design

12.7.1 Separation Principle. II

Solving the second problem, the unmeasured linear state $x(t)$, satisfying (21), is replaced with its mean-module estimate $m(t)$ over linear observations $y(t)$ (22), which is obtained using the mean-module sliding mode filter (15),(16)

$$\dot{m}(t) = a(t)m(t) + B(t)u(t) + K(t)A^T(t)(B(t)B^T(t))^{-1}\times \tag{46}$$

$$A(t)\mathrm{sign}[A^T(t)(A(t)A^T(t))^{-1}y(t) - m(t)].$$

$$m(t_0) = m_0 = E(x(t_0) \mid F^Y_{t_0}),$$

$$\dot{K}(t) = b(t)b^T(t) + a(t)K(t), \tag{47}$$

$$K(t_0) = E[(x(t_0) - m(t_0)(\mathrm{sign}(A^T(t)(A(t)A^T(t))^{-1}A(t)x(t_0) - m(t_0)))^T \mid F^Y_{t_0}].$$

Here, $m(t)$ is the mean-module estimate for the state vector $x(t)$, based on the observation process $Y(t) = \{y(s), t_0 \le s \le t\}$, that minimizes the mean-module norm

$$J = E[(\mid x(t) - \hat{x}(t) \mid) \mid F^Y_t]$$

at every time moment t.

It is readily verified (see [21,22]) that the optimal control problem for the system state (21) and cost function (24) is equivalent to the optimal control problem for the estimate (46) and the cost function J_2 represented as

$$J_2 = \sum_{i=1}^{n} \psi_{ii} \mid m_i(T) \mid + \int_{t_0}^{T} \frac{1}{2}(u^T(s)R(s)u(s))ds + \sum_{i=1}^{n} L_{ii}(s) \mid m_i(s) \mid ds +$$

$$\frac{1}{2}\int_{t_0}^{T} tr[K(s)L(s)]ds + tr[K(T)\psi], \tag{48}$$

where $tr[A]$ denotes trace of a matrix A. Since the latter part of J_2 does not depend on control $u(t)$ or state $x(t)$, the reduced effective cost function M_2 to be minimized takes the form

$$M_2 = \sum_{i=1}^{n} \psi_{ii} \mid m_i(T) \mid + \int_{t_0}^{T} \frac{1}{2}(u^T(s)R(s)u(s))ds + \sum_{i=1}^{n} L_{ii}(s) \mid m_i(s) \mid ds. \tag{49}$$

Thus, the solution to the optimal control problem specified by (21),(24) can be found solving the optimal control problem given by (46),(49). Finally, the minimal value of the criterion J_2 should be determined using (48). This conclusion presents the separation principle for linear systems with a non-quadratic criterion (24).

12.7.2 Optimal Controller Problem Solution. II

The optimal solution to the control problem defined by (46),(49) is given in [14]. Applying the separation principle from the previous subsection to the sliding mode mean-module filter (45),(46) and the sliding mode optimal regulator in [14], the optimal controller solving the original problem (21),(22),(24) is given by the following theorem.

Theorem 12.4. *The optimal controller for a linear system (21) over linear observations (22) with respect to a non-quadratic criterion (24) is given by the control law*

$$u(t) = R^{-1}(t)B^T(t)Q(t)sign[m(t)], \tag{50}$$

where the matrix function $Q(t)$ is the solution of the matrix equation

$$\dot{Q}(t) = L(t) - a^T(t)Q(t). \tag{51}$$

The terminal condition for the equation (51) is defined as $Q(T) = -\psi$, if the state $x(t)$ does not reach the sliding manifold $m(t) = 0$ within the time interval $[t_0, T]$, $m(t) \neq 0, t \in [t_0, T]$. Otherwise, if the state $m(t)$ reaches the sliding manifold $m(t) = 0$ within the time interval $[t_0, T]$, then the terminal condition for $Q(t)$ is set to zero at the time moment t^*, $Q(t^*) = 0$, where t^* is the maximum possible time of reaching the sliding manifold $m(t) = 0$. In other words, there exists no such solution to the system of equations (21), (50), (51) satisfying the conditions $m(t_0) = m_0$ and $Q(t_1) = 0, t_1 > t^*$, that $m(t) \neq 0$ for $t < t_1$ and $m(t) = 0$ for some $t \geq t_1$.

Upon substituting the optimal control (50) into the equation (46), the following optimally controlled state estimate equation is obtained

$$\dot{m}(t) = a(t)m(t) + B(t)R^{-1}(t)B^T(t)Q(t)\text{sign}[m(t)] + K(t)A^T(t)(B(t)B^T(t))^{-1} \times A(t)\text{sign}[A^T(t)(A(t)A^T(t))^{-1}y(t) - m(t)], \tag{52}$$

with the initial condition $m(t_0) = E(x(t_0) \mid F_t^Y)$.

Proof. Readily follows applying the separation principle from the previous subsection to the sliding mode mean-module filter (45),(46) and the sliding mode optimal regulator in [14]. □

Thus, the optimally controlled state estimate equation (52), the control gain matrix equation (51), the optimal control law (50), and the filter gain matrix equation (47) give the complete solution to the optimal controller problem for linear systems over linear observations and a non-quadratic cost function (24).

12.7.3 Example 4

This section presents an example of designing the optimal sliding mode controller for a linear system (21) over linear observations (22) with a non-quadratic criterion (24), using the controller (47),(50)–(52), and comparing it to the best available LQG controller.

Consider a linear state equation

$$\dot{x}(t) = x(t) + u(t) + \psi_1(t), \quad x(0) = 1, \tag{53}$$

and a linear observation process

$$y(t) = x(t) + \psi_2(t), \tag{54}$$

where $\psi_1(t)$ and $\psi_2(t)$ are white Gaussian noises.

The controller problem is to find the control $u(t)$, $t \in [0,T]$, $T = 1.2$, that minimizes the criterion

$$J_2 = 50 \mid x(T) \mid + \int_0^T \frac{1}{2}(u^2(t)) + \mid x(t) \mid dt, \tag{55}$$

In other words, the control problem is to minimize the overall energy of the state x using the minimal overall energy of control u.

Applying the sliding-mode controller (47),(50)–(52), the control law (50) is given by

$$u(t) = Q(t)\text{sign}[x(t)], \tag{56}$$

where $m(t)$ satisfies the equation

$$\dot{m}(t) = m(t) + u(t) + K(t)\text{sign}[y(t) - m(t)], \tag{57}$$

with the initial condition $m(0) = E(x(0) \mid y(0)) = m_0$, $K(t)$ satisfies the equation

$$\dot{K}(t) = K(t) + 1, \tag{58}$$

with the initial condition $K(0) = E((x(0) - m(0))(\text{sign}(x(0) - m(0)))^T \mid y(0))$, and $Q(t)$ satisfies the equation

$$\dot{Q}(t) = 1 - Q(t), \tag{59}$$

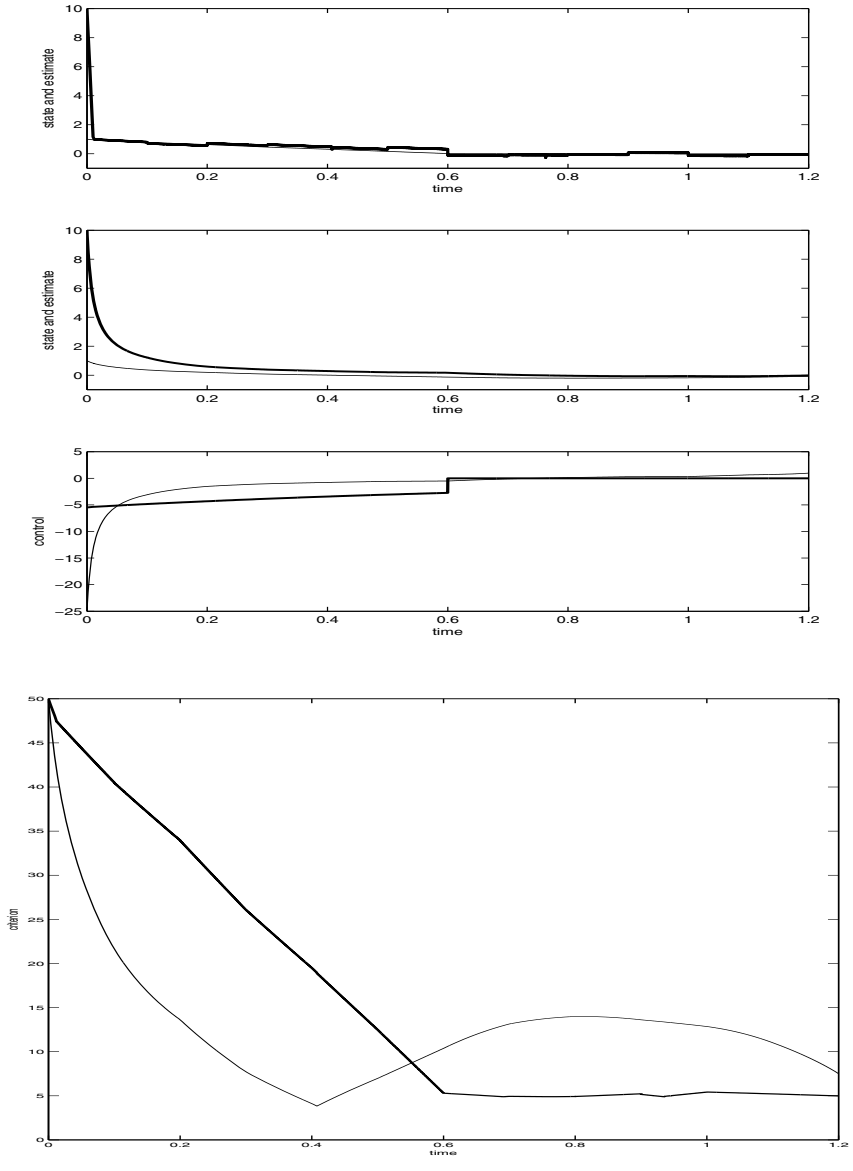

Fig. 12.4 Sliding mode controller optimal with respect to criterion J_1 vs. linear feedback controller in the entire simulation interval $[0, 1.2]$. **1. Sliding mode controller.** Graphs of the controlled state (32) $x(t)$ (thin solid line) and the controlled estimate (39) $m(t)$ (thick solid line); **2. Linear feedback controller.** Graphs of the controlled state (32) $x(t)$ (thin solid line) and the controlled estimate (45) $m(t)$ (thick solid line); **3. Control.** Graphs of the sliding mode control (35) $u^*(t)$ (thick solid line) and the linear feedback control (41) $u(t)$ (thin solid line); **4. Criterion.** Graphs of the criterion (34) J_1 produced by the sliding mode controller (thick solid line) and by the linear feedback controller (thin solid line).

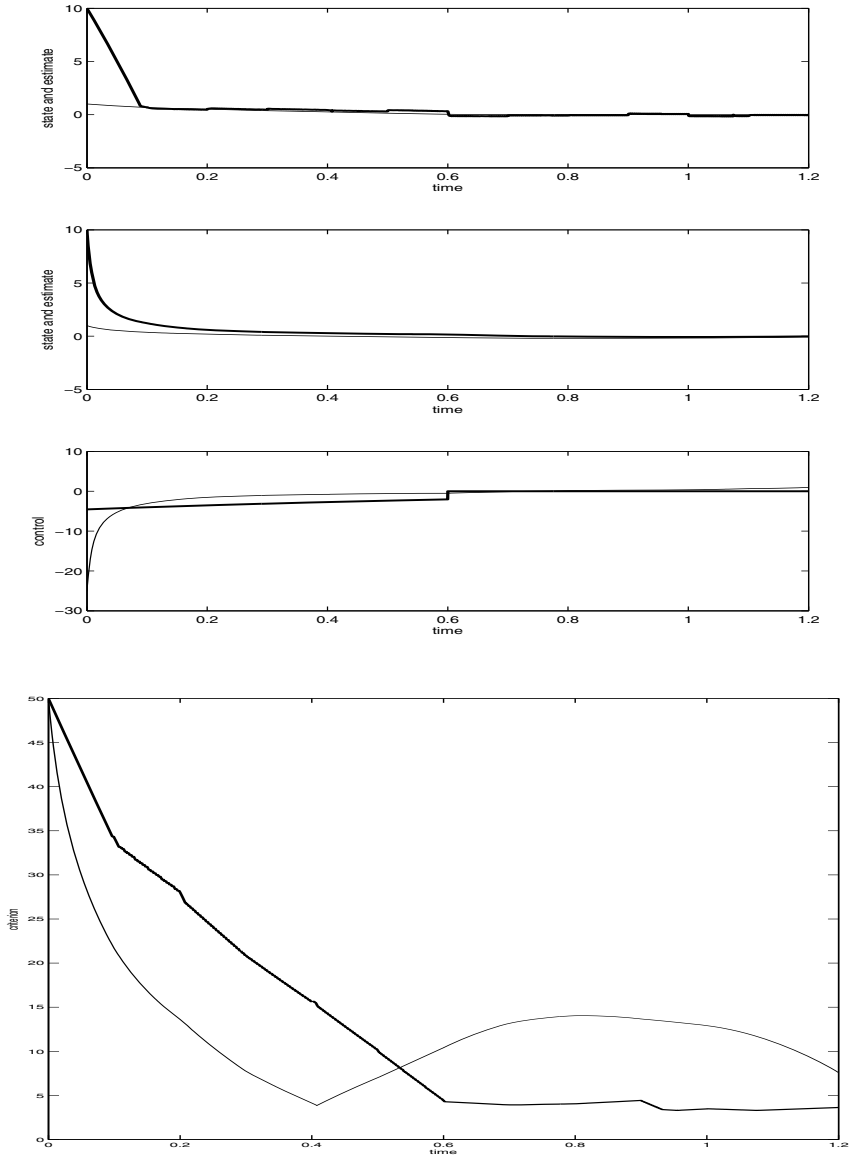

Fig. 12.5 Sliding mode controller optimal with respect to criterion J_1 vs. linear feedback controller in the entire simulation interval $[0, 1.2]$. **1. Sliding mode controller.** Graphs of the controlled state (53) $x(t)$ (thin solid line) and the controlled estimate (60) $m(t)$ (thick solid line); **2. Linear feedback controller.** Graphs of the controlled state (53) $x(t)$ (thin solid line) and the controlled estimate (45) $m(t)$ (thick solid line); **3. Control.** Graphs of the sliding mode control (56) $u^*(t)$ (thick solid line) and the linear feedback control (41) $u(t)$ (thin solid line); **4. Criterion.** Graphs of the criterion (55) J_1 produced by the sliding mode controller (thick solid line) and by the linear feedback controller (thin solid line).

with the terminal condition $Q^*(t^*) = 0$, where t^* is the maximum possible time of reaching the sliding manifold $m(t) = 0$ by the state estimate $m(t)$.

Upon substituting the control (56) and the obtained expressions for $K(t)$ and $Q(t)$ into (53), the optimally controlled state estimate equation takes the form

$$\dot{m}(t) = m(t) + Q(t)\text{sign}[m(t)] + K(t)\text{sign}[y(t) - m(t)], \tag{60}$$

with the initial condition $m(0) = E(x(0) \mid y(0)) = m_0$.

For numerical simulation of the system (53),(54) and the controller (56)–(60), the initial values $x(0) = 1$, $m(0) = 10$, and $P(0) = 100$ are assigned. The final time is set to $T = 1.2$. The disturbances $\psi_1(t)$ in (53) and $\psi_2(t)$ in (54) are realized using the built-in MatLab white noise function.

The results obtained applying the controller (56)–(60) to the system (53) are shown in Fig. 5, which presents the graphs of the controlled state (53) $x(t)$, the controlled estimate (60) $m(t)$, the control (56) $u(t)$, and the criterion (55) $J_2(t)$ in the interval $[0, 1.2]$. The value of the criterion (55) at the final moment $T = 1.2$ is $J_2(1.2) = 5.634$.

The optimal sliding-mode controller (47),(50)–(52) is compared to the best linear regulator (41)–(45) for the criterion (40) J_3.

Again, the comparison of the designed sliding mode controller (47),(50)–(52) to the best LQG controller (41)–(45) with respect to the criterion (40) is conducted for illustration purposes, since the controller (47),(50)–(52) should theoretically yield a better result, as follows from Theorem 12.4.

The results obtained applying the controller (47),(50)–(52) to the system (53),(54) are shown in Fig. 5, which presents the graphs of the controlled state (53) $x(t)$, the controlled estimate (60) $m(t)$, the control (56) $u(t)$, and the criterion (55) $J_2(t)$ in the interval $[0, 1.2]$. The value of the criterion (55) at the final moment $T = 1.2$ is $J_2(1.2) = 7.586$.

It can be observed that the sliding mode controller (47),(50)–(52) yields a certainly better value of the criterion (55) in comparison to the linear feedback LQG controller (41)–(45). Note again that the classical linear feedback LQG controller fails to provide a causal optimal control for the criterion (45).

12.8 Conclusions

This paper presents the mean-square and mean-module filtering problems and designs the solutions as filters based on a sliding mode gain. Both filtering problems are considered for linear systems with Gaussian white noises. It is shown that the designed sliding mode mean-square filter generates the mean-square estimate, which has the same minimum estimation error variance as the best estimate given by the classical Kalman-Bucy filter, although the gain matrices of both filters are different. It is numerically verified in an example that the estimates produced by the designed sliding mode mean-square filter and the Kalman-Bucy filter yield the same minimum estimation error variance. On the other hand, the designed sliding mode mean-module filter generates the mean-module estimate, which yields a better value

of the mean-module criterion in comparison to the mean-square Kalman-Bucy filter. This conclusion is theoretically proved and numerically verified in an example. The proposed approach based on involving a sliding mode innovations term is expected to be applicable to other filtering problems with non-mean-square criteria, where the conventional Kalman-Bucy linear filter would not work, in particular, to polynomial systems. Then, the paper presents two optimal controller problems, whose solutions are given by sliding mode controllers, each consisting of a sliding mode filter and a sliding mode regulator. The optimal controller problems are considered for a linear system over linear observations with respect to two different Bolza-Meyer criteria, where 1) the integral control and state energy terms are quadratic and the non-integral term is of the first degree or 2) the control energy term is quadratic and the state energy terms are of the first degree. It is shown that the optimal solutions are given by causal sliding mode controllers, whereas the conventional linear feedback controller fails to provide feasible solutions. The proposed approach based on a sliding mode control is expected to be applicable to optimal controller problems for nonlinear polynomial systems with non-quadratic criteria, where the conventional linear feedback controller would not work.

Acknowledgements. The author thanks the Mexican National Science and Technology Council (CONACyT) for financial support under Grant 55584 and joint Mexico-EU FONCICyT Grant 93302.

References

1. Utkin, V.I.: Sliding Modes in Control and Optimization. Springer, Heidelberg (1992)
2. Edwards, C., Spurgeon, S.K.: Sliding Mode Control: Theory and Applications. Taylor and Francis, London (1998)
3. Fridman, L., Levant, A.: Higher order sliding modes. In: Perruquetti, W., Barbot, J.P. (eds.) Sliding Mode Control in Engineering, pp. 53–101. Marcel Dekker, Inc., New York (2002)
4. Utkin, V.I., Guldner, J., Shi, J.: Sliding Mode Control in Electromechanical Systems. Taylor and Francis, London (1999)
5. Suzuki, S., Pan, Y., Furuta, K., Hatakeyama, S.: VS-control with time-varying sliding sector: Design and application to pendulum. Asian Journal of Control 6, 307–316 (2004)
6. Castaños, F., Fridman, L.: Analysis and design of integral sliding manifolds for systems with unmatched perturbations. IEEE Trans. Automatic Control 51, 853–858 (2006)
7. Baev, S., Shtessel, Y.B., Edwards, C., Spurgeon, S.K.: Output feedback tracking in causal nonminimum-phase nonlinear systems using HOSM techniques. In: Proc. 10th International Workshop on Variable Structure Systems, pp. 209–214 (2008)
8. Azemi, A., Yaz, E.: Sliding mode adaptive observer approach to chaotic synchronization. ASME Transactions. J. Dynamic Systems, Measurements and Control 122, 758–765 (2000)
9. Spurgeon, S.K.: Sliding mode observers: A survey. Intern. Journal of Systems Science 39, 751–764 (2008)
10. Boiko, I., Fridman, L., Pisano, A., Usai, E.: Analysis of chattering in systems with second order sliding modes. IEEE Trans. Automatic Control 52, 2085–2102 (2007)

11. Utkin, V.I., Shi, L.: Integral sliding mode in systems operating under uncertainty conditions. In: Proc. 35th Conference on Decision and Control, Kobe, Japan, pp. 4591–4596 (1996)
12. Bartolini, G., Ferrara, A., Levant, A., Usai, E.: On second order sliding mode controllers. In: Young, K.D., Ozguner, U. (eds.) Variable Structure Systems, Sliding Mode and Nonlinear Control. LNCIS, vol. 247, pp. 329–350. Springer, Heidelberg (1999)
13. Basin, M.V., Ferrara, A., Calderon-Alvarez, D.: Sliding mode regulator as solution to optimal control problem. In: Proc. 47th Conference on Decision and Control, Cancun, Mexico, pp. 2184–2189 (2008)
14. Basin, M.V., Ferrara, A., Calderon-Alvarez, D., Dinuzzo, F.: Sliding mode optimal regulator for a Bolza-Meyer criterion with non-quadratic state energy terms. In: Proc. 2009 American Control Conference, St. Louis, MO, pp. 4951–4955 (2009)
15. Xia, Y., Jia, Y.: Robust sliding mode control for uncertain stochastic time-delay systems. IEEE Trans. Automatic Control 48, 1086–1092 (2003)
16. Niu, Y., Ho, D.W.C., Lam, J.: Robust integral sliding mode control for uncertain stochastic systems with time-varying delay. Automatica 41, 873–880 (2005)
17. Shi, P., Xia, Y., Liu, G.P., Rees, D.: On designing of sliding mode control for stochastic jump systems. IEEE Trans. Automatic Control 51, 97–103 (2006)
18. Basin, M.V., Fridman, L., Skliar, M.: Optimal and robust sliding mode filter for systems with continuous and delayed measurements. In: Proc. 41st Conference on Decision and Control, Las Vegas, NV, pp. 2594–2599 (2002)
19. Basin, M.V., Fridman, L., Rodriguez-Gonzalez, J.G., Acosta, P.: Integral sliding mode design for robust filtering and control of linear stochastic time-delay systems. Intern. J. Robust Nonlinear Control 15, 407–421 (2005)
20. Kalman, R.E., Bucy, R.S.: New results in linear filtering and prediction theory. ASME Trans., Part D (J. of Basic Engineering) 83, 95–108 (1961)
21. Kwakernaak, H., Sivan, R.: Linear Optimal Control Systems. Wiley Interscience, New York (1972)
22. Fleming, W.H., Rishel, R.W.: Deterministic and Stochastic Optimal Control. Springer, Heidelberg (1975)
23. Pugachev, V.S., Sinitsyn, I.N.: Stochastic Systems: Theory and Applications. World Scientific, Singapore (2001)
24. Åström, K.J.: Introduction to Stochastic Control Theory. Academic Press, New York (1970)
25. Filippov, A.F.: Differential Equations with Discontinuous Righthand Sides. Kluwer, Dordrecht (1988)

Chapter 13
Output Tracking and Observation in Nonminimum Phase Systems via Classical and Higher Order Sliding Modes

Y. Shtessel, S. Baev, C. Edwards, S. Spurgeon, and A. Zinober

Abstract. The problem of causal output tracking and observation in non-minimum phase nonlinear systems is studied. The extended method of Stable System Center (ESSC) is used in two-fold manner: i) to generate reference profile for unstable internal states; ii) to estimate states of unstable internal dynamics. Two applications of the proposed technique are considered for illustration purposes: output voltage tracking in a nonminimum phase DC/DC electric power converter and output tracking in SISO systems with time-delayed output feedback. A variety of traditional and higher-order sliding mode (HOSM) control and observation methods is employed in the majority of algorithms. Most of the theoretical results are covered by numerical simulations.

Yuri Shtessel
University of Alabama in Huntsville, 301 Sparkman Drive, Huntsville, AL 35899, USA
e-mail: shtessel@eng.uah.edu

Simon Baev
Georgia SouthWestern State University, 800 GSW University Drive,
Americus, GA 31709, USA
e-mail: sbaev@canes.gsw.edu

Christopher Edwards
Department of Engineering, University of Leicester, University Road,
Leicester LE1 7RH UK
e-mail: ce14@le.ac.uk

Sarah Spurgeon
Department of Electronics, University of Kent, Canterbury, Kent, CT2 7NZ UK
e-mail: S.K.Spurgeon@kent.ac.uk

Alan Zinober
Department of Applied Mathematics, University of Sheffield, S10, 2TN Sheffield, UK
e-mail: a.zinober@sheffield.ac.uk

L. Fridman et al. (Eds.): Sliding Modes, LNCIS 412, pp. 351–380.
springerlink.com

13.1 Introduction

The problem of nonminimum phase output tracking is a challenging and nontrivial control problem. However, it keeps generating new ideas and control techniques with continuously improving contributions. Originally introduced as a purely theoretical problem, it has found itself applicable to many real-life applications including DC/DC power converters [25] and aircraft control [15, 14]. The control problem handles a class of dynamical systems, where the internal or zero-dynamics are unstable, making traditional and powerful control methods such as feedback linearization [11] and sliding mode control [22, 7, 23, 5] difficult to apply.

Tremendous efforts have been applied to address many of the issues mentioned above. Several control techniques have been proposed for the *noncausal* case where the *tracking reference profile is assumed to be known beforehand*. An approximate solution for a special class of systems and trajectories is proposed in [9]. Exact tracking of a known trajectory given by a noncausal system is achieved via a stable nonlinear inverse in [6]. The problem of nonminimum phase output tracking of nonlinear systems is handled in [10] through redefinition of the control.

A successful attempt to improve the *causality* of the tracking has been made in [16]. The authors address the problem of asymptotic output tracking for a class of nonlinear uncertain systems, where the output reference profile together with unmatched external disturbances are defined by an unknown linear exosystem with *known* characteristic polynomial. The proposed method improves the causality with respect to the existing state of art, but the assumption that the characteristic polynomial of the exogenous system is known means its impact is a theoretical breakthrough. An extension to the result of [16] has been proposed in [3, 2], where the exogenous system, responsible for generating the output reference profile is assumed to be *unknown*, but of given order. Its characteristic polynomial is identified online via a higher order sliding mode (HOSM) parameter observer [12, 1] and it is used for generating the reference profile for the internal state. The real restriction of the method proposed in [3, 2], is the unrealistic assumption of internal state availability.

In this paper, a multistage observer is employed to recover the unstable internal state. It relaxes the limitations of the previous work and converts the tracking problem to an output feedback oriented one. The contributions of the proposed work, with respect to the cornerstone results, published in [16], are summarized as follows:

1. A causal output reference profile is assumed to be generated by an *unknown* linear exosystem of given order. The coefficients of the corresponding characteristic polynomial, which are used in the controller design, are recovered by a higher order sliding mode parameter observer [1];
2. Employing the multistage observer along with a HOSM differentiator [12], allows estimation of the full state vector, including the unstable internal state;

3. Using the estimated state vector allows:
   a. asymptotic output feedback tracking of the causal reference profile;
   b. identification of the unknown input, forcing the I/O dynamics;

13.2 System Description

Consider a nonlinear plant model, presented in the form of *input/output dynamics*

$$\begin{pmatrix} y_1^{(r_1)} \\ \vdots \\ y_m^{(r_m)} \end{pmatrix} = \phi(\xi,\eta) + \mathbf{f}(t) + \mathbf{u}(\xi,\eta), \tag{13.1}$$

with *internal dynamics*

$$\dot{\eta} = \mathbf{Q}\,\eta + \mathbf{G}\,\xi \tag{13.2}$$

where

$\mathbf{u} \triangleq \{u_1, u_2, \ldots, u_m\} \in \mathbb{R}^m$ is the control input;
$\mathbf{y} \triangleq \{y_1, y_2, \ldots, y_m\} \in \mathbb{R}^m$ is the commanded output (available for measurement);
$[r_1, r_2, \ldots, r_m] \in \mathbb{R}^m$ is the vector relative degree;
$r = r_1 + r_2 + \cdots + r_m$ is the total relative degree;
n is the total order of the system ($n > r$);
$p = n - r$ is the order of the internal dynamics ($p > 0$);
$\eta \in \mathbb{R}^p$ are the states of the *unstable* internal dynamics (**not available for measurement**);
$\xi \in \mathbb{R}^r$ is the combined *output state* vector;
$\phi(\cdot) \triangleq \{\phi_1, \phi_2, \ldots, \phi_m\}^T \in \mathbb{R}^m$ is a known smooth and bounded vector field;
$\mathbf{f}(t) \in \mathbb{R}^m$ is a sufficiently smooth, bounded *unknown input/disturbance*;
$\mathbf{Q} \in \mathbb{R}^{p\times p}$ is a known *non-Hurwitz* gain matrix;
$\mathbf{G} \in \mathbb{R}^{p\times r}$ is a known gain matrix.

Remark 13.1. The system (13.1),(13.2) is *nonminimum phase* due to the non-Hurwitz nature of $\mathbf{Q}$.

The output state vector is constructed from all the outputs along with an appropriate number of their time derivatives:

$$\xi = \{\underbrace{y_1, \ldots, y_1^{(r_1-2)}, \ldots, y_m, \ldots, y_m^{(r_m-2)}}_{\xi_1 \in \mathbb{R}^{r-m}}, \underbrace{y_1^{(r_1-1)}, \ldots, y_m^{(r_m-1)}}_{\xi_2 \in \mathbb{R}^m}\}^T \tag{13.3}$$

Remark 13.2. The input-output (I/O) substates given by equation (13.3) are available for the controller design since they can be reconstructed in finite time using the exact HOSM differentiator of r_i-order [12]:

$$
\begin{aligned}
\dot{z}_{i,0} &= \nu_{i,0} \\
\nu_{i,0} &= -\lambda_{i,0}\,|z_{i,0}-y_i|^{r_i/(r_i+1)}\,\mathrm{sign}\,(z_{i,0}-y_i)+z_{i,1} \\
&\vdots \\
\dot{z}_{i,j} &= \nu_{i,j}, \quad j=\overline{1,r_i-1} \\
\nu_{i,j} &= -\lambda_{i,j}\,|z_{i,j}-\nu_{i,j-1}|^{(r_i-j)/(r_i-j+1)}\,\mathrm{sign}\,(z_{i,j}-\nu_{i,j-1})+z_{i,j+1}, \\
&\vdots \\
\dot{z}_{i,r_i} &= -\lambda_{i,r_i}\,\mathrm{sign}\,(z_{i,r_i}-\nu_{i,r_i-1})
\end{aligned}
\tag{13.4}
$$

where $|y_i^{(r_i+1)}| \le L_i$ ($\forall i=\overline{1,m}$) and the positive design constants $\lambda_{i,j} > \lambda_{i,j+1}$ ($\forall i=\overline{1,m}$ and $\forall j=\overline{0,r_i-1}$) should be selected sufficiently large to provide finite time convergence $z_{i,j-1} \to y_i^{(j-1)}$ ($\forall i=\overline{1,m}$ and $\forall j=\overline{1,r_i+1}$)

Without loss of generality, the nonlinear vector field $\phi(\xi,\eta)$ can be written as

$$
\phi(\xi,\eta) = \mathbf{D}_{11}\,\xi_1 + \mathbf{D}_{12}\,\xi_2 + \mathbf{D}_2\,\eta + \phi_0(\xi_1,\xi_2,\eta), \tag{13.5}
$$

which after being substituted into (13.1) provides a redefined form of the I/O dynamics:

$$
\dot{\xi}_1 = \mathbf{A}_{11}\,\xi_1 + \mathbf{A}_{12}\xi_2 \tag{13.6a}
$$

$$
\dot{\xi}_2 = \mathbf{D}_{11}\,\xi_1 + \mathbf{D}_{12}\,\xi_2 + \mathbf{D}_2\,\eta + \phi_0(\xi_1,\xi_2,\eta) + f(t) + \mathbf{u} \tag{13.6b}
$$

where $\phi_0(\cdot)$ is a known nonlinear vector field. The internal dynamics (13.2) can be rewritten in a form

$$
\dot{\eta} = \mathbf{Q}\,\eta + \mathbf{G}_1\,\xi_1 + \mathbf{G}_2\,\xi_2 \tag{13.7}
$$

where $\mathbf{G}=[\mathbf{G}_1,\mathbf{G}_2]$, $\mathbf{G}_1 \in \mathbb{R}^{p\times(r-m)}$, $\mathbf{G}_2 \in \mathbb{R}^{p\times m}$.

The I/O dynamics (13.6) are now written in a canonical form where the first $(r-m)$ differential equations implicitly represent the geometry of the output state vector in a phase variable format, while the last m equations reflect dynamical properties.

Such an observation imposes the structure on the gain matrices: $\mathbf{A}_{11} \in \mathbb{R}^{(r-m)\times(r-m)}$, $\mathbf{A}_{12} \in \mathbb{R}^{(r-m)\times m}$. Each of them can be presented in a block format:

$$
\mathbf{A}_{11} = \mathrm{diag}\{\mathbf{A}_{11}^1,\mathbf{A}_{11}^2,\ldots,\mathbf{A}_{11}^m\}, \quad \mathbf{A}_{12} = \mathrm{col}\{\mathbf{A}_{12}^1,\mathbf{A}_{12}^2,\ldots,\mathbf{A}_{12}^m\}, \tag{13.8}
$$

where

$$
\mathbf{A}_{11}^i = \begin{bmatrix} 0 & 1 & 0 & \ldots & 0 & 0 \\ 0 & 0 & 1 & \ldots & 0 & 0 \\ \vdots & \vdots & \vdots & \ddots & \vdots & \vdots \\ 0 & 0 & 0 & \ldots & 0 & 1 \\ 0 & 0 & 0 & \ldots & 0 & 0 \end{bmatrix} \in \mathbb{R}^{(r_i-1)\times(r_i-1)}, \quad \mathbf{A}_{12}^j = \begin{bmatrix} 0 & \ldots & 0 & \mathbf{0} & \ldots & 0 & 0 \\ 0 & \ldots & 0 & \mathbf{0} & \ldots & 0 & 0 \\ \vdots & \ddots & \vdots & \vdots & \ddots & \vdots & \vdots \\ 0 & \ldots & 0 & \mathbf{0} & \ldots & 0 & 0 \\ 0 & \ldots & 0 & \mathbf{1} & \ldots & 0 & 0 \end{bmatrix} \in \mathbb{R}^{(r_j-1)\times(r_j-1)}
$$

(j^{th} column)

(13.9)

13.3 Problem Formulation

The problem is to design an output-feedback based control law that provides asymptotic tracking of the *causal* output reference profile $\mathbf{y}_c$ in the nonminimum phase nonlinear system (13.6),(13.7) in the presence of a bounded disturbance $\mathbf{f}(t)$

$$\lim_{t\to\infty} \|\mathbf{y}_c(t) - \mathbf{y}(t)\| = 0 \tag{13.10}$$

where t stands for time.

13.4 Sliding Mode Control Design

Assume that the output reference profiles y_{c_j} $(j = \overline{1,m})$ along with time derivatives up to r_j-order are given in real time. The command $\xi_c = \left[\xi_{c_1}^T, \xi_{c_2}^T\right]^T$ to the full output reference state vector (13.3) can be constructed by analogy to ξ, according to (13.3). Furthermore, the full output state tracking error $\mathbf{e}_\xi$ can be constructed by analogy to (13.3), employing the HOSM differentiator (13.4) [12]:

$$\mathbf{e}_\xi = \{\underbrace{e_{y_1}, \ldots, e_{y_1}^{(r_1-2)}, \ldots, e_{y_m}, \ldots, e_{y_m}^{(r_m-2)}}_{\mathbf{e}_{\xi_1}}, \underbrace{e_{y_1}^{(r_1-1)}, \ldots, e_{y_m}^{(r_m-1)}}_{\mathbf{e}_{\xi_2}}\}^T \tag{13.11}$$

The output tracking problem (13.10) is transformed to

$$\lim_{t\to\infty} \|\xi_c(t) - \xi(t)\| = \lim_{t\to\infty} \|\mathbf{e}_\xi(t)\| = 0 \tag{13.12}$$

This problem cannot be addressed using just the I/O dynamics given by (13.6), since the *causal* internal dynamics given by (13.7) are unstable. Therefore, the output tracking problem (13.12) is reduced to the state tracking problem that comprises (13.12) and

$$\lim_{t\to\infty} \|\eta_c(t) - \eta(t)\| = \lim_{t\to\infty} \|\mathbf{e}_\eta(t)\| = 0 \tag{13.13}$$

where $\eta_c(t)$ is a bounded particular solution of the unstable internal dynamics

$$\dot{\eta}_c = \mathbf{Q}\,\eta_c + \theta \tag{13.14}$$

forced by a causal input $\theta = \mathbf{G}_1\,\xi_{1_c} + \mathbf{G}_2\,\xi_{2_c}$ that is available in current time. Using the *extended method of stable system center* (ESSC), a *bounded* estimate $\hat{\eta}_c$ can be generated online, such that $\hat{\eta}_c$ asymptotically converges to a true bounded solution η_c of (13.14) as time increases, with a prescribed convergence rate.

13.4.1 The Extended Method of Stable System Center

The ESSC method numerically solves the unstable differential equation (13.14) without explicit integration, where $\eta_c \in \mathbb{R}^p$, $\mathbf{Q} \in \mathbb{R}^{p\times p}$ is non-Hurwitz, and $\theta \in \mathbb{R}^p$ is a causal forcing term available for measurement.

The basis for the ESSC method — the method of Stable System Center (SSC) [16], assumes that the unstable differential equation (13.14) is forced by a *causal* (available in current time) term θ, which can be piece-wise modeled by an LTI exogenous system with *known characteristic polynomial*. An extension, that turns the SSC into the **E**SSC, relaxes this assumption, and requires knowing only the order of the above mentioned exogenous system. A corresponding characteristic polynomial is reconstructed online using a HOSM-based parameter observer [1]. This innovation *significantly* improves the causality of the problem. The development of the proposed ESSC method is based on the following Lemma.

Lemma 13.1 (Reconstruction of the Characteristic Polynomial). *Given an LTI system of known order k*

$$\dot{z} = A z, \quad \theta = C z \tag{13.15}$$

where $z \in \mathbb{R}^k$, $\theta \in \mathbb{R}^p$, $k > p$ *so that:*

i. the output θ *available for measurement;*

ii. the unknown matrices $A \in \mathbb{R}^{k\times k}$, $C \in \mathbb{R}^{p\times k}$ *are supposed to satisfy the observability condition:*

$$\operatorname{rank}(M) = k, \quad M = \left[C^T, A^T C^T, \ldots, \left(A^{k-1}\right)^T C^T\right]^T \in \mathbb{R}^{pk\times k}, \tag{13.16}$$

iii. the eigenvalues of the matrix A are located in the left half of the complex plane or on the imaginary axis (non-repeated).

then

a. there exists a constant matrix $\tilde{A}$, *similar to the matrix A, that satisfies an algebraic equation:*

$$\gamma(t) = \tilde{A}\,\psi(t), \tag{13.17}$$

where

$$\psi(t) = D\omega^1(t), \quad \gamma(t) = D\omega^2(t), \quad \omega^1(t) = \left[\theta^T, \dot{\theta}^T, \ldots, \left(\theta^{(k-1)}\right)^T\right]^T \in \mathbb{R}^{pk}, \quad \omega^2 = \dot{\omega}^1, \tag{13.18}$$

and the vectors $\omega^1(t)$, $\omega^2(t)$ *are obtained in real time by differentiating the output* $\theta(t)$ *using HOSM differentiators [12] that are similar to (13.4). The arbitrary, but known constant matrix* $D \in \mathbb{R}^{k\times mk}$ *is assumed to be of full rank, i.e.* $\operatorname{rank}(D) = k$.

b. the entries of the matrix $\tilde{A}$ *can be reconstructed as:*

$$\tilde{A} = \int_{t-k\Delta}^{t} \det(\Psi(\tau))\,\Gamma(\tau)\,\operatorname{adj}(\Psi(\tau))\,d\tau \Big/ \int_{t-k\Delta}^{t} [\det(\Psi(\tau))]^2\,d\tau \tag{13.19}$$

where

$$\Psi(t) = \left[\psi(t_0)\ \psi(t_1)\ \ldots\ \psi(t_{k-1})\right], \qquad \Gamma(t) = \left[\gamma(t_0)\ \gamma(t_1)\ \ldots\ \gamma(t_{k-1})\right], \tag{13.20}$$

with $t_i = t - i\Delta$, and $\Delta > 0$ is a constant time interval.

Proof. The k^{th} order exact HOSM differentiator is applied to the j^{th} component of the output vector $\theta \in \mathbb{R}^p$ of system (13.15)

$$\begin{aligned}
&\dot{\omega}_{0,j} = v_{0,j}, \quad v_{0,j} = -\lambda_0 \left|\omega_{0,j} - \theta_j\right|^{\frac{k}{k+1}} \operatorname{sign}\left(\omega_{0,j} - \theta_j\right) + \omega_{1,j} \\
&\dot{\omega}_{i,j} = v_{i,j}, \quad v_{i,j} = -\lambda_i \left|\omega_{i,j} - v_{i-1,j}\right|^{\frac{k-i}{k-i+1}} \operatorname{sign}\left(\omega_{i,j} - v_{i-1,j}\right) + \dot{\omega}_{i+1,j}, \quad i = \overline{1,k-1} \\
&\dot{\omega}_{k,j} = -\lambda_k \operatorname{sign}\left(\omega_{k,j} - v_{k-1,j}\right)
\end{aligned} \tag{13.21}$$

where the equality $\omega_{i,j} = \theta_j^{(i)}$ holds after finite time convergence, affected by the selection [12] of coefficients λ_i. Combining components $\omega_{i,j}$ gives

$$\left[\omega_{0,1}, \ldots, \omega_{0,m}, \ldots \omega_{k,1}, \ldots, \omega_{k,m}\right]^T = \left[\theta^T, \dot{\theta}^T, \ldots, \left(\theta^{(k)}\right)^T\right]^T \tag{13.22}$$

Introduce two auxiliary vectors:

$$\omega^1 = \left[\omega_{0,1}, \ldots, \omega_{0,p}, \ldots \omega_{k-1,1}, \ldots, \omega_{k-1,p}\right]^T, \quad \omega^2 = \left[\omega_{1,1}, \ldots, \omega_{1,p}, \ldots \omega_{k,1}, \ldots, \omega_{k,p}\right]^T \tag{13.23}$$

which are related as $\omega^2 = \dot{\omega}^1$.

Combining eqs. (13.15), (13.16), and (13.23)

$$\omega^1 = Mz \tag{13.24}$$

Introduce an arbitrary constant matrix $D \in \mathbb{R}^{k \times pk}$ of full rank, i.e. $\operatorname{rank}(D) = k$. Pre-multiplying the left and right hand sides of (13.24) by D yields

$$D\omega^1 = DMz \tag{13.25}$$

Note that $DM \in \mathbb{R}^{k \times k}$ is a square, nonsingular matrix. Therefore, the following expression can be derived from (13.25):

$$z = (DM)^{-1} D\omega^1 \tag{13.26}$$

Differentiating (13.25) and taking into account (13.26) gives

$$D\dot{\omega}^1 = (DM)\dot{z} = (DM)Az = (DM)A(DM)^{-1} D\omega^1. \tag{13.27}$$

Denoting

$$\psi(t) = D\omega^1(t), \quad \gamma(t) = D\omega^2(t) = D\dot{\omega}^1(t) \tag{13.28}$$

and introducing matrix $\tilde{A}$ connected to the A by a similarity transformation $\tilde{A} = (DM)A(DM)^{-1}$, eq. (13.27) is reduced to the form

$$\gamma(t) = \tilde{A}\psi(t) \tag{13.29}$$

and item i) of Lemma 13.1 is proven.

Note that the vectors $\gamma(t)$, and $\psi(t)$ are known online, and eq. (13.29) can be treated as a system of k linear equations in a regressive form with respect to the unknown matrix $\tilde{A}$ that comprises k^2 unknown terms $\tilde{a}_{i,j}$ for $i, j = \overline{1,k}$ which are to be identified. Since there are k^2 unknowns and only k equations, this problem can not be solved uniquely. Since $\gamma(t)$, and $\psi(t)$ are vector functions given in real time (measured or computed), k measurements of these vectors could be performed. Then, each pair of measurements $\gamma(t_i)$, and $\psi(t_i)$, taken at the same time $t = t_i$ are supposed to satisfy eq. (13.29). Therefore, eq. (13.29) can be extended to the following linear matrix equation

$$\Gamma = \tilde{A}\Psi \tag{13.30}$$

where Ψ and Γ are defined by (13.20). A unique solution of system (13.30) can be easily obtained as

$$\tilde{A} = \Gamma\Psi^{-1} = \frac{\Gamma\,\mathrm{adj}(\Psi)}{\det(\Psi)} \tag{13.31}$$

However, if the vectors $\gamma(t)$ and $\psi(t)$ are measured/estimated online with noise, the computation error in (13.31) could be large. In this case, it is beneficial to identify the matrix $\tilde{A}$ using the least square parameter estimation (LSPE) method. The measurement/estimation instants are varied with time, keeping a certain time interval between them, i.e. $t_i = t - i\Delta$, where $\Delta > 0$ is a constant time-interval. The matrix $\tilde{A}$ reconstruction in (13.31) can be averaged, while a norm of the estimation error is minimized

$$\tilde{A} = \int_{t-k\Delta}^{t} \det(\Psi(\tau))\,\Gamma(\tau)\,\mathrm{adj}(\Psi(\tau))\,d\tau \Big/ \int_{t-k\Delta}^{t} [\det(\Psi(\tau))]^2\,d\tau \tag{13.32}$$

and the Lemma is proven. □

Remark 13.3. It is worth noting that if the entire vector z in system (13.15) is measured then the matrix A in eq. (13.15) can be estimated using the sliding mode parameter observer proposed in the work [24]. The algorithm formulated in Lemma 13.1 assumes that only the output vector θ, whose dimension is less than the dimension of the state vector z, is available for measurement. Also, a use of the LSPE method in the proposed algorithm allows minimizing the effect of measurement noise to the matrix $\tilde{A}$ estimation.

Remark 13.4. Once the matrix $\tilde{A}$ estimated, it is straightforward to identify its characteristic polynomial

$$P_k(\lambda) = \lambda^k + p_{k-1}\lambda^{k-1} + \cdots + p_1\lambda + p_0, \tag{13.33}$$

which coincides with the one for A in equation (13.15) due to the similarity of $\tilde{A}$ and A. Eigenvalues of both matrices A and $\tilde{A}$ are considered to be located in the left half of the complex plane or on the imaginary axis (non-repeated).

The remainder of the ESSC method development is computing a bounded particular solution of the unstable differential equation (13.14), is presented in the following Theorem.

Theorem 13.1 (Extended Method of Stable System Center). *Given the unstable differential equation (13.14), driven by a causal signal $\theta(\cdot)$, which is available for measurement, and the following set of conditions:*

i. the matrix $\mathbf{Q}$ in (13.14) is nonsingular;
ii. the internal dynamics forcing term $\theta(\cdot)$ can be piece-wise modeled as the output of a dynamical process given by the unknown LTI system of differential equations (13.15) of known order k

***then**, the estimate $\hat{\eta}_c \in \mathbb{R}^p$ for the internal state command $\eta_c \in \mathbb{R}^p$ can be generated by a matrix differential equation:*

$$\hat{\eta}_c^{(k)} + C_{k-1}\,\hat{\eta}_c^{(k-1)} + \ldots + C_1\,\dot{\hat{\eta}}_c + C_0\,\hat{\eta}_c = -\left(\mathbf{P}_{k-1}\,\theta^{(k-1)} + \ldots + \mathbf{P}_1\,\dot{\theta} + \mathbf{P}_0\,\theta\right) \tag{13.34}$$

where the numbers $C_0, C_1, \ldots, C_{k-1}$ are chosen to provide desired eigenvalue placement of convergence $\hat{\eta}_c \to \eta_c$, and the matrices $\mathbf{P}_{k-1}, \ldots, \mathbf{P}_1, \mathbf{P}_0 \in \mathbb{R}^{p\times p}$ are given by:

$$\begin{aligned}
\mathbf{P}_{k-1} &= \left(\mathbf{I} + C_{k-1}\,\mathbf{Q}^{-1} + \cdots + C_0\,\mathbf{Q}^{-k}\right)\cdot\left(\mathbf{I} + p_{k-1}\,\mathbf{Q}^{-1} + \ldots + p_0\,\mathbf{Q}^{-k}\right)^{-1} - \mathbf{I} \\
\mathbf{P}_{k-2} &= C_{k-2}\,\mathbf{Q}^{-1} + \cdots + C_0\,\mathbf{Q}^{-(k-1)} - (\mathbf{P}_{k-1} + \mathbf{I})\cdot\left(p_{k-2}\,\mathbf{Q}^{-1} + \ldots + p_0\,\mathbf{Q}^{-(k-1)}\right) \\
&\vdots \\
\mathbf{P}_1 &= C_1\,\mathbf{Q}^{-1} + C_0\,\mathbf{Q}^{-2} - (\mathbf{P}_{k-1} + \mathbf{I})\cdot(p_1\,\mathbf{Q}^{-1} + p_0\,\mathbf{Q}^{-2}) \\
\mathbf{P}_0 &= C_0\,\mathbf{Q}^{-1} - (\mathbf{P}_{k-1} + \mathbf{I})\,p_0\,\mathbf{Q}^{-1}
\end{aligned} \tag{13.35}$$

where the coefficients $p_0, p_1, \ldots, p_{k-1}$ of the characteristic polynomial (13.33) are reconstructed based on Lemma 13.1.

Proof. Construct an auxiliary system

$$\dot{\hat{\eta}}_c = \mathbf{Q}\,\hat{\eta}_c + \theta(\cdot) + g(t) \tag{13.36}$$

where $\hat{\eta}_c \in \mathbb{R}^p$; $\mathbf{Q} \in \mathbb{R}^{p\times p}$ is non-Hurwitz; $\theta(\cdot) \in \mathbb{R}^p$ is a causal forcing term described by the *unknown* LTI system of differential equations (13.15). Assume conditions i. and ii. of Lemma 13.1 are satisfied and the coefficients $p_0, p_1, \ldots, p_{k-1}$ of the characteristic polynomial (13.33) of system (13.15) can be computed online.

The vector $g(t) \in \mathbb{R}^p$ is constrained by

$$\hat{\eta}_c^{(k)} + p_{k-1}\,\hat{\eta}_c^{(k-1)} + \cdots + p_1\,\dot{\hat{\eta}}_c + p_0\,\hat{\eta}_c = \mathbf{F}_{k-1}\,g(t)^{(k-1)} + \cdots + \mathbf{F}_1\,\dot{g}(t) + \mathbf{F}_0\,g(t), \tag{13.37}$$

where the numbers $p_0, p_1, \ldots, p_{k-1}$ are the coefficients of the characteristic polynomial (13.33), and the matrices $\mathbf{F}_{k-1}, \ldots, \mathbf{F}_1, \mathbf{F}_0 \in \mathbb{R}^{p\times p}$ are to be selected.

It is possible to uncouple (13.36) and (13.37) with respect to $g(t)$ as

$$(\mathbf{I} - \mathbf{F}_{k-1})\,g(t)^{(k)} + (p_{k-1}\mathbf{I} + \mathbf{Q}\mathbf{F}_{k-1} - \mathbf{F}_{k-2})\,g(t)^{(k-1)} + \cdots + (p_1\mathbf{I} + \mathbf{Q}\mathbf{F}_1 - \mathbf{F}_0)\,\dot{g}(t) + (p_0\mathbf{I} + \mathbf{Q}\mathbf{F}_0)\,g(t) = -\left(\theta^{(k)} + p_{k-1}\,\theta^{(k-1)} + \cdots + p_1\,\dot{\theta} + p_0\,\theta\right) \tag{13.38}$$

and

$$(\mathbf{I} - \mathbf{F}_{k-1})\,\hat{\eta}_c^{(k)} + (p_{k-1}\mathbf{I} + \mathbf{F}_{k-1}\mathbf{Q} - \mathbf{F}_{k-2})\,\hat{\eta}_c^{(k-1)} + \cdots + (p_1\mathbf{I} + \mathbf{F}_1\mathbf{Q} - \mathbf{F}_0)\,\dot{\hat{\eta}}_c + (p_0\mathbf{I} + \mathbf{F}_0\mathbf{Q})\,\hat{\eta}_c = -\left(\mathbf{F}_{k-1}\,\theta^{(k-1)} + \cdots + \mathbf{F}_1\,\dot{\theta} + \mathbf{F}_0\,\theta\right). \tag{13.39}$$

Since the term θ can be piece-wise modeled by an unknown linear exosystem (13.15) of known order k with characteristic polynomial (13.33), and the polynomial coefficients can be identified online, then

$$\theta^{(k)} + p_{k-1}\,\theta^{(k-1)} + \cdots + p_1\,\dot{\theta} + p_0\,\theta \equiv 0$$

almost everywhere. The matrices $\mathbf{F}_0, \mathbf{F}_1, \ldots, \mathbf{F}_{k-1}$ are selected to ensure $g \to 0$ asymptotically by enforcing the following equality:

$$g(t)^{(k)} + (\mathbf{I} - \mathbf{F}_{k-1})^{-1}(p_{k-1}\mathbf{I} + \mathbf{Q}\mathbf{F}_{k-1} - \mathbf{F}_{k-2})\,g(t)^{(k-1)} + \cdots + (\mathbf{I} - \mathbf{F}_{k-1})^{-1}(p_1\mathbf{I} + \mathbf{F}_1\mathbf{Q} - \mathbf{F}_0)\,\dot{g}(t) + (\mathbf{I} - \mathbf{F}_{k-1})^{-1}(p_0\mathbf{I} + \mathbf{F}_0\mathbf{Q})\,g(t) = g(t)^k + C_{k-1}\,g(t)^{(k-1)} + \cdots + C_1\,\dot{g}(t) + C_0\,g(t) \tag{13.40}$$

where the coefficients $C_0, C_1, \ldots, C_{k-1}$ are selected to provide given eigenvalue placement of the $g(t) \to 0$ convergence.

The matrices $\mathbf{F}_{k-1}, \ldots, \mathbf{F}_1, \mathbf{F}_0$ are calculated by equating similar terms in the left and right hand sides of (13.40). Specifically

$$\begin{aligned}
\mathbf{F}_0 &= [\mathbf{I} - \mathbf{F}_{k-1}]\,\left(C_0\,\mathbf{Q}^{-1}\right) - \left(p_0\,\mathbf{Q}^{-1}\right)\\
\mathbf{F}_1 &= [\mathbf{I} - \mathbf{F}_{k-1}]\,\left(C_1\,\mathbf{Q}^{-1} + C_0\,\mathbf{Q}^{-2}\right) - \left(p_1\,\mathbf{Q}^{-1} + p_0\,\mathbf{Q}^{-2}\right)\\
&\vdots\\
\mathbf{F}_{k-1} &= [\mathbf{I} - \mathbf{F}_{k-1}]\,\left(C_{k-1}\,\mathbf{Q}^{-1} + \cdots + C_0\,\mathbf{Q}^{-(k-1)}\right) - \left(p_{k-1}\,\mathbf{Q}^{-1} + \cdots + p_0\,\mathbf{Q}^{-(k-1)}\right)
\end{aligned} \tag{13.41}$$

from where

$$\mathbf{F}_{k-1} = \mathbf{I} - \left(\mathbf{I} + p_{k-1}\mathbf{Q}^{-1} + \cdots + p_0\mathbf{Q}^{-k}\right) \cdot \left(\mathbf{I} + C_{k-1}\mathbf{Q}^{-1} + \ldots + C_0\mathbf{Q}^{-k}\right)^{-1} \tag{13.42}$$

Substituting (13.41) and (13.42) into (13.39) gives (13.34) and (13.35). Since $g(t) \to 0$ asymptotically with a given convergence rate, then

$$\dot{\hat{\eta}}_c = \mathbf{Q}\,\hat{\eta}_c + \theta(\cdot) + g(t) \quad \therefore \quad \dot{\eta}_c = \mathbf{Q}\,\eta_c + \theta(\cdot) \tag{13.43}$$

and $\hat{\eta}_c \to \eta_c$ as time increases and the theorem is proven. □

Remark 13.5. The ESSC method consists of two successive procedures:

1. the identification of the coefficients $p_0, p_1, \ldots, p_{k-1}$ of the characteristic polynomial (13.33);
2. the use of the SSC method to design the linear filter (13.34) that generates $\hat{\eta}_c(t)$ on the basis of $\theta(t)$ being available in current time.

13.4.2 Sliding Variable and Sliding Mode Control

The following tracking error dynamics are identified:

$$\begin{aligned}
\dot{\mathbf{e}}_{\xi_1} &= \dot{\xi}_{c_1} - \dot{\xi}_1 = \mathbf{A}_{11}\,\mathbf{e}_{\xi_1} + \mathbf{A}_{12}\,\mathbf{e}_{\xi_2} + \left(\dot{\xi}_{c_1} - \mathbf{A}_{11}\,\xi_{c_1} + \mathbf{A}_{12}\,\xi_{c_2}\right) \\
\dot{\mathbf{e}}_{\xi_2} &= \dot{\xi}_{c_2} - \dot{\xi}_2 = \mathbf{D}_{11}\,\mathbf{e}_{\xi_1} + \mathbf{D}_{12}\,\mathbf{e}_{\xi_2} + \mathbf{D}_2\,\mathbf{e}_\eta - \phi_0(\xi_1, \xi_2, \eta) - \mathbf{f}(t) - \mathbf{u} + \left(\dot{\xi}_{2_c} - \mathbf{D}_2\,\eta_c - \mathbf{D}_{11}\,\xi_{c_1} - \mathbf{D}_{12}\,\xi_{c_2}\right) \\
\dot{\mathbf{e}}_\eta &= \dot{\eta}_c - \dot{\eta} = \mathbf{Q}\,\mathbf{e}_\eta + \mathbf{G}_1\,\mathbf{e}_{\xi_1} + \mathbf{G}_2\,\mathbf{e}_{\xi_2} + (\dot{\eta}_c - \mathbf{Q}\,\eta_c - \mathbf{G}_1\,\xi_{c_1} - \mathbf{G}_2\,\xi_{c_2})
\end{aligned} \tag{13.44}$$

It is worth noting that $\dot{\xi}_{c_1} - \mathbf{A}_{11}\,\xi_{c_1} + \mathbf{A}_{12}\,\xi_{c_2} \equiv 0$ and $\dot{\eta}_c - \mathbf{Q}\,\eta_c - \mathbf{G}_1\,\xi_{c_1} - \mathbf{G}_2\,\xi_{c_2} \to 0$ as time increases. Therefore, the asymptotic dynamics for the system (13.44) can be presented as

$$\begin{aligned}
\dot{\mathbf{e}}_{\xi_1} &= \mathbf{A}_{11}\,\mathbf{e}_{\xi_1} + \mathbf{A}_{12}\,\mathbf{e}_{\xi_2} \\
\dot{\mathbf{e}}_{\xi_2} &= \mathbf{D}_{11}\,\mathbf{e}_{\xi_1} + \mathbf{D}_{12}\,\mathbf{e}_{\xi_2} + \mathbf{D}_2\,\mathbf{e}_\eta - \phi_0(\xi_1, \xi_2, \eta) - \mathbf{f}(t) - \mathbf{u} + \left(\dot{\xi}_{2_c} - \mathbf{D}_2\,\eta_c - \mathbf{D}_{11}\,\xi_{c_1} - \mathbf{D}_{12}\,\xi_{c_2}\right) \\
\dot{\mathbf{e}}_\eta &= \mathbf{Q}\,\mathbf{e}_\eta + \mathbf{G}_1\,\mathbf{e}_{\xi_1} + \mathbf{G}_2\,\mathbf{e}_{\xi_2}
\end{aligned} \tag{13.45}$$

Introduce a vector *sliding variable*

$$\sigma \triangleq \mathbf{S}\,\mathbf{e}_{\xi_1} + \mathbf{e}_{\xi_2} + \mathbf{T}\,\mathbf{e}_\eta, \tag{13.46}$$

where $\mathbf{S} \in \mathbb{R}^{m\times(r-m)}$ and $\mathbf{T} \in \mathbb{R}^{m\times p}$ are design matrices (see Theorem 13.2 for details). The internal variable η is assumed to be available at this moment (it is estimated via the asymptotic observer that is presented in Section 13.5).

The sliding variable dynamics are identified as follows:

$$\dot{\sigma} = \Psi_0 - \mathbf{f}(t) - \mathbf{u} \tag{13.47}$$

where

$$\Psi_0 \triangleq (\mathbf{SA}_{11}+\mathbf{D}_{11}+\mathbf{TG}_1)\,\mathbf{e}_{\xi_1}+(\mathbf{SA}_{12}+\mathbf{D}_{12}+\mathbf{TG}_2)\,\mathbf{e}_{\xi_2}+(\mathbf{D}_2+\mathbf{TQ})\,\mathbf{e}_\eta- \phi_0(\xi_1,\xi_2,\eta)+\left(\dot{\xi}_{2_c}-\mathbf{D}_2\,\eta_c-\mathbf{D}_{11}\,\xi_{c_1}-\mathbf{D}_{12}\,\xi_{c_2}\right) \tag{13.48}$$

is the *known* part of the σ-dynamics that can be compensated algebraically in the control law. The following sliding mode control law [22, 7]

$$\begin{aligned}&\mathbf{u}=\mathbf{u}_1+\mathbf{u}_2\\&\mathbf{u}_1=\Psi_0,\quad \mathbf{u}_2=\rho\,\frac{\sigma}{\|\sigma\|},\quad \|\mathbf{f}(t)\|<\rho\end{aligned} \tag{13.49}$$

drives $\sigma \to 0$ in finite time.

13.4.3 The Nonminimum Phase System Output Tracking Error Dynamics in the Sliding Mode

The dynamics of system (13.6),(13.7) in the sliding mode ($\sigma = 0$) are given by the following Theorem

Theorem 13.2. *Given the system described by (13.6),(13.7), and the control designed according to (13.49),* ***then*** *the tracking errors* $\mathbf{e}_\xi$ *and* $\mathbf{e}_\eta$ *will approach zero as time increases, in accordance with the linear differential equation*

$$\begin{bmatrix}\dot{\mathbf{e}}_{\xi_1}\\ \dot{\mathbf{e}}_\eta\end{bmatrix}=\left[\begin{array}{c|c}\mathbf{A}_{11}-\mathbf{A}_{12}\mathbf{S} & -\mathbf{A}_{12}\mathbf{T}\\ \hline \mathbf{G}_1-\mathbf{G}_2\mathbf{S} & \mathbf{Q}-\mathbf{G}_2\mathbf{T}\end{array}\right]\begin{bmatrix}\mathbf{e}_{\xi_1}\\ \mathbf{e}_\eta\end{bmatrix} \tag{13.50}$$
$$\mathbf{e}_{\xi_2}=-\mathbf{T}\mathbf{e}_\eta-\mathbf{S}\mathbf{e}_{\xi_1}$$

where $\mathbf{e}_\xi=\left[\mathbf{e}_{\xi_1}^T,\mathbf{e}_{\xi_2}^T\right]^T$ *and the design matrices* $\mathbf{S}$ *and* $\mathbf{T}$*, introduced in (13.46), are chosen to provide a desirable convergence rate (eigenvalues placement) to the compensated error dynamics (13.50).*

Proof. The sliding mode has been established by the control law in (13.49) in a finite time

$$\sigma \triangleq \mathbf{S}\mathbf{e}_{\xi_1}+\mathbf{e}_{\xi_2}+\mathbf{T}\mathbf{e}_\eta=0 \quad \therefore \quad \mathbf{e}_{\xi_2}=-\mathbf{S}\mathbf{e}_{\xi_1}-\mathbf{T}\mathbf{e}_\eta \tag{13.51}$$

Substitution of $\mathbf{e}_{\xi_2}$ into the first and third equations of system (13.45) and replacement of the second equation in (13.45) by (13.51) yields equation (13.50). Next, the design matrices $\mathbf{S}$ and $\mathbf{T}$, introduced in (13.46), are to be selected to provide given eigenvalues placement of the system matrix of the compensated error dynamics (13.50)

$$\bar{A} = \left[\begin{array}{c|c} \mathbf{A}_{11} - \mathbf{A}_{12}\mathbf{S} & -\mathbf{A}_{12}\mathbf{T} \\ \hline \mathbf{G}_1 - \mathbf{G}_2\mathbf{S} & \mathbf{Q} - \mathbf{G}_2\mathbf{T} \end{array}\right] \tag{13.52}$$

and the theorem is proven. □

13.5 Observer for the Unstable Internal Dynamics

The control law (13.46), (13.49) has been designed under the temporary assumption of known internal dynamics η, which are not available according to the problem formulation. The design of a feedback-oriented observer for the nonminimum phase system (13.6),(13.7) is studied in this section.

The proposed implementation employs basic ideas of *Luenberger* observers along with the *extended method of stable system center* (see Section 13.4.1). The complete solution allows asymptotic identification of the unstable internal state η and the unknown bounded input $\mathbf{f}(t)$ based on the measurement of the output states ξ.

First, a traditional Luenberger observer for system (13.6),(13.7) is designed. The estimation errors do not converge to zero due to disturbance $\mathbf{f}(t)$. The *computable*, but non-vanishing output state estimation errors $\hat{\mathbf{e}}_{\xi_1} = \xi_1 - \hat{\xi}_1$ and $\hat{\mathbf{e}}_{\xi_2} = \xi_2 - \hat{\xi}_2$ drive the *non-computable* internal state estimation error $\hat{\mathbf{e}}_\eta = \eta - \hat{\eta}$ that has to be estimated in order to recover the internal state η.

Second, the ESSC method is employed to reconstruct the internal state estimation error $\hat{\mathbf{e}}_\eta$, which is used for recovering the internal state η as $\hat{\mathbf{e}}_\eta + \hat{\eta}$.

13.5.1 Luenberger Observer Design

Consider the dynamics of the Luenberger observer

$$\begin{aligned}
\dot{\hat{\xi}}_1 &= \mathbf{A}_{11}\hat{\xi}_1 + \mathbf{A}_{12}\hat{\xi}_2 + \mathbf{L}_{11}\hat{\mathbf{e}}_{\xi_1} + \mathbf{L}_{12}\hat{\mathbf{e}}_{\xi_2} \\
\dot{\hat{\xi}}_2 &= \mathbf{D}_{11}\hat{\xi}_1 + \mathbf{D}_{12}\hat{\xi}_2 + \mathbf{D}_2\hat{\eta} + \phi_0(\xi_1, \xi_2, \hat{\eta}) + \mathbf{u} + \mathbf{L}_{21}\hat{\mathbf{e}}_{\xi_1} + \mathbf{L}_{22}\hat{\mathbf{e}}_{\xi_2} \\
\dot{\hat{\eta}} &= \mathbf{Q}\hat{\eta} + \mathbf{G}_1\hat{\xi}_1 + \mathbf{G}_2\hat{\xi}_2 + \mathbf{L}_{31}\hat{\mathbf{e}}_{\xi_1} + \mathbf{L}_{32}\hat{\mathbf{e}}_{\xi_2}
\end{aligned} \tag{13.53}$$

where $\mathbf{L}_{i,j}$ are the observer design matrices of appropriate dimension.

Consider the error dynamics of the Luenberger observer (13.53):

$$\begin{bmatrix} \dot{\hat{\mathbf{e}}}_{\xi_1} \\ \dot{\hat{\mathbf{e}}}_{\xi_2} \\ \dot{\hat{\mathbf{e}}}_\eta \end{bmatrix} = \begin{bmatrix} \mathbf{A}_{11} - \mathbf{L}_{11} & \mathbf{A}_{12} - \mathbf{L}_{12} & 0 \\ \mathbf{D}_{11} - \mathbf{L}_{21} & \mathbf{D}_{12} - \mathbf{L}_{22} & \mathbf{D}_2 \\ \mathbf{G}_1 - \mathbf{L}_{31} & \mathbf{G}_2 - \mathbf{L}_{32} & \mathbf{Q} \end{bmatrix} \begin{bmatrix} \hat{\mathbf{e}}_{\xi_1} \\ \hat{\mathbf{e}}_{\xi_2} \\ \hat{\mathbf{e}}_\eta \end{bmatrix} + \begin{bmatrix} 0 \\ \mathbf{f}(t) + \left[\phi_0(\xi_1, \xi_2, \eta) - \phi_0(\hat{\xi}_1, \hat{\xi}_2, \hat{\eta})\right] \\ 0 \end{bmatrix} \tag{13.54}$$

The design matrices $\mathbf{L}_{i,j}$ are to be selected to provide a desirable rate of asymptotic convergence for the *homogenous* component of the observation errors.

13.5.2 Reconstruction of the Internal State

Only the *homogenous* component of estimation errors $\hat{\mathbf{e}}_{\xi_1}$, $\hat{\mathbf{e}}_{\xi_2}$, and $\hat{\mathbf{e}}_{\eta}$ converge to the origin from proper selection of the observer matrices $\mathbf{L}_{i,j}$. However, the unknown term $\mathbf{f}(t)$ directly excites the I/O dynamics (13.6) and makes the estimation errors obey some forced trajectory.

The last equation in (13.54) can be rewritten as

$$\dot{\hat{\mathbf{e}}}_{\eta} = \mathbf{Q}\hat{\mathbf{e}}_{\eta} + \hat{\theta}(\cdot) \tag{13.55}$$

where $\hat{\theta}(\cdot) = (\mathbf{G}_1 - \mathbf{L}_{31})\,\hat{\mathbf{e}}_{\xi_1} + (\mathbf{G}_2 - \mathbf{L}_{32})\,\hat{\mathbf{e}}_{\xi_2}$ which falls into the format of equation (13.14). Therefore, the ESSC method (see Section 13.4.1) can be used to estimate a bounded particular solution of the unstable differential equation (13.55). The estimated solution $\bar{\mathbf{e}}_{\eta}$ asymptotically converges to the internal state estimation error $\hat{\mathbf{e}}_{\eta}$ as time increases, i.e.

$$\lim_{t\to\infty} \|\bar{\mathbf{e}}_{\eta}(t) - \hat{\mathbf{e}}_{\eta}(t)\| = 0, \tag{13.56}$$

with a given convergence rate.

Finally, due to the equality $\eta = \hat{\mathbf{e}}_{\eta} + \hat{\eta}$, a *true estimate* $\bar{\eta}$ of the internal state η can be derived as

$$\bar{\eta} = \bar{\mathbf{e}}_{\eta} + \hat{\eta}, \quad \lim_{t\to\infty} \|\bar{\eta}(t) - \eta(t)\| = 0, \tag{13.57}$$

with t being the time variable.

13.5.3 Reconstruction of the External Disturbance

Disturbance reconstruction is considered in many works, see for instance [23, 8]. In this paper the external disturbance $\mathbf{f}(t)$ is asymptotically reconstructed using the second equation in (13.54)

$$\hat{\mathbf{f}}(t) = \dot{\hat{\mathbf{e}}}_{\xi_2} - (\mathbf{D}_{11} - \mathbf{L}_{21})\,\hat{\mathbf{e}}_{\xi_1} - (\mathbf{D}_{12} - \mathbf{L}_{22})\,\hat{\mathbf{e}}_{\xi_2} - \mathbf{D}_2\,\bar{\mathbf{e}}_{\eta} - \left[\phi_0(\xi_1, \xi_2, \eta) - \phi_0(\hat{\xi}_1, \hat{\xi}_2, \hat{\eta})\right] \tag{13.58}$$

where $\dot{\hat{\mathbf{e}}}_{\xi_2}$ is exactly reconstructed in finite time by differentiating $\hat{\mathbf{e}}_{\xi_2}$ using the HOSM differentiator (13.4), with entry-wise substitution of $\hat{\mathbf{e}}_{\xi_2}$ instead of $\mathbf{y}$. The last term in (13.58) converges to zero asymptotically since $\hat{\eta} \to \eta$, $\hat{\xi}_1 \to \xi_1$ and $\hat{\xi}_2 \to \xi_2$ as time increases.

Note that $\lim_{t\to\infty} \|\hat{\mathbf{f}}(t) - \mathbf{f}(t)\| = 0$, since the observation error $\hat{\mathbf{e}}_{\eta}$ can only be estimated asymptotically.

13.6 Case Study 1: Output Voltage Tracking in Nonminimum Phase DC/DC Electric Power Converter

Switched power DC/DC converters are used in a big variety of real life applications [22, 7, 20], including generation of a set of DC voltages from one DC power

supply [17, 25]. Not only a constant DC voltage, but also given in real time *commanded voltage profile* of the preserved polarity, can be generated using mentioned power converters [17, 25, 19]. In the case of *boost* DC/DC converter, the *nonminimum phase* nature of the problem requires special attention: *direct* regulating of the output voltage results in unstable growing of the phase current and finally causes damage of the converter.

The proposed solution is based on the ESSC method and HOSM control/observation algorithms [12]. Not only it maintains boundedness of the unstable internal state while tracking desired voltage profile, but also estimates uncertainty in the internal impedance of the voltage source and load resistance.

13.6.1 Model of the Boost DC/DC Converter

A boost DC/DC electric power converter (Fig. 13.1) can be modeled according to the following system of nonlinear differential equations:

$$\begin{cases} L\dfrac{di}{d\tau} = -ir + E - V_0 u \\ C\dfrac{dV_0}{d\tau} = -\dfrac{1}{R}V_0 + iu \end{cases} \tag{13.59}$$

where $u \in [0,1]$ is the control input; i is the inductor current (available for measurement); V_0 is the output voltage (available for measurement); L is a known input inductance; r is an impedance of the DC voltage source; C is a known output capacitance; R is an equivalent load resistance; τ is real time.

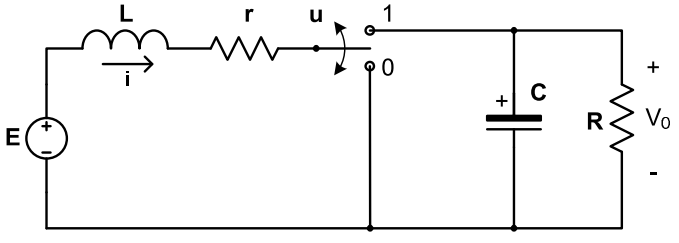

Fig. 13.1 Boost DC/DC converter circuit

Model (13.59) is presented in *natural* coordinates, where the input current and the output voltage are the model states. This particular presentation of the plant model does not make its nonminimum phase nature to show up. More convenient presentation of the converter dynamics, from the control law design standpoint, is to be used. Introduce a normalization of the model parameters along with the new state vector, which allows writing the model (13.59) in the *normal canonical form* [11]:

$$\frac{dy}{dt} = \dot{y} = -\frac{2}{\gamma_R} y + \sqrt{y(\eta - y)} + v\sqrt{y(\eta - y)} \tag{13.60a}$$

$$\frac{d\eta}{dt} = \dot{\eta} = -2\gamma_r(\eta - y) + 2\sqrt{\eta - y} - \frac{2}{\gamma_R} y \tag{13.60b}$$

where

$y = \frac{1}{E^2} V_0^2$ is the *output* state;

$\eta = \frac{1}{E^2} V_0^2 + \frac{L}{CE^2} i^2$ is the *internal* state;

$v \in [-1, 1]$ is the "new" control, defined as $v = 2u - 1$;

$\gamma_r = r\sqrt{C/L}$ is the source quality factor;

$\gamma_R = R\sqrt{C/L}$ is the load factor;

$t = \frac{\tau}{\sqrt{LC}}$ is the "new" (scaled) model time.

System (13.60) is presented in a form of *input/output dynamics* (13.60a), and *internal (forced zero) dynamics* (13.60b). Due to instability of the latter, the system is of *nonminimum phase*.

The internal dynamics (13.60b) appear to be presented as highly nonlinear differential equation which does not allow to apply the proposed methodology (ESSC method). The linearization of the latter in a small vicinity of some *operating point* $\{y_0, \eta_0\}^T$ is proposed to overcome such an issue. The idea is to present the nonlinear dynamics (13.60b) in the linearized form

$$\dot{\eta} = Q\eta + Ky + S, \tag{13.61}$$

where *piece-wise constant* coefficients $Q > 0$, K, and S are functions of γ_r, γ_R, y_0, η_0 and are assumed to be known.

Consider a small vicinity of the operating point, where the linearized form (13.61) is valid (fairly presents nonlinear internal dynamics). The pair (y_0, η_0) is supposed to be a solution of the right-hand-side of (13.60b)

$$\eta_0 = y_0 + \left(\frac{1}{2\gamma_r} - \sqrt{\frac{1}{4\gamma_r^2} - \frac{y_0}{\gamma_r \gamma_R}} \right)^2 \tag{13.62}$$

which is real, only if the *solvability condition* holds

$$\frac{1}{4\gamma_r^2} - \frac{y_0}{\gamma_r \gamma_R} \geq 0 \quad \therefore \quad y_0 \leq \frac{R}{4r} \tag{13.63}$$

The coefficients of the linearized internal dynamics, given by (13.61), can now be evaluated as follows

$$Q = -2\gamma_r + \frac{1}{\sqrt{\eta_0 - y_0}} > 0, \quad S = \sqrt{\eta_0 - y_0}, \quad K = 2\gamma_r - \frac{2}{\gamma_R} - \frac{1}{\sqrt{\eta_0 - y_0}}. \tag{13.64}$$

Remark 13.6. An uncertainty of the generally unknown parameters γ_r and γ_R may become a reason of significant reduction of the linearization quality since they directly effect coefficients Q and K. This issue can be addressed by employing a sliding mode parameter observer (SMPO), presented in Section 13.6.5, which allows asymptotic reconstruction of γ_r and γ_R.

13.6.2 The Problem Formulation

The problem is in designing of a control law $v(t)$, which will provide *causal output tracking* of a *causal* commanded (reference) output profile $y_c(t)$:

$$\lim_{t\to\infty} \|y(t) - y_c(t)\| = 0 \tag{13.65}$$

in the presence of bounded uncertainties of converter parameters γ_r and γ_R, whose nominal values γ_{r_0} and γ_{R_0} are assumed to be known.

Remark 13.7. Output reference profile $y_c(t)$ is assumed to be generated by unknown linear exogenous system of given order. Its characteristic polynomial is identified online and then is used in the control law design.

13.6.3 Sliding Mode Controller Design

The originally introduced problem of direct output voltage tracking is reduced to the conventional state tracking. In other words, *given* reference profile y_c is used twice: as a desirable trajectory for the output state y, and as an input of the ESSC filter which generates a *bounded* reference profile η_c for the unstable internal state η (see Section 13.6.4 for details on ESSC filter design).

Assume that profile η_c, satisfying the linear differential equation (13.61), is *known*. A sliding mode control law, forcing the asymptotic state tracking

$$\lim_{t\to\infty} \|y(t) - y_c(t)\| = 0, \qquad \lim_{t\to\infty} \|\eta(t) - \eta_c(t)\| = 0 \tag{13.66}$$

can now be designed. First of all, the two state tracking errors are introduced

$$e_y = y_c - y, \qquad e_\eta = \eta_c - \eta, \tag{13.67}$$

and their dynamics are identified along the system trajectory

$$\dot{e}_y = \dot{y}_c + \frac{2}{\gamma_R} y - \sqrt{y(\eta - y)} - v\sqrt{y(\eta - y)}, \qquad \dot{e}_\eta = Q e_\eta + K e_y. \tag{13.68}$$

Introduce a sliding variable $\sigma = e_y + T e_\eta$, where the design constant $T \in \mathbb{R}$ is to be selected to provide a desirable rate of compensated error stabilization in the sliding mode.

The σ-dynamics are identified as

$$\dot{\sigma} = \psi - b\,v, \qquad \psi = \dot{y}_c + \frac{2}{\gamma_R}\,y - \sqrt{y(\eta - y)} + T\,Q\,e_\eta + T\,K\,e_y, \qquad b = \sqrt{y(\eta - y)}. \tag{13.69}$$

The traditional sliding mode control law [22, 7]

$$v = \text{sign}(\sigma) \tag{13.70}$$

stabilizes σ at the origin in a finite time. In the sliding mode ($\sigma = 0$), the following dynamics of a reduced order describes the motion of the system

$$\dot{e}_\eta = Q\,e_\eta + K\,e_y, \qquad e_y = -T\,e_\eta. \tag{13.71}$$

The design constant T can now be selected to provide a *desirable* eigenvalue placement of $(Q - KT)$, which is responsible for the compensated error stabilization rate.

Remark 13.8. Finite time stabilization of the sliding variable σ guarantees, that the tracking errors (especially e_η whose dynamics are purely unstable due to $Q > 0$) will not diverge tremendously during the reaching phase. Instead, they will take some bounded values — starting point for asymptotic convergence to the origin with the selected eigenvalue $(Q - KT)$.

13.6.4 Generation of a Bounded Profile η_c

It was assumed for the purpose of the controller design, that bounded profile η_c satisfies the *unstable* differential equation (13.61), therefore, the generation process is equivalent to the finding of a bounded particular solution of

$$\dot{\eta}_c = Q\,\eta_c + K\,y_c + S, \tag{13.72}$$

The instability of (13.72) does not allow direct numerical integration. Instead, the extended method of stable system center (ESSC) is to be employed to estimate/generate η_c. The method is covered in details in Section 13.4.1.

13.6.5 Sliding Mode Parameter Observer

The sliding mode parameter obserever is used to estimate values of uncertain parameters γ_r and γ_R. Such values are then used for evaluation of the linearized internal dynamics' coefficients Q and K as (13.64) in (13.61). The "hat" notation is *introduced* here to differentiate the *estimates* and the *real* (existing) values, e.g. $\hat{\gamma}_r$ stands for the estimate of γ_r. That "hat"-noted estimations are to be used in (13.64) and thereafter instead of γ_r and γ_R respectively, making all following derivations dependant on the output of SMPO.

Consider the original nonlinear dynamics of the converter given in (13.60), where *uncertain* parameters γ_r and γ_R are assumed to be piece-wise constants with *known* nominal values γ_{r_0} and γ_{R_0} respectively.

Introduce a sliding mode observer dynamics:

$$\begin{cases} \dot{\hat{y}} = -\frac{2}{\gamma_{R_0}}\hat{y} + \sqrt{y(\eta - y)} + \nu\sqrt{y(\eta - y)} + \mu_1 \\ \dot{\hat{\eta}} = -2\gamma_{r_0}(\hat{\eta} - \hat{y}) + 2\sqrt{\eta - y} - \frac{2}{\gamma_{R_0}}\hat{y} + \mu_2 \end{cases} \tag{13.73}$$

where $\hat{y}$, $\hat{\eta}$ are the observer states, and $\mu = \{\mu_1, \mu_2\}^T$ is a vector injection term *to be designed*. Introduce an observation error:

$$\hat{\mathbf{e}} = \{\hat{e}_y, \hat{e}_\eta\}^T, \quad \hat{e}_y = y - \hat{y}, \quad \hat{e}_\eta = \eta - \hat{\eta} \tag{13.74}$$

which dynamics are identified as follows

$$\dot{\hat{\mathbf{e}}} = \begin{bmatrix} \hat{y} & 0 \\ \hat{y} & \hat{\eta} - \hat{y} \end{bmatrix} \begin{bmatrix} 2/\gamma_{R_0} \\ 2\gamma_{r_0} \end{bmatrix} - \begin{bmatrix} y & 0 \\ y & \eta - y \end{bmatrix} \begin{bmatrix} 2/\gamma_R \\ 2\gamma_r \end{bmatrix} - \mu \tag{13.75}$$

The injection term μ is proposed to be designed according to *unit vector control* (UVC) approach [22, 7]:

$$\mu = \rho \frac{\hat{\mathbf{e}}}{\|\hat{\mathbf{e}}\|} \tag{13.76}$$

where design constant $\rho > 0$ should be selected big enough to provide a finite time stabilization of the observation error $\mathbf{e}$.

In the sliding mode ($\mathbf{e} = \mathbf{0}$), which is established by injection (13.76) in finite time, the following equality holds:

$$\begin{bmatrix} \hat{y} & 0 \\ \hat{y} & \hat{\eta} - \hat{y} \end{bmatrix} \begin{bmatrix} 2/\gamma_{R_0} - 2/\gamma_R \\ 2\gamma_{r_0} - 2\gamma_r \end{bmatrix} = \mu_{eq} \tag{13.77}$$

where μ_{eq} is the *equivalent* injection that can be asymptotically reconstructed by entry-wise low-pass filtering (LPF) of the discontinuous vector term μ:

$$\hat{\mu}_{eq_j} = \mathrm{LPF}(\mu_j), \quad j = 1, 2 \tag{13.78}$$

Finally, estimates $\hat{\gamma}_r$ and $\hat{\gamma}_R$ can be reconstructed from the solution of linear system (13.77):

$$\hat{\gamma}_R = \left(\frac{1}{\gamma_{R_0}} - \frac{z_1}{2}\right)^{-1}, \qquad \hat{\gamma}_r = \gamma_{r_0} - \frac{z_2}{2}, \qquad \begin{bmatrix} z_1 \\ z_2 \end{bmatrix} = \begin{bmatrix} \hat{y} & 0 \\ \hat{y} & \hat{\eta} - \hat{y} \end{bmatrix}^{-1} \hat{\mu}_{eq}. \tag{13.79}$$

13.6.6 Numerical Simulations

Boost converter model in the normal canonical form (13.60) has been used for simulation purposes. Reference profile y_c is assumed to be constructed as sinusoidal

signal of arbitrary piece-wise magnitude and frequency, shifted by arbitrary positive piece-wise constant DC level. Such level is estimated by feeding signal y_c through a low-pass filter, and is used to calculate the operating point component y_0. The other component η_0 is calculated according to (13.62).

A 3^{rd} order linear exogenous system can be used to describe the dynamics of y_c profile, which yields the same 3^{rd} order of the ESSC filter.

For simulation purposes, output reference profile y_c and uncertain parameters γ_r and γ_R are defined as:

$$y_c(t) = \begin{cases} 5+0.5\sin(3t), & t \le 20 \\ 10, & 20 < t \le 60 \\ 10+\sin(1.5t), & 60 < t \le 75 \\ 15+1.5\sin(5t), & t > 75 \end{cases}, \quad \gamma_R = \begin{cases} 2.53, & t \le 40 \\ 3.79, & t > 40 \end{cases}, \quad \gamma_r = \begin{cases} 3.79\times10^{-3}, & t \le 40 \\ 2.53\times10^{-3}, & t > 40 \end{cases} \tag{13.80}$$

while the *nominal* values are known as $\gamma_{R_0} = 3.16$ and $\gamma_{r_0} = 3.16\times10^{-3}$ respectively.

Simulation plots are shown in Figures 13.2–13.4.

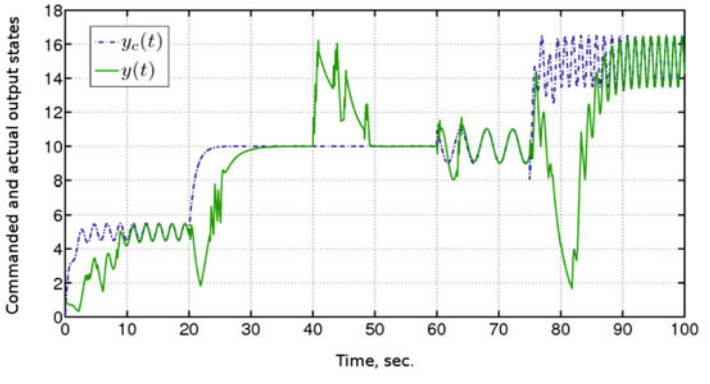

Fig. 13.2 Tracking performance of the *output state* states

The first two plots illustrate the *output* (Figure 13.2) and *internal* (Figure 13.3) state tracking performance. There are number of brakes during the tracking process, caused by abrupt change of either circuit parameters or tracking profile dynamics. Each break is detected as a destruction of the sliding mode, and is followed by the *reconstruction phase*, where all major coefficients are recalculated and are used for further tracking.

Sliding variable of the state tracking controller, shown in Figure 13.4, clearly illustrates time intervals of "good" tracking (σ is bounded by some layer, proportional to the simulation step size) and the ones, where tracking is broken.

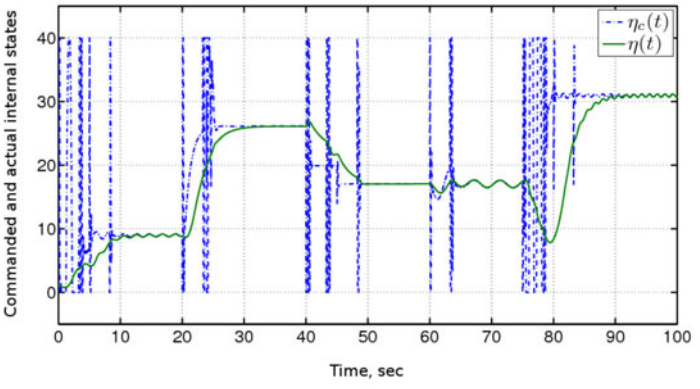

Fig. 13.3 Tracking performance of the *internal state* states

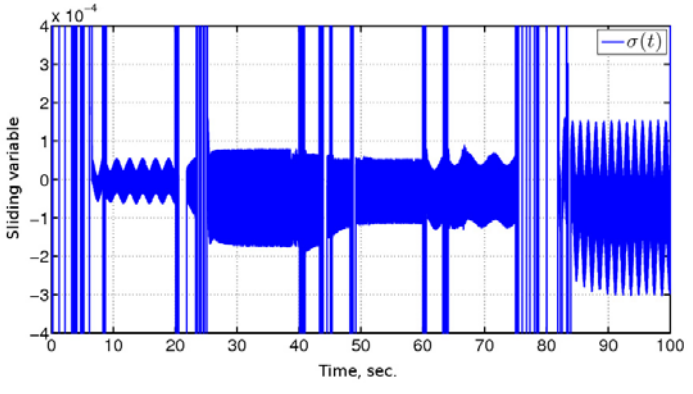

Fig. 13.4 Sliding variable of the state tracking controller

13.7 Case Study 2: SISO Output Tracking in Systems with Time Delay in Control Feedback

Output or measurement delay a is common feature in many technical systems and must be taken into account while designing control law. The causal output tracking problem in such systems can be accomplished by reducing the output-delay system into a nonminimum phase one [18, 13] by means of Padé approximation. The *accuracy* of the approximation is *proportional* to the order of the introduced unstable internal dynamics. Once the system is approximated, the previously introduced approach for output tracking in nonminimum phase systems is employed: (i) the output tracking problem is reduced to state tracking one; (ii) the method of stable system center (SSC) is used to generate a bounded reference profile for unstable

internal state (introduced as a result of Padé approximation); (iii) sliding mode control is used for state tracking.

13.7.1 Preliminaries

Consider a controllable fully feedback linearizable nonlinear SISO system:

$$\dot{x} = f(x,t) + g(x,t)\,u, \quad y = h(x) \tag{13.81}$$

where $x(t) \in \mathbb{R}^n$ is a state vector, $y(t) \in \mathbb{R}$ is a controlled output, and $u(t) \in \mathbb{R}$ is a control input. The output tracking profile $y_c(t) \in \mathbb{R}$ is given in realtime for the output $y(t)$ to be tracked asymptotically, i.e. $y(t) \to y_c(t)$ as time increases. It is assumed that $y_c(t)$ is generated by a linear exogenous system with a *known characteristic polynomial*. It is important to note that lack of knowledge about such an exosystem turns out the output tracking problem to be a *causal* one. The characteristic polynomial of power k, presenting dynamics of y_c is given as

$$P_k(\lambda) = \lambda^k + p_{k-1}\lambda^{k-1} + \cdots + p_1\lambda + p_0 \tag{13.82}$$

Remark 13.9. The causality of the problem can be further improved by using *Extended Method of Stable System Center* which relaxes requirements in such a way that only order k of the characteristic polynomial needs to be known while coefficients p_j ($j = \overline{0,k-1}$) of the polynomial can be reconstructed by means of identification algorithm presented in Section 13.4.1.

13.7.1.1 Reduction of the Relative Degree

Assuming system (13.81) has relative degree n, so it can be represented [11] as

$$y^{(n)} = \phi(\xi,t) + b(\xi,t)\,u \tag{13.83}$$

where $\xi = [y, \dot{y}, \ldots, y^{(n-1)}] \in \mathbb{R}^n$ and $\phi(\cdot)$ and $b(\cdot) \neq 0$ are smooth and bounded functions of their parameters.

Following the approach developed by Gopalswamy and Hedrick in [9], the dynamics of the system (13.83) can be rewritten in a form of *arbitrary relative degree* $r < n$ via *redefinition of the output*. Such a transformation appears to be well presented in many works [18, 13] and is not covered in details here.

A particular case of $r = 2$ is studied in this work. The *internal dynamics* are stable and can be disregarded from consideration with respect to output tracking problem. The *input/output dynamics* are given as

$$\begin{cases} \dot{q}_1 = q_2 \\ \dot{q}_2 = \hat{\phi}(\cdot) + b(\cdot)\,u \end{cases} \tag{13.84}$$

where $q_1(t) = y^{(n-2)}(t) + a_{n-3}y^{(n-3)} + \cdots + a_1\dot{y} + a_0 y$ is the new (redefined) output and $\hat{\phi}(\cdot)$ is a smooth and bounded function of its parameters. System function $\hat{\phi}(\cdot)$ can be derived from $\phi(\cdot)$ honoring to the relative degree reduction procedure. More details can be found in [18, 13].

The output reference profile $y_c(t)$ also needs to be *redefined*

$$q_{1_c}(t) = y_c^{(n-2)}(t) + a_{n-3}y_c^{(n-3)} + \cdots + a_1\dot{y}_c + a_0 y_c \tag{13.85}$$

Remark 13.10. The dynamics of the reference profile is immutable to output redefinition and the same characteristic polynomial (13.82) is about to be used.

13.7.1.2 Time Delayed Output

The root of the problem is caused by a time delay in the measurements of the controlled output. Opposite to so-called *in-system delay* which appears in the structural definition of the system, i.e. in function $\hat{\phi}(\cdot)$ and can be compensated by means of robust control, the *output delay* comes out to be a really challenging problem: control function calculated from the most recent but delayed measurement gets outdated at the time of being applied and does not properly affect the system's trajectory.

One of the ways to deal with the problem is to use *Padé approximation* [4] system's to turn the output-delayed system out into a nonminimum phase one. It introduces *extra internal dynamics*, which are unstable, but vanishes out the delay effect. The accuracy of the approximation is bound to its order that comes out to be the order of introduced internal dynamics.

The delayed output can be described as

$$\hat{y}(t) = q_1(t - \tau) \tag{13.86}$$

where τ is *small* and *known*.

13.7.2 Problem Formulation

Given a minimum phase SISO system of relative degree two, presented by its input/output dynamics (13.84) and the delayed output measurements (13.86). The problem is to provide asymptotic output tracking

$$\lim_{t\to\infty} |\hat{y}(t) - q_{1_c}(t)| = 0 \tag{13.87}$$

where reference profile's dynamics are described by a known characteristic polynomial (13.82).

13.7.3 Padé Approximation

Applying Laplace transformation to (13.86) yields $\hat{y}(s)/q_1(s) = e^{-s\tau}$ where time-delay transfer function $e^{-s\tau}$ can be presented by means of *first-*, *second-* or *third* order Padé approximation [4] correspondingly as

$$e^{-s\tau} \approx \frac{2-s\tau}{2+s\tau}, \quad e^{-s\tau} \approx \frac{12-6s\tau+s^2\tau^2}{12+6s\tau+s^2\tau^2}, \quad e^{-s\tau} \approx \frac{120-60s\tau+12s^2\tau^2-s^3\tau^3}{120+60s\tau+12s^2\tau^2+s^3\tau^3}. \tag{13.88}$$

Once the approximation applied, the delayed output $\hat{y}(t)$ turns out into approximated one $\tilde{y}(t)$ which is to be used in place of $\hat{y}(t)$ thereafter.

In general approximating dynamics can be written in a normal form [11] as

$$\begin{cases} \dot{\eta} = Q_1\eta + Q_2\tilde{y} \\ \dot{\tilde{y}} = \dot{\eta}_1 + (-1)^m q_2 \\ \dot{q}_2 = \hat{\phi}(\cdot) + b(\cdot)u \end{cases} \tag{13.89}$$

where m is the order of Padé approximation, $\eta = [\eta_1, \eta_2, \ldots]^T \in \mathbb{R}^m$ is the vector of internal states, and $\eta_1 = \tilde{y} - (-1)^m q_1$. Matrices $Q_1 \in \mathbb{R}^{m\times m}$ and $Q_2 \in \mathbb{R}^{m\times 1}$ are respectively defined with respect to the order of approximation. For the first order:

$$Q_1 = \frac{2}{\tau}, \quad Q_2 = -\frac{4}{\tau} \tag{13.90}$$

for the second order

$$Q_1 = \begin{bmatrix} 0 & 1 \\ -\frac{12}{\tau^2} & \frac{6}{\tau} \end{bmatrix}, \quad Q_2 = -\frac{12}{\tau}\begin{bmatrix} 1 \\ \frac{6}{\tau} \end{bmatrix} \tag{13.91}$$

and for the third order

$$Q_1 = \begin{bmatrix} 0 & 1 & 0 \\ 0 & 0 & 1 \\ \frac{120}{\tau^3} & -\frac{60}{\tau^2} & \frac{12}{\tau} \end{bmatrix}, \quad Q_2 = -\frac{1}{\tau}\begin{bmatrix} 24 \\ \frac{288}{\tau} \\ \frac{2256}{\tau^2} \end{bmatrix} \tag{13.92}$$

Since matrices Q_1 in (13.90)–(13.92) are *non-Hurwitz*, equation (13.89) represents a *nonminimum phase* system without time delay.

The original output-delay-system tracking problem has been reduced to a nonminimum-phase-system tracking problem by means of Padé approximation. Such a control problem is addressed in the following subsection.

13.7.4 Design of a Sliding Mode Controller for Causal Output Tracking

The method of Stable System Center (SSC) [16] is used in this section to address the output tracking problem in a nonminimum phase system. First of all the problem is to be reduced to a state-tracking by means of introducing a bounded reference profile η_c for the unstable internal state η. For control purposes (will be seen in the next subsection) such a reference profile should satisfy differential equation presenting unstable internal dynamics:

$$\dot{\eta}_c = Q_1\,\eta_c + Q_2\,q_{1_c} \tag{13.93}$$

where q_{1_c} is an output reference profile given in (13.85). The dimension of vector η_c fits the one of the internal state η and is equal to the order of Padé approximation m.

13.7.4.1 Method of Stable System Center

The method of Stable System Center allows finding a *bounded particular solution* of the unstable differential equation (13.93) on the basis of known dynamics of the reference profile $q_{1_c}(t)$.

Assume that characteristic polynomial (13.82) is given as

$$P_3(\lambda) = \lambda^3 + 0\cdot\lambda^2 + \omega_n^2\,\lambda + 0 = \lambda\left(\lambda^2 + \omega_n^2\right)$$

which in general describes a harmonical signal with a DC bias:

$$q_{1_c} = A + B\sin\omega_n t + C\cos\omega_n t \tag{13.94}$$

with A, B, C, and ω_n being piecewise constants.

According to the method of stable system center, a *bounded particular solution* η_c can be *estimated* as $\hat{\eta}_c$ which is generated by a matrix differential equation:

$$\hat{\eta}_c^{(3)} + c_2\,\hat{\eta}_c^{(2)} + c_1\,\hat{\eta}_c^{(1)} + c_0\,\hat{\eta}_c = -\left(P_2\,\theta_c^{(2)} + P_1\,\theta_c^{(1)} + P_0\,\theta_c\right) \tag{13.95}$$

where $\theta_c = Q_2\,q_{1_c}$ and matrices P_0, P_1, and P_2 are computed as follows:

$$\begin{cases} P_0 = c_0\,Q_1^{-1} \\ P_1 = \left[(c_1 - \omega_n^2)Q_1^{-1} + (c_0 - c_2\,\omega_n^2)Q_1^{-2}\right]\left(I + \omega_n^2\,Q_1^{-2}\right)^{-1} \\ P_2 = \left[c_2\,Q_1^{-1} + (c_1 - \omega_n^2)Q_1^{-2} + c_0\,Q_1^{-3}\right]\left(I + \omega_n^2\,Q_1^{-2}\right)^{-1} \end{cases} \tag{13.96}$$

Coefficients c_0, c_1, and c_2 are chosen to provide *desired eigenvalues* of the homogeneous differential equation

$$\hat{\eta}_c^{(3)} + c_2\,\hat{\eta}_c^{(2)} + c_1\,\hat{\eta}_c^{(1)} + c_0\,\hat{\eta}_c = 0$$

describing asymptotic convergence of $\hat{\eta}_c$ to η_c.

13.7.4.2 Second Order Sliding Mode Control

Once the reference profile for the unstable internal state η is computed (estimated as $\hat{\eta}_c$ by means of SSC method), a state tracking problem can be addressed. It is proposed to use the *second order sliding mode control* algorithm [12] as the system under consideration has relative degree equal to two.

The sliding variable is defined as

$$\sigma = e_q + C\, e_\eta \tag{13.97}$$

where $e_q = q_{1_c} - \tilde{y}$ and $e_\eta = \hat{\eta}_c - \eta$. Its 2^{nd}-order time-derivative is identified along the system's trajectory as

$$\ddot{\sigma} = \ddot{q}_{1_c} - \ddot{\tilde{y}} + C\left(\ddot{\hat{\eta}}_c - \ddot{\eta}\right) = \underbrace{\ddot{q}_{1_c} - \ddot{\eta}_1 - (-1)^j \ddot{\hat{\phi}} + C\left(\ddot{\hat{\eta}}_c - \ddot{\eta}\right)}_{\Psi} - (-1)^j b u = \Psi - (-1)^j b u \tag{13.98}$$

and the second order sliding mode control [12] can be designed as

$$u = (-1)^m b^{-1} \rho \operatorname{sign}\left(\dot{\sigma} + \lambda\, |\sigma|^{1/2} \operatorname{sign}(\sigma)\right) \tag{13.99}$$

where ρ is a sufficiently large positive gain and λ is a positive constant. Existence of the sliding mode as well as detailed guideline on selection of ρ and λ are given in [12].

Assume existence of the *second order sliding mode* ($\sigma = \dot{\sigma} = 0$) which will take place in a *finite time* upon proper selection of controller parameters ρ and λ. Accounting to (13.93) and description of the internal dynamics in (13.89) the following DAE system is used to describe the motion of the system in sliding mode:

$$\begin{cases} \dot{e}_\eta = \dot{\hat{\eta}}_c - \dot{\eta} = Q_1\, e_\eta + Q_2\, e_y \\ e_y = -C\, e_\eta \end{cases} \quad \therefore \quad \dot{e}_\eta = (Q_1 - Q_2 C)\, e_\eta \tag{13.100}$$

so matrix C can be selected to provide *desired asymptotic convergence* of $e_\eta(t)$ which results in convergence of $e_y(t)$ at the same time.

13.7.5 Numerical Example

The proposed methodology can be illustrated on the example of second order system with relative degree two:

$$\begin{cases} \dot{x}_1 = x_2 \\ \dot{x}_2 = -x_2 + u \\ y = x_1 \end{cases} \tag{13.101}$$

which naturally fits form (13.84) so no output redefinition is needed.

The controlled output $y(t)$ is assumed to be accessible with a time delay τ such that $\hat{y} = y(t - \tau)$. Applying the first order Padé approximation to the output-delayed system (13.101) yields the following dynamics:

$$\begin{cases} \dot{\eta}_1 = \dfrac{2}{\tau}\eta_1 - \dfrac{4}{\tau}\tilde{y} \\ \dot{\tilde{y}} = \dot{\eta}_1 - z_2 \\ \dot{z}_1 = z_2 \\ \dot{z}_2 = -z_2 + u \end{cases} \tag{13.102}$$

where $\tilde{y}$ is an approximation to the delayed output y, accessible with no delay; z_1, z_2 are states of the input/output dynamics; and η_1 is the state of unstable internal dynamics.

The two simulations[1] with *different feedback signals* have been conducted: the one that uses $\tilde{y}(t)$ (approximation of the delayed output which can be estimated, for example, by means of Smith Predictor [21]) and the one that uses $y(t-\tau)$ (real output of the system measured with a delay). In both cases the same set of parameters has been used: $c_0 = 1000$, $c_1 = 300$, $c_2 = 30$, $\omega_n = 2$, $A = 1$, $B = 2$, $C_1 = -0.75$, $\tau = 0.2$, $\rho = 25$, $\lambda = 1$, which yields control the following control law:

$$u = -25\,\mathrm{sign}\left(\dot{\sigma} + |\sigma|^{1/2}\mathrm{sign}\,(\sigma)\right) \tag{13.103}$$

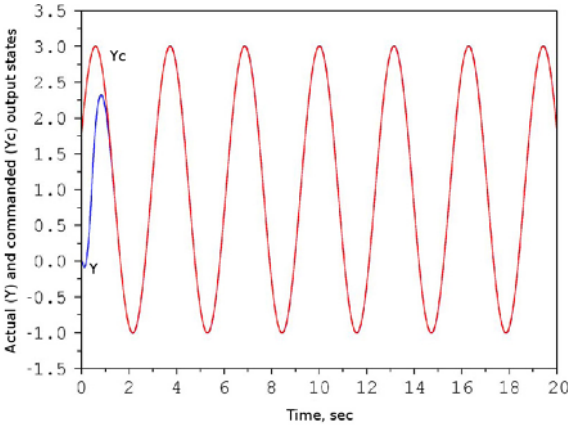

Fig. 13.5 Output tracking via SOSM control: output approximation $\tilde{y}(t)$ as feedback

It is obvious from observing the simulation plots shown on Figures 13.5 and 13.6, that the best output tracking performance can be achieved by using *non-existent* approximation $\tilde{y}(t)$ of the system's output (Figure 13.5) rather than via using *delayed output* (Figure 13.6) as a feedback.. Identification of $\tilde{y}(t)$ by means of measurement delayed output can be accomplished via using Smith Predictor [21].

[1] Simulation plots are taken from [13].

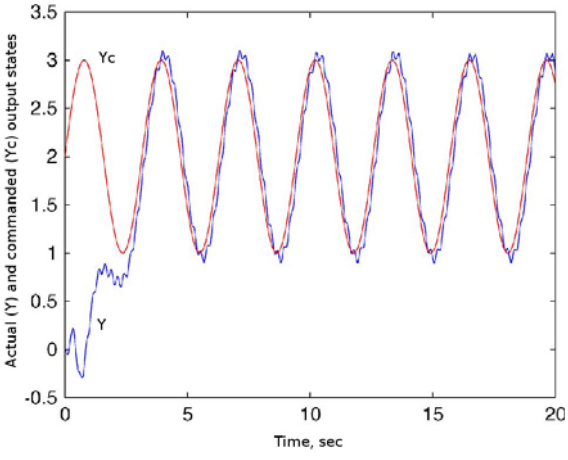

Fig. 13.6 Output tracking via SOSM control: delayed output $y(t-\tau)$ as feedback

13.8 Conclusions

The modern approach of *causal output feedback tracking* in a class of *nonminimum phase nonlinear systems* has been studied. The main contributions of the work can be summarized as follows: **(i)** The unmeasurable unstable internal states have been recovered together with the unknown input using the proposed observer; **(ii)** Output feedback stabilization of the tracking error has been accomplished using *sliding mode control*; **(iii)** The *extended method of stable system center* has been used in the internal state observer and for generation of the internal state bounded reference profile; **(iv)** The efficiency of the proposed output feedback tracking methodology for causal non-minimum phase nonlinear systems has been confirmed via two *case studies*:

1. Causal output voltage tracking for nonminimum phase boost DC/DC converter;
2. Causal output tracking in systems with time-delayed control feedback.

The former case explicitly illustrates the majority of algorithms proposed in the work while the latter introduces an approach of reducing a nonlinear system with time-delayed output to a nonminimum phase system via *Padé approximation*. The reduced system is then handled by means of method of stable system center and higher-order sliding mode control algorithm.

References

1. Baev, S., Shkolnikov, I., Shtessel, Y., Poznyak, A.: Sliding mode parameter identification of dynamic systems with measurement noise. International Journal of Systems Science 38(11), 871–878 (2007) Special Issue on Advances in Sliding Mode Observation and Estimation (part two)

2. Baev, S., Shtessel, Y., Shkolnikov, I.: HOSM driven output tracking in the nonminimum-phase causal nonlinear systems. In: Proceedings of CDC 2007, New Orleans, LA, USA (2007)
3. Baev, S., Shtessel, Y., Shkolnikov, I.: Nonminimum-phase output tracking in causal systems using higher order sliding modes. International Journal of Robust and Nonlinear Control 18(4-5), 454–467 (2008) Special Issue on Advances in Higher Order Sliding Mode Control
4. Baker, G.: Recursive Calculation of Padé Approximation, Padé Approximants and Their Applications. Academic, New York (1973)
5. Boiko, I., Fridman, L., Castellanos, M.: Analysis of second-order sliding-mode algorithms in the frequency domain. IEEE Transactions on Automatic Control 49, 946–950 (2004)
6. Devasia, S., Chen, D., Paden, B.: Nonlinear inversion-based output tracking. IEEE Transactions on Automatic Control 41, 930–942 (1996)
7. Edwards, C., Spurgeon, S.: Sliding Mode Control. Taylor & Francis, Bristol (1998)
8. Fridman, L., Levant, A., Davila, J.: Observation of linear systems with unknown inputs via high-order sliding-modes. International Journal of Systems Science 38(10) (October 2007)
9. Gopalswamy, S., Hedrick, J.: Tracking nonlinear non-minimum phase systems using sliding control. International Journal of Control 57, 1141–1158 (1993)
10. Hu, A., Sadegh, N.: Nonlinear non-minimum phase output tracking via output redefinition and learning control. In: Proceedings of ACC 2001, Arlington, VA, USA (2001)
11. Isidori, A., Byrnes, C.: Output regulation of nonlinear systems. IEEE Transactions on Automatic Control 35, 131–140 (1990)
12. Levant, A.: Higher order sliding modes, differentiation and output feedback control. International Journal of Control 26(9), 924–942 (2003)
13. Liu, G., Zinober, A., Shtessel, Y.: Second-order sm approach to siso time-delay system output tracking. IEEE Transactions on Industrial Electronics 56(9), 3638–3645 (2009)
14. Lu, X., Spurgeon, S., Postlethwaite, I.: Robust variable structure control of a PVTOL aircraft. International Journal of Systems Science 28(6), 547–558 (1997)
15. Shkolnikov, I., Shtessel, Y.: Aircraft nonminimum phase control in dynamic sliding manifolds. AIAA Journal on Guidance, Control, and Dynamics 24(3), 566–572 (2001)
16. Shkolnikov, I., Shtessel, Y.: Tracking in a class of nonminimum-phase systems with nonlinear internal dynamics via sliding mode control using method of system center. Automatica 38, 837–842 (2002)
17. Shtessel, Y., Raznopolov, O., Ozerov, L.: Control of multiple modular DC/DC power converters in conventional and dynamic sliding surfaces. IEEE Transactions on Circuits and Systems 45(10), 1091–1101 (1998)
18. Shtessel, Y., Zinober, A., Shkolnikov, I.: Sliding mode control for nonlinear systems with output delay via method of stable system center. Journal of Dynamic Systems, Measurement, and Control 125, 253–257 (2003)
19. Shtessel, Y., Zinober, A., Shkolnikov, I.: Sliding mode control of boost and buck-boost power converters using method of stable system centre. Automatica 39(6), 1061–1067 (2003)
20. Sira-Ramirez, H., Rios-Bolivar, M.: Sliding mode control of DC/DC power converters via extended linearization. IEEE Transactions on Circuits and Systems 41(10), 652–661 (1994)

21. Smith, O.: A controller to overcome dead time. ISA Journal 6, 28–33 (1957)
22. Utkin, V., Gulder, J., Shijun, M.: Sliding Mode Control in Electromechanical Systems, 2nd edn. Taylor & Francis, Abington (1999)
23. Yan, X., Edwards, C., Spurgeon, S.: Output feedback sliding mode control for nonminimum phase systems. International Journal of Control 77, 1353–1361 (2004)
24. Yong-Wha, K., Rizzoni, G., Utkin, V.: Automotive engine diagnosis and control via nonlinear estimation. Control Systems Magazine 18(5), 84–99 (1998)
25. Zinober, A., Shtessel, Y., Fossas, E., Olm, J., Patterson, B.: Nonminimum phase output tracking control strategies for DC/DC power converters. In: Fossas, E., Edwards, C., Fridman, L. (eds.) Modern Sliding Mode Control Theory: New Perspectives and Applications. LNCIS, pp. 447–482. Springer, Berlin (2006)

Chapter 14
Discrete-Time Sliding Mode Control Using Output Feedback and Nonlinear Surface

Bijnan Bandyopadhyay and Fulwani Deepak

Abstract. In this chapter, a nonlinear sliding surface is discussed to improve the transient response for general discrete-time multiple input multiple output linear systems with matched perturbations. The nonlinear surface modulates the closed loop damping ratio from an initial low to final high value to achieve better transient performance. The control law is based on the discrete-time sliding mode equivalent control and thus eliminates chattering. The control law is proposed based on two approaches: (1) reaching law based approach which needs only disturbance bounds and (2) disturbance observer based approach. Multirate output feedback is used to relax the need of the entire state vector for implementation of the control law. A possible extension of the nonlinear surface to input-delay systems is also presented.

14.1 Introduction

Beginning in the late 1970s and continuing today, the sliding mode control has received plenty of attention due to its insensitivity to disturbances and parameter variations. The well known *sliding mode control* is a particular type of Variable Structure Control System (VSCS). Recently many successful practical applications of sliding mode control (SMC) have established the importance of sliding mode theory which has mainly been developed in the last three decades. This fact is also witnessed by many special issues of learned journals focusing on sliding mode control [8, 10]. The research in this field was initiated by Emel'yanov and his colleagues [19, 20] in the former USSR, and the design paradigm now forms a mature and an established approach for robust control and estimation. The idea of sliding mode control (SMC)

Bijnan Bandyopadhyay
Indian Institute of Technology Bombay, India
e-mail: bijnan@ee.iitb.ac.in

Fulwani Deepak
Indian Institute of Technology Guwahati, India
e-mail: fulwani@iitg.ernet.in, fulwani@gmail.com

L. Fridman et al. (Eds.): Sliding Modes, LNCIS 412, pp. 381–405.
springerlink.com

was not known to the control community at large until a survey article published by Utkin [40] and a book by Itkis [27].

SMC design can be divided into two subparts viz. (1) the design of a stable surface and (2) the design of a control law to force the system states onto the chosen surface in finite time. The design of the surface should address all the constraints and required specifications therefore it should be designed optimally to meet all the requirements. The initial phase when the state trajectory is directed towards a sliding surface is called *reaching phase*. During the reaching phase, the system is sensitive to all types of disturbances. However, a control law can be designed which ensures finite time reaching of sliding surface even in the presence of uncertainties and disturbances. The effectiveness of SMC in the robust control of linear uncertain systems prompted the research on sliding mode control in other types of systems. Thus, a few researchers worked on the sliding mode control of nonlinear systems [5,37] and time delay systems [43,44]. To relax the need for measuring the entire state vector, an output feedback based sliding mode concept is also proposed in [17, 18, 16] which widens the scope of sliding mode control. However, due to the flexibility of implementation, most of the controllers are implemented through digital signal processor or high end microcontrollers. Due to this reason study and research on discrete sliding mode has received a considerable amount of attention (e.g., see [7, 4, 23, 3] and [28], among many).

In SMC, the sliding surface decides closed loop dynamics, therefore it should be designed such that it addresses all the requirements. One of the key requirements in many applications like robotics, electric drives, process control, vehicle and motion control is the high performance in an uncertain environment. To enhance the performance of the system with sliding mode control algorithms, a time-varying switching surface is proposed by many researchers in [14, 6, 15, 9]. Majority of these solutions are for second order and third order systems. In [15], an algorithm based on moving switching line is presented for second order system to enhance the performance and to eliminate the reaching phase. However, in [6] it is shown that this method does not ensure complete insensitivity to external disturbances and model mismatches. This happens because switching line slope changes in discrete steps and between two consecutive steps the state trajectory is in the reaching phase, therefore the system loses invariance during the transient phase when the switching line slope is being changed. In [34], a strategy based on fuzzy logic is devised to change the parameters of switching surfaces of higher order systems. Some researchers proposed nonlinear surfaces to improve the performance. In [46, 26], proximate time optimal control is used to design the switching line for hard disc drive seek control applications. This approach is applicable to second-order systems only. In a paper [30], the authors proposed a nonlinear sliding surface and they also noted that for higher order system their approach becomes computationally intensive. Most of the existing solutions to improve the performance are applicable to second and third order system, although some are very important from the practical point of view (e.g., see [9]). To the best of our knowledge, a few results are devoted to enhance the performance of higher order systems. These observations motivate us to search for a better technique to ensure high performance in an uncertain environment.

To ensure high performance, system should settle quickly without any overshoot. It is well understood that a low overshoot can be achieved at the cost of high settling time. Low settling time is also necessary for a quick response. Thus, most of the design schemes make a tradeoff between these two transient performance indices, and the damping ratio is chosen as a fixed number. Notable exceptions exist, of course, in [31], the authors proposed a seminal idea of composite nonlinear feedback (CNF) for a class of second order systems subject to actuator saturation. CNF uses a variable damping ratio to achieve high performance. CNF control consists of a linear feedback law and a nonlinear law without any switching element. The linear part is designed for a small damping ratio to achieve a quick response. The nonlinear feedback is used to increase the damping ratio as the output approaches the commanded target reference and thus overshoot is avoided. CNF applies more control efforts when the output is closer to the commanded target reference, resulting in a better utilization of the actuator capacity.

Subsequently, CNF controller was extended for general higher order SISO and MIMO systems in [39, 38, 12, 25] for the state feedback and output feedback cases. However, all these methods ensure performance only for perfectly known systems or when disturbance is constant. In [11], an enhanced CNF controller is proposed by adding integral action in the forward path. However, in [13], it is shown that integral action in forward path does not give robust performance for all types of disturbances. To solve this problem, in [13], a robust CNF controller is proposed based on constant disturbance estimation which is observed by an observer, and the effect of constant bias is compensated.

In general, model uncertainty and disturbances are inevitable in actual applications, which would restrict the applicability of aforementioned results in practice. To be effective in practice, along with the change of damping ratio, the controller should reject all kinds of disturbances. The existing CNF based algorithms have addressed the issue of robustness partially, i.e., by considering only constant disturbances. CNF algorithm also needs an inversion of plant model which may not be possible for an uncertain system. To solve the problem of achieving high performance with robustness, in this work a nonlinear sliding surfaces based algorithm for a discrete-time uncertain system is proposed. The proposed nonlinear surface change the closed loop damping ratio of the system as the output approaches a setpoint. Initially, the nonlinear surface keeps the damping ratio to a low value to ensure a quick response and as the output approaches the setpoint, the system is made highly damped to avoid the overshoot. The nonlinear surface continuously changes the damping ratio of system from its initial low value to the final high value. A control law to ensure the existence of sliding mode with the nonlinear surface is proposed. During the sliding mode, the system dynamics is governed by the sliding surface parameters. Therefore, the system becomes insensitive towards matched perturbations and thus robustness is achieved. The results reported in this chapter are based on our work in [1].

The brief outline of this chapter is as follows. Section 14.2 contains a brief review of the multirate output feedback strategy. The structure of nonlinear sliding surface and the proof of its stability is given in Section 14.3. Section 14.4 discusses

two approaches to design the control law, of which the first is based on a reaching law approach and the second is based on disturbance observer. A possible extension to input-delay system is discussed in Section 14.5. Application and simulation results are presented in Section 14.6 followed by a brief summary of the chapter in Section 14.7.

14.2 Multirate Output Feedback

The implementation of SMC law requires the availability of the entire state vector. However, the complete state vector is seldom available. One of the ways to overcome this problem is to construct an observer. However, this may add additional complexity in the system. Moreover, it is not always desirable to construct observer for an uncertain system. Hence one has to resort to output feedback design. It is well known that a complete pole placement can not be achieved using *static* output feedback. A concept known as multirate output feedback technique [3, 28] is of static output feedback kind and at the same time gives any arbitrary closed loop pole configuration. In what follows, we briefly review Multirate Output Feedback (MROF) technique.

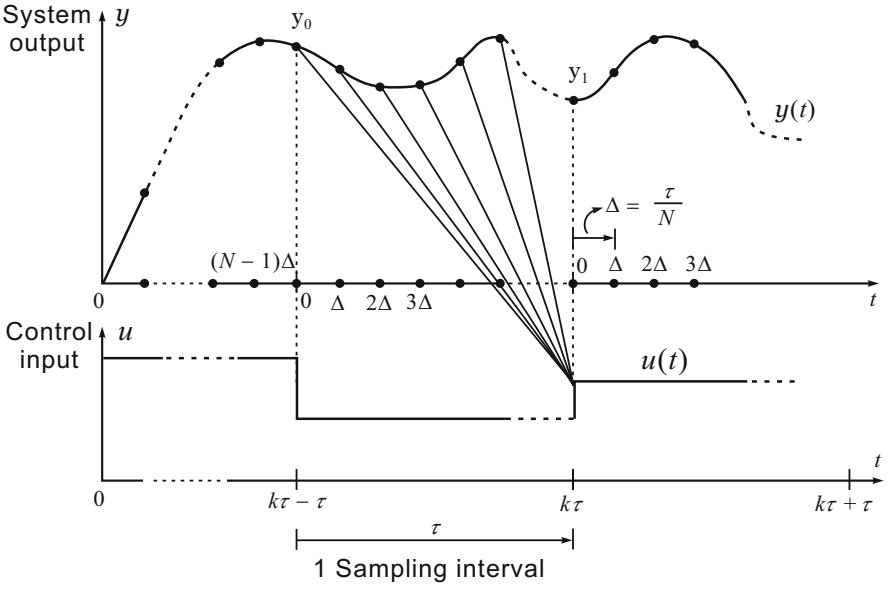

Fig. 14.1 Visualization of multirate sampling process

In MROF technique, the output is sampled at faster rate as compared to the control input. Consider the system described by the following equations

$$\dot{x}(t) = Ax(t) + Bu(t) + Bd(t) \tag{14.1a}$$
$$y(t) = C_1 x(t). \tag{14.1b}$$

Let the above continuous system be sampled at τ period and under the assumption that disturbance does not change in relatively small sampling period. Discrete equivalent of the above continuous plant can be written as follows

$$x(k+1) = \Phi x(k) + \Gamma u(k) + \Gamma d(k) \tag{14.2a}$$
$$y(k) = C_1 x(k). \tag{14.2b}$$

where $x(k) \in \mathbb{R}^n$, $u(k) \in \mathbb{R}^m$, $y(k) \in \mathbb{R}^p$ are respectively the state, input, and controlled output of the system. C_1 is output matrix, $\Phi = e^{A\tau}$, $\Gamma = \int_0^\tau (e^{A\lambda} d\lambda)B$, and $d(k)$ is a matched uncertainty. The principle of MROF technique is shown in the Figure 14.1. The following assumptions are made:

A1. Disturbance remains constant during a sampling period τ.
A2. The pair (Φ, Γ) is stabilizable.
A3. The pair (Φ, C_1) is observable.

A1 is necessary because the matched perturbation is considered. It should be noted that without the assumption A1 matched perturbation in continuous time becomes unmatched in discrete-time. Moreover, if the sampling rate is sufficiently high, then, it is reasonable to assume that disturbance remains constant over a sampling period τ. Let the input u be applied with a sampling interval of τ seconds and the system output is sampled with a faster sampling period of $\Delta = \tau/N$ seconds, where N is an integer greater than or equal to the observability index [3] of the system. Let the triplet $(\Phi_\Delta, \Gamma_\Delta, C_1)$ represents the system in (14.1) sampled at Δ rate. Using the fact that u is unchanged in the interval $\tau < t < (k+1)\tau$, the τ system state dynamics can be constructed from the Δ system dynamics. Further, if the past N multirate-sampled system outputs are represented as

$$Y_k = \begin{bmatrix} y(k\tau - \tau) \\ y(k\tau - \tau + \Delta) \\ \vdots \\ y(k\tau - \Delta) \end{bmatrix} \tag{14.3}$$

then τ system with multirate output samples can be represented as follows:

$$x(k+1) = \Phi x(k) + \Gamma u(k) + \Gamma d(k) \tag{14.4}$$
$$Y_{k+1} = C_0 x(k) + D_0 u(k) + D_0 d(k). \tag{14.5}$$

Where

$$C_0 = \begin{bmatrix} C_1 \\ C_1\Phi_\Delta \\ \vdots \\ C_1\Phi_\Delta^{N-1} \end{bmatrix}, D_0 = \begin{bmatrix} 0 \\ C_1\Gamma_\Delta \\ \vdots \\ C_1\Sigma_{j=0}^{N-2}\Phi_\Delta^j\Gamma_\Delta \end{bmatrix}. \tag{14.6}$$

From (14.4) and (14.5), $x(k)$ can be expressed using the past multirate output samples Y_k and the immediate past control input $u(k-1)$ as

$$x(k) = L_y Y_k + L_u u(k-1) + L_u d(k-1) \tag{14.7}$$

where

$$L_y = \Phi(C_0^T C_0)^{-1} C_0^T \tag{14.8}$$
$$L_u = \Gamma - \Phi(C_0^T C_0)^{-1} C_0^T D_0. \tag{14.9}$$

It is clear from the above explanation that by the previous samples of output, immediate previous input and disturbance value, one can exactly compute the states of system. The visualization of multirate sampling is shown in Figure 14.1.

14.3 Nonlinear Sliding Surface

This section discusses the design of sliding surface for general MIMO case with matched perturbation. Without loss of generality, the plant described by (14.2) can be transformed into regular form by using some orthogonal transformation matrix T_r as

$$z_1(k+1) = \Phi_{11} z_1(k) + \Phi_{12} z_2(k) \tag{14.10}$$
$$z_2(k+1) = \Phi_{21} z_1(k) + \Phi_{22} z_2(k) + \Gamma_2 u(k) + \tilde{d}(k) \tag{14.11}$$
$$y(k) = C z(k). \tag{14.12}$$

Where $z_1 \in \mathbb{R}^{n-m}$, $z_2 \in \mathbb{R}^m$, $C = C_1 (T_r)^{-1}$,
$\tilde{d}(k) = T_r \Gamma d(k) \in \mathbb{R}^m$, Γ_2 is a full rank $m \times m$ matrix, $z = T_r x = \begin{bmatrix} z_1 \\ z_2 \end{bmatrix}$. Define

$$\Phi_{reg} := \begin{bmatrix} \Phi_{11} & \Phi_{12} \\ \Phi_{21} & \Phi_{22} \end{bmatrix}. \tag{14.13}$$

Let the desired trajectory be $z_d := \begin{bmatrix} z_{1d} \\ z_{2d} \end{bmatrix}$. For notational simplicity let us define the following:

$$c_1(k) := F - \Psi(y(k)) \Phi_{12}^T P(\Phi_{11} - \Phi_{12} F), \tag{14.14a}$$
$$c^T := \begin{bmatrix} c_1(k) & I_m \end{bmatrix} \tag{14.14b}$$
$$e_1(k) := z_1(k) - z_{1d}(k) \tag{14.14c}$$
$$e_2(k) := z_2(k) - z_{2d}(k), \tag{14.14d}$$

where I_m is an identity matrix of $m \times m$, $\Psi(y(k))$ is an $m \times m$ diagonal matrix with non-positive entries and F is chosen such that $(\Phi_{11} - \Phi_{12}F)$ has stable eigenvalues and dominant poles have a low damping ratio.

The sliding surface for the system in regular form is proposed as

$$s(k) := c^T(k)e(k), \tag{14.15a}$$

$$= \begin{bmatrix} c_1(k) & I_m \end{bmatrix} \begin{bmatrix} z_1(k) - z_{1d}(k) \\ z_2(k) - z_{2d}(k) \end{bmatrix} \tag{14.15b}$$

$$= \begin{bmatrix} F - \Psi(y(k))\Phi_{12}^T P(\Phi_{11} - \Phi_{12}F) & I_m \end{bmatrix} \times \begin{bmatrix} e_1(k) \\ e_2(k) \end{bmatrix} \tag{14.15c}$$

The diagonal matrix $\Psi(y(k))$ is used to change the damping ratio of the closed-loop system. P is an $(n-m) \times (n-m)$ positive definite matrix, obtained from the solution of the following Lyapunov equation

$$P = (\Phi_{11} - \Phi_{12}F)^T P(\Phi_{11} - \Phi_{12}F) + W \tag{14.16}$$

for some positive definite matrix W. Such a matrix P exists because $(\Phi_{11} - \Phi_{12}F)$ is a stable matrix. Furthermore, $s(k) \in \mathbb{R}^m$ is a vector comprising of m sliding surfaces defined as

$$s(k) = \begin{bmatrix} s_1 & s_2 & \cdots & s_m \end{bmatrix}^T \tag{14.17}$$

where $s_i \in \mathbb{R}, \quad i = 1, 2, \cdot \cdot \cdot m$.

Matrix of Nonlinear Functions $\Psi(y(k))$:

The diagonal matrix of nonlinear function is used to change the system's closed loop damping ratio as the output(s) approaches the setpoint. It is chosen such that its elements change from 0 to -β_i according to some chosen nonlinear function. One possible choice of $\Psi(y(k))$ is as follows

$$\Psi(y(k)) = \begin{bmatrix} \Psi(y(k))_1 & \ldots & 0 \\ \vdots & . & \vdots \\ 0 & \ldots & \Psi(y(k))_m \end{bmatrix}.$$

where

$$\Psi(y(k))_i = -\beta_i \frac{|\,|y(k-1)_i - r(k)_i|^{\alpha_i} - |y(0)_i - r(0)_i|^{\alpha_i}|}{|y(0)_i - r(0)_i|^{\alpha_i}}, \quad i = 1 \cdots m. \tag{14.18}$$

In the above equation, $r(k)_i$ is a reference trajectory, β_i is used as a tuning parameter which contributes in deciding the final damping ratio and α_i decides the rate (speed) of change of damping ratio. The aforementioned choice of $\Psi(y(k))$ is similar in structure as suggested in [13] with reduced dimension. To compute the function

$\Psi(y(k))$ at $k=0$, the output $y(-1)$ can be approximated with $y(0)$. It should be noted that the choice of $\Psi(y(k))$ is not unique and any function with the above mentioned property can be used. Another possible choice [31] is as follows

$$\Psi(y(k))_i = -\beta_i e^{-\bar{k}_i|y(k-1)_i - r(k)_i|} \tag{14.19}$$

where $\bar{k}_i$ is a positive constant. The nonlinear function should ideally have zero initial value. So, initially damping ratio remains small which is contributed by F. Initial value of function given by (14.18) is zero but needs more computation while (14.19) has some small non-zero initial value but from the implementation viewpoint is simpler. The matrix $\Psi(y(k))$ is chosen so that it satisfies the following condition

$$2\Psi(y(k)) + \Psi(y(k))\Phi_{12}^T P \Phi_{12} \Psi(y(k)) \leq 0. \tag{14.20}$$

The above condition essentially limits the absolute maximum value of the function $\Psi(y(k))_i$. This limitation occurs because in discrete-time system closed loop poles have to be inside the unit circle unlike a continuous-time system where the closed-loop poles can be shifted into a deep left of complex plane. During sliding mode $s(k)=0$. So from (14.15),

$$e_2(k) = -c_1(k)e_1(k). \tag{14.21}$$

From (14.10) and (14.21) the system equation in sliding mode becomes

$$\begin{aligned} e_1(k+1) = \Phi_{11eq} e_1(k) + \Phi_{12}\Psi(y(k))\Phi_{12}^T P \Phi_{11eq} e_1(k) + \\ \Phi_{11} z_{1d}(k) + \Phi_{12} z_{2d}(k) - z_{1d}(k+1) \end{aligned} \tag{14.22}$$

where $\Phi_{11eq} = (\Phi_{11} - \Phi_{12}F)$. For the tracking problem, the desired trajectory is consistently generated using the system equations given in 14.10 [33,21] and due to this there exist some control $u_d(k)$ such that

$$\begin{aligned} z_{1d}(k+1) &= \Phi_{11} z_{1d}(k) + \Phi_{12} z_{2d}(k) \\ z_{2d}(k+1) &= \Phi_{21} z_{1d}(k) + \Phi_{22} z_{2d}(k) + \Gamma_2 u_d(k). \end{aligned} \tag{14.23}$$

Using (14.22) and (14.24), closed loop system (14.22) becomes

$$e_1(k+1) = \Phi_{11eq} e_1(k) + \Phi_{12}\Psi(y(k))\Phi_{12}^T P \Phi_{11eq} e_1(k). \tag{14.24}$$

To prove the stability of the sliding surface, the stability of the above subsystem need to be proved which is proved in the following theorem. In further discussion, for notational simplicity, the argument k for some variables is dropped i.e f stands for $f(k)$.

Theorem 14.1. *If $(\Phi_{11} - \Phi_{12}F)$ is stable and $\Psi(y(k))$ is defined by (14.18) or (14.19) which satisfies (14.20) then, the subsystem in (14.24) is stable.*

Proof. Let a Lyapunov function for system (14.24) be defined as follows

$$V(k) = e_1^T(k)Pe_1(k).$$

Increment of $V(k)$ becomes

$$\begin{aligned}
\Delta V(k) &= V(k+1) - V(k) \\
\Rightarrow \Delta V(k) &= e_1^T(k+1)Pe_1(k+1) - e_1^T(k)Pe_1(k) \\
&= \{\Phi_{11eq}e_1(k) + \Phi_{12}\Psi(y(k))\Phi_{12}^T P\Phi_{11eq}e_1(k)\}^T \times \\
&\quad P\{\Phi_{11eq}e_1(k) + \Phi_{12}\Psi(y(k))\Phi_{12}^T P\Phi_{11eq}e_1(k)\} - e_1(k)^T Pe_1(k) \\
&= e_1^T\Phi_{11eq}^T P\Phi_{12}\Psi(y(k))\Phi_{12}^T P\Phi_{11eq}e_1 + e_1^T\Phi_{11eq}^T P\Phi_{11eq}e_1 - e_1^T Pe_1 + \\
&\quad e_1^T\Phi_{11eq}^T P\Phi_{12}\Psi(y(k))\Phi_{12}^T P\Phi_{11eq}e_1 + \\
&\quad e_1^T\Phi_{11eq}^T P\Phi_{12}\Phi_{12}^T\Phi_{12}\Psi(y(k))\Phi_{12}^T P\Phi_{11eq}e_1 \\
&= -e_1^T We_1 + e_1^T\Phi_{11eq}^T P\Phi_{12}\{2\Psi(y(k)) \\
&\quad + \Psi(y(k))\Phi_{12}^T P\Phi_{12}\Psi(y(k))\}\Phi_{12}^T P\Phi_{11eq}e_1
\end{aligned}$$

Let $e_1^T\Phi_{11eq}^T P\Phi_{12} = M^T$ therefore

$$\Delta V(k) = M^T\{2\Psi(y(k)) + \Psi(y(k))\Phi_{12}^T P\Phi_{12}\Psi(y(k))\}M - e_1^T We_1.$$

From the condition (14.20) it follows

$$\Delta V(k) \leq -e_1^T We_1.$$

So the system represented by (14.24) is stable. Hence the nonlinear surface is stable and thus the theorem is proved. □

It should be noted that the system in sliding mode can be stabilized by any negative function $\Psi(y(k))$ which satisfies (14.20).

Remark 14.1. During sliding, the system dynamics is decided by the subsystem described by (14.24). It can be observed that the poles of subsystem (14.24) changes as $\Psi(y(k))_i$ changes from 0 to $-\beta_i$. The main purpose of adding a nonlinear component in the sliding surface is to add significant value to control input as the output reaches closer to the set point. The subsystem is stable for any non-positive value of $\Psi(y(k)_i$ where $i = 1...m$ which satisfy (14.20). Function $\Psi(y(k))_i$ changes from 0 to $-\beta_i$ as output tracks the reference signal. For any intermediate value of $\Psi(y(k))_i$ also the system (14.24) is stable. It is proved in [12] that introduction of this function changes damping ratio of system from an initial value ζ_1 to a final value ζ_2 where $\zeta_2 > \zeta_1$. Initially, when $\Psi(y(k)_i) = 0$, the damping ratio is determined by F which is designed for a low damping ratio. When output reaches closer to the reference, the function $\Psi(y(k)_i)$ contributes (adds) significantly to the damping ratio of the system and the steady state value of $\Psi(y(k)_i)$ becomes, $\Psi(y(k))_i \approx -\beta_i$. Therefore, the subsystem (14.24) can be written as

$$e_1(k+1) = (\Phi_{11} - \Phi_{12}F - \Phi_{12}\beta\Phi_{12}^T P(\Phi_{11} - \Phi_{12}F))e_1(k) \qquad (14.25)$$

where

$$\beta = \begin{bmatrix} \beta_1 & \dots & 0 \\ \vdots & \ddots & \vdots \\ 0 & \dots & \beta_m \end{bmatrix}.$$

Equation (14.25) decides the final damping ratio, therefore the parameter β and matrix P should be so designed that the dominant poles of (14.25) have the desired damping ratio.

One possible way to design P and β is by trial and error. Choose a diagonal matrix W and solve (14.16) for P. Through simulation, adjust the diagonal weight of W until a satisfactory response is obtained. This technique generally gives better response after proper tuning. To design the matrix P, an LMI based formulation can also be used. While formulating LMI, the condition (14.20) needs to be satisfied to ensure stability along with the other constraints.

14.4 Control Laws

The sliding surface discussed in the previous section is nonlinear. Here the surface parameters are changing at every instant. The control law should be chosen in such a way that from any initial condition, the system trajectory is attracted towards the sliding surface in finite time. To ensure the attractiveness of sliding surface, the condition $|s_i(k+1)| < |s_i(k)| \quad i = 1, 2, \cdot \cdot \cdot m$ should be satisfied. In discrete-time system, the equivalent control [42, 41] ensures attractiveness of sliding surface and keeps the trajectory on sliding surface at each sampling instant. However, to implement the equivalent control law for an uncertain discrete-time system, the actual value of uncertainty is needed. In practice it is difficult to obtain the exact value of an uncertainty and this gives rise to a boundary layer around the sliding surface $s(k) = 0$. The width of the boundary layer depends on how the unknown disturbance is estimated. In this section we present two methods to design a controller which brings sliding motion (a boundary layer around the surface for an uncertain system) in finite time. In the first method, a controller is designed based on the so called *reaching law approach* proposed in [35] which estimates an unknown disturbance by its average value. The second method estimates the current disturbance by its previous sampling instant disturbance value [45, 36]. The first method is simple from the implementation viewpoint and the width of the boundary layer is bounded by the spread of the disturbance. While the second method requires a disturbance observer and the width of the boundary layer is bounded by the rate of change of the disturbance. Furthermore, it ensures almost complete rejection of slowly varying disturbances. In what follows multi-rate output feedback control law based on these two approaches is discussed. In the following analysis a subscript i can take any integer value between 1 to m; recall m stands for the number of inputs.

14.4.1 Control Law Based on Reaching Law Approach

In this subsection a control law is derived using a reaching law approach. The control law requires only disturbance bounds. Reaching law is so constructed that it replaces the actual unknown disturbance terms in control law by its respective average values. From (14.15), $s(k+1)$ can be expressed as

$$\begin{aligned} s(k+1) &= c^T(k+1)T_r\{(x(k+1)) - x_d(k+1)\} \\ \Rightarrow s(k+1) &= c^T(k+1)T_r\Phi x(k) + c^T(k+1)T_r\Gamma u(k) + c^T(k+1)T_r\Gamma \\ &\quad d(k) - c^T(k+1)T_r x_d(k+1) \end{aligned} \tag{14.26}$$

Using (14.7) and (14.26), the switching function $s(k+1)$ can be written in terms of output as follows

$$\begin{aligned} s(k+1) = {} & c^T(k+1)T_r\Phi L_y Y_k + c^T(k+1)T_r\Phi L_u u(k-1) + \\ & c^T(k+1)T_r\Phi L_u d(k-1) + c^T(k+1)T_r\Gamma u(k) + \\ & c^T(k+1)T_r\Gamma d(k) - \tilde{x}_d(k+1), \end{aligned} \tag{14.27}$$

where

$$\tilde{x}_d(k+1) = c^T(k+1)T_r x_d(k+1). \tag{14.28}$$

To reach the sliding surface in one sampling instant the reaching law becomes

$$s(k+1) = 0.$$

If control law is obtained from the above reaching law then it contains uncertain terms. However, in general, only bounds of uncertainty are known, therefore as a remedy reaching law is constructed so that the actual unknown disturbance is replaced (estimated) by its average value. To simplify the notation let us assume without loss of generality
$d_m(k) := c^T(k+1)T_r\Phi L_u d(k-1)$,
$d_n(k) := c^T(k+1)T_r\Gamma d(k)$.
It should be noted that $d_m(k) \in \mathbb{R}^m$ and $d_n(k) \in \mathbb{R}^m$. Let us assume elements of $d_m(k)$ and $d_n(k)$ defined as:

$$\begin{aligned} d_m(k) &:= \begin{bmatrix} d_{m1}(k) & d_{m2}(k) & \cdots & d_{mm}(k) \end{bmatrix}^T \\ d_n(k) &:= \begin{bmatrix} d_{n1}(k) & d_{n2}(k) & \cdots & d_{nm}(k) \end{bmatrix}^T \end{aligned}$$

Let us also assume that d_{mLi}, d_{mUi} and d_{nLi}, d_{nUi} are the lower and upper bounds of $d_{mi}(k)$ and $d_{ni}(k)$ respectively where $i = 1, 2, \cdots m$. Thus the mean and the spread of $d_{mi}(k)$ and $d_{ni}(k)$ can be computed as

$$d_{mMi} = \frac{d_{mLi} + d_{mUi}}{2}, \quad d_{mSi} = \frac{d_{mUi} - d_{mLi}}{2} \tag{14.29a}$$

$$d_{nMi} = \frac{d_{nUi} + d_{nLi}}{2}, \quad d_{nSi} = \frac{d_{nUi} - d_{nLi}}{2}. \tag{14.29b}$$

In the above equation the subscript M is to specify the mean value and the subscript S is used to specify the spread. Now consider a modified reaching law [35]

$$s_i(k+1) = d_{mi}(k) - d_{mMi} + d_{ni}(k) - d_{nMi} \tag{14.30}$$

With the above modification of reaching law, the deviation of the state trajectory from $s_i(k) = 0$ reduces in the presence of disturbance. Using the reaching law (14.30) and $s(k+1)$ from (14.27), a control law can be derived as

$$\begin{aligned} u(k) = &-(c^T(k+1)T_r\Gamma)^{-1}\{c^T(k+1)T_r\Phi L_y Y_k + \\ &c^T(k+1)T_r\Phi L_u u(k-1) + d_{mM} + d_{nM} - \tilde{x}_d(k+1)\}. \end{aligned} \tag{14.31}$$

From the reaching law (14.30), the magnitude of sliding mode band is given as

$$|s_i(k)| \leq |d_{mSi}| + |d_{nSi}|. \tag{14.32}$$

Control law (14.31) does not require the entire state vector. To implement the control law, controller uses past outputs, immediate past inputs and disturbance bounds are needed; and to evaluate $c^T(k+1)$ only $y(k)$ is needed. It should be noted that there is no switching term in the control law unlike that used in [24]. For the system without disturbance, the trajectory with the proposed law does not deviate from the sliding surface.

14.4.1.1 Existence of Sliding Mode

With the proposed control law (14.31), boundary layer (the band of quasi sliding mode) for $s_i(k)$ is given in (14.32). It can be shown that in the reaching phase i.e. for $|s_i(k)| > |d_{mSi}| + |d_{nSi}|$, the condition $|s_i(k+1)| < |s_i(k)|$ is satisfied.

Let a Lyapunov function $v_i(k)$ be defined as $v_i(k) = |s_i(k)|$

$$\Rightarrow \Delta v_i(k) = |s_i(k+1)| - |s_i(k)|$$

substituting $s_i(k+1)$ from (14.30)

$$\Delta v_i(k) = |d_{mi}(k) - d_{mMi} + d_{ni}(k) - d_{nMi}| - |s_i(k)|$$

$$\Rightarrow \Delta v_i(k) \leq |d_{mi}(k) - d_{mMi}| + |d_{ni}(k) - d_{nMi}| - |s_i(k)|$$

Further using (14.29)

$$\Delta v_i(k) \leq |d_{mSi}| + |d_{nSi}| - |s_i(k)|$$

So during the reaching phase i.e. for $|s_i(k)| > |d_{mSi}| + |d_{nSi}|$.

$$\begin{aligned} &\Delta v_i(k) < 0 \\ \Rightarrow &|s_i(k+1)| < |s_i(k)| \end{aligned}$$

It can be concluded from the above that during reaching phase when $|s_i(k)| > |d_{mSi}| + |d_{nSi}|$, reaching condition $|s_i(k+1)| < |s_i(k)|$ is satisfied by the control law (14.31), therefore the existence of DSM is proved. By considering the bounded control input, the existence condition is also proved in [4, 41] using equivalent control approach for state feedback case. A similar approach can be used to prove the same result for the output feedback case.

14.4.2 Control Law with Disturbance Observer

In the previous subsection the control law is obtained from a reaching law in which an actual unknown disturbance is estimated by its average value. In this subsection a method is discussed in which the actual disturbance is approximated (estimated) by a disturbance at the previous sampling instant. The state vector of the system and the previous instant disturbance can be expressed in terms of previous outputs as proposed in [3, 29].

$$x(k) = \tilde{L}_y Y_k + \tilde{L}_u u(k-1) \tag{14.33}$$

$$d(k-1) = G_2 Y_k - G_2 D_0 u(k-1) \tag{14.34}$$

Where $\tilde{L}_y = \Phi G_1 + \Gamma G_2 \quad \tilde{L}_u = \Gamma - (\Phi G_1 + \Gamma G_2) D_0$

While $\begin{bmatrix} G_1 \\ G_2 \end{bmatrix} = G = \begin{bmatrix} C_0 \; D_0 \end{bmatrix}^\dagger$ is obtained by taking the generalized inverse (Moor-Penrose inverse) of $\begin{bmatrix} C_0 \; D_0 \end{bmatrix}$ and Y_k, C_0, D_0 can be computed from (14.3) and (14.6). To obtain the control law, reaching law $s(k+1) = 0$ is used. From (14.26) and reaching law $s(k+1) = 0$ one can write input $u(k)$ as follows

$$\begin{aligned} u(k) = &-(c^T(k+1)T_r\Gamma)^{-1}\{c^T(k+1)T_r\Phi x(k) - \\ &c^T(k+1)T_r x_d(k+1) + d_n(k)\} \end{aligned} \tag{14.35}$$

where $d_n(k) = c^T(k+1)T_r\Gamma d(k)$ as defined earlier. In the above equation, except $d_n(k)$ everything is known. To obtain $d_n(k)$, one needs the actual disturbance $d(k)$ therefore as proposed in [45, 36], $d_n(k)$ can be estimated with $d_n(k-1)$. To compute $d_n(k-1)$ one requires $d(k-1)$. To estimate $d_n(k)$, one can use its previous sampling instant disturbance $d_n(k-1)$ [36]. Substituting the value of $x(k)$ from (14.33), the control law can be written in terms of past output as follows

$$\begin{aligned} u(k) = &-(c^T(k+1)T_r\Gamma)^{-1}\{c^T(k+1)T_r\Phi(\tilde{L}_y Y_k + \tilde{L}_u u(k-1)) - \\ &\tilde{x}_d(k+1) + d_n(k-1)\} \end{aligned} \tag{14.36}$$

where $\tilde{x}_d(k+1)$ can be computed from (14.28) and

$$d_n(k-1) = c^T(k)T_r\Gamma(G_2Y_k - G_2D_0). \tag{14.37}$$

Using (14.26), (14.33), (14.36), (14.37) leads to

$$s(k+1) = d_n(k) - d_n(k-1).$$

From the above equation it follows

$$s_i(k+1) = d_{ni}(k) - d_{ni}(k-1).$$

From the above expression it is straightforward to verify that the switching function $s_i(k)$ is bounded by the rate of change of disturbance. For constant and slowly varying disturbances this method almost completely eliminates the effect of disturbances on the system performance and thus ensures invariance. Taking into account the availability of high speed DSP and microcontrollers, the sampling time can be chosen sufficiently small and this leads to small value of boundary layer thickness $(d_{ni}(k) - d_{ni}(k-1))$.

14.5 Extension to Input-Delay Systems

The nonlinear surfaces and corresponding control laws can also be used for a system with input delay. Consider the following system

$$x(k+1) = \Phi x(k) + \Gamma u(k-h) + D\rho(k) \tag{14.38a}$$
$$y(k) = C_1 x(k) \tag{14.38b}$$
$$u(k) = \Theta(k) \quad k = -h, -h+1, \ldots 0 \tag{14.38c}$$

where $x(k) \in \mathbb{R}^n$, $u(k) \in \mathbb{R}$, $y(k) \in \mathbb{R}$ are respectively the state, the input, and the output of the system. Φ, Γ, C_1 are matrices of appropriate dimensions, h is an integer which denotes the amount of delay and $\Theta(k)$ denotes an initial condition. $\Theta(k)$ is generally available because it refers to past inputs which were applied to the system in past. D is a column matrix and $\rho(k) \in \mathbb{R}$. The term $D\rho(k)$ accounts for an uncertainty which has both matched and unmatched components. In input-delay systems a control input applied at the k^{th} sampling instant becomes effective at the $(k+h)^{th}$ sampling instant due to the delay in the input. This situation demands that at the k^{th} instant the controller should know the future value of the state at the $(k+h)^{th}$ instant. This can be accomplished by predicting the state from the plant dynamics. Consider a predictor [32]

$$\hat{x}(k) := x(k+h) := \Phi^h x(k) + \sum_{i=-h+1}^{0} \Phi^{-i}\Gamma u(k+i-1). \tag{14.39}$$

From (14.38) and (14.39), the system can be described in $\hat{x}$ coordinates as follows

$$\hat{x}(k+1) = \Phi\hat{x}(k) + \Gamma u(k) + \Phi^h D\rho(k). \tag{14.40}$$

It should be noted that the predicted state and the actual state are generated from the same dynamical system and there is always an 'h' time step difference between them. The value of the predicted state $\hat{x}$ at any sampling instant k, is the value of the actual state at the $(k+h)^{th}$ sampling instant. We can write the output in terms of the predicted state as follows

$$\hat{y}(k) = C_1\hat{x}(k). \tag{14.41}$$

The system described in (14.40) is similar to the system in (14.2) except the presence of unmatched perturbations. If the uncertain term $\Phi^h D\rho(k)$ is assumed to be matched then surface and control law (state feedback based) can be designed in a similar way as it is discussed in the previous section. Interested readers are encouraged to refer our work in [2] for a detailed discussion with unmatched perturbations.

14.6 Magnetic Tape Position Tracking

In this section a magnetic-tape-drive servo is presented to illustrate the proposed method. The control of tension and position of a moving tape is a generic control problem in industries. Applications vary widely from digital tape transport to thin film manufacturing. For position control of read-write head, the detailed dynamics are given in [22]. A schematic diagram is given in Figure 14.2. Here the control system requirement is to achieve the commanded position of tape over read-write head. While achieving the required position, the control system should maintain a specific tension in the tape.

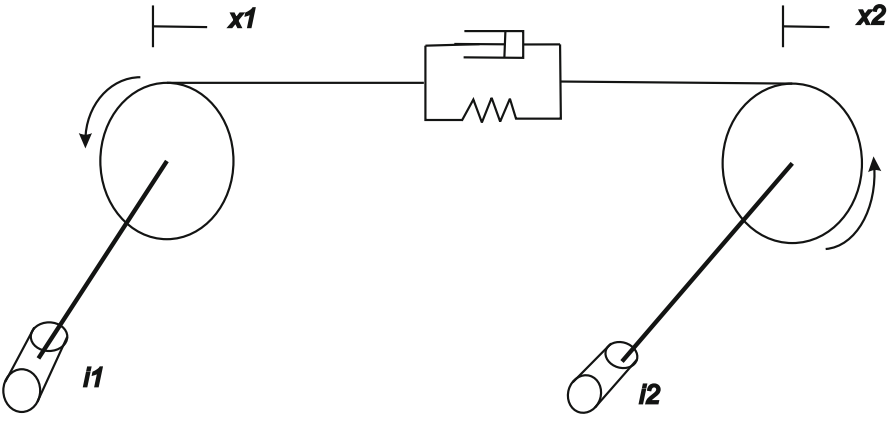

Fig. 14.2 Schematic diagram of magnetic tape position control

The continuous time model of the system is given as

$$\dot{x} = Ax + Bu + Bd$$
$$y = C_1 x$$

where

$$A = \begin{bmatrix} 0 & 0 & -10 & 0 \\ 0 & 0 & 0 & 10 \\ 3.3150 & -3.3150 & -0.5882 & -0.5882 \\ 3.3150 & -3.3150 & -0.5882 & -0.5882 \end{bmatrix},$$
$$B = \begin{bmatrix} 0 & 0 \\ 0 & 0 \\ 8.5330 & 0 \\ 0 & 8.5330 \end{bmatrix},$$
$$C_1 = \begin{bmatrix} 0.5 & 0.5 & 0 & 0 \\ -2.113 & 2.113 & 0.375 & 0.375 \end{bmatrix}.$$

Here $x = [x_1 \;\; x_2 \;\; \omega_1 \;\; \omega_2]^T$ x_1, x_2 are the positions of the tape at capstans (in mm) and ω_1, ω_2 are angular velocities motor/capstan assemblies; $u = [i_1 \;\; i_2]^T$ i_1 and i_2 are currents supplied to drive motors and $d(t)$ is smooth disturbance. The output of the system is given by

$$y(t) = \begin{bmatrix} y_1(t) \\ y_2(t) \end{bmatrix} = \begin{bmatrix} f_p(t) \\ T_e(t) \end{bmatrix}$$

where f_p is the position of the tape over read-write head in mm, and T_e is the tension in the tape in N. The following control objectives need to be achieved.

1. Magnetic tape should achieve commanded position over read-write head.
2. Settling time t_s should be less than 2.5 seconds
3. Overshoot should be less than 20 %.
4. The tape tension, T_e should be 2N with the constraint $0 < T_e < 4N$.
5. Input current should not exceed 3A at each drive motor.
6. The controlled system should be robust.

To design a discrete sliding mode controller, discretize the model with sampling rate $\tau = 0.05$ as suggested in [22]. Discrete model of the plant under assumption A_1 is given as follows

$$x(k+1) = \Phi x(k) + \Gamma u(k) + \Gamma d(k), \tag{14.42}$$
$$y(k) = C_1 x(k) \tag{14.43}$$

where

$$\Phi = \begin{bmatrix} 0.9599 & 0.0401 & -0.4861 & 0.0139 \\ 0.0401 & 0.9599 & -0.0139 & 0.4861 \\ 0.1566 & -0.1566 & 0.9321 & -0.0679 \\ 0.1566 & -0.1566 & -0.0679 & 0.9321 \end{bmatrix},$$

$$\Gamma = \begin{bmatrix} -0.1049 & 0.0017 \\ -0.0017 & 0.1049 \\ 0.4148 & -0.0118 \\ -0.0118 & 0.4148 \end{bmatrix}.$$

$$C_1 = \begin{bmatrix} 0.5000 & 0.5000 & 0 & 0 \\ -2.1130 & 2.1130 & 0.3750 & 0.3750 \end{bmatrix}. \tag{14.44}$$

First consider $d(k) = 0$ to show the improvement with the proposed nonlinear sliding surface then a disturbance will added to show robustness of the controller.

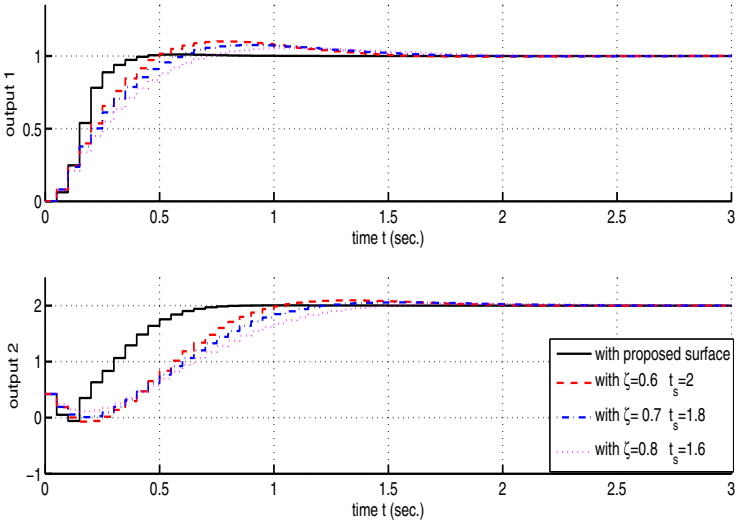

Fig. 14.3 Response of output $y(k)$ with different sliding surfaces

Step 1: Transform the system in regular form by an appropriate T_r matrix
Let $z = T_r x$ therefore in regular form the system equations becomes

$$z_1(k+1) = \Phi_{11} z_1 + \Phi_{12} z_2, \tag{14.45}$$

$$z_2(k+1) = \Phi_{21} z_1 + \Phi_{22} z_2 + \Gamma_2 u + \tilde{d}(k), \tag{14.46}$$

$$y = Cz. \tag{14.47}$$

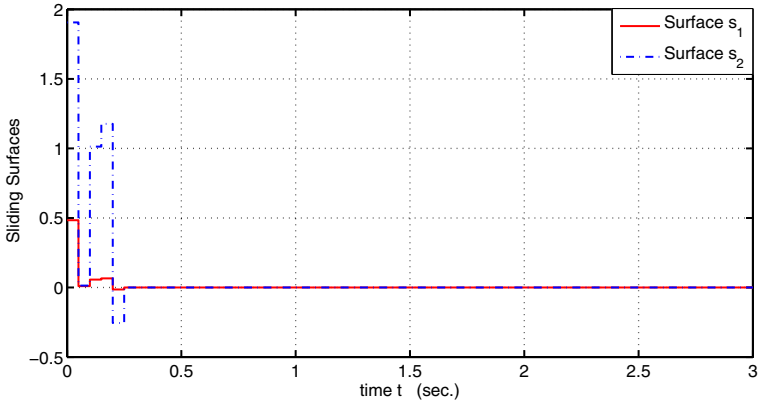

Fig. 14.4 Plot of nonlinear function with time.

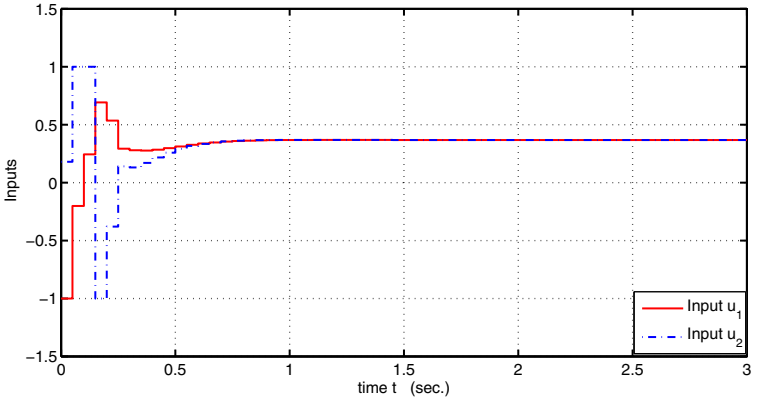

Fig. 14.5 Plot of inputs when nonlinear sliding surface is used

where $\Phi_{11} = \begin{bmatrix} 0.8802 & -0.0021 \\ -0.0021 & 0.8803 \end{bmatrix}$, $\Phi_{12} = \begin{bmatrix} -0.4727 & 0.0237 \\ 0.0185 & 0.4728 \end{bmatrix}$, $\Phi_{21} = \begin{bmatrix} 0.1678 & 0.1325 \\ -0.1476 & -0.1709 \end{bmatrix}$, $\Phi_{22} = \begin{bmatrix} 1.0177 & 0.1057 \\ 0.1057 & 1.0059 \end{bmatrix}$, $\Gamma_2 = \begin{bmatrix} 0.4281 & -0.0238 \\ -0.0000 & -0.4274 \end{bmatrix}$. $C = \begin{bmatrix} 0.4768 & -0.4932 & -0.1246 & -0.1179 \\ -1.9866 & -1.9208 & 0.8623 & -0.9116 \end{bmatrix}$

Based on output requirement $y_d = [1 \;\; 2]^T$ the required constant state trajectory is $x_d = [0.5267 \;\; 1.4733 \;\; 0 \;\; 0]^T$ and $r(k) = [1 \;\; 2]^T$

Step 2: Design of nonlinear sliding surface

Nonlinear sliding surface is composed of a constant and a nonlinear term. Initially the nonlinear term is zero, therefore the constant term decides initial damping ratio

(ζ_1) and settling time (t_{s1}). For initial settling time $t_{s1} = 1.3sec.$ and initial damping ratio $\zeta_1 = 0.7054$ gain matrix F can be computed as

$F = \begin{bmatrix} -0.0847 & -0.2713 \\ -0.2809 & 0.0815 \end{bmatrix}$.
For $W = \begin{bmatrix} 3.0336 & 0 \\ 0 & 3.0336 \end{bmatrix}$ solving the Lyapunov equation (14.16) for P gives

$$P = \begin{bmatrix} 3.7682 & 0 \\ 0 & 3.7682 \end{bmatrix}.$$

Matrix P is positive definite as required. Matrix $\Psi(y(k))$ is given as follows $\Psi(y(k)) = \begin{bmatrix} \Psi(y(k))_1 & 0 \\ 0 & \Psi(y(k))_2 \end{bmatrix}$. Functions $\Psi(y(k))_1$ and $\Psi(y(k))_2$ can be computed from (14.18) with the following parameters
$\beta_1 = 0.4$, $\alpha_1 = 8$, $\beta_2 = 0.15$, $\alpha_2 = 8$. From the above values switching function $s(k)$ can be computed.

Step 3: Design of control law.
From (14.31) control law with $d(k) = 0$

$$u(k) = -(c^T T_r \Gamma)^{-1}\{c^T(k+1)T_r \Phi L_y Y_k + c^T(k+1)T_r \Phi L_u u(k-1) - \tilde{x}_d(k+1)\}. \tag{14.48}$$

In the above equation $c^T(k+1)$ is computed from $y(k)$. The observability index for the system is 4, therefore N is chosen 4. Let $L_y = [L_1 \ : \ L_2]$

$$L_1 = \begin{bmatrix} -0.5000 & 0.0178 & 0.0000 & -0.0339 \\ -0.5000 & -0.0178 & 0.0000 & 0.0339 \\ 2.4000 & -0.5594 & 0.8000 & -0.1870 \\ -2.4000 & -0.5594 & -0.8000 & -0.1870 \end{bmatrix}$$

$$L_2 = \begin{bmatrix} 0.5000 & -0.0845 & 1.0000 & -0.1336 \\ 0.5000 & 0.0845 & 1.0000 & 0.1336 \\ -0.8000 & 0.1819 & -2.4000 & 0.5436 \\ 0.8000 & 0.1819 & 2.4000 & 0.5436 \end{bmatrix}$$

$$L_u = \begin{bmatrix} -0.0231 & 0.0102 \\ -0.0102 & 0.0231 \\ 0.1903 & -0.0764 \\ -0.0764 & 0.1903 \end{bmatrix}$$

$\tilde{x}_d(k+1)$ can be computed from (14.28).

Design of linear sliding surfaces:
Performance of the proposed nonlinear sliding surface is compared with the controller designed with different linear sliding surfaces. The system output response is plotted for different sliding surfaces and the proposed nonlinear sliding surface. Parameters of linear sliding surface(ζ and t_s) are chosen based on the values of corresponding parameters of the nonlinear surface at different instants. When the nonlinear sliding surface is used, the poles of the closed loop system changes as output approaches the reference. This changes the damping ratio and settling time from its initial values ζ_1 and t_{s1} to final values ζ_2 and t_{s2}. During the course of change, at different instants, the system has different damping ratios and settling times; linear surfaces are designed based on these parameters at some time instants. The following three different linear sliding surfaces are designed

Linear surface 1 with $\zeta = 0.6, t_s = 2.0$
Linear surface 2 with $\zeta = 0.7, t_s = 1.8$
Linear surface 3 with $\zeta = 0.8, t_s = 1.6$

Responses obtained by these three different sliding surfaces are compared with that of obtained by the nonlinear sliding surface. A control law for linear sliding surface is given as follows

$$u(k) = -(\bar{c}^T T_r \Gamma)^{-1}\{\bar{c}^T T_r \Phi L_y Y_k + \bar{c}^T T_r \Phi L_u u(k-1) + d_{m0} + d_{10} - \tilde{x}_d(k+1)\}. \tag{14.49}$$

where

$$\tilde{x}_d(k+1) = \bar{c}^T T_r x_d(k+1).$$

In the above control law $\bar{c}^T$ can be designed to obtain a desired damping ratio by using regular form and pole placement approach.

14.6.1 Comparison with Different Linear Sliding Surfaces

Responses of tape position $y_1(k)$ and tension in tape $y_2(k)$ are plotted which are obtained using the nonlinear sliding surface and different linear sliding surfaces. Figure 14.3 shows the response of $y(k)$ with the controller designed with different sliding surfaces. The plot clearly shows that with the nonlinear sliding surface performance improves significantly. With the proposed surface position settles in 0.5 seconds without any overshoot. The minimum improvement in settling time for position is 50%. It can be seen that the proposed surface ensures quick response without any overshoot. Switching function $s(k)$ goes to zero in two sampling instants which can be seen from Figure 14.4. Plot of input is shown in Figure 14.5 which confirms that chattering is eliminated because of equivalent control.

Table 14.1 Settling time of tape position obtained by the proposed sliding surface versus surfaces with different ζ

Type of sliding surface	Peak (%) overshoot	Settling t_s(sec.) Time
surface with ζ=0.6 and $t_s = 2$	10 %	2.4
surface with ζ=0.7 and $t_s = 1.8$	7.5%	1.5
surface with ζ=0.8 and $t_s = 1.6$	5.4%	1.7
Proposed surface	1%	0.5

14.6.2 Nonlinear Sliding Surface with Disturbance

Plant is perturbed by external matched disturbance $d(k) = 0.04sin(8\pi k\tau)$ to validate robustness of the proposed surface. The responses obtained by the control law designed based on the reaching law approach (14.31) and the control law with disturbance observer(14.36) are compared.

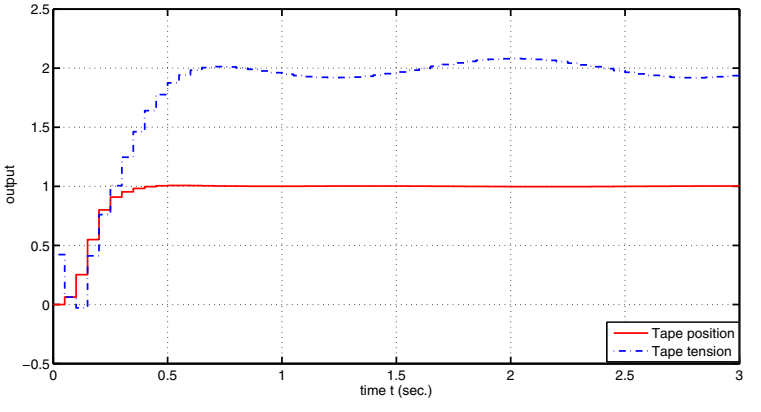

Fig. 14.6 Plot of outputs, when nonlinear sliding surface is used with plant disturbance and control is based on reaching law approach.

14.6.2.1 Control Law Designed Based on Reaching Law Approach

Response of the outputs and sliding surfaces are plotted in Figures 14.6 and 14.7. The control law in (14.31) is implemented. In symmetric disturbance upper and lower bounds are same, therefore $d_{mM} = d_{nM} = 0$ Amplitude of sliding mode band is

$$|d_{mS1}| + |d_{nS1}| = 0.0545$$
$$|d_{mS2}| + |d_{nS2}| = 0.0559$$

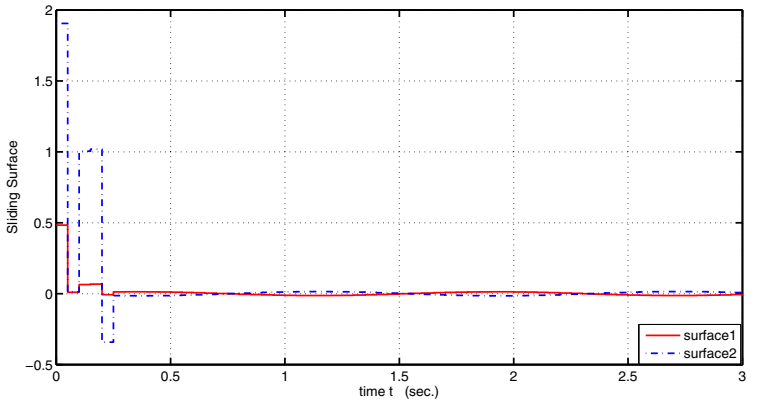

Fig. 14.7 Plot of the nonlinear switching function with disturbance and control is based on reaching law approach.

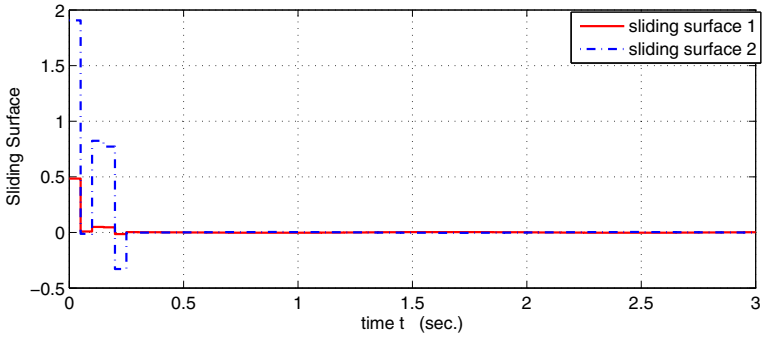

Fig. 14.8 Plot of outputs, when nonlinear sliding surface is used with plant disturbance and control law with disturbance observer.

The first equation corresponds to the first sliding surface band size and the second equation is the band size for the second sliding surface.

14.6.2.2 Control Law Designed Based on Disturbance Observer

Following the procedure described in Section 14.4 control law as per (14.36) is designed. To implement the control law constant matrices $\tilde{L}_y$,$\tilde{L}_u$,G_1,G_2 are obtained as discussed in Section 14.4. Figure 14.8 shows plot of tape position and tension in the tape when the plant is subjected to a disturbance. It can be seen that the effect of disturbance is very small on both outputs. Figure 14.9 shows evolution of switching function. It can be verified that the band is significantly reduced because of the disturbance observer.

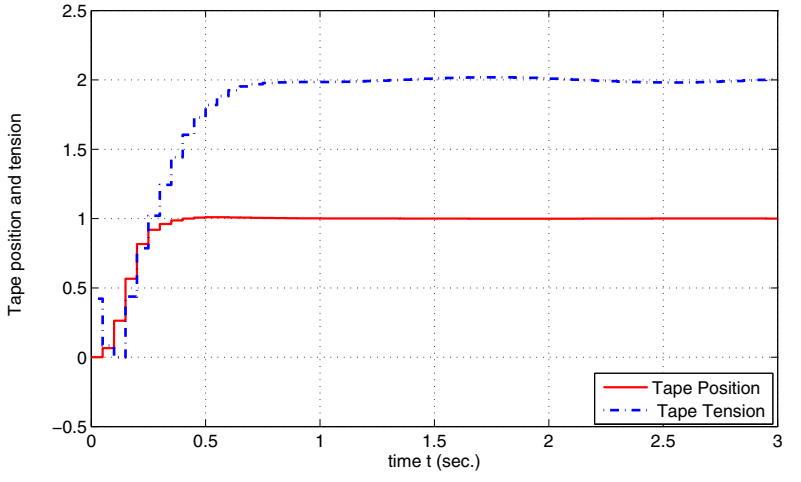

Fig. 14.9 Plot of the nonlinear switching function with disturbance and control law with disturbance observer.

14.7 Summary

The design of a nonlinear sliding surface, which allows the closed-loop system to simultaneously achieve low overshoot and low settling time, has been presented in this chapter. It has been shown how this high performance can be combined with high robustness (to matched uncertainty) and effective disturbance rejection. By application, it has been shown (Table I) that the nonlinear surface gives a minimum of 50% improvement in settling time (and negligible overshoot) when compared to linear surfaces.

References

1. Bandyopadhyay, B., Fulwani, D.: High performance tracking controller for discrete plant using non-linear sliding surface. IEEE Transaction on Ind. Electronics 9, 3628–3637 (2009)
2. Bandyopadhyay, B., Deepak, F., Kim, K.S.: Sliding Mode Control Using Novel Sliding Surfaces. LNCIS, vol. 392. Springer, Heidelberg (2009)
3. Bandyopadhyay, B., Janardhanan, S.: Discrete-Time Sliding Mode Control. LNCIS, vol. 323. Springer, Heidelberg (2006)
4. Bartolini, G., Ferrara, A., Utkin, V.I.: Adaptive sliding mode control in discrete-time systems. Automatica 31(5), 679–773 (1995)
5. Bartolini, G., Pisano, A., Usai, E., Levant, A.: On the robust stabilization of nonlinear uncertain systems with incomplete state availability. Journal of Dynamic Systems, Measurement and Control, Transactions of the ASME 122(4), 738–745 (2000)
6. Bartoszewicz, A.: Time-varying sliding modes for second-order systems. IEE Proc.-Control Theory Appl. 143(5), 455–462 (1996)

7. Bartoszewicz, A.: Discrete-time quasi-sliding-mode control strategies. IEEE Trans. on Industrial Electronics 45(3), 633–637 (1998)
8. Bartoszewicz, A., Kaynak, O., Utkin, V.I.: Special section on sliding mode control in industrial applications. IEEE Transactions on Industrial Electronics 55(11), 3806–4074 (2008)
9. Bartoszewicz, A., Nowacka-Leverton, A.: Time-Varying Sliding Modes for Second and Third Order Systems. LNCIS, vol. 382. Springer, Heidelberg (2009)
10. Bartoszewicz, A., Patton, R.J.: sliding mode control: Special issue. Int. Journal of Adaptive Control and Signal Processing 21(635822) (2007)
11. Chen, B.M., Cheng, G., Lee, T.H.: Modeling and compensation of nonlinearities and friction in a micro hard disk servo system with nonlinear control. IEEE Trans. on Control Systems Technology 13(5), 708–721 (2005)
12. Chen, B.M., Lee, T.H., Peng, K., Venkataramanan, V.: Composite nonlinear feedback control for linear systems with input saturation: theory and an applications. IEEE Trans. on Automatic Control 48(3), 427–439 (2003)
13. Cheng, G., Peng, K.: Robust composite nonlinear feedback control with application to a servo positioning system. IEEE Transaction on Ind. Electronics 54(2), 1132–1140 (2007)
14. Choi, S.B., Cheong, C.C., Park, D.W.: Moving switching surfaces for robust control of second-order variable structure systems. International Journal of Control 58, 229–245 (1993)
15. Choi, S.B., Park, D.W., Jayasuriya, S.: A time-varying sliding surface for fast and robust tracking control of second order uncertain systems. Automatica 30(5), 899–904 (1994)
16. Edwards, C., Akoachere, A., Spurgeon, S.K.: Sliding-mode output feedback controller design using linear matrix inequalities. IEEE Transactions on Automatic Control 46(1), 115–119 (2001)
17. Edwards, C., Spurgeon, S.K.: Sliding mode stabilization of uncertain systems using only output information. International Journal of Control 62(5), 1129–1144 (1995)
18. Edwards, C., Spurgeon, S.K.: Robust output tracking using a sliding-mode controller/observer scheme. International Journal of Control 64(5), 967–983 (1996)
19. Emel'yanov, S.V.: Method of designing complex control algorithm using an error and its first time derivative only. Automation and Remote Control 18(10) (1957) (in Russian)
20. Emel'yanov, S.V., Burovoi, I.A., et al.: Mathematical models of process in technology and development of variable structure control system. Metallurgy 18(07) (1964) (in Russian)
21. Eun, Y., Kim, J.H., Cho, D.I.: Discrete-time variable structure controller with a decoupled disturbance compensator and its application to a CNC servomechanism. IEEE Trans. on Control Systems Technology 7(4), 414–423 (1999)
22. Franklin, G., Powell, J.D., Workman, M.L.: Digital Control of Dynamic Systems. Addision-Wesley, Reading (1990)
23. Furuta, K.: Sliding mode control of a discrete system. Systems and Control Letters 14, 145–152 (1990)
24. Gao, W., Wang, Y., Homaifa, A.: Discrete-time variable structure control systems. IEEE Transactions on Industrial Electronics 42(2), 117–122 (1995)
25. He, Y., Chen, B.M., Wu, C.: Improving transient performance in tracking control for linear multivariable discrete-time systems with input saturation. Systems and Control Letters 56, 25–33 (2007)
26. Hu, Q., Du, C., Xie, L., Wang, Y.: Discrete-time sliding mode control with time varying surface for hard disc drives. IEEE Transactions on Control System Technology 17(1), 175–183 (2009)
27. Itkis, U.: Control Systems of Variable Structure. Wiley, New Yark (1976)

28. Janardhanan, S., Bandyopadhyay, B.: Output feedback sliding-mode control for uncertain systems using fast output sampling technique. IEEE Transactions on Industrial Electronics 53(5), 1677–1682 (2006)
29. Janardhanan, S., Kariwala, V.: Multirate output feedback based LQ optimal discrete-time sliding mode control. IEEE Transactions on Automatic Control 53(1), 367–373 (2008)
30. Lee, D.S., Youn, M.J.: Controller design of variable structure systems with nonlinear sliding surface. Electronics Letters 25(25), 1715–1717 (1989)
31. Lin, Z., Pachter, M., Banda, S.: Towards improvement of tracking performance-nonlinear feedback for linear systems. International Journal of Control 70(1), 1–11 (1998)
32. Lozano, R., Castillo, P., Garcia, P., Dzul, A.: Robust prediction-based control for unstable delay systems: application to the yaw control of a mini-helicopter. Automatica 40, 603–612 (2004)
33. Misawa, E.A.: Discrete-time sliding mode control: The linear case. Journal of Dynamic Systems, Measurement, and Control 119(2), 819–821 (1997)
34. Park, D.W., Choi, S.B.: Moving sliding surfaces for high-order variable structure systems. International Journal of Control 72, 960–970 (1999)
35. Reddy, G.D., Bandyopadhyay, B., Tiwari, A.P.: Multirate output feedback based sliding mode spatial control for a large PHWR. IEEE Trans. on Nuclear Science 54(6), 2677–2686 (2007)
36. Su, W.C., Drakunov, S.V., Ozguner, U.: An O(T^2) boundary layer in sliding mode for sampled-data systems. IEEE Trans. on Automatic Control 45(3), 482–485 (2000)
37. Tunay, I., Kaynak, O.: New variable structure controller for affine nonlinear systems with non-matching uncertainties. International Journal of Control 62(4), 917–939 (1995)
38. Turner, M.C., Postlethwaite, I.: Nonlinear regulation in constrained input discrete-time linear systems. International Journal of Control 77(15), 1330–1342 (2004)
39. Turner, M.C., Postlethwaite, I., Walker, D.J.: Non-linear tracking control for multivariable constrained input linear systems. International Journal of Control 73(12), 1160–1172 (2000)
40. Utkin, V.I.: Variable structure system with sliding mode. IEEE Transaction on Automatic Control 22(2), 212–221 (1977)
41. Utkin, V.I.: Sliding mode control in discrete-time and difference systems. In: Zinober, A.S. (ed.) Variable Structure and Lyapunov Control, ch.5, pp. 87–107. Springer, U.K (1993)
42. Utkin, V.I., Guldner, J., Shi, J.: Sliding Mode Control in Electromechanical Systems. Taylor and Francis, Abington (1999)
43. Xia, Y., Liu, G.P., Shi, P., Chen, J., Rees, D., Liang, J.: Sliding mode control of uncertain linear discrete-time systems with input delay. IET Control Theory Appl. 1(4), 1169–1175 (2007)
44. Yan, M., Shi, Y.: Robust discrete-time sliding mode control for uncertain systems with time-varying state delay. IET Control Theory Appl. 2(8), 662–674 (2008)
45. Young, K.D., Utkin, V.I., Ozguner, U.: A control engineer's guide to sliding mode control. IEEE Trans. Control System Technology 7(3), 328–342 (1999)
46. Zhang, D.Q., Guo, G.X.: Discrete-time sliding mode proximate time optimal seek control of hard disc drives. IEE Proceedings 147(4), 440–446 (2000)

Part III
Applications

Chapter 15
Higher Order Sliding Modes in Collaborative Robotics

Michael Defoort, Thierry Floquet, Anne-Marie Kökösy, and Wilfrid Perruquetti

Abstract. In this chapter, a scheme for real time motion planning and robust control of a swarm of nonholonomic mobile robots evolving in an uncertain environment is derived. This scheme consists of two main parts: (i) a real time collision-free motion planner; (ii) a trajectory tracking controller. In implementation, the motion planner dynamically generates the optimal trajectory while the robot runs. High precision motion tracking is achieved by the design of a higher order sliding mode controller based on geometric homogeneity properties. Experimental investigations have been conducted using several test benchmarks of mobile robots in order to demonstrate the effectiveness of the proposed strategy.

15.1 Introduction

The coordinated control of multiple autonomous mobile robots has become an important robotics research field. Cooperative robotics concerns a network of robots exchanging information in order to tackle a common problem and there are many potential advantages of such systems over a single robot, including greater flexibility, adaptability and robustness. It can provide solutions to several applicative fields

Michael Defoort
Univ Lille Nord de France, 59000 Lille
LAMIH, CNRS, FRE 3304, UVHC, 59313 Valenciennes, France
e-mail: michael.defoort@univ-valenciennes.fr

T. Floquet · W. Perruquetti
LAGIS, CNRS, FRE 3303, Ecole Centrale de Lille, Cité Scientifique, BP 48,
59651 Villeneuve-d'Ascq Cedex, France and Project ALIEN, INRIA Lille - Nord Europe
e-mail: {thierry.floquet,wilfrid.perruquetti}@ec-lille.fr

A. Kökösy
ISEN, 41 bvd Vauban, 59 046 Lille Cedex, France and LAGIS, CNRS, FRE 3303, BP 48,
Cité Scientifique, 59651 Villeneuve-d'Ascq, Cedex, France
e-mail: annemarie.kokosy@isen.fr

L. Fridman et al. (Eds.): Sliding Modes, LNCIS 412, pp. 409–437.
springerlink.com

including manufacturing, supervision (forest fire, military applications, . . .), space or underwater exploration, medical applications, . . .

Among all the topics of study in this field, this chapter focuses on the problem of the navigation of a swarm of autonomous mobile robots evolving in a partially known or unknown environment with obstacles. In many cooperative tasks such as surveillance mapping, search, rescue or area data acquisition, the swarm must navigate between known initial and final points without collisions.

Wheeled mobile robots have been widely studied in the last two decades due to their practical importance and theoretically interesting properties. Indeed, there are considerable research efforts toward solving mobile robot navigation in different applications in indoor and outdoor environments (see [1, 2] and the survey paper [3]). For some navigation tasks like planetary exploration, robots are required to travel long distances within constrained resources (energy, time. . .). In such cases, efficient motion planning and control algorithms are needed in order to achieve the goal while meeting certain performance issue, such as geometric-based or time-based criteria. Although motion planning and control are closely related in the robot navigation problem, they are usually addressed as two separate problems in most of the existing literature. Motion planning consists in generating a collision-free trajectory from the initial to the final desired positions and control is the determination of the physical inputs to the robot motion components, so that the robots accurately track the reference trajectories in spite of model uncertainties and external perturbations. These two problems are typically solved using methods from different areas such as those in artificial intelligence and control theory. Such a separation makes it difficult to address robot performances in a complete application, since the planned trajectory may not be efficiently tracked. This fact can imply that the meaning of optimization in each step is lost. For instance, in a typical time optimal trajectory planning, the open-loop control schemes result in bang-bang or bang-singular-bang controls [4]. However, the discontinuities of the planned open-loop control may not produce a satisfactory path tracking result in practice and will not be applicable to high speed traveling. In this research, path planning and motion control are designed accordingly.

A survey of nonholonomic control problems can be found in [5]. Obstacles to the tracking of nonholonomic systems are the uncontrollability of their linear approximation and the fact that the Brockett necessary condition to the existence of a smooth time-invariant state feedback is not satisfied [6]. To overcome these difficulties, various methods have been investigated: homogeneous and time-varying feedbacks [7, 8], sinusoidal and polynomial controls [9], piecewise continuous controls [10]. However, most of these methods do not provide both fast convergence and good robustness properties. Most of the control laws ensuring exponential or finite time convergence [11] are known to be non-robust under disturbances or modeling errors. On the other hand, control design methodologies like smooth time varying feedback [8], are quite insensitive to perturbations but imply a slow convergence.

In many other works about the stabilization of nonholonomic systems [12, 13, 14, 15], the derived control laws are of discontinuous type, providing for fast convergence and robustness properties, but can lead to discontinuous velocities in practice. This difficulty can be overcome by adding cascade integrators in the path of the usual control inputs so that the discontinuous part of the control is embedded in higher time derivatives of the variables associated to the mechanical parts. Furthermore, applying a discontinuous control on electrical inputs appears relevant since the latter are most of time made of switching electrical devices.

The discussed claims for discontinuous actions, cascade integrators and robustness properties naturally suggest the use of higher order sliding modes in control problems of wheeled mobile robots. This discontinuous control technique consists in constraining the system motion along manifolds of reduced dimensionality in the state space and is applicable to a broad variety of practical applications. In higher order sliding mode theory, the sliding surface is defined by the vanishing of a corresponding sliding variable s and its successive time derivatives up to a certain order, i.e. the r^{th} order sliding set:

$$\mathscr{S}^r = \left\{ x \in \mathbb{R}^n : \sigma = \dot{\sigma}(x) = \ldots = \sigma^{(r-1)}(x) = 0 \right\},$$

where x is the state vector of the system. A control law leading to such a behavior is called a r^{th} order ideal sliding mode algorithm with respect to s. Higher order sliding modes, that are characterized by a discontinuous control acting on the r^{th}, $r > 1$, time derivatives of the sliding variable (instead of the first time derivative in classical sliding mode, $r = 1$), can reduce the chattering phenomenon while preserving the robustness properties. This control technic has been recently applied in several fields such as in mechanics [16], [17], [18], mobile robotics [13], [19], [20] or electric machines [21], [22].

In Section 17.4, a higher order sliding mode control algorithm is proposed for a class of uncertain multi-input multi-output nonlinear systems. This problem can be seen as the finite time stabilization of a higher order input-output dynamical system with bounded uncertainties. The control scheme is based on geometric homogeneity and sliding mode control. The proposed procedure provides explicit conditions on the controller parameters and guarantees robustness against uncertainties.

Section 15.3 deals with the problem of real time motion planning and robust control of a swarm of nonholonomic mobile robots evolving in an uncertain environment. General control issues in collaborative robotics are first briefly discussed. Then, the path planning problem is formulated as a constrained receding horizon planning problem and is solved in real time with an efficient computational method that combines nonlinear control theory, B-spline basis function and nonlinear programming. After that, the robust tracking control problems without and with coordination are solved using the algorithm developed in Section 17.4. The efficacy, good performance of obstacle avoidance, real time and high robustness properties are demonstrated by experimental results.

15.2 Some Contributions on Higher Order Sliding Mode

15.2.1 Problem Formulation

A constructive algorithm that combines a finite time controller based on geometric homogeneity with a discontinuous controller based on SMC in order to ensure the robustness with respect to the uncertainties is derived. Consider the following general multi-input multi-output nonlinear uncertain system:

$$\begin{cases} \dot{x} &= f(x) + \sum_{i=1}^{m} g_i(x)u_i \\ y_1 &= \sigma_1(x) \\ &\vdots \\ y_m &= \sigma_m(x) \end{cases} \tag{15.1}$$

where $x \in \mathbb{R}^n$ and $u = [u_1, \ldots, u_m]^T \in \mathbb{R}^m$ are the state variable and the control input, respectively. $f(x)$ and $g(x) = [g_1(x), \ldots, g_m(x)]^T$ are uncertain smooth functions. $\sigma(x) = [\sigma_1(x), \ldots, \sigma_m(x)]^T \in \mathbb{R}^m$ is a smooth measurable output vector. The uncertainties on $f(x)$ and $g(x)$ are due to parameter variations, unmodeled dynamics or external disturbances and do not necessarily satisfy the matching condition. The control objective consists in the vanishing of the output $\sigma(x)$ in finite time.

Assumption 15.1. *The relative degree vector $r = [r_1, \ldots, r_m]^T$ of the system (15.1) with respect to $\sigma(x)$ is assumed to be constant and known. It means that the $m \times m$ matrix:*

$$B(x) = \begin{bmatrix} L_{g_1} L_f^{r_1 - 1} \sigma_1(x) & \ldots & L_{g_m} L_f^{r_1 - 1} \sigma_1(x) \\ \vdots & & \vdots \\ L_{g_1} L_f^{r_m - 1} \sigma_m(x) & \ldots & L_{g_m} L_f^{r_m - 1} \sigma_m(x) \end{bmatrix}$$

is nonsingular and $L_{g_j} L_f^k \sigma_i(x) = 0$, for $1 \leq i \leq m$, $1 \leq j \leq m$ and $0 \leq k < r_i - 1$. Moreover, it is supposed that the associated zero dynamics is asymptotically stable.

Definition 15.1. [23] Consider the nonlinear system (15.1) and the sliding variable $\sigma(x)$. Assume that the time derivatives σ_i, $\dot{\sigma}_i, \ldots,$ $\sigma_i^{(r_i - 1)}$ for all $i = 1, \ldots, m$ are continuous functions. The manifold defined as:

$$\mathscr{S}^r = \left\{ x : \begin{array}{c} \sigma_1(x) = \dot{\sigma}_1(x) = \ldots = \sigma_1^{(r_1 - 1)}(x) = 0 \\ \vdots \\ \sigma_m(x) = \dot{\sigma}_m(x) = \ldots = \sigma_m^{(r_m - 1)}(x) = 0 \end{array} \right\}$$

is called the r^{th} order sliding set. If it is non empty and locally an integral set in the Filippov sense [24], the motion on $\mathscr{S}^r$ is called r^{th} order sliding mode with respect to the sliding variable σ.

The r^{th} order SMC approach allows the finite time stabilization of the system on $\mathscr{S}^r$ by defining a suitable discontinuous control law. The r_i^{th} time derivative of each function σ_i yields:

$$\left[\sigma_1^{(r_1)}(x),\ldots,\sigma_m^{(r_m)}(x)\right]^T = A(x)+B(x)u \tag{15.2}$$

with

$$A(x)=\left[L_f^{r_1}\sigma_1(x),\ldots,L_f^{r_m}\sigma_m(x)\right]^T.$$

Assumption 15.2. *Solutions of the state differential equation (15.2) with discontinuous right-hand side are defined in the sense of Filippov [24].*

Assumption 15.3. *The vector $A(x)$ and the matrix $B(x)$:*

$$\begin{cases} A(x) = \overline{A}(x)+\Delta_A(x) \\ B(x) = \overline{B}(x)+\Delta_B(x) \end{cases} \tag{15.3}$$

are partitioned into a nominal part, $\overline{A}$ and $\overline{B}$, known a priori, and uncertain bounded functions Δ_A and Δ_B. The matrix $\overline{B}$ is non-singular. Furthermore, there exist an a priori known nonlinear function $\rho(x)$ and an a priori known constant $1 \geq \alpha > 0$ such that the uncertain functions satisfy the following inequalities:

$$\begin{cases} \| \Delta_A(x)-\Delta_B(x)\overline{B}^{-1}(x)\overline{A}(x) \| \leq \rho(x) \\ \| \Delta_B(x)\overline{B}^{-1}(x) \| \leq 1-\alpha \end{cases} \tag{15.4}$$

for $x \in \mathscr{X} \subset \mathbb{R}^n$, $\mathscr{X}$ being an open subset of $\mathbb{R}^n$ within which the boundedness of the system trajectories is ensured.

Apply to the system (15.2) the following preliminary feedback:

$$u = \overline{B}^{-1}\{-\overline{A}+w\} \tag{15.5}$$

where $w=[w_1,\ldots,w_m]^T \in \mathbb{R}^m$ is the auxiliary control input. This feedback partially decouples the nominal system (i.e. without uncertainties). Thus, the system (15.2) can be expressed as follows:

$$\left[\sigma_1^{(r_1)},\ldots,\sigma_m^{(r_m)}\right]^T = \left[I_m+\Delta_B\overline{B}^{-1}\right]w-\Delta_B\overline{B}^{-1}\overline{A}+\Delta_A \tag{15.6}$$

where I_m denotes the $m \times m$ identity matrix.

The r^{th} order SMC of system (15.1) with respect to the sliding variable σ is equivalent to the finite time stabilization of the multivariable uncertain system:

$$\begin{aligned} \dot{z}_{1,i} &= z_{2,i} \\ &\vdots \qquad\qquad , \quad \forall i=\{1,\ldots,m\} \\ \dot{z}_{r_i-1,i} &= z_{r_i,i} \\ [\dot{z}_{r_1,1},\dot{z}_{r_2,2},\ldots,\dot{z}_{r_m,m}]^T &= \left[I_m+\Delta_B\overline{B}^{-1}\right]w-\Delta_B\overline{B}^{-1}\overline{A}+\Delta_A \end{aligned} \tag{15.7}$$

with $1 \leq i \leq m$, $1 \leq j \leq r_i$, $z_{j,i}=\sigma_i^{(j-1)}$, $z_i=[z_{1,i},z_{2,i},\ldots,z_{r_i,i}]^T$ and $z=\left[z_1^T,\ldots,z_m^T\right]^T$.

15.2.2 Design of a Higher Order Sliding Mode Controller

The resolution of the finite time stabilization is a delicate task which has generally been studied for homogeneous systems of negative degree with respect to a flow of a complete vector field. Indeed, for this kind of systems, finite time stability is equivalent to asymptotic stability (see [25, 26, 27, 28, 29, 30] for more details). However, the existing techniques are generally neither constructive nor robust with respect to uncertainties. To the authors' knowledge, a constructive feedback control law for finite time stabilization of all-dimension chain of integrators without uncertainty has only been proposed in [26]. Before designing a robust finite time controller, let us recall the algorithm given in [26].

15.2.2.1 Finite Time Stabilization of an Integrator Chain System

Consider the nominal system of (15.7) (i.e. $\Delta_A = 0$ and $\Delta_B = 0$), which is represented by m single-input single-output independent integrator chains, defined as follows:

$$\forall i \in \{1,\dots,m\}, \quad \begin{cases} \dot{z}_{1,i} &= z_{2,i} \\ &\vdots \\ \dot{z}_{r_i-1,i} &= z_{r_i,i} \\ \dot{z}_{r_i,i} &= w_{nom,i} \end{cases} \tag{15.8}$$

The following result, introduced in [26], proves the existence of a continuous finite time stabilizing feedback controller for system (15.8) by giving an explicit construction involving a small parameter. This controller makes the closed-loop system asymptotically stable and homogeneous of negative degree with respect to a suitable dilation so that finite time stability follows. Note that the proof of asymptotic stability along with a continuity argument is based on the existence of a nonempty compact set that is strictly positively invariant with respect to the closed-loop vector field. One can refer to [26] for further details.

Theorem 15.1. *(Theorem 8.1 in [26]) Let the positive constants $k_{1,i},\dots,k_{r_i,i}$ be such that polynomial $p^{r_i} + k_{r_i,i}p^{r_i-1} + \dots + k_{2,i}p + k_{1,i}$ is Hurwitz. There exists $\varepsilon_i \in (0,1)$ such that, for every $\nu_i \in (1-\varepsilon_i, 1)$, the system (15.8) is stabilized at the origin in finite time under the feedback:*

$$w_{nom,i}(z_i) = -k_{1,i}\,\mathrm{sign}\,(z_{1,i})\,|z_{1,i}|^{\nu_{1,i}} - \dots - k_{r_i,i}\,\mathrm{sign}\,(z_{r_i,i})\,|z_{r_i,i}|^{\nu_{r_i,i}} \tag{15.9}$$

where the standard notation $\mathrm{sign}\,(.)$ *denotes the signum function and $\nu_{1,i},\dots,\nu_{r_i,i}$ satisfy:*

$$\nu_{j-1,i} = \frac{\nu_{j,i}\nu_{j+1,i}}{2\nu_{j+1,i} - \nu_{j,i}},\ j \in \{2,\dots,r_i\}$$

with $\nu_{r_i+1,i} = 1$ and $\nu_{r_i,i} = \nu_i$.

Let us generalize the results given in [26] by designing a robust discontinuous control law which ensures the finite time stabilization of system (15.7).

15.2.2.2 Robust Finite Time Controller Design

The higher order SMC algorithm is designed in two steps:

1. the design of a finite time controller $w_{nom}(z)$ which guarantees the finite time stabilization of the nominal system (15.8) at the origin,
2. the design of a discontinuous control law $w_{disc}(z)$ which enables to reject the uncertainties of the system (15.7) and ensures that the control objectives are fulfilled.

In order to stabilize in finite time the uncertain system (15.7), define the following control law:

$$\begin{cases} w(z) &= w_{nom}(z) + w_{disc}(z, z_{aux}) \\ \dot{z}_{aux} &= -w_{nom}(z) \end{cases} \tag{15.10}$$

The auxiliary function $z_{aux} \in \mathbb{R}^m$ will be used in the design of the sliding variable associated with the discontinuous control law $w_{disc}(z, z_{aux}) \in \mathbb{R}^m$. The control law $w_{nom}(z) = [w_{nom,1}(z_1), \ldots, w_{nom,m}(z_m)]^T \in \mathbb{R}^m$ is given by equation (15.9).

Define the sliding variable $s(z) \in \mathbb{R}^m$, associated with w_{disc}, as follows:

$$s(z) = [z_{r_1,1}, z_{r_2,2}, \ldots, z_{r_m,m}]^T + z_{aux} \tag{15.11}$$

The time derivative of s along the system trajectories is given by:

$$\begin{aligned} \dot{s} &= [\dot{z}_{r_1,1}, \dot{z}_{r_2,2}, \ldots, \dot{z}_{r_m,m}]^T + \dot{z}_{aux} \\ &= \left[I_m + \Delta_B \overline{B}^{-1}\right] w - \Delta_B \overline{B}^{-1} \overline{A} + \Delta_A - w_{nom} \\ &= \left[I_m + \Delta_B \overline{B}^{-1}\right] w_{disc} - \Delta_B \overline{B}^{-1} \overline{A} + \Delta_A + \Delta_B \overline{B}^{-1} w_{nom} \end{aligned}$$

The control law w_{disc} is defined to ensure the sliding motion on $\{x \in \mathscr{X} : s(x) = 0\}$ is guaranteed in spite of uncertainties and is of the following form:

$$w_{disc} = -G(z)\,\mathrm{sign}\,(s) \tag{15.12}$$

where the gain satisfies:

$$G(z) \geq \frac{(1-\alpha)\|w_{nom}(z)\| + \rho + \eta}{\alpha} \tag{15.13}$$

with $\eta > 0$. The notation $\mathrm{sign}\left([s_1, \ldots s_m]^T\right)$ denotes $[\mathrm{sign}\,(s_1), \ldots, \mathrm{sign}\,(s_m)]^T$.

Theorem 15.2. *[31] Consider the nonlinear system (15.1) and assume that assumptions 15.1-15.3 are fulfilled. Then, the control law*

$$u = \overline{B}^{-1}\left\{-\overline{A} + w_{nom}(z) + w_{disc}(z, z_{aux})\right\} \tag{15.14}$$

where $\dot{z}_{aux} = -w_{nom}(z)$, $w_{nom}(z)$ and $w_{disc}(z, z_{aux})$ are given by equations (15.9) and (15.12), respectively, ensures the establishment of a higher order sliding mode with respect to σ in finite time.

Proof. Choose the following Lyapunov function:

$$V = \frac{1}{2} s^T s$$

The time derivative of V along the system trajectories is expressed as:

$$\begin{aligned}\dot{V} &= s^T \left(\left[I_m + \Delta_B \overline{B}^{-1} \right] w_{disc} - \Delta_B \overline{B}^{-1} \overline{A} + \Delta_A + \Delta_B \overline{B}^{-1} w_{nom} \right) \\ &= s^T \left(-G \left[I_m + \Delta_B \overline{B}^{-1} \right] \text{sign}(s) - \Delta_B \overline{B}^{-1} \overline{A} + \Delta_A + \Delta_B \overline{B}^{-1} w_{nom} \right)\end{aligned}$$

Under the bounding relations in Assumption 15.3 and the choice of the gain (15.13), one obtains:

$$\begin{aligned}\dot{V} &\leq -G\|s\| + (1-\alpha)G\|s\| + (1-\alpha)\|w_{nom}\|\|s\| + \rho\|s\| \\ &\leq (-\alpha G + (1-\alpha)\|w_{nom}\| + \rho)\|s\| \\ &\leq -\eta\|s\| \\ &\leq -\eta\sqrt{2}\sqrt{V}\end{aligned}$$

Thus, the system trajectories evolve on the manifold $\{x \in \mathscr{X} : s(x) = 0\}$ in finite time and remains there in spite of the uncertainties. According to Assumption 15.3, the matrix $I_m + \Delta_B \overline{B}^{-1}$ is invertible. In sliding mode, the equivalent control of w_{disc}, denoted w_{disc}^{eq}, obtained by writing $\dot{s} = 0$ (see [32] for further details), is given by:

$$w_{disc}^{eq} = \left[I_m + \Delta_B \overline{B}^{-1} \right]^{-1} \left(\Delta_B \overline{B}^{-1} \overline{A} - \Delta_A - \Delta_B \overline{B}^{-1} w_{nom} \right). \tag{15.15}$$

Substituting $w = w_{nom} + w_{disc}^{eq}$ into (15.7), one obtains the equivalent closed-loop dynamics, in sliding mode, similar to the nominal system (15.8). Since the control law w_{nom} is designed using Theorem 15.1, the system trajectories converge to zero in finite time. Therefore, a r^{th} order sliding mode with respect to σ is established in finite time. □

Remark 15.1. The missing derivatives of σ_i $(1 \leq i \leq m)$ can be estimated on-line by the means of the robust exact finite time convergent differentiator [33].

Remark 15.2. Note that the higher order sliding mode controller is designed to obtain the finite time stabilization of the uncertain chain of integrators (and hence, to increase the convergence accuracy) but does not alleviate the chattering phenomenon. Indeed, because of the new choice of the sliding variable, the discontinuous control is still applied on the control input, as in the classical first order sliding mode case. Nevertheless, a super-twisting algorithm can be used in (15.12) in order to alleviate the chattering phenomenon and the proof of the finite time convergence onto the manifold $\{x \in \mathscr{X} : s(x) = 0\}$ can also be shown using Lyapunov arguments.

15.3 Collaborative Robotics Issues

15.3.1 Context

Cooperative robotics is concerned with a network of robots exchanging information in order to tackle a common problem. Thus, cooperative multi-robot systems have the possibility to solve problems more efficiently than a single one, but also problems that cannot be handled by a single one. Such deployment of large scale networks of cooperative robots can also provide complex behaviors by using simple agent based behaviors.

Tasks of cooperative robotics concern socially useful applications of robotics that can be found in the military, civil and spatial domains. It concerns missions which were historically automated, either because they represent a danger or a certain difficulty for a human being, or because a machine is more adapted and more effective than human operators. Robotics service (handling, cleaning, surveillance) covers certain needs untreated today, because they are difficult to be handled by operators. Thus, cooperative robotics, strongly imbricated with service robotics, concerns a lot of applications in which the researchers are particularly interested:

1. The carriage of loads and the collection of objects in dangerous areas.
2. The use of cooperative machines on building zones may speed up their achievement, increase security and allow operations that are impracticable for humans.
3. For the detection and the coordinated neutralization of land mines, the cooperation would allow to cover the widest zone without involving more human operators, while reducing the duration of the operation.
4. The security/surveillance of private properties: the surveillance and the detection of intrusion are tasks that robots can typically carry out. Cooperation allows the surveillance of a larger area.

Beyond the scientific interest to make cooperative robots interacting rationally with their environment and the fundamental research problems to be tackled, the considered problem has important social and economic stakes. Today, mobile robots become more and more complex, integrate capacities of perception, communication and adaptation to various operation domains and aim at meeting better and better robustness, ergonomics and safety requirements.

15.3.2 Control Issues

The results presented in this chapter have been obtained within a multidisciplinary research framework, the Robocoop project, started in 2003 at the LAGIS laboratory, which deals with issues in cooperative mobile robots. The software architecture of each robot of the swarm proposed in this paper is depicted in figure 15.1.

The blocks “Perception” and “Localization” receive information from the proprioceptive and exteroceptive sensors of the robot. In the “Localization” block, the information is processed in order to obtain the robot position and orientation. In the “Perception” block, the measurements obtained from the sensors are used in

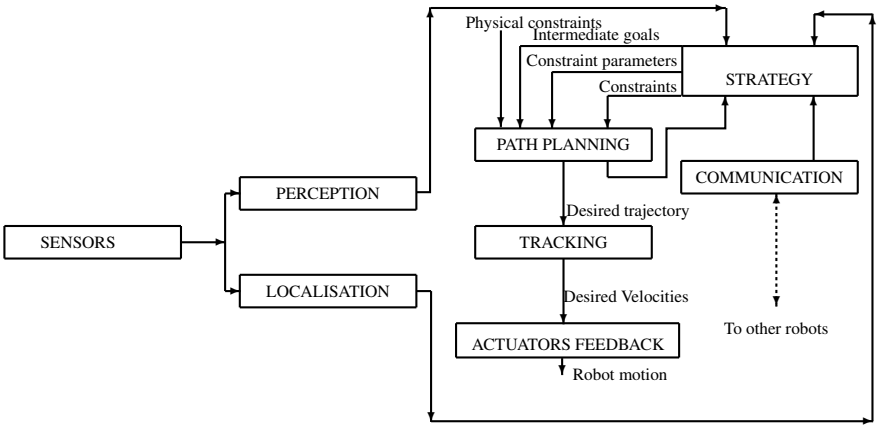

Fig. 15.1 Software architecture for an autonomous mobile robot.

order to obtain information about the position and the shape of the obstacles in the robot neighborhood. The block "Strategy" receives information about the robot localization and the environment, and about the internal state of the robot. With this information, it must evaluate the robot situation, and if necessary, it can ask complementary information to the robots in its neighborhood in order to make a decision about the direction of the robot movement.

Aspects such as localization and strategy designs are currently under investigation. In this chapter, under the assumption that the robots have the knowledge of their localization on the map and information about the obstacles in their neighborhood, algorithms are proposed to solve the problems of:

- collaborative path planning,
- higher order sliding mode based collaborative control design for mobile robots including robust path tracking control.

15.3.3 Problem Formulation and Navigation Strategy

15.3.3.1 Dynamic Model of the Robots

Each robot $\mathscr{A}_n$, $n \in (1,\ldots,N)$, shown in Fig. 15.2, is of unicycle-type. Its two fixed driving wheels of radius r_n, separated by $2\rho_n$, are independently controlled by two actuators (DC motors) and the passive wheel prevents the robot from tipping over as it moves on a plane. Its configuration is given by:

$$\eta_n = [x_n, y_n, \theta_n]^T$$

where (x_n, y_n) is the position of its center of mass C_n and θ_n is its orientation in the global frame.

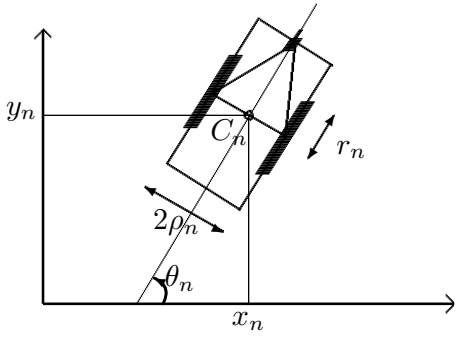

Fig. 15.2 Unicycle-type robot.

Under the pure rolling and non slipping condition [34], the ideal kinematic equations are:

$$\dot{\eta}_n = \begin{bmatrix} \cos\theta_n & 0 \\ \sin\theta_n & 0 \\ 0 & 1 \end{bmatrix} \begin{bmatrix} v_n \\ w_n \end{bmatrix} \tag{15.16}$$

where v_n and w_n are the linear and angular velocities, respectively.

Remark 15.3. Due to practical limitations, the speed $u_n = [\dot{x}_n, \dot{y}_n]^T$ of $\mathscr{A}_n$ is restricted to lie in a closed interval $\mathscr{S}_n$

$$\mathscr{S}_n = \left\{ u_n \in \mathbb{R}^2 \mid \|u_n\| \leq u_{n,max} \right\} \tag{15.17}$$

15.3.3.2 Assumptions and Control Objective

Assumption 15.4. *The following assumptions are made in this study:*

- *Each robot $\mathscr{A}_n$ ($n \in \{1,\ldots,N\}$) knows its position $p_n = [x_n, y_n]^T$, its velocity $u_n = [\dot{x}_n, \dot{y}_n]^T$ and its goal position $p_{n,des} = p_n(t_{fin})$ (t_{fin} is the final time instant). Note that the task location $p_{n,des}$ is chosen by some kind of high-level directive, for instance, the output of a task allocation problem.*
- *Each mobile robot has a physical safety area which is centered at C_n with a radius R_n, and has a circular communication area which is also centered at C_n with a radius $\bar{R}_n$. Note that $\bar{R}_n$ is strictly larger than $R_n + R_j$, $j \in (1,\ldots,N), j \neq n$.*
- *Robots have on-board sensors which can detect surrounding objects and vehicles within a range with a small margin of error.*
- *The obstacles are static and convex. Without loss of any generality[1], the i^{th} ($i = 1,\ldots$) obstacle in the environment is included in a 2-D circle, denoted by $\mathscr{B}_i(p_{obs_i}, R_{obs_i})$ where $p_{obs_i} = (X_i, Y_i)$ is its center and R_{obs_i} is its radius.*

[1] It is trivial to allow the envelope of an obstacle to be represented by union/intersection of several circles. The envelopes could also be polygonal. Mathematically, circular envelopes can be represented by second order inequalities while polygonal envelopes can be described by first order linear inequalities.

- *Each robot $\mathscr{A}_n$ can reliably communicate with the other robots $\mathscr{A}_j$ ($j \neq n$, $j \in \{1,\ldots,N\}$) of the swarm in its communication area.*

Definition 15.2. $\forall t_k \in \left[t_{ini}, t_{fin}\right]$ (t_{ini} is the initial time instant), $\forall \mathscr{A}_n$ ($n \in \{1,\ldots,N\}$), the detected obstacle set $\mathscr{O}_n(t_k)$ is defined as the subset

$$\mathscr{O}_n(t_k) \subset \{\mathscr{B}_1(p_{obs_1}, R_{obs_1}), \mathscr{B}_2(p_{obs_2}, R_{obs_2}), \ldots,\}$$

of obstacles in the range of the robot sensors.

Note that the detected obstacle set is time dependent and evolves as long as the robot moves and discovers new obstacles (see Fig. 15.3-15.4). In order to ensure the collision avoidance with obstacles, for all $t \geq 0$, the distance between the robot and the detected obstacles (i.e $O_{m_n} \in \mathscr{O}_n(t)$), $\|p_n(t) - p_{obs_{m_n}}\|$ must satisfy:

$$\|p_n(t) - p_{obs_{m_n}}\| \geq R_n + R_{obs_{m_n}} \tag{15.18}$$

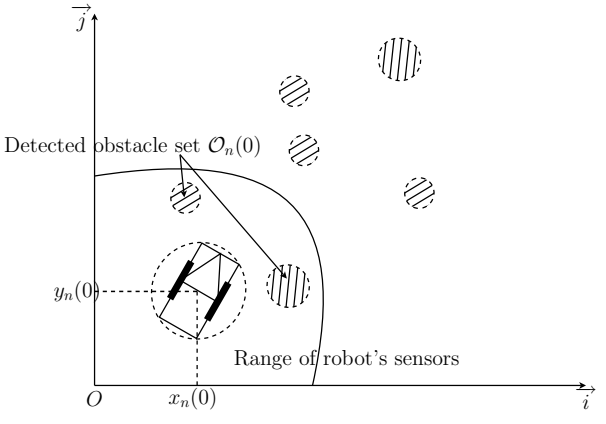

Fig. 15.3 Detected obstacle set at time $t_k = 0s$.

The objective is to find the control input τ_n for each robot $\mathscr{A}_n$ such that, under Assumption 15.4:

- $\mathscr{A}_n$ is stabilized toward its desired point $p_{n,des}$, i.e.

$$\lim_{t \to \infty} \|p_n(t) - p_{n,des}\| = 0 \tag{15.19}$$

- collisions between robots are avoided,
- obstacles avoidance is ensured,
- physical limitations of robots are satisfied,
- all computations are done on board in a decentralized cooperative way.

In order to solve this problem, reference trajectories that satisfy the above requirements and that can be computed on-line are designed. Then, sliding mode control laws that ensure the robust tracking of the reference trajectories are derived.

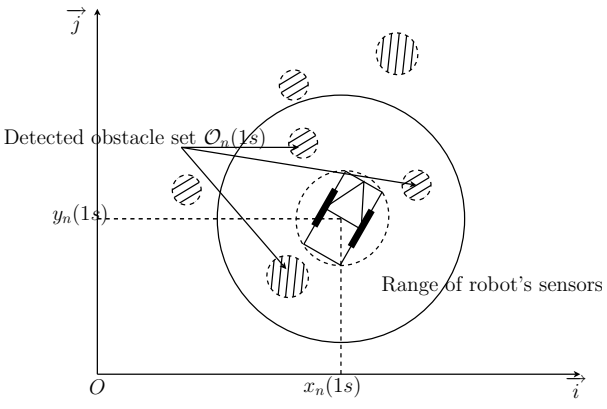

Fig. 15.4 Detected obstacle set at time $t_k = 1s$.

15.3.4 Path Planning

The aim of path planning is to compute admissible trajectories for a swarm of mobile robots such that they can evolve in an unknown environment from an initial configuration to a final configuration without collision and, eventually, in minimal time respecting an acceptable geometrical shape during the movement. Some constraints must be taken into account:

- constraints due to physics (energy limitation, maximal velocity and acceleration of the robots)
- obstacle avoidance,
- collision avoidance with the robots and other mobile objects,
- distances between robots (communication constraints),
- geometry of the formation,
- time constraints (in the case of rescue missions), energy constraints (batteries duration, ...).

The path planning problem is expressed as an optimal problem under constraints: find the optimal control and the optimal trajectory of each robot which minimize a cost function (i.e. minimal time or minimal energy or a mix between minimal time and minimal energy) and which satisfies the constraints enumerated above. In order to solve this problem in real time, we proposed an approach based on dynamical optimization over a sliding horizon and based on the flatness property.

First a scheme of coordination according to the method described above was designed *via* a global supervisor, which can be seen as a the leader of the swarm (centralized approach). In that case, the supervisor generates trajectories for all the vehicles by solving an optimization problem of large dimension. However, the lack of autonomy of robots with regard to the supervisor, the centralization of the information and the costs in terms of calculation time make difficult the on-line implementation of this strategy.

In order to get rid of these drawbacks, and to strongly decentralize the path planning algorithm, we propose an on-line decentralized algorithm on a sliding horizon, based only on the available local information for each robot. It consists in decomposing the problem of path planning of each robot into two steps. In the first one, every robot builds an intuitive trajectory using local information and taking only the obstacles into account. In the same time, each robot analyzes, by using its sensors, the potential problems which may appear (loss of communication or collision with another robot). In the second one, the robots which can be in collision or loose the communication with the other robots of the swarm adjust their intuitive trajectories by taking constraints of communication and of collision avoidance with the robots into account. This distributed implementation increases not only the autonomy of robots, but also reduces the complexity in term of calculations with regard to a centralized implementation.

The purpose of the distributed receding horizon planner is to decompose the overall problem into a family of simple receding horizon planning problems which are implemented on each robot $\mathscr{A}_n$.

Definition 15.3. [36] (*conflict*) A conflict occurs between two cooperative robots $\mathscr{A}_n$ and $\mathscr{A}_j$ at time $t_k \geq t_{ini}$ if they are not in collision at t_k, but at some future time, a collision may occur.

The following proposition, based on the concept of velocity obstacle [37], is useful to check the occurence of conflicts.

Lemma 15.1. *[38] Define for each pair $(\mathscr{A}_n, \mathscr{A}_j)$, the following variables depicted in Fig. 15.5:*

$$\beta_{nj}(t_k) = \arg(u_n(t_k) - u_j(t_k)) - \arg(p_j(t_k) - p_n(t_k))$$
$$\alpha_{nj}(t_k) = \arcsin\left(\frac{R_n + R_j}{\|p_j(t_k) - p_n(t_k)\|}\right)$$

A necessary and sufficient condition for no conflict between $\mathscr{A}_n$ and $\mathscr{A}_j$ at t_k is:

$$|\beta_{nj}(t_k)| \geq \alpha_{nj}(t_k) \tag{15.20}$$

Definition 15.4. (*conflict subset*) For each $\mathscr{A}_n$, the conflict subset $\mathscr{N}_n(t_k)$ at time $t_k \geq t_{ini}$ is the set of all robots which are in the communication area of $\mathscr{A}_n$ and in conflict with $\mathscr{A}_n$.

In every distributed optimal control problem, the same constant planning horizon $T_p \in \mathbb{R}^+$ and constant update period $T_c \in \mathbb{R}^+$ ($T_c < T_p$) are used. In practice, T_c is typically the time allocated for the resolution of the distributed optimal control problem. At each update, denoted t_k ($k \in \mathbb{N}$),

$$t_k = t_{ini} + kT_c \tag{15.21}$$

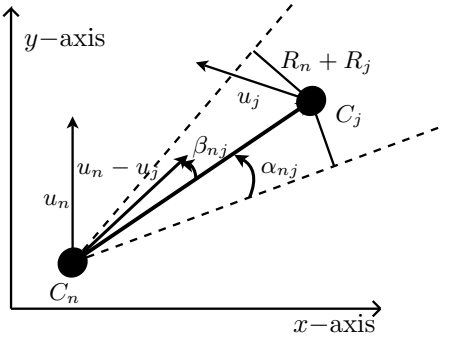

Fig. 15.5 Velocity obstacle concept

each robot computes, in parallel, an optimal planned collision-free trajectory. The distribution is achieved by having each vehicle exchanging its presumed information with other vehicles. A key element of this work is that the vehicles must only exchange information with robots belonging to the conflict set, enabling the local optimization to be based on local information. This is important because it reduces the communication requirements and the computational complexity.

First, every vehicle $\mathscr{A}_n$ must presume some preferred trajectories for robots $\mathscr{A}_j$ belonging to the conflict subset in order to plan its optimal conflict-free trajectory. Two difficulties can be stated:

- the definition of a unique presumed trajectory for each robot,
- the coherence between what a vehicle plans to do (the real optimal planned trajectory) and what the other robots believe that the vehicle will plan to do (the presumed trajectory).

The proposed solution is to divide each receding horizon planning problem into two steps. In each time interval $[t_{k-1}, t_k)$,

Step 1. Each robot $\mathscr{A}_n$ computes its **presumed trajectory**, denoted by $\widehat{p}_n(t, t_k)$ and its corresponding velocity, denoted by $\widehat{u}_n(t, t_k)$. This trajectory is obtained without taking the coupling constraints (i.e. collision avoidance between robots) into account.

Step 2. The robots which may produce collision adjust their presumed trajectory by taking the collision avoidance constraint into account and using local exchanged information. This new trajectory, denoted by $p_n^*(t, t_k)$, is called the **optimal planned trajectory** and is evaluated over the planning horizon T_p, i.e. $t \in [t_k, t_k + T_p]$. It is the trajectory that the robot must track during the time interval $[t_k, t_{k+1}]$. The associated velocities are denoted by $u_n^*(t, t_k)$.

Remark 15.4. Note that the first argument of p_n^*, $\widehat{p}_n$, u_n^* and $\widehat{u}_n$ denotes time. The second argument is only added to distinguish at which receding horizon update the trajectory and velocity are computed.

The collection of distributed receding horizon planning problems is formally defined as Problems 1-2 for each robot $\mathscr{A}_n$.

Problem 1: Over each interval $[t_{k-1}, t_k)$, let the following optimal control problem associated with the n^{th} robot which consists in determining the presumed velocity $\widehat{u}_n(t,t_k)$ and the presumed trajectory $\widehat{p}_n(t,t_k)$ which do not take the coupling constraint into account:
Find: the feasible presumed pair $(\widehat{p}_n(t,t_k), \widehat{u}_n(t,t_k))$ subject to $\forall t \geq t_k$:

$$\begin{cases} \widehat{p}_n(t_k,t_k) & = p_n^*(t_k,t_{k-1}) \\ \widehat{u}_n(t_k,t_k) & = u_n^*(t_k,t_{k-1}) \\ \|\widehat{p}_n(t,t_k) - p_{obs_{m_n}}\| & \geq R_n + R_{obs_{m_n}}, \ \forall O_{m_n} \in \mathscr{O}_n(t_{k-1}) \\ \widehat{u}_n(t,t_k) & \in \mathscr{S}_n \end{cases} \tag{15.22}$$

Remark 15.5. During the initialization step, that is to say before the robots move, we denote:

$$\begin{cases} t_{-1} & = t_{ini} \\ p_n^*(t_0,t_{-1}) & = p_n(t_{ini}) \\ u_n^*(t_0,t_{-1}) & = u_n(t_{ini}) \end{cases}$$

Problem 2: For each robot $\mathscr{A}_n$, define the optimal control problem over each interval $[t_{k-1}, t_k)$, which consists in:

Given: the conflict subset $\mathscr{N}_n(t_{k-1})$, the presumed pairs $(\widehat{p}_i(t,t_k), \widehat{u}_i(t,t_k))$, $\forall i \in \{i \in \mathbb{N} \mid \mathscr{A}_i \in \mathscr{N}_n(t_{k-1})\}$.

Find: the feasible optimal collision-free trajectory and velocity pairs $(p_n^*(t,t_k), u_n^*(t,t_k))$ that minimizes:

$$\int_{t_k}^{t_k+T_p} \left(a_n \sum_i U_{ni,rep}(t) + \|p_n^*(t,t_k) - \widehat{p}_n(t,t_k)\| \right) dt \tag{15.23}$$

subject to $\forall t \in [t_k, t_k + T_p]$:

$$\begin{cases} p_n^*(t_k,t_k) & = p_n^*(t_k,t_{k-1}) \\ u_n^*(t_k,t_k) & = u_n^*(t_k,t_{k-1}) \\ \|p_n^*(t,t_k) - p_{obs_{m_n}}\| & \geq R_n + R_{obs_{m_n}}, \ \forall O_{m_n} \in \mathscr{O}_n(t_{k-1}) \\ u_n^*(t,t_k) & \in \mathscr{S}_n \end{cases} \tag{15.24}$$

where

$$\begin{aligned} U_{ni,rep}(t) &= \begin{cases} 0 & \text{if } d_{ni}(t) \geq b_n \\ \frac{1}{2}\left(\frac{1}{d_{ni}(t)} - \frac{1}{b_n}\right)^2 & \text{else} \end{cases} \\ d_{ni}(t) &= \|p_n^*(t,t_k) - \widehat{p}_i(t,t_k)\| - (R_n + R_i) \end{aligned} \tag{15.25}$$

a_n and b_n are strictly positive factors which can vary among robots to reflect differences in aggressiveness ($a_n < 1$, $b_n \ll 1$) and shyness ($a_n > 1$, $b_n \gg 1$).

Remark 15.6. One can note that the first part of the cost (15.23) is designed to enforce the collision avoidance between cooperative robots. This term, based on artificial potential fields [2], is designed such that it equals to infinity when a collision between robots occurs and decreases according to the relative distance between robots.

The second part of the cost (15.23), i.e. the term $\|p_n^*(t,t_k) - \widehat{p}_n(t,t_k)\|$, is a way of penalizing the deviation of the optimal planned trajectory $p_n^*(t,t_k)$ from the presumed trajectory $\widehat{p}_n(t,t_k)$, which is the trajectory that other robots rely on. In previous work, this term was incorporated into the decentralized receding horizon planner as a constraint [39]. The formulation presented here is an improvement over this past formulation, since the penalty yields an optimization problem that is much easier to solve.

Remark 15.7. One can note that the constraints (15.24) which guarantee the continuity of the trajectory and control inputs require the optimal trajectory $p_n^*(t_k,t_{k-1})$ and velocity $u_n^*(t_k,t_{k-1})$ computed in the previous step. Therefore, the proposed planner is not able to reject external disturbances or inherent discrepancies between the model and the real process. However, it takes the real time constraint into account. Indeed, each robot has a limited time to plan its trajectory. The time allocated to make its decision depends on its perception sensors, its computation delays, etc. and is less than the update period T_c (see Fig. 15.6).

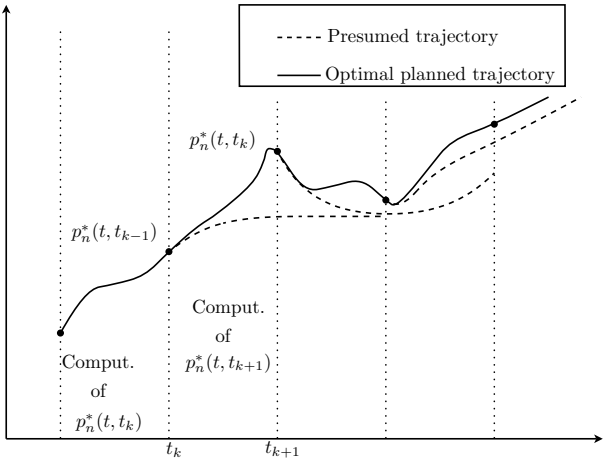

Fig. 15.6 Implementation of the receding horizon planner

Remark 15.8. A compromise must be done between reactivity and computation time. Indeed, the planning horizon must be sufficiently small in order to have good enough results in terms of computation time. However, it must be higher than the update period to guarantee enough reactivity.

To numerically solve Problems 1-2, a nonlinear trajectory generation algorithm [40] is applied. It is based on finding trajectory curves in a lower dimensional space

using the flatness property (see [35]). Flatness means that all the state variables and the inputs of a dynamical system can be parameterized in terms of so-called flat outputs (or linearizing outputs) and a finite number of their successive time derivatives. This is the case of most of mobile robots, for which the flat outputs are the coordinates of the center of gravity up to a translation. For example, for the unicycle type mobile robot which model is described by equations (15.16). The flat outputs are (x_n, y_n). Indeed, one has: $\theta_n = \arctan\left(\frac{\dot{y}_n}{\dot{x}_n}\right)$, $v_n = \pm\sqrt{\dot{x}_n^2 + \dot{y}_n^2}$ and $w_n = \frac{\dot{x}_n\ddot{y}_n - \dot{y}_n\ddot{x}_n}{\dot{x}_n^2 + \dot{y}_n^2}$. Using this property, all the dynamics of the vehicles, as well as the constraints, can be expressed as functions of the flat outputs and their time derivatives.

Then, the problem is to minimize a criteria that only depends on the flat outputs and their time derivatives. This optimal problem can be easily transformed into a nonlinear programming problem, using B-spline functions in order to approximate the trajectory of the flat outputs (a constrained feasible sequential quadratic optimization algorithm is used to find the B-splines coefficients that optimize the performance objective while respecting the constraints), and also to deduce the optimal control $u(t) = [v(t), w(t)]^T$ and the optimal trajectory $p^*(t) = [x^*(t)\ y^*(t)\ \theta^*(t)]^T$.

This algorithms was tested and compared with other existing methods (the details of these results can be found in [39]) and advantages of the approach were highlighted in terms of low computation time, communication resources, easiness of implementation (such as the number of parameters), high performances and the fact that there is no supervisor.

15.3.5 Path Tracking

Due to the use of the flatness property, the reference trajectory $(x_n^*, y_n^*, \theta_n^*)$, generated by the motion planner, fulfills the differential system:

$$\begin{bmatrix} \dot{x}_n^* \\ \dot{y}_n^* \\ \dot{\theta}_n^* \end{bmatrix} = \begin{bmatrix} \cos\theta_n^* & 0 \\ \sin\theta_n^* & 0 \\ 0 & 1 \end{bmatrix} \begin{bmatrix} v_n^* \\ w_n^* \end{bmatrix} \tag{15.26}$$

By directly applying v_n^* and w_n^*, the robots do not follow the reference trajectory. Indeed, in practical applications, they operate under uncertainty conditions. Once the desired trajectories have been computed, robust control algorithms must be designed so that the robots accurately track the reference trajectories in spite of model uncertainties and external perturbations. Two different cases are described here: tracking with and without coordination between robots.

15.3.5.1 Tracking Problem without Coordination

The simplest scenario for the swarm navigation is to assume that the robots have to track accurately the planned trajectory without any constraints with respect to their relative positions. In this subsection, the index n is dropped to simplify the notation. In order to express the unicycle type model (15.16) in a form more suitable for the control design, the global invertible transformation is defined [42]:

$$\left[z, X^T\right]^T = T \quad \left[\widetilde{x}, \widetilde{y}, \widetilde{\theta}\right]^T \tag{15.27}$$

where the transformation matrix T is defined as:

$$T = \begin{bmatrix} \widetilde{\theta}\cos\theta - 2\sin\theta & \widetilde{\theta}\sin\theta + 2\cos\theta & 0 \\ 0 & 0 & 1 \\ \cos\theta & \sin\theta & 0 \end{bmatrix} \tag{15.28}$$

where $z \in \mathbb{R}$ and $X = [x_1, x_2] \in \mathbb{R}^2$ are auxiliary tracking error variables, $\widetilde{x}$, $\widetilde{y}$, $\widetilde{\theta}$ are the difference between the actual and the reference trajectories, i.e:

$$\widetilde{x} = x - x^* \quad \widetilde{y} = y - y^* \quad \widetilde{\theta} = \theta - \theta^* \tag{15.29}$$

After taking the time derivative of (15.27), the error dynamics can be expressed as:

$$\begin{cases} \dot{z} &= Y^T JX + P \\ \dot{X} &= Y \end{cases} \tag{15.30}$$

where J is a constant, skew symmetric matrix defined as:

$$J = \begin{bmatrix} 0 & -1 \\ 1 & 0 \end{bmatrix}$$

and $P = -2\left(w^* x_2 - v^* \sin x_1\right)$.
The auxiliary variable $Y = [y_1, y_2]^T$ introduced in (15.30) is defined as follows:

$$\begin{cases} y_1 &= w - w^* \\ y_2 &= v - w\left(\widetilde{x}\sin\theta - \widetilde{y}\cos\theta\right) - v^*\cos\ \widetilde{\theta} \end{cases} \tag{15.31}$$

In many works about the stabilization of nonholonomic systems, the derived control laws are of discontinuous type and may lead to discontinuous velocities in practice. This difficulty can be overcome by taking into account the dynamic model of the mobile robot such that the discontinuous part of the control is embedded in the higher time derivatives of the mechanical parts. This remains to add integrators in the model as follows:

$$\begin{cases} \dot{z} &= Y^T JX + P \\ \dot{X} &= Y \\ \dot{Y} &= U \end{cases} \tag{15.32}$$

where $U \in \mathbb{R}^2$ is the new control input.

Due to the presence of uncertainties, it is of practical interest to study the following uncertain nonlinear system:

$$\dot{z} = Y^T JX + \pi_1(\Xi, t) \tag{15.33}$$

$$\dot{X} = Y + \pi_2(\Xi, t) \tag{15.34}$$

$$\dot{Y} = U + \pi_3(\Xi, t) \tag{15.35}$$

where the state vector is $\Xi = [z, X^T, Y^T]^T \in \mathbb{R}^5$ and the control input is $U \in \mathbb{R}^2$. $\pi_i(\Xi,t)$ represent parametric uncertainties or disturbances and are assumed to be sufficiently smooth functions such that:

$$\begin{array}{l} \|\pi_i(\Xi,t)\| \leq \Pi_i(\Xi),\ i=1,2,3 \\ \|\dot{\pi}_i(\Xi,t)\| \leq \bar{\Pi}_i(\Xi),\ i=1,2 \end{array} \tag{15.36}$$

where Π_i and $\bar{\Pi}_i$ are known nonnegative functions. It is worth stressing, that if $\pi_1(\Xi,t) \neq 0$ and $\pi_2(\Xi,t) \neq 0$, the disturbance is not satisfying the well-known matching condition and is not assumed to be vanishing.

The system (15.33)-(15.35), if undisturbed, can be seen as the interconnection of two subsystems: a 4^{th} order one represented by a chain of two $2-$dimensional integrators with drift terms, and a scalar nonlinear system whose dynamics is entirely driven by the subsystem (15.33).

Remark 15.9. It can be noticed that it is essential to stabilize z first. Indeed, if $\pi_1(\Xi,t) = 0$, once X and Y are stabilized, one can no longer set the $z-$dynamics.

The problems considered is to find stabilizing control laws for (15.33)-(15.35) in spite of the presence of uncertainties.

Since z has to be stabilized first, it appears interesting to set the following sliding variable $[\sigma_1, \sigma_2]^T \in \mathbb{R}^2$ as:

$$\begin{array}{l} \sigma_1 = \dot{z} + k_1 z \\ \sigma_2 = \dot{\psi} + k_2 \psi \end{array} \tag{15.37}$$

with

$$\psi = \frac{1}{2} X^T X - \varphi(z) - \frac{1}{2}\varepsilon \tag{15.38}$$

k_1, k_2 are strictly positive constants, $0 < \varepsilon \ll 1$ and $\varphi : \mathbb{R} \to \mathbb{R}_{>0}$ is a twice differentiable positive definite function. Applying a second order sliding mode controller as defined in Section 17.4, the practical stabilization of the tracking errors is ensured. The details of these results can be found in [41, 42]).

15.3.5.2 Tracking Problem with Coordination

Here, it is assumed that a specific geometric shape of the swarm of robots has to be kept. For this, a control scheme based on a leader-follower approach is developed and the following model, that take into account the independent actuators of the wheels and the uncertainties, is considered (see [43]):

$$\begin{bmatrix} \ddot{x}_n \\ \ddot{y}_n \\ \ddot{\theta}_n \end{bmatrix} = \begin{bmatrix} -\dot{y}_n \dot{\theta}_n \\ \dot{x}_n \dot{\theta}_n \\ 0 \end{bmatrix} + \begin{bmatrix} \cos\theta_n & 0 \\ \sin\theta_n & 0 \\ 0 & 1 \end{bmatrix} (I_2 + \Delta_n)\, T_n + \pi_n \tag{15.39}$$

where

- the control input is $T_n = \left[\frac{F_n}{m_n}, \frac{\tau_n}{J_n}\right]^T$. m_n and J_n are the known nominal robot mass and moment of inertia. F_n and τ_n denotes the force and the torque, respectively.

- I_2 denotes the 2×2 identity matrix,
- π_n stands for the disturbances (slipping or skidding effects),
- $\Delta_n = \begin{bmatrix} \varepsilon_n & 0 \\ 0 & \varepsilon_n' \end{bmatrix}$ where ε_n and ε_n' represents variations on the mass and the inertia of the robot, respectively.

To achieve the coordinated tracking control without using GPS systems for each robot, a decentralized strategy based on a leader-follower approach is proposed. Figure 15.7 presents the motion on a plane for two neighboring unicycles. Let $l_{ik} \in \mathbb{R}_{>0}$ be the relative distance between $\mathscr{A}_i$ and $\mathscr{A}_k$:

$$l_{ik} = \sqrt{(x_i - x_k - d\cos\theta_k)^2 + (y_i - y_k - d\sin\theta_k)^2} \tag{15.40}$$

where d is the distance between C_k and the front of the robot. The coordinates $(x_k + d\cos\theta_k, y_k + d\sin\theta_k)$ denote the position of the camera of $\mathscr{A}_k$. Let $\psi_{ik} \in (-\pi, \pi]$ be the relative bearing defined as:

$$\psi_{ik} = \pi + \zeta_{ik} - \theta_i \tag{15.41}$$

and $\zeta_{ik} = \arctan \frac{y_i - y_k - d\sin\theta_k}{x_i - x_k - d\cos\theta_k}$.

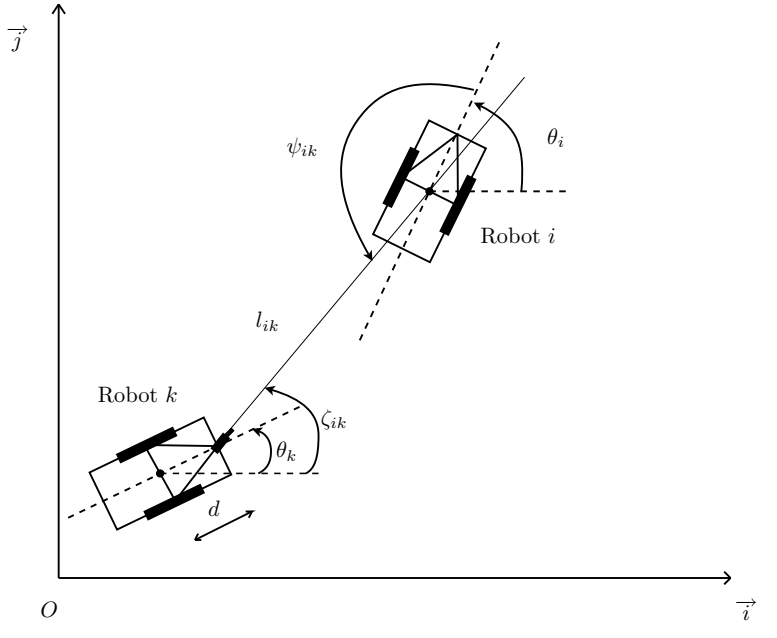

Fig. 15.7 Leader-follower pair.

Remark 15.10. If each robot is equipped with a pan-controlled monochromatic camera, the relative coordinates l_{ik} and ψ_{ik} can be estimated from a single image [44].

Definition 15.5. *(Formation geometry)* The required geometry of the formation is given by:

- $\eta_1^* = (x_1^*, y_1^*, \theta_1^*)$ being tracked by the formation's leader[2]
- the desired relative distance l_{ik}^* and angle ψ_{ik}^* between $\mathscr{A}_i$ and $\mathscr{A}_k$. These desired time-varying parameters are computed from the optimal planned trajectories using equations (15.40)-(15.41).

Let $h_{ik} = [l_{ik}, \psi_{ik}]^T$ be the relative configuration of $\mathscr{A}_k$ with respect to $\mathscr{A}_i$. Differentiating twice l_{ik} and ψ_{ik} yields:

$$\ddot{h}_{ik} = \Upsilon(I_2 + \Delta_k)T_k + F + P \tag{15.42}$$

where

- $\Upsilon = \begin{bmatrix} \cos\varphi_{ik} & d\sin\varphi_{ik} \\ \frac{-\sin\varphi_{ik}}{l_{ik}} & \frac{d\cos\varphi_{ik}}{l_{ik}} \end{bmatrix}$ is a non-singular matrix,
- $\varphi_{ik} = \psi_{ik} + \theta_{ik}$,
- $\theta_{ik} = \theta_i - \theta_k$,
- P reflects the disturbances and the parameter variations.

The control objective is to design a robust control law T_k that allows $\mathscr{A}_k$ to track its leader $\mathscr{A}_i$ with a desired relative configuration $h_{ik}^* = \left[l_{ik}^*, \psi_{ik}^*\right]^T$.

Define the tracking error vector $e_{ik} \in \mathbb{R}^4$ as:

$$e_{ik} = \left[e_{ik,1}^T, e_{ik,2}^T\right]^T \tag{15.43}$$

where $e_{ik,1}$ and $e_{ik,2} \in \mathbb{R}^2$ are defined by:

$$\begin{cases} e_{ik,1} = h_{ik}^* - h_{ik} \\ e_{ik,2} = \dot{h}_{ik}^* - \dot{h}_{ik} \end{cases} \tag{15.44}$$

The tracking error dynamics is expressed as:

$$\dot{e}_{ik} = \begin{bmatrix} e_{ik,2} \\ \ddot{h}_{ik}^* - \Upsilon(I_2 + \Delta_k)T_k - F - P \end{bmatrix} \tag{15.45}$$

Assumption 15.5. *It is assumed that each robot knows:*

- *its relative position* $[l_{ik}, \psi_{ik}]$,
- *its relative orientation* θ_{ik}.

[2] For a unicycle type mobile robot, a saturated robust controller has been proposed in [45] to asymptotically stabilize the tracking errors $x_1^* - x_1$, $y_1^* - y_1$ and $\theta_1^* - \theta_1$ in spite of the uncertainties.

Define the sliding variable as follows:

$$\sigma_k = \begin{bmatrix} \sigma_{1,k} \\ \sigma_{2,k} \end{bmatrix} = e_{ik,1} \tag{15.46}$$

The control objective is to generate a second order SMC on the suitable sliding surface σ_k for each follower, that is to say to constrain the system trajectories to evolve on:

$$\{e_{ik} : \sigma_k = \dot{\sigma}_k = 0\}.$$

The second time derivative of σ_k yields:

$$\ddot{\sigma}_k = \ddot{h}^*_{ik} - \Upsilon(I_2 + \Delta_k)T_k - F - P \tag{15.47}$$

Define the following state feedback control:

$$T_k = -\Upsilon^{-1}\left(\begin{bmatrix} v_{1,k} \\ v_{2,k} \end{bmatrix} - \ddot{h}^*_{ik} + F\right) \tag{15.48}$$

such that one gets:

$$\ddot{\sigma}_k = \left(I_2 + \Upsilon\Delta_k\Upsilon^{-1}\right)\tau_k - \overline{P} \tag{15.49}$$

where

$$\overline{P} = P + \Upsilon\Delta_k\Upsilon^{-1}\ddot{h}^*_{ik}$$

Assumption 15.6. *It is supposed that there are an a priori known nonlinear function* $\rho(e_{ik})$ *and an a priori known constant* $1 \geq \alpha > 0$ *such that the parameter variations satisfy the following inequalities:*

$$\begin{cases} \| \overline{P} \| & \leq \rho(e_{ik}) \\ \| \Upsilon\Delta_k\Upsilon^{-1} \| & \leq 1 - \alpha \end{cases} \tag{15.50}$$

Apply the proposed sliding mode controller defined in Section 17.4:

$$\begin{cases} \tau_k &= \tau_{nom,k} + \tau_{disc,k} \\ \dot{z}_{aux} &= -\tau_{nom,k} \\ \tau_{nom,k} &= -k_{1,k}\,\mathrm{sign}\,(\sigma_k)\,|\sigma_k|^{v_{1,k}} - k_{2,k}\,\mathrm{sign}\,(\dot{\sigma}_k)\,|\dot{\sigma}_k|^{v_{2,k}} \\ \tau_{disc,k} &= -\Upsilon\,\mathrm{sign}\,(\dot{\sigma}_k + z_{aux}) \end{cases}$$

where the term τ_{nom} is obtained via Theorem 15.1 and the gain Υ is tuned in order to satisfy condition (15.13). Then, the swarm of the robots is asymptotically stabilized to the desired formation. The details of these results can be found in [43].

15.3.6 Experimental Results

The experiments are performed with a team of three nonholonomic mobile robots which are two wheels differentially driven robots as shown in Fig. 15.8. The geometrical shape of each robot $\mathscr{A}_n$ is included in a circle of radius $R_n = 0.2$m. The

Fig. 15.8 The Pekee nonholonomic mobile robots.

robot Pekee is equipped with 15 infra-red telemeters sensors, two encoders, a WiFi wireless cartridge and a miniature color vision camera C-Cam8.

A limitation of the embedded vision camera is that its resolution quickly decreases with the distance of the objects. Indeed, the range of this sensor is about 1.5m. The localization and mapping method reported in [46] are applied.

We also consider communication constraints given by:

$$\begin{cases} \|p_1(t) - p_2(t)\| \leq d_{com}, \\ \|p_2(t) - p_3(t)\| \leq d_{com}, \end{cases} \tag{15.51}$$

where $d_{com} = 2.5$m is the broadcasting range of each robot. The associated communication graph is depicted in Fig. 15.9.

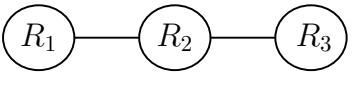

Fig. 15.9 Communication graph for the experiment.

The parameters used in the experiment for the decentralized receding horizon motion planner are given in Table 15.1. At the beginning, the geometrical shape of the group is triangular. The task is to drive these robots to form a desired triangular shape while avoiding collisions and maintaining the communication constraints.

Table 15.1 Parameters of the receding horizon planners.

T_p	2s
T_c	0.5s
a_n	1s
b_n	2

Due to the existence of obstacles, robots must pass through narrow ways and constraint each other in the team. In order to track the optimal planned trajectory, each robot uses the robust closed-loop controller described in the Section Path Tracking. Fig. 15.10 shows six snapshots of our experiment. During the motion, each robot computes its optimal planned trajectory using local exchanged information. Fig. 15.10(a) depicts the three robots at the beginning. In Fig. 15.10(a)-(f), they approach their goal positions to form the desired geometrical shape while avoiding collision and maintaining communication links. This experiment demonstrates that the proposed receding horizon planner manages to accomplish the desired objectives.

Another experiment using 7 Miabot robots (see Fig. 15.11) has been realized. The Miabot robot is produced by Merlin Robotics System. This 8cm*8cm

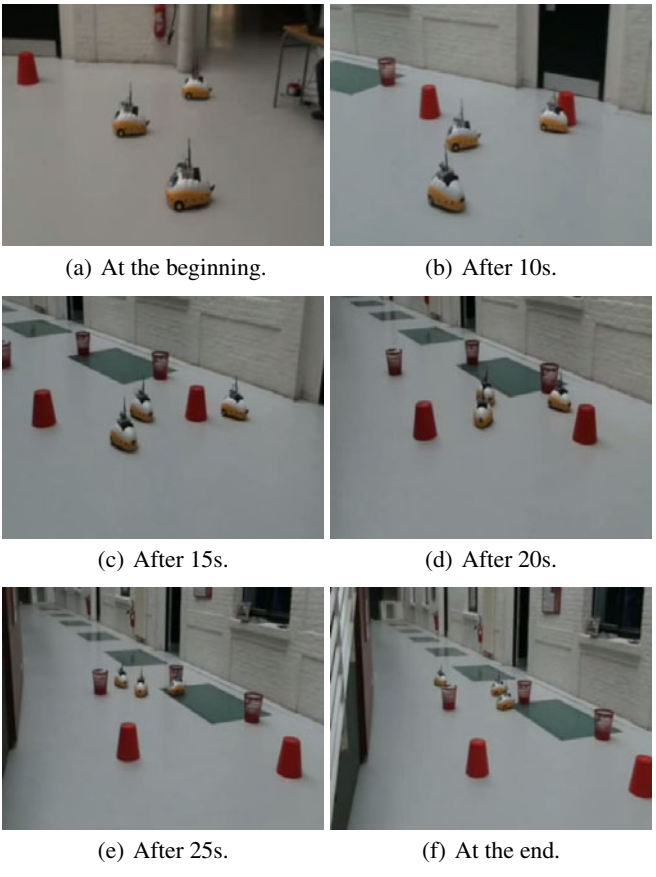

(a) At the beginning. (b) After 10s.

(c) After 15s. (d) After 20s.

(e) After 25s. (f) At the end.

Fig. 15.10 Three Pekee mobile robots flocking from initial configurations to a desired region, avoiding collisions and maintaining communication constraints.

Fig. 15.11 The Miabot nonholonomic mobile robots.

robot is nonholonomic, has two encoder sensors for the position and a bluetooth connection with the PC. Each robot has a range vision of 0.8m. The path planning horizon sampling time is $T_c = 250$ ms, the maximum linear speed is $u_{n_{max}} = 0.1m.s^{-1}$ the maximum acceleration is $a_{n_{max}} = 0.2m.s^{-2}$, and the maximum angular speed is $w_{n_{max}} = \frac{\pi}{2} rad.s^{-1}$. The minimum distance between each robot and the obstacles, and the distance between each robot and its neighbors are $d(\mathscr{A}_n, \mathscr{O}_{m_n}) > 0.2$m, $d(\mathscr{A}_n, \mathscr{A}_p) > 0.2$m In this experiment, the path planning algorithm is associated with a high level algorithm, which guarantees that robots can navigate without collision in an environment with obstacles which have a general shape. One can refer to [47] for more details.

15.4 Conclusion

During the Robocoop project, several tools have been proposed in order to perform the autonomous navigation of a swarm of mobiles robots. It is important to plan in real time a trajectory for each robot that takes into account the obstacles in the robot neighborhood, the physical robot limitations (maximal acceleration, maximal velocities), the robot model (kinematic or dynamic), the broadcasting range, some optimal constraints such as time or energy. The proposed decentralized path planning algorithm was considered as a constrained optimal problem with a receding horizon. The use of the flatness property of the robot allows the use of this algorithm for a large class of robots. Higher order sliding modes based control algorithms have also been designed such that each robot tracks accurately and robustly the desired optimal trajectory. All the proposed algorithms were implemented on several mobile robot benchmarks.

Current research is concerned with robot perception and localization which are some of the most important challenges for autonomous navigation of swarms. Strategies are also studied in order to increase the efficiency of the swarm (for instance, any robot can help its neighbors if they are in a critical situation).

References

1. Laumond, J.-P.: Robot Motion planning and Control. Springer, Heidelberg (1998)
2. Latombe, J.-C.: Robot Motion Planning. Kluwer Academic Publishers, Norwell (1991)
3. Salichs, M., Moreno, L.: Navigation of mobile robots: open questions. Robotica 18, 227–234 (2000)
4. Chen, Y., Desrochers, A.: Structure of Minimum-Time Control Law for Robotic Manipulators with Constrained Paths. In: IEEE International Conference on Robotics and Automation, pp. 971–976 (1989)
5. Kolmanovsky, I., McClamroch, N.H.: Developments in nonholonomic control problems. IEEE Control Systems Magazine 15(6), 20–36 (1995)
6. Brockett, R.W.: Asymptotic stability and feedback stabilization. In: Brockett, R.W., Millman, R.S., Sussmann, H.J. (eds.) Differential Geometric Control Theory. Birkhäuser, Basel (1983)
7. Pomet, J.-B.: Explicit design of time-varying stabilizing control laws for a class of controllable systems without drift. Systems and Control Letters 18, 147–158 (1992)
8. Samson, C.: Control of chained systems: Application to path following and time varying point-stabilization of mobile robots. IEEE Transactions on Automatic Control 40(1), 64–77 (1995)
9. Murray, R., Sastry, S.: Nonholonomic motion planning:steering using sinusoids. IEEE-Transactions on Automatic Control 38, 700–716 (1993)
10. Hespanha, J.P., Morse, A.S.: Stabilization of nonholonomic integrators via logic-based switching. Automatica 35, 385–393 (1999)
11. Monaco, S., Normand-Cyrot, D.: An introduction to motion planning under multirate digital control. In: Proceedings of the IEEE Conference on Decision and Control, Tucson, USA, pp. 1780–1785 (1992)
12. Bloch, A.M., Drakunov, S.V., Kinyon, M.K.: Stabilization of Nonholonomic Systems Using Isospectral Flows. SIAM J. on Control and Optimization 38(3), 855–874 (2000)
13. Floquet, T., Barbot, J.P., Perruquetti, W.: Higher order sliding mode stabilization for a class of nonholonomic perturbed systems. Automatica 39(6), 1077–1083 (2003)
14. Marchand, N., Alamir, M.: Discontinuous exponential stabilization of chained form systems. Automatica 39, 343–348 (2003)
15. Prieur, C., Astolfi, A.: Robust stabilization of chained systems via hybrid control. IEEE Trans. Automat. Control 48, 1768–1772 (2003)
16. Bartolini, G., Pisano, A., Punta, E., Usai, E.: A survey of applications of second-order sliding mode control to mechanical systems. International Journal of Control 76(9-10), 875–892 (2003)
17. Martinez, R., Alvarez, J., Orlov, Y.: Hybrid sliding mode-based control of underactuated systems with dry friction. IEEE Transactions on Industrial Electrononics 55(11), 3998–4003 (2008)
18. Riachy, S., Orlov, Y., Floquet, T., Santiesteban, R., Richard, J.P.: Second order sliding mode control of underactuated mechanical systems I: local stabilization with application to an inverted pendulum. International Journal of Robust Nonlinear Control 18(4-5), 529–543 (2008)
19. Drakunov, S.V., Floquet, T., Perruquetti, W.: Stabilization and tracking control for an extended Heisenberg system with a drift. Systems & Control Letters 54, 435–445 (2005)
20. Canale, M., Fagiano, L., Ferrara, A., Vecchio, C.: Vehicle yaw control via second-order sliding-mode technique. IEEE Transactions on Industrial Electrononics 55(11), 3908–3916 (2008)

21. Defoort, M., Nollet, F., Floquet, T., Perruquetti, W.: A third order sliding mode controller for a stepper motor. IEEE Transactions on Industrial Electronics 56(9), 3337–3346 (2009)
22. Pisano, A., Davila, A., Fridman, L., Usai, E.: Cascade control of PM DC drives via second order sliding mode technique. IEEE Transactions on Industrial Electronics 55(11), 3846–3854 (2008)
23. Fridman, L., Levant, A.: Higher order sliding modes. In: Perruquetti, W., Barbot, J.P. (eds.) Sliding Mode Control in Engineering, pp. 53–101. Marcel Dekker, New York (2002)
24. Filippov, A.: Differential equations with discontinuous right hand sides. Kluwer, Dordrecht (1988)
25. Bhat, S., Bernstein, D.: Continuous finite-time stabilitization of the translational and rotational double integrators. IEEE Trans. on Automatic Control 43(5), 678–682 (1998)
26. Bhat, S., Bernstein, D.: Geometric homogeneity with applications to finite time stability. Mathematics of Control, Signals and Systems 17, 101–127 (2005)
27. Hong, Y.: Finite time stabilization and stabilizability of a class of controllable systems. Syst. Cont. Let. 46(4), 231–236 (2002)
28. Moulay, E., Perruquetti, W.: Finite time stability and stabilization of class of continuous systems. J. Math. Analysis Applications 323, 1430–1443 (2006)
29. Moulay, E., Dambrine, M., Yeganefar, N., Perruquetti, W.: Finite time stability and stabilization of time delay systems. Syst. Cont. Let. 57(7), 561–566 (2008)
30. Moulay, E., Perruquetti, W.: Finite time stability of non autonomous non linear systems. Int. J. of Control 81(5), 797–803 (2008)
31. Defoort, M., Floquet, T., Kokosy, A., Perruquetti, W.: A novel higher order sliding mode control scheme. Systems and Control Letters 58(2), 102–108 (2009)
32. Utkin, V.I., Guldner, J., Shi, J.: Sliding Modes Control in Electromechanical Systems. Taylor and Francis, London (1999)
33. Levant, A.: Higher-order sliding modes, differentiation and output-feedback control. Int. J. of Control 76(9), 924–941 (2003)
34. Canudas de Wit, C., Sordalen, O.: Exponential stabilization of mobile robots with nonholonomic constraints. IEEE Trans. on Automatic Control 37(11), 1791–1797 (1992)
35. Fliess, M., Levine, J., Martin, P., Rouchon, P.: Flatness and defect of nonlinear systems: introductory theory and examples. Int. J. Control 61(6), 1327–1361 (1995)
36. Lalish, E., Morgansen, K., Tsukamaki, T.: Decentralized reactive collision avoidance for mutiple unicycle-type vehicles. In: Proc of IEEE American Control Conference (2008)
37. Fiorini, P., Shiller, Z.: Motion planning in dynamic environments using velocity obstacles. Int. J. Robot. Res. 17(7), 760–772 (1998)
38. Defoort, M., Doniec, A., Bouraqadi, N.: A decentralized collision avoidance algorithm for multi-robots navigation. In: Int. Conf. on Informatics in Control, Automation and Robotics, Milan, Italie (2009)
39. Defoort, M., Kokosy, A., Floquet, T., Perruquetti, W., Palos, J.: Motion planning for cooperative unicycle-type mobile robots with limited sensing ranges: A distributed receding horizon approach. Robotics and Autonomous Systems 57(11), 1094–1106 (2009)
40. Defoort, M., Palos, J., Kokosy, A., Floquet, T., Perruquetti, W.: Performance-based reactive navigation for non-holonomic mobile robots. Robotica 27(2), 281–290 (2009)
41. Defoort, M., Palos, J., Floquet, T., Kokosy, A., Perruquetti, W.: Practical Stabilization and Tracking of a Wheeled Mobile Robot With Integral Sliding Mode Controller. In: Proc of IEEE Int. Conf. on Decision and Control (2007)
42. Defoort, M., Floquet, T., Perruquetti, W., Drakunov, S.V.: Integral sliding mode control of extended Heisenberg system. IET Control Theory and Applications 3(10), 1409–1424 (2009)

43. Defoort, M., Floquet, T., Kokosy, A., Perruquetti, W.: Sliding mode formation control for cooperative autonomous mobile robots. IEEE Transactions on Industrial Electronics 55(11), 3944–3953 (2008)
44. Orqueda, O., Fierro, R.: Visual tracking of mobile robots in formation. In: American Control Conference, New York City, USA (2007)
45. Defoort, M., Floquet, T., Kökösy, A., Perruquetti, W.: Integral sliding mode control for trajectory tracking of a unicycle type mobile robot. Integrated Computer Aided Engeneering 13(3), 277–288 (2006)
46. Defoort, M., Palos, J., Kokosy, A., Floquet, T., Perruquetti, W., Boulinguez, D.: Experimental Motion Planning and Control for an Autonomous Nonholonomic Mobile Robot. In: Proc. IEEE Conf. Robotics and Automation (2007)
47. Sert, H., Kokosy, A., Perruquetti, W., Palos, J., Gaillard, F.: Decentralized Cooperative Strategy for an autonomous mobile robots swarm. In: IROS 2010 (2010)

Chapter 16
Two Applications of Sliding Mode Control in Energy Generation and Power Electronics

D. Biel, A. Dòria-Cerezo, E. Fossas, R.S. Muñoz-Aguilar, and R. Ramos-Lara

16.1 Introduction

Power electronics is concerned with electromechanical systems that carry power. In a wide sense, power electronics includes the analysis, synthesis and implementation of electrical motors and generators, as well as power converters. Several controllers designed in the framework of Sliding Mode can be found in specialized literature; in particular it is worth to quote the book of V.I. Utkin, J. Guldner and J. Shi [8] where several motors, generators and power converters were studied in the SMC domain. The authors took benefit of these systems to explain the advantages of SM as a robust control methodology and to show most of its applications in dynamical systems: as estimators, observers, ... This chapter is also devoted to electrical generators and power converters stressing implementation issues. We want to emphasize implementation procedures based on theory in front of the trial and error, a tuning method widely used even at universities. On the other way around, we are also interested in theoretical problems appeared when implementing algorithms.

The chapter is organized in two sections. In the first one, a Wound Rotor Synchronous Machine is analysed as an isolated energy generator. Three SMC control schemes are considered. The first sliding surface is a cylinder and for the second and third cases two control loops are considered: in both cases the sliding surface for the inner loop is a plane and the outer loop contains an integral term which is

D. Biel · R. Ramos-Lara
Institute of Industrial and Control Engineering (IOC) and Dpt. of Electronics
e-mail: {biel,lara}@eel.upc.edu

A. Dòria-Cerezo · R.S. Muñoz-Aguilar
IOC and Dpt. of Electrical Engineering
e-mail: {arnau.doria,raul.munoz-aguilar}@upc.edu

E. Fossas
IOC and Dpt. of Automatic Control
e-mail: enric.fossas@upc.edu

L. Fridman et al. (Eds.): Sliding Modes, LNCIS 412, pp. 439–463.
springerlink.com

implemented as a standard PI in the second case and through a dynamics extension in the third one. In all the three cases, stability of the equilibrium points were analysed and SMC were derived to guarantee local fulfilment of the reaching condition. Simulations were used to select which of the designed controllers was the most suitable to be implemented. Finally, the robustness of the closed loop system is experimentally shown. The second section is devoted to a problem that comes from SMC implementation in power converters. Power converters, because its topology on/off, are particularly suitable to be controlled using SM. However, as it is widely reported, the implementation of SMC in actual plants produces chattering. Even in most of the cases this chattering can be highly reduced by several procedures, none of them is appropriate for switched systems. Recently, V. Utkin and co-workers proposed a new methodology in [5] based on interleaving techniques that are very common in power electronics. A Field Parallel Gate Arrays (FPGA) based implementation of this new methodology is reported here. Utkin and co-workers methodology depends on specific gains that are parameter dependent, we used FPGA to make a robust implementation of that methodology. A section of conclusions ends the chapter.

16.2 Sliding Mode Control of a Wound Rotor Synchronous Generator

Electrical energy is mainly generated interconnecting electric generators driven by prime-movers which are basically wind, hydro, steam turbines or internal combustion engines. The standard power systems are composed mainly by Wound Rotor Synchronous Generators (WRSG) connected in parallel setting up a theoretical infinite bus. Hence, this kind of machine uses to be studied connected to an infinite bus called "power grid" [1]. Thus, the own grid determines the stator voltage and frequency, while the rotor voltage helps to improve the power factor and to compensate the reactive power at the connection point. A significantly different scenario is when the WRSG is isolated from the grid. For this insulated configuration, the mechanical speed determines the frequency, and the rotor voltage is used to set the stator voltage amplitude.

Sliding Mode Control has been proposed as a suitable method for controlling electrical machines [8]. In this Section we present a set of SMC for a stand-alone WRSG feeding a resistive load. In the first case, a sliding surface directly based on the error of the stator voltage amplitude is intended [7]. The switching function results in a polynomial of degree 2 and the equivalent control can not be defined in the whole sliding surface. A second and third switching surfaces consist in the error in the d-component of the stator voltage [4] and an outer I and PI loops respectively.

All the controllers are robust to variations in machine and load parameters. Local stability of the closed loop dynamics is proved invoking small-signal methods. It worth to mention the simplicity of the proposed controllers, they only require voltage measurements and are easily implementable. To conclude, some comparative simulations allow to determine the benefits and the handicaps of each controller

even that, in general, the first and the third sliding controllers provide very satisfactory responses. Experimental results are included.

16.2.1 System Description

Figure 16.1 shows the proposed scenario: a primary mover drags a WRSG, which acts as a generator to fed an isolated load. ω_m is the mechanical speed, v_s, v_F, i_s and i_F are the stator and field voltages and currents. On the one hand the system is assumed to be in an isolated connection and the mechanical speed externally regulated by the primary mover. On the other hand, the voltage amplitude must be regulated through the rotor field voltage.

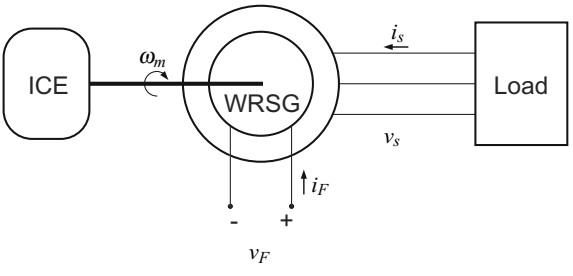

Fig. 16.1 Scheme of a stand-alone wound rotor synchronous generator.

The electrical part of the WRSG can be described, using the dq coordinates [3], as

$$L\frac{\mathrm{d}x}{\mathrm{d}t} = \begin{pmatrix} -R_s & \omega L_s & 0 \\ -\omega L_s & -R_s & -\omega L_m \\ 0 & 0 & -R_F \end{pmatrix} x + \begin{pmatrix} v_d \\ v_q \\ v_F \end{pmatrix} \tag{16.1}$$

where

$$L = \begin{pmatrix} L_s & 0 & L_m \\ 0 & L_s & 0 \\ L_m & 0 & L_F \end{pmatrix}$$

is the inductance matrix, $x^T = (i_d, i_q, i_F) \in \mathbb{R}^3$ are the dq-stator and field currents, R_s and R_F are the stator and field resistances, L_s, L_m and L_F are the stator, magnetizing and field inductances, ω is the electrical speed ($\omega = n_p\omega_m$, where n_p is the number of pole pairs), v_d, v_q are the dq-stator voltages and v_F is the field voltage which will be used as a control input.

In order to have the complete model of a WRSG connected to a resistive load R_L, let $v_L^T = (v_{Ld}, v_{Lq}) \in \mathbb{R}^2$ and $i_L^T = (i_{Ld}, i_{Lq}) \in \mathbb{R}^2$ be the dq load voltages and currents, related by

$$\begin{pmatrix} v_{Ld} \\ v_{Lq} \end{pmatrix} = R_L \begin{pmatrix} i_{Ld} \\ i_{Lq} \end{pmatrix}, \tag{16.2}$$

and R_L, the resistance value. According to the interconnection rules, $v_s = v_L$, $i_L = -i_s$, hence from (16.1) and (16.2), the full system can be written as

$$L\frac{\mathrm{d}x}{\mathrm{d}t} = Ax + Bv_F, \tag{16.3}$$

where L is the inductance matrix defined before,

$$A = \begin{pmatrix} -(R_s+R_L) & \omega L_s & 0 \\ -\omega L_s & -(R_s+R_L) & -\omega L_m \\ 0 & 0 & -R_F \end{pmatrix} \quad \text{and} \quad B = \begin{pmatrix} 0 \\ 0 \\ 1 \end{pmatrix}.$$

The equilibrium points parametrized by the control input v_F result in a straight line defined by

$$x^{*T}(v_F) = \left[-\frac{\omega^2 L_s L_m}{R_F |Z_s|^2}, -\frac{\omega L_m (R_s+R_L)}{R_F |Z_s|^2}, \frac{1}{R_F} \right] v_F \tag{16.4}$$

where $|Z_s|^2 = \omega^2 L_s^2 + (R_s+R_L)^2$.

It is supposed that the synchronous machine feeds the load with a nominal stator voltage amplitude and frequency. The stator frequency, directly given by the mechanical speed, is assumed to be externally regulated; the stator voltage amplitude $V_s = \sqrt{v_d^2 + v_q^2} = R_L\sqrt{i_d^2 + i_q^2}$ is the control objective and the control input is the field voltage v_F. Note that $V_s = V_{ref}$ defines a cylinder in the state space then, the desired equilibrium points are the intersection of the straight line (16.4) and this cylinder. Using polar coordinates $(i_d, i_q) = I_s \cdot (\cos\delta, \sin\delta)$ where, $I_s = \frac{V_s}{R_L}$, it is easy to obtain $i_d^* = \frac{V_{ref}}{R_L}\cos\delta^*$, $i_q^* = \frac{V_{ref}}{R_L}\sin\delta^*$ and $i_F^* = -\frac{V_{ref}}{R_L}\frac{L_s}{L_m \cos\delta^*}$. Hence, $\delta^* = \arctan\left((R_s+R_L)/(\omega L_s)\right)$. Actually, there are two equilibrium points δ^*, given by the two values of the arctan function. Furthermore, the value of the field voltage in equilibria is $v_F^* = \pm\left[(R_F L_s)/(R_L L_m \cos\delta^*)\right] V_{ref}$.

16.2.2 Direct Sliding Mode Controller

A SMC based on the error in the stator voltage amplitude is synthesized here. It will result in an easily implementable and reduced cost single control loop. The switching function $s(x)$ is defined as follows:

$$s(x) = V_s^2 - V_{ref}^2 = R_L^2(i_d^2 + i_q^2) - V_{ref}^2. \tag{16.5}$$

The equivalent control results in

$$u_{eq} = -\left(\frac{\partial s}{\partial x}L^{-1}B\right)^{-1}\frac{\partial s}{\partial x}L^{-1}Ax. \tag{16.6}$$

By replacing matrices and partial derivatives in (16.6), we have

$$u_{eq} = R_F i_F - \frac{L_F}{L_m}(R_s + R_L) i_d + \omega L_m i_q - \frac{\mu}{L_s}\left(\frac{(R_s + R_L)}{L_m} i_q + \omega i_F\right)\frac{i_q}{i_d}, \qquad (16.7)$$

where $\mu = L_s L_F - L_m^2$ is always positive. In the three dimensional space (i_d, i_q, i_F), the sliding surface is a cylinder. Sliding motion can be expected only in the cylinder subset defined by $i_d \neq 0$ where transversallity condition holds. The smaller the i_d, the higher the equivalent control. Therefore, a closed subset of the sliding domain must be taken to obtain a bounded control effort u_{eq}.

Adding and subtracting Bu_{eq} to $s \cdot \dot{s} = s\frac{\partial s}{\partial x} L^{-1}(Ax + Bv_F)$ and thanks to de definition of u_{eq} it can be proved that the control action defined by

$$v_F = u_{eq} - k \cdot \text{ sign}\left(s \cdot \frac{\partial s}{\partial x} \cdot L^{-1} B\right), \qquad (16.8)$$

with $k > 0$, fulfils the stability condition $s \cdot \dot{s} < 0$. Evaluating $\left(s \cdot \frac{\partial s}{\partial x} \cdot L^{-1} B\right)$ in (16.8) and taking into account that $\frac{2R_L^2 L_m}{L_s L_F - L_m^2} > 0$, (16.8) can be simplified as $v_F = u_{eq} - k \,\text{sign}(-s \cdot i_d)$. The control action v_F is implemented using a DC-DC power converter which commutes between two discrete signal values, $-V_{DC}$ and V_{DC}. Hence, the actual rotor voltage applied is

$$v_F = \begin{cases} V_{DC} & \text{if } s\, i_d < 0 \\ -V_{DC} & \text{if } s\, i_d > 0 \end{cases} \qquad (16.9)$$

Furthermore, since voltages are accessible variables and are used to compute the switching function, the switching policy in (16.9) is given in voltage terms, *i.e.* $v_F = \text{sign}(s \cdot v_d) \cdot V_{DC}$. Then, the closed loop shows sliding modes on the subset of $s = 0$ defined by the transversallity condition and $-V_{DC} < u_{eq} < V_{DC}$. Moreover, it is robust to plant parameter and load variations. The proposed control scheme is depicted in Figure 16.2. θ is the rotor position (required to compute the dq-transformation) and v_{abc} are the three-phase stator voltages. A hysteresis block is added to limit the switching frequency.

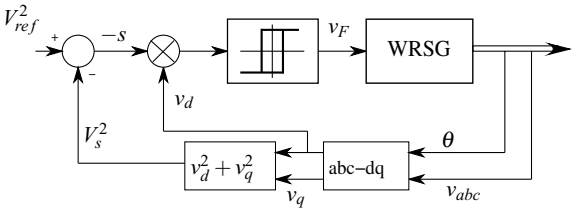

Fig. 16.2 Control scheme for a stand-alone wound rotor synchronous generator: Direct SMC

The subset of the cylinder where the transversallity condition holds has two connected components and there is a symmetry between the dynamics on each component. Taking (i_q, i_F) as local variables the ISD is given by

$$\frac{\mathrm{d}i_q}{\mathrm{d}t} = -\omega\sqrt{Y^2 - i_q^2} - ai_q - \omega\frac{a}{c}i_F, \tag{16.10}$$

$$\frac{\mathrm{d}i_F}{\mathrm{d}t} = -\frac{1}{\sqrt{Y^2 - i_q^2}}\left(cY^2 + \omega i_q i_F\right). \tag{16.11}$$

where $a = \frac{R_s+R_L}{L_s}$, $c = \frac{R_s+R_L}{L_m}$ and $Y^2 = \frac{V_{ref}^2}{R_L^2}$ are positive. There is a unique equilibrium point, (i_q^*, i_F^*), in each connected component at

$$(i_d^*, i_F^*) = \left(Y\sin\delta^*, -cY\left(\frac{\cos\delta^*}{a} + \frac{\sin\delta^*}{\omega}\right)\right).$$

that is locally asymptotically stable. Figure 16.3 shows the trajectory through $(i_q(0), i_F(0)) = (0,0)$ in the phase portrait of ISD defined in the subset $\{(i_d, i_q, i_F) \in \mathbb{R}^3 \,|\, i_d = +\sqrt{((V_{ref}^2 - R_L^2 \cdot i_q^2)/R_L^2)}$ and $-V_{ref} < i_q \cdot R_L < V_{ref}\}$. The parameter values are those in Subsections 16.2.5 and 16.2.6 where numerical simulations and experiments are performed. The equilibrium point is $i_q^* = -2.41$A and $i_F^* = 10.06$A.[1]

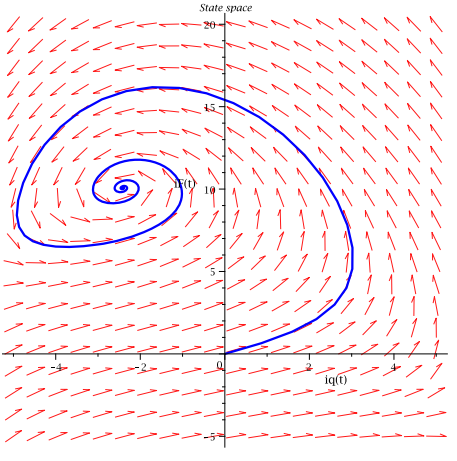

Fig. 16.3 Ideal Sliding Dynamics: phase portrait and trajectory with initial condition $i_q(0) = 0$ and $i_F(0) = 0$.

Notice the local stability of the equilibrium point. However, trajectories starting close to $i_q = -\frac{V_{ref}}{R_L}$ and $i_F > \frac{V_{ref}(R_s+R_L)}{\omega L_m R_L}$, and to $i_q = \frac{V_{ref}}{R_L}$ and $i_F < -\frac{V_{ref}(R_s+R_L)}{\omega L_m R_L}$ escape from the cylinder.

[1] In this analysis, the rotor parameters are referred to the stator; in the real application, the rotor current applied to the machine at the equilibrium point becomes, 2.515A.

16.2.3 Sliding Mode Control with an Outer-PI Loop

Figure 16.4 shows a control algorithm based on two loops; a SMC inner-loop and a PI outer-loop which provides v_d^{ref}, the reference of the d-component stator voltage amplitude to reach V_{ref}. Roughly speaking, when the system is faced with a perturbation, the PI loop places the sliding surface in the appropriate regulation point.

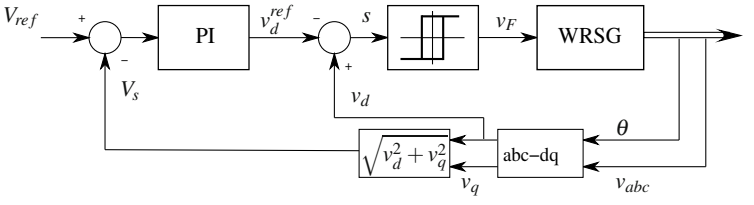

Fig. 16.4 Control scheme for a wound rotor synchronous generator: SMC with an outer-PI loop.

The whole stability proof is based on the assumption of a fast inner-loop, with respect to the PI dynamics. The switching surface, $s(x) = 0$ is given by

$$s(x) = v_d(x) - v_d^{ref} = R_L \cdot i_d - v_d^{ref} \tag{16.12}$$

and v_d^{ref} is defined by the PI outer-loop controller. $s(x) = 0$ defines the plane $i_d = v_d^{ref}/R_L$. The equivalent control, u_{eq} results in

$$u_{eq} = \frac{1}{L_m}(-L_F(R_s + R_L)i_d + \omega L_s L_F i_q + L_m R_F i_F). \tag{16.13}$$

There is sliding motion on $s(x) = 0$ provided that the $s \cdot \frac{ds}{dt} < 0$ holds. From (16.3)

$$s \cdot \frac{ds}{dt} = s \cdot \frac{\partial s}{\partial x} L^{-1} \cdot (Ax + Bv_F) < 0 \tag{16.14}$$

which, thanks to the definition of u_{eq}, can be written as $-s \cdot (R_L L_m)) \cdot (v_F - u_{eq})/\mu < 0$. Finally, as R_L ,L_m and μ are positive, the reachability condition yields $s \cdot (u_{eq} - v_F) < 0$. Using $v_F = \pm V_{DC}$, the switching policy $v_F = V_{DC}\text{sign}(s)$ provides sliding modes in the subset of $s = 0$ where $-V_{DC} < u_{eq} < V_{DC}$. The ISD results in the stable linear system

$$\frac{di_q}{dt} = -\frac{R_s + R_L}{L_s} i_q - \frac{\omega L_m}{L_s} i_F - \frac{\omega}{R_L} v_d^{ref} \tag{16.15}$$

$$\frac{di_F}{dt} = \frac{\omega L_s}{L_m} i_q - \frac{R_s + R_L}{L_m R_L} v_d^{ref}. \tag{16.16}$$

The outer-loop consists in a simple PI controller. Considering a fast inner-loop, the closed-loop system reduces to (16.15) and (16.16), where v_d^{ref} and V_s are the control input and the output respectively. The linearisation of V_s around (v_d^{ref}, i_q^*) so that $V_{ref} = \sqrt{(v_d^{ref*})^2 + R_L^2 i_q^{*2}}$ results in

$$V_s \simeq V_{ref} + \frac{v_d^{ref*}}{V_{ref}}(v_d^{ref} - v_d^{ref*}) + \frac{R_L^2 i_q^*}{V_{ref}}(i_q - i_q^*) \tag{16.17}$$

where $v_d^{ref*} = V_{ref}\cos\delta^*$. Additionally, equation (16.17) can be rewritten as $V_s \simeq v_d^{ref}\cos\delta^* + R_L i_q \sin\delta^*$ which is a function of (v_d^{ref}, i_q) but it is independent of the voltage component of the point around which function V_s is linearised. The transfer function[2] $G(s) = V_s(s)/v_d^{ref}(s)$ and the closed loop transfer function $W(s)$ result in

$$G(s) = \frac{\cos^2\delta^* s^2 + \omega^2}{\cos\delta^* s^2 + \omega\sin\delta^* s + \omega^2\cos\delta^*}, \qquad W(s) = \frac{c_3 s^3 + c_2 s^2 + c_1 s + c_0}{b_3 s^3 + b_2 s^2 + b_1 s + b_0} \tag{16.18}$$

where $c_3 = k_p\cos^2\delta^*$, $c_2 = k_i\cos^2\delta^*$, $c_1 = k_p\omega^2$, $c_0 = k_i\omega^2$, $b_3 = \cos\delta^*(k_p\cos\delta^* + 1)$, $b_2 = (\omega\sin\delta^* + k_i\cos^2\delta^*)$, $b_1 = \omega^2(k_p + \cos\delta^*)$ and $b_0 = k_i\omega^2$. Stability conditions for the PI controller can be obtained through the Routh-Hurwitz criterion. Namely, $k_p > -1/\cos\delta^*$, $0 < k_i < \omega\cdot(k_p\sin\delta^* + \cos\delta^*)/(\cos\delta^*\sin\delta^*)$.

16.2.4 Dynamic Sliding Mode Controller

The third SMC is defined in a dynamic extension of system (16.3). The error dynamics in the d-component of the stator voltage is extended by an integral term. The switching function is obtained by adding the error in the d-component of the stator voltage and the integral of this error. This results in a robust controller which block diagram is shown in Figure 16.5. Let the dynamic extension given by a new variable z defined by $\dot{z} = V_s^2 - V_{ref}^2$. Then, the proposed switching surface is $s_z(x) = v_d - v_d^{ref} + k\cdot z$ where $v_d^{ref} = V_{ref}\cos\tilde{\delta}^*$ is the v_d nominal value[3] for a given V_{ref}. The equivalent control $u_{zeq} = u_{eq} + \frac{\mu}{L_m R_L} k\cdot\dot{z}$ is equal to the former equivalent control plus the error in the d-component of the stator voltage. Tacking into account that $R_L, L_m, \mu > 0$ and proceeding as usual, reachability condition yields $s_z(u_{zeq} - v_F) < 0$ and, consequently, the switching control policy $v_F = V_{DC}\cdot\text{sign}(s_z)$ guaranties sliding motion on the subset of $s_z = 0$ defined by $-V_{DC} < u_{zeq} < V_{DC}$.

Let us define $\xi = v_d^{ref} - kz$, then the ideal sliding dynamics can be written as

[2] This transfer function takes the form $G(s) = 1 + Q(s)$. Hence, a jump in v_d^{ref} results in a jump in a V_s. But this only occurs presuming ideal sliding dynamics. In a real application, V_{DC} limitations and the own dynamics of the inner loop will filter the output signal V_s.

[3] The tilde denotes that this value depends on R_L, R_s and L_s estimations.

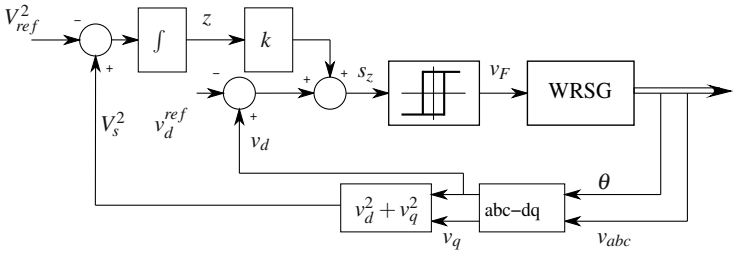

Fig. 16.5 Control scheme for a wound rotor synchronous generator: Direct SMC.

$$\frac{\mathrm{d}i_q}{\mathrm{d}t} = -\frac{R_s+R_L}{L_s}i_q - \frac{\omega L_m}{L_s}i_F - \frac{\omega}{R_L}\xi \tag{16.19}$$

$$\frac{\mathrm{d}i_F}{\mathrm{d}t} = \frac{kL_sR_L}{\mu L_m}i_q^2 + \frac{\omega L_s}{L_m}i_q + \frac{kL_s}{\mu L_mR_L}\xi^2 - \frac{R_s+R_L}{L_mR_L}\xi - \frac{kL_s}{\mu L_mR_LR_L}V_{ref}^2 \tag{16.20}$$

$$\frac{\mathrm{d}\xi}{\mathrm{d}t} = -\frac{kR_L^2}{\mu}i_q^2 - \frac{k}{\mu}\xi^2 + \frac{k}{\mu}V_{ref}^2. \tag{16.21}$$

Local stability can be analysed by means of the small signal model around the equilibrium point.

16.2.5 Simulations

The controllers presented above ensure regulation of the stator voltage amplitude of a WRSG to a given reference. The three control algorithms were simulated using the same conditions (parameters values, initial conditions, numerical methods...) in order to select the candidate to be tested in the experimental platform.

The parameters of the WRSG correspond to the machine used in the experimental results (see next subsection). Mechanical speed is set to $\omega_m = 1500$rpm and $V_{DC} = 35$V. Initial conditions are $V_{ref} = 200\sqrt{2}$V with a resistive load $R_L = 120\Omega$. Simulation tests show the response of the closed loop system under a load change to $R_L = 64\Omega$ at $t = 0.05$s. The controller gains are: $k_p = 1000$, $k_i = 100$ (for the SMC+PI controller) and $k = 0.2$ (for the Dynamic SMC scheme). Simulations have been performed using a variable step integration method. The ON/OFF controller was simulated by means of a 10kHz sampling frequency zero order holder.

Figure 16.6 shows the three-phase stator voltages and the switching function for each control algorithm. Notice that the Dynamic SMC approach, has a slower response than the other controllers. This can also be noticed in Figure 16.7, where the stator voltage amplitude is plotted. Additional plots in Figure 16.8 help to discard the Dynamic SMC, and suggest that both the Direct SMC and the SMC+PI schemes are good candidates to be experimentally tested. The former is implemented in the

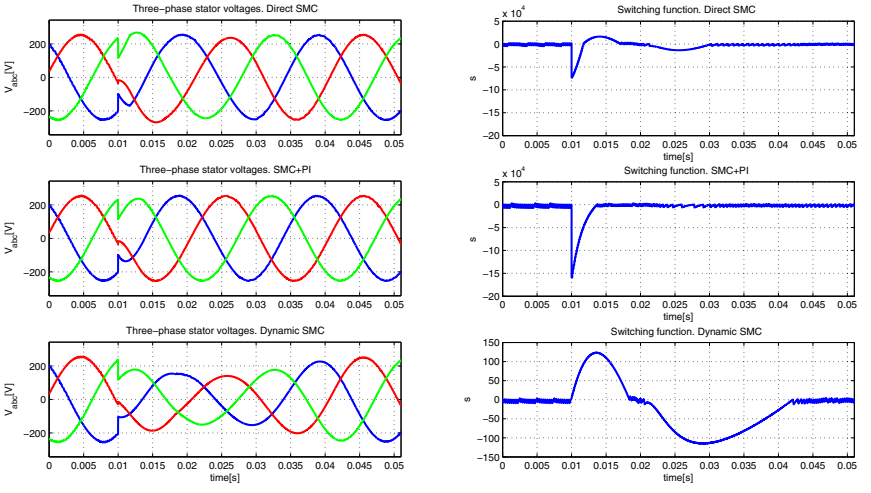

Fig. 16.6 Comparative simulation: three-phase stator voltages and switching function for a change from one half to full load value.

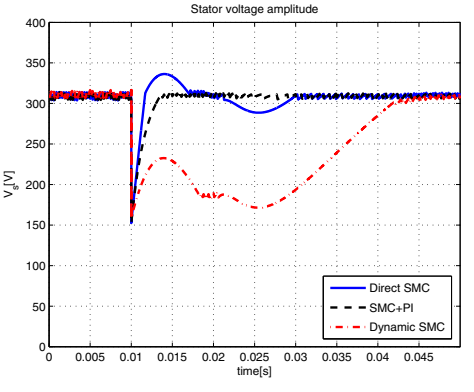

Fig. 16.7 Comparative simulation: Stator voltage amplitude for a change from one half to full load value.

next subsection because it performs similarly to the SMC+PI controller but the implementation is easier.

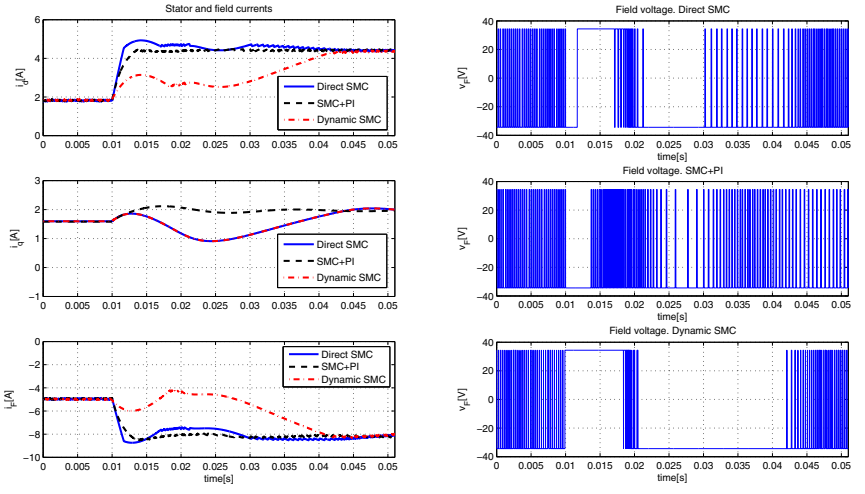

Fig. 16.8 Comparative simulation: stator and field currents, and the field voltage applied for a change from one half to full load value.

16.2.6 Experimental Results

The Direct Sliding Mode Controller has been tested in a real (2.4kVA, 4 poles three-phase) WRSG. The nominal characteristics and the WRSG parameters are shown in Table 16.1[4], respectively.

Table 16.1 WRSG Characteristics and parameters.

Motor Characteristics			Parameters		
$f = 50$Hz	$n = 1500$rpm	$P = 2.4$kVA	$R_s = 3.06\Omega$	$L_s = 0.48$H	$R_F = 39.65\Omega$
3ph	Δ/Y	$V_F = 100$V	$L_m = 0.31$H	$L_F = 3.87$H	$n = 4$
$I_F = 2.4$A	$V_s = 220/380$V	$I_s = 6.3/3.65$A	$R'_F = 2.48\Omega$	$L'_F = 0.24$H	

In this case, the WRSG is dragged by a DC motor which emulates the primary mover proposed in subsection 16.2.1. This machine, employed to provide a constant speed of 1500rpm to the WRSG (which corresponds to a frequency of 50Hz), is a 3kW machine with the 4Q2 commercial speed controller from Control Techniques Drives Ltd. The power converter connected to the field circuit is a full bridge DC/DC converter that can provide $\pm V_{DC}$ voltages. The V_{DC} voltage is obtained from the power grid with a diode rectifier, a L filter and a capacitor DC bus. For the experimental tests the bus voltage is set to $V_{DC} = 137.5$V. The resistive load is composed of

[4] The apostrophe signal indicates that the parameters are referred from the rotor to the stator, and n is the transformation relationship.

two interconnected banks, with a half or full load values (equivalent to $R_L = 128\Omega$ and $R_L = 64\Omega$ for the nominal voltage).

The control algorithm is programmed into a Texas Instruments floating point 150Mhz Digital Signal Processor (DSP TMS 320F28335). The DSP has 16 ADC channels with 12-bit resolution, with a maximum conversion speed of 12.5MSPS, 6 PWM and 6 HRPWM outputs and 88 GPIO pins which can be used to communication purposes. Three phase stator voltages are measured using two differential sensors and assuming a balanced load. Position is measured as well in order to compute the dq transformation. These measures are acquired through a DSP which is programmed from a personal computer. Real Time Workshop C code generation from Matlab/Simulink is used in order to simplify the code implementation to the DSP without needing a C code editor. Also Texas Target support package is used to configure the ADC, PWM, SPI, GPIO ports and interruptions. The sliding mode controller has been implemented so that a maximum 10kHz switching frequency is allowed.

In a first experiment, the reference line voltage is set to 380Vrms (which corresponds to $V_s = 220\sqrt{2}$V), and the load is suddenly increased from one half to the full load value. Results for the three-phase stator voltages and switching function are shown in Figure 9(a). A zero error in the stator voltage amplitude with a fast time response is achieved. The controller needs less than one stator voltage cycle to recover the reference (details are zoomed at the bottom of Figure 9(a)). Actually, the switching function oscillates around zero but the resulting chattering phenomenon is not reflected in the experimental test due to the filter effect of the digital to analog converter. Simulation results show that chattering is less than 2-3% of the stator voltage amplitude. The stator voltage amplitude, reference voltage, actual and equivalent controls are depicted in Figure 9(b). Note that, as it was expected from the simulations, experimental results reveal a good performance.

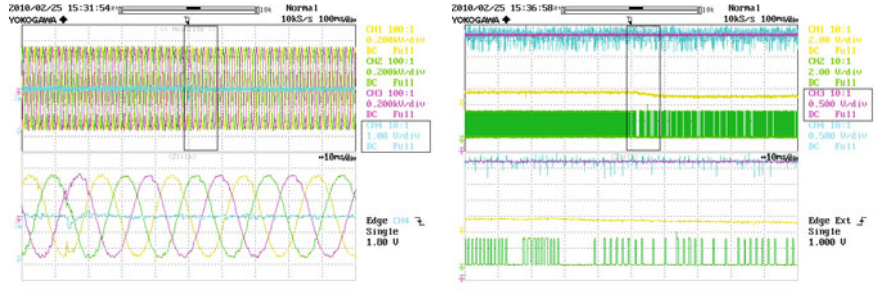

(a) (b)

Fig. 16.9 Experimental results: load change from one half to full load value. (a) Three-phase stator voltages and switching function for a change from one half to full load value. (b) Stator voltage amplitude and its reference and, switching control police, and its filtered value, for a change from half to full load value.

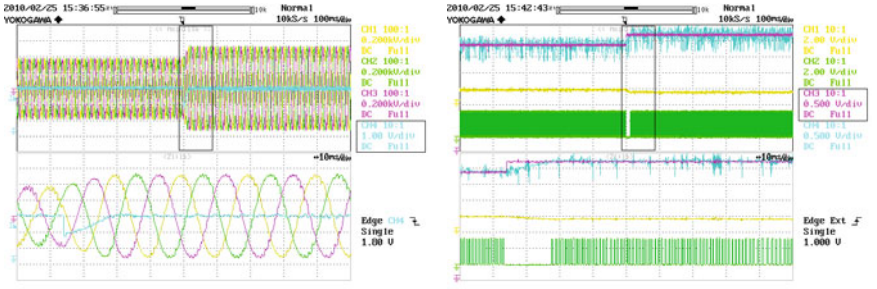

(a) (b)

Fig. 16.10 Experimental results: V_ref changes from 250Vrms to 380Vrms (a) Three-phase stator voltages and switching function. (b) Switching control policy, and its filtered value.

In the second experiment, a step change in the stator voltage amplitude reference is performed. From an initial line value of 250Vrms, the reference is set to 380Vrms. In this case, the load is kept at its half load value ($R_L = 128\Omega$). Again, experimental tests (Figures 10(a) and 10(b)) show good stator voltage regulation. The field voltage and the switch driver signal and its filtered value are shown in Figure 10(b). It is interesting to note that sliding mode is lost for a short period when the reference voltage changes. However, it recovers quickly, and the equivalent control returns to the operation strip.

The third experiment shows that the controller, firstly designed to be robust to resistive loads, is also robust to inductive-resistive ones. The reference line voltage is set to 380Vrms. The initial load is the half load value used in the previous tests and, suddenly, a 736W induction motor is connected. The three phase stator voltages and the switching action are depicted in Figure 11(a). Stator voltage regulation is lost while sliding motion is not achieved. In the meantime the actual control saturates. The stator voltage amplitude and the reference are shown in Figure 11(b). It is worth noticing again the good performance of the closed loop system.

16.3 Implementing ON/OFF Controllers by Field Parallel Gate Arrays (FPGA)

Sliding Mode Control stands out for its properties of robustness in front of parameter variations and external disturbances. It has been successfully applied in power electronics however, the ripple ("chattering") caused by actual implementations constitutes its main drawback. Several solutions to suppress the aforementioned chattering can be found in technical literature but, unfortunately, they can not be applied to switched systems. Recently, Hoon Lee et al. proposed a new methodology in [5] to

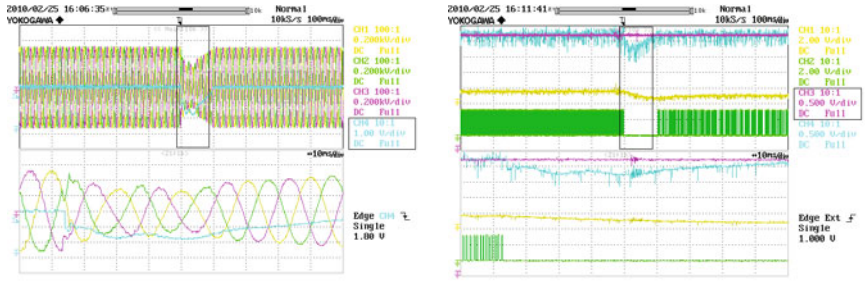

(a) (b)

Fig. 16.11 Experimental results: load change from one half load value to IM connection (a) Three-phase stator voltages and switching function. (b) Stator voltage amplitude and its reference, and, switching control police, and its filtered value.

reduce chattering in power converters. This section is devoted to a specific implementation of that methodology. The on/off control action is implemented through Field Parallel Gate Arrays (FPGA). FPGA allows to compute the on/off switching frequency which is used to tune an integral gain, this yielding the closed loop system robust in front of line and load perturbations.

16.3.1 Chattering Reduction

Let us consider a system which is in charge of regulating an output y by means of a relay as in Figure 16.12, where the Phase-1 block corresponds to a relative degree 1, first order transfer function with time-constant τ and canonical gain k_0. Thus,

$$\frac{ds}{dt} = \frac{dy_{ref}}{dt} - \frac{dy}{dt} = a - M\text{sign}(s) \tag{16.22}$$

where $a = a(t) = \frac{dy_{ref}}{dt} + \frac{y}{\tau}$ and $M = \frac{k_0}{\tau}$. Note that there is sliding motion on $s = 0$ provided that $|a| < M$. However, since the switching frequency is finite, actual trajectories do not slide, they evolve on a sawtooth around the switching surface producing *chattering*.

Several solutions to reduce the chattering were reported in the literature. In [8] a solution to totally eliminate the chattering utilize observers. Another way to decrease the chattering without designing any asymptotic observers is to implement state-dependent switching gain for discontinuous control [6]. However, for SMC of power converter systems with "on/off" as the only admissible switching operation mode, any of the above methodologies cannot be applicable, and a natural way to reduce chattering is increasing switching frequency. This is not always possible due to the limitation of switching frequency or losses in power converters. New results by

Hoon Lee et al. in [5] show that taking benefit of interleaving processes, chattering can be reduced. The key points of that new procedure are:

- a multi-phase inner loop instead of a 1-phase one,
- modifying the reference appropriately, *i.e.* taking as a new reference $y_{ref_0} = \frac{y_{ref}}{m}$,
- some properties of the Fourier expansions.

Two structures named phase interconnected and phase master-slave systems were described in [5]. The underlying theory is summarized here for the 2-phase master-slave model in Figure 16.13. As in the single phase case,

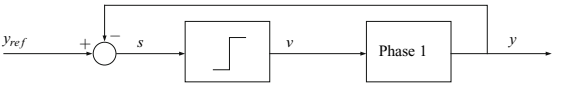

Fig. 16.12 Inner loop in a 1-phase system.

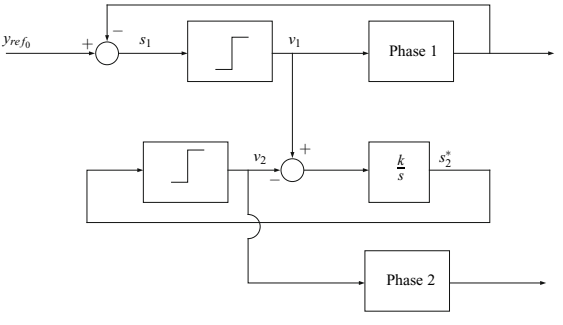

Fig. 16.13 A 2-phase master-slave system.

$$\frac{ds_1}{dt} = a - M\text{sign}(s_1) \tag{16.23}$$

$$\frac{ds_2^*}{dt} = kM\left[\text{sign}(s_1) - \text{sign}(s_2^*)\right] \tag{16.24}$$

where now

$$s_1 = y_{ref_0} - y_1 \tag{16.25}$$

$$s_2^* = k\int M\left[\text{sign}(s_1) - \text{sign}(s_2^*)\right] dt, \tag{16.26}$$

presumed that the relay gains and the dynamics in the two phases are identical.

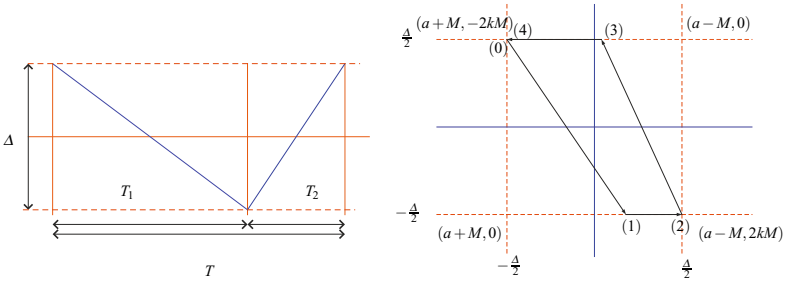

(a) Periodic s_1 dynamics. (b) Periodic (s_1, s_2^*) dynamics.

Fig. 16.14 (a) Periodic s_1 dynamics. (b) Periodic (s_1, s_2^*) dynamics.

Figure 14(a) shows the s_1 dynamics in steady-state. Presuming that $\frac{dy_{ref_0}}{dt}$, and state variables are practically constant[5], s_1 period can be computed from the figure as

$$T = T_1 + T_2 = \frac{\Delta}{M-a} + \frac{\Delta}{M+a} = \frac{2\Delta M}{M^2 - a^2} \tag{16.27}$$

In figure 14(b), a periodic trajectory in the (s_1, s_2^*)-plane is drawn for $a > 0$. Based on this trajectory, the phase shift results in

$$T_\phi = \frac{\Delta}{2kM} \tag{16.28}$$

which is equal to the time from changing s_2^* from (2) to (3) in figure 14(b).

The block diagram in Figure 16.13 allows implementing a phase shift between phases 1 and 2 while $\frac{\Delta}{2kM}(M + |a|) < \Delta$ where Δ is the hysteresis width and k and M are the integral and relay gains respectively. This is equivalent to

$$M + |a| < 2kM. \tag{16.29}$$

Note that the ideal sliding dynamics in the interconnected system results in $y_1 = y_2 = y_{ref_0}$. Suppose that a master-slave $m-$phases linear system is designed so that the period chattering is the same in each phase, and two consecutive phases have the same phase-shift $\frac{T}{m}$. Since chattering is a periodic function, it can be represented using Fourier series with frequencies $\omega_n = \frac{2\pi n}{T}$, for $n = 1, 2, \ldots, \infty$. It can be proved that all harmonics except for $n = l \cdot m$, $l \in \mathbb{Z}$ are suppressed in the output signal. Hence, chattering amplitude can be reduced to desired level by increasing the number of phases. Additionally, since the $T-$average of the sliding surface is zero, there is no continuous component in the Fourier expansion. See [5] for details.

[5] The dominant term in $\dot{s}_1$ is $M\text{sign}(s_1)$.

16.3.2 A $m-$Phases Parallel Buck Converter

The results just summarized will be applied here to a parallel buck converter. It is modeled by the system of ODE

$$L\frac{di_1}{dt} = -R_L i_1 - v_C + Eu_1 \tag{16.30}$$

$$\vdots\ \vdots\ \vdots \tag{16.31}$$

$$L\frac{di_m}{dt} = -R_L i_m - v_C + Eu_m \tag{16.32}$$

$$C\frac{dv_C}{dt} = i_1 + \cdots + i_m - \frac{v_C}{R} \tag{16.33}$$

where i_l refers to the current in the $l-$th phase inductor, v_C refers to the output voltage and $u_l \in \{0,1\}$ are the switches. Inductances L and losses resistors R_L are presumed to be the same for all phases. Let us assume we deal with a $m-$phase buck converter which phases are shifted $T_\phi = \frac{T}{m}$. Then from equations (16.27) and (16.28) the value of k can be obtained. Finally, replacing it in equation (16.29) and using $|a| < M$, this bound on a can be improved. It yields $|a| < M\left(1 - \frac{2}{m}\right)$. Particularizing this bound for the half-bridge DC-DC buck converter gives

$$\frac{1}{L}\left|\frac{E}{2} - \left(\frac{R_L}{mR} + 1\right)v_C^*\right| < \frac{E}{2L}\left(1 - \frac{2}{m}\right) \tag{16.34}$$

which, in turn, taking $v_C^* = \alpha E$ and defining $\hat{\alpha} = \alpha\left(\frac{R_L}{mR} + 1\right)$ yields the necessary and sufficient conditions $\hat{\alpha} > \frac{1}{m}$ if $\hat{\alpha} < 0.5$ and $\hat{\alpha} < 1 - \frac{1}{m}$ if $\hat{\alpha} > 0.5$.

16.3.2.1 FPGA Implementation Issues and Experimental Results

An analogue implementation of sliding mode control of a step-down multi-phase converter was presented in [2]. The switches were power Mosfets IRF9530, managed by Driver ICL7667, and diodes BYW29. Switching frequency was set at 100kHz for a load resistance of 2Ω. The current reference I_{ref} used in the first switching surface was generated by means of a PI controller in order to regulate the output voltage to a selected reference. As it was reported in that paper, the current ripple cancellation (the switching chattering) was properly minimized for nominal parameters, but the current ripple was considerably increased when the input voltage, the load or the reference voltage vary from their nominal value. Experimental measures confirmed the loss of robustness predicted by the theory, which was due to setting a constant value for parameters k and M. To fix this problem, these two parameters must be properly adapted to the changes of the equivalent control. With this aim, a digital implementation approach, which minimizes the current ripple and is robust with respect to load perturbations and changes in the input and reference voltages, is performed.

The approach is based on measuring the switching period of the Master switching surface and on using this measure adapt the value of parameter k of the Slaves switching surfaces. To this end, a digital device in charge of real-time measuring the switching signal and determining its period is required. The period value is then used to calculate the phase-shift among phases $T_\Phi = T_s/m$ and, finally, parameter k is obtained as $k = \Delta/T_\Phi$. Additionally, in order to get a proper adaptation of parameter M, a feed-forward loop is added to take into account input voltage changes. It is worth to denote the assumptions that have been considered:

- It is assumed that all phases are identical, this leading to the same equivalent control.
- Since digital device needs several clock periods to calculate parameter k value, an overall delay must be taken into account. It is assumed that this delay does not significantly modify the controlled system dynamics. Anyway, an accurate implementation can lead to neglect this delay. Specifically, the use of a Spartan-XC3S200 FPGA for implementation issues gives rise to a delay lower than 0.2% with respect the switching period (the clock frequency was 100MHz and the switching frequency of 100kHz was adjusted for the nominal parameters).
- $K = k \cdot M$ is used as the parameter to be adapted in the real implementation.

An electronic prototype of $4-$phase converter was built with the nominal parameters: $E = 10\text{V}, L = 22\mu\text{H}, C = 10\mu\text{F}, R = 2\Omega$ and $R_L = 700\,m\Omega$. The Master switching surface, the hysteresis width comparator and the PI outer loop were implemented by means of analogue devices such as amplifier operational. The Slaves switching surfaces and their hysteresis comparators were programmed within a Spartan-XC3S200 FPGA. The FPGA has several advantages (high processing speed, high device capability, user-friendly design environment and low device cost) with respect to other digital platforms such as general-purpose microprocessors or Digital Signal Processors (DSP). Parallel architecture execution performed by FPGA devices leads to designs with low processing time and, additionally, gives flexibility and modularity. Actually, the proposed design can be easily extended to control more phases and to add new algorithms such as power management or fault-tolerance procedures. Spartan-XC3S200 FPGA has 1920 Slices, twelve 18K-bit block RAMs, twelve 18x18 hardware multipliers and four Digital Clock Managers (DCM). This design spent 821 Slices (42% of the available Slices resources), 1 block RAM (8%), 8 hardware multiplier (66%) and 1 DCM (25%).

The following tests were performed to validate the proposed K-adaptive control:

A. First set of experimental results: Input voltage variation test

In this case the control proposal was tested when the input voltage takes values from $E = 7.5\text{V}$ to $E = 14\text{V}$. The reference voltage and the load were set to $V_{ref} = 5\text{V}$ and $R = 2\Omega$, respectively. Experimental results when parameter K was fixed to the value which eliminates the chattering ($E = 10\text{V}, V_{ref} = 4.59\text{V}$) and when the dynamical adaptation of K was used are shown in the following figures. Figure 16.15 shows the master inductor current and the control signal of the slaves converters for an input voltage of $E = 7.5\text{V}$ when K remains constant and when it is adapted through the proposed procedure. As it can be seen in these figures, there is a 65kHz

switching frequency approximately and the phase-shift is equally distributed when K is properly adapted. The output voltage, the reference voltage (scaled by 0.5), the master current and the sum of the currents are displayed in Figures 16.16 and 16.17 for a nominal K and when K is dynamically adapted. Parameters were set to $E = 10$V and $E = 14$V, respectively. In these plots it can be easily observed how the switching frequency is of 100kHz and 120kHz for $E = 10$V and $E = 14$V, respectively and the ripple of the sum of currents was lower when the K-adaptive control is used, this providing an equitable phase-shift among phases. In the case when K remains fixed the ripple of the sum of currents increases as duty cycle moves away from 0.5, since K was adjusted for ripple cancelation for this value. In the case of a dynamically adapted K, the sum of currents supports the same ripple as it can be verified by comparing Figures 16.16 and 16.17.

B. Second set of experimental results: Load variation test
Figure 16.18 shows the transient response when the reference voltage is set to $V_{ref} = 5$V and the load varies from $R = 2\Omega$ to $R = 1\Omega$ and from $R = 1\Omega$ to $R = 2\Omega$. Simulation results agree with the theoretical predictions: the converter presents a fast transient response and the output voltage recovers the reference one. For both load values the current ripple has been minimized.

C. Third set of experimental results: Reference voltage variation test
The controllers were also tested when the reference voltage changes from $V_{ref} = 4$V to $V_{ref} = 6$V and from $V_{ref} = 8$V to $V_{ref} = 6$V when the load was of $R = 2\Omega$. Figure 16.19 depicts the output voltage, the reference voltage (scaled by 0.5), the sum of the currents and the master current when the reference voltage changes from $V_{ref} = 4$V to $V_{ref} = 6$V and from $V_{ref} = 8$V to $V_{ref} = 6$V. As it can be seen in the plots, the converter acquires the desired value with a brief transient and the ripple of sum of currents remains small due to the adaptive control action on K.

16.4 Conclusions

Two applications of SMC in power electronics were presented in this chapter: the design of a controller for a stand alone Wound Rotor Synchronous Machine and a robust FPGA based implementation of a new technique to reduce chattering. Both show the applicability of SMC and the good features it provides: ease of implementation, robustness, response velocity, ...

SMC provided solutions for the stand alone WRSG from different perspectives. Slight modifications in the control design transforms each algorithm in a completely new scheme. For instance, the addition of an integral term can be done adding an outer loop with a standard PI or dynamically extending the initial system. The performances these controllers set are highly different.

As for the power converters, a SMC FPGA-based approach to reduce chattering as well as to improve line and load robustness in a step-down multi-phase converter was presented. This approach allows both to regulate the output voltage to a selected reference and to minimize the current ripple. This last goal is obtained by means of

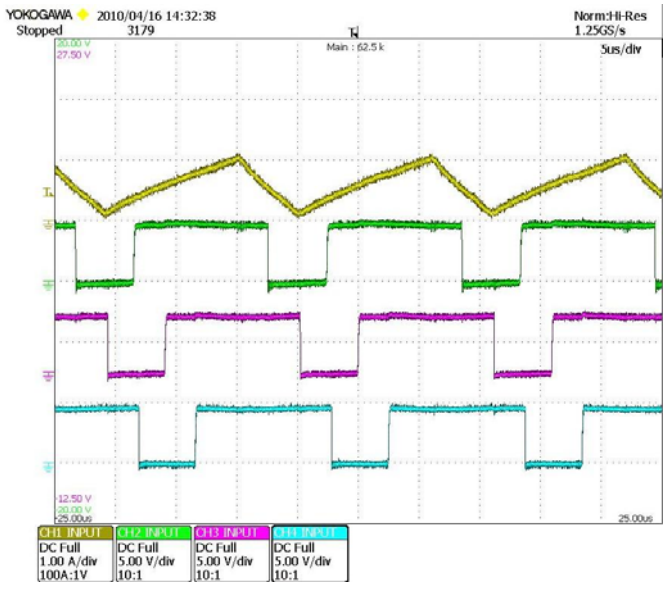

(a)

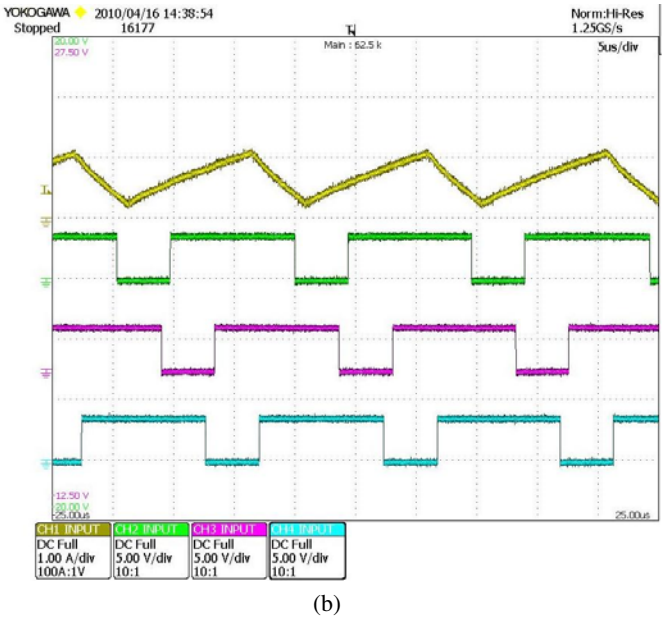

(b)

Fig. 16.15 Steady-state master current and slaves control signal for $E = 7.5\text{V}$ and $V_{ref} = 5\text{V}$ (a) when K remains fixed, (b) when K is dynamically adapted.

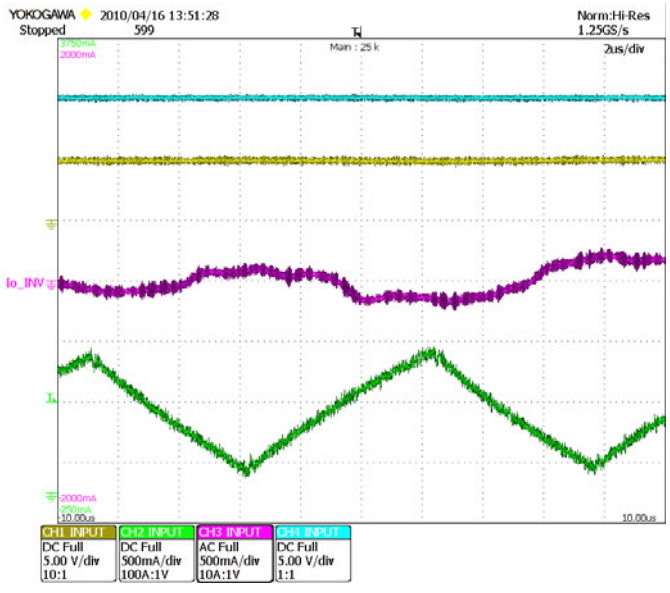

(a)

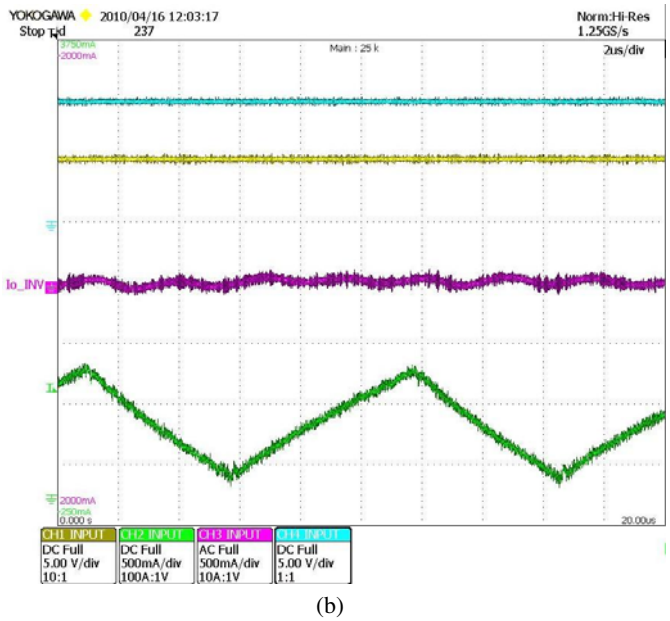

(b)

Fig. 16.16 Input voltage, output voltage, sum of the currents and master current for $E = 10$V and $V_{ref} = 5$V (a) when K remains fixed, (b) when K is dynamically adapted.

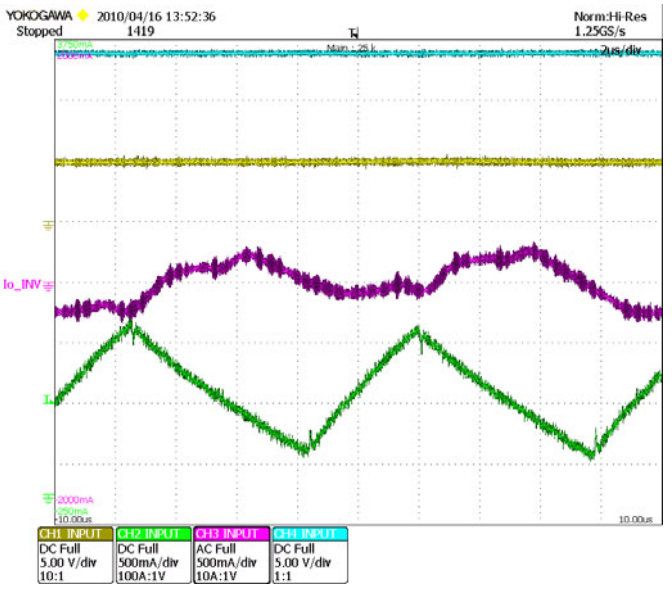

(a)

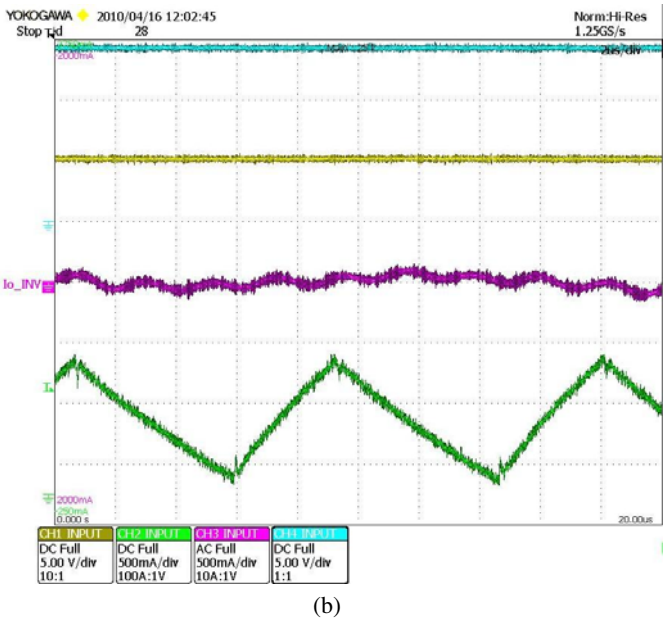

(b)

Fig. 16.17 Input voltage, output voltage, sum of the currents and master current for $E = 14$V and $V_{ref} = 5$V (a) when K remains fixed, (b) when K is dynamically adapted.

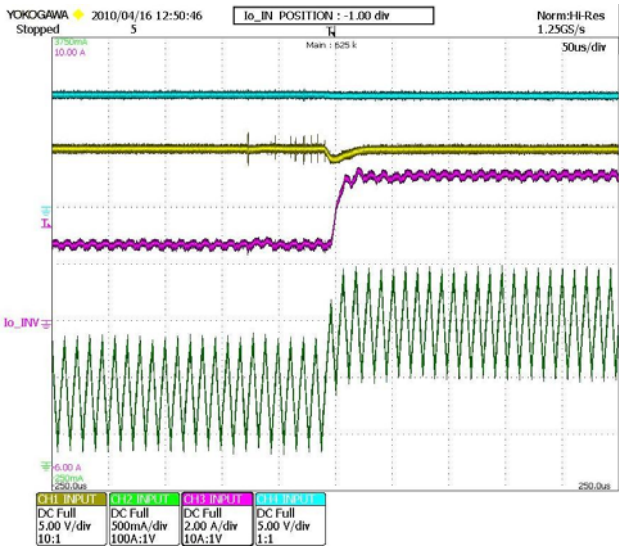

(a)

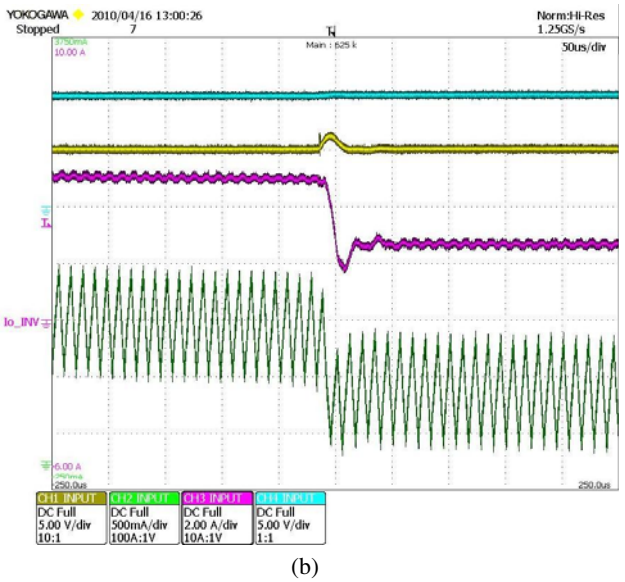

(b)

Fig. 16.18 Load variation. Input voltage, output voltage, sum of currents and master current when the load changes (a) from $R = 2\,\Omega$ to $R = 1\,\Omega$; (b) from $R = 1\,\Omega$ to $R = 2\,\Omega$.

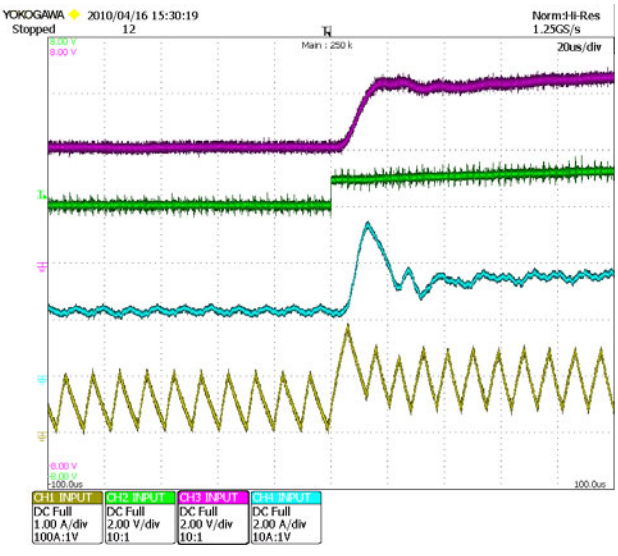

(a)

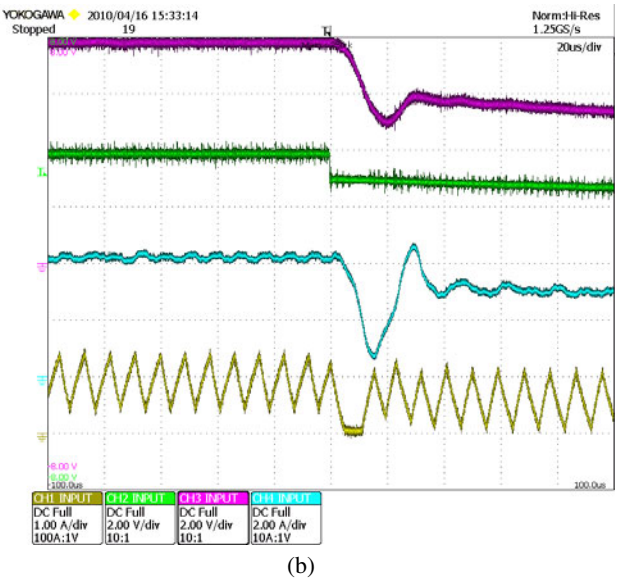

(b)

Fig. 16.19 Reference voltage variation. Output voltage, reference voltage (scaled by 0.5), sum of currents and master current (a) when the reference voltage changes from 4V to 6V; (b) when the reference voltage changes from 8V to 6V.

dynamically adjusting a specific gain which is characteristic of the SMC of multiphase converters [5], [2].

Acknowledgements. R. S. Muñoz-Aguilar and A. Dòria-Cerezo were partially supported by the Spanish government research projects ENE2008-06841-C02-01/ALT, and DPI2007-62582, respectively, while E. Fossas was partially supported by the Spanish government research projects DPI2008-01408 and DPI2010-15110. D. Biel was partially supported by the Spanish government research projects DPI2009-14713-C03-03 and DPI2010-15110. The authors would like to express their gratitude to Prof. Vadim I. Utkin for its comments during the controller design and experimental steps, and to Rafel Cardoner and Enric Miró for helping in the implementation of the power converter control stages.

References

1. Anderson, P., Fouad, A.: Power System Control and Stability. The Iowa State University Press (1977)
2. Biel, D., Fossas, E.: Some experiments on chattering suppression in power converters. In: Proc. IEEE Conference on Control Applications (CCA 2009), pp. 1523–1528 (2009)
3. Chiasson, J.: Modeling and High Performance Control of Electric Machines. John Wiley & Sons Inc., Chichester (2005)
4. Dòria-Cerezo, A., Utkin, V., Muñoz-Aguilar, R., Fossas, E.: Two sliding mode control approaches for the stator voltage amplitude regulation of a stand-alone wrsm. In: Proc. of the 11th Int. Workshop on Variable Structure Systems (2010)
5. Lee, H., Malinin, A., Utkin, V.: Chattering suppresion in multiphase power converters. International Journal of Control 8(9), 1720–1737 (2009)
6. Lee, H., Utkin, V.: The Chattering Analysis. LNCIS, vol. 334, pp. 107–124. Springer, Berlin (2006)
7. Muñoz-Aguilar, R., Dòria, A., Fossas, E., Cardoner, R.: Sliding mode control of a stand-alone wound rotor synchronous generator. IEEE Transactions on Industrial Electronics (2011), doi:10.1109/TIE.2011.2116754
8. Utkin, V., Guldner, J., Shi, J.: Sliding Mode Control in Electromechanical Systems. Taylor and Francis, Abington (1999)

Chapter 17
Advances in High Order and Adaptive Sliding Mode Control – Theory and Applications

F. Plestan, V. Brégeault, A. Glumineau, Y. Shtessel, and E. Moulay

Abstract. The objective of this chapter is to present advanced control methodologies of uncertain nonlinear systems. Firstly, adaptive sliding mode controller that retains the system's robustness in the presence of the bounded uncertainties/perturbations with unknown bounds is proposed. Due to the on-line adaptation, the proposed approach allows reducing control chattering. Secondly, a high order sliding mode control strategy that features a priory knowledge of the convergence time is presented. Finally, the output feedback second order sliding mode controller is presented and discussed. The control algorithms are applied to experimental set-up equipped by electrical or electropneumatic actuators.

17.1 Introduction

The objective of this chapter is to display major results obtained at IRCCyN, Nantes, France in the last 5 years, on sliding mode control of nonlinear uncertain systems, and the perspectives of future research works. The presented results are dedicated to two topics : the first one is about the very recent results on adaptive sliding mode control, whereas the second part of the chapter presents methodologies for high order sliding mode control (HOSM) of uncertain nonlinear systems. In the third part of the chapter, the results of the applications of the several newly developed sliding mode control laws to the real experimental set-ups (electropneumatic and electrical actuators) are demonstrated.

F. Plestan · V. Brégeault · A. Glumineau
IRCCyN, UMR CNRS 6597 - Ecole Centrale de Nantes, Nantes, France
e-mail: Franck.Plestan@irccyn.ec-nantes.fr

Y. Shtessel
The University of Alabama in Huntsville, Huntsville, USA
e-mail: shtessel@eng.uah.edu

E. Moulay
Xlim, UMR CNRS 6172 - Université de Poitiers, Futuroscope Chasseneuil, France
e-mail: Emmanuel.Moulay@univ-poitiers.fr

L. Fridman et al. (Eds.): Sliding Modes, LNCIS 412, pp. 465–492.
springerlink.com

The main purpose of the proposed adaptive sliding mode control approach is to retain a robustness feature of the controller to the bounded uncertainties/perturbations *without knowledge* of their bounds. The proposed sliding mode control with the *on-line* gain adaptation law allows not to overestimate the control gains. A direct consequence of the limitation of the gain value limitation is the chattering reduction.

Concerning HOSM control, all the presented results have been obtained in order to achieve the following objectives. Firstly, given that one of the features of HOSM control is the finite time convergence, the convergence time is precisely known and arbitrarily tuned *a priori*; secondly, the sliding mode occurs as early as the initial time, which ensures robustness features all over the entire response of the system. Finally, the strategy can be applied any order of sliding mode (greater or equal to the relative degree).

The chapter is organized as follows. Section 17.2 states the problem of high order sliding mode control for uncertain nonlinear systems. This section introduces the definitions of high order sliding surface, real sliding mode and shows that the HOSM control problem can be viewed as the stabilization at the origin (or in a vicinity of the origin) of an uncertain nonlinear system. Section 17.3 presents a solution for adaptive control, only for "standard" (first order) sliding mode control. Section 17.4 presents two approaches for HOSM control. The first one is based on the concept of integral sliding mode whereas the second one uses precomputed trajectories. A subsection devoted to an original output feedback second order sliding mode control completes the section. Finally, Section 17.5 establishes the applicability of all the control approaches by applying them to real experimental set-ups equipped by electrical or electropneumatic actuators.

17.2 Problem Statement

In this section, the problem of HOSM control of an uncertain nonlinear system is stated and written as the stabilization of an uncertain chain of integrators. Consider an uncertain nonlinear system[1]

$$\begin{aligned} \dot{x} &= f(x) + g(x)u \\ y &= h(x) \end{aligned} \tag{17.1}$$

where $x \in \mathbf{X} \subset \mathbb{R}^n$ is the state variable, $u \in \mathbb{R}$ is the input control and $y \in \mathbb{R}$ is the output function. $\mathbf{X}$ is a bounded open subset of $\mathbb{R}^n$ within which the boundedness of the system dynamics is ensured. Let $\sigma(x,t)$ denote the sliding variable defined as

$$\sigma(x,t) = h(x) - h_d(t) \tag{17.2}$$

with $h_d(t)$ being the smooth and differentiable enough desired trajectory. $\sigma(x,t)$, $f(x)$ and $g(x)$ are smooth functions, $f(x)$ and $g(x)$ being uncertain. Assume that

[1] For a sake of clarity, only SISO systems are considered in this chapter.

H1. The sliding mode order r is equal to the relative degree of σ w.r.t. (17.1). ■

Remark 17.1. The problem of zero dynamics stability is not studied here. ■

Remark 17.2. In case of sliding mode order larger than the relative degree of σ, the problem is a natural development of the current work, through the extension of system (17.1) by introduction of successive time derivatives of control input (see for example [10, 15]). All the results displayed in the sequel can then be applied to the extended system. ■

The control objective is to fulfill the constraint $\sigma(x,t) = 0$ *in finite time and then to keep it exactly at 0 by some feedback.* The r^{th} order sliding mode is defined as

Definition 17.1. [11] Consider the nonlinear system (17.1), and let the system be closed by some possibly-dynamical discontinuous feedback. The variable σ is a continuous function. The set

$$\mathbf{S} = \{x \in \mathbf{X},\ t > 0 \mid \sigma(x,t) = \dot{\sigma}(x,t) = \cdots = \sigma^{(r-1)}(x,t) = 0\} \tag{17.3}$$

is called "r^{th} order sliding surface", is non-empty and is locally an integral set in the Filippov sense [2], *i.e.* it consists of Filippov's trajectories of the discontinuous dynamical system. The motion on $\mathbf{S}$ is called "r^{th} order sliding mode" with respect to the sliding variable σ. ■

In real applications, due to the use of sampled control and neglected dynamics, the "ideal" sliding mode as defined in Definition 17.1 can not be established. Then, it is necessary to introduce the concept of "real" sliding mode. For a sake of clarity, only the "first order" real sliding mode concept is introduced here.

Definition 17.2. [11] Given the sliding variable $\sigma(x,t)$, the "real sliding surface" associated to (17.1) is defined as (with $\delta > 0$)

$$\mathbf{S}^* = \{x \in \mathbf{X},\ t > 0 \mid |\sigma| < \delta\}. \tag{17.4}$$

■

Definition 17.3. [11] Consider the non-empty real sliding surface $\mathbf{S}^*$ given by (17.4), and assume that it is locally an integral set in the Filippov sense. The corresponding behavior of system (17.1) on (17.4) is called "real sliding mode" with respect to the sliding variable $\sigma(x,t)$. ■

The r^{th} order sliding mode control approach allows the finite time stabilization to zero of the sliding variable σ and its $r-1$ first time derivatives by defining a suitable discontinuous control function. The output σ satisfies equation [13]

$$\sigma^{(r)} = \bar{\Phi}(x) + \Gamma(x)u - h_d^{(r)}(t) = \Phi(x,t) + \Gamma(x)u \tag{17.5}$$

with $\Gamma(x) = L_g L_f^{r-1} h(x)$, $\bar{\Phi}(x) = L_f^r h(x)$ and $\Phi(x,t) = \bar{\Phi}(x) - h_d^{(r)}(t)$. Assume that

H2. The solutions are understood in the Filippov sense [2], and the system trajectories are supposed to be infinitely extendible in time for any bounded Lebesgue measurable input. ■

Then, the r^{th} order sliding mode control of (17.1) with respect to the sliding variable σ is equivalent to the finite time stabilization of

$$\begin{aligned} \dot{Z}_1 &= A_{11}Z_1 + A_{12}Z_2 \\ \dot{Z}_2 &= \Phi + \Gamma u \end{aligned} \tag{17.6}$$

with

$$Z_1 = [Z_{10}\ Z_{11}\ \cdots\ Z_{1r-2}]^T := [\sigma\ \dot{\sigma}\ \cdots\ \sigma^{(r-2)}]^T,\ \ Z_2 = \sigma^{(r-1)}.$$

A_{11} ($(r-1)\times(r-1)$ matrix) and A_{12} ($(r-1)\times 1$ vector) are such that Z_1 dynamics are the ones of chain of integrators. For a sake of clarity in the sequel, consider the following hypothesis

H3. Uncertain functions Φ and Γ can be decomposed

$$\Phi = \Phi_n + \Delta\Phi, \qquad \Gamma = \Gamma_n + \Delta\Gamma \tag{17.7}$$

with Φ_n and Γ_n the nominal bounded values (well-known), and $\Delta\Phi$ and $\Delta\Gamma$ the bounded uncertainties for $x \in \mathbf{X}$ and $t \geq 0$. Furthermore, the function Γ_n is invertible for $x \in \mathbf{X}$ and $t \geq 0$. ■

By applying the deterministic feedback controller

$$u = \Gamma_n^{-1} \cdot (-\Phi_n + v), \tag{17.8}$$

system (17.6) becomes

$$\begin{aligned} \dot{Z}_1 &= A_{11}Z_1 + A_{12}Z_2 \\ \dot{Z}_2 &= \underbrace{\left[\Delta\Phi - \Delta\Gamma \cdot \Gamma_n^{-1} \cdot \Phi_n\right]}_{\varphi(\cdot)} + \underbrace{\left[1 + \Delta\Gamma \cdot \Gamma_n^{-1}\right]}_{\gamma(\cdot)} \cdot v \end{aligned} \tag{17.9}$$

H4. Functions $\varphi(x,t)$ and $\gamma(x)$ are bounded uncertain functions, and, without loss of generality, let also $\gamma(x)$ be strictly positive. Thus, there exist constants $K_m > 0$, $K_M > 0$ and $C_0 \geq 0$ such that $0 < K_m \leq \gamma(x) \leq K_M$ and $|\varphi(x,t)| \leq C_0$ for $x \in \mathbf{X}$. ■

Then, the r^{th} order sliding mode control of (17.1) with respect to the sliding variable σ is equivalent to the finite time stabilization of

$$\begin{aligned} \dot{Z}_1 &= A_{11}Z_1 + A_{12}Z_2 \\ \dot{Z}_2 &= \varphi + \gamma v \end{aligned} \tag{17.10}$$

Under Assumption H4, system (17.10) can be viewed as a chain of integrators with uncertain bounded terms φ and γ. Then, the problem can be stated as the finite time

stabilization of (17.10) in a linear uncertain context when considering the nonlinear functions γ and φ as bounded non structured parametric uncertainties.

In case of a "standard" (first order) sliding mode, the previous problem can be reduced to the design of a discontinuous controller v such that the system

$$\dot{\sigma} = \varphi + \gamma v \tag{17.11}$$

is stabilized in a vicinity of the origin. In the following section, an adaptive solution of the form $v = -K(t) \cdot \text{sign}(\sigma)$ is proposed.

17.3 Adaptive Sliding Mode Control

In this section, an adaptive sliding mode controller is proposed: this result is given in the case of first order sliding mode control ($r = 1$). The previously presented bounds K_m, K_M and C_0 are supposed to *exist but are not known*. The control gain has therefore to be *dynamically tuned* in order to be adapted to perturbations and uncertainties. The solution proposed in [16] is displayed in the sequel. Consider the controller

$$v = -K(t) \cdot \text{sign}(\sigma(x,t)) \tag{17.12}$$

with the gain $K(t)$ defined such that

$$\dot{K} = \begin{cases} \bar{K} \cdot |\sigma(x,t)| \cdot \text{sign}(|\sigma(x,t)| - \varepsilon) & \text{if } K > \mu \\ \mu & \text{if } K \leq \mu \end{cases} \tag{17.13}$$

with $K(0) > 0$, $\bar{K} > 0$, $\varepsilon > 0$ and $\mu > 0$ very small. The parameter μ is introduced in order to get only positive values for K.

Discussion. (see Figure 17.1) Suppose that $K(0) > \mu$ and, at $t = 0$, $|\sigma(x(0),0)| > \varepsilon$. Then, from (17.13), the gain $K(t)$ is increasing, *i.e.*

$$\dot{K} = \bar{K} \cdot |\sigma(x,t)|.$$

There exists a time instant t_1 (see Figure 17.1) such that $|\sigma(x(t_1),t_1)| < \varepsilon$, *i.e.* t_1 is a reaching time. As a real sliding mode is established, it means that the gain $K(t)$ is large enough with respect to uncertainties and perturbations. Then, it can be decreased in order to limit control magnitude and then to attenuate the chattering. Then, from $t = t_1$, K-gain adaptation law reads as

$$\dot{K} = -\bar{K} \cdot |\sigma(x,t)|.$$

The gain $K(t)$ is decreasing and then is adjusted by allowing to get a more adequate value with respect to uncertainties/perturbations magnitude. However, if disturbances/uncertainties contained in φ and γ exceed some value that makes $|\sigma(x,t)| > \varepsilon$ (from $t = t_2$ - see Figure 17.1), then the adaptation law becomes again

$$\dot{K} = \bar{K} \cdot |\sigma(x,t)|$$

until the next reaching time t_3 (see Figure 17.1), *i.e.* from $t = t_3$, $|\sigma(x(t),t)| < \varepsilon$, and so on. ■

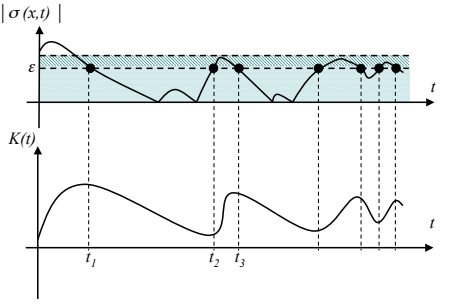

Fig. 17.1 Behavior of $\sigma(x,t)$ and $K(t)$ versus time around ε-convergence domain.

Lemma 17.1. **[16]** *Given the nonlinear uncertain system (17.1) with the sliding variable $\sigma(x,t)$ dynamics (17.5) with $r = 1$ controlled by (17.8)-(17.12)-(17.13), the gain $K(t)$ has an upper-bound, i.e. there exists a positive constant K^* so that*

$$K(t) \leq K^*, \ \ \forall t > 0.$$

■

Theorem 17.1. **[16]** *Given the nonlinear uncertain system (17.1) with the sliding variable $\sigma(x,t)$ dynamics (17.5) with $r = 1$ controlled by (17.8)-(17.12)-(17.13), there exists a finite time $t_F > 0$ so that a real sliding mode is established for all $t \geq t_F$, i.e. $|\sigma(x,t)| < \delta$ for $t \geq t_F$, with*

$$\delta = \sqrt{\varepsilon^2 + \frac{C_0^2}{\bar{K} K_m}}. \tag{17.14}$$

■

Sketch of proof. [16] The proof detailed in [16] is based on Lyapunov's approach and shows that, when $|\sigma| > \varepsilon$, then the control strategy ensures that $|\sigma| < \varepsilon$ in a finite time. Furthermore, it is proved that, once σ has reached ε-domain, system trajectories are such that $|\sigma|$ is evolving in a vicinity of ε whose the bound is given by δ. Therefore, the proof shows that there is the establishment of a real sliding mode given that, in a finite time, $|\sigma| < \delta$. Consider the following Lyapunov candidate function

$$V = \frac{1}{2}\sigma^2 + \frac{1}{2\alpha}(K - K^*)^2 \tag{17.15}$$

By introducing $\beta_\sigma = -C_0 + K_m \cdot K^*$ and

$$\xi = -K_m \cdot |\sigma| + \frac{\bar{K}}{\alpha} \cdot |\sigma| \cdot \text{sign}(|\sigma| - \varepsilon) - \beta_K$$

with $\beta_K > 0$ a positive constant, it yields from [16]

$$\begin{aligned}\dot{V} &\leq -\beta_\sigma \cdot |\sigma| - \beta_K \cdot |K - K^*| - \xi \\ &= -\beta_\sigma \cdot \sqrt{2}\frac{|\sigma|}{\sqrt{2}} - \beta_K \cdot \sqrt{2\alpha}\frac{|K-K^*|}{\sqrt{2\alpha}} - \xi \\ &\leq -\min\{\beta_\sigma\sqrt{2}, \beta_K\sqrt{2\alpha}\}\left(\frac{|\sigma|}{\sqrt{2}} + \frac{|K-K^*|}{\sqrt{2\alpha}}\right) - \xi \leq -\beta \cdot V^{1/2} - \xi\end{aligned} \tag{17.16}$$

with $\beta = \sqrt{2}\min\{\beta_\sigma, \beta_K\sqrt{\alpha}\}$.

- Suppose that $|\sigma| > \varepsilon$. ξ is positive if

$$-K_m \cdot |\sigma| + \frac{\bar{K}}{\alpha} \cdot |\sigma| - \beta_K > 0 \Rightarrow \alpha < \frac{\bar{K} \cdot \varepsilon}{K_m \cdot \varepsilon + \beta_K}. \tag{17.17}$$

  From (17.16), one gets $\dot{V} \leq -\beta \cdot V^{1/2}$. It is always possible to choose α such that the previous inequality fulfills. Therefore, finite time convergence to a domain $|\sigma| \leq \varepsilon$ is guaranteed from any initial condition $|\sigma(0)| > \varepsilon$.
- **Case 2.** Suppose now that $|\sigma| < \varepsilon$. Function ξ in (17.16) can be negative. It means that $\dot{V}$ would be sign indefinite, and it is not possible to conclude on the closed-loop system stability. Therefore, $|\sigma|$ can increase over ε. As soon as $|\sigma|$ becomes greater than ε, $\dot{V} \leq -\beta \cdot V^{1/2}$ and V starts decreasing. Decrease of V can be achieved via increase of K allowing $|\sigma|$ to increase before it starts decreasing down to $|\sigma| \leq \varepsilon$. Without loss of generality, by supposing $\sigma_0 = \sigma(0) = \varepsilon^+$ and $K_0 = K(0) > 0$, the overshoot can be estimated from $\sigma(t)$ and $K(t)$. In the "worst" case, these both latter functions read as [16]

$$\begin{aligned}\sigma(t) &= \sqrt{\sigma_0^2 + \frac{(C_0 - K_0K_m)^2}{\bar{K}K_m}}\sin\left(\sqrt{\bar{K}K_m}t + \Theta_\sigma\right) \\ K(t) &= \sqrt{\sigma_0^2\frac{\bar{K}}{K_m} + \left(K_0 - \frac{C_0}{K_m}\right)^2}\sin\left(\sqrt{\bar{K}K_m}t + \Theta_K\right) + \frac{C_0}{K_m}.\end{aligned} \tag{17.18}$$

  with Θ_σ and Θ_K constants depending on all the parameters. It appears from (17.18) that, when $\sigma_0 = \varepsilon^+ \to \varepsilon$, the maximum value δ of σ_M reads as

$$\delta = \sqrt{\varepsilon^2 + \frac{C_0^2}{\bar{K}K_m}}. \tag{17.19}$$

Finally, σ converges to the domain $|\sigma| \leq \varepsilon$ in a finite time, but could be sustained in the bigger domain $|\sigma| \leq \delta$. Therefore, the real sliding mode exists in the domain $|\sigma| \leq \delta$. ■

The previously presented adaptive control law is only usable for first order sliding mode establishment. Future researches can be made in order to extend this results to high order sliding mode control. Note that some of the authors have still obtained

preliminary results for second order sliding mode control, which allow to get more accurate results without any information on the uncertainties and perturbations (only the boundness feature is known).

17.4 High Order Sliding Mode Control

17.4.1 A Unified Approach

The two controllers presented in this section allow the establishment of a r^{th} order sliding mode by knowing the bounds of the uncertainties and perturbations. The control laws stabilize system (17.5) (or system (17.10)) to zero (or near zero) in an *a priori* finite time in spite of uncertainties / perturbations. For each developed control algorithm, the design procedure takes place in two stages

Stage 1. Trajectories of (17.5) (or system (17.10)) are forced to converge to the origin (or its vicinity), *i.e.* for (17.10), $[Z_1^T \; Z_2]^T = 0_{r\times 1}$ in a finite time t_F.

Stage 2. From $t = t_F$, trajectories of (17.5) (or system (17.10)) are forced to stay at the origin (or its vicinity).

The design of the control law is then as follows. First-of-all, the *sliding surface* is defined such that, if the system is evolving on it, one ensures $\sigma = \dot{\sigma} = \cdots = \sigma^{(r-1)} = 0$ in a finite time. Furthermore, the discontinuous control law is designed to make the sliding surface attractive in spite of the uncertainties and perturbations. The way to state the high order sliding mode controller design in terms of specific trajectories tracking contributes to the originality of the approaches.

17.4.1.1 Sliding Surface Design

From the *sliding variable* $\sigma(x,t)$ (17.2), let S be the so-called *switching variable* defined as

$$S = \sigma^{(r-1)} + \mathscr{F}(\cdot) \tag{17.20}$$

with $\mathscr{F}$ a function depending on time t and/or state vector x. This latter function has a key-role in the design of the proposed solutions for high order sliding mode control. Associated to this switching variable, the *sliding surface* $\mathbf{S}_S$ is defined as

$$\mathbf{S}_S = \{x \in \mathbf{X} \mid S = 0\}, \tag{17.21}$$

The main idea consists in an adequate choice for the function $\mathscr{F}$. By supposing that the control law forces the system trajectories to evolve on $\mathbf{S}_S$, it ensures that, from a finite time (*a priori* defined), the system trajectories are evolving on $\mathbf{S}$. As mentioned previously, this latter behavior ideally induces a high order sliding mode with respect to σ.

Remark 17.3. In the case of a dynamical sliding mode [3,21], function $\mathscr{F}$ is defined as

$$\mathscr{F} = \lambda_{r-2}\sigma^{(r-2)} + \lambda_{r-3}\sigma^{(r-3)} + \cdots + \lambda_0\sigma \tag{17.22}$$

with $\lambda_{r-2}, \cdots, \lambda_0$ chosen such that $P(z) = z^{r-1} + \lambda_{r-2} z^{r-2} + \cdots + \lambda_0$ is Hurwitz. A control law $v = -K \cdot \text{sign}(\sigma^{(r-1)} + \mathscr{F})$ ensures a finite time convergence to $\mathbf{S}_S$ if gain K is well-tuned with respect to uncertainties and perturbations. On the other hand side, this choice of function $\mathscr{F}$ does not allow a finite time convergence to $\mathbf{S}$: there is no establishment of high order sliding mode with respect to σ. ■

17.4.1.2 Controller Design

The control law v is now divided into two terms[2]: a continuous one v_0 and a discontinuous one v_1 such that

$$v = v_0 + v_1. \tag{17.23}$$

In order to make the surface $\mathbf{S}_S$ attractive, the discontinuous term v_1 reads as, for $0 \leq t \leq t_F$,

$$v_1 = -K \cdot \text{sign}(S) = -K \cdot \text{sign}\left(Z_2 + \mathscr{F}\right) = -K \cdot \text{sign}\left(s^{(r-1)} + \mathscr{F}\right) \tag{17.24}$$

with K tuned by taking into account uncertainties and perturbations, bounds of time derivatives of $\mathscr{F}$ and the bound of continuous term v_0 (see details in [8, 9, 10, 15]), such that the sliding condition

$$S \cdot \dot{S} < -\eta \, |S| \tag{17.25}$$

is fulfilled, with $\eta > 0$. One has

$$\begin{aligned} S \cdot \dot{S} &= S \cdot \left(\varphi + \gamma \cdot (v_0 + v_1) + \dot{\mathscr{F}}\right) \\ &= S \cdot \left(\varphi + \gamma \cdot [v_0 - K \cdot \text{sign}(S)] + \dot{\mathscr{F}}\right). \end{aligned}$$

Suppose that $S > 0$ (the computations would be similar for $S < 0$): one gets

$$\varphi - K \cdot \gamma + v_0 \cdot \gamma + \dot{\mathscr{F}} < -\eta \quad \Rightarrow \quad K > \frac{\varphi + v_0 \cdot \gamma + \dot{\mathscr{F}} + \eta}{\gamma}.$$

Knowing the bounds C_0, K_m and denoting $\mathscr{F}_M = \text{Max}_{0 \leq t \leq t_F} \left[\left|\dot{\mathscr{F}}(t)\right|\right]$ and $v_{0_M} = \text{Max}_{0 \leq t \leq t_F} \left[|v_0|\right]$, one gets the following condition on the gain K ensuring the convergence of the system to the surface $\mathbf{S}_S$

$$K > \frac{C_0 + v_{0_M} + \mathscr{F}_M + \eta}{K_m}. \tag{17.26}$$

In the sequel, the design of two specified function $\mathscr{F}$ is given, as well as the corresponding control terms v_0 and v_1.

[2] This decomposition will be used in the sequel, for the description of the proposed algorithms.

17.4.2 Control Solutions and Design of Functions $\mathscr{F}$

In the sequel, two different approaches for the design of the function $\mathscr{F}$ are proposed. As written previously, the function $\mathscr{F}$ is designed in order to allow the controller to ensure the establishment, in a finite time, of a high order sliding mode behaviour. In each control solution, the computation of $\mathscr{F}$ is based on a linear control law with finite time convergence. In this section, two control solutions are presented[3]

- The first one [10] is based on the concept of *Integral sliding mode* [24], which introduces dynamics in the control algorithm. One of its advantages is the cancelation of the reaching phase: the system is evolving on the surface early from $t = 0$, which allows to perfectly know the convergence time.
- The second one uses precomputed trajectories derived from open-loop linear control law. These trajectories are computed such that the system evolves on the sliding surface early from $t = 0$.

17.4.2.1 Integral Sliding Mode Control [10]

The use of the concept of the *Integral Sliding mode* for the synthesis of high order sliding mode control makes the result original because it is the first result using this concept in a such context. This concept developed in [24] consists in considering first-of-all the "ideal" system (*i.e.* the system without uncertainties and perturbations) for which a continuous control law v_0 is designed in order to drive it to 0 in a finite time. Then, considering that the control law reads as (17.23), the discontinuous part v_1 is added to the continuous one v_0 in order to perfectly track, early from $t = 0$, "ideal" system trajectories, in spite of perturbations and uncertainties.

Design of the continuous term v_0. The term v_0 is designed on the assumption that there is no uncertainty nor perturbation; in this case, the system (17.1) is equivalent to the system (17.10) with $\varphi = 0$ and $\gamma = 1$. One gets

$$\Sigma_{ref} \begin{cases} \dot{Z}_1 = A_{11}Z_1 + A_{12}Z_2 \\ \dot{Z}_2 = v_0 \end{cases} \Rightarrow \dot{Z} = A \cdot Z + B \cdot v_0 \qquad (17.27)$$

with[4] $Z = [Z_1^T \; Z_2]^T$. The term v_0 allows to force the trajectories of system (17.27) to reach the origin in a finite time, and to maintain them at this point. A solution for v_0 used in [10] is given by [18] and is based on a H_2 optimal feedback control over a finite time interval with fixed final states; this solution is displayed in the following theorem.

[3] In [8,9], the solution is based on a *LQ* control law. This strategy, which will be not detailed in this chapter because of the lack of space, only allows the establishment of a "real" sliding mode.

[4] Recall that, in the current context, $Z = [\sigma(x,t) \; \dot{\sigma}(x,t) \; \cdots \; \sigma^{(r-1)}(x,t)]^T$.

Theorem 17.2. [18] *Consider linear system (17.27) with (A,B) reachable. A control law v_0 minimizing the criteria*

$$J = \frac{1}{2}\int_0^{t_F} Z^T QZ + v_0^2 \, \mathrm{d}t \tag{17.28}$$

with $t_F < +\infty$, $|Z(0)| < +\infty$ and Q a symmetric positive definite matrix under the fixed final state constraint $Z(t_F) = 0$ and driving system (17.27) to $Z(t) = 0$ at $t = t_F$ from $Z(0)$ is given by

$$v_0 = -B^T MZ(t) + B^T \delta(t) \tag{17.29}$$

with $\delta(t)$ and M defined by

$$\begin{aligned} \dot{\delta} &= -(A^T - MBB^T)\,\delta, \\ 0 &= MA + A^T M - MBB^T M + Q. \end{aligned} \tag{17.30}$$

Initial condition $\delta(0)$ of $\delta(t)$ is selected in order to satisfy the terminal condition $Z(t_F) = 0$. ∎

Design of the discontinuous term v_1. As mentioned previously, the objective consists in forcing the "real" system (17.10) to behave like the "ideal" linear system (17.27), early from $t = 0$, by rejecting uncertainties and perturbations thanks to the discontinuous term v_1. A solution consists in defining the switching variable S as

$$S = \sigma^{(r-1)} + \underbrace{\sigma_{0,r-1}(t)}_{\mathscr{F}} \tag{17.31}$$

with $\sigma_{0,r-1}(t)$ an exogenous variable defined as

$$\dot{\sigma}_{0,r-1} = -v_0, \quad \sigma_{0,r-1}(0) = -\sigma^{(r-1)}(0) \tag{17.32}$$

It implies that $S(0) = 0$: then, the system is in sliding motion on $\mathbf{S}$ from $t = 0$. Thanks to an adequate tuning of the gain K (equation (17.26)), the discontinuous control v_1

$$v_1 = -K\,\mathrm{sign}(S)$$

forces the system (17.10) to evolve on the surface $\mathbf{S}$ and then to follow the "ideal" system (17.27): dynamics of (17.10) allows the establishment of an ideal high order sliding mode behavior from $t = t_F$.

Remark 17.4. The switching variable (17.31) only depends on $\sigma^{(r-1)}$ and then requires its highly accurate knowledge: this time derivative is obtained by differentiating $r-1$ times the sliding variable σ (by supposing that it is measured) for example through the use of robust time differentiators [12]. Then, by a practical point-of-view, the sampling allows to obtain a real sliding mode. However, it yields to a delayed and noised information which can strongly decrease the performances of the controller in term of finite time convergence, accuracy, ... This drawback can be limited thanks to the choice of the switching variable defined as a function of σ, $\dot{\sigma}$,

$\ldots, \sigma^{(r-1)}$. The control law v reads as $v = v_0 + v_1$ with v_0 defined as previously and v_1 as

$$v_1 = -K\text{sign}\left(\sigma^{(r-1)} + \underbrace{\sigma_{0,r-1} + \lambda_{r-2}(\sigma^{(r-2)} + \sigma_{0,r-2}) + \cdots + \lambda_0(\sigma + \sigma_{0,0})}_{\mathscr{F}}\right) \tag{17.33}$$

with $\sigma_{0,r-1}(t),\ \sigma_{0,r-2}(t), \ldots,\ \sigma_{0,0}(t)$ exogenous variables defined by

$$\begin{array}{ll} \dot{\sigma}_{0,0} = \sigma_{0,1}, & \sigma_{0,0}(0) = -\sigma(0) \\ \dot{\sigma}_{0,1} = \sigma_{0,2}, & \sigma_{0,1}(0) = -\dot{\sigma}(0) \\ \qquad\qquad \vdots & \\ \dot{\sigma}_{0,r-1} = -v_0, & \sigma_{0,r-1}(0) = -\sigma^{(r-1)}(0) \end{array} \tag{17.34}$$

The coefficients λ_* in $\mathscr{F}$ are chosen such that the polynomial $P(s) = s^{r-1} + \lambda_{r-2}s^{r-2} + \ldots + \lambda_0 s$ (s being a complex variable) is Hurwitz. From (17.34), $S(0)$ and each of its terms equal 0. In [4, 6], it has been proved that the proposed control law ensures the establishment of a r^{th} order sliding mode behavior for the "ideal" case and of a real r^{th} order sliding mode for a sampled control. ■

One of the advantages of the integral sliding mode approach is the absence of reaching phase to the sliding surface, given that the system is evolving in the surface early from the initial time. It implies that the convergence time is *a priori* known. However, this approach requires the use of an auxiliary dynamical system, which could be a drawback for example in case of embedded systems because of online computations. The approach developed in the next section will allow to remove the use of auxiliary dynamical system.

17.4.2.2 Precomputed Trajectories [15]

The objective of this control law strategy consists in providing a solution without use of an auxiliary dynamical system while keeping the features

- Robustness versus uncertainties and perturbations,
- Establishment in finite time of a high order sliding mode behavior with *a priori* knowledge of the finite time convergence,
- The system evolves on the sliding surface *early from* the initial time.

Let us recall that the switching variable S reads as

$$S = \sigma^{(r-1)} + \mathscr{F}(t)$$

with $\mathscr{F}$ a time-varying function. Define the function $\overline{\mathscr{F}}$ as $\overline{\mathscr{F}}^{(r-1)} = \mathscr{F}$. $\overline{\mathscr{F}}(t)$ has to verify the following features

- The system is evolving early from the initial time on the sliding surface

$$\overline{\mathbf{S}}_S = \{x \in \mathbf{X} \mid \sigma + \overline{\mathscr{F}}(\cdot) = 0,\ \dot{\sigma} + \dot{\overline{\mathscr{F}}}(\cdot) = 0,\ \ldots,\ \sigma^{(r-1)} + \overline{\mathscr{F}}^{(r-1)}(\cdot) = 0\}$$

  which removes the transient phase required to reach the surface, *i.e.*

$$\overline{\mathscr{F}}(0) = -\sigma(x(0),0), \dot{\overline{\mathscr{F}}}(0) = -\dot{\sigma}(x(0),0), \ldots, \overline{\mathscr{F}}^{(r-1)}(0) = -\sigma^{(r-1)}(x(0),0). \tag{17.35}$$

  This first constraint is not strong ; only the knowledge of the initial conditions of the sliding variable and its $r-1$ first time derivatives is required.
- The second constraint consists in stating that the system has to reach an r^{th} order sliding mode behavior with respect to $\sigma(x,t)$ at *exactly* $t = t_F$ by evolving on $\overline{\mathbf{S}}_S$. From the definition of this latter, one has

$$\sigma(x(t_f),t_f) = 0,\ \dot{\sigma}(x(t_f),t_f) = 0,\ \ldots,\ \sigma^{(r-1)}(x(t_f),t_f) = 0 \tag{17.36}$$

  which implies

$$\overline{\mathscr{F}}(t_f) = 0,\ \dot{\overline{\mathscr{F}}}(t_f) = 0,\ \ldots,\ \overline{\mathscr{F}}^{(r-1)}(t_f) = 0. \tag{17.37}$$

Suppose that the following hypothesis is fulfilled

H5. There exists *at least* one $j \in \mathbb{N}$ such that $0 \leq j \leq r-1$ and $\sigma^{(j)}(0) \neq 0$. ■

Under H5, it is always possible [15] to find a function $\overline{\mathscr{F}}(t)$ (and then $\mathscr{F}(t)$) satisfying (17.35)-(17.37). A solution[5] proposed in [15] reads as (with k arbitrarily chosen such that $0 \leq k \leq r-1$ and $\sigma^{(k)}(x(0),0) \neq 0$)

$$\overline{\mathscr{F}}(t) = K_{\mathscr{F}} e^{Ft} T \sigma^{(k)}(x(0),0) \Rightarrow \mathscr{F}(t) = K_{\mathscr{F}} F^{r-1} e^{Ft} T \sigma^{(k)}(x(0),0) \tag{17.38}$$

with F a stable $r \times r$-matrix (all its eigenvalues are negative), T a $2r \times 1$-vector and $0 \leq k \leq r-1$.

Lemma 17.2. **[15]** *Suppose that Hypothesis H5 is fulfilled. Then, there always exists a stable matrix F and a matrix T such that matrix $K_{\mathscr{F}}$ defined as (with $0 \leq k \leq r-1$)*

$$K_{\mathscr{F}} = \left[F^{r-1} T \sigma^{(k)}(0) \mid F^{r-1} e^{Ft_F} T \mid F^{r-2} T \sigma^{(k)}(0) \mid F^{r-2} e^{Ft_F} T \mid \ldots \mid T \sigma^{(k)}(0) \mid e^{Ft_F} T\right]$$

is invertible. ■

Then, a control law v ensuring the establishment of an r-th order sliding mode behavior with respect to the sliding variable $\sigma(x,t)$ in a finite time t_F is defined as $v = v_0 + v_1$ with [15] $v_0 = 0$ and

[5] In [19], a time-varying polynomial function is used. The advantage of an exponential function $\overline{\mathscr{F}}(t) = K_{\mathscr{F}} e^{Ft} T \sigma^{(k)}(x(0),0)$, $k \in \mathbb{N}$ is that it is usable for all sliding mode order whereas, in the case of a polynomial function, its order has to be adapted to the sliding mode order.

$$v_1 = \begin{cases} -K\text{sign}(\sigma^{(r-1)} + \mathscr{F}(t)) & \text{for } 0 \leq t \leq t_F \\ -K\text{sign}(\sigma^{(r-1)}) & \text{for } t > t_F \end{cases} \tag{17.39}$$

K and $\mathscr{F}(t)$ being respectively defined by (17.26) and (17.35)-(17.37)-(17.38).

Remark 17.5.

- One recalls that this control strategy can be easily used for practical applications (no auxiliary dynamical system, off-line computation of the function $\mathscr{F}(t)$, constructive condition for gain computation [15]).
- As previously for *Integral Sliding Mode*, in the case of application (finite sampling frequency), the switching variable must be adapted in order to take into account the "approached" time derivatives of the sliding variable. A real HOSM is then obtained. Then, in [6], a control law u defined as $v = v_0 + v_1$ with $v_0 = 0$ and

  $$v_1 = -K\text{sign}\left(\sigma^{(r-1)} + \overline{\mathscr{F}}^{(r-1)} + \lambda_{r-2}(\sigma^{(r-2)} + \overline{\mathscr{F}}^{(r-2)}) + \ldots + \lambda_0(\sigma + \overline{\mathscr{F}})\right).$$

  Given initial and final (at $t = t_F$) conditions on $\overline{\mathscr{F}}$, this control law u ensures the establishment of r-th order sliding mode behavior at *exactly* $t = t_F$.

17.4.3 Second Order Sliding Mode Control by Static Output Feedback [17]

A drawback of the HOSM controllers is the requirement of high order time derivatives of the switching variable. Then, the use of time differentiators is required : however, they introduce noisy informations in the controller, which can be harmful for the closed-loop system. An other solution consists in using static output feedback, *i.e.* the controller is using the sliding variable, and no time derivative of it. One of the most popular solutions is the "Super-Twisting" algorithm [11]. This algorithm is a second order sliding mode one but is only applicable to nonlinear systems with a sliding variable whose relative degree equals 1. This drawback has been removed in [17]: the proposed controller is applicable to systems with sliding variable whose relative degree equals 1 or 2. The control law is also using a switching strategy for the gain, which allows the finite time convergence in a vicinity of the origin, and then the establishment of a real second order sliding mode. The control law is developed in the case of finite sampling frequency. In the sequel, we first give the main idea of this output feedback controller through its application to a double integrator. Then, one proposes a solution for system (17.1) with $r = 2$.

17.4.3.1 Control of a Double Integrator

Consider the following system

$$\begin{aligned} \dot{z}_1 &= z_2 \\ \dot{z}_2 &= u \end{aligned} \tag{17.40}$$

with

$$u = -K(t)\,\mathrm{sign}\,(z_1(kT_e)) \tag{17.41}$$

and T_e the sampling period, $K > 0$ and $k \in I\!N$ (k can be viewed as a time counter). Gain K is constant on the time interval $t \in [k \cdot T_e, (k+1) \cdot T_e[$, and $k(0) = 0$.

Comments. The commutation of the gain $K(t)$, at an adequate time, between K_s and K_L, is crucial for the convergence and allows the system to reach a trajectory closer from the origin. As described in Figure 17.2, system (17.40) is starting from the point O and then follows the parabola (O,B) with the control gain equal to K_s. Given the sampling period, the control law is re-evaluated at each black point of the parabola. Due to this sampling period, the system takes into account the z_1-sign change only at B, which introduces a delay for the commutation of the control law. It is obvious that, if the gain $K(t)$ is maintained to the value K_s, the trajectory will follow the parabola (B,D) which yields to divergence. By using a sufficiently high gain K_L, it allows the system to reach the point C which is over the symmetric parabola of $(0,A)$ with respect to vertical axis, and then which is on a parabola closer from the origin. The use of a large gain K_L allows to compensate the delay due the sampling period by adding a sufficiently large energy to the system.

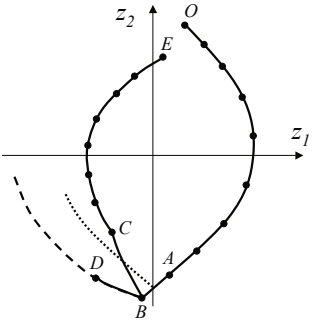

Fig. 17.2 Phase portrait of system (17.40).

Theorem 17.3. [17] *Consider system (17.40) controlled by (17.41) and a gain $K_s > 0$. Then, there always exists a sufficiently large gain K_L with $0 < K_s < K_L < \infty$ such that the gain $K(t)$ defined as*

$$K(t) = \begin{cases} K_s & \text{if } t \notin \mathscr{T} \\ K_L & \text{if } t \in \mathscr{T} \end{cases} \tag{17.42}$$

with $\mathscr{T} = \{t \mid \mathrm{sign}(z_1(kT_e)) \neq \mathrm{sign}(z_1((k-1)T_e))\}$ and the control law (17.41) ensures the establishment of a real second order sliding mode for system (17.40) with respect to z_1, i.e. there exists a finite time t_F such that, for $t \geq t_F$,

$$
\begin{aligned}
|z_1| &\leq \left[(K_L - K_s) + \frac{(K_L + K_s)^2}{2K_L}\right] \cdot T_e^2, \\
|z_2| &\leq \frac{K_L + K_s}{2} \cdot T_e
\end{aligned}
\tag{17.43}
$$

■

17.4.3.2 Extension to Uncertain Nonlinear Systems Control

This result has been extended for the second order sliding mode control of uncertain nonlinear systems, through the following theorem.

Theorem 17.4. [17] *Consider nonlinear system (17.1) with sliding variable $\sigma(x,t)$. Suppose that assumptions H1-H4 are fulfilled with $r = 2$, and state the gain K_s such that $K_s > C_0/K_m$. Then, there always exists a sufficiently large gain K_M with $0 < K_m < K_M < \infty$ such that the gain $K(t)$ defined as*

$$
K(t) = \begin{cases} K_s & \text{if } t \notin \mathscr{T} \\ K_L & \text{if } t \in \mathscr{T} \end{cases}
\tag{17.44}
$$

with $\mathscr{T} = \{t \mid \text{sign}(s(kT_e)) \neq \text{sign}(s((k-1)T_e))\}$, $k \in \mathbb{N}$ and the control input

$$
u = -K(t) \cdot \text{sign}(s(kT_e))
\tag{17.45}
$$

ensures the establishment of a real second order sliding mode for system (17.1) with respect to sliding variable $\sigma(x,t)$. ■

17.5 Applications

This section presents some practical applications of the previous high order sliding mode controllers. The main objectives of the following works were, not only to develop new methodologies for such kind of controllers, but also to evaluate their feasibility and their behaviors in case of real applications. In the sequel, results obtained by the authors for the control of electrical and electropneumatic actuators are recalled.

17.5.1 Control of Electropneumatic Actuator

Control of pneumatic actuators is a challenging problem, viewed their increasing popularity (law maintenance cost, lightweight and good force/weight ratio), in spite of their traditional drawbacks (friction, variation of the actuators dynamics due to large change of load and piston position along the cylinder stroke, nonlinearities, ...). Due to uncertainties on the model, robust controllers are necessary to ensure position tracking with high precision. In that way, sliding mode controllers have been used for electropneumatic actuators [1, 14, 26, 22]. However, since the sampling frequency of the controller is limited and dynamics of the servodistributor

is neglected, chattering will be produced. The spool of the valve is excited which induced noise due to the air going from source to exhaust and an undesirable deterioration of the servodistributor. Then, there is a real interest to control such actuators with robust controllers, in SISO (only the position of the electropneumatic actuator is controlled) or MIMO (both position and pressure in one of the chambers are controller) cases.

17.5.1.1 Actuator Description and Model

The considered experimental set-up (Figure 17.3) consists of two actuators, respectively named the "main" actuator and the "perturbation" one. Only multivariable control of the "main" one is considered here (the "perturbation" actuator is used to generate the varying load (external force).

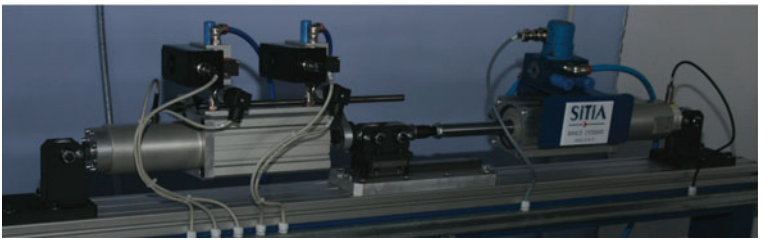

Fig. 17.3 Photo of electropneumatic system. On the left hand side is the "main" actuator whose position and pressure in a chamber can be controlled. On the right hand side is the "perturbation" actuator which provides varying load force.

The "main" actuator is a double effect pneumatic cylinder with two chambers respectively denoted P (as positive) and N (negative). The air mass flow rate entering inside each chamber is regulated by two 3 ways servovalve; these latter are voltage-controlled (control input u_P for P-chamber and control input u_N for N-chamber). The pneumatic jack horizontally moves a load carriage of mass M. This carriage is coupled to the "perturbation" actuator[6]. The control objective is to drive the position of the main actuator, and the mean pressures of the "main" actuator to desired trajectories whereas the "perturbation" actuator provides an external unknown force. The mathematical model of the controlled "main" actuator is given by (for details, see [6, 7])

$$\dot{x} = f(x) + g(x)\bar{u} \tag{17.46}$$

with $x = [p_P \;\; p_N \;\; \mathrm{d}y \;\; y]^T$, $\bar{u} = [u_P \; u_N]^T$ the control input,

[6] No detail is given here on the "perturbation" actuator and its control. Its goal is to provide a dynamical load external force versus the main actuator. In some results displayed in the sequel, this "perturbation" actuator has been modeled by 4 springs in order to simulate an aerodynamic load.

$$f(x) = \begin{bmatrix} \frac{krT}{V_P(y)}[\varphi_P - \frac{S}{rT}p_P \mathrm{d}y] \\ \frac{krT}{V_N(y)}[\varphi_N + \frac{S}{rT}p_N \mathrm{d}y] \\ \frac{1}{M}[Sp_P - Sp_N - b_v \mathrm{d}y - F] \\ \mathrm{d}y \end{bmatrix}, \quad g(x) = \begin{bmatrix} \frac{krT}{V_P(y)}\psi_P & 0 \\ 0 & \frac{krT}{V_N(y)}\psi_N \\ 0 & 0 \\ 0 & 0 \end{bmatrix}$$

where p_X is the pressure inside the chamber X (X being N or P), y and $\mathrm{d}y$ are the piston position and the piston velocity respectively of the "main" actuator, V_X is the volume in the chamber X, S is the piston area, and φ_X and ψ_X are both 5^{th}-order experimentally obtained polynomials with respect to p_X [20] so that the mass flow rate provided from the servodistributor X reads as $q_{mX} = \varphi_X + \psi_X \cdot u_X$; k is the polytropic constant, r is the perfect gas constant and T is the temperature in the chambers (supposed to be equal to the external temperature). It is assumed that uncertainties in the values of polytropic constant k, mass flow q_{mX}, temperature T, mass M, and viscous friction coefficient b_v are additive and bounded with unknown bounds, *i.e.* for example, $M = M_n + \Delta M$ with M_n the nominal mass and ΔM the mass uncertainty such that $|\Delta M| < M_M$. The external perturbation F is also bounded with an unknown bound. Then, system (17.46) is rewritten as

$$\dot{x} = (f_n(x) + \Delta f(x)) + (g_n(x) + \Delta g(x)) \cdot \bar{u} \tag{17.47}$$

with $f_n(x)$, $g_n(x)$ to be the nominal dynamical terms, and $\Delta f(x)$, $\Delta g(x)$ to be the uncertain terms (details on these vector and matrix are displayed in [8]). The position, pressures and control are limited by the physical domain $\mathbf{X}$ defined as

$$\mathbf{X} = \{x \in I\!R \mid -70\,\mathrm{mm} \le y \le +70\,\mathrm{mm}, -1\mathrm{m/s} \le \mathrm{d}y \le 1\ \mathrm{m/s}, 1\,\mathrm{bar} \le p_{P,N} \le 7\,\mathrm{bar}\}.$$

Furthermore, one has $-10\ V \le u_P \le 10\ V$ and $-10\ V \le u_N \le 10\ V$. Note also that $\forall x \in \mathbf{X}$, $V_P(y) > 0$ and $V_N(y) > 0$.

17.5.1.2 Adaptive Sliding Mode Control [16]

Design of the controller. Defining

$$\sigma = \begin{bmatrix} \sigma_1 \\ \sigma_2 \end{bmatrix} = \begin{bmatrix} \dot{\mathrm{d}y} + \lambda_v \cdot \mathrm{d}y + \lambda_y \cdot (y - y_d) \\ \frac{p_P + p_N}{2} - p_d \end{bmatrix}, \tag{17.48}$$

the σ-dynamics reads as

$$\begin{bmatrix} \dot{\sigma}_1 \\ \dot{\sigma}_2 \end{bmatrix} = \bar{\Phi}(x,t) + \bar{\Gamma}(x) \cdot \begin{bmatrix} u_P \\ u_N \end{bmatrix} \tag{17.49}$$

with $\bar{\Phi}(x,t)$ and $\bar{\Gamma}(x)$ derived from (17.46)-(17.47). From (17.47), one has $\bar{\Phi} = \bar{\Phi}_n + \Delta\bar{\Phi}$ and $\bar{\Gamma} = \bar{\Gamma}_n + \Delta\bar{\Gamma}$. Matrix $\bar{\Gamma}_n$ is invertible for all $x \in \mathbf{X}$ given that both volumes V_P and V_N can not be equal to zero. Then $\bar{u}$ reads as

$$\bar{u} = \bar{\Gamma}_n^{-1} \cdot \left(-\bar{\Phi}_n + \begin{bmatrix} v_1 \\ v_2 \end{bmatrix} \right). \tag{17.50}$$

It yields

$$\dot{\sigma} = \left(\Delta\bar{\Phi} - \Delta\bar{\Gamma}\bar{\Gamma}_n^{-1}\bar{\Phi}_n\right) + \left(\mathbf{I} + \Delta\bar{\Gamma}\bar{\Gamma}_n^{-1}\right) \cdot \bar{v} \tag{17.51}$$

with $\bar{v} = [v_1\ v_2]^T$. Thanks to the identification process, the uncertainties are limited to reasonable values such that $\Gamma = \mathbf{I} + \Delta\bar{\Gamma} \cdot \bar{\Gamma}_n^{-1}$ is still positive definite and diagonally dominant. Furthermore, $\left(\Delta\bar{\Phi} - \Delta\bar{\Gamma}\bar{\Gamma}_n^{-1}\bar{\Phi}_n\right)$ and $\left(\mathbf{I} + \Delta\bar{\Gamma}\bar{\Gamma}_n^{-1}\right)$ are bounded for all $x \in \mathbf{X}$. Then, from (17.12)-(17.13), control input v_i is defined as (with $i = \{1,2\}$)

$$v_i = -K_i(t) \cdot \text{sign}(\sigma_i) \tag{17.52}$$

with the gain $K_i(t)$ defined by (17.13).

Experimentations. They have been made with a sampling period $T = 0.1$ ms. Measured are the position y and both pressures p_P and p_N. The speed is reconstructed by means of a simple filtered differentiator. Mechanical and physical parameters of the "main" actuator, and controller parameters are detailed in [16]. Figures 17.4 displays position and pressure, and their respective errors with respect to their desired values in spite of perturbation force (unknown by the controller); this latter force is displayed by Figure 17.5 - Bottom. Furthermore, Figure 17.5-Left displays control inputs u_P and u_N. The position chattering is much lower than the pressure one, which is due to the smaller parameter ε_1 with respect to ε_2. A more precise regulation of the pressure would require the reduction of ε_2. Note that there are no strong saturations or chattering effects. Figure 17.5-Right displays the evolution of $K(t)$ and shows the adaptation of the gain $K(t)$ with respect to uncertainties and perturbations.

17.5.1.3 Integral Sliding Mode Control [4]

The objective consists in designing a robust (with respect to uncertainties/ disturbances) position controller: in this case, the problem appears as a SISO one which implies that $u_P = -u_N = u$. Define σ the sliding variable as $\sigma = y - y_d(t)$: from (17.46), its relative degree with respect to u equals 3. One has

$$\sigma^{(3)} = \Phi(x,t) + \Gamma(x)u \tag{17.53}$$

with $\Phi(x,t)$ and $\Gamma(x)$ derived from (17.46)-(17.47). From (17.47), one has $\Phi = \Phi_n + \Delta\Phi$ and $\Gamma = \Gamma_n + \Delta\Gamma$. The control law is defined as

$$u = \Gamma_n^{-1} \cdot [-\Phi_n + v]$$

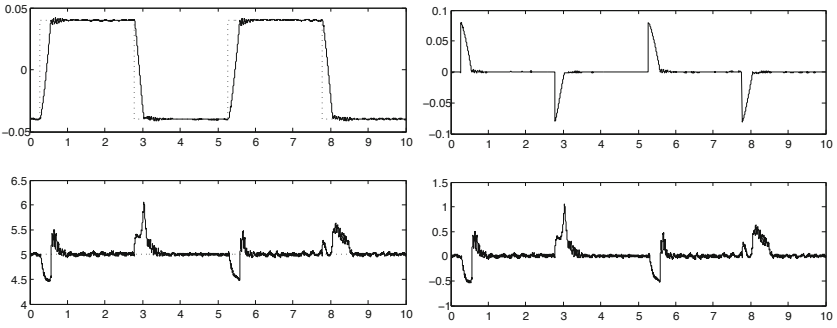

Fig. 17.4 LEFT. Top. Position y (m) versus time (sec) - **Bottom.** Mean pressure in the two chambers (*bar*) versus time (sec). **RIGHT Top.** Error (m) between current and desired positions of the actuator versus time (sec) - **Bottom.** Error (*bar*) between current and desired mean pressures in the two chambers versus time (sec).

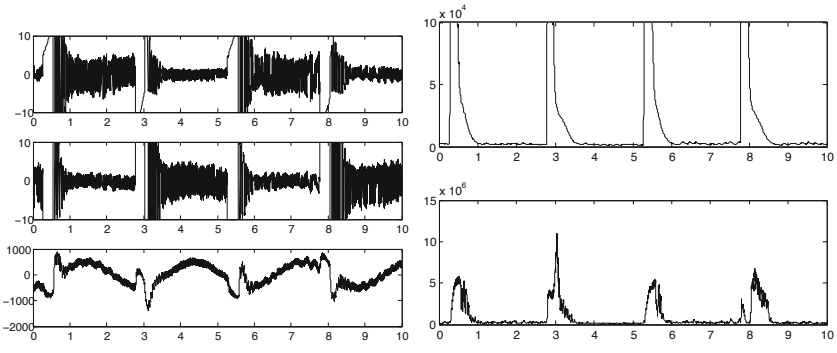

Fig. 17.5 LEFT Top. Control input u_P (V) versus time (sec) - **Middle.** Control input u_N (V) versus time (sec) - **Bottom.** Perturbation force (N) versus time (sec). **RIGHT Top.** Adaptive gain $K_1(t)$ versus time (sec) - **Bottom.** Adaptive gain $K_2(t)$ versus time (sec).

with Γ_n (resp. Φ_n) the nominal value of Γ (resp. Φ). Then, one gets

$$\sigma^{(3)} = \left(\Delta\Phi - \Delta\Gamma\Gamma_n^{-1}\Phi_n\right) + \left(1 + \Delta\Gamma\Gamma_n^{-1}\right)\cdot v \tag{17.54}$$

Consider the so-called "nominal" system (with $Z = [\sigma\ \dot{\sigma}\ \ddot{\sigma}]^T$, and $\Delta\Phi = \Delta\Gamma = 0$)

$$\dot{Z} = \underbrace{\begin{bmatrix} 0 & 1 & 0 \\ 0 & 0 & 1 \\ 0 & 0 & 0 \end{bmatrix}}_{A} Z + \underbrace{\begin{bmatrix} 0 \\ 0 \\ 1 \end{bmatrix}}_{B} v \tag{17.55}$$

which has the same form than system (17.27). As mentioned in Section 17.4.2.1, the integral sliding mode controller v reads as $v = v_0 + v_1$.

Continuous part v_0. Given the matrix Q (see details in [4]), from (17.30), one gets the matrix M. From (17.30), one gets $\delta(t) = e^{A_m t}\delta(0)$ with $A_m = -\left[A^T - MBB^T\right]$. Then, given $\delta(t)$, and from (17.55)-(17.29), one gets $\dot{Z} = -A_m^T Z + BB^T e^{A_m t}\delta(0)$. By multiplying both side of previous equation by $e^{A_m^T t}$, and integrating from $t = 0$ to $t = t_F$, with $Z(t_F) = 0$, one gets

$$Z(0) = -\underbrace{\left[\int_0^{t_F} e^{A_m^T t} BB^T e^{A_m t}\mathrm{d}t\right]}_{H} \cdot \delta(0)$$

Matrix H is the partial reachability Gramian of linear system $\dot{x} = A_m x + Bv$ and is, viewed the form of A_m, B and $t_F < \infty$, invertible. Then, the initial condition $\delta(0)$ ensuring that $Z(t_F) = 0$ can be derived from $\delta(0) = -H^{-1}Z(0)$. The matrix H is evaluated using an algorithm from [25] which yields $\delta_1(0) = -3.6034e4$, $\delta_2(0) = -3.6034e3$ and $\delta_3(0) = -1.2002e2$ for $\sigma(0) = [0.016\ 0\ 0]^T$ and a convergence time fixed to $t_F = 0.2\ sec$. Then, v_0 reads as (with $|v_0| < v_{0M} = 120$)

$$v_0 = \begin{cases} -B^T M\sigma(t) + B^T\delta(t) & \text{for } 0 \le t \le t_F \\ -B^T M\sigma(t) & \text{for } t > t_F \end{cases} \tag{17.56}$$

with δ verifying (17.30).

Discontinuous part v_1. Let introduce now S as

$$S = \ddot{\sigma} + \sigma_{0,2}(t) + 2\xi\omega_n(\dot{\sigma} + \sigma_{0,1}(t)) + \omega_n^2(\sigma + \sigma_{0,0}(t))$$

with

$$\dot{\sigma}_{0,2} = -v_0,\ \dot{\sigma}_{0,1} = \sigma_{0,2},\ \dot{\sigma}_{0,0} = \sigma_{0,1}$$

and $\sigma_{0,2}(0) = -\ddot{\sigma}(x(0),0)$, $\sigma_{0,1}(0) = -\dot{\sigma}(x(0),0)$, $\sigma_{0,0}(0) = -\sigma(x(0),0)$. From (17.33), one gets $v_1 = -K \cdot \mathrm{sign}(S)$.

Experimentations. They have been made by choosing $\xi = 0.7$, $\omega_n = 200\ rad \cdot s^{-1}$ and $K = 10^5$, this latter allowing to ensure the sliding conditions by taking into account the uncertainties. The convergence time has been fixed at $t_F = 0.5\ s$. For the results displayed in the sequel, the load actuator has been changed into "unknown" load composed by springs (for details, see [6]). The actuator position (Figure 17.6-Left) converges to the desired trajectory in $0.5s$ (which is the stated convergence time t_F) controller without overshoot. The maximum error position in steady state is $0.18mm$. During all trajectory tracking, input is realistic even if there is some saturation phenomena (Figure 17.6-Right).

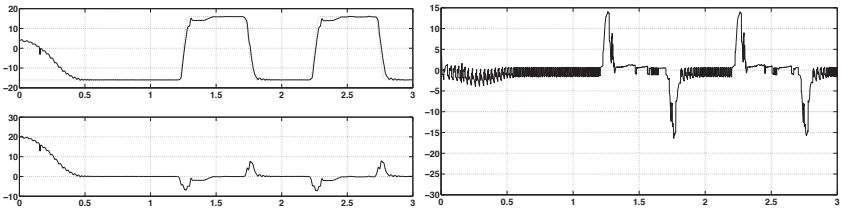

Fig. 17.6 LEFT. Top. Desired and current positions (*mm*) versus time (*sec*). **Bottom.** Positions errors (*mm*) versus time (*sec*). **RIGHT.** Control input $u_P = -u_N$ (V) versus time (*sec*).

17.5.2 Control of Induction Motor [23]

This section, which is entirely based on [23], is devoted to robust control of induction motors, in order to evaluate the applicability and the performances of the "pre-computed trajectories" high order sliding mode approach. In [23], an adaptive interconnected observer and high order sliding mode control of induction motors without mechanical sensors (speed sensor and load torque sensor) are proposed and experimentally evaluated. Only controller is displayed in the sequel of the chapter. Note that the adaptive interconnected observer developed in [23] estimates fluxes, angular velocity, load torque and the stator resistance, whereas the speed-flux control law is based on previously described control law with "pre-computed trajectories". Furthermore, in [23], the stability of closed-loop system (with controller and observer) based on Lyapunov theory is proved. Note finally that these results take place in "sensorless control" of electrical motors.

17.5.2.1 Model of an Induction Motor

The model is based on the motor equations in a rotating **d** and **q**-axis and reads as

$$\begin{bmatrix} \dot{i}_{sd} \\ \dot{i}_{sq} \\ \dot{\phi}_{rd} \\ \dot{\phi}_{rq} \\ \dot{\Omega} \end{bmatrix} = \begin{bmatrix} ba\phi_{rd} + bp\Omega\phi_{rq} - \gamma i_{sd} + \omega_s i_{sq} \\ ba\phi_{rq} - bp\Omega\phi_{rd} - \gamma i_{sq} - \omega_s i_{sd} \\ -a\phi_{rd} + (\omega_s - p\Omega)\phi_{rq} + aM_{sr} i_{sd} \\ -a\phi_{rq} - (\omega_s - p\Omega)\phi_{rd} + aM_{sr} i_{sq} \\ m(\phi_{rd} i_{sq} - \phi_{rq} i_{sd}) - c\Omega - \frac{1}{J} T_l \end{bmatrix} + \begin{bmatrix} m_1 & 0 \\ 0 & m_1 \\ 0 & 0 \\ 0 & 0 \\ 0 & 0 \end{bmatrix} \begin{bmatrix} u_{sd} \\ u_{sq} \end{bmatrix} \tag{17.57}$$

with $i_{sd}, i_{sq}, \phi_{rd}, \phi_{rq}, u_{sd}, u_{sq}, \Omega$, T_l and ω_s respectively the stator currents, the rotor fluxes, the stator voltage inputs, the angular speed, the load torque and the stator frequency (defined in Section 17.5). The subscripts s and r refer to the stator and rotor. The parameters a, b, c, γ, m, and m_1 are defined in [23]. M_{sr} is the mutual inductance between the stator and rotor windings, p the number of pole-pair, J the inertia of the system (motor and load) and f_v the viscous damping coefficient.

17.5.2.2 Precomputed Trajectories High Order Sliding Mode Controller

As introduced before, the goal is to design a robust (with respect to uncertainties/disturbances) flux and speed controller. Define σ_ϕ and σ_Ω the sliding vector as

$$\sigma = \begin{bmatrix} \sigma_\phi \\ \sigma_\Omega \end{bmatrix} = \begin{bmatrix} \phi_{rd} - \phi^* \\ \Omega - \Omega^* \end{bmatrix} \tag{17.58}$$

with ϕ^* and Ω^* respectively the flux and speed references. From (17.57), it yields that the relative degree of σ_ϕ and σ_Ω with respect to u equals 2 ($r = 2$), which implies that at least a 2^{nd} order sliding mode controller is required. In order to avoid the "chattering" effect and to improve the robustness of the controller, according to previous design, 3^{rd} order HOSM controllers are designed for the two outputs, which means that the discontinuous term is applied to $\sigma_\phi^{(3)}$ and $\sigma_\Omega^{(3)}$ through $\dot{u}$. One has

$$\begin{bmatrix} \sigma_\phi^{(2)} \\ \sigma_\Omega^{(2)} \end{bmatrix} = \begin{bmatrix} \Phi_\phi(\cdot) \\ \Phi_\Omega(\cdot) \end{bmatrix} + \Gamma_{\phi,\Omega}(\cdot) \begin{bmatrix} u_{sd} \\ u_{sq} \end{bmatrix} \tag{17.59}$$

with each component Φ_ϕ, Φ_Ω and $\Gamma_{\phi,\Omega}$ detailed in [23]. As the previous applications, one considers that each previous function can be written as a nominal part and an uncertain one,

$$\Phi_\phi = \Phi_{\phi_n} + \Delta_\phi, \quad \Phi_\Omega = \Phi_{\Omega_n} + \Delta_\Omega, \quad \Gamma_{\phi,\Omega} = \Gamma_n + \Delta_\Gamma \tag{17.60}$$

such that Φ_{ϕ_n}, Φ_{Ω_n} and Γ_n are the well-known nominal terms whereas Δ_ϕ, Δ_Ω and Δ_Γ contain all the uncertainties due to parameters variations and disturbance. Suppose that these uncertainties are bounded. The control input u reads as (note that matrix Γ_n is invertible on the work domain)[7]

$$\begin{bmatrix} u_{sd} \\ u_{sq} \end{bmatrix} = \Gamma_n^{-1} \left[- \begin{bmatrix} \Phi_{\phi_n} \\ \Phi_{\Omega_n} \end{bmatrix} + \begin{bmatrix} v_{sd} \\ v_{sq} \end{bmatrix} \right]. \tag{17.61}$$

From (17.59)-(17.61), and by time-differentiating[8] system (17.59), one gets

$$\begin{bmatrix} \sigma_\phi^{(3)} \\ \sigma_\Omega^{(3)} \end{bmatrix} = \Phi + \Gamma \cdot \begin{bmatrix} \dot{v}_{sd} \\ \dot{v}_{sq} \end{bmatrix}. \tag{17.62}$$

The control law design takes 2 steps: the design of the switching variable and the discontinuous input.

[7] The interest of a such feedback is the minimization of the control discontinuous function gain.

[8] Details are available in [23], especially on the features of system (17.59), these features allowing time differentiation.

Switching vector. The switching vector S reads as

- **For** $t \leq t_F$.

$$\begin{aligned} S_\phi &= \sigma_\phi^{(2)} - \ddot{\mathscr{F}}_\Phi + 2\zeta_\phi \omega_{n\phi}(\dot{\sigma}_\phi - \dot{\mathscr{F}}_\Phi) + \omega_{n\phi}^2(\sigma_\phi - \mathscr{F}_\Phi) \\ S_\Omega &= \sigma_\Omega^{(2)} - \ddot{\mathscr{F}}_\Omega + 2\zeta_\Omega \omega_{n\Omega}(\dot{\sigma}_\Omega - \dot{\mathscr{F}}_\Omega) + \omega_{n\Omega}^2(\sigma_\Omega - \mathscr{F}_\Omega) \end{aligned} \tag{17.63}$$

with $\mathscr{F}_\Phi = K_\phi e^{Ft} T \sigma_\phi(0)$ and $\mathscr{F}_\Omega = K_\Omega e^{Ft} T \sigma_\Omega(0)$. The choice of these very specific both reference functions has to be made for their C^∞ class ; the tuning method for F and T is displayed in [15], which allows to calculate

- **For** $t > t_F$.

$$\begin{aligned} S_\phi &= \sigma_\phi^{(2)} + 2\zeta_\phi \omega_{n\phi} \dot{\sigma}_\phi + \omega_{n\phi}^2 \sigma_\phi \\ S_\Omega &= \sigma_\Omega^{(2)} + 2\zeta_\Omega \omega_{n\Omega} \dot{\sigma}_\Omega + \omega_{n\Omega}^2 \sigma_\Omega \end{aligned} \tag{17.64}$$

Discontinuous input. The control discontinuous input reads as

$$\begin{bmatrix} \dot{v}_{sd} \\ \dot{v}_{sq} \end{bmatrix} = \begin{bmatrix} -K_\phi . \text{sign}(S_\phi) \\ -K_\Omega . \text{sign}(S_\Omega) \end{bmatrix} \tag{17.65}$$

Experimentations. [23] The sliding mode controller parameters are chosen such that $t_F = 0.3sec$ and

- $t \leq 5$ *sec.* $\zeta_\phi = 0.35$, $\omega_{n\phi} = 316$ rad/s, $\alpha_\phi = 6.10^4$, $\zeta_\Omega = 1.56$, $\omega_{n\Omega} = 32$ rad/s, $\alpha_\Omega = 8.10^4$,
- $t > 5$ *sec.* $\zeta_\phi = 0.35$, $\omega_{n\phi} = 447$ rad/s, $\alpha_\phi = 15.10^4$, $\zeta_\Omega = 0.7$, $\omega_{n\Omega} = 200$ rad/s, $\alpha_\Omega = 8.10^6$

Rotor speed and flux amplitude are provided by observers whereas flux angle is provided by estimator. The experimental sampling time T equals $200\mu s$. The experimental results[9] of the nominal case with identified parameters (except stator resistance) are shown in Fig. 17.7. These figures show the good performance of the complete system observer-controller in trajectory tracking and disturbance rejection. The estimated motor speed (Fig. 17.7**b**) converges to the measured speed (Fig. 17.7**a**) near and under conditions of unobservability (details of these latter conditions are displayed in [23]). It is the same conclusion for estimated flux (Fig. 17.7**f**) with respect to reference flux (Fig. 17.7**e**). The estimated load torque (Fig. 17.7**d**) converges to the measured load torque (Fig. 17.7**c**), under conditions of observability and at very low frequency (conditions of unobservability) (between 7 and 9 sec). Nevertheless, it appears a small static error when the motor speed increases (between 4 and 6 sec). The load torque is well rejected excepted at the time when it is applied (Fig. 17.7**h** and **j** at time 1.5s and 5s) and when it is removed (Fig. 17.7**h** and

[9] For each figure, each line is refereed to a, c: measured speed and load torque, e: reference flux, b, d, f, g: estimated speed, load torque, flux and stator resistance, h, i, j: speed, load torque and flux estimation error.

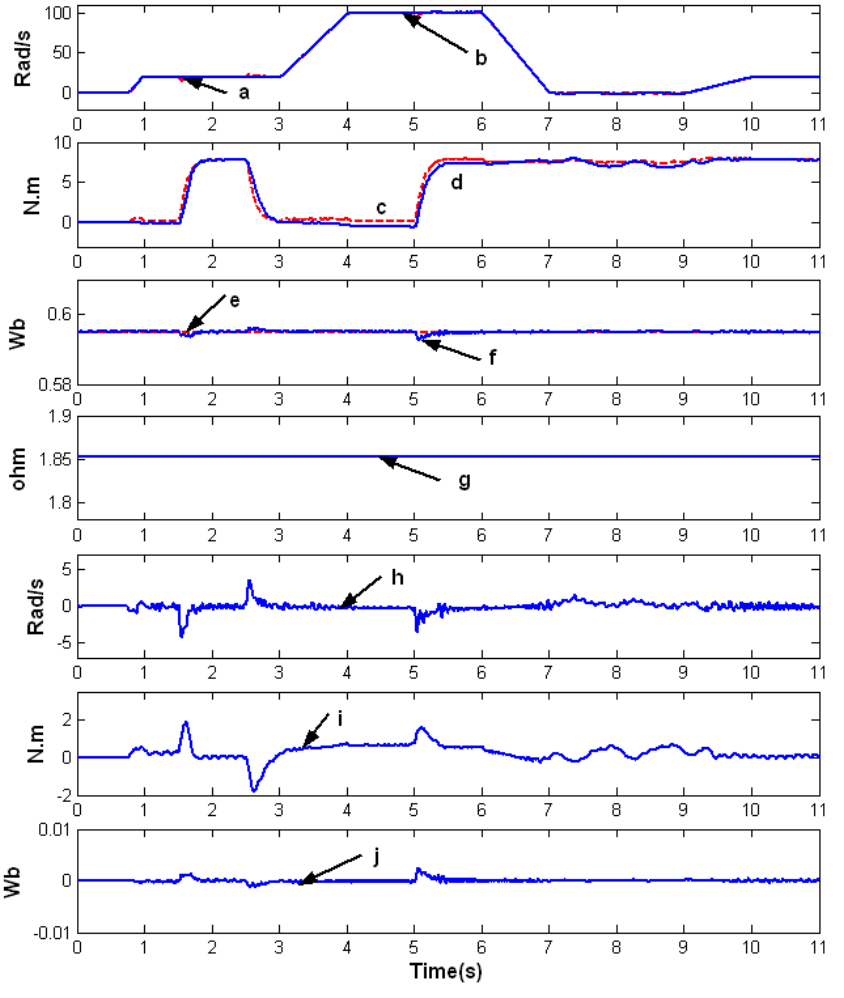

Fig. 17.7 Experimental result in nominal case.

j at time 2.5s). On Figure 17.7**g**, it can be viewed that the stator resistance estimation remains almost constant despite of noise and transient dynamics of speed and load torque. This test shows the capability of the proposed controller to guarantee flux and speed tracking of slowly varying speed reference with excitation frequency close to zero (between 7 and 9 sec).

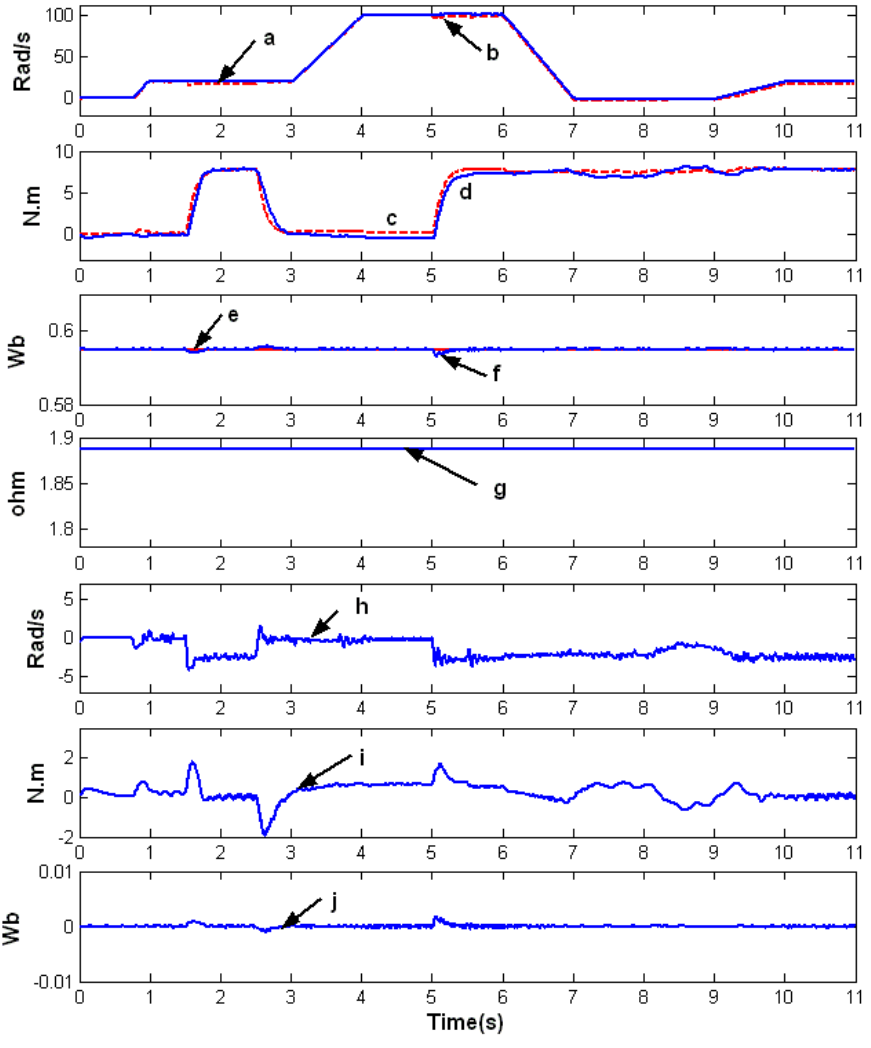

Fig. 17.8 Experimental result with rotor resistance variation (+50%).

17.6 Conclusion

This chapter presents control methodologies for controlling uncertain nonlinear systems, all these results being developed through joined works including Control group of IRCCyN, Nantes, France. The presented methods can be divided in two groups : adaptive solutions for standard (first order) sliding mode control, and high order sliding mode control solutions (including static output feedback for second order sliding mode). The proposed adaptive sliding mode controller allows

retaining robustness and accuracy without knowledge of the uncertainties / perturbations bounds, while dynamically adapting the gain versus the current-time uncertainties magnitude. Then, two high order sliding mode strategies are presented, one of their features being the *a priori* knowledge of the convergence time. An output feedback second order sliding mode controller is also presented: it ensures the establishment of a second order sliding mode without using the time derivative of the switching variable. The efficacy of these control algorithms has been verified on experimental set-up equipped with electrical or electropneumatic actuators.

Acknowledgements. Franck Plestan and Alain Glumineau thank their Ph.D. students Alexis Girin and Salah Laghrouche for their important contributions on the presented results. These works have been financially supported by *Délégation Générale de l'Armement* (DGA-French Defense Ministry) (R.E.I. project no. 06 34 032 00 470 75 65 connected to Alexis Girin's Ph.D.), *Centrale Initiatives Foundation* (for sabbatical of Franck Plestan at UAH, in 2009) and FONCICyT Project 93302 "Automation of energy production processes via sliding mode control and monitoring".

References

1. Bouri, M., Thomasset, D.: Sliding control of an electropneumatic actuator using an integral switching surface. IEEE Trans. Control Syst. Tech. 9, 368–375 (2001)
2. Filippov, A.F.: Differential Equations with Discontinuous Right-Hand side. Kluwer Academic Publishers, Dordrecht (1992)
3. Fliess, M.: Generalized controller canonical form for linear and nonlinear dynamics. IEEE Trans. Autom. Control 35, 994–1000 (1990)
4. Girin, A., Plestan, F., Brun, X., Glumineau, A.: A third order sliding mode controller based on integral sliding mode for an electropneumatic system. In: IEEE Conference on Decision and Control CDC 2006, San Diego, California (2006)
5. Girin, A.: Contribution à la commande non linéaire d'un système électropneumatique pour une utilisation aéronautique: application sur un benchmark dédié (In French). Ph.D. Thesis, Ecole Centrale and University of Nantes (2007)
6. Girin, A., Plestan, F., Brun, X., Glumineau, A.: Robust control of an electropneumatic actuator: application to an aeronautical benchmark. IEEE Trans. Control Syst. Tech. 17, 633–645 (2009)
7. Girin, A., Plestan, F.: A new experimental setup for a high performance double electropneumatic actuators system. In: American Control Conference ACC 2009, Saint Louis, Missouri (2009)
8. Laghrouche, S., Plestan, F., Glumineau, A.: Practical higher order sliding mode control: optimal control based approach and application to electromechanical systems. In: Edwards, C., Fossas Colet, E., Fridman, L. (eds.) Advances in Variable Structure and Sliding Mode Control. LNCIS, vol. 334, pp. 169–191. Springer, Berlin (2006)
9. Laghrouche, S., Smaoui, M., Plestan, F., Brun, X.: Higher order sliding mode control based on optimal approach of an electropneumatic actuator. Int. J. Control 79, 119–131 (2006)
10. Laghrouche, S., Plestan, F., Glumineau, A.: Higher order sliding mode control based on integral sliding surface. Automatica 43, 531–537 (2007)
11. Levant, A.: Sliding order and sliding accuracy in sliding mode control. Int. J. Control 58, 1247–1263 (1993)

12. Levant, A.: Robust exact differentiation via sliding mode technique. Automatica 34, 379–384 (1998)
13. Levant, A.: Homogeneity approach to high-order sliding mode design. Automatica 41, 823–830 (2005)
14. Paul, A.K., Mishra, J.K., Radke, M.G.: Reduced order sliding mode control for pneumatic actuator. IEEE Trans. Control Syst. Tech. 2, 271–276 (1994)
15. Plestan, F., Glumineau, A., Laghrouche, S.: A new algorithm for high order sliding mode control. International Journal of Robust and Nonlinear Control 18, 441–453 (2008)
16. Plestan, F., Shtessel, Y., Brégeault, V., Poznyak, A.: New methodologies for adaptive sliding mode control. International Journal of Control 83, 1907–1919 (2010)
17. Plestan, F., Moulay, E., Glumineau, A., Cheviron, T.: Output feedback sampling control: a robust solution based on second order sliding mode. Automatica 46, 1096–1100 (2010)
18. Rekasius, Z.V.: An alternate approach to the fixed terminal point regulator problem. IEEE Trans. Automat. Control 9, 290–292 (1964)
19. Rengifo-Rodas, C., Plestan, F., Aoustin, Y.: Optimal control of a neuromusculoskeletal model: a second order sliding mode solution. In: Int. Workshop on Variable Structure Systems (VSS), Antalya, Turkey (2008)
20. Sesmat, S., Scavarda, S.: Static characteristics of a three way servovalve. In: Conf. Fluid Power Tech., Aachen, Germany (1996)
21. Sira-Ramirez, H.: An algebraic approach to sliding mode control. In: Zinober, A.S.I. (ed.) Variable Structure and Lyapunov Control. LNCIS, vol. 193, pp. 23–49. Springer, London (1994)
22. Smaoui, M., Brun, X., Thomasset, D.: Robust position control of electropneumatic system using second order sliding mode. In: IEEE International Symposium on Industrial Electronics, Ajaccio, France (2004)
23. Traoré, D., Plestan, F., Glumineau, A., de Léon-Morales, J.: Sensorless induction motor: high order sliding mode controller and adaptative interconnected observer. IEEE Trans. Indus. Electron. 55, 3818–3827 (2008)
24. Utkin, V.I., Shi, J.: Integral sliding mode in systems operating under uncertainty. In: IEEE Conference on Decision and Control CDC 1996, Kobe, Japan (1996)
25. VanLoan, C.F.: Computing integrals involving the matrix exponential. IEEE Trans. Automat. Control 23, 395–404 (1978)
26. Yang, L., Lilly, J.H.: Sliding mode tracking for pneumatic muscle actuators in bicep/triceps pair configuration. In: American Control Conference ACC 2003, Denver, Colorado (2003)

Chapter 18
Sliding Mode Controllers and Observers for Electromechanical Systems

J. de Leon-Morales

Abstract. Controllers and observers for electromechanical systems are widely used and implemented in the industry in order to improve its performance. Among different electromechanical systems we can find interesting domains of application such as power systems, UAVs, teleoperation. This paper intents to show the advantages of the control and observer design using sliding mode techniques. These domains are related with the research topics of the Mechatronics laboratory of the Nuevo Leon University, in the CIIDIT-UANL Research Institute.

18.1 Introduction

During the last two decades significant interest on sliding mode control has been generated in the research community. The success of sliding mode techniques is the significative performance of the system due to the insensitivity to parameters variations and the complete rejection of disturbances ([13]). However, some challenges are present due to the so-called chattering phenomenon. Several efforts to explain and reduce the effects of the chattering have been done in order to avoid this limitation. The propose of this paper is to provide some illustrative applications of the sliding-mode design which have been developed recently in the Mechatronics laboratory of the CIIDIT-UANL Research Institute ([17], [25], [28], [29]).

An overview of the applications of the sliding modes to electromechanical systems is presented in this work. The control of electrical machines in power systems, UAVs like small helicopters and the most recent applications in teleoperation of the electromechanical systems like a robots or machines, are probably the most challenging topics. We focus on the control of systems using directly or indirectly the theoretical concepts of sliding mode to achieve stability, regulation or tracking.

J. de Leon-Morales
Facultad de Ingeniería Mecánica y Eléctrica
Universidad Autónoma de Nuevo León, Cd. Universitaria,
66450 San Nicolás de los Garza, N.L., México
e-mail: drjleon@gmail.com

L. Fridman et al. (Eds.): Sliding Modes, LNCIS 412, pp. 493–516.
springerlink.com

18.1.1 Application Domains of Sliding Mode

18.1.1.1 Power Systems: Synchronous Machine and Multi-machine Systems

The transient stability of power systems is a classical dynamical control system problem. The application of nonlinear control methods to design the excitation control has been investigated for improving the transient stability of a power system. A survey on power systems control shows that most existing controllers are designed assuming that power systems have fixed structure and constant parameters. However, in power systems uncertainties always exist and they are due to sudden load shedding, generation tripping, occurrence of faults, change of parameters and network configuration among others. These problems are some of the typical conditions found in power systems which must be taken into account for control and observer design (see [11], [12], [14], [16], [17], [18]). In this work, a synchronous machine connected to an infinity bus (SMIB) and a multi-machine system are considered for illustrating the control design using sliding mode techniques to improve the transient stability of such systems.

18.1.1.2 UAV: Twin Rotor System

Recently, a lot of works related with the control of the UAV have been published. The main objective is to design controllers stabilizing UAV's taking into account the perturbations and tracking a specific trajectory. Furthermore, the helicopter is an aircraft that is lifted, propelled and maneuvered by vertical and horizontal rotors. All twin rotor aircraft have high cross-coupling in all degrees of motion. For this reason, this system poses very challenging problem of precise maneuvering in the presence of cross-coupling ([19], [20]). In this work, some results are presented by applying a sliding mode control which is implemented in a setup of a twin rotor system.

18.1.1.3 Teleoperation

The evolution of important technologies and the development of computational tools have allowed the implementation of robotic systems in the industry. Recently, the application of robots in telesurgery and the use the images have permitted to improve accuracy and performance and helping surgeon in complex and delicate surgeries, saving time and money. Furthermore, the stability and transparency are two of the most important topics in teleoperation. In particular, maintain stability of the closed-loop system irrespective of the behavior of the operator or the environment, is one of the most important tasks to be considered if a communication medium (wireless or wired) is included in the scheme. The complexity of the overall system introduces distortion, delays and losses that impact in the stability and performance. Several schemes have been proposed to study such systems, for example those based on passivity, which is inspired in the network theory in transmission lines. However, sliding-mode control has been used extensively in robotics to cope with

parametric uncertainties and hard nonlinearities, in particular for time delay teleoperators, which have gained gradual acceptance due to technological advances. In this work, a scheme to design a sliding mode teleoperator controller to guarantee robust tracking under unknown constant time delay is presented (see for more details [1], [8], [9]).

18.1.2 Paper Structure

The rest of the work is organized as follows. Section 18.2 shows the general ideas of sliding modes techniques used to design an observer and a controller of a power system, where a mathematical model of one machine connected to the transmission line to the infinity bus and multi-machine power system are presented. In Section 18.3, the model of a twin rotor system is presented, where results are given for illustrating the performance of this methodology. Furthermore, using a master-slave configuration, the teleoperation problem is analyzed in Section 18.4. A control scheme using a super twisting algorithm based on sliding-modes is given to solve the bilateral problem which is robust in presence of unknown constant time-delays. Finally, conclusions are presented in Section 18.5.

18.2 Power Systems: Synchronous Machine and Multi-machine Systems

Most of the electrical power systems are operating closer to their technical limits putting restrictions to supply electrical energy to all customers which represent a big challenge to the electrical industry. Conventional controllers based on approximated linearized models are usually tuned at one particular operating point. Nevertheless, due to nonlinear nature of power systems it may be required to be re-tuned when the operating point changes, assuring in this way a satisfactory dynamic performance. Furthermore, in case of severe disturbances, the configuration of power system may be drastically changed. Under such changing conditions, nonlinear controllers offer an alternative to traditional controllers, allowing to improve the performance of power systems under such uncertain conditions. In what follows, we present a control scheme based on sliding mode techniques in order to guarantee the stability under disturbances present in the line or parametric uncertainties.

18.2.1 Synchronous Machine

Although the existing classical controllers have good dynamical performance for a wide range of operating conditions and disturbances, however, the real electric power system have been experimenting a dramatic change in recent years. Because

of that, a lot of attention has been paid to the application of advanced control techniques in power systems as one of the most promising application areas.

In this Section, the control objective is to design a sliding mode controller for a synchronous machine connected to an infinity bus (SMIB) in such a way to regulate the terminal voltage and improve the transient stability of the system over a wide operating region and under external perturbations.

The equations describing the electromechanical transient behavior of a synchronous machine with flux linkage variations, machine damping and transient saliency included are the following

$$\begin{aligned}
\dot{\delta} &= \omega - \omega_s \\
\dot{\omega} &= \frac{\omega_s}{2H}\left(T_M - \frac{X''_d - X_{ls}}{\left(X'_d - X_{ls}\right)}E'_q I_q - \frac{X'_d - X''_d}{\left(X'_d - X_{ls}\right)}\psi_d I_q - \frac{X''_q - X_{ls}}{\left(X'_q - X_{ls}\right)}E'_d I_d \right. \\
&\quad \left. + \frac{X'_q - X''_q}{\left(X'_q - X_{ls}\right)}\psi_q I_q - \left(X''_q - X''_d\right) I_d I_q - D\left(\omega - \omega_s\right)\right) \\
\dot{E}'_q &= \frac{1}{T'_{doi}}\left(-E'_q - \left(X_d - X'_d\right)\left[I_d - \frac{X'_d - X''_d}{\left(X'_d - X_{ls}\right)^2}\left(\psi_d + \left(X'_d - X_{ls}\right) I_d - E'_q\right)\right] + E_{fd}\right) \\
\dot{E}'_d &= \frac{1}{T'_{qo}}\left(-E'_d + \left(X_q - X'_q\right)\left[I_q - \frac{X'_d - X''_d}{\left(X'_q - X_{ls}\right)^2}\left(\psi_q + \left(X'_q - X_{ls}\right) I_q + E'_d\right)\right)\right] \\
\dot{\psi}_d &= \frac{1}{T''_{do}}\left(-\psi_d + E'_q - \left(X'_d - X_{ls}\right) I_d\right) \\
\dot{\psi}_q &= \frac{1}{T''_{qo}}\left(-\psi_q - E'_d - \left(X'_q - X_{ls}\right) I_q\right)
\end{aligned} \tag{18.1}$$

together with the linear algebraic relations between currents and flux linkages:

$$\begin{aligned}
0 &= \left(R_s + R_e\right) Id - \left(X''_q - X_{ep}\right) I_q - \frac{X''_q - X_{ls}}{\left(X'_q - X_{ls}\right)}E'_d + \frac{X'_q - X''_q}{\left(X'_q - X_{ls}\right)}\psi_q + V_s sin\left(\delta - \theta_{vs}\right) \\
0 &= \left(R_s + R_e\right) I_q - \left(X''_d - X_{ep}\right) I_d - \frac{X''_d - X_{ls}}{\left(X'_d - X_{ls}\right)}E'_q + \frac{X'_d - X''_d}{\left(X'_d - X_{ls}\right)}\psi_d + V_s cos\left(\delta - \theta_{vs}\right),
\end{aligned}$$

$$\begin{aligned}
T_e &= \frac{X''_d - X_{ls}}{\left(X'_d - X_{ls}\right)}E'_q I_q + \frac{X'_d - X''_d}{\left(X'_d - X_{ls}\right)}\psi_d I_q + \frac{X''_q - X_{ls}}{\left(X'_q - X_{ls}\right)}E'_d I_d \\
&\quad + \frac{X'_q - X''_q}{\left(X'_q - X_{ls}\right)}\psi_q I_q + \left(X''_q - X''_d\right) I_d I_q
\end{aligned} \tag{18.2}$$

where

$\delta(t)$	Rotor angle, in radians;
$\omega(t)$	Relative speed, in rad/s;
$\omega_s = 2\pi f_s$,	Synchronous machine speed, in rad/s;
H	Inertia constant, in seconds;
D	Damping factor;
T_m	Mechanical power input, in p.u.
T_e	Electrical power output, in p.u.;
E_f	Excitation system voltage, in p.u.
T'_{do}	Open circuit d-axis time constant, in sec;
T'_{qo}	Open circuit q-axis time constant, in sec;
T''_{do}	d-axis sub-transient time constant, in sec;
T''_{qo}	q-axis sub-transient time constant, in sec;
x_d	d-axis synchronous reactance, in p.u.;
x_q	q-axis synchronous reactance, in p.u.;
x'_d	d-axis transient reactance, in p.u.;
x'_q	q-axis transient reactance, in p.u.;
x''_d	d-axis sub-transient reactance, in p.u.;
x''_q	q-axis sub-transient reactance, in p.u.;
$I_q(t)$ and $I_d(t)$	Currents in d-q reference frame of the generator,
$E'_d(t)$	Transient EMF in the direct axis,
$E'_q(t)$	Transient EMF in the quadrature axis,
ψ_d and ψ_q	Flux linkages, direct and quadrature.

where p.u. stands per unit.

18.2.2 One Axes Model

In power systems, models of reduce dimension are frequently used which take into account some physical considerations in order to study the transient stability of the synchronous machine and design a controller.

One of the most used model for designing a nonlinear controller is the so-called the one axes model. Assuming that the stator sub-transient dynamics and those of the transmission line are neglected, taking into account that T''_{qo}, T''_{do} and T'_{qo} are sufficiently small, and neglecting the dynamics driven the turbines assuming the mechanical torque T_M is constant, and taking into account the assumption that the impedance are constant and $X_q = X'_d$. Then, a 6th order model of the generator is represented by the following one axes model

$$\begin{cases} \dot{\delta} &= \omega - \omega_s \\ \dot{\omega} &= \frac{\omega_s}{2H}\left(P_m - D(\omega - \omega_s) - E'_{q_i} I_{q_i}\right) \\ \dot{E}'_q &= \frac{1}{T'_d}(E_f - E'_q - (X_d - X'_d)I_d) \end{cases} \tag{18.3}$$

with the linear algebraic relations:

$$0 = (R_s + R_e) Id - \left(X'_q + X_{ep}\right) I_q + V_s sin\left(\delta - \theta_{vs}\right) \tag{18.4}$$

$$0 = (R_s + R_e) Iq - \left(X'_d + X_{ep}\right) I_d - E'_q + V_s cos\left(\delta - \theta_{vs}\right) \tag{18.5}$$

where $T_e = E'_q I_q$, and $E_f(t)$ is the input of the system. Taking the system described by (18.1), the control problem can be formulated as follows:

Control objective: Considering the dynamical system (18.1) and using the only available information, design a control law $u(t)$ such that the rotor angle achieves the prescribed behavior with all the internal variables of the system being bounded. Then, in order to design a controller some assumptions are introduced.

Assumptions
A1. δ is available by measurement and the operating point (δ^*, 0, E'^*_q) is known.
A2. The mechanical power P_m is constant and known and all system parameters are known.
A3. No saturation in the model is considered.

18.2.3 Sliding-Mode Controller Design

Now, we introduce the most important results related to high order sliding mode which will be considered in the sequel (see [3], [4], for more details).

Consider systems belonging to a class of single-input-single-output systems with a known relative degree r, which are represented by

$$\dot{x} = f(x) + g(x)u, \qquad \sigma = \sigma(t,x) \tag{18.6}$$

where $x(t_0) = x_0$, $t_0 \geq 0$, $x \in B_x \subset \mathbb{R}^3$ is the *state vector*, $u \in \mathbb{R}^n$ is the *control input vector*, the field vectors f and g are assumed to be bounded with their components being smooth function of x and $\sigma : \mathbb{R}^{n+1} \to \mathbb{R}$ are unknown smooth functions. B_x denotes a closed and bounded subset, centered at the origin. In order to design a finite-time convergent controller some conditions are required. Since the relative degree r of the system is assumed to be constant and known, the control explicitly appears first time in rth total time derivative of σ and

$$\sigma^{(r)} = h(t,x) + m(t,x)u \tag{18.7}$$

where $h(t,x) = \sigma^{(r)}|_{u=0}$, $m(t,x) = (\partial/\partial u)\sigma(r) \neq 0$. It is supposed that for some $K_m, K_M, C > 0$

$$0 < K_m \leq \frac{\partial}{\partial u}\sigma^{(r)} \leq K_M \qquad |\sigma^{(r)}|_{u=0} \leq C \tag{18.8}$$

which is always true at least locally. From (18.7) and (18.8),

$$\sigma^{(r)} \in [-C, C] + [K_m, K_M]u \tag{18.9}$$

The closed differential inclusion is understood here in the Filippov sense, which means that the right-hand vector set is enlarged in a special way, in order to satisfy certain and semi-continuity conditions. The inclusion only requires to know the constants r, C, K_m and K_M of the system (18.6). These conditions allow to give a solution to this control problem (see [4]).

To design a high order sliding mode control for the system, we consider the following n-dimensional nonlinear surface defined by

$$\sigma(x, x^*) = 0 \tag{18.10}$$

where x^* is equilibrium point of the system and each function $\sigma_i : \mathbb{R}^3 \to \mathbb{R}, i = 1, ..., n$, is a C^1 function such that $\sigma_i(0) = 0$. Then, provided that successive total time derivatives σ, $\dot{\sigma}$, ...,$\sigma^{(r-1)}$ are continuous functions of the closed-system state-space variables, and

$$\sigma = \dot{\sigma} = ... = \sigma^{(r-1)} = 0 \tag{18.11}$$

is a nonempty integral set, the motion of (18.11) is called r-sliding mode. Under the above considerations the controller which will be designed for finite-time stabilization of smooth systems at an equilibrium point, is a quasi-continuous high order sliding mode controller, which is discontinuous at least (18.11), and $r-$ sliding homogeneous (see [3] and [4] for more details). This controller can be determined as follows. Let us $i = 0, ..., r-1$. Denote $\varphi_{0,r} = \sigma \quad N_{0,r} = |\sigma|, \quad \Psi_{0,r} = \varphi_{0,r}/N_{0,r} = sign\sigma$,

$$\varphi_{i,r} = \sigma^{(i)} + \beta_i N_{i-1,r}^{(r-i+1)} \Psi_{i-1,r} \tag{18.12}$$

$$N_{i,r} = |\sigma^{(i)}| + \beta_i N_{i-1,r}^{(r-i)/(r-i+1)} \tag{18.13}$$

$$\Psi_{i,r} = \varphi_{i,r}/N_{i,r} \tag{18.14}$$

where $\beta_i, ..., \beta_{r-1}$, α are positive numbers, which are chosen sufficiently large in the list order, the controller

$$u = -\alpha \Psi_{r-1,r}(\sigma, \dot{\sigma}, ..., \sigma^{r-1}) \tag{18.15}$$

is r-sliding homogeneous and provided for the finite-time stability, $\sigma = 0$. Each choice of parameters $\beta_1, ..., \beta_{r-1}$ determines a controller family applicable to all systems (21.13) of relative degree r.

18.2.3.1 Differentiator Design

It is clear that in order to implement the control law (18.15), it is necessary to know the real time exact calculation or direct measurement of $\sigma, \dot{\sigma}, \ddot{\sigma}$ or all components of the state vector. However, in order to reduce the number of sensors, the only measurable signal in the system is the rotor angle δ. Combining the controller (18.15) and the homogeneous differentiator (see [3]) given by

$$\begin{aligned}
\dot{z}_0 &= v_0 \\
v_0 &= -\lambda_r L^{1/r}|z_0-\sigma|^{(r-1)/r} sign(z_0-\sigma)+z_1 \\
&\vdots \\
\dot{z}_k &= v_k \\
v_k &= -\lambda_{r-k} L^{1/(r-k)}|z_k-v_{k-1}|^{(r-k-1)/(r-k)} sign(z_k-v_{k-1})+z_{k+1} \\
\dot{z}_{r-1} &= -\lambda_1 L sign(z_{r-1}-v_{r-2})
\end{aligned} \tag{18.16}$$

for k = 1,..., r-2; where z_0, z_1,..., z_k are estimates of the k-th derivatives of σ.

18.2.3.2 Sliding-Mode Control for SMIB Power Systems

Now, the proposed methodology is applied to the SMIB system (18.1) as shown in Figure 18.1. Since system (21.13) has relative degree equal to 3 and $x^* = (x_1^*, x_2^*, x_3^*)$ is a stable equilibrium point of system (21.13). Consider the following nonlinear switching surface defined by $\sigma(x,x^*) = x_1 - x_1^*$, where

$$\begin{aligned}
\dot{\sigma}(x,x^*) &= x_2 \\
\ddot{\sigma}(x,x^*) &= a_1 - a_2 x_2 - \frac{a_3}{a_4 + a_5(x_3 - a_6)} sin(x_1)
\end{aligned}$$

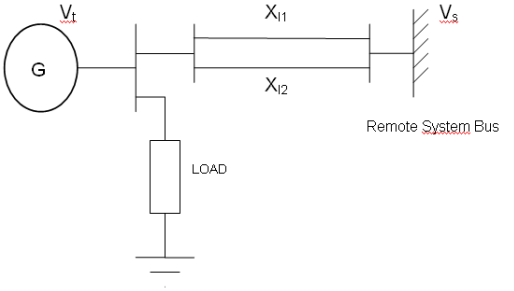

Fig. 18.1 Synchronous generator connected to a infinity bus.

Remark 18.1. It is clear that other switching surfaces can be defined.

Simulations results obtained using the following system parameters. Generator: $\omega_s = 377$ rad/s, $D = 0$, $H = 3.542$, $T_m = 0.6$ pu, $T'_{do} = 6.66$, $T'_{qo} = 0.44$, $T''_{do} = 0.03$, $T''_{qo} = 0.05$, $x_d = 1.7572$, $x_q = 1.5845$, $x'_d = 0.4245$, $x'_q = 1.04$, $x''_d = 0.25$, $x''_q = 0.25$, $Re = 0$. Infinite bus: $V_s = 1$. Transmission line: $R = 0$, $X_{l1} = 0.45$, $X_{l2} = 0.30$. For the differentiator: $\lambda_1 = 1.1$, $\lambda_2 = 1.5$, $\lambda_3 = 2$ and $L = 200$. Control input u_B: $\alpha_1 = 0.7$. Control input E_f : $\alpha_2 = -20$. The initial conditions were chosen as follows. $\delta_o = .744 rad$; $\omega_o = 377$ rad/s ; $E'_{qo} = 1.34$ p.u., $E'_{do} = 0.165$ p.u.; $\psi_{qo} = -0.48$ p.u.; $\psi_{do} = 1.109$ p.u. It is worth mentioning that the sliding-mode differentiator-controller is computed form the 3er model and it is implemented in the 6th order model.

The simulation results using the sliding mode control are shown in the Figure 18.2 and Figure 18.3, where we can appreciate the good performance of such controller under of the presence of a triphasic failure in the line. Notice that the controller stabilize all variables around the equilibrium point and damps out the angle oscillations. It is clear that the proposed scheme has a good performance inreducing overshoots and oscillations in few cycles.

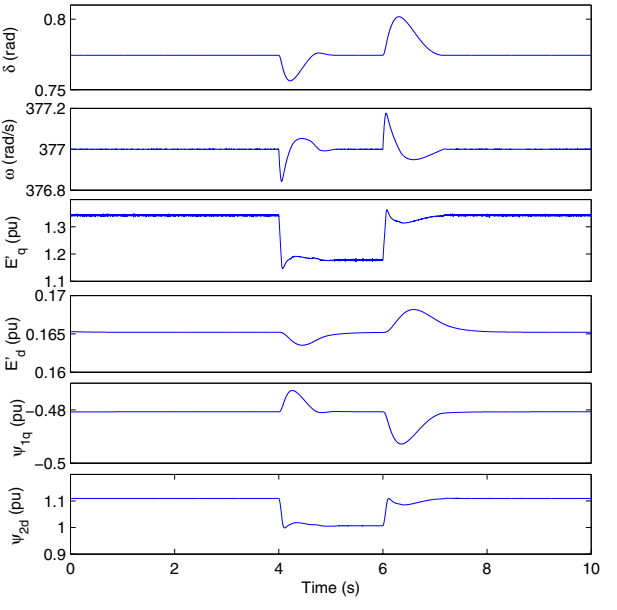

Fig. 18.2 Responses of the system in closed-loop.

18.2.4 Multi-machine Mathematical Model

Now, we study, under some standard assumptions, the dynamics of n interconnected generators through a transmission network can be described by the one axes model (21.13), (see [11]). The network has been reduced to internal bus representation assuming the loads to be constant impedances and taking into account the presence of transfer conductances. Then, the dynamical model of the i-th machine is represented by

$$\begin{cases} \dot{\delta}_i &= \omega_i - \omega_s \\ \dot{\omega}_i &= \frac{\omega_s}{2H_i}\left(P_{m_i} - D_i(\omega_i - \omega_s) - E'_{q_i} I_{q_i}\right) \\ \dot{E}'_{q_i} &= \frac{1}{T'_{d_i}}(E_{f_i} - E'_{q_i} - (X_{d_i} - X'_{d_i})I_{d_i}) \end{cases} \tag{18.17}$$

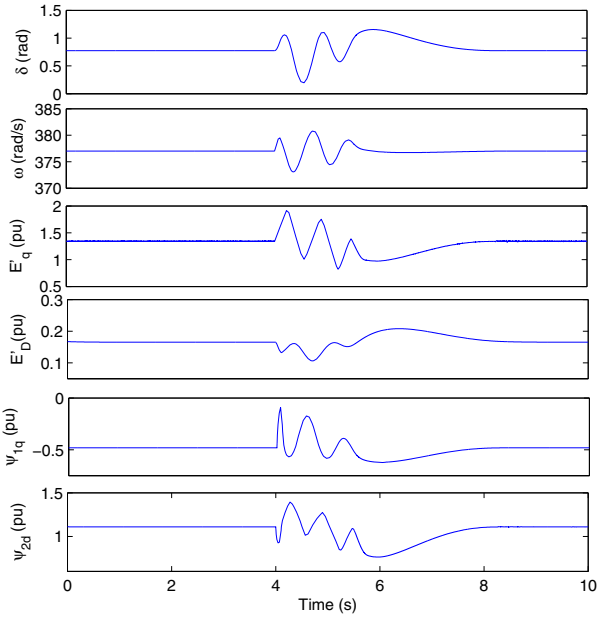

Fig. 18.3 Responses under triphasic failure.

where

$$I_{q_i} = G_{ii}E'_{q_i} + \sum_{j=1, j\neq i}^{n} E'_{q_j}\left\{G_{ij}cos(\delta_j - \delta_i) - B_{ij}sin(\delta_j - \delta_i)\right\}$$

$$I_{d_i} = -B_{ii}E'_{q_i} - \sum_{j=1, j\neq i}^{n} E'_{q_j}\left\{G_{ij}sin(\delta_j - \delta_i) + B_{ij}cos(\delta_j - \delta_i)\right\}$$

I_{q_i}, I_{d_i}	Currents in d-q reference frame of the i-th generator,
$E'_{q_i}(t)$	Transient EMF in the quadrature axis,
$E_{f_i}(t)$	The equivalent EMF in the excitation coil,
X_{d_i}, X'_{d_i}	Direct axis and direct axis transient reactance, respectively,
P_{m_i}	Mechanical input power,in p.u.
D_i	Damping factor; in p.u.
H_i	inertia constant, in seconds;
T'_{d_i}	Direct axis transient short circuit time constant, in seconds;
$\delta_i(t)$	Rotor angle, in radians;
$\omega_i(t)$	Relative speed,
$\omega_s = 2\pi f_s$	Synchronous machine speed, in rad/s;
G_{ij}, B_{ij}	$\{ij\}$ nodal conductance and susceptance matrices, respectively,

which are symmetric; at the internal nodes after eliminating all physical buses, in p.u.. Then, the state space representation of the multi-machine power system is given by

$$\begin{cases} \dot{x}_{i1} &= x_{i2} \\ \dot{x}_{i2} &= f_{i1}(X) \\ \dot{x}_{i3} &= f_{i2}(X) + u_i \end{cases}$$

where

$$f_{i1}(X) = a_i - b_i x_{i2} - c_i x_{i3}^2 - d_i x_{i3} \sum_{j=1, j\neq i}^{n} x_{j3} \left\{ G_{ij} cos(x_{j1} - x_{i1}) - B_{ij} sin(x_{j1} - x_{i1}) \right\}$$

$$f_{i2}(x) = -e_i x_{i3} + h_i \sum_{j=1, j\neq i}^{n} x_{j3} \left\{ G_{ij} sin(x_{j1} - x_{i1}) + B_{ij} cos(x_{j1} - x_{i1}) \right\}$$

$$\begin{array}{lll} a_i = (\omega_s/2H_i)P_{m_i}, & b_i = (\omega_s/2H_i)D_i, & c_i = (\omega_s/2H_i)G_{ii} \\ d_i = \omega_s/2H_i, & e_i = (1 + (X_{d_i} - X_{d_i}^{'})B_{ii})/T_{d_i}^{'}, & h_i = (X_{d_i} - X_{d_i}^{'})/T_{d_i}^{'} \end{array}$$

are the system parameters, $X_i = [x_{i1}, x_{i2}, x_{i3}]^T = [\delta_i(t), \omega_i(t), E_{q_i}^{'}(t)]^T$ for $i = 1, ..., n$, represents the state vector of i-th subsystem, thus $X = [X_1, X_2, ..., X_n]^T$ is the state vector of multi-machine system and the control inputs is given by $u_i = (1/T_{d_i}^{'})E_{fi}(t)$.

The control objective can be established as follows: Considering the model (18.17) and assuming that the currents $I_{q_i}(t)$ and $I_{d_i}(t)$ and the rotor angle $\delta_i(t)$ of each generator are available for measurement. Then, design a robust excitation control law for the system (18.17) in such a way the transient stability properties of system's operating point are guarantee improving its behavior under presence of noise in the measurable signals and faults in the network.

18.2.4.1 Sliding-Mode Control for Multi-machine Power Systems

Now, we design a control law for n interconnected machines based on sliding mode technique in such a way the stability properties of the system are improved. Since each subsystem (18.17) has relative degree equal to 3, then the resulting control law is given by

$$u = -\alpha \frac{\ddot{\sigma} + 2(|\dot{\sigma}| + |\sigma|^{2/3})^{-1/2}(\dot{\sigma} + |\sigma|^{2/3} sign\sigma)}{|\ddot{\sigma}| + 2(|\dot{\sigma}| + |\sigma|^2/3)1/2} \tag{18.18}$$

Now, considering the following nonlinear switching surface defined by $\sigma(X - X^*) = (\sigma_1(X - X^*), \sigma_2(X - X^*), \sigma_3(X - X^*))^T = 0$, where

$$\begin{aligned} \sigma_i(X) &= x_{i1} - x_{i1}^* \\ \dot{\sigma}_i(X) &= x_{i2} \\ \ddot{\sigma}_i(X) &= a_i - b_i x_{i2} - c_i x_{i3}^2 - d_i x_{i3} I_{qi} \end{aligned}$$

for $i = 1, 2, 3$, $X_i^* = (x_{i1}^*, x_{i2}^*, x_{i3}^*)$ is an equilibrium point.

Remark 18.2. It is worth noticing that the controller is expressed only in terms of local measurable variables (x_{i1}, x_{i2}, x_{i3}) and I_{qi} for $i = 1,2,3$. Consequently, the resulting controller is a decentralized output feedback (see [3], [14]).

Now, assuming that the only measurable signals in the system are the rotor angle δ_i, in order to reduce the number of sensors. Then, the control objective is to implement a finite-time convergent differentiator based on high order sliding mode, when the outputs $\sigma_i = \delta_i - \delta_i^*$ are available to estimate the values of $\dot{\sigma}_i$ and $\ddot{\sigma}_i$. The robust control law stabilizing the synchronous machine i, for $i = 1,2,3$; is given by

$$u_i = -\alpha_i \Psi_{r-1,r}(z_{i0}, z_{i1}, z_{i2}) \tag{18.19}$$

where z_{i0}, z_{i1}, and z_{i2} are given by the differentiator

$$\begin{aligned} \dot{z}_{i0} &= v_{i0} \\ v_{i0} &= -\lambda_{i3} L_i^{1/3} |z_{i0} - \sigma_i|^{2/3} sign(z_{i0} - \sigma_i) + z_{i1} \\ \dot{z}_{i1} &= v_{i1} \\ v_{i1} &= -\lambda_{i2} L_i^{1/2} |z_{i1} - v_{i0}|^{1/2} sign(z_{i1} - v_{i0}) + z_{i2} \\ \dot{z}_{i2} &= -\lambda_{i1} L_i sign(z_{i2} - v_{i1}) \end{aligned} \tag{18.20}$$

and the parameters of the differentiator (18.20) are chosen according to the condition $|\sigma_i^{(r)}| \leq L_i$, when L_i satisfies $L_i \geq C_i + \alpha_i K_M$. Finally, taken the following computer-tested values $\lambda_{i1} = 1.1$, $\lambda_{i2} = 1.5$ and $\lambda_{i3} = 2$ (see [3] for more details).

Notice that in the differentiator not appear the terms of interconnection, therefore the control scheme is completely decentralized. Furthermore, the order of the differentiator is not associated with number of machines interconnected in the network, it depends only on the relative degree of the model of the generator used for achieving the control objective. Furthermore, finite-time convergence of the observer allows to design the observer and the control law separately, i.e. the separation principle is satisfied.

18.2.4.2 Simulation Results

Now, we present some simulation results when the proposed scheme is implemented in a multi-machine system. In Figure 18.4 is shown the multi-machine system considered which represent a system of 3 generators interconnected. The numerical values of the generators parameters are presented in the Table 1.

Table 1 Generators parameters.

Parameter	Gen_1	Gen_2	Gen_3
$H(seg)$	23.64	6.4	3.01
$X_d(pu)$	0.146	0.8958	1.3125
$X'_d(pu)$	0.0608	0.1198	0.1813
$D(pu)$	0.3100	0.5350	0.6000
$P_m(pu)$	0.7157	1.6295	0.8502
$T'_{do}(seg)$	8.96	6.0	5.89

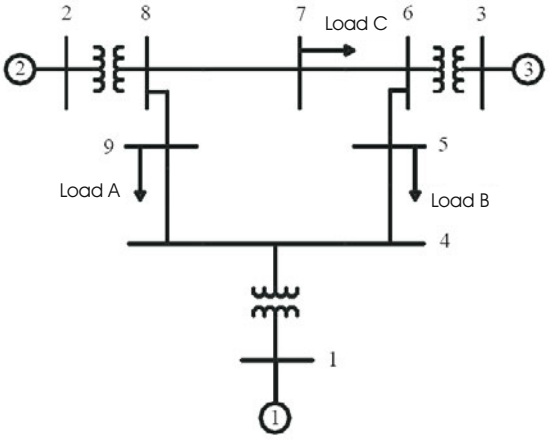

Fig. 18.4 Three-machine system.

Furthermore, the topology of the network has been represented by the conductance and susceptance nodal matrices

$$G = \begin{bmatrix} 0.8453 & 0.2870 & 0.2095 \\ 0.2870 & 0.4199 & 0.2132 \\ 0.2095 & 0.2132 & 0.2770 \end{bmatrix}, \qquad B = \begin{bmatrix} -2.9882 & 1.5130 & 1.2256 \\ 1.5130 & -2.7238 & 1.0879 \\ 1.2256 & 1.0879 & -2.3681 \end{bmatrix}$$

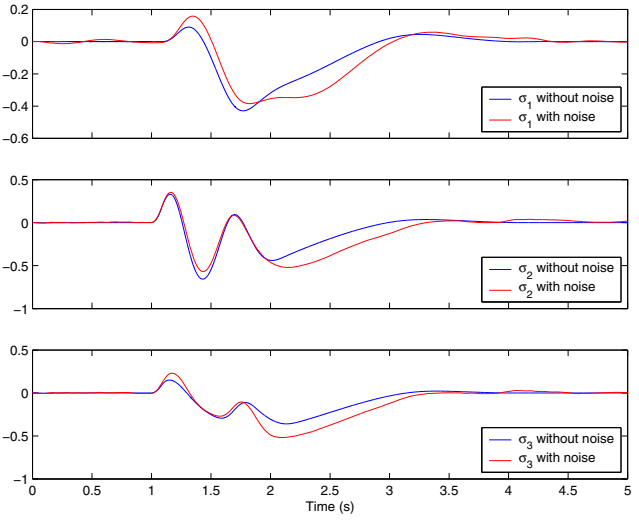

Fig. 18.5 Responses of the three-machine system.

In order to implement the controller, the following equilibrium point of the three-machine system is considered.

$$EP_1 : \begin{cases} x_{11}^* = 0.0396 \; x_{12}^* = 0 \; x_{13}^* = 1.0566 \\ x_{21}^* = 0.3444 \; x_{22}^* = 0 \; x_{23}^* = 1.0502 \\ x_{31}^* = 0.2300 \; x_{32}^* = 0 \; x_{33}^* = 1.017 \end{cases}$$

The parameters of the differentiators were selected as follows: $\lambda_{i1} = 1.1$, $\lambda_{i2} = 1.5$, $\lambda_{i3} = 2$, $L = 500$, for $i = 1, 2, 3$.

The performance of the proposed scheme is illustrated in Figure 18.5, where the responses of all state variables of the multi-machine system are shown. Notice that the good performance of the proposed controller has a better performance and stabilizes the machine variables and damps out the oscillations few cycles after.

18.3 Helicopter: Twin Rotor System

Helicopter is an aircraft that is lifted, propelled and maneuvered by vertical and horizontal rotors. All twin rotor aircrafts have high cross-coupling in all their degrees of motion. Especially the gyroscopic effect on azimuth dynamics prevents precise maneuvers by the operator emphasizing the need to compensate cross-coupling, a task that clearly adds to the workload for the pilot if done manually.

The twin rotor system recreates a simplified behavior of a real helicopter with fewer degrees of freedom. In real helicopters the control is generally achieved by tilting appropriately blades of the rotors with the collective and cyclic actuators, while keeping constant rotor speed. To simplify the mechanical design of the system, the twin rotor system setup considered in this presentation, is designed slightly differently. In this case, the blades of the rotors have a fixed angle of attack, and control is achieved by controlling the speeds of the rotors. As a consequence of this, the twin rotor system has highly nonlinear coupled dynamics. Additionally, it tends to be non-minimum phase system exhibiting unstable zero dynamics. This system poses very challenging problem of precise maneuvering in the presence of cross-coupling. It has been extensively investigated under the algorithms ranging from linear robust control to nonlinear control domains.

In this Section, the control objective is to design a robust controller for a twin rotor system taking into account the cross-couplings residing in the helicopter dynamics in such a way the improve its stability under external disturbances.

18.3.1 Dynamical Model of a Twin Rotor System

The dynamical model of the 2-DOF twin rotor system is described by the following equations

$$\begin{aligned}
\dot{x}_1 &= x_2 \\
\dot{x}_2 &= \frac{\{g\,[(A-B)\cos(x_1)-C\sin(x_1)]+l_m F_v-[A+B+C]\sin(x_1)\cos(x_1)x_4^2\}}{J_v} \\
&\quad -\frac{\{f_v x_2-a_1|\omega_m|x_2+k_{hv}u_h\}}{J_v} \\
\dot{x}_3 &= x_{i4} \\
\dot{x}_4 &= \frac{l_t F_h\cos(x_1)-f_h x_4-a_2|\omega_t|x_4+k_{vh}u_v}{D\sin(x_1)^2+E\cos(x_1)^2+F}
\end{aligned} \tag{18.22}$$

where $X=[x_1,...,x_4]^T$ represents the state vector of the system such as $X=[\theta,\dot{\theta},\psi,\dot{\psi}]$.
θ,ψ represent vertical and horizontal angles, respectively.
$\dot{\theta},\dot{\psi}$ represent vertical and horizontal velocities.
A,B,C,D,E,F are inertial constants taken from experimental setup measures.
l_m,l_t are the lengths of the main and tail parts of the beam.
f_v,f_h are viscous friction terms relative to vertical and horizontal axes.
ω_m,ω_t are angular velocities from main and tail rotors. Relationship has been experimentally determined, depends on the input voltage.
J_v is the sum of moments of inertia relative to the horizontal axis.
F_v,F_h denote the dependence of the propulsive force on the angular velocity of the main and tail rotors (experimentally determined).
a_1,a_2 are model constants.
k_{hv} and k_{vh} represent cross-coupling constant terms.
u_v and u_h represent the voltage applied to motors.
The angles θ and ψ are the measurable outputs.
Velocities $\dot{\theta}$ and $\dot{\psi}$ are assumed to be non-measurable states.

In the control system and robotic communities have gained interest for the development of observers applied to UAVs due to the important developments of embedded electronics and micro-controllers. This technological improvement has motivated the testing of more sophisticated algorithms in real time.

Motivated by previous arguments, in what follows a differentiator will be designed in order to solve the problem of speed estimation of a twin rotor system, when the vertical and horizontal angles are available from measurements.

18.3.1.1 Observer Design

Form the model (18.22), and knowing that the outputs of the system $y_1=x_1$ and $y_2=x_3$ are measurable, we use a differentiator in order to estimate the non measurable state components. For that

$$\begin{aligned}
\dot{z}_{i,0} &= \nu_{i,0} \\
\nu_{i,0} &= -\lambda_{i,2}L_i^{1/2}|z_{i,0}-\sigma_i|^{1/2}sign\,(z_{i,0}-\sigma_i)+z_{i,1} \\
\dot{z}_{i,1} &= -\lambda_{i,1}L_i sign\,(z_{i,1}-\nu_{i,0})
\end{aligned} \tag{18.23}$$

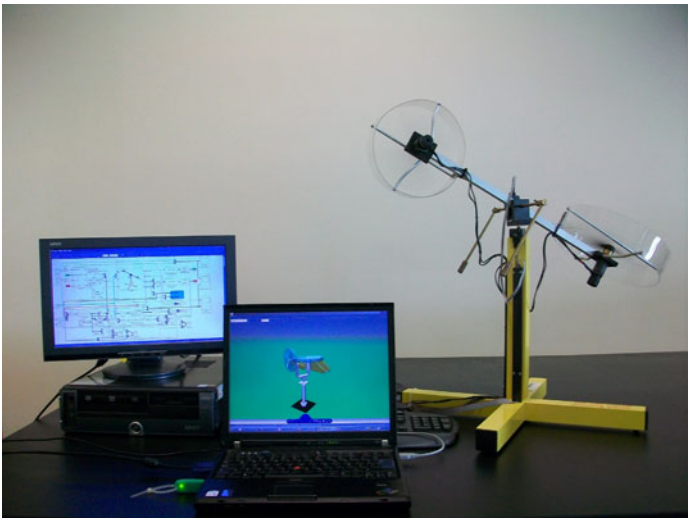

Fig. 18.6 Helicopter: twin rotor system setup.

for $i = 1, 2$. Then, the controller is of the form.

$$u_i = -\alpha_i sign(z_{i,1}) + |z_{i,0}|^{1/2} sign(z_{i,0})) \tag{18.24}$$

where $u_1 = u_h$ and $u_2 = u_v$.

18.3.1.2 Simulation Results

In this Section, we provide simulation results to illustrate the effectiveness of the proposed methodology when applied to the twin rotor systems.

The case of study concerns the design of a robust control for twin rotor system of a 2-DOF helicopter setup (see Figure 18.6).

Platform consists of a beam pivoted on its base in such a way that it can rotate freely both in the horizontal and vertical planes. At both ends of the beam there are rotors (main and tail rotors) driven by DC motors. A counterbalance arm with a weight at its end is fixed to the beam at the pivot. The state of the beam is described by four process variables: horizontal and vertical angles measured by position sensors fitted at the pivot, and two corresponding angular velocities. Two additional state variables are the angular velocities of the rotors, measured by tacho-generators coupled with the driving DC motors.

The numerical values from the system parameters were $J_v = 0.02421, m = 0.5920, l_m = 0.202, l_t = 0.216, g = 9.8, A = 1.0671, B = 1.4678, C = 0.0044, D = 0.0006225, E = 0.0224, F = 0.0021, f_v = 45, f_h = 90, a_1 = 0.1, a_2 = 0.1, k_{vh} = 20, k_{hv} = 18$.

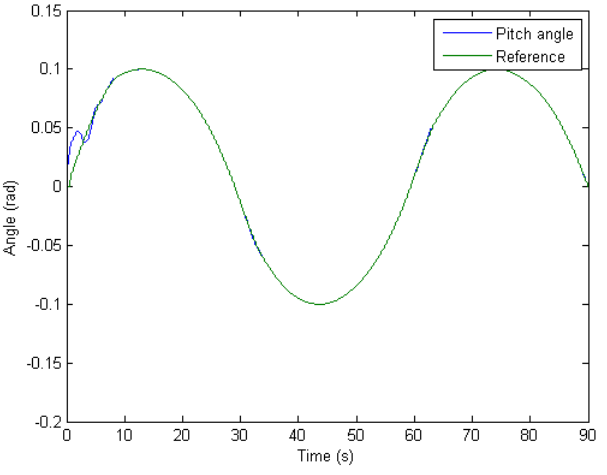

Fig. 18.7 Reference and horizontal response of helicopter system with 2-DOF.

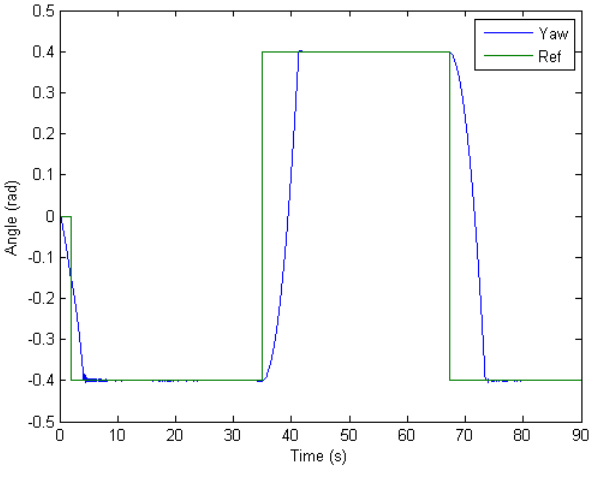

Fig. 18.8 Reference and vertical response of helicopter system with 2-DOF.

Defining $\sigma_1 = y1 - y_{ref,1}$ and $\sigma_1 = y3 - y_{ref,2}$, where $y_{ref,1} = 0.1sin(wt)$ of 1/60 Hz frequency and $y_{ref,2} = 0.4Square(t)$ of 1/0.015 Hz frequency. Assuming the helicopter starts moving from a rest point, initial value of the states variables were $x_1(0) = 0.01$, $x_3(0) = 0.01$, $x_2(0) = 0.01$, $x_4(0) = 0.01$. Furthermore, the differentiator parameters were chosen as follows: $\lambda_{1,1} = 1.5$, $\lambda_{1,2} = 1.1$, $\lambda_{2,1} = 1.85$, $\lambda_{2,2} = 1.81$, $L_1 = 20$, $L_2 = 20$. Finally, the control parameters were chosen as follows: $\alpha_1 = 18.02$, $\alpha_2 = 450.02$.

In Figure 18.7 and Figure 18.8 are plotted the responses of vertical and horizontal angles, respectively; tracking the desired reference and which are obtained from the twin rotor system setup. In all simulations, we can see that the output controller tracks the desired time varying references of the horizontal and vertical angles. Furthermore, we can see that the position and speed converges to the desired references in finite-time. It is clear that the proposed controller has a good performance in terms of rate of convergence.

18.4 Teleoperation Bilateral: Master-Slave Systems

18.4.1 Introduction

Recently, the application of nonlinear control theory has attracted the attention of the research community to understand and overcome problems in bilateral teleoperation. Furthermore, teleoperation over the internet has introduced new problems due to the effects of delays in communications, which may cause instability in the system.

In a system which is teleoperated basically, a human operator interacts with an interface, called master teleoperator, and drives it in order to govern the remote counterpart, on the opposite side, while another interface (slave operator) is in charge of directly implementing commands received from the operator on the remote environment (see [8], [9]).

Several teleoperation schemes considering time-delays have been proposed in the last decades. However, stability problems have found in these schemes, so that important improvements have been suggested. Recently, an increased interest on sliding-mode control has been developed to address the problem of delays in teleoperation, which has generated and inspired a line of research in designing controllers to compensate the effects of these delays in real time (see [26] [27], [25]).

The control objective is to design a robust control for a teleoperator system taking into account a fixe delay time in the communication system. The scheme applied contains an impedance control for the master system combined with a second order sliding mode control and differentiator for the slave system. Thus, this scheme provides a better performance over a wide range of constant time-delays.

18.4.2 Teleoperation System

In a teleoperation general setting, the human imposes a force on the master manipulator which in turn results in a displacement that is transmitted to the slave that mimics that movement. If the slave possess force sensors, then it can reflect or transmit back to the master reaction forces from the task being performed, which enters into the input torque of the master, and the teleoperator is said to be controlled bilaterally.

For sake of simplicity, we consider the dynamics of the 1-DOF master/slave systems are represented as a mass-damper system

$$M_m\ddot{x}_m(t) + C_m\dot{x}_m(t) = u_m(t) + f_h(t) \tag{18.25}$$

$$M_s\ddot{x}_s(t) + C_s\dot{x}_s(t) = u_s(t) - f_e(t) \tag{18.26}$$

where x and u denote the position and the input torque, respectively; subscript m and s denote the master and the slave; f_h and f_e are the force applied at the master by the human operator, and the force exerted on the slave by the environment, respectively. Also M_i and C_i represent mass and viscous friction coefficient, respectively, with $i = m,s$ denoting master and slave. Furthermore, a time delay imposed on the communication channels is assumed to be constant and unknown.

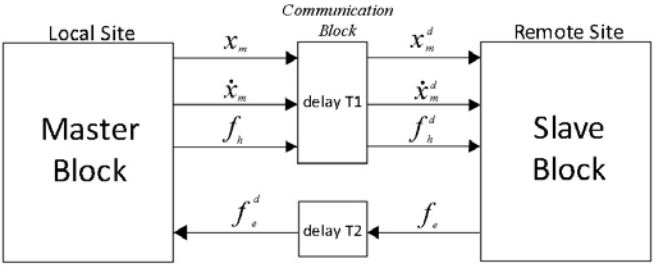

Fig. 18.9 A block diagram of bilateral teleoperation

This bilateral teleoperation system scheme can be represented by the block diagram shown in Figure 18.9. Furthermore, the position and force of the master are transmitted to the slave and the contact force of the slave is sent to the master through the communication channel, where there is a time delay in the communication channel. The signals from and to the channel are related as

$$\begin{aligned} x_m^d(t) &= x_m(t - T_1) & f_h^d(t) &= f_h(t - T_1) \\ \dot{x}_m^d(t) &:= \dot{x}_m(t - T_1) & f_e^d(t) &:= f_e(t - T_2) \end{aligned} \tag{18.27}$$

where x_m^d, $\dot{x}_m^d$, and f_h^d are the position and velocity of the master, and the force exerted by a human operator, respectively, which are transmitted to the slave through the communication channel; f_e^d is the external force at the slave transmitted to the slave through the master; T_1 is a time delay of the signal flowing from master to the slave, and T_2 is in the opposite direction.

This delayed signals out of the communication block are then scaled up or down by some factors, then the position/velocity command to the slave and the force signal to the master are modified such that $x_s = K_p x_m^d$ and $f_h = K_f f_e^d$, where K_p and K_f are position and force scale factors, respectively. Then, the state space representation of (18.25) and (18.26) are given as follows.

$$\begin{cases} \dot{x}_{m1} = x_{m2} \\ \dot{x}_{m2} = -\frac{C_m}{M_m} x_{m2} + \frac{1}{M_m} u_m + \frac{1}{M_m} f_h \end{cases} \tag{18.28}$$

$$\begin{cases} \dot{x}_{s1} = x_{s2} \\ \dot{x}_{s2} = -\frac{C_s}{M_s} x_{s2} + \frac{1}{M_s} u_s - \frac{1}{M_s} f_e \end{cases} \tag{18.29}$$

In what follows, a robust impedance controller as well as a differentiator in order to estimate the speed and acceleration are designed. It is clear that an extension of theses results for the multi-variable case can be obtained.

18.4.3 Controller Design

Now, an impedance controller and a sliding-mode based impedance controller are designed for the master and the slave, respectively.

Consider the following master control structure

$$u_m = -f_h + C_m \dot{x}_m + \frac{M_m}{\bar{M}_m}(f_h - K_f f_e^d - \bar{C}_m \dot{x}_m - \bar{K}_m x_m) \tag{18.30}$$

where $\bar{M}_m$, $\bar{C}_m$, $\bar{K}_m > 0$ are desired inertia, damping coefficient, and stiffness, respectively; of a desired impedance. Substituting (18.30) into (18.25), the closed-loop impedance error is given by

$$\bar{M}_m \ddot{x}_m + \bar{C}_m \dot{x}_m + \bar{K}_m x_m = f_h - K_f f_e^d \tag{18.31}$$

Consider the slave control design based on second order sliding mode approach to produce a desired impedance behavior modulated by the environmental contact force and robust to unknown time-delay. To this end, consider the desired slave impedance

$$\bar{M}_s \ddot{\tilde{x}}_s + \bar{C}_s \dot{\tilde{x}}_s + \bar{K}_s \tilde{x}_s = -f_e \tag{18.32}$$

where $\bar{M}_s$, $\bar{C}_s$, $\bar{K}_s > 0$ are the desired inertia, damping, and stiffness, respectively, and $\ddot{\tilde{x}}_s := \ddot{x}_s - K_p \ddot{x}_m^d$, $\dot{\tilde{x}}_s := \dot{x}_s - K_p \dot{x}_m^d$, $\tilde{x}_s := x_s - K_p x_m^d$ are the slave tracking errors for acceleration, velocity and position, respectively.

Since we want to obtain (18.32) in closed-loop, then defining the following sliding surface

$$I_e = \bar{M}_s \ddot{\tilde{x}}_s + \bar{C}_s \dot{\tilde{x}}_s + \bar{K}_s \tilde{x}_s + f_e = 0 \tag{18.33}$$

Now, let us define the extended error variable as follows

$$\Omega = \frac{1}{\bar{m}_s} \left[\int_0^t I_e(\tau) d\tau + K_i \int_0^t \int_0^\sigma sign(I_e(\tau)) d\tau d\sigma \right] \tag{18.34}$$

where $K_i > 0$ is the sliding mode gain. Substituting (18.33) into (18.34) and integrating, we finally obtain

$$\Omega = \dot{\tilde{x}}_s + \frac{\bar{C}_s}{\bar{M}_s}\tilde{x}_s + \frac{1}{\bar{M}_s}\int_0^t [\bar{K}_s\tilde{x}_s + f_e]d\tau + \frac{K_i}{\bar{M}_s}\int_0^t\int_0^\sigma sign(I_e(\tau))d\tau d\sigma \tag{18.35}$$

The slave controller u_s has the following form

$$\begin{aligned} u_s = & -\tfrac{M_s}{\bar{M}_s}\left(\bar{C}_s\dot{\tilde{x}}_s + \bar{K}_s\tilde{x}_s + f_e + K_i\int_0^t sign(I_e(\tau))d\tau\right) \\ & + \tfrac{M_s}{\bar{M}_m}kK_p\left(f_h^d - K_f f_e^{dd} - \bar{C}_m\dot{x}_m^d - \bar{K}_m x_m^d\right) + f_e + C_s\dot{x}_s - K_g\Omega \end{aligned} \tag{18.36}$$

where $f_e^{dd} = f_e(t-2T)$, the superscript dd stands for the round trip delay: $2T$, $K_g > 0$, and $sign(\cdot)$ is the discontinuous signum function. The term $K_g\Omega$ has been added to achieve stability as it will be seen afterwards. Also, notice that (18.35) requires acceleration measurement because I_e depends on acceleration. To deal with this inconvenience, acceleration and velocity are estimated, at master and slave sides, by means of super twisting observers.

18.4.4 Super Twisting Observer Design

The elimination of sensors to measure velocity and acceleration is an advantage in robotics because expensive and bulky tachometers are avoided. Then, to reduce the number of sensors we add to the control scheme a nonlinear super twisting sliding mode observer (see [6]). This sliding mode observer is based on structural conditions and the iterative use of the super twisting algorithm. The importance of such observer is that it can be used as a tool to solve several difficult problems of observation.

Now, a finite time observer for slave system (18.29) is designed. Consider the following canonical form.

$$\begin{cases} \dot{x}_1 = x_2 \\ \dot{x}_2 = F(x_1, x_2, u, y) \end{cases} \tag{18.37}$$

with $F(x_1,x_2,u,y) = -\frac{C_s}{M_s}x_2 + \frac{1}{M_s}u_s - \frac{1}{M_s}f_h$.

Notice that the term F can be seen as unknown input, which must be estimate in such a way to estimate the acceleration of the slave system.

The super twisting observer for system (18.37) has the following form

$$\begin{aligned} \dot{\hat{x}}_1 &= \tilde{x}_2 + \lambda_1\sqrt{|\tilde{x}_1 - \hat{x}_1|}sign(\tilde{x}_1 - \hat{x}_1) \\ \dot{\tilde{x}}_2 &= \alpha_1 sing(\tilde{x}_1 - \hat{x}_1) \\ \dot{\hat{x}}_2 &= E_1[\tilde{\Theta} + \lambda_2(\sqrt{|\tilde{x}_2 - \hat{x}_2|})sign(\tilde{x}_2 - \hat{x}_2)] \\ \dot{\tilde{\Theta}} &= E_2\alpha_2 sign(\tilde{x}_2 - \hat{x}_2) \end{aligned} \tag{18.38}$$

where α_1 and α_2 are the observer gains, λ_1 and λ_2 are the corrections factors designed for convergence of the estimation error, which are defined as $e_i = \tilde{x}_i - \hat{x}_i$, for $i = 1,2$. Also the scalar functions E_i for $i = 1,2$ are defined as: $E_i = 1$ if $e_i \leq \varepsilon_i$, else $E_i = 0$, where ε_i are small positive constants.

18.4.5 Simulation Results

Simulation results are obtained using the following parameter values. The parameter values of the each system are the following. Master System: $C_m = 0.9$, $M_m = 1.9$, $\bar{M}_m = 1.8641$, $\bar{C}_m = 1.5$, $K_f = .9$, $\bar{K}_m = 0.01$. Slave system: $C_s = 0.9$, $M_s = 7$, $\bar{C}_s = 0.5$, $\bar{M}_s = 0.3$, $\bar{K}_s = 15$. The parameters of the controller: $K_p = 1$, $K_g = 500$, $K_i = 0.1$, and the observer: $\alpha_1 = 100$, $\alpha_2 = 200$, $\lambda_1 = 10$, $\lambda_2 = 750$, $E_1 = 1$, $E_2 = 0$.

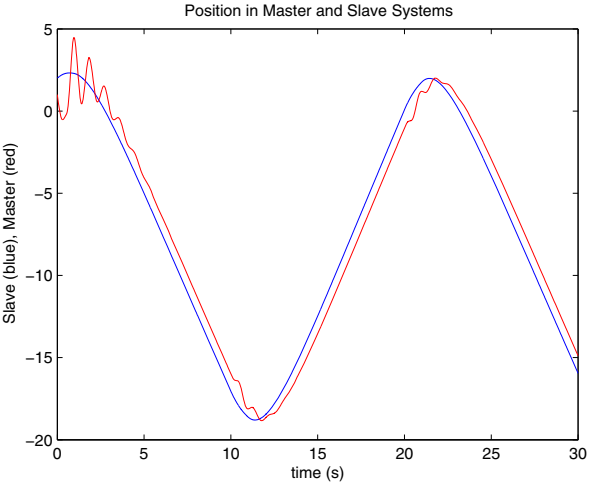

Fig. 18.10 Position responses of Master-Slave system.

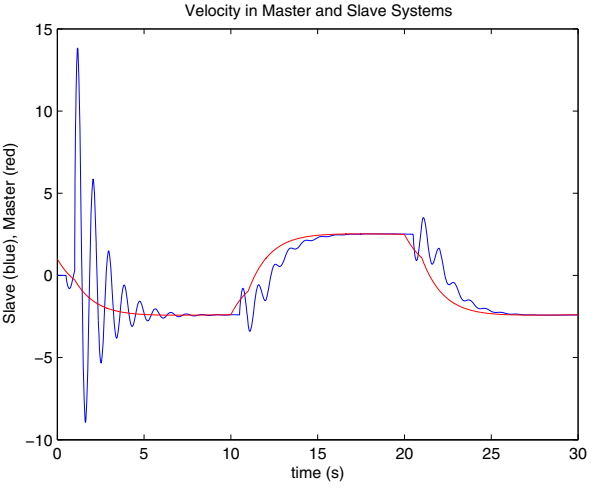

Fig. 18.11 Velocity responses of Master-Slave system.

In Figure 18.10 and Figure 18.11, the position and velocity responses are plotted. We can see the performance of the control when the master system tracks a desired trajectory and the slave system tracks the master system signal sent by the communication system with a time delay T, which was chosen of $T = 0.5$sec..

18.5 Conclusions

In this paper, an overview about the strategies of control and observation based on sliding modes techniques has been presented and implemented in electrical power systems (synchronous machine and multi-machines systems), in a twin rotor system (Helicopter of 2-DOF), and in a master-slave teleoperated bilaterally system, which are the research fields of the Mechatronics laboratory of the Universidad Autónoma de Nuevo León, in the CIIDIT-UANL Research Institute.

Furthermore, in all applications presented in this paper, the tested control-observer strategies based on sliding mode have been demonstrated the good performance as well as the finite-time convergence and robustness under external disturbances.

Acknowledgements. The author gratefully acknowledges the financial support by the Mexican CONACyT (Consejo Nacional de Ciencia y Tecnología) grant number 105799, by the FONCyT (Fondo Nacional para la Ciencia y la Tecnología) project number 93302.

References

1. Cho, H.C., Park, J.H.: Stable bilateral teleoperator under a time delay using a robust impedance control. Mechatronics 15, 611–625 (2005)
2. Young, K.D., Utkin, V., Özgüner, Ü.: A control engineer's guide to sliding mode control. IEEE Transactions on Control Systems Technology 7(3) (May 1999)
3. Levant, A.: High-order sliding modes, differentiation and output feedback control. Int. J. Control 76(9/10), 924–941 (2003)
4. Levant, A.: Quasi-continuous high order sliding-mode controllers. IEEE Transactions on Automatic Control 50(11), 1812–1816 (2005)
5. Davila, J., Fridman, L., Poznyak, A.: Observation and identification of mechanical systems via second order sliding modes. In: International workshop on variable structure systems, Aleghero, Italy, June 5 -7, pp. 232–237 (2006)
6. Floquet, T., Barbot, J.P.: Super twisting algorithm based step-by-step sliding mode observers nonlinear systems with unknown inputs. International Journal of Systems Science 38(10), 803–815 (2007)
7. Walcott, B.L., Żak, S.H.: State observation of nonlinear uncertain dynamical systems. IEEE Transactions on Automatic Control 32, 88–104 (1987)
8. Slotine, J.J., Hedrick, J.K., Misawa, E.A.: On sliding observers for nonlinear systems. ASME Journal Dynamical Systems Measurement Control 109, 245–252 (1987)
9. Hoyakem, P.F., Spong, M.W.: Bilateral Teleoperation: An historical survey. Automatica 42, 2035–2057 (2006)
10. Li, C., Elbuluk, M.: A sliding mode observer for sensorless control of permanent magnet synchronous motors. In: Industry Applications Conference (2001)

11. Bergen, A.: Power System Analysis. Prentice-Hall, Englewood Cliffs (1986)
12. Utkin, V.I., Guldner, J., Shi, J.: Sliding mode control in electromechanical systems. Taylor & Francis, Abington (1999)
13. Utkin, V.I.: Sliding modes in control and optimization. Comunications and Control Engineering Series. Springer, Heidelberg (1992)
14. Chapman, J.W., Ilic, M.D., King, C.A., Eng, L., Kaufman, H.: Stabilizing a multimachine power system via decentralized feedback linearizing excitation control. IEEE Trans. on Power Systems 8(1), 830–839 (1993)
15. Ortega, R., Galaz, M., Astolfi, A., Sun, Y., Shen, T.: Transient stabilization of multimachine power systems with nontrivial transfer conductances. IEEE Trans. on Automatic Control 50(1), 60–75 (2005)
16. Taore, D., Plestan, F., Glumineau, A., de Leon, J.: Sensroless induction motor: Hihg sliding mode controller and adaptive interconnected observer. IEEE Trans. Ind. Electron 55(1), 3818–3827 (2008)
17. Colbia-Vega, A., de Leon-Morales, J., Fridman, L., Salas-Pena, O., Mata-Jimenez, M.T.: Robust excitation control design using sliding-mode technique for multimachine power systems. Electric Power Systems Research 78(1), 1627–1634 (2008)
18. Loukianov, A.G., Caedo, J.M., Utkin, V.I., Cabrera-Vazquez, J.: Discontinuous Controller for Power System: Sliding-Mode Block Control Approach. IEEE Trans. On Industrial Electronics 51(2), 340–353 (2004)
19. Valavanis, K.P.: Advances in Unmanned Aerial Vehicle, University of south Florida Tampa, Florida. Springer, Heidelberg (2007)
20. Stengel, R.: Flight Dynamics, November 2004. Princeton University Press, Princeton (2004)
21. Zyskowky, M.K.: Aircraft Simulation Techniques Used in Low-Cost, Commercial Software. In: AIAA 2003, vol. 5818 (August 2003)
22. Melin, T.: A Vortex Lattice Matlab Implementation for linear Aerodynamic Wing Applications. Masters Thesis, Royal Institute of Technology, KTH (2000)
23. Etkin, B.: Dynamics of Flight Stability and Control, 3rd edn. John Wiley and Sons, Inc., Chichester (1996)
24. Naveed, U., Whidborne, J.F.: A lateral Directional Flight Control System for the MOB Blended Wing Body. Departament of Aerospace Sciences. Cranfield University, Bedfordshire MK45 OAL, UK
25. Guerra-Torres, C., de Leon-Morales, J., Glumineau, A., Traore, D., Boisliveau, R.: Teleoperation of an Experimental Platform of Electrical Machines through the Internet. International Journal of Online Engineering (iJOE) 42(1) (2121) ISSN 1861-2121
26. Garcia-Valdovinos, L.G., Parra-Vega, V., Arteaga, M.: Higher-order sliding mode impedance bilateral teleoperation with robust state estimation under constant unknown time delay. In: Proceedings IEEE/ASME Int. Conf. on Advanced Intelligent Mechatronics, pp. 1293–1298 (2005)
27. Cho, H.C., Park, J.H.: Stable bilateral teleoperatin under a time delay using a robuste impedance control. Mechatronics 15, 611–625 (2005)
28. Rodriguez, A., De Leon, J., Fridman, L.: Quasi-continuous high-order sliding-mode controllers for reduced-order chaos synchronization. International Journal of Non-Linear Mechanics 43, 948–961 (2008)
29. Rodriguez, A., De Leon, J., Fridman, L.: Synchronization in reduced-order of chaotic systems via control approaches based on high-order sliding-mode observer. Chaos, Solitons and Fractals 42, 3219–3233 (2009)

Chapter 19
Synthesis of Canonical Elements for Power Processing Based on Sliding-Mode Control

Luis Martínez-Salamero and Angel Cid-Pastor

Abstract. Inducing sliding motions in appropriate converters allows a systematic design of the three canonical elements for power processing, i.e., DC transformer, power gyrator and loss-free resistor (LFR). A search of candidates is performed by studying a great number of converters with topological constraints imposed by the nature of each canonical element. Several examples ranging from DC impedance matching by means of a DC transformer to LFR-based power factor correction illustrate the application of the synthesis.

19.1 Introduction

The domain of Power Electronics lies in the field of conversion and control of electric energy for industrial, commercial or domestic applications. Many times identified with Industrial Electronics, Power Electronics is the result of the interaction of independent disciplines with a high degree of maturity, such as Control Theory and Circuit Theory, with technological subjects in permanent change such as Analogue and Digital Electronics, Microprocessors, Semiconductor Power Devices, VLSI circuits and Electrical Machines [24].

Power Electronics has been a key element in the regulation and control of electrical machines during more than sixty years, and it was initially associated with high power and high current processes. Later, at the end of the sixties of last century, it underwent an alternative development in high frequency, low power, and low current systems with the appearance of the DC-DC switching converters in the electrical architecture of satellites and other spacecrafts systems.

DC-DC switching converters were gradually becoming the basic core of power supplies for terrestrial applications, where computer and telecommunication industries are their greatest debtors, and nowadays they are key elements in the electrical

L. Martínez-Salamero · A. Cid-Pastor
Escola Técnica Superior d'Enginyeria, Universitat Rovira i Virgili, Tarragona, 43007 Spain
e-mail: luis.martinez@urv.cat

L. Fridman et al. (Eds.): Sliding Modes, LNCIS 412, pp. 517–540.
springerlink.com

architecture of any electronic instrumentation equipment. The importance of this development has had its correlation in a very dynamic market, in constant expansion and with permanent attractive challenges for engineers.

The design of switching converters requires interdisciplinary knowledge to fusion notions of analysis and modeling, simulation and control with technological expertise in magnetic design, capacitive components and power devices employed in the converter realization [12].

The most simple way to describe a switching converter is by means of a two-port element, so that in the input port energy is extracted from a non-regulated DC source, i.e., battery, photovoltaic (PV) panel, rectifier or fuel cell, to be supplied according to specifications to a load connected at the output port. Thus, we can find stable consume and strict margins of output voltages in instrumentation equipments, pulsating consume in laser supplies or large consume margins in motor supplies.

The electrical architecture of power supplied has evolved from an initial centralized configuration to a present distributed configuration [20]. Centralized power systems use only one converter with multiple outputs with different voltage values and regulation levels, these output being connected to their respective loads by means of individual buses .Their main advantage lies in the concentration in a single box of all the technology for power processing , this including the thermal management. However, their adaptation to the requirements of the new generation of power equipments is very limited. On the other hand, distributed power systems are of modular type, employ multiple converters located in different points, and combine voltages and currents to satisfy the load specifications. They are specially indicated for high-power applications and can be easily standardized, so that low power techniques can be used in their design. They employ an input converter that provides an intermediate DC bus whereto multiple converters acting as interface with their respective loads are connected. These converters are located at the point of load, and are used to provide the local voltages required by their respective loads. This type of architecture shows significant advantages over the centralized approach in terms of thermal management and encapsulating, decrease of the basic modular element, reduction of harmonic components and electromagnetic interference (EMI), design standardization, maintenance and flexibility to design complex architectures. Distributed power architectures are nowadays the best candidate to fulfill the requirements of the new power supply architectures among which we have to point out the one corresponding to microprocessors which should operate with clock frequencies of gigahertz from a power converter delivering voltages low of a 1 V and nominal current loads of 30 A or more.

There are two families of converters, namely, the hard switching converters and the resonant converters. The hard switching converters are dominant in the industrial area of electrical architectures for power supplies and will be the subject of this paper.

19.2 Power Processing Systems

Power Processing is a technical field defined by some of the pioneers in power supplies almost 40 years ago with the aim to organize systematically both teaching and research in the area of power electronics that at that time had already achieved maturity. The name was by analogy with and in contrast to Signal Processing, in which the information content is processed by electronic devices at the expense of some power consumption. In Power Processing the main objective is to minimize energy loss in transforming one form of electrical power into another according to some signal control [24]. If we observe the elements used in an analogue signal processor, we will find resistors, capacitors and semiconductors in linear operation, the inductors being excluded because they are bulky, heavy and do not fit to integrated circuits. In a clear cut contrast, in a Power Processing system the basic elements are inductors, capacitors and semiconductors operating in switched mode, the resistor being the forbidden element in any configuration.

The basic electronic functions of a power processing system are 1) voltage regulation 2) DC impedance matching 3) capability of association with other processors 4) generation of power signals by tracking variable reference signals. Converter association constitutes the key element of modern power distribution structures due basically to the employ of modular systems whose use is justified by reasons of efficiency and standardization. There are five basic distribution structures to provide functions of paralleling, cascading, stacking, source splitting and load splitting [20].

DC impedance matching in power processing basically means to match a PV generator and a DC load. In most of the cases found in the technical literature, the converter has implicitly performed the canonical function of a DC transformer. However, there are other canonical elements in power processing [27], namely, the power gyrator and the loss-free resistor that can be used to improve the efficiency and versatility of power distribution systems and can also provide impedance matching in photovoltaic systems.

In this paper, a systematic procedure for the synthesis of canonical elements for power processing is presented in a unified way. The three basic elements, i.e., DC transformer, power gyrator and loss-free resistor are designed by inducing sliding motions in appropriate DC-DC switching converters whose respective equilibrium states are characterized by the corresponding descriptive equation of the canonical element. This paper is organized as follows. A generalized canonical element for the synthesis is presented in Section 19.3. DC Transformers are analyzed in Section 19.3. Power gyrators and loss-free resistors are studied in Sections 19.5 and 19.6 respectively. The PV impedance matching problem is analyzed in Section 19.7 with experimental results for a boost converter with output filter acting as a DC transformer interfacing a PV generator and a battery. DC-AC conversion in a modular chain for PV systems is studied in Section 19.8. Power distribution based on gyrators is covered in Section 19.9. Power factor correction by means of loss-free resistors is investigated in Section 19.10. Finally, conclusions and discussion on future research are given in Section 19.11.

19.3 Generalized Canonical Element

Fig. 19.1 shows the block diagram of a generalized canonical element for power processing. It consists of a switching converter, which is controlled by means of a sliding mode regulation loop [22]. The switching surface is given by $S(x) = K_1 i_1 + K_2 i_2 + K_3 v_1 + K_4 v_2$ and can be particularized in the following cases: a) $K_3 = K_4 = 0$, b) $K_1 = K_2 = 0$, c) $K_1 = K_4 = 0$, d) $K_2 = K_3 = 0$, e) $K_2 = K_4 = 0$. Cases a) and b) result in a DC transformer, cases c) and d) lead to a power gyrator and case e) yields a loss-free resistor.

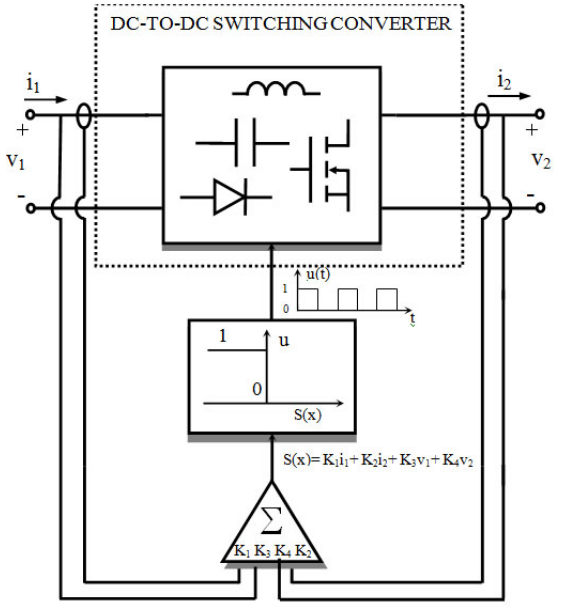

Fig. 19.1 Block diagram of a generalized canonical element for power processing

There are two main approaches in the use of sliding-mode control in switching power converters. The first one is based on the fact that for single input systems a suitable Lyapunov function is $V(t,x) = s^2(x)/2$, which is positive definite. If the switched feedback gains are chosen so that

$$\frac{dV(t,x)}{dt} = s\frac{ds}{dt} < 0 \tag{19.1}$$

in the domain of attraction, then the state trajectory converges to the surface and is restricted to the surface for all subsequent time. This procedure is used in the works of Bilalovic [1], Venkataraman et al. [36, 37], Malesani et al. [21] and Tan et al. [31, 30]. The second approach is based on Filippov's method [13] and its immediate corollary, which is known as the method of the equivalent control [32, 33, 34] and can

be easily applicable to multi-input systems. This technique has been used by Sira-Ramirez [28] considering sliding surfaces of the form $x_j = K$, for some state variable that is desired to be regulated at the level K. It has been also used in [23, 8, 6, 10] for surfaces that are a linear combination of the converter state variables yielding interesting results for the design of new power devices.

On the other hand, it has to be pointed out that imposing a sliding mode regime using a combination of voltages and currents requires the corresponding variables to be either continuous function of time or represent independent generators [36]. Therefore, this condition establishes the main topological constraint in all the above mentioned cases and will be the base for searching the candidates to implement the different canonical elements.

19.4 Synthesis of DC Transformers

The goal of the synthesis is to design a switching structure whose equations in steady-state are given by

$$\begin{aligned} V_2 &= nV_1 \\ I_2 &= \frac{I_1}{n} \end{aligned} \tag{19.2}$$

where I_1, V_1, and I_2, V_2 are the steady-state averaged values of input and output variables respectively.

Equations (19.2) define a DC transformer, which can be synthesised particularising the block diagram of Fig. 19.1 in cases A or B.

CASE A

The sliding surface is given by $S_(x) = K_1 i_1 + K_2 i_2$. In steady-state $S(x) = 0$, i.e., $I_2 = -\frac{K_1 I_1}{K_2} = \frac{I_1}{n}$ with $n = -\frac{K_2}{K_1}$. On the other hand, since the converter in Fig. 19.1 is ideal and therefore is a POPI structure (DC Power output=DC Power input) [27], equation (19.2) will be automatically satisfied.

The sliding constraint requires both i_1 and i_2 to be continuous function of time, this implying the existence of a series inductor in both ports. The most simple converters with such constraints at both ports are fourth order, namely, buck with input filter (BIF), boost with output filter (BOF), Ćuk converter and Ćuk converter with galvanic isolation (Fig. 19.2).

Example of Case A

a) *Equivalent Control.* Fig. 19.3 shows the block diagram of a Ćuk converter with a feedback loop forcing the converter dynamics to evolve on the surface $S_(x) = K_1 i_1 + K_2 i_2$ where $\frac{-K_2}{K_1} = K$. The absence of external periodic signal together with the ideal comparator makes this system self-oscillating [23].

In the continuous conduction mode the converter has only one structural change during a switching period and therefore it can be represented by two piecewise-linear vector differential equations as follows:

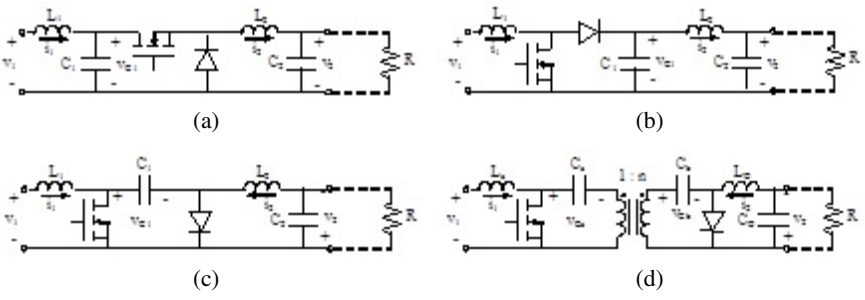

Fig. 19.2 Fourth order converters with non-pulsating input and output currents. (a) buck converter with input filter (b) boost converter with output filter (c) Ćuk converter (d) Ćuk converter with galvanic isolation

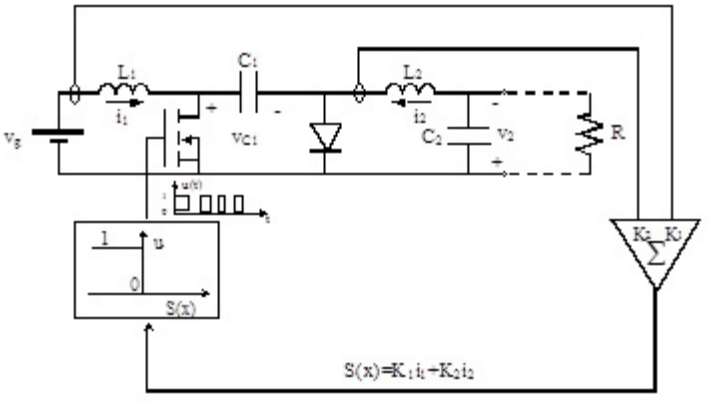

Fig. 19.3 Self-oscillating Ćuk converter with sliding-mode control

$$\dot{X} = A_1 X + B_1 \qquad \text{during } T_{ON} \tag{19.3}$$

$$\dot{X} = A_2 X + B_2 \qquad \text{during } T_{OFF} \tag{19.4}$$

where $X = [i_1, i_2, v_{C1}, v_2]^+$ is the state vector and matrices A_1, B_1, A_2, B_2 are given by

$$A_1 = \begin{bmatrix} 0 & 0 & 0 & 0 \\ 0 & 0 & 1/L_2 & 1/L_2 \\ 0 & -1/C_1 & 0 & 0 \\ 0 & -1/C_1 & 0 & -1/RC_2 \end{bmatrix} \qquad B_1 = \begin{bmatrix} V_g/L_1 & 0 & 0 & 0 \end{bmatrix} \tag{19.5}$$

Equations (19.3) and (19.4) can be combined in only one bilinear expression

$$\dot{X} = (A_1 X + B_1)\, u + (A_2 X + B_2)\,(1 - u) \tag{19.6}$$

where $u = 1$ during T_{ON} and $u = 0$ during T_{OFF}. Equation (19.4) can be expressed as follows:

$$\dot{X} = A_2 X + B_2 + (A_1 - A_2)\, X\, u + (B_1 - B_2)\, u \tag{19.7}$$

From (19.3) and (19.5), the following set of differential equations is derived

$$\begin{aligned} \frac{di_1}{dt} = -\frac{v_{C1}}{L_1} + \frac{v_{C1}}{L_1}u + \frac{V_g}{L_1}\frac{di_2}{dt} &= -\frac{v_2}{L_2} + \frac{v_{C1}}{L_2}u\frac{dv_{C1}}{dt} \\ &= \frac{i_1}{C_1} - \frac{i_1}{C_1}u - \frac{i_2}{C_1}u\frac{dv_2}{dt} = \frac{i_2}{C_2} - \frac{v_2}{RC_2} \end{aligned} \tag{19.8}$$

Assuming $S(x) = K_1 i_1 + K_2 i_2$ as sliding surface and imposing the invariance conditions [28] $S(x) = 0$ and $\frac{dS(x)}{dt} = 0$ in (19.8) lead to the following expression of the equivalent control $u_{eq}(x)$

$$u_{eq}(x) = \frac{K_1 L_2 (v_{C1} - V_g) + K_2 L_1 v_2}{v_{C1}(K_1 L_2 + K_2 L_1)} \tag{19.9}$$

From (19.9) we conclude that a sliding regime will exist if the following condition is fulfilled

$$\frac{K_2}{K_1} \neq \frac{L_2}{L_1} \tag{19.10}$$

Now, the discrete variable u is substituted by a continuous variable $u_{eq}(x)$ which can take all the values between 0 and 1. This variable $u_{eq}(x)$ represents the control law that describes the behavior of the system restricted to the switching surface where the system motion takes place on the average [32, 33, 34, 13]. Therefore, $u_eq(x)$ is bounded by the minimum and maximum values of u

$$0 < u_{eq}(x) < 1 \tag{19.11}$$

b) *Equilibrium Point.* Substituting u by $u_{eq}(x)$ in (19.8) and taking into account the constraint $i_2 = -\frac{K_1 i_1}{K_2}$ imposed by the switching surface will result in the following ideal sliding dynamics:

$$g_1(x) = \frac{di_1}{dt} - \frac{v_{C1}}{L_1} + \frac{K_1 L_2 (v_{C1} - V_g) + K_2 L_1 v_2}{L_1 (L_2 K_1 + L_1 K_2)} + \frac{V_g}{L_1} \tag{19.12}$$

$$g_2(x) = \frac{dv_{C1}}{dt} = \frac{i_1}{C_1} - \frac{i_1}{C_1}\left(1 - \frac{K_1}{K_2}\right) \frac{\frac{K_1}{L_1}(v_{C1} - V_g) + \frac{K_2}{L_2} v_2}{v_{C1}\left(\frac{K_1}{L_1} + \frac{K_2}{L_2}\right)} \tag{19.13}$$

$$g_3(x) = \frac{dv_2}{dt} = -\frac{K_1 i_1}{K_2 C_2} - \frac{v_2}{RC_2} \tag{19.14}$$

The coordinates of the equilibrium point $x^* = [I_1,\ I_2,\ V_{C1},\ V_2]^+$ are given by

$$x^* = \left[\left(\frac{K_2}{K_1} \right)^2 \frac{V_g}{R},\ -\frac{K_2}{K_1}\frac{V_g}{R},\ \left(1 - \frac{K_2}{K_1}\right) V_g,\ -\frac{K_2}{K_1} V_g \right] \tag{19.15}$$

Note that

$$V_2 = -\frac{K_2}{K_1} V_g \tag{19.16}$$

$$I_2 = -\frac{K_1}{K_2} \mathrm{I}_1 \tag{19.17}$$

Expressions (19.16) and (19.17) define the transformer behavior of the converter in steady-state. It has to be pointed out that K_2/K_1 must be negative due to the sign inversion in the output voltage of the Ćuk converter.

Hence, the sliding domain for the output voltage will be expressed as

$$V_2 < V_g \quad \text{if} \quad -\frac{K_2}{K_1} < 1 \qquad \text{(step-down behavior)} \tag{19.18}$$

$$V_2 > V_g \quad \text{if} \quad -\frac{K_2}{K_1} > 1 \qquad \text{(step-up behavior)} \tag{19.19}$$

From (19.9) and (19.15), the expression of the equivalent control in the equilibrium point $u_{eq}(x^*)$ can be derived

$$u_{eq}(x*) = \frac{V_2}{V_{C1}} \tag{19.20}$$

which is bounded by the minimum and maximum values of u

$$0 < \frac{V_2}{V_{C1}} < 1 \tag{19.21}$$

c) *Stability Analysis.* The ideal sliding dynamics given by equations (19.12)-(19.14) is nonlinear. In order to study the stability of the system, equations (19.12)-(19.14) will be linearized around the equilibrium point x^*. The corresponding Jacobian matrix J can be expressed as follows

$$J = \begin{bmatrix} \frac{\partial g_1(x)}{\partial i_1}\Big|_{x*} & \frac{\partial g_1(x)}{\partial v_{C1}}\Big|_{x*} & \frac{\partial g_1(x)}{\partial v_2}\Big|_{x*} \\ \frac{\partial g_2(x)}{\partial i_1}\Big|_{x*} & \frac{\partial g_2(x)}{\partial v_{C1}}\Big|_{x*} & \frac{\partial g_2(x)}{\partial v_2}\Big|_{x*} \\ \frac{\partial g_3(x)}{\partial i_1}\Big|_{x*} & \frac{\partial g_3(x)}{\partial v_{C1}}\Big|_{x*} & \frac{\partial g_3(x)}{\partial v_2}\Big|_{x*} \end{bmatrix} \tag{19.22}$$

where

$$J = \begin{bmatrix} 0 & -\frac{K_2}{L_1K_2+L_2K_1} & \frac{K_2}{L_1K_2+L_2K_1} \\ 0 & -\frac{K_2\left(L_1K_2^2+L_2K_1^2\right)}{C_1RK_1(K_1-K_2)(L_1K_2+L_2K_1)} & \frac{K_2}{L_1K_2+L_2K_1} \\ -\frac{K_1}{C_2K_2} & 0 & -\frac{1}{C_2R} \end{bmatrix} = \begin{bmatrix} 0 & a & -a \\ 0 & b & c \\ d & 0 & e \end{bmatrix} \tag{19.23}$$

Therefore, the characteristic equation of the linearized system will be given by

$$\begin{pmatrix} s & -a & a \\ 0 & s-b & -c \\ -d & 0 & s-e \end{pmatrix} = s^3 + ms^2 + ns + p = 0 \tag{19.24}$$

where

$$\begin{aligned} m &= \frac{C_1K_1(K_1-K_2)(L_1K_2+L_2K_1) - C_2K_2\left(L_1K_2^2+L_2K_1^2\right)}{C_1C_2RK_1(K_1-K_2)(L_1K_2+L_2K_1)} \\ n &= \frac{C_1R^2K_1^2(K_1-K_2) - K_2\left(L_1K_2^2+L_2K_1^2\right)}{C_1C_2R^2K_1(K_1-K_2)(L_1K_2+L_2K_1)} \\ p &= -\frac{K_1K_2}{C_1C_2R(K_1-K_2)(L_1K_2+L_2K_1)} \end{aligned} \tag{19.25}$$

The application of the Routh Criterium to the characteristic equation (19.24) reveals that all the roots will be located in the left-half plane if the following condition is fulfilled

$$L_1K_2 + L_2K_1 > 0 \qquad \text{with } K_1 > 0 \text{ and } K_2 < 0 \tag{19.26}$$

Condition (19.24) guarantees the system stability for small perturbations around the equilibrium point.

d) *Control Implementation.* The control law must force $S(x) \cdot dS(x)/dt < 0$ to guarantee that a sliding mode exists on the sliding surface and is reachable in finite time from all initial states in the state space [37]. This requirement leads to the following switching control law

$$u = 1 \text{ if } S(x) < 0, u = 0 \text{ if } S(x) > 0 \tag{19.27}$$

e) *Experimental Results.* Fig. 19.4 shows the experimental behavior of input and output variables in steady-state. In such figure, V_o, V_{in}, I_o and I_in correspond respectively to V_2, V_g, I_2 and I_1 in the converter analysis. The converter has voltage step-up behavior delivering -27.30 V at the output port for a DC input voltage of 11.59 V which corresponds to a voltage dc gain of 2.35. Input current I_1 is 5.05 A while output current I_2 is 2.02 A, this representing a current DC gain of 0.4. Note that the inverse of the current DC gain (2.5) is practically the voltage DC gain, which demonstrates the transformer characteristics of the proposed circuit. The slight difference between 2.35 and 2.5 is due to the converter power losses of approximately 3 W. The transient behavior of the converter when the load has pulsating characteristics of step type changing periodically every 14 ms between R = 14Ω and R = 28Ω is depicted in Fig. 19.5. Note that the output voltage remains practically constant during the transient-state and that the load perturbations are absorbed by the input current.

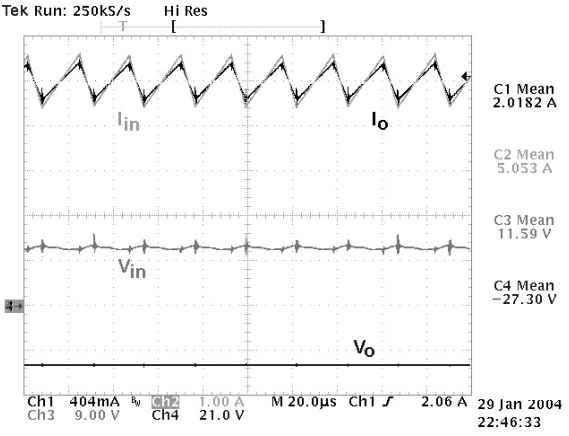

Fig. 19.4 Steady-state waveforms of the circuit depicted in Fig. 19.3.

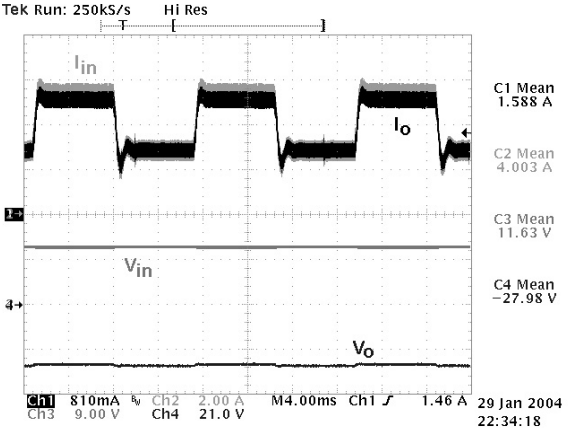

Fig. 19.5 Converter behavior for pulsating load perturbations of the circuit depicted in Fig. 19.3.

A similar analysis of the sliding-mode regime in BIF and BOF converters reveals that both of them have an equilibrium point with transformer characteristics but only BOF is stable [23].

CASE B

Similarly, the surface $S(x) = K_3 v_1 + K_4 v_2$ will result in a DC transformer using both input and output voltages. In this case, the sliding constraint only requires v_2 to be a continuous function of time because the continuous nature of the input voltage is ensured by the different DC energy sources, i.e., battery, PV panel, rectifier bridge, fuel cell etc. The continuous nature of the output voltage is also guaranteed in all

voltage to voltage converters due to the existence of a capacitor connected in parallel with the output load.

The analysis of the sliding-mode regime in the elementary converters shows that boost and buck-boost exhibit an unstable equilibrium point with transformer characteristics. The buck converter, in turn, does not admit a sliding regime but it yields a stable limit cycle [28,15,16]. A sliding-mode leading to a stable equilibrium point with transformer characteristics can be induced in the two-inductor voltage step-down converter depicted in Fig. 19.6(a) [14].

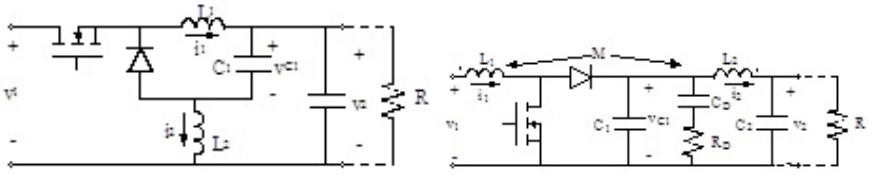

Fig. 19.6 (a) Two inductor voltage step down-converter, (b) Boost converter with output filter, magnetic coupling and capacitive damping.

Finally, a DC transformer with voltage step-up characteristics can be implemented using a BOF converter with magnetic coupling and capacitive damping as illustrated in Fig. 19.6(b) [3]. The hysteretic control does not result in a sliding-mode regime but it yields a stable limit cycle as in the buck converter.

19.5 Power Gyrator

A power gyrator is a two-port structure characterized by any of the following set of equations

$$I_1 = gV_2, I_2 = gV_1 \tag{19.28}$$

$$V_1 = rI_2, V_2 = rI_1 \tag{19.29}$$

where V_1,V_2, I_1, and I_2 have been previously defined.

The set of equations (19.28) defines a power gyrator of type G whereas the set (19.29) corresponds to a gyrator of type R [8]. Both types of gyrator can be implemented by particularizing the block diagram of Fig. 19.1 in cases C and D.

CASE C

The surface $S(x) = K_2 i_2 + K_3 v_1$ results in a G-gyrator with controlled output current. The sliding constraint requires i_2 to be a continuous function of time, this implying the existence of a series inductor at the output port. Moreover, in order to minimize EMI levels, a pulsating current will not be allowed at the input port and therefore the power gyrator will also require a series inductor at the input port. The most simple converters with such constraints are represented in Fig. 19.2. It was shown in [6] that

both BIF and Ćuk converter can exhibit stable G-gyrator characteristics if capacitive damping are inserted and certain parametric conditions are satisfied.

CASE D

The sliding surface $S(x) = K_1 i_1 + K_4 v_2$ can lead to a G-gyrator with controlled input current or to a gyrator of type R. In the first case we impose a sliding behavior to i_1 considering v_2 as independent voltage. The best candidate for this type of gyrator is the Ćuk converter which provides a sliding regime with an unconditionally stable point of equilibrium [8]. In the second case, i_1 is an input current source i_g that will be transformed into an output voltage source by means of the gyrator action. The current source at the input port precludes the existence of a series inductor in that port. On the other hand, in order to minimize EMI levels, a pulsating current will not be allowed at the output port and therefore the R-gyrator will require a series inductor at the output port. The most simple converters with these topological constraints are shown in Fig. 19.7. Such converters are derived by slight modification of the BOF converter, Ćuk converter and Ćuk converter with galvanic isolation.

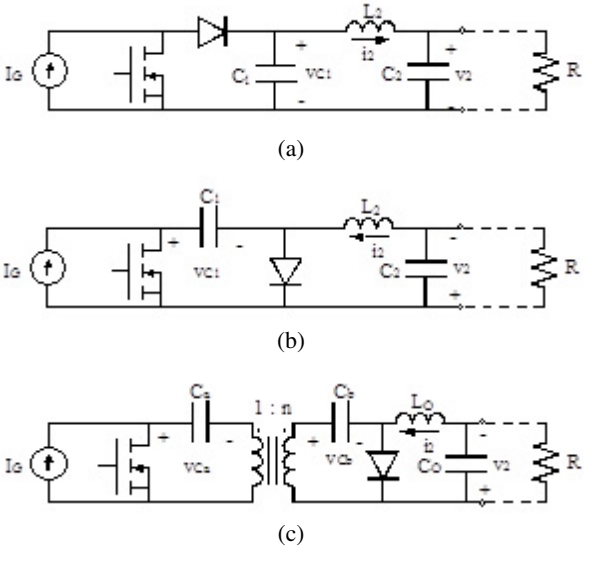

Fig. 19.7 Current to voltage DC-DC switching converters with non-pulsating input and output currents a) boost converter with output filter b) Ćuk converter c) Ćuk converter with galvanic isolation.

19.6 Loss-Free Resistors

The case E corresponds to the synthesis of a loss-free resistor whose notion was introduced by Singer [26] and, so far, it has been limited to the recognition that certain switching converters exhibit resistive input impedance in steady-state in

discontinuous conduction mode. This is the case of the buck-boost, SEPIC and Ćuk converter, which have been employed, due to this property, as power factor correctors by including only one loop of voltage regulation with pulse width modulation [18,4,11,17,25,2,29].

On the other hand, the introduction of sliding-mode control in the power factor correction has its main antecedent in the work of Rossetto et al. [35], in which a switching surface defined as a linear combination of the input current error and output voltage error was proposed in the Ćuk converter with galvanic isolation. Depending on the relative values of the coefficients multiplying each error, the input current or the output voltage can be more precisely regulated. The result is a good example of the existing trade-off between the increase of the circuit response velocity and the reduction of the input current distortion. A loss-free resistor is defined by the following equations

$$V_1 = rI_1 \tag{19.30}$$

$$V_1 I_1 = V_2 I_2 \tag{19.31}$$

It can be implemented as shown in Fig. 19.8 by means of the sliding surface $S(x) = K_1 i_1 + K_3 v_1$, where i_1 represents the controlled variable and v_1 is the independent voltage. The sliding constraint in this design requires i_1 to be a continuous function of time, this implying the existence of a series inductor at the input port. The simplest converters with this constraint at the input port are the boost converter and the fourth order structures BOF, BIF, Ćuk converter with galvanic isolation and SEPIC. It has been demonstrated in [10] that the boost converter has unconditionally stable equilibrium point with loss-free resistor characteristics.

A similar analysis of the sliding-mode regime in Ćuk, BOF and SEPIC converters reveals that all of them have an equilibrium point with LFR characteristics. BOF and Ćuk converters are unconditionally stable and SEPIC is stable provided that certain parametric conditions are fulfilled.

19.7 Impedance Matching

In the last years, a significant increase of photovoltaic (PV) installations has taken place around the world mainly due to the progressive decrease of solar panel cost, and also to certain government policies establishing attractive purchase prices for the electric energy produced by renewable energies. These new market conditions make visible a production map of electric energy where small companies and individuals are melted together with great investment groups.

A key technical issue in this new production map is the optimization of the energy transfer in PV conversion chains, where extracting the maximum power from the panel (DC matching) is one the most important aspects of such optimization.

Fig. 19.10 illustrates the problem of matching a PV generator to a DC load. The interface element can be indistinctly a DC transformer, a power gyrator or a loss-free resistor. The DC load can be modeled by means of the function $v_2 = f_o(i_2)$,

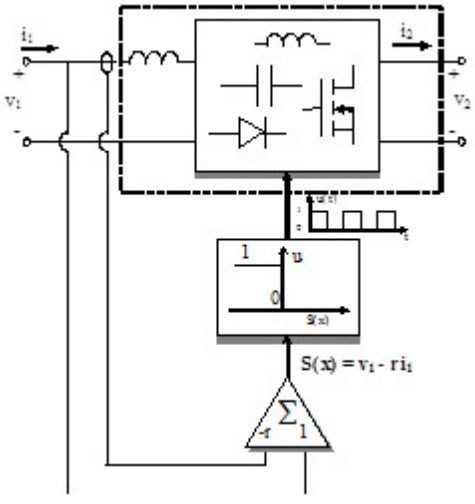

Fig. 19.8 Block diagram of a DC-DC switching converter with LFR characteristics

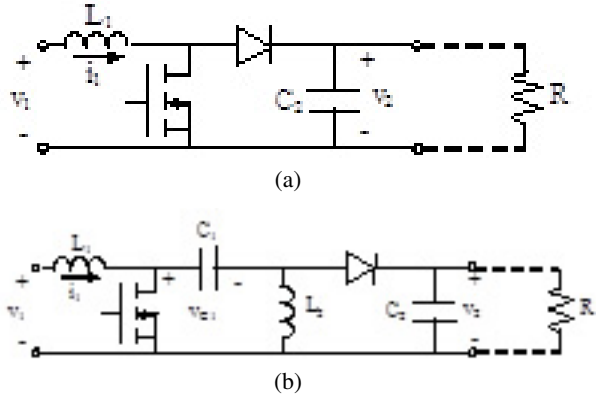

Fig. 19.9 Other converters with non pulsating input current (a) boost converter, (b) SEPIC converter.

which corresponds to the one-port description of the usual DC loads supplied by a PV generator and can be expressed as

$$v_2 = f_0(i_2) = V_B + R_L i_2$$

where $V_B > 0$ and $R_L > 0$.

We will analyze the three possible solutions of impedance matching in the case that the load is battery with a very small equivalent series resistance ($R_L \to 0$).

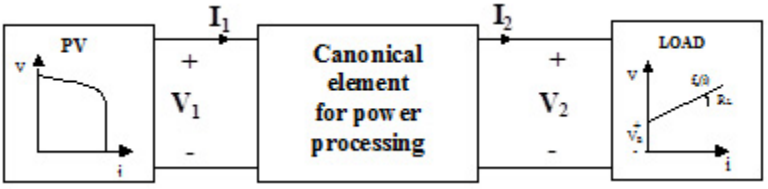

Fig. 19.10 Matching a PV generator to a DC load using a canonical element for power processing.

A) *DC Transformer.* Equations (19.1) and (19.7) lead to

$$v_1 = f_{in}(i_1) \approx \frac{V_B}{n} \tag{19.32}$$

Fig. 19.11(a) shows the intersection of characteristics $f_o(i_2)$ and $f_i n(i_1)$ with the PV curve under different hypotheses. We assume that the direct connection of the load to the panel would correspond to an operating point (VB) where the output current of the PV generator is zero. This is due to the fact that the battery voltage is greater than the open circuit voltage of the PV generator. It can be deduced from (19.32) that $f_{in}(i_1)$ will be placed below $f_o(i_2)$ if $n > 1$. Therefore, the intersection point C could be placed at the left side of M for a certain value of the transformer ratio $n_1 > 1$. On the other hand, the intersection point D will correspond to a transformer ratio $n_2 > n_1$. Finally, it has to be pointed out that the objective of a DC impedance matching design is to achieve a f_{inopt} characteristics so that it intersects the PV curve at the maximum power point M.

B) *Power Gyrator.* Assuming a G-gyrator with either controlled input or output current, the variation of the gyrator conductance changes the PV panel operating point as depicted in Fig. 19.11(b). In such figure the operating points P_1 and P_2 correspond respectively to conductances g_1 and g_2 with $g_2 > g_1$. As in the DC transformer case, we have supposed that the battery voltage is greater than the open circuit voltage of the PV generator. The objective of the matching is to find an optimal value of the conductance, so that $f_{in}(g)$ characteristics intersects the PV curve at the maximum power point.

C) *Loss-Free Resistor.* Similarly, the variation of the parameter r of a loss-free resistor changes the operating point of the solar panel as illustrated in Fig. 19.11(c). Operating points A and B correspond respectively to resistances r_1 and r_2 with $r_1 > r_2$. The goal of the matching is to find an optimal value of the resistance that leads to an intersection of PV and $f_{in}(r)$ characteristics at the maximum power point.

D) *Time-Varying Parameters.* The transformer ratio, the gyrator conductance or the loss-free resistor resistance can be made time varying and periodic in steady-state as illustrated in Fig. 19.12(a) where $\alpha(t)$ indistinctly represents any of these parameters.

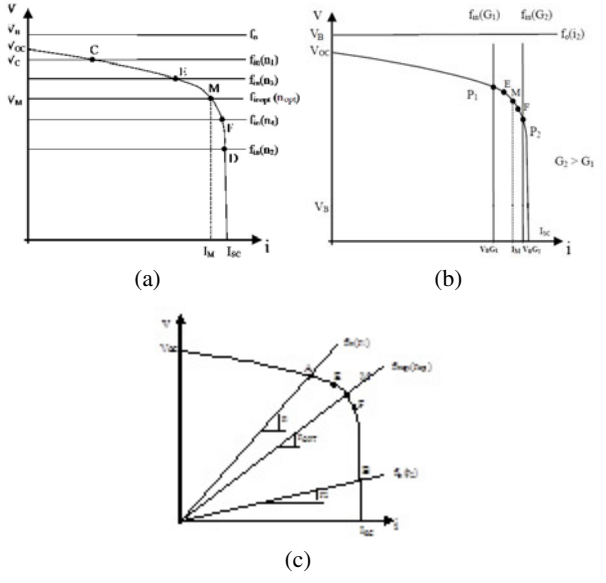

Fig. 19.11 PV panel operating points for an impedance matching with (a) a DC transformer, (b) a power gyrator, (c) a loss-free resistor.

The insertion of maximum power point tracking (MPPT) in the control loop should generate the signal $\alpha(t)$ with the aim of eventually yielding a stable oscillation around the maximum power point M regardless of the system initial conditions and atmospheric variations. E and F illustrate in Fig. 19.12 the nearest points to M allowing this stable oscillation. Fig. 19.12(b) and 19.12(c) show respectively the corresponding waveforms of panel voltage and panel current assuming a first-order Taylor development for both variables. It can be observed that $\alpha(t)$ and $v(t)$ are in phase while $i(t)$ is in opposite phase.

Also, it can be observed that the instant corresponding to $\alpha(t) = \alpha_{opt}$ corresponds in Fig 11 to $f_i n(\alpha_{opt})$, this resulting in voltage V_M and current I_M of the maximum power point indicated in Fig. 19.12(b) and Fig. 19.12(c). Among the different MPPT techniques, the extremum-seeking control offers robustness and large-signal stability and guarantees a stable oscillation around the maximum power point in spite of changes of initial conditions and atmospheric parameters [19]. In our case, signal $\alpha(t)$ is obtained in the block diagram of the extremum-seeking control system depicted in Fig. 19.13.

The equations describing the system behavior are governed by an integrator, a differentiator and a logic circuit. The output of the integrator is $\alpha(t)$ whereas the differentiator output is the time-derivative of the power panel. The logic circuit provides a signal $\varepsilon(t)$ that can be ± 1. The sign of $\varepsilon(t)$ is changed when the differentiator output is negative and the sign is held when the differentiator output is positive.

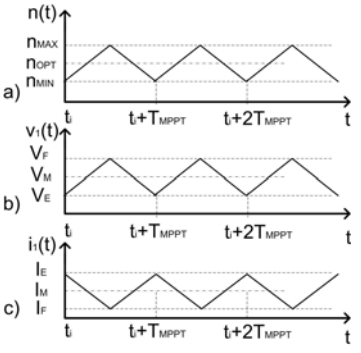

Fig. 19.12 (a) Periodic behaviour in steady-state of the defining parameter of a canonical power processing element, (b) panel voltage, (c) panel current

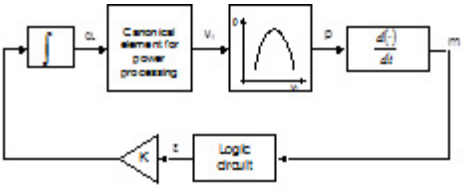

Fig. 19.13 Generation of $\alpha(t)$ by means of means of a maximum power point tracking scheme based on extremum-seeking control

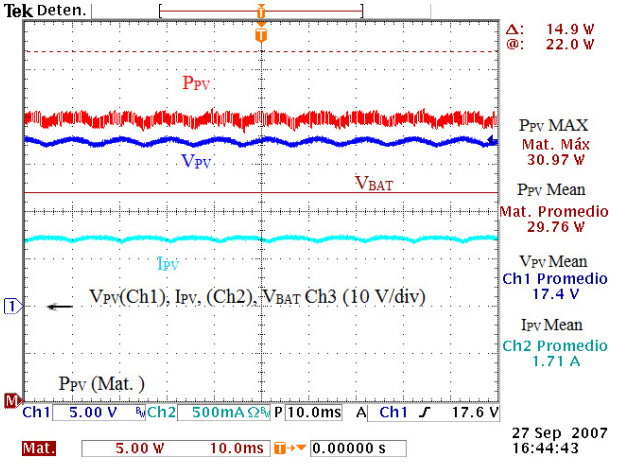

Fig. 19.14 Steady-state behavior of PV array variables

Fig. 19.14 illustrates the results of applying the scheme of Fig. 19.13 in a DC transformer implemented by a boost converter with output filter.

19.8 DC-AC Conversion

A key technical element in the photovoltaic market is the DC-AC PV inverter whose optimal topology is still an open problem. Fig. 19.15 shows the basic structure of a modular one-phase inverter consisting in the connection of three cascaded stages. The first stage is a step boost converter-based loss-free resistor with maximum power point tracking. The second stage uses a power G-gyrator and transforms a DC voltage into a fully rectified current of 100 Hz. The H-bridge performs the DC-AC conversion and subsequently a 50 Hz transformer with a 1:13 transformer ratio provides the connection to the mains.

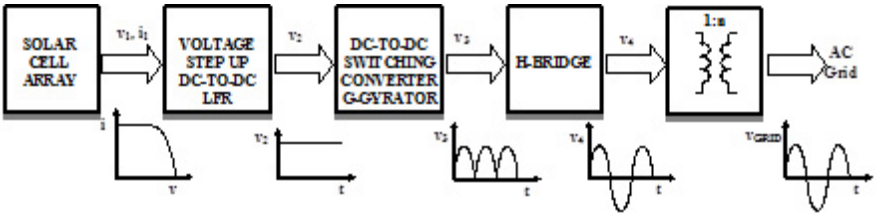

Fig. 19.15 Block diagram of a modular one-phase PV inverter

A. *Voltage Step-Up Stage with MPTT Function.* This stage has two objectives, i.e., absorbing the maximum power from the solar panel and step-up the voltage in order to decrease the conduction losses. Note that the impedance matching in a solar is the electronic function that imposes the panel operation at the maximum power point. The impedance matching is performed by a loss-free resistor as shown in Fig. 19.16.

B. *Buck Converter Stage.* The aim of this stage is to transform the DC voltage at the output of the LFR into a fully rectified sinusoidal waveform of 100 Hz (Fig. 19.17). A buck converter acting as a G-semi-gyrator with controlled output current is used to perform the transformation. It is shown in [9] that buck converter exhibit stable G-gyrator characteristics. The output port of this semi-gyrator can be modeled as a current source. This fact facilitates the connection in parallel of the output ports of this type of semi-gyrators. [7].

A classification and synthesis of power gyrators was presented in [8] where the notion of semi-gyrator was also defined. Note that a semi-gyrator satisfies the same equations (19.28) and (19.29) than the gyrator but the current can be discontinuous in either the input or output port. Thus, a semi-gyrator of type G with controlled output current has a pulsating input current whose steady-state average value is proportional to the steady-state average output voltage and whose output current is a continuous function with a steady-state value proportional to the DC input voltage. Fig. 19.17 illustrates the block diagram of a semi-gyrator of type G with controlled output current where the gyrator conductance g is a fully rectified sinusoidal waveform of 100 Hz. Therefore, the output current will

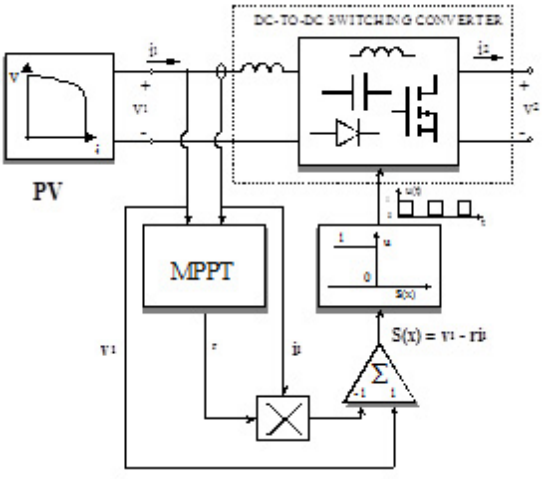

Fig. 19.16 Block diagram of switching converter with LFR characteristics acting as a PV impedance matching stage

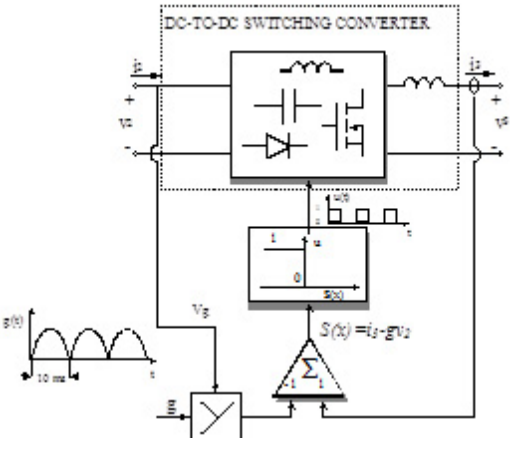

Fig. 19.17 Block diagram of a switching converter in sliding-mode operation with semi-gyrator characteristics

be proportional to the input voltage, the proportionality constant being a time-varying function $g(t)$. Since $g(t)$ is a fully rectified waveform, the output current will have the same shape and its amplitude will depend on both $g(t)$ and input voltage whose value will in turn depend on the power supplied by the PV panel.

C. *H-Bridge and Grid Connection.* An H-bridge is used to perform the conversion of the DC fully rectified sinusoidal current of 100 Hz at the gyrator output port into a sinusoidal voltage of 50 Hz which eventually is delivered to the grid by means of a low frequency transformer.

D. *Parallel Connection of Additional PV Modules.* The parallel connection of the output ports of gyrators of type G with controlled output current yields the addition of their respective output currents. Fig. 19.18 illustrates the application of the proposed modular structure in the case of n independent solar panels. Note that each solar panel is connected to an LFR with MPPT function in order to deliver the maximum power. On the other hand, each LFR is connected in cascade with a semi-gyrator of type G with controlled output current. Subsequently, the semi-gyrator output ports are connected in parallel to obtain a high current level, which eventually is transformed into a high power sinusoidal voltage and sent to the mains.

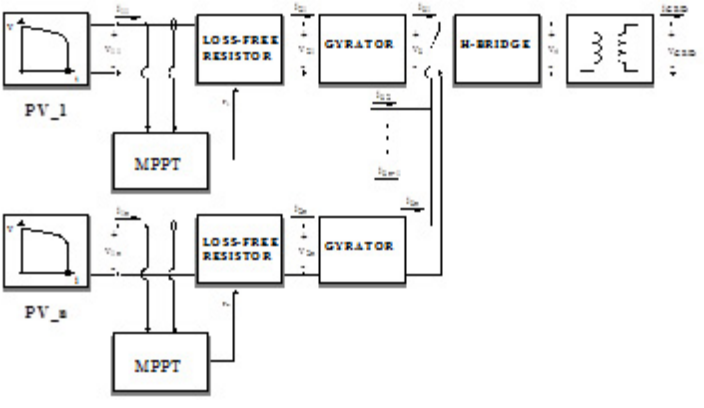

Fig. 19.18 Block diagram of the parallel connection of n solar panels

19.9 Power Distribution

Distributed power systems (DPS) and distributed generation systems (DGS) are increasingly used in advanced electronic systems. While DPS are becoming a key issue in the power supply configuration of computer and information systems, DGS have been increasing dramatically in recent years due to the growing importance of renewable energy systems. The bus voltage of a DPS can be either DC or AC, this leading to two different DPS architectures. In DGS, the distribution is mainly carried out in AC because most of these systems are connected to the utility grid.

In this section, we illustrate the use of power gyrators to implement a DC bus architecture for power distribution using power gyrators as shown in Fig. 19.19.

The DC bus architecture consists in the cascade connection of a G-gyrator-based source splitting structure and an R-gyrator stage [8]. The source splitting is performed by paralleling the N output ports of the G-gyrators whose corresponding input ports are excited by independent sources that can model batteries, fuel cells or photovoltaic panels. Currents $i_{21}, i_{22}, \ldots, i_{2n}$ are proportional to $v_{g1}, v_{g2}, \ldots, v_{gn}$ respectively, this resulting in the input current of the R-gyrator given by $i_{2T} = g_1 v_{g1} + g_2 v_{g2} + \ldots + g_n v_{gn}$. The R-gyrator stage performs the current to

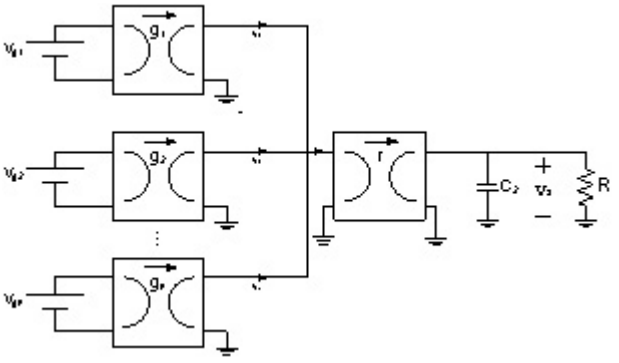

Fig. 19.19 Cascade connection of n-paralleled power G-gyrators and a power R-gyrator

voltage $(i-v)$ conversion yielding the output DC voltage given by $v_o = ri_{2T}$ with inherent voltage regulation in the case of load perturbation. This means that although a load perturbation results in an output current change of the R-gyrator and therefore in an input voltage variation, the output voltage remains constant. Perturbations in the output voltage due to changes in the input voltage values $v_{g1}, v_{g2}, \ldots, v_{gn}$ can be minimized by adding a simple regulation loop that will lead the output voltage to recover its DC steady-state value with a small overshoot after a fast transient state. Also, the output current perturbations in the G-gyrators due to input voltage changes can be distributed among the different gyrators of the source splitting stage by adding a current regulation loop for active current sharing as reported in [5].

The most suitable converter structures for a G-gyrator realization are either a buck converter with input filter (BIF) or a Ćuk converter whereas an R-gyrator stage can be only implemented by means of a boost converter with output filter (BOF).

19.10 Power Factor Correction

All electronic equipments supplied by the AC mains should present at the input port a sinusoidal current waveform with negligible total harmonic distortion. Power factor correction is then mandatory for these systems that should fulfill strict specifications given by different norms.

A direct application of a boost converter-based LFR analyzed in Section 19.6 is a power factor correction (PFC) pre-regulator as shown in Fig. 19.20. The rectified bridge is supplied by an AC source of 22 Vrms and 50 Hz. Fig. 19.21(a) and 19.21(b) show the PSIM simulated responses in steady and transient-states respectively.

The simulation parameters are $V_{AC} = 22$ V_{rms} 50Hz, R=60 Ω, L=100 μH, C=1000 μF and r=3.75 Ω. Note that the phase-shift between LFR input voltage and current is zero in Fig. 19.21(a), this implying a unity power factor at the rectifier input.

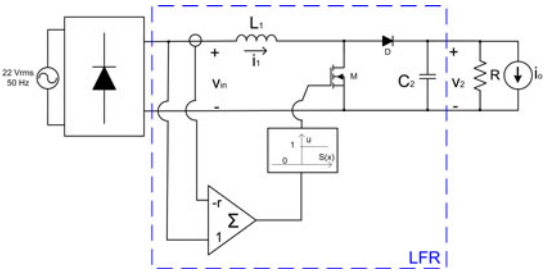

Fig. 19.20 Pre-regulator for power factor correction based on a loss-free resistor in sliding operation.

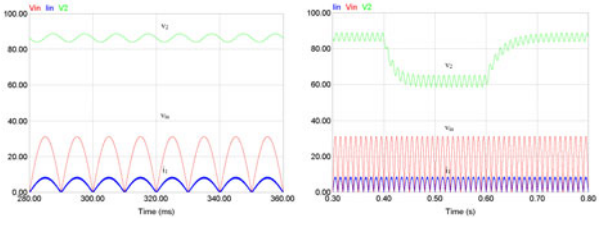

(a) (b)

Fig. 19.21 (a) Steady-state response of the boost converter-based LFR acting as PFC pre-regulator, (b) Transient response of the PFC pre-regulator depicted in Fig. 19.20 to load perturbations of step type (60 Ω-30 Ω-60 Ω).

19.11 Conclusions

The three types of canonical elements for power processing can be implemented following the systematic procedure described in this paper. The basic functions defining each canonical element have been designed by means of a simple sliding-mode regulation loop. All canonical elements have "sliding inside". The disclosed elements can be designed as standardized modules to facilitate their association and the implementation of modern electrical architectures for either distributed power systems or distributed generation systems. The implementation and test of each element is simple and requires low-power techniques. High-power can be achieved by increasing the number of elements in specific associations. The modularity of the elements has been demonstrated in the realization of a DC-AC inverter for photovoltaic applications and in the power distribution by means of gyrators in a DC bus. All canonical elements can be successfully used to solve the DC matching problem in PV systems. A DC transformer with an appropriate MPPT algorithm has illustrated the application. Finally, it has been shown that pre-regulation for power factor correction is a direct application of LFRs.

References

1. Bilalovic, F., Music, O., Sabanovic, A.: Buck converter regulator operating in the sliding mode. In: Proceedings of the 1983 Seventh International PCI Conference, pp. 331–340 (1983)
2. Brkovic, M., Ćuk, S.: Input current shaper using ćuk converter. In: INTELEC Conf. Proc., pp. 532–539 (1992)
3. Calvente, J., Martínez-Salamero, L., Garcés, P., Leyva, R., Capel, A.: Dynamic optimization of bidirectional topologies for battery charge/discharge in satellite. In: IEEE Power Electronics Specialists Conference, PESC 2001, Vancouver (2001)
4. Cascio, J., Nalbant, M.: Active power factor correction using a flyback topology. In: PCIM Conf. Proc., pp. 10–17 (1990)
5. Cid-Pastor, A., Martinez-Salamero, L., Alonso, C., El Aroudi, A., Valderrama-Blavi, H.: Power distribution based on gyrator. IEEE Trans. On Power Electronics 24(12), 2907–2909 (2009)
6. Cid-Pastor, A., Martínez-Salamero, L., Alonso, C., Estibals, B., Alzieu, J., Schweitz, G., Shmilovitz, D.: Analysis and design of power gyrators in sliding-mode operation. IEE Proceedings Electric Power Applications 152(4), 821–826 (2005)
7. Cid-Pastor, A., Martinez-Salamero, L., Alonso, C., Leyva, R., Singer, S.: Paralleling dc-dc switching converters by means of power gyrators. IEEE Trans. On Power Electronics 22(6), 2444–2453 (2007)
8. Cid-Pastor, A., Martinez-Salamero, L., Alonso, C., Schweitz, G., Calvente, J., Singer, S.: Classification and synthesis of power gyrators. IEE Proc. Electric Power Applications 153(6), 802–808 (2006)
9. Cid-Pastor, A., Martinez-Salamero, L., El Aroudi, A., Hernando-Ureta, D.: Analysis of a modular one-phase pv inverter. In: 6th International Multi-Conference on Systems, Signals and Devices, SSD 2009, March 23-26, 2009, pp. 23–26 (2009)
10. Cid-Pastor, A., Martinez-Salamero, L., Ribes, U., El Aroudi, A.: Analysis and design of a loss-free resistor based on a boost converter in sliding-operation. In: Proceedings of the 14th Internacional symposium on Power Electronics, Novi Sad, Serbia (2007)
11. Erickson, R., Madigan, M., Singer, S.: Design of a simple high-power-factor rectifier based on the flyback converter. In: APEC Conf. Proc., pp. 792–801 (1990)
12. Erickson, R., Maksimovic, D.: Fundamental of Power Electronics, 2nd edn. Kluwer Academic Publishers, USA (2001)
13. Filippov, A.: Differential equations with discontinuous right hand sides. Am. Math. Soc. Transl. 42, 199–231 (1964)
14. Garcés, P., Calvente, J., Leyva, R., Martínez-Salamero, L.: Análisis de un convertidor reductor de dos inductores como mdulo regulador de voltaje. In: Actas del SAAEI 2002, Alcal de Henares, pp. 69–72 (2002)
15. Bábáa, I.M., Wilson, I.M.H., Yu, T.G.,, Y.: Analitic solutions of limit cycles in a feedbackregulated converter system with hysteresis. IEEE Trans. Autom. Contr. 13, 524–531 (1968)
16. Judd, F., Cheng, C.: Analysis and optimal design of self-oscillating dc-dc converters. IEEE Transact. On Circuit Theory 18(6), 651–658 (1971)
17. Liu, K.H., Liu, Y.L.: Current waveform distortion in power factor correction circuits employing discontinuous-mode boost converters. In: PESC Conf. Proc., pp. 825–829 (1989)
18. Kocher, M., Steigerwald, R.: An ac-to-dc converter with high quality input wave-forms. IEEE Trans. on Industry Applications 19(4), 586–599 (1983)

19. Leyva, R., Alonso, C., Queinnec, I., Cid-Pastor, A., Lagrange, D., Martínez-Salamero, L.: Mppt of photovoltaic systems using extremum seeking control. IEEE Transactions on Aerospace and Electronic Systems 42(1), 249–258 (2006)
20. Luo, S., Batarseh, I.: A review of distributed power systems. part i: Dc distributed power system. IEEE Aerospace and Electronic Systems Magazine 20(8), 5–15 (2005)
21. Malesani, L., Rossetto, L., Spiazzi, G., Tenti, P.: Performance optimization of Ćuk converters by sliding-mode control. In: Proceeding of the 7th Annual Applied Power Electronics Conference and Exposition, APEC 1992, pp. 23–27 (1992)
22. Martínez-Salamero, L.: Syntheis of canonical elements for power processing. In: Proceedings of the 6th International Multi-Conference on Systems, Signals and Devices, SSD 2009, pp. 23–26 (2009)
23. Martinez-Salamero, L., Valderrama-Blavi, H., Giral, R., Alonso, C., Estibals, B., Cid-Pastor, A.: Self-oscillating dc-to-dc switching converters with transformer characteristics. IEEE Transactions on Aerospace and Electronic Systems 41, 710–716 (2005)
24. Middlebrook, R.: Power electronics: An emerging discipline, advances in switched-mode power conversion. TESLAco 1, 11–15 (1981)
25. Simonetti, D., Sebastian, J., dos Reis, F., Uceda, J.: Design criteria for sepic and ćuk converters as power factor preregulators in discontinuous conduction mode. In: IECON Conf. Proc., pp. 283–288 (1992)
26. Singer, S.: Realization of loss-free resistive elements. IEEE Transactions on Circuits and Systems 37(1), 54–60 (1990)
27. Singer, S., Erickson, R.W.: Canonical modeling of power processing circuits based on the popi concept. IEEE Transactions on Power Electronics 7(1), 37–43 (1992)
28. Sira-Ramírez, H.: Sliding-motions in bilinear switched networks. IEEE Transactions on Circuit and Systems 34, 919–933 (1987)
29. Spiazzi, G., Rossetto, L.: High-quality rectifier based on coupled-inductor sepic topology. In: PESC Conf. Proc., pp. 336–341 (1994)
30. Tan, S.: Development of sliding-mode controllers for dc-dc converters. Ph.D. thesis, Hong Kong Polytechnic University (2005)
31. Tan, S.C., Lai, Y., Tse, C.: Implementation of pulse-width-modulation based sliding mode controller for boost converters. IEEE Power Electronics Letters 3(4), 130–135 (2005)
32. Utkin, V.: Sliding modes and their applications in variable structure systems. Mir, Moscow, Russia (1978)
33. Utkin, V.: Sliding Modes in Control and Optimization. Springer, London (1992)
34. Utkin, V., Guldner, J., Shi, J.: Sliding Mode Control in Electro-Mechanical Systems, 2nd edn. CRC Press, Boca Raton (2009)
35. Valderrama-Blavi, H., Alonso, C., Martinez-Salamero, L., Singer, S., Estibals, B., Maixe-Altes, J.: Ac-lfr concept applied to modular photovoltaic power conversion chains. IEE Proceedings on Electric Power Applications, 149(6), 441–448 (2002)
36. Venkataraman, R.: Sliding mode control of power converters. Ph.D. thesis, California Institute of Technology (1986)
37. Venkataramanan, R., Sabanovic, A., Ćuk, S.: Sliding mode control of dc-to-dc converters. In: Proceeding of the 1985 IEEE Conference On Industrial Electronics, Control and Instrumentations (IECON), pp. 251–258 (1985)

Chapter 20
Second Order Sliding Modes to Control and Supervise Industrial Robot Manipulators

Antonella Ferrara and Luca Massimiliano Capisani

Abstract. On the basis of classical studies in robotics, it seems that the conventional sliding mode approach is not a suitable technique to design robotic controllers, due to the presence of the so-called chattering effect. However, studies have shown that a good reduction of the chattering effect can be achieved by relying on higher order sliding modes. This chapter presents the application of the Second Order Sliding Mode (SOSM) design methodology to the control and supervision of industrial manipulators, by proposing a robust control scheme and a diagnostic scheme to detect and, possibly, isolate and identify faults acting on the components of the system. The proposed SOSM motion controller and the SOSM observers designed to construct the diagnostic scheme are theoretically developed, and their practical application is suitably described. Indeed, the proposed approaches are experimentally verified on a COMAU SMART3-S2 industrial robot manipulator, obtaining satisfactory results.

20.1 Introduction

Motion control of rigid robot manipulators is a complex problem, mainly because of the nonlinearities and the coupling effects typical of robotic systems. In the past years, different approaches have been proposed in order to solve this problem, such as, for instance, decentralized control [2, 43, 24, 60], feedback linearization [44, 45, 1, 62, 36, 18], model predictive control [58, 42, 57], adaptive control [3, 26, 52, 50, 25, 53, 21, 18, 59, 66, 9, 61], as well as sliding mode control [60, 2, 62, 36, 39, 61, 23, 67, 41, 5, 11, 10, 27, 67].

Sliding mode control [65, 33] has the advantage of being robust versus a significant class of parameter uncertainties and bounded disturbances. Yet, it is a common opinion that sliding mode control is not appropriate to be applied in the robotic field, due to its major drawback, the so-called chattering phenomenon, see [38, 13, 12, 14].

A. Ferrara · L.M. Capisani
Department of Computer Engineering and Systems Science,
University of Pavia, via A. Ferrata 1, 27100 Pavia (PV), Italy
e-mail: {antonella.ferrara,luca.capisani}@unipv.it

L. Fridman et al. (Eds.): Sliding Modes, LNCIS 412, pp. 541–567.
springerlink.com

In case of conventional (i.e. first order) sliding mode control laws, chattering can be circumvented by approximating, with a continuous function, the sign function. Yet, in this way, only pseudo-sliding modes are generated and the positive features of sliding mode control, among which robustness, are lost. Recent studies have shown that a good reduction of the chattering effect can be achieved by relying on higher order sliding modes [49, 46, 31]. In particular, by adopting the so-called second order sliding mode control approach [6, 4, 7, 8, 11, 13, 14], the chattering effect can be made less critical by confining the discontinuity necessary to enforce sliding modes to the derivative of the control law. The idea underlying such an approach is that of enforcing a sliding mode on the manifold $s[x(t)] = \dot{s}[x(t)] = 0$ in the system state space, by using a signal function of $s[x(t)]$, but directly acting only on $\ddot{s}[x(t)]$. In case of relative degree one systems, this signal, which turns out to be discontinuous, is the derivative of the actual control signal.

The aim of this chapter is to investigate the possibility of applying the sliding mode design methodology also in robotics. In the first part of the chapter, an inverse dynamics-based second order sliding mode control scheme to perform the motion control of robot manipulators is proposed. The theoretical analysis is developed and an experimental verification is made to evaluate the performances of the proposal.

The second part of the chapter is devoted to fault diagnosis. The purpose is to verify if the robot, controlled via the proposed SOSM approach, can also be supervised in order to detect, and possibly isolate and identify faults occurring on the actuators or on the sensors. In a robotic system, faults can be modelled as an unexpected change of the dynamics of the system or as an unexpected presence of unknown signals affecting the components of the system [55, 56, 30, 32, 37, 35, 28, 29]. Sliding mode based techniques are frequently adopted to accomplish the state observation [54, 34, 40] so as to generate suitable residuals which are useful to indicate the presence of faults. Usually, the fault diagnosis is possible by combining multiple sliding mode state observers [35, 64, 63, 22].

The proposed fault diagnosis approach is based on an Unknown Input Observer (UIO) (see [34]) to detect and identify actuator faults, and on a Generalized Observer Scheme (GOS) [37] to detect sensor faults. Robustness of the observers is enhanced by considering as input law of each observer a SOSM law, in particular of Sub-Optimal type [7].

Experimental results which confirm the satisfactory performances of the proposal are presented in the chapter. The experimental tests have been performed on a COMAU SMART3-S2 industrial robot manipulator.

20.2 Problem Formulation

This chapter deals with two main problems which have been theoretically and experimentally investigated.

1. Design a robust motion controller for robotic manipulators, able to steer a position tracking error to zero exponentially.

2. Design a fault diagnosis approach in order to make the fault detection, the fault isolation, and the fault identification possible while the robotic manipulator is operating under the previously designed control. The considered faults can occur on the actuators (even multiple and simultaneous faults are acceptable) or on a particular sensor of the system (multiple sensor faults which are not simultaneous are also possible).

20.2.1 The Manipulator Model

In absence of faults the dynamics of a n-joints robot manipulator can be written in the joint space, by using the Lagrangian approach, as

$$\tau(t) = B(q)\ddot{q} + C(q,\dot{q})\dot{q} + g(q) + F_v\dot{q} = B(q)\ddot{q} + n(q,\dot{q}) \tag{20.1}$$

(see [60]) where $q \in \mathbb{R}^n$, $B(q) \in \mathbb{R}^{n\times n}$ is the inertia matrix, $C(q,\dot{q})\dot{q} \in \mathbb{R}^n$ represents centripetal and Coriolis torques, $F_v \in \mathbb{R}^{n\times n}$ is the viscous friction diagonal matrix, and $g(q) \in \mathbb{R}^n$ is the vector of gravitational torques. In this chapter, it is assumed that the term $n(q,\dot{q})$ in (20.1) can be identified, while the term $B(q)$ is regarded as known. Then, the following relationship holds

$$\tau = B(q)\ddot{q} + \hat{n}(q,\dot{q}) + \eta = \hat{\tau} + \eta, \quad \eta = n - \hat{n} \tag{20.2}$$

where η is uncertain. Yet by virtue of the particular application considered, η can be assumed to be bounded. Obviously, model (20.1) includes a number of parameters which need to be identified [19].

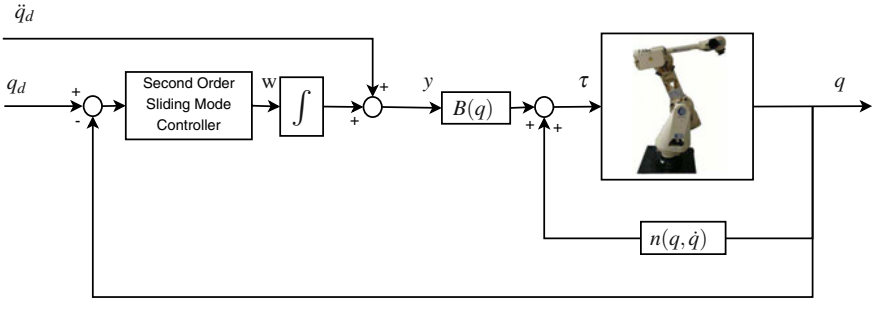

Fig. 20.1 The proposed SOSM control scheme for the industrial robot.

20.3 Solution to the Problem 1: Robust Motion Control for Robot Manipulators

One of the aims of this chapter is to show the efficacy of sliding mode control as a robust methodology to design motion controllers for robot manipulators, in contrast to a rather common opinion which judges it as inappropriate because of the vibration

it can induce due to the chattering effect. The proposal object of the present chapter, based on [20], consists in coupling a classical inverse dynamics control scheme with a multi-input multi output (MIMO) sliding mode controller. To circumvent the problems tied to the use of a discontinuous control law, SOSM methodology is adopted to design such a controller. The overall control scheme is illustrated in Fig. 20.1.

20.3.1 Design of the Inverse Dynamics Part of the Control Scheme

The inverse dynamics control consists in transforming the nonlinear system (20.1) into a linear and decoupled system by means of a suitable nonlinear feedback, see [2, 62, 60]. More specifically, by choosing

$$\tau = B(q)y(t) + n(q,\dot{q}) \tag{20.3}$$

with $n(q,\dot{q}) = C(q,\dot{q})\dot{q} + F_v\dot{q} + F_s sign(\dot{q}) + g(q)$, system (20.1) simply becomes $\ddot{q}(t) = y(t)$.

Note that, even if the term $n(q,\dot{q})$ in (20.3) is accurately identified, it can be quite different from the real one because of uncertainties and unmodelled dynamics, unmodelled frictions effects, elasticity and joint plays. Now assume that the term $\hat{n}(q,\dot{q})$ includes the identified centripetal, Coriolis, gravity and friction torques terms, while the inertia matrix $B(q)$ is assumed to be known. So letting

$$\tau = B(q)y(t) + \hat{n}(q,\dot{q}) \tag{20.4}$$

the compensated system becomes

$$\ddot{q} = y(t) + B(q)^{-1}\tilde{n}(q,\dot{q}) = y(t) - \eta(t) \tag{20.5}$$

where $\eta = -B^{-1}(q)\tilde{n}(q,\dot{q})$ and $\tilde{n}(q,\dot{q}) = \hat{n}(q,\dot{q}) - n(q,\dot{q})$. The $y(t)$ signal is regarded as an auxiliary input signal which is obtained by combining two different actions

$$y(t) = y_{sm}(t) + \ddot{q}_d(t) \tag{20.6}$$

where q_d is a continuous reference signal that has to be tracked with $\dot{q}_{di}$ Lispchitz, and $y_{sm}(t)$ has to be designed so as to enforce the robust tracking.

20.3.2 Design of the Proposed Second Order Sliding Mode Controller

To design the motion controller for robot manipulators here proposed, the so-called Sub-Optimal Sliding Mode Control (SOSMC) approach, introduced in [6], and extended to the multi-input case in [8] has been followed. Thus, taking into account the system dynamics (20.5) and the error state vector

$$x_i = \begin{bmatrix} x_{1i} \\ x_{2i} \end{bmatrix} = \begin{bmatrix} e_i \\ \dot{e}_i \end{bmatrix}, \quad e_i = q_{di} - q_i \tag{20.7}$$

an auxiliary second order state can be introduced, by letting

$$\xi_i(t) = \begin{bmatrix} \xi_{i1}(t) \\ \xi_{i2}(t) \end{bmatrix} = \begin{bmatrix} s_i(t) \\ \dot{s}_i(t) \end{bmatrix} \tag{20.8}$$

where s_i is the sliding variable, i.e.

$$s_i = s(x_i) = x_{2i} + \beta x_{1i}, \qquad \beta > 0. \tag{20.9}$$

In this case, the following auxiliary system can be formulated for each joint i

$$\begin{cases} \dot{\xi}_{i1}(t) = \xi_{i2}(t) \\ \dot{\xi}_{i2}(t) = \dot{\eta}_i(t) + \beta\eta_i(t) - \beta y_i(t) + \beta\ddot{q}_{di}(t) - \dot{y}_{smi}(t) \\ \dot{y}_{smi}(t) = w_i(t) + \beta\ddot{e}_i(t) \end{cases} \tag{20.10}$$

where $y_{sm}(t)$ can be determined, for each joint i, as follows

$$y_{smi}(t) = \int_{t_0}^{t} w_i(t)dt + \beta\dot{e}_i(t) \tag{20.11}$$

t_0 being the initial time instant. Note that in (20.10), $w_i(t)$ can be regarded as an auxiliary control signal still to be designed and $\dot{\eta}_i(t)$ can be regarded as an uncertain term. To apply the second order sliding mode design methodology, we require that $\dot{\eta}_i(t)$ is bounded, i.e. we assume that

$$| \dot{\eta}_i(t) | < \overline{F}_i \qquad \forall i \tag{20.12}$$

this means that to perform the synthesis procedure we are now considering a model which is simplified with respect to the model of the robot manipulator indicated in (20.1). In other terms, in the design of the second order sliding mode controller the dry friction term is neglected. In spite of this simplification, it will be shown that the proposed controller provides satisfactory performance even in experimental cases in which dry friction is surely present.

The design of the second order MIMO sliding mode control law can be carried out separately for each joint and the following result can be proved.

Theorem 20.1. *Given system (20.1) where $\tau(t)$ is selected as in (20.4) and y_i as in (20.6), (20.11), choosing the control signal w_i as*

$$w_i(t) = +\alpha_i W_{iMAX} sign\left\{\xi_{i1}(t) - \frac{1}{2}\xi_{i1MAX}\right\} \tag{20.13}$$

with

$$W_{iMAX} > \left(\frac{\overline{F}_i}{\alpha^*}; \frac{4\overline{F}_i}{3-\alpha^*}\right), \qquad \alpha^* \in (0,1] \tag{20.14}$$

where ξ_{i1MAX} is the last extremal value of $\xi_{i1}(t)$ and α_i is chosen according with the algorithm described in [7], then, starting from any initial condition $x_i(t_0) = x_{0i}$, the second order sliding manifold $[s_i, \dot{s}_i]^T = 0$ is reached in finite time for each i-th subsystem, and the origin of the state space of the error system is an asymptotically stable equilibrium point of the controlled system.

Proof. By applying Theorem 1 in [7], it can be claimed that the choice of the auxiliary control signal w_i ensures the finite reaching of

$$\xi_{i1} = \xi_{i2} = 0 \tag{20.15}$$

As in the case of first order sliding mode control, by virtue of (20.8) one has that also $s_i = 0$, i.e. the sliding manifold, is reached in finite time. Moreover, $s_i = 0$ implies that,

$$s_i = x_{2i} + \beta x_{1i} = \dot{e}_i + \beta e_i = 0 \tag{20.16}$$

Then the dynamical behavior of the error can be described by $\dot{e}_i = -\beta e_i$. Consequently, the manipulator asymptotically tracks the desired trajectory for each joint. □

Remark 20.1. The actual control signal acting on joint i, namely, $y_{smi}(t)$, is continuous, so attaining the requirement of avoiding the possible generation of vibrations.

Remark 20.2. Note that the weak point of the Sub-Optimal controller is the need to detect, in real time, the extremal values ξ_{i1MAX} of the sliding variable $\xi i1(t)$. In practical applications, the extremal values are not detected with ideal precision. If such values are detected with a delay, due to discrete sampling, in absence of measurement noise, then, it is possible to prove that a vicinity of the origin of the ξ_{i1}, ξ_{i2} state plane can be reached in finite time, see [6]. Yet, if some measurement noise exists, as it is reasonable in practice, the sampling interval needs to be chosen taking into account the measurement noise magnitude, to avoid performance degradation. More specifically, according to [46] and [48], the sampling interval has to be proportional to the square root of the measurement noise magnitude. In the experiments described in the next section, this requirement has been taken into account in selecting the sampling interval, relying on a rough estimation of the measurement errors. A possible alternative, to circumvent this problem, is to use a different approach to detect ξ_{i1MAX}. Indeed, one could use a "Robust exact differentiator" such as that is defined by [47] which is based on second order sliding modes to determine ξ_{i2}. Then, ξ_{i1MAX} is the value of ξ_{i1} when $\xi_{i2} = 0$. The value ξ_{i1MAX} determined in this way can be used in the control law (20.13).

20.4 Experimental Results on Motion Control

In this section, the results obtained by applying the proposed control scheme to a COMAU SMART3-S2 industrial robot are presented. They are also compared with those obtained by applying the Super Twisting second order sliding mode strategy

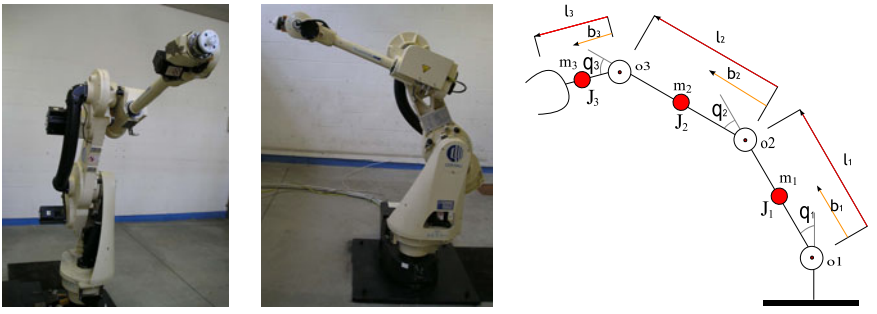

Fig. 20.2 The COMAU SMART3-S2 robot manipulator.

(see [46] and [47]), conventional first order sliding mode control law, and a classical PID controller.

20.4.1 The Considered Industrial Robot

The control and the supervision approaches described in this chapter have been experimentally tested on the SMART3-S2 industrial anthropomorphic rigid robot manipulator by COMAU, located at the Department of Electrical Engineering of the University of Pavia, and shown in Fig. 20.2. It consists of six links and six rotational joints driven by brushless electric motors. For the sake of simplicity, in this chapter it is assumed that the robot is constrained to move in a vertical plane and joints 1, 4 and 6 are not used. As a result, it is possible to consider the robot as a three link-three joint, in the sequel numbered as $\{1, 2, 3\}$, planar manipulator as schematically represented in Fig. 20.2. Yet, the proposed methods are general and can be applied to a n-joints robot.

In Fig. 20.2 and in Table 20.1, the following symbols will be used: m_i is the mass, J_i is the inertia, q_i is the angular position, l_i represents the link length and b_i the center of mass position with respect to the i-th link.

The six electrical motors of the COMAU SMART3-S2 robot are actuated by using as input signal six currents generated by the PWM power suppliers which are present in the COMAU C3G-900 Control Unit. This actuation system can be controlled via a Personal Computer by sending to the PWM six integer values belonging to the interval [-2047, 2047]. These values are converted by the PWM into six values of current in the interval [-30,30] (A). In this chapter we assume that the torques generated by actuators depend linearly on the currents generated by the power suppliers and that such currents are provided with accuracy. This assumption can appear rather strong. Yet, by executing experimental tests, it can be seen that for low to medium frequency input signals, the generated torque signals are very precise. Clearly, in the case of the first order sliding mode controller, high frequency control signals are generated. Then, it can happen that the actuators do not generate exactly the prescribed torque. In particular, one can observe a reduction of the frequency

of the torque signals with respect to the sampling frequency, which can produce performance degradation due to chattering effect. By using the second order sliding mode controllers, continuous input signals are generated, hence an accurate torque generation by the motors becomes feasible.

The considered industrial robot can be modelled as in (20.1). To perform the identification, the dynamical model (20.1) has been written in the following form

$$Y = \Phi(q, \dot{q}, \ddot{q})\theta^o + V \tag{20.17}$$

where the nonlinear matrix function $\Phi(\cdot) \in \mathbb{R}^{3N \times 9}$ represents the model (20.1) in a parametrized linear form, N being the number of sampled data, and 3 being the number of the considered joints. The term $\theta^o = [\gamma_1, \ldots, \gamma_9]^T$, $\gamma_i \in \mathbb{R}$, represents the unknown parameter vector to be estimated, while $Y \in \mathbb{R}^{3N}$ is the torque applied by the actuators, and $V \in \mathbb{R}^{3N}$ is the noise acting on Y, which is the input of the robotic system. The parametrization of θ^o and the values of the parameters determined via the Maximum Likelihood method (expressed in SI units) for the considered robot are shown in Table 20.1, see [19].

Table 20.1 (Left) Parametrization of the manipulator model. (Right) Average value and variance for the estimated parameters.

Parameter	Meaning	Identified Value	Variance
γ_1	$m_3 b_3^2 + J_3$	0.297	0.003
γ_2	$J_3 + m_3(l_2^2 + b_3^2) + J_2 + m_2 b_2^2$	10.07	0.04
γ_3	$J_3 + m_3(l_1^2 + l_2^2 + b_3^2) + J_2 + m_2(l_1^2 + b_2^2) + J_1 + m_1 b_1^2$	87.91	0.2
γ_4	$m_1 b_1 + m_2 l_1 + m_3 l_1$	57.03	0.06
γ_5, γ_6	$m_2 b_2 + m_3 l_2,\ m_3 b_3$	9.21, 0.316	0.02, 0.003
$\gamma_7, \gamma_8, \gamma_9$	F_{v1}, F_{v2}, F_{v3}	66.3, 14.71, 8.29	0.3, 0.1, 0.02

As for the controller, it has a sampling time of 0.001 (s), a 12 bit D/A and a 16 bit A/D converters. The joints positions are acquired by resolvers, fastened on the three motors, holding mechanical reducers with ratio $\{207, 60, 37\}$ respectively, while the maximum torques are $\{1825, 528, 71\}$ (Nm). Note that in applying the auxiliary control signal in (20.13), the following parameters values have been used: $\alpha^* = 0.8$, $W_{1MAX} = 362$, $W_{2MAX} = 607$, $W_{1MAX} = 10286$. Apart from the features of the experimental setup already mentioned, it is necessary to note that the evaluation of the sliding variable requires the evaluation of the derivative of the error signal, i.e., x_{2i} in (20.9). In order to avoid estimation errors a robust exact differentiator is used. This differentiator is described in [47].

20.4.2 The Experiments

The proposed control strategy has been tested with the following reference trajectories:

- A fifth order polynomial which consists in a fast and large but smooth enough variation of the three set point signals.
- A step reference signal, which consists in a discontinuous signal in order to emphasize the performances in the reaching phase of the algorithm.
- A sinusoidal reference signal, in order to emphasize the exact tracking performances typical of the sliding mode control.
- A spline reference signal, which consists in fast tracking and positioning phases in order to test the reaching capability of the algorithm when a discontinuous velocity signal is imposed.

Finally, an experimental evaluation of the good properties of the proposed second order sliding mode control strategy can be made relying on the a Root Mean Square Error Index, i.e.,

$$e_{RMSi} = \sqrt{\sum_{j=1}^{N} \frac{(q_{dij} - q_{ij})^2}{N-1}} \tag{20.18}$$

where N is the number of sampled data. The results obtained for the first order and the second order sliding mode controllers are reported in Table 20.2.

Table 20.2 Comparison of the Root Mean Square Errors for the three joints using First Order Sliding Mode Control (FOSMC) and second order sliding mode control when the reference trajectories described above are imposed to the robot (experimental results).

	5-th order polynomial st. RMSE (deg)	Two degrees step RMSE (deg)
PID	2.252 1.455 2.076	0.0022 0.0013 0.0026
FOSMC	0.0178 0.1384 0.0630	0.0128 0.0524 0.0739
Super-Twisting	0.1423 0.1801 0.0875	0.0016 0.0108 0.0157
Sub-Optimal	0.0037 0.0133 0.0465	0.0019 0.0162 0.0213
	Sinusoidal signal RMSE (deg)	Spline signal RMSE (deg)
PID	1.234 1.800 2.964	0.0064 0.0099 0.0036
FOSMC	0.0322 0.2135 0.2617	0.0173 0.0484 0.0299
Super-Twisting	0.0126 0.1125 0.1649	0.0068 0.0445 0.0641
Sub-Optimal	0.0125 0.0737 0.1365	0.0051 0.0051 0.1051

20.4.2.1 Experimental Results Obtained with the Fifth Order Polynomial Reference

The first reference signal is designed as to respect the boundedness requirements introduced to develop the theoretical treatment

$$\begin{aligned} [\text{pol5d}(0), \tfrac{d}{dt}\text{pol5d}(0), \tfrac{d^2}{dt^2}\text{pol5d}(0)] &= [0,0,0] \\ [\text{pol5d}(1), \tfrac{d}{dt}\text{pol5d}(1), \tfrac{d^2}{dt^2}\text{pol5d}(1)] &= [1,0,0] \end{aligned} \tag{20.19}$$

obtaining the reference multiplier

$$\text{pol5d}(t) = \begin{cases} 0 & t < 0 \\ 10t^3 - 15t^4 + 6t^5 & 0 \leq t \leq 1 \\ 1 & t > 1 \end{cases} \tag{20.20}$$

the three reference signals for the joints are obtained as follows

$$q_{di}(t) = A_i \text{pol5d}(t-1) \tag{20.21}$$

where $A_i = (70, 50, 70)$ (deg).

The results obtained with the proposed SOSMC applied to the robot manipulator are showed in Fig. 20.3. One can observe that the tracking performances are satisfactory in both the dynamic and static phase. The RMSE values for this experiment are compared with those obtained using a first order sliding mode controller, a super twisting second order sliding mode controller and a classical PID control law in Table 20.2. These values are obtained by considering only the time interval starting from 1.5 (s) to 2.5 (s), i.e. the time interval in which a fast movement of the entire robot is performed. It is clear that, in this way, a very good enhancement of the tracking performances can be obtained by relying on a SOSM controller, at least for the first and the second joint considered. The third joint, however, results affected by a highly uncertain friction effect, function of the angular position q_3 of the joint, leading to a higher switching action of $w_3(t)$. Note that with this reference signal, the sliding condition can be guaranteed at every time instant of the control phase.

20.4.2.2 Experimental Results Obtained with the Step Reference Signal

In this case, a 2 (deg) discontinuous step is imposed simultaneously as a reference signal for the three considered joints. It can be noted that using the proposed SOSMC strategy, the discretization chatter effect, see [67], and the audible chattering (audible noise) result very low, compared with those obtained with the first order sliding mode control (see [20]). In Fig. 20.4 the tracking performances of the three considered joints and the corresponding error signals are shown, while in Table 20.2 the RMS Errors relevant to the three joints are reported. Note that they have been evaluated in the steady state, when the sliding manifold has been reached. From the results, it is clear that the sub-optimal and the super-twisting algorithm reach approximatively the same precision for the tracking error. The comparison with the first order sliding mode control algorithm show that a very good enhancement of the results can be obtained with the second order sliding modes control algorithms.

20.4.2.3 Experimental Results Obtained with the Sinusoidal and the Spline Reference Signals

The sinusoidal reference trajectory is given by

$$q_{di}(t) = A_i' \sin\left(2\pi \frac{t}{b_i}\right) \tag{20.22}$$

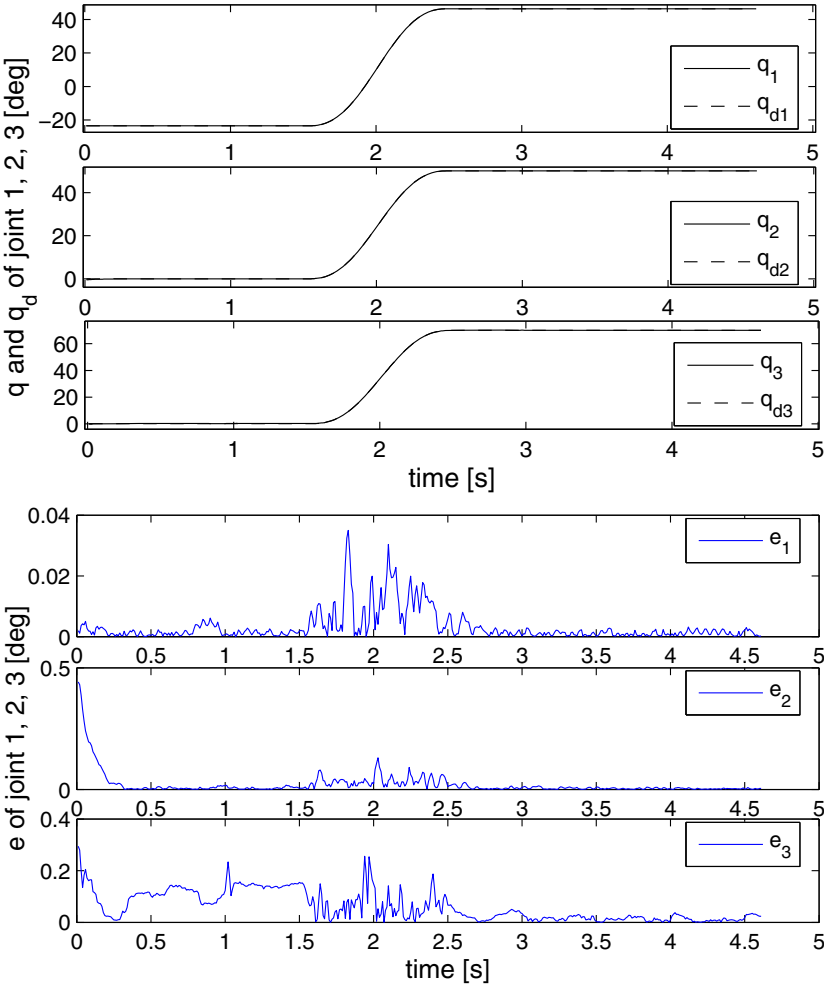

Fig. 20.3 Good tracking of the continuous polynomial reference trajectory using the proposed control scheme applied to the COMAU SMART3-S2 robot (the reference trajectories versus the measured joint angular positions on the first three plots; the tracking errors on the last three plots).

with $i = 1,2,3$, where A_i' are respectively $(30,30,40)$ (deg) and b_i are $(3,2,1.5)$ (s) while the spline reference trajectory is chosen as

$$\dot{q}_{di}(t) = \begin{cases} A_i'' & \text{if } t - \mathcal{N}P \leq 1 \\ 0 & \text{if } 1 < t - \mathcal{N}P \leq 3 \\ -A_i'' & \text{if } 3 < t - \mathcal{N}P \leq 4 \\ 0 & \text{if } 4 < t - \mathcal{N}P < 6 \end{cases} \tag{20.23}$$

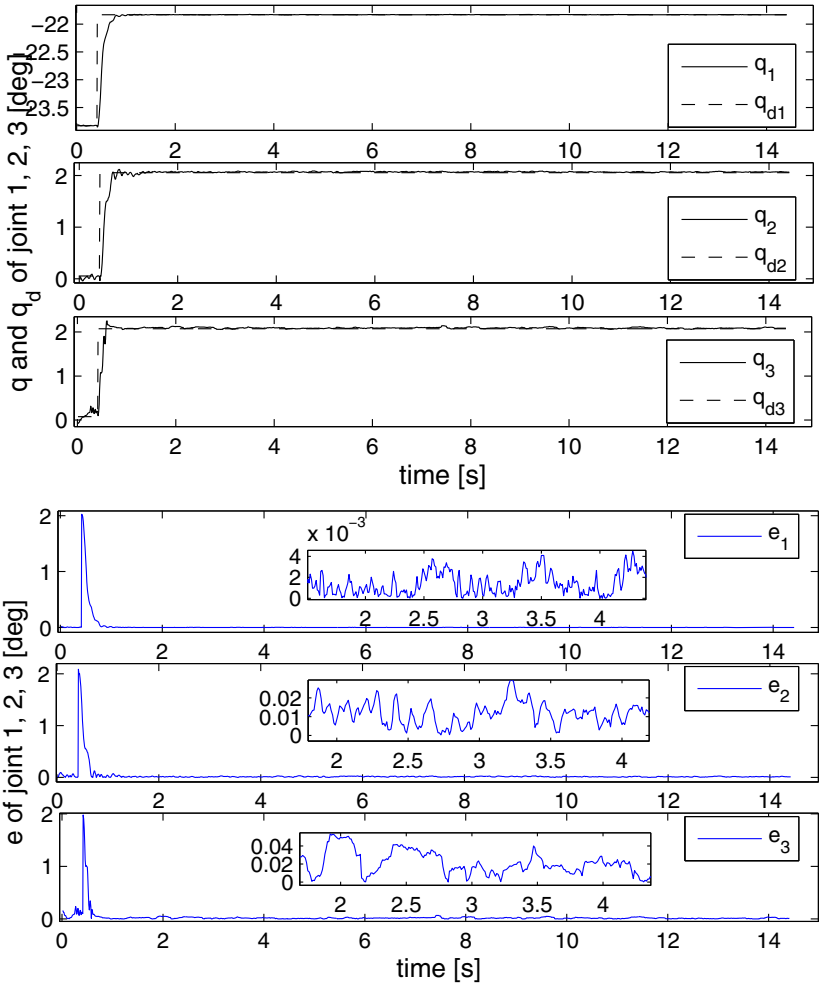

Fig. 20.4 Fast tracking of the discontinuous step reference trajectory using the proposed SOSMC (20.11) applied to the COMAU SMART3-S2 robot.

where $\mathscr{N} = \lfloor (\frac{t}{P}) \rfloor$, t represents the time instant, $q_d(0) = (-20, 0, 0)$ (deg), $P = 6$ (s) is the period, and A_j'' is the derivative amplitude, $(70, 40, 60)$ (deg/s) for each joint respectively. In practice this signal provides four different stages: a first increasing stage, a positioning stage, a decreasing stage and finally a positioning stage, such that it is possible to test tracking rapidity, precision and repeatability for the controlled system.

In Figures 20.5 and 20.6 it can be seen that the reaching phase results relatively short in both cases, and that the sliding phase (i.e. when the reference tracking is accomplished) starts after a small interval of time. In Table 20.2 the Root Mean Square tracking Errors are compared in a time interval in which the sliding manifold

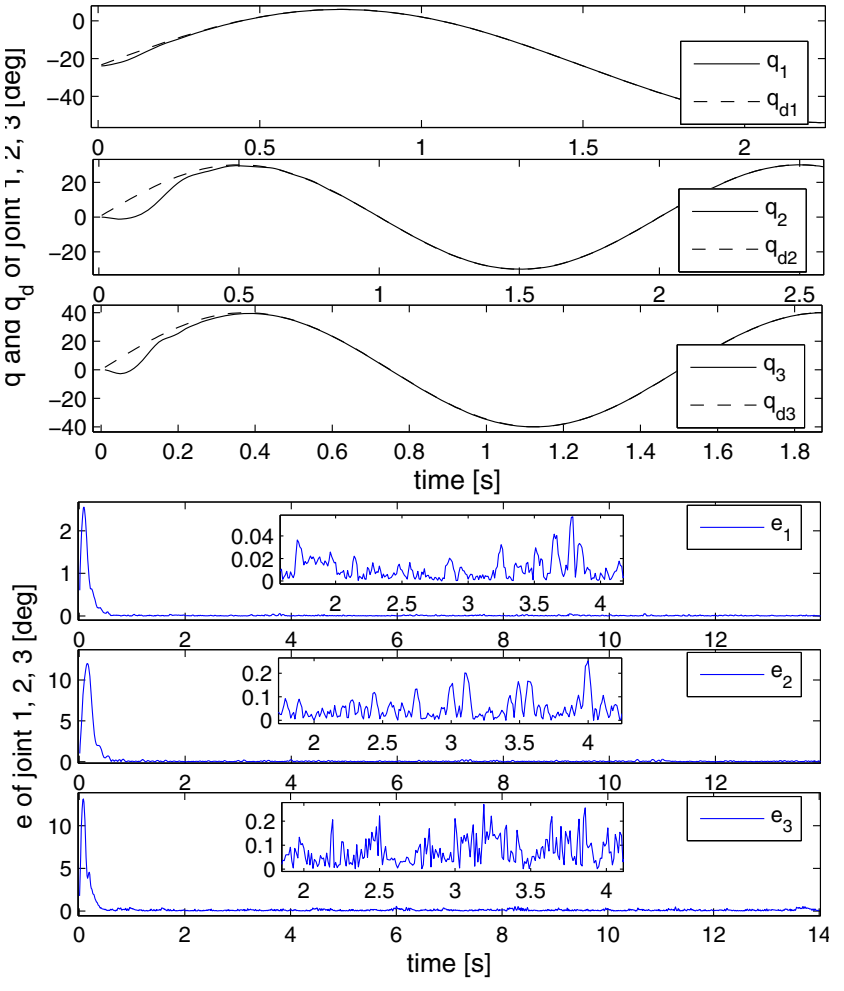

Fig. 20.5 Tracking of the sinusoidal reference trajectory using the proposed SOSMC (20.11) applied to the COMAU SMART3-S2 robot.

has been reached. Also in this case, the second order algorithms showed very good tracking performances, even if unpredictable frictions, especially on the third joint are present.

20.4.3 Comparison with the Super Twisting Second Order Sliding Mode Algorithm

In order to make a comparison with the Super Twisting second order sliding mode control, all the presented experiments have been performed applying also the

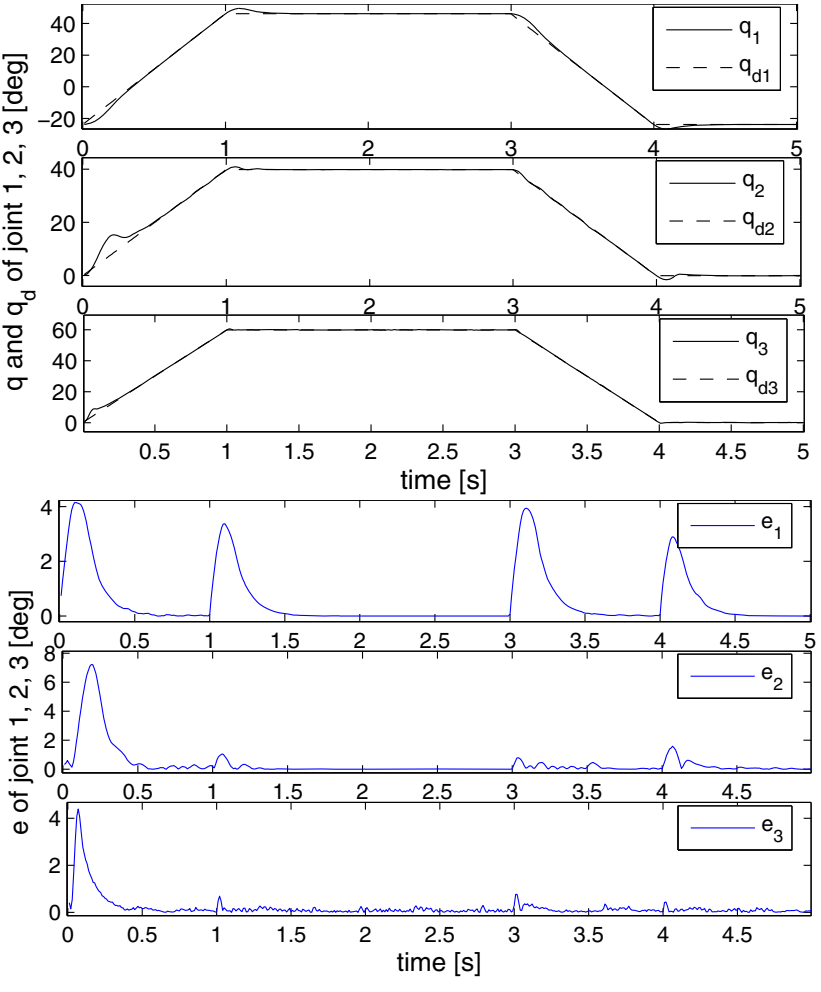

Fig. 20.6 Tracking of the spline reference trajectory using the proposed SOSMC (20.11) applied to the COMAU SMART3-S2 robot.

Super Twisting second order sliding mode algorithm, showing similar results as those obtained when the Sub-Optimal sliding mode control method is considered. In particular, after a very fine tuning of the controller parameters, good performances have been obtained for the spline signal, as it can be seen in Table 20.2. However, the Sub-Optimal control strategy showed a lower audible chattering in all the experiments and a easier tuning procedure.

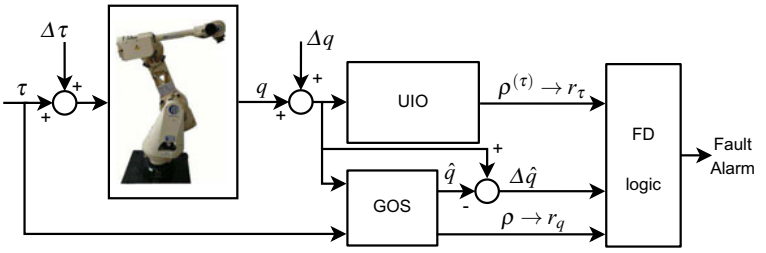

Fig. 20.7 The proposed fault diagnois scheme for actuator and sensor faults.

20.5 Solution to Problem 2: Fault Diagnosis for Robot Manipulators

20.5.1 The Considered Fault Scenarios

In this chapter, the presence of faults on the inputs or on the outputs of the controlled robot manipulator is considered. More precisely, the following combinations of faults are considered:

1. The case of multiple faults, even simultaneous, occurring on the actuators of the manipulator.
2. The case of single faults occurring on one of the actuators or on one of the sensors. The case of multiple and non simultaneous sensor faults is also admissible.

20.5.2 Actuator and Sensor Faults

Consider the robot manipulator model (20.1). If actuator faults are present, the real torque applied by the actuators is unknown. That is the actual torque vector which is the input to the robotic system can be expressed as $\overline{\tau}(t) = \tau(t) + \Delta\tau(t)$, where $\tau \in \mathbb{R}^n$ is the nominal torque calculated by the robot controller, while $\Delta\tau \in \mathbb{R}^n$ ($\Delta\tau_i$ being its i-th component) is the input fault. In practice, this type of fault can be caused by a damage that can occur on power supply systems, or actuator mechanisms, or wirings (but we will not distinguish among them).

Instead, when sensor faults occur, the control system cannot determine the exact angular displacements of the joints. Let $q \in \mathbb{R}^n$ be the true but unknown output (i.e. the joints displacements), while $\Delta q \in \mathbb{R}^n$ (Δq_i being its i-th component) be the vector of the fault signals acting on it. Then, $\bar{q} \in \mathbb{R}^n$ represents the measurement that the control system receives, i.e., $\bar{q}(t) = q(t) + \Delta q(t)$.

20.5.3 The Proposed Diagnostic Scheme

The proposed diagnostic scheme, derived from [15, 17, 16], is illustrated in Fig. 20.7. It includes an Uncertain Input Observer (UIO) to deal with actuator faults,

and a generalized observer scheme, to perform the detection and isolation (when possible) of sensor faults.

20.5.4 Actuator Faults Detection Strategy

Suitable estimators of the input torques can be designed taking into account the observability issues discussed in [30], [51]. We propose to detect the actuator faults by means of an UIO of sliding mode type. The possibility of using this kind of observers in the fault detection context has already been investigated, for instance, in [34]. The UIO we propose is a multi-input-multi-state second order sliding mode observer, i.e.,

$$\begin{cases} \dot{\hat{\chi}}_1^{(\tau)} = \hat{\chi}_2^{(\tau)} \\ \dot{\hat{\chi}}_2^{(\tau)} = \hat{f}(\hat{\chi}_1^{(\tau)}, \hat{\chi}_2^{(\tau)}, \tau) + \rho^{(\tau)} \end{cases} \tag{20.24}$$

where $\hat{\chi}^{(\tau)} = [\hat{\chi}_1^{(\tau)}, \hat{\chi}_2^{(\tau)}]^T$ is the observer state, with $\hat{\chi}_1^{(\tau)} \in \mathbb{R}^n, \hat{\chi}_2^{(\tau)} \in \mathbb{R}^n$, and $f(\cdot)$ is defined as

$$\hat{f}(\cdot) = B^{-1}(\hat{\chi}_1^{(\tau)})[\tau - \hat{C}(\hat{\chi}_1^{(\tau)}, \hat{\chi}_2^{(\tau)})\hat{\chi}_2^{(\tau)} - \hat{F}_v\hat{\chi}_2^{(\tau)} - \hat{g}(\hat{\chi}_1^{(\tau)})] \tag{20.25}$$

where $\rho^{(\tau)}$ is the observer input law, determined according to the so-called SOSM Sub-Optimal approach [4,6,7] as

$$\begin{cases} \dot{\rho}_i^{(\tau)}(t) = \alpha_i W_{iMAX} \operatorname{sign}\left\{ s_i^{(\tau)}(t) - 0.5 s_{iMAX}^{(\tau)} \right\} \\ s_i^{(\tau)}(t) = \tilde{\chi}_{2i}^{(\tau)} + \beta \tilde{\chi}_{1i}^{(\tau)} \\ \tilde{\chi}_1^{(\tau)} = q(t) - \hat{\chi}_1^{(\tau)}, \quad \tilde{\chi}_2^{(\tau)} = \dot{\tilde{\chi}}_1^{(\tau)} \end{cases} \tag{20.26}$$

where $\tilde{\chi}_1^{(\tau)} = [\tilde{\chi}_{11}^{(\tau)}, \ldots, \tilde{\chi}_{1n}^{(\tau)}]^T$, $\tilde{\chi}_2^{(\tau)} = [\tilde{\chi}_{21}^{(\tau)}, \ldots, \tilde{\chi}_{2n}^{(\tau)}]^T$. In (20.26), $s_i^{(\tau)}(t)$ is the so-called sliding variable, that is the variable to steer to zero in order to perform the observation task, i is the index of the component of the state vector coinciding with the actuator number, $s_{iMAX}^{(\tau)}$ represents the last extremal value of the sliding variable $s_i^{(\tau)}(t)$, and β is a strictly positive design parameter. It can be proved that a suitable choice of $\alpha_i W_{iMAX}$ exists such that the Sub-Optimal input law guarantees the exponential stability of the tracking error of this observer (the proof of this claim can be developed as in [7]).

Note that in case of actuator faults, the dynamics of the robotic system given by (20.1) can be expressed as

$$\ddot{q} = f(q, \dot{q}, \tau + \Delta\tau) \tag{20.27}$$

The exponential stability of the observation error, implies that $\tilde{\chi}_1^{(\tau)} \to 0$, i.e.

$$\left[f(q, \dot{q}, \tau + \Delta\tau) - \hat{f}(\hat{\chi}_1^{(\tau)}, \hat{\chi}_2^{(\tau)}, \tau) - \rho^{(\tau)} \right] \to 0 \tag{20.28}$$

By virtue of the structure of model (20.1), it is apparent that an actuator fault $\Delta\tau$ can be modeled as a signal Δy acting at the acceleration level of the model, with $\Delta\tau(t) = B(q)\Delta y(t)$, because of the existence of the matrix $B^{-1}(q)$, $\forall q \in \mathbb{R}^n$. Then, (20.28) can be rewritten as

$$\left\{B(q)^{-1}[\tau - n(q,\dot{q})] + \Delta y(t) - B^{-1}(\hat{\chi}_1)[\tau - \hat{n}(q,\dot{q})] - \rho^{(\tau)}\right\} \to 0 \qquad (20.29)$$

which implies the exponential convergence of $\rho^{(\tau)}$ to $\Delta y(t) - B^{-1}(q)\eta$. Then, by determining $B(q)\rho^{(\tau)}$, one has $B(q)\Delta y - \eta$ that is $B(q)\rho^{(\tau)} = \widehat{\Delta\tau} \approx \Delta\tau$ provided that the magnitude of η is acceptable. Since the $B^{-1}(q)\eta$ term is bounded, suitable thresholds can be defined in order to enable the actuator faults detection. Note that, because of the fact that we assume that the modeling error η exists (which is quite realistic, as confirmed by the experimental tests), only faults exceeding the pre-specified thresholds can be detected, in contrast to the ideal case in which η is assumed to be zero and $\rho^{(\tau)} \to \Delta y(t)$, i.e. $B(q)\rho^{(\tau)} = \Delta\tau$, so that any fault is detectable. Thresholds are selected so as to minimize misdetections and false alarms, on the basis of experimental tests.

20.5.5 Sensor Faults Detection Strategy

To perform the detection of sensor faults, n observers are used, one for each sensor. The resulting scheme can be regarded as a Generalized Observer Scheme (GOS) [37]. The peculiarity of our proposal lies in the fact that the observers of the designed GOS are of sliding mode type.

The input law of the i-th GOS observer is calculated relying on all the sensor measurements, apart from the measurement coming from the i-th sensor (see Fig. 20.8). That is, the input law of the i-th GOS observer has the i-th component equal to zero.

Thus, the i-th GOS observer in our proposal is defined as

$$\begin{cases} \dot{\hat{\chi}}_1^{(i)} = \hat{\chi}_2^{(i)} \\ \dot{\hat{\chi}}_2^{(i)} = \hat{f}(\hat{\chi}_1^{(i)}, \hat{\chi}_2^{(i)}, \tau) + \rho^{(i)}(t) \end{cases} \qquad (20.30)$$

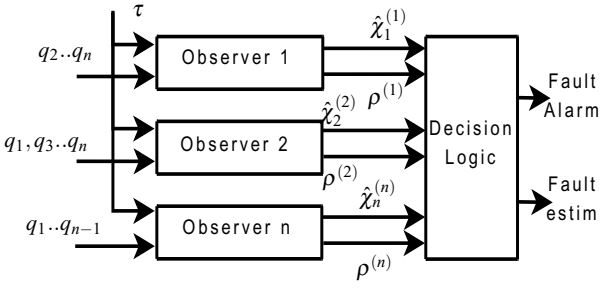

Fig. 20.8 Generalized Observer Scheme (GOS) for a n sensors system.

where $\hat{\chi}_1^{(i)} \in \mathbb{R}^n$ is the vector of the estimate of the $\bar{q}$ vector made by the i-th observer, with $\hat{\chi}_1^{(i)} = \left[\hat{\chi}_{1,1}^{(i)},\ \hat{\chi}_{1,2}^{(i)},\ \ldots,\ \hat{\chi}_{1,n}^{(i)}\right]^T$, $\hat{f}(\cdot)$ has the structure indicated in (20.25), while $\rho^{(i)} \in \mathbb{R}^n$ is the input law of observer i. Note that the form of the observer is analogous to that adopted in [27] in the general case of mechanical systems.

The considered error vector signal for the i-th observer is given by

$$e^{(i)} = q + \Delta q - \hat{\chi}_1^{(i)} \tag{20.31}$$

Then, also in this case, we design the observer input law $\rho^{(i)}(t)$ in (20.30) according to the Sub-Optimal Algorithm [7], by posing, in addition, the i-th component of $\rho^{(i)}(t)$ equal to zero, i.e.,

$$\begin{cases} \dot{\rho}_j^{(i)} = \alpha_j W_{jMAX} \text{sign}\left\{s_j^{(i)}(t) - 0.5 s_{jMAX}^{(i)}\right\}, \quad j \neq i \\ \rho_i^{(i)} = 0 \\ s^{(i)}(t) = \dot{e}^{(i)} + \beta e^{(i)} \end{cases} \tag{20.32}$$

In (20.32), $s^{(i)}(t)$ is the so-called sliding variable, that is the variable to steer to zero in order to perform the observation task, j is the index of the component of the state vector coinciding with the sensor number, $s_{jMAX}^{(i)}$ represents the last extremal value of the sliding variable $s_j^{(i)}(t)$, and β is a strictly positive design parameter. It can be proved that a suitable choice of $\alpha_j W_{jMAX}$ exists such that the Sub-Optimal input law guarantees the exponential stability of the tracking error of this observer (the proof of this claim can be developed as in [7]). Note that, with this input law, the observer (20.30) has the i-th component in open loop. This can imply stability problems also in absence of faults, if the system is not open loop stable by itself. However, this component of the i-th observer is just that useful, in case of fault on the i-th sensor, in order to give an estimate of the fault signal. To circumvent stability problems while avoiding to significantly alterate the detection, in the experimental tests, a local small gain proportional feedback is closed to generate the i-th input law component of the i-th observer (20.32). That is,

$$\rho_i^{(i)}(t) = K\left(q_i + \Delta q_i - \hat{\chi}_{1,i}^{(i)}\right),\ \forall i,\ K > 0 \tag{20.33}$$

with K sufficiently small.

If $\hat{f}(\cdot)$ can be assumed to be a quite accurate estimate of $f(\cdot)$ in absence of noise and faults, the GOS observers would be a perfect copy of the robot model. Thus, each input law could be zero to allow for a null error $e^{(i)}$. This means that where a component of the input law $\rho^{(i)}$ is different from zero, a fault is present somewhere. Assuming that faults can occur only on sensors, a fault can be detected considering Table 20.3. As it can be seen from this table, when a single sensor fault occurs, only $n-1$ of the n GOS observers have their input laws, i.e. $\rho^{(i)}$, sensitive to the fault, since the observer j, associated with the sensor where the fault has occurred, has

the j-th component of the input law, i.e. $\rho_j^{(j)}$, always set equal to zero. During the robot operation, one can observe the n vectors $\rho^{(i)}$. If the situation is that depicted in a generic column of Table 20.3, say the j-th, then one can conclude that the fault has occurred on sensor j. The value r_{qj}, called residual associated with sensor j, is set equal to 1 in that case (note that in practice, each component of $\rho^{(i)}$ is suitably filtered in order to determine $r_q = [r_{q1}, \ldots, r_{qn}]^T$ as will be mentioned in Subsection 20.5.6).

If, in contrast, $\hat{f}(\cdot)$ differs from $f(\cdot)$ of the bounded quantity $B^{-1}(q)\eta$, as mentioned in Subsection 20.5.4, again thresholds need to be introduced to perform the fault detection. For instance, the entries of Table 20.3 expressed as $\rho^{(i)} \neq 0$ can be replaced by the condition

$$\text{if} \quad \exists\, k \text{ s.t. } \left[\text{sign}\left\{\rho^{(i)}\right\} \odot \rho^{(i)}\right]_k > T_k^q \tag{20.34}$$

while the entries of Table 20.3 expressed as $\rho^{(i)} = 0$ become

$$\left[\text{sign}\left\{\rho^{(i)}\right\} \odot \rho^{(i)}\right]_k < T_k^q,\ \forall k = 1, \ldots, n \tag{20.35}$$

where $\text{sign}\left\{\rho^{(i)}\right\}$ is the vector containing the sign of each component of $\rho^{(i)}$, the symbol $\odot$ denotes the Schur product, $[\cdot]_k$ denotes the k-th component of a vector, and T_k^q is a positive real number representing the selected threshold. As in the case addressed in Subsection 20.5.4, the values of the thresholds depend on the magnitude of the uncertain term $B^{-1}(q)\eta$. Obviously, now the fact that a fault has occurred on sensor j can be inferred when (20.35) is true for $i = j$ and (20.34) is true $\forall\, i \neq j$.

Table 20.3 Signature table for sensor faults isolation.

Sensor 1 fault $r_{q1} = 1$	Sensor 2 fault $r_{q2} = 1$	$\ldots$ $\ldots$	Sensor n fault $r_{qn} = 1$
$\rho^{(1)} = 0$	$\rho^{(1)} \neq 0$	$\ldots$	$\rho^{(1)} \neq 0$
$\rho^{(2)} \neq 0$	$\rho^{(2)} = 0$	$\ldots$	$\rho^{(2)} \neq 0$
$\vdots$	$\vdots$	$\vdots$	$\vdots$
$\rho^{(n)} \neq 0$	$\rho^{(n)} \neq 0$	$\ldots$	$\rho^{(n)} = 0$

20.5.6 Residual Generation

Fig. 20.7 shows the complete diagnostic scheme for robot manipulators. where the residual vector r_q associated with the sensors and the residual vector r_τ associated with the actuators are indicated.

The residual vector r_τ is given by

$$r_{\tau i} = \begin{cases} 0 & \text{if } |\mathscr{F}(t) * \rho_i^\tau| < T_i^\tau \\ 1 & \text{if } |\mathscr{F}(t) * \rho_i^\tau| \geq T_i^\tau \end{cases} \qquad \forall\, i \tag{20.36}$$

where it is assumed that, to deal with measurement noise in experiments, the following 5-th order low-pass filter is introduced (z is the unitary delay operator)

$$\mathscr{F}(z) = \frac{b}{1 - az^{-1} - az^{-2} - az^{-3} - az^{-4} - az^{-5}} \tag{20.37}$$

with $a = 0.1993$ and $b = 1 - 5a$.

The residual vector r_q is obtained by filtering the $\rho_{j\neq i}^{(i)}(t)$ signals through the filter (20.37) and comparing these signals with their thresholds T_k^q, according to Table 20.3. Thresholds T_i^τ and T_k^q take into account the presence of uncertainties and discrete time sampling. To choose suitable thresholds, tuning experiments have been executed.

20.5.7 Fault Isolation for Single Faults

To isolate a fault means to determine if the fault has occurred on a specific actuator or on a specific sensor. This is a complex task which may be possible only for single faults occurring on both actuators or sensors, or for multiple faults occurring only on actuators. In this second case it is sufficient to check the residual r_τ and claim that the fault has occurred on the actuators corresponding to the components of r_τ equal to 1. In the first case, instead it can be useful to compare the binary residual vector $\left[r_\tau^T, r_q^T\right]^T$ with the the rows of the fault signature Table 20.4. The row which coincides with the residual vector identifies the device affected by fault. Note that, in general, an actuator fault can produce relevant residuals on all the n sensor faults observers and a sensor fault can produce relevant residuals associated with the actuators. However, for a small fault on sensors, i.e., for small Δq, for small velocities and accelerations of the robot manipulator system, and in the absence of uncertainties, the actuator residual r_τ is not sensitive to a sensor fault Δq if the magnitude of $[B(q+\Delta q)\ddot{q} - B(q)\ddot{q} + n(q+\Delta q, \dot{q}+\Delta\dot{q}) - n(q,\dot{q})]_k$ is less than the

Table 20.4 Fault signature table, where p represents a value that can be 0 or 1.

Fault	$r_{\tau 1}$	$r_{\tau 2}$	$r_{\tau n}$	r_{q1}	r_{q2}	r_{qn}
None	0	0	0	0	0	0
Act. 1	1	0	0	p	p	p
Act. 2	0	1	0	p	p	p
Act. n	0	0	1	p	p	p
Sen. 1	p	p	p	1	0	0
Sen. 2	p	p	p	0	1	0
Sen. n	p	p	p	0	0	1

k-th actuator fault threshold. The binary values p in Table 20.4, take into account this fact, and, in general, a single fault cannot be exactly isolated if the fault induces the detection of one actuator fault and one sensor fault. From a theoretical point of view, it can be shown that, in case of exact identification of the manipulator model, and in particular working conditions, a single fault occurring on the actuators or on the sensors can be correctly isolated, as expressed by the following result.

Theorem 20.1. *Under the assumptions of single fault, of exact knowledge of the manipulator model (20.1) and the absence of noise on sensor measurements, a sensor fault Δq_i can be isolated from an actuator fault $\delta\tau_i$ if the following conditions hold:*

- *the n degree of freedom manipulator belongs to a vertical plane, and each link has a non null gravitational contribution on each actuator;*
- *the sensor fault signal Δq_i is time invariant, i.e. $\Delta\dot{q}_i = \Delta\ddot{q}_i = 0$;*
- *the robot manipulator represented by the model (20.1) is in static working conditions, i.e. $\dot{q} = \ddot{q} = 0$.*

In particular, when a single fault occurs on a specified component of the vector q, the former conditions assure that it is impossible to detect a non-existent single fault $\Delta\tau_j$, (which represents a false alarm situation).

Observation 20.1. Note that the conditions stated in Theorem 20.1 can appear a little restrictive, but these conditions are only sufficient. In practice, a fault can be isolated in several situations, especially when $\|\dot{q}\|$ and $\|\ddot{q}\|$ are small.

20.5.8 Experimental Results on Fault Diagnosis

In this subsection the proposed scheme is experimentally tested on the COMAU SMART3-S2 manipulator. The faults presence is introduced in the control system by adding a fault signal to the control variable (in case of actuator fault) or to the sensor signal (in case of sensor fault).

Clearly, to carry on the experiments on the COMAU SMART3-S2 manipulator it is necessary to control the robot. In this case, the COMAU SMART3-S2 manipulator is controlled via the control scheme described in Section 20.3.

20.5.9 Experimental Test in Presence of Actuator Faults

Experiments in presence of actuator faults have been developed through the introduction of abrupt faults on each joint. To show the properties of the proposed scheme, a 10 (Nm) fault signal on the third actuator is considered. Note that this fault is below the 20% of the maximum torque allowed by the corresponding actuator. As it can be seen from Fig. 20.9, the fault is correctly detected (since $|\widehat{\Delta\tau}_3|$ exceeds the threshold T_3^{τ}) and identified, since the actual shape of the fault signal is recognizable from $\widehat{\Delta\tau}_3$.

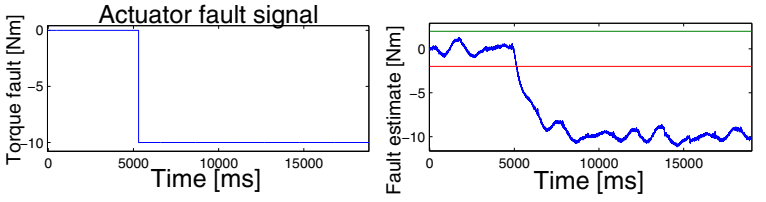

Fig. 20.9 Experiment with fault on the third actuator (the actual fault signal $\Delta\tau_3$ on the left and the fault estimate $\widehat{\Delta\tau}_3 = [B(q)\rho^{(\tau)}]_3$ on the right).

20.5.10 Experimental Tests in Presence of Sensor Faults

In the experimental case, the presence of nonlinear and unmodelled effects leads to a corruption of the signals useful for the fault analysis. The modified input law (20.33) for the GOS has been considered in this case.

Relying on the modified structure, the following experiment is performed: an abrupt fault of -30 (deg) on the first joint sensor measurement is introduced starting from time instant 3.1 (s). In order to identify the joint on which the fault has occurred, the proposed fault signature table (Table 20.4) is considered. Figs. 20.11, 20.12, and 20.13 show the two components different from zero of the input laws of the three GOS observers. The fault isolation can be accomplished considering the second and the third observer signals since only these (in particular one of their components) exceed the thresholds. So, one can conclude that the fault has occurred

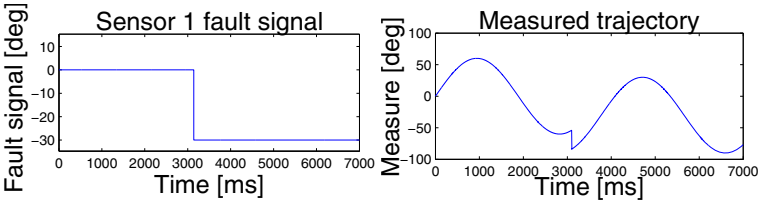

Fig. 20.10 Experiment with fault on the first sensor (the actual fault signal Δq_1 on the left and the measurement $\bar{q} = q_1 + \Delta q_1$ on the right).

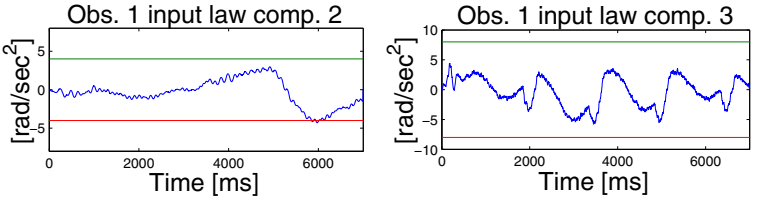

Fig. 20.11 Sensor fault detection experiments: $\rho_2^{(1)}$ and $\rho_3^{(1)}$ signals in (20.30) for a fault on sensor 1.

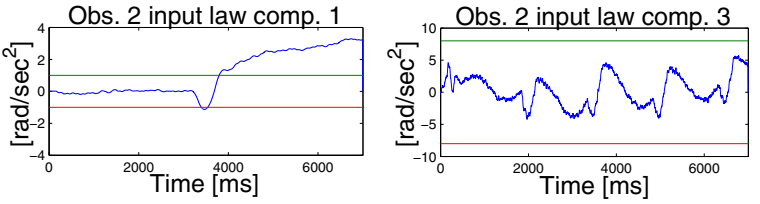

Fig. 20.12 Sensor fault detection experiments: $\rho_1^{(2)}$ and $\rho_3^{(2)}$ signals in (20.30) for a fault on sensor 1.

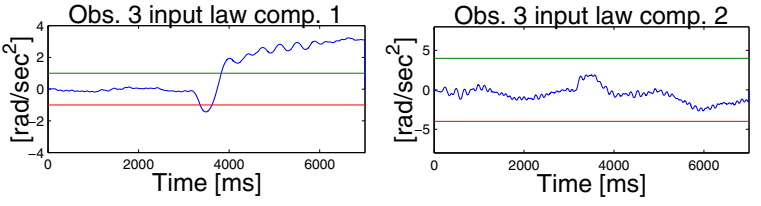

Fig. 20.13 Sensor fault detection experiments: $\rho_1^{(3)}$ and $\rho_2^{(3)}$ signals in (20.30) for a fault on sensor 1.

on sensor 1. In contrast to the case illustrated in Subsection 20.5.9, now the fault identification is not allowed.

20.6 Conclusions

The possibility of applying the sliding mode design methodology also in robotics is investigated in this chapter. The idea is to use such a methodology to design both a control scheme to perform the robot motion control, and a diagnostic scheme to detect and, possibly, identify and isolate actuator and sensor faults. It has been pointed out that a second order sliding mode approach is surely more appropriate than conventional first order sliding mode.

The proposed control scheme provides robustness versus bounded uncertainties and disturbances and therefore it allows to compensate possible errors or imprecisions coming from the identification phase. Moreover, it allows to mitigate the chattering problem by virtue of the design of a continuous control signal. This makes the proposed sliding mode controller actually applicable to an industrial robot, by virtue of the practical absence of induced vibrations.

Also fault diagnosis results in being practicable via a second order sliding mode approach. The experimental tests performed on a COMAU SMART3-S2 robot demonstrate that the position tracking error is actually enforced to zero, ensuring good tracking performances of the controlled system, and that, while the robot is controlled through the proposed scheme, an efficient fault diagnosis can be performed.

Note that the theoretical development presented in this chapter allows one to deal with the following cases: faults (even multiple) occurring only on the actuators; single faults occurring on the actuators or on the sensors (the knowledge of the type of the device affected by the fault can be non available). Yet, in practical experiments we have observed that the detection and isolation of multiple sensor faults is possible, provided that they are not simultaneous. The possibility of solving the problem of fault diagnosis also in more general cases is presently under investigation.

References

1. Abdallah, C.T., Dawson, D.M., Dorato, P., Jamshidi, M.: Survey of robust control for rigids robots. IEEE Control Systems Magazine 11(2), 24–30 (1991)
2. Asada, H., Slotine, J.J.E.: Robot Analysis and Control. John Wiley & Sons, New York (1986)
3. Balestrino, A., De Maria, G., Sciavicco, L.: An adaptive model following control for robotic manipulators. ASME Journal of Dynamic Systems, Measurement, and Control 105, 143–151 (1983)
4. Bartolini, G., Ferrara, A., Levant, A., Usai, E.: On second order sliding mode controllers. In: Young, K.D., Ozguner, U. (eds.). LNCIS, vol. 247, pp. 329–350 (1999)
5. Bartolini, G., Ferrara, A., Punta, E.: Multi-input second-order sliding-mode hybrid control of constrained manipulators. Dynamics and Control 10(3), 277–296 (2000)
6. Bartolini, G., Ferrara, A., Usai, E.: Output tracking control of uncertain nonlinear second-order systems. Automatica 33(12), 2203–2212 (1997)
7. Bartolini, G., Ferrara, A., Usai, E.: Chattering avoidance by second order sliding mode control. IEEE Transactions on Automatic Control 43(2), 241–246 (1998)
8. Bartolini, G., Ferrara, A., Usai, E., Utkin, V.I.: On multi-input chattering-free second-order sliding mode control. IEEE Transactions on Automatic Control 45(9), 1711–1717 (2000)
9. Bartolini, G., Ferrara, A., Utkin, V.I.: Adaptive sliding mode control in discrete-time systems. Automatica 31(5), 763–769 (1995)
10. Bartolini, G., Pisano, A.: Global output-feedback tracking and load disturbance rejection for electrically-driven robotic manipulators with uncertain dynamics. International Journal of Control 76(12), 1201–1213 (2003)
11. Bartolini, G., Pisano, A., Punta, E., Usai, E.: A survey of applications of second-order sliding mode control to mechanical systems. International Journal of Control 76(9), 875–892 (2003)
12. Boiko, I., Fridman, L.M.: Analysis of chattering in continuous sliding-mode controllers. IEEE Transactions on Automatic Control 50(9), 1442–1446 (2005)
13. Boiko, I., Fridman, L.M., Castellanos, M.I.: Analysis of second-order sliding-mode algorithms in the frequency domain. IEEE Transactions on Automatic Control 49(6), 946–950 (2004)
14. Boiko, I., Fridman, L.M., Pisano, A., Usai, E.: Performance analysis of second-order sliding-mode control systems with fast actuators. IEEE Transactions on Automatic Control 52(6), 1053–1059 (2007)
15. Brambilla, D., Capisani, L.M., Ferrara, A., Pisu, P.: Actuators and sensors fault detection for robot manipulators via second order sliding mode observers. In: Proc. 10th IEEE/IFAC International Workshop on Variable Structure Systems, Antalya, Turkey, pp. 61–66 (2008)

16. Brambilla, D., Capisani, L.M., Ferrara, A., Pisu, P.: Fault detection for robot manipulators via second-order sliding modes. IEEE Transactions on Industrial Electronics 55(11), 3954–3963 (2008)
17. Brambilla, D., Capisani, L.M., Ferrara, A., Pisu, P.: Second order sliding modes observers for fault detection of robot manipulators. In: Proc. 47th IEEE Conference on Decision and Control, Cancun, Mexico, pp. 2949–2954 (2008)
18. Calanca, A., Capisani, L.M., Ferrara, A., Magnani, L.: An inverse dynamics-based discrete-time sliding mode controller for robot manipulators. In: Kozlowski, K. (ed.) Robot Motion and Control 2007. LNCIS, pp. 137–146. Springer, London (2007)
19. Capisani, L.M., Ferrara, A., Magnani, L.: MIMO identification with optimal experiment design for rigid robot manipulators. In: Proc. IEEE/ASME International Conference on Advanced Intelligent Mechatronics, Zürich, Switzerland, pp. 1–6 (2007)
20. Capisani, L.M., Ferrara, A., Magnani, L.: Design and experimental validation of a second-order sliding-mode motion controller for robot manipulators. International Journal of Control 82(2), 365–377 (2009)
21. Cheah, C.C., Liu, C., Slotine, J.J.E.: Adaptive tracking control for robots with unknown kinematic and dynamic properties. The International Journal of Robotics Research 25(3), 283–296 (2006)
22. Chen, W., Saif, M.: Robust fault detection and isolation in constrained nonlinear systems via a second order sliding mode observer. In: Proc. 15th IFAC World Congress, Barcelona, Spain, pp. 1498–1500 (2002)
23. Chen, Y., Chang, J.L.: Sliding-mode force control of manipulators. National Science Council ROC(A) 23(2), 281–289 (1999)
24. Chiacchio, P., Pierrot, F., Sciavicco, L., Siciliano, B.: Robust design of independent joint controllers with experimentation on a high-speed parallel robot. IEEE Transactions on Industrial Electronics 40(4), 393–403 (1993)
25. Colbaugh, R.D., Bassi, E., Benzi, F., Trabatti, M.: Enhancing the trajectory tracking performance capabilities of position-controlled manipulators. In: Proc. IEEE Industry Applications Conference, Rome, Italy, vol. 2, pp. 1170–1177 (2000)
26. Craig, J.J.: Adaptive Control of Mechanical Manipulators. Addison-Wesley, New York (1988)
27. Davila, J.A., Fridman, L.M., Levant, A.: Second-order sliding-mode observer for mechanical systems. IEEE Transactions on Automatic Control 50(11), 1785–1789 (2005)
28. De Luca, A., Mattone, R.: Actuator failure detection and isolation using generalized momenta. In: Proc. IEEE International Conference on Robotics and Automation, Taipei, Taiwan, vol. 1, pp. 634–639 (2003)
29. De Luca, A., Mattone, R.: An identification scheme for robot actuator faults. In: Proc. IEEE/RSJ International Conference on Intelligent Robots and Systems, Alberta, Canada, pp. 1127–1131 (2005)
30. De Persis, C., Isidori, A.: A geometric approach to nonlinear fault detection and isolation. IEEE Transactions on Automatic Control 46(6), 853–865 (2001)
31. Dinuzzo, F., Ferrara, A.: Higher order sliding mode controllers with optimal reaching. IEEE Transactions on Automatic Control 54(9), 2126–2136 (2009)
32. Dixon, W.E., Walker, I.D., Dawson, D.M., Hartfranft, J.P.: Fault detection for robot manipulators with parametric uncertainty: A prediction-error-based approach. IEEE Transactions on Robotics and Automation 16(6), 689–699 (2000)
33. Edwards, C., Spurgeon, S.K.: Sliding Mode Control: Theory and Applications. Taylor & Francis, London (1998)
34. Edwards, C., Spurgeon, S.K., Hebden, R.G.: On development and applications of sliding mode observers. In: Xu, J., Xu, Y. (eds.) Variable Structure Systems: Toward 21st Century. LNCIS, pp. 253–282. Springer, Berlin (2002)

35. Edwards, C., Spurgeon, S.K., Patton, R.J.: Sliding mode observers for fault detection and isolation. Automatica 36(4), 541–553 (2000)
36. Ferrara, A., Magnani, L.: Motion control of rigid robot manipulators via first and second order sliding modes. Journal of Intelligent and Robotic Systems 48(1), 23–36 (2007)
37. Frank, P.M.: Fault diagnosis in dynamic systems via state estimation - a survey. In: Tzafestas, Singh, Schmidt (eds.) System Fault Diagnostics, Reliability and Related Knowledge-based Approaches, pp. 35–98. Reidel Press, Dort (1987)
38. Fridman, L.M.: An averaging approach to chattering. IEEE Transactions on Automatic Control 46(8), 1260–1264 (2001)
39. Guldner, J., Utkin, V.I., Hashimoto, H., Harashima, F.: Obstacle avoidance in r^n based on artificial harmonic potential fields. In: Proc. IEEE Conference on Robotics and Automation, Nagoya, Aichi, Japan, vol. 3, pp. 3051–3056 (1995)
40. Hermans, F.J.J., Zarrop, M.B.: Sliding mode observers for robust sensor monitoring. In: Proc. 13th IFAC World Congress, San Francisco, California, USA, pp. 211–216 (1997)
41. Jafarov, E.M., Parlakçi, A.M.N., Istefanopulos, Y.: A new variable structure pid-controller design for robot manipulators. IEEE Transactions on Control Systems Technology 13(1), 122–130 (2000)
42. Juang, J.N., Eure, K.W.: Predictive feedback and feedforward control for systems with unknown disturbance. NASA/Tm-1998-208744 pp. 1–35 (1998)
43. Koivo, A.J.: Fundamentals for Control of Robotic Manipulators. Wiley & Sons, New York (1989)
44. Kreutz, K.: On manipulator control by exact linearization. IEEE Transactions on Automatic Control 34(7), 763–767 (1989)
45. Kuo, C.Y., Wang, S.P.T.: Nonlinear robust industrial robot control. Transactions of the ASME Journal of Dynamic Systems, Measurement and Control 111(1), 24–30 (1989)
46. Levant, A.: Sliding order and sliding accuracy in sliding mode control. International Journal of Control 58(6), 1247–1263 (1993)
47. Levant, A.: Robust exact differentiation via sliding mode technique. Automatica 34(3), 379–384 (1998)
48. Levant, A.: Variable measurement step in 2-sliding control. Kybernetika 36(1), 77–93 (2000)
49. Levant, A.: Homogeneity approach to high-order sliding mode design. Automatica 41(5), 823–830 (2005)
50. Liu, M.: Decentralized control of robot manipulators: Nonlinear and adaptive approaches. IEEE Transactions on Automatic Control 44(2), 357–363 (1999)
51. Mattone, R., De Luca, A.: Fault detection and isolation in mechanical systems. Tech. rep., Department of Computer and System Science, University of La Sapienza, Rome, Italy (2004)
52. Ortega, R., Spong, M.W.: Adaptive motion control of rigid robots: a tutorial. Automatica 25(6), 877–888 (1989)
53. Perk, J.S., Han, G.S., Ahn, H.S., Kim, D.H.: Adaptive approaches on the sliding mode control of robot manipulators. Transactions on Control, Automation and Systems Engineering 3(2), 15–20 (2001)
54. Pisu, P., Ferrara, A.: An observer-based second order sliding mode vehicle control strategy. In: Proc. IEEE 4th Intelligent Vehicles Symposium, Dearborn, Michigan, USA, pp. 180–185 (2000)
55. Pisu, P., Rizzoni, G.: A framework for model-based fault diagnosis with application to vehicle systems. In: Proc. 2nd IFAC Conference on Mechatronic Systems, Berkeley, California, USA (2002)

56. Pisu, P., Serrani, A., You, S., Jalics, L.: Adaptive threshold based diagnostics for steer-by-wire systems. ASME Transactions on Dynamics Systems, Measurement and Control 128(2), 428–435 (2006)
57. Poignet, P., Gautier, M.: Nonlinear model predictive control of a robot manipulator. In: Proc. 6th International Workshop on Advanced Motion Control, Nagoya, Japan, pp. 401–406 (2000)
58. Richalet, J., Abu, E., Ata-Doss, S., Arber, C.: Predictive functional control. application to fast and accurate robots. In: Proc. 10th IFAC World Congress, Munich, Germany, pp. 251–258 (1997)
59. Sarpturk, S.Z., Istefanopulos, Y., Kaynak, O.: On the stability of discrete-time sliding mode control systems. IEEE Transactions on Automatic Control 32(10), 930–932 (1987)
60. Sciavicco, L., Siciliano, B.: Modelling and Control of Robot Manipulators, 2nd edn. Springer, London (2000)
61. Shyu, K.K., Chu, P.H., Shang, L.J.: Control of rigid robot manipulators via combination of adaptive sliding mode control and compensated inverse dynamics approach. In: Proc. IEE Control Theory and Application, vol. 143, pp. 283–288 (1996)
62. Spong, M.W., Lewis, F.L., Abdallah, C.T.: Robot Control: Dynamics, Motion Planning, and Analysis. IEEE Press, Piscataway (1993)
63. Sreedhar, F., Fernández, B., Masada, G.Y.: Robust fault detection in nonlinear systems using sliding mode observers. In: Proc. IEEE Conference on Control Applications, Vancouver, British Columbia, Canada, vol. 2, pp. 715–721 (1993)
64. Tan, C.P., Edwards, C.: Sliding mode observers for detection and reconstruction of sensor faults. Automatica 38(10), 1815–1821 (2002)
65. Utkin, V.I.: Sliding modes in control and optimization. Springer, Berlin (1992)
66. Utkin, V.I., Drakunow, S.V.: On discrete-time sliding modes control. In: Preprints IFAC Conference on Nonlinear Control, Capri, Italy, pp. 484–489 (1989)
67. Utkin, V.I., Guldner, J., Shi, J.: Sliding Mode Control in Electromechanical Systems. Taylor & Francis, London (1999)

Chapter 21
Sliding Block Control of Electrical Machines (Motors and Generators)

Alexander G. Loukianov, Jose M. Cañedo,
B. Castillo-Toledo, and Edgar N. Sanchez

21.1 Introduction

The dynamics of the electric motors and generators (synchronous and induction) are highly nonlinear and content uncertainties including plant parameters variations magnetic saturation and external disturbances (load torque). On the other hand, the electric machine models are described by a class of nonlinear minimum phase systems which include the strict-feedback form or the nonlinear block controllable form (NBC-form) and stable residual stable. Therefore, in this case, to design a stabilized controller it is naturally to applied some feedback linearization (FL) technique: input-output (IO) linearization [9], backstepping (BS) [11] or block control (BC) ([13]- [15]). It is interesting to note that the BC approach has some advantage comparing with the IO and BS ones. This advantige can be shown by designing of a FL controller for the following second order triangular system:

$$\begin{aligned} \dot{x}_1 &= x_2 \\ \dot{x}_2 &= f_2(x_1, x_2) + u \end{aligned}$$

Applying the IO, BS and BC algorithms, respectively,

$$\begin{aligned} u_{IO} &= -f_2(x_1,x_2) - k_1 z_1 - k_2 z_2, && z_1 = x_1, \quad z_2 = x_2, \\ u_{BS} &= -f_2(x_1,x_2) - k_1(k_1 z_1 + z_2)x_2 - k_2 z_2 - z_1 && z_1 = x_1, \quad z_2 = x_2 + k_1 x_1, \\ u_{BC} &= -f_2(x_1,x_2) - k_1(k_1 z_1 + z_2) - k_2 z_2 && z_1 = x_1, \quad z_2 = x_2 + k_1 x_1 \end{aligned}$$

the matrices of the linearized closed-loop system

$$\dot{\mathbf{z}} = \mathbf{A}_i \mathbf{z}, \quad i = IO,\ BS,\ BC$$

Alexander G. Loukianov · Jose M. Cañedo · B. Castillo-Toledo · Edgar N. Sanchez
CINVESTAV- IPN, Unidad Guadalajara
A. P. 31-438,C.P. 44550, Guadalajara, Jal., México

L. Fridman et al. (Eds.): Sliding Modes, LNCIS 412, pp. 569–595.
springerlink.com

are as follows

$$\mathbf{A}_{IO} = \begin{bmatrix} 0 & 1 \\ -k_1 & -k_2 \end{bmatrix}, \mathbf{A}_{BS} = \begin{bmatrix} -k_1 & 1 \\ -1 & -k_2 \end{bmatrix}, \mathbf{A}_{BC} = \begin{bmatrix} -k_1 & 1 \\ 0 & -k_2 \end{bmatrix},$$

where $\mathbf{z} = (z_1, z_2)^T$, $k_1 > 0$ and $k_2 > 0$ are the controller gains. It easy to see that only in the BC controller case the controller gains $-k_1$ and $-k_2$ coincide with the eigenvalues of the closed-loop system matrix, that facilities to adjust these gains. Moreover, the eigenvalues of the matrix $\mathbf{A}_{BC}$ are real while the BS matrix $\mathbf{A}_{BS}$ has comlex eigenvalues.

However, the chief drawback of FL approaches is that, they rely on exact cancellation of non-linear terms in order to get linear behavior of the closed-loop system. Therefore, in the case of modelling errors it is useful to combine these approaches with the sliding mode (SM) control [23] which ensures robustness in a realistic setting of inexact models.

This chapter proposes the control schemes for the electric machines based on the combination of the block FL control and SM control techniques. For this propose, the chapter is organized as follows. In Section 21.2, the synchronous motor controller design based on the complete 7-th order plant model, is presented. Section 21.3 deals with electric power system (EPS) control. First, the block integral SM control approach is proposed for a class of nonlinear minimum phase MIMO systems presented in NBC- form with stable residual dynamics. Then, this approach is aplied to design a controller for multi machine EPS. Section 21.4 describes the block SM controller for an induction motor with saturation effect. Discrete time (DT) block SM controllers for an induction motor based on approximately and exactly discretized plant models are presented in Sections 21.5 and 21.6, respectively. Finally, Section 21.7 describes a neural network block DT SM controller for an induction motor.

21.2 Synchronous Motor SM Block Control

21.2.1 Plant Model

For the SM control, we use the complete dynamic model of a synchronous motor given in the rotor coordinate frame, the (d,q) coordinates, with stator current components i_q, i_d and rotor flux $\psi_{fd}, \psi_{kd}, \psi_{1q}, \psi_{2q}$ as state variables [19]

$$\dot{\mathbf{x}}_1 = \mathbf{f}_1(\mathbf{x}_1, \mathbf{x}_2) + \mathbf{B}_1\mathbf{u} + \mathbf{D}_1 w \tag{21.1}$$

$$\dot{\mathbf{x}}_2 = \mathbf{f}_2(\mathbf{x}_1, \mathbf{x}_2) \tag{21.2}$$

where $\mathbf{x} = (\mathbf{x}_1, \mathbf{x}_2)^T$, $\mathbf{x}_1 = (\omega_m, i_q, i_d, \psi_{fd})^T$, $\mathbf{x}_2 = (\psi_{kd}, \psi_{1q}, \psi_{2q})^T$,

$u = (V_q, V_d, V_{fd})^T$, ω_m is the angular velocity, $w = T_L$ is the load torque, i_q and i_d are the quadrature-axis stator and direct-axis currents; ψ_{fd} is the field flux; V_q, V_d and V_{fd} are the quadrature-axis and direct-axis stator voltages control inputs and the

excitation voltage control input, respectively; ψ_{kd}, ψ_{1q} and ψ_{2q} are the direct-axis and quadrature-axis damper windings fluxes, respectively;

$$\mathbf{f}_1 = \begin{bmatrix} f_1 \\ f_2 \\ f_3 \\ f_4 \end{bmatrix} = \begin{bmatrix} -a_{12} i_q i_d + a_{14} i_q \psi_{fd} + a_{15} i_q \psi_{kd} + a_{16} i_d \psi_{1q} + a_{17} i_d \psi_{2q} \\ -a_{21} \omega_m i_d - a_{22} i_q + \omega_m (a_{24} \psi_{fd} + a_{25} \psi_{kd}) + a_{26} \psi_{1q} + a_{27} \psi_{2q} \\ a_{31} \omega_m i_d - a_{33} i_d + a_{34} \psi_{fd} + a_{35} \psi_{kd} + \omega_m (a_{36} \psi_{1q} + a_{37} \psi_{2q}) \\ -a_{41} i_d - a_{44} \psi_{fd} + a_{45} \psi_{kd} \end{bmatrix},$$

$$\mathbf{f}_2 = \begin{bmatrix} -a_{53} i_d - a_{54} \psi_{fd} - a_{55} \psi_{kd} \\ -a_{62} i_q - a_{66} \psi_{1q} + a_{67} \psi_{2q} \\ -a_{72} i_q + a_{76} \psi_{fd} - a_{77} \psi_{2q} \end{bmatrix}, \mathbf{B}_1 = \begin{bmatrix} 0 & 0 & 0 \\ b_{21} & 0 & 0 \\ 0 & b_{32} & b_{33} \\ 0 & 0 & b_{43} \end{bmatrix}, \mathbf{D}_1 = \begin{bmatrix} -a_L \\ 0 \\ 0 \\ 0 \end{bmatrix}.$$

The control goal is to make the motor speed ω_m be equal to a reference signal ω_{ref}. Hence, the main control error can be defined as

$$\varepsilon_\omega = \omega_m - \omega_{ref}(t) \tag{21.3}$$

with the speed reference $\omega_{ref}(t)$. Having three control inputs V_q, V_d and V_{fd}, we can choose two additional outputs to be controlled: the flux ψ_{fd} in the winding excitation and the current i_d. Thus, we define the following auxiliary control errors:

$$\varepsilon_\psi = \psi_{fd} - \psi_{ref} \tag{21.4}$$

$$\varepsilon_d = i_d - i_{ref} \tag{21.5}$$

where ψ_{ref} and i_{ref} are, respectively, reference signals for the flux and the current. Because of the auxiliary control outputs ψ_{fd} and i_d have relative degree be equal to one while the main control output ω_m has relative degree two, first, the flux linkage ψ_{fd} control loop is designed, and then the current i_d control loop is formulated, and, finally, the speed ω_m control loop is designed, in order to simplify the control design and closed-loop stability analysis procedures.

21.2.2 The Flux Linkage ψ_{fd} Control Loop

Using (21.4) and (21.1) the dynamics for ε_ψ are derived as

$$\dot{\varepsilon}_\psi = f_4(\mathbf{x}_1, \mathbf{x}_2) + b_{43} V_{fd}.$$

Now, the control strategy of the form

$$V_{fd} = -U_{fd0} sign(\varepsilon_\psi),\ U_{fd0} > 0 \tag{21.6}$$

under the condition $U_{fd0} > \left| V_{fdeq} \right|$, $V_{fdeq} = -b_{43}^{-1} f_4(\mathbf{x}_1, \mathbf{x}_2)$ ensures that the error $\varepsilon_\psi(t)$ reaches zero in finite time t_{s1}.

Note that the voltage may be supplied by a separate converter with closed loop voltage control, thus underlining the characteristics of a low impedance voltage source. It would of course be possible also to substitute a control loop for the field current in order to eliminate the effect of changing field winding resistance due

temperature. The drive would then respond faster in the field winding range, but the damping effect by transient currents induced in the low impedance field circuit would be reduced.

21.2.3 The Current i_d Control Loop

Since in the absence of d-axis stator current there is no reluctance torque and only the q-axis reactance is involved in finding the terminal voltage, i.e. there is no direct magnetization or demagnetization of d-axis, only the field winding acts to produce flux in this direction, we choose the reference signal in (21.5) as $i_{ref} = 0$. For this situation, the field current in the d-axis and the stator current in the q-axis are 90° apart as is the case in the d.c. machine, that results in the following dynamics of ε_d after the time t_{s1} :

$$\dot{\varepsilon}_d = f_3(\mathbf{x}_1, \mathbf{x}_2) + b_{32} V_d + b_{33} V_{fdeq},\ V_{fdeq} = -b_{43}^{-1} f_2(\mathbf{x}_1, \mathbf{x}_2). \tag{21.7}$$

The following discontinuous control is selected:

$$V_d = -U_{d0} sign(\varepsilon_d),\ U_{d0} > 0. \tag{21.8}$$

It is known that the plant (21.1) is input-to-state stable. Therefore, during the time period $[0,\ t_{s1}]$ the closed-loop system (21.1) with the bounded controls (21.6) and (21.8), is stable. After this time we have (21.7). Hence, the SM stability condition for this case can be derived of the following form:

$$U_{d0} > \left| -b_{32}^{-1} [f_3(\mathbf{x}_1, \mathbf{x}_2) - b_{33} b_{43}^{-1} f_2(\mathbf{x}_1, \mathbf{x}_2)] \right|.$$

Under this condition the current i_d converges to zero in finite time t_{s2}, $t_{s2} > t_{s1}$.

21.2.4 The Speed ω_m Control Loop

After the time t_{s2}, the SM motion occurs on the manifold $\varepsilon_\psi = 0$ (21.4) and $\varepsilon_d = 0$ (21.5) yielding $\psi_{fd} = \psi_{ref}$ and $i_d = 0$. As result, the dynamics of ε_ω together with dynamics of i_q fit the NBS-form consisting of two blocks:

$$\begin{aligned} \frac{d\varepsilon_\omega}{dt} &= \bar{f}_1(T_L, t) + b_\omega(\mathbf{x}) i_q \\ \frac{di_q}{dt} &= \bar{f}_2(\mathbf{x}_1, \mathbf{x}_2) + b_{21} V_q \end{aligned}$$

where $\bar{f}_1(T_L, t) = a_L T_L - \omega_{ref}(t)$, $b_\omega = a_{14}\psi_{fd} + a_{15}\psi_{kd}$, $\bar{f}_2 = -a_{22} i_q + \omega_m(a_{24}\psi_{fd} + a_{25}\psi_{ref}) + a_{26}\psi_{1q} + a_{27}\psi_{2q}$.

To design a speed SM controller, first, exploring the block control (BC) technique a nonliear sliding manifold is formed as

$$s_q = i_q - i_q^* = 0, \quad i_q^* = b_\omega^{-1}(\mathbf{x})(\bar{f}_1 - c_1 \varepsilon_\omega),\ c_1 > 0. \tag{21.9}$$

Then, the proposed discontinuous control law is designed as

$$V_d = -U_{d0} sign(\varepsilon_d),\ U_{d0} > 0 \tag{21.10}$$

ensures the sliding manifold $s_q = 0$ (21.9) be attractive. A SM motion on this manifold is governed by first order linear system

$$\dot{\varepsilon}_\omega = -c_1 \varepsilon_\omega$$

with the desired eigenvalue $-c_1$.

A crucial property of the SM control (21.6), (21.8) and (21.10) when applied to (21.1) and (21.2) is that, it yields the invariant subspace $\{\xi = (0,0,0,0)^T,\ \mathbf{x}_2 \in R^3\}$ where $\xi = (\varepsilon_\omega, s_q, \varepsilon_d, \varepsilon_\psi)^T$. The dynamics of $\mathbf{x}_2$ on this invariant subspace are referred to as the *zero dynamics*. To derive these dynamics, the vector $\mathbf{x}_1$ in (21.2) is changed by $\xi = \varphi(\mathbf{x}) : \dot{\mathbf{x}}_2 = \bar{\mathbf{f}}_2(\xi, \mathbf{x}_2, \omega_{ref}, \psi_{ref}, T_L)$ where mapping φ is defined by (21.3)-(21.5) and (21.9). Then the vector ξ is zeroed resulting in

$$\dot{\mathbf{x}}_2 = \bar{\mathbf{f}}_2(0, \mathbf{x}_2, \omega_{ref}, \psi_{ref}, T_L).$$

An equilibrium point for this system defined by ω_{ref}, ψ_{ref} and the value of the load torque T_L is asymptotically stable providing the system 8) and() is minimum phase.

The detailed controller scheme including the rotor flux observer design and simulation results can be found in [19].

21.3 The Synchronous Generator Control

21.3.1 Plant Model

The synchronous generator (multi machine power system) state space model is given by the following differential algebraic equation [7]:

$$\begin{bmatrix} \dot{\mathbf{x}}_{1i} \\ \dot{\mathbf{x}}_{2i} \end{bmatrix} = \begin{bmatrix} \mathbf{f}_{1i}(\mathbf{x}_i, \mathbf{i}_i) \\ \mathbf{f}_{2i}(\mathbf{x}_i, \mathbf{i}_i) \end{bmatrix} + \begin{bmatrix} \mathbf{b}_{1i} \\ \mathbf{0} \end{bmatrix} \upsilon_{fi} + \begin{bmatrix} \mathbf{g}_{1i}(\mathbf{x}_i, \mathbf{i}_i, T_{mi}) \\ \mathbf{0} \end{bmatrix} \tag{21.11}$$

$$\mathbf{i}_i = \mathbf{A}_{3i}^{-1}(x_{2i})[\mathbf{f}_{3i}(\mathbf{x}_i) + \mathbf{H}_i \mathbf{V}_i] \tag{21.12}$$

where $\mathbf{x}_i = (\mathbf{x}_{1i}, \mathbf{x}_{2i})^T$, $\mathbf{x}_{1i} = (x_{1i}, x_{2i}, x_{3i})^T = (\delta_i, \omega_i, \psi_{fi})^T$; $\mathbf{x}_{2i} = (x_{4i}, x_{5i}, x_{6i})^T = (\psi_{gi}, \psi_{kdi}, \psi_{kqi})^T$, $\mathbf{i}_i = (i_q, i_d)^T$, $\mathbf{V}_i = (V_{di}, V_{qi})^T$, δ_i is the relative power angle with respect to the first generator; ω_i is the angular speed; ω_b is the reference speed, T_{mi} is the mechanical torque; ψ_{fi}, ψ_{gi}, ψ_{kdi} and ψ_{kqi} are the field flux, the direct-axis and quadrature-axis damper windings fluxes, respectively; i_{di} and i_{qi} are the direct-axis and quadrature-axis stator currents, respectively; υ_{fi} is the generator excitation voltage (control input); V_{di} and V_{qi} are the quadrature-axis and direct-axis stator voltages;

$$\mathbf{f}_{1i}=\begin{bmatrix} x_{2i}-\omega_b \\ f_{2i,nom}(\mathbf{x}_i,\mathbf{i}_i)-q_{2i}(\mathbf{i}_i)x_{3i} \\ f_{3i}(\mathbf{x}_i,\mathbf{i}_i)\end{bmatrix},\ \mathbf{b}_{1i}=\begin{bmatrix}0\\0\\b_{4i}\end{bmatrix},$$
$$f_{2i,nom}(\cdot)=a_{2i}x_{4i}i_{di}+a_{3i}x_{5i}i_{qi}-a_{4i}x_{6i}i_{di}+a_{5i}i_{di}i_{qi},\ q_{2i}(\mathbf{i}_i)=a_{1i}i_{qi},$$
$$\mathbf{g}_{1i}(\mathbf{x}_i,\mathbf{i}_i)=(0,g_{2i}(\mathbf{x}_i,\mathbf{i}_i,T_{mi}),0)^T,\ f_{3i}(\mathbf{x}_i,\mathbf{i}_i)=-b_{1i}x_{3i}+b_{2i}x_5-b_{3i}i_{di},$$
$$\mathbf{f}_{2i}(\mathbf{x}_i,\mathbf{i}_i)=\mathbf{A}_{2i}\mathbf{x}_{2i}+\mathbf{d}_{1i}x_{3i}+\mathbf{D}_i\mathbf{i}_i,$$
$$\mathbf{A}_{2i}=\begin{bmatrix}c_{1i}&0&c_{2i}\\0&d_{2i}&0\\r_{2i}&0&r_{2i}\end{bmatrix},\ \mathbf{d}_{1i}=\begin{bmatrix}0\\d_{1i}\\1\end{bmatrix},\ \mathbf{D}_i=\begin{bmatrix}0&c_{3i}\\d_{3i}&0\\0&e_{3i}\end{bmatrix},\ \mathbf{A}_{3i}=\begin{bmatrix}h_{7i}&k_{6i}x_{2i}\\h_{6i}x_{2i}&k_{7i}\end{bmatrix},\ \mathbf{H}_i=$$
$$\begin{bmatrix}h_{1i}&0\\0&k_{1i}\end{bmatrix},\ \mathbf{f}_{3i}=\begin{bmatrix}h_{2i}x_{3i}+h_{3i}x_{5i}+h_{4i}x_{2i}x_{4i}+h_{5i}x_{2i}x_{6i}\\k_{2i}x_{4i}+k_{3i}x_{6i}+k_{4i}x_{2i}x_{3i}+k_{5i}x_{2i}x_{5i}\end{bmatrix}.$$

The unmatched perturbation term $g_{2i}(\mathbf{x}_i,\mathbf{i}_i)$ includes parameters variations, and the mechanical torque T_{mi} (external disturbance), i. e. $g_{2i}(\cdot)=d_{mi}T_{mi}-(\Delta a_{2i}x_{4i}i_{di}+\Delta a_{3i}x_{5i}i_{qi}-\Delta a_{4i}x_{6i}i_{di}+\Delta a_{15}i_{di}i_{qi})$, $a_{ji}=a_{ji,nom}+\Delta a_{ji}$, $j=2,...,5$; where $a_{ji,nom}$ and Δa_{ji} are the nominal value and variation, respectively, of the parameter a_{ji}. Moreover $\mathbf{A}_{3i}$ is a Hurwitz matrix.

21.3.2 The Idea of Block Integral SM Controllers

In this Subsection, the method and underlying ideas are described in generic terms to show the generality of our approach which will be applied to generator control. Consider a class of nonlinear MIMO system presented (possibly after a nonlinear transformation) in the nonlinear BC form consisting of r blocks subject to uncertainties

$$\dot{\mathbf{x}}_i=\mathbf{f}_i(\bar{\mathbf{x}}_i)+\mathbf{B}_i(\bar{\mathbf{x}}_i)\mathbf{x}_{i+1}+\mathbf{g}_i(\bar{\mathbf{x}}_i,\mathbf{x}_{r+1},t),\quad i=1,\dots,r-1 \tag{21.13}$$
$$\dot{\mathbf{x}}_r=\mathbf{f}_r(\bar{\mathbf{x}}_r,\bar{\mathbf{x}}_{r+1})+\mathbf{B}_r(\bar{\mathbf{x}}_r,\mathbf{x}_{r+1})\mathbf{u}+\mathbf{g}_r(\bar{\mathbf{x}}_r,\mathbf{x}_{r+1},t)$$
$$\dot{\mathbf{x}}_{r+1}=\mathbf{f}_{r+1}(\bar{\mathbf{x}}_r,\mathbf{x}_{r+1},t) \tag{21.14}$$
$$\mathbf{y}=\mathbf{x}_1 \tag{21.15}$$

where the state vector $\mathbf{x}\in\mathbf{R}^n$ is decomposed as $\mathbf{x}=(\mathbf{x}_1,\dots,\mathbf{x}_r,\mathbf{x}_{r+1})^T=(\bar{\mathbf{x}}_r,\mathbf{x}_{r+1})^T$, $\bar{\mathbf{x}}_i=(\mathbf{x}_1,\dots,\mathbf{x}_i)^T$, $i=1,\dots,r$; $\mathbf{u}\in\mathbf{R}^m$; $\mathbf{f}_i(\cdot)$ and $\mathbf{B}_i(\cdot)$ are known sufficiently smooth functions of their arguments, $\mathbf{g}_i(\cdot)$ is an uncertain but bounded function, and $rank\mathbf{B}_i(\cdot)=n_i$ over the set $D_1\times D_2$:

$$D_1=\left\{\bar{\mathbf{x}}_r\in\mathbf{R}^{\bar{n}_r}\mid\|\bar{\mathbf{x}}_r\|_2\le r_1,\ \ r_1>0\right\}r_1 \tag{21.16}$$
$$D_2=\left\{\mathbf{x}_{r+1}\in\mathbf{R}^{n-r}\mid\|\bar{\mathbf{x}}_{r+1}\|_2\le r_2,\ \ r_2>0\right\} \tag{21.17}$$

$n_1\le n_2\le\dots\le n_r=m$, $\sum_{i=1}^{r}n_i=\bar{n}_r$, $\bar{n}_r+n_{r+1}=n$. Suppose

A1) The set

$$\|\mathbf{x}_{r+1}\|_2\le d_0<r_2,\ \ d_0>0 \tag{21.18}$$

is uniformly attractive with respect to the set D_2 , i.e. for any solution to the system

$$\dot{\mathbf{x}}_{r+1} = \mathbf{f}_{r+1}(0, \mathbf{x}_{r+1}, t) \tag{21.19}$$

describing zero dynamics in (21.13)-(21.15) with any initial conditions from D_2 there exists T such that for all $t > T$ we will have $\|\mathbf{x}_{r+1}(t)\|_2 \leq d_0$.

The control problem is to determine a controller such that the output $\mathbf{y}$ in (21.13)-(21.15) tracks a desired reference $\mathbf{y}_{ref}$ with bounded derivatives, in spite of the presence of unknown bounded perturbations. To induce quasi sliding mode in the each block of the system (21.13)-(21.15), the continuously differentiable sigmoid function $sigm\left(\frac{s}{\gamma}\right)$ defined as

$$sigm\left(\frac{s}{\gamma}\right) = \tanh\left(\frac{s}{\gamma}\right), \ \tanh\left(\frac{s}{\gamma}\right) = \frac{e^{\frac{s}{\gamma}} - e^{-\frac{s}{\gamma}}}{e^{\frac{s}{\gamma}} + e^{-\frac{s}{\gamma}}}$$

where $\frac{1}{\gamma}$ is the slope of the sigmoid function at $s = 0$, will be used since $\lim_{\gamma \to 0} sigm\left(\frac{s}{\gamma}\right) = sigm\left(\frac{s}{\gamma}\right)$.

Remark 21.1. The class of nonlinear systems (21.13)-(21.15) is more general than the considered one in ([13]- [15]), since the perturbation term $\mathbf{g}_i(\cdot)$, depends also on the state vector $\mathbf{x}_{r+1}$.

Defining the control error as

$$\mathbf{z}_1 = \mathbf{y} - \mathbf{y}_{ref} = \mathbf{x}_1 - \mathbf{y}_{ref}$$

where $\mathbf{y}_{ref}$ is a reference signal. Then, designing the following BC linearized transformation:

$$\begin{aligned} \mathbf{z}_{i+1} &= \bar{\mathbf{B}}_i(\bar{\mathbf{x}}_i)\mathbf{x}_{i+1} + \begin{bmatrix} \tilde{\mathbf{f}}_i(\bar{\mathbf{x}}_i) - k_i\varphi_i(\bar{\mathbf{x}}_i) - \rho_i \mathbf{sigm}\left(\frac{\mathbf{s}_i}{\gamma_i}\right) \\ 0 \end{bmatrix} \equiv \varphi_i(\bar{\mathbf{x}}_{i+1}) \\ \mathbf{s}_i &= \mathbf{z}_i + \sigma_i \\ \dot{\sigma}_i &= k_i\mathbf{z}_i - \mathbf{E}_i\mathbf{z}_{i+1}, \ \sigma_i(0) = -\mathbf{z}_i(0), \ k_i > 0, \ i = 1, ..., r-1 \end{aligned} \tag{21.20}$$

and the control law

$$\begin{aligned} \mathbf{u} &= -\rho_0\bar{\mathbf{B}}_r^{-1}\mathbf{sign}(\mathbf{s}_r) - \bar{\mathbf{B}}_r^{-1}\left[\tilde{\mathbf{f}}_r(\bar{\mathbf{z}}_r, \mathbf{x}_{r+1}) - k_r\mathbf{z}_r\right], \ \rho_0 > 0, \ k_r > 0 \\ \mathbf{s}_r &= \mathbf{z}_r + \sigma_r \\ \dot{\sigma}_r &= k_r\mathbf{z}_r, \ \sigma_r(0) = -\mathbf{z}_r(0) \end{aligned} \tag{21.21}$$

the closed-loop system (21.13)-(21.14) with (21.21) becomes of the form

$$\dot{\mathbf{z}}_i = -k_i\mathbf{z}_i + \mathbf{E}_i\mathbf{z}_{i+1} - \rho_i \mathbf{sigm}\left(\frac{\mathbf{s}_i}{\gamma_i}\right) + \tilde{\mathbf{g}}_i(\bar{\mathbf{z}}_i, \mathbf{x}_{r+1}, t) \tag{21.22}$$

$$\dot{\mathbf{s}}_i = -\rho_i \mathbf{sigm}\left(\frac{\mathbf{s}_i}{\gamma_i}\right) + \tilde{\mathbf{g}}_i(\bar{\mathbf{z}}_i, \mathbf{x}_{r+1}, t), \quad i = 1, \ldots, r-1 \tag{21.23}$$

$$\dot{\mathbf{z}}_r = -k_r\mathbf{z}_r - \rho_0 \mathbf{sign}(\mathbf{s}_r) + \tilde{\mathbf{g}}_r(\bar{\mathbf{z}}_r, \mathbf{x}_{r+1}, t) \tag{21.24}$$

$$\dot{\mathbf{s}}_r = -\rho_0 \mathbf{sign}(\mathbf{s}_r) + \tilde{\mathbf{g}}_r(\bar{\mathbf{z}}_r, \mathbf{x}_{r+1}, t) \tag{21.25}$$

$$\dot{\mathbf{x}}_{r+1} = \mathbf{f}_{r+1}(\bar{\mathbf{z}}_r, \mathbf{x}_{r+1}, t) \tag{21.26}$$

where $\mathbf{z}_i = (\mathbf{z}_1, \ldots, \mathbf{z}_r)^T$, $\bar{\mathbf{z}}_i = (\mathbf{z}_1, \ldots, \mathbf{z}_i)^T$, $i = 1, \ldots, r$; $k_i > 0$, $\rho_i > 0$, $\gamma_i > 0$, $i = 1, \ldots, r$ and $\bar{\mathbf{B}}_i = \mathbf{B}_1\mathbf{B}_2 \cdots \mathbf{B}_i$.

Theorem 21.1. *If assumption A1 holds then a solution of the closed-loop system (21.22)- (21.26) under the following condition:*

$$\rho_i > \|\tilde{\mathbf{g}}_i(\bar{\mathbf{z}}_i, \mathbf{x}_{r+1}t,)\|, \quad i = 1, \ldots, r-1$$
$$\rho_0 > \|\tilde{\mathbf{g}}_r(\bar{\mathbf{z}}_r, \mathbf{x}_{r+1}, t)\|$$

is uniformly ultimately bounded, i.e.

$$\limsup_{t\to\infty} \|\mathbf{z}_i(t)\| \leq h_i, \; i = 1, ..., r-1$$
$$\limsup_{t\to\infty} \|\mathbf{x}_{r+1}(t)\| \leq h_{r+1}, \; i = 1, ..., r-1.$$

In the following we present the application of the proposed method to control the electric power system.

21.3.3 Block Integral SM Speed Stabilizer

Note that the first part of the generator dynamic model (21.11) has the NBC-form (21.13)-(21.15) while the second part presents the stable residual dynamics. Therefore, to achieve the first control objective, that is, the rotor speed stability enhancement, we applied the control method described in Subsection 21.3.2. Define the control error as

$$z_{2i} = x_{2i} - \omega_b \equiv \varphi_{2i}(x_{2i}). \tag{21.27}$$

Using the first subsystem in (21.11) and then (21.27), straightforward calculations result in

$$\dot{z}_{1i} = z_{2i} \tag{21.28}$$

$$\dot{z}_{2i} = f_{2i,nom}(\mathbf{x}_i, \mathbf{i}_i) - q_{2i}(\mathbf{i}_i)x_{3i} + g_{2i}(\mathbf{x}_i, \mathbf{i}_i, T_{mi}) \tag{21.29}$$

$$\dot{x}_{3i} = f_{3i}(\mathbf{x}_{2i}) + b_{4i}\upsilon_{fi} \tag{21.30}$$

where $z_{1i} = x_{1i} \equiv \varphi_{1i}(x_{1i})$. The change of variables (21.20) takes the form

$$x_{3i} = q_i^{-1}(\mathbf{i}_i)[f_{i,nom}(\mathbf{x}_i, \mathbf{i}_i, T_{mi}) + k_{2i}z_{2i} - z_{3i}] + \rho_{2i} sigm\left(\frac{s_{2i}}{\gamma_{2i}}\right) \tag{21.31}$$

$$s_{2i} = z_{2i} + \sigma_{2i} \tag{21.32}$$

$$\dot{\sigma}_{2i} = -k_{2i}z_{2i} + z_{3i} \tag{21.33}$$

where z_3 is a new variable, the term $-k_{2i}z_{2i}$ presents the desired dynamics for the control error z_2, $k_2 > 0$, and the term $\rho_i sigm\left(\frac{s_{2i}}{\gamma_{2i}}\right)$ is designed to reject the perturbation $g_{2i}(\mathbf{x}_i, \mathbf{i}_i, T_{mi})$ in (21.29); s_{2i} is a quasi sliding variable and σ_{2i} is an integral variable defined by (21.33). Now, the new variable z_{3i} can be defined from (21.31) as

$$z_{3i} = q_i(\mathbf{i}_i)x_{3i} + f_{i,nom}(\mathbf{x}_i, \mathbf{i}_i) + k_{2i}(x_{2i} - \omega_b) \equiv \varphi_{3i}(\mathbf{x}_i, \mathbf{i}_i). \tag{21.34}$$

Using (21.34) and (21.28) - (21.30), the dynamics for z_{3i} are derived of the form

$$\dot{z}_{3i} = \bar{f}_{3i}(\mathbf{x}_i, \mathbf{i}_i) - q_{3i}(\mathbf{i}_i)\upsilon_{fi} + g_{3i}(\mathbf{x}_i, \mathbf{i}_i, T_{mi})$$

where $\bar{f}z_{3i3i}(\cdot) = \frac{\partial \varphi_{3i}}{\partial \mathbf{x}_{1i}}\mathbf{f}_{1i}(\mathbf{x}_{1i}, \mathbf{x}_{i2}) + \frac{\partial \varphi_{3i}}{\partial \mathbf{x}_{2i}}\mathbf{f}_{2i}(\mathbf{x}_{1i}, \mathbf{x}_{2i})$ is a continuous function, $q_{3i}(\cdot) = q_{2i}(\cdot)b_{4i}$, and $q_{3i}(t)$ is a positive function of the time. To reject the perturbation $g_{3i}(\mathbf{x}_i, \mathbf{i}_i, T_{mi})$ and induce the desired dynamics $(-k_{3i}z_{3i},\ k_{3i} > 0)$ for z_{3i} the excitation control υ_{fi} is chosen similar to (21.21):

$$\upsilon_{fi} = q_{3i}^{-1}(\mathbf{i}_i)[\bar{f}_{3i}(\mathbf{x}_i, \mathbf{i}_i) + k_{3i}z_{3i}] + \rho_{3i} sign\,(s_{3i}) \tag{21.35}$$

$$s_{3i} = z_{3i} + \sigma_{3i} \tag{21.36}$$

$$\dot{\sigma}_{3i} = k_{3i}z_{3i}. \tag{21.37}$$

Then, the system (21.28) - (21.30) with (21.34)-(21.37) can be represented of the form

$$\dot{z}_{1i} = z_{2i} \tag{21.38}$$

$$\dot{z}_{2i} = -k_{2i}z_{2i} + z_{3i} - \rho_{2i}q_{2i}(\mathbf{i}_i) sigm\left(\frac{s_{2i}}{\gamma_{2i}}\right) + g_{2i}(\mathbf{x}_i, \mathbf{i}_i, T_{mi}) \tag{21.39}$$

$$\dot{s}_{2i} = -\rho_{2i}q_{2i}(\mathbf{i}_i) sigm\left(\frac{s_{2i}}{\gamma_{2i}}\right) + g_{2i}(\mathbf{x}_i, \mathbf{i}_i, T_{mi}) \tag{21.40}$$

$$\dot{z}_{3i} = -k_{3i}z_{3i} - \rho_{3i}q_{3i}(\mathbf{i}_i) sign\,(s_{3i}) + g_{3i}(\mathbf{x}_i, \mathbf{i}_i, T_{mi}) \tag{21.41}$$

$$\dot{s}_{3i} = -\rho_{3i}q_{3i}(\mathbf{i}_i) sign\,(s_{3i}) + g_{3i}(\mathbf{x}_i, \mathbf{i}_i, T_{mi}). \tag{21.42}$$

Under the condition

$$\rho_{3i}q_{3i} > |g_{3i}(\mathbf{x}_i, \mathbf{i}_i, T_{mi})| \tag{21.43}$$

$$\rho_{2i}q_{2i} > |g_{2i}(\mathbf{x}_i, \mathbf{i}_i, T_{mi})| \tag{21.44}$$

the state vector of the closed-loop system (21.38) - (21.42) converges to the set

$$s_{3i} = 0, \quad s_{2i} = 0 \tag{21.45}$$

in finite time, and sliding mode starts on (21.45) from this time. The conditions (21.43) and (21.44) defines the closed-loop system stability region and obviously holds for all the possible values of T_{mi}. The sliding motion on (21.45) is described by the unperturbed SM equation

$$\dot{z}_{1i} = z_{2i} \tag{21.46}$$
$$\dot{z}_{2i} = -k_{2i}z_{2i} + z_{3i} \tag{21.47}$$
$$\dot{z}_{3i} = -k_{3i}z_{3i} \tag{21.48}$$
$$\dot{\mathbf{x}}_{2i} = \mathbf{f}_{2i}(z_{1i}, z_{2i}, z_{3i}, \mathbf{x}_{2i}, \mathbf{i}_i, \omega_b) \tag{21.49}$$

with desired eigenvalues $-k_{2i}$ and $-k_{3i}$.

Note that sliding mode dynamics (21.46)-(21.49) can be considered as particular case of the SM equation (21.22)- (21.26) while the internal dynamics (21.49) reduce on the space $\{z_{1i} = \delta_{ssi},\ z_{2i} = 0,\ z_{3i} = 0,\ \mathbf{x}_{2i} \in \mathbf{R}^{3N}\}$ to the asymptotically stable zero dynamics due to the matrix $\mathbf{A}_{2i}$ is Hurwitz. Hence, a solution of (21.46)-(21.49) by Theorem 21.1 is ultimately bounded and, moreover, the control error $z_{2i}(t)$ (21.27) converges exponentially to zero.

21.3.4 SM Voltage Regulator

The second control objective is to regulate the terminal voltage, V_{gi}, defined as

$$V_{gi}^2 = V_{di}^2 + V_{qi}^2. \tag{21.50}$$

Using (21.12) we have

$$\mathbf{V}_i = \begin{bmatrix} V_{di} \\ V_{qi} \end{bmatrix} = \mathbf{H}_i^{-1}\mathbf{A}_{3i}(x_{2i})\mathbf{i}_i + \mathbf{f}_{3i}(\mathbf{x}_i, \mathbf{i}_i) + \mathbf{H}_i\mathbf{V}_i] \tag{21.51}$$

Then, the dynamics for terminal voltage can be obtained from (21.50), (21.51), (21.11) and (21.12) as

$$\dot{V}_{gi} = f_{vi}(\mathbf{x}_i, \mathbf{i}_i) + b_{vi}(\mathbf{x}_i, \mathbf{i}_i)\upsilon_{fi} + g_{vi}(\mathbf{x}_i, \mathbf{i}_i, T_{mi}) \tag{21.52}$$

where $f_{vi}(\mathbf{x}_i, \mathbf{i}_i)$ is a continuous function while the term $g_{vi}(\mathbf{x}_i, \mathbf{i}_i, T_{mi})$ contains parameter variations and external disturbance T_{mi}, $b_{vi}(t) > 0$ for all $t \geq 0$. Defining the voltage regulation error as

$$\varepsilon_{gi} = V_{gi} - V_{refi} \tag{21.53}$$

we design the excitation control υ_{fi} of the form

$$\upsilon_{fi} = b_{vi}^{-1}(\mathbf{x}_i, \mathbf{i}_i)\left[f_{vi}(\mathbf{x}_i, \mathbf{i}_i) - k_{gi}\varepsilon_{gi}\right] - \rho_v sign(s_{vi}),\ k_{gi} > 0,\ \rho_v > 0 \tag{21.54}$$
$$s_{vi} = \varepsilon_{vi} + \sigma_{vi}$$
$$\dot{\sigma}_{vi} = k_{gi}\varepsilon_{gi}.$$

Then, the closed-loop system (21.53), (21.52) with (21.54) becomes

$$\begin{aligned}\dot{\varepsilon}_{gi} &= -k_{gi}\varepsilon_{gi} - \rho_v b_{vi}(\mathbf{x}_i, \mathbf{i}_i) sign(s_{vi}) + g_{vi}(\mathbf{x}_i, \mathbf{i}_i, T_{mi}) \\ \dot{s}_{vi} &= -\rho_v b_{vi}(\mathbf{x}_i, \mathbf{i}_i) sign(s_{vi}) + g_{vi}(\mathbf{x}_i, \mathbf{i}_i, T_{mi}).\end{aligned}$$

If the condition

$$\rho_v b_{vi} > |g_{vi}(\mathbf{x}_i, \mathbf{i}_i, T_{mi})|$$

holds then a SM motion occurs on the manifold $s_{vi} = 0$ on which we have

$$-\rho_v b_{vi}(\mathbf{x}_i, \mathbf{i}_i) sign(s_{vi}) + g_{vi}(\mathbf{x}_i, \mathbf{i}_i, T_{mi}) = 0$$

resulting in the following desired SM equation:

$$\dot{\varepsilon}_{gi} = -k_{gi}\varepsilon_{gi},\ k_{gi} > 0$$

which is asymptotically stable.

21.3.5 Control Switching Logic

Having just one control input υ_{fi} in each generator for two outputs ω_i and V_{gi}, the control strategy is formulated finally as

$$\upsilon_{fi} = \begin{cases} q_{3i}^{-1}(\mathbf{i}_i)[f_{3i} + k_{3i} z_{3i}] + \rho_{3i} sign\,(s_{3i}) & if\ |s_{3i}| > e_i \\ b_{vi}^{-1}(\mathbf{x}_i, \mathbf{i}_i)\,[f_{vi}(\mathbf{x}_i, \mathbf{i}_i) - k_{gi}\varepsilon_{gi}] - \rho_v sign(s_{vi}) & if\ |s_{3i}| \le e_i \end{cases}$$

$$e_i = \begin{cases} e_{1i}\ if\ |s_{vi}| > e_{3i} \\ e_{2i}\ if\ |s_{vi}| \le e_{3i} \end{cases}$$

with $e_{2i} < e_{3i}$. Therefore, we propose a hierarchical control action through the proposed logic (56). Since the mechanical dynamics are slower than the electrical ones, we spend the control resources, at first, to stabilize s_{3i}. When s_{3i} reaches the boundary layer with width e_{1i}, the control resources will be spending to stabilize s_{vi}. After s_{vi} convergence of such that $|s_{vi}| < e_{3i}$, the control action reduces the s_{3i} boundary layer width from e_{1i} to e_{2i}. Thus, the controller maintains the value of s_{3i} within desired accuracy $|s_{3i}| \le e_{2i}$ and $|s_{vi}| \le e_{3i}$.

21.4 Induction Motor with Magnetic Saturation Control

It is known that the magnetic saturation effect, allowing an induction motor to produce higher torque, can cause a bad performance of the dynamic response of the motor, if it is not taken into account in controller design. Most of studies concerning the saturation effect tried to find special models with varying parameters We present an extended order model of the motor with constant parameters. Based on this model, and applying the SM and BC techniques, a discontinuous observed based control law can be derived.

21.4.1 Mathematical Model of Induction Motor with Saturation

To include the saturation effect in the motor model, we approximate this curve with a function $f(\lambda_m)= \lambda_m^3$. The established saturated model can be described by the mechanical equation

$$\begin{aligned}
\frac{dw_r}{dt} &= c_1(c_2(\lambda_\alpha i_\beta - \lambda_\beta i_\alpha) - T_L)\\
\frac{d\lambda_\alpha}{dt} &= -n_p w_r \lambda_\beta - c_3(\lambda_\alpha - \lambda_{m\alpha})\\
\frac{d\lambda_\beta}{dt} &= -n_p w_r \lambda_\alpha - c_3(\lambda_\beta - \lambda_{m\beta})\\
\frac{di_\alpha}{dt} &= c_{71} w_r \lambda_\beta + c_{81}\lambda_\alpha - c_{81}\lambda_{m\alpha} - (c_{91} - c_5) i_\alpha + (c_4 - c_{61}) V_\alpha\\
\frac{di_\beta}{dt} &= -c_{72} w_r \lambda_\alpha + c_{82}\lambda_\beta - c_{82}\lambda_{m\beta} + (c_{92} - c_5) i_\alpha + (c_4 - c_{62}) V_\beta\\
\frac{d\lambda_{m\alpha}}{dt} &= L_s\left(-c_{71} w_r \lambda_\beta - c_{81}\lambda_\alpha + c_{81}\lambda_{m\alpha} - c_{91} i_\alpha + c_{61} V_\alpha\right)\\
\frac{d\lambda_{m\beta}}{dt} &= L_s\left(c_{72} w_r \lambda_\alpha - c_{82}\lambda_\beta + c_{82}\lambda_{m\beta} - c_{92} i_\alpha + c_{62} V_\beta\right)
\end{aligned} \tag{21.55}$$

where w_r is the rotor velocity, λ_α and λ_β are the rotor magnetic fluxes; $\lambda_{m\alpha}$ and $\lambda_{m\beta}$ are the magnetizing fluxes; i_α and i_β are the stator currents; u_α and u_β are the stator voltages; T_L is the load torque, $c_1 = \frac{1}{J_r}$, $c_2 = \frac{3n_pM}{2L_r}$, $c_2 = \frac{R_r}{L_r}$, $c_4 = \frac{1}{L_s}$, $c_5 = \frac{R_s}{L_s}$, $c_{61} = \frac{M}{d_1 L_s^2}$, $c_{61} = \frac{M}{d_2 L_s^2}$, $c_{71} = \frac{n_pM}{d_1 L_s L_s}$, $c_{72} = \frac{n_pM}{d_2 L_s L_s}$, $c_{81} = \frac{MR_r}{d_1 L_r^2 L_s}$, $c_{82} = \frac{MR_r}{d_2 L_r^2 L_s}$, $c_{91} = \frac{MR_s}{d_1 L_s^2}$, $c_{92} = \frac{MR_s}{d_2 L_s^2}$, $d_1 = 1 + \frac{M}{L_s} + \frac{M}{L_r} + 3c\lambda_{m\alpha}^2$, $d_2 = 1 + \frac{M}{L_s} + \frac{M}{L_r} + 3c\lambda_{m\beta}^2$.

Let us define the control errors as

$$\mathbf{x}_1 = \begin{bmatrix} x_1 \\ x_2 \end{bmatrix} = \begin{bmatrix} \omega_r - \omega_{ref}(t) \\ \varphi - \varphi_{ref}(t) \end{bmatrix},\ \mathbf{x}_2 = \begin{bmatrix} x_3 \\ x_4 \end{bmatrix} = \begin{bmatrix} i_\alpha \\ i_\beta \end{bmatrix},\ \mathbf{x}_3 = \begin{bmatrix} x_5 \\ x_6 \end{bmatrix} = \begin{bmatrix} \lambda_{m\alpha} \\ \lambda_{m\beta} \end{bmatrix}$$

where $\varphi = (\lambda_\alpha\ \lambda_\beta)^T(\lambda_\alpha\ \lambda_\beta)$ is the flux square module, $\omega_{ref}(t)$ and $\varphi_{ref}(t)$ are reference signals. Then the system (21.55) can be represented in quasi NBC-form with perturbation and residual ynamics:

$$\dot{\mathbf{x}}_1 = \mathbf{f}_1(\mathbf{x}_1) + \mathbf{B}_1(\mathbf{x}_1)\begin{bmatrix} \mathbf{x}_2 \\ \mathbf{x}_3 \end{bmatrix} - \mathbf{d}_1 T_L - \mathbf{w}_1(t) \tag{21.56}$$

$$\begin{bmatrix} \dot{\mathbf{x}}_2 \\ \dot{\mathbf{x}}_3 \end{bmatrix} = \begin{bmatrix} \mathbf{f}_2(\mathbf{x}) \\ \mathbf{f}_3(\mathbf{x}) \end{bmatrix} + \begin{bmatrix} \mathbf{B}_2 \\ \mathbf{B}_3 \end{bmatrix}\mathbf{u} \tag{21.57}$$

where $\mathbf{x} = (\mathbf{x}_1, \mathbf{x}_2, \mathbf{x}_3)^T$, $\mathbf{w}_1 = (\dot{\omega}_{ref}(t), \dot{\varphi}_{ref}(t))^T$, $\mathbf{u} = (u_\alpha, u_\beta)^T$, $\mathbf{f}_1 = \begin{bmatrix} f_1 \\ f_2 \end{bmatrix} = \begin{bmatrix} 0 \\ 2c_3\varphi \end{bmatrix}$,

$$\mathbf{B}_1 = \begin{bmatrix} -c_1c_2\lambda_\beta & c_1c_2\lambda_\alpha & 0 & 0 \\ 0 & 0 & 2c_3\lambda_\alpha & 2c_3\lambda_\beta \end{bmatrix},$$

$$\mathbf{f}_2 = \begin{bmatrix} f_3 \\ f_4 \end{bmatrix} = \begin{bmatrix} c_{71} w_r \lambda_\beta + c_{81}\lambda_\alpha - c_{81}\lambda_{m\alpha} - (c_{91} - c_5) i_\alpha \\ -c_{72} w_r \lambda_\alpha + c_{82}\lambda_\beta - c_{82}\lambda_{m\beta} + (c_{92} - c_5) i_\alpha \end{bmatrix},$$

$$\mathbf{f}_3 = \begin{bmatrix} f_5 \\ f_6 \end{bmatrix} = \begin{bmatrix} L_s\left(c_{71} w_r \lambda_\beta + c_{81}\lambda_\alpha - c_{81}\lambda_{m\alpha} - (c_{91} - c_5) i_\alpha\right) \\ L_s\left(-c_{72} w_r \lambda_\alpha + c_{82}\lambda_\beta - c_{82}\lambda_{m\beta} + (c_{92} - c_5) i_\alpha\right) \end{bmatrix},$$

$$\mathbf{B}_2 = \begin{bmatrix} (c_4 - c_{61}) & 0 \\ 0 & (c_4 - c_{62}) \end{bmatrix},\ \mathbf{B}_3 = \begin{bmatrix} L_s c_{61} & 0 \\ 0 & L_s c_{62} \end{bmatrix}.$$

Then using BC algorithm the following nonsingular change of variables can be proposed:

$$\mathbf{z}_1 = \mathbf{x}_1,\ \ \mathbf{z}_2 = \mathbf{f}_1(\mathbf{x}_1) + \mathbf{B}_1(\mathbf{x}_1)\begin{bmatrix}\mathbf{x}_2\\ \mathbf{x}_3\end{bmatrix} - \mathbf{d}_1 T_L - \mathbf{w}_1(t) + k_1\mathbf{z}_1,\ k_1 > 0$$

where $(-k_1\mathbf{z}_1,\ k_1 > 0)$ is the desired dynamics for the control error $\mathbf{z}_1$. Then the equations (21.56) and (21.57) are represented in the new variables $\mathbf{z}_1$ and $\mathbf{z}_2$ of the form

$$\begin{aligned}\dot{\mathbf{z}}_1 &= -k_1\mathbf{z}_1 + \mathbf{z}_2\\ \dot{\mathbf{z}}_2 &= \mathbf{f}_2(\mathbf{z}_1,\mathbf{z}_2,\eta) + \bar{\mathbf{B}}_2(\mathbf{z}_1)\mathbf{u} + \mathbf{d}_2 T_L - \mathbf{w}_2(t)\\ \dot{\eta} &= \mathbf{A}_\eta\eta + \mathbf{B}_\eta(\mathbf{z}_1)\mathbf{u} + \mathbf{g}_\eta(\mathbf{z},\eta)\end{aligned}$$

where $\mathbf{f}_2(\mathbf{z}_1,\mathbf{z}_2,\eta)$, $\mathbf{B}_\eta(\mathbf{z}_1)$ and $\mathbf{g}_\eta(\mathbf{z},\eta)$ are continuos functions, $\bar{\mathbf{B}}_2 = \mathbf{B}_1\begin{bmatrix}\mathbf{B}_2\\ \mathbf{B}_3\end{bmatrix}$, $\mathbf{w}_2(t) = k_1\mathbf{w}_1(t) - \dot{\mathbf{w}}_1(t)$.

The selected control

$$\mathbf{u} = -U_0\mathbf{sign}(\mathbf{B}_2^T\mathbf{z}_2),\ U_0 > 0$$

under the condition $U_0 > \left\|\mathbf{u}_{eq}\right\|$, $\mathbf{u}_{eq} = \bar{\mathbf{B}}_2^{-1}[\mathbf{f}_2 + \mathbf{d}_2 T_L - \mathbf{w}_2(t)]$ ensures a SM motion will appear on the manifold $\mathbf{z}_2 = 0$. Then closed-loop system motion reduces on this manifold to

$$\begin{aligned}\dot{\mathbf{z}}_1 &= -k_1\mathbf{z}_1\\ \dot{\eta} &= \mathbf{A}_\eta\eta + \bar{\mathbf{g}}_\eta(\mathbf{z}_1,\eta,t)\end{aligned}$$

where $\bar{\mathbf{g}}_\eta(\mathbf{z}_1,\eta,t) = \mathbf{B}_\eta\mathbf{u}_{eq}(\mathbf{z}_1,\eta,t) + \mathbf{g}_\eta(\mathbf{z}_1,\eta)$. The zero dynamics governed on subspace $\{\mathbf{z}_1 = 0,\ \eta \in \mathbf{R}^3\}$ by $\dot{\eta} = \mathbf{A}_\eta\eta + \bar{\mathbf{g}}_\eta(\mathbf{0},\eta,t)$ are stable since the matrix $\mathbf{A}_\eta$ is Hurwitz and $\bar{\mathbf{g}}_\eta(\mathbf{z}_1,\eta,t)$ is a continuos function bounded on a compact set. Therefore, a solution of the closed-loop system is ultimately uniformly bounded, and the control error $\mathbf{z}_1(t)$ converges exponentially to zero.

The detailed stability analysis including the rotor flux observer design and simulation results can be found in [14], [22], [2], [6], [7] and [8].

21.5 Induction Motor Discrete Time Control

21.5.1 Plant Model

Under the assumptions of equal mutual inductance and a linear magnetic circuit, an induction motor model is given by

$$\begin{aligned}\dot{\theta} &= \omega \\ \dot{\omega} &= \mu I^T \Im \phi - \frac{1}{J} C_L \\ \dot{\phi} &= -\alpha\phi + p\omega\Im\phi + \alpha L_m I \\ \dot{I} &= \alpha\beta\phi - p\beta\omega\Im\phi - \gamma I + \frac{1}{\sigma}u\end{aligned} \tag{21.58}$$

where θ and ω are the rotor position and angular velocity, $\phi = (\phi_\alpha, \phi_\beta)^T$ is the rotor flux vector, $I = (i_\alpha, i_\beta)^T$ is the stator current vector, $u = (u_\alpha, u_\beta)^T$ is the control input voltage vector, C_L is the load torque, J is the rotor moment of inertia, and $\Im = \begin{bmatrix} 0 & -1 \\ 1 & 0 \end{bmatrix}$, $\alpha = \frac{R_r}{L_r}, \beta = \frac{L_m}{\sigma L_r}, \gamma = \frac{L_m^2 R_r}{\sigma L_r^2} + \frac{R_s}{\sigma}, \sigma = L_s - \frac{L_m^2}{L_r}, \mu = \frac{3}{2}\frac{L_m p}{J L_r}$, and L_s, L_r L_m are the stator, rotor and mutual inductance respectively, R_s and R_r are the stator and rotor resistance respectively, and p is the number of pole pairs.

The digital control scheme here considered has a sampling period δ. In what follows it is considered the following hypothesis, which will be instrumental for the next developments

(H1) *The load torque C_L is piece-wise constant over the sampling period δ.*

Hypothesis (H1) holds for all cases in which C_L slowly varies with respect to the system dynamics. As far as the reduced-model is concerned, making use of the following globally defined change of coordinate

$$\begin{bmatrix} \theta \\ \omega \\ Y \\ X \end{bmatrix} = \begin{bmatrix} \theta \\ \omega \\ e^{-p\theta\Im}\phi \\ e^{-p\theta\Im} I \end{bmatrix} \tag{21.59}$$

where $e^{-p\theta\Im}$ is a rotational matrix that rotate with the mechanical velocity. Considering as new input X, one obtains the following bilinear model:

$$\begin{aligned}\dot{\theta} &= \omega \\ \dot{\omega} &= \mu X^T \Im Y - \frac{1}{J} C_L \\ \dot{Y} &= -\alpha Y + \alpha L_m X.\end{aligned} \tag{21.60}$$

The advantage of considering (21.59) is that the equation regarding Y, related to the flux ϕ, becomes linear and, hence easily discretized.

From here after we derive the sampling of (21.60). Considering X constant over the sampling period δ, we integrate the third of (21.60) over $[t_0 = k\delta,\ t \le (k+1)\delta]$, then one has

$$Y(t) = e^{-\alpha(t-k\delta)} Y_k + L_m \left(1 - e^{-\alpha(t-k\delta)}\right) X_k \tag{21.61}$$

where $Y_k = Y(k\delta)$, $X_k = X(k\delta)$. Now, under (H1), the integration of the second of (21.60) gives

$$\omega(t) = \omega_k + \mu X_k^T \Im \int_{k\delta}^{t} Y(\xi) d\xi - \frac{1}{J} C_{L,k} \int_{k\delta}^{t} d\xi \tag{21.62}$$

where $\omega_k = \omega(k\delta)$ and

$$\int_{k\delta}^{t} Y(\xi) d\xi = \frac{1}{\alpha}\left(1 - e^{-\alpha(t-k\delta)}\right) Y_k + L_m (t-k\delta) X_k - \frac{1}{\alpha} L_m \left(1 - e^{-\alpha(t-k\delta)}\right) X_k. \tag{21.63}$$

Replacing (21.63) in (21.62), one obtains

$$\omega(t) = \omega_k + \frac{\mu}{\alpha}\left(1 - e^{-\alpha(t-k\delta)}\right) X_k^T \Im Y_k - \frac{1}{J} C_{Lk}(t-k\delta) \ , \ t \le (k+1)\delta. \tag{21.64}$$

By integrating over $[t_0 = k\delta,\ t \le (k+1)\delta]$ the first of (21.60), one obtains

$$\theta(t) = \theta_k + \int_{k\delta}^{t} \omega(\xi) d\xi \tag{21.65}$$

where $\theta_k = \theta(k\delta)$ and

$$\begin{aligned} \int_{k\delta}^{t} \omega(\xi) d\xi \ = \ & \omega_k (t-k\delta) + \frac{\mu}{\alpha} X_k^T \Im Y_k \left((t-k\delta) + \frac{1}{\alpha}\left(e^{-\alpha t} - e^{-\alpha k\delta}\right) e^{\alpha k\delta} \right) \\ & - \frac{1}{J} C_{L,k} \left(\frac{1}{2}(t-k\delta)^2 \right). \end{aligned} \tag{21.66}$$

Using (21.66), for $t = (k+1)\delta$, (21.65), (21.64) and (21.61) yields

$$\begin{aligned} \theta_{k+1} &= \theta_k + \omega_k \delta + \frac{\mu}{\alpha}\left(\delta - \frac{1}{\alpha}(1-a)\right) X_k^T \Im Y_k - \frac{\delta^2}{2J} C_{L,k} \\ \omega_{k+1} &= \omega_k + \frac{\mu}{\alpha}(1-a) X_k^T \Im Y_k - \frac{\delta}{J} C_{L,k} \\ Y_{k+1} &= a Y_k + (1-a) L_m X_k \end{aligned} \tag{21.67}$$

where $a = e^{-\alpha\delta}$. In the old coordinates $\left[\ \theta\ \ \omega\ \ \phi\ \right]^T$ equations in (21.67) are written as

$$\begin{aligned} \theta_{k+1} &= \theta_k + \omega_k \delta + \frac{\mu}{\alpha}\left(\delta - \frac{1}{\alpha}(1-a)\right) I_k^T \Im \phi_k - \frac{\delta^2}{2J} C_{L,k} \\ \omega_{k+1} &= \omega_k + \frac{\mu}{\alpha}(1-a) I_k^T \Im \phi_k - \frac{\delta}{J} C_{L,k} \\ \phi_{k+1} &= \begin{bmatrix} \cos p\theta_{k+1} & -\sin p\theta_{k+1} \\ \sin p\theta_{k+1} & \cos p\theta_{k+1} \end{bmatrix} \begin{bmatrix} \rho_1(\theta_k,\ \phi_k,\ I_k) \\ \rho_2(\theta_k,\ \phi_k,\ I_k) \end{bmatrix} \end{aligned} \tag{21.68}$$

where

$$\begin{bmatrix} \rho_1(\theta_k,\ \phi_k,\ I_k) \\ \rho_2(\theta_k,\ \phi_k,\ I_k) \end{bmatrix} = a \begin{bmatrix} \cos p\theta_k & \sin p\theta_k \\ -\sin p\theta_k & \cos p\theta_k \end{bmatrix} \phi_k + (1-a) L_m \begin{bmatrix} \cos p\theta_k & \sin p\theta_k \\ -\sin p\theta_k & \cos p\theta_k \end{bmatrix} I_k.$$

The discretization of the whole system (21.58) can be obtained considering the stator current equations in (21.58). More precisely, the equation for I can be sampled as

$$I_{k+1} = e^{\delta L_F}(I)\,|_{k\delta}, \quad F = \alpha\beta\phi - p\beta\omega\Im\phi - \gamma I + \frac{1}{\sigma}u$$

with L_F the usual Lie derivative. In this expression the control u appears nonlinearly. This clearly complicates the derivation of the control law. In order to simplify this derivation, we will consider only terms up to δ. Clearly this approximation introduced in the current dynamic equations determines, in the mechanical and flux equations, an error of order $O(\delta^2)$. Then, using the usual notations, one has

$$I_{k+1} = I_k + \delta\left(\alpha\beta\phi_k - p\beta\omega_k\Im\phi_k - \gamma I_k + \frac{1}{\sigma}u_k\right). \tag{21.69}$$

Note that the variable X previously introduced, is constant over δ. Therefore, the sampled model of the induction motor model is given by (21.68), (21.69)

$$\begin{aligned}
\theta_{k+1} &= \theta_k + \omega_k\delta + \frac{\mu}{\alpha}\left(\delta - \frac{1}{\alpha}(1-a)\right)(i_{\beta,k}\phi_{\alpha,k} - i_{\alpha,k}\phi_{\beta,k}) - \frac{\delta^2}{2J}C_{L,k}\\
\omega_{k+1} &= \omega_k + \frac{\mu}{\alpha}(1-a)(i_{\beta,k}\phi_{\alpha,k} - i_{\alpha,k}\phi_{\beta,k}) - \frac{\delta}{J}C_{L,k}\\
\phi_{\alpha,k+1} &= \rho_1(\theta_k,\ \phi_k,\ I_k)\cos p\theta_{k+1} - \rho_2(\theta_k,\ \phi_k,\ I_k)\sin p\theta_{k+1}\\
\phi_{\beta,k+1} &= \rho_1(\theta_k,\ \phi_k,\ I_k)\sin p\theta_{k+1} + \rho_2(\theta_k,\ \phi_k,\ I_k)\cos p\theta_{k+1}\\
i_{\alpha,k+1} &= i_{\alpha,k} + \delta\left(\alpha\beta\phi_{\alpha,k} + p\beta\omega_k\phi_{\beta,k} - \gamma i_{\alpha,k} + \frac{1}{\sigma}u_{\alpha,k}\right)\\
i_{\beta,k+1} &= i_{\beta,k} + \delta\left(\alpha\beta\phi_{\beta,k} - p\beta\omega_k\phi_{\alpha,k} - \gamma i_{\beta,k} + \frac{1}{\sigma}u_{\beta,k}\right).
\end{aligned}$$

21.5.2 Control Algorithm

Let us define the following change of coordinates:

$$\begin{aligned}
x_{1,k} &= \begin{pmatrix} x_{11,k} \\ x_{12,k} \end{pmatrix} = \begin{pmatrix} \omega_k - \omega_{r,k} \\ \phi_k - \phi_{r,k} \end{pmatrix}\\
x_{2,k} &= \begin{pmatrix} x_{21,k} \\ x_{22,k} \end{pmatrix} = \begin{pmatrix} i_{\alpha,k} \\ i_{\beta,k} \end{pmatrix}\\
x_{3,k} &= \begin{pmatrix} x_{31,k} \\ x_{32,k} \end{pmatrix} = \begin{pmatrix} \arctan\dfrac{\phi_{\beta,k}}{\phi_{\alpha,k}} \\ \theta_k \end{pmatrix}
\end{aligned} \tag{21.70}$$

where $\phi_k = \phi_{\alpha,k}^2 + \phi_{\beta,k}^2$ is the squared rotor flux magnitude, $\omega_{r,k}$ and $\phi_{r,k}$ are bounded references signals. If the resulting control drives the state $x_{1,k}$ toward zero, then ω_k and ϕ_k will track exactly their respective reference signals. Clearly,

$$\begin{aligned}
\omega_k &= x_{11,k} + \omega_{r,k} \\
\phi_{\alpha,k} &= \sqrt{x_{12,k} + \phi_{r,k}} \cos x_{31,k}, \quad \phi_{\beta,k} = \sqrt{x_{12,k} + \phi_{r,k}} \sin x_{31,k} \\
i_{\alpha,k} &= x_{21,k} \quad i_{\beta,k} = x_{22,k} \\
\theta_k &= x_{32,k}.
\end{aligned}$$

Due to (21.70), the motor equations can be rewritten as follows

$$\begin{aligned}
x_{11,k+1} &= x_{11,k} + c_1 \sqrt{x_{12,k} + \phi_{r,k}} \left(x_{22,k} \cos x_{31,k} - x_{21,k} \sin x_{31,k} \right) \\
&\quad - \frac{\delta}{J} C_{L,k} + \omega_{r,k} - \omega_{r,k+1} \\
x_{12,k+1} &= a^2 x_{12,k} + c_2 \left(x_{21,k}^2 + x_{22,k}^2 \right) \\
&\quad + c_3 \sqrt{x_{12,k} + \phi_{r,k}} \left(x_{21,k} \cos x_{31,k} + x_{22,k} \sin x_{31,k} \right) + a^2 \phi_{r,k} - \phi_{r,k+1} \\
x_{21,k+1} &= \varphi_{\alpha,k} \left(x_k \right) + \frac{\delta}{\sigma} u_{\alpha,k} \\
x_{22,k+1} &= \varphi_{\beta,k} \left(x_k \right) + \frac{\delta}{\sigma} u_{\beta,k} \\
x_{31,k+1} &= p x_{32,k+1} + \arctan \frac{\rho_2 \left(x_k \right)}{\rho_1 \left(x_k \right)} \\
x_{32,k+1} &= x_{32,k} + x_{11,k} \delta + c_4 \sqrt{x_{12,k} + \phi_{r,k}} (x_{22,k} \cos x_{31,k} - x_{21,k} \sin x_{31,k}) \\
&\quad - \frac{\delta^2}{2J} C_{Lk} + \omega_{r,k} \delta
\end{aligned}$$

with

$$\begin{aligned}
c_1 &= \frac{\mu}{\alpha} (1-a), \; c_2 = (1-a)^2 L_m^2, \; c_3 = 2a(1-a) L_m, \; c_4 = \frac{\mu}{\alpha} \left(\delta - \frac{1}{\alpha} (1-a) \right) \\
\rho_1 \left(x_k \right) &= a \sqrt{x_{12,k} + \phi_{r,k}} \cos \left(x_{31,k} - p x_{32,k} \right) \\
&\quad + (1-a) L_m \left(x_{21,k} \cos p x_{32,k} + x_{22,k} \sin p x_{32,k} \right) \\
\rho_2 \left(x_k \right) &= a \sqrt{x_{12,k} + \phi_{r,k}} \sin \left(x_{31,k} - p x_{32,k} \right) \\
&\quad + (1-a) L_m \left(x_{22,k} \cos p x_{32,k} - x_{21,k} \sin p x_{32,k} \right) \\
\varphi_{\alpha,k} \left(x_k \right) &= (1 - \delta\gamma) x_{21,k} + \delta\beta \sqrt{x_{12,k} + \phi_{r,k}} \left(\alpha \cos x_{31,k} + p \left(x_{11,k} + \omega_{r,k} \right) \sin x_{31,k} \right) \\
\varphi_{\beta,k} \left(x_k \right) &= (1 - \delta\gamma) x_{22,k} + \delta\beta \sqrt{x_{12,k} + \phi_{r,k}} \left(\alpha \sin x_{31,k} - p \left(x_{11,k} + \omega_{r,k} \right) \cos x_{31,k} \right)
\end{aligned}$$

and $x_k = \left(x_{1,k}^T, x_{2,k}^T, x_{3,k}^T \right)^T$. These equations are in the form

$$\begin{aligned}
x_{1,k+1} &= f_1 \left(k, x_k \right) + B \left(k, x_k \right) x_{2,k} \\
x_{2,k+1} &= f_2 \left(k, x_k \right) + \frac{\delta}{\sigma} u_k \\
x_{3,k+1} &= f_3 \left(k, x_k \right)
\end{aligned} \tag{21.71}$$

where

$$f_1(k,x_k) = \begin{pmatrix} x_{11,k} - \dfrac{\delta}{J}C_{L,k} + \omega_{r,k} - \omega_{r,k+1} \\ a^2 x_{12,k} + a^2\phi_{r,k} - \phi_{r,k+1} + c_2\left(x_{21,k}^2 + x_{22,k}^2\right) \end{pmatrix}$$

$$f_2(k,x_k) = \begin{pmatrix} \varphi_{\alpha,k}(x_k) \\ \varphi_{\beta,k}(x_k) \end{pmatrix},\ f_3(k,x_k) = \begin{pmatrix} \psi_{\alpha,k}(x_k) \\ \psi_{\beta,k}(x_k) \end{pmatrix}$$

$$B(k,x_k) = \sqrt{x_{12,k}+\phi_{r,k}} \begin{pmatrix} c_1 & 0 \\ 0 & c_3 \end{pmatrix} \begin{pmatrix} -\sin x_{31,k} & \cos x_{31,k} \\ \cos x_{31,k} & \sin x_{31,k} \end{pmatrix}$$

with $\psi_{\alpha,k}(x_k) = px_{32,k+1} + \arctan\dfrac{\rho_2(x_k)}{\rho_1(x_k)}$ and $\psi_{\beta,k}(x_k) = x_{32,k} + x_{11,k}\delta + c_4\sqrt{x_{12,k}+\phi_{r,k}}(x_{22,k}\cos x_{31,k} - x_{21,k}\sin x_{31,k}) - \dfrac{\delta^2}{2J}C_{Lk} + \omega_{r,k}\delta$.

In what follows we exploit the NBC-form of the first two equations of (21.71) in order to derive a sliding mode controller, using a block control procedure. To this aim, note first that the matrix $B(k,x_k)$ is bounded under the hypothesis that $\phi_{r,k} \in L_\infty$. Moreover, $B(k,x_k)$ is invertible if $\phi_{r,k} \neq 0$. These are conditions always verified in practical situations. Then imposing in the first of (21.71)

$$x_{1,k+1} = f_1(k,x_k) + B(k,x_k)x_{2,k} = K_1 x_{1,k}$$

and considering $x_{2,k}$ as fictitious input, one works out

$$x_{2,d,k} = B^{-1}(k,x_k)\left(K_1 x_{1,k} - f_1(k,x_k)\right).$$

We use this signal for defining a time-varying change of coordinates

$$z_{1,k} = \begin{pmatrix} z_{11,k} \\ z_{12,k} \end{pmatrix} = x_{1,k}$$

$$z_{2,k} = \begin{pmatrix} z_{21,k} \\ z_{22,k} \end{pmatrix} = x_{2,k} - B^{-1}(k,x_k)\left(K_1 x_{1,k} - f_1(k,x_k)\right)$$

$$z_{3,k} = \begin{pmatrix} z_{31,k} \\ z_{32,k} \end{pmatrix} = x_{3,k}$$

so that if $z_{2,k} = 0$, also $z_{1,k} = 0$ for K_1 with eigenvalues inside the unit circle. In these error variables the dynamics are written as follows

$$\begin{aligned} z_{1,k+1} &= K_1 z_{1,k} + B(k,z_k)z_{2,k} \\ z_{2,k+1} &= x_{2,k+1} - B^{-1}(k,x_{k+1})\left(K_1 x_{1,k+1} - f_1(k,x_{k+1})\right) \\ &= \bar{f}_2(k,z_k) + \frac{\delta}{\sigma}u_k - B^{-1}(k,z_{k+1})\left(K_1^2 z_{1,k} + K_1 B(k,z_k)z_{2,k} - \bar{f}_1(k,z_k)\right) \end{aligned}$$

with $\bar{f}_1(k,z_k) = \begin{pmatrix} \bar{f}_{11}(k,z_k) \\ \bar{f}_{12}(k,z_k) \end{pmatrix}$, $\bar{f}_2(k,z_k) = \begin{pmatrix} \bar{\varphi}_{\alpha,k}(z_k) \\ \bar{\varphi}_{\beta,k}(z_k) \end{pmatrix}$,

$\bar{f}_{11}(k,z_k) = z_{11,k} + c_1\sqrt{z_{12,k}+\phi_{r,k}}(x_{22,k}\cos z_{31,k} - x_{21,k}\sin z_{31,k}) - \frac{\delta}{J}C_{L,k} - \frac{\delta}{J}C_{L,k+1} + \omega_{r,k} - \omega_{r,k+2}$, $\bar{f}_{12}(k,z_k) = a^4 z_{12,k} + a^2 c_2\left(x_{21,k}^2 + x_{22,k}^2\right)$,

$+a^2 c_3\sqrt{z_{12,k}+\phi_{r,k}}\left(x_{21,k}\cos z_{31,k} + x_{22,k}\sin z_{31,k}\right) + c_2\left(x_{21,k+1}^2 + x_{22,k+1}^2\right) + a^4\phi_{r,k} - \phi_{r,k+2}$,

$\bar{\varphi}_{\alpha,k}(z_k) = (1-\gamma)x_{21,k} + \delta\beta\sqrt{z_{12,k}+\phi_{r,k}}\left(\alpha\cos z_{31,k} + p\left(z_{11,k}+\omega_{r,k}\right)\sin z_{31,k}\right)$,

$\bar{\varphi}_{\beta,k}(z_k) = (1-\gamma)x_{22,k} + \delta\beta\sqrt{z_{12,k}+\phi_{r,k}}\left(\alpha\sin z_{31,k} - p\left(z_{11,k}+\omega_{r,k}\right)\cos z_{31,k}\right)$

$B(k,z_k) = \sqrt{z_{12,k}+\phi_{r,k}}\begin{pmatrix} c_1 & 0 \\ 0 & c_2 \end{pmatrix}\begin{pmatrix} -\sin z_{31,k} & \cos z_{31,k} \\ \cos z_{31,k} & \sin z_{31,k} \end{pmatrix}$.

Finally, the error dynamics reduce to

$$\begin{aligned} z_{1,k+1} &= K_1 z_{1,k} + B(k,z_k)\, z_{2,k} \\ z_{2,k+1} &= \overline{f}_3(k,z_k) + \frac{\delta}{\sigma}u_k \end{aligned} \tag{21.72}$$

with

$$\overline{f}_3(k,z_k) = \bar{f}_2(k,z_k) - B^{-1}(k,z_{k+1})\left(K_1^2 z_{1,k} + K_1 B(k,z_k)\, z_{2,k} - \bar{f}_1(k,z_k)\right).$$

The next step is to design the control law from the last results. The first step in sliding mode control is to choose the surface $S_k = 0$, and, a smart selection is

$$S_k = z_{2,k} = 0.$$

This surface will be zeroing as the state trajectories reach the surface, and then the control objectives will be accomplished. The transformed system (21.72) is redefined as

$$\begin{aligned} z_{1,k+1} &= K_1 z_{1,k} + B(k,z_k)\, S_k \\ S_{k+1} &= \overline{f}_3(k,z_k) + \frac{\delta}{\sigma}u_k. \end{aligned} \tag{21.73}$$

In order to design a control law, a discrete-time sliding mode version ([23]), is implemented where the equivalent u_{keq} is calculated from $S_{k+1} = 0$ as

$$u_{keq} = \frac{\sigma}{\delta}\left(\overline{f}_3(k,z_k)\right)$$

and u_0 is the control resources that bound the control. The stability analysis is similar to the one presented in the above section, where the sliding mode equations are:

$$z_{1,k+1} = K_1 z_{1,k}.$$

It is an obvious fact that the proposed control u_k depends of $\overline{f}_3(k,z_k)$ in order to eliminate old dynamics, but this function depends of control u_k squared, due to terms $x_{21,k+1}^2 + x_{22,k+1}^2$, that appears in $\bar{f}_1(k,z_k)$, making the system in that way,

unsolvable. To solve this problem, it is designed an observer with current measurements for the new variable current modulus defined as $I_{m,k} = \sqrt{x_{21,k}^2 + x_{22,k}^2}$. It is assumed that $I_{m,k}$ is constant, i.e., $I_{m,k+1} = I_{m,k}$, then the observer is presented as the original plant plus a tracking error

$$\widehat{I}_{m,k+1} = \widehat{I}_{m,k} + g e_{I,k}$$

where $e_{I,k} = I_{m,k} - \widehat{I}_{m,k}$ is the tracking error. Taking one step ahead

$$z_{I,k+1} = (1-g) e_{I,k}$$

where $2 > g > 0$ for the observer error to asymptotically decay to zero, and the estimation $\widehat{I}_{m,k}$ will track the real value $I_{m,k}$, avoiding in that way the control dependency of u_k squared.

The detailed stability analysis including the rotor flux observer design and simulation results can be found in [5].

21.6 Induction Motor Hybrid Control

In order to obtain sampled dynamics of the system dynamics in closed form, let us consider first the following feedback:

$$u = u_f(t) + e^{p\theta\Im} v_k, \quad u_f = pL_\sigma \omega \Im (I_s + \beta \phi_r) \tag{21.74}$$

with u_f the continuous control which makes the system finite discretizable, and v_k the new control input.

Remark 21.2. Note that u_f in (21.74) and the term $e^{p\theta\Im}$ must be implemented by analog devices, while the new control $v_k = v(k\delta) =^T$, designed on the basis of the discrete time representation of the system derived in the following, can be implemented by a digital computer and a zero–order holder. The resulting controller will be hybrid, namely it will contain discrete and continuous time terms.

With the continuous feedback (21.74) and under (H_1) the following controlled dynamics are obtained:

$$\begin{aligned} \dot{\phi} &= -\alpha\phi + p\omega\Im\phi + \alpha L_m I_s \\ \dot{I}_s &= \alpha\beta\phi - p\beta\omega\Im\phi - \gamma I_s + \frac{1}{\sigma} u \\ \dot{\omega} &= \mu I_s^T \Im\phi - \frac{1}{J} C_L \\ \dot{\theta} &= \omega. \end{aligned} \tag{21.75}$$

With the continuous feedback (21.74), considering hereinafter a change of coordinates in an appropriate rotating frame,

$$\begin{pmatrix} \Phi = e^{p\theta\Im}\phi_r \\ I \end{pmatrix} = \begin{pmatrix} e^{p\theta\Im}\phi_r \\ e^{p\theta\Im}I_s \end{pmatrix}, \quad e^{-p\theta\Im} = \begin{pmatrix} \cos p\theta & \sin p\theta \\ -\sin p\theta & \cos p\theta \end{pmatrix}$$

with $e^{-p\theta\Im}$ as an orthogonal matrix, under (H_1) the following controlled dynamics are now obtained:

$$\dot{\Phi} = -\alpha\Phi + \alpha L_m I \tag{21.76}$$

$$\dot{I} = \alpha\beta\Phi - -\gamma I + \frac{1}{L_\sigma}v_k \tag{21.77}$$

$$\dot{\omega} = \mu I^T \Im\Phi - \frac{1}{J}C_L \tag{21.78}$$

$$\dot{\theta} = \omega. \tag{21.79}$$

The transformed variables Φ, I in (21.76)-(21.79) are the rotor flux and the stator current rotated according to the electrical rotor angular position $p\theta$. Note that equations (21.76)-(21.79) are nonlinear, but the sampled closed form is now easily obtained noting that the dynamics for Φ and I are linear, and the control v_k will be designed to be constant over the sampling period δ. Denoting $\Phi_k = \Phi(k\delta)$, $I_k = I(k\delta)$, $\omega_k = \omega(k\delta)$ and $C_k = C(k\delta)$, and considering as outputs to be controlled the rotor angular velocity and the rotor flux square modulus, some calculations yield the *closed representation* for the sampled dynamics of system (21.76)-(21.79)

$$\Phi_{k+1} = a_{11}\Phi_k + a_{12}I_k + b_1\upsilon_k \tag{21.80}$$

$$I_{k+1} = a_{21}\Phi_k + a_{22}I_k + b_2\upsilon_k \tag{21.81}$$

$$\omega_{k+1} = \omega_k + \eta_1 I_k^T \Im\Phi_k + (\eta_2\Phi_k + \eta_3 I_k)\Im\upsilon_k - \frac{\delta}{J}C_k \tag{21.82}$$

$$\theta_{k+1} = \theta_k + \delta\omega_k + k_1 I_k^T \Im\Phi_k + (k_2\Phi_k + k_3 I_k)\Im\upsilon_k - \frac{\delta^2}{2J}C_k \tag{21.83}$$

where a_{11}, a_{12}, a_{21}, a_{22}, b_1, b_2, η_i, κ_i, $i = 1,2,3$, are constants.

21.6.1 Discrete–Time Controller

The control problem is to force the rotor angular velocity ω_k and the rotor flux modulus $\Phi_k^T\Phi_k$ to track some desired references $\omega_{r,k}$, $\Phi_{r,k}$, ensuring at the same time disturbance rejection. We assume that these references are bounded with bounded increments. Moreover, also the load torque C_k is bounded by a value $C_{\max}$. Furthermore, we assume that the C_k has bounded increments. Finally, we need to ensure that this increment vanishes when δ is zero. This can be formalized with the following assumption.

(H_2) The piece–wise load torque C_k is such that $C_{k+1} = C_k + \Delta C(k,\delta)$ with, for each integer $\bar{k}$

$$10pt|\Delta C(\bar{k},\delta)| \le \Delta C_{\max}\Delta(\delta), \quad \lim_{\delta\to 0}\Delta(\delta) = 0.05cm.$$

The discrete time control v_k in (21.74) is designed hereinafter, in order to solve the posed control problem, following the SM approach. For, we first derive the expression of the tracking error dynamics $e_{1,k} = \omega_k - \omega_{r,k}$, $e_{2,k} = \Phi_k^T \Phi_k - \Phi_{r,k}$, which are the new outputs which we want to force to zero. Using (21.80)-(21.83), the error dynamics can be written as follows

$$e_{1,k+1} = \omega_k + \eta_1 I_k^T \Im \Phi_k + \lambda_{1,k}^T \upsilon_k - \frac{\delta}{J} C_k - \omega_{r,k+1} \tag{21.84}$$

$$e_{2,k+1} = a_{11}^2 \Phi_k^T \Phi_k + 2a_{11}a_{12}\Phi_k^T I_k + a_{12}^2 I_k^T I_k + \lambda_{2,k}^T \upsilon_k + b_1^2 \upsilon_k^T \upsilon_k - \Phi_{r,k+1} \tag{21.85}$$

where

$$\lambda_{1,k} = -\Im(\eta_2 \Phi_k + \eta_3 I_k),\ \lambda_{2,k} = 2b_1(a_{11}\Phi_k + a_{12} I_k). \tag{21.86}$$

It is interesting to note that $\lambda_{1,k}$ represents the vector $\eta_2 \Phi_k + \eta_3 I_k$ rotated $\pi/2$ clockwise.

Notice that the system (21.84)-(21.85), depends on quadratic terms of the control signal v_k since $b_1 > 0$ for all sampling time $\delta > 0$. This complicates the control design procedure. In order to simplify the design of a control law, one considers as new control

$$\mathscr{V}_k = \begin{pmatrix} \mathscr{V}_{a,k} \\ \mathscr{V}_{b,k} \end{pmatrix} = \mathscr{T}_k v_k, \quad \mathscr{T}_k = \begin{pmatrix} \lambda_{1,k}^T \\ \lambda_{2,k}^T \end{pmatrix} \tag{21.87}$$

$v_k = \mathscr{T}_k^{-1} \mathscr{V}_k$. It can be verified that the transformation $\mathscr{T}_k$ is invertible for all k. With such a control transformation, $e_{1,k+1}$, $e_{2,k+1}$ depend only on $\mathscr{V}_{a,k}$, $\mathscr{V}_{b,k}$, respectively, and equations (21.84)-(21.85) become

$$e_{1,k+1} = \omega_k + \eta_1 I_k^T \Im \Phi_k - \frac{\delta}{J} C_k - \omega_{r,k+1} + \mathscr{V}_{a,k} \tag{21.88}$$

$$e_{2,k+1} = a_k \mathscr{V}_{b,k}^2 + b_k \mathscr{V}_{b,k} + c_k \tag{21.89}$$

where

$$a_k = \frac{b_1^2}{d_k^2} \lambda_{1,k}^T \lambda_{1,k} \geq 0,\ b_k = 1 - \frac{b_1^2}{d_k^2} \lambda_{1,k}^T \lambda_{2,k} \mathscr{V}_{a,k},$$

$$b_{ck} = \frac{1}{4b_1^2} \lambda_{2,k}^T \lambda_{2,k} + \frac{b_1^2}{d_k^2} \lambda_{2,k}^T \lambda_{2,k} \mathscr{V}_{a,k}^2 - \Phi_{r,k+1}.$$

It is worth noting that a_k is zero when $\Phi_k = -\eta_3 I_k / \eta_2$.

A discrete time sliding–mode control will be designed hereinafter, to force to zero the error dynamics. A natural choice as sliding functions are the errors $e_{1,k}$, $e_{2,k}$.

Since the control objective is to design a controller for angular velocity tracking and disturbance rejection, considering $e_{1,k}$ as sliding surface, one can impose that this tracking error be zeroed in one step, namely $e_{1,k+1} = 0$. Considering (21.88), this is achieved considering

$$\mathscr{V}_{a,k} = -\omega_k - \eta_1 I_k^T \Im \Phi_k + \frac{\delta}{J} C_k + \omega_{r,k+1}. \tag{21.90}$$

Usually, such a control is called equivalent control, and is such that the sliding manifold $e_{1,k} = 0$ is rendered invariant. Analogously, we determine $\mathscr{V}_{b,k}$ in (21.89) as

$$\mathscr{V}_{b,k} = \begin{cases} -\frac{b_k}{2a_k} \pm \frac{\sqrt{\Delta_k}}{2a_k} & \text{if } a_k > 0 \text{ and } \Delta_k \geq 0 \\ -\frac{b_k}{2a_k} & \text{if } a_k > 0 \text{ and } \Delta_k < 0 \\ -\frac{c_k}{2a_k} & \text{if } a_k = 0 \end{cases}$$

with $\Delta_k = b_k^2 - 4a_k c_k$,. With this choice the tracking flux error $e_{2,k}$ tends asymptotically to zero.

We have shown that $e_{1,k}, e_{2,k}$ are forced to zero asymptotically. One should ensure that I_k does not diverge to infinity. This aspect is correlated with the stability of what are called the zero dynamics which, roughly speaking, are those dynamics obtained when the output of the system is zero.

The detailed stability analysis including the rotor DT flux observer design and simulation results can be found in [4].

21.7 Induction Motor Neural Network SM Block Control

In this section we design robust controller using discrete-time Recurrent High Order Neural Network (RHONN) [10] and block control technique combined with DT SM control [21].

21.7.1 Identification

To identify the motor model the following RHONN identifier is proposed:

$$\begin{aligned} &x_{1,k+1} = w_{11,k} S(\omega_k) \\ &+ w_{12,k} S(\omega_k) S\left(\phi_{\beta,k+1}\right) i_{\alpha,k} + w_{13} S(\omega_k) S\left(\phi_{\alpha,k+1}\right) i_{\beta,k} \end{aligned} \tag{21.91}$$

$$\begin{cases} x_{2,k+1} = w_{21,k} S(\omega_k) S\left(\phi_{\beta,k}\right) S\left(i_{\alpha,k}\right) + w_{22} i_{\beta,k} \\ x_{3,k+1} = w_{31,k} S(\omega_k) S\left(\phi_{\alpha,k}\right) S\left(i_{\alpha,k}\right) + w_{32} i_{\alpha,k} \end{cases} \tag{21.92}$$

$$\begin{cases} x_{4,k+1} = w_{41,k} S\left(\phi_{\alpha,k}\right) + w_{42,k} S\left(\phi_{\beta,k}\right) + w_{43,k} S\left(i_{\alpha,k}\right) + w_{44} u_{\alpha,k} \\ x_{5,k+1} = w_{51,k} S\left(\phi_{\alpha,k}\right) + w_{52,k} S\left(\phi_{\beta,k}\right) + w_{53,k} S\left(i_{\beta,k}\right) + w_{54} u_{\beta,k} \end{cases} \tag{21.93}$$

where $x_{i,k}$, $i = 1,...,5$ is the state of the ith neuron; $x_{1,k}$ is the estimate of the speed ω_k; $x_{2,k}$ and $x_{3,k}$ are the estimates of the rotor fluxes $\phi_{\alpha,k}$ and $\phi_{\beta,k}$, respectively; $x_{4,k}$ and $x_{5,k}$ are the estimates of the stator currents $i_{\alpha,k}$ and $i_{\beta,k}$, respectively;; $w_{11,k}, w_{12,k}, w_{13,k}, w_{21,k}, w_{31,k}, w_{41,k}$ and $w_{51,k}$ are the respective on-line adapted weights. The weights $w_{13}, w_{22}, w_{32}, w_{44}$ and w_{54} are constant positive values, which are selected initially via simulations and are adjusted on real-time in

order to reduce the identification error. These weights are called the controllability weights [20]. Finally $S(\bullet)$ is defined by

$$S(\chi_k) = \frac{1}{1+exp(-\beta\chi_k))}, \ \beta > 0. \tag{21.94}$$

We use a neural model due to the fact that the plant parameters and external disturbances (the load torque) are unknown; then, to approximate the plant complete model with the load torque, we propose a neural identifier which reproduces the behavior of the plant, without the identification of the plant parameters. Moreover, we propose a neural identifier structure based on the plant model structure, and the structure (21.91)-(21.93) uses the smallest quantity of weights needed to obtain an adequate identification and reduces computational requirements.

For the neural identifier training we use the Extended Kalman Filtering (EKF) algorithm described by

$$w_{i,k+1} = w_{i,k} + \eta_i K_{i,k} e_k, \ \ i = 1, \cdots, 5 \tag{21.95}$$

where

$$K_{i,k} = P_{i,k} H_{i,k} M_{i,k} \tag{21.96}$$

$$P_{i,k+1}(k+1) = P_{i,k} - K_{i,k} H_{i,k}^T P_{i,k} + Q_i$$

$$M_{i,k} = \left[R_i + H_{i,k}^T P_{i,k} H_{i,k}\right]^{-1}, \tag{21.97}$$

$e_k = (e_{1,k}, e_{4,k}, e_{5,k})^T$, $e_{4,k} = x_{1,k+1} - \omega_k$, $e_{5,k} = x_{4,k+1} - i_{\alpha,k}$, $e_{5,k} = x_{5,k+1} - i_{\beta,k}$; $P_{i,k} \in \mathbb{R}^{L_i \times L_i}$ is the prediction error covariance matrix at step k, $w_{i,k} \in \mathbb{R}^{L_i}$ is the weight (state) vector, L_i is the respective number of NN weights

$$\begin{aligned} w_{1,k} &= (w_{11,k}, w_{12,k}, w_{13,k})^T, \\ w_{2,k} &= w_{21,k}, \\ w_{3,k} &= w_{31,k}, \\ w_{4,k} &= (w_{41,k}, w_{42,k}, w_{43,k})^T, \\ w_{4,k} &= (w_{41,k}, w_{42,k}, w_{43,k})^T, \end{aligned}$$

η_i is a design parameter, $K_{i,k}(k) \in \mathbb{R}^{L_i \times 5}$ is the Kalman gain matrix, $Q_i \in \mathbb{R}^{L_i \times L_i}$ is the NN associated state noise covariance matrix, $R_i \in \mathbb{R}^{5\times 5}$ associated measurement noise covariance matrix; $H_i \in \mathbb{R}^{L_i}$ is a vector, in which each entry (H_{ij}) is the derivative of one of the NN state $\left(x_{i,k}\right)$, with respect to one NN weight, $\left(w_{ij,k}(k)\right)$, as follows

$$H_{ij,k} = \left[\frac{\partial x_{i,k}}{\partial w_{ij,k}}\right]^T_{w_{i,k}=\hat{w}_{i,k+1}} \tag{21.98}$$

where $i = 1, \cdots, 5$ and $j = 1, \cdots L_i$. Usually $P_{i,k}$, Q_i and R_i are diagonal matrices. The matrix $P_{i,k}$ has its initial value as $P_{i,0}$. It is important to remark that $H_{i,k}$, $K_{i,k}$ and $P_{i,k}$ for the EFK are bounded; for a detailed explanation of this fact see [21].

The training is performed on-line, using a series-parallel configuration. All the NN states are initialized in a random way as well as the weights vectors. It is important to note that the initial conditions of the NN are completely different from the initial conditions for the plant.

21.7.2 Controller Design

The control objective is to develop speed and field amplitude tracking for the induction motor. Therefore we define the following state variables

$$x_k^1 = \begin{bmatrix} x_{1,k} - \omega_{ref,k} \\ \phi_k - \phi_{ref,k} \end{bmatrix}, \; x_k^2 = \begin{bmatrix} x_{\alpha,k} \\ x_{\beta,k} \end{bmatrix} = \begin{bmatrix} i_{\alpha,k} \\ i_{\beta,k} \end{bmatrix}. \tag{21.99}$$

Then we have

$$\begin{aligned} \phi_{1,k+1} = {} & w_{21,k}^2 S^2(\omega_k) S^2\left(\phi_{\beta,k+1}\right) + \left(w_{22} i_{\beta,k}\right)^2 + \left(w_{22} i_{\alpha,k}\right)^2 + \left(w_{32} i_{\alpha,k}\right)^2 \\ & + w_{31,k}^2 S^2(\omega_k) S^2\left(\phi_{\alpha,k+1}\right) + 2 w_{21,k} S(\omega_k) S\left(\phi_{\beta,k}\right) w_{22} i_{\beta,k} \\ & + 2 w_{31} S(\omega_k) S\left(\phi_{\alpha,k+1}\right) w_{32} i_{\alpha,k}. \end{aligned}$$

Using (21.99) the system (21.91)-(21.93) can be represented as the NBC form consisting of two blocks:

$$x_{k+1}^1 = f_1(x_k, k) + B_1\left(x_k^1\right) x_{2,k} \tag{21.100}$$

$$x_{k+1}^2 = f_2(x_k, k) + B_2 u_k \tag{21.101}$$

where $x_k = (x_{k+1}^1, x_{k+1}^1)$, $B_1 \equiv \begin{bmatrix} w_{12,k} S(\omega_k) S\left(\phi_{\beta,k+1}\right) & w_{13} S(\omega_k) S\left(\phi_{\alpha,k+1}\right) \\ 2 w_{31} w_{32} S(\omega_k) S\left(\phi_{\alpha,k+1}\right) & 2 w_{21,k} w_{22} S(\omega_k) S\left(\phi_{\beta,k}\right) \end{bmatrix}$, $B_2 \equiv \begin{bmatrix} w_{44} & 0 \\ 0 & w_{44} \end{bmatrix}$, $f_1(x_k, k)$ and $f_2(x_k, k)$ a continuos functions.

At the first step, introducing the desired dynamics for x_k^1 as $k_1 x_k^1$, $|k_1| < 1$, the desired value $x_{d,k}^2$ for x_k^2 in (21.100) is chosen as

$$x_{d,k}^2 = \begin{bmatrix} x_{\alpha d,k} \\ x_{\beta d,k} \end{bmatrix} = \left[B_1\left(x_k^1\right)\right]^{-1} \left[-f_1(x_k, k) + k_1 x_k^1\right].$$

At the second step, given $x_{\alpha d,k}$ and $x_{\beta d,k}$ as the desired values for the stator currents $x_{\alpha,k}$ and field $x_{\beta,k}$ currents, respectively, a second current error vector $\varepsilon_{2,k}$ is defined as

$$\varepsilon_k^2 \equiv \begin{bmatrix} \varepsilon_{\alpha,k} \\ \varepsilon_{\beta,k} \end{bmatrix} = \begin{bmatrix} x_{\alpha,k} - x_{\alpha d,k} \\ x_{\beta,k} - x_{\beta d,k} \end{bmatrix}. \tag{21.102}$$

Thus, the system (21.100)-(21.101) in the new variables x_k^1, $\varepsilon_{\alpha,k}$ and $\varepsilon_{\alpha,k}$ is presented of the form

$$\left\{x_{k+1}^1 = k_1 x_k^1 + B_1\left(x_k^1\right)\varepsilon_2(k) \right. \tag{21.103}$$

$$\left\{\begin{array}{l} \varepsilon_{\alpha,k+1} = \tilde{f}_\alpha(x_k^1, x_k^2, k) + w_{44}u_{\alpha,k} \\ \varepsilon_{\beta,k+1} = \tilde{f}_\beta\left(x_k^1, x_k^2, k\right) + w_{44}u_{\beta,k}(k) \end{array}\right. \tag{21.104}$$

where $\tilde{f}_2(\cdot)$ and $\tilde{f}_3(\cdot)$ are continuous functions of the state vector and time. Selecting the sliding variables as $s_2(k) = \varepsilon_2(k)$ and $s_3(k) = \varepsilon_3(k)$, and taking into account saturation values $\left\|u_{\alpha,k}\right\| \leq u_0$ and $\left\|u_{\alpha,k}\right\| \leq u_0$ of the voltages, respectively, the following control is implemented:

$$u_{i,k} = \left\{\begin{array}{ll} u_{i,k,eq} & \text{for } \left\|u_{i,k,eq}\right\| \leq u_0 \\ u_0 \frac{u_{i,k,eq}}{\left\|u_{i,k,eq}\right\|} & \text{for } \left\|u_{i,k,eq}\right\| > u_0 \end{array}\right. \tag{21.105}$$

with

$$u_{i,k,eq} = -w_{44}^{-1}\tilde{f}_i(x_k^1, x_k^2, k), \;\; i = \alpha, \beta.$$

The control (21.105) is able to drive the system (21.104) on the sliding manifold $\varepsilon_k^2 = 0$ where the control errors satisfies

$$x_{k+1}^1 = k_1 x_k^1, \;\; |k_1| < 1.$$

Thus, the control error asymptotically tends to zero.

The detailed controller scheme including stability analysis, simulation and real time implementation results can be found in [21] and [20].

References

1. Anderson, P.M., Fouad, A.: Power System Control and Stability. IEEE Press, New York (1994)
2. Cabrera-Vázquez, J., Loukianov, A.G., Cañedo, J.M., Utkin, V.I.: Robust controller for synchronous generator with local load via VSC. International Journal of Electrical Power & Energy Systems 29(4), 348–359 (2007)
3. Cañedo, J.M., Fridman, L., Loukianov, A.G., Valenzuela, F.A.: High-Order Sliding-Mode Controllers in Induction Motors with Magnetic Saturation Effect, Memorias del Congreso Latinoamericano de Control Automático. In: 13th CLCA/VI CAC, Mérida - Venezuela, pp. 1110–1117 (2008)
4. Castillo-Toledo, B., Di Gennaro, S., Loukianov, A.G., Rivera, J.: Hybrid Control of Induction Motors via Sampled Closed Representation. IEEE Transactions on Industrial Electronics 55(10), 3758–3771 (2008)
5. Castillo-Toledo, B., Di Gennaro, S., Loukianov, A.G., Rivera, J.: Discrete-Time Sliding Mode Block Control: Application to the Induction Motor. The IFAC Journal Automatica 44, 3036–3045 (2008)
6. Huerta, H., Loukianov, A., Cañedo, J.M.: Integral Sliding Modes with Block Control and its Application to Electric Power Systems. In: Structure and Control, pp. 83–110. Petr Husek, The Croatia (2008)
7. Huerta, H., Loukianov, A.G., Cañedo, J.M.: Multimachine Power-System Control: Integral-SM Approach. IEEE Transactions on Industrial Electronics 56(6), 2229–2236 (2009)

8. Huerta, H., Loukianov, A.G., Cañedo, J.M.: Decentralized Sliding Mode Block Control of Multimachine Power Systems. International Journal of Electrical Power and Energy Systems 32(1), 1–11 (2010)
9. Isidori, A.: Nonlinear control systems. Springer, London (1992)
10. Kosmatopoulos, E.B.: Dynamical neural networks that ensure exponential identification error convergence. Neural Networks 1(2), 299–314 (1997)
11. Krstic, M., Kanellakopoulos, I., Kokotovic, P.: Nonlinear and adaptive control design. Wiley-Interscience, New York (1995)
12. Levant, A.: Higher-order sliding modes, differentiation and output-feedback control. International Journal of Control 76(9/10), 924–941 (2003)
13. Luk'yanov, A.G.: A Block Method of Synthesis of Nonlinear Systems at Sliding Mode. Automation and Remote Control 59(7), 916–933 (1998)
14. Loukianov, A.G., Cañedo, J.M., Utkin, V.I., Cabrera-Vázquez, J.: Discontinuous controller for power system: sliding-mode block control approach. IEEE Trans. On Industrial Electronics 51(2), 340–353 (2004)
15. Loukianov, A.G.: Robust block decomposition sliding mode control design. Int. Jorn. Mathematical Problems in Engineering: Theory, Methods and Applications 8(4-5), 349–365 (2002)
16. Loukianov, A.G., Sanchez, E.N., Felix, R.A.: Induction motor VSC control using neural networks. In: Proceedings of the 15th IFAC World Congress, Barcelona (July 2002)
17. Loukianov, A.G., Cañedo, J.M., Coronado Mendoza, A.: Sliding mode observer-based control of induction motor with magneting saturation effect. In: Proceedings of the 7th International Workshop on Variable Structure Systems, Sarajevo, pp. 235–245 (July 2002)
18. Loukianov, A., Cañedo, J.M., Fridman, L., Soto-Cota, A.: High order sliding mode controller for synchronous generator with exciter system. IEEE Trans. On Industrial Electronics (2010) (to appear)
19. Aguilar, O., Loukianov, A.G., Cañedo, J.M.: Observer-Based Sliding Mode Control of Synchronous Motors. In: Memorias del Congreso Latinoamericano de Control Automático, Guadalajara, México (December 2002)
20. Sanchez, E.N., Loukianov, A.G., Felix, R.A.: Recurrent neural block form control. Automatica 39, 1275–1282 (2003)
21. Sanchez, E.N., Alanis, A.Y., Loukianov, A.G.: Discrete-Time High Order Neural Control Trained with Kalman Filtering. SCI, vol. 112, p. 110. Springer, Berlin (2008)
22. Soto-Coto, A., Fridman, L.M., Loukianov, A.G., Cañedo, J.M.: Variable structure control of synchronous generator: singularly perturbed analysis. International Journal of Control 79(1), 1–13 (2006)
23. Utkin, V.I., Guldner, J., Shi, J.: Sliding Mode control in Electromechanical Systems. Taylor & Francis, London (1999)